PETER MARTI

THEORY OF STRUCTURES

FUNDAMENTALS
FRAMED STRUCTURES
PLATES AND SHELLS

PETER MARTI

THEORY OF STRUCTURES

FUNDAMENTALS
FRAMED STRUCTURES
PLATES AND SHELLS

WILEY
Ernst & Sohn
A Wiley Company

Prof. Dr. Peter Marti
ETH Zurich
Institute of Structural Engineering (IBK)
8093 Zurich
Switzerland
marti@ibk.baug.ethz.ch

Translated by Philip Thrift, German2English Language Services, Hanover, Germany

Cover: Static and kinematic variables and their relationships, Peter Marti

Library of Congress Card No.:
applied for

British Library Cataloguing-in-Publication Data
A catalogue record for this book is available from the British Library.

Bibliographic information published by the Deutsche Nationalbibliothek
The Deutsche Nationalbibliothek lists this publication in the Deutsche Nationalbibliografie; detailed bibliographic data are available on the Internet at <http://dnb.d-nb.de>.

Coverdesign: Sophie Bleifuß, Berlin, Germany
Production: HillerMedien, Berlin, Germany
Typesetting: Hagedorn Kommunikation, Viernheim, Germany
Printing and Binding: AZ Druck und Datentechnik GmbH, Berlin, Germany
Binding: Stein+Lehmann, Berlin, Germany
Printed in the Federal Republic of Germany.
Printed on acid-free paper.

ISBN 978-3-433-02991-6

// ePDF ISBN 978-3-433-60260-7 // ePub ISBN 978-3-433-60261-4 //
// mobi ISBN 978-3-433-60262-1 // oBook ISBN 978-3-433-60263-8 //

PREFACE

This book grew out of the lectures I gave at the University of Toronto between 1982 and 1987 and those I have been giving at the Swiss Federal Institute of Technology Zurich (ETH Zurich) since 1990. The lectures in Toronto were entitled "Energy methods in structural engineering" and "Structural stability", those in Zurich "Theory of structures I-III" and "Plate and shell structures". In addition, the book contains material from my lectures on "Applied mechanics" and "Plasticity in reinforced concrete" (Toronto) as well as "Conceptual design", "Bridge design", "Building structures" and "Structural concrete I-III" (Zurich).

The book is aimed at students and teaching staff as well as practising civil and structural engineers. Its purpose is to enable readers to model and handle structures sensibly, and to provide support for the planning and checking of structures.

These days, most structural calculations are carried out by computers on the basis of the finite element method. This book provides only an introduction to that topic. It concentrates on the fundamentals of the theory of structures, the goal being to convey appropriate insights into and knowledge about structural behaviour. Framed structures and plate and shell structures are treated according to elastic theory and plastic theory. There are many examples and also a number of exercises for the reader to solve independently. On the whole, the aim is to provide the necessary support so that the reader, through skilful modelling, can achieve meaningful results just adequate for the respective engineering issue, using the simplest means possible. In particular, such an approach will enable the reader to check computer calculations critically and efficiently – an activity that is always necessary, but unfortunately often neglected. Moreover, the broader basis of more in-depth knowledge focuses attention on the essentials and creates favourable conditions for the synthesis of the structural, constructional, practical realisation and creative issues so necessary in structural design.

Chapters 3 and 4, which deal with the general principles of structural engineering, have been heavily influenced by my work as the head of the "Swisscodes" project of the Swiss Engineers & Architects Association (SIA). The purpose of this project, carried out between 1998 and 2003, was to revise fully the structures standards of the SIA, which were subsequently republished as Swiss standards SIA 260 to 267. I am grateful to the SIA for granting permission to reproduce Fig. 1 and Tab. 1 from SIA 260 "Basis of structural design" as Fig. 3.1 and Tab. 4.1 in this book. Further, I would also like to thank the SIA for consenting to the use of the service criteria agreement and basis of design examples, which formed part of my contribution to the introduction of SIA 260 in document SIA D 0181, as examples 3.1 and 3.2 here.

In essence, the account of the theory of structures given in this book is based on my civil engineering studies at ETH Zurich. Hans Ziegler, professor of mechanics, and Bruno Thürlimann, professor of theory of structures and structural concrete, and also my dissertation advisor and predecessor, had the greatest influence on me. Prof. Thürlimann was a staunch advocate of the use of plastic theory in structural engineering and enjoyed support from Prof. Ziegler for his endeavours in this respect. I am also grateful to the keen insights provided by Pierre Dubas, professor of theory of structures and structural steelwork, and Christian Menn, professor of theory of structures and design, especially with regard to the transfer of theory into practice. Many

Theory of Structures. First Edition. Peter Marti

examples and forms of presentation used in this book can be attributed to all four of these teachers, whom I hold in high esteem, and the Zurich school of theory of structures, which they have shaped to such a great extent.

During my many years as a lecturer in Toronto and Zurich, students gave me many valuable suggestions for improving my lectures; I am deeply obliged to all of them. Grateful thanks also go to my current and former assistants at ETH Zurich. Their great dedication to supervising students and all their other duties connected with teaching have contributed greatly to the ongoing evolution of the Zurich school of theory of structures.

Susanna Schenkel, dipl. Ing. ETH, and Matthias Schmidlin, dipl. Arch. ETH/dipl. Ing. ETH, provided invaluable help during the preparation of the manuscript. Mr. Schmidlin produced all the figures and Mrs. Schenkel coordinated the work, maintained contact with the publisher and wrote all the equations and large sections of the text; I am very grateful to both for their precise and careful work. Furthermore, I would like to thank Maya Stacey for her typing services. A great vote of thanks also goes to my personal assistant, Regina Nöthiger, for her help during the preparations for this book project and for always relieving me from administrative tasks very effectively. Philip Thrift translated the text from German into English. I should like to thank him for the care he has taken and also for his helpful suggestions backed up by practical experience. Finally, I would like to thank the publisher, Ernst & Sohn, for the pleasant cooperation and the meticulous presentation of this book.

Zurich, February 2013 Peter Marti

CONTENTS

Preface V

I INTRODUCTION

1 THE PURPOSE AND SCOPE OF THEORY OF STRUCTURES 1
1.1 General 1
1.2 The basis of theory of structures 1
1.3 Methods of theory of structures 2
1.4 Statics and structural dynamics 3
1.5 Theory of structures and structural engineering 3

2 BRIEF HISTORICAL BACKGROUND 5

II FUNDAMENTALS

3 DESIGN OF STRUCTURES 11
3.1 General 11
3.2 Conceptual design 11
3.3 Service criteria agreement and basis of design 14
3.4 Summary 26
3.5 Exercises 27

4 STRUCTURAL ANALYSIS AND DIMENSIONING 29
4.1 General 29
4.2 Actions 29
4.2.1 Actions and action effects 29
4.2.2 Models of actions and representative values 30
4.3 Structural models 31
4.4 Limit states 31
4.5 Design situations and load cases 32
4.6 Verifications 33
4.6.1 Verification concept 33
4.6.2 Design values 33
4.6.3 Verification of structural safety 34
4.6.4 Verification of serviceability 35
4.7 Commentary 35
4.8 Recommendations for the structural calculations 36
4.9 Recommendations for the technical report 38
4.10 Summary 40
4.11 Exercises 41

5 STATIC RELATIONSHIPS 43
5.1 Force systems and equilibrium 43
5.1.1 Terminology 43
5.1.2 Force systems 44
5.1.3 Equilibrium 45
5.1.4 Overall stability 45
5.1.5 Supports 47
5.1.6 Hinges 50
5.1.7 Stress resultants 51
5.2 Stresses 53
5.2.1 Terminology 53
5.2.2 Uniaxial stress state 53
5.2.3 Coplanar stress states 54
5.2.4 Three-dimensional stress states 57
5.3 Differential structural elements 61
5.3.1 Straight bars 61
5.3.2 Bars in single curvature 62
5.4 Summary 68
5.5 Exercises 69

6 KINEMATIC RELATIONSHIPS 71
6.1 Terminology 71
6.2 Coplanar deformation 72
6.3 Three-dimensional deformation state 74
6.4 Summary 76
6.5 Exercises 77

7 CONSTITUTIVE RELATIONSHIPS 79
7.1 Terminology 79
7.2 Linear elastic behaviour 81
7.3 Perfectly plastic behaviour 83
7.3.1 Uniaxial stress state 83
7.3.2 Three-dimensional stress states 84
7.3.3 Yield conditions 85
7.4 Time-dependent behaviour 90
7.4.1 Shrinkage 90
7.4.2 Creep and relaxation 91
7.5 Thermal deformations 94
7.6 Fatigue 94
7.6.1 General 94
7.6.2 *S-N* curves 95
7.6.3 Damage accumulation under fatigue loads 96
7.7 Summary 98
7.8 Exercises 99

Theory of Structures. First Edition. Peter Marti

8 ENERGY METHODS 101
8.1 Introductory example 101
8.1.1 Statically determinate system 101
8.1.2 Statically indeterminate system 103
8.1.3 Work equation 104
8.1.4 Commentary 105
8.2 Variables and operators 105
8.2.1 Introduction 105
8.2.2 Plane framed structures 107
8.2.3 Spatial framed structures 109
8.2.4 Coplanar stress states 110
8.2.5 Coplanar strain state 111
8.2.6 Slabs 111
8.2.7 Three-dimensional continua 113
8.2.8 Commentary 114
8.3 The principle of virtual work 115
8.3.1 Virtual force and deformation variables 115
8.3.2 The principle of virtual deformations 115
8.3.3 The principle of virtual forces 115
8.3.4 Commentary 116
8.4 Elastic systems 118
8.4.1 Hyperelastic materials 118
8.4.2 Conservative systems 119
8.4.3 Linear elastic systems 125
8.5 Approximation methods 128
8.5.1 Introduction 128
8.5.2 The RITZ method 129
8.5.3 The GALERKIN method 132
8.6 Summary 134
8.7 Exercises 135

III LINEAR ANALYSIS OF FRAMED STRUCTURES

9 STRUCTURAL ELEMENTS AND TOPOLOGY 137
9.1 General 137
9.2 Modelling of structures 137
9.3 Discretised structural models 140
9.3.1 Description of the static system 140
9.3.2 Joint equilibrium 141
9.3.3 Static determinacy 142
9.3.4 Kinematic derivation of the equilibrium matrix 144
9.4 Summary 147
9.5 Exercises 147

10 DETERMINING THE FORCES 149
10.1 General 149
10.2 Investigating selected free bodies 150
10.3 Joint equilibrium 154
10.4 The kinematic method 156
10.5 Summary 158
10.6 Exercises 158

11 STRESS RESULTANTS AND STATE DIAGRAMS 159
11.1 General 159
11.2 Hinged frameworks 160
11.2.1 Hinged girders 161
11.2.2 Hinged arches and frames 163
11.2.3 Stiffened beams with intermediate hinges 165
11.3 Trusses 166
11.3.1 Prerequisites and structural topology 166
11.3.2 Methods of calculation 169
11.3.3 Joint equilibrium 169
11.3.4 CREMONA diagram 171
11.3.5 RITTER method of sections 172
11.3.6 The kinematic method 173
11.4 Summary 174
11.5 Exercises 175

12 INFLUENCE LINES 177
12.1 General 177
12.2 Determining influence lines by means of equilibrium conditions 178
12.3 Kinematic determination of influence lines 179
12.4 Summary 183
12.5 Exercises 183

13 ELEMENTARY DEFORMATIONS 185
13.1 General 185
13.2 Bending and normal force 185
13.2.1 Stresses and strains 185
13.2.2 Principal axes 187
13.2.3 Stress calculation 189
13.2.4 Composite cross-sections 190
13.2.5 Thermal deformations 192
13.2.6 Planar bending of curved bars 193
13.2.7 Practical advice 194
13.3 Shear forces 194
13.3.1 Approximation for prismatic bars subjected to pure bending 194
13.3.2 Approximate coplanar stress state 196
13.3.3 Thin-wall cross-sections 197
13.3.4 Shear centre 199
13.4 Torsion 200
13.4.1 Circular cross-sections 200
13.4.2 General cross-sections 201
13.4.3 Thin-wall hollow cross-sections 204
13.4.4 Warping torsion 207
13.5 Summary 216
13.6 Exercises 218

14 SINGLE DEFORMATIONS 221
14.1 General 221
14.2 The work theorem 222
14.2.1 Introductory example 222
14.2.2 General formulation 223
14.2.3 Calculating the passive work integrals 223
14.2.4 Systematic procedure 226

14.3 Applications 226
14.4 MAXWELL's theorem 230
14.5 Summary 231
14.6 Exercises 231

15 DEFORMATION DIAGRAMS 233
15.1 General 233
15.2 Differential equations for straight bar elements 233
15.2.1 In-plane loading 233
15.2.2 General loading 235
15.2.3 The effect of shear forces 235
15.2.4 Creep, shrinkage and thermal deformations 235
15.2.5 Curved bar axes 235
15.3 Integration methods 236
15.3.1 Analytical integration 236
15.3.2 MOHR's analogy 238
15.5 Exercises 243

16 THE FORCE METHOD 245
16.1 General 245
16.2 Structural behaviour of statically indeterminate systems 245
16.2.1 Overview 245
16.2.2 Statically determinate system 246
16.2.3 System with one degree of static indeterminacy 247
16.2.4 System with two degrees of static indeterminacy 249
16.2.5 In-depth analysis of system with one degree of static indeterminacy 250
16.2.6 In-depth analysis of system with two degrees of static indeterminacy 253
16.3 Classic presentation of the force method 254
16.3.1 General procedure 254
16.3.2 Commentary 255
16.3.3 Deformations 257
16.3.4 Influence lines 259
16.4 Applications 262
16.5 Summary 272
16.6 Exercises 274

17 THE DISPLACEMENT METHOD 277
17.1 Independent bar end variables 277
17.1.1 General 277
17.1.2 Member stiffness relationship 277
17.1.3 Actions on bars 278
17.1.4 Algorithm for the displacement method 280
17.2 Complete bar end variables 281
17.2.1 General 281
17.2.2 Member stiffness relationship 282
17.2.3 Actions on bars 283
17.2.4 Support force variables 283
17.3 The direct stiffness method 284
17.3.1 Incidence transformation 284
17.3.2 Rotational transformation 285
17.3.3 Algorithm for the direct stiffness method 286
17.4 The slope-deflection method 290
17.4.1 General 290
17.4.2 Basic states and member end moments 292
17.4.3 Equilibrium conditions 293
17.4.4 Applications 294
17.4.5 Restraints 298
17.4.6 Influence lines 303
17.4.7 CROSS method of moment distribution 305
17.5 Summary 309
17.6 Exercises 310

18 CONTINUOUS MODELS 311
18.1 General 311
18.2 Bar extension 311
18.2.1 Practical examples 311
18.2.2 Analytical model 312
18.2.3 Residual stresses 314
18.2.4 Restraints 315
18.2.5 Bond 316
18.2.6 Summary 320
18.3 Beams in shear 321
18.3.1 Practical examples 321
18.3.2 Analytical model 321
18.3.3 Multi-storey frame 321
18.3.4 VIERENDEEL girder 323
18.3.5 Sandwich panels 324
18.3.6 Summary 326
18.4 Beams in bending 326
18.4.1 General 326
18.4.2 Analytical model 327
18.4.3 Restraints 327
18.4.4 Elastic foundation 329
18.4.5 Summary 332
18.5 Combined shear and bending response 333
18.5.1 General 333
18.5.2 Shear wall - frame systems 334
18.5.3 Shear wall connection 338
18.5.4 Dowelled beams 342
18.5.5 Summary 344
18.6 Arches 345
18.6.1 General 345
18.6.2 Analytical model 345
18.6.3 Applications 346
18.6.4 Summary 350
18.7 Annular structures 350
18.7.1 General 350
18.7.2 Analytical model 351
18.7.3 Applications 352
18.7.4 Edge disturbances in cylindrical shells 353
18.7.5 Summary 354
18.8 Cables 354
18.8.1 General 354
18.8.2 Analytical model 355
18.8.3 Inextensible cables 357

18.8.4 Extensible cables 358
18.8.5 Axial stiffness of laterally loaded cables 360
18.8.6 Summary 360
18.9 Combined cable-type and bending response 361
18.9.1 Analytical model 361
18.9.2 Bending-resistant ties 362
18.9.3 Suspended roofs and stress ribbons 363
18.9.4 Suspension bridges 368
18.9.5 Summary 368
18.10 Exercises 369

19 DISCRETISED MODELS 371
19.1 General 371
19.2 The force method 372
19.2.1 Complete and global bar end forces 372
19.2.2 Member flexibility relation 372
19.2.3 Actions on bars 374
19.2.4 Algorithm for the force method 374
19.2.5 Comparison with the classic force method 376
19.2.6 Practical application 376
19.2.7 Reduced degrees of freedom 376
19.2.8 Supplementary remarks 379
19.3 Introduction to the finite element method 381
19.3.1 Basic concepts 381
19.3.2 Element matrices 381
19.3.3 Bar element rigid in shear 381
19.3.4 Shape functions 385
19.3.5 Commentary 386
19.4 Summary 386
19.5 Exercises 387

IV NON-LINEAR ANALYSIS OF FRAMED STRUCTURES

20 ELASTIC-PLASTIC SYSTEMS 389
20.1 General 389
20.2 Truss with one degree of static indeterminacy 389
20.2.1 Single-parameter loading 389
20.2.2 Dual-parameter loading and generalisation 395
20.3 Beams in bending 398
20.3.1 Moment-curvature diagrams 398
20.3.2 Simply supported beams 399
20.3.3 Continuous beams 403
20.3.4 Frames 404
20.3.5 Commentary 405
20.4 Summary 406
20.5 Exercises 407

21 LIMIT ANALYSIS 409
21.1 General 409
21.2 Upper- and lower-bound theorems 410
21.2.1 Basic concepts 410
21.2.2 Lower-bound theorem 410
21.2.3 Upper-bound theorem 411
21.2.4 Compatibility theorem 411
21.2.5 Consequences of the upper- and lower-bound theorems 411
21.3 Static and kinematic methods 412
21.3.1 General 412
21.3.2 Simply supported beams 413
21.3.3 Continuous beams 415
21.3.4 Plane frames 416
21.3.5 Plane frames subjected to transverse loads 421
21.4 Plastic strength of materials 426
21.4.1 General 426
21.4.2 Skew bending 426
21.4.3 Bending and normal force 428
21.4.4 Bending and torsion 432
21.4.5 Bending and shear force 434
21.5 Shakedown and limit loads 435
21.6 Dimensioning for minimum weight 437
21.6.1 General 437
21.6.2 Linear objective function 438
21.6.3 FOULKES mechanisms 438
21.6.4 Commentary 440
21.7 Numerical methods 441
21.7.1 The force method 441
21.7.2 Limit load program 442
21.7.3 Optimum design 444
21.8 Summary 446
21.9 Exercises 447

22 STABILITY 449
22.1 General 449
22.2 Elastic buckling 449
22.2.1 Column deflection curve 449
22.2.2 Bifurcation problems 453
22.2.3 Approximation methods 454
22.2.4 Further considerations 460
22.2.5 Slope-deflection method 465
22.2.6 Stiffness matrices 469
22.3 Elastic-plastic buckling 471
22.3.1 Concentrically loaded columns 471
22.3.2 Eccentrically loaded columns 474
22.3.3 Limit loads of frames according to second-order theory 477
22.4 Flexural-torsional buckling and lateral buckling 480
22.4.1 Basic concepts 480
22.4.2 Concentric loading 482
22.4.3 Eccentric loading in the strong plane 483
22.4.4 General loading 485
22.5 Summary 488
22.6 Exercises 489

V PLATES AND SHELLS

23 PLATES 491
23.1 General 491
23.2 Elastic plates 491
23.2.1 Stress function 491

23.2.2 Polar coordinates 493
23.2.3 Approximating functions for displacement components 496
23.3 Reinforced concrete plate elements 496
23.3.1 Orthogonal reinforcement 496
23.3.2 General reinforcement 500
23.4 Static method 501
23.4.1 General 501
23.4.2 Truss models 501
23.4.3 Discontinuous stress fields 505
23.4.4 Stringer-panel model 511
23.5 Kinematic method 512
23.5.1 Applications in reinforced concrete 512
23.5.2 Applications in geotechnical engineering 517
23.6 Summary 520
23.7 Exercises 522

24 SLABS 525
24.1 Basic concepts 525
24.1.1 General 525
24.1.2 Static relationships 525
24.1.3 Kinematic relationships 531
24.2 Linear elastic slabs rigid in shear with small deflections 533
24.2.1 Fundamental relationships 533
24.2.2 Methods of solution 535
24.2.3 Rotationally symmetric problems 536
24.2.4 Rectangular slabs 539
24.2.5 Flat slabs 543
24.2.6 Energy methods 546
24.3 Yield conditions 547
24.3.1 VON MISES and TRESCA yield conditions 547
24.3.2 Reinforced concrete slabs 550
24.4 Static method 557
24.4.1 Rotationally symmetric problems 557
24.4.2 Moment fields for rectangular slabs 560
24.4.3 Strip method 563
24.5 Kinematic method 567
24.5.1 Introductory example 567
24.5.2 Calculating the dissipation work 568
24.5.3 Applications 569
24.6 The influence of shear forces 572
24.6.1 Elastic slabs 572
24.6.2 Rotationally symmetric VON MISES slabs 574
24.6.3 Reinforced concrete slabs 575
24.7 Membrane action 575
24.7.1 Elastic slabs 575
24.7.2 Perfectly plastic slab strip 577
24.7.3 Reinforced concrete slabs 578
24.8 Summary 581
24.9 Exercises 583

25 FOLDED PLATES 587
25.1 General 587
25.2 Prismatic folded plates 588
25.2.1 Sawtooth roofs 588
25.2.2 Barrel vaults 589
25.2.3 Commentary 593
25.3 Non-prismatic folded plates 594
25.4 Summary 594
25.5 Exercises 594

26 SHELLS 595
26.1 General 595
26.2 Membrane theory for surfaces of revolution 596
26.2.1 Symmetrical loading 596
26.2.2 Asymmetric loading 600
26.3 Membrane theory for cylindrical shells 601
26.3.1 General relationships 601
26.3.2 Pipes and barrel vaults 602
26.3.3 Polygonal domes 604
26.4 Membrane forces in shells of any form 606
26.4.1 Equilibrium conditions 606
26.4.2 Elliptical problems 607
26.4.3 Hyperbolic problems 608
26.5 Bending theory for rotationally symmetric cylindrical shells 613
26.6 Bending theory for shallow shells 615
26.6.1 Basic concepts 615
26.6.2 Differential equation for deflection 616
26.6.3 Circular cylindrical shells subjected to asymmetric loading 617
26.7 Bending theory for symmetrically loaded surfaces of revolution 620
26.7.1 Basic concepts 620
26.7.2 Differential equation for deflection 620
26.7.3 Spherical shells 621
26.7.4 Approximation for shells of any form 623
26.8 Stability 623
26.8.1 General 623
26.8.2 Bifurcation loads 624
26.8.3 Commentary 626
26.9 Summary 627
26.10 Exercises 628

APPENDIX

A1 DEFINITIONS 631
A2 NOTATION 637
A3 PROPERTIES OF MATERIALS 643
A4 GEOMETRICAL PROPERTIES OF SECTIONS 645

A5 MATRIX ALGEBRA 649
A5.1 Terminology 649
A5.2 Algorithms 650
A5.3 Linear equations 652
A5.4 Quadratic forms 652
A5.5 Eigenvalue problems 653
A5.6 Matrix norms and condition numbers 654

A6 TENSOR CALCULUS 655
A6.1 Introduction 655
A6.2 Terminology 655
A6.3 Vectors and tensors 656
A6.4 Principal axes of symmetric second-order tensors 658
A6.5 Tensor fields and integral theorems 658

A7 CALCULUS OF VARIATIONS 661
A7.1 Extreme values of continuous functions 661
A7.2 Terminology 661
A7.3 The simplest problem of calculus of variations 662
A7.4 Second variation 663
A7.5 Several functions required 664
A7.6 Higher-order derivatives 664
A7.7 Several independent variables 665
A7.8 Variational problems with side conditions 665
A7.9 The RITZ method 666
A7.10 Natural boundary conditions 667

REFERENCES 669

NAME INDEX 671

SUBJECT INDEX 673

EXAMPLECOLLECTION

Example 3.1 Service criteria agreement for industrial building XY in Z 15
Example 3.2 Basis of design for industrial building XY in Z 19
Example 5.1 Cantilever retaining wall 45
Example 5.2 Support envelope 47
Example 5.3 Steel plate 56
Example 5.4 Stress tensor 59
Example 5.5 Hoop stress formula 63
Example 5.6 Thrust line 63
Example 5.7 Three-hinged arch 65
Example 5.8 Beam as circular arc 67
Example 6.1 Measuring grid 73
Example 7.1 Time-independent restraint 93
Example 7.2 Time-dependent restraint 93
Example 7.3 Prestressing 93
Example 7.4 Loss of prestress 93
Example 7.5 Fatigue of reinforcing steel 97
Example 8.1 Determining internal force variables 116
Example 8.2 Determining external deformation variables 116
Example 8.3 Geometric and material non-linearity 117
Example 8.4 Tie 119
Example 8.5 Beam with one degree of static indeterminacy 121
Example 8.6 Geometric non-linearity 122
Example 8.7 Cantilever beam 122
Example 8.8 Cantilever beam 124
Example 8.9 Calibration ring 124
Example 8.10 Simply supported beam 126
Example 8.11 Simply supported beam 128
Example 8.12 Tie 129
Example 8.13 Cantilever beam 130
Example 8.14 Ideal cantilever column 130
Example 8.15 Cantilever beam column 131
Example 8.16 Simply supported beam column 133
Example 10.1 Plane truss 152
Example 10.2 Plane frame 153
Example 10.3 Plane truss 154
Example 10.4 Plane frame 154
Example 10.5 Three-hinged arch 156
Example 10.6 Plane frame 157
Example 11.1 Hinged girder 162
Example 11.2 Three-hinged frame with tie 164
Example 11.3 Plane truss 169
Example 11.4 Plane truss 171
Example 11.5 Plane truss 172
Example 11.6 Plane truss 172
Example 12.1 Hinged girder 180
Example 12.2 Three-hinged arch 180
Example 12.3 Plane truss 182
Example 13.1 Unequal leg angle 188
Example 13.2 Rectangular cross-section – kern 190
Example 13.3 Reinforced concrete slab – bending 191
Example 13.4 Reinforced concrete slab – shrinkage 192
Example 13.5 Rectangular cross-section – shear stress distribution 195
Example 13.6 Wide-flange beam 197
Example 13.7 Unequal leg angle 198

Example 13.8 Elliptical bar 202
Example 13.9 Narrow rectangular cross-section 203
Example 13.10 Reinforced concrete box girder 205
Example 13.11 Twin-cell box girder 206
Example 13.12 Twisted I beam – concentrated load 208
Example 13.13 Twisted I beam – distributed load 209
Example 13.14 Reinforced concrete beam 213
Example 14.1 SIMPSON's rule 225
Example 14.2 Beam with one degree of static indeterminacy 226
Example 14.3 Hinged girder 227
Example 14.4 Cantilever beam 228
Example 14.5 Cranked cantilever beam 228
Example 14.6 Plane truss 229
Example 14.7 Rectangular cross-section – area shear factor 229
Example 14.8 Thin-wall hollow cross-section 230
Example 15.1 Simply supported beam 236
Example 15.2 Beam fixed at both ends 236
Example 15.3 Beam with one degree of static indeterminacy 237
Example 15.4 Beam with spring restraint 239
Example 15.5 Cantilever beam 239
Example 15.6 Beam with one degree of static indeterminacy 240
Example 15.7 Hinged girder 240
Example 16.1 Plane frame 257
Example 16.2 Bar fixed at both ends 258
Example 16.3 Beam with one degree of static indeterminacy 259
Example 16.4 Continuous beam 260
Example 16.5 Beam fixed at both ends 262
Example 16.6 Continuous beam of infinite length 263
Example 16.7 Continuous beam – support settlement 267
Example 16.8 Arch fixed at both ends 268
Example 16.9 Beam on skew supports 269
Example 16.10 Beam as circular arc 270
Example 16.11 Considering subsystems 271
Example 17.1 Cantilever beam rigid in shear 280
Example 17.2 Cantilever beam rigid in shear 283
Example 17.3 Plane frame 287
Example 17.4 Non-sway frame 294
Example 17.5 Grandstand frame 295
Example 17.6 Multi-storey sway frame 296
Example 17.7 Multi-storey non-sway frame 297
Example 17.8 Non-sway frame – settlement of supports 299
Example 17.9 Non-sway frame – uniform rise in temperature 299
Example 17.10 Non-sway frame – temperature difference 301
Example 17.11 Sway frame – uniform rise in temperature 301
Example 17.12 Three-span frame 304
Example 17.13 Continuous beam 306
Example 18.1 Bar restrained at both ends 313
Example 18.2 Bar with spring restraint at one end 313
Example 18.3 Reinforced concrete column – change in temperature 314
Example 18.4 Reinforced concrete column – shrinkage 314
Example 18.5 Pulling out a reinforcing bar 317
Example 18.6 Multi-storey frame 322
Example 18.7 Externally statically indeterminate VIERENDEEL girder 323
Example 18.8 Plastic panel with bonded sheet steel outer faces 325
Example 18.9 Simply supported beam – sinusoidal line load 327
Example 18.10 Bar fixed at both ends – linear temperature gradient 328

Example 18.11 High-rise building 335
Example 18.12 High-rise building with outrigger 337
Example 18.13 Shear wall 340
Example 18.14 Shear wall – influence of wall extensions 341
Example 18.15 Two-hinged arch – uniformly distributed load 347
Example 18.16 Two-hinged arch – sinusoidal load 348
Example 18.17 Two-hinged arch – constant load segment by segment 349
Example 18.18 Displacement of the abutments to a concrete arch 350
Example 18.19 Stiffened pipe subjected to internal pressure 354
Example 18.20 Single strand – uniformly distributed load 359
Example 18.21 Single strand – thermal action 359
Example 18.22 Single strand – prestress 359
Example 18.23 Single strand – constant loads on both halves of the span 360
Example 18.24 Cable with wheel load 362
Example 18.25 Stresses in stay cable 363
Example 18.26 Suspended roof – uniformly distributed load 364
Example 18.27 Suspended roof – asymmetric imposed load 365
Example 18.28 Stress ribbon – asymmetric imposed load 365
Example 18.29 Suspended roof – central point load 367
Example 18.30 Stress ribbon – thermal action 367
Example 19.1 Plane frame 374
Example 19.2 Orthogonalised restraint states 379
Example 19.3 Beam with one degree of static indeterminacy 384
Example 21.1 Unequal leg angle 427
Example 21.2 Two-span beam – repeated variable actions 436
Example 21.3 Plane frame 442
Example 21.4 Plane frame – static program 443
Example 21.5 Plane frame – kinematic program 444
Example 21.6 Plane frame – minimum weight 445
Example 22.1 Beam column 451
Example 22.2 Cantilever column 455
Example 22.3 Ideal column 455
Example 22.4 Beam column 456
Example 22.5 Ideal column 456
Example 22.6 Ideal column with one degree of static indeterminacy 457
Example 22.7 Column with abrupt change in stiffness 458
Example 22.8 Load applied to top of cantilever column 458
Example 22.9 Statically determinate frame 459
Example 22.10 Elastically supported inclined leg frame 463
Example 22.11 Two-hinged frame 467
Example 22.12 Non-sway frame 468
Example 22.13 Sway frame 468
Example 22.14 Elastically restrained vertical cantilever 468
Example 22.14 Vertical cantilever 477
Example 22.15 Lateral buckling of an I section 486
Example 22.16 Lateral buckling – shifting the point of load application 486
Example 23.1 Cantilever beam 492
Example 23.2 Cylindrical pipe 495
Example 23.3 Beam in the form of a circular arc 495
Example 23.4 Uniaxial tension 498
Example 23.5 Vertical embankment 505
Example 23.6 Strip foundation on TRESCA half-space 506
Example 23.7 Curtailed reinforcement in tension chord 514
Example 23.8 Web crushing failure 516
Example 23.9 Dissipation at hyperbolic slip line 517
Example 23.10 Strip foundation on TRESCA half-space 519

Example 24.1 Square slab supported at the corners 528
Example 24.2 Square slab supported in the centre 529
Example 24.3 Rectangular slab supported at the corners 529
Example 24.4 Simply supported square slab 547
Example 24.5 Fixed square slab 547
Example 24.6 Simply supported circular slab 549
Example 24.7 Fixed circular slab 550
Example 24.8 Reinforced concrete slab – dimensioning for bending 553
Example 24.9 Slab element subjected to pure twist 554
Example 24.10 Fixed circular slab 558
Example 24.11 Annular slab fixed at its inner edge and loaded on its outer edge by m_u 558
Example 24.12 Simply supported rectangular slab 561
Example 24.13 Square slab simply supported along two adjacent edges 561
Example 24.14 Simply supported regular polygonal slabs 561
Example 24.15 Cantilever slab with point load on edge 563
Example 24.16 Fixed rectangular slab 569
Example 24.17 Square slab simply supported along two adjacent edges 569
Example 24.18 Fixed square slab 570
Example 24.19 Slab strip subjected to a central point load 570
Example 24.20 Cantilever slab with point load on edge 570
Example 24.21 Flat slab 571
Example 24.22 Semi-infinite rectangular slab subjected to edge loads 573
Example 24.23 Buckling of simply supported rectangular slabs 575
Example 24.24 Rectangular slab with initial deformation 576
Example 24.25 Square membrane 577
Example 25.1 Barrel vault – membrane theory 590
Example 25.2 Barrel vault – bending theory 591
Example 26.1 Spherical shells 597
Example 26.2 Spherical tanks 598
Example 26.3 Conical shell 598
Example 26.4 Spherical shell – dead load 599
Example 26.5 Spherical shell – wind pressure 600
Example 26.6 Conical shell – wind pressure 601
Example 26.7 Dome with circular cylindrical sectors – self-weight 605
Example 26.8 Pipe subjected to end loads 613
Example 26.9 Cylindrical tank 614
Example 26.10 Pipe subjected to thermal action 614
Example 26.11 Chimney subjected to wind pressure 618
Example 26.12 Fixed spherical shell subjected to internal pressure 622
Example 26.13 Pressure vessel 622
Example A7.1 Cantilever beam rigid in shear 666
Example A7.2 Cantilever beam – uniformly distributed load plus load at free end 667

1 THE PURPOSE AND SCOPE OF THEORY OF STRUCTURES

1.1 General

Theory of structures is a subdiscipline of applied mechanics which is configured to suit the needs of civil and structural engineers. The purpose of theory of structures is to present systematically the knowledge about the behaviour of structures at rest, to expand that knowledge and to prepare it for practical applications. It forms the basis for the design of every new structure and the examination of every existing one.

The terms and methods used in the theory of structures enable the engineer to adopt a uniform approach not tied to any particular type of construction (concrete, steel, composite, timber or masonry). With the advent of the computer in the third quarter of the 20th century, this approach gradually became *structural mechanics*, the discipline to which theory of structures belongs today.

At the heart of every theory of structures exercise there is a *structural model*, which is obtained through isolation and idealisation and takes into account the geometry of the structure, the properties of the construction materials and the possible actions. Determining the action effects, i. e. the structure's responses to the actions, is carried out with the help of *analytical models* that link the governing force and deformation variables via equilibrium and compatibility conditions plus constitutive equations.

Without doubt, many are convinced that the calculations should determine the dimensions unequivocally and conclusively. However, in the light of the impossibility of taking into account all secondary circumstances, every calculation constitutes only a basis for the design engineer, who thus has to grapple with those secondary circumstances...

A totally simple form of calculation alone is therefore possible and sufficient.

Robert MAILLART (1938)

1.2 The basis of theory of structures

Structural behaviour is expressed in the form of *internal* and *external force* and *deformation variables* (loads and stresses plus displacements and strains). Static relationships (equilibrium conditions and static boundary conditions, see chapter 5) link the force variables, kinematic relationships (kinematic relationships and boundary conditions, see chapter 6) link the deformation variables, and constitutive relationships (see chapter 7) link the internal force and deformation variables. The most general statements within the scope of theory of structures are obtained when the internal and external force and deformation variables are rigorously associated in the form of *work-associated variables* (see chapter 8) [1].

Statics is based on three fundamental principles of mechanics. According to the *principle of virtual work*, a (statically admissible) force state (equilibrium set of force variables) fulfilling the static relationships in conjunction with a (kinematically admissible) deformation state (compatibility set of deformation variables) fulfilling the kinematic relationships does not perform any work. Added to this are the *reaction principle* (for every force there is a equal and opposite reaction with the same direction of action) and the *free-body principle* (every part removed from a system in equilibrium undergoing compatible deformation is itself in equilibrium and undergoes compatible deformation).

Looking beyond its link with mechanics, theory of structures has a special significance for *structural engineering* (see chapters 3 and 4). It is a tool for assessing the stability, strength and stiffness of a structure that either exists or is being designed. This application of theory of structures manifests itself in specific methods developed for ascertaining structural behaviour in general and (numerical) treatment in individual cases.

Theory of Structures. First Edition. Peter Marti

1.3 Methods of theory of structures

The principle of virtual work can be expressed as the principle of virtual deformations or the principle of virtual forces. The systematic application of these two principles leads to a series of *dual* kinematic or static *methods*. On the kinematic side it is important to mention LAND's method for determining influence lines (section 12.3), the displacement method for solving statically indeterminate framed structures (chapter 17 and section 19.3) and the kinematic method of limit analysis (sections 21.3 and 21.7). On the static side we have the work theorem for determining single deformations (section 14.2), the force method for solving statically indeterminate framed structures (chapter 16 and section 19.2) and the static method of limit analysis (sections 21.3 and 21.7).

Assuming linear elastic behaviour and small deformations leads to linear statics, in which all the force and deformation variables may be superposed. This possibility of superposition is used extensively in theory of structures, especially in the force and displacement methods. Introducing unknown force or deformation variables and superposing their effects on those of external actions results in sets of linear equations for the unknowns.

However, the *superposition law* no longer applies in the case of non-linear materials problems (chapters 20 and 21) and non-linear geometrical problems (chapter 22). In such instances an (incremental) *iterative procedure* is generally necessary. Errors caused by simplifications at the beginning are evaluated step by step and successively reduced through appropriate corrections.

Analogies can often be used to make complex situations more accessible, or to reduce them to simpler, known situations. Examples of this are the membrane analogy (section 13.4.2) and the sand hill analogy (section 21.4.4) for dealing with elastic or plastic torsion problems, and MOHR's analogy for determining deformation diagrams (section 15.3.2). Combined warping and pure torsion problems (section 13.4.4) can be approached in a similar way to combined shear and bending problems (section 18.5.2) or bending problems in beams with tension (section 18.9). Edge disturbance problems in cylindrical shells (sections 18.7.4 and 26.5) can be reduced to the theory of beams on elastic foundation (section 18.4.4); this theory is also useful for approximating edge disturbance problems in spherical (section 26.7.3) and other shells (section 26.7.4). Furthermore, plates (chapter 23) can be idealised as plane trusses, slabs (chapter 24) as grillages, and folded plates (chapter 25) and shells (chapter 26) as space trusses or spatial frameworks

The development of powerful numerical methods has led to the methods of *graphical statics* (section 10.1) gradually losing the importance they had in the past. However, graphical aids still represent an unbeatable way of illustrating the flow of the forces in structures, e. g. with thrust lines (section 5.3.2, Figs. 17.19 and 21.7) or truss models (section 23.4.2). They represent an indispensable foundation for conceptual design (section 3.2) and the detailing of structural members and their connections.

The development of numerical methods has also brought about a change in the significance of *experimental statics*. From the 1920s through to the 1970s, loading tests on scale models made from celluloid, acrylic sheet and other materials were central to understanding the elastic loadbearing behaviour of complex structures. Such tests are no longer significant today. What continues to be important, however, is scientific testing to verify theoretical models, primarily in conjunction with non-linear phenomena, new materials or forms of construction and accidental actions. In structural design, physical models are not only useful for form-finding and detailing, but also very helpful when assessing the quality of the structural behaviour of the design. During the dimensioning, tests are a sensible backup if, for example, there are no appropriate analytical models available or a large number of identical structural members is required.

Finally, specific measurements during and after execution enable extremely valuable comparisons with the predicted behaviour of a structure – a source of experience that is all too often neglected.

In the *numerical methods* of theory of structures, it is the *finite element method* (FEM) that plays the leading role (section 19.3). These days FEM is the basis of almost all structural calculations. Users have extremely powerful tools at their disposal in the shape of appropriate modern computer programs. But to be able to deploy such programs responsibly, designers should at least understand the basics of the algorithms on which they are based. First and foremost, however, the engineer 's knowledge of theory of structures should enable him or her to check the computer output critically. The crucial thing here is the ability to be able to approximate complex issues by reducing them to simple, understandable problems. Adequate training in the classical methods of theory of structures, which this book aims at, will supply the foundation for that ability.

1.4 Statics and structural dynamics

When it comes to dynamic problems, the principle of virtual work has to be formulated taking into account *inertial forces* (proportional to acceleration): the motion in a system is such that at any point in time the internal, external and inertial forces are in equilibrium. Appropriate additional terms in the equilibrium conditions turn them into *equations of motion*, and can be included, for example, within the scope of the finite element method by way of local and global *mass matrices*. Instead of a set of linear equations, this leads to a set of simultaneous ordinary second-order differential equations for the (time-dependent) node displacement parameters. Assuming constant coefficients, the differential equations can be decoupled according to the method of *modal analysis*. The associated eigenvalue problem leads to a solution in the form of superposed *natural vibrations*.

Generally, damping forces must also be taken into account in the equations of motion. In order that the differential equations remain linear, it is usual to assume that these forces are proportional to velocity. And so that a modal analysis remains possible with decoupled natural vibrations, we use a so-called *modal damping* for simplicity.

Structural dynamics is essentially readily accessible via statics. However, adding the dimension of time makes a more in-depth examination necessary so that dynamic processes become just as familiar as static phenomena. In the end, engineers prepared to make the effort obtain a broader view of theory of structures.

1.5 Theory of structures and structural engineering

For *structural engineering*, theory of structures is an ancillary discipline, like materials science. The knowledge and experience of practising design engineers in this and other relevant special subjects, e. g. geotechnics and construction technology, must be adequate for the complexity and significance of the jobs to which they are assigned. Furthermore, appropriate practical experience with the respective types of construction is an essential requirement for managing the design and execution of construction projects.

Theory of structures plays a role in all phases of conventional project development, from the preliminary design and tender design to the detail design, but in different ways, to suit the particular phase. Whereas for the conceptual design rough structural calculations are adequate, the subsequent phases require analyses of structural safety and serviceability that can be verified by others – and not just for the final condition of the structure, but especially for critical conditions during construction.

Besides new-build projects, the conservation and often the deconstruction of structures also throw up their share of interesting theory of structures problems. Frequently such tasks are far more demanding than those of new structures because fewer, if any, standards are available to help the engineer, and appraising the current condition of a structure is often difficult and associated with considerable uncertainties. The development of appropriate structural and actions models in such cases can be extremely tricky yet fascinating.

Looking beyond the immediate uses of structural design, there are various applications that can be handled with the methods of theory of structures, especially in mechanical engineering, shipbuilding and automotive manufacture, aerospace engineering, too. We are thus part of the great interdisciplinary field of *structural mechanics*.

2 BRIEF HISTORICAL BACKGROUND

Apart from a few minor modifications, this chapter is based on an earlier essay by the author [19]. Readers who wish to find out more should consult references [10], [16], [32] and [33].

Until well into the 19th century, the practical experience of architects, builders and engineers far exceeded their theoretical knowledge. The scientifically founded knowledge of structural behaviour that prevails today had its beginnings in antiquity and the Middle Ages and evolved with the development of mechanics. However, it was not until the 18th century that the first attempts were made to use the new findings in practical construction.

We have to thank the Greek mathematician ARCHIMEDES (*c.* 287 – *c.* 212 BC) for the discovery of hydrostatic buoyancy and for formulating the lever principle for unequal straight levers subjected to vertical forces. Besides formulating theories for the functions of the "simple machines" lever, wedge, screw, pulley and wheel and axle, Archimedes is also credited with inventing technical artefacts such as the screw pump.

Jordanus DE NEMORE (*c.* 1200) is thought to have written various treatises that draw on the works of Greek scholars. But he also added new observations on the cranked lever and the inclined plane.

Leonardo DA VINCI (1452 – 1519) recognised the principle of resolving a force into two components, and also applied the term "moment" (force $\times$ lever arm) to skew forces. He also investigated the breakage of a rope due to its own weight (specific strength), the bending of beams and columns and the equilibrium and failure mechanisms of arches. His extremely imaginative and diverse, yet unsystematic, insights went apparently largely unnoticed during his lifetime.

Simon STEVIN's (1548 – 1620) approach to the concept of moments and the resolution of forces into components cannot be faulted. He worked on many practical applications and provided very vivid descriptions, e. g. the funicular polygon and the "wreath of spheres" experiment to prove the law of the inclined plane.

Pierre VARIGNON (1654 – 1722) identified the connection between the force and funicular polygons and formulated the theorem of the summability of moments.

Giovanni POLENI (1683 – 1761) analysed the load transfer of the 42 m span of the dome to St. Peter's in Rome by constructing the funicular polygon for the weights corresponding to the individual segments of the vaulting. He selected the funicular polygon that passed through the centres of the springing and crown joints and established that the inverted funicular polygon must lie within the arch profile. In 1743 POLENI was appointed to investigate the damage to the dome of St. Peter's, just as one year before the three mathematicians Ruggiero Giuseppe BOŠCOVIĆ (1711 – 1787), Thomas LE SEUR (1703 – 1770) and François JACQUIER (1711 – 1788) had been commissioned to do. Based on the crack pattern observed, the three mathematicians analysed an assumed mechanism and hence determined a deficit in the resistance with respect to the thrust in the arch. They recommended adding further horizontal iron hoops (to resist the tension) around the dome to the three already in place. Although POLENI did not agree with the cause of the damage

Theory of Structures. First Edition. Peter Marti

as described by the mathematicians, he did agree with the proposed strengthening measures.

GALILEO Galilei (1564 – 1642) founded the discipline of strength of materials through his studies of the failure of the cantilever beam. Starting with the tensile test as a "thought experiment" and the associated question of the specific strength, he analysed the equilibrium of a cantilever beam as a cranked lever with its fulcrum at the bottom edge of the fixed-end cross-section. Applying similitude theory, he determined the failure load relationships of simple beam structures with different geometries. He realised that no structure can exceed a certain given size (maximum span) determined by the limits of strength and remarked that hollow cross-sections and cross-sections that vary over the length of the beam can make better use of the strength than prismatic, solid cross-sections.

Edmé MARIOTTE (1620 – 1684) and Pieter van MUSSCHENBROEK (1692 – 1761) carried out tensile and bending strength tests on various materials, the latter also buckling strength tests. Applying similitude theory, it became possible to design a beam. In the bending failure problem, MARIOTTE, like GALILEO, initially assumed that the cantilever beam rotates about the bottom edge of the fixed-end cross-section, but presumed a triangular distribution of the tensile force over the depth of the cross-section. In a further step, he introduced the "axe d'équilibre" (neutral axis) in the middle of the depth of the cross-section and distinguished between zones in tension and compression, with triangular distributions of the tensile and compressive forces above and below this axis. Instead of the theoretically correct reduction factor of 3 of GALILEO's strength studies, he mistakenly arrived at a value of 1.5; his tests resulted in a reduction factor of about 2.

Antoine PARENT (1666 – 1716) recognised that the tensile and compressive forces due to bending must be equal in magnitude and that there are also shear forces acting on the cross-section. Based on MARIOTTE's tests, PARENT positioned the neutral axis somewhat below the middle, i. e. at 45% of the depth of the cross-section, which when compared with GALILEO's work leads to a reduction factor of 2.73 for an equal tensile strength.

Robert HOOKE (1635 – 1703) undertook experiments with springs and reached the conclusion that the forces in elastic bodies are proportional to the corresponding displacements. He also recognised that some of the fibres in a beam subjected to bending are pulled and hence extended and some are compressed and hence shortened. Further, he recommended giving arches the form of an inverted catenary.

Jacob BERNOULLI (1654 – 1705) investigated the deformation of elastic bars with the help of the infinitesimal calculus introduced by Isaac NEWTON (1643 – 1727) and Gottfried Wilhelm LEIBNIZ (1646 – 1716). He assumed that the cross-sections of the bar remain plane during the deformation and discovered that the change in curvature is proportional to the bending forces. However, as he was not yet aware of the stress concept, the integration of the internal forces over the cross-section, which is taken for granted today, is missing from his deductions.

The principle of virtual displacements, already used in a simple form by DE NEMORE, STEVIN and GALILEO, was stated in general form in 1717 by Johann BERNOULLI (1667 – 1748).

Following a proposal by Daniel BERNOULLI (1700 – 1782), Leonhard EULER (1707 – 1783) showed that Jacob BERNOULLI's differential equation of the elastic curve corresponds to a variational problem. According to this, the integral of the squares of the curvatures over the length of the bar is a minimum; for homogeneous prismatic bars, this integral is proportional to the elastically stored deformation work. EULER's detailed treatises on elastic curves led to the solution of the eigenvalue problems of buckling and laterally vibrating bars. Apart from the concept of hydrostatic

stress, we also have EULER to thank for the free-body principle at the root of all mechanics. This principle states that every free body separated with an imaginary cut from a body in equilibrium is itself in equilibrium; internal forces are thus externalised and can therefore be dealt with. Starting by considering the individual mass elements of a body, EULER formulated NEWTON's law of motion in the form of the theorem of linear momentum, and also postulated the theorem of angular momentum. Therefore, equilibrium conditions for forces and moments became special cases of the equations of motion.

The designation "engineer" had already been used in isolated cases in the Middle Ages to describe the builders of military apparatus and fortifications. The direct predecessors of civil engineers as we know them today were French engineering officers who were called upon to carry out civil as well as military tasks. At the suggestion of the most outstanding of these engineering officers, Sébastien le Prêtre de VAUBAN (1633 – 1707), the "Corps des ingénieurs du génie militaire" was set up in 1675. The "Corps des ingénieurs des ponts et chaussées" followed around 1720.

The French engineering officers received scientific, primarily mathematical, training at state schools. The "Ecole des ponts et chaussées" in Paris, founded in 1747 by Daniel Charles TRUDAINE (1703 – 1769) and reorganised in 1760 by Jean Rodolphe PERRONET (1708 – 1794), was at that time unique in Europe. The "Ecole polytechnique", which opened in Paris in 1794, was followed by the polytechnic schools of Prague (1806), Vienna (1815), Karlsruhe (1825) and other cities.

PERRONET was primarily active as a builder of stone bridges. He reduced the widths of the piers in order to improve the flow cross-section, employed very shallow three-centred arches and introduced various other new ideas into the design and construction of such bridges.

Charles Augustin de COULOMB (1736 – 1806) was another French engineering officer. He set down his practical experience in the building of fortifications in the "Essai sur une application des règles de maximis et minimis à quelques problèmes de statique relatifs à l'architecture", which was published in 1776. Based on the tensile tests of samples of stone, he determined the resistance to cleavage fracture per unit area, a property that he termed "cohesion". Although shearing-off tests gave a somewhat larger resistance, COULOMB ignored this difference and, considering possible failure planes in masonry piers, introduced a friction resistance proportional to the normal compression on the failure plane. By varying the inclination of the failure plane, he discovered the smallest possible and hence critical ratio between compressive strength and cohesion. He proceeded in a similar way when investigating active and passive earth pressure problems and when determining the upper and lower limits for arch thrust. COULOMB also concluded the strength problem of the beam in bending. Using the example of the cantilever beam, he distinguished between internal forces normal to and parallel with the cross-section and formulated the equilibrium conditions for the free body separated by the cross-section being studied. In doing so, he assumed a generally non-linear distribution of the internal forces over the depth of the beam. For the special case of the rectangular cross-section with linear force distribution, as with GALILEO's strength studies, he obtained the right result with a reduction factor of 3.

Claude Louis Marie Henri NAVIER (1785 – 1836) was appointed professor at the "Ecole des ponts et chaussées" in 1819 and the "Ecole polytechnique" in 1831. It is him we have to thank for today's form of the differential equation for the beam in bending, with the modulus of elasticity of the construction material and the principal moment of inertia of the cross-section. His published lecture notes bring together the scattered knowledge of his predecessors in a form suitable for practical building applications. He solved numerous problems of static indeterminacy, investigated the buckling of elastic bars subjected to eccentric loads and also became involved with

suspension bridges and many other issues. As a design engineer, NAVIER also had to cope with setbacks: his Pont des Invalides in Paris, spanning 160 m across the Seine, was abandoned shortly before completion (1826) because of various difficulties encountered during construction.

Augustin Louis CAUCHY (1789 – 1857) abandoned the notion that the stress vector must be orthogonal to the surface of the section, which applies in hydrostatics, and established the concept of the stress tensor. He also introduced the strain tensor and recognised that the linear elastic theory of homogeneous isotropic materials requires two material constants. Important contributions to the ongoing expansion of elastic theory were supplied by Siméon Denis POISSON (1781 – 1840), Gabriel LAMÉ (1795 – 1870), Benoît Pierre Emile CLAPEYRON (1799 – 1864), Adhémar Jean Claude Barré de SAINT-VENANT (1797 – 1886) and others.

Karl CULMANN (1821 – 1881), a professor at Zurich Polytechnic, which had opened in 1855, established graphical statics, i. e. the geometric/graphic treatment of theory of structures problems which is especially suitable for trusses. The rigorous application of force and funicular polygons enabled him to reduce beam statics to cable statics and obtain a universally applicable method of integration by adding the closing line to the funicular polygon. Antonio Luigi Gaudenzio Giuseppe CREMONA (1830 – 1903), Maurice LÉVY (1838 – 1910) and Karl Wilhelm RITTER (1847 – 1906) were firm advocates of the use of graphical statics.

Emil WINKLER (1835 – 1888) made important contributions to the elastic theory foundations of theory of structures. He introduced the axial and shear stiffnesses of elastic bars, investigated thermal deformations, analysed the arch fixed on both sides, studied beams on elastic foundation and worked on how "stress curves" indicate the effects of travelling loads, for which Johann Jacob WEYRAUCH (1845 – 1917) coined the term influence line.

Otto Christian MOHR (1835 – 1918) discovered the analogy between line loads and bending moments on the one hand and curvatures and deflections of beams on the other, thus paving the way for the graphical determination of deflection curves. He introduced his circle diagrams for presenting general stress and strain conditions and proposed a universal failure hypothesis based on COULOMB's approach. His studies of the secondary stresses in trusses, which are due to the fact that the connections between the members are actually rigid and not hinged as assumed in theory, gave him the idea of considering joint and bar rotations as unknowns. It was not until the first decades of the 20th century that this idea was exploited, in the form of the slope-deflection method for dealing with statically indeterminate systems.

James Clerk MAXWELL (1831 – 1879) regarded elastic trusses as machines working without energy losses and discovered that the displacement caused by a first unit force at the position and in the direction of a second unit force is equal to the displacement caused by the second unit force at the position and in the direction of the first unit force. This reciprocal theorem is a special case of the interaction relationship for linear elastic systems named after Enrico BETTI (1823 – 1892). According to this relationship, a first force system does the same work on the displacements of a second force system as the second system does on the displacements of the first. It is Carlo Alberto CASTIGLIANO (1847 – 1884) we have to thank for the theorem that the force variables in an elastic system are equal to the derivatives of the deformation work with respect to the corresponding deformation variables. Mathias KOENEN (1849 – 1924) transferred the work theorem for the displacement calculation, introduced by MOHR for trusses, to beams in bending. Friedrich ENGESSER (1848 – 1931) highlighted the difference between deformation work and complementary work and thus paved the way for the treatment of non-linear elastic systems in the theory of structures.

Heinrich Franz Bernhard MÜLLER-BRESLAU (1851 – 1925) placed the concept of work at the focus of the formulation of structural analysis theories and developed the force method for dealing with statically indeterminate systems. Robert LAND (1857 – 1899) created a method for determining influence lines based on a unit displacement imposed on the structural system at the position and in the direction of the relevant force variable. The development of the deformation method by Asger Skovgaard OSTENFELD (1866 – 1931) concluded the theory of elastic framed structures with small deformations.

The further evolution of the theory of structures in the 20th century primarily concerned plate and shell structures, stability theory, plastic theory and the development of computer-aided methods for analysing structures by means of discretised structural models.

3 DESIGN OF STRUCTURES

3.1 General

Fig. 3.1 [31] summarises the relationships between various design elements. The terminology in the figure is defined in appendix A1 (together with further specialist terminology that, generally, is highlighted in italics the first time it is used or explained in the text).

Fig. 3.1 applies to all *construction works* or their *structures* erected in the natural and built environments, i. e. all the structural members and all the subsoils that are necessary for their equilibrium and for retaining their form. The figure refers to the total life cycle of the construction works, which extends from *design* to *execution*, *use* and *conservation* right up to *deconstruction*. *Construction works documents* corresponding to the individual phases are listed in a separate column.

Fig. 3.1 and the associated terminology assist in understanding the subject and enable a uniform, systematic approach to theory and practice for all design, site management and construction work specialists engaged in the areas of structures and geotechnics. The figure is not a flow diagram, nor does it refer directly to the conventional course of a project from *preliminary design* to *tender design* and *detail design*. Rather, it gives an order to the steps in the process and the relationships between various design elements, and can be used to understand the connections between and the categorisation of the specialist terminology used.

The design of a structure encompasses the *conceptual design*, the *structural analysis* and the *dimensioning*. The conceptual design is all the activities and developments, and the outcomes thereof, that lead from the service criteria to the structural concept. The structural analysis uses structural models to determine action effects, i. e. the responses of the structure to potential actions as a result of execution and use as well as environmental influences. Dimensioning establishes the sizes, construction materials and detailing of the structure; the basis for this are structural and construction technology considerations plus numerical verifications.

The quality of a structure primarily depends on its conceptual design, its detailing and its execution. The importance of structural analyses and numerical verifications is often overrated; they are merely tools for guaranteeing an appropriate reliability, i. e. the behaviour of a structure with respect to structural safety and serviceability within specified limits.

Key aspects of conceptual design and the associated construction works documents (service criteria agreement and basis of design) are described below. Structural analysis and dimensioning are covered in chapter 4.

3.2 Conceptual design

The aim of the draft design is to develop a suitable *structural concept*, which specifies the structural system, the most important dimensions, construction material properties and construction details plus the intended method of construction. It is developed as part of the integrative planning of the construction works in consultation with all the specialists involved. The structural concept is based on the overall planning, the

Theory of Structures. First Edition. Peter Marti

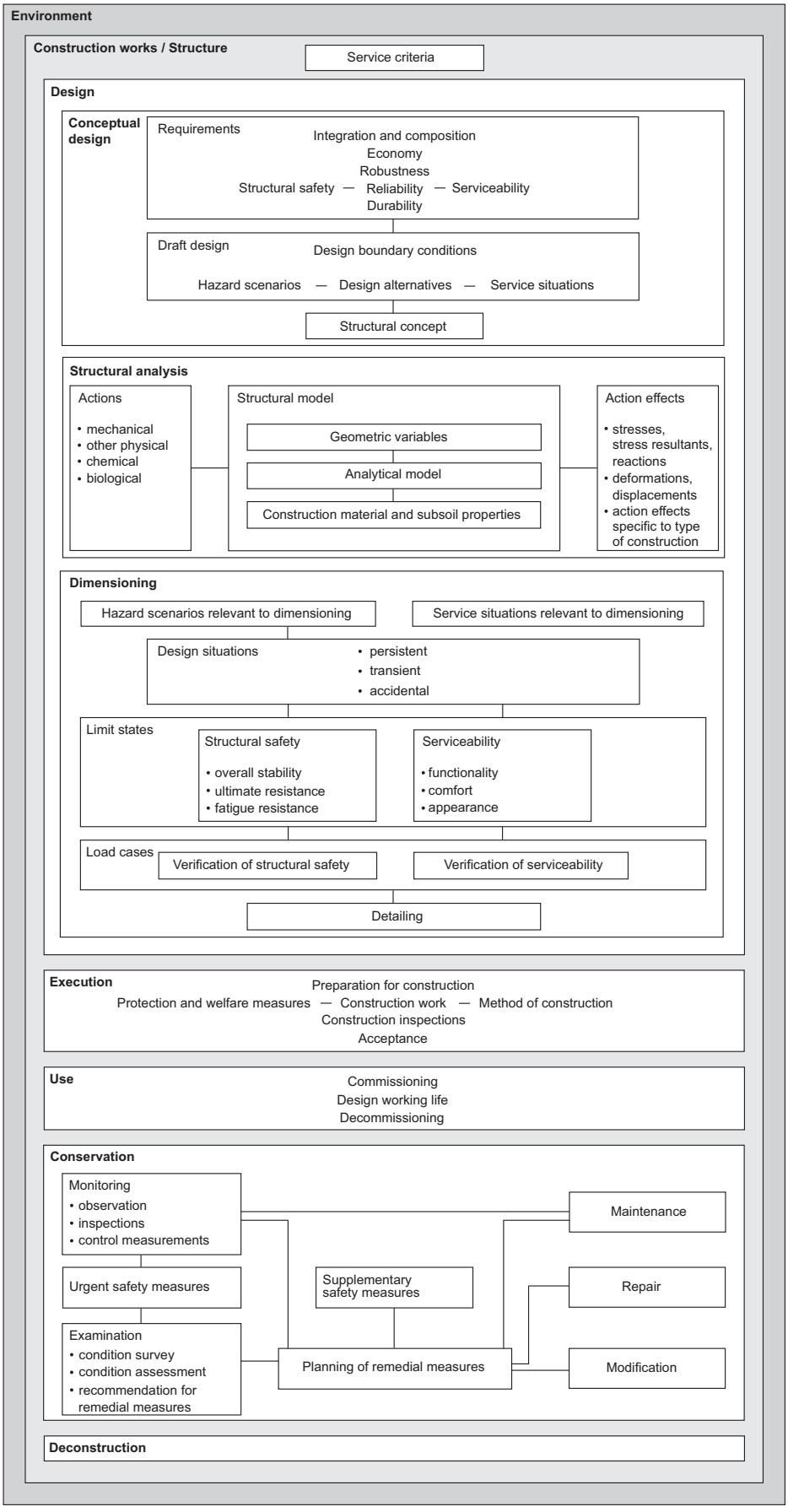

Fig. 3.1 Relationships between various design elements

architecture and operational issues and takes into account the boundary conditions dictated by the environment, legislation, etc.

The draft design includes producing a number of alternatives, taking into account the relevant *design boundary conditions*, checking their feasibility and assessing whether they fulfil the design requirements. In doing so, foreseeable execution and *service situations*, also potentially critical situations (*hazard scenarios*), are reviewed and experience gained from similar construction projects is incorporated. The structural concept finally decided upon is the result of an iterative process that presumes equal amounts of expertise and ingenuity.

The draft design corresponds to a consolidation process, which manifests itself in successively better sketches. Such sketches should be drawn freehand but to scale as far as possible. The instincts of the design engineer can therefore be directly integrated into the conceptual design, where they are further refined. The dimensions are chosen based on experience, estimates and rough structural calculations and checked against the sketches to establish their structural and construction technology feasibility. In order to assess the effect in three dimensions and to create a basis for the composition of a design, it is expedient to make use of (physical) working models right from the early stages of the conceptual design. Perspective drawings produced by a computer are also very helpful, but cannot replace the tactile experience of a model.

Subjective ideas and decisions based on experience and intuition help to progress the conceptual design; but they must stand up to objective criticism and therefore must be checked and should undergo further development. A systematic procedure is therefore to be recommended, which addresses the following points in succession:

- Clarifying the design boundary conditions and examining their relevance
- Establishing the principal actions and action effects
- Considering potential hazard scenarios and specifying suitable measures for dealing with the critical hazards
- Considering the foreseeable service situations and specifying appropriate measures for guaranteeing serviceability
- Estimating potential deterioration of the structure and specifying appropriate measures to guarantee durability.

The *design boundary conditions* include, for example:

- Location, hazard zone, topography, alignment, clearances, distances to boundaries, maximum and minimum dimensions
- Restrictions regarding design and construction time, design working life
- Statutory instruments (legislation, regulations, directives)
- Budgetary framework
- Quality, availability and reuse of construction materials
- Subsoil properties
- Applicability of methods of construction, transport and erection options
- Maintaining the use of rights of way and services
- Arrangements for monitoring and maintenance measures.

Any of the following influences can represent a *hazard*, for example:

- Deviations from the assumed values of actions
- Actions arising in the subsoil
- Chemical actions, e. g. as a result of de-icing salt or groundwater
- Resonance effects
- Deviations from the planned values of the ultimate resistance of the structure or the subsoil
- Curtailment of the ultimate resistance through corrosion, embrittlement or fatigue
- Curtailment of the ultimate resistance through fire, explosion, impact, broken service lines or earthquake.

Hazards can be dealt with by applying one or more of the following measures:

- Eliminating, preventing or minimising the hazard
- Inspection or warning systems
- Choosing structural systems with a low susceptibility to the hazards concerned
- Choosing structural systems that can handle local damage or the failure of an individual structural member or a whole part of the structure without collapsing completely
- Choosing structural systems that do not fail without warning
- Limiting the spread of fire to fire compartments
- Choosing suitable construction materials
- Appropriate structural analyses and dimensioning
- Careful detailing
- Careful execution according to plan
- Allowing for particular protective measures
- Appropriate monitoring and maintenance.

Every conceptual design must satisfy the requirements resulting from the intended use. This is primarily the *durability* over the design working life taking into account the *reliability* with respect to structural safety and serviceability as demanded by society or the client. Further, adequate *robustness* is necessary in order to limit potential deterioration or failure to an extent not disproportionate to its cause.

The true marks of quality of a conceptual design are to be found in its *economy*, *integration* and *composition*. Economy is to be understood as the moderate use of financial and natural resources, related to the total life cycle of the construction works. Integration is the compatible incorporation of the construction works into its natural and built environment. Composition is the creation of an aesthetic manifestation through spatial arrangement, shaping and choice of materials.

Economy is primarily influenced by the choice of the structural system and the intended method of construction. It is possible to avoid unnecessary ballast and achieve a more or less consistent utilisation of the construction materials across the entire structure by segmenting and shaping the structural members in a way that takes into account the construction work and is based on a rigorous adherence to the flow of the forces, and also by resolving and, if necessary, prestressing the cross-sections. The synthesis of structural and construction technology considerations therefore gives rise to an efficient, essentially well-proportioned primary form for the structure which can be further refined to achieve the best possible integration and composition.

In terms of the aesthetic quality of a design, special attention should be paid to its transparency, slenderness, regularity and proportions. In this respect, a critical examination of the overall three-dimensional appearance viewed from different locations is always essential, especially with respect to the most unfavourable angles. And in terms of architectural design aids, limiting the choice to a few simple and distinct measures, e. g. profiling to emphasize the flow of the forces, is generally to be recommended.

3.3 Service criteria agreement and basis of design

The requirements regarding the properties and behaviour of the construction works arising from the intended use should be specified at the start of the design work in the *service criteria agreement*, which is based on a dialogue between the client and the project realisation team. The agreement specifies the general objectives for the use of the construction works, the surroundings and the demands of third parties, the requirements regarding operation and maintenance, special stipulations of the client, protection objectives, special risks and the provisions of standards.

Producing a service criteria agreement is part of the preliminary design. In principle, it is necessary to record all decisions that are not the sole responsibility of the project realisation team in a manner that can be understood by the client.

Drawing up the service criteria agreement carefully and prudently is very important to the orderly progress of the project. Modifications and supplements to the service criteria agreement within the scope of the tender design and detail design should be avoided as far as possible.

The basic concepts and requirements for further design, execution, use and conservation which arise out of the conceptual design are described in the *basis of design*. This lays down the design working life, the service situations and hazard scenarios considered, the requirements placed on structural safety, serviceability and durability, and measures intended to guarantee these (including responsibilities, procedures, inspections and corrective mechanisms), the assumed subsoil conditions, the main assumptions regarding the structural and analytical models, the accepted risks and further conditions relevant to the project. The scope and content of the basis of design must be appropriate to the significance and hazard of the construction works plus the risks it poses for the environment.

The basis of design describes the implementation of the service criteria agreement specific to the construction works in the jargon of the project realisation team. It is part of the preliminary design and is successively supplemented and refined as the project undergoes further development in the tender design and detail design stages.

Example 3.1 Service criteria agreement for industrial building XY in Z

1 General objectives for use

1.1 Description of construction and intended use

The project concerns a new industrial building in which household goods are to be manufactured and sold. The building, rectangular on plan and measuring 25 × 50 m, is to have four storeys above and two below ground, with storey heights of 4 m and 3 m respectively. The basement storeys intended as parking facilities for motor cars are to be accessed via ramps on the north side of the building. The ground floor and first upper floor will be used for storage and production; later usage for retailing (shopping centre) is not ruled out. Access for goods vehicles is required on the north side of the building. The second and third upper floors are intended to accommodate display and sales facilities plus offices. The roof is only accessible for maintenance work; the addition of further storeys at a later date is not envisaged.

The subsoil is an approx. 15 m thick surface stratum of silty gravel above a deep boulder bed. The water table is 4 to 5 m below ground level.

For dimensions and intended uses, see Fig. 3.2 to Fig. 3.5.

1.2 Design working life

– Structure	50 years
– Waterproofing, floor finishes and carriageway joints	25 years
– Crash barriers	25 years
– Façade	25 years
– Roof covering	25 years

1.3 Supplementary stipulations regarding use

– BL: Plant rooms plus parking areas for vehicles up to 3.5 t, imposed load = 2 kN/m^2

– GF/1st UF: - Storage and production, imposed load = 8 kN/m^2
- Use of fork-lifts of type ... with a total (laden) weight of 6 t is possible [1]
- The machines cause no significant vibrations
- The intended subdivision of the floor areas may change over time

– 2nd UF: Sales, imposed load = 5 kN/m^2

– 3rd UF: Offices, imposed load = 3 kN/m^2

– Roof: Accessible for maintenance only.

2 Surroundings and third-party requirements

– The A-road (including footway) must remain open for traffic in two directions during the entire construction period.
– The B-road shall serve as access to the construction site. It is to be kept open for single-lane traffic from ... onwards and for third-party traffic in both directions from ... onwards.

3 Operational and maintenance requirements

– BL: - Imperviousness to water despite the lack of external insulation, injection of individual cracks as required is accepted by the client [2]
- Protection against the effects of de-icing salts for floor slabs, walls and columns
- No ponding
– GF/1st UF: Abrasion-resistant floor covering
– 2nd/3rd UF: Sound insulation to protect against the noise of storage/production
– Roof: Flawless waterproofing and drainage
– Façade: Inspection of fixing elements must be possible.

4 Particular stipulations of the client

– The client requests suspended floors in the form of flat slabs with a maximum depth of 300 mm. Small column heads beneath the suspended floors will be accepted.
– The type of façade has already been selected. The edges of the suspended floors carry a dead load of 4 kN/m due to non-structural elements and may not deflect by more than 15 mm [3].
– The building must be ready for use 18 months after commencing work on site.

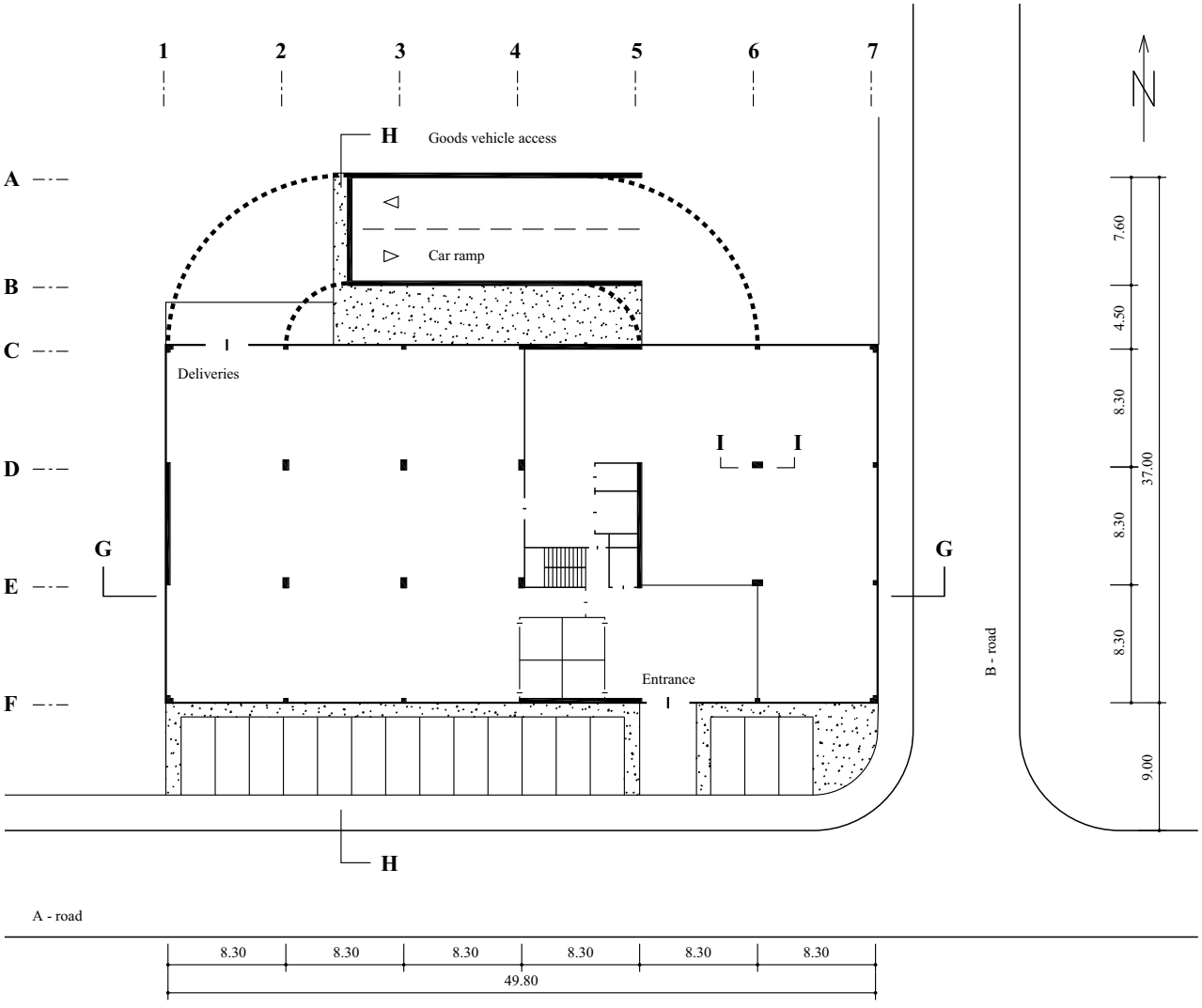

Fig. 3.2 GF plan (dimensions in m)

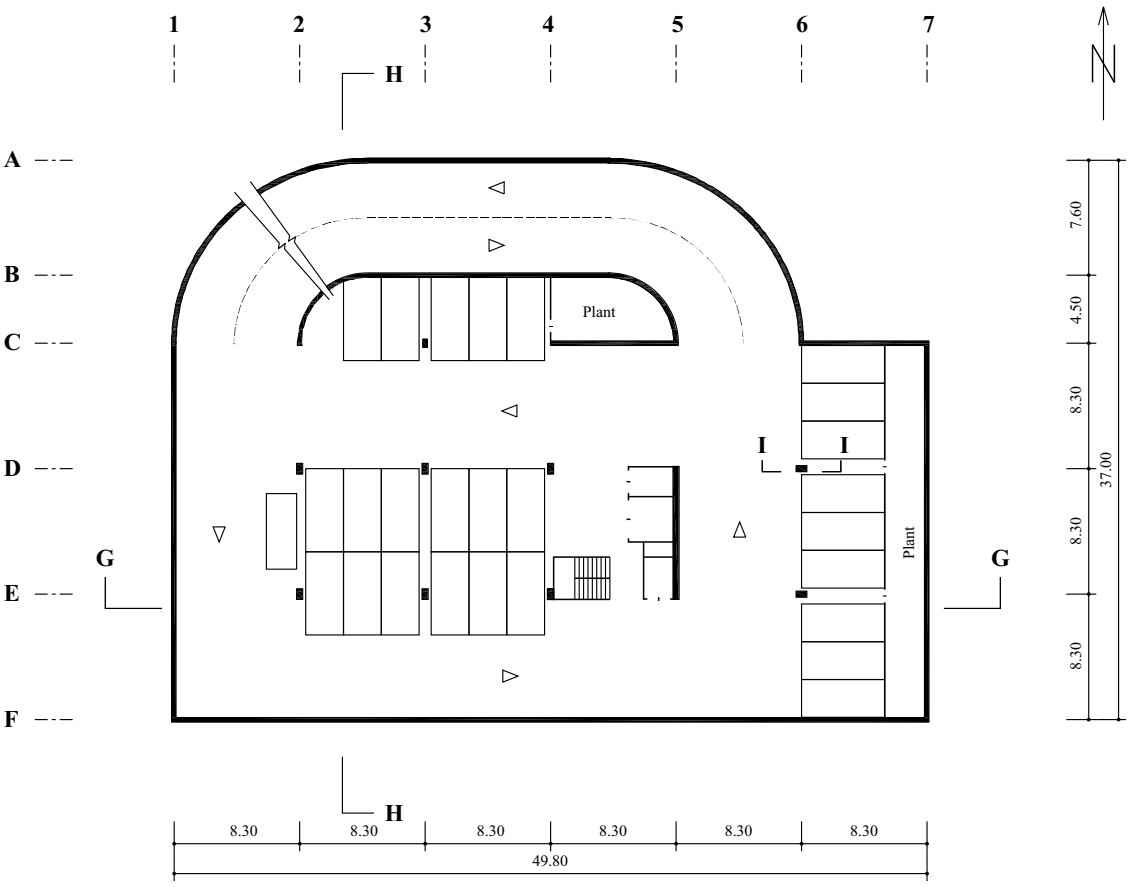

Fig. 3.3 1st BL plan (dimensions in m)

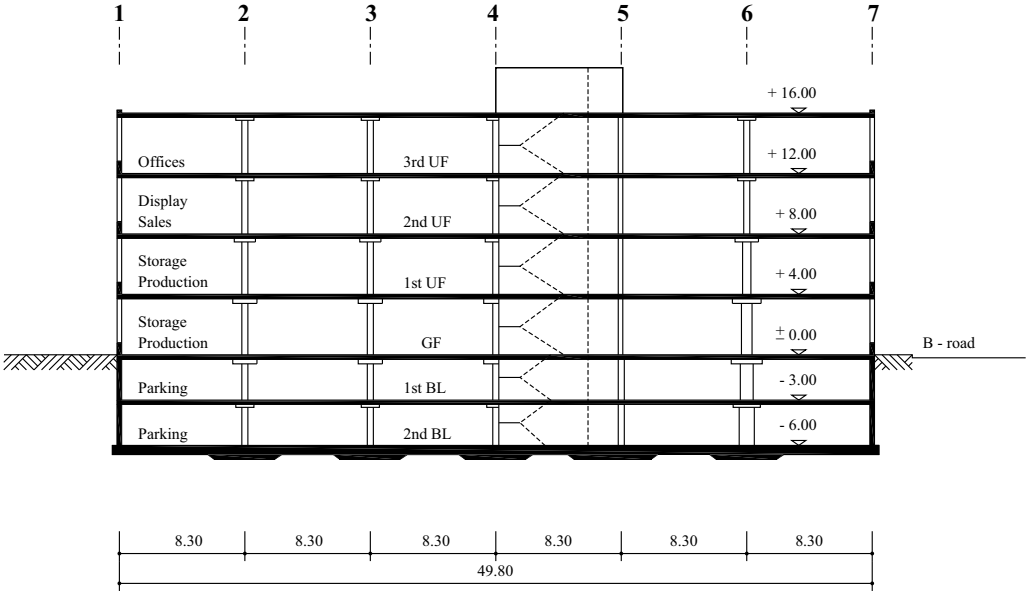

Fig. 3.4 Section G-G (dimensions in m)

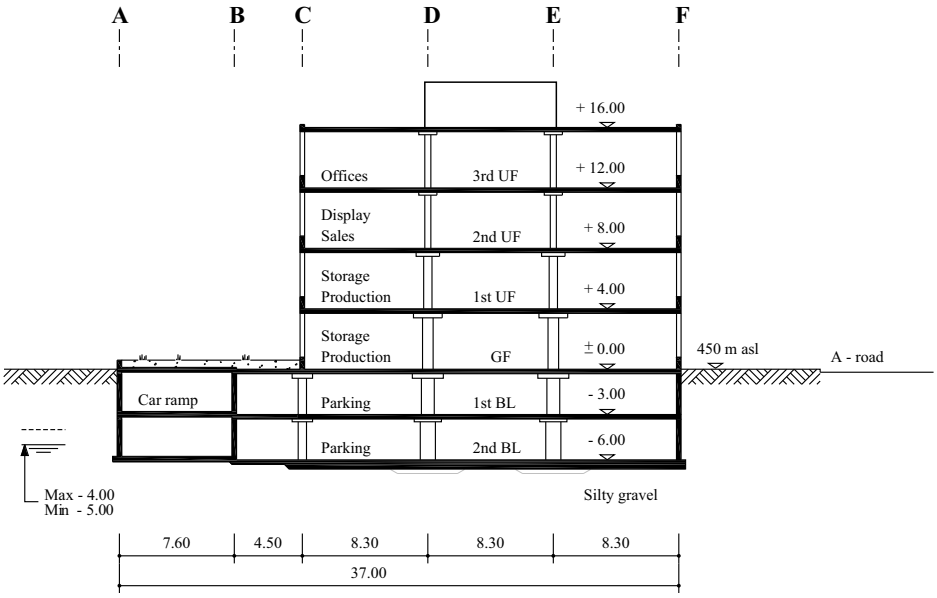

Fig. 3.5 Section H-H (dimensions in m)

5 Protection objectives and special risks

– A risk assessment has resulted in a fire resistance of R90 being specified [4].
– With respect to earthquake resistance, the building is classified as class II according to SIA 261. Later use as a shopping centre (GF to 2nd UF) is therefore possible without the need for strengthening measures.
– The possibility of flooding caused by rising waters in the neighbouring river is a risk accepted by the client.

6 Provisions of standards

The goods vehicle access is to be designed for road traffic loads according to section 10 of SIA 261. The reduction coefficient according to section 10.3.3 shall be 0.65.

7 Governing documentation

[1] Minutes of meeting No. … of …
[2] Minutes of meeting No. … of …
[3] Minutes of meeting No. … of …
[4] Minutes of meeting No. … of …

8 Signatures

[place], [date] Client: … (company XY) Project realisation team: … (consulting engineers xy)

Example 3.2 Basis of design for industrial building XY in Z

1 General

– The service criteria agreement forms the starting point for the basis of design [1].
– The design working life of the structure is 50 years. The design working life for replaceable structural members is 25 years.
– Conditions during construction, especially in connection with excavations, must be investigated in detail at the tender design and detail design stages.
– The construction inspection plan can essentially be restricted to regulating the responsibilities and the flow of information. The requirements of SIA 262 and SIA 118-262 apply in all other circumstances; these are given in the "Checklists for concrete works" [4].

2 Structural concept

2.1 Structural system

– See description of building in service criteria agreement (Fig. 3.2 to Fig. 3.5).
– In the finished state, a monolithic reinforced concrete construction with loadbearing walls and internal columns continuous from raft foundation to roof; perimeter and corner columns supported on peripheral basement walls; raft foundation strengthened below internal columns and service core (lift shafts); column heads around internal columns, spandrel panels on GF to 3rd UF.
– Prestressed raft foundation and suspended floors (bonded tendons, 4 No. Ø15.7 mm in 75 × 21 mm steel ducts, concentrated in column strips in N-S direction, distributed in E-W direction).

2.2 Dimensions

– Raft foundation 600 mm, increased locally to 900 mm
– Basement walls 300 mm (wall 5DE 400 mm)
– Internal columns 400 × 400 to 1000 mm, see Tab. 3.1
– Perimeter columns 400 × 300 mm
– Corner columns 300 × 300 mm, L-form on GF, 500 mm leg length
– Loadbearing walls 300 mm
– Suspended floors 280 or 300 mm, see Tab. 3.1
– Spandrel panels 800 × 200 or 250 mm, see Tab. 3.1.

2.3 Construction materials

– Concrete C 30/37 f_{cd} = 20 N/mm^2 τ_{cd} = 1.1 N/mm^2
– Reinforcing steel B500B f_{sd} = 435 N/mm^2 k_s = 1.08, ε_{ud} = 4.5 %
– Prestressing steel Y1770S7-15.7 f_{pk} = 1770 N/mm^2 f_{pd} = 1320 N/mm^2, ε_{ud} = 2 %

Tab. 3.1 Dimensions in mm

Storey	Internal columns	Column head	Suspended floor	Spandrel panel thickness
3rd UF	400 × 400	200 × 1200 × 1200	280	200
2nd UF	400 × 400	200 × 1200 × 1200	280	200
1st UF	400 × 550	250 × 1400 × 1550	280	250
GF	400 × 700	300 × 1600 × 1900	300	250
1st BL	400 × 850	300 × 1600 × 2050	300	-
2nd BL	400 × 1000	200 × 1200 × 1800	280	-

2.4 Construction details

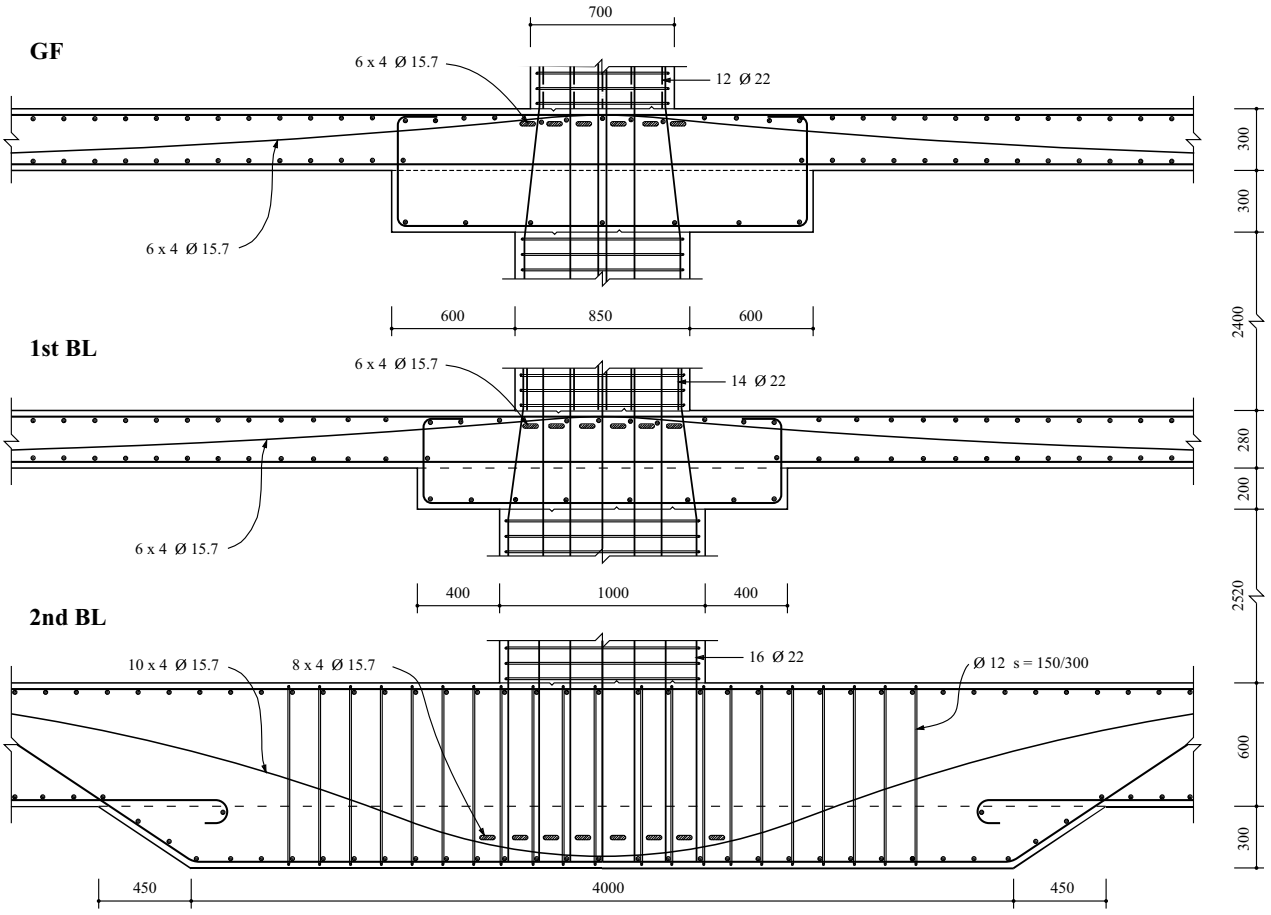

Fig. 3.6 Section I-I (dimensions in mm)

2.5 Method of construction

– Sides to excavation partly sloping, partly supported by sheet piles, temporary dewatering
– Conventional execution of walls and suspended floors with large-panel formwork and concrete placed by crane or pump
– Construction joints with coupled tendons in raft foundation, basement walls and suspended floors in bay 3-4 along grid-line 4, construction of eastern part of building to proceed ahead of western part
– Staged prestressing of raft foundation according to progress on site
– Construction of ramp structure after completion of basement levels.

3 Permanent actions

Tab. 3.2 Permanent actions

Actions	Measures	Further work	Assumptions for structural analysis and dimensioning
Dead loads	- Dimensioning - Construction inspections	Structural calculations Construction inspection plan	Body load = 25 kN/m^3
Self-weight of non-structural elements	- Dimensioning - Construction inspections - Monitoring during use with respect to modifications	Structural calculations Construction inspection plan Monitoring plan	2nd BL to 3rd UF 3 kN/m^2 Roof 3 kN/m^2 Perimeter of floor slabs 4 kN/m Car ramp 3 kN/m^2 Fill, ramp 15 kN/m^2 Goods vehicle access 5 kN/m^2
Prestress	- Dimensioning - Construction inspections	Structural calculations Construction inspection plan	$\sigma_{p0} = 0.7 f_{pk} = 1239$ N/mm^2 $\mu = 0.2$ $\Delta\varphi = 4$ mrad/m
Earth pressure	- Dimensioning - Construction inspections (excavations, sheet piles) - Checking the assumed subsoil conditions during execution - Comparing measured and calculated sheet pile wall displacements - Checking anchor forces - Inspecting backfill material	Structural calculations Construction inspection plan Construction inspection plan Construction inspection plan Construction inspection plan Construction inspection plan	$\gamma_{ek} = 19$ kN/m^3 [2] $\varphi_k' = 28°$ $c_k' = 0$
Hydrostatic pressure	- Dimensioning - Checking the water level before and during execution - Groundwater lowering/construction inspections	Structural calculations Tender design/ construction inspection plan Tender & detail design/ construction inspection plan	$\gamma_{wk} = 10$ kN/m^3 $h_{wd,\max} = -4.0$ m [2]

4 Structural safety, serviceability and durability

Tab. 3.3 Structural safety

Hazard scenario	Measures	Further work	Assumptions for structural analysis and dimensioning
Failure of excavation shoring	- Tab. 3.2, earth/hydrostatic pressure - Restricting storage of materials behind excavation shoring	Structural calculations Construction inspection plan	Tab. 3.2
Anchor failure	- Dimensioning - Construction inspections/monitoring	Structural calculations Construction inspection plan	Tab. 3.2
Ground heave	- Tab. 3.2, hydrostatic pressure	Structural calculations Construction inspection plan	$\gamma_{G,\text{sup}} = 1.6$ $\gamma_{G,\text{inf}} = 0.9$ $h_{wd,\text{min}} = -7.5$ m
Buoyancy, BL	- Powerful pumps - Flood BL as last resort (opening left adjacent to ramp until floor above 1st BL completed)	Construction inspection plan	
Punching, raft foundation	- Dimensioning - Prestressing in stages - Construction inspections	Structural calculations Construction inspection plan	
Punching, suspended floors during construction	- Dimensioning - Prestressing of column strip - Propping - Construction inspections	Structural calculations Construction inspection plan	
Blocked roof drainage	- Height of parapet 100 mm - Inspections/regular cleaning of outlets	 Monitoring plan Maintenance plan	Ponding considered in imposed load Snow not critical
Wind	- Dimensioning (only critical for façade incl. fixing elements)	Structural calculations	$q_{p0} = 0.9$ kN/m^2 $z_g = 450$ m $\alpha_r = 0.23$ $z = 16$ m $q_p = 1.0$ kN/m^2
Imposed loads/ traffic loads	- Dimensioning - Signs indicating permissible imposed loads in building - Traffic signs and constructional measures at car ramp - Checking in the event of changes to the machinery for storage/production	Structural calculations Monitoring plan Monitoring plan Monitoring plan	Roof cat. H $q_k = 1$ kN/m^2 3rd UF cat. B $q_k = 3$ kN/m^2 2nd UF cat. D $q_k = 5$ kN/m^2 1st UF cat. E $q_k = 8$ kN/m^2 GF cat. E $q_k = 8$ kN/m^2 1st BL cat. F $q_k = 2$ kN/m^2, $Q_k = 20$ kN 2nd BL cat. F $q_k = 2$ kN/m^2, $Q_k = 20$ kN Car ramp $q_k = 2$ kN/m^2, $Q_k = 20$ kN Goods vehicle access $b = 11$ m, $\alpha = 0.65$

Tab. 3.3 Structural safety (Continued)

Hazard scenario	Measures	Further work	Assumptions for structural analysis and dimensioning
Impact, parking, A-road	- Concrete perimeter wall - Reinforced concrete spandrel panel F17 on GF	Detail design	
Impact, B-road	- Dimensioning - Columns C7 and F7 L-form on GF - Reinforced concrete spandrel panel 7CF on GF	Structural calculations	Q_{dx} = 750 kN Q_{dy} = 300 kN
Impact, goods vehicle access	- Dimensioning - Speed $\leq$ 30 km/h - Ramp wall A35 - Unloading platform C12 for deliveries	Structural calculations	Q_d = 300 kN
Impact, ramp/BL	- Dimensioning	Structural calculations	Q_d = 60 kN
Impact, fork-lift, GF/1st UF	- Dimensioning - Perimeter reinforced concrete spandrel panel - Impact protection for internal columns	Structural calculations	G_k = 60 kN Q_d = 300 kN h = 0.8 m
Fire	- Fire compartments (staircase/individual storeys, GF to 3rd UF, divided along C4-E4-E45-F45) - Fire resistance R90 - Fire detection system - Instruction of personnel - Regular checking of fire protection concept	Tender/detail design Monitoring plan Monitoring plan	Concrete cover $\geq$ 30 mm
Earthquake	- Dimensioning - Measures according to SIA 261	Structural calculations	Earthquake zone Z1 Subsoil class E Construction works class II ξ = 0.05 γ_f = 1.2 q = 2.0
Explosion, BL	- Possibly pressure-relief openings - Inspecting service lines at risk	Tender design Monitoring plan	Construction works category 1 No verification
Explosion, GF/UF	- Regulations for storing hazardous goods	Monitoring plan	Construction works category 1 No verification
Pipe breakage	- Construction inspections - Inspecting and maintaining service lines at risk	Construction inspection plan Monitoring plan Maintenance plan	

Tab. 3.4 Serviceability and durability

Requirement	Measures	Further work	Assumptions for structural analysis and dimensioning
Watertightness, BL	- Special requirements for concrete - Suitable concreting pours - Careful curing - Prestressing - Waterstops in construction joints - Installing injection hoses for waterproofing at a later date - Construction inspections - Checking the watertightness - Injection of cracks if required	Tender /detail design Construction inspection plan Monitoring plan Maintenance plan	
Drainage, BL	- Fall 2 % - Properly positioned/adequately sized outlets - Construction inspections - Regular cleaning	Tender/detail design Construction inspection plan Maintenance plan	
Waterproof roof	- Waterproofing - Fall 2 % - Properly positioned/adequately sized outlets - Construction inspections	Tender/detail design Construction inspection plan	
Stiffness of suspended floors	- Dimensioning - Prestressing - Spandrel panels	Structural calculations	SIA 260, Tab. 3 Suspended floor edges: $w \leq 15$ mm
Crack limitation	- Minimum reinforcement - Suitable concreting pours - Careful curing - Prestressing - Construction inspections	Structural calculations Detail design	BL/ramp: higher requirements GF/UF: normal requirements
Sound insulation, 1st UF/2nd UF	- Consult specialist	Tender design	
Abrasion resistance, finishes, GF/1st UF	- Granolithic finish, 40 mm	Tender/detail design	
Corrosion protection, reinforcement, BL	- Dense finish (asphalt) - Impregnation/coating of walls and columns - Thick concrete cover (exposure class XC4/XD1) - Concrete cover 40 mm - Construction inspections - Regular cleaning - Checking the chloride content	Tender/detail design Construction inspection plan Maintenance plan Monitoring plan	

Tab. 3.4 Serviceability and durability (Continued)

Requirement	Measures	Further work	Assumptions for structural analysis and dimensioning
Corrosion protection, reinforcement, car ramp/ goods vehicle access	- Fall ≥ 2 % - Effective drainage - Waterproofing/finishes - Dense cover concrete (exposure class XC4/XD3) - Concrete cover 55 mm - Construction inspections - Regular cleaning	Tender/detail design Construction inspection plan Maintenance plan	
Corrosion protection, reinforcement, GF/UF	- Dense cover concrete (exposure class XC1) - Concrete cover 30 mm - Construction inspections	Tender/detail design Construction inspection plan	
Corrosion protection, façade fixings	- Stainless steel - Construction inspections - Regular inspections	Tender/detail design Construction inspection plan Monitoring plan	

5 Accepted risks

– Tanker accident with fire on A-road

– Pressure wave caused by explosion in neighbouring tank farm on A-road

6 Further conditions relevant to the project

– The agreement [3] applies with respect to tensioned and non-tensioned anchorage components in the areas of the A- and B-roads.

– Plant room BC45 in the basement is continuous over both basement levels without an intermediate floor and must be accessible from above as well as from both basement levels (opening closed off with Ø 2 m hatch).

7 Basic information

7.1 Standards

SIA 260 (2003)	Basis of structural design
SIA 261 (2003)	Actions on structures
SIA 261/1 (2003)	Actions on structures – Supplementary specifications
SIA 262 (2003)	Concrete structures
SIA 262/1 (2003)	Concrete structures – Supplementary specifications
SIA 263 (2003)	Steel structures
SIA 263/1 (2003)	Steel structures – Supplementary specifications
SIA 267 (2003)	Geotechnical design
SIA 267/1 (2003)	Geotechnical design – Supplementary specifications.

7.2 Information specific to the project

[1] Service criteria agreement for the industrial building XY in Z, dd.mm.yy, … pp.

[2] Geotechnical report for the industrial site XY in Z, practice of Dr. …, z, dd.mm.yy, … pp.

[3] Contractual agreement between the XY company and the Z local authority concerning anchorage components in the areas of the A- and B-roads, z, dd.mm.yy, … pp.

7.3 General information

[4] Checklists for concrete structures, consulting engineers xy, z, yy, … pp.

8 Signature

[place], [date] Project realisation team: … (consulting engineers xy)

Drawing up the service criteria agreement and the basis of design compels the project realisation team to follow an orderly procedure for the conceptual design. Of course, this does not compensate for lack of creativity and decisiveness. Applied properly and limited to the essentials, however, the two documents are very welcome inclusions that support the conceptual design process. They simplify the overview and pave the way for discovering useful potential solutions to given problems.

3.4 Summary

1. The design of a structure embraces diverse elements whose relationships with each other are summarised in Fig. 3.1. The corresponding terminology is defined in appendix A1.
2. Fig. 3.1 and the associated terminology assist in understanding the subject and enable a uniform, systematic approach to theory and practice for all design, site management and construction work specialists engaged in the areas of structures and geotechnics.
3. The quality of a structure primarily depends on its conceptual design, its detailing and its execution. Structural analyses and numerical verifications are merely tools for guaranteeing the behaviour of a structure with respect to structural safety and serviceability within specified limits.
4. The aim of the draft design is to develop a suitable structural concept, which specifies the structural system, the most important dimensions, construction material properties and construction details plus the intended method of construction. It is developed as part of the integrative planning of the construction works in consultation with all the specialists involved.
5. Subjective ideas and decisions based on experience and intuition help to progress the conceptual design; but they must stand up to objective criticism and therefore must be checked and should undergo further development.
6. Drawing up the service criteria agreement and the basis of design compels the project realisation team to follow an orderly procedure for the conceptual design.
7. All decisions that are not the sole responsibility of the project realisation team must be recorded in the service criteria agreement in a manner that can be understood by the client. Modifications and supplements to the service criteria agreement within the scope of the tender design and detail design should be avoided as far as possible.
8. The basis of design describes the implementation of the service criteria agreement specific to the construction works in the jargon of the project realisation team. It is part of the preliminary design and is successively supplemented and refined as the project undergoes further development in the tender design and detail design stages.
9. Every conceptual design must satisfy the basic requirements concerning adequate durability, reliability and robustness. The true marks of quality of a conceptual design are to be found in its economy, integration and composition.
10. Economy is primarily influenced by the choice of the structural system and the intended method of construction. The synthesis of structural and construction technology considerations gives rise to an efficient, essentially well-proportioned primary form for the structure which can be further refined to achieve the best possible integration and composition.

3.5 Exercises

3.1 A new, approx. 20 km long footpath is to be built in an Alpine region about 1000 m above sea level. This project calls for the erection of a number of small structures, in particular:
- 6 footbridges with spans between 6 and 30 m, usable width 1.2 m
- 1 viewing platform of 20 m^2 overlooking a gorge
- 1 lookout tower on a tree-covered hill with a platform of 20 m^2 at a height of 20 m
- 2 canopies each of 60 m^2 over barbecue areas.

You work for the consulting engineers appointed to design these structures and have been invited to a first (all-day) meeting with the client (including a site visit).

What preliminary clarifications would you carry out in your office beforehand?

3.2 How would you prepare for the meeting? What would you take with you?

3.3 Draw up a list of questions relevant to the compilation of the service criteria agreement as a basis for the dialogue with the client.

3.4 What additional information would you like to acquire during the site visit as a basis for the structural design work and for compiling the basis of design?

4 STRUCTURAL ANALYSIS AND DIMENSIONING

4.1 General

We learned in chapter 3 that dimensioning is only one of a number of different measures for dealing with potential hazards and hence assuring *structural safety.* Similarly, dimensioning is only one of a number of different measures for taking into account foreseeable service situations and hence assuring *serviceability.*

Where dimensioning is an adequate measure, we speak of a *design situation*, see Fig. 3.1. Dimensioning is then carried out on the basis of *limit states* by specifying the *load cases* appropriate to the design situations and supplying appropriate *verifications*.

An indispensable part of dimensioning, besides the analytical determination or confirmation of the dimensions and the construction material properties as a result of the verifications, is *detailing* based on structural and construction technology considerations. Detailing is the process of determining and coordinating the construction details.

The *structural analysis* forms the starting point for dimensioning. It enables the behaviour of a structure to be understood with respect to the design situations requiring investigation taking into account the critical influences. The methods of structural analysis, such as those presented in this book, must be based on acknowledged theory and engineering practice, confirmed by experimental testing where necessary.

The basic concepts and the results of the structural analysis and the dimensioning must be included in the *structural calculations* and the *technical report*.

Checking the plausibility of the results of the structural analysis and the dimensioning is essential in every case. Equilibrium checks, examining appropriately simplified structural systems and comparisons with known structural solutions to similar problems are all excellent ways of carrying out plausibility checks.

4.2 Actions

4.2.1 Actions and action effects

The term *actions* corresponds to the normal use of the word. It refers to all the mechanical (loads, forces), other physical (temperature, humidity), chemical (salts, acids, alkalis, organic compounds) and biological (bacteria, insects, fungi, algae) effects experienced by a structure as a result of execution, use and environmental influences.

Action effects are the structure's response to the actions. Examples of such effects are stresses, stress resultants, support force variables, strains, displacements and rotations as well as effects connected with the type of construction, e. g. cracks, corrosion, rot, etc.

Whether a certain variable is to be regarded as an action or an action effect depends on the *system bounds*. If, for example, in a retaining structure the subsoil is regarded as part of the structure, then the bearing pressure is an action effect, but otherwise an action applied to the subsoil or the retaining structure. Another example is the post-tensioning of structural members made from reinforced concrete; during post-tensioning, the stressing force is considered as an action applied to the reinforced con-

Theory of Structures. First Edition. Peter Marti

crete member without the prestressing tendon, but when verifying the structural safety, it can be interpreted as an action effect.

Deformations are the primary action effects caused by actions such as temperature changes or the shrinkage or swelling of materials. If these effects are prevented as a result of kinematic constraints, secondary action effects in the form of *residual stresses*, and in the case of statically indeterminate systems, *restraints*, are the result, see sections 7.5, 13.2.5, 14.3 and 16.2.

Actions are classified according to how they change over time, how they change with position and according to their dynamic effect.

Permanent actions G are those actions that remain approximately constant over a reference period or tend towards a limit value, e. g. dead loads, self-weight of non-structural elements, prestressing forces. *Variable actions Q*, e. g. snow loads, wind loads, imposed loads, are those actions that are not permanently applied, are not constant or do not tend towards a limit value over a reference period. *Accidental actions A* are those actions with a low probability of occurrence, which are generally of short duration but have a significant effect, e. g. the effects of impacts, fires, earthquakes and explosions.

Actions are designated as *fixed* when their distribution over the structure is defined, i. e. when their magnitude and direction, e. g. in snow and wind load models, are uniquely determined by the value at one point. And vice versa, actions are designated as *free* when their distribution over the structure is not defined, e. g. imposed loads in buildings or the effects of traffic; in such cases the actions are assumed to be applied at the most unfavourable positions.

When there are no or at best negligible accelerations due to an action, the action is designated as *static*, otherwise as *dynamic*. In the latter case, dynamic effects are often considered in simplified form as surcharges, by applying equivalent static forces or by including dynamic factors.

4.2.2 Models of actions and representative values

The relevant standards specify easy-to-use *models of actions* for the numerical formulation of conventional actions. The magnitude of an action is determined by one or more scalar indications, which can assume various *representative values* F_{rep}. The most important representative value of an action is the *characteristic value* F_k. It stands for a certain fractile for permanent actions G_k and for a certain probability of occurrence for variable actions Q_k. In the case of accidental actions, the design value A_d is specified directly.

The mean value is mostly used for G_k in the case of permanent actions. In the case of sensitive structures or when G can vary over a wider range (coefficient of variation $> 5\,\%$), upper and lower values $G_{k,inf}$ and $G_{k,sup}$ should be used (the 5 % and 95 % fractiles of the statistical distribution of G). Dead loads are generally determined on the basis of intended dimensions and average body loads. Mean, upper or lower values are used for the characteristic values P_k of prestressing forces depending on the point in time considered and the type of prestressing.

In the case of variable actions, Q_k is generally specified in such a way that the probability of this value being exceeded over a period of one year is 2 % (corresponding to a 50-year return). The reduction factors ψ_0, ψ_1 and ψ_2 for rare, frequent or quasi permanent values of variable actions take into account the lower probability of the simultaneous occurrence of the most unfavourable values of several independent actions, see sections 4.6.3 and 4.6.4.

Actions arising in the subsoil, especially earth and hydrostatic pressures as well as subsoil deformations not related to the construction works, must be treated as permanent, variable or accidental actions depending on their variability, duration and probability of occurrence. The characteristic value of an action arising in the subsoil can be calculated through soil mechanics analyses, conclusions drawn from the behaviour of the subsoil or structure, large-scale tests, testing of scale models or by applying empirical values to the case being considered. An upper or lower value of an action may be critical depending on the particular design situation.

4.3 Structural models

According to Fig. 3.1, a *structural model* links the actions to the action effects and includes the geometrical properties plus the properties of the construction materials and the subsoil. Linking the individual variables (e. g. forces and deformations) takes place in an *analytical model* using appropriate mathematical/physical relationships (e. g. static and kinematic relationships plus constitutive relationships) as presented in this book, for example.

The structural model is the result of defining and idealising the structural system. It must be suitable for predicting the structural behaviour for the design situations that are to be investigated. Different structural models are suitable depending on the particular problem. Idealisation as a *rigid body* is often sufficient, and in many cases for complex structures the global structural behaviour at least can be idealised with acceptable accuracy as a (one-dimensional elastic or plastic) *framed structure*. On the other hand, in order to analyse local effects, it may be necessary to work with more elaborate (two- or three-dimensional) models in the form of *plate and shell* or *three-dimensional structures*. The art of handling structural analysis problems manifests itself in skilful modelling, using the simplest approach possible, which leads to meaningful results just adequate for the respective problem. By presenting the appropriate principles and including many examples plus exercises for readers to work through themselves, it is precisely that approach that this book wishes to communicate.

The characteristic value of a *geometric variable* normally corresponds to the nominal value a_{nom} (e. g. for planned dimensions), sometimes a prudent estimate (e. g. water table, height of dumped goods). Imperfections are taken into account directly by way of design values a_d .

The *properties of construction materials* and *subsoils* are generally represented by upper or lower characteristic values X_k (generally the 5 % and 95 % fractiles), which are determined by way of standardised test methods. If necessary, conversion factors η are used in order to convert the results of tests into values that we can assume are representative for the structure or the subsoil (e. g. to take into account humidity, temperature or scale effects, the type of failure or the duration of the action).

4.4 Limit states

According to Fig. 3.1, we distinguish between ultimate limit states (structural safety) and serviceability limit states.

The *ultimate limit states* concern the safety of the structure and its ancillary elements plus the safety of persons. We distinguish between four types:

- Type 1 is the *overall stability* of the structure (lateral buckling, uplift or buoyancy as a rigid body).
- Type 2 is reaching the *ultimate resistance* of the structure or one of its parts (failure due to rupture, excessive deformations, conversion of the structure into a mechanism or loss of stability).

– Type 3 is reaching the *ultimate resistance of the subsoil* (landslide, slope failure, ground failure).
– Type 4 is reaching the *fatigue resistance* of the structure or one of its parts.

The *serviceability limit states* concern the functionality of the construction works, the comfort of persons using the construction works and the appearance of the construction works. The design criteria for serviceability can refer to:

– Deformations that impair the functionality or appearance of the construction works or its ancillary elements or cause damage to non-loadbearing components
– Vibrations that limit the functionality of the construction works or impair the comfort of persons using the construction works
– Sealing defects that limit the functionality of the construction works or impair the comfort of persons using the construction works
– Action effects specific to the type of construction, e. g. cracks or slip at connections, which impair the appearance of the construction works and the durability of the structure
– Limit values for environmental impacts, e. g. obstructing the flow of groundwater.

From the point of view of *durability*, the requirements regarding structural safety and serviceability must be fulfilled within the scope of the intended use and the foreseeable actions without unforeseeable maintenance and repair costs. Employing suitable measures during design can create favourable conditions, but durability of the construction works is essentially influenced by the effective use, monitoring and maintenance of the construction works. These activities exceed the responsibilities of the project realisation team. It should be in the interests of the owner and user, and also their responsibility, to ensure that their construction works are used and monitored as intended and also properly maintained.

4.5 Design situations and load cases

According to Fig. 3.1, there is a hazard scenario or service situation at the bottom of every design situation. We distinguish between *persistent* and *transient design situations* depending on whether a given design situation governs during a period of time equal to the design working life or governs during a much shorter period. There are also *accidental design situations*, which involve exceptional conditions for the structure; they include either an accidental situation itself or relate to the situation immediately after an exceptional event (e. g. following an earthquake).

The *load cases* associated with the design situations must be specified. Every load case is characterised by a *leading action* corresponding to the *leading hazard* in the hazard scenario and the *accompanying actions* occurring simultaneously with it. Generally, it is sufficient to consider one variable accompanying action.

Dimensioning in no way means trying to “cover as many situations as possible” with a multitude of load cases and accompanying actions, as is very often attempted. Instead, it means determining the load cases governing a limit state for the structure. This mostly involves just a few, physically compatible arrangements of actions that occur simultaneously. The consideration of individual actions as “load cases” (e. g. “snow load case”, “wind load case”, etc.) and their thoughtless superposition with the help of the superposition law for geometric and material linear systems (without taking account of the physical compatibility of the actions) is an approach often encountered in practice – and is senseless.

4.6 Verifications

4.6.1 Verification concept

The verification of structural safety and serviceability is generally carried out on the basis of *design values* that are specified directly or calculated from characteristic or other representative values or using a design value function in conjunction with *partial factors*. The partial factors take into account uncertainties in the individual variables but also uncertainties in the models of the actions and resistances. The aim of this is to achieve a certain reliability, i. e. a certain probability that the requirements regarding structural safety and serviceability are fulfilled over a given length of time. The partial factors are specified based on the methods of *reliability theory* taking into account construction practice and experience.

In principle, structural safety and serviceability must be verified in every case. However, a particular verification may not be needed if it can be established that it is not critical. In addition, one or both of the verifications may not be necessary if it can be shown that the corresponding requirements are of only minor significance or can be achieved with structural or construction technology measures; the procedure adopted must be recorded in the basis of design in such instances.

4.6.2 Design values

The following generally applies for the design value of an action effect:

$$E_d = \gamma_S E\{F_d, X_d, a_d\} \tag{4.1}$$

where $F_d = \gamma_f F_{\text{rep}}$, $X_d = \eta X_k / \gamma_m$ and $a_d = a_{\text{nom}}$ or $a_d = a_{\text{nom}} \pm \Delta a$. The partial factor γ_S takes into account uncertainties in the model at the transition from the actions to the action effects, γ_f allows for possibly unfavourable discrepancies between the magnitude of the action F and the representative value F_{rep}, and γ_m takes into account unfavourable discrepancies between the properties of the construction material or the subsoil X and the characteristic value X_k. The conversion factor η and the nominal value a_{nom} of a geometrical property have already been introduced in section 4.3; Δa denotes the difference between the nominal and design values of a geometrical property for the case that such deviations exert a substantial influence on the reliability of the structure.

The curly brackets $\{\ldots\}$ used in (4.1) and in the following signify a design value function. Depending on the verification, some of the design values given between the brackets may be omitted, i. e. the relevant variables must be specified from case to case when applying the equation.

The following generally applies for the design value of the ultimate resistance:

$$R_d = \frac{R\{X_d, a_d\}}{\gamma_R} \tag{4.2}$$

where the partial factor γ_R takes into account the uncertainties in the model of resistance.

As a rule, γ_S and γ_f can be combined, according to $\gamma_F = \gamma_S\, \gamma_f$, to form one *load factor* γ_F. Further, γ_R and γ_m can normally be combined, according to $\gamma_M = \gamma_R\, \gamma_m$, to form one *resistance factor* γ_M. Instead of (4.1) and (4.2), the following then applies:

$$E_d = E\left\{\gamma_F F_{\text{rep}}\,,\ \frac{\eta X_k}{\gamma_m}\,,\ a_d\right\} \quad , \quad R_d = R\left\{\frac{\eta X_k}{\gamma_M}\,,\ a_d\right\} \tag{4.3}$$

Tab. 4.1 contains, for example, the load factors given in [31].

The design values C_d for *serviceability limits* (e. g. permissible deflections, sway, eigenfrequencies, etc.) are generally specified or agreed specifically for each project and take account of the recommended values given in the standards.

Tab. 4.1 Load factors for the verification of structural safety

Actions	γ_F	Limit state		
		Type 1	Type 2	Type 3
Permanent actions				
- unfavourable effect	$\gamma_{G,\mathrm{sup}}$	1.10 [1)]	1.35 [1)]	1.00
- favourable effect	$\gamma_{G,\mathrm{inf}}$	0.90 [1)]	0.80 [1)]	1.00
Variable actions				
- generally	γ_Q	1.50	1.50	1.30
- road traffic loads	γ_Q	1.50	1.50	1.30
- railway traffic loads	γ_Q	1.45	1.45	1.25
Actions arising in the subsoil				
Earth surcharges				
- unfavourable effect	$\gamma_{G,\mathrm{sup}}$	1.10	1.35 [2) 3)]	1.00
- favourable effect	$\gamma_{G,\mathrm{inf}}$	0.90	0.80	1.00
Earth pressure				
- unfavourable effect	$\gamma_{G,Q,\mathrm{sup}}$	1.35	1.35	1.00
- favourable effect [4)]	$\gamma_{G,Q,\mathrm{inf}}$	0.80	0.70	1.00
Hydrostatic pressure				
- unfavourable effect	$\gamma_{G,Q,\mathrm{sup}}$	1.05	1.20 [3)]	1.00
- favourable effect	$\gamma_{G,Q,\mathrm{inf}}$	0.95	0.90	1.00

[1)] G is either multiplied by $\gamma_{G,\mathrm{sup}}$ or by $\gamma_{G,\mathrm{inf}}$ depending on whether the overall effect is favourable or unfavourable.

[2)] $\gamma_{G,\mathrm{sup}}$ may be reduced linearly from 1.35 to 1.2 for heights of dumped goods from 2 to 6 m.

[3)] According to SIA 267, lower values are permissible in certain cases when using the observation method.

[4)] According to SIA 267, $F_d = R_d$ is valid for passive earth pressure as a favourable action.

4.6.3 Verification of structural safety

The following *design criterion* must be fulfilled for type 1 limit states (see section 4.4):

$$E_{d,\mathrm{dst}} \leq E_{d,\mathrm{stb}} \tag{4.4}$$

where $E_{d,\mathrm{dst}}$ and $E_{d,\mathrm{stb}}$ denote the design values of the destabilising and stabilising action effects respectively.

The following design criterion must be fulfilled for type 2 and 3 limit states:

$$E_d \leq R_d \tag{4.5}$$

Here, the design values of the action effects for persistent and transient design situations are to be calculated according to

$$E_d = E\left\{\gamma_G G_k,\ \gamma_P P_k,\ \gamma_{Q1} Q_{k1},\ \psi_{0i} Q_{ki},\ X_d,\ a_d\right\} \tag{4.6}$$

and for accidental design situations according to

$$E_d = E\{G_k, P_k, A_d, \psi_{2i}Q_{ki}, X_d, a_d\} \tag{4.7}$$

Please see appendix A2 for the notation used here.

The verification of structural safety for type 4 limit states is carried out essentially according to (4.5), although special rules for determining the effects of *fatigue loads* and the corresponding resistances are applied (see also section 7.6.3).

4.6.4 Verification of serviceability

Verifications of serviceability must be carried out for persistent and transient design situations, in exceptional cases for accidental design situations as well (e. g. for vital infrastructure elements such as hospitals, fire stations and ambulance stations following an earthquake).

Serviceability is deemed to be satisfied when the design criterion

$$E_d \leq C_d \tag{4.8}$$

is fulfilled, where E_d is generally to be calculated according to $(4.3)_1$, with $\gamma_F = \gamma_m = 1$.

We distinguish between three types of load case for persistent and transient design situations, and determine the governing action effects as follows:

Rare load cases

$$E_d = E\{G_k, P_k, Q_{k1}, \psi_{0i}Q_{ki}, X_d, a_d\} \tag{4.9}$$

Frequent load cases

$$E_d = E\{G_k, P_k, \psi_{11}Q_{k1}, \psi_{2i}Q_{ki}, X_d, a_d\} \tag{4.10}$$

Quasi permanent load cases

$$E_d = E\{G_k, P_k, \psi_{2i}Q_{ki}, X_d, a_d\} \tag{4.11}$$

Eq. (4.7) applies to the earthquake design situation, although the value used for A_d should be reduced by 50 % compared with that used in the verification of structural safety.

4.7 Commentary

Until the 1960s, the dimensioning of structures was carried out using *permissible stresses* for the stress resultants calculated based on the elastic system at serviceability level. The focus was on the behaviour of the structure in the serviceability state. The aim of limiting the stress was to limit deformations and also to create a sufficient safety margin against failure.

The introduction of plastic methods of calculation in the 1960s and 1970s brought about a paradigm change; the focus shifted to the ultimate resistance. Verification of the stress was replaced by *verification of the ultimate load*, with the limit load determined according to plastic theory being divided by a global safety factor (in the order of magnitude of 1.8, but varying depending on the type of construction) to obtain the permissible load at the serviceability state. It was recognised that every stress and deformation calculation at the serviceability state is complicated, and essentially called into question, by the diverse initial stress states caused by, for example, the production process, and is impossible, at best very difficult, to ascertain in practice. On the other hand, the limit load is independent of the loading history in the presence of adequately ductile behaviour and the absence of stability problems.

Regarding verification of structural safety, further developments led to the introduction of the *design level* lying between the serviceability and ultimate levels. The global safety factor was split into a load factor and a resistance factor, with the actions and resistances being increased and decreased accordingly. The practical significance of the behaviour at the serviceability state (which had been forced somewhat into the

background by the ultimate load verification approach) was rediscovered, given a differentiated formulation and by calling it the "limit state of serviceability" placed on the same level as the established consideration of the limit state of structural safety. This development was concluded around 1990 and, following further refinements over the next 10 years, culminated in the design concept presented in this chapter.

The procedure for dimensioning structures as outlined here, which is common these days, will not be referred to further in the following chapters. The focus will be on the structural behaviour of structures subjected to mechanical and significant physical actions at the serviceability and ultimate limit states. It is easy to incorporate appropriate models in the design concept presented here for practical applications, and such models will still retain their usefulness even in any future adaptations of this design concept.

The design concept described here is primarily suitable for the definitive structural calculations during detail design. Simplifications are justified for the tender design, and principally the preliminary design. A method for the conceptual design and the rough checking of concrete structures, used successfully by the author over many years, is briefly described here as an example of such a simplification.

The method basically returns to the concept of permissible stresses and can be referred to as dimensioning based on *representative stresses*. All verifications are carried out according to (4.5) at the serviceability level using conventional modelling by setting $\gamma_F = 1$ in $(4.3)_1$ and including an additional factor of 1.4 in the denominator of the first expression in brackets on the right-hand side of $(4.3)_2$, which corresponds to a mean γ_F for limit state 2 according to Tab. 4.1. For reinforcing steel, this leads to a limit stress of $0.62 f_{sk}$, where f_{sk} denotes the characteristic value of the yield strength of the reinforcing steel. For prestressing steel, the limit stress is $0.62 f_{p0.1k}$, where $f_{p0.1k}$ = characteristic value of yield strength of prestressing steel. For the compressive stresses in the concrete, bond stresses and tensile or shear stresses, the result is limit values of about $5 f_{ctm}$, $0.65 f_{ctm}$ and $0.17 f_{ctm}$, where f_{ctm} = mean concrete tensile strength. In the case of second-order effects in compressive members, the curvatures are to be increased by a factor of 1.4.

In contrast to the concept of permissible stresses, which is based rigorously on elastic theory, dimensioning based on representative stresses is much less restrictive and makes full use of the accomplishments of plastic methods of calculation. These methods result in simplified calculations for the stress resultants, which can largely be confined to considering the equilibrium, and also in simplified cross-sectional considerations, e. g. assuming a rectangular distribution of the concrete compressive stress over 85 % of the depth of the bending compression zone.

Dimensioning based on representative stresses presumes that ductile structural behaviour is assured. This requirement can be achieved by choosing suitable construction materials, including a minimum amount of reinforcement and through careful detailing. Using this as a starting point, the method outlined here enables the user to design or check structural members quickly and sufficiently accurately for conceptual design purposes, freed from unnecessary analytical ballast.

4.8 Recommendations for the structural calculations

Producing clearly organised structural calculations that are easy for others to follow is an important engineering activity. The following recommendations should be applied appropriately depending on the scope of the project and its status (preliminary/tender/detail design).

Tab. 4.2 shows one possible way of organising the structural calculations and contains remarks regarding individual sections.

Tab. 4.2 One possible way of organising the structural calculations

Content	Commentary
Title page Contents	
Contents	
1 Basic information	
1.1 Documents	List of all relevant construction works documents
Reports	e. g. description of construction works, previous technical reports
Drawings	
Preliminary calculations	e. g. preliminary structural analysis
Service criteria agreement	
Basis of design	
Surveys	e. g. geotechnical report
Standards	
Regulations	e. g. official directives
Publications	full details (author, title, publisher, location, year, page Nos.)
Computer programs	name, version
1.2 Geometry	Description of geometry of structural system
Overview	three-dimensional structural system with principal dimensions, construction states
Notation	system of coordinates, sign conventions, structural member designations
Cross-sections	numbering, cross-sectional values
Prestressing	cable geometry and numbering
1.3 Construction materials	Material designations and summary of characteristic values
Concrete	
Reinforcing steel	
Prestressing steel	
Structural steel	
Timber	
Connectors	
Masonry	
1.4 Subsoil	Implementation of soil survey data
Subsoil model	
Subsoil parameters	
Permissible stresses	e. g. ground bearing pressures
Permissible deformations	e. g. settlement, wall displacements
1.5 Actions	Summary of load models, characteristic values and factors
Dead loads	
Self-weight of non-structural elements	
Prestressing	
Subsoil	dead loads, earth pressure, hydrostatic pressure, soil-structure interaction
Snow	
Wind	
Temperature	
Shrinkage	
Creep	
Imposed loads	dynamic effects
Impact	
Fire	
Earthquake	earthquake zone, construction works and subsoil classes

Tab. 4.2 One possible way of organising the structural calculations (Continued)

Content		Commentary
2	Structural analysis and dimensioning	Separate presentation of individual parts of the structure (e. g. superstructure, substructure), also construction states and temporary structures
2.1	Structural models	Description of structural systems considered and assumptions made
	Structural systems	hinges, degrees of fixity
	Prerequisites	behaviour of construction materials and subsoil, effective widths
2.2	Design situations	Description of physical circumstances and conditions considered
	Relevant hazard scenarios	leading hazard, accompanying situations
	Relevant service situations	design working life
	Governing limit states	structural safety, serviceability
	Load cases	physically compatible application of actions occurring simultaneously
2.3	Action effects	Determining the structural behaviour
	Support force variables	checking equilibrium
	Stress resultants	graphic presentations, envelopes
	Stresses	e. g. boundary forces, stress differences, principal stresses
	Displacements	e. g. deflections, displacements at supports
	Deformations	
2.4	Verifications	Confirmation that design criteria have been fulfilled
	Design values	partial and conversion factors
	Structural safety	overall stability, ultimate resistance, fatigue resistance
	Serviceability	functionality, comfort, appearance
2.5	Detailing	Construction details, sketches to scale
3	Appendix (computer calculations)	
3.1	General	Scope, analytical models, overview
3.2	Inputs	
3.3	Outputs	Preferably graphic presentations
	Structural analysis	treatment of the individual parts of the structure (structural members), preferably in direction of flow of forces
	Verifications	
3.4	File	CD (incl. overview) with detailed data

Write on only one side of each sheet of the structural calculations; add the date and the initials of the author to each sheet. Number the sheets consecutively section by section; sheets added at a later date with supplementary data or modifications should be given the number of the page being supplemented/modified plus a letter, e. g. 2.3.17 B.

Give equations in algebraic form when they appear for the first time. Add a cross-reference in the case of equations that are not generally in use.

Describe the calculation procedure, at least in abbreviated form, and mention important considerations (e. g. concerning modelling) and consequences.

Adding cross-references makes it a lot easier to follow the structural calculations. In doing so, specify the significance and source of variables that are being used again.

Highlight results so that they are clearly identifiable as such at first glance. Always include units of measurement with the results and round them off to two or three significant places. (Do not make them appear more accurate than they really are!)

4.9 Recommendations for the technical report

The technical report should include the essentials of a project described as simply and briefly as possible. Tab. 4.3 shows one possible way of organising the report and includes non-exhaustive lists of remarks and keywords regarding the individual sections. As with the structural calculations (section 4.8), the following recommendations should be applied accordingly depending on the scope and status of the project.

Tab. 4.3 One possible way of organising a technical report

Content	Commentary, keywords
Title page Contents	
Contents	
1 Introduction	
Brief	Situation, scope of project, surroundings Possibly a brief historical review Preliminary work, status of project
Aims of project	Highlight the most important requirements of the service criteria agreement (use, environment, operation/maintenance, durability, economy, integration, composition)
2 Overall concept	
Important boundary conditions	Highlight the relevant design boundary conditions (see section 3.2)
Development of concept and reasoning	Summary of the main steps in the draft design (examining alternatives, choice of concept, durability, economy, integration and composition)
3 Description of construction works	
Geometry	Principal dimensions, alignment, surroundings
Construction materials	Material selected for each structural member
Environment	E. g. consideration of nature conservation stipulations, relationship with neighbouring construction works, immissions during construction, energy balance
Structural composition	Principles, individual structural members
Durability and maintenance	Scheduled renewals, particular aspects of maintenance
Special aspects	E. g. supplementary soil surveys, preliminary testing
4 Structural calculations	As a rule, this section is first added for the tender design. For the preliminary design, it is generally sufficient to include rough structural calculations.
Overview	Structural systems, principal assumptions
Most important results	E. g. settlement, deflections, stresses Graphic or tabular presentation
5 Construction work	
Concept	Construction programme, construction concept
Construction site infrastructure	Access, space requirements
Excavations and foundations	Securing excavations, piles, pilecaps, etc.
Superstructure	E. g. abutments, piers, bridge superstructure or walls, columns, suspended floors
Deconstruction	Possible deconstruction of existing construction works or individual superseded structural members
6 Costs	
Quantities	Removal of topsoil, excavation, demolition, deconstruction Fill, topsoil, concrete, reinforcing steel, prestressing steel, structural steel, timber, masonry, floor finishes Round off quantities sensibly Cover uncertainties by adding a “contingencies” item
Cost of construction	Preliminary design: estimate (accuracy ± 20 %) based on preliminary quantities or experience Tender design: estimate (accuracy ± 10 %) based on quantities and unit prices
Cost of maintenance and operation	
7 Summary	Structural concept, integration and composition, economy, design, foundations, construction work, costs

In the "Description of construction works", it is expedient to include a land register map (if available) that shows a plan plus longitudinal and transverse sections of the construction works and specifies the most important dimensions of the structure. Alternatively, or as a supplement to the land register map, a general arrangement drawing can be used which shows the construction works and the relevant surroundings. To ensure clarity and legibility, it is worthwhile including excerpts from the general arrangement drawing in the technical report, e. g. typical cross-sections or schematic views of the layout of the prestressing tendons. The same applies to describing construction procedures in the "Construction work" section. Finally, conceptual design sketches, perspective views, photomontages and, in particular, photos of models can be skilfully used to improve the quality of a technical report.

4.10 Summary

1. Dimensioning is only one of a number of different measures for assuring structural safety and serviceability.
2. Dimensioning is carried out on the basis of considering limit states by specifying the load cases associated with particular design situations and supplying appropriate verifications. In addition, detailing based on structural and construction technology considerations enables the construction details to be determined and coordinated.
3. The structural behaviour in the design situations to be considered is investigated by means of the methods of structural analysis. The focus here is the transition from the true structure to the structural model, which links actions and action effects and takes into account geometrical properties as well as the properties of the construction materials and the subsoil.
4. The art of handling structural analysis problems manifests itself in skilful modelling, using the simplest approach possible, which leads to meaningful results just adequate for the respective problem.
5. Verification of structural safety and serviceability is generally carried out on the basis of design values.
6. A particular verification may not be needed if it can be established that it is not critical. In addition, a particular verification may not be necessary if it can be shown that the corresponding requirements are of only minor significance or can be achieved with structural or construction technology measures.
7. The dimensioning concept common these days, based on a design level between the serviceability and ultimate levels, is primarily suited to definitive structural calculations. Simplifications are possible and advisable for the conceptual design and for quick structural checks, e. g. in the sense of dimensioning based on representative stresses.
8. The principles and the results of the structural analysis and the dimensioning must be included in the structural calculations and the technical report. Recommendations for the organisation and contents of structural calculations and technical reports can be found in sections 4.8 and 4.9.
9. It is essential to check the plausibility of the results of the structural analysis and the dimensioning in every case. Equilibrium checks, examining simplified structural systems and comparisons with known solutions to similar problems are all excellent ways of carrying out plausibility checks.

4.11 Exercises

4.1 Consider the "Buoyancy, BL" hazard scenario given in example 3.2. Discuss the effect of the proposed opening adjacent to the ramp taking into account the groundwater levels given in Fig. 3.5.

4.2 Consider the "Punching, suspended floors" hazard scenario during construction given in example 3.2. Discuss the effect of the proposed measures, especially propping.

4.3 Describe the design situation on which the punching verification for the final condition (normal use) is based and identify the associated load case together with leading and accompanying actions according to (4.6). How should the imposed load be applied in order to achieve the most unfavourable action effects?

4.4 Consider the design situation associated with the "Impact, fork-lift" hazard scenario for internal columns on the ground floor and discuss the corresponding load case according to (4.7).

4.5 Discuss the requirement that the edges of the suspended floors may deflect no more than 15 mm with the help of (4.8) to (4.11).

5 STATIC RELATIONSHIPS

5.1 Force systems and equilibrium

5.1.1 Terminology

Forces are perceived through their effects. They correspond to physical interactions that cause or modify states of deformation or motion in material systems. The effect of a force depends on its point of application, its magnitude and its direction. Therefore, according to Fig. 5.1(a), a force can be represented as a point-based vector $\boldsymbol{F}$ with point of application A, magnitude F and line of action f.

The line of action f and an arbitrary reference point O define one plane. If we imagine a body connected to this one plane, then it is clear that $\boldsymbol{F}$ would cause a rotation of the body about the axis n perpendicular to the plane and passing through O. The tendency to rotate is proportional to the magnitude F and the distance a of force $\boldsymbol{F}$ from O. The *position vector* $\boldsymbol{r}$ of the point of application A of $\boldsymbol{F}$ expresses the tendency to rotate with the *moment*

$$\boldsymbol{M} = \boldsymbol{r} \times \boldsymbol{F} \tag{5.1}$$

correctly in terms of magnitude and direction; $|\boldsymbol{M}| = Fa$ applies and the vectors $\boldsymbol{M}$, $\boldsymbol{r}$ and $\boldsymbol{F}$ constitute a right-hand screw, see Fig. 5.1(b). As can be seen, the moment $\boldsymbol{M}$ remains unaltered if force $\boldsymbol{F}$ is translated along its line of action f.

Every force $\boldsymbol{F}$ has a corresponding *reaction* $-\boldsymbol{F}$ with the same line of action. According to this so-called *reaction principle*, a force without its reaction cannot exist.

Remote forces (e. g. gravity) exhibit points of application different to those of their reactions; the interaction between two bodies with mass generally takes place without contact. But in the case of *contact forces* (e. g. support forces), the points of application of forces and reactions are geometrically identical (although not materially identical); the interaction between support and supported body comes about through contact – if the contact is eliminated, so the contact force disappears as well.

The *inertial forces* that must be considered in dynamics (see section 8.3.4) do not have any reactions. They do not correspond to any physical interactions, instead are mathematical auxiliary variables.

Contact forces are generally in the form of *surface forces* (*surface loads*) distributed over a finite area. The contact force related to the unit of surface area, the *force per unit area*

$$\boldsymbol{t} = \frac{\mathrm{d}\boldsymbol{F}}{\mathrm{d}A} \tag{5.2}$$

is also known as a *stress vector*, see Fig. 5.2(a) and section 5.2.1.

Similarly, remote forces distributed over a finite three-dimensional space are called *body forces* (*body loads*) with a *force per unit volume* of

$$\boldsymbol{q} = \frac{\mathrm{d}\boldsymbol{F}}{\mathrm{d}V} \tag{5.3}$$

see Fig. 5.2(b).

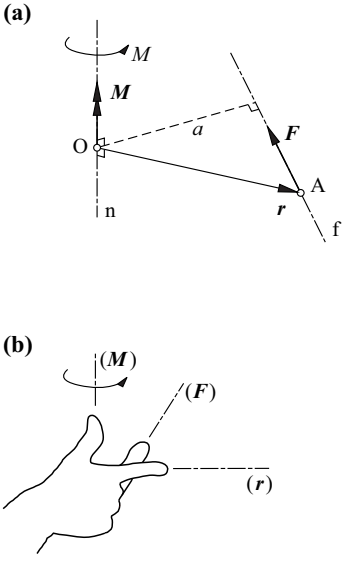

Fig. 5.1 Force and moment: (a) reference point O, point of application A, line of action f, axis of rotation n, (b) right-hand screw rule

Theory of Structures. First Edition. Peter Marti

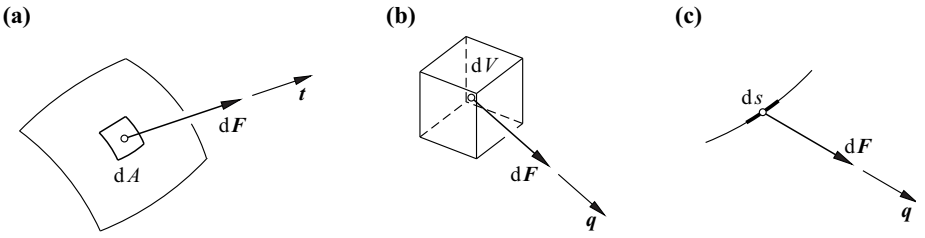

Fig. 5.2 Distributed forces: (a) force per unit area, (b) force per unit volume, (c) force per unit length

If, ultimately, a body such as a beam or cable is idealised as one-dimensional and if distributed forces act on this in the form of *line forces* (*line loads*), we get a *force per unit length*

$$\boldsymbol{q} = \frac{\mathrm{d}\boldsymbol{F}}{\mathrm{d}s} \tag{5.4}$$

see Fig. 5.2(c).

In the SI or MKS systems, the unit used for specifying the magnitude of a force is the *newton* [1 N = 1 mkgs^{-2}] or [kN] or [MN]. Correspondingly, the unit used for moments is [Nm] or [kNm] or [MNm]. To distinguish between forces and moments, we indicate the latter with double arrows, see Fig. 5.1(a). The units for forces per unit length, area and volume are therefore [Nm^{-1}], [Nm^{-2} = Pa] and [Nm^{-3}].

5.1.2 Force systems

We shall now consider *force systems* (groups of forces) whose material points of application lie within the arbitrary limits of a body or system. A body isolated from a body or system (or part thereof) by means of an imaginary cut is known as a *free body* (FB). By introducing all the forces that act on the free body, we obtain a *free-body diagram* (FBD).

The *resultant force* of a force system is obtained by adding together the vectors acting on the free body:

$$\boldsymbol{R} = \sum_{\mathrm{FB}} \boldsymbol{F} \tag{5.5}$$

Likewise, the *resultant couple* of a force system with respect to an arbitrary reference point O is

$$\boldsymbol{M}_{\mathrm{O}} = \sum_{\mathrm{FB}} \boldsymbol{r} \times \boldsymbol{F} \tag{5.6}$$

see Fig. 5.3 and (5.1).

If instead of O we select a different reference point O′, then according to Fig. 5.3, with $\boldsymbol{r}' = \boldsymbol{r} - \boldsymbol{r}''$ and considering (5.5) and (5.6), it follows that

$$\boldsymbol{M}_{\mathrm{O}'} = \sum_{\mathrm{FB}} \boldsymbol{r}' \times \boldsymbol{F} = \sum_{\mathrm{FB}} \boldsymbol{r} \times \boldsymbol{F} - \boldsymbol{r}'' \times \sum_{\mathrm{FB}} \boldsymbol{F} = \boldsymbol{M}_{\mathrm{O}} - \boldsymbol{r}'' \times \boldsymbol{R} \tag{5.7}$$

The pair of vectors $\{\boldsymbol{R}, \boldsymbol{M}_{\mathrm{O}}\}$ or $\{\boldsymbol{R}, \boldsymbol{M}_{\mathrm{O}'}\}$ is called the *force-couple system* of the force system at O or O′.

Two force systems are *equivalent* when their force-couple systems are identical with respect to an arbitrary reference point. According to (5.7), the equivalence of two force systems need only be verified for one reference point; the identity of the resultant couple is then given for all points.

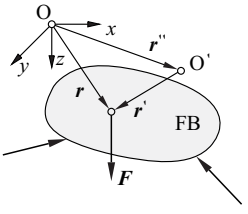

Fig. 5.3 Free body diagram with reference points O and O′

5.1.3 Equilibrium

A force system is *in equilibrium* when its force-couple system sums to zero:

$$\boldsymbol{R} = \boldsymbol{0} \quad , \quad \boldsymbol{M}_{\mathrm{O}} = \boldsymbol{0} \tag{5.8}$$

The *equilibrium conditions* (5.8) result in six scalar equations in the case of force systems in three dimensions, i. e. three *force-balance equations* and three *moment-balance equations*. In the case of coplanar force systems, this number is reduced to three, i. e. two force-balance equations in the plane of the force system and one moment-balance equation perpendicular to that plane.

If (5.8) applies, then according to (5.7), $\boldsymbol{M}_{\mathrm{O}'} = \boldsymbol{0}$. Consequently, the force-balance equations can be replaced by moment-balance equations about a second reference point. Generally, in the three-dimensional case, moment-balance equations can be formulated about six non-collinear axes and in the coplanar case about three points not lying in a straight line. In practice, this is often easier than setting up the force-balance equations. Depending on the particular problem, in the coplanar case only one, and in the three-dimensional case only one or two, force-balance equations are replaced by moment-balance equations, as is explained further in chapter 10.

Applying (5.8) to differential structural elements results in differential equations for the equilibrium, as dealt with in section 5.3.

When defining free bodies and applying the equilibrium conditions to those bodies, we generally use the so-called *free-body principle*: if we remove arbitrary parts from a compatibly deformed body or system in equilibrium by way of imaginary cuts, each one of those parts is in equilibrium and compatibly deformed.

Forces acting on arbitrary free bodies are known as *internal* or *external forces* depending on whether the material point of application of the reaction to a force lies inside or outside the free body.

According to the reaction principle, the internal forces form an *equilibrium system* (i. e. a force system in equilibrium), and so the external forces must themselves be in equilibrium if the free body is in equilibrium in its entirety. This assertion is known as the *fundamental theorem of statics*.

If the equilibrium conditions – at best following a suitable breakdown of the system – are sufficient for determining the unknowns in a problem, we speak of a *statically determinate* system, otherwise a *statically indeterminate* system.

5.1.4 Overall stability

Structures must be *stable*, i. e. they must not fail in their entirety (e. g. due to buoyancy, sliding or overturning). Their *rigid body equilibrium*, or rather their overall stability, must be assured (see section 4.4, limit state type 1).

Example 5.1 Cantilever retaining wall

The cantilever retaining wall shown in Fig. 5.4(a) is to be investigated for overturning about its toe O. To do this, we consider the cantilever retaining wall as a free body isolated from its surroundings according to Fig. 5.4(b) and add all the forces acting on it in order to create a free body diagram. Those forces are the dead loads of the base (G_1) (related to the unit length perpendicular to the yz plane) and the vertical stem (G_2), the surcharges due to the earth above the cantilevering parts of the base (G_3 and G_4), the active and passive earth pressures (E_a and E_p) plus a contact force A acting on the underside of the base. For simplicity, hydrostatic pressures are neglected. Further, the calculation with the earth surcharges G_3 and G_4 represents a considerable idealisation. Actually, in the event of an overturning failure, a wedge-shaped mass of soil would form in the ground behind the wall. And this would be linked with the mobilisation of further forces that are neglected here; a similar consideration applies to the soil in front of the wall.

The contact force A can easily be determined with (5.8) according to magnitude, direction and point of application, e. g. by setting up the two force-balance equations in the y and z directions and the moment-balance equation about O. Alternatively, A can also be determined graphically. Fig. 5.4(c) shows

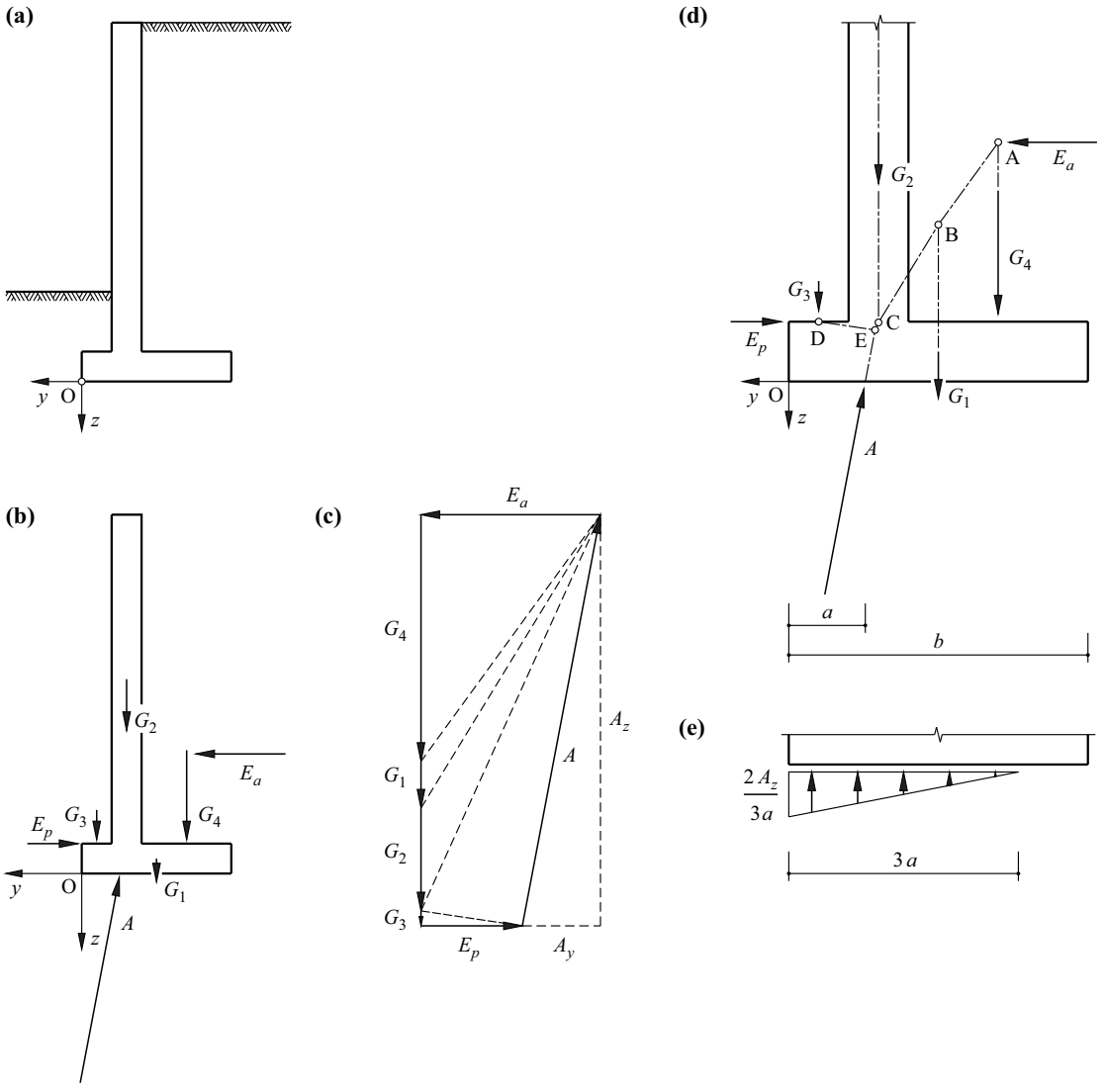

Fig. 5.4 Overall stability of a cantilever retaining wall: (a) overview, (b) free body diagram, (c) force polygon, (d) funicular polygon, (e) possible distribution of ground pressure

the associated addition of the force vectors in the so-called *force polygon*; for equilibrium, the force polygon must be closed, which determines the magnitude and direction of A. The point of application of A follows from the *funicular polygon* according to Fig. 5.4(d). This is done by successively forming the interim resultants (shown as dotted lines in the force polygon) of forces E_a and G_4 etc., drawing their lines of action starting from point A, the intersection of E_a and G_4, and extending this to intersect with the next force G_1 at B etc. This approach enables us to establish point E, the intersection of the lines of action CE and DE for (E_a, G_4, G_1, G_2) or (E_p, G_3), and hence determine the line of action of A.

For overall stability, A must act on the base, i. e. $0 \leq a \leq b$, see Fig. 5.4(d). For the limit case $a = 0$ (or $a = b$), the bearing pressure would be infinitely large, which is of course impossible because the strength of the subsoil is finite. Fig. 5.4(d) shows one practical possibility and Fig. 5.4(e) shows a statically equivalent linear bearing pressure distribution with a maximum value of $2A_z/(3a)$ at O. As can be seen, $3a < b$, i. e. in the range $-3a > y \geq -b$ the foundation experiences *partial uplift* with the contact force tending towards zero.

It is not possible to reach any conclusion about the distribution of the horizontal component A_y of A at the underside of the base solely on the basis of static considerations. For simplicity, a distribution proportional to A_z is assumed, which in this particular case means a triangular distribution.

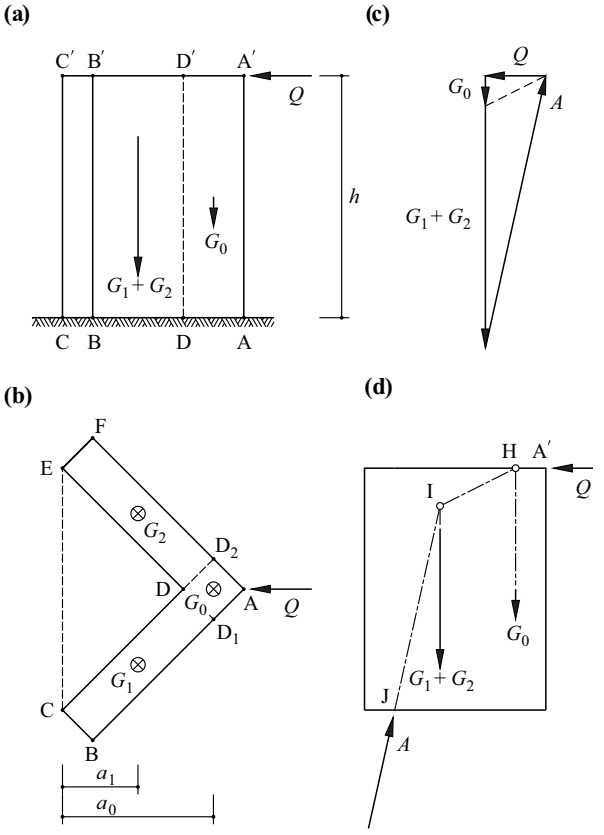

Fig. 5.5 Upturned right-angled element on horizontal surface: (a) elevation, (b) plan, (c) force polygon, (d) funicular polygon

Example 5.2 Support envelope

The upturned right-angled element supported on a horizontal surface shown in Fig. 5.5(a) and (b) is loaded at A′ by a horizontal force Q. In Fig. 5.5(b) we must distinguish between the *area of contact* ABCDEF and the *support envelope* ABCEF. The latter is the smallest convex envelope enclosing the former.

The overall stability of the right-angled element can be checked with the help of a moment-balance equation about axis CE. The overturning moment Qh due to Q acting about CE may not exceed the resisting moment $G_0 a_0 + (G_1 + G_2)a_1$ due to the dead load components $G_0(\mathrm{AD_1DD_2})$, $G_1(\mathrm{D_1BCD})$ and $G_2(\mathrm{DEFD_2})$, otherwise the element will overturn.

Fig. 5.5(c) and (d) show the alternative graphical examination with the help of the force and funicular polygons. For overall stability, the point of application J of the contact force A must lie within the support envelope.

The contact force A is assumed to be distributed equally over the end zones of the two legs of the element. In the limit case, the force is concentrated at points C and E, which means that the local bearing pressure is then infinitely large.

5.1.5 Supports

Supports correspond to the locally inhibited displacement and rotation capabilities (*degrees of freedom*) of structures. They can be classified according to the inhibited (restrained) displacement and rotation capabilities or the passive degrees of freedom, i. e. according to whether the displacements u, v, w and the rotations φ_x, φ_y, φ_z in the x, y, z directions are possible or prevented, see Fig. 5.6. The number of passive (restrained) degrees of freedom (or the number of components in the *support force-couple system*) is known as the *determinacy* of the support.

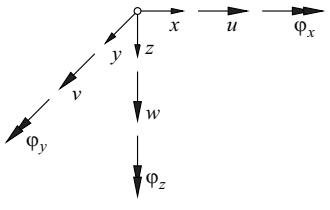

Fig. 5.6 Displacements and rotations

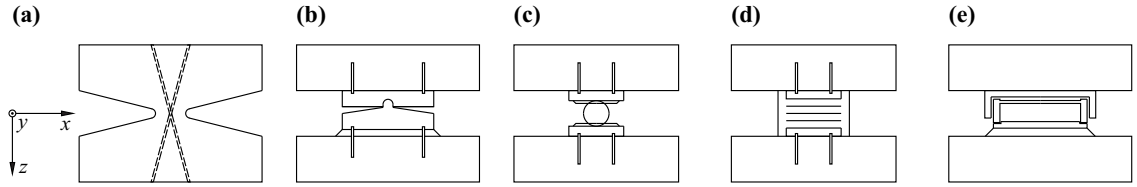

Fig. 5.7 Types of bearing: (a) concrete hinge, (b) steel linear rocker bearing, (c) steel roller bearing, (d) laminated elastomeric bearing, (e) elastomer pot sliding bearing

Fig. 5.7 shows a number of different types of support. If the concrete hinge shown in Fig. 5.7(a) is in the form of a linear support (long in the y direction), it inhibits displacements u, v, w and rotations φ_x, φ_z; in the form of a discrete support (short in the y direction), both φ_y and also φ_x and φ_z are practically not inhibited at all. It is notable that with respect to the forces, the support acts bilaterally in all three directions, i. e. positive and negative forces can occur in the body of the bearing sliced through at the horizontal joint, especially in the z direction, too, because of the reinforcement intersecting the horizontal joint. The steel linear rocker bearing shown in Fig. 5.7(b) acts bilaterally with respect to u and unilaterally with respect to w – the support would lift up in the z direction when the force tends towards zero; with respect to v, it works bilaterally up to a certain amount, either via friction or with lugs at the sides (after overcoming the play between lug and body of bearing); rotation φ_y is practically unrestrained, and rotations φ_x, φ_z are inhibited. In the case of the steel roller bearing shown in Fig. 5.7(c), u and φ_y are not inhibited and the support acts unilaterally with respect to w; guide rails at the side inhibit displacement v and rotation φ_z; rotation φ_x is inhibited because of the long roller in the y direction. The laminated elastomeric bearing shown in Fig. 5.7(d) functions unilaterally with respect to w and, depending on the particular type, enables displacements u, v as well as rotations φ_y, φ_x. The same is true for the elastomer pot sliding bearing shown in Fig. 5.7(e).

A closer look at Fig. 5.7 shows that, depending on the particular design, the displacement and rotation capabilities of supports always lie within certain limits and are never enabled or prevented in absolute terms. Likewise, the components of the support force-couple system associated with the inhibited displacement and rotation capabilities are restricted to certain limit values. In practice, it is certainly necessary to consider these limits carefully every time.

In theory of structures, we assume the appropriate idealisations shown in Fig. 5.8 for the coplanar case. Fig. 5.8(a) shows a unilaterally or bilaterally functioning *sliding support* (hinged support capable of displacement) that only inhibits w and whose support force-couple system is limited to the force component in the z direction. In the case of the *hinged support* shown in Fig. 5.8(b), u is also inhibited and the corresponding force component in the x direction is added to the support force-couple system. Considering the *fixed support* shown in Fig. 5.8(c), φ_y is finally inhibited as well; the support force-couple system also exhibits a moment about the y axis. Extending these considerations to the general three-dimensional case is easily possible with the help of Fig. 5.6.

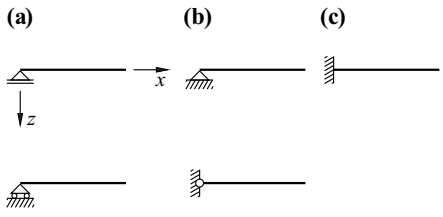

Fig. 5.8 Support idealisations: (a) sliding support, (b) hinged support, (c) fixed support

Static equivalents to the types of support shown in Fig. 5.8 can be realised according to Fig. 5.9 with *pin-jointed members*. These are straight, weightless bars connected concentrically on both sides with frictionless hinges. With such assumptions, only forces can be transferred from the bars, whose lines of action coincide with the axes of the bars. So a statically equivalent substitute for a sliding support, as shown in Fig. 5.9(a), could be a pin-ended strut; the force component in the x direction caused by the inclination of the pin-ended strut as a result of a displacement u is negligible in comparison to the force component in the z direction, assuming infinitesimally small dis-

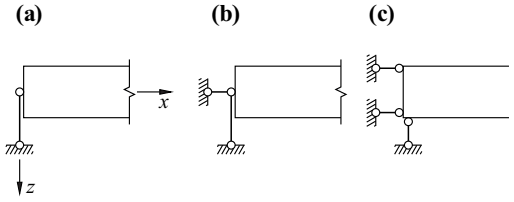

Fig. 5.9 Equivalent supports with pin-jointed members: (a) sliding support, (b) hinged support, (c) fixed support.

placements (first-order theory, see section 6.1). The support force component possible in the x direction with a hinged support requires a corresponding second pin-jointed member, as shown in Fig. 5.9(b). Ultimately, a third pin-jointed member is required to achieve fixity, as shown in Fig. 5.9(c); here, the first two pin-jointed members exhibit different lines of action and the axis of the third may not pass through the intersection of the first two, otherwise the support would not provide fixity, instead function like a hinged support at this point.

For the general three-dimensional case, six pin-jointed members are necessary for a braced support. With the force-couple system $\{\boldsymbol{R}, \boldsymbol{M}_\mathrm{O}\}$, the coordinates r_{ij} of one point on the axis of the pin-jointed member i and the direction cosine c_{ij} of the six pin-jointed members and the forces in those members N_i, then according to (5.5) and (5.6) the following applies:

$$\begin{bmatrix} c_{1x} & c_{2x} & \cdots & c_{6x} \\ c_{1y} & c_{2y} & \cdots & c_{6y} \\ c_{1z} & c_{2z} & \cdots & c_{6z} \\ r_{1y}c_{1z} - r_{1z}c_{1y} & r_{2y}c_{2z} - r_{2z}c_{2y} & \cdots & r_{6y}c_{6z} - r_{6z}c_{6y} \\ r_{1z}c_{1x} - r_{1x}c_{1z} & r_{2z}c_{2x} - r_{2x}c_{2z} & \cdots & r_{6z}c_{6x} - r_{6x}c_{6z} \\ r_{1x}c_{1y} - r_{1y}c_{1x} & r_{2x}c_{2y} - r_{2y}c_{2x} & \cdots & r_{6x}c_{6y} - r_{6y}c_{6x} \end{bmatrix} \begin{Bmatrix} N_1 \\ N_2 \\ N_3 \\ N_4 \\ N_5 \\ N_6 \end{Bmatrix} = \begin{Bmatrix} R_x \\ R_y \\ R_z \\ M_{\mathrm{O}x} \\ M_{\mathrm{O}y} \\ M_{\mathrm{O}z} \end{Bmatrix} \tag{5.9}$$

In order that (5.9) can have a solution $\boldsymbol{N}$ for any force-couple system, the matrix on the left must be invertible, i. e. its determinant may not be zero.

Let us select the origin of coordinates O for the coplanar case (three bars in the xz plane) with R_x, R_z, $M_{\mathrm{O}y}$ to be the intersection of bars 1 and 2 ($\boldsymbol{r}_1 = \boldsymbol{r}_2 = \boldsymbol{0}$) and consider the point of pin-jointed member axis 3 on the z axis ($r_{3x} = 0$, $r_{3z} \neq 0$). In this case, removing the second, fourth and sixth rows as well as the fourth, fifth and sixth columns from the matrix in (5.9) gives us the following matrix:

$$\begin{bmatrix} c_{1x} & c_{2x} & c_{3x} \\ c_{1z} & c_{2z} & c_{3z} \\ 0 & 0 & r_{3z}c_{3x} \end{bmatrix} \tag{5.10}$$

and hence

$$\det = r_{3z}c_{3x}(c_{1x}c_{2z} - c_{1z}c_{2x}) \neq 0 \tag{5.11}$$

must apply. Without restricting the universal applicability, it is possible to place the x axis in the direction of bar axis 1, i. e. $c_{1x} = 1$, $c_{1z} = 0$. Consequently, $c_{3x} \neq 0$, $c_{2z} \neq 0$ must be true, i. e. bar axis 3 may not pass through O and bars 1 and 2 may not be collinear. The above requirements are therefore confirmed.

It is often not possible to idealise supports as fully restrained, as has been assumed up to now; instead, it is necessary to consider their flexibility. To this end, in accordance with Fig. 5.10, we use appropriate *translational* and *rotational springs* and in the simplest case presume a linear relationship between the components of the support force-couple system and the corresponding displacements and rotations:

$$A_x = -k_x u_\mathrm{A} \quad , \quad A_z = -k_z w_\mathrm{A} \quad , \quad M_\mathrm{A} = -k_y \varphi_{y\mathrm{A}} \tag{5.12}$$

where k_x, k_z and k_y denote the *stiffnesses of the translational* and *rotational springs*.

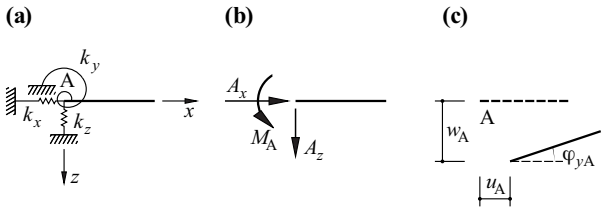

Fig. 5.10 Flexible supports: (a) translational and rotational springs, (b) support force-couple system, (c) translation-rotation system at support

5.1.6 Hinges

Hinges (or connections) correspond to local displacement and rotation capabilities within structures. Fig. 5.11 shows theory of structures hinge idealisations for the coplanar case. We speak of *expansion*, *shear* and *flexural hinges* depending on which component of the *hinge forces* is zero. As with supports, the *determinacy* of a hinge defines the number of components in the hinge forces. Hinges with one degree of determinacy can be combined from the basic types shown in Fig. 5.11, and the generalisation for hinges functioning in three dimensions is readily possible.

Flexural hinges can be formed not only as *full hinges*, as shown in Fig. 5.12(a), but also as *semi-hinges*, see Fig. 5.12(b). In doing so, a second bar is connected to an unweakened continuous first bar with an articulated joint.

In compression elements such as arches and columns, hinges can be formed in a similar manner to supports, e. g. as concrete hinges. In tension elements or connections subjected to shear only, simple pinned and bolted connections with adequate play in the holes can be considered. Fig. 5.13 shows a few examples of hinges selected from the huge variety of potential forms.

The connection between two beams with *dapped ends* shown in Fig. 5.13(a) is widely used with precast concrete components, for example; the connection can function not only as a flexural hinge, but also as an expansion hinge depending on the type of bearing (hinged or sliding) between the two beams. The shear connection between a *secondary beam* and a *primary beam* in structural steelwork shown in Fig. 5.13(b) is achieved with cleats and bolts; in this detail the secondary beam is connected via its web only, not via its flanges. Fig. 5.13(c) shows one possible form for the ridge joint in a timber roof structure.

As with the supports (Fig. 5.7), a closer look at Fig. 5.13 reveals that ideal hinge conditions cannot be realised in practice. Displacement capabilities are always either enabled or inhibited between certain limits; further, the wanted components of the hinge

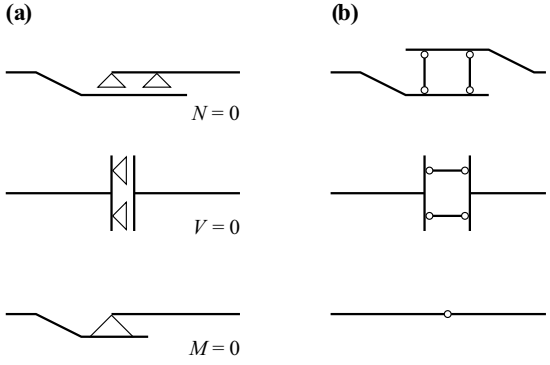

Fig. 5.11 Idealised hinges: (a) expansion, shear and flexural hinges, (b) alternative presentation with pin-jointed members, or rather full hinge

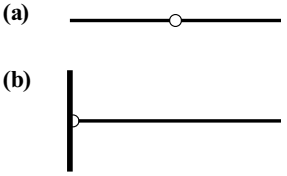

Fig. 5.12 Flexural hinges: (a) full hinge, (b) semi-hinge

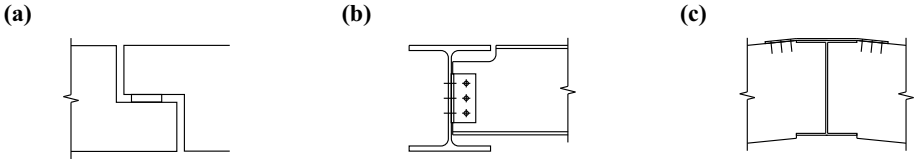

Fig. 5.13 Hinge forms: (a) connection between beams with dapped ends, (b) shear connection for a secondary beam, (c) ridge joint in a timber roof structure

forces are, on the one hand, accompanied by unwanted components and, on the other hand, contained within certain limits. The aim is to use skilful detailing to try to reduce the unwanted components to a negligible level. In any case, it is important to consider carefully how the form of the construction itself limits the forces and deformations, and their consequences.

As with supports, hinges always correspond to a weakening of the construction. Structurally, their design can be more or less awkward, they can prove to be expensive, may require maintenance or might be problematic in terms of their durability. Therefore, the positioning of supports and hinges must always be well thought out and the necessary precautions must be taken when considering the structural concept in order to achieve trouble-free functioning over the design working life.

5.1.7 Stress resultants

5.1.7.1 Framed structures

If we cut a linear-type beam into two parts I and II with a plane cut perpendicular to its axis according to Fig. 5.14, then the resultant force $\boldsymbol{R}$ and the resultant couple $\boldsymbol{M}$ of the internal forces must be introduced at the cut face of part I, related to the centroid O as a reference point on the cut face. At the cut face of part II, the force-couple system $\{-\boldsymbol{R}, -\boldsymbol{M}\}$ acts according to the reaction principle. According to (5.8), (5.5) and (5.6), for equilibrium of part II

$$-\boldsymbol{R} + \sum_{\text{II}} \boldsymbol{F} = \boldsymbol{0} \quad , \quad -\boldsymbol{M} + \sum_{\text{II}} \boldsymbol{r} \times \boldsymbol{F} = \boldsymbol{0}$$

hence

$$\boldsymbol{R} = \sum_{\text{II}} \boldsymbol{F} \quad , \quad \boldsymbol{M} = \sum_{\text{II}} \boldsymbol{r} \times \boldsymbol{F} \tag{5.13}$$

i. e. the force-couple system $\{\boldsymbol{R}, \boldsymbol{M}\}$ is obtained by reducing the forces acting on part II to reference point O.

If we introduce a system of Cartesian coordinates with the x axis in the direction of the member axis, then the components of the resultant force $\boldsymbol{R}$ are the *normal force* N in the x direction and the *shear forces* V_y and V_z in the y and z directions. The corresponding components of the resultant couple $\boldsymbol{M}$ are the *torque* T and the *bending moments* M_y and M_z.

Normal and shear forces plus torques and bending moments are known as *stress resultants*. They are positive when they act in the positive x, y or z direction on the positive side of the cut (normal = positive x axis), or when they act in the negative x, y or

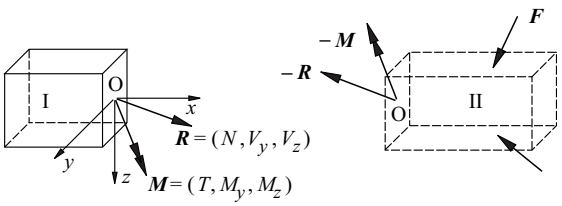

Fig. 5.14 Stress resultants

z direction on the negative side of the cut (normal = negative x axis). Fig. 5.15 uses the example of an **I** beam to show the stress resultants with their corresponding displacements u, v, w and rotations φ_x, φ_y, φ_z. The stress resultants and the associated deformation variables are so-called *state variables*. Their distribution along the axis of the member is described by way of so-called *state diagrams*, see chapters 11 and 15.

The *bar axis*, i. e. the line connecting the centroids of the cross-sectional areas, is generally in single or double curvature, and the geometry of the cross-section generally varies along the bar axis. However, the direction of the axis and the geometry of the cross-section are often constant, at least over certain sections, or can be approximated in this way with good accuracy. In order to justify being idealised as a *bar*, it is assumed that the dimensions of the cross-section (b and h in Fig. 5.15) are small in comparison with the dimensions along the bar axis.

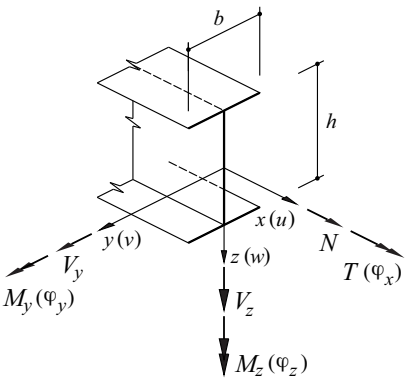

Fig. 5.15 State variables in framed structures

5.1.7.2 Plate and shell structures

In *plate and shell structures*, the bar axis is replaced by the *middle surface* or *middle plane* acting as the reference surface. The dimension of the structure h perpendicular to the reference surface at every point is presumed to be small in comparison with the dimensions in the reference surface.

Fig. 5.16 includes a local system of Cartesian coordinates x, y, z tangential or perpendicular to the reference surface. The stress resultants at the side faces of an (infinitesimally small) structural element with length 1 in the x and y directions are the *membrane forces*

$$n_x = \int_{-h/2}^{h/2} \sigma_x \, dz \quad , \quad n_y = \int_{-h/2}^{h/2} \sigma_y \, dz \quad , \quad n_{xy} = n_{yx} = \int_{-h/2}^{h/2} \tau_{xy} \, dz \tag{5.14}$$

the *shear forces*

$$v_x = \int_{-h/2}^{h/2} \tau_{zx} \, dz \quad , \quad v_y = \int_{-h/2}^{h/2} \tau_{zy} \, dz \tag{5.15}$$

and the *bending* and *twisting moments*

$$m_x = \int_{-h/2}^{h/2} \sigma_x z \, dz \quad , \quad m_y = \int_{-h/2}^{h/2} \sigma_y z \, dz \quad , \quad m_{xy} = m_{yx} = \int_{-h/2}^{h/2} \tau_{xy} z \, dz \tag{5.16}$$

(all related to the unit length). The normal and shear stresses σ_x, σ_y, $\tau_{xy} = \tau_{yx}$ in the plane of the element as well as the shear stresses τ_{zx}, τ_{zy} perpendicular to the plane of the element, which are introduced in section 5.2, are used here. The units of the membrane and shear forces (related to the unit length) and the bending and twisting moments are [N/m] and [Nm/m = N] or [kN/m] and [kNm/m = kN]. Incidentally, it is worth noting that at the side faces of the element in Fig. 5.16 there are no moments about the z axis (because of the infinitesimally small size of the element).

A *plate* is a form of plane structure that carries in-plane loads only, where a coplanar stress state constant over h is assumed ($\tau_{zx} = \tau_{zy} = 0$). Accordingly, the result is membrane forces n_x, n_y, $n_{xy} = n_{yx}$only.

A *slab* is a form of plane structure that carries loads perpendicular to its plane and is primarily or exclusively subjected to bending and twisting moments m_x, m_y, $m_{xy} = m_{yx}$ plus shear forces v_x, v_y.

A *folded plate structure* is a structure in three dimensions made up of plates structurally connected along their longitudinal sides and further braced by the inclusion of end plates. The global or local structural behaviour of a folded plate is dominated by membrane or bending effects.

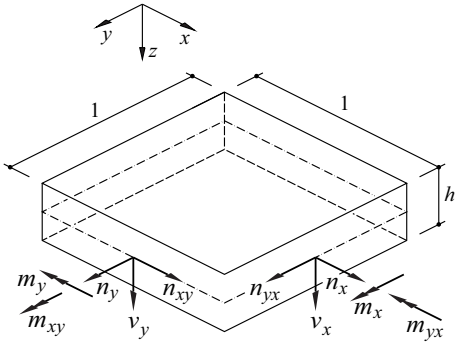

Fig. 5.16 Stress resultants in plate and shell structures

A *shell* is a form of structure in single or double curvature which as a rule is subjected to general loads (perpendicular to and parallel with the middle surface) and stress resultants (membrane and shear forces plus bending and twisting moments). An idealisation as a *membrane shell* or *membrane* with dominant membrane forces and negligible shear forces as well as bending and twisting moments is often justified. Further, shells can always be approximated by using suitable folded plates.

5.2 Stresses

5.2.1 Terminology

Fig. 5.17(a) reiterates the terms introduced in section 5.1.1: *force per unit area* and *stress vector* $\boldsymbol{t}$, see (5.2). We shall consider an infinitesimally small surface element dA with an external unit normal vector $\boldsymbol{n}$ which has been separated from a body by an arbitrary cut. The force-couple system of the internal forces acting on the surface element is reduced at the passage to the limit $\mathrm{d}A \to 0$ to the stress resultant $\mathrm{d}\boldsymbol{F} = \boldsymbol{t}\,\mathrm{d}A$ with a generally finite force per unit area $\boldsymbol{t} = \mathrm{d}\boldsymbol{F}/\mathrm{d}A$; the moment per unit area $\mathrm{d}\boldsymbol{M}/\mathrm{d}A$ is zero because when $\mathrm{d}A \to 0$, not only d$\boldsymbol{F}$, but also the lever arm of the corresponding couple d$\boldsymbol{M}$ is zero.

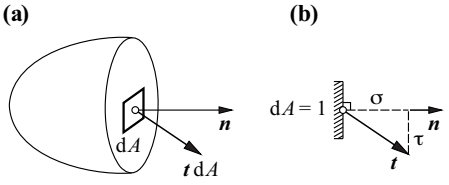

Fig. 5.17 Definition of stress: (a) stress vector, (b) normal and shear stresses

The stress vector $\boldsymbol{t}$ is resolved according to Fig. 5.17(b) into the *normal stress*

$$\sigma = \boldsymbol{t} \cdot \boldsymbol{n} \tag{5.17}$$

in the n direction and the *shear stress* perpendicular to this

$$\tau = \sqrt{\boldsymbol{t} \cdot \boldsymbol{t} - \sigma^2} \tag{5.18}$$

The associated vectors are $\sigma\boldsymbol{n}$ and $\boldsymbol{t} - \sigma\boldsymbol{n}$.

5.2.2 Uniaxial stress state

The prismatic bar shown in Fig. 5.18(a) and (b), with cross-sectional area A, is subjected to a constant normal force N in the y direction, which corresponds to a uniform tensile stress $\sigma_1 = N/A$ = const over A.

Fig. 5.18(c) shows a free body cut out of the bar with thickness 1 in the z direction. The free body is defined by cuts parallel to the xz, yz and tz planes, with the cut at an angle of φ to the y axis having a length 1 in the t direction. The force $\sigma_1 \sin\varphi$ acts in the negative y direction at the cut face with length $\sin\varphi$ perpendicular to the y axis, whereas the cut face perpendicular to the x axis is not subjected to any forces.

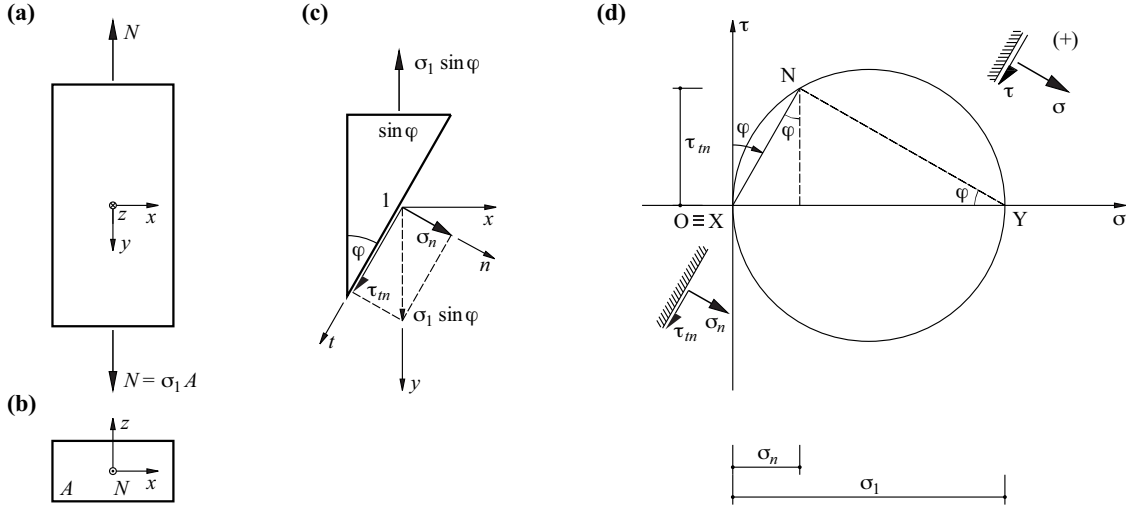

Fig. 5.18 Uniaxial stress state: (a) elevation on bar, (b) plan on bar, (c) free body diagram, (d) MOHR's stress circle

For equilibrium, the cut face perpendicular to the n axis requires a force $\sigma_1 \sin\varphi$ opposite to the first force acting in the positive y direction. Resolving this vector into its components in the n and t directions according to (5.17) and (5.18) supplies the *stress components*

$$\sigma_n = \sigma_1 \sin^2\varphi \quad , \quad \tau_{tn} = \sigma_1 \sin\varphi \cos\varphi \tag{5.19}$$

Here, the normal stress σ_n is given the index n corresponding to its direction. In the case of the shear stress τ_{tn}, the first index t designates its direction and the second index n the direction of the normal to the element on which it acts.

The equations in (5.19) can be interpreted geometrically using the MOHR*'s stress circle* given in Fig. 5.18(d). The surface element with the normal direction n in Fig. 5.18(c) corresponds to the stress point N in Fig. 5.18(d). This results from drawing a line parallel to the surface element (the t direction) which passes through the origin O of the system of coordinates σ, τ and continuing the line so that it intersects the circle with its centre on the positive σ axis and diameter σ_1 which touches the τ axis.

Fig. 5.18(d) shows a general case with $0 \leq \varphi \leq \pi/2$. For $\varphi = 0$, i. e. a cut perpendicular to the x axis, N = X coincides with the origin O of the system of coordinates; $\sigma_n = \tau_{tn} = 0$ applies for such a cut and the cut face is not subjected to any stress. For $\varphi = \pi/2$, i. e. a cut perpendicular to the y axis, the result is point N = Y at position $\sigma_n = \sigma_y = \sigma_1$, $\tau_{tn} = \tau_{xy} = 0$; a pure normal stress σ_1 in the y direction is the result, as assumed.

Point O $\equiv$ X in Fig. 5.18(d) plays the role of the *pole* in MOHR's stress circle. Lines parallel with the surface elements and passing through the pole intersect with the MOHR's stress circle at the associated stress points.

MOHR*'s sign convention* for the stress components can be seen in Fig. 5.18(d): normal stresses σ are classed as positive when they are tensile. Shear stresses τ are positive when they rotate clockwise about points within the free body.

5.2.3 Coplanar stress states

The elemental prism with side length 1 shown in Fig. 5.19(a) in the xyz system of coordinates is free from stresses on the cut faces perpendicular to the z axis. Following on from the thinking of Fig. 5.18, the stress components σ_x, τ_{yx} and σ_y, τ_{xy} have to be introduced at the cut surfaces perpendicular to the x and y axes. For equilibrium of moments about the line parallel with the z axis and passing through the centre of the element, where the normal stresses intersect, then

$$\tau_{xy} = \tau_{yx} \tag{5.20}$$

If we consider, similar to Fig. 5.18(c), a wedge-shaped element defined by the angle φ according to Fig. 5.19(b), then equilibrium of forces in the n and t directions results in the following when considering (5.20):

$$\sigma_n = \sigma_x \cos^2\varphi + \sigma_y \sin^2\varphi + 2\tau_{xy} \sin\varphi \cos\varphi$$

$$\tau_{tn} = (\sigma_y - \sigma_x) \sin\varphi \cos\varphi + \tau_{xy}(\cos^2\varphi - \sin^2\varphi)$$

Similarly, from Fig. 5.19(c) we get

$$\sigma_t = \sigma_x \sin^2\varphi + \sigma_y \cos^2\varphi - 2\tau_{xy} \sin\varphi \cos\varphi$$

$$\tau_{nt} = (\sigma_y - \sigma_x) \sin\varphi \cos\varphi + \tau_{xy}(\cos^2\varphi - \sin^2\varphi)$$

and hence, in summary, the *stress transformation relationships*

$$\begin{Bmatrix} \sigma_n \\ \sigma_t \\ \tau_{tn} \end{Bmatrix} = \begin{bmatrix} \cos^2\varphi & \sin^2\varphi & 2\sin\varphi\cos\varphi \\ \sin^2\varphi & \cos^2\varphi & -2\sin\varphi\cos\varphi \\ -\sin\varphi\cos\varphi & \sin\varphi\cos\varphi & \cos^2\varphi - \sin^2\varphi \end{bmatrix} \begin{Bmatrix} \sigma_x \\ \sigma_y \\ \tau_{xy} \end{Bmatrix} \tag{5.21}$$

and

$$\tau_{tn} = \tau_{nt} \tag{5.22}$$

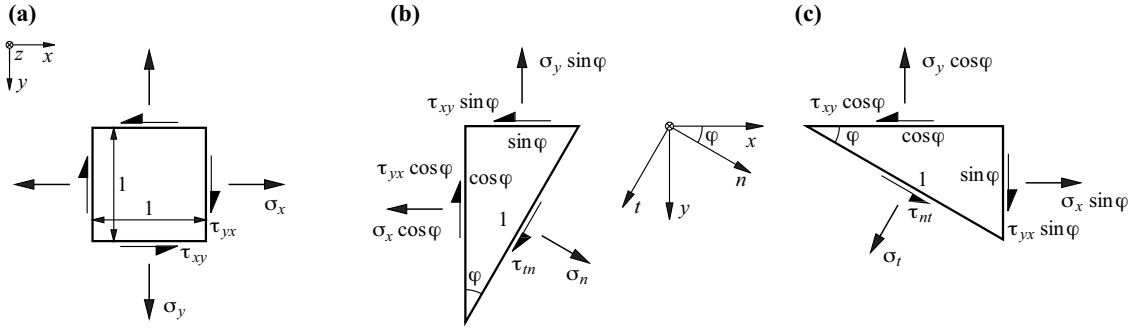

Fig. 5.19 Coplanar stress states: (a) designations, (b) and (c) free body diagrams

If we wish to find out the directions t and n, for which the shear stresses are zero, $\tau_{tn} = 0$, eq. (5.21) initially gives us angle φ_1 with

$$\tan(2\varphi_1) = \frac{2\tau_{xy}}{\sigma_x - \sigma_y} \tag{5.23}$$

Substituting angle φ_1 back into the equations for σ_n and σ_t results in the *principal stresses* σ_1 and σ_2 with

$$\sigma_{1,2} = \frac{\sigma_x + \sigma_y}{2} \pm \sqrt{\left(\frac{\sigma_x - \sigma_y}{2}\right)^2 + \tau_{xy}^2} \tag{5.24}$$

and the *principal directions* 1 and 2 defined by φ_1 and $\varphi_1 + \pi/2$ according to (5.23).

Eq. (5.21), (5.23) and (5.24) can be interpreted geometrically with the help of a MOHR's stress circle similar to Fig. 5.18(d), see Fig. 5.20. The two terms on the right in (5.24) correspond to the abscissa of the centre and the radius of the MOHR's stress circle. The principal stresses σ_1 and σ_2 are extremal; they represent the upper and lower bounds for all possible normal stresses. The construction of the stress points N etc. in the $\sigma\tau$ plane with the help of the pole is carried out as described in section 5.2.2, i. e. by drawing a line parallel with the respective surface element which passes through the pole and intersects with the MOHR's stress circle, see Fig. 5.20(a) und (c). MOHR's sign convention for stress components, given in Fig. 5.18(d), still applies, see Fig. 5.20(b).

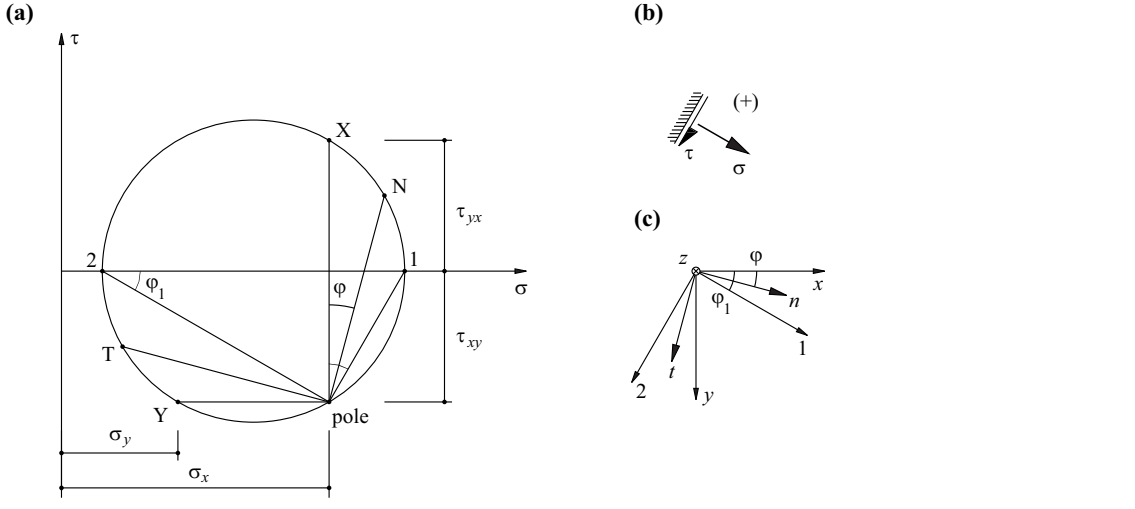

Fig. 5.20 Coplanar stress states: (a) MOHR's stress circle, (b) sign convention, (c) directions of axes

Incidentally, it can be seen that the variables

$$\sigma_n + \sigma_t = \sigma_x + \sigma_y = \sigma_1 + \sigma_2 = \sigma_I \tag{5.25}$$

and

$$\tau_{xy}^2 - \sigma_x\sigma_y = \tau_{xy}^2 + \left(\frac{\sigma_x - \sigma_y}{2}\right)^2 - \left(\frac{\sigma_x + \sigma_y}{2}\right)^2 = -\sigma_1\sigma_2 = \sigma_{II} \tag{5.26}$$

remain unaffected by the rotation of the system of coordinates, i. e. are *invariant*.

According to appendix A6, the stress components σ_x, σ_y, $\tau_{xy} = \tau_{yx}$ can be grouped together in the (planar) *stress tensor*

$$\boldsymbol{\sigma} = \begin{bmatrix} \sigma_x & \tau_{xy} \\ \tau_{yx} & \sigma_y \end{bmatrix} \tag{5.27}$$

The two columns of the matrix on the right in (5.27) contain the stress components at the surface elements with the normals x and y given in Fig. 5.19(a). Here, similarly to the sign convention for stress resultants (see Fig. 5.14), we use the *tensorial sign convention*, which states that stress components are positive when they act on surface elements with positive (negative) external normals in the positive (negative) direction of an axis.

According to (A6.7), the stress vector $\boldsymbol{t}$ at a surface element defined by the unit normal vector $\boldsymbol{n} = (\cos\varphi, \sin\varphi)$ has the components $\sigma_x\cos\varphi + \tau_{xy}\sin\varphi$ and $\tau_{yx}\cos\varphi + \sigma_y\sin\varphi$ in the x and y directions; eq. (5.17) and (5.18) are used, taking account of (5.20), to return to σ_n and τ_{tn} according to (5.21).

According to (A6.20), the variables σ_I and σ_{II} according to (5.25) and (5.26) correspond to the *basic invariants* of the stress tensor. The first of these is the trace and the second the negative determinant of the matrix in (5.27).

Example 5.3 Steel plate

The stress state $\sigma_x = 160\,\text{N/mm}^2$, $\sigma_y = 0$, $\tau_{xy} = 60\,\text{N/mm}^2$ prevails locally in a steel plate, see Fig. 5.21(a). Eq. (5.23) supplies $\tan\varphi_1 = 1/3$, and from (5.24) it follows that $\sigma_1 = 180\,\text{N/mm}^2$, $\sigma_2 = -20\,\text{N/mm}^2$. Fig. 5.21(b) shows the corresponding MOHR's stress circle, and the principal stresses and their directions are shown in Fig. 5.21(c).

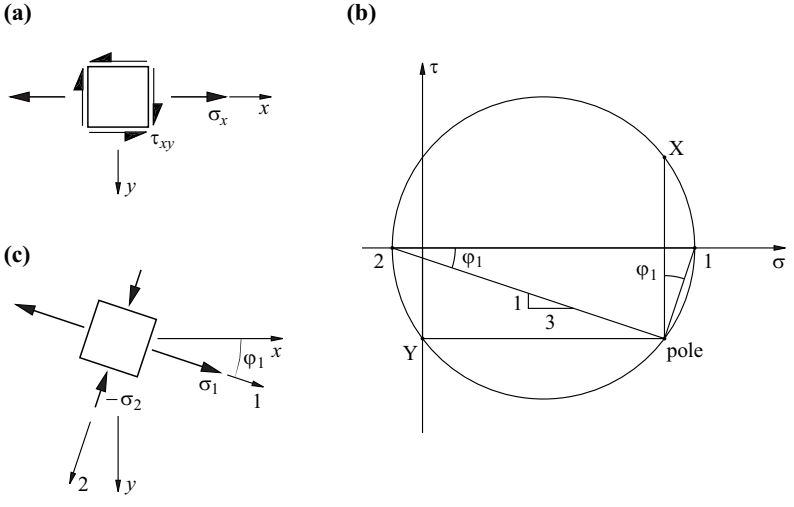

Fig. 5.21 A steel plate in a coplanar stress state: (a) stress components $\sigma_x = 160\ \text{N/mm}^2$, $\sigma_y = 0$, $\tau_{xy} = 60\ \text{N/mm}^2$; (b) MOHR's stress circle; (c) principal stresses $\sigma_1 = 180\ \text{N/mm}^2$, $\sigma_2 = -20\ \text{N/mm}^2$

5.2.4 Three-dimensional stress states

The volume element shown in Fig. 5.22 is subjected to a force per unit volume of $\boldsymbol{q} = (q_x, q_y, q_z)$. The stress components σ_x etc. act on the side faces with external normals in the negative directions of the axes; similarly to (5.27), these components are grouped together in columns in the three-dimensional stress tensor

$$\boldsymbol{\sigma} = \begin{bmatrix} \sigma_x & \tau_{xy} & \tau_{xz} \\ \tau_{yx} & \sigma_y & \tau_{yz} \\ \tau_{zx} & \tau_{zy} & \sigma_z \end{bmatrix} \tag{5.28}$$

The differentials $(\partial\sigma_x/\partial x)\mathrm{d}x$ etc. must be considered at the surface elements with external normals in the positive direction of the axes.

For equilibrium of forces in the three axis directions

$$\left(\frac{\partial\sigma_x}{\partial x} + \frac{\partial\tau_{xy}}{\partial y} + \frac{\partial\tau_{xz}}{\partial z} + q_x\right)\mathrm{d}x\,\mathrm{d}y\,\mathrm{d}z = 0$$

$$\left(\frac{\partial\tau_{yx}}{\partial x} + \frac{\partial\sigma_y}{\partial y} + \frac{\partial\tau_{yz}}{\partial z} + q_y\right)\mathrm{d}x\,\mathrm{d}y\,\mathrm{d}z = 0$$

$$\left(\frac{\partial\tau_{zx}}{\partial x} + \frac{\partial\tau_{zy}}{\partial y} + \frac{\partial\sigma_z}{\partial z} + q_z\right)\mathrm{d}x\,\mathrm{d}y\,\mathrm{d}z = 0$$

Obviously, the three expressions in brackets must be zero. Using the index notation given in section A6.2 results in the following shortened form

$$\sigma_{ij,j} + q_i = 0 \tag{5.29}$$

for the three *equilibrium conditions of the continuum*. Here, the indexes i and j denote the axis directions x, y and z; the doubled (dummy) index j stands for a summation via the values x, y, z, and the comma before the second index j stands for a partial differentiation with respect to the corresponding coordinates.

The first index i of a stress component σ_{ij} generally denotes its direction and the second index j the direction of the normal to the element on which it acts. As a result, with the normal stress components, except when using the index notation, one of the identical indexes continues to be suppressed because a mix-up is ruled out, i. e. we write σ_x instead of σ_{xx} etc.

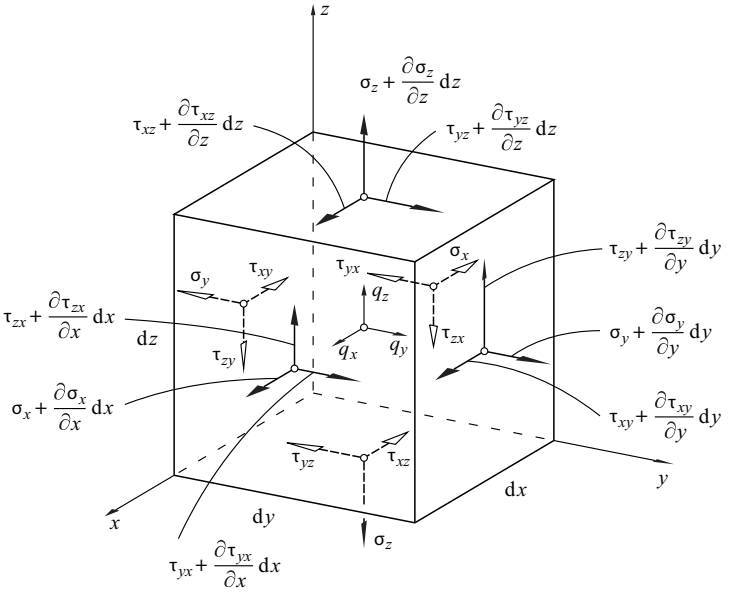

Fig. 5.22 Stress components and force per unit volume $\boldsymbol{q}$ on a volume element

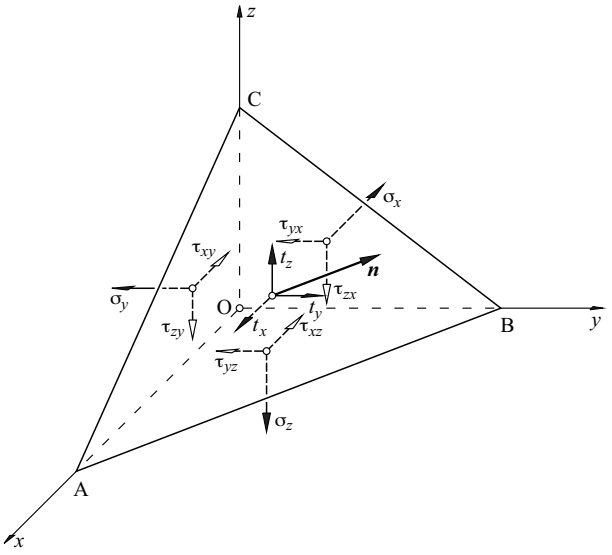

Fig. 5.23 Tetrahedron with surface ABC = 1, unit normal vector $\boldsymbol{n}$ and associated stress vector $\boldsymbol{t}$

For equilibrium of moments about the straight lines parallel with the axes and passing through the centre of the element

$$\sigma_{ij} = \sigma_{ji} \tag{5.30}$$

i. e. the stress tensor is symmetric; this result is known as the *theorem of associated shear stresses*. Note that the contribution of the differentials $(\partial\tau_{xy}/\partial y)\mathrm{d}y$ etc. to the respective moments is small of a higher order compared with that of τ_{xy} etc. It can be ignored in the passage to the limit.

The three partial differential equations (5.29) are supplemented by *static boundary conditions* resulting from the load on the surface of the body being investigated. If $\boldsymbol{n}$ is the local unit normal vector and $\boldsymbol{t}$ the given force per unit area, then $\boldsymbol{t} = \boldsymbol{\sigma}\bullet\boldsymbol{n}$ or

$$t_i = \sigma_{ij} n_j \tag{5.31}$$

see (A6.7).

Eq. (5.31) can be illustrated by Fig. 5.23 for any points (on the surface or within a body). Let us consider the equilibrium of forces for the tetrahedron OABC, whose surface ABC with the unit normal vector $\boldsymbol{n}$ has a surface area of 1. The surfaces OBC, OAC, OAB then have the areas n_x, n_y, n_z, which are equal to the components of $\boldsymbol{n}$. For the components of the stress vector $\boldsymbol{t}$ belonging to $\boldsymbol{n}$, equilibrium of forces in the three axis directions then results in

$$\begin{aligned} t_x &= \sigma_x n_x + \tau_{xy} n_y + \tau_{xz} n_z &= \sigma_{xj} n_j \\ t_y &= \tau_{yx} n_x + \sigma_y n_y + \tau_{yz} n_z &= \sigma_{yj} n_j \\ t_z &= \tau_{zx} n_x + \tau_{zy} n_y + \sigma_z n_z &= \sigma_{zj} n_j \end{aligned}$$

i. e. (5.31).

If one stress field satisfies the equilibrium conditions (5.29) and the boundary conditions (5.31), it is regarded as *statically admissible*.

If we wish to know (according to section A6.4) the *principal directions* $\boldsymbol{n}$ for which $\boldsymbol{t} = \sigma\boldsymbol{n}$ applies, i. e. there are no shear stresses, we get the following *characteristic equation*

$$\sigma^3 - \sigma_{\mathrm{I}}\sigma^2 - \sigma_{\mathrm{II}}\sigma - \sigma_{\mathrm{III}} = 0 \tag{5.32}$$

with the *basic invariants*

$$\begin{aligned}
\sigma_{\mathrm{I}} &= \sigma_x + \sigma_y + \sigma_z && = \sigma_1 + \sigma_2 + \sigma_3 \\
\sigma_{\mathrm{II}} &= \tau_{yz}^2 + \tau_{zx}^2 + \tau_{xy}^2 - \sigma_y\sigma_z - \sigma_z\sigma_x - \sigma_x\sigma_y && = -\sigma_2\sigma_3 - \sigma_3\sigma_1 - \sigma_1\sigma_2 \\
\sigma_{\mathrm{III}} &= 2\tau_{yz}\tau_{zx}\tau_{xy} - \sigma_x\tau_{yz}^2 - \sigma_y\tau_{zx}^2 - \sigma_z\tau_{xy}^2 + \sigma_x\sigma_y\sigma_z = \sigma_1\sigma_2\sigma_3
\end{aligned} \tag{5.33}$$

where σ_1, σ_2 and σ_3 denote the principal stresses belonging to the principal directions, see (A6.20). The principal stresses are obtained by solving the characteristic equation (5.32), and their directions follow from (A6.21).

Example 5.4 Stress tensor

The principal stresses are given: $\sigma_1 = 4\,\mathrm{N/mm^2}$, $\sigma_2 = 2\,\mathrm{N/mm^2}$, $\sigma_3 = 1\,\mathrm{N/mm^2}$; the directions of those stresses in the *xyz* system are given by the unit vectors collected in the columns of the transformation matrix

$$\boldsymbol{c} = \frac{1}{65}\begin{bmatrix} 60 & 0 & -25 \\ 20 & 39 & 48 \\ 15 & -52 & 36 \end{bmatrix}$$

see (A5.17) and (A6.1). The task is to determine the stress tensor in the *xyz* system.

The stress vectors on the principal axes system associated with the *x*, *y*, z directions follow from the rows of the transformation matrix by multiplying each element by the associated principal stress; e. g. for the *x* direction, the result is the vector $(240/65,\ 0,\ -25/65)\,\mathrm{N/mm^2}$. According to (A5.18), the stress vectors in the *xyz* system are obtained from the products of the transformation matrix and these vectors, and hence the stress tensor follows row by row:

$$\begin{bmatrix} 3.56 & 0.85 & 0.64 \\ 0.85 & 1.64 & -0.27 \\ 0.64 & -0.27 & 1.80 \end{bmatrix}\ \mathrm{N/mm^2}$$

As is easily confirmed by (5.33), the basic invariants $\sigma_{\mathrm{I}} = 7\,\mathrm{N/mm^2}$, $\sigma_{\mathrm{II}} = -14\,(\mathrm{N/mm^2})^2$, $\sigma_{\mathrm{III}} = 8\,(\mathrm{N/mm^2})^3$ are obtained for this tensor. As supposed, (5.32) provides us with the principal stresses $\sigma_1 = 4\,\mathrm{N/mm^2}$, $\sigma_2 = 2\,\mathrm{N/mm^2}$, $\sigma_3 = 1\,\mathrm{N/mm^2}$, and (A6.21) supplies the principal directions collected in the given transformation matrix $\boldsymbol{c}$.

The geometric interpretation of uniaxial and coplanar stress states with MOHR's stress circles described in sections 5.2.2 and 5.2.3 can be expanded to three-dimensional stress states according to Fig. 5.24(a). To do this, we select the *z* axis according to Fig. 5.24(b) in the direction of the principal stress σ_3 and divide the stress tensor into a coplanar part and a hydrostatic part:

$$\begin{bmatrix} \sigma_x & \tau_{xy} & 0 \\ \tau_{yx} & \sigma_y & 0 \\ 0 & 0 & \sigma_3 \end{bmatrix} = \begin{bmatrix} \sigma_x - \sigma_3 & \tau_{xy} & 0 \\ \tau_{yx} & \sigma_y - \sigma_3 & 0 \\ 0 & 0 & 0 \end{bmatrix} + \begin{bmatrix} \sigma_3 & 0 & 0 \\ 0 & \sigma_3 & 0 \\ 0 & 0 & \sigma_3 \end{bmatrix} \tag{5.34}$$

With respect to the coplanar part, in Fig. 5.24(a) this division corresponds to a translation of the τ axis by σ_3 to the right to position τ'. Surface elements N parallel with the *z* axis with a normal direction φ according to Fig. 5.24(b) correspond to stress points N in Fig. 5.24(a), which can be obtained on the circle defined by the principal values σ_1 and σ_2 in the usual way via its pole. If we rotate the surface element through an angle ψ about the *t* axis, then we obtain the normal stress $\sigma_n\cos^2\psi$ at the inclined element S as a result of σ_n plus the shear stress $\sigma_n\sin\psi\cos\psi$ perpendicular to the *t* axis and, further, as a result of τ_{tn}, the shear stress $\tau_{tn}\cos\psi$ parallel with the *t* axis, i. e. in total

$$\sigma = \sigma_n\cos^2\psi \quad , \quad \tau = \sqrt{\sigma_n^2\sin^2\psi + \tau_{tn}^2}\ \cos\psi \tag{5.35}$$

As can be seen, (5.35) describes the circle 3SN centred on the σ axis, tangential to the τ' axis and passing through N. The stress point S with coordinates σ and τ is obtained via the auxiliary circle centred on the σ axis, tangential to the τ' axis and passing through the point $(\sigma_n, 0)$. This is done by determining point T via ψ, as indicated in Fig. 5.24(a), and drawing the vertical line TS through T to intersect with circle 3N at S.

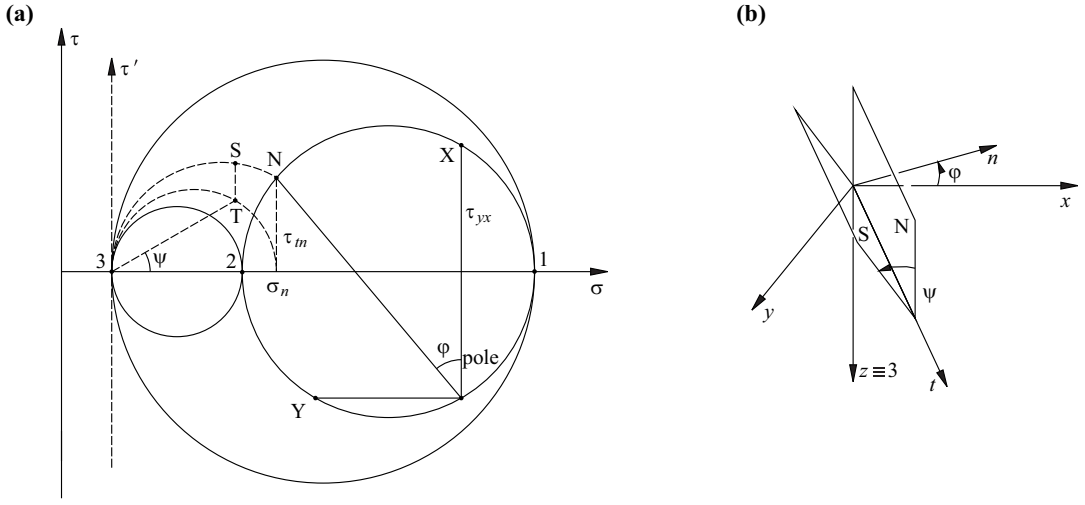

Fig. 5.24 Three-dimensional stress state: (a) MOHR's stress circles, (b) axes, normal plane N and inclined plane S

All of the stress points S lie in the crescent-shaped zone between the three MOHR's stress circles defined by the principal values σ_1, σ_2, σ_3 or the corresponding points 1, 2, 3 in Fig. 5.24(a). Superimposing the hydrostatic stress state $\sigma_x = \sigma_y = \sigma_z = \sigma_3$ finally brings axis τ' back to position τ.

It should also be noted that the *maximum shear stress* is equal to the radius of the largest MOHR's stress circle:

$$\tau_{\max} = \frac{1}{2}|\sigma_1 - \sigma_3| \quad , \quad \sigma_1 \geq \sigma_2 \geq \sigma_3 \tag{5.36}$$

Generally, we may resolve a stress tensor into a *hydrostatic* and a *deviatoric component*, i. e.

$$\begin{bmatrix} \sigma_x & \tau_{xy} & \tau_{xz} \\ \tau_{yx} & \sigma_y & \tau_{yz} \\ \tau_{zx} & \tau_{zy} & \sigma_3 \end{bmatrix} = \begin{bmatrix} \sigma_o & 0 & 0 \\ 0 & \sigma_o & 0 \\ 0 & 0 & \sigma_o \end{bmatrix} + \begin{bmatrix} s_x & \tau_{xy} & \tau_{xz} \\ \tau_{yx} & s_y & \tau_{yz} \\ \tau_{zx} & \tau_{zy} & s_z \end{bmatrix} \tag{5.37}$$

where

$$\sigma_o = \frac{\sigma_I}{3} \tag{5.38}$$

denotes the so-called *octahedral normal stress*.

The basic invariants of the *deviator*

$$s_{ij} = \sigma_{ij} - \sigma_o \delta_{ij} \tag{5.39}$$

where the KRONECKER symbol δ_{ij} according to (A6.3) is used, are obtained similarly to (5.33):

$$\begin{aligned} s_I &= 0 \\ s_{II} &= \frac{1}{3}\left(\sigma_x^2 + \sigma_y^2 + \sigma_z^2 - \sigma_y\sigma_z - \sigma_z\sigma_x - \sigma_x\sigma_y\right) + \tau_{yz}^2 + \tau_{zx}^2 + \tau_{xy}^2 = \sigma_{II} + \frac{1}{3}\sigma_I^2 \\ s_{III} &= \sigma_{III} + \frac{1}{3}s_{II}\sigma_I - \frac{1}{27}\sigma_I^3 \end{aligned} \tag{5.40}$$

In the principal stress space $\sigma_1, \sigma_2, \sigma_3$, it is possible to represent any vector $\boldsymbol{\sigma} = (\sigma_1, \sigma_2, \sigma_3)$ as the sum of a vector $\boldsymbol{\sigma}_o = \sigma_o(1, 1, 1)$ lying on the *hydrostatic axis* $\sigma_1 = \sigma_2 = \sigma_3$ and a vector $\boldsymbol{s}(s_1, s_2, s_3)$ perpendicular to this lying in the *deviatoric plane* $\sigma_I = 0$, see Fig. 5.25(a):

$$\boldsymbol{\sigma} = \boldsymbol{\sigma_o} + \boldsymbol{s} \tag{5.41}$$

Projecting $\boldsymbol{s}$ in the deviatoric plane gives us

$$\mathrm{OP}_1 = (\sigma_1, \sigma_2, \sigma_3) \bullet (2, -1, -1) \cdot \frac{1}{\sqrt{6}} = 3s_1 \frac{1}{\sqrt{6}} = \sqrt{\frac{3}{2}} s_1, \ldots \tag{5.42}$$

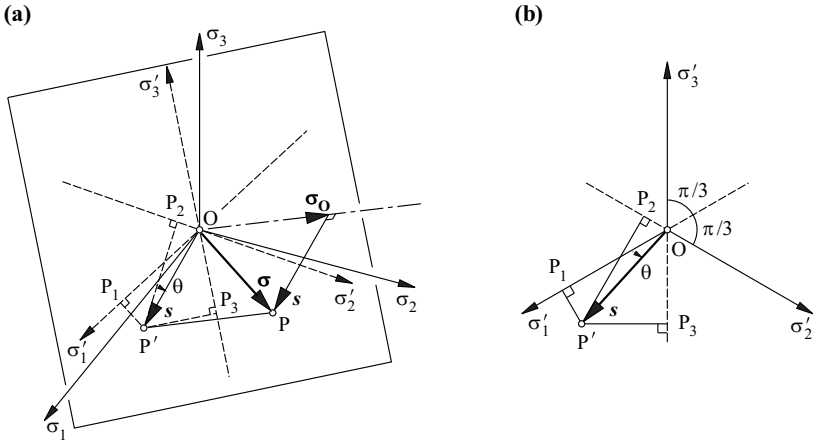

Fig. 5.25 Principal stress space: (a) hydrostatic axis and deviatoric plane, (b) deviatoric plane

see Fig. 5.25(b). Vector $\boldsymbol{s}$ has a magnitude of

$$|\boldsymbol{s}| = \sqrt{2s_{II}} = \sqrt{3}\tau_o \tag{5.43}$$

where

$$\tau_o = \sqrt{\frac{2}{3}s_{II}} \tag{5.44}$$

denotes the so-called *octahedral shear stress*. As is readily apparent from (5.31), (5.17), (5.38), (5.18) and (5.40), σ_o and τ_o correspond to the normal and shear stresses on the surfaces of a regular octahedron drawn in the octants of the system of principal axes.

We obtain

$$\cos\theta = \frac{s_1}{\sqrt{2}\tau_o} = \frac{\sqrt{2}(2\sigma_1 - \sigma_2 - \sigma_3)}{6\tau_o} \tag{5.45}$$

for the angle θ.

Specifying σ_o, τ_o and θ determines the stress state $\boldsymbol{\sigma}$ in the principal stress space unequivocally. Of the original six components of the symmetric stress tensor, the three variables "lost" during the principal axis transformation describe the position of the system of principal axes with respect to the original coordinates.

5.3 Differential structural elements

Only the differential elements of framed structures are considered below. Similar considerations for plate and shell structures can be found in section 8.2 and chapters 23 to 26.

5.3.1 Straight bars

5.3.1.1 Pure bending

The differential element of a straight bar with bar axis x shown in Fig. 5.26 has the principal cross-section axes y and z (see section 13.2.1) and is merely loaded by a line load with a force per unit length of $q_z = q$ in the z direction. Bearing these assumptions in mind, of the six stress resultants shown in Fig. 5.15, only the shear force $V_z = V$ and the bending moment $M_y = M$ are relevant; all other stress resultants are zero or are constant and do not need to be considered any further here. In such a case, where the resultant moment vector coincides with a principal cross-section axis, we speak of *pure bending*.

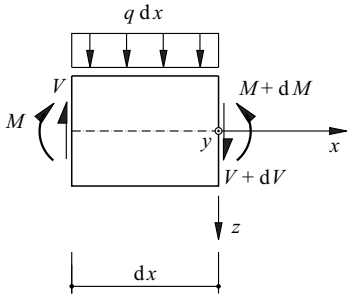

Fig. 5.26 Differential bar element subjected to pure bending

For equilibrium of the free body shown in Fig. 5.26, $q\mathrm{d}x + \mathrm{d}V = 0$ and $-V\mathrm{d}x + \mathrm{d}M = 0$, i. e.

$$\frac{\mathrm{d}V}{\mathrm{d}x} = -q \quad , \quad \frac{\mathrm{d}M}{\mathrm{d}x} = V \tag{5.46}$$

and hence

$$\frac{\mathrm{d}^2M}{\mathrm{d}x^2} + q = 0 \tag{5.47}$$

5.3.1.2 Skew bending

Skew bending is present when the resultant moment vector at one section of a bar does not coincide with a principal axis of the cross-section, i. e. in the notation of Fig. 5.26, has components M_y and M_z, which stem from line loads q_z and q_y. Instead of (5.46) and (5.47), the following applies with the corresponding shear forces V_z and V_y:

$$\frac{\mathrm{d}V_z}{\mathrm{d}x} = -q_z \quad , \quad \frac{\mathrm{d}M_y}{\mathrm{d}x} = V_z \quad ; \quad \frac{\mathrm{d}V_y}{\mathrm{d}x} = -q_y \quad , \quad \frac{\mathrm{d}M_z}{\mathrm{d}x} = -V_y \tag{5.48}$$

and hence

$$\frac{\mathrm{d}^2M_y}{\mathrm{d}x^2} + q_z = 0 \quad ; \quad \frac{\mathrm{d}^2M_z}{\mathrm{d}x^2} - q_y = 0 \tag{5.49}$$

The reason for the minus sign in $(5.48)_4$ is that both the couple $V_y\,\mathrm{d}x$ and also the differential $\mathrm{d}M_z$ act in the positive z direction.

5.3.1.3 General stress resultants

Normally, it is necessary to consider line loads in the x direction (q_x) as well as those in the z and y directions, plus *line load moments* (m_x, m_y, m_z) about the three axes. Similar considerations to those given above lead to the result summarised in (8.26).

5.3.2 Bars in single curvature

5.3.2.1 Loads in the plane of curvature

Fig. 5.27(a) shows a point on an axis of a bar in single curvature whose position is given by the arc length s related to a certain origin. We shall introduce the axes tangential t or normal n to the bar at this point. With a radius of curvature $\rho = \rho(s)$ inclined at an angle φ to the vertical, then $\mathrm{d}s = \rho\mathrm{d}\varphi$.

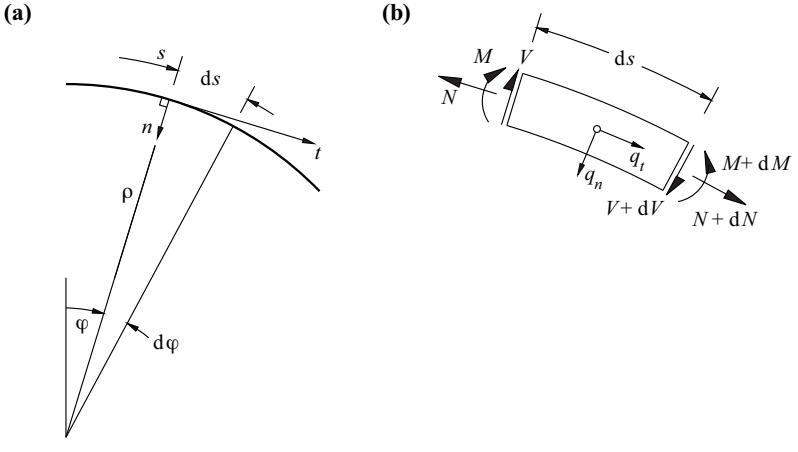

Fig. 5.27 A bar curved and loaded in one plane: (a) overview, (b) free body diagram

The free body diagram in Fig. 5.27(b) enables us to find the equilibrium conditions

$$\mathrm{d}N - V\,\mathrm{d}\varphi + q_t\,\mathrm{d}s = 0 \quad , \quad \mathrm{d}V + N\,\mathrm{d}\varphi + q_n\,\mathrm{d}s = 0 \quad , \quad \mathrm{d}M - V\,\mathrm{d}s = 0$$

and therefore, if differentiation with respect to s is designated with a superscript dash ($'$), then

$$N' - \frac{V}{\rho} + q_t = 0 \quad , \quad V' + \frac{N}{\rho} + q_n = 0 \quad , \quad M' - V = 0 \tag{5.50}$$

For a given load q_t, q_n, the bar axis can be selected in such a way that the bending moment M and the shear force V both disappear, i. e. only normal forces N occur. A bar axis determined in this way is called a *thrust line*. It corresponds to the *funicular polygon* used in Fig. 5.4(d) and Fig. 5.5(d). With $M = V = 0$, eq. (5.50) can be used to obtain the differential equation of the thrust line

$$(\rho\, q_n)' = q_t \tag{5.51}$$

from which it is possible to determine $\rho(s)$ for a given q_t and q_n.

If $q_t = 0$ and $q_n = \text{const}$, then we obtain $\rho = \text{const}$ directly from (5.51), and $(5.50)_2$ supplies the so-called *hoop stress formula*

$$N = -\,q_n \rho = \text{const} \tag{5.52}$$

see $(18.99)_1$.

Example 5.5 Hoop stress formula

The hoop stress formula can be used for many different applications in construction. For example, let us consider one ring of an empty, cylindrical tank for an offshore drilling rig at a water depth of 150 m, see Fig. 5.28(a). The hydrostatic pressure acting on the ring from outside amounts to about $1.5\,\mathrm{N/mm^2} = 1.5\,\mathrm{MN/m^2}$. With a cylinder radius of $\rho = 12\,\mathrm{m}$, it follows from (5.52) that the normal force (compressive force) amounts to $1.5 \cdot 12 = 18\,\mathrm{MN}$ per metre height of ring. Assuming the concrete wall of the cylinder is 0.8 m thick, this results in a mean compressive stress of $18/0.8 = 22.5\,\mathrm{N/mm^2}$.

As a second example we could consider a cylindrical containment structure, topped by a hemispherical dome, for a nuclear power station. In the event of an incident this structure is subjected to an overpressure of $0.5\,\mathrm{N/mm^2}$, see Fig. 5.28(b). With a cylinder radius of $\rho = 20\,\mathrm{m}$, according to (5.52), normal forces (tensile forces) amounting to $0.5 \cdot 20 = 10\,\mathrm{MN}$ per metre height of ring ensue. The cylinder is precompressed in order to prevent cracking, or rather decompression, of the concrete wall of the cylinder. To do this, tendons made from high-strength steel, arranged in a ring, are prestressed. The anchorages for the tendons are located in buttresses on the outside of the concrete structure, which then enable the cylinder to be precompressed.

Example 5.6 Thrust line

An arch is subjected to a line load $q_z = \text{const}$ according to Fig. 5.29(a). The task is to find the associated thrust line $z(x)$. With $\mathrm{d}x = \mathrm{d}s \cos\varphi = \rho \cos\varphi\,\mathrm{d}\varphi$, resolving the force $q_z \mathrm{d}x$ into its components in the n and t directions results in

$$q_n = \frac{q_z \mathrm{d}x \cos\varphi}{\mathrm{d}s} = q_z \cos^2\varphi \quad , \quad q_t = \frac{q_z \mathrm{d}x \sin\varphi}{\mathrm{d}s} = q_z \sin\varphi \cos\varphi \tag{5.53}$$

Using (5.51), we first obtain

$$\frac{\mathrm{d}\rho}{\mathrm{d}s} q_n + \rho \frac{\mathrm{d}q_n}{\mathrm{d}s} = q_t$$

and by substituting (5.53) and simplifying we get the differential equation

$$\frac{\mathrm{d}\rho}{\rho} = 3 \tan\varphi\,\mathrm{d}\varphi \tag{5.54}$$

with the solution

$$\rho \cos^3\varphi = \text{const} \tag{5.55}$$

As $\cos\varphi = \mathrm{d}x/\mathrm{d}s = \mathrm{d}x/\sqrt{(\mathrm{d}x)^2 + (\mathrm{d}z)^2} = [1 + (\mathrm{d}z/\mathrm{d}x)^2]^{-1/2}$, the following therefore applies:

$$\rho = \rho_0 \left[1 + \left(\frac{\mathrm{d}z}{\mathrm{d}x} \right)^2 \right]^{3/2} \tag{5.56}$$

where ρ_0 is a constant.

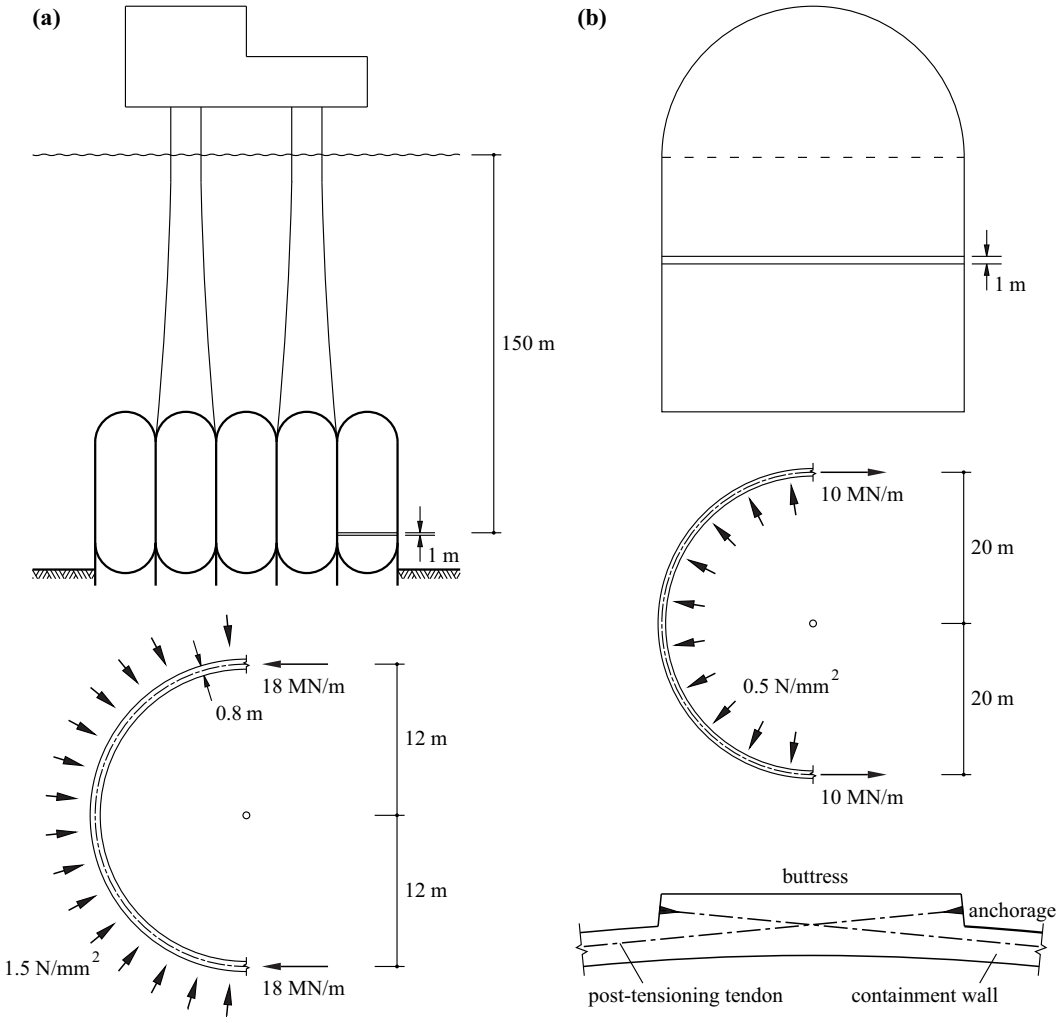

Fig. 5.28 Examples of the use of the hoop stress formula: (a) offshore drilling rig, (b) containment structure for nuclear power station

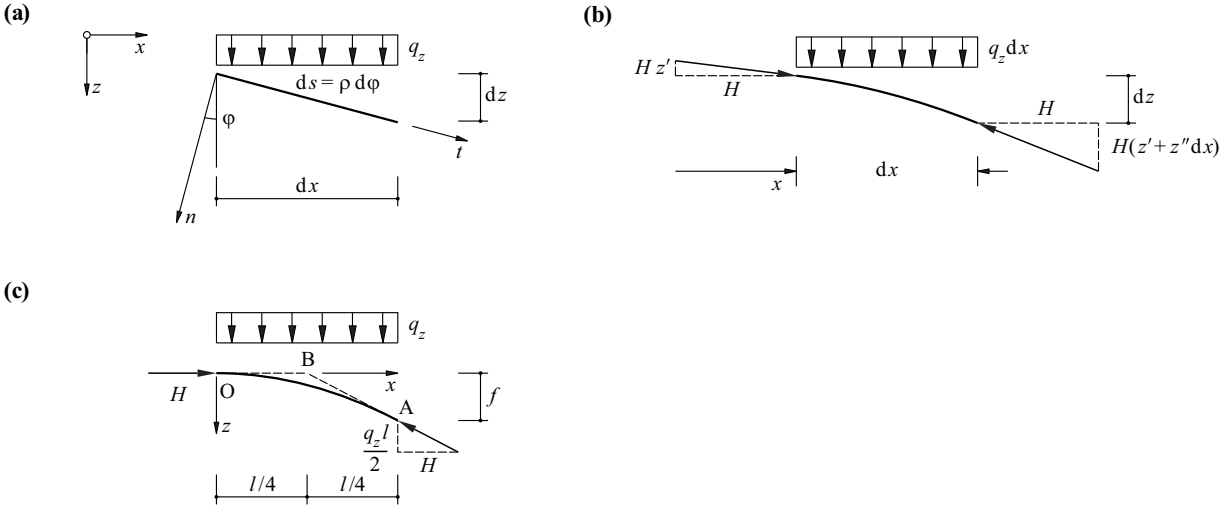

Fig. 5.29 Arch subjected to q_z = const: (a) arch element, (b) free body diagram, (c) parabolic arch

According to the theory of plane curves, the following applies for the radius of curvature:

$$\rho = \frac{\left[1 + \left(\frac{dz}{dx}\right)^2\right]^{3/2}}{\frac{d^2z}{dx^2}} \tag{5.57}$$

and the comparison with (5.56) shows that $d^2z/dx^2 = \rho_0^{-1} = \text{const}$. The function $z(x)$ is therefore a quadratic parabola with the following equation:

$$z = \frac{x^2}{2\rho_0} \tag{5.58}$$

if we place the origin of the xz system of coordinates at the vertex of the parabola.

The result (5.58) can be obtained much more easily by considering the free body diagram shown in Fig. 5.29(b). As the arch is loaded in the z direction only, the horizontal component H of the normal force (compressive force) in the arch is constant. The vertical components of the normal force at the ends of the element are Hz' and $H(z' + z''dx)$, where a superscript dash means differentiation with respect to x. For equilibrium of the forces in the vertical direction, $q_z dx - Hz''dx = 0$, i. e. $z'' = q_z/H = \text{const}$, and therefore we get

$$z = \frac{q_z x^2}{2H} \tag{5.59}$$

if, again, the origin of the xz system of coordinates is placed at the vertex of the parabola.

A comparison of (5.58) and (5.59) reveals that $H = \rho_0 q_z$. We also get this result when we apply $(5.50)_2$ to the vertex of the parabola, where $q_n = q_z$, and because $z' = 0$, then $N = -H$ and $\rho = \rho_0$, too, see (5.56). As $z(x)$ should be a thrust line, V' is zero, and we get $H = \rho_0 q_z$ again.

Fig. 5.29(c) shows half of a parabolic arch with span l and *rise f*. The parabolic form is given by $z = 4fx^2/l^2$, and a comparison with (5.59) results in

$$H = \frac{q_z l^2}{8f} \tag{5.60}$$

This result is also easily obtained from a moment-balance equation applied to the free body diagram shown in Fig. 5.29(c).

The line of action of the normal force at the *springing* (point A, $x = l/2$, $z = f$) intersects the x axis at the point $x = l/4$ (point B). If the load q_z is not uniformly distributed but rather applied as a (statically equivalent) point load amounting to $q_z l/2$ at B, then instead of the parabola OA, the result would be the polygonal thrust line OBA, which is made up of the end tangents of the parabola at O and A.

Example 5.7 Three-hinged arch

The three-hinged arch A′OA shown in Fig. 5.30(a), with the form $z = 4fx^2/l^2$, is loaded with a uniformly distributed permanent load g and a uniformly distributed imposed load q on one half of the arch. According to example 5.6, the permanent load causes purely normal forces (compressive forces) with a constant horizontal component $H = gl^2/(8f)$, see (5.60).

With an asymmetric imposed load, a *rearrangement of the load* is carried out by dividing it into a symmetric part and an antisymmetric part according to Fig. 5.30(b). The symmetric part acts like g and causes additional normal forces with horizontal component $ql^2/(16f)$. The antisymmetric part causes opposing vertical forces of $ql/8$ at the springings according to Fig. 5.30(c); the antisymmetric distributed forces result in an anticlockwise moment of $(q/2)\cdot(l/2)^2 = ql^2/8$, which is kept in equilibrium by the clockwise couple of the springing forces $ql/8$ with the lever arm l. According to section 5.1.7, this results in the following bending moments at an arbitrary section x in arch OA:

$$M = -\frac{ql}{8}\left(\frac{l}{2} - x\right) + \frac{q}{2}\left(\frac{l}{2} - x\right)^2 \cdot \frac{1}{2} = -\frac{qx\left(\frac{l}{2} - x\right)}{4} \qquad \left(0 \le x \le \frac{l}{2}\right)$$

with the minimum $M_{\min} = -ql^2/64$ at point $x = l/4$. Considering arch OA′ similarly leads to

$$M = \frac{ql}{8}\left(\frac{l}{2} + x\right) - \frac{q}{2}\left(\frac{l}{2} + x\right)^2 \cdot \frac{1}{2} = -\frac{qx\left(\frac{l}{2} + x\right)}{4} \qquad \left(-\frac{l}{2} \le x \le 0\right)$$

with the maximum $M_{\max} = ql^2/64$ at point $x = -l/4$, see Fig. 5.30(d).

Carrying the asymmetric imposed load q can be illustrated in another way, see Fig. 5.31. As arch OA is not loaded and has a hinge at both ends, the line of action of the force it carries must pass through O and A; arch OA functions like a pin-jointed member coinciding with the chord of the arch. The vertical load $ql/2$ can be replaced by a statically equivalent point load at $x = -l/4$, and the intersection of the line of action of this force with chord OA supplies point B. Consequently, the line of action A′B of the support reaction at A′ is also found and we get the support force components shown in Fig. 5.31. As the load in zone $-l/2 \le x \le 0$ is uniformly distributed and not concentrated at

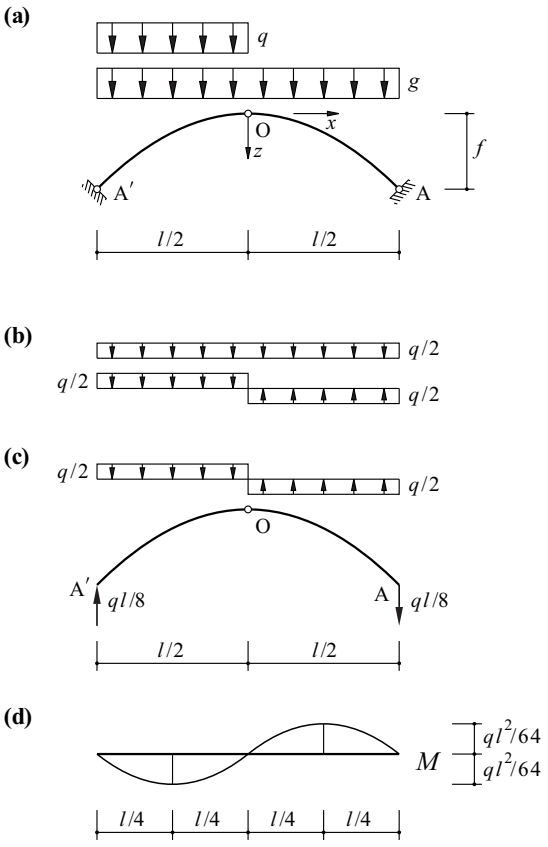

Fig. 5.30 Three-hinged arch: (a) system and loads, (b) resolving the asymmetric imposed load into a symmetric part and an antisymmetric part, (c) free body diagram for antisymmetric part of imposed load, (d) bending moment diagram for asymmetric imposed load

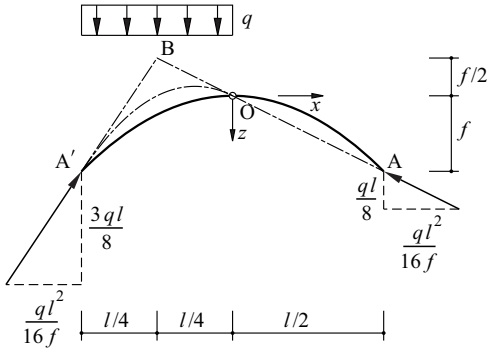

Fig. 5.31 Thrust line for an asymmetric imposed load

$x = -l/4$, the thrust line in this zone is not line A′BO, but rather parabolic; the relationship $z = 2fx(l + 4x)/l^2$ applies here. The deviation of the arch form $z = 4fx^2/l^2$ from the thrust line, both in this zone and also along OA (where the thrust line coincides with chord OA), illustrates very vividly the occurrence of the bending moments shown in Fig. 5.30(d). At every point on this arch, the bending moment is equal to the product of the normal force and the distance of the axis of the arch from the thrust line.

In practice, arch structures are designed to match the thrust line for permanent actions as closely as possible in order to minimise the bending moments. However, as a result of variable actions, certain bending moments (and hence the associated shear forces) must always be accepted. Such bending moments can either be accommodated by the arch itself (*stiff arch*) or partly or totally assigned to a stiffening member (*deck-stiffened polygonal arch*).

5.3.2.2 Load perpendicular to plane of curvature

The beam element shown in Fig. 5.32, with radius of curvature ρ and length $\mathrm{d}s = \rho\,\mathrm{d}\varphi$, is loaded by the line load q and the line load moment m. Forces in the plane of curvature and moments perpendicular to the plane of curvature are irrelevant, i. e. we can limit our investigation to considering shear force V, bending moment M and torque T.

For equilibrium of forces perpendicular to the plane of curvature and equilibrium of moments about the n and t axes

$$q\,\mathrm{d}s + \mathrm{d}V = 0 \quad , \quad \mathrm{d}M + T\,\mathrm{d}\varphi - V\,\mathrm{d}s = 0 \quad , \quad \mathrm{d}T - M\,\mathrm{d}\varphi + m\,\mathrm{d}s = 0$$

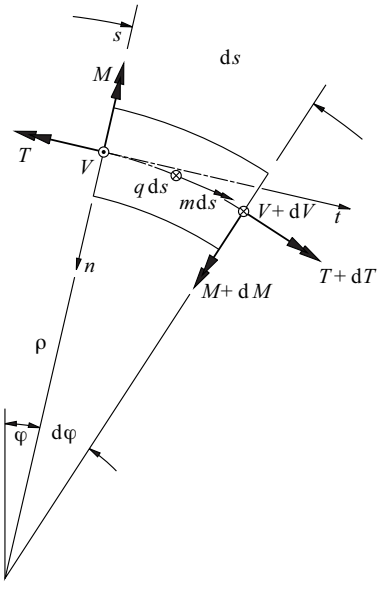

Fig. 5.32 Beam element loaded perpendicular to plane of curvature

which results in the following simultaneous differential equations

$$-q = V' \quad , \quad M' + \frac{T}{\rho} = V \quad , \quad T' = \frac{M}{\rho} - m \tag{5.61}$$

where a superscript dash ($'$) means differentiation with respect to s.

Generally, the radius of curvature $\rho(s)$ is variable. However, assuming an average, constant radius of curvature (at least span by span) mostly results in a good approximation and hence allows the beam to be treated as a circular arc with $\rho = r = \text{const}$. Linking the differential equations (5.61) then gives

$$M'' + \frac{M}{r^2} = \frac{m}{r} - q \tag{5.62}$$

Example 5.8 Beam as circular arc

The beam shown in Fig. 5.33(a) is supported by a transverse beam at A and discretely at B. The transverse beam enables shear forces V_A as well as torques T_A to be carried, but on the other hand $M_A = 0$. And at B only shear forces V_B can be carried, $M_B = T_B = 0$. The measures required to support the beam in such a way that it is braced in three dimensions will not be discussed here. For example, a point support with three degrees of determinacy and a sliding support with one degree of determinacy at A plus a sliding support with two degrees of determinacy at B (preventing displacement in the radial direction) would result in a statically determinate support situation.

If the beam is loaded over its (developed) length $l = r\varphi_0$ with a uniformly distributed line load $q = \text{const}$, $m = 0$, integrating (5.62), taking into account the static boundary conditions mentioned, results in

$$M = qr^2\left(\sin\varphi\frac{1-\cos\varphi_0}{\sin\varphi_0} + \cos\varphi - 1\right) \tag{5.63}$$

and $(5.61)_3$, considering $T(\varphi_0) = 0$, results in

$$T = qr^2\left[\sin\varphi - \sin\varphi_0 + \frac{1-\cos\varphi_0}{\sin\varphi_0}(\cos\varphi_0 - \cos\varphi) + \varphi_0 - \varphi\right] \tag{5.64}$$

and from $(5.61)_2$ it follows that

$$V = qr\left(\cos\varphi_0\frac{1-\cos\varphi_0}{\sin\varphi_0} - \sin\varphi_0 + \varphi_0 - \varphi\right) \tag{5.65}$$

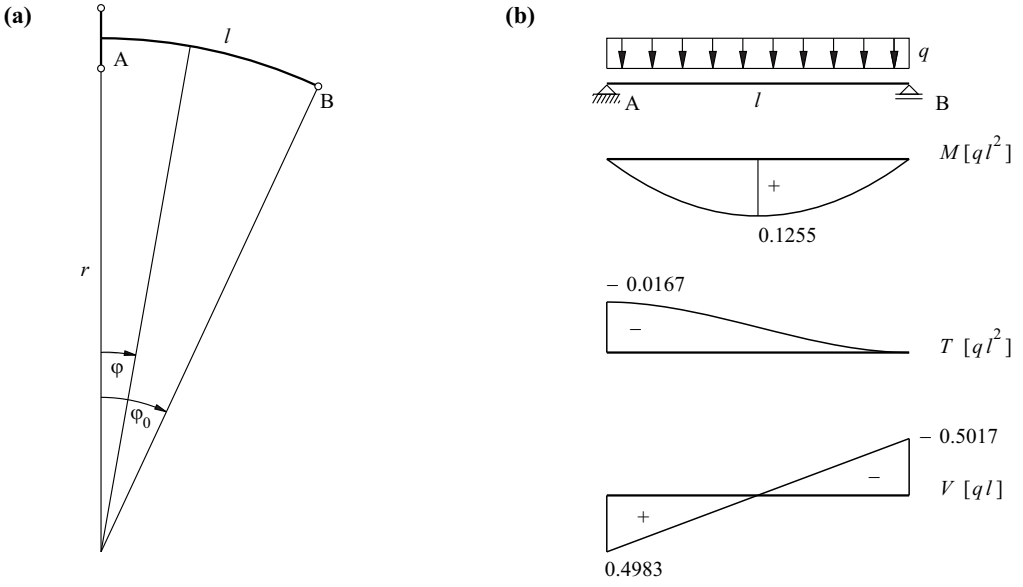

Fig. 5.33 Simply supported beam as circular arc with torsion-resistant support at one end and carrying a load $q = \text{const}$: (a) system and notation, (b) stress resultants

The diagrams of the stress resultants according to (5.63) to (5.65) are shown in Fig. 5.33(b) for the case of $\varphi_0 = l/r = 0.2$. As can be seen, these stress resultants are very well approximated by the stress resultants M, V and T determined on a developed straight beam of span l for q and M/r. This can be easily explained by the development of the TAYLOR series for the expressions on the right in (5.63) to (5.65). If we consider only the first term or the first two terms of the series in each case, we get

$$V \approx qr(\varphi_0/2 - \varphi) \quad , \quad M \approx qr^2\varphi(\varphi_0 - \varphi)/2 \quad , \quad T \approx qr^2\left(-\varphi_0^3 + 3\varphi_0\varphi^2 - 2\varphi^3\right)/12 \tag{5.66}$$

which with $x = r\varphi$ and $l = r\varphi_0$ corresponds exactly with the stress resultants of the straight beam:

$$V = q(l/2 - x) \quad , \quad M = qx(l - x)/2 \quad , \quad T = q(-l^3 + 3lx^2 - 2x^3)/(12r) \tag{5.67}$$

5.4 Summary

1. Forces are perceived through their effects on material systems, can be represented as vectors and always occur together with their reactions (except inertial forces, which are mathematical auxiliary variables). Depending on the point of application of the reactions, we distinguish between remote and contact forces as well as internal and external forces.
2. Reducing a force system to one reference point produces the force-couple system (the resultant force and the resultant couple) related to the reference point. The force system is in equilibrium when the force-couple system equals zero.
3. Any free body isolated from a system, together with all the forces acting on it, constitutes a free body diagram. According to the free body principle, any free body removed from a compatibly deformed body or system in equilibrium by way of imaginary cuts is itself in equilibrium and compatibly deformed; the external forces are in equilibrium in themselves because the internal forces constitute a group in equilibrium (fundamental theorem of statics).
4. A system is statically determinate when the equilibrium conditions – if necessary after resolving the system appropriately – are adequate for determining the unknowns. Otherwise it is statically indeterminate.
5. Structures must not fail in their entirety (as rigid bodies). Their overall stability must be assured.
6. Force and funicular polygons are excellent graphic engineering tools for understanding equilibrium conditions.
7. Supports and hinges correspond to the locally inhibited or released degrees of freedom of structures. Their arrangement should be well thought out as part of the structural concept. The limit values of the associated force and deformation variables must be carefully considered in every case.
8. The stress resultants in framed structures (normal and shear forces plus torques and bending moments) are obtained by reducing the forces acting on the section to the centroid of the cut face under consideration. In plate and shell structures, the stress resultants related to points on the middle surface are generally made up of membrane and shear forces as well as bending and twisting moments.
9. The stress state at one point in a continuum is described by a symmetric second-order tensor and can be represented with MOHR's stress circles in the plane of stress σ, τ (normal and shear stresses). Alternatively, the stress state can be described through its principal axes and principal values (the principal stresses). Resolving into hydrostatic and deviatoric components is often helpful.
10. Applying the equilibrium approach to differential structural elements results in differential equations for the equilibrium in the respective model space – generally three-dimensional, see (5.29), two-dimensional in the case of plate and shell structures (plates, slabs, folded plates, shells) and one-dimensional in the case of framed structures. In this respect, this chapter confines itself to straight and single-curvature bars.
11. In order to minimise the bending moments in an arch structure, it should be designed so that its axis matches the thrust line for permanent actions as closely as possible.

12. Beams with a radius of curvature r loaded perpendicular to the plane of curvature can be approximated by considering similar straight beams with the same (developed) span and by introducing line load moments M/r.

5.5 Exercises

5.1 The masonry wall shown in section in Fig. 5.34(a) has a thickness $b = 1\,\text{m}$ and is subjected to a mean body load of $\gamma_m = 24\,\text{kN/m}^3$. The active earth pressure varies linearly over h and at the base of the wall amounts to $e_h = \gamma_e h/3$, where γ_e = body load of soil = $20\,\text{kN/m}^3$. Assume a linear distribution for the ground bearing pressure and calculate the permissible height h plus the associated ground bearing pressure distribution (assuming no partial uplift at the base). How does the permissible height change when partial uplift is present and the bearing pressure is max. $200\,\text{kN/m}^2$?

5.2 Draw the force and funicular polygons for the two situations in exercise 5.1. Divide the height h into four equal parts and indicate the associated masonry loads and earth pressures.

5.3 A steel plate, see Fig. 5.34(b), is formed by two parts welded together along $x = y$ and exhibits stresses of $\sigma_x = -30\,\text{N/mm}^2$, $\sigma_y = 90\,\text{N/mm}^2$ and $\tau_{xy} = -45\,\text{N/mm}^2$. Determine the stress components along the weld seam.

5.4 A timber member is made up of two parts joined together via a glued finger joint, as shown in Fig. 5.34(c). With a mean tensile stress of $\sigma = 10\,\text{N/mm}^2$ in the timber member, what is the maximum permissible opening angle 2α if neither the tensile stresses nor the shear stresses in the glued joint are to exceed $1\,\text{N/mm}^2$?

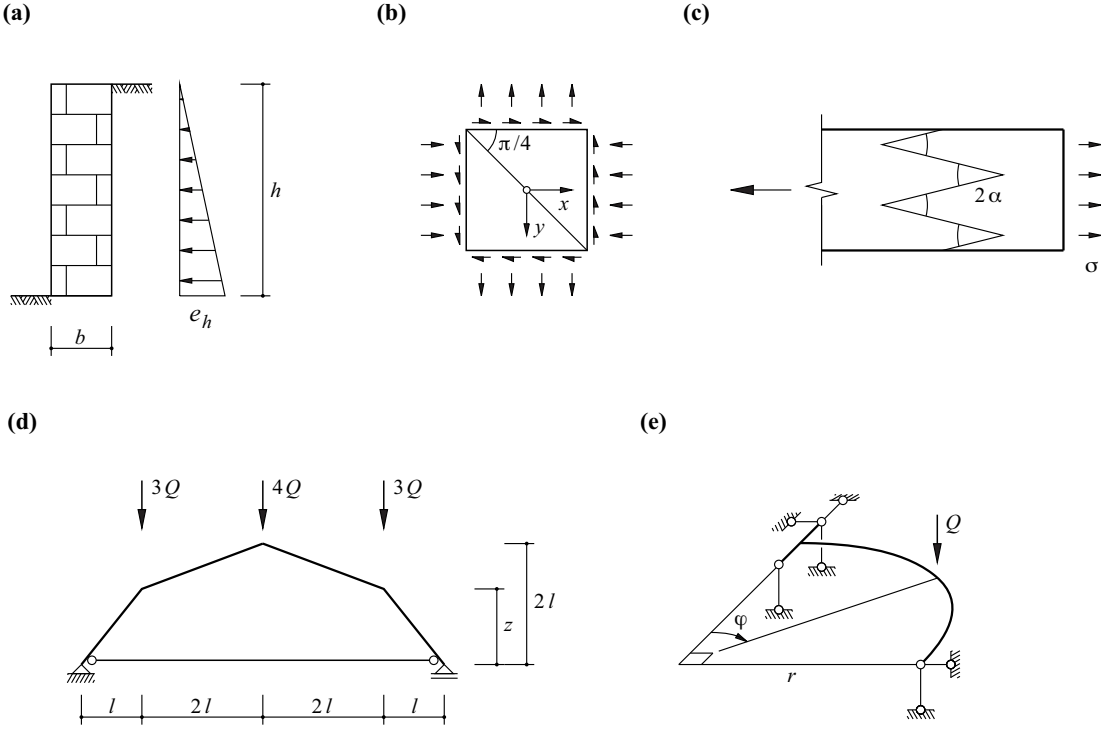

Fig. 5.34 Figures for section 5.5

5.5 Using the stress tensor

$$\boldsymbol{\sigma} = \begin{bmatrix} 2 & 6 & -4 \\ 6 & -2 & 2 \\ -4 & 2 & 5 \end{bmatrix} \text{N/mm}^2$$

determine the corresponding principal stresses and their directions and illustrate the stress state according to Fig. 5.24 and Fig. 5.25.

5.6 Determine the height z in Fig. 5.34(d) such that the shape of the frame corresponds to the thrust line for the given loads. What is the magnitude of the force in the tie connecting the two supports?

5.7 Determine the stress resultants for the quarter-circle beam shown in Fig. 5.34(e). As a comparison, consider a similar straight beam with a (developed) span of $l = r\pi/2$ and a line load moment of M/r.

6 KINEMATIC RELATIONSHIPS

6.1 Terminology

The points P and $\overline{\text{P}}$ in Fig. 6.1 designate the positions of a material point of a system in the undeformed and deformed states. The difference

$$\boldsymbol{u} = \overline{\boldsymbol{r}} - \boldsymbol{r} \tag{6.1}$$

between the corresponding position vectors is known as the *displacement vector* for P. Generally, $\boldsymbol{u}$ depends on P or $\boldsymbol{r}$, i. e. we have to consider the *displacement field* $\boldsymbol{u}(\boldsymbol{r})$, which we presume is continuous and differentiable. As a rule, this field is described by the position functions $u(x, y, z)$, $v(x, y, z)$, $w(x, y, z)$ for the three Cartesian displacement components. The designations u_x, u_y, u_z are often used instead of u, v, w.

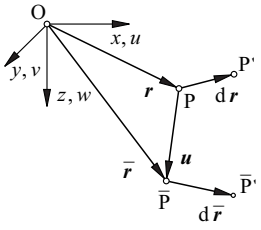

Fig. 6.1 Displacement field

The displacement state of a system described by the displacement field can always be divided into *rigid body motion* and *deformations* independent of that motion. When dealing with structures in the service situation, it is generally the aim to rule out the former, or limit it to small (local) rigid body deformation components such as bar rotations, by choosing a suitable system (appropriate supports in particular), and to keep the latter reasonably small, bearing in mind functionality. However, for specific conditions during construction, e. g. transverse launching, incremental launching or rotation of beams, raising or lowering suspended floors and roofs as well as rotating arches into position, (global) rigid body motion that can be carried out in a controlled way is not only desirable, but intrinsic to the concept.

The rigid body motion is fully described by the *translation* $\boldsymbol{u}_\text{O}$ of a reference point O and the *rotation* $\boldsymbol{\omega}$, see Fig. 6.2. The translation $\boldsymbol{u}$ of an arbitrary point P with the position vector $\boldsymbol{r}$ related to O is given by

$$\boldsymbol{u} = \boldsymbol{u}_\text{O} + \boldsymbol{\omega} \times \boldsymbol{r} \tag{6.2}$$

The pair of vectors $\{\boldsymbol{u}_\text{O}, \boldsymbol{\omega}\}$ is called the *translation-rotation system* at O.

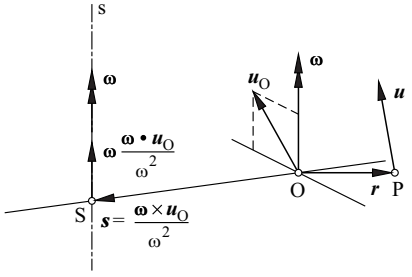

Fig. 6.2 Rigid body motion

The simplest way of understanding rigid body motion is as a *wrench deformation* about the *wrench axis* s parallel with $\boldsymbol{\omega}$, see Fig. 6.2. The wrench axis intersects the plane passing through O orthogonal to $\boldsymbol{\omega}$ at point S with the position vector

$$\boldsymbol{s} = \frac{\boldsymbol{\omega} \times \boldsymbol{u}_\text{O}}{\omega^2} \tag{6.3}$$

All the points on the wrench axis exhibit the same translation-rotation system $\{\boldsymbol{\omega}\ (\boldsymbol{\omega} \cdot \boldsymbol{u}_\text{O})/\omega^2, \boldsymbol{\omega}\}$, which is called a *wrench*.

The coplanar state of deformation is first discussed below, followed by the general spatial state of deformation. In doing so, *small deformations* are always presumed, i. e. the derivatives $u_{i,j}$ of the displacement components u_i with respect to the coordinates x_j (the elements of the displacement gradient introduced in section 6.3) should be infinitesimally small compared to 1.

If both the derivatives $u_{i,j}$ and also the displacement component u_i itself are small (compared with the dimensions of the relevant part of the structure, e. g. deflection $\ll$ span), then we speak of *first-order theory.* In this case the equilibrium conditions may be formulated for the undeformed (rigid) system. Furthermore, presuming linear elastic material behaviour according to section 7.2 results in *linear statics*; all state variables may then be superimposed according to the *superposition law.*

Theory of Structures. First Edition. Peter Marti

In the case of stability problems (chapter 22) and similar issues, it is no longer possible to consider all displacement components as small, and the equilibrium conditions must be formulated for the deformed system (*second-order theory*). The superposition law no longer applies to such problems with *geometric non-linearity*; similarly, the superposition law does not apply to problems with *material non-linearity* (e. g. the elastic-plastic and rigid-plastic systems dealt with in chapters 20 and 21).

6.2 Coplanar deformation

If we consider a *plane displacement field* with the displacement components $u(x,y)$, $v(x,y)$ and $w = 0$, then the result for a differential element in the xy plane is the situation depicted in Fig. 6.3.

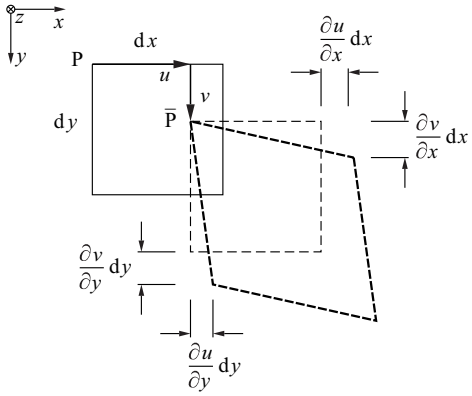

Fig. 6.3 Coplanar deformation

The elongations or *normal strains* related to the original lengths dx and dy in the x and y directions are

$$\varepsilon_x = \frac{\partial u}{\partial x} \quad , \quad \varepsilon_y = \frac{\partial v}{\partial y} \tag{6.4}$$

The angle between dx and dy, originally a right-angle, is reduced by the *shear strain*

$$\gamma_{xy} = \frac{\partial u}{\partial y} + \frac{\partial v}{\partial x} \tag{6.5}$$

and there is also a rotation about the z axis

$$\omega_z = \frac{1}{2}\left(\frac{\partial v}{\partial x} - \frac{\partial u}{\partial y}\right) \tag{6.6}$$

in addition to the displacement $\boldsymbol{u} = (u, v)$ of the element. Summing up, the deformation state is described by the translation $\boldsymbol{u}$, the rotation ω_z according to (6.6) and a *change in volume* and *form* (dilatation and distortion) characterised by the *kinematic relations* (6.4) and (6.5).

According to (A6.1) and (A6.4), the relationship between the original coordinates $\boldsymbol{x} = (x,y)$ and the $\overline{\boldsymbol{x}} = (n,t)$ coordinates rotated through the angle φ about the z axis is described by

$$\boldsymbol{x} = \boldsymbol{c} \bullet \overline{\boldsymbol{x}} \quad , \quad \overline{\boldsymbol{x}} = \boldsymbol{c}^{\mathrm{T}} \bullet \boldsymbol{x} \quad , \quad \boldsymbol{c} = \begin{bmatrix} \cos\varphi & -\sin\varphi \\ \sin\varphi & \cos\varphi \end{bmatrix} \tag{6.7}$$

Similarly, the following applies for the displacements $\boldsymbol{u} = (u,v)$ and $\overline{\boldsymbol{u}} = (n,t)$:

$$\overline{\boldsymbol{u}} = \boldsymbol{c}^{\mathrm{T}} \bullet \boldsymbol{u} \tag{6.8}$$

and according to $(6.7)_1$, the elements of the rotation matrix $\boldsymbol{c}$ correspond to the derivatives

$$c_{ij} = \frac{\partial x_i}{\partial \overline{x}_j} \tag{6.9}$$

Thus, from the relations analogous with (6.4) and (6.5)

$$\varepsilon_n = \frac{\partial u_n}{\partial n} \quad , \quad \varepsilon_t = \frac{\partial u_t}{\partial t} \quad , \quad \gamma_{nt} = \frac{\partial u_n}{\partial t} + \frac{\partial u_t}{\partial n} \tag{6.10}$$

the transformation relationship analogous with (5.21)

$$\begin{Bmatrix} \varepsilon_n \\ \varepsilon_t \\ \frac{1}{2}\gamma_{tn} \end{Bmatrix} = \begin{bmatrix} \cos^2\varphi & \sin^2\varphi & \sin\varphi\cos\varphi \\ \sin^2\varphi & \cos^2\varphi & -\sin\varphi\cos\varphi \\ -\sin\varphi\cos\varphi & \sin\varphi\cos\varphi & \cos^2\varphi - \sin^2\varphi \end{bmatrix} \begin{Bmatrix} \varepsilon_x \\ \varepsilon_y \\ \frac{1}{2}\gamma_{xy} \end{Bmatrix} \tag{6.11}$$

follows by applying the chain rule.

The normal strains ε_x, ε_y and the halved shear strains $\gamma_{xy}/2 = \gamma_{yx}/2$ can therefore be grouped together in the (planar) *strain tensor* similarly to the stress tensor (5.27)

$$\boldsymbol{\varepsilon} = \begin{bmatrix} \varepsilon_x & \frac{1}{2}\gamma_{xy} \\ \frac{1}{2}\gamma_{yx} & \varepsilon_y \end{bmatrix} \tag{6.12}$$

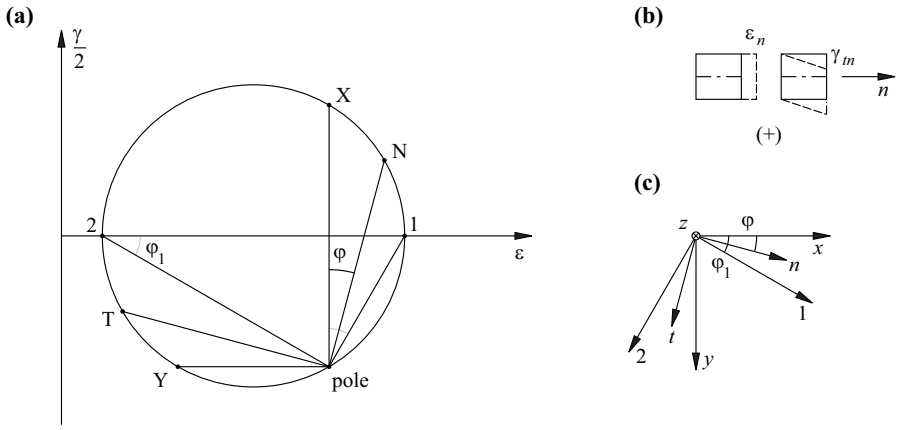

Fig. 6.4 Coplanar deformation state: (a) MOHR's strain circle, (b) sign convention, (c) system of coordinates

Its principal values, the *principal strains*

$$\varepsilon_{1,2} = \frac{\varepsilon_x + \varepsilon_y}{2} \pm \sqrt{\left(\frac{\varepsilon_x - \varepsilon_y}{2}\right)^2 + \frac{\gamma_{xy}^2}{4}} \tag{6.13}$$

occur in the φ_1 and $\varphi_1 + \pi/2$ directions with

$$\tan(2\varphi_1) = \frac{\gamma_{xy}}{\varepsilon_x - \varepsilon_y} \tag{6.14}$$

and the variables

$$\varepsilon_n + \varepsilon_t = \varepsilon_x + \varepsilon_y = \varepsilon_1 + \varepsilon_2 = \varepsilon_{\mathrm{I}} \tag{6.15}$$

and

$$\frac{1}{4}\gamma_{nt}^2 - \varepsilon_n\varepsilon_t = \frac{1}{4}\gamma_{xy}^2 - \varepsilon_x\varepsilon_y = -\varepsilon_1\varepsilon_2 = \varepsilon_{\mathrm{II}} \tag{6.16}$$

are invariant.

Coplanar strain states can be interpreted geometrically with the help of MOHR's circles in a similar way to Fig. 5.20, see Fig. 6.4.

Example 6.1 Measuring grid

The measuring bolts A, B, C and D are arranged on a 200 mm square grid in the undeformed state on the side face of a test specimen according to Fig. 6.5(a). Measurements of the distances AB, CD, AC, BD and BC with the help of instruments to measure the permanent strain in the deformed state reveal elongations of 1, 1.2, 0.2, 0.4 and 0.566 mm. What elongation does distance AD undergo and what are the principal strains and their directions?

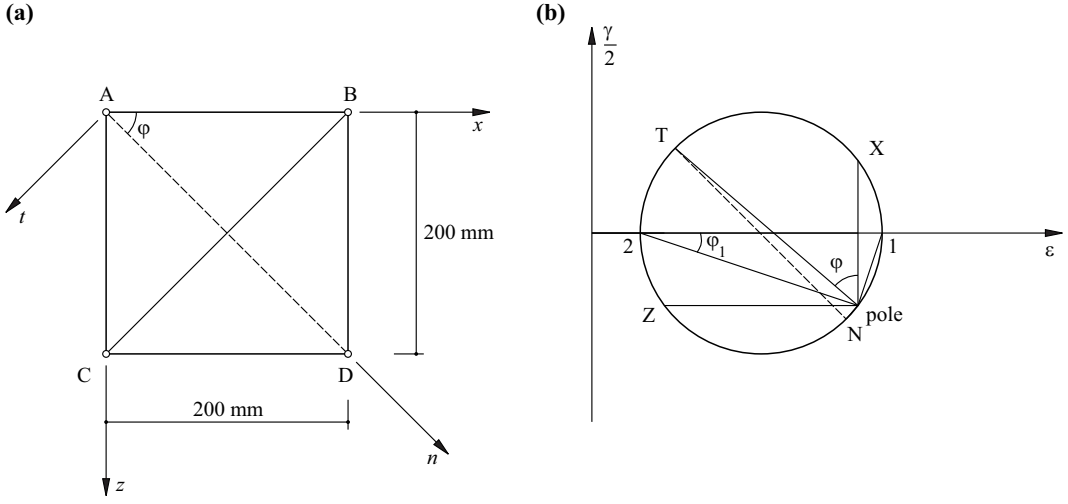

Fig. 6.5 Permanent strain measurements: (a) measuring grid and axes, (b) MOHR's strain circle

The measurements of the distances AB, CD and AC, BD result in the average strains

$$\varepsilon_x = \frac{1}{2}(\varepsilon_{AB} + \varepsilon_{CD}) = \frac{1 + 1.2}{2 \cdot 200} = 5.5\,‰$$

$$\varepsilon_z = \frac{1}{2}(\varepsilon_{AC} + \varepsilon_{BD}) = \frac{0.2 + 0.4}{2 \cdot 200} = 1.5\,‰$$

and the result for diagonal BC is

$$\varepsilon_{BC} = \varepsilon_t = \frac{0.566}{\sqrt{2} \cdot 200} = 2\,‰$$

From (6.15) it follows that $\varepsilon_{AD} = \varepsilon_n = \varepsilon_x + \varepsilon_z - \varepsilon_t = 5‰$, and from $(6.11)_3$, with $\varphi = \pi/4$, the shear strain is $\gamma_{tn} = -4‰$. MOHR's circle can therefore be drawn as shown in Fig. 6.5(b). Eq. (6.16) supplies $\gamma_{yx} = 3‰$, and from (6.13) and (6.14) it follows that $\varepsilon_1 = 6‰$, $\varepsilon_2 = 1‰$ and $\varphi_1 = 18.4°$.
In the diagonal direction AD, the measurement should be $\varepsilon_n = 5‰$. But actually, owing to unavoidable measuring errors, the result would almost certainly deviate slightly from this. The redundant measurement AD plays the role of a *restraint* and enables an error to be compensated for, i. e. enables the measurements to be improved.
In surveying, errors are compensated for by requiring that the sum of the squares of the improvements multiplied by the weighting of the individual measurements should be a minimum. If we regard the measuring grid as a statically indeterminate, linear elastic truss with bar stiffnesses of $k_i = (EA/l)_i$ according to (8.5), then this complies with the requirement that the energy stored elastically in the n bars of the truss

$$\Pi_i = \sum_{i=1}^{n} \left(\frac{EA}{l}\right)_i \frac{(\delta l_i)^2}{2}$$

should be a minimum, where δl_i = improvement to the ith measurement, see (8.73) and (8.74); it can be seen that the external potential Π_e is zero for the purely restraint condition of this example. The stiffnesses of the truss members correspond to the weighting of the measurements, and the (minimal) sum of the weighted squares of the improvements corresponds to the (minimal) internal potential Π_i. Compensating for surveying errors in a grid of linear measurements is carried out in a similar way to the treatment of a truss with enforced deformations in theory of structures.

6.3 Three-dimensional deformation state

Referring to Fig. 6.1, let us consider a point P′ at an infinitesimally small distance d$\boldsymbol{r}$ from P in the undeformed state. As deformation takes place, so the two points are displaced to the positions $\overline{\mathrm{P}}$ and $\overline{\mathrm{P}}'$ at a distance of

$$\mathrm{d}\overline{\boldsymbol{r}} = \overline{\boldsymbol{r}}_{,i}\,\mathrm{d}x_i \tag{6.17}$$

Substituting (6.1), it follows that

$$\mathrm{d}\overline{x} = \left(1 + \frac{\partial u_x}{\partial x}\right)\mathrm{d}x + \frac{\partial u_x}{\partial y}\mathrm{d}y + \frac{\partial u_x}{\partial z}\mathrm{d}z, \ldots \tag{6.18}$$

where the ellipsis indicates the cyclic alternation of the indexes. The derivatives $u_{i,j}$, presumed to be infinitesimally small, form the *displacement gradient*

$$u_{i,j} = \begin{bmatrix} \dfrac{\partial u_x}{\partial x} & \dfrac{\partial u_x}{\partial y} & \dfrac{\partial u_x}{\partial z} \\ \dfrac{\partial u_y}{\partial x} & \dfrac{\partial u_y}{\partial y} & \dfrac{\partial u_y}{\partial z} \\ \dfrac{\partial u_z}{\partial x} & \dfrac{\partial u_z}{\partial y} & \dfrac{\partial u_z}{\partial z} \end{bmatrix} \tag{6.19}$$

The normal and shear strains that occur can be read off from the infinitesimally small cube shown in Fig. 6.6. In a first approximation, the new side length $\mathrm{d}\overline{x}$ is $\mathrm{d}x(1 + \partial u_x/\partial x)$, and, consequently, the normal strain $\varepsilon_x = (\mathrm{d}\overline{x} - \mathrm{d}x)/\mathrm{d}x$ is $\partial u_x/\partial x$. Likewise, for the shear strain γ_{xy} (= decrease in the initially 90° angle between dx and dy), the expression is $\partial u_y/\partial x + \partial u_x/\partial y$.

The displacement gradient (6.19) can be divided into a symmetric part and an antisymmetric part according to (A6.9):

$$u_{i,j} = u_{(i,j)} + u_{[i,j]} \tag{6.20}$$

Here, the symmetric part

$$u_{(i,j)} = \varepsilon_{ij} = \begin{bmatrix} \varepsilon_x & \frac{1}{2}\gamma_{xy} & \frac{1}{2}\gamma_{xz} \\ \frac{1}{2}\gamma_{yx} & \varepsilon_y & \frac{1}{2}\gamma_{yz} \\ \frac{1}{2}\gamma_{zx} & \frac{1}{2}\gamma_{zy} & \varepsilon_z \end{bmatrix} \tag{6.21}$$

with the normal strains and (halved) shear strains given by the *kinematic relations*

$$\varepsilon_x = \frac{\partial u_x}{\partial x} \quad , \quad \ldots \quad , \quad \gamma_{yz} = \gamma_{zy} = \frac{\partial u_z}{\partial y} + \frac{\partial u_y}{\partial z} \quad , \quad \ldots \tag{6.22}$$

denotes the (spatial) *strain tensor*. And according to (A6.27), the antisymmetric part

$$u_{[i,j]} = \begin{bmatrix} 0 & \frac{1}{2}\left(\frac{\partial u_x}{\partial y} - \frac{\partial u_y}{\partial x}\right) & \frac{1}{2}\left(\frac{\partial u_x}{\partial z} - \frac{\partial u_z}{\partial x}\right) \\ -\frac{1}{2}\left(\frac{\partial u_x}{\partial y} - \frac{\partial u_y}{\partial x}\right) & 0 & \frac{1}{2}\left(\frac{\partial u_y}{\partial z} - \frac{\partial u_z}{\partial y}\right) \\ -\frac{1}{2}\left(\frac{\partial u_x}{\partial z} - \frac{\partial u_z}{\partial x}\right) & -\frac{1}{2}\left(\frac{\partial u_y}{\partial z} - \frac{\partial u_z}{\partial y}\right) & 0 \end{bmatrix} \tag{6.23}$$

corresponds to the dual vector

$$\boldsymbol{\omega} = \frac{1}{2}\operatorname{curl}\boldsymbol{u} = \frac{1}{2}\nabla \times \boldsymbol{u} \tag{6.24}$$

whose components

$$\omega_x = \frac{1}{2}\left(\frac{\partial u_z}{\partial y} - \frac{\partial u_y}{\partial z}\right) \quad , \quad \omega_y = \frac{1}{2}\left(\frac{\partial u_x}{\partial z} - \frac{\partial u_z}{\partial x}\right) \quad , \quad \omega_z = \frac{1}{2}\left(\frac{\partial u_y}{\partial x} - \frac{\partial u_x}{\partial y}\right) \tag{6.25}$$

describe a rigid body rotation of the region around P. Eq. $(6.25)_3$ is identical with (6.6).

Summing up, the spatial deformation state in the vicinity of a point P is described by the translation $\boldsymbol{u}$, the rotation $\boldsymbol{\omega}$ and the strain state $\boldsymbol{\varepsilon}$.

The strain tensor (6.21) has the following basic invariants

$$\begin{aligned} \varepsilon_{\mathrm{I}} &= \varepsilon_x + \varepsilon_y + \varepsilon_z && = \varepsilon_1 + \varepsilon_2 + \varepsilon_3 \\ \varepsilon_{\mathrm{II}} &= \left(\frac{\gamma_{yz}}{2}\right)^2 + \left(\frac{\gamma_{zx}}{2}\right)^2 + \left(\frac{\gamma_{xy}}{2}\right)^2 - \varepsilon_y\varepsilon_z - \varepsilon_z\varepsilon_x - \varepsilon_x\varepsilon_y && = -\varepsilon_2\varepsilon_3 - \varepsilon_3\varepsilon_1 - \varepsilon_1\varepsilon_2 \\ \varepsilon_{\mathrm{III}} &= \frac{1}{4}\gamma_{yz}\gamma_{zx}\gamma_{xy} - \varepsilon_x\left(\frac{\gamma_{yz}}{2}\right)^2 - \varepsilon_y\left(\frac{\gamma_{zx}}{2}\right)^2 - \varepsilon_z\left(\frac{\gamma_{xy}}{2}\right)^2 + \varepsilon_x\varepsilon_y\varepsilon_z = \varepsilon_1\varepsilon_2\varepsilon_3 \end{aligned} \tag{6.26}$$

and the principal strains and their directions follow from the characteristic equation

$$\varepsilon^3 - \varepsilon_{\mathrm{I}}\varepsilon^2 - \varepsilon_{\mathrm{II}}\varepsilon - \varepsilon_{\mathrm{III}} = 0 \tag{6.27}$$

or (A6.21).

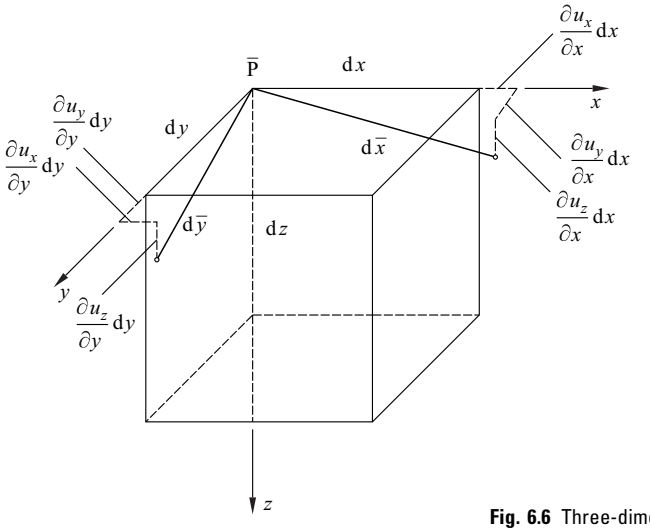

Fig. 6.6 Three-dimensional deformation state

Using the *octahedral normal strain*

$$\varepsilon_o = \frac{\varepsilon_I}{3} \tag{6.28}$$

the strain tensor can be divided into a hydrostatic part and a deviatoric part, similarly to (5.37):

$$\begin{bmatrix} \varepsilon_x & \frac{1}{2}\gamma_{xy} & \frac{1}{2}\gamma_{xz} \\ \frac{1}{2}\gamma_{yx} & \varepsilon_y & \frac{1}{2}\gamma_{yz} \\ \frac{1}{2}\gamma_{zx} & \frac{1}{2}\gamma_{zy} & \varepsilon_z \end{bmatrix} = \begin{bmatrix} \varepsilon_o & 0 & 0 \\ 0 & \varepsilon_o & 0 \\ 0 & 0 & \varepsilon_o \end{bmatrix} + \begin{bmatrix} e_x & \frac{1}{2}\gamma_{xy} & \frac{1}{2}\gamma_{xz} \\ \frac{1}{2}\gamma_{yx} & e_y & \frac{1}{2}\gamma_{yz} \\ \frac{1}{2}\gamma_{zx} & \frac{1}{2}\gamma_{zy} & e_z \end{bmatrix} \tag{6.29}$$

The hydrostatic part describes purely a change in volume (*dilatation*) without a change in form, and the deviatoric part purely a change in form (*distortion*) without a change in volume. The basic invariants of the deviator

$$e_{ij} = \varepsilon_{ij} - \varepsilon_o \delta_{ij} \tag{6.30}$$

are similar to (5.40)

$$e_I = 0 \quad , \quad e_{II} = \varepsilon_{II} + \frac{1}{3}\varepsilon_I^2 \quad , \quad e_{III} = \varepsilon_{III} + \frac{1}{3}e_{II}\varepsilon_I - \frac{1}{27}\varepsilon_I^3 \tag{6.31}$$

Using the *octahedral shear strain* γ_o, where

$$\frac{\gamma_o}{2} = \sqrt{\frac{2}{3}e_{II}} \tag{6.32}$$

and the angle θ, where

$$\cos\theta = \frac{\sqrt{2}e_1}{\gamma_o} = \frac{\sqrt{2}(2\varepsilon_1 - \varepsilon_2 - \varepsilon_3)}{3\gamma_o} \tag{6.33}$$

enables a presentation with hydrostatic axis and deviatoric plane similar to Fig. 5.25 in the principal strain space ε_1, ε_2, ε_3, see (5.44) and (5.45).

The kinematic relations (6.22) are supplemented by *kinematic boundary conditions*, which result in prescribed *boundary displacements* $\boldsymbol{r}$ at the edge of the structure. The displacement $\boldsymbol{u}$ of a point on the edge of the structure must match the corresponding boundary displacement, i. e. $\boldsymbol{r} = \boldsymbol{u}$, or, when using (A6.3)

$$r_i = \delta_{ij} u_j \tag{6.34}$$

A displacement field that satisfies the kinematic relations (6.22) and the kinematic boundary conditions (6.34) is regarded as *kinematically admissible*.

6.4 Summary

1. The displacement state of a system can be divided into rigid body motion and deformations independent of that motion. Apart from specific conditions during construction, for structures it is generally the aim to rule out the former or limit it to small (local) rigid body deformation components such as bar rotations, and to keep the latter reasonably small.
2. Rigid body motion is fully described by the translation of a reference point and the rotation of the body. The simplest way of understanding this is as a wrench deformation about the wrench axis.
3. Where the elements of the displacement gradient are infinitesimally small and the displacements are negligible in comparison with the dimensions of the relevant part of the structure, then the equilibrium conditions may be formulated for the undeformed system according to first-order theory; if, in addition, linear elastic material behaviour is assumed, then the superposition law applies (linear statics). If individual displacement components can no longer be considered as small, then the equilibrium must be investigated according to second-order theory for the deformed system.
4. The general spatial state of deformation in the vicinity of a point is described by its translation, the rotation given by the antisymmetric part of the displacement gradient and the strain state given by the symmetric part of the displacement gradient.

5. All the considerations relevant for the stress tensor (MOHR's circles, basic invariants, principal axes and values, division into hydrostatic and deviatoric parts, etc.) can be readily transferred to the strain tensor.
6. The octahedral normal strain corresponds to purely a change in volume (dilatation) and the octahedral shear strain purely a change in form (distortion).

6.5 Exercises

6.1 A beam in the form of a helix ($x = a\cos\varphi$, $y = a\sin\varphi$, $z = b\varphi$) is constructed using incremental launching by successively adding segments of length s and sliding the beam forward by an amount s. Show that the end cross-sections of a segment related to the bar axis are rotated through $sb/(a^2 + b^2)$ with respect to each other.

6.2 The sides of an equilateral triangle ABC (considered anticlockwise) undergo normal strains $\varepsilon_{AB} = 2.44\,‰$, $\varepsilon_{BC} = 0.36\,‰$, $\varepsilon_{AC} = -0.40\,‰$. Determine the principal strains and their directions.

6.3 Can the theory of structures analogy regarding compensating errors in surveying, which was discussed in connection with example 6.1, also be used for angular measurements in triangulated grids? Assume a triangular mesh and use the sine law of trigonometry.

6.4 Show that the ratio γ_o/γ_{max}, where $\gamma_{max} = \text{Max}\,(|e_2 - e_3|,|e_3 - e_1|,|e_1 - e_2|)$, is limited by the values $\sqrt{2/3}$ and $\sqrt{8/9}$.

6.5 Use the identity $\cos(3\theta) = 4\cos^3\theta - 3\cos\theta$ to show that

$$\cos(3\theta) = \frac{3\sqrt{3}}{2} \cdot \frac{e_{III}}{e_{II}^{3/2}}$$

6.6 Determine the rotation $\boldsymbol{\omega}$, strains $\boldsymbol{\varepsilon}$ (including principal values and directions), γ_{max}, octahedral normal strain ε_o and octahedral shear strain γ_o belonging to the displacement gradient

$$u_{i,j} = \begin{bmatrix} 0.1 & 0.2 & -0.4 \\ -0.2 & 0.25 & 0.15 \\ -0.4 & 0.3 & 0.3 \end{bmatrix} \cdot 10^{-3}$$

7 CONSTITUTIVE RELATIONSHIPS

7.1 Terminology

The aim of this chapter is to bring together the stress and strain variables introduced in chapters 5 and 6 by way of *constitutive relationships*, or rather, *constitutive equations*, which are obtained through idealisation based on the results of experiments. This chapter will address those deformations that are dependent on loads, but also the deformations not dependent on loads (e. g. due to shrinkage, swelling or thermal actions) as well as the fatigue of materials caused by repetitive loadings.

Fig. 7.1(a) shows a uniaxial tensile test on a bar-type element and Fig. 7.1(b) shows a typical *stress-strain diagram* for an *air-hardened* steel; a steadily increasing load results in the line OABCD. The material behaves *elastically* between O and A, and the line returns to O upon removing the load. The segment AB is a so-called *yield plateau*, which corresponds to dislocations within the crystal lattice of the material; removing the load at this stage would result in a line parallel with OA, and a certain *plastic* strain would remain for $\sigma = 0$. The segment BC with σ increasing further represents a *strain hardening* of the material; removing the load (and applying it again) at this stage would again result in a line roughly parallel with OA. The decrease in the load after reaching the maximum load in the test (indicated by point C) up to fracture at point D leads to an apparent decrease in the stress because the force applied is related to the original cross-sectional area ($A = 1$); in fact, there is a local decrease in the cross-section (*necking*) and the stress at the point of fracture continues to increase.

The transition from elastic to plastic behaviour is not as distinct as point A in Fig. 7.1(b) might lead us to believe, even with air-hardened steels. In reality, the stress-strain diagram starts to deviate from the linear progression at the *limit of proportionality*, which is reached just before the *yield limit* f_y (point A). *Cold-formed* steels do not exhibit a yield plateau at all and instead of the yield limit f_y we use the *yield point* $f_{0.2}$ (also $f_{0.1}$), i. e. the point at which a permanent (plastic) strain of 0.2 % (0.1 %) or 2 ‰ (1 ‰) occurs.

By way of a comparison, Fig. 7.2 shows typical stress-strain diagrams for various concretes (normal-, high-strength), reinforcing steels (air-hardened, cold-formed) and prestressing steels (bars, wires, strands) used in concrete structures. The prestressing steels exhibit strengths that are two to three times greater than those of the reinforcing steels and at the same time elongations at rupture that are two to three times smaller. The strengths and elongations at rupture of the concretes are much smaller than those

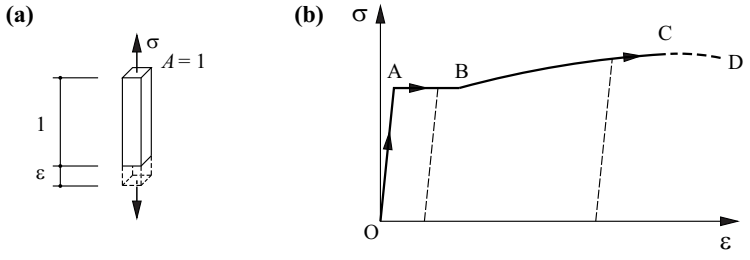

Fig. 7.1 Uniaxial tensile test: (a) bar element, (b) stress-strain diagram

Theory of Structures. First Edition. Peter Marti

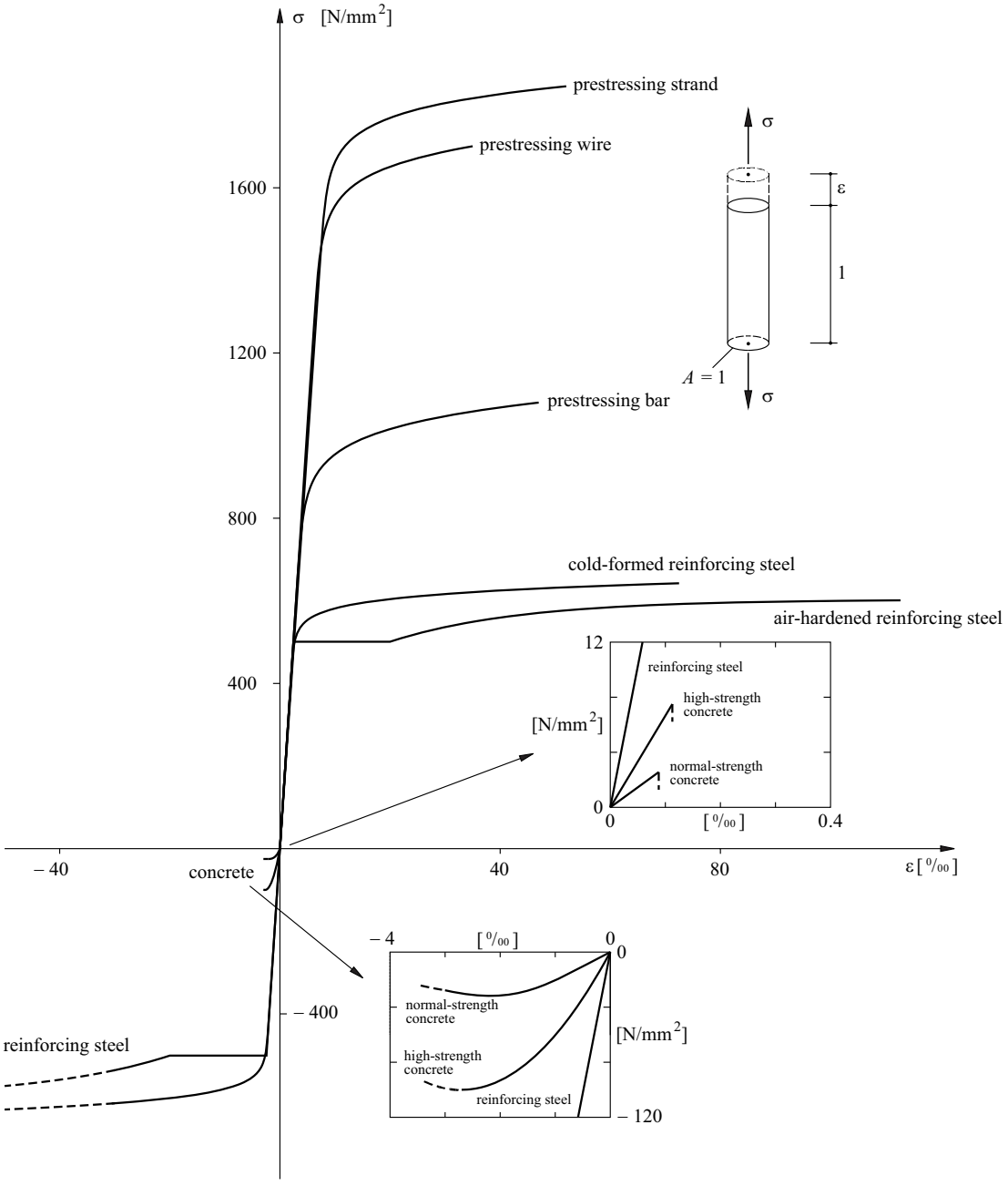

Fig. 7.2 Stress-strain diagrams for reinforcing steel and concrete

of the reinforcing steels. Normal-strength concretes subjected to compression exhibit a distinctly non-linear behaviour that decreases with increasing strength. Subjected to tension, all concretes exhibit an approximately linear behaviour that concludes with a *brittle* failure, similar to glass. The tensile strength of concrete is only about one-tenth of its compressive strength, and is subject to a relatively large scatter.

Fig. 7.3 shows a number of important idealisations of stress-strain relationships for materials. The *(hyper)elastic* behaviour shown in Fig. 7.3(a) is characterised by a distinct, reversible σ-ε relationship; applying and relieving the load follow the same (non-linear) path, all the energy stored in the material during deformation is released again upon reversing the deformation. Fig. 7.3(b) illustrates *(hyper)elastic-plastic* behaviour – a type of behaviour that is not reversible; the loading and unloading paths are different, plastic strains remain and part of the energy required for the deformation

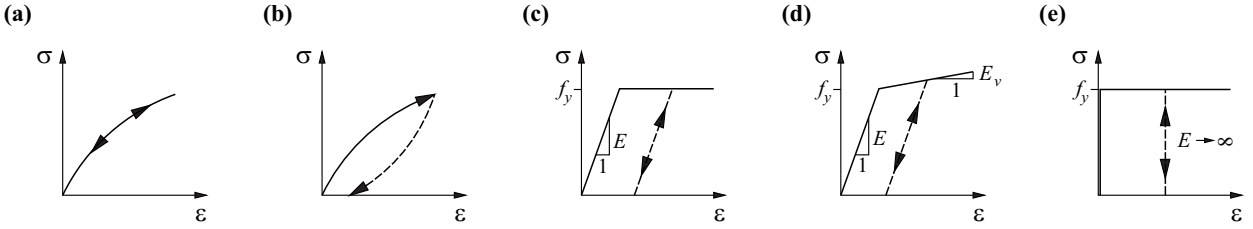

Fig. 7.3 Idealised stress-strain diagrams: (a) elastic, (b) elastic-plastic, (c) linear elastic - perfectly plastic, (d) linear elastic - linearly hardening plastic, (e) rigid - perfectly plastic

is *dissipated*, i. e. converted into heat. Fig. 7.3(c) shows the *linear elastic - perfectly plastic* idealisation very often assumed in construction applications; the initial elastic portion characterised by the *modulus of elasticity E* is followed by a yield plateau determined by f_y, and relieving the load takes place purely elastically, parallel with the initial loading; the strain that remains once the load has been fully relieved ($\sigma = 0$) corresponds to the plastic portion ε_r, but the strain reversed upon relieving the load corresponds to the elastic portion ε_e of the total strain $\varepsilon = \varepsilon_e + \varepsilon_r$, see (20.17). The *linear elastic - linearly hardening plastic* behaviour shown in Fig. 7.3(d) does not exhibit a yield plateau, but rather a further rise in the σ-ε line characterised by the *modulus of strain hardening* E_v; otherwise, the behaviour is identical with the linear elastic - perfectly plastic model. Finally, Fig. 7.3(e) shows the *rigid - perfectly plastic* idealisation, which is a further development of the linear elastic - perfectly plastic behaviour in which the modulus of elasticity exceeds all limits, $E \to \infty$.

7.2 Linear elastic behaviour

In this section we shall confine ourselves to *isotropic* behaviour, i. e. behaviour not dependent on the choice of the system of coordinates; we shall also presume a linear relationship between stresses and strains. Assuming isotropic behaviour means that the principal axes of the stresses and strains coincide.

If we make the x axis a bar axis in Fig. 7.1(a), then according to the information in section 7.1, $\varepsilon_x = \sigma_x / E$. In line with our premise, there will normally be strains transverse to the bar axis which are likewise proportional to σ_x; assuming isotropic behaviour means that $\varepsilon_y = \varepsilon_z = -\nu\varepsilon_x$, where ν = POISSON*'s ratio*. If σ_x is joined by σ_y and σ_z as well, then the generalisation of these considerations results in the following strains

$$\varepsilon_x = \frac{1}{E}\left[\sigma_x - \nu\left(\sigma_y + \sigma_z\right)\right] \quad , \quad \varepsilon_y = \frac{1}{E}\left[\sigma_y - \nu(\sigma_z + \sigma_x)\right]$$
$$\varepsilon_z = \frac{1}{E}\left[\sigma_z - \nu\left(\sigma_x + \sigma_y\right)\right] \tag{7.1}$$

Fig. 7.4(a) examines a state of pure shear $\tau_{xz} = \tau_{zx} = \tau$. According to Fig. 7.4(b), the principal stresses corresponding to this state are $\sigma_1 = -\sigma_2 = \tau$ at 45° to the x and z axes, as is easily confirmed by the free bodies shown in Fig. 7.4(c) and Fig. 7.4(d), or the MOHR's circle of Fig. 7.4(e). Fig. 7.4(f) shows the associated deformation. The diagonals of the element shown in Fig. 7.4(a) are stretched or shortened by the amount $\varepsilon_1 = -\varepsilon_2 = (\sigma_1 - \nu\sigma_2)/E = \tau(1 + \nu)/E$ according to (7.1), and the initially 90° angle between the x and z axes is reduced by $-2\varepsilon_2 = 2\tau\ (1 + \nu)/E$. This means that the shear strain is $\gamma_{xz} = \tau_{xz}/G$, where

$$G = \frac{E}{2(1 + \nu)} \tag{7.2}$$

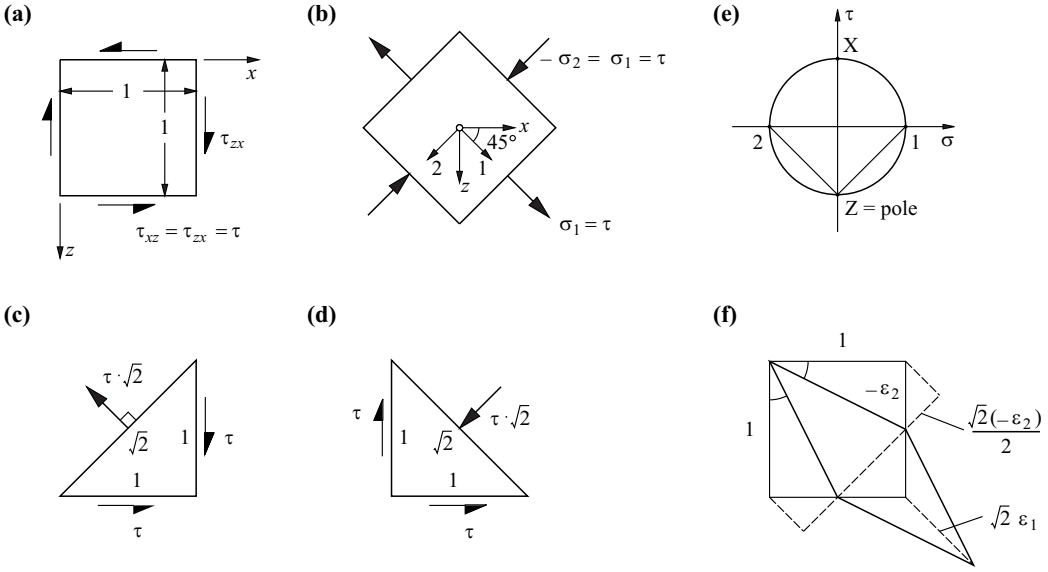

Fig. 7.4 State of pure shear: (a) notation, (b) principal stresses, (c) and (d) free bodies, (e) MOHR's circle, (f) shear strain γ_{xz}

is the *shear modulus*. Generally, as well as (7.1), we have

$$\gamma_{xy} = \frac{\tau_{xy}}{G} \quad , \quad \gamma_{xz} = \frac{\tau_{xz}}{G} \quad , \quad \gamma_{yz} = \frac{\tau_{yz}}{G} \tag{7.3}$$

The six equations of (7.1) and (7.3) are known as the *generalised* HOOKE*'s law.*

Summing the expressions of (7.1) and applying $(5.33)_1$, (5.38) and $(6.26)_1$ results in

$$\varepsilon_I = \frac{\sigma_o}{K} \tag{7.4}$$

where

$$K = \frac{E}{3(1-2\nu)} \tag{7.5}$$

is the *bulk modulus*. On the other hand, applying (5.37), (5.38), (6.28), (6.29), (7.1) and (7.3), it becomes clear that there is a relationship

$$s_{ij} = 2Ge_{ij} \tag{7.6}$$

between the elements of the stress deviator and those of the strain deviator.

The bulk modulus K describes the change in volume, and the shear modulus G the change in form. The factor $2G = E/(1 + \nu)$ in (7.6) corresponds to the ratio of the diameters in the associated MOHR's stress and strain circles.

The outcome for the *specific strain energy* (8.67) is

$$\pi_i = \frac{3K}{2}\left(\sqrt{3}\varepsilon_o\right)^2 + G\left(\frac{\sqrt{3}\gamma_o}{2}\right)^2 \tag{7.7}$$

and for the *specific complementary energy* (8.69)

$$\pi_i^* = \frac{1}{6K}\left(\sqrt{3}\sigma_o\right)^2 + \frac{1}{4G}\left(\sqrt{3}\tau_o\right)^2 \tag{7.8}$$

Eq. (7.7) and (7.8) describe rotational ellipsoids in the principal strain and principal stress space respectively, with the hydrostatic axis as the axis of rotation. The expressions $|\boldsymbol{\varepsilon}_\mathbf{o}| = \sqrt{3}\varepsilon_o$ and $e = |\boldsymbol{e}| = \sqrt{3}\gamma_o/2$ or $|\boldsymbol{\sigma}_\mathbf{o}| = \sqrt{3}\sigma_o$ and $s = |\boldsymbol{s}| = \sqrt{3}\tau_o$ correspond to the magnitudes of the hydrostatic and deviatoric components of the strain and stress vectors $\boldsymbol{\varepsilon}$ and $\boldsymbol{\sigma}$, see (6.28) and (6.32) or (5.38) and (5.43). Deriving (7.7) or (7.8) with respect to these expressions and making use of (7.4) and (7.6) confirms (8.68) and (8.70). The functions $\pi_i = \text{const}$ and $\pi_i^* = \text{const}$ correspond to potential surfaces whose gradients at arbitrary strain or stress points are the associated stress or strain vectors, see Fig. 7.5.

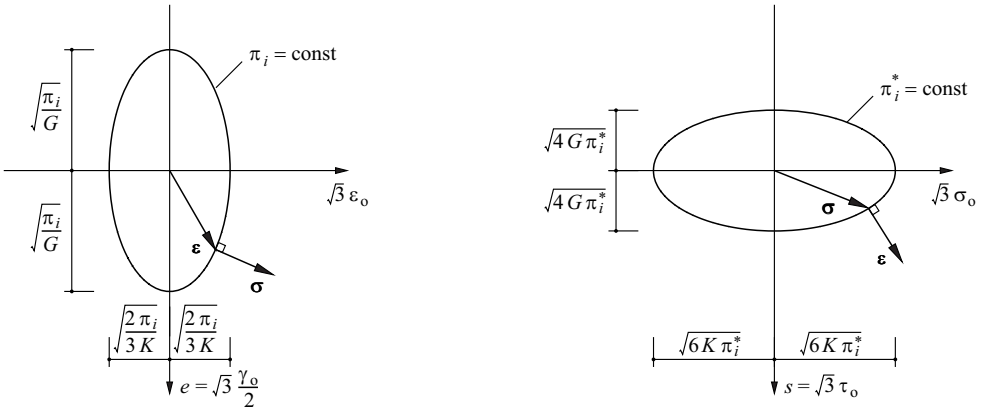

Fig. 7.5 Potential functions π_i (specific strain energy) and π_i^* (specific complementary energy)

The linear elastic, isotropic behaviour is fully characterised by two material constants; K and G can be used as an alternative to E and ν. The use of the LAMÉ *constants* μ and λ represents yet another alternative, see (8.53).

From (7.4) and (7.5) it follows that using $\nu = 0.5$, the material is *incompressible*; the change in volume tends to zero irrespective of σ_o. Values of ν exceeding 0.5 are obviously impossible because otherwise the result for a positive σ_o value would be a negative ε_I (or ε_o) value, $\nu \leq 0.5$. Applying the same reasoning, according to (7.2) and (7.3), $\nu \geq -1$ is essential because otherwise a positive τ value would result in a negative γ value. In practice, ν varies between 0 and 0.5 depending on the material. The value of ν is about 0.3 for the majority of metals, about 0.4 for most polymers and can be approximated with $\nu = 0.2$ for concrete, see appendix A3.

7.3 Perfectly plastic behaviour

7.3.1 Uniaxial stress state

The *perfectly plastic* behaviour shown in Fig. 7.3(c) and (e) is characterised by the fact that plastic deformations can occur where $\sigma = f_y$, whereas, at best, elastic changes in deformation are possible where $\sigma < f_y$. The magnitudes of the plastic deformations at the yield limit f_y remain indefinite; the only thing that is clear is that they cannot decrease. Obviously, it is not possible to make any assertion about the total plastic strains, only about possible *plastic strain increments* $\dot{\varepsilon}$. It is true that $\dot{\varepsilon} \geq 0$ where $\sigma = f_y$ and $\dot{\varepsilon} = 0$ where $\sigma < f_y$; stresses $\sigma > f_y$ are impossible.

We often speak of plastic strain rates instead of plastic strain increments and therefore we use a superscript dot ($\dot{}$) to indicate these, as is usual when differentiating with respect to time t. It should be pointed out that a true differentiation with respect to time is not the case here; the velocity is irrelevant, i. e. t could be multiplied by any positive factor. To keep the notation tidy, the superscript dot will be used in the following, but always referring to the strain increments ($\dot{\boldsymbol{\varepsilon}}$), displacement increments ($\dot{\boldsymbol{u}}$) and incremental dissipation energy ($\dot{D}$).

Fig. 7.6 summarises the considerations so far, to which a yield limit for compression (f_{yc}) will be added to the one for tension (f_{yt}). Using the *yield functions*

$$Y_t = \sigma - f_{yt} \quad , \quad Y_c = -\sigma - f_{yc} \tag{7.9}$$

it is true that where $\kappa \geq 0$

$$\dot{\varepsilon} = \kappa \frac{\mathrm{d}Y_t}{\mathrm{d}\sigma} \quad \text{for } Y_t = 0 \quad , \quad \dot{\varepsilon} = 0 \quad \text{for } Y_t < 0 \tag{7.10}$$

and

$$\dot{\varepsilon} = \kappa \frac{\mathrm{d}Y_c}{\mathrm{d}\sigma} \quad \text{for } Y_c = 0 \quad , \quad \dot{\varepsilon} = 0 \quad \text{for } Y_c < 0 \tag{7.11}$$

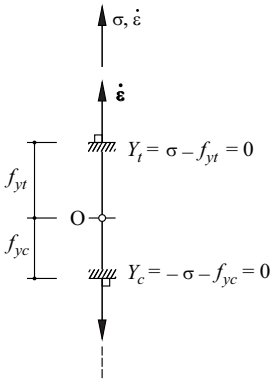

Fig. 7.6 Yield conditions and plastic strain increments in the uniaxial stress state

Stress states with $Y_t > 0$ or $Y_c > 0$ are not permissible; possible stress states are confined to the zone between the two yield limits.

7.3.2 Three-dimensional stress states

A *yield surface* defined by the *yield condition* $Y(\sigma_{ij}) = 0$ is assumed in the following in the six-dimensional stress space according to Fig. 7.7(a); this yield surface contains the origin O and should be *non-concave*; in the planar case the yield surface is reduced to a *yield locus*. The function Y is normalised in such a way that $Y < 0$ for points within the yield surface (in the so-called *non-plastic domain*). Points outside the yield surface ($Y > 0$) are not permissible.

The *flow rule*

$$\dot{\boldsymbol{\varepsilon}} = \kappa \operatorname{grad} Y \quad (Y = 0\,,\ \kappa \geq 0) \quad , \quad \dot{\boldsymbol{\varepsilon}} = 0 \quad (Y < 0) \tag{7.12}$$

is postulated in the following, i. e. plastic strain increments, which correspond to orthogonal vectors outward from the yield surface, can occur for stress points on the yield surface, whereas no plastic strain increments are possible for any point within the yield surface. Accordingly, the yield function Y plays the role of a *plastic potential* and (7.12) is called an *associated flow rule*.

Applications in soil and rock mechanics often make use of *non-associated flow rules* in which the plastic potential is different from the yield function. Such cases are not considered further here.

Eq. $(7.12)_1$ must be generalised when yield surfaces are made up of several segments described by various yield conditions $Y_i = 0$:

$$\dot{\boldsymbol{\varepsilon}} = \sum_i \kappa_i \operatorname{grad} Y_i \quad (Y_i = 0,\ \kappa_i \geq 0) \tag{7.13}$$

Fig. 7.7(b) shows characteristic points with different conditions on the yield surface. At B, the yield surface is strictly convex and smooth, and therefore regular. At C, it is singular, i. e. strictly convex, but not smooth. And at point E on segment AD it is also singular, i. e. smooth, but only weakly convex. In all cases, the *specific incremental dissipation energy*

$$\dot{D} = \boldsymbol{\sigma} \bullet \dot{\boldsymbol{\varepsilon}} = \dot{D}(\dot{\boldsymbol{\varepsilon}}) \geq 0 \tag{7.14}$$

is a single-valued function of $\dot{\boldsymbol{\varepsilon}}$. Further, when $c > 0$

$$\dot{D}(c\,\dot{\boldsymbol{\varepsilon}}) = c\,\dot{D}(\dot{\boldsymbol{\varepsilon}}) \tag{7.15}$$

i. e. $\dot{D}$ is a homogeneous function of degree one in the $\dot{\boldsymbol{\varepsilon}}$.

Generally, a function $f(\boldsymbol{r})$ is homogeneous of degree n when $f(c\boldsymbol{r}) = c^n f(\boldsymbol{r})$. According to EULER's homogenous function theorem, $\boldsymbol{r} \bullet \operatorname{grad} f = n f(\boldsymbol{r})$. Where $n = 1$, $f = \dot{D}$ and $\boldsymbol{r} = \dot{\boldsymbol{\varepsilon}}$, it follows that

$$\dot{\boldsymbol{\varepsilon}} \bullet \operatorname{grad} \dot{D} = \dot{D} \tag{7.16}$$

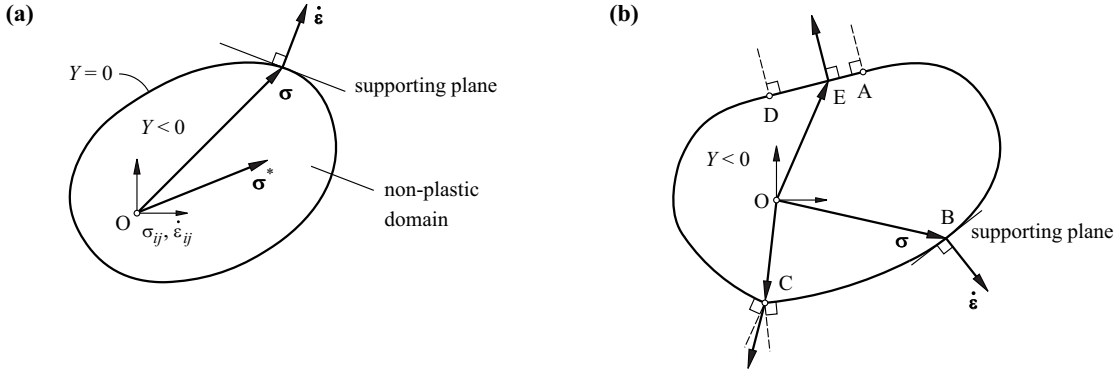

Fig. 7.7 Yield conditions in the stress space: (a) regular yield surface, (b) yield surface with singularities

and the comparison with $(7.14)_1$ supplies

$$\boldsymbol{\sigma} = \operatorname{grad} \dot{D} \tag{7.17}$$

Eq. $(7.12)_1$ and (7.17) are similar to (8.70) and (8.68). The plastic potential plays the same role in plastic theory as the specific complementary energy plays in elastic theory, and the specific incremental dissipation energy corresponds to the specific deformation energy.

Fig. 7.7(a) also shows that the relationship

$$(\boldsymbol{\sigma} - \boldsymbol{\sigma}^*) \bullet \dot{\boldsymbol{\varepsilon}} = \dot{D}(\dot{\boldsymbol{\varepsilon}}) - \boldsymbol{\sigma}^* \bullet \dot{\boldsymbol{\varepsilon}} \geq 0 \tag{7.18}$$

applies for any stress states $\boldsymbol{\sigma}$ on the yield surface and $\boldsymbol{\sigma}^*$ in the non-plastic domain. This relationship is known as the *principle of the maximum* (incremental specific) *dissipation energy* because $\boldsymbol{\sigma}^* \bullet \dot{\boldsymbol{\varepsilon}}$ can be interpreted as a fictitious specific dissipation energy. Instead of the convexity of the yield surface and the orthogonality of the plastic strain increments, the validity of (7.18) is often presumed in order to infer convexity of the yield surface and orthogonality of the strain increments.

Stress states $\boldsymbol{\sigma}$ at the yield surface and associated incremental strain states $\dot{\boldsymbol{\varepsilon}}$ according to Fig. 7.7(a) are referred to as *compatible*. For B in Fig. 7.7(b), the regular case, there is a one-to-one correspondence between $\boldsymbol{\sigma}$ and $\dot{\boldsymbol{\varepsilon}}$. For C, the singular case, only the allocation of $\boldsymbol{\sigma}$ to $\dot{\boldsymbol{\varepsilon}}$ is unambiguous and, vice versa, in the case of E merely the allocation of $\dot{\boldsymbol{\varepsilon}}$ to $\boldsymbol{\sigma}$.

The term *supporting plane* is often useful. This plane is a plane orthogonal to $\dot{\boldsymbol{\varepsilon}}$ at the end-point of the vector $\boldsymbol{\sigma}$ compatible with this, see Fig. 7.7(a). As can be seen, the supporting planes envelop the non-plastic domain. The distance of a supporting plane from the origin is $\dot{D}/|\dot{\boldsymbol{\varepsilon}}|$.

These observations are confined to a perfectly plastic behaviour of the material. A fixed function Y determines the yield surface. On the other hand, in a material with strain hardening, both the position of the non-plastic domain in the stress space as well as its form and extent generally vary. Such circumstances will not be discussed any further here.

The *theory of plastic potential* presented here for a three-dimensional element is discussed further in chapters 20 and 21 using *generalised force* and *deformation variables*. The theory remains valid for generalised variables if it is assumed to be correct for all the elements of a system.

7.3.3 Yield conditions

Only *isotropic* materials will be considered below. Corresponding yield conditions can be presented as a function of the basic invariants of the stress tensor, i. e.

$$Y(\sigma_{\mathrm{I}}, \sigma_{\mathrm{II}}, \sigma_{\mathrm{III}}) = 0 \tag{7.19}$$

The principal axes of the stresses and the strain increments coincide because isotropy is presumed.

7.3.3.1 VON MISES and TRESCA yield conditions

When a material is *incompressible*, $\dot{\varepsilon}_{\mathrm{I}} = 0$, and the resulting yield surfaces are cylinders

$$Y(s_{\mathrm{II}}, s_{\mathrm{III}}) = 0 \tag{7.20}$$

parallel with the hydrostatic axis, see (5.40). Examples of this are the VON MISES yield condition

$$Y = s_{\mathrm{II}} - \frac{f_y^2}{3} = 0 \tag{7.21}$$

or the TRESCA yield condition

$$Y = 4s_{\mathrm{II}}^3 - 27s_{\mathrm{III}}^2 - 9f_y^2 s_{\mathrm{II}}^2 + 6f_y^4 s_{\mathrm{II}} - f_y^6 = 0 \tag{7.22}$$

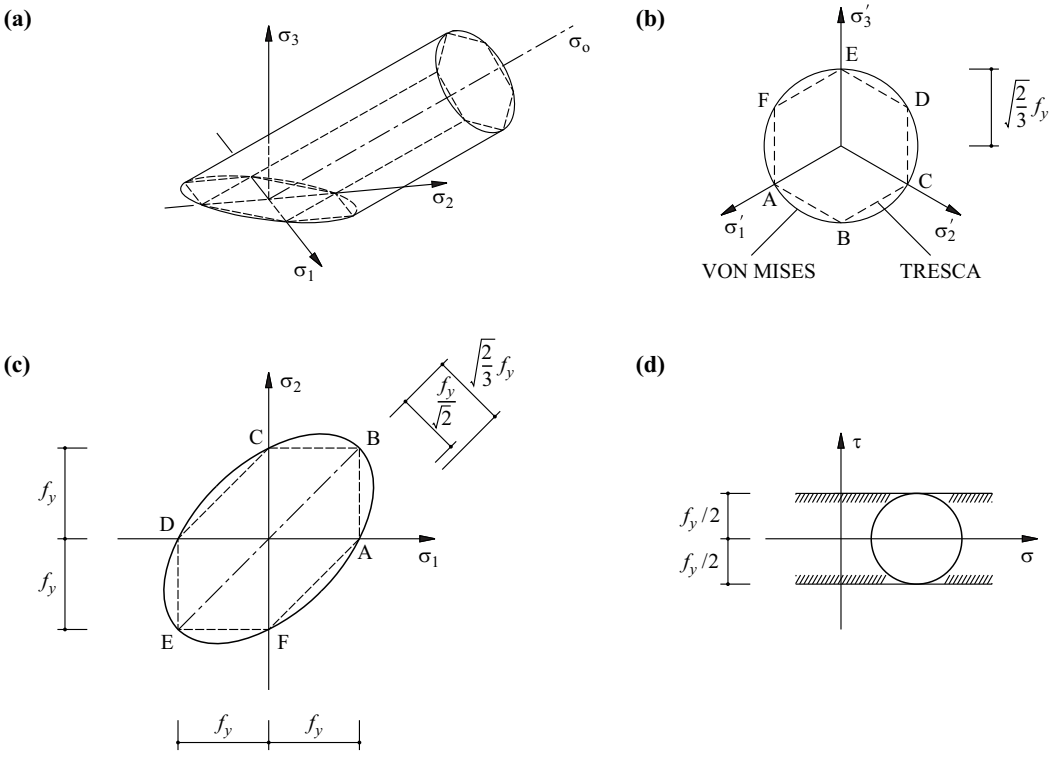

Fig. 7.8 VON MISES and TRESCA yield conditions: (a) principal stress space, (b) deviatoric plane, (c) coplanar stress state, (d) TRESCA yield condition in the stress plane

which can also be written in the form

$$Y = \mathrm{Max}(|s_2 - s_3|, |s_3 - s_1|, |s_1 - s_2|) - f_y = 0 \tag{7.23}$$

or, even simpler, as

$$Y = \tau_{\max} - \frac{f_y}{2} = 0 \tag{7.24}$$

where, as before, f_y denotes the uniaxial yield limit.

According to (7.21) and (5.43), in the principal stress space the VON MISES yield condition corresponds to a cylinder of radius $\sqrt{2/3}\, f_y$ about the hydrostatic axis, see Fig. 7.8(a). The TRESCA yield condition (assuming the same uniaxial yield limit f_y) corresponds to a regular hexagonal prism inscribed within the VON MISES cylinder. Fig. 7.8(b) shows the intersection between the cylinder/prism and the deviatoric plane, and Fig. 7.8(c) shows the yield loci in the coplanar stress state ($\sigma_3 = 0$). The result for the VON MISES ellipse circumscribing the TRESCA hexagon ABCDEF is

$$Y = \sigma_1^2 - \sigma_1\sigma_2 + \sigma_2^2 - f_y^2 = 0 \quad (\sigma_3 = 0) \tag{7.25}$$

Finally, Fig. 7.8(d) shows the TRESCA yield condition in the stress plane σ, τ; the diameters of the MOHR's stress circles cannot exceed f_y but any points on the σ axis may serve as the centres of the circles.

7.3.3.2 PRAGER and DRUCKER yield conditions

The simplest generalisation of (7.21) for a *compressible* material can be seen in the PRAGER yield condition

$$Y = s_{\mathrm{II}} - \frac{f_y^2}{3}\left(1 - \frac{\sigma_{\mathrm{I}}}{k}\right) = 0 \quad \left(|k| > f_y\right) \tag{7.26}$$

shown in Fig. 7.9, with the yield limits $f_y/(1 + f_y/k)$ or $-f_y/(1 + f_y/k)$ in uniaxial tension or compression respectively.

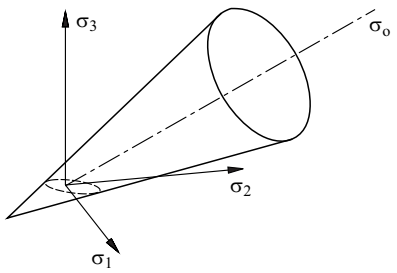

Fig. 7.9 PRAGER yield condition

The similar generalisation

$$Y = \tau_{\max} - \frac{f_y}{2}\left(1 - \frac{\sigma_I}{k}\right) = 0 \quad \left(|k| > f_y\right) \tag{7.27}$$

of (7.24) was formulated by DRUCKER. The yield limits in uniaxial tension or compression are the same as for the PRAGER yield condition.

In the principal stress space, (7.26) corresponds to a regular cone and (7.27) to the inscribed regular hexagonal pyramid. The intersections of these surfaces with the deviatoric plane are identical to the yield conditions of VON MISES and TRESCA, see Fig. 7.8(b).

7.3.3.3 COULOMB yield condition

The COULOMB yield condition widely used in soil mechanics

$$Y = |\tau| + \sigma \tan\varphi - c = 0 \tag{7.28}$$

becomes

$$Y = \sigma_i(1 + \sin\varphi) - \sigma_k(1 - \sin\varphi) - 2c\cos\varphi = 0 \quad \left(\sigma_i \geq \sigma_j \geq \sigma_k\right) \tag{7.29}$$

when formulated for the principal stresses because the radius $(\sigma_i - \sigma_k)/2$ of the governing MOHR's circle is equal to $[c\cot\varphi - (\sigma_i + \sigma_k)/2]\sin\varphi$, where c is the *cohesion* and φ the *angle of internal friction.* For uniaxial stresses, according to Fig. 7.10(a), the yield limits are

$$f_c = \frac{2c\cos\varphi}{1 - \sin\varphi} = 2c\tan\left(\frac{\pi}{4} + \frac{\varphi}{2}\right) \quad , \quad f_t = \frac{2c\cos\varphi}{1 + \sin\varphi} = 2c\tan\left(\frac{\pi}{4} - \frac{\varphi}{2}\right) \tag{7.30}$$

According to (7.29), the mean principal stress σ_j has no effect on the plastic deformation. Consequently, applying the flow rule $(7.12)_1$ gives us the relationship $\dot{\varepsilon}_j = 0$, i. e. a coplanar strain state is present; where $\varphi > 0$ and κ is positive, there is a dilatation according to $\dot{\varepsilon}_I = \dot{\varepsilon}_i + \dot{\varepsilon}_j + \dot{\varepsilon}_k = 2\kappa\sin\varphi$. In Fig. 7.10(b), σ_3 is the mean principal stress. The yield condition (7.29) is given by two planes perpendicular to the $\sigma_1\sigma_2$ plane or parallel with the σ_3 axis, with traces GAF and GCD.

For a coplanar stress state where $\sigma_3 = 0$, the resulting yield locus is the irregular hexagon ABCDEF in Fig. 7.10(b); $\dot{\varepsilon}_3 = 0$ applies along AF and CD. Similarly to these two lines, there are also boundary lines CB and EF (where $\dot{\varepsilon}_1 = 0$) which ensue due to the intersection of plane $\sigma_3 = 0$ with the two side planes of the COULOMB yield surface perpendicular to the $\sigma_2\sigma_3$ plane in the principal stress space. Likewise, the boundary lines AB und ED (where $\dot{\varepsilon}_2 = 0$) ensue from the intersection of plane $\sigma_3 = 0$ with the two side planes of the COULOMB yield surface perpendicular to the $\sigma_1\sigma_3$ plane. As can be seen, with coplanar stress states at the corners of the non-plastic domain, the result according to the generalised flow rule (7.13) is normally a three-dimensional strain state. Further, for stress states along DE and EF, the $\dot{\varepsilon}_3$ component orthogonal to the stress plane is positive, and the same component along AB and BC is negative.

In the deviatoric plane, the COULOMB yield surface according to Fig. 7.10(c) manifests itself as an irregular hexagon ABCDEF. The distances OA and OB are equal to $2c\cos\varphi\sqrt{6}/(3 + \sin\varphi)$ and $2c\cos\varphi\sqrt{6}/(3 - \sin\varphi)$. When $\varphi = 0$, the COULOMB yield condition is reduced to that of TRESCA, and the irregular hexagon ABCDEF becomes the trace AGCHEI of the regular hexagonal TRESCA prism. And vice versa, the hexagon ABCDEF becomes the equilateral triangle AJCKEL in the theoretical limiting case $\varphi = \pi/2$.

The COULOMB yield condition in the principal stress space of Fig. 7.10(d) corresponds to an irregular hexagonal pyramid with pairs of side planes parallel with the axes. By displacing the vectors $\dot{\boldsymbol{\varepsilon}}$ orthogonal to the yield surface to the apex of pyramid G, we see that the scalar product of the specific incremental dissipation energy defined by $(7.14)_1$ for the general case (i. e. for side planes and edges as well as for the apex of the pyramid) can be described by

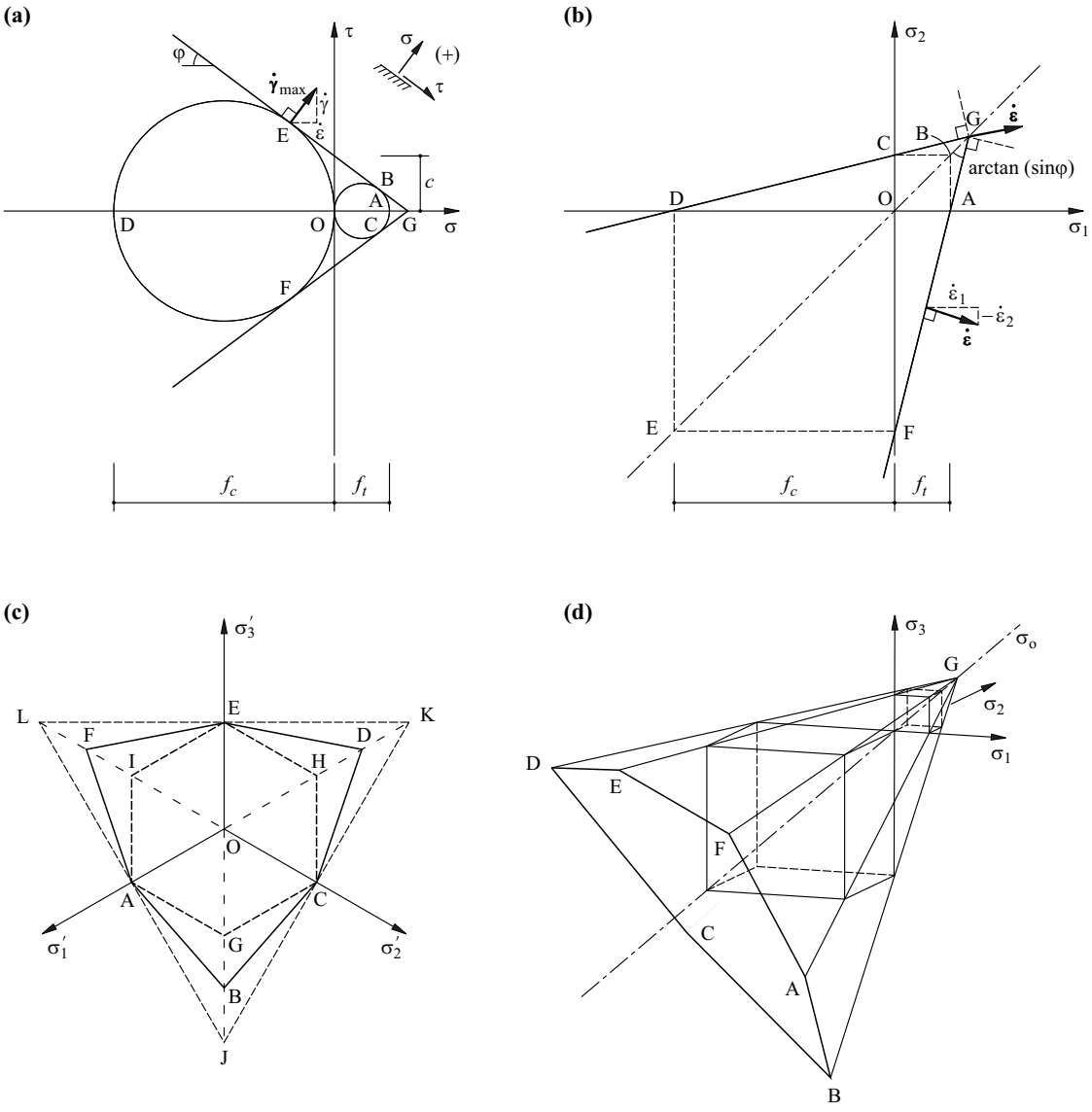

Fig. 7.10 COULOMB yield condition: (a) stress plane, (b) coplanar stress or strain state, (c) deviatoric plane, (d) principal stress space

$$\dot{D} = c\cot\varphi\ \dot{\varepsilon}_I \tag{7.31}$$

Therefore, owing to (7.29) and $(7.12)_1$, $\dot{\varepsilon}_I = 2\kappa\sin\varphi$ and $\dot{\gamma}_{max} = \dot{\varepsilon}_i - \dot{\varepsilon}_k = 2\kappa$, and therefore

$$\dot{D} = c\cos\varphi\ \dot{\gamma}_{max} \tag{7.32}$$

applies for the side planes, where $\dot{\gamma}_{max}$ is the diameter of the MOHR's circle for strain increments.

7.3.3.4 Modified COULOMB yield condition

The COULOMB yield condition is often modified by the condition

$$\sigma \leq f_{ct} \tag{7.33}$$

(based on RANKINE) where $f_{ct} < 2c\cos\varphi/(1 + \sin\varphi)$ because otherwise the values for uniaxial tensile strength would be too large compared with those for uniaxial compressive strength. For example, assuming $\tan\varphi = 3/4$ for concrete is sensible, but inserting that into (7.30) results in the generally unrealistic ratio $f_t/f_c = 1/4$; indeed, $f_t/f_c \approx 1/10$, and the tensile strength is often completely neglected, i. e. $f_{ct} = 0$.

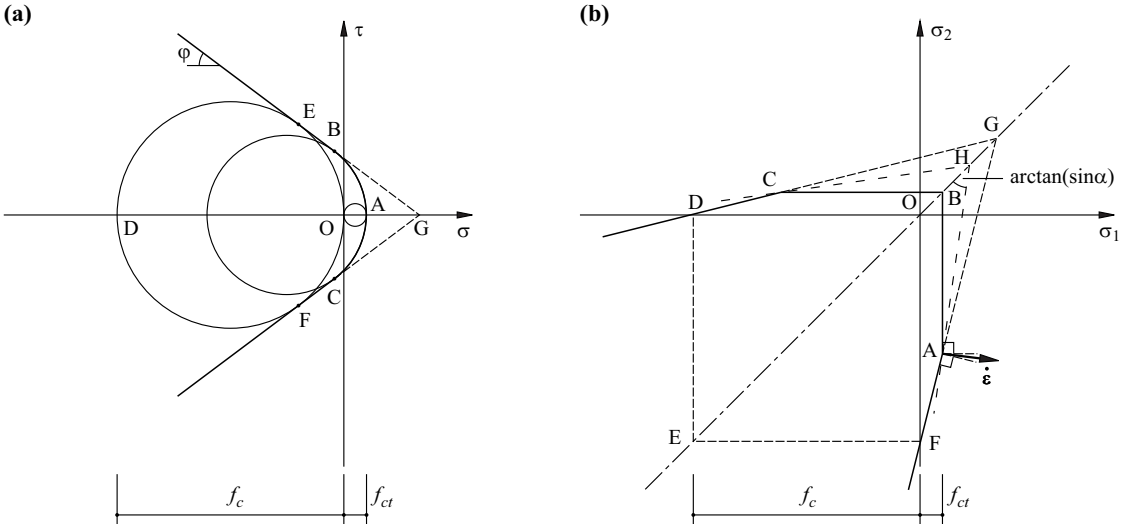

Fig. 7.11 Modified COULOMB yield condition: (a) stress plane, (b) coplanar stress or strain state

Compared with Fig. 7.10(a) and (b), (7.33) leads to the modifications shown in Fig. 7.11. The circle BAC completing the yield limit in Fig. 7.11(a) has the diameter $f_c - 2\sin\varphi\, f_{ct}/(1 - \sin\varphi)$, which corresponds to points A and C in Fig. 7.11(b). According to the generalised flow rule (7.13), these two points can be allocated to the COULOMB yield loci AHC with apexes H between points B and G and fictitious angles of internal friction α where $\pi/2 \geq \alpha \geq \varphi$. The associated specific incremental dissipation energy is calculated similarly to (7.32):

$$\dot{D} = \left[\frac{f_c(1 - \sin\alpha)}{2} + \frac{f_{ct}(\sin\alpha - \sin\varphi)}{1 - \sin\varphi}\right]\dot{\gamma}_{\max} \qquad \left(\frac{\pi}{2} \geq \alpha \geq \varphi\right) \tag{7.34}$$

When $\alpha = \pi/2$, the result is $\dot{D} = f_{ct}\dot{\gamma}_{\max}$, and when $\alpha = \varphi$, eq. (7.34) is reduced to (7.32) because of $(7.30)_1$.

7.3.3.5 MOHR's envelopes

The COULOMB yield condition (7.28) can be generalised according to MOHR as follows:

$$Y = |\tau| - f(\sigma) = 0 \tag{7.35}$$

see Fig. 7.12(a). In doing so, the function f should become zero for a certain, non-negative value σ. Further, the first and second derivative of f should not be positive, and f for $\sigma \to -\infty$ should tend towards a finite limit value, i. e. should switch to a TRESCA yield condition.

As indicated in Fig. 7.12(a), any point B on the envelope can be assigned to a circumscribed COULOMB yield condition with a fictitious angle of internal friction α and a fictitious cohesion c. The distance of the associated straight line DB from the origin O is $c\cos\alpha$. If we consider a *kinematic discontinuity* such that a relative displacement of 1 occurs at an angle α to a certain surface, then in a thin zone of thickness d the mean normal strain increment is $\dot{\varepsilon} = \sin\alpha/d$ along the discontinuity surface. Further, the mean shear strain increment perpendicular to and parallel with the discontinuity surface is $\dot{\gamma} = \cos\alpha/d$, whereas no normal strain increments occur parallel with the discontinuity surface. This strain state corresponds to a mean maximum shear strain increment $\dot{\gamma}_{\max}$ of $1/d$, and according to (7.32), it follows that $\dot{D} = c\cos\alpha/d$. Integrating over the thickness d supplies the incremental dissipation work

$$\dot{D} = c\cos\alpha \tag{7.36}$$

related to a unit surface area of the discontinuity and valid for a unit displacement, which in Fig. 7.12(a) is equal to the distance of the straight line DB from the origin O.

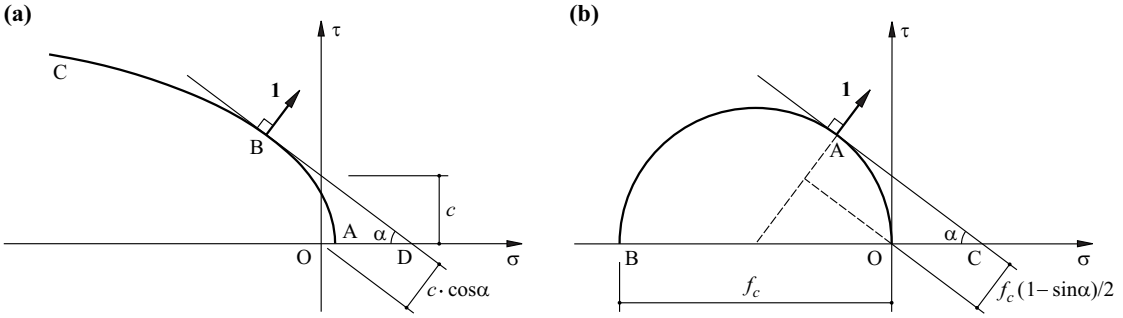

Fig. 7.12 MOHR's envelopes: (a) general presentation in the stress plane, (b) quadratic yield condition in the coplanar stress state

As the thickness d disappears from the equation, in contrast to Fig. 7.10(a), where the vector $\dot{\boldsymbol{\gamma}}_{max}$ and the components $\dot{\varepsilon}$ and $\dot{\gamma}$ are given at point E, the unit displacement vector at an angle α to the τ axis can be given directly at point B in Fig. 7.12(a). Applying $(7.14)_1$ allows (7.32) and (7.36) to be confirmed geometrically.

Neglecting the tensile strength f_{ct} according to Fig. 7.11(b) results in the square yield locus ODEF in the coplanar stress state, which can also be described by

$$-f_c \leq \sigma \leq 0 \tag{7.37}$$

Owing to the square form of the non-plastic domain, (7.37) is normally called the *square yield condition*. In the stress plane, (7.37) can be drawn as a circle OAB according to Fig. 7.12(b), and applying (7.36) supplies

$$\dot{D} = \frac{f_c(1 - \sin\alpha)}{2} \tag{7.38}$$

Apart from $\dot{\gamma}_{max}$, this expression corresponds to the value given by (7.34) for $f_{ct} = 0$. However, in contrast to (7.34), α in (7.38) is not confined to the interval $\pi/2 \geq \alpha \geq \varphi$, instead can assume all values between $-\pi/2$ and $\pi/2$.

Incidentally, it should be noted that the above requirements placed on MOHR's envelopes are only partly fulfilled for (7.37). But as in this case we are dealing with a coplanar stress state and not a coplanar strain state, this is unimportant. The important thing is that (7.38) can be obtained geometrically in a similar way to (7.36).

7.4 Time-dependent behaviour

Many construction materials, especially concrete and timber, experience deformations that change over time. We distinguish here between load-dependent *creep deformations* and load-independent *shrinkage*, *swelling* and *thermal deformations*. Creep and shrinkage processes are discussed below using concrete as an example.

7.4.1 Shrinkage

Shrinkage describes a decrease in the volume of the concrete caused by drying processes, and also through hydration of the cement in the case of low water/cement ratios (as are used, for example, in the production of high-strength concretes). The *shrinkage strain* can be estimated as follows:

$$\varepsilon_s(t) = \varepsilon_{s,\infty}\beta(t - t_s) \tag{7.39}$$

The *final shrinkage strain* $\varepsilon_{s,\infty}$, which lies between about – 0.2 and – 0.7 ‰, primarily depends on the concrete mix and the ambient humidity; considerable differences can occur depending on weather conditions and curing measures – suitable curing can reduce the shrinkage strain. The $\beta(t - t_s)$ factor for taking into account the onset of shrinkage has a value of 0 for the age $t = t_s$ when shrinkage begins and a value of 1 for $t \to \infty$; relatively thin components with a small volume in relation to their surface area shrink considerably faster than thicker components.

We generally assume that the loss in volume due to shrinkage is isotropic, i. e. $\varepsilon_1 = \varepsilon_2 = \varepsilon_3 = \varepsilon_s(t)$.

7.4.2 Creep and relaxation

Creep is a change in the strain state that varies over time as a result of persistent loading. *Relaxation* is the inverse process which involves a time-dependent change in the stress state as a result of a specified persistent deformation.

If we confine ourselves to the typical stresses at the serviceability state, whose magnitude does not exceed about 40 % of the uniaxial concrete compressive strength, and if we exclude a strain reversal, then, assuming constant humidity and temperature, a good approximation is to idealise the concrete as an ageing, *linear viscoelastic* material. Creep strains are proportional to the applied stress and can be superposed linearly over time. For the uniaxial case, the load-dependent strains are given by

$$\varepsilon_\sigma(t) = \int_0^t J(t,\tau)\mathrm{d}\sigma(\tau) \tag{7.40}$$

where the *creep function*

$$J(t,\tau) = \frac{1 + \varphi(t,\tau)}{E(\tau)} \tag{7.41}$$

denotes the strain at time t as a result of a unit stress applied at time τ, see Fig. 7.13(a). The *creep coefficient* $\varphi(t,\tau)$ corresponds to the ratio of the creep strain at time t (with a constant stress) to the initial elastic strain at time τ; it can be estimated as follows

$$\varphi(t,\tau) = \varphi_\infty \beta(t-\tau) \tag{7.42}$$

The *final creep coefficient* φ_∞, which is in the order of magnitude of about 2 to 3, depends, in particular, on the age of the concrete at the onset of the action, the concrete mix, the relative thickness of the component, the ambient humidity and the temperature. The $\beta(t-\tau)$ factor for taking into account the duration of the load has a value of 0 for $t = \tau$ and a value of 1 for $t \to \infty$; as with shrinkage, relatively thin components creep at a faster rate than thicker components, but the difference is not so pronounced.

Instead of (7.40), it is possible to use the equivalent equation

$$\sigma(t) = \int_0^t R(t,\tau)\,\mathrm{d}\varepsilon_\sigma(\tau) \tag{7.43}$$

where the *relaxation function* $R(t,\tau)$ designates the strain at time t due to a load-dependent unit strain applied at time τ, see Fig. 7.13(b).

The relationship between the functions J and R is obtained, for example, by considering the strain history $\varepsilon_\sigma = 0$ for $t < t_0$, and $\varepsilon_\sigma = 1$ for $t \geq t_0$, which, according to the definition, results in $\sigma(t) = R(t,t_0)$. Eq. (7.40) supplies a linear inhomogeneous

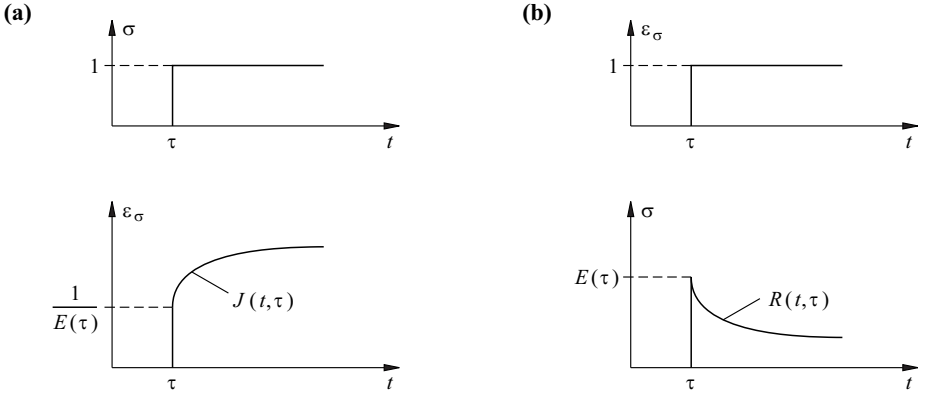

Fig. 7.13 Creep and relaxation: (a) creep function, (b) relaxation function

VOLTERRA integral equation for the numerical calculation of the relaxation function R for a known creep function J:

$$1 = J(t,t_0)E(t_0) + \int_{t_0}^{t} J(t,\tau)\frac{\partial R(\tau,t_0)}{\partial \tau}d\tau \tag{7.44}$$

And vice versa, considering the strain history $\sigma = 0$ for $t < t_0$, and $\sigma = 1$ for $t \geq t_0$, which, according to the definition, results in $\varepsilon_\sigma(t) = J(t,t_0)$, we obtain

$$1 = \frac{R(t,t_0)}{E(t_0)} + \int_{t_0}^{t} R(t,\tau)\frac{\partial J(\tau,t_0)}{\partial \tau}d\tau \tag{7.45}$$

from (7.43), which is the inverse relation to (7.44). If we assume that the load-dependent strain follows from the equation

$$\varepsilon_\sigma = c_1 + c_2\varphi(t,t_0) \tag{7.46}$$

for $t \geq t_0$, and that the stress is zero ($\sigma = 0$) for $0 < t < t_0$, where c_1 and c_2 are arbitrary constants, then $\sigma(t)$ varies linearly with $R(t,t_0)$. Taking $\Delta\sigma = \sigma(t) - \sigma(t_0)$ and $\Delta\varepsilon_\sigma = \varepsilon_\sigma(t) - \varepsilon_\sigma(t_0)$, the incremental elastic stress-strain relationship is

$$\Delta\sigma(t) = E_a(t,t_0)\left[\Delta\varepsilon_\sigma(t) - \frac{\sigma(t_0)\,\varphi(t,t_0)}{E(t_0)}\right] \tag{7.47}$$

where

$$E_a(t,t_0) = \frac{E(t_0)}{1 + \chi(t,t_0)\,\varphi(t,t_0)} \tag{7.48}$$

denotes the *age-adjusted effective elastic modulus* with the *ageing coefficient*

$$\chi = \left[1 - \frac{R(t,t_0)}{E(t_0)}\right]^{-1} - \frac{1}{\varphi(t,t_0)} \tag{7.49}$$

Using $\varphi(t,t_0) = E(t_0)\,J(t,t_0) - 1$, (7.48) and (7.49) initially result in $E_a = [E(t_0) - R(t,t_0)]/\varphi(t,t_0)$. If we enter this expression into (7.47) and use (7.46) and $\sigma(t_0) = c_1E(t_0)$, then

$$\sigma(t) = \sigma(t_0) + [E(t_0) - R(t,t_0)](c_2 - c_1) \tag{7.50}$$

for $t \geq t_0$, i. e. the asserted linear variation of $\sigma(t)$ with $R(t,t_0)$. If we use (7.50) together with (7.46), it follows from (7.40) that

$$c_1 + c_2[E(t_0)\,J(t,t_0) - 1] = J(t,t_0)\,\sigma(t_0) - (c_2 - c_1)\int_{t_0}^{t} J(t,\tau)\frac{\partial R(\tau,t_0)}{\partial \tau}\mathrm{d}\tau$$

and by rearranging it follows that

$$(c_2 - c_1)\left[1 - E(t_0)\,J(t,t_0) - \int_{t_0}^{t} J(t,\tau)\frac{\partial R(\tau,t_0)}{\partial \tau}\mathrm{d}\tau\right] = 0 \tag{7.51}$$

As the expression in the square brackets on the left in (7.51) disappears according to (7.44), the equations (7.47) to (7.49) apply for any value of c_1 and c_2.

Using typical assumptions for J and R (or φ and E) generally results in ageing coefficients χ in the order of magnitude of about 0.7 to 1; as an average we may assume $\chi = 0.85$.

The assumption (7.46) corresponds to linear combinations of the cases $\sigma(t) = \text{const}$ and $\varepsilon_\sigma(t) = \text{const}$ shown in normalised form in Fig. 7.13. The majority of strain histories can therefore be at least approximated with this. In the light of the inherent uncertainties in the assumptions for J and R (or φ and E), using (7.48) leads to a practical, simple method [2], [37].

Example 7.1 Time-independent restraint

A prismatic, initially stress-free homogeneous bar undergoes the subsequent restraint $\varepsilon_\sigma(0)$ at time $t_0 = 0$ corresponding to $\sigma(0) = E(0)\varepsilon_\sigma(0)$. Eq. (7.47), using $\Delta\varepsilon_\sigma(t) = 0$ and (7.48), supplies

$$\frac{\Delta\sigma(t)[1 + \chi(t)\,\varphi(t)]}{E(0)} + \frac{\sigma(0)\,\varphi(t)}{E(0)} = 0$$

and therefore

$$\sigma(t) = \sigma(0) + \Delta\sigma(t) = \sigma(0)\left[1 - \frac{\varphi(t)}{1 + \chi(t)\,\varphi(t)}\right]$$

The creep considerably reduces the time-independent restraint.

Example 7.2 Time-dependent restraint

The time-independent restraint examined in example 7.1 can be caused, for example, by a single support displacement. A time-dependent restraint affecting the system which is initially free from stress and strain is considered below. This restraint is caused by a gradual support displacement, e. g. settlement, and it is assumed that this exhibits an identical chronological progression to that of the creep, i. e. $\Delta\varepsilon_\sigma(t) = \varepsilon_\sigma(t) = \varepsilon_{\sigma,\infty}\,\varphi(t)/\varphi_\infty$. Using (7.47) and (7.48), it follows that

$$\sigma(t) = \Delta\sigma(t) = \frac{\varepsilon_{\sigma,\infty}E(0)\varphi(t)}{\varphi_\infty[1 + \chi(t)\,\varphi(t)]}$$

The creep gives rise to a much lower value for the time-dependent restraint than is the case with purely elastic behaviour.

Example 7.3 Prestressing

If a prestressing force (compressive force) P, which is assumed to be constant, acts on the bar with cross-sectional area A used in examples 7.1 and 7.2, then on the one hand, with $t = 0$ we get a time-independent restraint $\varepsilon_\sigma(0) = -P/(EA)$, and on the other, a time-dependent restraint where $\varepsilon_{\sigma,\infty} = \varphi_\infty\,\varepsilon_\sigma(0) = \varphi_\infty\,\sigma(0)/E(0)$.

By combining the solutions for $\sigma(t)$ from the two examples above, it follows that

$$\sigma(t) = \sigma(0)\left[1 - \frac{\varphi(t)}{1 + \chi(t)\,\varphi(t)}\right] + \sigma(0)\frac{\varphi(t)}{1 + \chi(t)\,\varphi(t)} = \sigma(0)$$

As assumed, the sum of the two components remains constant, $\sigma(0) = -P/A = \text{const}$.

Example 7.4 Loss of prestress

In reality, owing to the shortening of the bar caused by creep, the concrete bar (with cross-sectional area A_c and modulus of elasticity $E_c(0) = E_c$) considered below experiences a loss of prestress ΔP in the tendon (with cross-sectional area A_p and modulus of elasticity E_p) embedded in and rigidly bonded to the concrete. Added to this is the influence of the shrinkage $\varepsilon_s(t) = \varepsilon_{cs}(t)$.

The prestressing force P_0 at time $t = 0$ causes a normal strain $\varepsilon_{p0} = P_0/(E_pA_p)$ in the tendon and a normal strain $\varepsilon_{c0} = -P_0/(E_cA_c)$ in the concrete, see Fig. 7.14.

The difference in the strains $\varepsilon_{p0} - \varepsilon_{c0}$ subsequently remains constant because of the rigid bond, i. e. we get the compatibility condition

$$\varepsilon_p(t) - \varepsilon_c(t) = \varepsilon_{p0} - \varepsilon_{c0} = \frac{P_0(1 + \rho n)}{E_pA_p} = \text{const}$$

where $\rho = A_p/A_c$ denotes the *geometric reinforcement ratio* and $n = E_p/E_c$ is the *modular ratio* between the material of the tendon and the concrete.

The following applies at time t

$$\varepsilon_c(t) = \varepsilon_{c0}[1 + \varphi(t)] + \frac{\Delta P}{E_cA_c}[1 + \chi(t)\,\varphi(t)] + \varepsilon_{cs}(t) \quad , \quad \varepsilon_p(t) = \frac{P_0 - \Delta P}{E_pA_p}$$

Substituting this in the above compatibility condition results in

$$\frac{\Delta P(t)}{P_0} = \frac{n\rho\left[\varphi(t) + \dfrac{\varepsilon_{cs}(t)}{\varepsilon_{c0}}\right]}{1 + n\rho[1 + \chi(t)\,\varphi(t)]}$$

It can be seen that both $\varepsilon_{cs}(t)$ and ε_{c0} are negative, i. e. the loss of prestress increases as a consequence of the shrinkage.

Using $\rho = 0.5\,\%$, $n = 6$, $\varphi(\infty) = 2$, $\varepsilon_{cs} = -0.4\,‰$, $\varepsilon_{c0} = -0.2\,‰$ and $\chi(\infty) = 0.85$, the ratio is $\Delta P(\infty)/P_0 = 11.1\,\%$, for example.

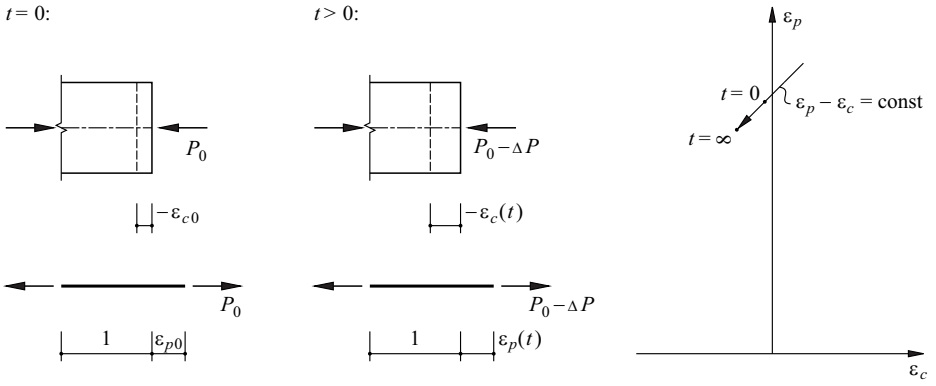

Fig. 7.14 Concentrically prestressed concrete bar

The deliberations up to now were confined to uniaxial stress and strain states. If we presume isotropic behaviour with a constant POISSON's ratio ν, then it is possible to deal with general three-dimensional stress and strain states according to (7.48), (7.2) and (7.5), e. g. using the *age-adjusted effective shear* and *bulk moduli*

$$G_a(t, t_0) = \frac{G(t_0)}{1 + \chi(t, t_0)\, \varphi(t, t_0)} \quad , \quad K_a(t, t_0) = \frac{K(t_0)}{1 + \chi(t, t_0)\, \varphi(t, t_0)} \tag{7.52}$$

7.5 Thermal deformations

If we confine ourselves to *thermally homogeneous* and *isotropic* materials and presume proportionality between changes in temperature and the associated deformations, then

$$\varepsilon = \alpha_T T \tag{7.53}$$

where α_T denotes the *coefficient of thermal expansion* and T the *change in temperature* (rise = positive) related to a certain initial temperature. Appendix A3 gives typical values for α_T.

According to (7.53), thermal actions lead solely to changes in volume without changes in form, i. e. $\varepsilon_1 = \varepsilon_2 = \varepsilon_3 = \alpha_T T$.

In bar cross-sections, general temperature distributions normally lead to *residual stresses* (see section 13.2.5), and in statically indeterminate systems thermal actions generally cause *restraints* (see section 16.3.3).

Changes to the mechanical and thermal properties of a structure (especially losses of strength and stiffness), in some instances very distinctive, can be expected at elevated temperatures, e. g. as caused by a fire. The deformations and restraints due to fires can reach considerable proportions.

7.6 Fatigue

7.6.1 General

It is normally necessary to investigate the *fatigue behaviour* of structures subjected to road, rail or crane loads, or vibrations. The frequent repetition of loads can cause cumulative and irreversible changes to the microstructure of a material, which corresponds to increasing *deterioration* and, ultimately, to *fracture*, similar to applying a single, steadily increasing (static) load to a brittle material up to failure. The *fatigue resistance* is regarded as the acceptable *stress difference* as a function of the *number of load cycles* and depending on the respective *construction details*.

Most of the knowledge we have about fatigue behaviour comes from tests on uniaxially loaded specimens that are generally subjected to a stress history of

$$\sigma = \sigma_m + \frac{\Delta\sigma}{2}\sin(\omega t) \tag{7.54}$$

(where σ_m = mean stress, $\Delta\sigma$ = stress difference, ω = angular frequency, t = time) carried out until failure occurs at a number of load cycles N_u. We speak of a *single-stage loading*; with a *fluctuating loading*, either $\sigma_m > \Delta\sigma/2$ or $-\sigma_m > \Delta\sigma/2$ applies (special case: *repeated loading*, $|\sigma_m| = \Delta\sigma/2$), and with a *reversed loading*, $-\Delta\sigma/2 < \sigma_m < \Delta\sigma/2$ (special case: fully reversed, $\sigma_m = 0$). In the case of a *multi-stage loading*, either the load is increased step by step, or the specimen is subjected to alternating high and low stresses. And finally, a *fatigue loading* is understood to be the load that occurs stochastically on a construction works.

7.6.2 *S-N* curves

Plotting the number of load cycles to failure N_u reached in fatigue tests with different stress differences $\Delta\sigma$ using a double logarithmic scale produces so-called *S-N curves* (WÖHLER diagrams) , as shown in Fig. 7.15(a). The results of such tests normally exhibit considerable scatter; the number of load cycles to failure N_u can deviate by a

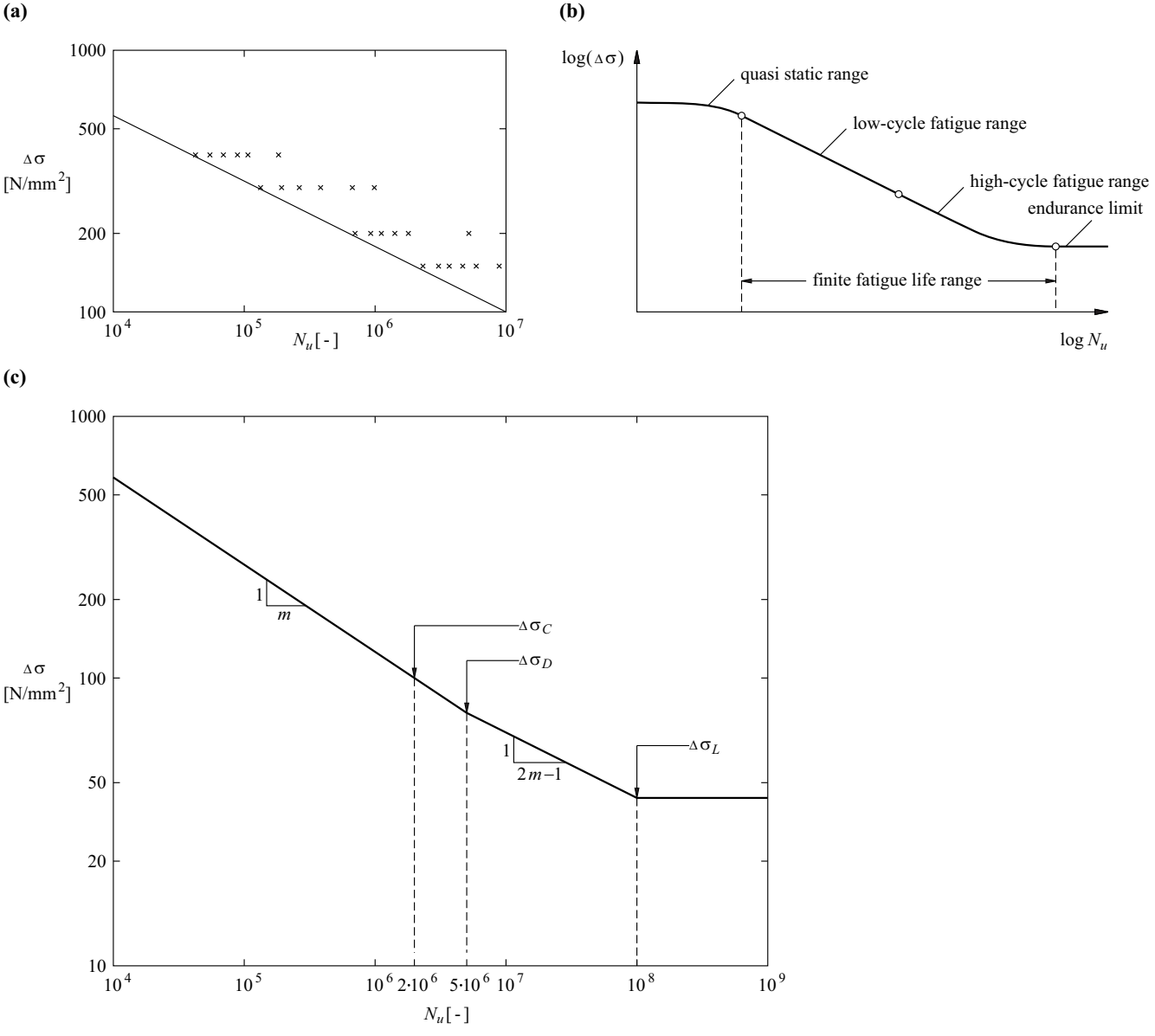

Fig. 7.15 *S-N* curves: (a) test results and evaluation, (b) distinguishing the different ranges, (c) standard fatigue resistance curve

factor of 10 or more with identical stress differences $\Delta\sigma$. *S-N* curves are generally evaluated by fitting straight lines having a certain probability of not being exceeded.

The so-called *finite fatigue life range* in the *S-N* curve is divided into the *low-cycle fatigue range* (about $10^2 < N_u < 10^5$) and the *high-cycle fatigue range* as shown in Fig. 7.15(b). The *endurance limit* is understood to be the stress difference that can be repeated an infinite number of times without causing failure.

The *S-N* curve is normalised for dimensioning purposes, something like that illustrated in Fig. 7.15(c). The *fatigue resistance* $\Delta\sigma_C$ is the stress difference at $2 \cdot 10^6$ load cycles depending on the construction detail or the notch category. The value m describing the slope of the fatigue resistance curve is, for example, $m = 3$ for structural steel, $m = 4$ for reinforcing and prestressing steel. Generally, the nominal endurance limit is assumed to be $5 \cdot 10^6$ load cycles, which with $m = 3$ or 4 leads to a $\Delta\sigma_D$ value of $0.737\Delta\sigma_C$ or $0.795\Delta\sigma_C$. When $N > 5 \cdot 10^6$ load cycles, the fatigue resistance curve continues with a slope of $1:(2m - 1)$ up to $N_u = 10^8$, which with $m = 3$ or 4 corresponds to fatigue resistance *thresholds* of $\Delta\sigma_L = 0.405\Delta\sigma_C$ or $0.518\Delta\sigma_C$.

7.6.3 Damage accumulation under fatigue loads

To reach a conclusion about the deterioration caused by arbitrary fatigue loads we consider a specimen with a cross-sectional area A subjected to a constant normal force difference $\Delta\sigma_0 A$. The deterioration D occurring after N load cycles is such that only a cross-sectional area of $A(1 - D)$ is still effective. The effective stress difference is then

$$\Delta\sigma = \frac{\Delta\sigma_0}{1 - D} \tag{7.55}$$

Assuming that the increase in D with N is proportional to $\Delta\sigma^m$, i. e.

$$\frac{\mathrm{d}D}{\mathrm{d}N} = c\,\Delta\sigma^m \tag{7.56}$$

where c = const, then using (7.55) results in

$$\frac{\mathrm{d}D}{\mathrm{d}N} = \frac{c\,\Delta\sigma_0^m}{(1 - D)^m}$$

from which it follows that

$$-\frac{(1 - D)^{m+1}}{m + 1} = Nc\Delta\sigma_0^m + \text{const}$$

and as $D(0) = 0$ and $D(N_u) = 1$, then

$$N_u = \frac{1}{c(m + 1)\Delta\sigma_0^m} \tag{7.57}$$

and

$$D = 1 - \left(1 - \frac{N}{N_u}\right)^{\frac{1}{m+1}} \tag{7.58}$$

see Fig. 7.16.

Fig. 7.16(a) shows that (7.57) corresponds to a straight *S-N* line with slope $1:m$, and Fig. 7.16(b) shows the D-(N/N_u) relationship (7.58). If m is constant for all values of $\Delta\sigma_0$, the result is a single D-(N/N_u) curve, and therefore the deterioration values for all values of $\Delta\sigma_{0i}$ can be superposed. Where N_i = number of load cycles causing $\Delta\sigma_{0i}$, and N_{ui} = number of load cycles to failure as a result of $\Delta\sigma_{0i}$, then the following applies upon reaching the fatigue failure:

$$\sum \frac{N_i}{N_{ui}} = 1 \tag{7.59}$$

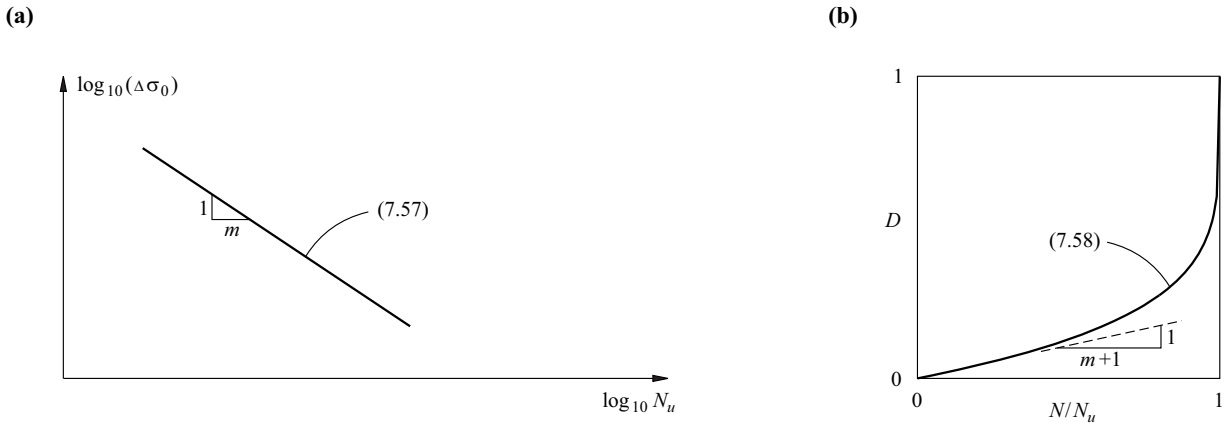

Fig. 7.16 Consequences of the assumptions (7.55) and (7.56): (a) fatigue resistance, (b) deterioration as a function of number of load cycles

Example 7.5 Fatigue of reinforcing steel

Fatigue tests on a reinforcing steel reveal that $1.6 \cdot 10^6$ load cycles at $\Delta\sigma = 150\,\mathrm{N/mm^2}$ lead to failure, whereas at $\Delta\sigma = 300\,\mathrm{N/mm^2}$ the failure occurs earlier, at 10^5 load cycles. (a) How many load cycles at $\Delta\sigma = 200\,\mathrm{N/mm^2}$ would lead to failure? (b) First of all, 10^6 load cycles are applied at $\Delta\sigma = 150\,\mathrm{N/mm^2}$; how many load cycles at $\Delta\sigma = 200\,\mathrm{N/mm^2}$ would then lead to failure?

Where $\log_{10}300 = 2.477$, $\log_{10}150 = 2.176$, $\log_{10}10^5 = 5$ and $\log_{10}(1.6 \cdot 10^6) = 6.204$, we initially obtain

$$m = \frac{6.204 - 5}{2.477 - 2.176} = 4$$

see Fig. 7.17.

(a) From (7.57) it follows that

$$N_u(\Delta\sigma = 200\,\mathrm{N/mm^2}) = 1.6 \cdot 10^6 \cdot \left(\frac{150}{200}\right)^4 = 506\,250$$

(b) According to (7.59),

$$\frac{10^6}{1.6 \cdot 10^6} + \frac{N_{200}}{506\,250} = 1$$

and therefore $N_{200} = 189\,844$. We also notice that according to (7.58), the initial 10^6 load cycles at $\Delta\sigma = 150\,\mathrm{N/mm^2}$ cause a deterioration D of 17.8 %, but already utilise 62.5 % of N/N_u.

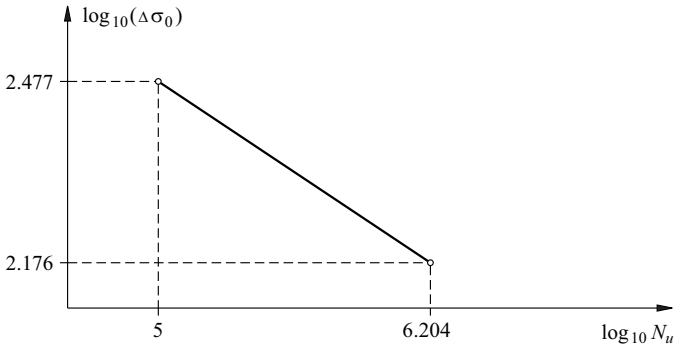

Fig. 7.17 *S-N* curve for example 7.5

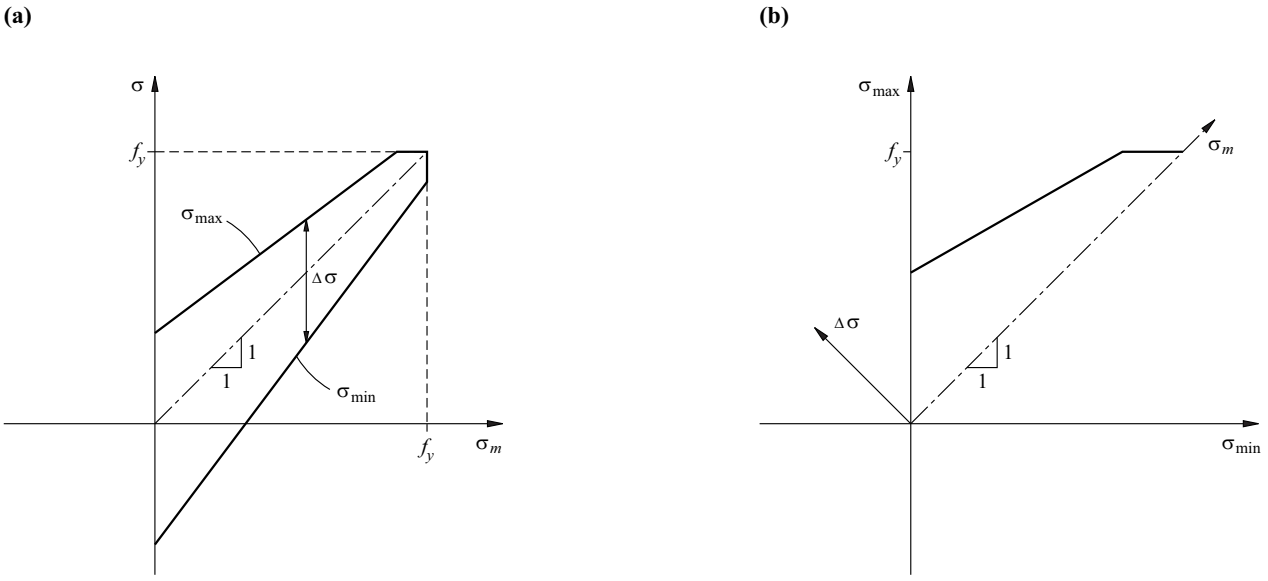

Fig. 7.18 How the mean stress influences the fatigue resistance: (a) SMITH diagram, (b) GOODMAN diagram

Using the *damage accumulation hypothesis* (7.59) named after PALMGREN and MINER presumes that we know the stress differences $\Delta\sigma_{0i}$ and the associated numbers of load cycles N_i in addition to the fatigue resistance $\Delta\sigma_C$ and the slope $1:m$ of the fatigue resistance curve. It is often sufficient to use simplified methods to verify fatigue resistance which show that the ensuing stress differences lie below the endurance limit.

Compared with the stress difference $\Delta\sigma$, the mean stress σ_m according to (7.54) mostly has only a minor influence on the fatigue strength. The dependence of the fatigue resistance on the mean stress (for a certain number of load cycles) can be presented as shown in Fig. 7.18; this dependence should be considered in the flexural compression zones of concrete structures, for instance.

7.7 Summary

1. Constitutive equations are obtained through idealisation based on experimental observations. Load-independent deformations (e. g. due to shrinkage, swelling or thermal actions) must be considered as well as load-dependent deformations.
2. Isotropic linear elastic behaviour can be described by means of two material constants. We normally use the modulus of elasticity and POISSON's ratio. The shear and bulk moduli or the LAMÉ constants can be used as alternatives.
3. The description of perfectly plastic behaviour is based on defining, or assuming, a yield condition, which describes a non-concave (at least weakly convex) non-plastic domain in the stress space.
4. According to the associated flow rule, the plastic strain increments are proportional to the gradient of the yield function. And vice versa, the stresses at the yield surface are equal to the gradient of the dissipation function.
5. The principle of maximum dissipation energy can be postulated as an alternative to presuming a convex yield surface and orthogonal plastic strain increments.
6. The yield conditions of isotropic materials can be presented as a function of the basic invariants of the stress tensor. For incompressible behaviour, the yield surfaces in the principal stress space are cylinders parallel with the hydrostatic axis, e. g. after VON MISES or TRESCA. For compressible behaviour, conical or pyramidal yield surfaces or corresponding generalisations are the result; for applications involving concrete, soil and rock, the COULOMB yield condition is the

favourite in this respect (possibly modified based on RANKINE), but its generalisation according to MOHR also plays a role in isolated cases.

7. The swelling or shrinkage of the material is normally treated as an increase or decrease in volume over time determined by various influences.
8. Creep and relaxation are two related processes which, for practical construction applications, can be described by a creep or relaxation function according to the theory of ageing linear viscoelastic materials; alternatively, the creep coefficient and the modulus of elasticity (as functions of time) can be used as basic variables. Any stress-strain histories can be approximated with good accuracy using the method of the age-modified effective elastic modulus.
9. When it comes to thermal deformations, construction materials are generally regarded as thermally homogeneous and isotropic, with deformations proportional to the change in temperature. In a similar way to shrinkage or swelling, the result is a change in volume only. However, residual stresses generally ensue in bar cross-sections and restraints in statically indeterminate systems.
10. At elevated temperatures, e. g. due to a fire, it is essential to take into account the changes to the material properties compared with their properties in the normal service situations of the construction works.
11. Fatigue behaviour must be investigated in structures that are subjected to repeated loading.
12. The fatigue resistance depends on the number of load cycles and the respective construction details.
13. The influence of fatigue loads can be taken into account via the damage accumulation hypothesis (7.59).
14. It is often sufficient to apply simplified methods to verify fatigue resistance which show that the ensuing stress differences lie below the endurance limit.

7.8 Exercises

7.1 Assuming a linear elastic behaviour ($E = 210\,\mathrm{kN/mm^2}$, $\nu = 0.3$), determine the strains associated with the coplanar stress state of exercise 5.3.

7.2 Using the same assumption as in exercise 7.1, determine the stresses associated with the strains of exercise 6.2. How do these stresses change when we consider a coplanar strain state instead of a coplanar stress state? Compare (8.35) and (8.37).

7.3 Show that in an oedometer test with $\varepsilon_x = \varepsilon_y = 0$, the relationship $\sigma_z = E\varepsilon_z(1 - \nu)/(1 - \nu - 2\nu^2)$ applies when we assume a linear elastic behaviour.

7.4 If a point load Q is applied to a homogeneous, isotropic and incompressible linear elastic half-space (E = const, $\nu = 1/2$), see Fig. 7.19(a), then according to BOUSSINESQ, the only principal stresses not equal to zero are the compressive stresses

$$\sigma_r = -\frac{3Qz}{2\pi r^3}$$

radial to the load Q. Show that the resultant of these stresses (integral over the hemispherical surface with radius r) is in equilibrium with Q.

7.5 Verify (7.7) and (7.8).

7.6 Verify (7.22).

7.7 A stress state is given by the tensor

$$\begin{bmatrix} 1.000 & -0.2041 & -0.3536 \\ -0.2041 & 0.7500 & -0.1443 \\ -0.3536 & -0.1443 & 1.2500 \end{bmatrix} \cdot f_y$$

Determine the principal stresses and their directions, and check whether the TRESCA yield condition has been infringed.

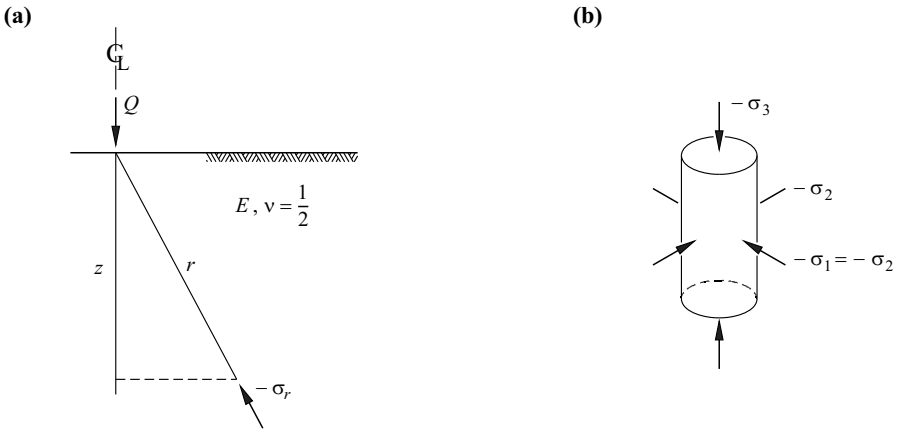

Fig. 7.19 Figures for section 7.8

7.8 Draw a sketch similar to Fig. 7.8(c) using the Cartesian system of coordinates $\sigma_x, \sigma_y, \tau_{xy}$.

7.9 Verify (7.29) and (7.30), and show that the angle OGA in Fig. 7.10(b) is equal to $\arctan(\sin\varphi)$.

7.10 Six triaxial compression tests on cylindrical soil samples according to Fig. 7.19(b) resulted in the failure stress combinations given in Tab. 7.1.
A hydrostatic stress state was initially applied in all tests. The lateral stresses $\sigma_1 = \sigma_2$ were subsequently kept constant, whereas the axial pressure $-\sigma_3$ was increased until failure. Based on the test data, use a regression line to determine the parameters c and φ according to the COULOMB yield condition. Discuss the result with the help of the parameters $p = -(\sigma_1 + \sigma_3)/2$, $q = (\sigma_1 - \sigma_3)/2$ used in soil mechanics.

7.11 Verify the expressions for OA and OB given in connection with Fig. 7.10(c).

7.12 Verify (7.34).

Tab. 7.1 Failure values from triaxial compression tests

Test	1	2	3	4	5	6
$-\sigma_1$ [kN/m^2]	26	33	40	62	78	101
$-\sigma_3$ [kN/m^2]	61	83	101	148	197	252

8 ENERGY METHODS

8.1 Introductory example

8.1.1 Statically determinate system

8.1.1.1 Statics and kinematics

The plane truss shown in Fig. 8.1(a) consists of six straight bars joined together and to wall 13 concentrically via five friction-free hinged joints. The idealisation assumes that the bars are weightless and that loads are applied at the joints only. Such properties are characteristic of an *ideal truss*.

Each joint has two degrees of freedom in the direction of the global axis system X_1, X_2. The support conditions at 1 and 3 mean that the *passive degrees of freedom* V_1, V_2 and V_5, V_6 are omitted, see Fig. 8.1(b). The *active degrees of freedom* V_3, V_4, V_7, V_8, V_9 and V_{10} are combined in one column vector $\boldsymbol{V}$. The corresponding bar extensions v_i are found from

$$\begin{Bmatrix} v_1 \\ v_2 \\ v_3 \\ v_4 \\ v_5 \\ v_6 \end{Bmatrix} = \begin{bmatrix} 1 & 0 & 0 & 0 & 0 & 0 \\ 0 & 0 & \sqrt{2}/2 & \sqrt{2}/2 & 0 & 0 \\ 0 & -1 & 0 & 1 & 0 & 0 \\ -\sqrt{2}/2 & -\sqrt{2}/2 & 0 & 0 & \sqrt{2}/2 & \sqrt{2}/2 \\ 0 & 0 & 1 & 0 & 0 & 0 \\ 0 & 0 & -1 & 0 & 1 & 0 \end{bmatrix} \begin{Bmatrix} V_3 \\ V_4 \\ V_7 \\ V_8 \\ V_9 \\ V_{10} \end{Bmatrix}$$

or in concise form

$$\boldsymbol{v} = \boldsymbol{a} \bullet \boldsymbol{V} \tag{8.1}$$

where the deformation variables v, V can be assumed to be infinitesimally small according to first-order theory.

Fig. 8.1(c) shows the loads Q_j corresponding to the active degrees of freedom V_j, which are numbered consecutively and combined in one column vector $\boldsymbol{Q}$. The figure also shows the forces in the bars s_i corresponding to the bar extensions v_i, which as tensile forces are regarded as positive. For equilibrium of the three unsupported joints, considered individually as free bodies,

$$\begin{Bmatrix} Q_3 \\ Q_4 \\ Q_7 \\ Q_8 \\ Q_9 \\ Q_{10} \end{Bmatrix} = \begin{bmatrix} 1 & 0 & 0 & -\sqrt{2}/2 & 0 & 0 \\ 0 & 0 & -1 & -\sqrt{2}/2 & 0 & 0 \\ 0 & \sqrt{2}/2 & 0 & 0 & 1 & -1 \\ 0 & \sqrt{2}/2 & 1 & 0 & 0 & 0 \\ 0 & 0 & 0 & \sqrt{2}/2 & 0 & 1 \\ 0 & 0 & 0 & \sqrt{2}/2 & 0 & 0 \end{bmatrix} \begin{Bmatrix} s_1 \\ s_2 \\ s_3 \\ s_4 \\ s_5 \\ s_6 \end{Bmatrix}$$

or in concise form

$$\boldsymbol{Q} = \boldsymbol{a}^{\mathrm{T}} \bullet \boldsymbol{s} \tag{8.2}$$

The columns of the *kinematic transformation matrix* $\boldsymbol{a}$ contain the bar extensions v_i as a result of unit displacements $V_j = 1$ on the otherwise undeformed system. Starting with a *kinematically determinate basic system* with all joints restrained ($V_1 = V_2 = ... = V_n = 0$), we obtain $\boldsymbol{a}$ column by column by imposing $V_j = 1$. It is important to note that the degree of static indeterminacy of the system is irrelevant.

Theory of Structures. First Edition. Peter Marti

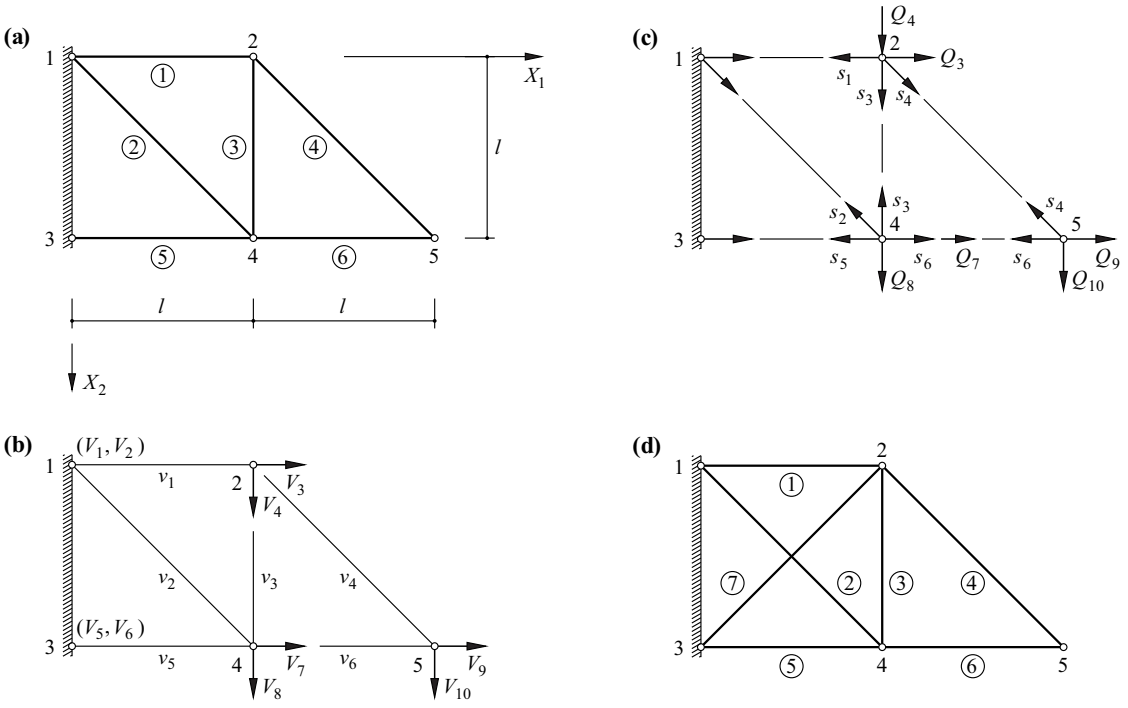

Fig. 8.1 Plane, ideal truss: (a) system and notation, (b) deformation variables, (c) force variables, (d) system with one degree of internal static indeterminacy

The equilibrium matrix above, which turns out to be $\boldsymbol{a}^{\mathrm{T}}$, is obtained row by row through joint equilibrium conditions in the direction of Q_j. In this case (which is a statically determinate, stable system), the equilibrium matrix is square and invertible, i. e. has an inverse matrix and therefore

$$\begin{Bmatrix} s_1 \\ s_2 \\ s_3 \\ s_4 \\ s_5 \\ s_6 \end{Bmatrix} = \begin{bmatrix} 1 & 0 & 0 & 0 & 0 & 1 \\ 0 & \sqrt{2} & 0 & \sqrt{2} & 0 & \sqrt{2} \\ 0 & -1 & 0 & 0 & 0 & -1 \\ 0 & 0 & 0 & 0 & 0 & \sqrt{2} \\ 0 & -1 & 1 & -1 & 1 & -2 \\ 0 & 0 & 0 & 0 & 1 & -1 \end{bmatrix} \begin{Bmatrix} Q_3 \\ Q_4 \\ Q_7 \\ Q_8 \\ Q_9 \\ Q_{10} \end{Bmatrix}$$

or in concise form

$$\boldsymbol{s} = \boldsymbol{b} \bullet \boldsymbol{Q} \tag{8.3}$$

Similarly to (8.2), $\boldsymbol{b}^{\mathrm{T}}$ provides the transition from $\boldsymbol{v}$ to $\boldsymbol{V}$

$$\begin{Bmatrix} V_3 \\ V_4 \\ V_7 \\ V_8 \\ V_9 \\ V_{10} \end{Bmatrix} = \begin{bmatrix} 1 & 0 & 0 & 0 & 0 & 0 \\ 0 & \sqrt{2} & -1 & 0 & -1 & 0 \\ 0 & 0 & 0 & 0 & 1 & 0 \\ 0 & \sqrt{2} & 0 & 0 & -1 & 0 \\ 0 & 0 & 0 & 0 & 1 & 1 \\ 1 & \sqrt{2} & -1 & \sqrt{2} & -2 & -1 \end{bmatrix} \begin{Bmatrix} v_1 \\ v_2 \\ v_3 \\ v_4 \\ v_5 \\ v_6 \end{Bmatrix}$$

or in concise form

$$\boldsymbol{V} = \boldsymbol{b}^{\mathrm{T}} \bullet \boldsymbol{v} \tag{8.4}$$

The transpose $\boldsymbol{b}^{\mathrm{T}}$ of the *static transformation matrix* $\boldsymbol{b}$, which is equal to the inverse matrix of $\boldsymbol{a}$ ($\boldsymbol{b}^{\mathrm{T}} = \boldsymbol{a}^{-1}$) for the statically determinate system, is obtained column by column by imposing $v_i = 1$, similarly to $\boldsymbol{a}$ by imposing $V_j = 1$.

8.1.1.2 Linear elasticity

Bar forces and bar extensions are combined with each other through the linear elastic relationships

$$s_i = \left(\frac{EA}{l}\right)_i v_i = k_i v_i \quad , \quad v_i = \left(\frac{l}{EA}\right)_i s_i = f_i s_i$$

which can be expressed in the form

$$\boldsymbol{s} = \boldsymbol{k} \bullet \boldsymbol{v} \quad , \quad \boldsymbol{v} = \boldsymbol{f} \bullet \boldsymbol{s} \tag{8.5}$$

when the *stiffnesses* $k_i = (EA/l)_i$ or the *flexibilities* $f_i = (l/EA)_i$ are arranged as elements of corresponding diagonal matrices $\boldsymbol{k}$ or $\boldsymbol{f}$. Combining equations (8.2), $(8.5)_1$ and (8.1) results in

$$\boldsymbol{Q} = \boldsymbol{a}^{\mathrm{T}} \bullet \boldsymbol{k} \bullet \boldsymbol{a} \bullet \boldsymbol{V} = \boldsymbol{K} \bullet \boldsymbol{V} \tag{8.6}$$

and combining equations (8.4), $(8.5)_2$ and (8.3) results in

$$\boldsymbol{V} = \boldsymbol{b}^{\mathrm{T}} \bullet \boldsymbol{f} \bullet \boldsymbol{b} \bullet \boldsymbol{Q} = \boldsymbol{F} \bullet \boldsymbol{Q} \tag{8.7}$$

where $\boldsymbol{K} = \boldsymbol{a}^{\mathrm{T}} \bullet \boldsymbol{k} \bullet \boldsymbol{a}$ designates the *global stiffness matrix* congruent to $\boldsymbol{k}$, and $\boldsymbol{F} = \boldsymbol{b}^{\mathrm{T}} \bullet \boldsymbol{f} \bullet \boldsymbol{b}$ the *global flexibility matrix* congruent to $\boldsymbol{f}$.

8.1.2 Statically indeterminate system

Adding a seventh bar as shown in Fig. 8.1(d) turns the system into one with one degree of static indeterminacy. Eq. (8.1) is still valid, but $\boldsymbol{a}$ is now a (7×6) matrix:

$$\begin{Bmatrix} v_1 \\ v_2 \\ v_3 \\ v_4 \\ v_5 \\ v_6 \\ v_7 \end{Bmatrix} = \begin{bmatrix} 1 & 0 & 0 & 0 & 0 & 0 \\ 0 & 0 & \sqrt{2}/2 & \sqrt{2}/2 & 0 & 0 \\ 0 & -1 & 0 & 1 & 0 & 0 \\ -\sqrt{2}/2 & -\sqrt{2}/2 & 0 & 0 & \sqrt{2}/2 & \sqrt{2}/2 \\ 0 & 0 & 1 & 0 & 0 & 0 \\ 0 & 0 & -1 & 0 & 1 & 0 \\ \sqrt{2}/2 & -\sqrt{2}/2 & 0 & 0 & 0 & 0 \end{bmatrix} \begin{Bmatrix} V_3 \\ V_4 \\ V_7 \\ V_8 \\ V_9 \\ V_{10} \end{Bmatrix}$$

Eq. (8.2) also continues to apply, but as $\boldsymbol{a}^{\mathrm{T}}$ is not square, there is no inverse matrix; there is a *row deficit* of one for determining the seven forces in the bars:

$$\begin{Bmatrix} Q_3 \\ Q_4 \\ Q_7 \\ Q_8 \\ Q_9 \\ Q_{10} \end{Bmatrix} = \begin{bmatrix} 1 & 0 & 0 & -\sqrt{2}/2 & 0 & 0 & \sqrt{2}/2 \\ 0 & 0 & -1 & -\sqrt{2}/2 & 0 & 0 & -\sqrt{2}/2 \\ 0 & \sqrt{2}/2 & 0 & 0 & 1 & -1 & 0 \\ 0 & \sqrt{2}/2 & 1 & 0 & 0 & 0 & 0 \\ 0 & 0 & 0 & \sqrt{2}/2 & 0 & 1 & 0 \\ 0 & 0 & 0 & \sqrt{2}/2 & 0 & 0 & 0 \end{bmatrix} \begin{Bmatrix} s_1 \\ s_2 \\ s_3 \\ s_4 \\ s_5 \\ s_6 \\ s_7 \end{Bmatrix}$$

According to the *force method*, a constraint is now released, e. g. by cutting through bar 7, which turns the system into a *statically determinate basic system*. We introduce a *statically indeterminate force variable* (*redundant variable*) X at this point in order to eliminate the *incompatibility* caused by $\boldsymbol{Q}$ and thus ensure compatibility. The known matrix $\boldsymbol{b}$ for the basic system is expanded by one row for s_7 and by one column for X, i. e.

$$\begin{Bmatrix} s_1 \\ s_2 \\ s_3 \\ s_4 \\ s_5 \\ s_6 \\ s_7 \end{Bmatrix} = \begin{bmatrix} 1 & 0 & 0 & 0 & 0 & 1 & -\sqrt{2}/2 \\ 0 & \sqrt{2} & 0 & \sqrt{2} & 0 & \sqrt{2} & 1 \\ 0 & -1 & 0 & 0 & 0 & -1 & -\sqrt{2}/2 \\ 0 & 0 & 0 & 0 & 0 & \sqrt{2} & 0 \\ 0 & -1 & 1 & -1 & 1 & -2 & -\sqrt{2}/2 \\ 0 & 0 & 0 & 0 & 1 & -1 & 0 \\ 0 & 0 & 0 & 0 & 0 & 0 & 1 \end{bmatrix} \begin{Bmatrix} Q_3 \\ Q_4 \\ Q_7 \\ Q_8 \\ Q_9 \\ Q_{10} \\ X \end{Bmatrix}$$

or in concise form

$$\boldsymbol{s} = \boldsymbol{b}_0 \bullet \boldsymbol{Q} + \boldsymbol{b}_1 \bullet \boldsymbol{X} \tag{8.8}$$

where matrix $\boldsymbol{b}_1$ and vector $\boldsymbol{X}$ represent the general case with several redundant variables X_k. The *compatibility condition* for the severed bar 7 (no incompatibility) is

$$\{-\sqrt{2}/2 \quad 1 \quad -\sqrt{2}/2 \quad 0 \quad -\sqrt{2}/2 \quad 0 \quad 1\} \begin{Bmatrix} v_1 \\ v_2 \\ v_3 \\ v_4 \\ v_5 \\ v_6 \\ v_7 \end{Bmatrix} = 0$$

or in concise form

$$\boldsymbol{b}_1^{\mathrm{T}} \bullet \boldsymbol{v} = \boldsymbol{0} \tag{8.9}$$

which again represents the general case. Using $(8.5)_2$ and (8.8), we therefore obtain

$$\boldsymbol{b}_1^{\mathrm{T}} \bullet \boldsymbol{v} = \boldsymbol{b}_1^{\mathrm{T}} \bullet \boldsymbol{f} \bullet \boldsymbol{s} = \boldsymbol{b}_1^{\mathrm{T}} \bullet \boldsymbol{f} \bullet \boldsymbol{b}_0 \bullet \boldsymbol{Q} + \boldsymbol{b}_1^{\mathrm{T}} \bullet \boldsymbol{f} \bullet \boldsymbol{b}_1 \bullet \boldsymbol{X} = \boldsymbol{0}$$

from which it follows that

$$\boldsymbol{X} = -\boldsymbol{F}_{11}^{-1} \bullet \boldsymbol{F}_{10} \bullet \boldsymbol{Q} \qquad (\boldsymbol{F}_{10} = \boldsymbol{b}_1^{\mathrm{T}} \bullet \boldsymbol{f} \bullet \boldsymbol{b}_0 \quad , \quad \boldsymbol{F}_{11} = \boldsymbol{b}_1^{\mathrm{T}} \bullet \boldsymbol{f} \bullet \boldsymbol{b}_1) \tag{8.10}$$

Subsituting (8.10) into (8.8) and comparing with (8.3) results in

$$\boldsymbol{b} = \boldsymbol{b}_0 - \boldsymbol{b}_1 \bullet \boldsymbol{F}_{11}^{-1} \bullet \boldsymbol{F}_{10} \tag{8.11}$$

and therefore from (8.4), $(8.5)_2$ and (8.8), taking into account the definition of $\boldsymbol{F}_{10}$ and the symmetry of $\boldsymbol{F}_{11}$, we get

$$\boldsymbol{V} = \boldsymbol{F} \bullet \boldsymbol{Q} \quad , \quad \boldsymbol{F} = \boldsymbol{F}_{00} - \boldsymbol{F}_{10}^{\mathrm{T}} \bullet \boldsymbol{F}_{11}^{-1} \bullet \boldsymbol{F}_{10} \qquad (\boldsymbol{F}_{00} = \boldsymbol{b}_0^{\mathrm{T}} \bullet \boldsymbol{f} \bullet \boldsymbol{b}_0) \tag{8.12}$$

Summing up, the force method requires the matrices $\boldsymbol{b}_0$, $\boldsymbol{b}_1$ and $\boldsymbol{f}$ to be set up for the given loads $\boldsymbol{Q}$. The displacements $\boldsymbol{V}$ follow from $(8.12)_1$ with the global flexibility matrix $\boldsymbol{F}$ defined in $(8.12)_2$ and the expressions for $\boldsymbol{F}_{00}$, $\boldsymbol{F}_{10}$ and $\boldsymbol{F}_{11}$ given in (8.12) and (8.10).

According to the *displacement method* (deformation method), we proceed as for statically determinate systems when dealing with statically indeterminate systems. Setting up the matrices $\boldsymbol{a}$ and $\boldsymbol{k}$ and subsequently inverting (8.6) results in $\boldsymbol{V} = \boldsymbol{K}^{-1} \bullet \boldsymbol{Q}$, and (8.1) and $(8.5)_1$ supply the internal deformation and force variables $\boldsymbol{v}$ and $\boldsymbol{s}$.

8.1.3 Work equation

Comparing (8.1), (8.2) or (8.3), (8.4) with (A5.18), (A5.21) shows that the kinematic variables $\boldsymbol{v}$, $\boldsymbol{V}$ and the static variables $\boldsymbol{s}$, $\boldsymbol{Q}$ undergo a *contragredient* transformation; $\boldsymbol{s}^{\mathrm{T}} \bullet \boldsymbol{v} = \boldsymbol{Q}^{\mathrm{T}} \bullet \boldsymbol{V}$ applies, i. e.

$$\boldsymbol{Q}^{\mathrm{T}} \bullet \boldsymbol{V} - \boldsymbol{s}^{\mathrm{T}} \bullet \boldsymbol{v} = 0 \tag{8.13}$$

This relationship is valid for any system irrespective of the material behaviour. Furthermore, different static and kinematic states $\boldsymbol{Q}_1$, $\boldsymbol{s}_1$ or $\boldsymbol{V}_2$, $\boldsymbol{v}_2$ may be involved. All that is required for these is that they are *in equilibrium* in themselves in accordance with (8.2) or (8.3), or are *compatible* according to (8.1) or (8.4):

$$\boldsymbol{Q}_1^{\mathrm{T}} \bullet \boldsymbol{V}_2 - \boldsymbol{s}_1^{\mathrm{T}} \bullet \boldsymbol{v}_2 = 0 \tag{8.14}$$

The two terms in (8.14) correspond to the *deformation work* of the *external* and *internal force variables* of state 1 done on the corresponding deformation variables of state 2:

$$W = W_e + W_i = 0 \quad , \quad W_e = \boldsymbol{Q}_1^{\mathrm{T}} \bullet \boldsymbol{V}_2 \quad , \quad W_i = -\boldsymbol{s}_1^{\mathrm{T}} \bullet \boldsymbol{v}_2 \tag{8.15}$$

According to the so-called *work equation* (8.14) or (8.15), the force variables of a state of equilibrium on the whole do no work on the deformation variables of a compatible deformation state.

8.1.4 Commentary

Combining (8.2) and (8.3) or (8.4) and (8.1) shows that the following identity applies:

$$\boldsymbol{a}^{\mathrm{T}} \bullet \boldsymbol{b} = \boldsymbol{b}^{\mathrm{T}} \bullet \boldsymbol{a} = \mathbf{I} \tag{8.16}$$

Owing to the *congruence transformation* with the $(m \times n)$ matrix $\boldsymbol{a}$ and the symmetric $(m \times m)$ matrix $\boldsymbol{k}$ $(\boldsymbol{k}^{\mathrm{T}} = \boldsymbol{k})$, the global stiffness matrix $\boldsymbol{K} = \boldsymbol{a}^{\mathrm{T}} \bullet \boldsymbol{k} \bullet \boldsymbol{a}$ defined by $(8.6)_2$ is square of order n and symmetric $(\boldsymbol{K}^{\mathrm{T}} = \boldsymbol{a}^{\mathrm{T}} \bullet \boldsymbol{k}^{\mathrm{T}} \bullet \boldsymbol{a} = \boldsymbol{a}^{\mathrm{T}} \bullet \boldsymbol{k} \bullet \boldsymbol{a} = \boldsymbol{K})$. Likewise, owing to the congruence transformation with the $(m \times n)$ matrix $\boldsymbol{b}$ and the symmetric $(m \times m)$ matrix $\boldsymbol{f}$ $(\boldsymbol{f}^{\mathrm{T}} = \boldsymbol{f})$, the global flexibility matrix $\boldsymbol{F} = \boldsymbol{b}^{\mathrm{T}} \bullet \boldsymbol{f} \bullet \boldsymbol{b}$ defined by $(8.7)_2$ is square of order n and symmetric $(\boldsymbol{F}^{\mathrm{T}} = \boldsymbol{b}^{\mathrm{T}} \bullet \boldsymbol{f}^{\mathrm{T}} \bullet \boldsymbol{b} = \boldsymbol{b}^{\mathrm{T}} \bullet \boldsymbol{f} \bullet \boldsymbol{b} = \boldsymbol{F})$.

If we consider only active degrees of freedom and associated external deformation and force variables in $\boldsymbol{V}$ and $\boldsymbol{Q}$, then $\boldsymbol{K}$ and $\boldsymbol{F}$ are invertible ($\det \boldsymbol{K} \neq 0$ and $\det \boldsymbol{F} \neq 0$) and positive definite ($\boldsymbol{V}^{\mathrm{T}} \bullet \boldsymbol{K} \bullet \boldsymbol{V} > 0$ and $\boldsymbol{Q}^{\mathrm{T}} \bullet \boldsymbol{F} \bullet \boldsymbol{Q} > 0$). It is also possible to include the passive degrees of freedom in $\boldsymbol{V}$, in which case $\boldsymbol{K}$ is singular ($\det \boldsymbol{K} = 0$) and positive semi-definite ($\boldsymbol{V}^{\mathrm{T}} \bullet \boldsymbol{K} \bullet \boldsymbol{V} = 0$); the nullity d of $\boldsymbol{K}$ corresponds here to the number of possible *rigid body deformations* of the system released from its support conditions. Contrasting with this, rigid body deformations must always be ruled out when determining $\boldsymbol{b}$ and $\boldsymbol{F}$ because otherwise equilibrium would be impossible.

The scalar product $\boldsymbol{V}^{\mathrm{T}} \bullet \boldsymbol{Q} = \boldsymbol{Q}^{\mathrm{T}} \bullet \boldsymbol{V}$ in (8.13) is equal to the quadratic forms $\boldsymbol{V}^{\mathrm{T}} \bullet \boldsymbol{K} \bullet \boldsymbol{V}$ or $\boldsymbol{Q}^{\mathrm{T}} \bullet \boldsymbol{F} \bullet \boldsymbol{Q}$ in the case of linear elastic behaviour according to (8.6) or (8.7). These expressions correspond to the doubled *active work* of the external force variables (loads) $\boldsymbol{Q}$ done on the external deformation variables (displacements) $\boldsymbol{V}$ they cause.

8.2 Variables and operators

8.2.1 Introduction

The example examined in section 8.1 introduced a number of basic concepts that will be referred to again in various ways in the next sections. It was possible to describe fully the structural behaviour of the system with just a few *work-associated force and deformation variables*, i. e. the internal variables s_i, v_i and the external variables Q_i, V_i at the discrete joints. Fig. 8.2 provides an overview of these variables and the transformations between them. The top part of the figure corresponds to the purely static considerations, the bottom part the purely kinematic (force or displacement method). This scheme forms the basis for the so-called *discontinua* (discretised structural models), see sections 9.3 and 17.1 to 17.3, also chapter 19.

The variables for *continua* and the operators that link them are discussed below with reference to the static, kinematic and constitutive relationships discussed in chapters 5 to 7. In doing so we make use of various results that will not be discussed in detail until chapters 13, 23 and 24. Fig. 8.3 shows a scheme similar to that of Fig. 8.2 which relates to a *model space* with volume V and surface area S according to Fig. 8.4.

The *external force variables* – i. e. forces whose reactions, according to the reaction principle, are applied outside V (see sections 5.1.1 and 5.1.3) – are divided into *loads* $\boldsymbol{q}$ (related to V) and the *boundary stresses* t specified on S_t (related to S). These are in equilibrium with the *internal force variables*, the *stresses* $\boldsymbol{\sigma}$:

$$\boldsymbol{q} = \boldsymbol{D}_s \bullet \boldsymbol{\sigma} \quad , \quad \boldsymbol{t} = \boldsymbol{T} \bullet \boldsymbol{\sigma} \tag{8.17}$$

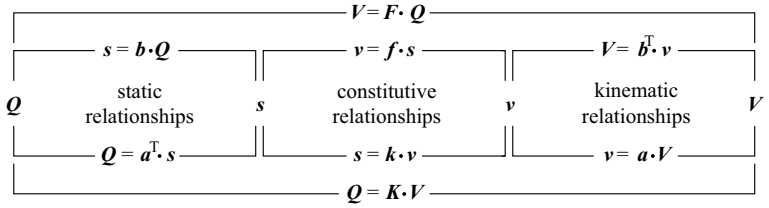

Fig. 8.2 Variables and transformations for discontinua

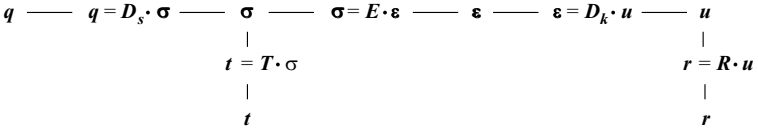

Fig. 8.3 Variables and operators for continua

The *static operator* $\boldsymbol{D_s}$ and the *boundary stress operator* $\boldsymbol{T}$ are matrices formed by differential operators and numbers.

The *external deformation variables* corresponding to $\boldsymbol{q}$ and $\boldsymbol{t}$ are the *displacements* $\boldsymbol{u}$ and the *boundary displacements* $\boldsymbol{r}$ specified on S_r. The displacements are compatible with the *internal deformation variables*, the *strains* $\boldsymbol{\varepsilon}$ and with the boundary displacements:

$$\boldsymbol{\varepsilon} = \boldsymbol{D_k} \bullet \boldsymbol{u} \quad , \quad \boldsymbol{r} = \boldsymbol{R} \bullet \boldsymbol{u} \tag{8.18}$$

The *kinematic operator* $\boldsymbol{D_k}$ and the *boundary displacement operator* $\boldsymbol{R}$, like $\boldsymbol{D_s}$ and $\boldsymbol{T}$, are matrices formed by differential operators and numbers.

Stresses and strains are combined by the *constitutive equations*, in the case of linear elastic behaviour by

$$\boldsymbol{\sigma} = \boldsymbol{\sigma}_0 + \boldsymbol{E} \bullet (\boldsymbol{\varepsilon} - \boldsymbol{\varepsilon}_0) \tag{8.19}$$

where $\boldsymbol{E}$ is the (symmetric) *elasticity matrix* and $\boldsymbol{\sigma}_0$ and $\boldsymbol{\varepsilon}_0$ are the *initial stresses* and *initial strains*.

The work equation (8.14) or (8.15) becomes

$$W = \int \boldsymbol{q}_1^{\mathrm{T}} \bullet \boldsymbol{u}_2 \, \mathrm{d}V + \int \boldsymbol{t}_1^{\mathrm{T}} \bullet \boldsymbol{r}_2 \, \mathrm{d}S - \int \boldsymbol{\sigma}_1^{\mathrm{T}} \bullet \boldsymbol{\varepsilon}_2 \, \mathrm{d}V = 0 \tag{8.20}$$

The generally three-dimensional model space becomes two-dimensional for plate and shell structures and one-dimensional for framed structures (see section 5.1.7). In these cases, V corresponds to the middle surface of plate and shell structures or the bar axis of framed structures, and S the edge of the structure or end-points of the structure. The reduction in the number of dimensions is compensated for by adapting the force variables appropriately. Body loads become surface or line loads, boundary stresses become length-related or effective boundary forces, and stresses become length-related or effective internal forces. It should also be remembered that moments can occur as force variables in addition to forces; the work-associated displacement and strain variables are then rotations and curvatures as well as twists.

Owing to the reduction in the number of dimensions for V and the need to take moments into account, the elasticity matrix $\boldsymbol{E}$ normally also contains parameters dependent on the cross-section as well as those dependent on the material.

It is often possible to assume that certain strain components are negligible, i. e. we consider the structural behaviour to be *rigid* when subjected to corresponding stress components of any magnitude; for example, we speak of bars that are *inextensible* or are *rigid in shear* (= have infinite shear stiffness) when the deformations corresponding to the normal or shear force can be neglected. And vice versa, it is also possible to assume that certain stress components are negligible; we then speak of a *flexible* behaviour in this context, e. g. a flexible cable that is unable to accommodate any bending moments. In both cases, the corresponding rows and columns disappear from the elasticity matrix. The *stiff* behaviour lying between the limit cases of infinitely large and negligibly small stiffness corresponds to the standard case and normally does not require any special consideration unless we want to emphasize that, for example, in bars or slabs with finite shear stiffness (= flexible in shear), an idealisation with infinite shear stiffness (the normal case) is not being assumed.

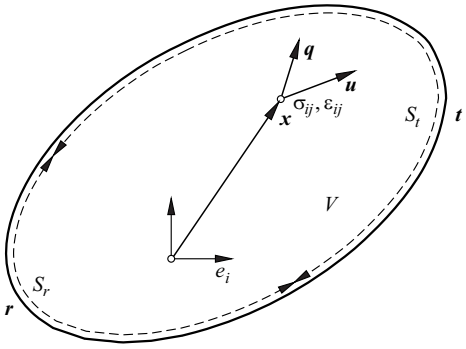

Fig. 8.4 Model space and variables for continua

In contrast to *resistant*, the designation flexible is also used in the context of perfectly plastic behaviour to indicate that certain stress components or internal force variables are neglected. For example, we speak of *torsionless* or *torsion-resistant* behaviour depending on whether torques are ignored or included.

8.2.2 Plane framed structures

8.2.2.1 Bars with finite shear stiffness

Fig. 8.5(a) shows a differential element of a framed structure lying in the xz plane. Equilibrium of forces in the x and z directions plus equilibrium of moments about the y axis results in

$$\boldsymbol{q} = \begin{Bmatrix} q_x \\ q_z \\ m_y \end{Bmatrix} = \begin{bmatrix} -\mathrm{d}_x & 0 & 0 \\ 0 & -\mathrm{d}_x & 0 \\ 0 & 1 & -\mathrm{d}_x \end{bmatrix} \begin{Bmatrix} N \\ V \\ M \end{Bmatrix} = \boldsymbol{D_s} \bullet \boldsymbol{\sigma} \tag{8.21}$$

where $\mathrm{d}_x = \mathrm{d}/\mathrm{d}x$. On the internal forces side, the *line loads* q_x, q_z and the *line load moment* m_y (all related to a unit length of the bar) correspond to the *normal force* N, the *shear force* V and the *bending moment* $M_y = M$. In the case of the moment equilibrium condition, the contribution of $\mathrm{d}V$ disappears because it is small of a higher order compared with the other values.

Fig. 8.5(b) shows the kinematic relationships corresponding to Fig. 8.5(a). Every point on the bar axis x experiences a displacement u in the x direction and a displacement w in the z direction. The associated cross-section originally perpendicular to the bar axis is rotated through an angle φ about the y axis and the element of length $\mathrm{d}x = \rho\mathrm{d}\varphi$ undergoes – besides a normal strain and a curvature – a *mean shear strain* γ combined with a corresponding change to the initially 90° angle between bar axis and cross-sectional areas. Assuming infinitesimally small deformations, the *normal strain* on the bar axis is $\varepsilon = \mathrm{d}_x u$, the shear strain is $\gamma = \varphi + \mathrm{d}_x w$ and the *curvature* is $\chi = 1/\rho = \mathrm{d}_x\varphi$ (where ρ = radius of curvature), i. e.

$$\boldsymbol{\varepsilon} = \begin{Bmatrix} \varepsilon \\ \gamma \\ \chi \end{Bmatrix} = \begin{bmatrix} \mathrm{d}_x & 0 & 0 \\ 0 & \mathrm{d}_x & 1 \\ 0 & 0 & \mathrm{d}_x \end{bmatrix} \begin{Bmatrix} u \\ w \\ \varphi \end{Bmatrix} = \boldsymbol{D_k} \bullet \boldsymbol{u} \tag{8.22}$$

As can be seen, apart from the sign of the (odd) differential operators d_x, $\boldsymbol{D_k}$ is equal to the transpose of $\boldsymbol{D_s}$ in (8.21).

The linear elastic constitutive equations (see sections 13.2.1 and 13.3.1) are

$$\boldsymbol{\sigma} = \begin{Bmatrix} N \\ V \\ M \end{Bmatrix} = \begin{bmatrix} EA & 0 & 0 \\ 0 & GA_v & 0 \\ 0 & 0 & EI \end{bmatrix} \begin{Bmatrix} \varepsilon \\ \gamma \\ \chi \end{Bmatrix} = \boldsymbol{E} \bullet \boldsymbol{\varepsilon} \tag{8.23}$$

where E is the modulus of elasticity, $G = E/[2(1 + \nu)]$ the shear modulus (where ν = POISSON's ratio), A the *cross-sectional area*, $A_v = \alpha_v A$ the *shear area* (where α_v = *area shear factor*) and $I = I_y$, the *moment of inertia* related to the principal axis of the cross-section y.

Using the variables $\boldsymbol{\sigma}$ and $\boldsymbol{u}$ introduced above, the boundary stress and boundary displacement operators $\boldsymbol{T}$ and $\boldsymbol{R}$ given in $(8.17)_2$ and $(8.18)_2$ are found to be identity matrices $\mathbf{I}$.

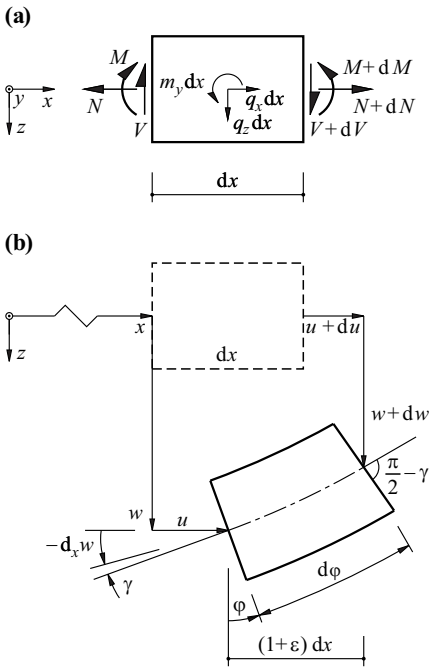

Fig. 8.5 Differential element of a plane framed structure: (a) statics, (b) kinematics

8.2.2.2 Bars rigid in shear

The theory of bars with *finite shear stiffness* dealt with up to now is named after TIMOSHENKO. The shear strains γ are often neglected according to a hypothesis formulated by Jacob BERNOULLI, i. e. we use the theory of bars that are *rigid in shear.* As $\gamma = \varphi + d_x w = 0$, φ depends on w. Instead of (8.22) we get

$$\boldsymbol{\varepsilon} = \begin{Bmatrix} \varepsilon \\ \chi \end{Bmatrix} = \begin{bmatrix} d_x & 0 \\ 0 & -d_x^2 \end{bmatrix} \begin{Bmatrix} u \\ w \end{Bmatrix} = \boldsymbol{D_k} \bullet \boldsymbol{u} \tag{8.24}$$

One consequence of the $\gamma = 0$ hypothesis is that m_y disappears from (8.21); $V = d_x M + m_y$ applies and (8.21) becomes

$$\boldsymbol{q} = \begin{Bmatrix} q_x \\ q_z \end{Bmatrix} = \begin{bmatrix} -d_x & 0 \\ 0 & -d_x^2 \end{bmatrix} \begin{Bmatrix} N \\ M \end{Bmatrix} = \boldsymbol{D_s} \bullet \boldsymbol{\sigma} \tag{8.25}$$

Again, apart from the sign of d_x, $\boldsymbol{D_k}$ is equal to the transpose of $\boldsymbol{D_s}$; V and φ remain as possible boundary specifications, $\boldsymbol{T}$ and $\boldsymbol{R}$ become (3×2) matrices, and the corresponding terms $d_x M$ or $-d_x w$ appear:

$$\boldsymbol{t} = \begin{bmatrix} 1 & 0 \\ 0 & d_x \\ 0 & 1 \end{bmatrix} \begin{Bmatrix} N \\ M \end{Bmatrix} \quad , \quad \boldsymbol{r} = \begin{bmatrix} 1 & 0 \\ 0 & 1 \\ 0 & -d_x \end{bmatrix} \begin{Bmatrix} u \\ w \end{Bmatrix}$$

Finally, $\boldsymbol{E}$ in (8.23) is reduced by the row for V and the column for γ.

8.2.2.3 Signs of elements of $\boldsymbol{D_s}$ and $\boldsymbol{D_k}$

If we switch from the differential equation $\varepsilon = d_x u$ in (8.24) to finite differences, then the function values u_i at the equidistant points $x = i\Delta$ ($i = 0, 1, \ldots, n$) result in the approximations $\varepsilon_i = (u_i - u_{i-1})/\Delta$, from the first differences, or in concise form $\Delta\boldsymbol{\varepsilon} = \boldsymbol{a} \bullet \boldsymbol{u}$, where the coefficients -1 and 1 occur along the diagonals in the $[n\times(n+1)]$ matrix $\boldsymbol{a}$, see (8.1). On the other hand, joint equilibrium results in $\Delta q_{x,i} = -(N_i - N_{i-1})$, or in concise form $\Delta\boldsymbol{q_x} = \boldsymbol{a}^{\mathrm{T}} \bullet \boldsymbol{N}$, where the coefficients 1 and -1 occur along the diagonals in the $[(n+1)\times n]$ matrix $\boldsymbol{a}^{\mathrm{T}}$, see (8.2):

$$\boldsymbol{a} = \begin{bmatrix} -1 & 1 & & & & \\ & -1 & 1 & & & \\ & & \cdot & \cdot & & \\ & & & \cdot & \cdot & \\ & & & & \cdot & \cdot \\ & & & & -1 & 1 \end{bmatrix} \quad , \quad \boldsymbol{a}^{\mathrm{T}} = \begin{bmatrix} -1 & & & & & \\ 1 & -1 & & & & \\ & \cdot & \cdot & & & \\ & & \cdot & \cdot & & \\ & & & \cdot & \cdot & \\ & & & & \cdot & \cdot \\ & & & & & 1 \end{bmatrix}$$

This is the reason for the negative sign in the differential equation $q_x = -d_x N$ in (8.25).

Similarly, instead of $\chi = -d_x^2 w$ in (8.24), we get the approximations $\chi_i = (-w_{i-1} + 2w_i - w_{i+1})/\Delta^2$ from the second differences, or in concise form $\Delta^2\boldsymbol{\chi} = \boldsymbol{a} \bullet \boldsymbol{w}$, with the coefficients -1, 2 and -1 along the diagonals of the matrix $\boldsymbol{a}$. On the other hand, joint equilibrium results in $q_{zi}\Delta = (M_i - M_{i-1})/\Delta - (M_{i+1} - M_i)/\Delta$, or in concise form $\Delta^2\boldsymbol{q_z} = \boldsymbol{a}^{\mathrm{T}} \bullet \boldsymbol{M} = \boldsymbol{a} \bullet \boldsymbol{M}$:

$$\boldsymbol{a} = \boldsymbol{a}^{\mathrm{T}} = \begin{bmatrix} \cdot & \cdot & & & & \\ \cdot & \cdot & \cdot & & & \\ & -1 & 2 & -1 & \cdot & \\ & & -1 & 2 & -1 & \\ & & & \cdot & \cdot & \cdot \\ & & & & \cdot & \cdot \end{bmatrix}$$

This is the reason why the same (negative) sign occurs in the differential equation $q_z = -d_x^2 M$ in (8.25) as in the corresponding differential equation $\chi = -d_x^2 w$ in (8.24).

It appears that $\boldsymbol{D_k} = \boldsymbol{D_s}^{\mathrm{T}}$ ($\boldsymbol{D_k} = -\boldsymbol{D_s}^{\mathrm{T}}$) generally applies for even (odd) differential operators as elements of $\boldsymbol{D_k}$ and $\boldsymbol{D_s}$.

8.2.3 Spatial framed structures

Fig. 8.6 summarises the variables that occur with spatial framed structures (see also Fig. 5.15). The following variables occur in addition to those for plane framed structures: line loads q_y and line load moments m_x, m_z; shear forces V_y, *torques* T and bending moments M_z; shear strains γ_y (= γ_{yx}), *twists* ϑ and curvatures χ_z; displacements v and *rotations* φ_x, φ_z. The non-indexed variables M, χ, φ and V, γ (= γ_{zx}) for plane framed structures are given the index y or z.

In generalising (8.21), considering equilibrium at the bar element results in

$$\boldsymbol{q} = \begin{Bmatrix} q_x \\ q_y \\ q_z \\ m_x \\ m_y \\ m_z \end{Bmatrix} = \begin{bmatrix} -\mathrm{d}_x & 0 & 0 & 0 & 0 & 0 \\ 0 & -\mathrm{d}_x & 0 & 0 & 0 & 0 \\ 0 & 0 & -\mathrm{d}_x & 0 & 0 & 0 \\ 0 & 0 & 0 & -\mathrm{d}_x & 0 & 0 \\ 0 & 0 & 1 & 0 & -\mathrm{d}_x & 0 \\ 0 & -1 & 0 & 0 & 0 & -\mathrm{d}_x \end{bmatrix} \begin{Bmatrix} N \\ V_y \\ V_z \\ T \\ M_y \\ M_z \end{Bmatrix} = \boldsymbol{D_s} \bullet \boldsymbol{\sigma} \tag{8.26}$$

and taking into account $\gamma_y = -\varphi_z + \mathrm{d}_x v$, $\gamma_z = \varphi_y + \mathrm{d}_x w$ instead of (8.22) results in

$$\boldsymbol{\varepsilon} = \begin{Bmatrix} \varepsilon \\ \gamma_y \\ \gamma_z \\ \vartheta \\ \chi_y \\ \chi_z \end{Bmatrix} = \begin{bmatrix} \mathrm{d}_x & 0 & 0 & 0 & 0 & 0 \\ 0 & \mathrm{d}_x & 0 & 0 & 0 & -1 \\ 0 & 0 & \mathrm{d}_x & 0 & 1 & 0 \\ 0 & 0 & 0 & \mathrm{d}_x & 0 & 0 \\ 0 & 0 & 0 & 0 & \mathrm{d}_x & 0 \\ 0 & 0 & 0 & 0 & 0 & \mathrm{d}_x \end{bmatrix} \begin{Bmatrix} u \\ v \\ w \\ \varphi_x \\ \varphi_y \\ \varphi_z \end{Bmatrix} = \boldsymbol{D_k} \bullet \boldsymbol{u} \tag{8.27}$$

Again, apart from the sign of d_x, $\boldsymbol{D_k}$ is equal to the transpose of $\boldsymbol{D_s}$. Finally, instead of (8.23), the following applies:

$$\boldsymbol{\sigma} = \begin{Bmatrix} N \\ V_y \\ V_z \\ T \\ M_y \\ M_z \end{Bmatrix} = \begin{bmatrix} EA & 0 & 0 & 0 & 0 & 0 \\ 0 & GA_{vy} & 0 & 0 & 0 & 0 \\ 0 & 0 & GA_{vz} & 0 & 0 & 0 \\ 0 & 0 & 0 & GI_x & 0 & 0 \\ 0 & 0 & 0 & 0 & EI_y & 0 \\ 0 & 0 & 0 & 0 & 0 & EI_z \end{bmatrix} \begin{Bmatrix} \varepsilon \\ \gamma_y \\ \gamma_z \\ \vartheta \\ \chi_y \\ \chi_z \end{Bmatrix} = \boldsymbol{E} \bullet \boldsymbol{\varepsilon} \tag{8.28}$$

where I_x is the *torsion constant*. Again, the variables $\boldsymbol{\sigma}$ and $\boldsymbol{u}$ introduced here mean that $\boldsymbol{T}$ und $\boldsymbol{R}$ become identity matrices $\mathbf{I}$.

For bars in three dimensions rigid in shear, where $\gamma_y = -\varphi_z + \mathrm{d}_x v = 0$ and $\gamma_z = \varphi_y + \mathrm{d}_x w = 0$ as well as $m_z = -V_y - \mathrm{d}_x M_z = 0$ and $m_y = V_z - \mathrm{d}_x M_y = 0$, the generalisation of (8.24) results in

$$\boldsymbol{\varepsilon} = \begin{Bmatrix} \varepsilon \\ \vartheta \\ \chi_y \\ \chi_z \end{Bmatrix} = \begin{bmatrix} \mathrm{d}_x & 0 & 0 & 0 \\ 0 & 0 & 0 & \mathrm{d}_x \\ 0 & 0 & -\mathrm{d}_x^2 & 0 \\ 0 & \mathrm{d}_x^2 & 0 & 0 \end{bmatrix} \begin{Bmatrix} u \\ v \\ w \\ \varphi_x \end{Bmatrix} = \boldsymbol{D_k} \bullet \boldsymbol{u} \tag{8.29}$$

and the generalisation of (8.25) results in

$$\boldsymbol{q} = \begin{Bmatrix} q_x \\ q_y \\ q_z \\ m_x \end{Bmatrix} = \begin{bmatrix} -\mathrm{d}_x & 0 & 0 & 0 \\ 0 & 0 & 0 & \mathrm{d}_x^2 \\ 0 & 0 & -\mathrm{d}_x^2 & 0 \\ 0 & -\mathrm{d}_x & 0 & 0 \end{bmatrix} \begin{Bmatrix} N \\ T \\ M_y \\ M_z \end{Bmatrix} = \boldsymbol{D_s} \bullet \boldsymbol{\sigma} \tag{8.30}$$

Once again, apart from the sign of d_x, $\boldsymbol{D_k}$ is equal to the transpose of $\boldsymbol{D_s}$. V_y, V_z and φ_y, φ_z remain as possible boundary specifications; $\boldsymbol{T}$ and $\boldsymbol{R}$ become (6×4) matrices, and the corresponding terms $-\mathrm{d}_x M_z$, $\mathrm{d}_x M_y$ or $-\mathrm{d}_x w$, $\mathrm{d}_x v$ appear. Finally, $\boldsymbol{E}$ is obtained from (8.28) by deleting the rows for V_y, V_z and the columns for γ_y, γ_z.

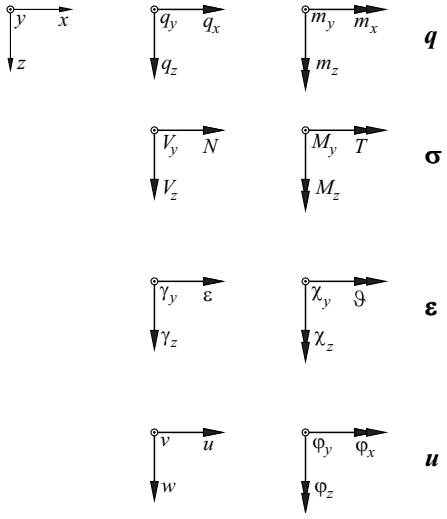

Fig. 8.6 Variables for spatial framed structures

8.2.4 Coplanar stress states

The plate element shown in Fig. 8.7(a) is assumed to be subjected to a constant *coplanar stress state* ($\sigma_z = \tau_{zy} = \tau_{zx} = 0$) over the depth h in the z direction, see sections 5.1.7.2 and 5.2.3. The remaining stress components σ_x, σ_y and $\tau_{xy} = \tau_{yx}$ correspond to the *in-plane forces* (membrane forces) $n_x = h\sigma_x$, $n_y = h\sigma_y$, $n_{xy} = n_{yx} = h\tau_{xy}$ according to (5.14). Equilibrium of forces in the x and y directions calls for

$$n_{ij,j} + q_i = 0 \tag{8.31}$$

or rather

$$\boldsymbol{q} = \begin{Bmatrix} q_x \\ q_y \end{Bmatrix} = \begin{bmatrix} -\partial_x & 0 & -\partial_y \\ 0 & -\partial_y & -\partial_x \end{bmatrix} \begin{Bmatrix} n_x \\ n_y \\ n_{xy} \end{Bmatrix} = \boldsymbol{D_s} \bullet \boldsymbol{\sigma} \tag{8.32}$$

From Fig. 8.7(b) it can be seen that with the displacement components u, v, the normal strains ε_x, ε_y and the shear strain γ_{xy} are given by

$$\boldsymbol{\varepsilon} = \begin{Bmatrix} \varepsilon_x \\ \varepsilon_y \\ \gamma_{xy} \end{Bmatrix} = \begin{bmatrix} \partial_x & 0 \\ 0 & \partial_y \\ \partial_y & \partial_x \end{bmatrix} \begin{Bmatrix} u \\ v \end{Bmatrix} = \boldsymbol{D_k} \bullet \boldsymbol{u} \tag{8.33}$$

where $\boldsymbol{D_k}$ is the negative transpose of $\boldsymbol{D_s}$, see (6.4) and (6.5).

As $\sigma_z = \tau_{zy} = \tau_{zx} = 0$, inverting the general linear elastic relationship

$$\boldsymbol{\varepsilon} = \begin{Bmatrix} \varepsilon_x \\ \varepsilon_y \\ \varepsilon_z \\ \gamma_{yz} \\ \gamma_{zx} \\ \gamma_{xy} \end{Bmatrix} = \frac{1}{E} \begin{bmatrix} 1 & -\nu & -\nu & 0 & 0 & 0 \\ -\nu & 1 & -\nu & 0 & 0 & 0 \\ -\nu & -\nu & 1 & 0 & 0 & 0 \\ 0 & 0 & 0 & 2(1+\nu) & 0 & 0 \\ 0 & 0 & 0 & 0 & 2(1+\nu) & 0 \\ 0 & 0 & 0 & 0 & 0 & 2(1+\nu) \end{bmatrix} \begin{Bmatrix} \sigma_x \\ \sigma_y \\ \sigma_z \\ \tau_{yz} \\ \tau_{zx} \\ \tau_{xy} \end{Bmatrix} = \boldsymbol{E}^{-1} \bullet \boldsymbol{\sigma} \tag{8.34}$$

according to (7.1) and (7.3), taking into account integration over h, results in

$$\boldsymbol{\sigma} = \begin{Bmatrix} n_x \\ n_y \\ n_{xy} \end{Bmatrix} = \frac{Eh}{1-\nu^2} \begin{bmatrix} 1 & \nu & 0 \\ \nu & 1 & 0 \\ 0 & 0 & \dfrac{1-\nu}{2} \end{bmatrix} \begin{Bmatrix} \varepsilon_x \\ \varepsilon_y \\ \gamma_{xy} \end{Bmatrix} = \boldsymbol{E} \bullet \boldsymbol{\varepsilon} \tag{8.35}$$

We also get $\varepsilon_z = -\nu(n_x + n_y)/(Eh)$, which generally corresponds to a certain variation in the depth of the plate and hence, strictly speaking, certain shear strains γ_{yz}, γ_{zx} and the associated stresses τ_{yz}, τ_{zx}, i. e. the stress state is only approximately planar. However, such effects may be neglected in plates that are thin in relation to their dimensions in the planar directions.

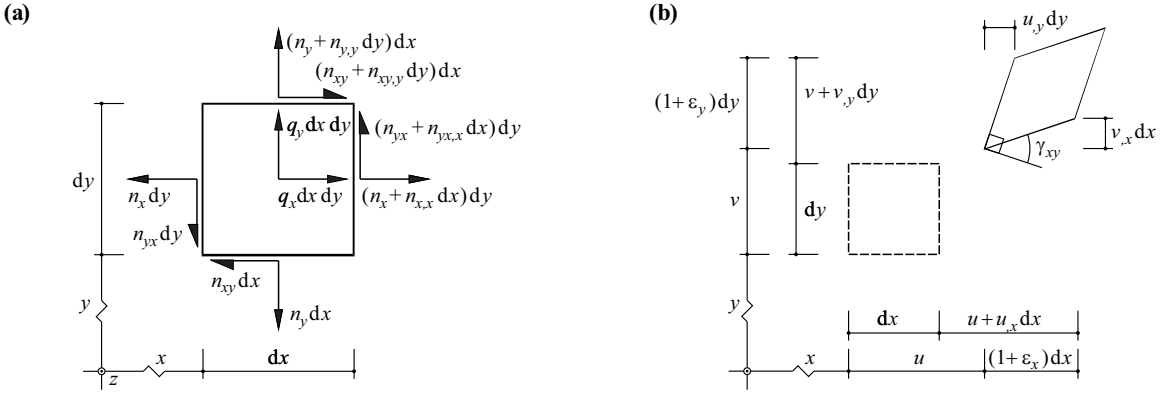

Fig. 8.7 Differential plate element: (a) statics, (b) kinematics

At an edge inclined at an angle of α to the y axis, *edge forces* occur with the components $n_x\cos\alpha + n_{xy}\sin\alpha$ and $n_{yx}\cos\alpha + n_y\sin\alpha$ in the x and y directions, where α is regarded as positive for rotation about the positive z axis. The edge force components normal and tangential to the edge are equal to $n_x\cos^2\alpha + n_y\sin^2\alpha + 2n_{xy}\sin\alpha\cos\alpha$ and $(n_y - n_x)\sin\alpha\cos\alpha + n_{xy}(\cos^2\alpha - \sin^2\alpha)$, see (5.21).

8.2.5 Coplanar strain state

When $\varepsilon_z = 0$, eq. (8.34) initially results in $\sigma_z = \nu(\sigma_x + \sigma_y)$ and therefore

$$\varepsilon_x = \frac{1+\nu}{E}\left[(1-\nu)\sigma_x - \nu\sigma_y\right] \quad , \quad \varepsilon_y = \frac{1+\nu}{E}\left[-\nu\sigma_x + (1-\nu)\sigma_y\right] \tag{8.36}$$

Considering $\gamma_{xy} = \tau_{xy}/G$ and inverting results in

$$\boldsymbol{\sigma} = \begin{Bmatrix} \sigma_x \\ \sigma_y \\ \tau_{xy} \end{Bmatrix} = \frac{E}{(1+\nu)(1-2\nu)} \begin{bmatrix} 1-\nu & \nu & 0 \\ \nu & 1-\nu & 0 \\ 0 & 0 & \dfrac{1-2\nu}{2} \end{bmatrix} \begin{Bmatrix} \varepsilon_x \\ \varepsilon_y \\ \gamma_{xy} \end{Bmatrix} = \boldsymbol{E} \bullet \boldsymbol{\varepsilon} \tag{8.37}$$

8.2.6 Slabs

The differential slab element shown in Fig. 8.8(a) is loaded by the surface load q perpendicular to its plane, i. e. in the z direction The depth of the slab h is presumed to be small in comparison with the dimensions in the plane of the slab, meaning that, as an approximation, we can assume a coplanar stress state varying (linearly) over h. In addition, all deformations are assumed to be infinitesimally small, which means that the equilibrium conditions according to first-order theory may be formulated on the undeformed system.

The *shear forces* related to the length v_x, v_y according to (5.15) are regarded as positive if they act in the positive (negative) z direction on the positive (negative) side of the section, i. e. correspond to positive shear stresses τ_{zx} or τ_{zy} according to section 5.2.4. The *bending moments* m_x, m_y and the *twisting moments* $m_{xy} = m_{yx}$ according to (5.16), also related to the length, are positive when they correspond to positive (negative) stresses σ_x, σ_y, $\tau_{xy} = \tau_{yx}$ in the lower (upper) half of the slab.

Equilibrium of forces in the z direction and equilibrium of moments about the y and x axes for the element in Fig. 8.8(a) calls for

$$q + v_{i,i} = 0 \quad , \quad -m_{ij,j} + v_i = 0 \tag{8.38}$$

or

$$\boldsymbol{q} = \begin{Bmatrix} q \\ 0 \\ 0 \end{Bmatrix} = \begin{bmatrix} 0 & 0 & 0 & -\partial_x & -\partial_y \\ -\partial_x & 0 & -\partial_y & 1 & 0 \\ 0 & -\partial_y & -\partial_x & 0 & 1 \end{bmatrix} \begin{Bmatrix} m_x \\ m_y \\ m_{xy} \\ v_x \\ v_y \end{Bmatrix} = \boldsymbol{D_s} \bullet \boldsymbol{\sigma} \tag{8.39}$$

when, as usual, we ignore variables that are small of a higher order and when the symmetry of the moment tensor is exploited ($m_{xy} = m_{yx}$).

Fig. 8.8(b) indicates the *deflection* w of a point P in the middle plane of a slab for a section y = const. A point P_ζ linked with point P at a distance of ζ is displaced – owing to the inclination $w_{,x}$ of the middle surface of the slab – by an amount $\zeta w_{,x}$ in the negative x direction when normals to the middle surface of the slab remain straight and orthogonal to the middle surface during the deformation. If a mean shear strain $\gamma_x = \gamma_{zx}$ corresponding to the shear force v_x is taken into consideration, the cross-section rotates through an angle $\varphi_x = \gamma_x - w_{,x}$ (given by the slope of the straight line $P'P_\zeta'$) about the y axis. In total, point P_ζ undergoes a displacement $u(\zeta) = \zeta(\gamma_x - w_{,x})$ in the x direction and a similar displacement $v(\zeta) = \zeta(\gamma_y - w_{,y})$

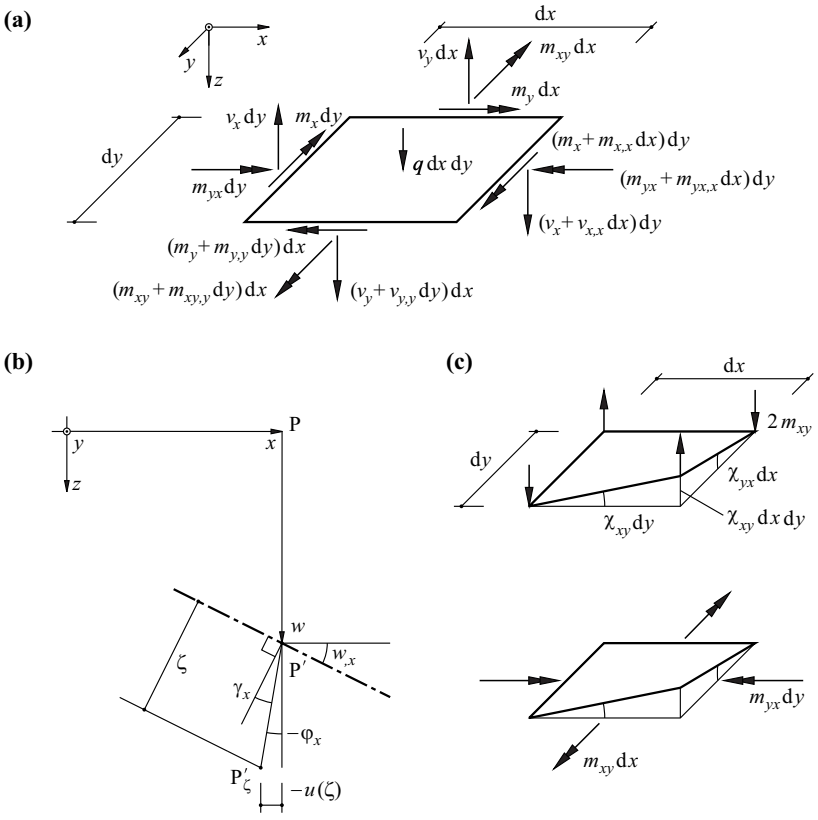

Fig. 8.8 Differential slab element: (a) statics, (b) kinematics, (c) twists and twisting moments

in the y direction. The corresponding strains $\varepsilon_x = u_{,x}$, $\varepsilon_y = v_{,y}$, $\gamma_{xy} = u_{,y} + v_{,x}$ are proportional to ζ and depend on the derivatives of φ_x and φ_y:

$$\varepsilon_x = \zeta\,\varphi_{x,x} = \zeta\,\chi_x \quad , \quad \varepsilon_y = \zeta\,\varphi_{y,y} = \zeta\,\chi_y$$
$$\gamma_{xy} = \zeta(\varphi_{x,y} + \varphi_{y,x}) = \zeta\,2\chi_{xy} \tag{8.40}$$

Using the *curvatures* χ_x, χ_y, the doubled *twist* $2\chi_{xy}$ and the *mean shear strains* γ_x, γ_y as variables corresponding to the generalised stresses in (8.39), we get

$$\boldsymbol{\varepsilon} = \begin{Bmatrix} \chi_x \\ \chi_y \\ 2\chi_{xy} \\ \gamma_x \\ \gamma_y \end{Bmatrix} = \begin{bmatrix} 0 & \partial_x & 0 \\ 0 & 0 & \partial_y \\ 0 & \partial_y & \partial_x \\ \partial_x & 1 & 0 \\ \partial_y & 0 & 1 \end{bmatrix} \begin{Bmatrix} w \\ \varphi_x \\ \varphi_y \end{Bmatrix} = \boldsymbol{D_k} \bullet \boldsymbol{u} \tag{8.41}$$

The factor of 2 that appears in conjunction with χ_{xy} can be easily verified with the help of Fig. 8.8(c). The twists $\chi_{xy} = \chi_{yx}$ correspond to rotations $\chi_{xy}\,dy$, $\chi_{yx}\,dx$ related to the lengths of an infinitesimal element at which the moments $m_{xy}dx$, $m_{yx}dy$ together do the elementary deformation work $2m_{xy}\chi_{xy}dx\,dy$. In the upper drawing, the twisting moments are replaced by statically equivalent *corner forces* $2m_{xy}$ in accordance with the observations in section 24.1.2.5; as expected, the only one of the four forces whose point of application is displaced also does the aforementioned elementary deformation work on the displacement $\chi_{xy}\,dx\,dy$.

Using

$$m_{ij} = \int_{-h/2}^{h/2} \sigma_{ij}\,\zeta\,d\zeta \tag{8.42}$$

and (8.40) and (8.35), with $h = 1$ in the latter, we get the following linear elastic constitutive equation

$$\boldsymbol{\sigma_m} = \begin{Bmatrix} m_x \\ m_y \\ m_{xy} \end{Bmatrix} = \frac{Eh^3}{12(1-\nu^2)} \begin{bmatrix} 1 & \nu & 0 \\ \nu & 1 & 0 \\ 0 & 0 & \dfrac{1-\nu}{2} \end{bmatrix} \begin{Bmatrix} \chi_x \\ \chi_y \\ 2\chi_{xy} \end{Bmatrix} = \boldsymbol{E_m} \bullet \boldsymbol{\varepsilon_m} \tag{8.43}$$

for the slab moments. By considering

$$v_i = \int_{-h/2}^{h/2} \tau_{zi} \mathrm{d}\zeta \tag{8.44}$$

and applying (8.34), the above relationships are completed for the slab shear forces by the corresponding equations

$$\boldsymbol{\sigma_v} = \begin{Bmatrix} v_x \\ v_y \end{Bmatrix} = \frac{Eh^3}{12(1-\nu^2)} \begin{bmatrix} \dfrac{6(1-\nu)}{h^2} & 0 \\ 0 & \dfrac{6(1-\nu)}{h^2} \end{bmatrix} \begin{Bmatrix} \gamma_x \\ \gamma_y \end{Bmatrix} = \boldsymbol{E_v} \bullet \boldsymbol{\varepsilon_v} \tag{8.45}$$

If we consider an area shear factor of 5/6 according to section 13.3.1, the factors of 6 in the elasticity matrix $\boldsymbol{E_v}$ are replaced by 5.

At the edges of the slab, it is possible to specify the deflection w and the rotations φ parallel with and perpendicular to the edge. On the static side, these variables correspond to the shear force and the bending and twisting moments parallel with and perpendicular to the edge of the slab.

Neglecting the shear strains γ_x, γ_y means that the rotations φ_x, φ_y – as independent external deformation variables – can be omitted; $\varphi_x = -w_{,x}$, $\varphi_y = -w_{,y}$ applies and (8.41) can be simplified to

$$\boldsymbol{\varepsilon} = \begin{Bmatrix} \chi_x \\ \chi_y \\ 2\chi_{xy} \end{Bmatrix} = \begin{bmatrix} -\partial_{xx} \\ -\partial_{yy} \\ -2\partial_{xy} \end{bmatrix} \{w\} = \boldsymbol{D_k} \bullet \boldsymbol{u} \tag{8.46}$$

and instead of (8.39) we get

$$\boldsymbol{q} = \{q\} = [\, -\partial_{xx} \quad -\partial_{yy} \quad -2\partial_{xy}\,] \begin{Bmatrix} m_x \\ m_y \\ m_{xy} \end{Bmatrix} = \boldsymbol{D_s} \bullet \boldsymbol{\sigma} \tag{8.47}$$

Eq. (8.43) together with (8.46) and (8.47) forms the core of the theory of slabs *rigid in shear*, which is named after KIRCHHOFF. The relation $\boldsymbol{q} = \boldsymbol{D_s} \bullet \boldsymbol{E_m} \bullet \boldsymbol{D_k} \bullet \boldsymbol{u}$ resulting from these relationships gives rise to the fourth-order partial differential equation

$$\frac{\partial^4 w}{\partial x^4} + 2\frac{\partial^4 w}{\partial x^2 \partial y^2} + \frac{\partial^4 w}{\partial y^4} = \Delta\Delta w = \frac{q}{D} \qquad \left[D = \frac{Eh^3}{12(1-\nu^2)}\right] \tag{8.48}$$

the solutions to which can be adapted to two boundary conditions per edge. In the case of free and simply supported edges, this results in a problem that is overcome by combining the shear forces and the derivatives of the twisting moments parallel with the edge to form *edge shear forces*. As is shown in section 24.1.2.4, such edges correspond to *static discontinuity lines* along which shear forces are carried that are equal to the difference between the twisting moments on both sides.

8.2.7 Three-dimensional continua

Chapters 5 to 7 discuss in detail the equilibrium conditions (5.29)

$$\sigma_{ij,j} + q_i = 0 \tag{8.49}$$

the static boundary conditions (5.31)

$$t_i = \sigma_{ij} n_j \tag{8.50}$$

the kinematic relations $(6.21)_1$ or (6.22)

$$\varepsilon_{ij} = u_{(i,j)} \tag{8.51}$$

the kinematic boundary conditions (6.34)

$$r_i = \delta_{ij} u_j \tag{8.52}$$

and the linear elastic constitutive relationship (7.1), (7.3) or

$$\sigma_{ij} = 2\mu\varepsilon_{ij} + \lambda\varepsilon_{ij}\varepsilon_{kk} \qquad \left(\mu = G = \frac{E}{2(1+\nu)} \quad , \quad \lambda = \frac{\nu E}{(1+\nu)(1-2\nu)}\right) \tag{8.53}$$

or

$$\varepsilon_{ij} = \frac{(1+\nu)\sigma_{ij} - \nu\delta_{ij}\sigma_{kk}}{E} \tag{8.54}$$

We shall confine ourselves here to using matrix notation to describe the relationships (8.49)

$$\boldsymbol{q} = \begin{Bmatrix} q_x \\ q_y \\ q_z \end{Bmatrix} = \begin{bmatrix} -\partial_x & 0 & 0 & 0 & -\partial_z & -\partial_y \\ 0 & -\partial_y & 0 & -\partial_z & 0 & -\partial_x \\ 0 & 0 & -\partial_z & -\partial_y & -\partial_x & 0 \end{bmatrix} \begin{Bmatrix} \sigma_x \\ \sigma_y \\ \sigma_z \\ \tau_{yz} \\ \tau_{zx} \\ \tau_{xy} \end{Bmatrix} = \boldsymbol{D_s} \bullet \boldsymbol{\sigma} \tag{8.55}$$

and (8.51)

$$\boldsymbol{\varepsilon} = \begin{Bmatrix} \varepsilon_x \\ \varepsilon_y \\ \varepsilon_z \\ \gamma_{yz} \\ \gamma_{zx} \\ \gamma_{xy} \end{Bmatrix} = \begin{bmatrix} \partial_x & 0 & 0 \\ 0 & \partial_y & 0 \\ 0 & 0 & \partial_z \\ 0 & \partial_z & \partial_y \\ \partial_z & 0 & \partial_x \\ \partial_y & \partial_x & 0 \end{bmatrix} \begin{Bmatrix} u \\ v \\ w \end{Bmatrix} = \boldsymbol{D_k} \bullet \boldsymbol{u} \tag{8.56}$$

Eq. (8.54) has already been presented in matrix form in (8.34).

8.2.8 Commentary

If we use $(8.17)_1$ to write the integrand in the first term on the right in (8.20) in the form $\boldsymbol{q_1}^{\mathrm{T}} \bullet \boldsymbol{u_2} = \boldsymbol{u_2}^{\mathrm{T}} \bullet \boldsymbol{q_1} = \boldsymbol{u_2}^{\mathrm{T}} \bullet \boldsymbol{D_s} \bullet \boldsymbol{\sigma_1}$ and take into account the relationship $(8.18)_1$ for $\boldsymbol{\varepsilon_2}$ in the third term, we then get

$$W = \int (\boldsymbol{u_2}^{\mathrm{T}} \bullet \boldsymbol{D_s} \bullet \boldsymbol{\sigma_1} - \boldsymbol{\sigma_1}^{\mathrm{T}} \bullet \boldsymbol{D_k} \bullet \boldsymbol{u_2})\, \mathrm{d}V + \int \boldsymbol{t_1}^{\mathrm{T}} \bullet \boldsymbol{r_2}\, \mathrm{d}S = 0 \tag{8.57}$$

The operators $\boldsymbol{D_s}$ and $\boldsymbol{D_k}$ have elements in the form of numbers and differential operators, and, as shown in section 8.2.2, $\boldsymbol{D_k} = \boldsymbol{D_s}^{\mathrm{T}}$ ($\boldsymbol{D_k} = -\boldsymbol{D_s}^{\mathrm{T}}$) applies for even (odd) differential operators. It is easy to prove that the two operators $\boldsymbol{D_s}$ and $\boldsymbol{D_k}$ are *adjoint* in framed structures. Corresponding expressions of the type $u_2\sigma_1 - \sigma_1 u_2$, $u_2\sigma_1' - \sigma_1 u_2'$, $u_2\sigma_1'' - \sigma_1 u_2''$ occur in the volume integral from (8.57) degenerated to a line integral ($' = \mathrm{d}/\mathrm{d}x$); of these, the first disappears and the second and third can be integrated through integration by parts. As an example, applying (8.24) and (8.25) results in

$$\boldsymbol{u_2}^{\mathrm{T}} \bullet \boldsymbol{D_s} \bullet \boldsymbol{\sigma_1} = -N_1' u_2 - M_1'' w_2 \quad , \quad -\boldsymbol{\sigma_1}^{\mathrm{T}} \bullet \boldsymbol{D_k} \bullet \boldsymbol{u_2} = -N_1 u_2' + M_1 w_2''$$

for a BERNOULLI bar, and hence, after integrating between the end-points x_l and $x_r > x_l$

$$(-N_1 u_2 - M_1' w_2 + M_1 w_2')\Big|_{x_l}^{x_r} = -(N_1 u_2 + V_1 w_2 + M_1 \varphi_2)\Big|_{x_l}^{x_r} = -\boldsymbol{t_1}^{\mathrm{T}} \bullet \boldsymbol{r_2}\Big|_{x_l}^{x_r}$$

Either GAUSS' theorem (A6.30) or GREEN's second identity (A6.34) can be used in a similar way to verify the adjointness of $\boldsymbol{D_s}$ and $\boldsymbol{D_k}$ for plate and shell structures and three-dimensional continua. The adjointness of the static and kinematic operators for continua corresponds to the identity relationship (8.16) between the static and kinematic transformation matrices for discontinua.

8.3 The principle of virtual work

8.3.1 Virtual force and deformation variables

Starting with the real deformation state $\boldsymbol{u}$, $\boldsymbol{\varepsilon}$, $\boldsymbol{r}$, let us consider the neighbouring states

$$\overline{\boldsymbol{u}} = \boldsymbol{u} + \delta\boldsymbol{u} \quad , \quad \overline{\boldsymbol{\varepsilon}} = \boldsymbol{\varepsilon} + \delta\boldsymbol{\varepsilon} \quad , \quad \overline{\boldsymbol{r}} = \boldsymbol{r} + \delta\boldsymbol{r} \tag{8.58}$$

according to (A7.4), which should be characterised by the fact that the kinematic relationships and boundary conditions

$$\overline{\boldsymbol{\varepsilon}} = \boldsymbol{D}_k \bullet \overline{\boldsymbol{u}} \text{ in } V \quad , \quad \overline{\boldsymbol{r}} = \boldsymbol{r} = \boldsymbol{r}_0 \text{ on } S_r \tag{8.59}$$

are fulfilled, see(8.18). Such states are known as *kinematically admissible*.

Further, starting from the real force state $\boldsymbol{q}$, $\boldsymbol{\sigma}$, $\boldsymbol{t}$, let us consider the neighbouring states

$$\underline{\boldsymbol{\sigma}} = \boldsymbol{\sigma} + \delta\boldsymbol{\sigma} \quad , \quad \underline{\boldsymbol{t}} = \boldsymbol{t} + \delta\boldsymbol{t} \tag{8.60}$$

that satisfy the equilibrium conditions and the static boundary conditions

$$\boldsymbol{q} = \boldsymbol{D}_s \bullet \underline{\boldsymbol{\sigma}} \text{ in } V \quad , \quad \underline{\boldsymbol{t}} = \boldsymbol{t} = \boldsymbol{t}_0 \text{ on } S_t \tag{8.61}$$

see (8.17). Such states are known as *statically admissible*.

8.3.2 The principle of virtual deformations

If we combine the real force state 1 and the virtual deformation state 2 in the work equation (8.20), the result is

$$\delta W = \int_V \boldsymbol{q}^{\mathrm{T}} \bullet \delta\boldsymbol{u} \, \mathrm{d}V + \int_{S_t} \boldsymbol{t}_0^{\mathrm{T}} \bullet \delta\boldsymbol{r} \, \mathrm{d}S - \int_V \boldsymbol{\sigma}^{\mathrm{T}} \bullet \delta\boldsymbol{\varepsilon} \, \mathrm{d}V = 0 \tag{8.62}$$

Using (8.57) and (8.59), the third integral in (8.62) can be rearranged as follows:

$$-\int_V \boldsymbol{\sigma}^{\mathrm{T}} \bullet \delta\boldsymbol{\varepsilon} \, \mathrm{d}V = -\int_V \boldsymbol{\sigma}^{\mathrm{T}} \bullet \boldsymbol{D}_k \bullet \delta\boldsymbol{u} \, \mathrm{d}V = -\int_V \delta\boldsymbol{u}^{\mathrm{T}} \bullet \boldsymbol{D}_s \bullet \boldsymbol{\sigma} \, \mathrm{d}V - \int_S \boldsymbol{t}^{\mathrm{T}} \bullet \delta\boldsymbol{r} \, \mathrm{d}S$$

Therefore,

$$\delta W = \int_V \delta\boldsymbol{u}^{\mathrm{T}} \bullet (\boldsymbol{q} - \boldsymbol{D}_s \bullet \boldsymbol{\sigma}) \, \mathrm{d}V - \int_{S_t} \delta\boldsymbol{r}^{\mathrm{T}} \bullet (\boldsymbol{t} - \boldsymbol{t}_0) \, \mathrm{d}S = 0 \tag{8.63}$$

According to the fundamental lemma of calculus of variations, the expressions in brackets in the integrands of (8.63) disappear, i. e. we get (8.61) as the equivalent conditions for the variational problem (8.62). The *principle of virtual deformations* is a global (weak) formulation of the equilibrium conditions and the static boundary conditions or, in other words, the equilibrium.

8.3.3 The principle of virtual forces

By combining the virtual force state 1 with the real deformation state 2 in (8.20), we get

$$\delta W = \int_{S_r} \delta\boldsymbol{t}^{\mathrm{T}} \bullet \boldsymbol{r}_0 \, \mathrm{d}S - \int_V \delta\boldsymbol{\sigma}^{\mathrm{T}} \bullet \boldsymbol{\varepsilon} \, \mathrm{d}V = 0 \tag{8.64}$$

The equilibrium condition $\mathbf{0} = \boldsymbol{D}_s \bullet \delta\boldsymbol{\sigma}$ can be considered as an auxiliary condition with the LAGRANGE multiplier $\boldsymbol{u}^{\mathrm{T}}$:

$$\delta W = \int_V \boldsymbol{u}^{\mathrm{T}} \bullet \boldsymbol{D}_s \bullet \delta\boldsymbol{\sigma} \, \mathrm{d}V - \int_V \delta\boldsymbol{\sigma}^{\mathrm{T}} \bullet \boldsymbol{\varepsilon} \, \mathrm{d}V + \int_{S_r} \delta\boldsymbol{t}^{\mathrm{T}} \bullet \boldsymbol{r}_0 \, \mathrm{d}S = 0 \tag{8.65}$$

Taking into account (8.57), the first integral in (8.65) can be rearranged:

$$\int \boldsymbol{u}^{\mathrm{T}} \bullet \boldsymbol{D}_s \bullet \delta\boldsymbol{\sigma} \, \mathrm{d}V = -\int \delta\boldsymbol{\sigma}^{\mathrm{T}} \bullet \boldsymbol{D}_k \bullet \boldsymbol{u} \, \mathrm{d}V - \int \delta\boldsymbol{t}^{\mathrm{T}} \bullet \boldsymbol{r} \, \mathrm{d}S$$

Therefore,

$$\delta W = \int_V \delta\boldsymbol{\sigma}^{\mathrm{T}} \bullet (\boldsymbol{D}_k \bullet \boldsymbol{u} - \boldsymbol{\varepsilon}) \, \mathrm{d}V - \int_{S_r} \delta\boldsymbol{t}^{\mathrm{T}} \bullet (\boldsymbol{r} - \boldsymbol{r}_0) \, \mathrm{d}S = 0 \tag{8.66}$$

According to the fundamental lemma of calculus of variations, the expressions in the brackets in the integrands of (8.66) disappear. We get (8.59) as the equivalent conditions for the variational problem (8.65). The *principle of virtual forces*, assuming infinitesimally small deformations, is a global (weak) formulation of the kinematic relationships and the kinematic boundary conditions or, in other words, the compatibility.

8.3.4 Commentary

The principle of virtual deformations and the principle of virtual forces are valid for any system irrespective of the material behaviour. It should be pointed out that (8.62) and (8.65) do not describe complete variations, but rather merely partial variations, either for the kinematic or the static variables.

In contrast to the principle of virtual forces, the principle of virtual deformations still applies to geometric non-linear problems (second-order theory). According to the principle of virtual forces (8.65), deformation variables occur directly, but according to the principle of virtual deformations (8.62), only in the form of their variations. The consequence of geometric non-linear effects according to the principle of virtual forces is therefore one order higher than according to the principle of virtual deformations.

According to the principle of virtual deformations, a force state is then, and only then, in equilibrium, when the total virtual deformation work for each permissible virtual deformation state (compatible with the constraints) disappears. In this form, the *principle of virtual work*, together with the *free-body principle* (section 5.1.3) and the *reaction principle* (section 5.1.1), forms the basis for the whole of *statics*. In *dynamics*, the principle of virtual work has to be formulated including the *inertial forces* of D'ALEMBERT: any arbitrary body moves in such a way that at any point in time, the internal, external and inertial forces are in equilibrium.

Example 8.1 Determining internal force variables

We can use the principle of virtual deformations to determine internal force variables (stresses or stress resultants) in statically determinate systems. For instance, if we want to find out the bar force s_5 in the system shown in Fig. 8.1(a), we consider bar 5 to be cut through at one point and assign the relative displacement δv_5 to the sides of the cut. The rest of the system, in the form of a parallelogram 1452, is thus a rigid body rotating through an angle $\delta v_5/l$ about joint 1, and displacements ensue in the direction of the active degrees of freedom V_3 to V_{10}, which apart from factor δv_5 correspond to the coefficients in the fifth column of the matrix $\boldsymbol{b}^{\mathrm{T}}$ leading to relationship (8.4). Eq. (8.62) becomes

$$\delta W = (-Q_4 + Q_7 - Q_8 + Q_9 - 2Q_{10} - s_5)\delta v_5 = 0$$

Owing to the fundamental lemma of calculus of variations, the expression in brackets must disappear and that therefore determines s_5, see also Fig. 10.9.

Instead of cutting through bar 5, we can subject the bar to an arbitrary virtual strain $\delta\varepsilon(x) = \delta u'(x)$ in which the x axis moves from joint 3 to joint 4. Taking into account the boundary condition $u_3 = 0$, the third integral in (8.62) results in the value $-s_5\delta u_4$. As expected, δu_4 takes on the role of the relative displacement δv_5, but otherwise there is no difference between this and the first procedure. Actually, the first procedure is a special case of the second with an infinitely large virtual strain at the point at which the bar is cut.

Example 8.2 Determining external deformation variables

We can use the principle of virtual forces to determine external deformation variables (displacements or rotations) provided the stresses or stress resultants are known. For instance, if we want to find out the deflection V_8 at joint 4 of the system shown in Fig. 8.1(a), we can apply a virtual load δQ_8 at the point and in the direction of this deflection, which according to matrix $\boldsymbol{b}$ which leads to (8.3) generates bar forces $s_2 = \sqrt{2}\delta Q_8$, $s_5 = -\delta Q_8$. If we presume flexibilities $f_2 = \sqrt{2}f_5$ according to (8.5) and temporarily treat V_8 as a specified edge displacement r_0 in the first integral of (8.64) (and consequently Q_8 as a reaction force), then this relationship – taking into account the second and fifth rows of matrix $\boldsymbol{b}$ – results in

$$\delta Q_8 V_8 = \sqrt{2}\,\delta Q_8\sqrt{2}f_5(\sqrt{2}Q_4 + \sqrt{2}Q_8 + \sqrt{2}Q_{10}) - \delta Q_8 f_5(-Q_4 + Q_7 - Q_8 + Q_9 - 2Q_{10})$$

and therefore

$$V_8 = f_5\left[(2\sqrt{2}+1)(Q_4 + Q_8) - (Q_7 + Q_9) + 2(\sqrt{2}+1)\,Q_{10}\right]$$

Example 8.3 Geometric and material non-linearity

Two identical bars, idealised as weightless and with constant axial stiffness EA, are connected concentrically with each other (B) and to rigid abutments (A, C) via frictionless joints as shown in Fig. 8.9(a). The length of the initially stress-free bars is $l/2$, i. e. the initial position of joint B is B_0 on the level of AC. A load Q applied at B causes the deflection w as well as normal forces N and corresponding strains ε in both bars. The strain is

$$\varepsilon = \sqrt{1 + \left(\frac{2w}{l}\right)^2} - 1 \approx \frac{2w^2}{l^2}$$

when higher terms in the TAYLOR series are neglected. A virtual additional deflection δw causes an additional strain $\delta\varepsilon = 2\Delta/l$. By taking into account $N = EA\varepsilon$ and the relationship between Δ and δw shown in Fig. 8.9(b), then applying the principle of virtual deformations (8.62) results in

$$\delta W = Q\,\delta w - N\,l\,\delta\varepsilon = Q\,\delta w - EA\frac{2w^2}{l^2}2\frac{2w}{l}\delta w = 0$$

and therefore

$$Q = \frac{8EAw^3}{l^3}$$

see Fig. 8.9(c).

The linear elastic system behaves with *geometric non-linearity*. This example shows that it is also possible to use the principle of virtual deformations in such situations.

It is easy to provide an exact solution in this case. If we call angle B_0CB $\alpha = \arctan(2w/l)$, then $\varepsilon = (\sec\alpha - 1)$ and

$$Q = 2N\sin\alpha = 2EA(\tan\alpha - \sin\alpha) \approx EA\,\alpha^3$$

if only the first two terms are considered in the TAYLOR series for $\tan\alpha$ and $\sin\alpha$. Compared with the exact solution, the approximation $8EA(w/l)^3$ for $2w/l = 0.1$ results in a discrepancy of 0.7 %.

If the stress $E\varepsilon$ reaches the yield limit f_y and if the material behaves perfectly plastically upon further deformation, the bar forces are $N = Af_y$, and the following applies:

$$Q = 2Af_y\sin\alpha \approx 4Af_y\frac{w}{l\left(1 + 2\frac{w^2}{l^2}\right)}$$

The system displays geometric and *material non-linearity*. The onset of yield is given by

$$w_y \approx l\sqrt{\frac{f_y}{2E}} \quad , \quad Q_y \approx 2Af_y\sqrt{\frac{2f_y}{E}}$$

see Fig. 8.9(c).

It is also possible to apply the principle of virtual deformations in the phase of plastic behaviour:

$$\delta W = Q\,\delta w - Nl\delta\varepsilon = Q\delta w - Af_y 2\Delta = \left[Q - \frac{4Af_y w}{l(1+\varepsilon)}\right]\delta w = 0$$

Once again, we arrive at the aforementioned expression for Q, and $Nl\delta\varepsilon = 2Af_y\,\Delta$ corresponds to the energy dissipated during the plastic deformation.

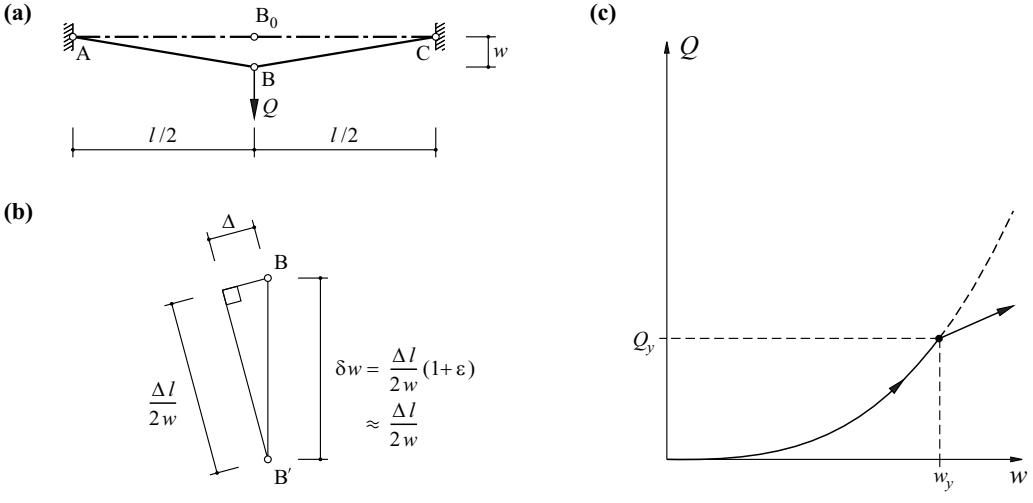

Fig. 8.9 Geometric and material non-linearity: (a) system and loads, (b) kinematics, (c) load-deflection curve

8.4 Elastic systems

8.4.1 Hyperelastic materials

The stress field $\boldsymbol{\sigma} = \boldsymbol{\sigma}(\boldsymbol{\varepsilon})$ is *conservative* in the case of *hyperelastic* material behaviour. The specific deformation work (related to the volume) of the internal forces (stresses)

$$-\int_{\boldsymbol{\varepsilon}_1}^{\boldsymbol{\varepsilon}_2} \boldsymbol{\sigma}^{\mathrm{T}} \bullet \mathrm{d}\boldsymbol{\varepsilon}$$

for a certain deformation process depends on the end-points $\boldsymbol{\varepsilon}_1$, $\boldsymbol{\varepsilon}_2$ only, not the path between those points. The integrand $\boldsymbol{\sigma}^{\mathrm{T}} \bullet \mathrm{d}\boldsymbol{\varepsilon}$ therefore corresponds to the total differential of a *potential function*

$$\pi_i = \int \boldsymbol{\sigma}^{\mathrm{T}} \bullet \mathrm{d}\boldsymbol{\varepsilon} \tag{8.67}$$

the so-called *specific strain energy*, and $\boldsymbol{\sigma}$ is equal to the gradient of this function:

$$\boldsymbol{\sigma} = \operatorname{grad} \pi_i \tag{8.68}$$

The term π_i represents a positive definite function of the strains $\boldsymbol{\varepsilon}$. The energy input π_i for a certain deformation process is stored and fully retrieved mechanically when subsequently relieving the load, i. e. no energy is dissipated. Fig. 8.10(a) shows a corresponding stress-strain relationship (one-to-one correspondence) for the uniaxial behaviour.

As a complement to π_i, it is possible to define the *specific complementary energy*

$$\pi_i^* = \boldsymbol{\sigma}^{\mathrm{T}} \bullet \boldsymbol{\varepsilon} - \pi_i = \int \boldsymbol{\varepsilon}^{\mathrm{T}} \bullet \mathrm{d}\boldsymbol{\sigma} \tag{8.69}$$

with the gradient

$$\boldsymbol{\varepsilon} = \operatorname{grad} \pi_i^* \tag{8.70}$$

see Fig. 8.10(b). In contrast to π_i, π_i^* is purely a mathematical auxiliary variable. Whereas π_i remains positive definite for any initial strains $\boldsymbol{\varepsilon}_0$, π_i^* can become negative depending on the initial strain, see Fig. 8.10(c).

Differentiating the relationships (8.68) and (8.70) results in the reciprocal relationships

$$\frac{\partial \sigma_{jk}}{\partial \varepsilon_{lm}} = \frac{\partial^2 \pi_i}{\partial \varepsilon_{jk}\, \partial \varepsilon_{lm}} = \frac{\partial \sigma_{lm}}{\partial \varepsilon_{jk}} \tag{8.71}$$

and

$$\frac{\partial \varepsilon_{jk}}{\partial \sigma_{lm}} = \frac{\partial^2 \pi_i^*}{\partial \sigma_{jk}\, \partial \sigma_{lm}} = \frac{\partial \varepsilon_{lm}}{\partial \sigma_{jk}} \tag{8.72}$$

i. e. the fields $\boldsymbol{\sigma}(\boldsymbol{\varepsilon})$ and $\boldsymbol{\varepsilon}(\boldsymbol{\sigma})$ are irrotational.

The relationships (8.68) and (8.70) correspond to local formulations of the *theorems of* CASTIGLIANO and ENGESSER, (8.72) corresponds to the local form of MAXWELL*'s generalised theorem*, and (8.71) to a dual proposition of this.

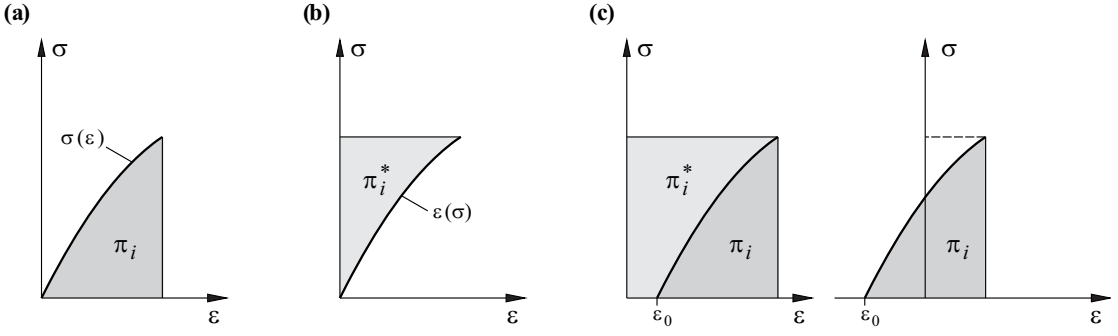

Fig. 8.10 Hyperelastic material behaviour: (a) specific strain energy π_i, (b) specific complementary energy π_i^*, (c) how initial strain ε_0 influences π_i^*

8.4.2 Conservative systems

8.4.2.1 Total potential

If in addition to the internal forces, the external forces are conservative, too, there is a *total potential*

$$\Pi = \int_V \pi_i \, \mathrm{d}V - \int_V \boldsymbol{q}^{\mathrm{T}} \bullet \boldsymbol{u} \, \mathrm{d}V - \int_S \boldsymbol{t}^{\mathrm{T}} \bullet \boldsymbol{r} \, \mathrm{d}S = \Pi_i + \Pi_e \tag{8.73}$$

whose first variation according to the principle of virtual deformations (8.62) must be equal to zero

$$\delta\Pi = \int_V \delta\pi_i \, \mathrm{d}V - \int_V \boldsymbol{q}^{\mathrm{T}} \bullet \delta\boldsymbol{u} \, \mathrm{d}V - \int_{S_t} \boldsymbol{t}_0^{\mathrm{T}} \bullet \delta\boldsymbol{r} \, \mathrm{d}S = 0 \tag{8.74}$$

We can see that the integral over S_r is omitted because the boundary displacements $\boldsymbol{r}$ on S_r are not varied.

The higher variations of Π_e disappear compared with the first variation $\delta\Pi_e$ because we assume small deformations. Using a TAYLOR series, the variation of Π at the stationary value Π_{stat} results in

$$\Pi = \Pi_{\mathrm{stat}} + \frac{1}{2}\delta^2\Pi_i + \ldots \geq \Pi_{\mathrm{stat}} \tag{8.75}$$

because Π_i is positive definite. The total potential, with the stationary value, therefore assumes a minimum.

This result can be summarised as the *theorem of least total potential*: of all the kinematically admissible deformation states of a conservative system, the one that occurs is the one in which the total potential Π is a minimum.

Example 8.4 Tie

The normal force - normal strain curve shown in Fig. 8.11(c) applies to every cross-section of the tie OA shown in Fig. 8.11(a). The total potential

$$\Pi = \int_0^l \pi_i \, \mathrm{d}x - \int_0^l qu \, \mathrm{d}x - Q_{\mathrm{A}} u_{\mathrm{A}}$$

has the (negligible) first variation

$$\delta\Pi = \int_0^l \delta\pi_i \, \mathrm{d}x - \int_0^l q \, \delta u \, \mathrm{d}x - Q_{\mathrm{A}} \delta u_{\mathrm{A}} = 0$$

Taking into account $\delta\pi_i = N\delta\varepsilon = N\delta(u') = N\,(\delta u)'$ allows us to integrate the first integral by parts and we get

$$\delta\Pi = -\int_0^l \delta u \, (N' + q) \, \mathrm{d}x + N \, \delta u \Big|_0^l - Q_{\mathrm{A}} \delta u_{\mathrm{A}} = 0$$

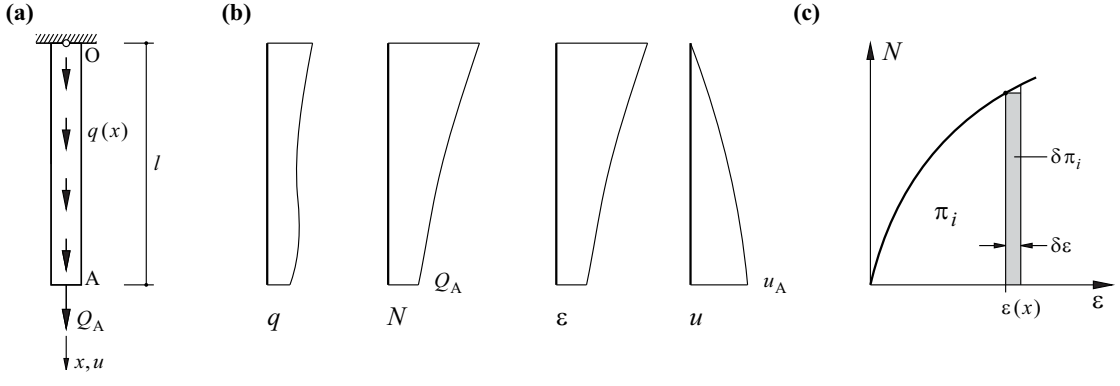

Fig. 8.11 Tie: (a) system and loads, (b) diagrams of loads, (generalised) stresses, strains and displacements, (c) normal force - normal strain curve

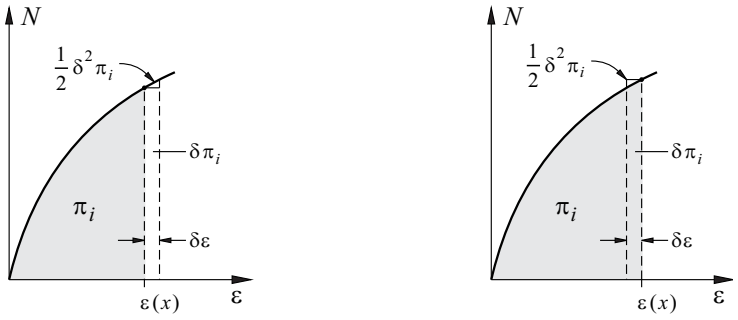

Fig. 8.12 Positive definiteness of π_i

Owing to the (essential) kinematic boundary condition $\delta u(0) = 0$, in accordance with the fundamental lemma of calculus of variations, the equilibrium condition $N' + q = 0$ and the (natural) static boundary condition $N(l) = Q_A$ remain in the end. Integrating q, starting from A, results in the normal force N, which means that the strain diagram ε is also known from the N-ε relationship; integrating ε, starting from O, then results in the displacement diagram u, see Fig. 8.11(b).
Where $Q_A = 0$, q = const and $N = EA\varepsilon$, the result is, for example

$$\Pi = \int_0^l EA\,\frac{\varepsilon^2}{2}\,\mathrm{d}x - \int_0^l qu\,\mathrm{d}x = \frac{EA}{2}\int_0^l (u')^2\,\mathrm{d}x - q\int_0^l u\,\mathrm{d}x$$

and therefore

$$\delta\Pi = EA\int_0^l u'\,\delta u'\,\mathrm{d}x - q\int_0^l \delta u\,\mathrm{d}x = EA\,u'\,\delta u\Big|_0^l - EA\int_0^l u''\,\delta u\,\mathrm{d}x - q\int_0^l \delta u\,\mathrm{d}x = 0$$

Consequently, according to the fundamental lemma of calculus of variations, $EAu'' + q = 0$, and owing to $\delta u(0) = 0$ also $u'(l) = 0$, i. e. ultimately,

$$\varepsilon = u' = \frac{q}{EA}(l - x) \quad , \quad u = \frac{qx(2l - x)}{2EA}$$

We get

$$\Pi = \frac{q^2}{2EA}\int_0^l [(l - x)^2 - x(2l - x)]\,\mathrm{d}x = -\frac{q^2 l^3}{6EA}$$

for the stationary value. Examining the second variation of Π results in

$$\delta^2\Pi = -EA\int_0^l (\delta u''\,\delta u + u''\,\delta^2 u)\,\mathrm{d}x - q\int_0^l \delta^2 u\,\mathrm{d}x = -EA\,\delta u'\,\delta u\Big|_0^l + EA\int_0^l (\delta u')^2\mathrm{d}x - \int_0^l \delta^2 u(EAu'' + q)\,\mathrm{d}x$$

As the first and third terms disappear and the second is positive, $\delta^2\Pi > 0$, and the stationary value corresponds to a minimum.
The integrand $EA(\delta u')^2 = EA(\delta\varepsilon)^2$, apart from the factor 1/2, corresponds to the third term $\delta^2\pi_i/2$ of the TAYLOR series for the specific strain energy, see (8.75). Fig. 8.12 illustrates this situation for positive and negative $\delta\varepsilon$ values assuming a general hyperelastic material behaviour.

8.4.2.2 Complementary total potential

Conservative external forces involve a *complementary total potential*

$$\Pi^* = \int_V \pi_i^*\,\mathrm{d}V - \int_{S_r} \boldsymbol{r}_0^{\mathrm{T}} \cdot \boldsymbol{t}\,\mathrm{d}S = \Pi_i^* + \Pi_e^* \tag{8.76}$$

and according to the principle of virtual forces (8.64), the first variation of that potential must equal zero:

$$\delta\Pi^* = \int_V \delta\pi_i^*\,\mathrm{d}V - \int_{S_r} \boldsymbol{r}_0^{\mathrm{T}} \cdot \delta\boldsymbol{t}\,\mathrm{d}S = 0 \tag{8.77}$$

The loads $\boldsymbol{q}$ and the boundary stresses $\boldsymbol{t}$ on S_t do not vary, and so the corresponding integrals can be omitted. Furthermore, the integral extending over S_r, the potential of the applied boundary displacements, is often omitted as well; this is the case when $\boldsymbol{r}_0 \equiv \boldsymbol{0}$, i. e. when the system is rigidly constrained. Eq. (8.77) is then reduced to the condition $\delta\Pi_i^* = 0$.

In a similar way to (8.75), it can be shown that Π_i^* with the stationary value given by (8.77) assumes a minimum and the result can be summarised as the *theorem of least complementary total potential*: of all the statically admissible force states in a conservative system, the one that occurs is the one in which the complementary total potential Π^* is a minimum.

Example 8.5 Beam with one degree of static indeterminacy

The beam AB shown in Fig. 8.13(a) is subjected to a line load q uniformly distributed over its length l. With, for example, two moment equilibrium conditions about A and B, the upper free body diagram in Fig. 8.13(b) results in the support reactions

$$A = \frac{ql}{2} - \frac{X}{l} \quad , \quad B = \frac{ql}{2} + \frac{X}{l}$$

dependent on the unknown fixity moment X. And the lower free body diagram results in the bending moment M

$$M = \frac{q}{2}x(l-x) + X\left(1 - \frac{x}{l}\right)$$

at point x. If we assume a linear elastic behaviour rigid in shear according to section 8.2.2 with EI = const, then only the bending moments need to be considered in the specific complementary energy π_i^*, see Fig. 8.13(c):

$$\pi_i^* = \frac{M^2}{2EI}$$

Noting that $\delta M = \delta X(1 - x/l)$, eq. (8.77) results in

$$\delta\Pi^* = \int_0^l \frac{\delta M^2}{2EI}\,\mathrm{d}x = \int_0^l \frac{M\delta M}{EI}\,\mathrm{d}x = \int_0^l \frac{\delta X}{EIl}\left[\frac{qx(l-x)^2}{2} + \frac{X(l-x)^2}{l}\right]\mathrm{d}x = 0$$

from which it follows that $X = -ql^2/8$ and therefore $A = 5ql/8$, $B = 3ql/8$. Fig. 8.13(d) shows the corresponding bending moments M and shear forces $V = M'$.

Subjecting the system to a displacement r_B at support B as shown in Fig. 8.13(e) is associated with a certain support reaction B and a corresponding moment $M = B(x - l)$ according to Fig. 8.13(f). Eq. (8.77) then results in

$$\delta\Pi^* = \int_0^l \frac{\delta M^2}{2EI}\,\mathrm{d}x - r_\mathrm{B}\,\delta B = \int_0^l \frac{M\delta M}{EI}\,\mathrm{d}x - r_\mathrm{B}\,\delta B = \int_0^l \frac{B\delta B(x-l)^2}{EI}\,\mathrm{d}x - r_\mathrm{B}\,\delta B = 0$$

from which it follows that $B = 3EIr_\mathrm{B}/l^3$.

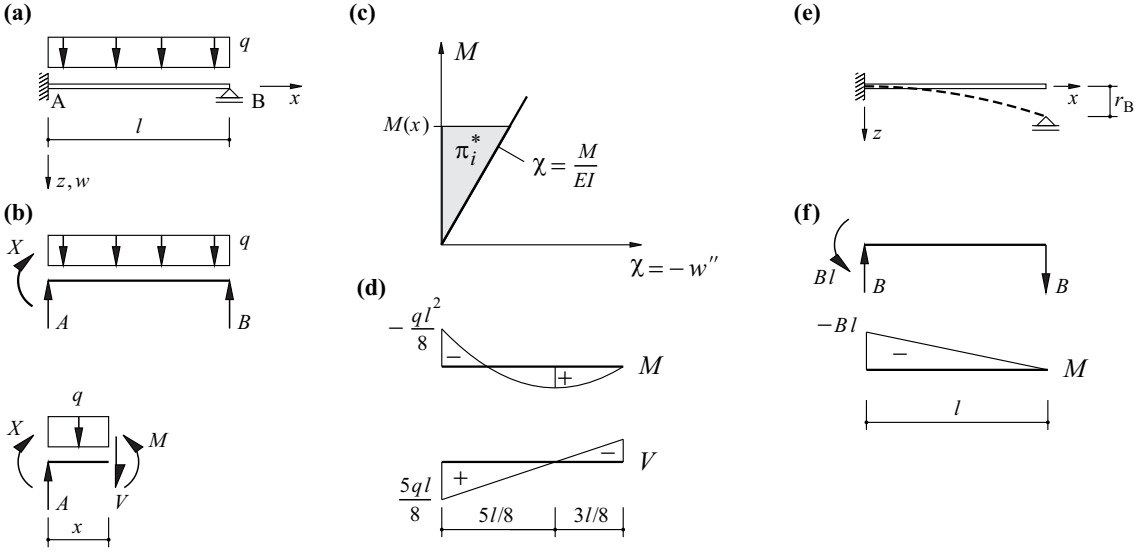

Fig. 8.13 Beam with one degree of static indeterminacy: (a) system and loads, (b) free body diagrams, (c) moment-curvature diagram, (d) stress resultants, (e) specified boundary displacement, (f) free body and moment diagrams

Fig. 8.13(e) and (f) correspond to a zero-load so-called *restraint state* of the system with one degree of static indeterminacy. The stress resultants $V = B$ and $M = B(x - l)$ due to the restraint are directly proportional to the applied boundary displacement r_B and the bending stiffness EI. Generally, in a system with n degrees of static indeterminacy, we can distinguish between n independent restraint states, the effects of which (stress resultants and deformations) are superimposed on those caused by the loads. Actions that cause restraints vary from case to case; for example, changes in temperature and humidity as well as material-dependent long-term deformations may need to be considered, see sections 4.2.1, 7.4 and 7.5.

8.4.2.3 CASTIGLIANO's theorem

The following discussion will be confined to systems subjected to displacements (or rotations) u_k in given directions at n points. The notation for the corresponding forces (or moments) is Q_k. The strains, and hence also the internal potential Π_i, depend on u_k via the kinematic relationships. Eq. (8.73) becomes

$$\Pi = \Pi_i(u_k) - Q_k u_k \tag{8.78}$$

and (8.74) results in

$$\delta\Pi = \frac{\partial \Pi_i}{\partial u_k}\delta u_k - Q_k \delta u_k = \left(\frac{\partial \Pi_i}{\partial u_k} - Q_k\right)\delta u_k = 0 \tag{8.79}$$

In accordance with the fundamental lemma of calculus of variations, the expression in brackets must disappear, i. e.

$$Q_k = \frac{\partial \Pi_i}{\partial u_k} \tag{8.80}$$

is CASTIGLIANO*'s theorem*: the partial differentiation of the internal potential with respect to a displacement variable u_k results in the corresponding force variable Q_k.

Example 8.6 Geometric non-linearity

The geometric non-linear problem in example 8.3 with the normal strain $\varepsilon = 2w^2/l^2$ has an internal potential of

$$\Pi_i = l\,EA\frac{\varepsilon^2}{2} = EA\frac{2w^4}{l^3}$$

Applying (8.80) results directly in

$$Q = \frac{8EAw^3}{l^3}$$

Example 8.7 Cantilever beam

Fig. 8.14(a) shows the cantilever beam, rigid in shear and with constant bending stiffness EI, examined in example A7.2. Assuming $w = c_1\xi^2 + c_2\xi^3$ for the deflection $w(\xi = x/l)$, see (A7.52), and $w(l) = w_0$, $-w'(l) = \varphi_0$, we first get $c_1 = 3w_0 + \varphi_0 l$, $c_2 = -2w_0 - \varphi_0 l$ and

$$w'' = [(6w_0 + 2\varphi_0 l) - 6\xi(2w_0 + \varphi_0 l)]\frac{1}{l^2}$$

Using the internal potential

$$\Pi_i = \int_0^l \frac{(w'')^2}{2} EI\,\mathrm{d}x$$

and applying (8.80), it follows that

$$\begin{Bmatrix} Q_0 \\ M_0 \end{Bmatrix} = \frac{2EI}{l^3}\begin{bmatrix} 6 & 3l \\ 3l & 2l^2 \end{bmatrix}\begin{Bmatrix} w_0 \\ \varphi_0 \end{Bmatrix}$$

The columns in the above stiffness matrix correspond to the boundary force variables entered in Fig. 8.14(b) and (c) for the unit displacements $w_0 = 1$ and $\varphi_0 = 1$.
Inverting the stiffness matrix gives us the flexibility relationship

$$\begin{Bmatrix} w_0 \\ \varphi_0 \end{Bmatrix} = \frac{l^3}{2EI}\begin{bmatrix} \frac{2}{3} & -\frac{1}{l} \\ -\frac{1}{l} & \frac{2}{l^2} \end{bmatrix}\begin{Bmatrix} Q_0 \\ M_0 \end{Bmatrix}$$

which is also easy to obtain from elementary observations according to Fig. 8.14(d) and (e). The boundary deformation variables in the figures due to unit loads $Q_0 = 1$ and $M_0 = 1$ correspond to the columns of the flexibility matrix.

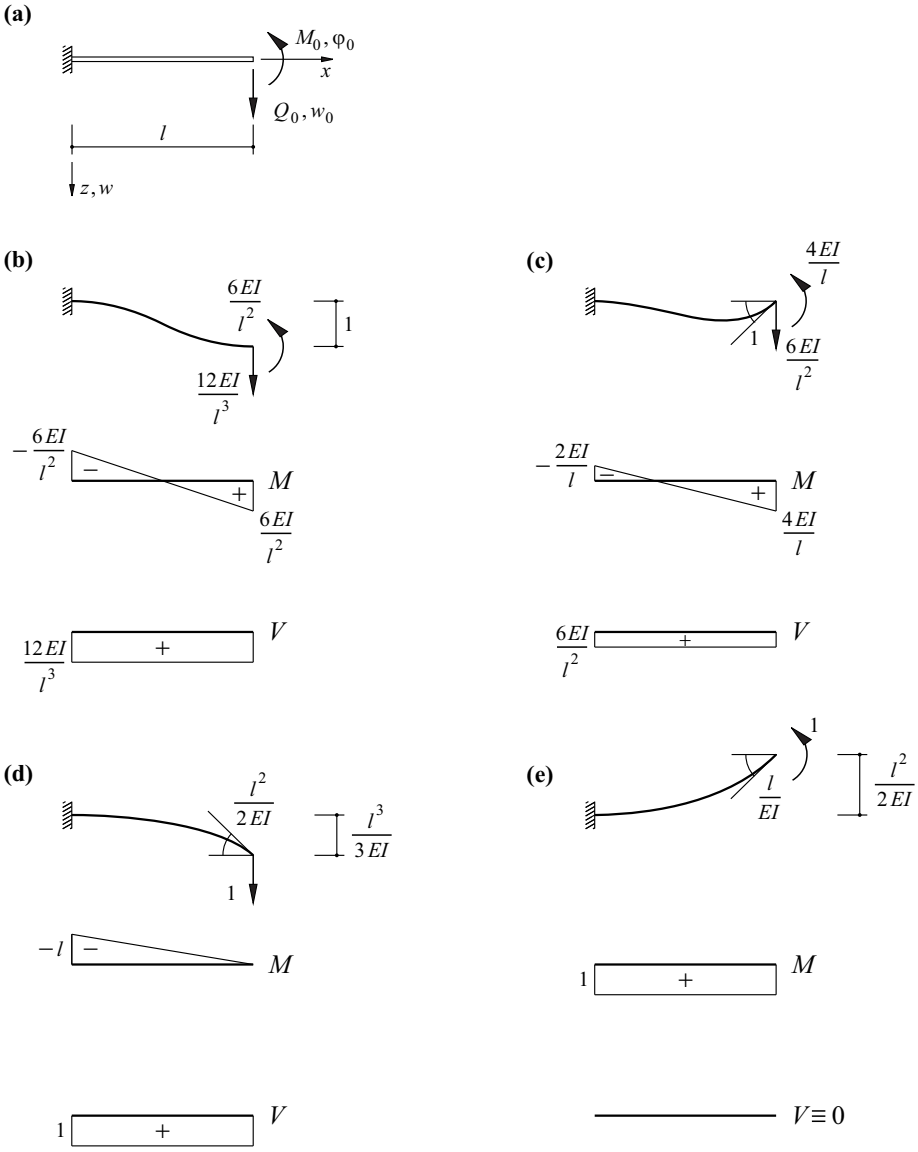

Fig. 8.14 Cantilever beam rigid in shear: (a) system and loads, (b) and (c) unit displacements, (d) and (e) unit loads

Superposing the cases considered in Fig. 8.14(d) and example A7.1 results in the beam with one degree of static indeterminacy of example 8.5. In order to eliminate the deflection $ql^4/(8EI)$ according to (A7.45) at the unsupported end of the cantilever ($\xi = 1$), we need the support force

$$B = \frac{3EI}{l^3} \cdot \frac{ql^4}{8EI} = \frac{3ql}{8}$$

see Fig. 8.13(d).

8.4.2.4 ENGESSER's theorem

We shall now consider systems that are subjected to forces (or moments) Q_k in given directions at n points in addition to the loads $\boldsymbol{q}_0$ in $V$and the boundary stresses $\boldsymbol{t}_0$ on S_t. The notation for corresponding displacements (or rotations) is u_k. The stresses, and hence the complementary internal potential Π_i^* as well, depend on Q_k via the equilibrium conditions. Eq. (8.76) becomes

$$\Pi^* = \Pi_i^*(Q_k) - Q_k u_k \tag{8.81}$$

and (8.77) results in

$$\delta\Pi^* = \frac{\partial \Pi_i^*}{\partial Q_k}\,\delta Q_k - u_k\,\delta Q_k = \left(\frac{\partial \Pi_i^*}{\partial Q_k} - u_k\right)\delta Q_k = 0 \tag{8.82}$$

from which, according to the fundamental lemma of calculus of variations, it follows that

$$u_k = \frac{\partial \Pi_i^*}{\partial Q_k} \tag{8.83}$$

i. e. ENGESSER*'s theorem*: the partial differentiation of the complementary internal potential with respect to a force variable Q_k results in the corresponding displacement variable u_k.

Example 8.8 Cantilever beam

The cantilever beam examined in example 8.7 is subjected to an additional line load q uniformly distributed over its length l (as in example A7.1). In order to determine the boundary deformation variables w_0 and φ_0, we use

$$M = M_0 - Q_0(l-x) - \frac{q}{2}(l-x)^2$$

to formulate the complementary internal potential

$$\Pi_i^* = \int_0^l \frac{M^2}{2EI}\,\mathrm{d}x$$

and apply (8.83):

$$\frac{\partial \Pi_i^*}{\partial Q_0} = \frac{1}{EI}\int_0^l \left[M_0 - Q_0(l-x) - \frac{q}{2}(l-x)^2\right](x-l)\,\mathrm{d}x = \frac{1}{EI}\left[-\frac{M_0 l^2}{2} + \frac{Q_0 l^3}{3} + \frac{q l^4}{8}\right] = w_0$$

$$\frac{\partial \Pi_i^*}{\partial M_0} = \frac{1}{EI}\int_0^l \left[M_0 - Q_0(l-x) - \frac{q}{2}(l-x)^2\right]\mathrm{d}x = \frac{1}{EI}\left[M_0 l - \frac{Q_0 l^2}{2} - \frac{q l^3}{6}\right] = \varphi_0$$

Example 8.9 Calibration ring

Fig. 8.15(a) shows a circular calibration ring that can be used for checking the accuracy of testing machines, for example. The ring with radius r has a constant bending stiffness EI and is subjected to two diametrically opposed loads Q.

For reasons of symmetry, it is sufficient to consider just one quarter AB of the ring, see Fig. 8.15(b). No shear force can act at B, and hence no normal force at A, and the normal force at B is a compressive force of magnitude $Q/2$. The bending moment at any point is

$$M = M_\mathrm{B} + \frac{Qr}{2}(1 - \cos\alpha)$$

where positive moments on the inside of the ring cause tensile stresses. Using

$$\Pi_i^* = 4\int_0^{\pi/2} \frac{M^2}{2EI} r\,\mathrm{d}\alpha$$

then (8.83) requires $\partial\Pi_i^*/\partial M_\mathrm{B} = 0$; the rotation corresponding to M_B must disappear. Therefore, it follows that

$$M_B = \frac{Qr}{2}\left(\frac{2}{\pi} - 1\right)$$

and thus

$$M = \frac{Qr}{\pi} - \frac{Qr}{2}\cos\alpha$$

Applying (8.83) again results in the mutual approximation of points A:

$$\frac{4Qr^3}{EI}\int_0^{\pi/2}\left(\frac{1}{\pi} - \frac{\cos\alpha}{2}\right)^2 \mathrm{d}\alpha = \frac{Qr^3}{4\pi EI}(\pi^2 - 8)$$

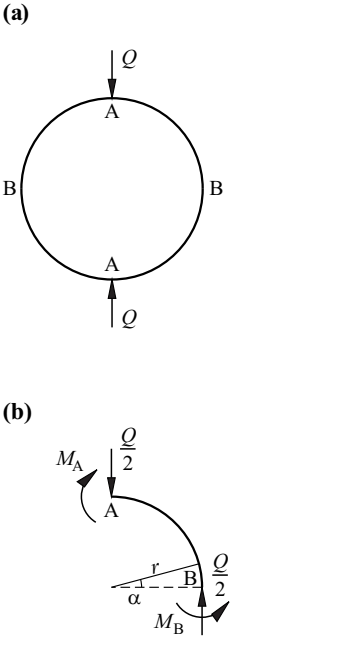

Fig. 8.15 Calibration ring: (a) elevation, (b) free body diagram

8.4.2.5 MAXWELL's generalised theorem

The partial differentiation of (8.83) with respect to a generalised force Q_l different from Q_k results in MAXWELL's *generalised theorem*

$$\frac{\partial^2 \Pi_i^*}{\partial Q_k \partial Q_l} = \frac{\partial u_k}{\partial Q_l} = \frac{\partial u_l}{\partial Q_k} \tag{8.84}$$

see (8.72); the field $\boldsymbol{u}(\boldsymbol{Q})$ is irrotational.

The partial differentiation of (8.80) with respect to a generalised displacement u_l different from u_k results in the dual relation of (8.84)

$$\frac{\partial^2 \Pi_i}{\partial u_k \partial u_l} = \frac{\partial Q_k}{\partial u_l} = \frac{\partial Q_l}{\partial u_k} \tag{8.85}$$

see (8.71); the field $\boldsymbol{Q}(\boldsymbol{u})$ is irrotational.

8.4.3 Linear elastic systems

When all the parts of the system are linear elastic and the deformations remain infinitesimally small, then various force and deformation states may be *superposed* because all the relationships describing the structural behaviour are linear, see section 6.1. This leads to significant simplifications when dealing with theory of structures issues.

8.4.3.1 MAXWELL's theorem

Every generalised displacement variable can be expressed as the sum of the effects of the generalised forces, i. e.

$$u_j = f_{jk} Q_k \quad \text{or} \quad \boldsymbol{u} = \boldsymbol{f} \bullet \boldsymbol{Q} \tag{8.86}$$

and, vice versa, every generalised force variable can be expressed as the sum of the effects of the generalised displacements, i. e.

$$Q_j = k_{jk} u_k \quad \text{or} \quad \boldsymbol{Q} = \boldsymbol{k} \bullet \boldsymbol{u} \tag{8.87}$$

The stiffness matrix $\boldsymbol{k}$ and the flexibility matrix $\boldsymbol{f}$ are inverse, $\boldsymbol{k} \bullet \boldsymbol{f} = \boldsymbol{f} \bullet \boldsymbol{k} = \mathbf{I}$.

According to ENGESSER's theorem (8.83), $u_j = \partial \Pi_i^* / \partial Q_j$, and according to (8.86), $\partial u_j / \partial Q_k = f_{jk} = \partial^2 \Pi_i^* / (\partial Q_j \partial Q_k)$. Owing to the interchangeability of the partial differentiations, MAXWELL's *theorem* applies:

$$f_{jk} = f_{kj} = \frac{\partial^2 \Pi_i^*}{\partial Q_j \partial Q_k} \tag{8.88}$$

The flexibility matrix $\boldsymbol{f}$ is symmetrical, and its coefficients result from the second derivatives of the complementary internal potential.

Similarly, applying CASTIGLIANO's theorem (8.80) and (8.87), we arrive at the dual proposition

$$k_{jk} = k_{kj} = \frac{\partial^2 \Pi_i}{\partial u_j \partial u_k} \tag{8.89}$$

The stiffness matrix $\boldsymbol{k}$ is symmetrical, and its coefficients result from the second derivatives of the internal potential.

Fig. 8.16 illustrates MAXWELL's theorem regarding the reciprocity of the displacements and the dual proposition regarding the reciprocity of the force variables for a system with two unit forces or displacements applied in given directions at points j and k.

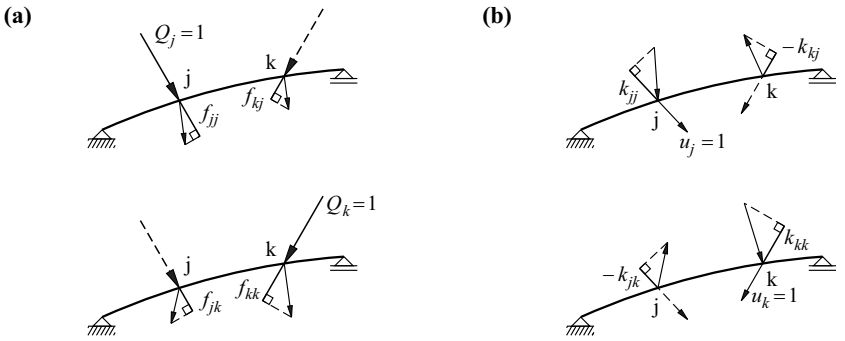

Fig. 8.16 MAXWELL's theorem: (a) reciprocity of displacements, (b) reciprocity of forces

Example 8.10 Simply supported beam

Determine the flexibility matrix $\boldsymbol{f}$ and the stiffness matrix $\boldsymbol{k}$ for the simply supported beam, rigid in shear and with constant bending stiffness EI, shown in Fig. 8.17.

The bending moment M for each section due to the unit loads can be determined from the moment diagrams shown in Fig. 8.17(a):

$$M = \frac{x}{2}Q_j + \frac{x}{4}Q_k \qquad (0 \le x \le l/2)$$

$$M = \frac{l-x}{2}Q_j + \frac{x}{4}Q_k \qquad (l/2 \le x \le 3l/4)$$

$$M = \frac{l-x}{2}Q_j + \frac{3(l-x)}{4}Q_k \qquad (3l/4 \le x \le l)$$

The quadratic form

$$\Pi_i^* = \int_0^l \frac{M^2}{2EI}\,\mathrm{d}x = \frac{l^3}{1536EI}(16Q_j^2 + 22Q_jQ_k + 9Q_k^2)$$

follows for the complementary internal potential. Applying (8.88) results in

$$\boldsymbol{f} = \frac{l^3}{768EI}\begin{bmatrix} 16 & 11 \\ 11 & 9 \end{bmatrix}$$

see Fig. 8.17(b). Inverting $\boldsymbol{f}$ results in

$$\boldsymbol{k} = \frac{768EI}{23l^3}\begin{bmatrix} 9 & -11 \\ -11 & 16 \end{bmatrix}$$

see Fig. 8.17(c), and from (8.89) we get the quadratic form for the internal potential

$$\Pi_i = \int_0^l \frac{\chi^2}{2}EI\,\mathrm{d}x = \frac{384EI}{23l^3}(9w_j^2 - 22w_jw_k + 16w_k^2)$$

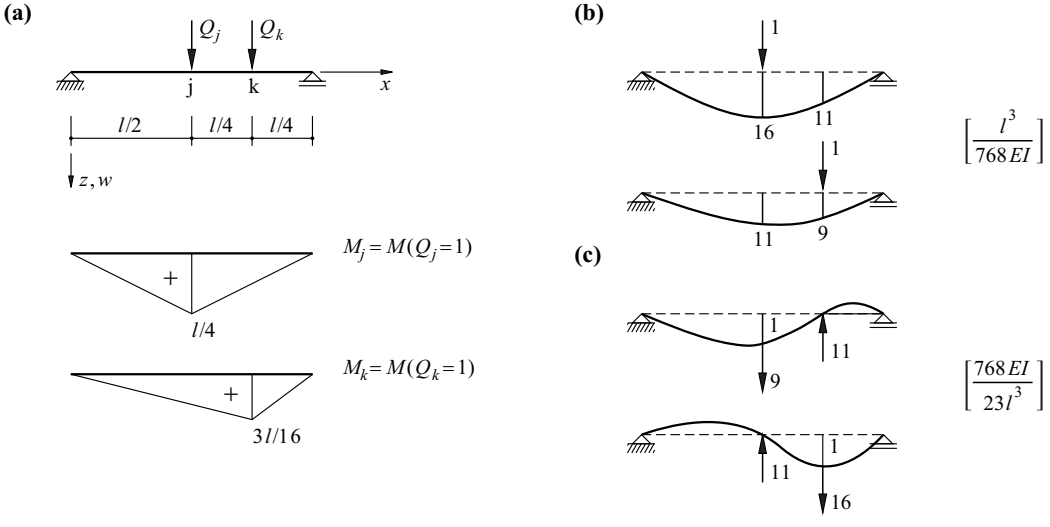

Fig. 8.17 Simply supported beam with two point loads: (a) system and moments due to unit loads, (b) flexibility coefficients, (c) stiffness coefficients

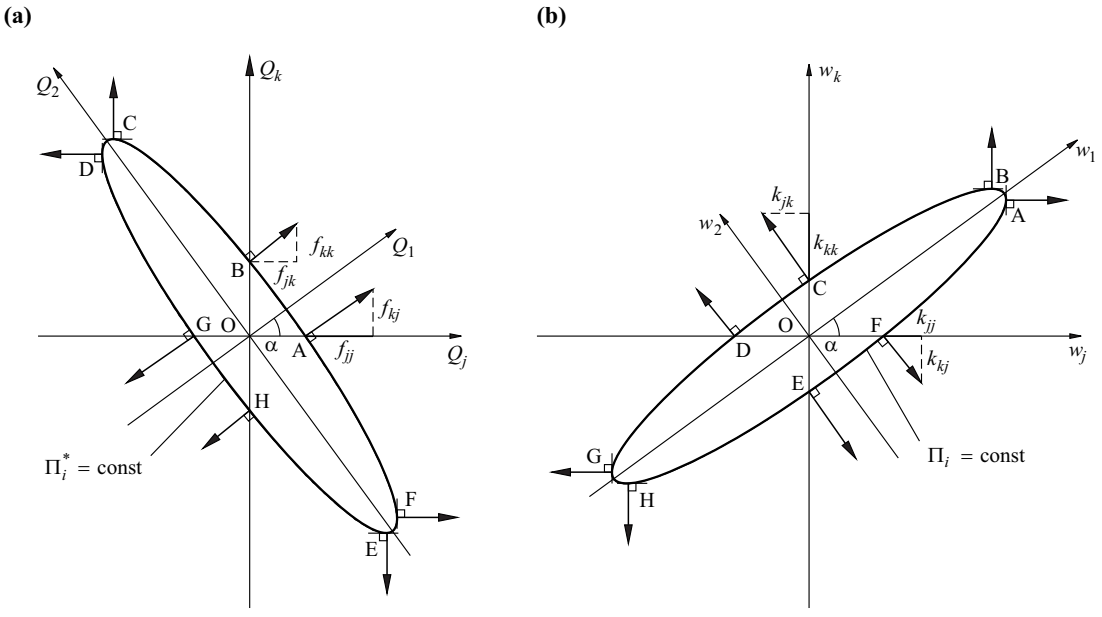

Fig. 8.18 Potential surfaces and gradients: (a) ENGESSER's theorem and flexibility coefficients, (b) CASTIGLIANO's theorem and stiffness coefficients

According to Fig. 8.18, the two quadratic forms can be represented as ellipses in the Q_j, Q_k or w_j, w_k planes The complementary internal potential is then as follows:

$$\Pi_i^* = \frac{l^3}{1536EI}(c_1^* Q_1^2 + c_2^* Q_2^2)$$

with the eigenvalues

$$c_{1,2}^* = \frac{16+9}{2} \pm \sqrt{\left(\frac{16-9}{2}\right)^2 + 11^2} = \left\{ \begin{array}{c} 24.043 \\ 0.957 \end{array} \right\}$$

and the directions of the principal axes follow from

$$\tan(2\alpha) = \frac{2 \cdot 11}{16-9} \quad \text{i. e.} \quad \alpha = 36.175°$$

Similarly, it follows that

$$\Pi_i = \frac{384EI}{23l^3}(c_1 w_1^2 + c_2 w_2^2)$$

where

$$c_{1,2} = \frac{9+16}{2} \mp \sqrt{\left(\frac{9-16}{2}\right)^2 + 11^2} = \left\{ \begin{array}{c} 0.957 \\ 24.043 \end{array} \right\}$$

and

$$\tan(2\alpha) = \frac{-2 \cdot 11}{9-16} \quad \text{i. e.} \quad \alpha = 36.175°$$

As can be seen, the eigenvalues c_1^*, c_2^* and c_1, c_2 are proportional to the inverses of the semi-axis squares ${Q_1}^2$, ${Q_2}^2$ and ${w_1}^2$, ${w_2}^2$, see (A5.40).

Fig. 8.18 illustrates the theorems of ENGESSER and CASTIGLIANO, according to which the displacements $\boldsymbol{u}$ ($\boldsymbol{w}$ in the example) and the loads $\boldsymbol{Q}$ are the gradients of the potential functions Π_i^* and Π_i. The corresponding points in the two figures have been given the same letters A to H. Points A and G correspond to the upper figure in Fig. 8.17(b), points B and H the lower figure. Likewise, points F and D correspond to the upper figure in Fig. 8.17(c), points C and E the lower figure.

8.4.3.2 BETTI's theorem

Starting with the work equation (8.20), we can interchange the roles of equilibrium state 1 and compatible deformation state 2:

$$\int \boldsymbol{q}_1^{\mathrm{T}} \cdot \boldsymbol{u}_2 \, \mathrm{d}V + \int \boldsymbol{t}_1^{\mathrm{T}} \cdot \boldsymbol{r}_2 \, \mathrm{d}S - \int \boldsymbol{\sigma}_1^{\mathrm{T}} \cdot \boldsymbol{\varepsilon}_2 \, \mathrm{d}V = 0$$

$$\int \boldsymbol{q}_2^{\mathrm{T}} \cdot \boldsymbol{u}_1 \, \mathrm{d}V + \int \boldsymbol{t}_2^{\mathrm{T}} \cdot \boldsymbol{r}_1 \, \mathrm{d}S - \int \boldsymbol{\sigma}_2^{\mathrm{T}} \cdot \boldsymbol{\varepsilon}_1 \, \mathrm{d}V = 0$$

Applying the symmetrical ($\boldsymbol{E}^{\mathrm{T}} = \boldsymbol{E}$) and positive definite ($\boldsymbol{\varepsilon}^{\mathrm{T}} \cdot \boldsymbol{E} \cdot \boldsymbol{\varepsilon} > 0$) elasticity matrix $\boldsymbol{E}$ according to (8.19), the third integrals in the two relationships above are identical:

$$\int \boldsymbol{\sigma}_1^{\mathrm{T}} \cdot \boldsymbol{\varepsilon}_2 \, \mathrm{d}V = \int \boldsymbol{\varepsilon}_2^{\mathrm{T}} \cdot \boldsymbol{E} \cdot \boldsymbol{\varepsilon}_1 \, \mathrm{d}V = \int \boldsymbol{\varepsilon}_1^{\mathrm{T}} \cdot \boldsymbol{E} \cdot \boldsymbol{\varepsilon}_2 \, \mathrm{d}V = \int \boldsymbol{\sigma}_2^{\mathrm{T}} \cdot \boldsymbol{\varepsilon}_1 \, \mathrm{d}V$$

and therefore BETTI*'s theorem*

$$\int \boldsymbol{q}_1^{\mathrm{T}} \cdot \boldsymbol{u}_2 \, \mathrm{d}V + \int \boldsymbol{t}_1^{\mathrm{T}} \cdot \boldsymbol{r}_2 \, \mathrm{d}S = \int \boldsymbol{q}_2^{\mathrm{T}} \cdot \boldsymbol{u}_1 \, \mathrm{d}V + \int \boldsymbol{t}_2^{\mathrm{T}} \cdot \boldsymbol{r}_1 \, \mathrm{d}S \tag{8.90}$$

applies. According to this theorem, the external deformation work of an equilibrium state 1 done on the (compatible) deformations of an equilibrium state 2 is equal to the external deformation work of state 2 done on the deformations of state 1.

If we use (8.17) to (8.19) to replace the loads $\boldsymbol{q}$ in (8.90) by $\boldsymbol{D}_s \cdot \boldsymbol{E} \cdot \boldsymbol{D}_k \cdot \boldsymbol{u} = \boldsymbol{D}_0 \cdot \boldsymbol{u}$, then after rearranging it follows that

$$\int \left(\boldsymbol{u}_1^{\mathrm{T}} \cdot \boldsymbol{D}_0 \cdot \boldsymbol{u}_2 - \boldsymbol{u}_2^{\mathrm{T}} \cdot \boldsymbol{D}_0 \cdot \boldsymbol{u}_1 \right) \mathrm{d}V = \int \left(\boldsymbol{t}_1^{\mathrm{T}} \cdot \boldsymbol{r}_2 - \boldsymbol{t}_2^{\mathrm{T}} \cdot \boldsymbol{r}_1 \right) \mathrm{d}S \tag{8.91}$$

an assertion similar to (8.57), according to which the *fundamental operator* $\boldsymbol{D}_0 = \boldsymbol{D}_s \cdot \boldsymbol{E} \cdot \boldsymbol{D}_k$ is *self-adjoint*.

Example 8.11 Simply supported beam

If we first apply Q_j to the beam examined in example 8.10 (Fig. 8.17), the result is the deflections $f_{jj}\, Q_j$ and $f_{kj}\, Q_j$ at j and k; in doing so, the force Q_j does the *active work* $Q_j f_{jj} Q_j / 2$ during its displacement. If, while still applying Q_j, we subsequently apply force Q_k, then the result is the additional displacements $f_{jk}\, Q_k$ and $f_{kk}\, Q_k$ at j and k; in this case the force Q_j does the *passive work* $Q_j f_{jk}\, Q_k$, and the force Q_k does the active work $Q_k f_{kk}\, Q_k / 2$ during its displacement.

Reversing the order of the loading results in the sequence of work values $Q_k f_{kk}\, Q_k / 2$, $Q_k f_{kj}\, Q_j$, $Q_j f_{jj}\, Q_j / 2$. As the system is conservative and the first and last terms result in the same sum, the two passive work values must be equal, i. e.

$$Q_j f_{jk} Q_k = Q_k f_{kj} Q_j$$

If we impose a deflection w_j on the system while restraining k, this requires the forces $k_{jj}\, w_j$ and $k_{kj}\, w_j$ at j and k; the work $w_j\, k_{jj}\, w_j / 2$ is done during this. Subsequently imposing w_k while maintaining w_j requires the forces $k_{jk}\, w_k$ and $k_{kk}\, w_k$ at j and k; in doing so, the force $k_{kj}\, w_j$ at k does the work $w_k\, k_{kj}\, w_j$, and the additional force for generating w_k contributes the work $w_k\, k_{kk}\, w_k / 2$. As before, reversing the order of the loading results in

$$w_k k_{kj} w_j = w_j k_{jk} w_k$$

8.5 Approximation methods

8.5.1 Introduction

Section 8.3 showed us that the principle of virtual deformations and the principle of virtual forces correspond to a global formulation of the equilibrium and the compatibility respectively, and section 8.4 provided the derivation of the theorems of least total potential and complementary total potential for conservative systems based on those principles. These two theorems are particularly suitable for devising approximate solutions for cases in which an exact answer to the static and kinematic relationships proves to be difficult or even impossible. The equilibrium conditions and the static boundary conditions, or the compatibility conditions and the kinematic boundary conditions, are therefore satisfied only approximately, i. e. infringed locally to a greater or lesser extent.

8.5.2 The RITZ method

The variational problem (8.74) can be overcome by applying

$$u = \sum_{i=1}^{n} c_i \omega_i \tag{8.92}$$

as described in section A7.9, where the approximating functions ω_i must fulfil the essential boundary conditions for u. The variational problem is turned into an ordinary extremal problem. The n unknown coefficients c_i follow from the linear equations

$$\frac{\partial \Pi}{\partial c_i} = 0 \qquad (i = 1, 2, ..., n) \tag{8.93}$$

By way of explanation, a number of simple examples are considered below which permit a direct comparison between the approximate and exact solutions. It is obvious that the real benefit of the RITZ *method* only really pays off in more complex cases when exact solutions cannot be found or found only with great difficulty.

Example 8.12 Tie

Fig. 8.19(a) shows the tie already examined in example 8.4, where q = const, EA = const and the total potential is

$$\Pi = \int_0^l \left[\frac{EA(u')^2}{2} - qu \right] \mathrm{d}x$$

As the highest derivative of the required function u has the order one in the integrand, the sole essential boundary condition results in a requirement for u at point $x = 0$: $u(0) = 0$. In the variational problem $\delta\Pi = 0$, functions with continuous derivatives up to order two are permitted for comparison. Approximating functions $\omega_i = x^i$ fulfil the essential boundary condition and it should be expected that when $n = 2$, the exact solution is reached according to (8.92).

Putting $n = 1$, i. e. working with the function $u = c_1 x$, then (8.93) results in

$$\frac{\mathrm{d}\Pi}{\mathrm{d}c_1} = \int_0^l (EAc_1 - qx)\,\mathrm{d}x = 0$$

and therefore $c_1 = ql/(2EA)$, see Fig. 8.19(b). Comparing this with the exact solution reveals consensus for $u(l)$; on the other hand, using EAu' only results in the mean value $ql/2$ of the exact linear progression of N.

When $n = 2$, the result is

$$\Pi = \int_0^l \frac{EA}{2} [(c_1 + 2c_2 x)^2 - q(c_1 x + c_2 x^2)]\,\mathrm{d}x$$

and (8.93) results in $c_1 = ql/(EA)$, $c_2 = -q/(2EA)$, see Fig. 8.19(c). We get the exact progression for both u and $N = EAu'$.

Putting $n = 2$ in the stationary case, we get the effective minimum $\Pi_2 = -q^2 l^3/(6EA)$ for Π. On the other hand, with $n = 1$, the answer is

$\Pi_1 = -q^2 l^3/(8EA) > \Pi_2$.

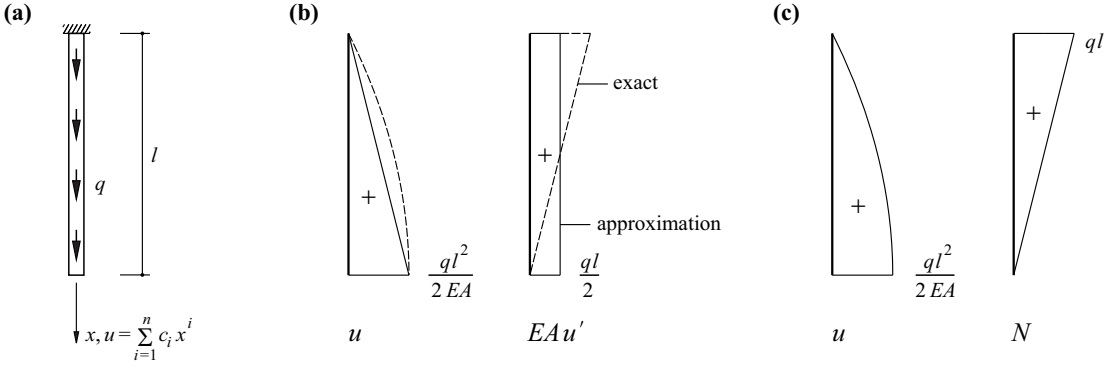

Fig. 8.19 Tie: (a) system, loads and approximating function, (b) $n = 1$, (c) $n = 2$, exact solution

Example 8.13 Cantilever beam

Fig. 8.20(a) shows the cantilever beam examined in example A7.1, with length l, EI = const, q = const and rigid in shear. Owing to the occurrence of the second derivative w'' of the required deflection function $w(x)$ in the integrand of the elastic potential (A7.43), it is necessary to consider the essential boundary conditions for w and w', i. e. $w(0) = w'(0) = 0$, and also to allow functions with continuous derivatives up to order four for comparison. (A7.44) fulfils these conditions and it is to be expected that an exact solution is reached when $n = 4$.

Fig. 8.20(b), (c) and (d) show the approximate solutions for $n = 2$ and $n = 3$ plus the exact solution for $n = 4$, see (A7.45). Fig. 8.20(b) and (c) illustrate, on the one hand, the improvement to the approximations when changing from $n = 2$ to $n = 3$, and, on the other, how the influence of the higher-order derivatives worsens the result – in contrast to the smoothing effect of integration, differentiation has a coarsening effect.

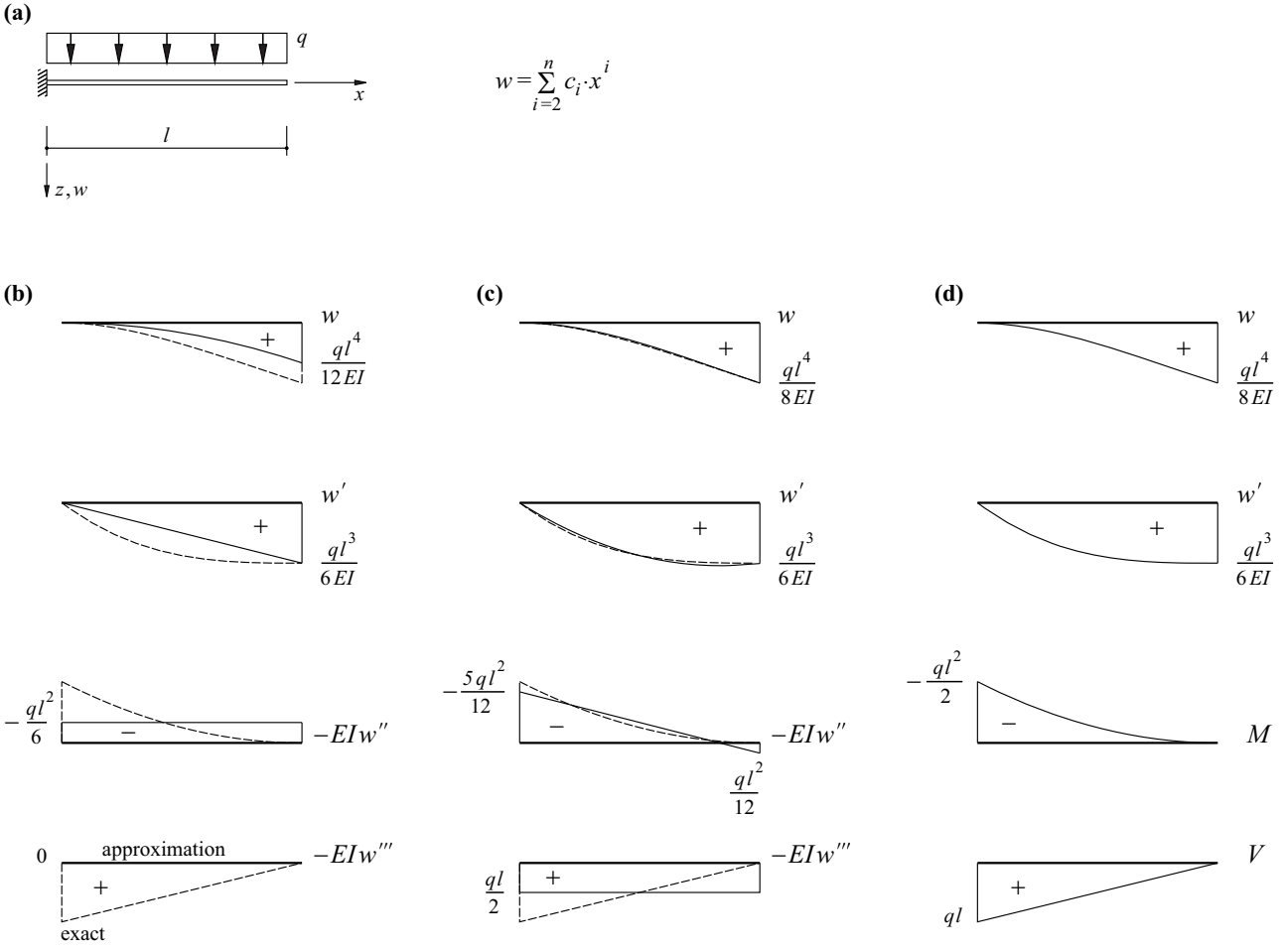

Fig. 8.20 Cantilever beam rigid in shear: (a) system, loads and approximating function, (b) $n = 2$, (c) $n = 3$, (c) $n = 4$, exact solution

Example 8.14 Ideal cantilever column

We shall again use (A7.44) with $n = 4$ for the inextensible, weightless *ideal column* ($q = 0$) shown in Fig. 8.21(a). From Fig. 8.21(b) we get the relationship $(\mathrm{d}u + \mathrm{d}x)^2 + (\mathrm{d}w)^2 = (\mathrm{d}x)^2$ and therefore $u' = -w'^2/2$, i. e.

$$\Pi_e = -\int_0^l \frac{Qw'^2}{2}\,\mathrm{d}x \quad , \quad \Pi = \int_0^l \left(\frac{EIw''^2}{2} - \frac{Qw'^2}{2}\right)\mathrm{d}x$$

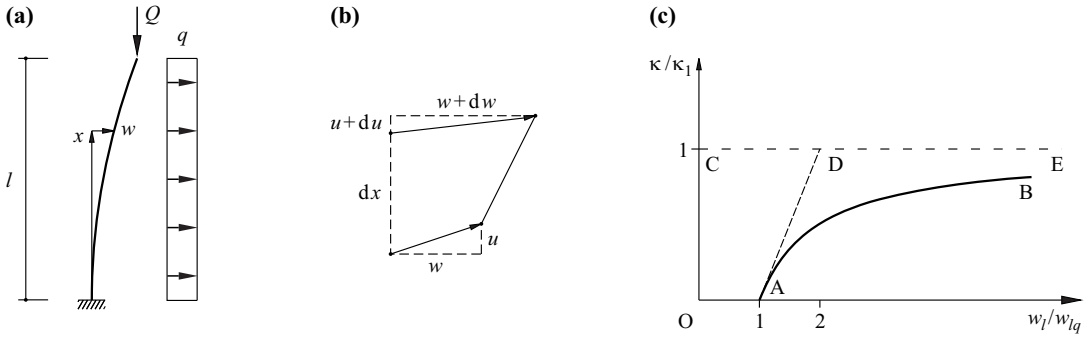

Fig. 8.21 Cantilever beam column subjected to transverse load: (a) notation, (b) kinematics of a differential element, (c) top deflection for uniform transverse load q

Substituting (A7.44) and applying (8.93) with EI = const and $\kappa = Ql^2/(EI)$ results in

$$\begin{bmatrix} 4-\frac{4}{3}\kappa & 6-\frac{3}{2}\kappa & 8-\frac{8}{5}\kappa \\ 6-\frac{3}{2}\kappa & 12-\frac{9}{5}\kappa & 18-2\kappa \\ 8-\frac{8}{5}\kappa & 18-2\kappa & \frac{144}{5}-\frac{16}{7}\kappa \end{bmatrix} \begin{Bmatrix} c_2 \\ c_3 l \\ c_4 l^2 \end{Bmatrix} = \begin{Bmatrix} 0 \\ 0 \\ 0 \end{Bmatrix}$$

Setting the determinant to zero leads to the characteristic polynomial

$$-\kappa^3 + 135\,\kappa^2 - 2880\,\kappa + 6300 = 0$$

with the eigenvalues

$$\kappa_1 = 2.4677 \quad , \quad \kappa_2 = 23.391 \quad , \quad \kappa_3 = 109.141$$

where the sole interesting minimum value κ_1 here lies only 0.014 % above the exact value $\pi^2/4 = 2.4674$ known for this problem.

Putting $n = 3$ eliminates the third row and the third column from the above matrix. The characteristic polynomial

$$\kappa^2 - \frac{104}{3}\kappa + 80 = 0$$

leads to the eigenvalues

$$\kappa_1 = 2.4860 \quad , \quad \kappa_2 = 32.18$$

where κ_1 lies 0.75 % above the exact value $\pi^2/4$.

When $n = 2$, only the first element of the matrix remains and we get $\kappa_1 = 3$, i. e. a value 21.6 % above $\pi^2/4$.

The smallest eigenvalue always lies above the exact value $\pi^2/4$, i. e. we approach the buckling load from above. It can be seen that we quickly achieve very good approximations with higher-value functions.

Example 8.15 Cantilever beam column

Combining the problems of the previous two examples, see Fig. 8.21(a), results in a *beam column* with the total potential

$$\Pi = \int_0^l \left(\frac{EIw''^2}{2} - \frac{Qw'^2}{2} - qw \right) \mathrm{d}x \tag{8.94}$$

To solve this, we first set up the function

$$w = c(6\xi^2 - 4\xi^3 + \xi^4)$$

proportional to the deflection function (A7.45), where $\xi = x/l$. And by applying (8.93) we get

$$c\left(\frac{24EI}{l^3} - \frac{60Q}{7l} \right) = ql$$

When $Q = 0$, this leads to the exact solution (A7.45), and when $q = 0$, we get the approximation $2.8\,EI/l^2$ for the buckling load, i. e. a value that is 13.5 % too high.

The relatively poor approximation for the buckling load can be explained by the fact that the deflection curve (A7.45) of the transversely loaded cantilever deviates considerably from the buckled shape.

If we insert the eigenvalue κ_1 determined in example 8.14 into the matrix, it is possible to determine

the coefficients c_2, c_3, c_4 apart from a common constant factor. We get $c_3 l = -0.06824\,c_2$, $c_4 l^2 = -0.13645\,c_2$ and therefore the form

$$w = c(3.772\xi^2 - 0.257\xi^3 - 0.515\xi^4)$$

comparable with the above approximation, which with $\xi = 1$ also results in $w = 3c$.

The exact solution to the bifurcation problem examined in example 8.14 leads to the buckled shape

$$w = c\left[1 - \cos\left(\frac{\pi\xi}{2}\right)\right]$$

which with a TAYLOR series and normalising to $w(1) = 3c$ can be approximated in the form

$$w = c\left(3.777\xi^2 - 0.777\xi^4\right)$$

The factor of 3.777 for ξ^2 is practically the same as the value of 3.772 found according to example 8.14.

In contrast to the bifurcation problem of example 8.14, using the general approximation (A7.44) for the second-order problem examined in the previous example does not result in a homogeneous, but rather an inhomogeneous, set of linear equations for determining the coefficients c_2, c_3, c_4 :

$$\begin{bmatrix} 4-\frac{4}{3}\kappa & 6-\frac{3}{2}\kappa & 8-\frac{8}{5}\kappa \\ 6-\frac{3}{2}\kappa & 12-\frac{9}{5}\kappa & 18-2\kappa \\ 8-\frac{8}{5}\kappa & 18-2\kappa & \frac{144}{5}-\frac{16}{7}\kappa \end{bmatrix} \begin{Bmatrix} c_2 \\ c_3 l \\ c_4 l^2 \end{Bmatrix} = \frac{ql^2}{EI} \begin{Bmatrix} \frac{1}{3} \\ \frac{1}{4} \\ \frac{1}{5} \end{Bmatrix}$$

This set of equations can be solved for any normal force level $\kappa/\kappa_1 < 1$, and it is possible to compare, for example, the top deflection $w(l) = w_l$ with the value $w_{lq} = ql^4/(8EI)$ which ensues for $Q = 0$, see Fig. 8.21(c). When $\kappa = \kappa_1/2$, we therefore get $c_2 = 0.4054\,ql^2/(EI)$, $c_3 = -0.1849\,ql/(EI)$, $c_4 = 0.0242\,q/(EI)$ and $w_l = 1.957\,w_{lq}$; when $\kappa = 3\kappa_1/4$, then $c_2 = 0.7084\,ql^2/(EI)$, $c_3 = -0.2097\,ql/(EI)$, $c_4 = -0.0151\,q/(EI)$ and $w_l = 3.869\,w_{lq}$.

Applying q moves the point in Fig. 8.21(c) from O to A. With a constant q and a steadily increasing Q, the point subsequently travels along curve AB. The slope of the initial tangent AD to curve AB is approximately 1, see Fig. 22.4(c). As can be seen, w_l is approximately two or four times w_{lq} when κ is equal to a half or three quarters of κ_1. The bifurcation load given in the figure by the asymptote CDE ($\kappa = \kappa_1$) cannot be reached; the deformations exceed all limits as Q rises further.

8.5.3 The GALERKIN method

If we replace u in (8.92) by w and apply (8.93) to (8.94), the outcome is n equations

$$\int_0^l (EIw''\omega_i'' - Qw'\omega_i' - q\omega_i)\,\mathrm{d}x = 0 \tag{8.95}$$

Double integration by parts of the term with EI and simple integration by parts of the term with Q, taking into account $M = -EIw''$ and $V = M'$, results in

$$\int_0^l [(EIw'')'' + Qw'' - q]\,\omega_i\,\mathrm{d}x - M\omega_i'\Big|_0^l + (V - Qw')\omega_i\Big|_0^l = 0 \tag{8.96}$$

The expression $V - Qw'$ denotes the shear force related to sections perpendicular to the undeformed bar axis; V is related to sections perpendicular to the deformed bar axis. When ω_i satisfies all boundary conditions, i. e. the natural (static) as well as the essential (kinematic) boundary conditions, the two boundary terms disappear from (8.96) and n equations

$$\int_0^l [(EIw'')'' + Qw'' - q]\,\omega_i\,\mathrm{d}x = 0 \tag{8.97}$$

remain.

According to (8.97), in general, the differential equation

$$(EIw'')'' + Qw'' - q = 0 \tag{8.98}$$

is not satisfied exactly, but merely approximately in an integral sense. The approximating functions ω_i play the role of weightings; the weighted means of the differential expressions in the square brackets in (8.97) disappear.

The equations (8.97) correspond to the *ordinary* GALERKIN *method*. The approximating functions must satisfy all boundary conditions. In the case of complex boundary conditions, we may use the *generalised* GALERKIN *method*. We use approximating functions that satisfy as many as possible, but not all, boundary conditions and take into account the corresponding boundary terms that do not disappear, see (8.96). This again provides us with a set of algebraic linear equations for determining the unknown coefficients c_i.

The methods of RITZ and GALERKIN are closely related. In fact, the former is a special case of the latter.

Example 8.16 Simply supported beam column

Fig. 8.22(a) shows a simply supported beam column with constant bending stiffness EI subjected to a uniform transverse load q. The approximation

$$w = c \sin\left(\frac{\pi x}{l}\right)$$

is set up to satisfy all boundary conditions: $w(0) = w(l) = w''(0) = w''(l) = 0$. Eq. (8.97) results in

$$\int_0^l \left[EIc\left(\frac{\pi}{l}\right)^4 \sin\left(\frac{\pi x}{l}\right) - Qc\left(\frac{\pi}{l}\right)^2 \sin\left(\frac{\pi x}{l}\right) - q \right] \sin\left(\frac{\pi x}{l}\right) \mathrm{d}x = 0$$

and therefore

$$EIc\left(\frac{\pi}{l}\right)^4 \frac{l}{2} - Qc\left(\frac{\pi}{l}\right)^2 \frac{l}{2} - q\frac{2}{\pi} l = 0$$

or

$$w = \frac{4ql^2}{\pi^3\left[\frac{\pi^2 EI}{l^2} - Q\right]} \sin\left(\frac{\pi x}{l}\right) = \frac{1}{1 - \frac{Ql^2}{\pi^2 EI}} \cdot \frac{4ql^4}{\pi^5 EI} \sin\left(\frac{\pi x}{l}\right)$$

We get the exact solution to the bifurcation problem ($q = 0$) with the buckling load $\pi^2 EI/l^2$. Turning to the pure transverse bending problem ($Q = 0$), the maximum deflection at $x = l/2$ is $4ql^4/(\pi^5 EI)$ instead of $5ql^4/(384EI)$, i. e. a value that is 0.4 % too high.

The comparison with a cantilever beam of only half the length in Fig. 8.22(b) shows that the solution to the bifurcation problem can be applied directly; a cantilever beam has the same buckling load as a beam twice as long and simply supported at both ends. However, we can see from Fig. 8.22(c) that the solution for the general second-order problem with axial and transverse loads cannot be used because of the different bending moment diagrams M.

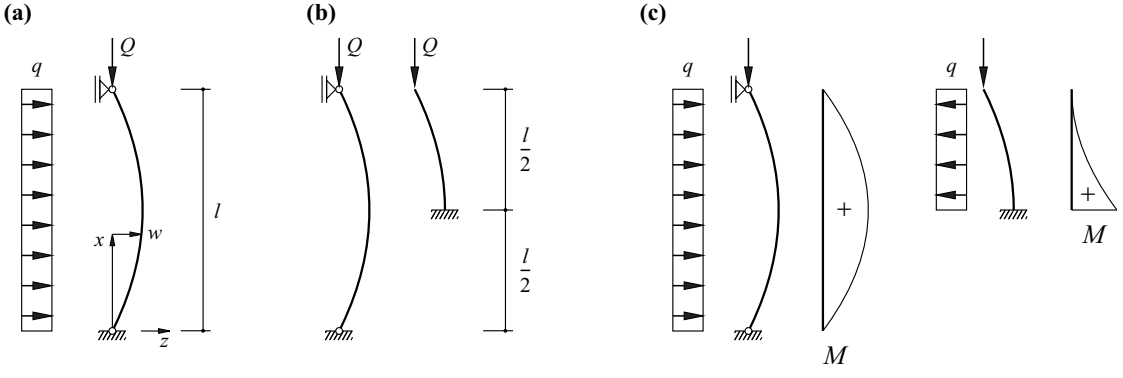

Fig. 8.22 Simply supported beam column: (a) system, (b) comparison with cantilever beam - bifurcation problem, (c) comparison with cantilever beam - transverse load

8.6 Summary

1. The introductory example using an ideal truss (Fig. 8.1) results in a basic scheme (Fig. 8.2 and Fig. 19.5) for discontinua. The structural behaviour is described by a finite number of work-associated force and deformation variables, i. e. the stresses $\boldsymbol{s}$, the strains $\boldsymbol{v}$, the loads $\boldsymbol{Q}$ and the displacements $\boldsymbol{V}$. The kinematic transformation matrix $\boldsymbol{a}$ describes the transition from $\boldsymbol{V}$ to $\boldsymbol{v}$, its transpose $\boldsymbol{a}^{\mathrm{T}}$ the transition from $\boldsymbol{s}$ to $\boldsymbol{Q}$. And vice versa, the static transformation matrix $\boldsymbol{b}$ describes the transition from $\boldsymbol{Q}$ to $\boldsymbol{s}$ and its transpose $\boldsymbol{b}^{\mathrm{T}}$ the transition from $\boldsymbol{v}$ to $\boldsymbol{V}$.
2. Irrespective of the material behaviour and the system, the force variables of an equilibrium state 1 on the whole do no work on the deformation variables of a compatible deformation state 2 (work equation $\boldsymbol{Q}_1{}^{\mathrm{T}} \cdot \boldsymbol{V}_2 - \boldsymbol{s}_1{}^{\mathrm{T}} \cdot \boldsymbol{v}_2 = 0$).
3. Statically indeterminate linear elastic systems can be analysed using the force method or the displacement method. The displacement method (chapter 17) requires the matrix $\boldsymbol{a}$ and the (diagonal) stiffness matrix $\boldsymbol{k}$ to be set up. The force method (chapter 16) requires the setting-up of matrices $\boldsymbol{b}_0$ and $\boldsymbol{b}_1$ for the influence of the loads, or rather the statically indeterminate force variables, for the statically determinate basic system as well as the (diagonal) flexibility matrix $\boldsymbol{f}$.
4. A scheme (Fig. 8.3) similar to Fig. 8.2 results for continua (chapter 18) with a three-, two- or one-dimensional model space, Fig. 8.4. For the adjoint operators linking the static and kinematic variables, $\boldsymbol{D}_k = \boldsymbol{D}_s{}^{\mathrm{T}}$ ($\boldsymbol{D}_k = -\boldsymbol{D}_s{}^{\mathrm{T}}$) for even (odd) differential operators as elements.
5. In preparation for chapters 13, 23 and 24, static, kinematic and (linear elastic) constitutive relationships are specified for planar and spatial framed structures with bars having finite or infinite shear stiffness, also for the coplanar stress state and the coplanar strain state as well as for slabs having finite or infinite shear stiffness, and three-dimensional continua.
6. The principle of virtual work, the fundamental principle of equilibrium, applies to any system irrespective of the material behaviour. It can be expressed as the principle of virtual deformations and as the principle of virtual forces. The principle of virtual deformations corresponds to a global formulation of the equilibrium, and the principle of virtual forces corresponds to a global formulation of the compatibility. In contrast to the principle of virtual forces, the principle of virtual deformations remains valid even for geometric non-linearity.
7. For conservative systems, the principle of virtual deformations results in the theorem of least total potential, and the principle of virtual forces results in the theorem of least complementary total potential. If we confine ourselves to a finite number of displacement or force variables in given directions, then we arrive at the theorems of CASTIGLIANO and ENGESSER, and through partial differentiation at MAXWELL's generalised theorem.
8. The various force and deformation states may be superposed for linear elastic systems with infinitesimally small deformations (first-order theory). The stiffness and flexibility matrices are symmetrical and their coefficients result from the second derivatives of the internal potential or the complementary internal potential. In addition, BETTI's theorem applies, which says that the external deformation work of an equilibrium state 1 done on the deformations of an equilibrium state 2 is equal to the external deformation work of state 2 done on the deformations of state 1.
9. Based on the theorems of least total potential and complementary total potential, it is possible to devise approximate solutions according to the methods of RITZ and GALERKIN using suitable approximating functions; such approximate solutions convert the associated variational problems into ordinary extremal problems. When using the RITZ method, a special case of the GALERKIN method, the approximating functions only have to satisfy the kinematic boundary conditions. However, when using the ordinary GALERKIN method, all the boundary conditions, i. e. including the static boundary conditions, must be fulfilled.

10. When using the generalised GALERKIN method, we use approximating functions that satisfy as many as possible, but not all, boundary conditions and take into account the corresponding boundary terms in the set of linear equations that ensues for the coefficients of the approximating functions. The differential equations corresponding to the variational problem are not solved exactly, but rather only in the weighted mean (with the approximating functions as weightings).

8.7 Exercises

8.1 The two bars of the system shown in Fig. 8.23 are rigid. Determine the relationship between Q and V according to the force method and the displacement method. To do this, use eq. (8.1) and (8.5) to (8.12). The internal force and deformation variables are the moments and the associated rotations at 1 and 2.

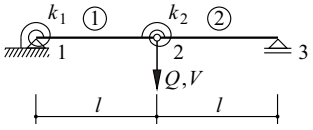

Fig. 8.23 Sketch of the static system for exercise 8.1

8.2 Verify the expressions for the boundary force components of plates given at the end of section 8.2.4 and show that combining (8.32), (8.33) and (8.35) leads to

$$\Delta\Delta u = -\frac{1}{Eh}\left[(1-\nu^2)q_{x,xx} + 2(1+\nu)q_{x,yy} - (1+\nu)^2 q_{y,xy}\right] \tag{8.99}$$

8.3 Verify the differential equation (8.48) for KIRCHHOFF slabs.

8.4 Based on section 8.2.8, verify the adjointness of the operators $\boldsymbol{D}_s$ and $\boldsymbol{D}_k$ in (8.32) and (8.33) for plates.

8.5 A semicircular cantilever beam is loaded at its unsupported end by a force Q acting perpendicular to the plane of the circle. Use the principle of virtual deformations to determine the diagrams of the stress resultants.

8.6 Use the principle of virtual forces to calculate the displacements and rotations at the unsupported end of the cantilever beam of exercise 8.5. Assume constant flexural, torsional and shear stiffnesses along the bar axis.

8.7 A straight cantilever beam of length l is loaded at its unsupported end ($x = l$) by a force Q_0 acting perpendicular to the bar axis. Present the total potential (8.73) graphically as a function of the deflection w_0 at the position and in the direction of Q_0. Use the approximations $w/w_0 = \xi^2$, ξ^3 and $3\xi^2/2 - \xi^3/2$ and only take into account deformations due to bending (EI = const, $\xi = x/l$). Discuss the result and compare it with examples A7.2 and 8.7.

8.8 Work out a presentation similar to Fig. 8.18 for example 8.7.

8.9 Using a similar approach to exercise 8.7, examine a simply supported beam (length l, EI = const, $\xi = x/l$) subjected to a uniform load q = const with the approximations $w = w_m \cdot 4\xi(1-\xi)$ or $w = w_m \cdot \sin(\pi\xi)$. Discuss the result using the exact deflection function $w = ql^4(\xi^4 - 2\xi^3 + \xi)/(24EI)$.

8.10 Examine example 8.15 under the assumption of a bending stiffness in the upper half of the bar ($l/2 \leq x \leq l$) which is reduced to $EI/2$. What changes are there to κ_1, w_{lq} and Fig. 8.21(c)?

9 STRUCTURAL ELEMENTS AND TOPOLOGY

9.1 General

This chapter deals exclusively with *framed structures*. Such structures are made up of *bar elements* that have *joints* at their ends connecting them to other bars or to supports. A *bar* is an idealised, linear structural component consisting of a *bar axis* and the *bar cross-sections* orthogonal to that axis; further, the dimensions of the bar cross-section are small in comparison with its span. The bar axis may be straight, or may be curved in one plane or in space, and the principal axes of the cross-sections (see section 13.2.1), element for element, may have a constant direction or may be twisted. In addition, the dimensions of the cross-sections and hence the bar stiffnesses, element for element, may be constant or variable.

The static and kinematic variables for the general case of spatial framed structures were introduced in section 8.2.3, after plane framed structures had been dealt with in section 8.2.2. Cases with general stress resultants in the bar elements and straight bar axes are known as *beams* or *columns*, and those with curved bar axes are known as *arches* or *curved beams*, see section 5.3.2. Where the bar elements are straight and connected concentrically to other elements via frictionless hinges and the loads are applied at the joints only, then we are dealing with an ideal (plane or spatial) *truss* (see section 8.1), in which the only stress resultants in the bars are normal forces. In a similar fashion, owing to their low bending stiffness, *cables*, with a curving axis, are practically only subjected to normal forces (tensile forces), apart from local effects, see section 18.8.

Combining beams, columns and arches produces *frameworks*, which must be clearly distinguished from trusses. Hybrid systems are often employed. Such systems consist of a combination of framework and truss or cable elements and, if need be, other types of element.

The reader should refer to sections 5.1.5 and 5.1.6 for information about *supports* and *hinges*.

9.2 Modelling of structures

Continuing on from the general information regarding modelling of structures given in section 4.3, we shall now begin by considering the bridge structure shown in the upper drawing of Fig. 9.1. The main span, with its raking piers, is connected to a continuous frame structure spanning over the slender foreshore piers to the abutments. The bridge beams and piers are primarily subjected to bending in the vertical plane. In addition, there are certain stress resultants due to horizontal actions such as wind and earthquake transverse to the bridge elevation plus torsional stress resultants caused by eccentric traffic loads.

The lower drawing of Fig. 9.1 shows the basis of one possible idealisation of the bridge structure, i. e. as a (plane) framed structure; this is the so-called *structural system*. The structural system describes the topology of the structure, in other words, the arrangement of the loadbearing elements (supports, columns, beams) and the way in which they work together. The raking piers supporting the main span, which taper

Theory of Structures. First Edition. Peter Marti

towards the base, are considered to have hinged joints at their foundations and to be fixed at the bridge beams. The foreshore piers are idealised as fixed at both ends (i. e. at bridge beams and foundations) and sliding bearings are assumed at the abutments.

The structural system contains neither information about the dimensions of the structure nor details of the construction materials or subsoil conditions. Such information, together with the structural system, forms part of the more comprehensive *structural model*, which in the following will also be referred to as a *static system*. We shall use diagrams and tables to achieve a precise mathematical definition of the static system (see Fig. 9.4 and Tab. 9.1).

Structures are assemblies in three dimensions which, however, can often be broken down into *plane subsystems*. For example, the single-storey shed structure shown in Fig. 9.2 can be broken down into the two *lattice girders* and the *wind bracing* in the roof and wall plates. Only in the case of true spatial structures, e. g. cable nets or shells in double curvature, is such a breakdown impossible.

Fig. 9.3 shows various examples of plane framed structures. The *cantilever beam* of Fig. 9.3(a) and the *simply supported beam* in Fig. 9.3(b) are basic types which can be combined in diverse ways and extended by introducing or releasing constraints. The simply supported beam with an overhang at one end shown in Fig. 9.3(c) has a *propped beam* in the second span connected to the first beam via a hinge. Fig. 9.3(d) shows a similar arrangement for a three-span beam, in this case with a *suspended beam* in the middle span. *Hinged girders*, as shown in Fig. 9.3(c) and (d), are sometimes called GERBER *beams*.

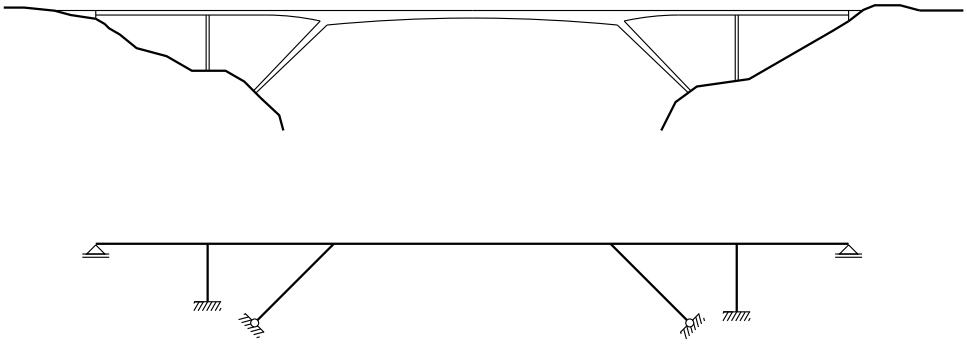

Fig. 9.1 Bridge structure and structural system

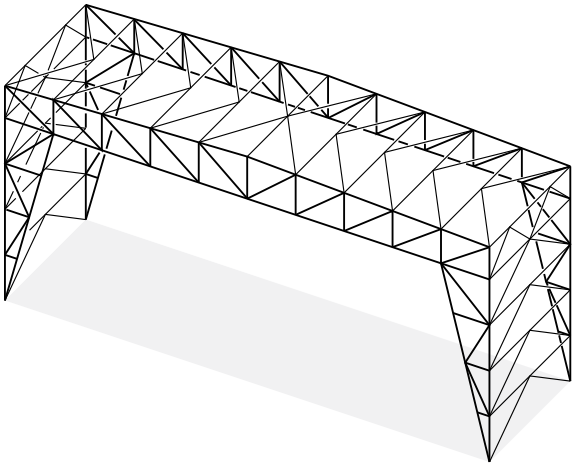

Fig. 9.2 Lattice girders and wind bracing

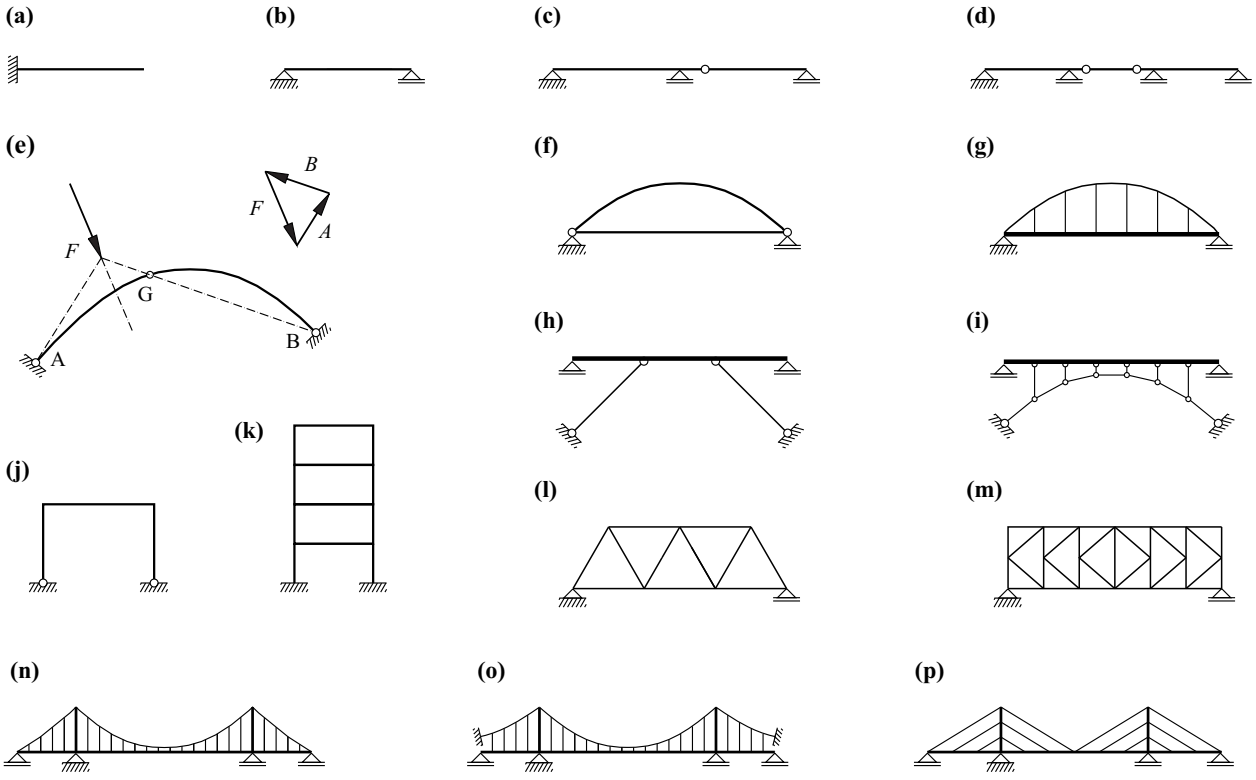

Fig. 9.3 Examples of plane framed structures: (a) cantilever beam, (b) simply supported beam, (c) hinged girder, (d) hinged girder with suspended beam, (e) three-hinged arch, (f) two-hinged arch with tie, (g) LANGER beam, (h) strutted beam, (i) deck-stiffened polygonal arch, (j) two-hinged frame, (k) multi-storey frame, (l) WARREN truss (m) K-truss, (n) self-anchored suspension bridge, (o) externally anchored suspension bridge, (p) cable-stayed bridge

The *three-hinged arch* of Fig. 9.3(e) is illustrated carrying a force $\boldsymbol{F}$ with the help of the force and funicular polygons introduced in section 5.1.4. As arc BG is not loaded, the line of action of the support force $\boldsymbol{B}$ coincides with chord BG, which also determines $\boldsymbol{A}$. The *two-hinged arch* with a *tie* (tied arch) shown in Fig. 9.3(f) essentially functions like a simply supported beam, at least externally. The same is true for the LANGER *beam* (arch-hanger-girder system) of Fig. 9.3(g), which is strengthened by a bar polygon and suspenders.

In the *strutted beam* of Fig. 9.3(h), the beam is propped and horizontally stabilised by two raking *pin-ended struts* connected to the beam via hinges. In the system shown in Fig. 9.3(i), the polygonal arch is stiffened by the deck beam so that it can accommodate asymmetric loads; see the remarks at the conclusion of example 5.7.

Fig. 9.3(j) and (k) correspond respectively to the *two-hinged frame* and *multi-storey frame* commonly used for buildings; these frames consist of columns (legs) and beams (frame beams).

Fig. 9.3(l) shows a simply supported beam in the form of a WARREN *truss*, and Fig. 9.3(m) in the form of a *K-truss*; the latter functions in a similar way to the wind bracing in Fig. 9.2.

In the *self-anchored suspension bridge* shown in Fig. 9.3(n), the horizontal component of the tension in the cable is brought into equilibrium by the compressive forces in the deck beam after completing the bridge. The bridge must be built on scaffolding – a disadvantage that is overcome in the *externally anchored suspension bridge* (genuine suspension bridge) of Fig. 9.3(o); here, the deck beam is built cantilevering out in both directions from the middle, or rather from the *pylons*, and successively connected via the *suspenders* to the *main cables*, which are spun in advance and are continuous over the pylons. Finally, Fig. 9.3(p) shows a *cable-stayed bridge* with a harp-type arrange-

ment of the cable stays, which are connected to the deck beam and the pylons via semi-hinges. As with the self-anchored suspension bridge, compressive forces ensue in the deck beam due to the horizontal component of the tensile forces in the cables, but the system can be built without scaffolding by using the *free cantilevering* method, which involves successively cantilevering out from and guying back to the pylons.

9.3 Discretised structural models

9.3.1 Description of the static system

Fig. 9.4(a) shows the *diagram of the static system* for a plane system consisting of five joints and four bar elements. The diagram includes the *global coordinates X*, *Z*, the designations of all joints and bars (consecutive numbering, bar numbers in circles), the dimensioning of all joints, support and hinge (none in this case) symbols, all the loads (M_2, F_3 and q_3 in this example) and the orientation of the *local coordinates x, z* of all bar elements (indicated by the dotted line on the positive z side), see Fig. 9.4(b).

The *support force variables* C_{ij} do not need to be included in the diagram of the static system if it has been agreed that positive support force variables are forces and moments acting in the positive global axis direction (j = *X, Y, Z*) on the system released from the supports i; in the case of sliding bearings inclined with respect to the global axes, one of the support force components must be considered as independent and the other as dependent (geometrically determinate). Including the support force variables in the diagram of the system would also be inadmissible because that (without removing the supports) would not result in a true free body diagram.

The diagram of the static system could be completed by adding the stiffnesses of all bar elements according to (8.23) or (8.28). This is possible in simple cases, but generally the diagram then seems to be overloaded, and it is more expedient to provide this data in a *table of the static system*, see Tab. 9.1.

As can be seen, Tab. 9.1 provides all the information contained in Fig. 9.4(a) plus the bar stiffnesses. Making these stiffnesses functions of x, as is the case with *haunched beams*, for example, with their varying cross-sectional geometry, would allow them to be described as varying bar loads q, for example, by specifying the boundary values. If existing constraints were to be released in the system of Fig. 9.4(a), e. g. by introducing a flexural hinge to the left of joint 3 (i. e. at the right-hand end of bar 2), then this would have to be taken into account by including a corresponding auxiliary condition in Tab. 9.1; the hinge creates an additional degree of freedom, the corresponding moment becomes zero.

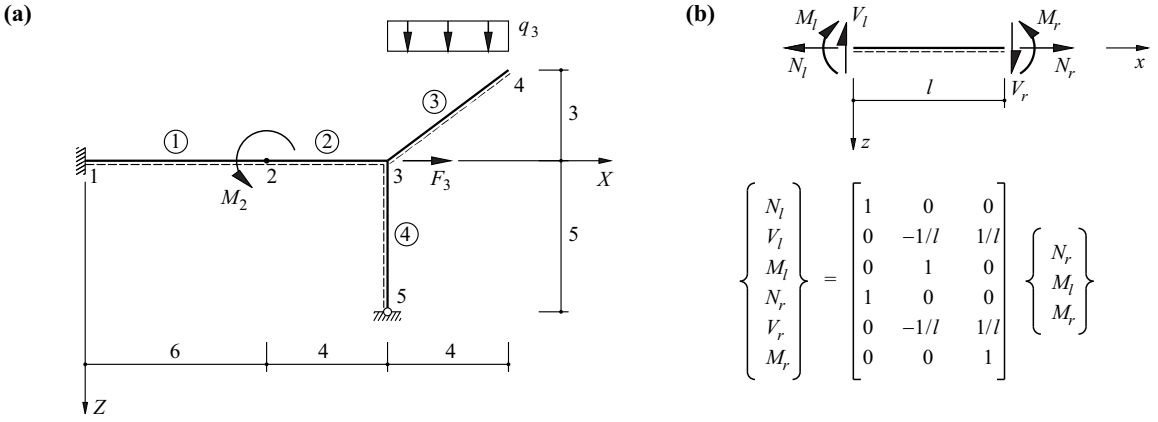

Fig. 9.4 Plane frame: (a) diagram of the static system (dimensions in m), (b) bar end forces

Tab. 9.1 Table of the static system – data of joints and bars

Joint	X	Z	Q_X	Q_Z	M_Y
1	0	0	C_{1X}	C_{1Z}	C_{1Y}
2	6	0			M_2
3	10	0	F_3		
4	14	– 3			
5	10	5	C_{5X}	C_{5Z}	
	m	m	kN	kN	kNm

Bar	l	r	l	EA	GA_v	EI	q_x	q_z
1	1	2	6	EA_1	GA_{v1}	EI_1		
2	2	3	4	EA_2	GA_{v2}	EI_2		
3	3	4	5	EA_3	GA_{v3}	EI_3	$-0.6\,q_3$	$0.8\,q_3$
4	3	5	5	EA_4	GA_{v4}	EI_4		
			m	MN	MN	MNm^2	kN/m	kN/m

Dividing the system into joints and bar elements is completely arbitrary. Each of the four bars shown in Fig. 9.4(a) could be further subdivided by introducing further joints; the ensuing new bar elements would then be explicitly defined by the choice of joint.

9.3.2 Joint equilibrium

Applying the equilibrium conditions enables three of the six bar end forces to be eliminated for each bar element, as shown in Fig. 9.4(b); N_r, M_l and M_r are chosen as *independent bar end forces*. In the general spatial case according to (8.28) with 12 bar end forces, it is expedient to choose the six variables N_r, T_r, M_{yl}, M_{yr}, M_{zl}, M_{zr} as independent bar end forces. The corresponding transformation of the *complete bar end forces* into independent bar end forces comes about without any further work by generalising the relationship given in Fig. 9.4(b).

The *internal force variables* N_r, M_l, M_r are supplemented by *external force variables* (forces and moments) at the joints, the so-called *joint loads* Q_i. These are introduced as positive in the direction of the positive global coordinates.

In the case of the bar element shown in Fig. 9.5(a), the local coordinates x, z coincide with the global coordinates X, Z. If we consider the two joints and the bar element between them separately as free bodies, see Fig. 9.5(b), then by considering the transformation given in Fig. 9.4(b), we get the *joint equilibrium conditions*

$$\begin{Bmatrix} Q_1 \\ Q_2 \\ Q_3 \\ Q_4 \\ Q_5 \\ Q_6 \end{Bmatrix} + \begin{bmatrix} 1 & 0 & 0 \\ 0 & -1/l & 1/l \\ 0 & 1 & 0 \\ -1 & 0 & 0 \\ 0 & 1/l & -1/l \\ 0 & 0 & -1 \end{bmatrix} \begin{Bmatrix} N_r \\ M_l \\ M_r \end{Bmatrix} = \begin{Bmatrix} 0 \\ 0 \\ 0 \\ 0 \\ 0 \\ 0 \end{Bmatrix} \tag{9.1}$$

Each joint load Q_i corresponds to a *degree of freedom* or an *external deformation variable* (displacement or rotation) V_i, see section 8.1.1. In order to restrain the bar element of Fig. 9.5(a), which is free to move in any direction, we need to introduce at least three constraints, i. e. three degrees of freedom must become passive. This converts the corresponding external force variables Q_i into support force variables C_i. For example, in the case of Fig. 9.5(c), these are the variables C_1, C_2, C_3 correspond-

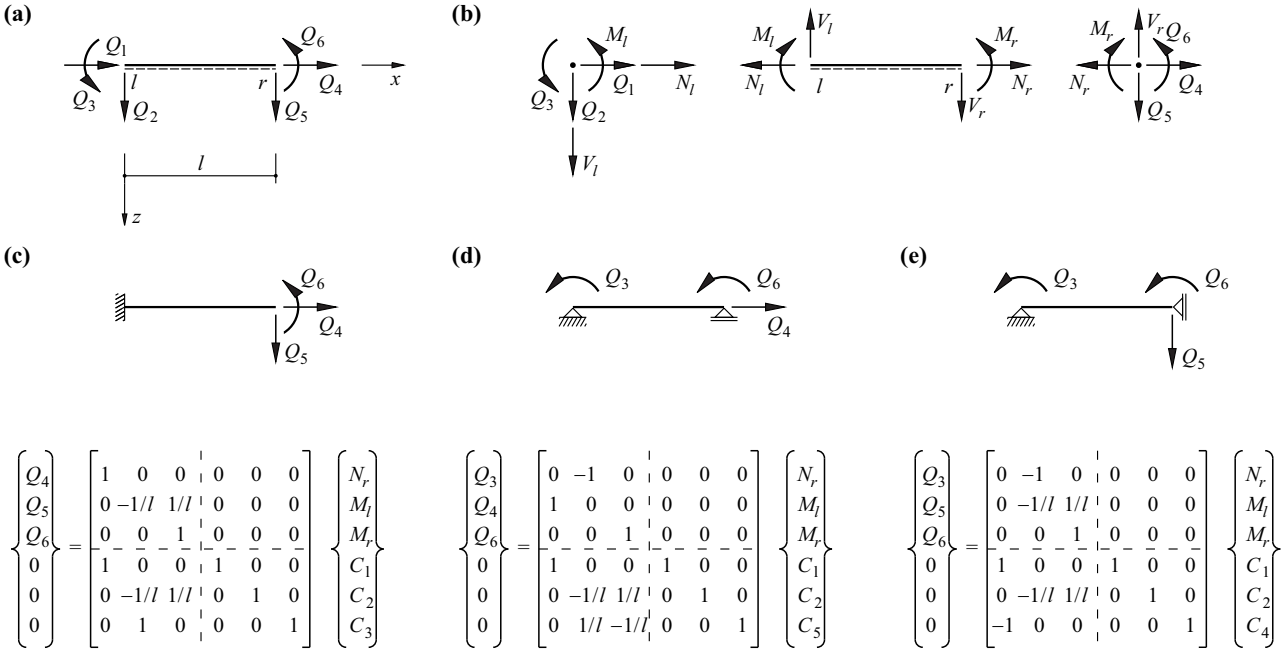

$$\begin{Bmatrix} Q_4 \\ Q_5 \\ Q_6 \\ 0 \\ 0 \\ 0 \end{Bmatrix} = \left[\begin{array}{ccc|ccc} 1 & 0 & 0 & 0 & 0 & 0 \\ 0 & -1/l & 1/l & 0 & 0 & 0 \\ 0 & 0 & 1 & 0 & 0 & 0 \\ \hline 1 & 0 & 0 & 1 & 0 & 0 \\ 0 & -1/l & 1/l & 0 & 1 & 0 \\ 0 & 1 & 0 & 0 & 0 & 1 \end{array}\right] \begin{Bmatrix} N_r \\ M_l \\ M_r \\ C_1 \\ C_2 \\ C_3 \end{Bmatrix} \qquad \begin{Bmatrix} Q_3 \\ Q_4 \\ Q_6 \\ 0 \\ 0 \\ 0 \end{Bmatrix} = \left[\begin{array}{ccc|ccc} 0 & -1 & 0 & 0 & 0 & 0 \\ 1 & 0 & 0 & 0 & 0 & 0 \\ 0 & 0 & 1 & 0 & 0 & 0 \\ \hline 1 & 0 & 0 & 1 & 0 & 0 \\ 0 & -1/l & 1/l & 0 & 1 & 0 \\ 0 & 1/l & -1/l & 0 & 0 & 1 \end{array}\right] \begin{Bmatrix} N_r \\ M_l \\ M_r \\ C_1 \\ C_2 \\ C_5 \end{Bmatrix}$$

$$\begin{Bmatrix} Q_3 \\ Q_5 \\ Q_6 \\ 0 \\ 0 \\ 0 \end{Bmatrix} = \left[\begin{array}{ccc|ccc} 0 & -1 & 0 & 0 & 0 & 0 \\ 0 & -1/l & 1/l & 0 & 0 & 0 \\ 0 & 0 & 1 & 0 & 0 & 0 \\ \hline 1 & 0 & 0 & 1 & 0 & 0 \\ 0 & -1/l & 1/l & 0 & 1 & 0 \\ -1 & 0 & 0 & 0 & 0 & 1 \end{array}\right] \begin{Bmatrix} N_r \\ M_l \\ M_r \\ C_1 \\ C_2 \\ C_4 \end{Bmatrix}$$

Fig. 9.5 Joint equilibrium conditions: (a) joint force variables, (b) free body diagrams for joints and bar elements, (c) cantilever beam, (d) simply supported beam, (e) kinematically unstable system

ing to the fixity of the cantilever beam at the left-hand end of the bar. If we rearrange the joint equilibrium conditions (9.1) as follows

$$\begin{Bmatrix} \boldsymbol{Q} \\ \mathbf{0} \end{Bmatrix} = \begin{bmatrix} \boldsymbol{g} & \mathbf{0} \\ \boldsymbol{g}_{sC} & \mathbf{I} \end{bmatrix} \cdot \begin{Bmatrix} \boldsymbol{s} \\ \boldsymbol{C} \end{Bmatrix} \tag{9.2}$$

the result is the relationship given below the figure in Fig. 9.5(c), where the vectors $\boldsymbol{Q}$, $\boldsymbol{s}$ and $\boldsymbol{C}$ contain the internal and external force variables or the support force variables, and $\boldsymbol{g}$ and $\boldsymbol{g}_{sC}$ denote corresponding *equilibrium matrices*. Inverting $\boldsymbol{g}$ gives us $\boldsymbol{s}$: $N_r = Q_4$, $M_l = -Q_5 l + Q_6$ and $M_r = Q_6$; substituting in (9.2) gives us $\boldsymbol{C}$: $C_1 = -Q_4$, $C_2 = -Q_5$, $C_3 = Q_5 l - Q_6$.

Similarly, the simply supported beam shown in Fig. 9.5(d) has the relationship (9.2) given below the figure. By inverting $\boldsymbol{g}$, it follows that $N_r = Q_4$, $M_l = -Q_3$, $M_r = Q_6$ and, furthermore, that $C_1 = -Q_4$, $-C_2 = (Q_3 + Q_6)/l = C_5$.

The matrices $\boldsymbol{g}$ and $\boldsymbol{g}_{sC}$ are singular for the case shown in Fig. 9.5(e), their determinants are zero and it is not possible to solve the set of equations. As we can see from the diagram of the static system, the reason for this is that the bar can rotate freely as a rigid body about the left-hand support within the limits of infinitesimal deformation variables (first-order theory). A similar case has already been dealt with in example 8.3 (Fig. 8.9); significant loads can only be carried in conjunction with large deformations.

9.3.3 Static determinacy

In order that the independent bar end forces $\boldsymbol{s}$ can be determined from the joint loads $\boldsymbol{Q}$ according to (9.2), the equilibrium matrix $\boldsymbol{g}$ must be square and invertible. This is the case, for example, in Fig. 9.5(c) and (d); both systems are *statically determinate*. Although $\boldsymbol{g}$ in Fig. 9.5(e) is square, it is also singular; the system is *kinematically unstable*.

Applying (9.2) to the system shown in Fig. 9.4(a) results in a vector $\boldsymbol{s}$ with $4 \cdot 3 = 12$ elements. However, owing to the three constraints at joint 1 and the two constraints at joint 5, vector $\boldsymbol{Q}$ has merely $5 \cdot 3 - 3 - 2 = 10$ elements, i. e. matrix $\boldsymbol{g}$ is rectangular,

with a row deficit of $n = 2$, see (9.10); the system is *statically indeterminate* to the second degree.

Generally, the *degree of static indeterminacy* of a plane frame structure follows from the *counting scheme*

$$n = 3s + c - 3k - g \tag{9.3}$$

where s, c, k and g stand for the number of bars, support force variables, joints (including support joints) and auxiliary conditions (hinge conditions) respectively. Similarly, for spatial framed structures

$$n = 6s + c - 6k - g \tag{9.4}$$

while for plane trusses

$$n = s + c - 2k \tag{9.5}$$

and for spatial trusses

$$n = s + c - 3k \tag{9.6}$$

We assume frictionless hinged joints in trusses and therefore the rotational degrees of freedom are irrelevant; two (plane case) or three (spatial case) degrees of freedom remain per joint.

Systems where $n = 0$ are statically determinate, systems where $n > 0$ are statically indeterminate. Systems with $n < 0$ are kinematically unstable and generally unusable. A kinematically unstable case, such as the one shown in Fig. 9.5(e), where $n \geq 0$ but the matrix $\boldsymbol{g}$ is singular, is known as an *exceptional case of statics*.

In the example shown in Fig. 9.3(c), $s = 2$, $c = 4$, $k = 3$, $g = 1$, and therefore according to (9.3), $n = 0$. Similarly, in Fig. 9.3(d), $s = 3$, $c = 5$, $k = 4$, $g = 2$, and therefore $n = 0$. The two hinged beams are statically determinate.

Turning to the three-hinged arch shown in Fig. 9.3(e), $s = 2$, $c = 4$, $k = 3$, $g = 1$, and therefore according to (9.3), $n = 0$. For Fig. 9.3(f), $s = 2$, $c = 3$, $k = 2$, $g = 2$, i. e. $n = 1$. Although the two-hinged tied arch is *externally statically determinate* (it functions externally like a simply supported beam); *internally*, however, it is *statically indeterminate* (to the first degree).

In the case of the strutted beam of Fig. 9.3(h), $s = 5$, $c = 6$, $k = 6$, $g = 2$, and therefore $n = 1$. The stiffened polygonal arch shown in Fig. 9.3(i) has $s = 20$, $c = 6$, $k = 16$, $g = 18$, and therefore $n = 0$; we note that the six hinges in the arch have a double action, i. e. act for both the arch and the vertical bars. For the case of the two-hinged frame in Fig. 9.3(j), $s = 3$, $c = 4$, $k = 4$, $g = 0$, and therefore $n = 1$, and for the multi-storey frame in Fig. 9.3(k), $s = 12$, $c = 6$, $k = 10$, $g = 0$, i. e. $n = 12$ according to (9.3); it has three degrees of static indeterminacy externally, nine degrees internally.

The truss shown in Fig. 9.3(l) has $s = 11$, $c = 3$, $k = 7$, and therefore $n = 0$ according to (9.5). Similarly, for Fig. 9.3(m), $s = 37$, $c = 3$, $k = 20$, and therefore $n = 0$.

Instead of determining the degree of static indeterminacy with the help of the counting scheme, it is possible to start with a system similar to the static system being investigated, generally a *statically determinate basic system* (or a system with a known degree of static indeterminacy) and to count the additional constraints. For example, the arch in Fig. 9.3(f) would work on its own as a (statically determinate) simply supported beam, and the tie connected via hinges at both ends corresponds to one additional constraint, i. e. $n = 1$. In a similar way, the multi-storey frame of Fig. 9.3(k) could, for example, be converted into a basic system consisting of two (statically determinate) cantilever beams by introducing hinges with three degrees of freedom into the four horizontal frame beams, i. e. $n = 4 \cdot 3 = 12$; we can achieve the same result by introducing three flexural hinges at each of the four storeys, i. e. by considering a stack of four (statically determinate) three-hinged frames.

9.3.4 Kinematic derivation of the equilibrium matrix

Fig. 9.6(a), like Fig. 9.4(b), includes the bar end forces, and the transformations of the complete to the independent bar end forces have been considered.

Fig. 9.6(b) shows the bar element in its undeformed and deformed states. Joints l, r undergo the displacements u_l, w_l and u_r, w_r respectively in the x and z directions, and the ends of the bars rotate through $\lambda + \psi$ and $\rho - \psi$ respectively about the y axis. Here, $\psi = (w_r - w_l)/l$ designates the *bar rotation*, and λ and ρ the *bar end rotations* related to the chord of the deformed bar.

According to (8.15), the deformation work W_i done by the internal force variables on the corresponding deformation variables is

$$W_i = -N_r(u_r - u_l) - M_l(\lambda + \psi) - M_r(\rho - \psi) - \frac{M_r - M_l}{l}(w_r - w_l)$$
$$= -N_r\Delta - M_l\lambda - M_r\rho \qquad (9.7)$$

where $\Delta = u_r - u_l$ designates the *bar extension*. The internal deformation variables v_i corresponding to the independent bar end forces s_i are therefore the bar extension and the two bar end rotations.

Instead of *sign convention* I (Fig. 9.6) used up until now, we shall now introduce *sign convention* II as illustrated in Fig. 9.7, according to which all bar end variables in the positive local system of coordinates are regarded as positive.

N_r continues to be positive when it acts in the direction of the positive x axis; however, M_l and M_r as well as λ and ρ are all regarded as positive when rotating anticlockwise (about the positive y axis). Instead of (9.7), we get

$$W_i = -N_r(u_r - u_l) - M_l(\lambda - \psi) - M_r(\rho - \psi) - \frac{M_l + M_r}{l}(w_r - w_l)$$
$$= -N_r\Delta - M_l\lambda - M_r\rho \qquad (9.8)$$

We shall now return to the structural system of Fig. 9.4(a) and introduce all the possible joint loads Q_j according to Fig. 9.8(a) and the external deformation variables V_j corresponding to those according to Fig. 9.8(b).

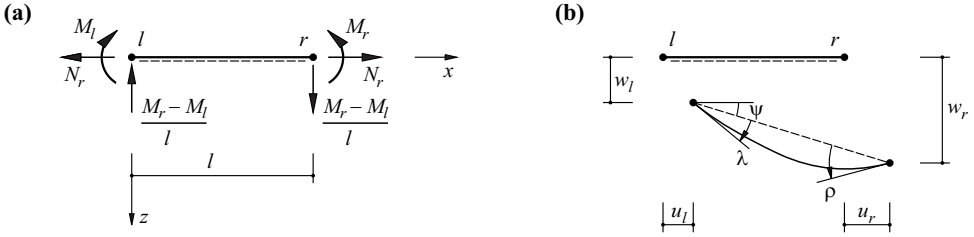

Fig. 9.6 Sign convention I: (a) bar end forces, (b) deformation variables

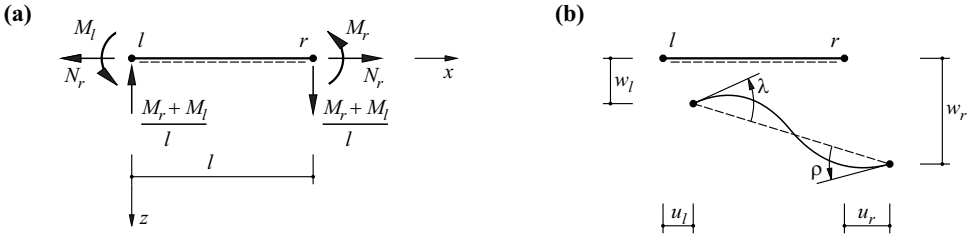

Fig. 9.7 Sign convention II: (a) bar end forces, (b) deformation variables

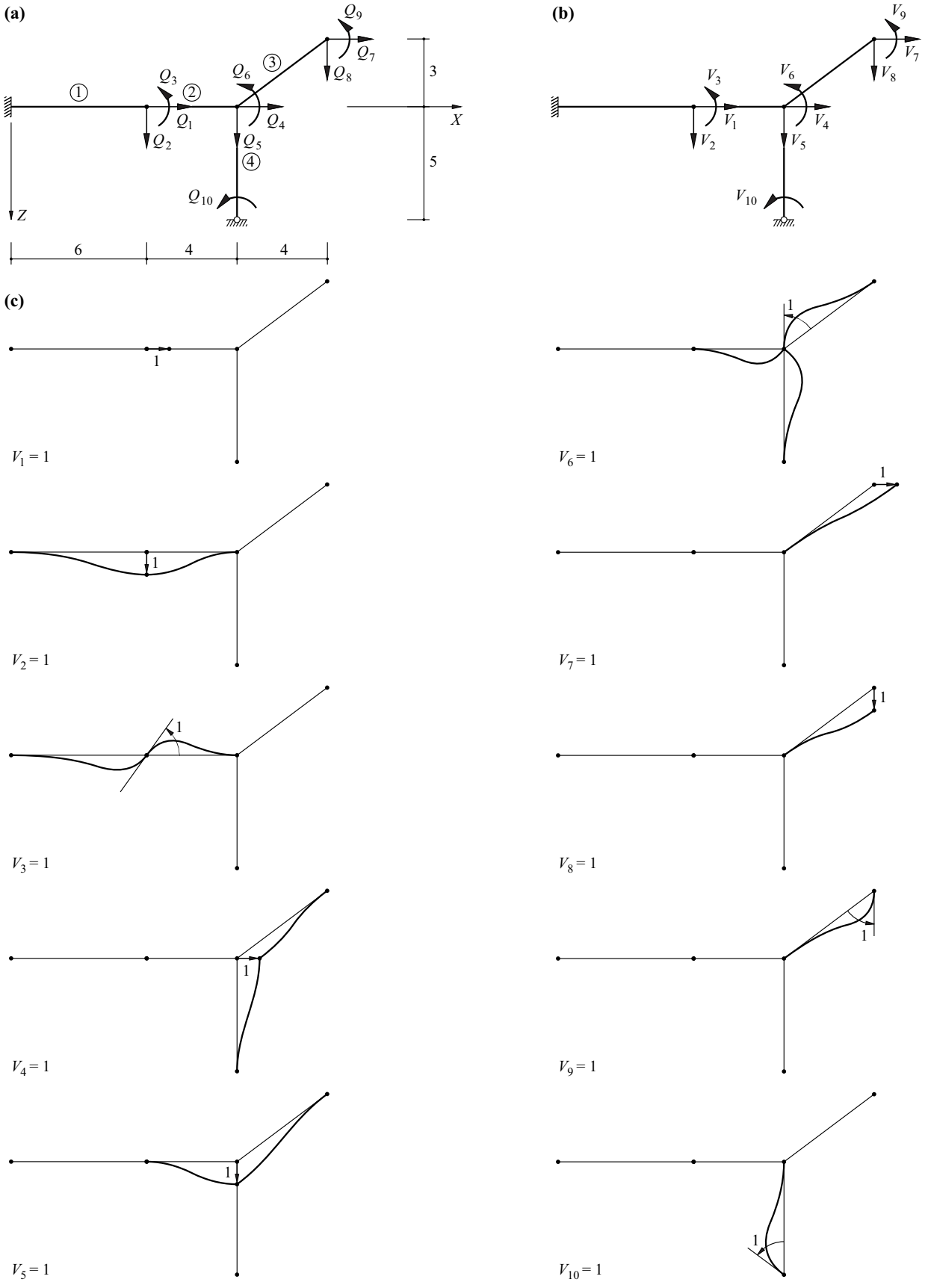

Fig. 9.8 Determining the kinematic transformation matrix ***a***: (a) joint loads, (b) degrees of freedom, (c) unit deformation states

If we apply successive unit deformation states to a *kinematically determinate basic system* (i. e. to the static system without any degree of freedom, $V_j \equiv 0$) as shown in Fig. 9.8(c), then we get the internal deformation variables of the four bars through the column-by-column setup of the kinematic transformation matrix $\boldsymbol{a}$ according to (8.1):

$$\begin{Bmatrix} \Delta_1 \\ \lambda_1 \\ \rho_1 \\ \Delta_2 \\ \lambda_2 \\ \rho_2 \\ \Delta_3 \\ \lambda_3 \\ \rho_3 \\ \Delta_4 \\ \lambda_4 \\ \rho_4 \end{Bmatrix} = \begin{bmatrix} 1 & 0 & 0 & 0 & 0 & 0 & 0 & 0 & 0 & 0 \\ 0 & 1/6 & 0 & 0 & 0 & 0 & 0 & 0 & 0 & 0 \\ 0 & 1/6 & 1 & 0 & 0 & 0 & 0 & 0 & 0 & 0 \\ -1 & 0 & 0 & 1 & 0 & 0 & 0 & 0 & 0 & 0 \\ 0 & -1/4 & 1 & 0 & 1/4 & 0 & 0 & 0 & 0 & 0 \\ 0 & -1/4 & 0 & 0 & 1/4 & 1 & 0 & 0 & 0 & 0 \\ 0 & 0 & 0 & -4/5 & 3/5 & 0 & 4/5 & -3/5 & 0 & 0 \\ 0 & 0 & 0 & -3/25 & -4/25 & 1 & 3/25 & 4/25 & 0 & 0 \\ 0 & 0 & 0 & -3/25 & -4/25 & 0 & 3/25 & 4/25 & 1 & 0 \\ 0 & 0 & 0 & 0 & -1 & 0 & 0 & 0 & 0 & 0 \\ 0 & 0 & 0 & 1/5 & 0 & 1 & 0 & 0 & 0 & 0 \\ 0 & 0 & 0 & 1/5 & 0 & 0 & 0 & 0 & 0 & 1 \end{bmatrix} \begin{Bmatrix} V_1 \\ V_2 \\ V_3 \\ V_4 \\ V_5 \\ V_6 \\ V_7 \\ V_8 \\ V_9 \\ V_{10} \end{Bmatrix} \tag{9.9}$$

and using (8.14), then (8.2) follows, i. e.

$$\begin{Bmatrix} Q_1 \\ Q_2 \\ Q_3 \\ Q_4 \\ Q_5 \\ Q_6 \\ Q_7 \\ Q_8 \\ Q_9 \\ Q_{10} \end{Bmatrix} = \begin{bmatrix} 1 & 0 & 0 & -1 & 0 & 0 & 0 & 0 & 0 & 0 & 0 & 0 \\ 0 & 1/6 & 1/6 & 0 & -1/4 & -1/4 & 0 & 0 & 0 & 0 & 0 & 0 \\ 0 & 0 & 1 & 0 & 1 & 0 & 0 & 0 & 0 & 0 & 0 & 0 \\ 0 & 0 & 0 & 1 & 0 & 0 & -4/5 & -3/25 & -3/25 & 0 & 1/5 & 1/5 \\ 0 & 0 & 0 & 0 & 1/4 & 1/4 & 3/5 & -4/25 & -4/25 & -1 & 0 & 0 \\ 0 & 0 & 0 & 0 & 0 & 1 & 0 & 1 & 0 & 0 & 1 & 0 \\ 0 & 0 & 0 & 0 & 0 & 0 & 4/5 & 3/25 & 3/25 & 0 & 0 & 0 \\ 0 & 0 & 0 & 0 & 0 & 0 & -3/5 & 4/25 & 4/25 & 0 & 0 & 0 \\ 0 & 0 & 0 & 0 & 0 & 0 & 0 & 0 & 1 & 0 & 0 & 0 \\ 0 & 0 & 0 & 0 & 0 & 0 & 0 & 0 & 0 & 0 & 0 & 1 \end{bmatrix} \begin{Bmatrix} N_{r1} \\ M_{l1} \\ M_{r1} \\ N_{r2} \\ M_{l2} \\ M_{r2} \\ N_{r3} \\ M_{l3} \\ M_{r3} \\ N_{r4} \\ M_{l4} \\ M_{r4} \end{Bmatrix} \tag{9.10}$$

A comparison of (8.2) and (9.2) shows that

$$\boldsymbol{g} = \boldsymbol{a}^{\mathrm{T}} \tag{9.11}$$

generally applies, i. e. the equilibrium matrix $\boldsymbol{g}$ can be derived from exclusively kinematic considerations.

Matrix $\boldsymbol{a}$ in (9.9) can be obtained through exclusively kinematic considerations because all (ten) degrees of freedom of the system were introduced as variables V_j; the problem is therefore *kinematically determinate*. Kinematically indeterminate systems are expressly excluded because all the independent degrees of freedom and the joint loads corresponding to those are used every time.

According to (8.3), the reciprocal transformation $\boldsymbol{s} = \boldsymbol{b} \bullet \boldsymbol{Q}$ is allocated to the equilibrium condition $\boldsymbol{Q} = \boldsymbol{g} \bullet \boldsymbol{s}$ according to (8.2) and (9.11) with the static transformation matrix $\boldsymbol{b}$. In the general case with n degrees of static indeterminacy, $\boldsymbol{b}$ has a column deficit of n. For statically determinate systems ($n = 0$), $\boldsymbol{b}$ is square and follows from the inversion of $\boldsymbol{g} = \boldsymbol{a}^{\mathrm{T}}$; in this case, $\boldsymbol{g} = \boldsymbol{b}^{-1}$ can also be obtained directly from exclusively static considerations instead of via $\boldsymbol{a}$. Generally, according to (8.16) und (9.11), the relationship $\boldsymbol{g} \bullet \boldsymbol{b} = \mathbf{I}$ applies, also $\boldsymbol{b} \bullet \boldsymbol{g} = \mathbf{I}$ for statically determinate systems.

9.4 Summary

1. Framed structures are composed of bars, connections (hinges) and supports. The properties of the bar are related to the (straight or curved) bar axis and the bar cross-sections orthogonal to that axis.
2. Depending on the stress resultants in the bar, we distinguish between frameworks (general stress resultants), trusses (normal forces) and hybrid systems (combined framework and truss structures, possibly using additional loadbearing elements such as cables).
3. The structural system describes the arrangement of the loadbearing components (supports, columns, beams) and the way in which they work together; it describes the structural topology.
4. The structural model, or static system, contains, in addition, precise details of the dimensions of the structure as well as details of the construction materials and subsoil properties. The model is presented in the form of diagrams and tables of the static system.
5. Structures are always three-dimensional assemblies which, however, can often be completely or at least partly broken down into plane subsystems.
6. Discretised structural models are especially suitable for dealing with the structural analysis. All the relevant data can therefore be related either to the (arbitrarily selected) joints or the bars between those joints.
7. Joint loads, bar end forces and support force variables are linked with each other in accordance with (9.2) via an equilibrium matrix. When this matrix is square and invertible, the system is statically determinate. Matrices with a row deficit indicate static indeterminacy, and singular matrices and those with a column deficit indicate kinematic instability.
8. We can use the counting schemes (9.3) to (9.6) to assess the degree of static indeterminacy of plane and spatial frameworks and trusses. Alternatively, we can start with a statically determinate basic system (or a system with known static indeterminacy) similar to the system being investigated and count the additional constraints.
9. The equilibrium matrix $\boldsymbol{g} = \boldsymbol{a}^{\mathrm{T}}$ can be obtained through the column-by-column setup of the kinematic transformation matrix $\boldsymbol{a}$ and subsequent transposition. The bar extensions Δ and the bar end rotations λ and ρ are the internal deformation variables $\boldsymbol{v} = \boldsymbol{a} \bullet \boldsymbol{V}$ corresponding to the independent bar end forces $\boldsymbol{s} = \boldsymbol{b} \bullet \boldsymbol{Q}$.
10. Generally, $\boldsymbol{g} \bullet \boldsymbol{b} = \mathbf{I}$ applies for the static transformation matrix $\boldsymbol{b}$, also $\boldsymbol{b} = \boldsymbol{g}^{-1}$ for statically determinate systems.

9.5 Exercises

9.1 Determine the degree of static indeterminacy of each of the systems shown in Fig. 9.9 and describe these as briefly and precisely as possible using the terminology of the theory of structures.

9.2 Determine the equilibrium matrix for the system of Fig. 9.9(a) in a similar way to (9.10).

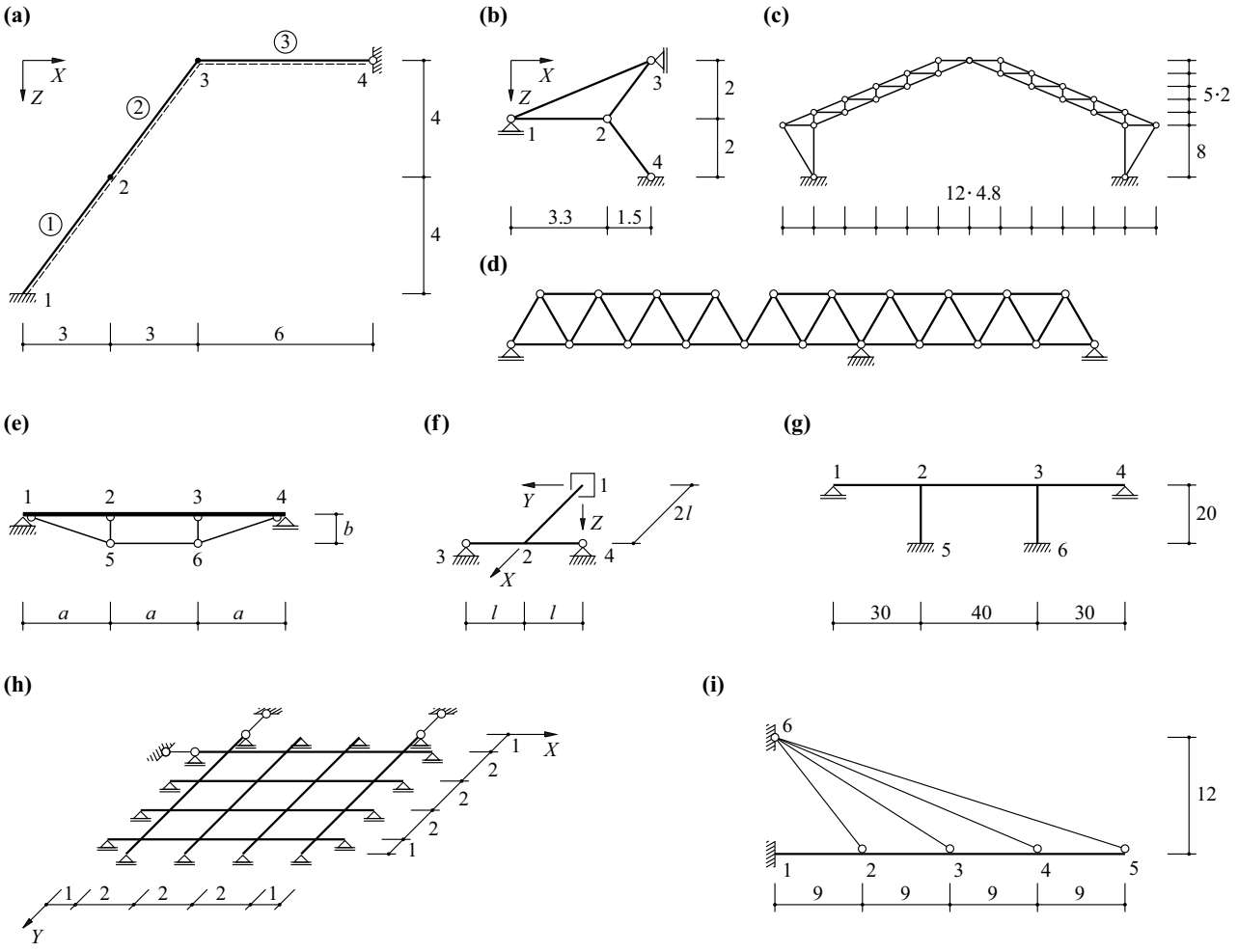

Fig. 9.9 Diagrams of the static systems for section 9.5 (dimensions in m)

10 DETERMINING THE FORCES

10.1 General

We shall only investigate statically determinate framed structures in this chapter. For such structures, as explained in section 9.3.3, we only need the equilibrium conditions in order to determine all the stress resultants and support force variables. This chapter therefore makes use of the concept of the free body diagram introduced in section 5.1.2, the equilibrium conditions (5.8) and the principle of virtual deformations discussed in section 8.3.2.

Depending on the formulation of the equilibrium conditions, we distinguish between the following methods for determining the forces:

- *Graphical statics*, based on the graphic presentation of the force vectors by means of funicular and force polygons according to section 5.1.4
- Applying the equilibrium conditions (5.8) to skilfully selected free bodies
- Systematic application of the equilibrium conditions (5.8) to the joints considered as free bodies
- Applying the principle of virtual deformations (kinematic method).

We were first introduced to the principle of the method of graphical statics – which is illustrated here briefly again with the help of Fig. 10.1 – through the examples shown in Figs. 5.4, 5.5, 5.31 and 9.3(e). Graphical statics has in the meantime been superseded by more powerful methods and so it is not intended to discuss this method in detail here. However, owing to their unsurpassed clarity, elements of graphical statics will be referred to from time to time in the following chapters. Graphical tools are particularly suitable for checking the equilibrium of individual system components removed from any system through skilful sectioning. They also permit the flow of the forces to be illustrated and form an indispensable basis for the creative act of conceiving a structural design, see section 3.2.

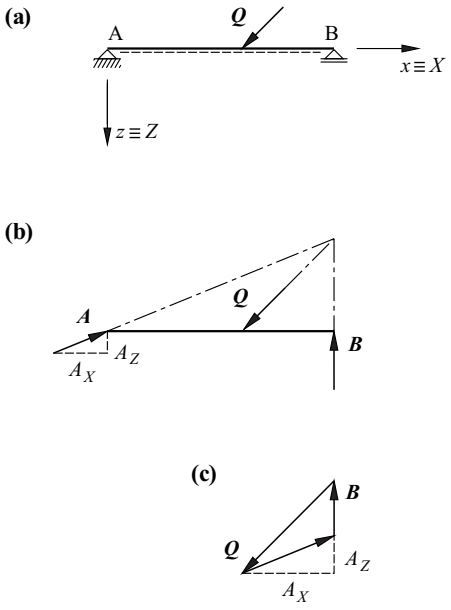

Fig. 10.1 Graphical statics: (a) system and loads, (b) funicular polygon, (c) force polygon

Fig. 10.1(b) shows the positions and directions of support forces ***A*** and ***B*** which are required to guarantee equilibrium. Component A_X acts in the positive X direction, whereas components A_Z and B act in the negative Z direction. In the following, as agreed in section 9.3.1, the positive support force variables will always be forces and moments acting on the system released from its supports in the positive global axis direction. According to (5.8), components A_Z and B introduced in the positive Z direction are found to be negative in this example, which means that the two vertical support forces actually act on the beam in the negative Z direction.

Sign convention I, already discussed with the help of Fig. 9.6(a), is used for the stress resultants of plane frameworks, see Fig. 10.2. According to this, a stress resultant (N, V, M) is then regarded as positive when it acts on the positive (negative) side of a bar element in the positive (negative) direction of the system of coordinates. The orientation of the local axes x, y, z is indicated by a dotted line on the positive z side.

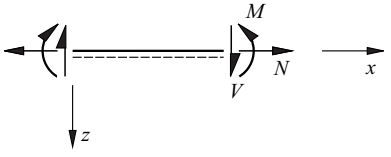

Fig. 10.2 Sign convention I for plane frameworks

Theory of Structures. First Edition. Peter Marti

10.2 Investigating selected free bodies

As an introductory example, we shall consider the cantilever beam shown in Fig. 10.3(a), which carries a point load Q at $x = a$ acting at an angle α to the x axis. Applying (5.8) to Fig. 10.3(b) results in

$$A_X + Q\cos\alpha = 0 \quad , \quad A_Z + Q\sin\alpha = 0 \quad , \quad M_A - a\,Q\sin\alpha = 0 \tag{10.1}$$

and similarly, considering the upper free body diagram in Fig. 10.3(c), we get

$$-N + Q\cos\alpha = 0 \quad , \quad -V + Q\sin\alpha = 0 \quad , \quad -M - (a-x)Q\sin\alpha = 0 \tag{10.2}$$

from which it follows that

$$N = -A_X = Q\cos\alpha \ , \ V = -A_Z = Q\sin\alpha \ , \ M = -M_A\left(1 - \frac{x}{a}\right) = -(a-x)Q\sin\alpha \tag{10.3}$$

see Fig. 10.3(d). The lower free body diagram in Fig. 10.3(c) can be used to check the equilibrium. Using $(10.3)_1$, $(10.3)_2$ and $(10.3)_3$ as well as $(10.1)_3$, it is possible to confirm that the relationships $A_X + N = 0, A_Z + V = 0$ and $M_A + M - xV = 0$ are fulfilled.

Looking at the three-hinged arch shown in Fig. 10.4(a), which carries a uniformly distributed line load q and is released from its supports A and B, it is easy to apply moment-balance equations about B or A to find that $A_Z = B_Z = -ql/2$. Equilibrium of forces in the X direction calls for $A_X = -B_X$, but the magnitudes of these two forces cannot be determined from the free body diagram of Fig. 10.4(a). If we cut through the system at hinge G, see Fig. 10.4(b), we get the moment-balance equation $ql^2/8 + A_X f + A_Z l/2 = 0$ about G. From this it follows that, using A_Z determined beforehand, the horizontal force is $A_X = ql^2/(8f)$, see (5.60). The hinge force components result from the equilibrium of forces in the X and Z directions: $G_X = -A_X$, $G_Z = 0$. We can also see that owing to the symmetry of the system and the load, it would have been sufficient to consider Fig. 10.4(b) in order to determine the support and hinge force variables. Indeed, symmetry calls for $G_Z = 0$, and therefore Fig. 10.4(b) contains only three unknown force variables, which can be determined directly with the help of the equilibrium conditions.

Likewise, for the hinged girder shown in Fig. 10.5(a), cutting through the system at hinge G according to Fig. 10.5(b) is the right approach. In addition to the hinge force, only vertical force Q and vertical support force C act on propped beam GC, and so the horizontal component of the hinge force does not apply, i. e. $G_X = 0$, $G_Z = G$. Applying the same approach to subsystem ABG results in $A_X = 0$, $A_Z = A$. Moment-balance

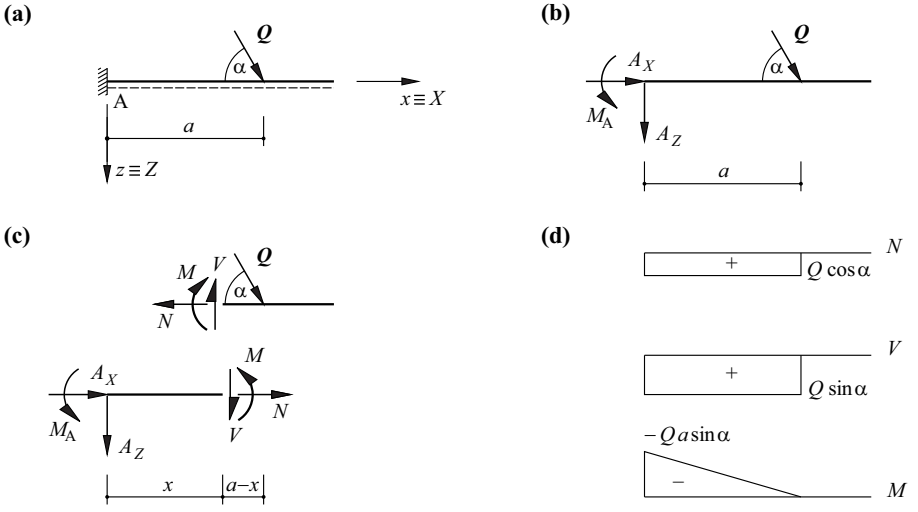

Fig. 10.3 Cantilever beam: (a) system and loads, (b) free body diagram for determining the support force variables, (c) free body diagrams for determining the stress resultants and for checking the equilibrium, (d) diagrams of stress resultants

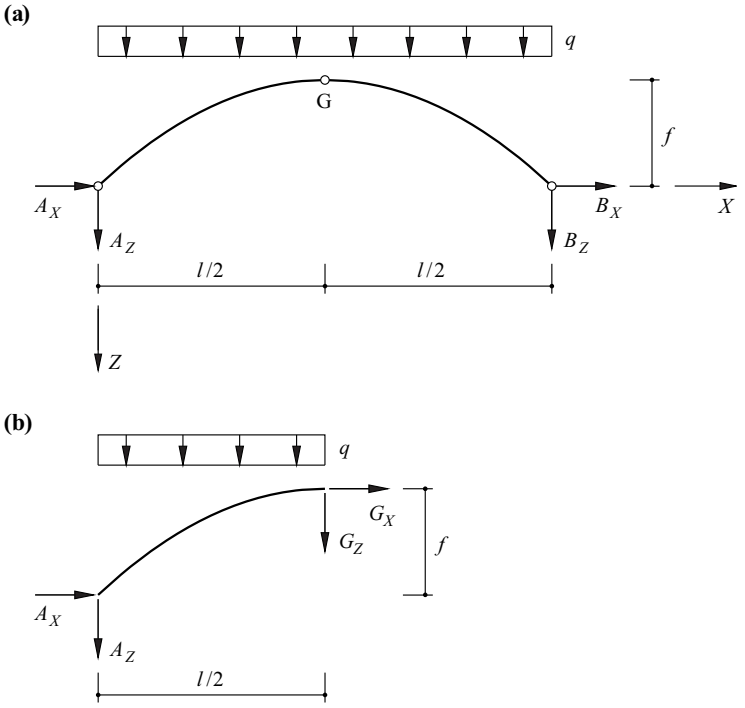

Fig. 10.4 Three-hinged arch: (a) free body diagram for determining A_Z and B_Z, (b) free body diagram for determining A_X

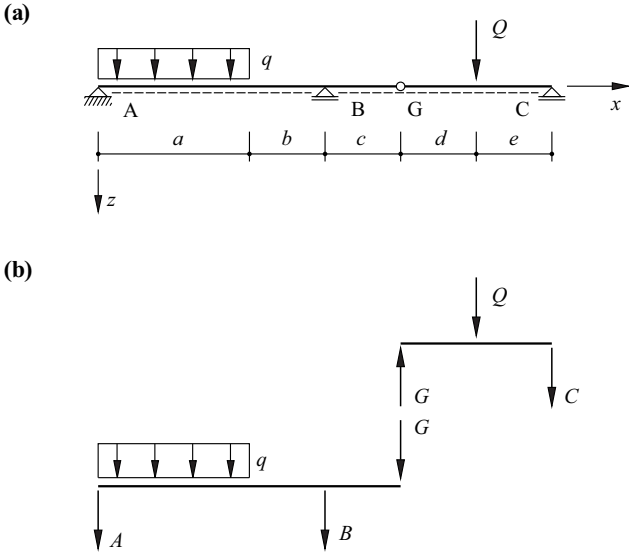

Fig. 10.5 Hinged girder: (a) system and loads, (b) free body diagrams

equations about G and C for subsystem GC result in $C = -Qd/(d + e)$ and $G = Qe/(d + e)$. Moment-balance equations about B and A for subsystem ABG then result in $A = [Qec/(d+e) - qa(a/2+b)]/(a+b)$ and $B = -[qa^2/2 + Qe(a+b+c)/(d+e)]/(a+b)$.

The procedure for determining the force variables of statically determinate framed structures, as illustrated in Fig. 10.3 to Fig. 10.5 can be summarised as follows:

1. Release the system from its supports and introduce the corresponding support force variables in the direction of the positive global coordinates.
2. Set up and resolve the equilibrium conditions for the released system.
3. If necessary, cut through the system at the hinges and apply the hinge force variables to the subsystems.

4. Set up and resolve the equilibrium conditions for the subsystems.
5. Determine the stress resultants N, V, M by considering free bodies according to Fig. 10.3(c) and applying the appropriate equilibrium conditions.
6. Draw the diagrams of the stress resultants according to Fig. 10.3(d) with the positive ordinates in the direction of the positive z axis.

As the example of Fig. 10.4(b) shows, it is often possible to make considerable simplifications when dealing with symmetrical systems and loads. Furthermore, the examples of Fig. 10.4 and Fig. 10.5 show that it is often advantageous to replace the force-balance equations by moment-balance equations about suitable reference points, see section 5.1.3; the force-balance equations can then be used for checking the equilibrium afterwards.

Example 10.1 Plane truss

Let us return to the plane truss of Fig. 8.1, see Fig. 10.6(a). There are two or three unknown bar forces (normal forces) N_i in the free bodies shown in Fig. 10.6(b) to (d). In accordance with Fig. 10.2, these forces are introduced as positive variables, i. e. as tensile forces, on either side of the section.

A moment-balance equation about joint 4 in Fig. 10.6(b) results in $N_4\, l/\sqrt{2} - Q_{10}\, l = 0$, and the moment-balance equation about joint 2 gives us $-N_6\, l + Q_9\, l - Q_{10}\, l = 0$. This therefore confirms the coefficients in the fourth and sixth rows of the matrix $\boldsymbol{b}$ leading to (8.3).

The moment-balance equation about joint 4 in Fig. 10.6(c) results in $N_1\, l - Q_3\, l - Q_{10}\, l = 0$, and the force-balance equation in the Z direction is $N_3 + Q_4 + Q_{10} = 0$, which confirms the coefficients in the first and third rows of matrix $\boldsymbol{b}$.

In Fig. 10.6(d), the force-balance equation in the Z direction calls for $-N_2/\sqrt{2} + Q_4 + Q_8 + Q_{10} = 0$, and the moment-balance equation about joint 1 leads to $-N_5\, l - Q_4\, l + Q_7\, l - Q_8\, l + Q_9\, l - 2Q_{10}\, l = 0$. Therefore, the coefficients in the second and fifth rows of matrix $\boldsymbol{b}$ are confirmed as well.

In section 8.1, the static transformation matrix $\boldsymbol{b}$ was established as the inverse matrix $\boldsymbol{b} = \boldsymbol{g}^{-1}$ of the equilibrium matrix $\boldsymbol{g} = \boldsymbol{a}^{\mathrm{T}}$ according to (8.11), where $\boldsymbol{g}$ was obtained row by row from joint equilibrium conditions in the direction of Q_j. The opposite is the case here, with $\boldsymbol{b}$ being determined row by row from skilfully formulated equilibrium conditions in which there is only one unknown bar force N_i in each case.

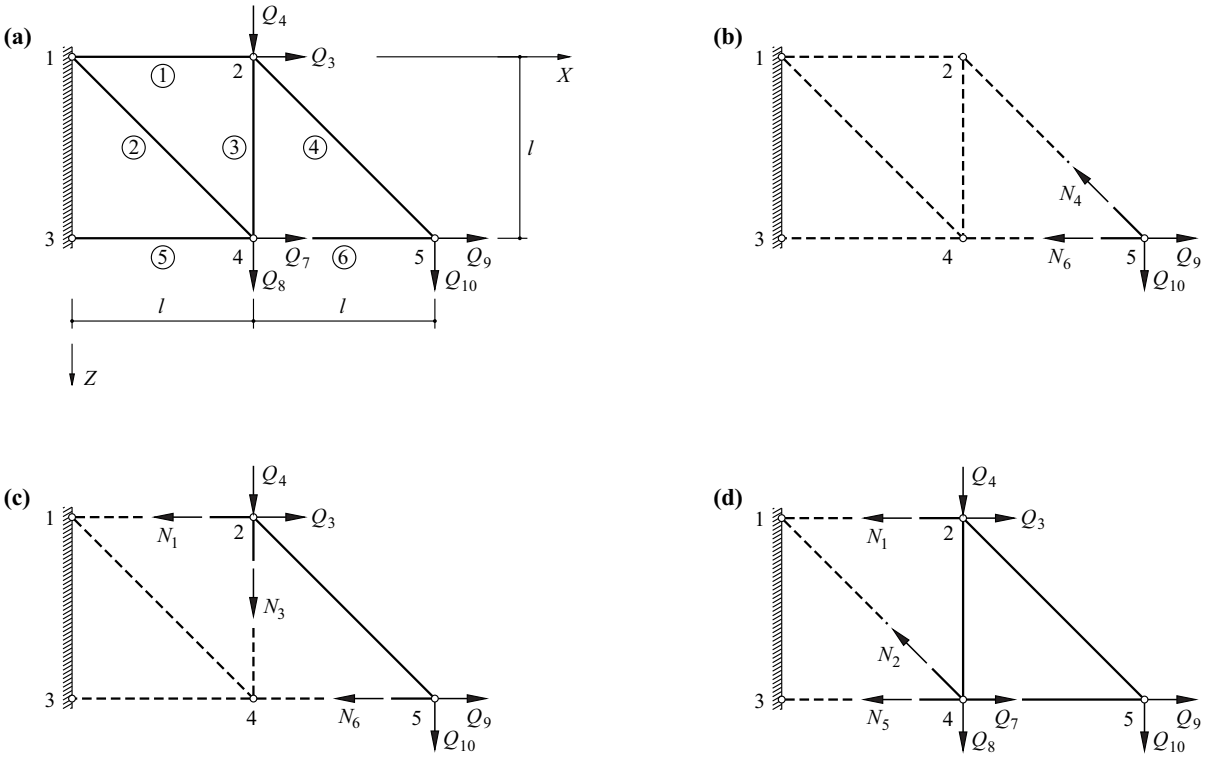

Fig. 10.6 Plane truss: (a) system and loads, (b) to (d) free body diagrams

Example 10.2 Plane frame

Consider the plane frame shown in Fig. 10.7(a); the free body diagram of Fig. 10.7(b) first of all gives us the support force variables C_{1X}, C_{1Z} and C_{4Z}. The force-balance equation in the X direction calls for $C_{1X} + 50\,\text{kN} = 0$, i. e. $C_{1X} = -50\,\text{kN}$. The moment-balance equation about joint 4 is $C_{1Z} \cdot 10\,\text{m} - 50\,\text{kN} \cdot 4\,\text{m} + 350\,\text{kN} \cdot 7\,\text{m} + 100\,\text{kNm} = 0$, from which it follows that $C_{1Z} = -235\,\text{kN}$. The force-balance equation $C_{1Z} + C_{4Z} + 350\,\text{kN} + 150\,\text{kN} = 0$ in the Z direction therefore results in $C_{4Z} = -265\,\text{kN}$.

Considering bar 1 as a free body according to Fig. 10.7(c), it follows first of all that the moment-balance equation $M_2 - 50\,\text{kN} \cdot 4\,\text{m} - 235\,\text{kN} \cdot 3\,\text{m} = 0$ about joint 2 results in the moment $M_2 = 905\,\text{kNm}$. The moment-balance equation $905\,\text{kNm} - V_1 \cdot 5\,\text{m} = 0$ about joint 1 then results in the shear force $V_1 = 181\,\text{kN}$. Finally, we get the normal force N_1 by projecting the support forces C_{1X} and C_{1Z} onto the bar axis: $N_1 = 50\,\text{kN} \cdot (3/5) - 235\,\text{kN} \cdot (4/5) = -158\,\text{kN}$. The bending moment M increases linearly from 0 to 905 kNm between joints 1 and 2.

The compressive force $N_3 = -265$ kN carried by bar 3 is reduced to 115 kN at joint 3 by the vertical load of 150 kN applied there. The remaining force of 115 kN is carried by bar 2 as a shear force $V_2 = -115\,\text{kN}$, see Fig. 10.7(c). The moment-balance equation for bar 2 about joint 2 is $-905\,\text{kNm} + 115\,\text{kN} \cdot 7\,\text{m} + 100\,\text{kNm} = 0$, and is actually fulfilled. Between joints 2 and 3, the moment M varies linearly between 905 kNm and 100 kNm.

The diagrams of the stress resultants N, V, M are shown in Fig. 10.7(d).

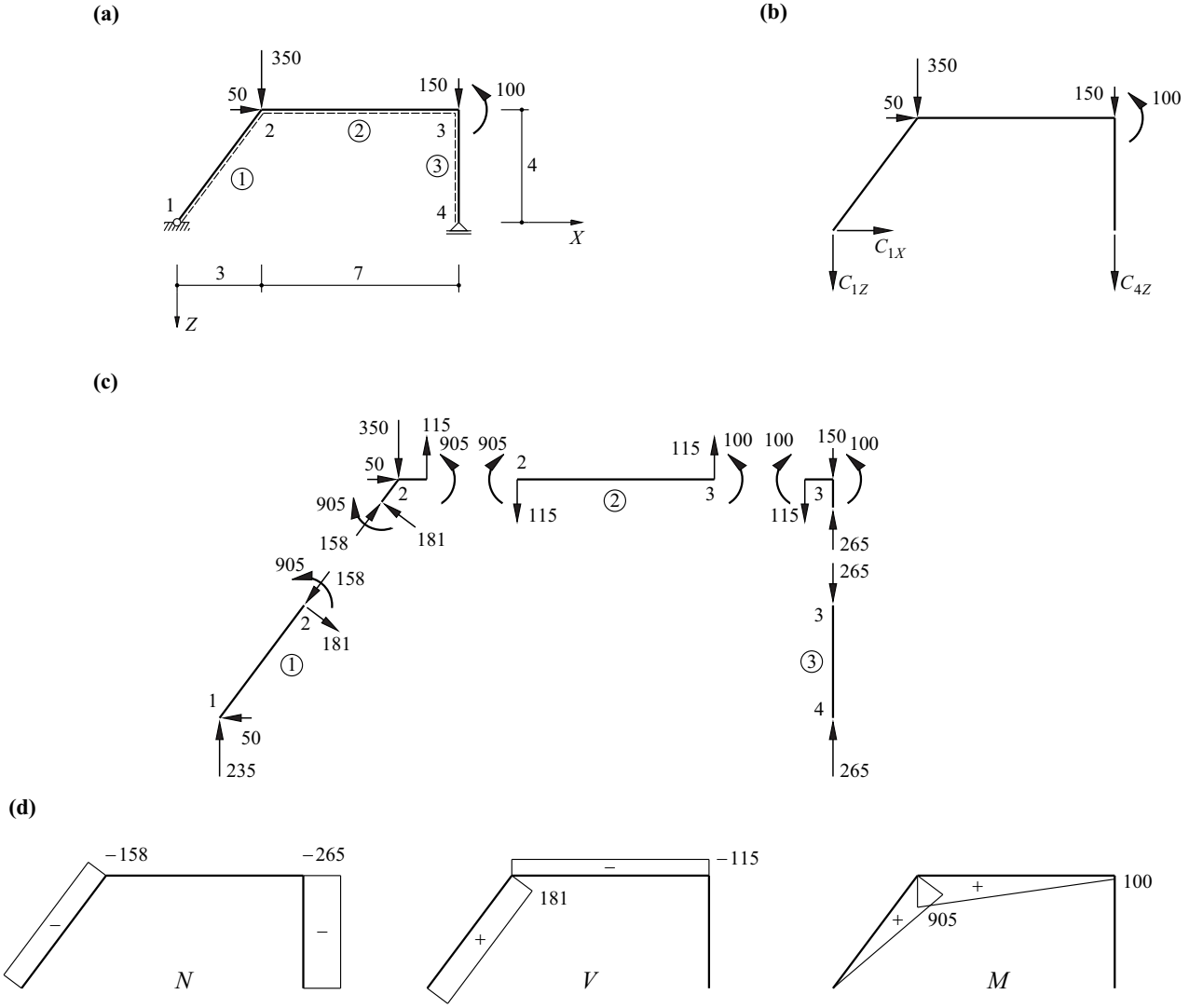

Fig. 10.7 Plane frame: (a) system and loads [m, kN], (b) and (c) free body diagrams, (d) diagrams of stress resultants

10.3 Joint equilibrium

A first method for determining the force variables of statically determinate framed structures was discussed in section 10.2. That method is based on considering skilfully chosen free bodies, can be easily adapted to diverse problems and is suitable for hand calculations. In this chapter, we start from (9.2) and determine the internal force variables $\boldsymbol{s}$ and the support force variables $\boldsymbol{C}$ with $\boldsymbol{b} = \boldsymbol{g}^{-1}$ according to

$$\boldsymbol{s} = \boldsymbol{b} \cdot \boldsymbol{Q} \quad , \quad \boldsymbol{C} = -\boldsymbol{g}_{s\boldsymbol{C}} \cdot \boldsymbol{b} \cdot \boldsymbol{Q} \tag{10.4}$$

This leads to a standardised method which, however, quickly results in large sets of equations and requires the use of a computer.

Example 10.3 Plane truss

Let us consider the plane truss of Fig. 8.1 once again. The joint loads of Fig. 10.6(a) corresponding to the six active degrees of freedom of Fig. 8.1(b) are given. The support force variables we are looking for, C_1, C_2, C_5, correspond to the passive degrees of freedom V_1, V_2, V_5 in Fig. 8.1(b); the support force variable C_6 corresponding to the passive degree of freedom V_6 disappears because of the hinges at both ends of bar 5 and can be ignored.

Considering the matrix $\boldsymbol{g} = \boldsymbol{a}^{\mathrm{T}}$ leading to (8.2), eq. (9.2) results in

$$\begin{Bmatrix} Q_3 \\ Q_4 \\ Q_7 \\ Q_8 \\ Q_9 \\ Q_{10} \\ 0 \\ 0 \\ 0 \end{Bmatrix} = \begin{bmatrix} 1 & & & -\sqrt{2}/2 & & & & & \\ & & -1 & -\sqrt{2}/2 & & & & & \\ & \sqrt{2}/2 & & & 1 & -1 & & & \\ & \sqrt{2}/2 & 1 & & & & & & \\ & & & \sqrt{2}/2 & & 1 & & & \\ & & & \sqrt{2}/2 & & & & & \\ 1 & \sqrt{2}/2 & & & & & 1 & & \\ & \sqrt{2}/2 & & & & & & 1 & \\ & & & & 1 & & & & 1 \end{bmatrix} \begin{Bmatrix} N_1 \\ N_2 \\ N_3 \\ N_4 \\ N_5 \\ N_6 \\ C_1 \\ C_2 \\ C_5 \end{Bmatrix} \tag{10.5}$$

where the empty spaces in the matrix are filled with zeros. The bar forces N_1 to N_6 follow from the matrix $\boldsymbol{b} = \boldsymbol{g}^{-1}$ according to $(10.4)_1$, which leads to (8.3) and is verified in example 10.1. According to $(10.4)_2$, the support force variables are

$$\begin{Bmatrix} C_1 \\ C_2 \\ C_5 \end{Bmatrix} = \begin{bmatrix} -1 & -1 & & -1 & & -2 \\ & -1 & & -1 & & -1 \\ & 1 & -1 & 1 & -1 & 2 \end{bmatrix} \begin{Bmatrix} Q_3 \\ Q_4 \\ Q_7 \\ Q_8 \\ Q_9 \\ Q_{10} \end{Bmatrix} \tag{10.6}$$

where the empty spaces in the matrix are again filled with zeros.

Example 10.4 Plane frame

Let us return to example 10.2 (Fig. 10.7). However, this time, in a similar way to Fig. 9.8, we shall introduce all the active degrees of freedom and the corresponding joint loads (see Fig. 10.8), and determine the equilibrium matrix $\boldsymbol{g} = \boldsymbol{a}^{\mathrm{T}}$ using kinematics, as described in section 9.3.4. Similarly to (9.9), we get

$$\begin{Bmatrix} \Delta_1 \\ \lambda_1 \\ \rho_1 \\ \Delta_2 \\ \lambda_2 \\ \rho_2 \\ \Delta_3 \\ \lambda_3 \\ \rho_3 \end{Bmatrix} = \begin{bmatrix} & 3/5 & -4/5 & & & & & & \\ 1 & 4/25 & 3/25 & & & & & & \\ & 4/25 & 3/25 & 1 & & & & & \\ & -1 & & & 1 & & & & \\ & & -1/7 & 1 & & 1/7 & & & \\ & & -1/7 & & & 1/7 & 1 & & \\ & & & & & -1 & & & \\ & & & & 1/4 & & 1 & -1/4 & \\ & & & & 1/4 & & & -1/4 & 1 \end{bmatrix} \begin{Bmatrix} V_3 \\ V_4 \\ V_5 \\ V_6 \\ V_7 \\ V_8 \\ V_9 \\ V_{10} \\ V_{12} \end{Bmatrix} \tag{10.7}$$

and therefore (9.2) is

$$\begin{Bmatrix} Q_3 \\ Q_4 \\ Q_5 \\ Q_6 \\ Q_7 \\ Q_8 \\ Q_9 \\ Q_{10} \\ Q_{12} \\ 0 \\ 0 \\ 0 \end{Bmatrix} = \begin{bmatrix} & 1 & & & & & & & & & & \\ 3/5 & 4/25 & 4/25 & -1 & & & & & & & & \\ -4/5 & 3/25 & 3/25 & & -1/7 & -1/7 & & & & & & \\ & & 1 & & 1 & & & & & & & \\ & & & 1 & & & & 1/4 & 1/4 & & & \\ & & & & 1/7 & 1/7 & -1 & & & & & \\ & & & & & 1 & & 1 & & & & \\ & & & & & & & -1/4 & -1/4 & & & \\ & & & & & & & & 1 & & & \\ 3/5 & 4/25 & 4/25 & & & & & & & 1 & & \\ -4/5 & 3/25 & 3/25 & & & & & & & & 1 & \\ & & & & & & -1 & & & & & 1 \end{bmatrix} \begin{Bmatrix} N_{r1} \\ M_{l1} \\ M_{r1} \\ N_{r2} \\ M_{l2} \\ M_{r2} \\ N_{r3} \\ M_{l3} \\ M_{r3} \\ C_1 \\ C_2 \\ C_{11} \end{Bmatrix} \tag{10.8}$$

Inverting the matrix $\boldsymbol{g} = \boldsymbol{a}^{\mathrm{T}}$ at upper left in (10.8) results in $\boldsymbol{b} = \boldsymbol{g}^{-1}$, and therefore, according to $(10.4)_1$,

$$\begin{Bmatrix} N_{r1} \\ M_{l1} \\ M_{r1} \\ N_{r2} \\ M_{l2} \\ M_{r2} \\ N_{r3} \\ M_{l3} \\ M_{r3} \end{Bmatrix} = \begin{bmatrix} -2/25 & 23/25 & -14/25 & -2/25 & 23/25 & & -2/25 & 3/5 & -2/25 \\ 1 & & & & & & & & \\ -7/10 & 14/5 & 21/10 & 3/10 & 14/5 & & 3/10 & 4 & 3/10 \\ & & & & 1 & & & 1 & \\ 7/10 & -14/5 & -21/10 & 7/10 & -14/5 & & -3/10 & -4 & -3/10 \\ & & & & & & 1 & 4 & 1 \\ 1/10 & -2/5 & -3/10 & 1/10 & -2/5 & -1 & 1/10 & & 1/10 \\ & & & & & & & -4 & -1 \\ & & & & & & & & 1 \end{bmatrix} \begin{Bmatrix} Q_3 \\ Q_4 \\ Q_5 \\ Q_6 \\ Q_7 \\ Q_8 \\ Q_9 \\ Q_{10} \\ Q_{12} \end{Bmatrix} \tag{10.9}$$

Finally, we get

$$\begin{Bmatrix} C_1 \\ C_2 \\ C_{11} \end{Bmatrix} = \begin{bmatrix} & -1 & & & -1 & & & -1 & \\ -1/10 & 2/5 & -7/10 & -1/10 & 2/5 & & -1/10 & & -1/10 \\ 1/10 & -2/5 & -3/10 & 1/10 & -2/5 & -1 & 1/10 & & 1/10 \end{bmatrix} \begin{Bmatrix} Q_3 \\ Q_4 \\ Q_5 \\ Q_6 \\ Q_7 \\ Q_8 \\ Q_9 \\ Q_{10} \\ Q_{12} \end{Bmatrix} \tag{10.10}$$

for the support force variables according to $(10.4)_2$.

The empty spaces in the matrices of relationships (10.7) to (10.10) are filled with zeros. In addition, it is important to remember that bar extensions and displacements are entered into the calculation in m, but forces in kN and moments in kNm.

As can be easily checked by substituting $Q_4 = 50\,\mathrm{kN}$, $Q_5 = 350\,\mathrm{kN}$, $Q_8 = 150\,\mathrm{kN}$ and $Q_9 = 100\,\mathrm{kNm}$ in (10.9) and (10.10), we get the support force variables and stress resultants given in Fig. 10.7(c) and (d).

The static transformation matrix $\boldsymbol{b}$ in (10.9) contains an abundance of information. The rows describe how the various loads Q_j influence a certain stress resultant. And vice versa, the columns describe the stress resultants as a result of a load $Q_j = 1$ in each case. There is much more information here than in the solution of example 10.2. However, much more work is required.

(a) **(b)**

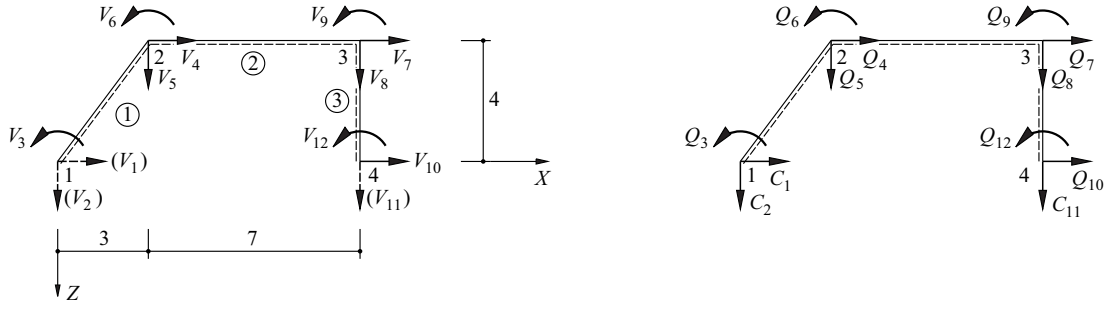

Fig. 10.8 Plane frame: (a) active and passive degrees of freedom, (b) joint loads and support force variables

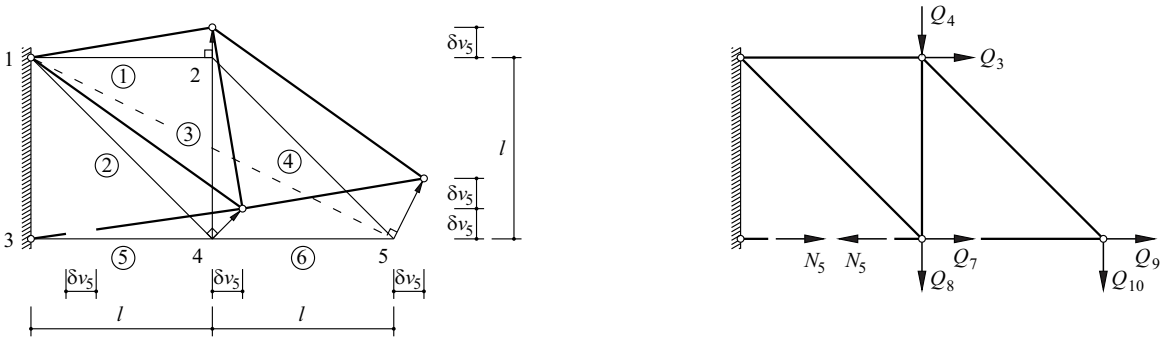

Fig. 10.9 The kinematic method – application according to example 8.1 ($N_5 = s_5$)

10.4 The kinematic method

Using the principle of virtual deformations to calculate internal force variables in statically determinate systems was introduced in example 8.1. In that example, we calculated force s_5 in bar 5 of the truss shown in Fig. 8.1(a) by introducing an imaginary cut through this bar at one point and applying the infinitesimally small relative displacement δv_5 to the sides of the cut, see Fig. 10.9.

As the relative displacement is infinitesimally small, joints 2, 4 and 5 do not move in an arc, but rather at 90° to the straight lines joining them, with the *instantaneous centre of rotation* of the planar movement of the subsystem 1452 at joint 1. So we consider merely the start of the movement and represent this (to an exaggerated scale) as shown in the diagram on the left of Fig. 10.9.

The two drawings in Fig. 10.9 make it easy to understand the relationship

$$\delta W = (-Q_4 + Q_7 - Q_8 + Q_9 - 2Q_{10} - s_5)\,\delta v_5 = 0$$

set up in example 8.1. Force Q_3 does no work because its point of application is displaced perpendicular to its direction. The displacements of the points of application of forces Q_4 to Q_{10} are clear from the drawing on the left in Fig. 10.9 and are taken into account in terms of sign and factor in the above expression in brackets. Bar force $s_5 = N_5$ is shown with two arrows in the drawing on the right in Fig. 10.9 (as tensile force positive) because it acts on both sides of the cut. With a virtual deformation, the left side of the cut does not undergo any movement, whereas the right side is displaced upwards and to the right by δv_5; the right-hand tensile force s_5 contributes the amount $-s_5\,\delta v_5$ to δW in this case.

Example 10.5 Three-hinged arch

In order to be able to calculate the support force B_X for the three-hinged arch shown in Fig. 10.4(a), we release the corresponding constraint, i. e. we introduce a sliding support at B, see Fig. 10.10. This turns the system into a mechanism with instantaneous centre of rotation A for arc AG and instantaneous centre of rotation C for arc GB. With a virtual rotation $\delta\varphi$ about C, the outcome is, on the one hand, that B undergoes a virtual displacement of $2f\,\delta\varphi$ in the X direction and, on the other, that the arch experiences a virtual settlement δw in the Z direction with a triangular distribution over l and a maximum value of $\delta\varphi\, l/2$ at G.

Applying the principle of virtual deformations results in

$$\delta W = (B_X \cdot 2f + ql \cdot l/4)\,\delta\varphi = 0$$

and therefore $B_X = -ql^2/(8f)$, see (5.60).

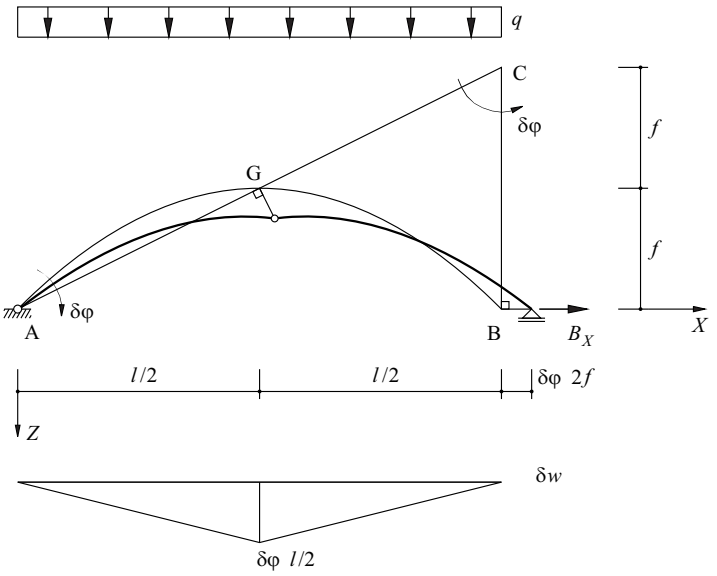

Fig. 10.10 The kinematic method applied to a three-hinged arch to calculate support force B_X

Example 10.6 Plane frame

In this next example we shall calculate the member end moment M_{l2} for the frame examined in example 10.4, see Fig. 10.11. First of all, we introduce a flexural hinge immediately to the right of joint 2 with a reciprocal virtual rotation of the bar ends amounting to δφ. This corresponds to a virtual rotation of bar 1 amounting to 0.7δφ about its instantaneous centre of rotation 1, whereas subsystem 234 rotates by 0.3δφ about the instantaneous centre of rotation 5.

Applying the principle of virtual deformations results in

$$\delta W = (M_{l2} - 0.7\,Q_3 + 2.8\,Q_4 + 2.1\,Q_5 - 0.7\,Q_6 + 2.8\,Q_7 + 0.3\,Q_9 + 4\,Q_{10} + 0.3\,Q_{12})\,\delta\varphi = 0$$

which confirms the coefficients in the fifth row of the matrix on the right in (10.9).

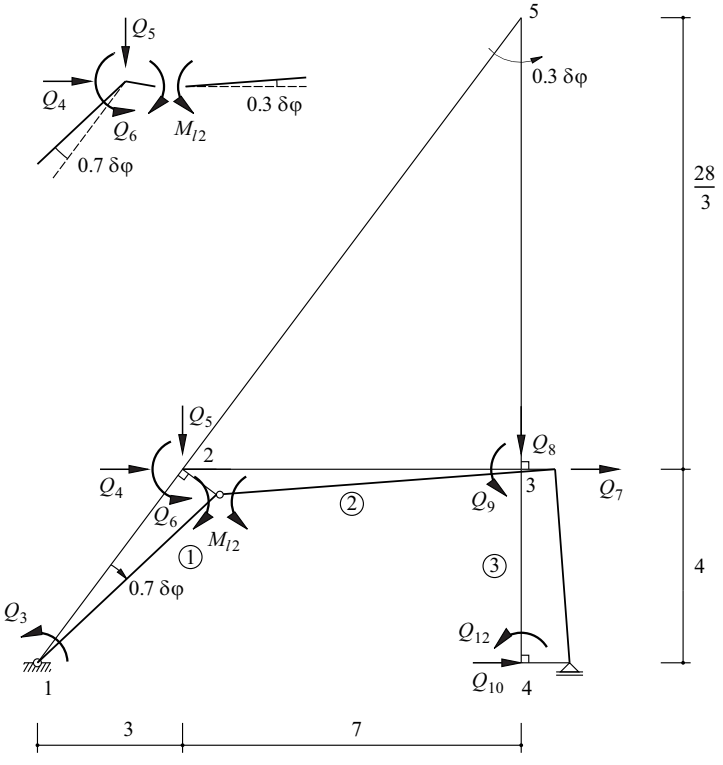

Fig. 10.11 The kinematic method applied to a plane frame to calculate member end moment M_{l2}

Summing up, the kinematic method for calculating force variables in statically determinate framed structures can be characterised by the following steps:

1. Release the corresponding constraint and by doing that convert the statically determinate system into a mechanism (with one degree of kinematic instability).
2. Introduce the released force variables.
3. Apply the principle of virtual deformations to the mechanism and calculate the force variable required from the expression $\delta W = 0$.

10.5 Summary

1. Although the methods of graphical statics have been superseded by more powerful methods, their unsurpassed clarity makes them still extremely valuable. They are particularly suitable for checking equilibrium, permit the flow of the forces to be illustrated and form an indispensable basis for the conceptual design of structures.
2. Considering skilfully selected free bodies and applying the equilibrium conditions (5.8) allows to determine individual force variables for any specific problems, mostly with the help of simple hand calculations.
3. Setting up the joint equilibrium conditions systematically leads to a standardised method that provides ample information but quickly requires the use of a computer. The internal and support force variables follow from (10.4), with the static transformation matrix $\boldsymbol{b}$ being very conveniently obtained from the kinematic transformation matrix $\boldsymbol{a}$ by inverting the equilibrium matrix $\boldsymbol{g} = \boldsymbol{a}^{\mathrm{T}}$.
4. The rows of the static transformation matrix $\boldsymbol{b}$ describe how a certain stress resultant is influenced by the various loads. And vice versa, the columns of the matrix describe the stress resultants due to individual unit load states.
5. Individual force variables of statically determinate systems can be determined by releasing the corresponding constraints, introducing the released force variable and applying the principle of virtual deformations to the system with one degree of kinematic instability.

10.6 Exercises

10.1 A point load with components Q_X and Q_Z in the X and Z directions respectively is applied to joint 2 of the system shown in Fig. 9.9(b). Determine the corresponding force in bar 24 purely graphically and by applying the principle of virtual deformations (kinematic method).

10.2 Set up the relationships (10.4) for the system of Fig. 9.9(b), see example 11.4.

10.3 Consider the system shown in Fig. 9.9(c). Show how the forces in the bars connected to both bases can be determined purely graphically for any point load applied to the system.

10.4 The system shown in Fig. 9.9(d) consists of a number of equally long bars (length l) and is loaded by vertical loads applied to the joints of the bottom chord. Discuss the application of the kinematic method for determining the support force at the right-hand end and the forces in the diagonal struts at the intermediate support.

10.5 Each of the 11 joints in the bottom chord of the system shown in Fig. 9.9(d) is loaded by a vertical point load Q. Consider the bottom chord joints as free bodies and draw a free body diagram for each one.

11 STRESS RESULTANTS AND STATE DIAGRAMS

11.1 General

Stress resultants, which are generally components of the resultant force and the resultant couple of the internal forces in plane sections normal to the bar axis, were introduced in section 5.1.7, see Fig. 5.14. Together with the associated deformation variables (displacements and rotations according to Fig. 5.15), the stress resultants constitute the so-called *state variables*, whose progression along the bar axis is described with the help of *state diagrams*. In such diagrams, positive (negative) state variables are generally drawn to scale in the direction of the positive (negative) z axis. The ensuing drawings are known as *diagrams of stress resultants*.

The reader has already encountered examples of diagrams of stress resultants, e. g. in Figs. 5.30 and 5.34, in Figs. 8.11, 8.13, 8.14, 8.17, 8.19, 8.20 and 8.22, and also in Figs. 10.3 and 10.7.

The differential relationships (8.21) and (8.26) between the stress resultants and the line loads and line load moments apply to the straight bar elements of plane or spatial framed structures respectively. These relationships can generally be applied to limit the calculation of the stress resultants to a few typical cross-sections and deduce the progression of the stress resultants between those cross-sections in a simple way.

According to (8.21),

$$q_x = -\frac{\mathrm{d}N}{\mathrm{d}x} \quad , \quad q_z = -\frac{\mathrm{d}V}{\mathrm{d}x} \quad , \quad V = \frac{\mathrm{d}M}{\mathrm{d}x} \tag{11.1}$$

applies for a plane framed structure where $m_y = 0$, the commonest case in practice. Accordingly, setting q_x, q_z, V to zero corresponds to setting N, V, M to extreme values; and in areas where q_x, q_z, V disappear or are constant or vary linearly, N, V, M are constant or vary linearly or to the power of two. Further, for positive V, M increases as x increases, whereas for positive q_x and q_z, N and V decrease as x increases. Point loads Q_x, Q_z or point load moments M_y cause corresponding abrupt changes in N, V, M; the result is a kink in the M diagram at the point of application of a point load Q_z. All these readily identifiable relationships are shown in Fig. 11.1.

If we use x_1 and x_2 to designate two points on a straight segment of bar where the moment is zero (e. g. flexural hinges), then according to $(11.1)_3$,

$$\int_{x_1}^{x_2} V \,\mathrm{d}x = 0 \tag{11.2}$$

provided no point load moments M_y occur between x_1 and x_2. This is useful when checking the shear force diagrams, for instance.

Pin-jointed bars not loaded transverse to the bar axis (see section 5.1.5 for definition) are obviously subjected to normal forces N only, $V = M = 0$.

A symmetrical three-hinged arch subjected to an asymmetric imposed load was investigated in example 5.7 (Fig. 5.30). The load was rearranged to divide it into symmetric and antisymmetric parts. Whereas the symmetric part caused normal forces with a symmetric distribution, the antisymmetric part gave rise to asymmetrically distributed bending moments and normal forces (with zeros on the axis of symmetry $x = 0$) plus symmetrically distributed shear forces. These findings can be generalised. In a

Theory of Structures. First Edition. Peter Marti

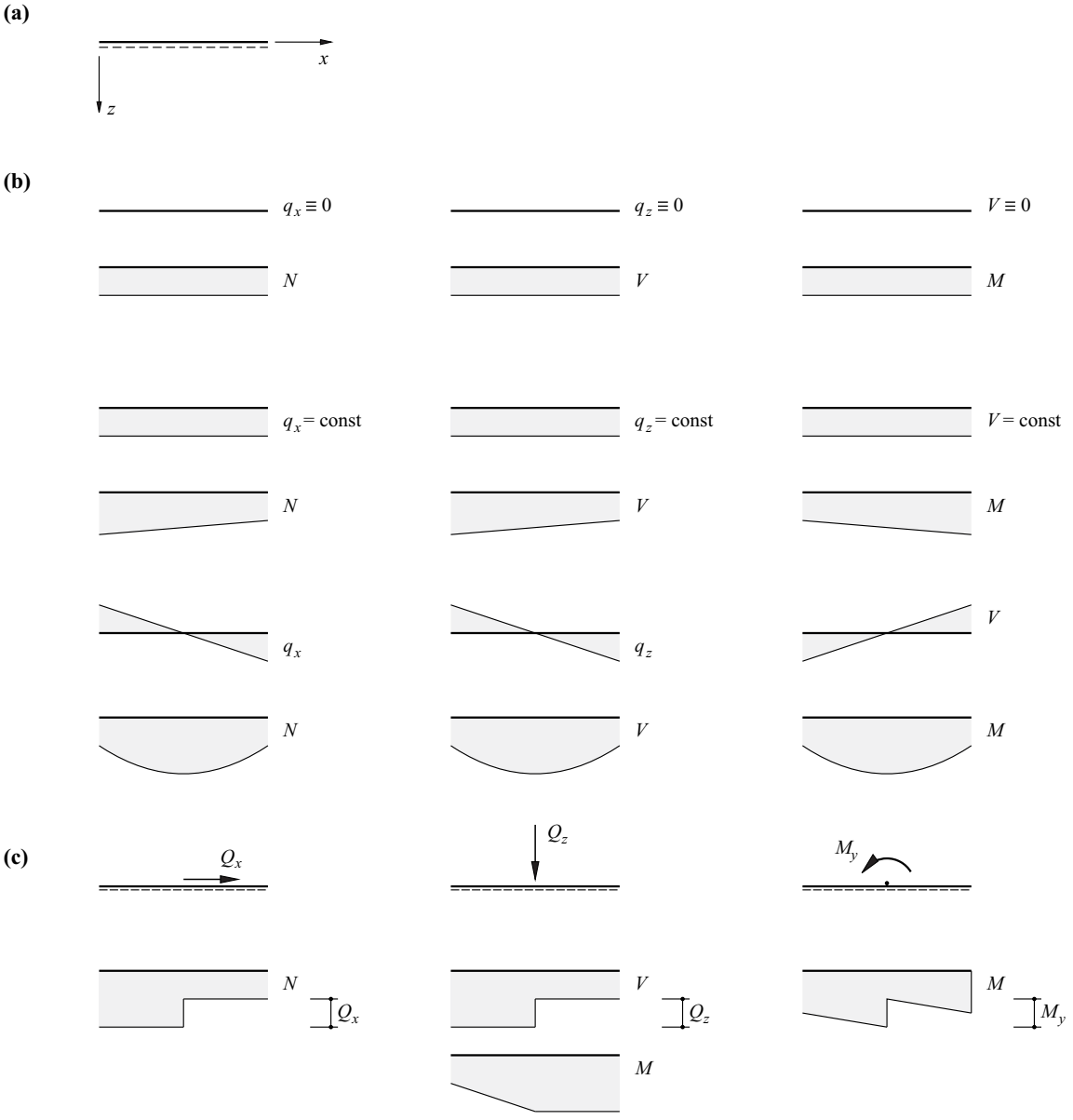

Fig. 11.1 Diagrams of stress resultants: (a) local coordinates, (b) the influence of q_x, q_z, V which are constant, linear or disappear over certain lengths, (c) the influence of point loads and point load moments

symmetric system, symmetric (antisymmetric) load components cause symmetric (antisymmetric) progressions of N and M as well as antisymmetric (symmetric) progressions of V, and the antisymmetric stress resultants become zero on the axis of symmetry.

11.2 Hinged frameworks

This section deals with systems such as the *hinged girders* (GERBER *beams*) of Figs. 9.3(c) and (d) and 10.5, *hinged arches* and *frames* such as those shown in Figs. 5.30, 5.31, 9.3(e), 10.4 and 10.10, and *stiffened beams with intermediate hinges*, similar to the structures depicted in Figs. 9.3(g), (i), (n) and (o). Such systems are statically determinate and therefore adapt without restraint to any support displacements and can also be erected without restraint. In addition, they are often employed as statically determinate basic systems when applying the force method to statically indeterminate systems (chapter 16).

11.2.1 Hinged girders

According to (9.3), a beam continuous over m spans becomes statically determinate when we introduce $m-1$ flexural hinges. For example, $s = 3$, $c = 5$, $k = 4$, $g = 2$, and therefore $n = 0$, for the system shown in Fig. 11.2(a) with its central *cantilever beam* EF (overhang at both ends) and *propped beams* AE, FD on either side. The system shown in Fig. 11.2(b), with the cantilever beam ABE (overhang at one end), the *coupling beam* EF and the propped beam FD, results in the same outcome when we apply the counting scheme (9.3): $n = 3 \cdot 3 + 5 - 3 \cdot 4 - 2 = 0$.

The flexural hinges must be introduced in such a way that they do not cause a *chain of hinges*. Therefore, interior spans may have no more than two hinges, end spans no more than one. In addition, with a *suspended beam*, there should be neither propped beams in the adjacent end spans nor suspended beams in the adjacent interior spans; Fig. 11.2(c) and (d) illustrate the mechanisms otherwise possible – both systems are kinematically unstable and their equilibrium matrices according to (9.2) are singular.

The three global equilibrium conditions and $m-1$ moment-balance equations (auxiliary conditions) about the intermediate hinges can be set up in order to determine the $m+2$ support forces. Once the corresponding sets of linear equations have been resolved, the diagrams of the stress resultants can be drawn simply by considering the individual parts of the system as free bodies and applying the equilibrium conditions according to section 10.2.

Alternatively, the system can be divided into its constituent parts at the outset by introducing cuts through the intermediate hinges. Starting with the suspended and propped beams, the system is then analysed successively by applying the equilibrium conditions.

Both procedures will be explained by means of the following example.

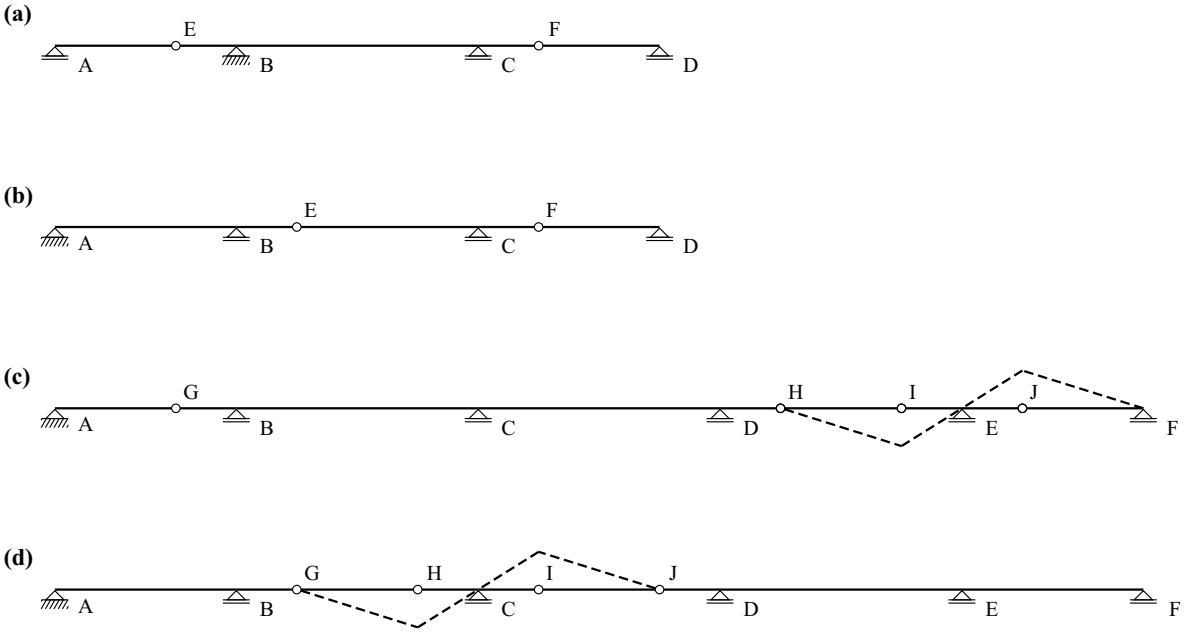

Fig. 11.2 Hinged girder: (a) cantilever beam EF with propped beams AE, FD, (b) coupling beam EF, (c) suspended beam HI with inadmissible hinge J in adjacent end span EF, (d) suspended beam GH with inadmissible suspended beam IJ in adjacent interior span CD

Example 11.1 Hinged girder

The system shown in Fig. 11.3(a) has the free body shown in Fig. 11.3(b) with equilibrium and auxiliary conditions that result in the following set of linear equations:

$$\begin{bmatrix} 0 & 0 & 0 & 0 & 0 & -1 \\ -1 & -1 & -1 & -1 & -1 & 0 \\ 0 & 5 & 11 & 17 & 22 & 0 \\ 0 & 0 & 0 & 1 & 6 & 0 \\ 0 & 0 & 0 & 5 & 10 & 0 \\ -4 & 0 & 0 & 0 & 0 & 0 \end{bmatrix} \begin{Bmatrix} A \\ B \\ C \\ D \\ E \\ K \end{Bmatrix} + \begin{Bmatrix} 10 \\ 50 \\ -680 \\ -80 \\ -200 \\ 20 \end{Bmatrix} = \begin{Bmatrix} 0 \\ 0 \\ 0 \\ 0 \\ 0 \\ 0 \end{Bmatrix}$$

from which it follows that $\{A, B, C, D, E, K\} = \{5, 7.5, 7.5, 20, 10, 10\}$. Therefore, it is easy to draw the diagrams of the stress resultants as shown in Fig. 11.3(c), taking into account the relationships discussed in section 11.1.

Fig. 11.3(d) shows the system divided into its constituent parts at the intermediate hinges. Equilibrium results directly in $A = F = 5$, $G = H = 10$, $I = J$ for the subsystems AF and GH. Equilibrium of subsystems FG and HE then calls for $B = 7.5$, $C = 7.5$, $J = K$ and $D = 20$, $E = 10$, $I = 10$, from which it follows that, in the end, $I = J = K = 10$. The diagrams of the stress resultants then ensue as before, see Fig. 11.3(c).

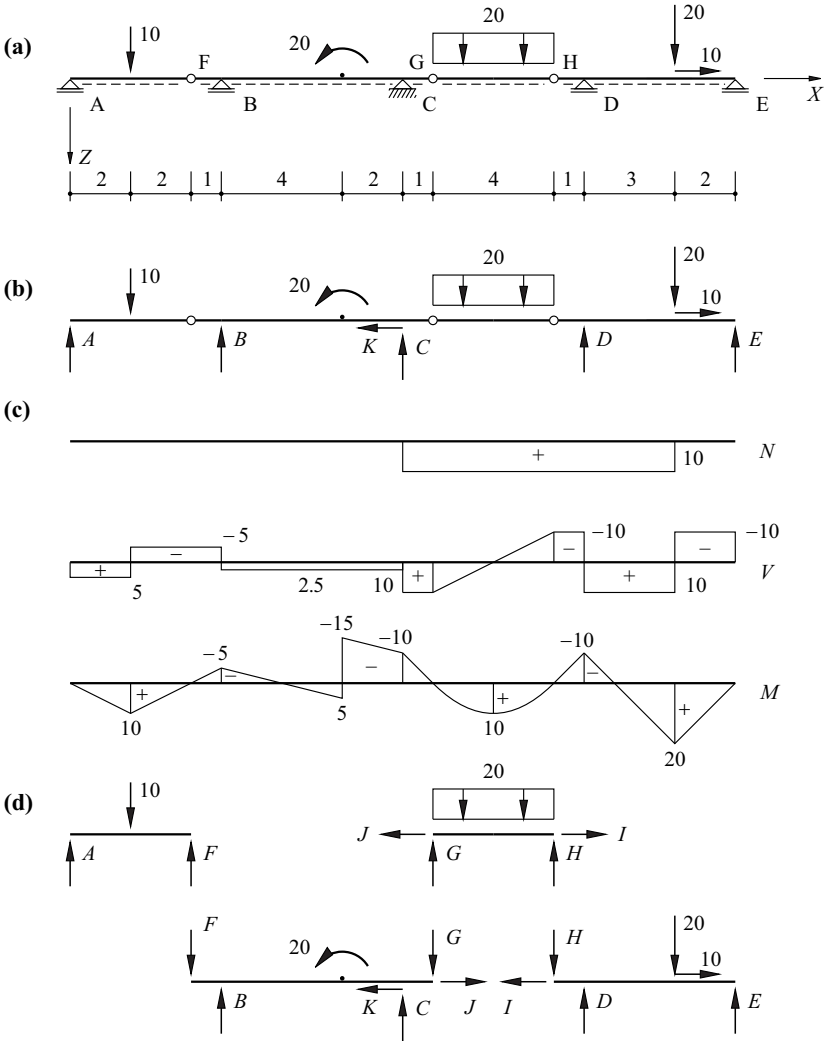

Fig. 11.3 Hinged girder: (a) diagram of static system [m, kN], (b) support forces, (c) diagrams of stress resultants, (d) subsystems

11.2.2 Hinged arches and frames

Three-hinged arches have already been examined in section 5.3.2 and example 10.5. Fig. 11.4(a) shows a general case in which the abutments A and B, known as the *springings*, are at different levels. Besides the *springing hinges*, there is a third hinge at the *crown* C of the arch. The *rise f* is the vertical distance of the *crown hinge* above a line joining the springings.

Where the subsoil is unsuitable for accommodating horizontal loads, a *tie* connecting the springings can be included, as shown in Fig. 11.4(b). The tie is usually suspended from the arch via regularly spaced *hangers*. In the case of a bridge structure, the deck beam serves as a tie. Externally, the system of Fig. 11.4(b) acts like a simply supported beam.

Fig. 11.4(c) shows a three-hinged arch with a propped deck. The deck DE is a statically determinate hinged framework, the loads of which are transferred via vertical *props* to the arch ACB.

Frames are cranked bar systems that have either rigid or hinged corners. Frames are generally statically indeterminate. We shall only examine statically determinate *hinged frames* here.

Fig. 11.4(d) shows a *three-hinged frame* with *frame legs* AD, BE, *frame beams* DC, EC, *base hinges* A, B and *ridge hinge* C. Similarly to Fig. 11.4(b), a tie connecting the bases of the frame legs can be included in a three-hinged frame as well, see Fig. 11.4(e). Fig. 11.4(f) shows a three-span hinged frame that consists of two three-hinged frames DEF, GHI either side of a central three-hinged frame ACB; it is also possible to design multi-span hinged arch structures in a similar way. Generally, setting up series of statically determinate subsystems, side by side or on top of each other, results in *multi-span hinged arches* or *frames*.

The four support forces of three-hinged arches and frames are obtained from three equilibrium conditions and the auxiliary condition such that the bending moment at the third hinge must be equal to zero. Afterwards, the stress resultants required can be calculated by considering corresponding free bodies in accordance with the principles of section 10.2. When dealing with arch structures, it is expedient to

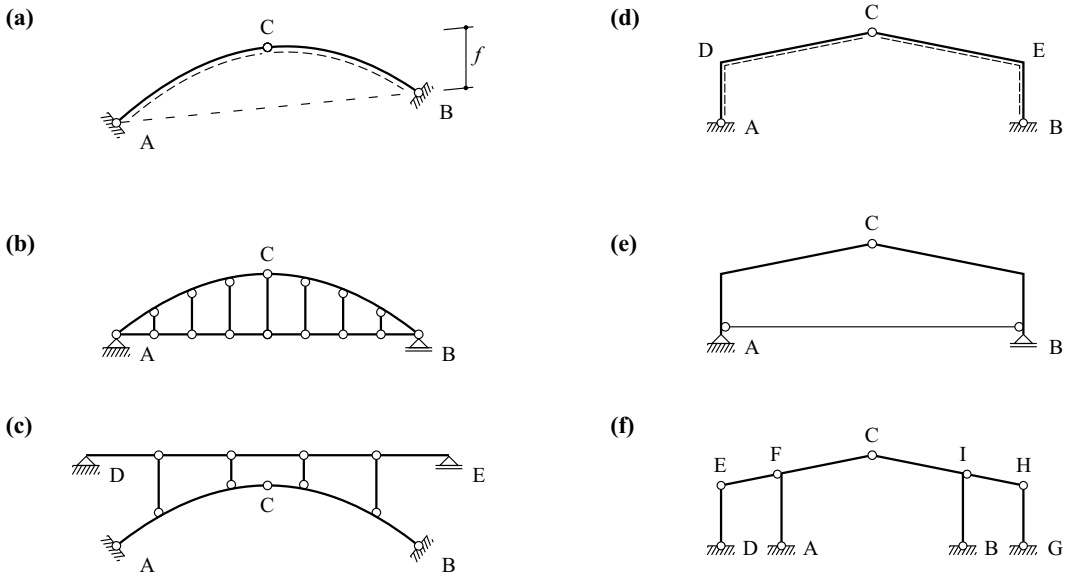

Fig. 11.4 Hinged arches and frames: (a) three-hinged arch, (b) three-hinged arch with tie, (c) three-hinged arch with propped deck, (d) three-hinged frame, (e) three-hinged frame with tie, (f) multi-span hinged frame

determine the stress resultants in the direction of the global coordinates first and then convert these to the local coordinates.

Hangers and props transfer normal forces only. These forces result from the support forces of the simply supported beams making up the associated transversely loaded ties or deck beams. In multi-span hinged arches and frames, all the stress resultants are calculated by considering the individual subsystems in succession, in a similar way to a hinged girder.

Example 11.2 Three-hinged frame with tie

Externally, the three-hinged frame ABCD with tie EFD shown in Fig. 11.5(a) functions like a simply supported beam. Equilibrium of moments about A initially results in a vertical support force of 100 kN at D. The force-balance equations then result in corresponding support forces at A of 54 kN in the horizontal direction and 86 kN in the vertical direction.

The normal force N_{DE} in the tie can be obtained using the kinematic method according to section 10.4, for example. If we make an imaginary cut through the tie and apply a horizontal displacement δu to

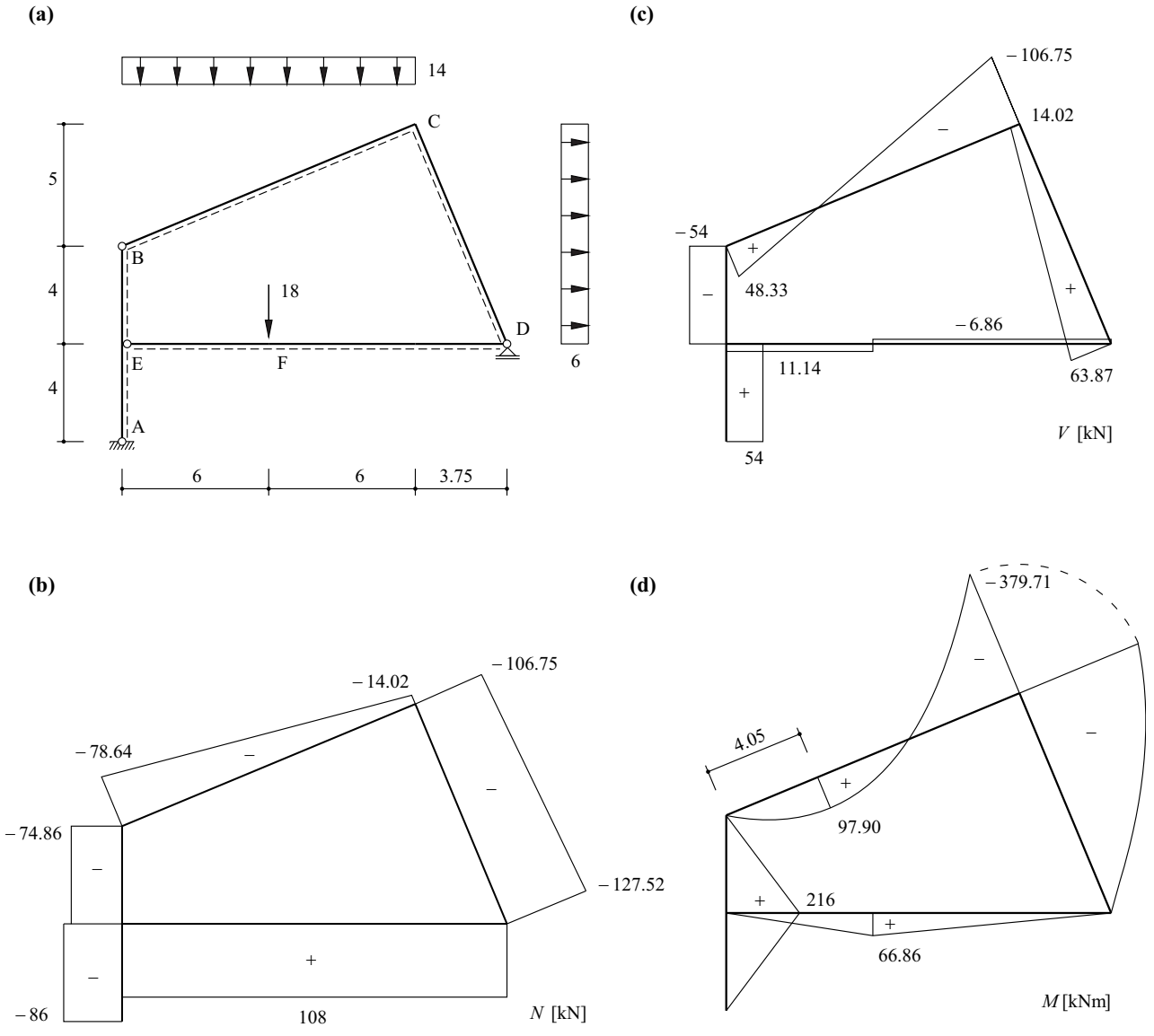

Fig. 11.5 Three-hinged frame with tie: (a) diagram of static system [m, kN], (b) to (d) diagrams of stress resultants

the right at point E, then subsystem BCD undergoes a horizontal translation of $2\delta u$, and at the point of the cut through the tie, the two sides of the cut undergo a relative displacement of δu. According to the principle of virtual deformations,

$$\delta W = (2 \cdot 9\ m \cdot 6\ kN/m - N_{DE})\,\delta u = 0$$

and therefore N_{DE} = 108 kN. We get the same result with a moment-balance equation about B for subsystem AEB: $N_{DE} \cdot 4\,m - 54\,kN \cdot 8\,m = 0$.

Considering the simply supported beam DE, applying the moment-balance equation about E for the transverse load at F results in a support force of $18\,kN \cdot 6\,m / 15.75\,m = 6.86\,kN$ at D and therefore a bending moment of $6.86\,kN \cdot 9.75\,m = 66.86\,kNm$ at F.

The compressive force amounting to 86 kN in frame leg AE is reduced to 74.86 kN in frame leg EB because of the shear force of 18 kN – 6.86 kN = 11.14 kN at E. The shear force in frame leg AB changes from 54 kN to – 54 kN at E, and a bending moment of 54 kN · 4 m = 216 kNm occurs at E. Resolving the forces at B and D results in normal and shear forces of – 78.64 kN and 48.33 kN and – 127.52 kN and 63.87 kN respectively. Considering subsystems BC and CD also leads to normal forces of – 14.02 kN and – 106.75 kN at C and, owing to the 90° crank in the bar axis, to corresponding shear forces of – 106.75 kN and 14.02 kN. Finally, we get a value of – 379.71 kNm for the bending moment at C.

The point of zero shear in frame beam BC lies at a distance of

$$\frac{48.33}{48.33 + 106.75}\sqrt{12^2 + 5^2}\,m = 4.05\,m$$

from B, and the associated maximum bending moment amounts to $48.33\,kN \cdot 4.05\,m\ /\ 2 = 97.9\,kNm$. As a check, we get the following corner moment at C:

$$97.9\,kNm - 106.75\,kN \cdot (\sqrt{12^2 + 5^2} - 4.05)\,m/2 = -379.7\,kNm$$

The diagrams of the stress resultants are shown in Fig. 11.5(b) to Fig. 11.5(d).

11.2.3 Stiffened beams with intermediate hinges

Fig. 11.6 shows various stiffening arrangements for beams achieved with *bar polygons* and vertical bars (posts and hangers) connected via hinges. If we presume that the joints of the bar polygon are not loaded (all loads are applied to the beam), then the horizontal component H of the forces in the bar polygon must be constant. This observation means that it is expedient to divide the systems by cutting through the intermediate hinges and setting up the six equilibrium conditions for the two subsystems in order to calculate the three support forces of the beam and H as well as the two hinge force components. All the forces in the vertical bars and the stress resultants in the beam then result from simple equilibrium considerations.

In the LANGER beam (arch-hanger-girder system) of Fig. 11.6(a), the bar polygon above the beam is in compression and connected to the beam via hangers. Fig. 11.6(b) shows the inversion of this system, with the bar polygon below the beam in tension and connected to the beam via *struts*.

The bar polygon of the *deck-stiffened polygonal arch* of Fig. 11.6(c) transfers its loads directly to the springings D and E. The system is closely related to the LANGER beam of Fig. 11.6(a). Instead of being loaded via hangers from below, the bar polygon in compression is loaded via struts from above.

Fig. 11.6(d) shows the bending moment diagram due to a point load Q applied to the deck-stiffened polygonal arch of Fig. 11.6(c). The bending moment for the unstiffened beam without intermediate hinge would be $M_0(x)$. Stiffening results in a reduction affine to the shape of the bar polygon such that M becomes zero at the point of the intermediate hinge C, see Fig. 5.31 and the associated discussion. If in the example of Fig. 5.31 the arch itself has to accommodate the bending moments, then this function is assigned to the beam according to Fig. 11.6(c); it stiffens the bar polygon, which is why the system is called a deck-stiffened polygonal arch.

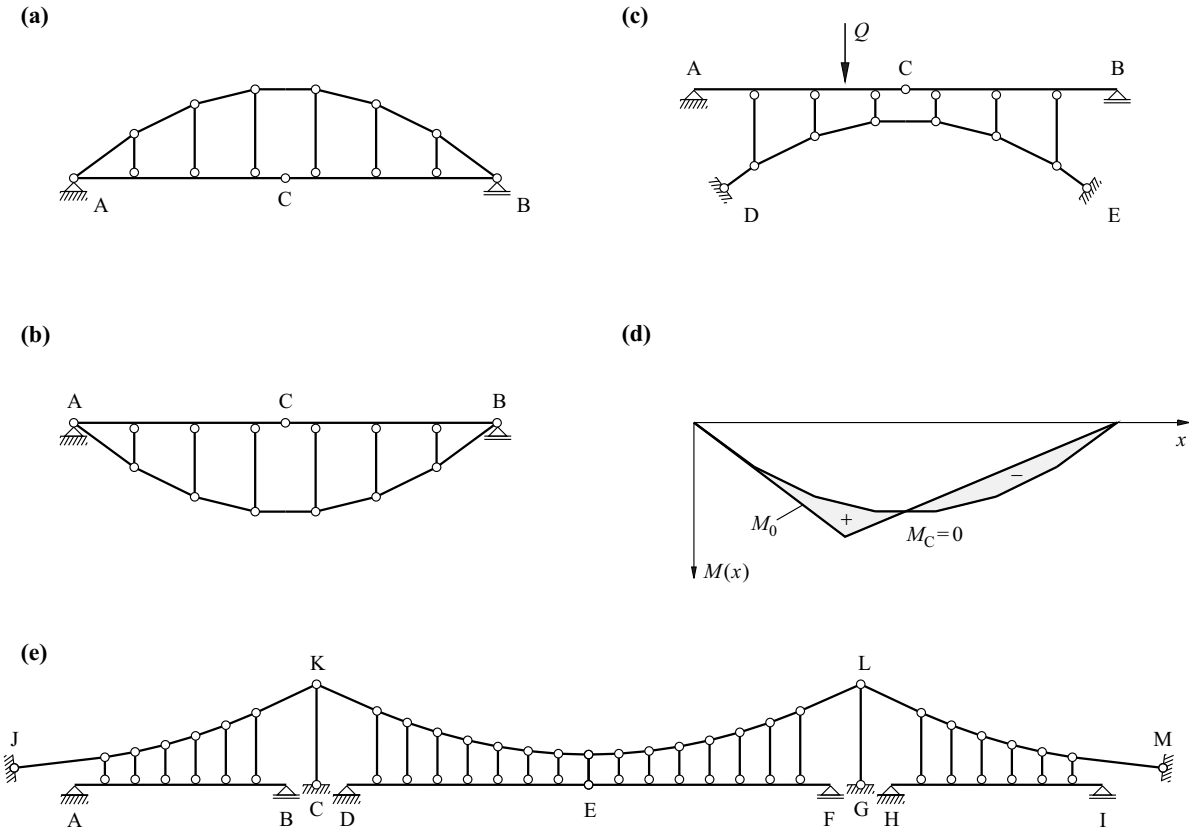

Fig. 11.6 Stiffened beams with intermediate hinges: (a) LANGER beam (arch-hanger-girder system), (b) underslung beam, (c) deck-stiffened polygonal arch, (d) bending moment diagram due to point load Q on deck-stiffened polygonal arch, (e) suspension bridge

The middle span DEF of the *suspension bridge* shown in Fig. 11.6(e) corresponds to an inversion of the deck-stiffened polygonal arch of Fig. 11.6(c). The bar polygon KL in tension continues over the hinged *pylons* CK, GL to the anchorages J, M and is used to suspend the side spans AB, HI.

The stiffened beams with intermediate hinges shown here have little significance in practice these days. Compared with the corresponding statically indeterminate systems without intermediate hinges, the intermediate hinges reduce both the stiffness and the strength, require maintenance and are uneconomic. However, discussing such statically determinate systems was necessary here in order to generate an understanding of the structural behaviour of the corresponding statically indeterminate systems; in these systems, H is not calculated from a hinge condition but rather from a deformation condition.

11.3 Trusses

11.3.1 Prerequisites and structural topology

The prerequisites for *ideal trusses* introduced by CULMANN (straight bars connected at the joints concentrically via frictionless hinges and loaded only at the joints) are only fulfilled approximately by trusses in practice. At the joints, the bars are generally connected rigidly together via *gusset plates*, see Fig. 11.7(a). In addition, eccentricities at the connections, both intended and unintended, can occur, also curvature of the bars, and the bars are loaded in bending by their self-weight at least and often also by external transverse loads. Apart from the intended transverse loads, which are considered in the dimensioning, the stresses caused by the various aforementioned effects can be regarded as *secondary stresses* and therefore ignored, provided it is not necessary

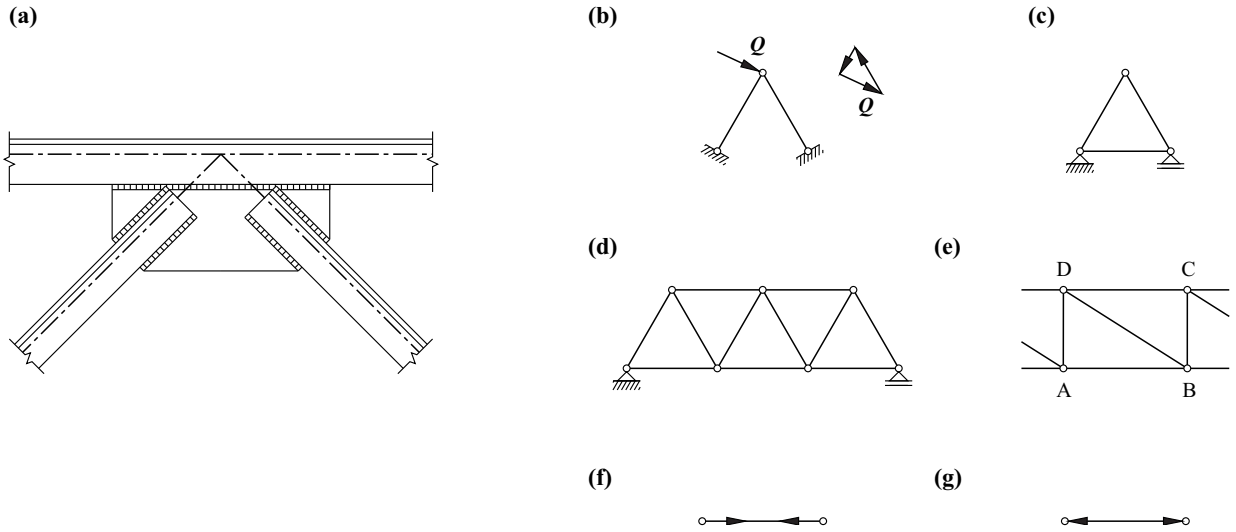

Fig. 11.7 Trusses: (a) typical joint, (b) resolving a joint load into two bar forces, (c) basic truss element, (d) connecting new joints via pairs of bars (WARREN truss), (e) PRATT truss , (f) tie, (g) strut

to verify the fatigue resistance; with adequate deformation capacity and no stability problems, such stresses have no influence on the limit load, see chapter 21.

In the two-dimensional case, any joint load $\boldsymbol{Q}$, see Fig. 11.7(b), can be resolved into two bar forces with non-concurrent axes. Assuming the basic triangular truss element as shown in Fig. 11.7(c), we can therefore create a statically determinate plane frame when each new joint is connected via two new bars not in a straight line (i. e. with a bipod), see Fig. 11.7(d). According to (9.5), $s + c = 2k$ applies.

In the three-dimensional case, instead of Fig. 11.7(b), we get a tripod made up of three bars not lying in one plane. Instead of the triangle of bars of Fig. 11.7(c), a tetrahedron of bars plays the role of the basic truss element. The result is a statically determinate space frame in which each new joint is connected via three new bars not lying in one plane (i. e. with a tripod). According to (9.6), $s + c = 3k$ applies.

The bars of a truss are divided into *chords* and *web members*. Referring to Fig. 11.7(e), the former includes the *bottom chord* AB and the *top chord* DC, and the latter includes the *posts* AD, BC and the *truss diagonal* DB.

To distinguish between ties and struts, the bar forces are indicated with arrows according to Fig. 11.7(f) and (g), which show how the forces act on the joints.

Fig. 11.8 provides an overview of various feasible *truss types*. Fig. 11.8(a) to Fig. 11.8(c) illustrate trusses with a simple triangulated frame. Trusses with a complex frame are shown in Fig. 11.8(d) to Fig. 11.8(f), whereas Fig. 11.8(g) is an example of a truss with a secondary frame.

Fig. 11.9 shows various forms of trussed girder used in bridges and buildings. Bowstring (PARKER), inverted bowstring and PAULI trusses are matched to the bending moment diagram in such a way that the result is approximately constant forces in the chords. In the PAULI truss (fish-belly truss), the forces in the web members are especially small. In the SCHWEDLER truss, the top chord is cranked in the centre in such a way that the diagonals are loaded in tension only, even when subjected to a travelling load. The POLONCEAU truss is actually a three-hinged frame with a tie. It is possible to construct further combined forms of trussed girders from those illustrated in Fig. 11.9, e. g. hinged girders, hinged frames, stiffened beams, and also *space trusses*, see Fig. 9.2.

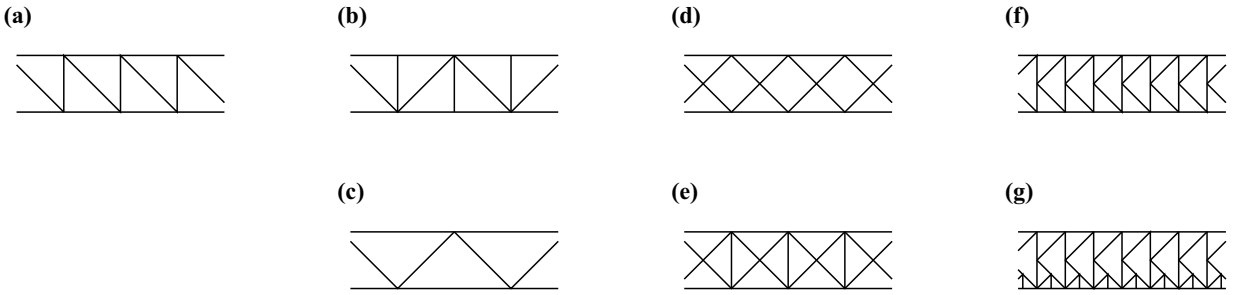

Fig. 11.8 Types of truss: (a) PRATT truss, (b) modified WARREN truss, (c) WARREN truss, (d) BROWN truss, (e) LONG truss, (f) K-truss, (g) K-truss with secondary diagonals and posts

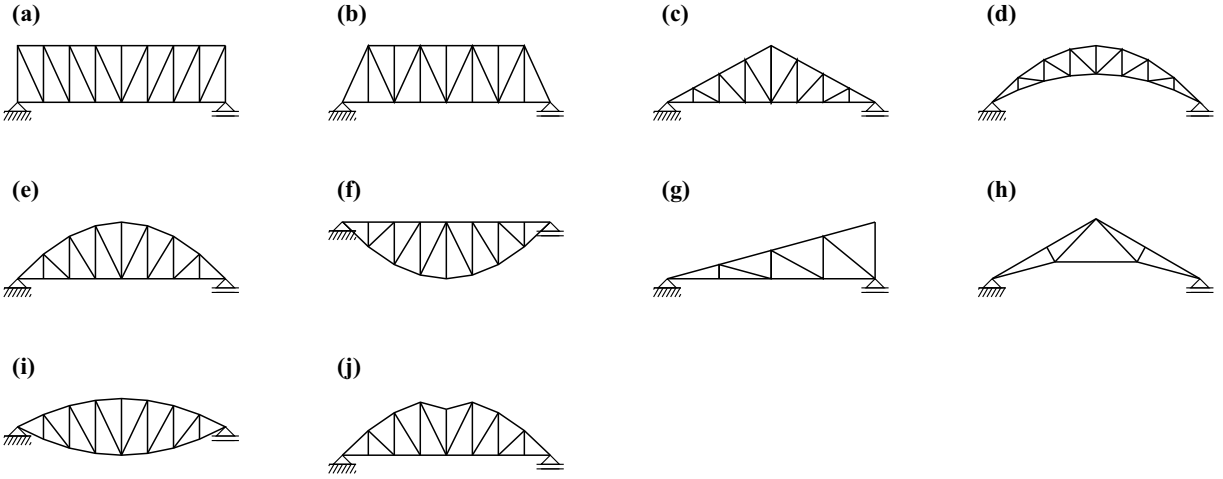

Fig. 11.9 Types of truss: (a) PRATT truss, (b) modified WARREN truss, (c) duopitch PRATT truss, (d) crescent truss, (e) bowstring truss(PARKER truss), (f) inverted bowstring truss, (g) monopitch truss, (h) POLONCEAU truss, (i) PAULI truss (fish-belly truss), (j) SCHWEDLER truss

The hexagonal SCHWEDLER dome shown in Fig. 11.10 consists of meridional *ribs* (rafters), horizontal *rings* and diagonals, which stiffen the individual trapezoidal panels. There is often a ring joining the bases as well, which means that one support force component per base joint can be omitted while maintaining the static determinacy; each second base joint could be supported in the vertical direction only, for instance. SCHWEDLER domes are often also built with diagonals in both directions (X-bracing), which turns them into statically indeterminate space trusses.

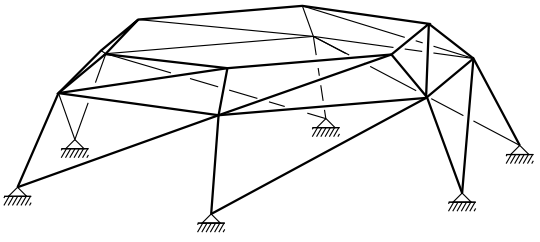

Fig. 11.10 SCHWEDLER dome

11.3.2 Methods of calculation

Basically, all the methods discussed in chapter 10 can be used for determining the bar forces of statically determinate trusses. The method whereby the joint equilibrium is systematically considered can be applied to any truss. For simple plane trusses, one graphical method, the CREMONA diagram, still plays a certain role. If we only require individual bar forces, considering selected free bodies or the kinematic method are quicker ways of achieving results than applying joint equilibrium conditions. The method of sections developed by August RITTER, which can be applied to any truss, is essentially based on moment-balance conditions about skilfully selected points or axes. The graphical method for simple plane trusses corresponding to this method and developed by CULMANN is of historical interest only.

11.3.3 Joint equilibrium

11.3.3.1 Considering individual joints in succession

Once we have determined the support forces, we can examine the equilibrium joint by joint. Where only two unknown bar forces occur, these are easy to calculate.

Example 11.3 Plane truss

The plane truss shown in Fig. 11.11(a) consists of $k = 6$ joints and $s = 9$ bars. With $c = 3$ support forces at 1 and 6, according to (9.5), $n = 0$. The load of 9 kN at 2 leads to vertical support forces of 6 kN at 1 and 3 kN at 6, as can be easily seen by way of the moment-balance conditions about 6 and 1 respectively. As there are no loads in the X direction, the corresponding support force at 1 is zero.

Equilibrium at joint 1 calls for forces of 10 kN (compression) and 8 kN (tension) in bars 1 and 2 respectively. The two remaining unknown bar forces 3 and 4 at joint 2 are therefore 3 kN (compression) and 8 kN (compression) respectively. Similarly, at joint 3 we get bar forces 5 (5 kN, tension) and 6 (4 kN, tension) and at joint 4 we get bar forces 7 (zero) and 8 (5 kN, compression). The force-balance condition in the X direction at joint 5 results in a tensile force of 4 kN in bar 9. The force-balance condition in the Z direction at joint 5, and the two equilibrium conditions at joint 6 are satisfied and can be regarded as a check.

Fig. 11.11(b) shows the free body diagrams for the six joints, and Fig. 11.11(c) summarises the results when using the notation according to Fig. 11.7(f) and (g).

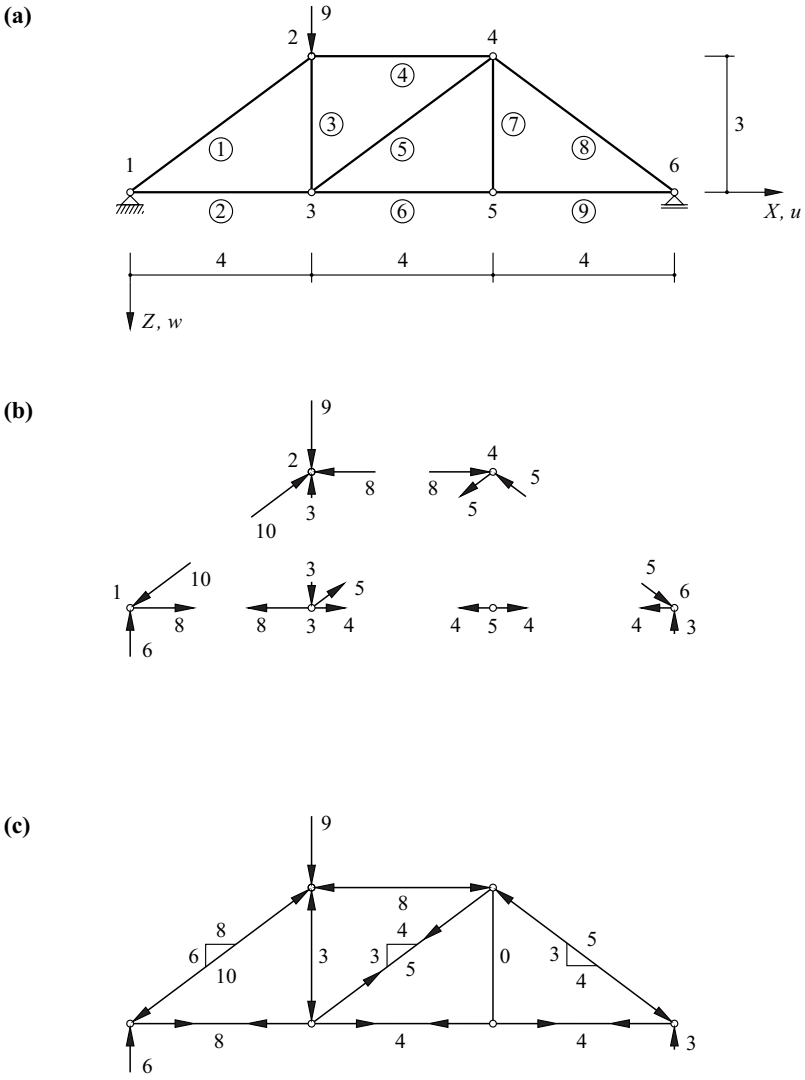

Fig. 11.11 Plane truss: (a) diagram of static system [m, kN], (b) joint equilibrium, (c) load, support forces and bar forces

11.3.3.2 Complex trusses

Complex trusses in which, unlike *simple trusses*, not every new joint is connected by two bars not in a straight line or three bars not lying in one plane, can sometimes be converted to simple trusses by way of *bar substitution*.

For example, the complex truss shown in Fig. 11.12(a) is converted to a simple truss by removing bars i, j and introducing bars $\bar{i}$, $\bar{j}$, see Fig. 11.12(b). The forces N_i, N_j in the bars removed follow from the condition that the bar forces s_i, s_j of the new bars must be equal to zero. If we designate the bar forces s_i, s_j as a result of external loads as well as $N_i = 1$ and $N_j = 1$ with s_{i0}, s_{ii}, s_{ij} and s_{j0}, s_{ji}, s_{jj} respectively, then

$$s_i = s_{i0} + N_i s_{ii} + N_i s_{ij} = 0$$

$$s_j = s_{j0} + N_j s_{ji} + N_i s_{jj} = 0$$

applies, or generalised

$$\{s_0\} + [s]\{N\} = \{0\} \tag{11.3}$$

which allows N_i, N_j to be calculated.

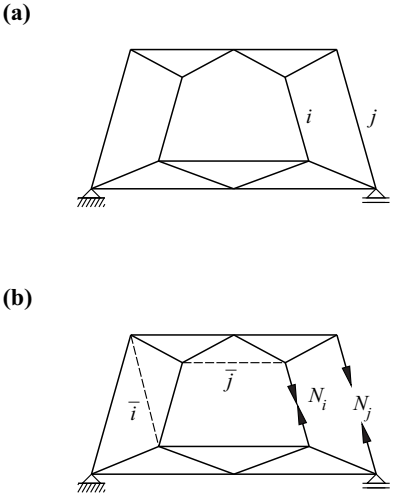

Fig. 11.12 Method of bar substitution: (a) complex, statically determinate truss, (b) conversion to a simple truss by removing bars i, j and introducing bars $\bar{i}$, $\bar{j}$.

11.3.3.3 General procedure

The general procedure according to (9.2) or (10.4) was explained in example 10.3 by means of the truss shown in Fig. 8.1. The procedure will be used again below for the system examined in example 11.3.

Example 11.4 Plane truss

Consider the system shown in Fig. 11.11(a). According to (8.1), we first get the bar extensions Δ_i as a result of the joint displacements u_j, w_j:

$$\begin{Bmatrix} \Delta_1 \\ \Delta_2 \\ \Delta_3 \\ \Delta_4 \\ \Delta_5 \\ \Delta_6 \\ \Delta_7 \\ \Delta_8 \\ \Delta_9 \end{Bmatrix} = \begin{bmatrix} 0.8 & -0.6 & & & & & & & & & & \\ & & 1 & & & & & & & & & \\ & -1 & & & 1 & & & & & & & \\ -1 & & & & & & 1 & & & & & \\ & & & -0.8 & 0.6 & 0.8 & -0.6 & & & & & \\ & & & -1 & & & & & 1 & & & \\ & & & & & & & -1 & & 1 & & \\ & & & & & & -0.8 & -0.6 & & & 0.8 & \\ & & & & & & & & -1 & & 1 & \end{bmatrix} \begin{Bmatrix} u_2 \\ w_2 \\ u_3 \\ w_3 \\ u_4 \\ w_4 \\ u_5 \\ w_5 \\ u_6 \end{Bmatrix}$$

The empty spaces in matrix $\boldsymbol{a}$ are filled with zeros in the above equation. We get the value $0.864 \neq 0$ for $\det\boldsymbol{a}$, i.e. $\boldsymbol{a}$ is invertible. According to (9.11), transposing $\boldsymbol{a}$ results in the equilibrium matrix $\boldsymbol{g} = \boldsymbol{a}^{\mathrm{T}}$, and inverting $\boldsymbol{g}$ results in the static transformation matrix $\boldsymbol{b} = \boldsymbol{g}^{-1}$ for this statically determinate system, and therefore according to $(10.4)_1$, we get the bar forces

$$\begin{Bmatrix} N_1 \\ N_2 \\ N_3 \\ N_4 \\ N_5 \\ N_6 \\ N_7 \\ N_8 \\ N_9 \end{Bmatrix} = \frac{1}{36} \begin{bmatrix} 15 & -40 & 0 & -40 & 15 & -20 & 0 & -20 & 0 \\ 24 & 32 & 36 & 32 & 24 & 16 & 36 & 16 & 36 \\ -9 & -12 & 0 & 24 & -9 & 12 & 0 & 12 & 0 \\ -24 & -32 & 0 & -32 & 12 & -16 & 0 & -16 & 0 \\ 15 & 20 & 0 & 20 & 15 & -20 & 0 & -20 & 0 \\ 12 & 16 & 0 & 16 & 12 & 32 & 36 & 32 & 36 \\ 0 & 0 & 0 & 0 & 0 & 0 & 0 & 36 & 0 \\ -15 & -20 & 0 & -20 & -15 & -40 & 0 & -40 & 0 \\ 12 & 16 & 0 & 16 & 12 & 32 & 0 & 32 & 36 \end{bmatrix} \begin{Bmatrix} 0 \\ 9 \\ 0 \\ 0 \\ 0 \\ 0 \\ 0 \\ 0 \\ 0 \end{Bmatrix} = \begin{Bmatrix} -10 \\ 8 \\ -3 \\ -8 \\ 5 \\ 4 \\ 0 \\ -5 \\ 4 \end{Bmatrix}$$

in kN. Using matrix $\boldsymbol{g}_{sC}$ according to (9.2), we get the support forces

$$\begin{Bmatrix} C_{1X} \\ C_{1Z} \\ C_{6Z} \end{Bmatrix} = \begin{bmatrix} -0.8 & -1 & 0 & 0 & 0 & 0 & 0 & 0 & 0 \\ 0.6 & 0 & 0 & 0 & 0 & 0 & 0 & 0 & 0 \\ 0 & 0 & 0 & 0 & 0 & 0 & 0 & 0.6 & 0 \end{bmatrix} \begin{Bmatrix} -10 \\ 8 \\ -3 \\ -8 \\ 5 \\ 4 \\ 0 \\ -5 \\ 4 \end{Bmatrix} = \begin{Bmatrix} 0 \\ -6 \\ -3 \end{Bmatrix}$$

in kN according to $(10.4)_2$.

11.3.4 CREMONA diagram

When dealing with simple plane trusses, there are no more than two unknown bar forces per joint. It is generally necessary to calculate the support forces and, possibly, the hinge forces beforehand in such systems in order to be able to begin at one joint with just two unknown bar forces. Afterwards, it is possible to draw the appropriate force polygons for each joint in succession and hence determine the unknown bar forces.

Instead of drawing each bar force twice with individual force polygons, all the force polygons can be combined into a single diagram, the CREMONA *diagram*. Doing this means that the forces acting on each joint are considered in turn by proceeding around the joint in a direction that is maintained for the entire truss. The support forces and loads acting externally on the plane system are arranged in the same rotational order and form a closed force polygon according to the fundamental theorem of statics.

As each bar force has two directions in the CREMONA diagram, depending on which of the two corresponding joints it acts on, the directions of the forces are specified either with a sign (+ tension, – compression) on the CREMONA diagram or with arrows according to Fig. 11.7(f) and (g) on the funicular polygon. As the three equilibrium conditions of the plane are initially used for determining the support forces, the final force polygons in the CREMONA diagram allow the equilibrium to be checked. Finally, we realise that bar forces whose bar axes form a triangle in the funicular polygon intersect at one point in the CREMONA diagram; force polygon and funicular polygon are in this sense reciprocal.

Example 11.5 Plane truss

Fig. 11.13 shows the CREMONA diagram for Fig. 11.11(c). Anticlockwise was chosen as the uniform direction for considering each joint. The bar numbers are taken from Fig. 11.11(a). The scale for the forces is specified by the load of 9 kN and the support forces of 6 kN and 3 kN.

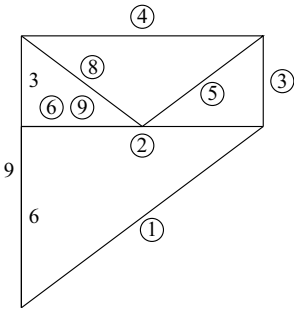

Fig. 11.13 CREMONA diagram for the truss of Fig. 11.11 [kN]

11.3.5 RITTER method of sections

Simple trusses can often be divided into subsystems such that only three unknown bar forces are affected. A moment-balance equation about the intersection of the bar axes of two of these forces then results in the third bar force. If two bar axes are approximately or truly parallel, their intersection lies well beyond the system or at infinity respectively; in such cases, the moment-balance equation must be replaced by a force-balance equation.

The RITTER *method of sections* presumes – like the method of CREMONA – that the support forces are determined beforehand. In contrast to the latter method, the method of sections can be applied to spatial trusses as well, although then the moment equilibrium about appropriate axes has to be formulated.

Example 11.6 Plane truss

Fig. 11.14 illustrates the RITTER method of sections for calculating bar forces 4, 5, 6 of the truss shown in Fig. 11.11(a). With a support force of 6 kN at joint 1, we get the vertical force-balance equation $-6\,\text{kN} + 9\,\text{kN} - 0.6N_5 = 0$ and the moment-balance equations $-6\,\text{kN}\cdot 4\,\text{m} - N_4 \cdot 3\,\text{m} = 0$ and $-6\,\text{kN}\cdot 8\,\text{m} + 9\,\text{kN}\cdot 4\,\text{m} + N_6 \cdot 3\,\text{m} = 0$ about points 3 and 4 respectively, from which it follows that $\{N_4, N_5, N_6\} = \{-8, 5, 4\}\,\text{kN}$.

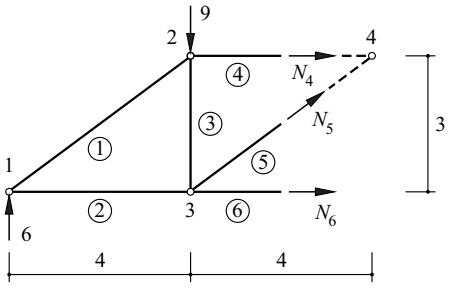

Fig. 11.14 RITTER method of sections [m, kN]

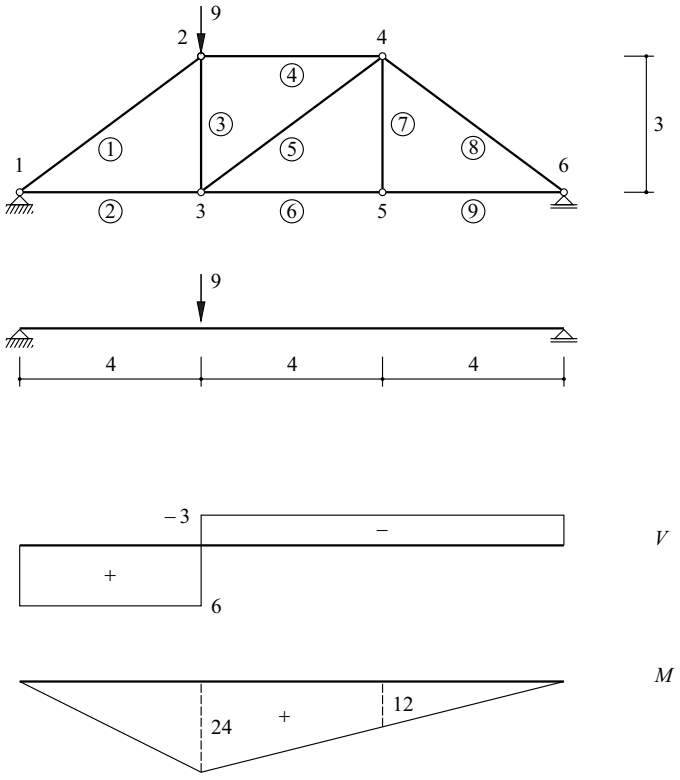

Fig. 11.15 Truss with equivalent beam and corresponding stress resultants [m, kN]

As can be seen, these bar forces can also be easily obtained from the stress resultants of an equivalent beam with the same span, load and support conditions, see Fig. 11.15. The force in the top chord N_4 is obtained by dividing the moment $M = 24\,\text{kNm}$ at the associated reference point 3 by the lever arm of 3 m. Likewise, the force in the bottom chord N_6 is obtained by dividing the moment $M = 12\,\text{kNm}$ at reference point 4 by the lever arm of 3 m. Finally, the vertical component of diagonal force N_5 must be equal to the amount of the associated shear force $V = -3\,\text{kN}$.

11.3.6 The kinematic method

To conclude, the kinematic method already explained for a truss using the example of Fig. 10.9 will be illustrated with a further example.

In order to determine the force O in the top chord of the truss shown in Fig. 11.16, we remove the corresponding bar and introduce force O as a compressive force acting on the adjacent joints. The mechanism that ensues as a result of removing the top chord bar is described by a virtual rotation ω about the right-hand support and an opposite rotation of 3.5ω about the left-hand support. The corresponding virtual displacement components of the two joints at which the forces O act with components $5O/\sqrt{26}$ and $O/\sqrt{26}$ are shown in Fig. 11.16. The point of application of force Q undergoes a virtual deflection of 9ω.

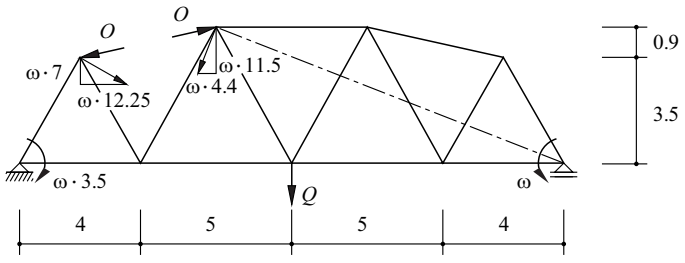

Fig. 11.16 Applying the kinematic method to determine the force O in the top chord (dimensions in m)

Applying the principle of virtual deformations results in

$$\delta W = Q \cdot 9\omega + O[(-5\,,1)\cdot(12.25\,,7) + (5\,,-1)\cdot(-4.4\,,11.5)]\omega/\sqrt{26} = 0$$

and therefore $O = 9\cdot\sqrt{26}Q/87.75 = 0.523Q$. If O had been introduced as a tensile force, the result would have been a negative sign, and the force in the top chord would have been identified as a compressive force.

11.4 Summary

1. Diagrams of stress resultants describe the progression of stress resultants along the bar axis. It is usually sufficient to limit the calculation of the stress resultants to a few typical cross-sections and deduce the progression of the stress resultants between those cross-sections in a simple way.
2. Pin-jointed members are subjected to normal forces only.
3. In symmetrical systems, symmetric (antisymmetric) load components cause symmetric (antisymmetric) progressions of N and M as well as antisymmetric (symmetric) progressions of V. Stress resultants with an antisymmetric progression disappear at the axis of symmetry.
4. Statically determinate hinged frameworks such as hinged girders, arches and frames, also stiffened beams with intermediate hinges, adapt to any support displacements without restraint and can be erected without restraints.
5. The equilibrium of hinged girders can be analysed either by setting up the global equilibrium conditions and the moment-balance equations (auxiliary conditions) about the intermediate hinges or by dividing the system at the intermediate hinges and considering the individual subsystems (starting from suspended and propped beams).
6. Hinged arches and frames can be treated in a similar way to hinged girders. In the case of arch structures, it is expedient to calculate the stress resultants in the direction of the global coordinates first and then convert these to local coordinates.
7. Stiffened beams with intermediate hinges have little significance in practice these days. However, they help us to understand the structural behaviour of the corresponding statically indeterminate systems.
8. Deviations from the conditions of ideal trusses (bent bars, rigid connections between bars, eccentric connections) lead to secondary stresses that can generally be ignored for the dimensioning. By contrast, intended transverse loads on the bars of trusses must be considered in the dimensioning.
9. Simple plane (spatial) trusses are created by connecting each new joint by two bars not lying in a straight line (three bars not lying in one plane). Complex trusses that do not comply with this requirement can sometimes be converted to simple trusses by way of bar substitution; the forces in the bars removed for the substitution procedure are then calculated from (11.3).
10. All the methods discussed in chapter 10 can be used to calculate the bar forces of statically determinate trusses. The method of systematically considering the joint equilibrium can be applied to any truss; the corresponding method according to CREMONA for simple plane trusses still plays a certain role these days. If we are only interested in individual bar forces, applying the kinematic method or the RITTER method of sections is advantageous.

11.5 Exercises

11.1 Fixed support 1 of the system shown in Fig. 9.9(a) is replaced by a hinge and hinged support 4 replaced by a support sliding in the X direction. Uniformly distributed loads of 100 kN and 60 kN act on bars 123 and 34 respectively in the Z direction; in addition, a uniformly distributed load of 15 kN acts on bar 123 in the X direction. Determine the corresponding diagrams of stress resultants.

11.2 The system of Fig. 9.9(c) is loaded over its entire width of $12 \cdot 4.8 = 57.6$ m by a uniformly distributed vertical load of 720 kN. Substitute this load by statically equivalent loads of 60 kN at each of the 11 inner joints of the top chord plus 30 kN at each of the end joints. Determine all the bar forces.

11.3 Solve exercise 11.2 for an asymmetric load of $1 \cdot 12$ kN, $5 \cdot 24$ kN, 0, $5 \cdot (-24$ kN), $1 \cdot (-12$ kN).

11.4 Solve exercises 11.2 and 11.3 for a modified system in which the 8 m high vertical columns are connected at the top by a 48 m long tie and the inclined member connected to the right-hand base is omitted. Discuss the effects of these modifications to the system.

11.5 Use Fig. 11.8 to discuss how the type of truss affects how a constant (positive or negative) shear force is carried in a parallel-chord truss.

11.6 Compare the structural behaviour of the systems in Fig. 11.9(a) and (e) subjected to a uniformly distributed load and a travelling point load applied to the bottom chord. Sum up the products of the bar lengths and the magnitude of the bar forces critical for the dimensioning. Select the depth of the beam to be equal to one-eighth of the span.

11.7 Compare the systems of Fig. 11.9(e) and (i) in a similar way to exercise 11.6.

11.8 On what does the crank in the top chord of the system in Fig. 11.9(j) depend and how should it be formed? Compare the structural behaviour with that of the system in Fig. 11.9(e) in a similar way to exercise 11.6.

12 INFLUENCE LINES

12.1 General

In contrast to diagrams of stress resultants, which apply to one particular load case, *influence lines* show how a moving (free) load affects certain state variables. Moving loads occur in conjunction with, for example, bridges, crane tracks and buildings, see section 4.2.1.

The simply supported beam AB shown in Fig. 12.1(a) with cantilever BC at one end is loaded momentarily by load Q_m at m. The moment-balance equation about A in the free body diagram of Fig. 12.1(b) results in the support force

$$B = \frac{Q_m x_m}{l} = Q_m \eta_{Bm} \qquad (0 \le x_m \le l + a)$$

where $\eta_{Bm} = x_m/l$ is the *influence ordinate* for B at m. The first index B denotes the position and nature of the state variable being considered, the second index m refers to the cause of the load. Fig. 12.1(c) shows the function $\eta_{Bm}(x_m)$ as an influence line for support force B starting from a reference axis parallel with the *loaded chord* ABC. With a *load train* according to Fig. 12.1(d), B is found using the superposition law as the sum of all the individual loads Q_m :

$$B = \sum_m Q_m \eta_{Bm}$$

As we can see, η_{Bm} corresponds to the progression of B as a result of $Q_m = 1$. This finding is easy to generalise. For the general case, an influence line η_{im} describes how an individual force variable of magnitude 1 acting in a specified direction at any point m influences a certain state variable s_i at point i.

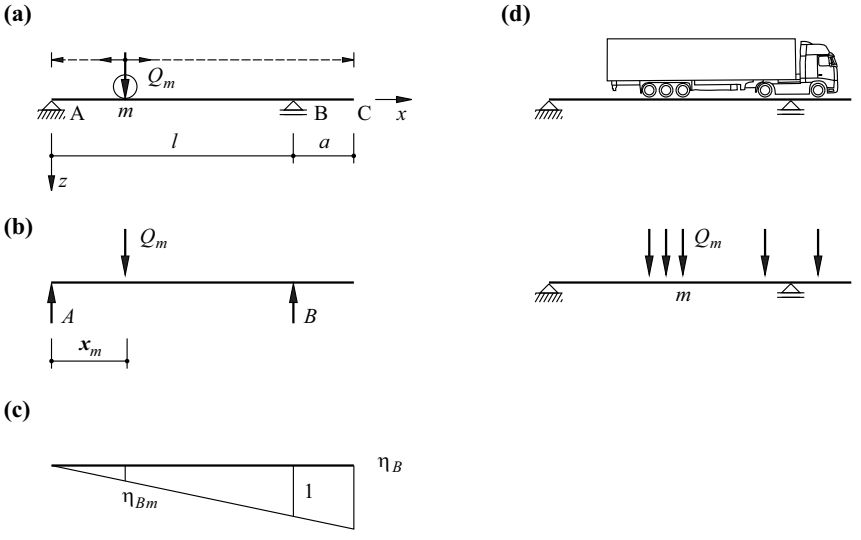

Fig. 12.1 Influence lines: (a) diagram of static system, (b) free body diagram, (c) influence line for support force B, (d) load train

Theory of Structures. First Edition. Peter Marti

Basically, influence lines can be assigned to individual force variables acting in any direction. However, influence lines are mostly confined to vertical point forces in order to be able to investigate the effects of imposed loads caused by traffic.

Influence lines are evaluated according to

$$s_\mathrm{i} = \sum_m Q_m \eta_{\mathrm{i}m} \tag{12.1}$$

for point loads, and according to

$$s_\mathrm{i} = \int q(x)\, \eta_\mathrm{i}(x)\, \mathrm{d}x \tag{12.2}$$

for line loads.

Influence lines help to identify *worst load positions* in particular, i. e. load positions that allow certain state variables to reach extreme values.

Also often interesting in addition to *influence lines for force variables* are the *influence lines for deformation variables*. By applying MAXWELL's theorem (8.88), the relationship (8.86), which is similar to (12.1), can be expressed as

$$u_\mathrm{i} = \sum_m Q_m \cdot f_{m\mathrm{i}} \tag{12.3}$$

by replacing the indexes j, k used there by the indexes i, m used here. In this case $f_{m\mathrm{i}}$ is the (generalised) displacement at the position and in the direction of Q_m as a result of the force variable $Q_\mathrm{i} = 1$ corresponding to u_i, see Fig. 8.16(a). Influence lines for deformation variables are therefore displacement curves that ensue when a corresponding unit force variable is applied at the position and in the direction of the deformation variable of interest.

12.2 Determining influence lines by means of equilibrium conditions

The shear force and bending moment influence lines for reference point i are to be determined for the simply supported beam shown in Fig. 12.2(a). To do this, we make use of the influence lines for the support forces A and B shown together in Fig. 12.2(b), which are produced in a similar way to Fig. 12.1(c). When load $Q_m = 1$ is to the left of reference point i ($x_m \leq x_\mathrm{i}$), the free body diagram on the right in the upper part of Fig. 12.2(c) results in $V_{\mathrm{i}m} = -B_m$ and $M_{\mathrm{i}m} = B_m b$. When load $Q_m = 1$ is to the right of reference point i ($x_m \geq x_\mathrm{i}$), the free body diagram on the left in the lower part of Fig. 12.2(c) results in $V_{\mathrm{i}m} = A_m$ and $M_{\mathrm{i}m} = A_m\, a$. It is therefore possible to draw the influence lines $\eta_{V\mathrm{i}}$ and $\eta_{M\mathrm{i}}$ shown in Fig. 12.2(d) by referring to Fig. 12.2(b). At point i, $\eta_{V\mathrm{i}}$ undergoes an abrupt change of magnitude 1 and $\eta_{M\mathrm{i}}$ has a kink of magnitude 1.

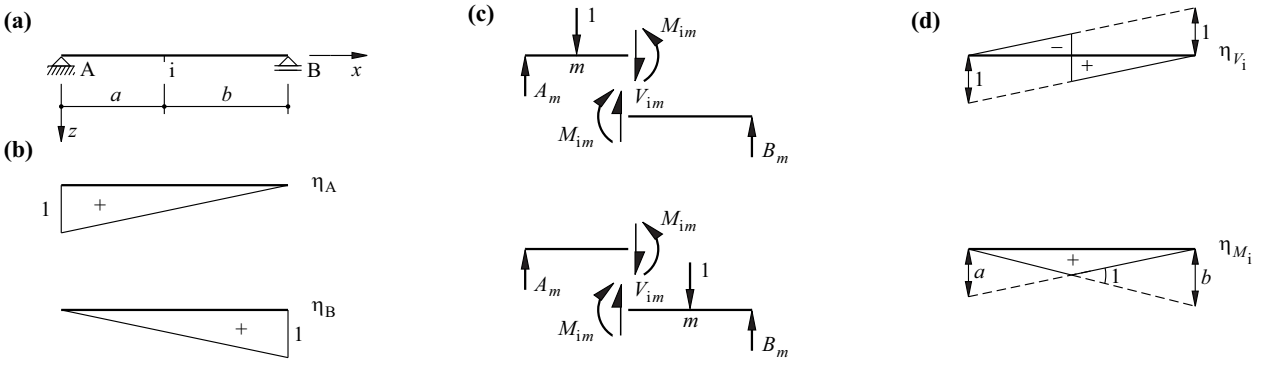

Fig. 12.2 Determining influence lines by means of equilibrium conditions: (a) diagram of static system with reference point i, (b) influence lines for support forces, (c) free body diagrams, (d) influence lines for shear forces and bending moments

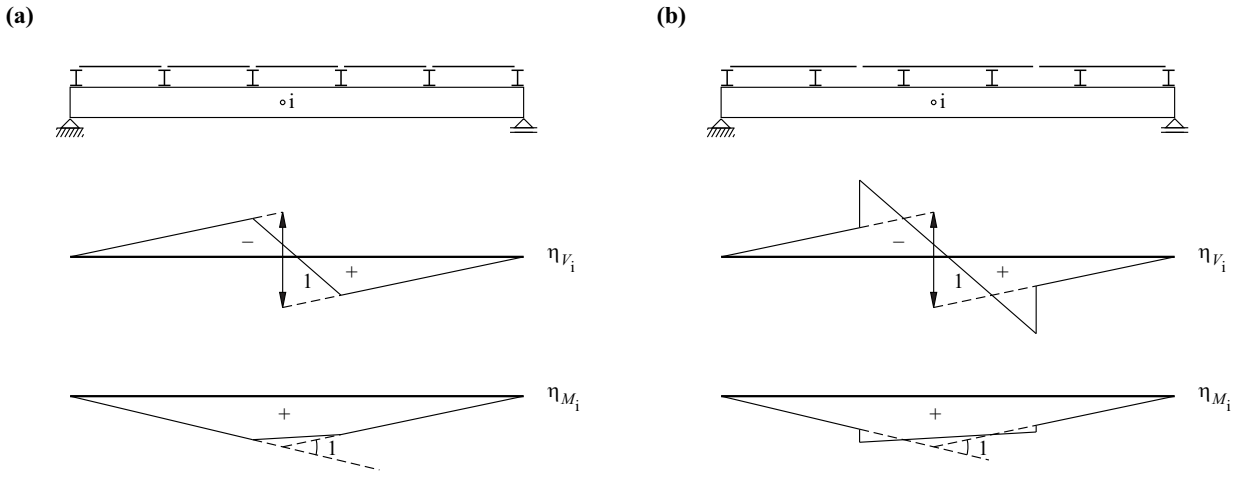

Fig. 12.3 Influence lines for shear forces and bending moments for indirect loading via longitudinal and transverse beams: (a) longitudinal members as simply supported beams, (b) longitudinal members with cantilevering ends

Loads that are not introduced directly but rather indirectly via transverse and longitudinal beams, as shown in Fig. 12.3, require the influence lines for the direct load transfer to be determined first. Owing to the assumption that the longitudinal beams are statically determinate, the influence ordinates at the locations of the transverse beams are then connected by straight lines that are continued as far as the ends of the longitudinal beams. As can be seen, depending on the configuration of the secondary structure, the influence ordinates of the primary structure can increase or decrease, see Fig. 12.3(a) and (b).

12.3 Kinematic determination of influence lines

The findings of section 12.2, i. e. that segments of influence lines are straight and exhibit discontinuities (abrupt changes or kinks) of magnitude 1 at the reference points, lead to an elegant option for determining the influence lines: the kinematic method named after LAND. If we release the constraint corresponding to force variable s_i at reference point i and apply the virtual deformation -1 (i. e. opposite to the positive force variable s_i) to the ensuing mechanism at i, then according to the principle of virtual deformations, we get

$$\delta W = Q_m \cdot \delta u_m - s_i \cdot 1 = 0 \tag{12.4}$$

where δu_m is the virtual displacement or rotation that occurs at the position and in the direction of load Q_m as a consequence of the mechanism. Comparing this with (12.1) shows that $\eta_{im} = \delta u_m$, i. e. the influence line results as a virtual displacement figure of the loaded chord in the direction of load Q_m due to the mechanism that ensues when the deformation variable corresponding to s_i is set to -1.

Eq. (12.4) only contains the two work components due to Q_m and s_i. This is because Q_m is the only load occurring and the internal force variables, except s_i, do not exhibit any corresponding deformations (the system components remain rigid in the mechanism).

Fig. 12.4 shows virtual deformations of -1 corresponding to the individual force variables (support forces, normal forces, shear forces and bending moments).

The kinematic method for determining influence lines also applies to statically indeterminate systems. Releasing the constraint corresponding to the force variable s_i does not produce a mechanism, but rather reduces the degree of static indeterminacy n by 1. The virtual deformation of -1 opposite to the positive force variable s_i cannot be applied without introducing restraints. Instead, it must be imposed on the statically

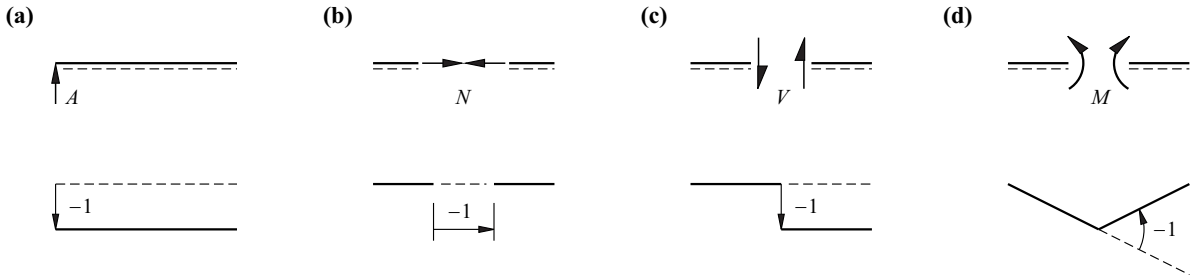

Fig. 12.4 Positive force variables and corresponding negative unit deformations: (a) support force, (b) normal force, (c) shear force, (d) bending moment

indeterminate system with $n-1$ degree(s) of static indeterminacy. The individual system components do not remain rigid, but are deformed. Nevertheless, (12.4) remains valid because according to the reduction theorem, the stress resultants of the restraint do not perform any virtual work on the whole, see section 14.3. In contrast to the influence lines with their straight segments for statically determinate systems, statically indeterminate systems produce curved influence lines; however, the discontinuities of magnitude 1 at the reference points remain.

Example 12.1 Hinged girder

The task is to determine the influence lines η_{Mi} and η_{Vi} for reference point i in the hinged girder of Fig. 12.5(a).

Introducing a flexural hinge at i with a virtual rotation of -1 leads directly to the upper virtual displacement figure of Fig. 12.5(b), which corresponds to η_{Mi}. The resulting lower influence line η_{Vi} in Fig. 12.5(b) has the abrupt change of -1 between the left-hand support and the intermediate support as for η_{Vi} in Fig. 12.2(d); the continuation into the right-hand span with the kink at the hinge easily follows from the mechanism considered.

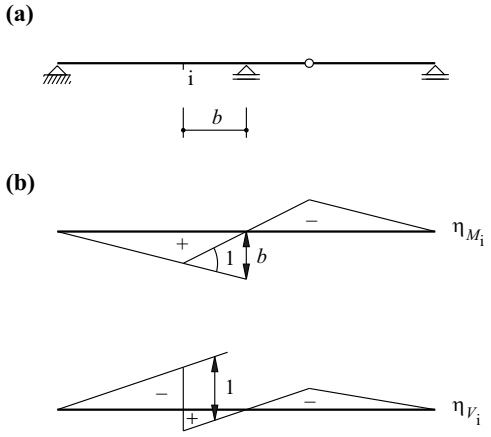

Fig. 12.5 Hinged girder: (a) static system, (b) influence lines

Example 12.2 Three-hinged arch

Fig. 12.6 illustrates how to determine the influence lines of a three-hinged arch according to the kinematic method.

Releasing the constraint for A_v according to Fig. 12.6(b) leads to a first geometric position for the instantaneous centre of rotation (pole) 1 of plate I; this must lie on the horizontal line passing through A. A second geometric position is given by the straight line passing through B and the hinge at the crown. The line that can be determined in this way for η_{Av} with the abrupt change of -1 at A is only valid between A and the crown hinge; between this point and B, η_{Av} approaches zero linearly because plate II rotates about its instantaneous centre of rotation $2 \equiv$ B.

Similar considerations for B_v lead to the kinematic diagram shown in Fig. 12.6(c) with the instantaneous centres of rotation 1 ≡ A and 2 for plates I and II respectively. The resulting straight line η_{Bv} between 2 and B with the abrupt change of –1 at B is only valid between B and the hinge at the crown; between this point and A, the influence line η_{Bv} approaches zero linearly because of the rotation of plate I about 1 ≡ A.

In order to determine the influence line for A_h, the corresponding constraint is released according to Fig. 12.6(d). The instantaneous centre of rotation 1 of plate I results from the intersection between the vertical line passing through A and the straight line passing through the crown hinge and B. The displacement –1 at A corresponds to a rotation of plate I about 1 amounting to $1/h$. Therefore, η_{Ah} has been found.

To determine η_{Ni}, the arch is forced apart at i according to Fig. 12.6(e) by the amount –1 in the direction of N_i. The reciprocal translation of plates I and II corresponds to a rotation about a relative pole (1, 2) at a distance of infinity in the direction perpendicular to N_i. Pole 2 of plate II therefore lies, on the one hand, on a line parallel with this direction passing through 1 (the pole of plate I) and, on the other, on the straight line passing through the crown hinge, i. e. the relative pole (2, 3), and 3 ≡ B (the pole of plate III). In the vertical direction, a displacement $\sin\alpha_i$, which occurs at η_{Ni} be-

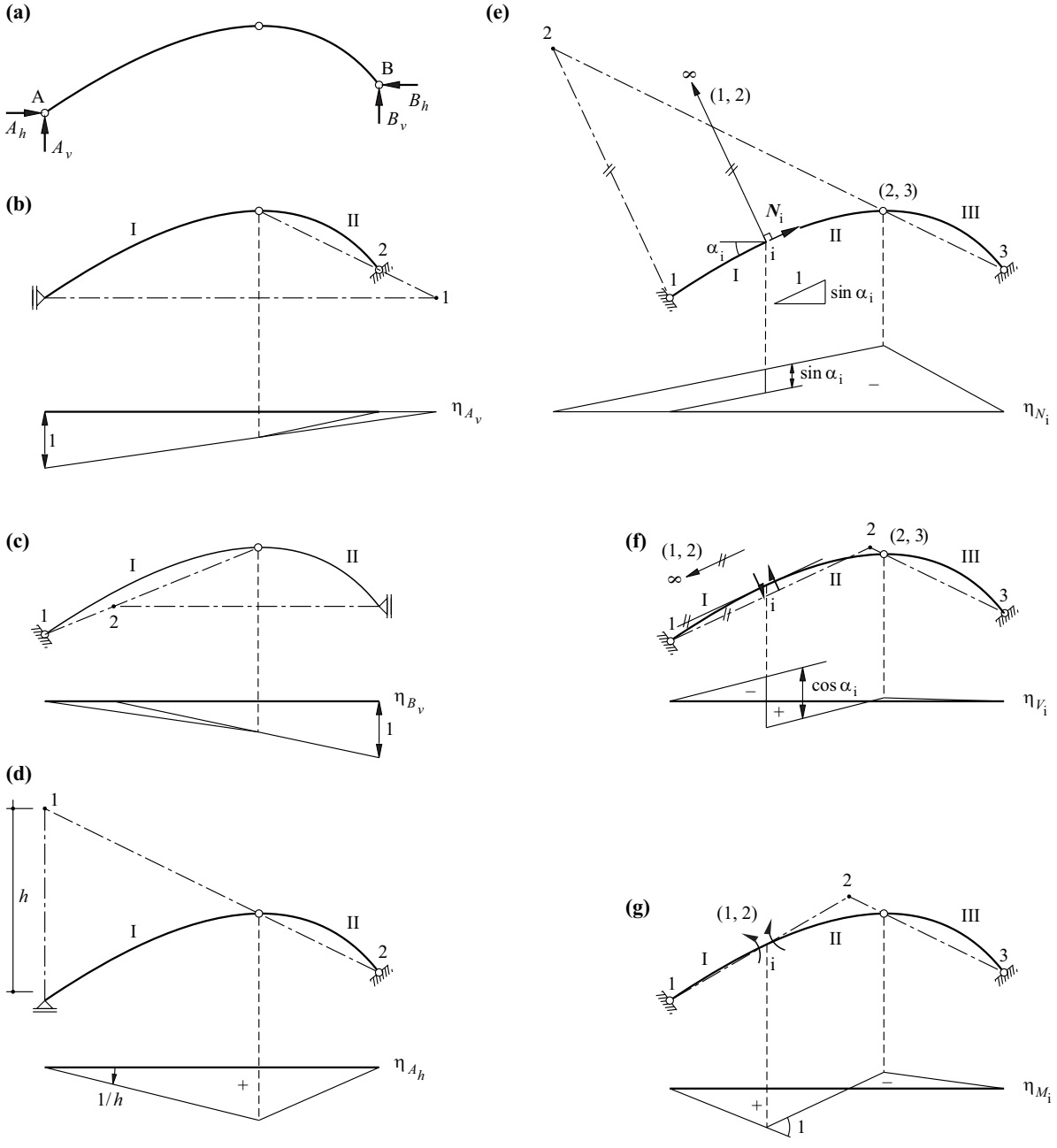

Fig. 12.6 Three-hinged arch: (a) support forces, (b) to (g) kinematic diagrams and influence lines

tween the two parallel straight lines for plates I and II, corresponds to the displacement −1. Therefore, η_{Ni} has been determined completely.

A relative displacement of −1 perpendicular to the arch axis at i is assumed for plates I and II when determining η_{Vi} in Fig. 12.6(f). Pole 2 of plate II is determined by the direction to the corresponding relative pole (1, 2) passing through 1 and the straight line passing through (2, 3) and 3. As the displacement −1 has the component $\cos\alpha_i$ in the vertical direction, the result is a corresponding abrupt change to η_{Vi} at i, and the influence line is therefore determined completely.

In the influence line case η_{Mi} shown in Fig. 12.6(g), i plays the role of the relative pole (1, 2). Pole 2 comes about in a similar way to that shown in Fig. 12.6(e) and (f). With the kink −1 at i, η_{Mi} is therefore determined completely.

Example 12.3 Plane truss

We require the influence line for the bottom chord force U of the truss of Fig. 12.7(a). The moving load travels along the bottom chord.

Removing the bottom chord bar results in the two plates I and II, which can rotate about 1 and 2 respectively. Applying a relative displacement of −1 to the points of application of the two forces U results in a reciprocal rotation of the two plates of $1/r$ about the relative pole (1, 2). The influence line for U can therefore be drawn, provided we also consider that, as shown in the lower drawing of Fig. 12.3(a), the ordinates at the ends of the two bars can be joined by a straight line owing to the indirect load transfer via the joints of the truss.

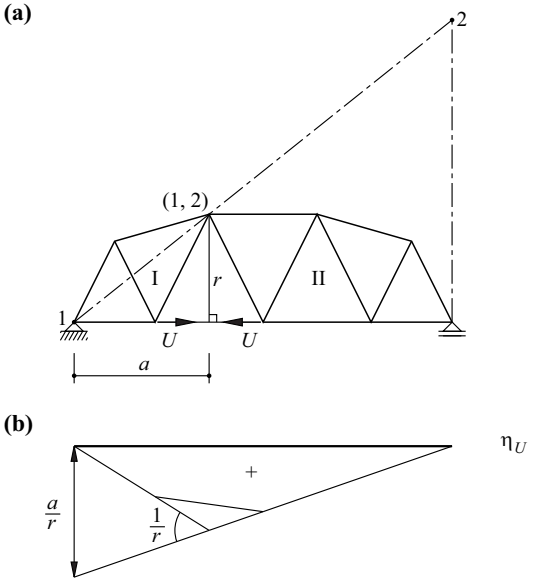

Fig. 12.7 Truss: (a) kinematic diagram, (b) influence line for bottom chord force U

12.4 Summary

1. Influence lines η_{im} show how a point force variable $Q_m = 1$ acting in a specified direction at any point m influences a certain state variable s_i at point i.
2. Influence lines are mostly confined to vertical point forces for examining the effects of imposed (traffic) loads.
3. Influence lines are particularly helpful for identifying worst load positions.
4. Influence lines are evaluated according to (12.1) and (12.2).
5. Influence lines can either be determined by applying equilibrium conditions or by using LAND's kinematic method, which is particularly convenient.
6. The segments of the influence lines of statically determinate systems are straight.
7. In the kinematic method, influence lines are virtual displacement figures of the loaded chord in the direction of load Q_m for the mechanism that ensues when the deformation variable corresponding to s_i is set to -1.
8. The kinematic method for determining influence lines remains valid for systems statically indeterminate to the nth degree. However, the influence lines are curved because the deformation variables of -1 corresponding to s_i must each be imposed on a statically indeterminate system with $n-1$ degree(s) of static indeterminacy.
9. In addition to influence lines for force variables, influence lines for deformation variables are often interesting, too. They are displacement curves that ensue when a corresponding unit force variable is applied at the position and in the direction of the deformation variable of interest.

12.5 Exercises

12.1 Determine the influence lines for the support forces and the bending moments at B and C in the system of Fig. 11.3(a).

12.2 Determine the influence line for the shear force to the left of support C in the system of Fig. 11.3(a).

12.3 Determine the influence lines for the bottom chord forces on both sides of the intermediate support of the system shown in Fig. 9.9(d).

12.4 Determine the influence line for the top chord force in the middle of the right-hand span of the system shown in Fig. 9.9(d).

13 ELEMENTARY DEFORMATIONS

13.1 General

The linear elastic constitutive equations for plane and spatial framed structures were introduced with eq. (8.23) and (8.28) without a detailed explanation. Fig. 13.1 illustrates the relationships between stress resultants (see section 5.1.7) and corresponding deformation variables (see sections 8.2.2 and 8.2.3). The relationship between the normal force N and the strain ε on the bar axis x is expressed by the *axial stiffness* EA, the relationship between the shear force V and the mean shear strain γ by the *shear stiffness* GA_v. Likewise, the *bending stiffness* EI and the *torsional stiffness* GI_x express the relationship between bending moment M and curvature χ, and between torque T and twist ϑ respectively. In order to present the relationships with the proper dimensions, the reference length used in the M-χ and T-ϑ diagrams is the depth of the section h.

The equations for bending, normal forces, shear forces and torsion will be examined separately on the following pages. It will generally be assumed that the idealisation as a bar (see section 5.1.7) and the treatment according to first-order theory (see section 6.1) are justified and that the materials exhibit linear elastic and isotropic behaviour (see section 7.2). Both homogeneous and composite cross-sections will be considered for bending and normal forces; thermal deformations and the effect of bar curvature will also be addressed.

13.2 Bending and normal force

13.2.1 Stresses and strains

The cantilever beam shown in Fig. 13.2 has a normal stress component σ_z that is in the same order of magnitude as the stress at the extreme fibre q; actually, $\sigma_z = q$ applies for $z = h/2$ and $\sigma_z = 0$ for $z = -h/2$. On the other hand, at the cross-section at the point of fixity $x = 0$, shear stresses τ_{zx} in the order of magnitude $qbl/(bh) = ql/h$ correspond to the shear force

$$V_z = \int \tau_{zx}\, \mathrm{d}A \tag{13.1}$$

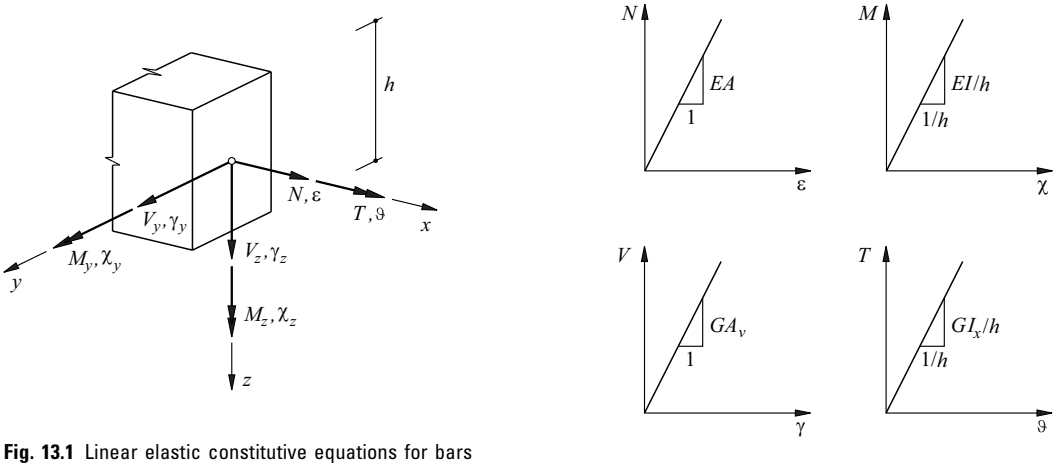

Fig. 13.1 Linear elastic constitutive equations for bars

Theory of Structures. First Edition. Peter Marti

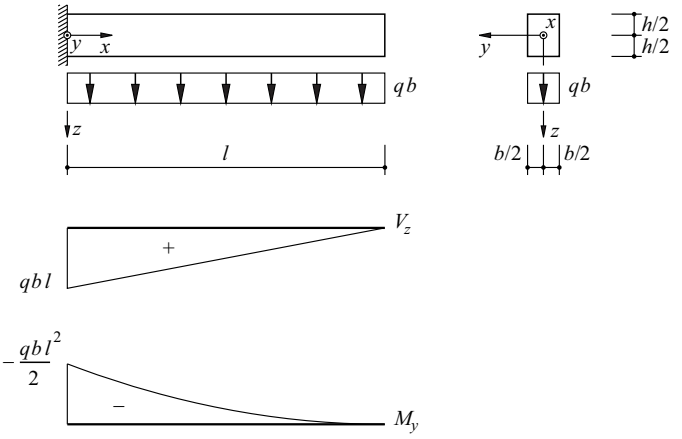

Fig. 13.2 Cantilever beam with suspended load

and normal stresses σ_x in the order of magnitude of $qbl^2/(bh^2) = q(l/h)^2$ correspond to the bending moment

$$M_y = \int z\,\sigma_x\,\mathrm{d}A \tag{13.2}$$

As l/h is large (as supposed), the normal stresses σ_x exceed the shear stresses τ_{zx} (and with general loading the shear stresses τ_{yx}, too) by one order of magnitude, and the normal stresses σ_z (and with general loading the normal stresses σ_y and the shear stresses τ_{yz}, too) by no less than two orders of magnitude. Therefore, in a first approximation, the stress state may be regarded as uniaxial (only σ_x is not equal to zero).

As compared with σ_x, shear stresses τ_{yx} and τ_{zx} can be ignored, then according to (7.3), the shear strains γ_{yx} and γ_{zx} disappear as well. This means that the bar cross-sections are approximately plane and remain perpendicular to the deformed bar axis. Considering two infinitesimally close bar cross-sections leads to the conclusion that the strains ε_x are distributed linearly over the bar cross-section, i. e.

$$\varepsilon_x = \varepsilon + \chi_y z - \chi_z y \tag{13.3}$$

Using the following relationship from (7.1)

$$\sigma_x = E\,\varepsilon_x \tag{13.4}$$

and

$$N = \int \sigma_x\,\mathrm{d}A \quad , \quad M_y = \int z\,\sigma_x\,\mathrm{d}A \quad , \quad M_z = -\int y\,\sigma_x\,\mathrm{d}A \tag{13.5}$$

it follows that

$$\begin{Bmatrix} N \\ M_y \\ M_z \end{Bmatrix} = E \begin{bmatrix} \int \mathrm{d}A & \int z\,\mathrm{d}A & -\int y\,\mathrm{d}A \\ \int z\,\mathrm{d}A & \int z^2\mathrm{d}A & -\int yz\,\mathrm{d}A \\ -\int y\,\mathrm{d}A & -\int yz\,\mathrm{d}A & \int y^2\mathrm{d}A \end{bmatrix} \begin{Bmatrix} \varepsilon \\ \chi_y \\ \chi_z \end{Bmatrix} \tag{13.6}$$

We choose the axes of the cross-section y, z to be the *principal axes* in such a way that

$$\int y\,\mathrm{d}A = \int z\,\mathrm{d}A = \int yz\,\mathrm{d}A = 0 \tag{13.7}$$

Eq. (13.6) then simplifies to

$$N = EA\,\varepsilon \quad , \quad M_y = EI_y\chi_y \quad , \quad M_z = EI_z\chi_z \tag{13.8}$$

where

$$A = \int \mathrm{d}A \quad , \quad I_y = \int z^2\mathrm{d}A \quad , \quad I_z = \int y^2\mathrm{d}A \tag{13.9}$$

The equations (13.5) and (13.3) are illustrated in Fig. 13.3(a) and (b) respectively. The integrals $S_z = \int y\,\mathrm{d}A$, $S_y = \int z\,\mathrm{d}A$ in (13.6) are called *first moments of area*, the integrals $I_z = \int y^2\,\mathrm{d}A$, $I_y = \int z^2\,\mathrm{d}A$ *moments of inertia* (second moments of area) and the integral $C_{yz} = -\int yz\,\mathrm{d}A$ is the *product of inertia* (composite moment of area).

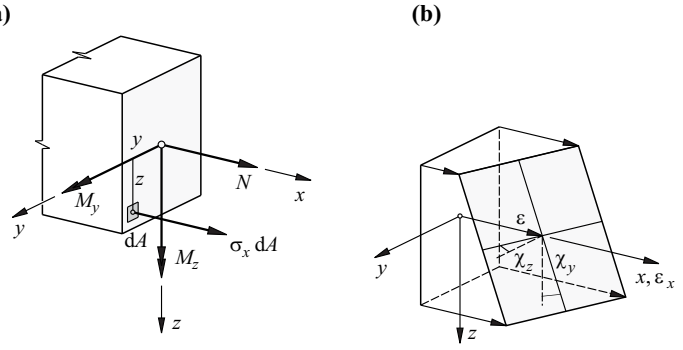

Fig. 13.3 Bending and normal force: (a) local stress and stress resultants, (b) linear strain distribution

The fundamental assumption (13.3) of Jacob BERNOULLI, i. e. that *cross-sections remain plane*, is retained, for example, when dealing with reinforced concrete cross-sections, also in non-linear stress-strain relationships $\sigma_x = \sigma_x(\varepsilon_x)$. For given deformation variables ε, χ_y, χ_z, we get the stress resultants N, M_y, M_z according to (13.5) by integrating once. And vice versa, calculating the deformation variables associated with a set of stress resultants is generally an iterative procedure; starting with an estimated set of deformation variables, it is possible to determine the associated stress resultants and improve the result through successive corrections until the desired accuracy is achieved.

13.2.2 Principal axes

Assuming arbitrary initial coordinates η, ζ according to Fig. 13.4(a), then

$$\begin{Bmatrix} y \\ z \end{Bmatrix} = \begin{bmatrix} \cos\varphi & \sin\varphi \\ -\sin\varphi & \cos\varphi \end{bmatrix} \begin{Bmatrix} \eta - \eta_C \\ \zeta - \zeta_C \end{Bmatrix} \tag{13.10}$$

applies. Eq. $(13.7)_1$ and $(13.7)_2$ call for

$$\begin{bmatrix} \cos\varphi & \sin\varphi \\ -\sin\varphi & \cos\varphi \end{bmatrix} \begin{Bmatrix} \int \eta \, dA - \eta_C A \\ \int \zeta \, dA - \zeta_C A \end{Bmatrix} = \begin{Bmatrix} 0 \\ 0 \end{Bmatrix}$$

from which we get the coordinates of the *centroid* C of the cross-section as follows:

$$\eta_C = \frac{\int \eta \, dA}{A} \quad , \quad \zeta_C = \frac{\int \zeta \, dA}{A} \tag{13.11}$$

Using the axes η', ζ' parallel with η, ζ and passing through C, then

$$\begin{aligned} C_{yz} &= -\int yz \, dA = -\int (\eta' \cos\varphi + \zeta' \sin\varphi)(-\eta' \sin\varphi + \zeta' \cos\varphi) \, dA \\ &= \sin\varphi \cos\varphi \int (\eta'^2 - \zeta'^2) \, dA - (\cos^2\varphi - \sin^2\varphi) \int \eta' \zeta' \, dA \\ &= \frac{1}{2} \sin(2\varphi)(I_{\zeta'} - I_{\eta'}) + \cos(2\varphi) C_{\eta'\zeta'} = 0 \end{aligned} \tag{13.12}$$

applies, from which it follows that

$$\tan(2\varphi) = \frac{2C_{\eta'\zeta'}}{I_{\eta'} - I_{\zeta'}} \tag{13.13}$$

We use the variables

$$I_{\eta'} = \int \zeta'^2 dA \quad , \quad I_{\zeta'} = \int \eta'^2 dA \quad , \quad C_{\eta'\zeta'} = -\int \eta' \zeta' \, dA \tag{13.14}$$

in this case.

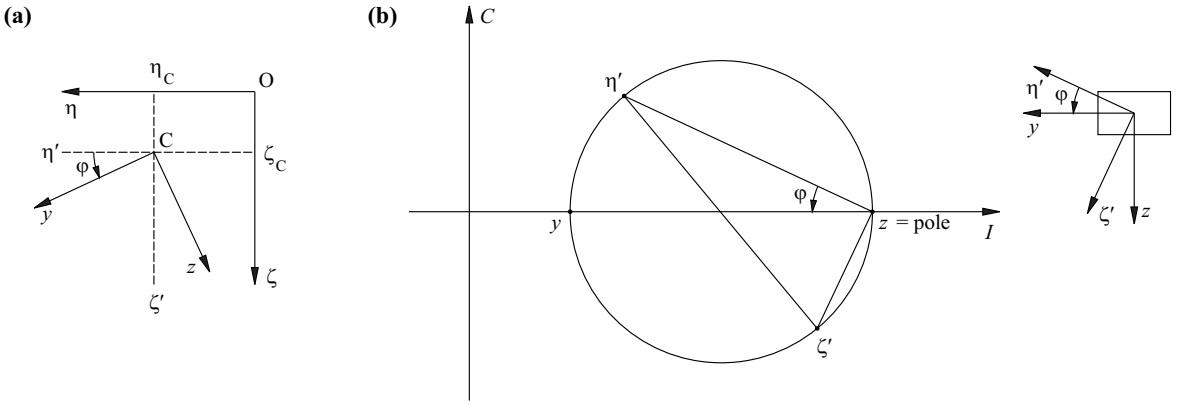

Fig. 13.4 Principal axes: (a) initial coordinates and principal axes, (b) MOHR's circle for second moments of area

The transformation equation $(13.12)_4$ for the products of inertia can be supplemented by similar equations for the moments of inertia according to $(13.9)_2$ and $(13.9)_3$:

$$\begin{Bmatrix} I_y \\ I_z \\ C_{yz} \end{Bmatrix} = \begin{bmatrix} \cos^2\varphi & \sin^2\varphi & 2\sin\varphi\cos\varphi \\ \sin^2\varphi & \cos^2\varphi & -2\sin\varphi\cos\varphi \\ -\sin\varphi\cos\varphi & \sin\varphi\cos\varphi & \cos^2\varphi - \sin^2\varphi \end{bmatrix} \begin{Bmatrix} I_{\eta'} \\ I_{\zeta'} \\ C_{\eta'\zeta'} \end{Bmatrix} \tag{13.15}$$

Eq. (13.15) and (13.13) are similar to (5.21) and (5.23). In a similar way to Fig. 5.20, it is therefore possible to present the transformation of second moments of area with the help of MOHR*'s circles for second moments of area*, see Fig. 13.4(b).

When the bending moment vector lies on a principal axis ($M_z = 0$ or $M_y = 0$), we speak of *pure bending*, but in the general case ($M_z \neq 0$ and $M_y \neq 0$) *skew bending*. In the latter case, the deflection gives rise to so-called *secondary torsion* because of the relative displacement of the shear forces in neighbouring cross-sections; this torsion may need to be considered in slender beams.

Example 13.1 Unequal leg angle

The task is to determine the geometrical properties and the principal axes of the unequal leg angle shown in Fig. 13.5(a).

First of all, we find the cross-sectional area: $A = (35 + 60)\cdot 5 = 475\,\text{mm}^2$. Eq. (13.11) supplies the coordinates of the centroid:

$$\eta_C = \frac{20\cdot 4\cdot 5 + 2.5\cdot 55\cdot 5}{475} = 9.87\ \text{mm} \quad , \quad \zeta_C = \frac{-2.5\cdot 35\cdot 5 - 30\cdot 60\cdot 5}{475} = -19.87\ \text{mm}$$

From (13.14) we get

$$I_{\eta'} = \frac{35\cdot 5^3}{12} + (19.87-2.5)^2\cdot 35\cdot 5 + \frac{5\cdot 60^3}{12} + (30-19.87)^2\cdot 5\cdot 60 = 173\,950\ \text{mm}^4$$

$$I_{\zeta'} = \frac{5\cdot 40^3}{12} + (20-9.87)^2\cdot 5\cdot 40 + \frac{55\cdot 5^3}{12} + (9.87-2.5)^2\cdot 55\cdot 5 = 62\,700\ \text{mm}^4$$

$$C_{\eta'\zeta'} = -(22.5-9.87)(19.87-2.5)\cdot 35\cdot 5 - (9.87-2.5)(30-19.87)\cdot 5\cdot 60 = -60\,789\ \text{mm}^4$$

and therefore using (13.13), we get $\tan\varphi = -0.440$. Fig. 13.5(b) shows the corresponding MOHR's circle with the principal values

$$I_{y,z} = \frac{173\,950 + 62\,700}{2} \pm \sqrt{\left(\frac{173\,950 - 62\,700}{2}\right)^2 + 60\,789^2} = \begin{Bmatrix} 200\,723\ \text{mm}^4 \\ 35\,927\ \text{mm}^4 \end{Bmatrix}$$

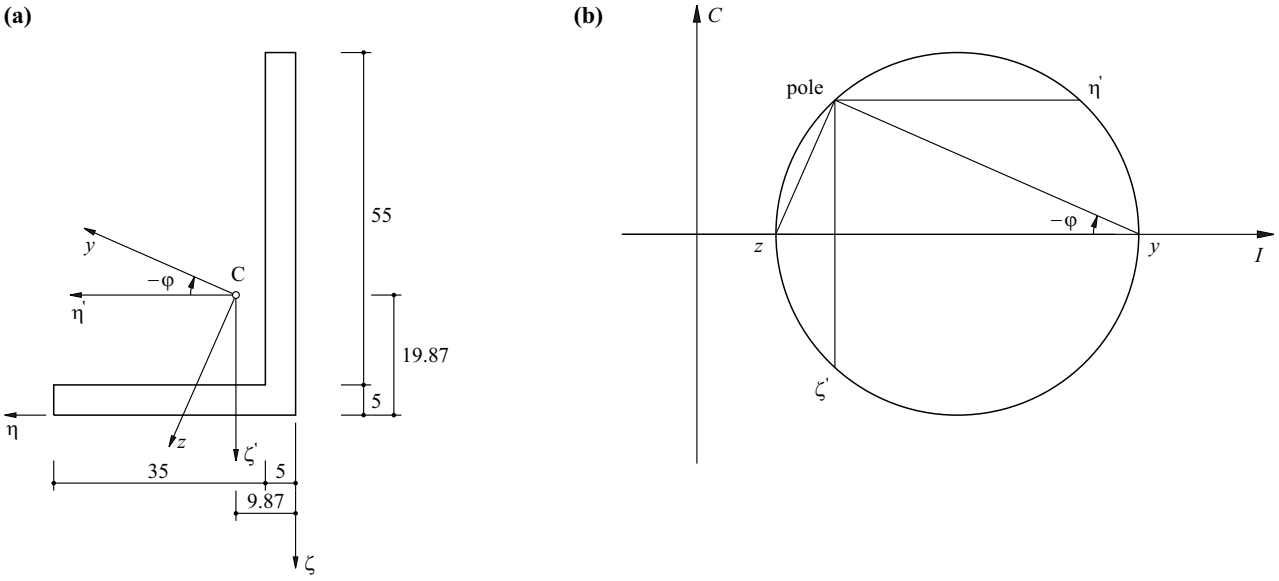

Fig. 13.5 Unequal leg angle: (a) notation and dimensions [mm], (b) MOHR's circle

13.2.3 Stress calculation

Combining (13.4) with (13.3) and (13.8) results in

$$\sigma_x = \frac{N}{A} + \frac{M_y}{I_y} z - \frac{M_z}{I_z} y \tag{13.16}$$

Instead of working with N, M_y, M_z, it is possible (see Fig. 13.6) to apply the normal force N at point A with the coordinates

$$y_A = \frac{-M_z}{N} \quad , \quad z_A = \frac{M_y}{N} \tag{13.17}$$

which is statically equivalent. Eq. (13.16) then becomes

$$\sigma_x = \frac{N}{A}\left(1 + \frac{z\, z_A}{i_y^2} + \frac{y\, y_A}{i_z^2}\right) \tag{13.18}$$

where the variables

$$i_y = \sqrt{\frac{I_y}{A}} \quad , \quad i_z = \sqrt{\frac{I_z}{A}} \tag{13.19}$$

denote the *radii of gyration*.

According to (13.18), the condition $\sigma_x = 0$ results in the straight-line equation

$$\frac{y\, y_A}{i_z^2} + \frac{z\, z_A}{i_y^2} + 1 = 0 \tag{13.20}$$

for the *neutral axis* n-n. If we develop this along the smallest convex envelope of the cross-section, as shown in Fig. 13.6, the coordinates of the intersections P and Q with the principal axes y, z result in the associated coordinates

$$y_A = \frac{-i_z^2}{y_P} \quad , \quad z_A = \frac{-i_y^2}{z_Q} \tag{13.21}$$

of the point of application A of normal force N. All points A determined in this way define the extent of the so-called *kern* of the cross-section. If N is applied within the kern, then σ_x has the same sign (tension or compression) over the entire cross-section. The concept of the kern is particularly useful for cross-sections made from materials that have little tensile strength (concrete, masonry) and also for foundations (partial uplift, see example 5.1).

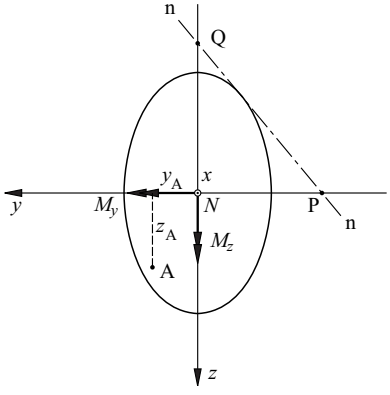

Fig. 13.6 Statically equivalent normal force and determining the points defining the extent of the kern

Example 13.2 Rectangular cross-section – kern

The rectangular cross-section shown in Fig. 13.7 has the properties $A = bh$, $I_y = bh^3/12$, $I_z = hb^3/12$, and therefore according to (13.19), $i_y^2 = h^2/12$, $i_z^2 = b^2/12$.

Where $y_P = -(b + h\tan\alpha)/2$ and $z_Q = -(h + b\cot\alpha)/2$, it follows from (13.21) that

$$y_A = \frac{b^2}{6(b + h\tan\alpha)} \quad , \quad z_A = \frac{h^2}{6(h + b\tan\alpha)}$$

When $\alpha = 0$, this gives us the coordinates of point A_1 :

$$y_{A_1} = b/6 \quad , \quad z_{A_1} = 0$$

and when $\alpha = \pi/2$, those of point A_2 :

$$y_{A_2} = 0 \quad , \quad z_{A_2} = h/6$$

When $0 < \alpha < \pi/2$, α can be omitted from the equations for y_P and z_Q:

$$(2y_P + b)(2z_Q + h) = bh$$

and therefore, using (13.21), we get the equation

$$\frac{y_A b}{2i_z^2} + \frac{z_A h}{2i_y^2} = 1$$

for the straight line joining points A_1 und A_2. As we can see, the corners of a cross-section correspond to a straight boundary to the kern. And vice versa, the straight edges of a cross-section correspond to the corners of the kern.

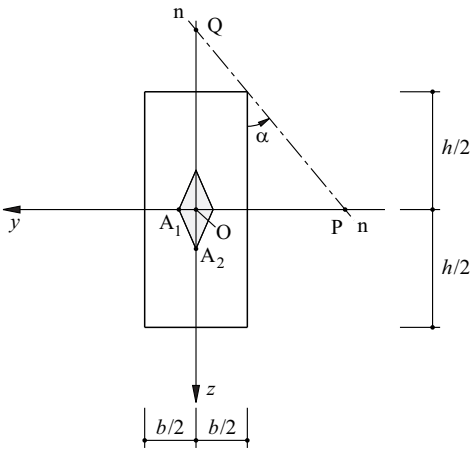

Fig. 13.7 Kern of a rectangular cross-section

13.2.4 Composite cross-sections

So far, we have presumed homogeneous material properties and a constant modulus of elasticity over the bar cross-section. When it comes to *composite cross-sections* made from various materials, such as the examples shown in Fig. 13.8, equations (13.6) to (13.9) must be generalised.

Eq. (13.3) to (13.5) remain valid, but the modulus of elasticity depends on the fibres:

$$E = E(y, z) = E_0 n(y, z) \tag{13.22}$$

The reference value E_0 for the modulus of elasticity is generally taken to be the modulus of elasticity of the dominant material, i. e. that of the structural steel E_a in the case of steel-concrete composite construction, or that of the concrete E_c in reinforced concrete beams, for example. The *modular ratio* $n = E/E_0$ enables any fibres to be considered corresponding to their stiffness. This is achieved by replacing their cross-sectional area dA by ndA. Instead of (13.6), we therefore get

$$\begin{Bmatrix} N \\ M_y \\ M_z \end{Bmatrix} = E_0 \begin{bmatrix} \int n\,\mathrm{d}A & \int zn\,\mathrm{d}A & -\int yn\,\mathrm{d}A \\ \int zn\,\mathrm{d}A & \int z^2 n\,\mathrm{d}A & -\int yzn\,\mathrm{d}A \\ -\int yn\,\mathrm{d}A & -\int yzn\,\mathrm{d}A & \int y^2 n\,\mathrm{d}A \end{bmatrix} \begin{Bmatrix} \varepsilon \\ \chi_y \\ \chi_z \end{Bmatrix} \tag{13.23}$$

Condition (13.7) for the principal axes y, z then becomes

$$\int yn\,\mathrm{d}A = \int zn\,\mathrm{d}A = \int yzn\,\mathrm{d}A = 0 \tag{13.24}$$

and instead of (13.8) we get

$$N = E_0 A_i \cdot \varepsilon \quad , \quad M_y = E_0 I_{yi} \cdot \chi_y \quad , \quad M_z = E_0 I_{zi} \cdot \chi_z \tag{13.25}$$

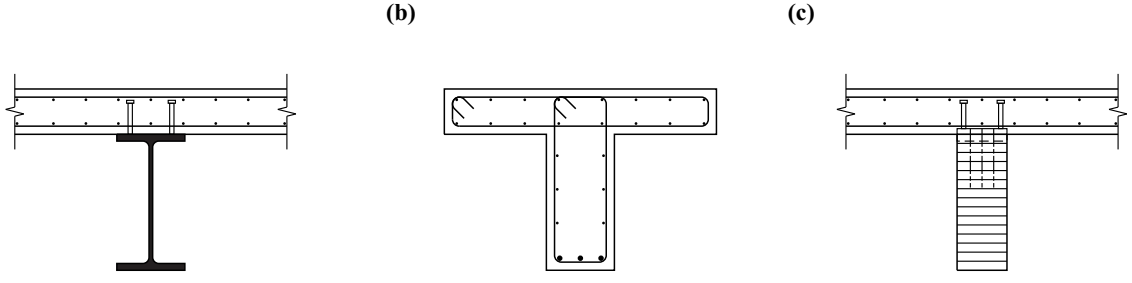

Fig. 13.8 Composite cross-sections: (a) steel-concrete composite construction, (b) reinforced concrete T-beam, (c) timber-concrete composite construction

with the *transformed section properties*

$$A_i = \int n\,\mathrm{d}A \quad , \quad I_{yi} = \int z^2 n\,\mathrm{d}A \quad , \quad I_{zi} = \int y^2 n\,\mathrm{d}A \tag{13.26}$$

The coordinates of the centroid of the transformed section are obtained from (13.11) by replacing dA by ndA and A by A_i. The directions of the principal axes are given by (13.13), with dA being replaced by ndA in (13.14).

Example 13.3 Reinforced concrete slab – bending

Fig. 13.9(a) shows part of a 240 mm deep reinforced concrete slab that is reinforced in the x direction with steel reinforcing bars near the soffit at a regular spacing of 150 mm. The reinforcing bars are 16 mm in diameter and are positioned with a concrete cover of 20 mm to the soffit of the slab. We shall assume a modulus of elasticity $E_c = 30\,\mathrm{kN/mm^2}$ for the concrete and $E_s = 205\,\mathrm{kN/mm^2}$ for the steel reinforcement. Accordingly, the modular ratio of the reinforcing steel to the concrete is $n = 205/30 = 6.83$.

The transformed cross-sectional area (per m slab width) according to $(13.26)_1$ is $A_i^{\mathrm{I}} = 240 \cdot 1000 + (1000/150) \cdot (16^2 \cdot \pi/4) \cdot (6.83 - 1) = 247\,819\,\mathrm{mm^2/m}$, i. e. about 3.3 % more than that of the cross-sectional area of the concrete alone, $A_c = 240\,000\,\mathrm{mm^2/m}$. The expression in brackets $(6.83 - 1)$ takes into account the stiffness of the reinforcement beyond that of the concrete, which is already included in the product $240 \cdot 1000$.

Eq. $(13.11)_2$, taking into account n, supplies the coordinates of the centroid $\zeta_C = [120 \cdot 240\,000 + (240 - 20 - 16/2) \cdot 7819]/247\,819 = 122.9\,\mathrm{mm}$. Eq. $(13.26)_2$ therefore results in $I_{yi}^{\mathrm{I}} = 240^3 \cdot 1000/12 + (122.9 - 120)^2 \cdot 240\,000 + (240 - 20 - 16/2 - 122.9)^2 \cdot 7819 = 1\,216.1 \cdot 10^6\,\mathrm{mm^4/m}$; this value is about 5.6 % higher than the value $I_{yc} = 1152 \cdot 10^6\,\mathrm{mm^4/m}$ of the concrete cross-section on its own.

In practice, the stiffening effect of the reinforcing steel in the uncracked state (I) can usually be ignored, i. e. as a rule we assume, for simplicity, the concrete's cross-sectional properties instead of the transformed section properties. However, the decrease in stiffness in the cracked state (II), caused by the cracking of the concrete, must always be considered.

If we assume that the concrete in the cracked state (II) carries only compressive stresses (modular ratio of concrete fibres in tension zone $n = 0$), then the situation illustrated in Fig. 13.9(b) ensues when the slab is subjected to a pure bending moment about the y axis. The y axis now coincides with the neutral axis at a distance c from the top edge of the cross-section. As the first moment of area about the neutral axis must be equal to 0, the following applies for a rectangular cross-section:

$$\frac{bc^2}{2} = (d - c)nA_s$$

from which it follows that

$$c = d\left(\sqrt{(\rho n)^2 + 2\rho n} - \rho n\right)$$

where $\rho = A_s/(bd)$, A_s denotes the cross-sectional area of the reinforcement over the width b of the cross-section ($b = 1\,\mathrm{m}$ and $A_s = 1340\,\mathrm{mm^2}$ in this example), d stands for the *effective depth* (distance of extreme fibre in compression from centroid of reinforcement, $d = 212$ mm in this example) and ρ represents the *geometric reinforcement ratio* ($\rho = 0.63$ % in this example). In this case, $c = 53.8\,\mathrm{mm}$, and $(13.26)_2$ results in $I_{yi}^{\mathrm{II}} = (53.8)^3 \cdot 1000/12 + (53.8/2)^2 \cdot 53\,800 + (212 - 53.8)^2 \cdot (1000/150) \cdot (16^2 \cdot \pi/4) \cdot (205/30) = 281.1 \cdot 10^6\,\mathrm{mm^4/m}$; this value is only 24.4 % of I_{yc} or 23.1 % of I_{yi}^{I}, i. e. cracking causes the bending stiffness to drop to less than one-quarter of the stiffness in the uncracked state (I).

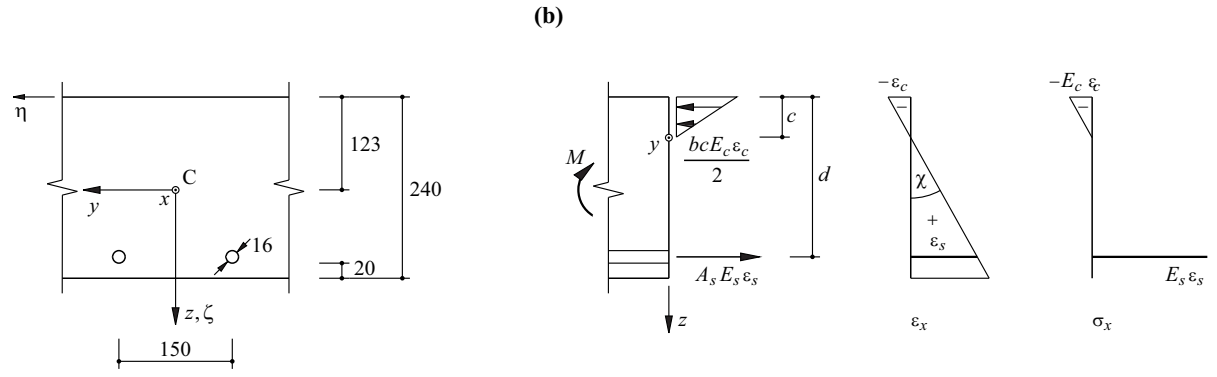

Fig. 13.9 Reinforced concrete slab: (a) uncracked state (I), (b) cracked state (II)

13.2.5 Thermal deformations

A temperature gradient $T = T(y, z)$, related to a certain basic value, e. g. the ambient temperature or an initial temperature, prevails over a bar cross-section. Using the coefficient of thermal expansion $\alpha_T = \alpha_T(y, z)$, the result is an unhindered elongation of the fibres of

$$\varepsilon_{xT} = \alpha_T T \tag{13.27}$$

according to (7.53). However, the concept of cross-sections remaining plane calls for (13.3) and therefore according to (13.4) and (13.22), the outcome is generally *residual stresses* of

$$\sigma_{xr} = E(\varepsilon_x - \varepsilon_{xT}) = E_0 n(\varepsilon + \chi_y z - \chi_z y - \alpha_T T) \tag{13.28}$$

The variables ε, χ_y, χ_z follow from the condition that the stress resultants (13.5) vanish; applying (13.26), it follows that

$$\varepsilon = \frac{\int \alpha_T T n \, dA}{A_i} \quad , \quad \chi_y = \frac{\int \alpha_T T z n \, dA}{I_{yi}} \quad , \quad \chi_z = -\frac{\int \alpha_T T y n \, dA}{I_{zi}} \tag{13.29}$$

We can deal with the effects of the shrinkage or swelling of materials in a similar way to thermal deformations. To do this, we only have to replace $\alpha_T T$ by the respective load-independent strain in (13.28) and (13.29).

Example 13.4 Reinforced concrete slab – shrinkage

The concrete of the reinforced concrete slab of example 13.3 experiences the final shrinkage strain $\varepsilon_{cs}(\infty) = -0.4\,‰$, see (7.39) and example 7.4. As the reinforcement resists the shrinkage deformation, the slab develops a downward curvature. And as the concrete not only shrinks over time but also creeps, for simplicity we use an effective modulus of elasticity of the concrete $E_c = 10\,\text{kN/mm}^2$ in our calculations. Therefore, using $n = 20.5$, we get new values of $A_i^{\text{I}} = 266\,138\,\text{mm}^2/\text{m}$, $\zeta_{\text{C}} = 129.0\,\text{mm}$ and $I_{yi}^{\text{I}} = 1\,351.5 \cdot 10^6\,\text{mm}^4/\text{m}$ instead of the values given in example 13.3.

Eq. $(13.29)_1$ results in $\varepsilon = -0.4\,‰ \cdot (240\,000 - 1340)/266\,138 = -0.359\,‰$, and from $(13.29)_2$ we get $\chi_y = -0.4\,‰ \cdot [(120 - 129) \cdot 240\,000 - (212 - 129) \cdot 1340]/\,1\,351.5 \cdot 10^6 = 0.675\,\text{mrad/m}$. Fig. 13.10 shows the corresponding distributions of strain and residual stress. In the reinforcing steel, the result is a compressive stress of $-62\,\text{N/mm}^2$. The tensile stress of $1.16\,\text{N/mm}^2$ in the concrete at the underside of the slab is, for common concrete strengths, well below the tensile strength of the concrete. Cracking of the concrete due to shrinkage is therefore unlikely in such conditions. If the amount of reinforcement in the concrete were to be increased, however, cracking as a result of shrinkage alone would have to be taken into account for a slab reinforced on one face only.

The neutral axis of the residual stresses in the concrete lies 67.8 mm below the top surface of the slab. It is easy to verify this result by considering the concrete cross-section on its own (with the principal axis y positioned in the centre of the slab). The compressive stresses in the reinforcing steel and the absence of tensile stresses in the concrete at the position of the reinforcement on the whole correspond to a compressive force at a distance of $z_{\text{A}} = 92\,\text{mm}$ from the middle plane. This force must be compensated for by a tensile force equal in magnitude and acting at the same depth on the concrete cross-section alone because it is on the whole a residual stress state. Using $i_y^2 = (240\,\text{mm})^2/12$, eq. (13.20) gives us a position of $z = -240^2/(12 \cdot 92) = -52.2\,\text{mm}$ for the neutral axis, i. e. the neutral axis is actually $120 - 52.2 = 67.8\,\text{mm}$ below the top surface of the slab.

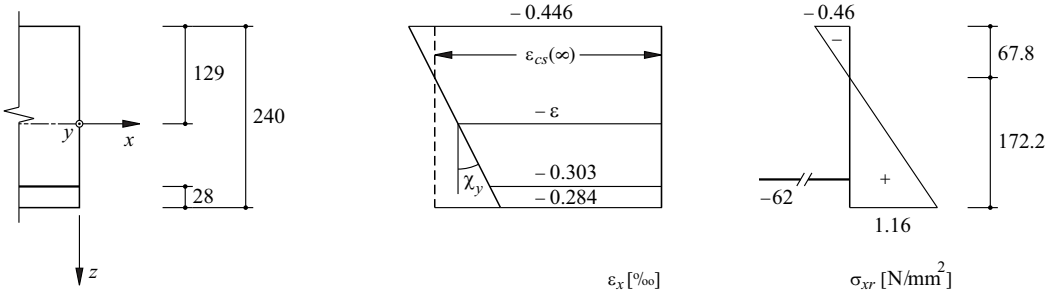

Fig. 13.10 How concrete shrinkage affects a reinforced concrete slab reinforced on one face only

13.2.6 Planar bending of curved bars

We shall now consider a bar curved and loaded in one plane as in section 5.3.2. Fig. 13.11 shows a differential bar element with the centroid axis s_C (radius of curvature ρ_C) at the level of the centroid of the cross-section C and the axis s_0 (radius of curvature ρ_0) at the level of the neutral axis for a pure bending moment $M_y = M$. The bar cross-section with depth h is symmetrical with respect to the plane of curvature and has a width $b(z)$ at the position z measured from s_0. The material is assumed to be homogenous, isotropic and linear elastic, with a modulus of elasticity E.

We also continue to assume that cross-sections remain plane. Therefore,

$$\varepsilon_s(\rho_0 - z)\,\mathrm{d}\varphi = \Delta \mathrm{d}s + z\,\Delta\mathrm{d}\varphi \tag{13.30}$$

applies, i. e. the strains ε_s and hence – owing to (13.4) – the stresses $\sigma_s = E\varepsilon_s$ do not exhibit a linear, but rather a hyperbolic distribution over the depth of the cross-section h.

For the case of pure bending ($N = 0$), $\Delta \mathrm{d}s$ disappears and according to (13.4), $(13.5)_1$ and $(13.5)_2$ as well as (13.30),

$$N = E \cdot \frac{\Delta\mathrm{d}\varphi}{\mathrm{d}\varphi} \int \frac{z}{\rho_0 - z}\,\mathrm{d}A = 0 \quad , \quad M = E \cdot \frac{\Delta\mathrm{d}\varphi}{\mathrm{d}\varphi} \int \frac{z^2}{\rho_0 - z}\,\mathrm{d}A \tag{13.31}$$

Substituting $\rho = \rho_0 - z$, then $(13.31)_1$ results in

$$\rho_0 \int \frac{\mathrm{d}A}{\rho} - \int \mathrm{d}A = 0$$

and therefore

$$\rho_0 = \frac{A}{\displaystyle\int \frac{\mathrm{d}A}{\rho}} \tag{13.32}$$

Considering the integral in $(13.31)_2$, using (13.32) and $\int \rho\,\mathrm{d}A = \rho_C A$ gives us

$$\int \frac{z^2}{\rho_0 - z}\,\mathrm{d}A = \int \frac{(\rho_0 - \rho)^2}{\rho}\,\mathrm{d}A = \rho_0^2 \frac{A}{\rho_0} - 2\rho_0 A + \rho_C A = (\rho_C - \rho_0)A$$

This therefore results in

$$\sigma_s(M) = \frac{E\,z\,\Delta\mathrm{d}\varphi}{(\rho_0 - z)\,\mathrm{d}\varphi} = \frac{Mz}{A(\rho_C - \rho_0)(\rho_0 - z)}$$

and taking into account a normal force N (related to C), then

$$\sigma_s = \frac{N}{A} + \frac{M_C\,z}{A(\rho_C - \rho_0)(\rho_0 - z)} \tag{13.33}$$

with the bending moment M_C related to C.

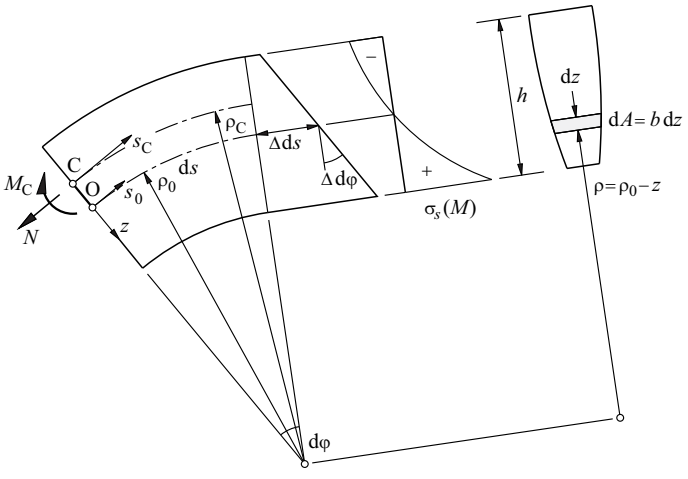

Fig. 13.11 Planar bending of a curved bar

For rectangular cross-sections where $\rho_C > h$, eq. (13.33) supplies results that deviate by less than 1 % from those of an elastic plate calculation. On the other hand, where $\rho_C > 10h$, the difference with respect to a calculation for the straight bar is practically negligible.

13.2.7 Practical advice

In practice, various cross-section programs and design tables are available which simplify the task of calculating stresses and deformations. In particular, design tables have been developed for structural steelwork and timber which specify the most important cross-sectional values for frequently used sections. Similar design tables for reinforced and prestressed concrete – for the cracked state (II) as in example 13.3, neglecting the tensile strength of the concrete – can also prove useful.

13.3 Shear forces

13.3.1 Approximation for prismatic bars subjected to pure bending

The prismatic bar shown in Fig. 13.12(a) is subjected to pure bending about the y axis. The width of the cross-section in the y direction is designated $b = b(z)$, and it is assumed that the shear stresses $\tau_{xz}(z_s)$ at section z_s are uniformly distributed over the width of the section $b(z_s)$. Equilibrium of forces in the x direction for the free body shown in Fig. 13.12(b) calls for

$$-\tau_{xz}(z_s)\cdot b(z_s)\,\mathrm{d}x + \int_{z_s}^{z_u} \mathrm{d}\sigma_x(z)\cdot b(z)\,\mathrm{d}z = 0 \tag{13.34}$$

As $N = M_z = 0$, eq. (13.16) results in $\sigma_x = M_y\, z/I_y$, and as $I_y = \text{const}$, eq. $(5.46)_2$, with $M = M_y$ and $V = V_z$, then provides

$$\frac{\mathrm{d}\sigma_x}{\mathrm{d}x} = \frac{V_z \cdot z}{I_y} \tag{13.35}$$

Using the shortened form

$$S(z_s) = \int_{z_s}^{z_u} z \cdot b(z)\,\mathrm{d}z \tag{13.36}$$

for the first moment of area of the portion of the cross-section cut off at z_s, combining (13.34) and (13.35) results in

$$\tau_{xz} = \frac{V_z S}{b\, I_y} \tag{13.37}$$

where τ_{xz}, b and S depend on z_s as discussed above.

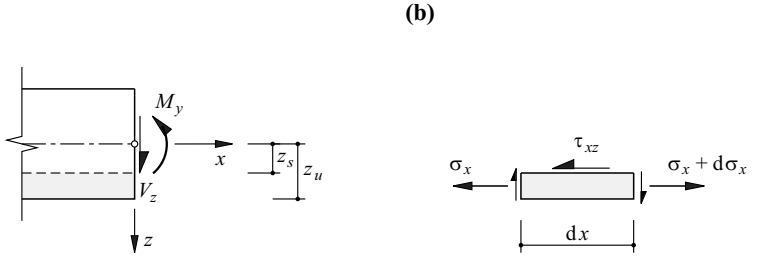

Fig. 13.12 Prismatic bar subjected to pure bending: (a) notation, (b) free body

Example 13.5 Rectangular cross-section – shear stress distribution

Consider the rectangular cross-section shown in Fig. 13.13, with $A = bh$, $I_y = bh^3/12$ and $S = b(h^2/4 - z^2)/2$. Taking into account (5.30), eq. (13.37) results in the parabolic shear stress distribution

$$\tau_{zx} = \frac{V_z}{bh} \cdot \frac{3}{2} \cdot \left(1 - \frac{4z^2}{h^2}\right)$$

over the depth of the cross-section h. The maximum shear stress τ_{max} exceeds the mean shear stress V_z/A by 50 %.

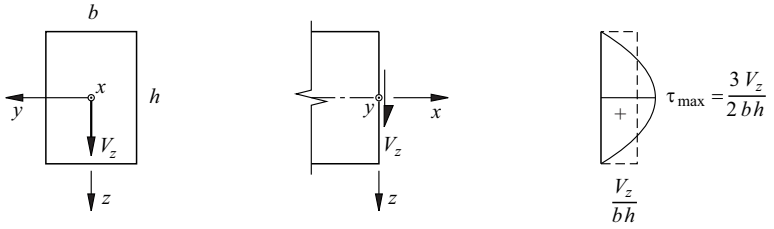

Fig. 13.13 Shear stress distribution in a rectangular cross-section subjected to pure bending

According to $(7.3)_2$ and (8.67), the shear stresses τ_{xz} resulting from (13.37) correspond to the specific deformation energy

$$\pi_i = \frac{\tau_{xz}^2}{2G} = \frac{V_z^2 S^2}{2Gb^2 I_y^2} \tag{13.38}$$

Integrating over a bar element results in the internal potential component

$$\Pi_i(V_z) = \int_x \int_A \pi_i \, dA \, dx = \int_x \frac{V_z^2}{2GA_v} \, dx \tag{13.39}$$

according to (8.73), where the shortened form

$$A_v = \left[\int \frac{S^2}{b^2 I_y^2} \, dA\right]^{-1} = \alpha_v A \tag{13.40}$$

was used for the shear area, see (8.23).

The *area shear factor* α_v, for example, for the rectangular cross-section examined in example 13.5, where

$$\int \frac{S^2}{b^2 I_y^2} \, dA = \int_{-h/2}^{h/2} \frac{b^2(h^2/4 - z^2)^2}{b^2(bh^3/12)^2} b \, dz = \frac{6}{5bh}$$

and $A = bh$, turns out to be a value of $\alpha_v = 5/6$. Appendix A4 contains the values for other cross-sections.

Compared with the extent to which the normal stresses σ_x contribute to the internal potential Π_i, the contribution of the shear stresses τ_{xz} is normally small and is therefore often ignored, i. e. the designer settles for a theory of bars rigid in shear according to section 8.2.2 or 8.2.3. In a similar way to (13.39), the contribution of the normal stresses σ_x or the bending moments M_y to Π_i is

$$\Pi_i(M_y) = \int_x \int_A \frac{\sigma_x^2}{2E} \, dA \, dx = \int_x \int_A \frac{M_y^2 z^2}{2EI_y^2} \, dA \, dx = \int_x \frac{M_y^2}{2EI_y} \, dx \tag{13.41}$$

Considering the example of the simply supported beam of Fig. 13.14(a) subjected to a uniformly distributed line load q, then $V_z = q(l - 2x)/2$ and $M_y = qx(l - x)/2$ applies. Taking into account (7.2), $(13.19)_1$ and $(13.40)_2$, using (13.39) and (13.41) results in the relationship

$$\frac{\Pi_i(V_z)}{\Pi_i(M_y)} = \frac{20(1 + \nu)}{\alpha_v} \cdot \left(\frac{i_y}{l}\right)^2 \tag{13.42}$$

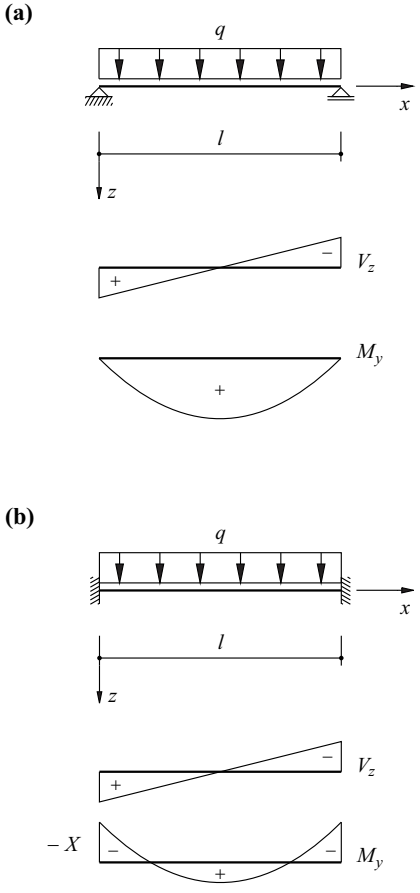

Fig. 13.14 Comparison of internal potential as a result of bending and shear force: (a) simply supported beam subjected to uniformly distributed line load, (b) fixed-end beam

If the beam is fixed at both ends, see Fig. 13.14(b), a fixed-end moment X is superimposed on the moment M_y of the simply supported beam. Similarly to example 8.5, the fixed-end moment can be determined with the theorem of least complementary total potential: $X = -ql^2/12$. Using the modified M_y, the factor in (13.42), which depends on static system and load, is 120 instead of 20; for a rectangular cross-section with $l = 20h$, $i_y^2 = h^2/12$, $\alpha_v = 5/6$ and $\nu = 0.2$, the result is therefore $\Pi_i(V_z) = 0.036\ \Pi_i(M_y)$, for example.

13.3.2 Approximate coplanar stress state

According to the elastic beam theory discussed in section 13.2.1, the stresses σ_z and τ_{xz} are negligible in comparison with σ_x. The beam with a narrow rectangular cross-section loaded along its top edge, see Fig. 13.15, is considered below on the basis of section 8.2.4. For τ_{xz}, we shall assume a parabolic distribution over the depth of the cross-section h as determined in example 13.5, i. e.

$$\tau_{xz} = \tau_{zx} = \frac{V_z}{2I_y}\left(\frac{h^2}{4} - z^2\right) \tag{13.43}$$

Applying the equilibrium condition (8.31) and taking into account $q_z = 0$, we get the equation $\partial\sigma_z/\partial z = -\partial\tau_{zx}/\partial x$ and therefore, owing to $(5.46)_1$ and $\sigma_z(h/2) = 0$ as well as $I_y = bh^3/12$, we get

$$\sigma_z = q\left(-\frac{1}{2} + \frac{3z}{2h} - \frac{2z^3}{h^3}\right) \tag{13.44}$$

If the load q were to be applied to the bottom instead of the top edge, the term $1/2$ in the brackets on the right of (13.44) would be positive instead of negative.

Replacing the y coordinate by the z coordinate and the displacement v by w in (8.33) and carrying out double differentiation of the strain components results in the relationship

$$\frac{\partial^2\varepsilon_x}{\partial z^2} + \frac{\partial^2\varepsilon_z}{\partial x^2} = \frac{\partial^2\gamma_{xz}}{\partial x\,\partial z} \tag{13.45}$$

Applying $(5.46)_1$, $(7.3)_2$ and (13.43), we get

$$\frac{\partial^2\gamma_{xz}}{\partial x\,\partial z} = \frac{qbz}{GI_y}$$

for the expression on the right in (13.45). Using $\nu = 0$ for POISSON's ratio, according to (7.1), $\varepsilon_x = \sigma_x/E$ and $\varepsilon_z = \sigma_z/E$ applies, and according to (7.2), $G = E/2$. If we also assume that $\partial^2 q/\partial x^2 = 0$, eq. (13.45) is reduced to

$$\frac{\partial^2\sigma_x}{\partial z^2} = \frac{2qbz}{I_y}$$

from which it follows that

$$\sigma_x = \frac{M_y\, z}{I_y} + \Delta\sigma_x \quad , \quad \Delta\sigma_x = \frac{q}{5h^3}(20z^3 - 3zh^2) \tag{13.46}$$

The additional stresses $\Delta\sigma_x$ form a residual stress state, and the following applies:

$$\int_{-h/2}^{h/2} \Delta\sigma_x b\,\mathrm{d}x = \int_{-h/2}^{h/2} z\Delta\sigma_x b\,\mathrm{d}x = 0$$

The equations (13.46), (13.44) and (13.43) describe an approximate coplanar stress state with which the stress relationships can be approximated apart from local zones such as beam ends and force transfer points.

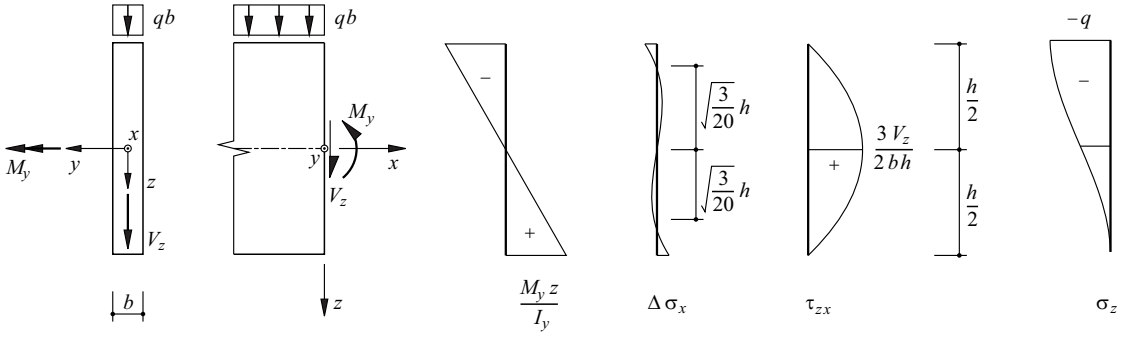

Fig. 13.15 Approximate coplanar stress state

13.3.3 Thin-wall cross-sections

From the derivation of (13.37), it follows that the shear stress distribution in thin-wall sections, e. g. those common in structural steelwork, can normally be determined in a similar way, provided the sections are perpendicular to the parts of the cross-section. Fig. 13.16 shows an I section in which the sections transverse to the flanges and the web lead to shear stresses τ_{yx} and τ_{zx} respectively as a result of shear force V_z. The first moment of area S is related to the sectioned parts, where the y axis is the reference axis.

We also notice that the shear stresses τ_{zx} determined with (13.37) are practically irrelevant for the flange of the I section shown in Fig. 13.16. They are purely fictitious variables that result from the simplified assumption of a shear stress distribution that is constant over the width of the section.

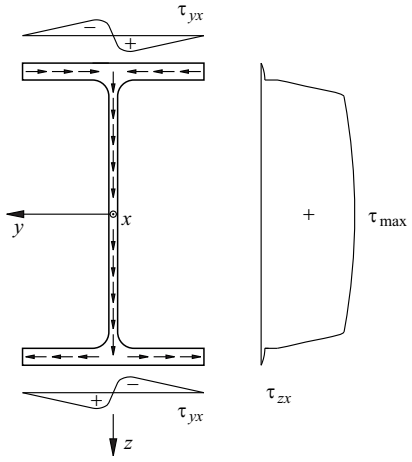

Fig. 13.16 Distribution of shear stress in an I section as a result of V_z

Example 13.6 Wide-flange beam

The HEB 300 wide-flange beam shown in Fig. 13.17 is subjected to a shear force $V_z = 200\,\text{kN}$. The task is to determine the shear stress distribution.

First of all, we get $A = 2\cdot 19\cdot 300 + 11\cdot 262 + (4-\pi)\cdot 27^2 = 14\,908\,\text{mm}^2$ for the cross-sectional area and $I_y = (300^4 - 289\cdot 262^3)/12 + 4\cdot(27^4/12 + 27^2\cdot 117.5^2 - \pi\cdot 27^4/16 - \pi\cdot 27^2\cdot 115.46^2/4) = 251.36\cdot 10^6\,\text{mm}^4$ for the moment of inertia.

The first moments of area for sections 1 to 3 are

$$S_1 = 140.5\cdot 19\cdot 117.5 = 313\,666\,\text{mm}^3$$

$$S_2 = 140.5\cdot 19\cdot 300 + 2\cdot(27^2\cdot 117.5 - \pi\cdot 27^2\cdot 115.46/4) = 839\,952\,\text{mm}^3$$

$$S_3 = S_2 + 52\cdot 104\cdot 11 = 899\,440\,\text{mm}^3$$

and from those we get the shear stresses

$$\tau_{yx1} = \frac{200\,000\cdot 313\,666}{19\cdot 251.36\cdot 10^6} = 13.1\,\text{N/mm}^2$$

$$\tau_{zx2} = \frac{200\,000\cdot 839\,952}{11\cdot 251.36\cdot 10^6} = 60.8\,\text{N/mm}^2$$

$$\tau_{zx3} = \frac{200\,000\cdot 899\,440}{11\cdot 251.36\cdot 10^6} = 65.1\,\text{N/mm}^2$$

Dividing the shear force by the area of the web (extending as far as the centre of each flange), we get a good approximate value for the shear stress in the web

$$\tau_{zx} \approx \frac{200\,000}{281\cdot 11} = 64.7\,\text{N/mm}^2$$

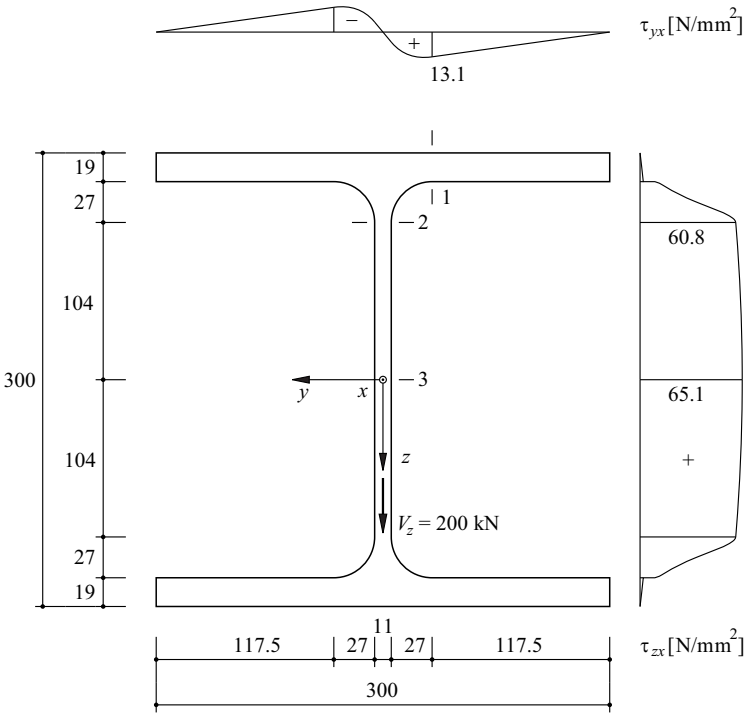

Fig. 13.17 Shear stress distribution for HEB 300 wide-flange beam

In asymmetric cross-sections, e. g. unequal leg angles, it is often better to work with axes parallel with the parts of the cross-section instead of with the principal axes. For example, considering the angle shown in Fig. 13.18 subjected to $V_{\zeta'}$, we get

$$\tau = \frac{V_{\zeta'}(I_{\zeta'} S_{\eta'} + C_{\eta'\zeta'} S_{\zeta'})}{t(I_{\eta'} I_{\zeta'} - C_{\eta'\zeta'}^2)} \tag{13.47}$$

This equation results when the y, z coordinates are replaced by η', ζ' in (13.6), and – applying (13.14) and (13.4) – the stresses σ_x as a result of $M_{\eta'}$, $M_{\zeta'}$ are calculated according to (13.3):

$$\sigma_x = M_{\eta'} \frac{I_{\zeta'}\zeta' + C_{\eta'\zeta'}\eta'}{I_{\eta'} I_{\zeta'} - C_{\eta'\zeta'}^2} - M_{\zeta'} \frac{I_{\eta'}\eta' + C_{\eta'\zeta'}\zeta'}{I_{\eta'} I_{\zeta'} - C_{\eta'\zeta'}^2} \tag{13.48}$$

As $V_{\zeta'} = \mathrm{d}M_{\eta'}/\mathrm{d}x$, eq. (13.47) follows from (13.34), as (13.37) did before.

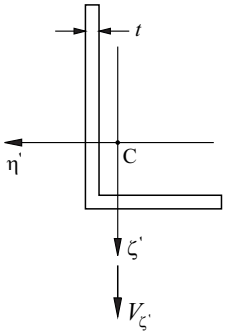

Fig. 13.18 Unequal leg angle

Example 13.7 Unequal leg angle

The unequal leg angle already examined in example 13.1 is subjected to a shear force $V_{\zeta'} = 15$ kN. The task is to determine the shear stress distribution with the simplification that the thickness of the leg is negligible in comparison with the length of the leg, i. e. the calculation is based on an L section reduced to the axes of the legs, see Fig. 13.19(a).

Using a leg thickness of 1, we first get $A = 37.5 + 57.5 = 95$ mm, and therefore (13.11) gives us the centroid coordinates $\eta_C = (37.5)^2/(2\cdot 95) = 7.40$ mm and $\zeta_C = -(57.5)^2/(2\cdot 95) = 17.40$ mm. Eq. (13.14) results in $I_{\eta'} = 37.5\cdot 17.40^2 + (57.5)^3/12 + 57.5\cdot(57.5/2 - 17.40)^2 = 34\,603\,\mathrm{mm}^3$, $I_{\zeta'} = 57.5\cdot 7.40^2 + (37.5)^3/12 + 37.5\cdot(37.5/2 - 7.40)^2 = 12\,374\,\mathrm{mm}^3$ and $C_{\eta'\zeta'} = -37.5\cdot(37.5/2 - 7.40)\cdot 17.40 - 57.5\cdot(57.5/2 - 17.40)\cdot 7.40 = -12\,235\,\mathrm{mm}^3$.

By applying (13.13), it follows that $\tan\varphi = -0.443$, and (13.15) results in $I_y = 40\,018\,\mathrm{mm}^3$, $I_z = 6\,959\,\mathrm{mm}^3$.

Fig. 13.19(b) shows the position of the neutral axis and the normal stresses σ_x as a result of $M_{\eta'}$. The neutral axis passes through the centroid C and the outermost third point of the leg along the η axis. Fig. 13.19(c) shows the corresponding shear stress distribution as a result of $V_{\zeta'}$ according to (13.47). The positive and negative shear stresses $\tau_{\eta' x}$ in the leg along the η axis cancel each other out, $-10.3\cdot 25\cdot 2/3 + (30.9 + 10.3)\cdot 25/3 - 10.3\cdot(25 - 12.5\cdot 2/3) = 0$, and the shear stresses $\tau_{\zeta' x}$ in the leg along the ζ axis correspond to $V_{\zeta'}$ in total:

$[71.6(32.78\cdot 2/3 + 24.72) - (71.6 - 30.9)\cdot 24.72/3]\cdot 5 = 15$ kN

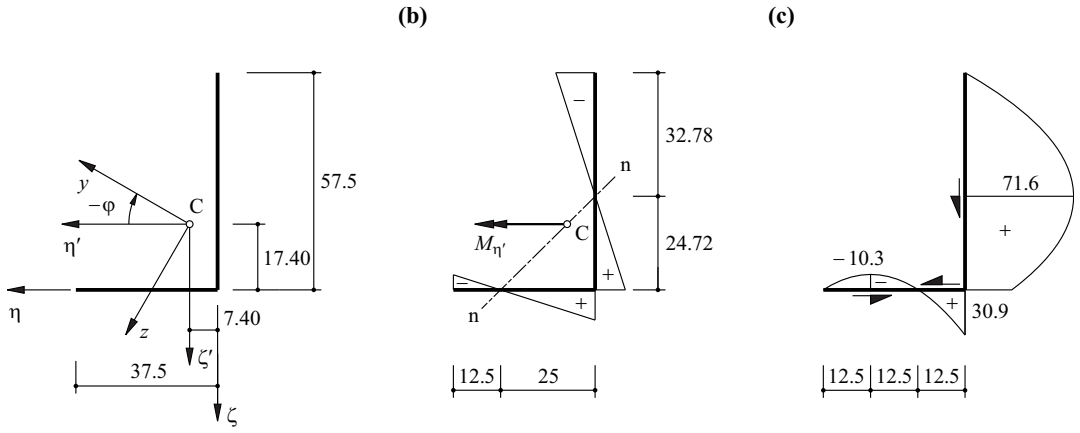

Fig. 13.19 Unequal leg angle: (a) dimensions [mm] and axes, (b) neutral axis and normal stress distribution as a result of $M_{\eta'}$, (c) shear stress distribution [N/mm^2]

The effective leg thickness $t = 5$ mm is used again when calculating the shear stresses at the corner of the cross-section according to (13.47):

$$\tau = \frac{15\,000 \cdot [12\,374 \cdot (57.5/2 - 17.4) \cdot 57.5 - 12\,235 \cdot 7.4 \cdot 57.5]}{5 \cdot (34\,603 \cdot 12\,374 - 12\,235^2)} = 30.9 \text{ N/mm}^2$$

Owing to the parabolic distribution of $\tau_{\eta' x}$, the extreme negative shear stress at the outermost third point of the leg along the η axis is one-third of the shear stress at the corner of the cross-section, i. e. 10.3 N/mm^2. On the other hand, the magnitude of the maximum positive shear stress in the leg along the ζ axis follows from knowing the shear stress at the corner of the cross-section and the position of the neutral axis:

$$30.9 \cdot [1 - (24.72/32.78)^2]^{-1} = 71.6 \text{ N/mm}^2$$

If instead of $V_{\zeta'}$, we were to apply a shear force $V_{\eta'}$, the neutral axis would pass through C and the outermost third point of the leg along the ζ axis. The distribution of the shear stress would then be similar to that given above. Superposing cases $V_{\zeta'}$ or $M_{\eta'}$ and $V_{\eta'}$ or $M_{\zeta'}$ therefore allows any case of skew bending to be dealt with.

13.3.4 Shear centre

The shear stresses τ_{yx} in the singly symmetric cross-section shown in Fig. 13.20 correspond to the resulting flange forces V_f, which with a lever arm d form a couple $d\,V_f$. On the other hand, the shear stresses τ_{zx} correspond to a resulting web force $V_w = V_z$. Moment equilibrium about the x axis calls for V_z to be applied at the *shear centre* M at a distance of

$$a = \frac{d\,V_f}{V_w} \tag{13.49}$$

from the web resultant V_w.

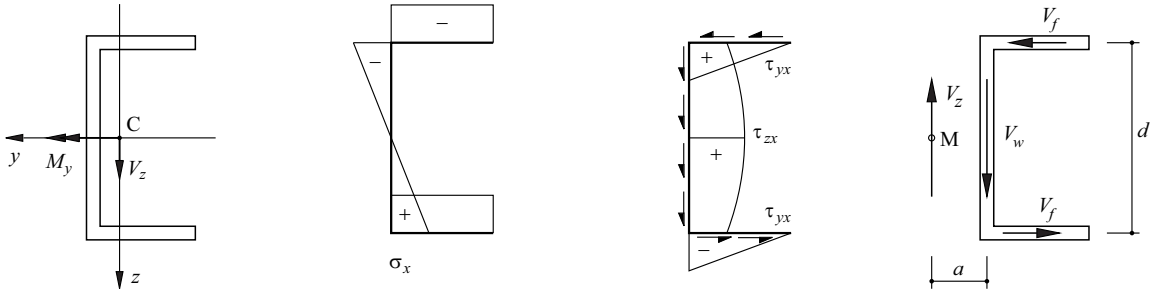

Fig. 13.20 Shear centre of a singly symmetric cross-section

The stress distribution assumed in beam theory is only possible when the shear force acts at the shear centre, i. e. the shear centre M and not the centroid C of a cross-section is the force application point for bending without rotation. On the other hand, M is also the fulcrum for rotation without bending, see section 13.4.4.

For general cross-sections, M can be obtained from the intersection of the lines of action of the resultants of the shear stresses for bending about the two principal axes y and z. With singly symmetric cross-sections, it is sufficient to consider bending about the axis of symmetry, as shown above.

Where a cross-section consists of a number of straight legs which, like with an angle, all meet at one point, then the shear centre is at this point. There is no *warping* in such cross-sections; they are said to be *free from warping*, see Fig. 13.21.

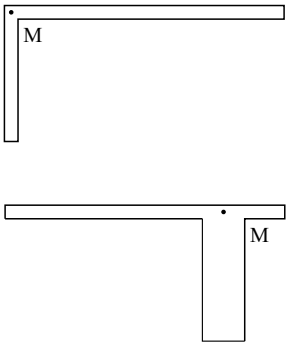

Fig. 13.21 Cross-sections free from warping

13.4 Torsion

13.4.1 Circular cross-sections

It is possible to solve a pure torsion problem exactly in the case of circular and annular cross-sections made from homogeneous and isotropic linear elastic materials with (at least segment by segment) constant radii and torques. With the specific rotation or twist $\vartheta = \mathrm{d}\varphi_x/\mathrm{d}x$ according to (8.27) and $\tau_{\varphi x} = G\gamma_{\varphi x}$ according to (7.3), the following applies:

$$\gamma_{\varphi x} = r\,\frac{\mathrm{d}\varphi_x}{\mathrm{d}x} = r\vartheta = \frac{\tau_{\varphi x}}{G} \tag{13.50}$$

see Fig. 13.22. It therefore follows that

$$T = \int_A \tau_{\varphi x} r^2 \mathrm{d}r\,\mathrm{d}\varphi = G2\pi\vartheta \int_{r_i}^{r_e} r^3 \mathrm{d}r = GI_p\vartheta \tag{13.51}$$

with the *polar moment of inertia*

$$I_p = \frac{\pi}{2}(r_e^4 - r_i^4) \tag{13.52}$$

Further, from $(13.50)_3$ and $(13.51)_3$ it follows that

$$\tau_{\varphi x} = \frac{Tr}{I_p} \tag{13.53}$$

The similarity with how the bending moments contribute to σ_x in (13.16) is obvious here.

The polar moment of inertia is only equal to the torsion constant I_x in the case of circular and annular cross-sections, see (8.28). Values of I_x for other cross-sections can be found in sections 13.4.2 and 13.4.3 as well as appendix A4.

If T, G or r_e, r_i change abruptly, the result is concentrations of stress at the points of abrupt change which have to be investigated separately. The above equations can be used to obtain approximate answers when variations in the torques, material properties and cross-section radii are only small in comparison with the length of the bar.

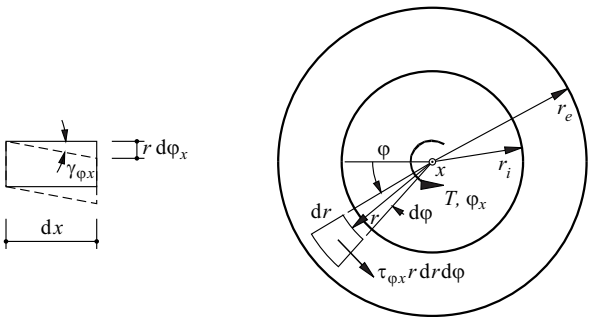

Fig. 13.22 Annular cross-section subjected to a pure torsional action

13.4.2 General cross-sections

Fig. 13.23(a) shows the cross-section through a solid prismatic bar that is subjected to a pure torque T. We shall continue to assume that the cross-section rotates through an angle of φ_x about the x axis, but also allows a displacement or a warping $u(y, z)$ independent of x in the x direction. The displacements v, w in cross-sectional plane y, z are

$$v = -z\,\varphi_x \quad , \quad w = y\,\varphi_x \tag{13.54}$$

Using $\vartheta = \mathrm{d}\varphi_x/\mathrm{d}x$, the kinematic relations (6.22) result in

$$\varepsilon_x = \varepsilon_y = \varepsilon_z = \gamma_{yz} = \gamma_{zy} = 0 \quad , \quad \gamma_{xy} = \gamma_{yx} = \frac{\partial u}{\partial y} - z\,\vartheta \quad , \quad \gamma_{xz} = \gamma_{zx} = \frac{\partial u}{\partial z} + y\,\vartheta \tag{13.55}$$

and therefore, according to (7.3), the following applies to the only two stress components not equal to zero:

$$\tau_{xy} = G\left(\frac{\partial u}{\partial y} - z\,\vartheta\right) \quad , \quad \tau_{xz} = G\left(\frac{\partial u}{\partial z} + y\,\vartheta\right) \tag{13.56}$$

Differentiating the first (second) of these relationships with respect to z (y) and subtracting results in the *compatibility condition*

$$\frac{\partial \tau_{xy}}{\partial z} - \frac{\partial \tau_{xz}}{\partial y} = -2G\vartheta \tag{13.57}$$

On the edge of the cross-section, the shear stress vector consisting of the τ_{yx}, τ_{zx} components must be parallel with the edge. With the n_y, n_z components of the unit vector $\boldsymbol{n}$ perpendicular to the edge, the following applies:

$$\tau_{xy} n_y + \tau_{xz} n_z = 0 \tag{13.58}$$

From the equilibrium conditions (5.29), it follows that

$$\frac{\partial \tau_{xy}}{\partial y} + \frac{\partial \tau_{xz}}{\partial z} = 0 \quad , \quad \frac{\partial \tau_{xy}}{\partial x} = \frac{\partial \tau_{xz}}{\partial x} = 0 \tag{13.59}$$

Combining $(13.59)_2$ and $(13.59)_3$ with (13.57), it must be that ϑ = const.

Introducing the *stress function* $\Phi(y,z)$ with

$$\tau_{xy} = \frac{\partial \Phi}{\partial z} \quad , \quad -\tau_{xz} = \frac{\partial \Phi}{\partial y} \tag{13.60}$$

means that $(13.59)_1$ is satisfied, and (13.57) gives us POISSON*'s differential equation*

$$\Delta\Phi = \frac{\partial^2 \Phi}{\partial y^2} + \frac{\partial^2 \Phi}{\partial z^2} = -2G\vartheta = \text{const} \tag{13.61}$$

Finally, by substituting (13.60) in the boundary condition (13.58), we realise that the gradient vector $\nabla\Phi$ of the stress function is proportional to the vector perpendicular to the edge $\boldsymbol{n}$. Therefore, Φ remains constant along the perimeter and we can set the constant to zero without compromising the generality, see Fig. 13.23(b).

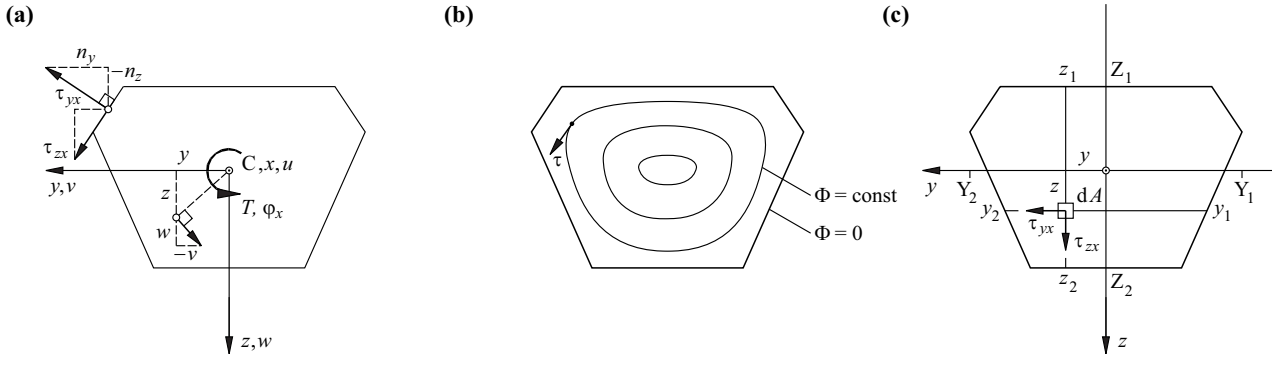

Fig. 13.23 Torsion in bars with a general cross-section: (a) notation, (b) stress function Φ, (c) determination of T

If, for a given cross-sectional form, we find a solution to differential equation (13.61) which satisfies the boundary condition $\Phi = 0$, the shear stress components τ_{xy}, τ_{xz} follow from (13.60) and the warping function u follows from (13.56). According to Fig. 13.23(c), the torque is

$$T = \int (\tau_{zx} y - \tau_{yx} z)\, \mathrm{d}A = -\int \left(\frac{\partial \Phi}{\partial y}\, y + \frac{\partial \Phi}{\partial z}\, z \right) \mathrm{d}A$$

where $\mathrm{d}A = \mathrm{d}y\,\mathrm{d}z$. Integrating by parts and considering the condition $\Phi = 0$ at the edge of the cross-section gives us

$$\int \frac{\partial \Phi}{\partial y}\, y\, \mathrm{d}A = \int_{Z_1}^{Z_2} \left(\int_{y_1(z)}^{y_2(z)} \frac{\partial \Phi}{\partial y}\, y\, \mathrm{d}y \right) \mathrm{d}z = -\int_{Z_1}^{Z_2} \left(\int_{y_1(z)}^{y_2(z)} \Phi\, \mathrm{d}y \right) \mathrm{d}z = -\int \Phi\, \mathrm{d}A$$

and

$$\int \frac{\partial \Phi}{\partial z}\, z\, \mathrm{d}A = \int_{Y_1}^{Y_2} \left(\int_{z_1(y)}^{z_2(y)} \frac{\partial \Phi}{\partial z}\, z\, \mathrm{d}z \right) \mathrm{d}y = -\int_{Y_1}^{Y_2} \left(\int_{z_1(y)}^{z_2(y)} \Phi\, \mathrm{d}z \right) \mathrm{d}y = -\int \Phi\, \mathrm{d}A$$

and therefore

$$T = 2 \int \Phi\, \mathrm{d}A \tag{13.62}$$

According to (13.62), the torque is equal to double the volume that ensues when we apply the stress function Φ as a curved surface over the cross-section, see Fig. 13.23(b). The contour lines Φ = const of the Φ surface parallel with the plane of the cross-section are tangential to the shear stress vector $\boldsymbol{\tau}$ at every point y, z because according to (13.60), the scalar product of $\boldsymbol{\tau}$ and the gradient vector $\nabla\Phi$ orthogonal to the contour lines disappears.

Every (closed) contour line Φ = const corresponds to a circumferential shear flow. The way of carrying torques shown here is therefore called *pure torsion* (in order to distinguish it from the warping torsion discussed in section 13.4.4). Where the contour lines are closer together, e. g. at re-entrant corners of the cross-section, the shear stresses due to pure torsion take on high values corresponding to the large gradient of Φ, see (13.60).

Example 13.8 Elliptical bar

The function

$$\Phi = c \left(1 - \frac{y^2}{a^2} - \frac{z^2}{b^2} \right)$$

satisfies the boundary condition $\Phi = 0$ for the elliptical cross-section shown in Fig. 13.24(a), with semi-axes a and b. The constant c results from substituting in (13.61):

$$c = \frac{G\vartheta a^2 b^2}{a^2 + b^2}$$

and (13.60) gives us the shear stress components

$$\tau_{xy} = -\frac{2G\vartheta a^2 z}{a^2 + b^2} \quad , \quad \tau_{xz} = \frac{2G\vartheta b^2 y}{a^2 + b^2}$$

Eq. (13.56) results in

$$\frac{\partial u}{\partial y} = \vartheta z \frac{b^2 - a^2}{a^2 + b^2} \quad , \quad \frac{\partial u}{\partial z} = \vartheta y \frac{b^2 - a^2}{a^2 + b^2}$$

and therefore

$$u = \frac{b^2 - a^2}{a^2 + b^2} \vartheta y z$$

The warping surface is a hyperbolic paraboloid, see Fig. 13.24(b). When $b = a$, i. e. the cross-section is circular, the warping is equal to zero.

Using (13.9), eq. (13.62) initially results in

$$T = \frac{2G\vartheta a^2 b^2}{a^2 + b^2} \left(A - \frac{I_z}{a^2} - \frac{I_y}{b^2} \right)$$

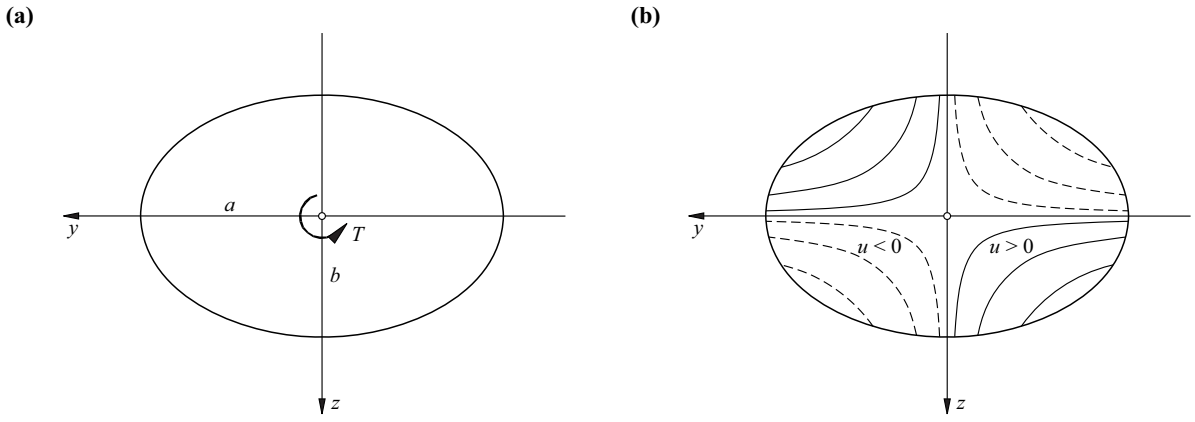

Fig. 13.24 Torsion in a bar with an elliptical cross-section: (a) notation, (b) warping

and therefore as $A = \pi ab$, $I_y = \pi ab^3/4$, $I_z = \pi ba^3/4$, then

$$T = GI_x\vartheta \quad , \quad I_x = \frac{\pi a^3 b^3}{a^2 + b^2}$$

As we can see, the torsion constant I_x for $a \neq b$ is smaller than the polar moment of inertia $I_p = I_y + I_z$ because $(a^2 - b^2)^2 > 0$.

Differential equation (13.61) is similar to the differential equation

$$\Delta u = \frac{\partial^2 u}{\partial y^2} + \frac{\partial^2 u}{\partial z^2} = -\frac{p}{n} = \text{const} \tag{13.63}$$

for a membrane with a constant tensile force per unit length n subjected to a small overpressure p, where u is the (small) displacement of the membrane perpendicular to the yz plane. Replacing N by n and $-q_n$ by p in the hoop stress formula (5.52) and considering the two directions y and z, we first get

$$\frac{n}{\rho_y} + \frac{n}{\rho_z} = p$$

The curvatures $\chi_y = 1/\rho_y$ and $\chi_z = 1/\rho_z$ are found in a similar way to (8.46):

$$\chi_y = -\frac{\partial^2 u}{\partial y^2} \quad , \quad \chi_z = -\frac{\partial^2 u}{\partial z^2}$$

from which (13.63) follows.

The torsion problem can therefore be handled according to PRANDTL's *membrane analogy* (soap film analogy) by considering a membrane that spans across an opening matching the cross-section of the bar in torsion.

Example 13.9 Narrow rectangular cross-section

The narrow rectangular cross-section shown in Fig. 13.25 has a width a that far exceeds its thickness b ($a \gg b$). The membrane analogy shows that apart from small areas at both ends of the cross-section, we can expect a curvature purely in the z direction.

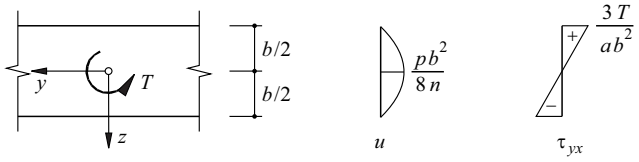

Fig. 13.25 Narrow rectangular cross-section subjected to a pure torque (thickness of cross-section $b \ll$ width of cross-section a)

The function

$$u = \frac{p}{2n}\left(\frac{b^2}{4} - z^2\right)$$

satisfies (13.63). Double the volume spanned by the membrane amounts to

$$2\int u \, dA = \frac{pb^2}{4n} \cdot \frac{2}{3} \cdot ab = \frac{pab^3}{6n}$$

and according to (13.62), this is proportional to T. The membrane slope, which according to $(13.60)_1$ is proportional to τ_{yx}, is

$$\frac{\partial u}{\partial z} = -\frac{pz}{n}$$

and therefore it follows that

$$\tau_{yx} = -\frac{pz}{n} \cdot \frac{6nT}{pab^3} = -\frac{6Tz}{ab^3}$$

Further, $\Delta u = -p/n$ is proportional to $-2G\vartheta$ according to (13.61), and from that we get

$$\vartheta = \frac{p}{2Gn} \cdot \frac{6nT}{pab^3} = \frac{3T}{Gab^3}$$

and thus a torsion constant of

$$I_x = \frac{ab^3}{3}$$

Where a thin-wall cross-section is made up of several narrow rectangles, its torsional stiffness can obviously be approximated with good accuracy by adding together the torsional stiffnesses of the individual cross-sections, i. e.

$$GI_x = \sum_i \frac{G_i a_i b_i^3}{3} \qquad (a_i \gg b_i) \tag{13.64}$$

13.4.3 Thin-wall hollow cross-sections

Simply-connected cross-sections with a single boundary curve have been dealt with in section 13.4.2. It was found that the stress function Φ along the boundary curve has to be constant and the constant was set to zero.

In the case of a *multiply-connected* cross-section, i. e. one with one or more openings, if on the outer edge $\Phi = 0$, then various constants Φ_1, Φ_2, etc. result at the edges of the openings. The Φ surface then contains horizontal segments at the corresponding levels in the opening areas.

The situation shown in Fig. 13.26(a) results with a thin-wall hollow cross-section. The shear stresses τ as a result of a torque may be assumed to be distributed uniformly over the thickness of the wall t and in the direction of the centre-line of the wall (indicated by the chain-dot line). Instead of (13.60), we get $\tau = \Phi_1/t$, or

$$S = \tau t = \text{const} \tag{13.65}$$

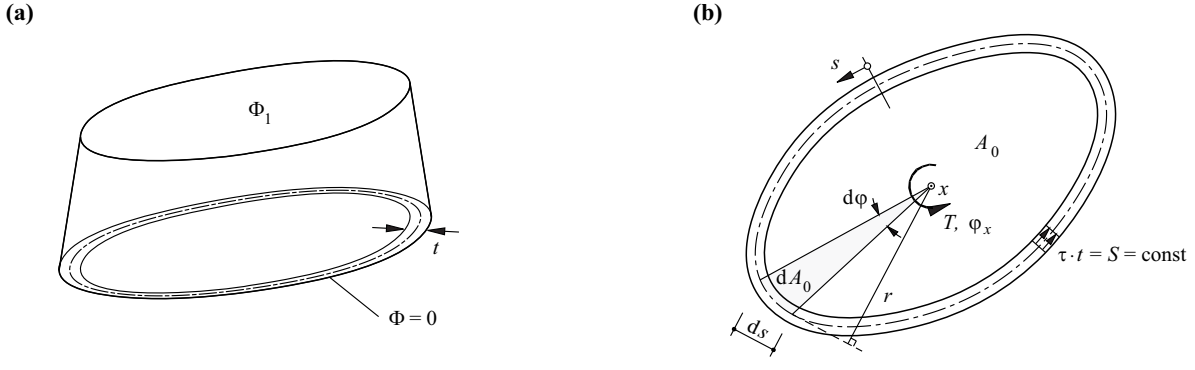

Fig. 13.26 Thin-wall hollow cross-section: (a) Φ surface, (b) designations

where $S = \Phi_1$, the *shear flow*. Using the surface A_0 enclosed by the centre-line of the wall of the cross-section, (13.62) results in BREDT's 1st equation:

$$T = 2A_0 S \tag{13.66}$$

This result is also obtained from the integral

$$T = \oint rS \, \mathrm{d}s = 2A_0 S$$

over the closed path along the perimeter of A_0 according to Fig. 13.26(b).

The rotation φ_x gives us the displacement $v = r\varphi_x$ at s in the s direction. Together with the displacement u in the x direction, using (6.22) and considering $\mathrm{d}\varphi_x/\mathrm{d}x = \vartheta$, we get the shear strain

$$\gamma_{xs} = \frac{\partial u}{\partial s} + r\vartheta$$

The contribution of the first term disappears in the integral

$$\oint \gamma_{xs} \, \mathrm{d}s = \oint \left(\frac{\partial u}{\partial s} + r\vartheta \right) \mathrm{d}s = 2A_0 \vartheta \tag{13.67}$$

Putting $\gamma_{xs} = \tau_{xs}/G$ according to (7.3) and $\tau_{xs} = T/(2A_0 t)$ according to (13.65) and (13.66), the result is therefore

$$T = GI_x \vartheta \quad , \quad I_x = \frac{4A_0^2}{\oint \dfrac{\mathrm{d}s}{t}} \tag{13.68}$$

Eq. $(13.68)_2$ is known as BREDT's 2nd equation.

Example 13.10 Reinforced concrete box girder

The task is to determine the torsion constant and the warping function $u(y,z)$ for the reinforced concrete box girder shown in Fig. 13.27.

Putting $A_0 = 4.8 \cdot 2.1 = 10.08\,\mathrm{m}^2$, then according to Fig. 13.27(b), eq. $(13.68)_2$ results in

$$I_x = \frac{4 \cdot 10.08^2}{2 \cdot \left(\dfrac{4.8}{0.3} + \dfrac{2.1}{0.4} \right)} = 9.563\ \mathrm{m}^4$$

Using $(13.56)_1$, with $y = 2.4\,\mathrm{m}$, $z = 1.05\,\mathrm{m}$ and $t_f = 0.3\,\mathrm{m}$, then initially

$$\frac{\tau_{yx}}{G} = -\frac{I_x \vartheta}{2A_0 t_f} = -1.581\ \mathrm{m} \cdot \vartheta$$

and consequently the following for the bottom flange of the box girder:

$$\frac{\partial u}{\partial y} = (-1.581\ \mathrm{m} + 1.05\ \mathrm{m}) \cdot \vartheta = -0.531\ \mathrm{m} \cdot \vartheta$$

Using $u(0, 1.05) = 0$ therefore results in a warping of $-0.531 \cdot 2.4 = -1.275\,\mathrm{m}^2 \cdot \vartheta$ at cross-section corner (2.4, 1.05).

Similarly, $(13.56)_2$, with $t_w = 0.4\,\mathrm{m}$, initially results in

$$\frac{\tau_{zx}}{G} = \frac{I_x \vartheta}{2A_0 t_w} = 1.186\ \mathrm{m} \cdot \vartheta$$

and consequently the following for the left-hand web of the box girder

$$\frac{\partial u}{\partial x} = (1.186\ \mathrm{m} - 2.4\ \mathrm{m}) \cdot \vartheta = -1.214\ \mathrm{m} \cdot \vartheta$$

which with $u(2.4, 0) = 0$ again leads to a warping of $-1.214 \cdot 1.05 = -1.275\,\mathrm{m}^2 \cdot \vartheta$ at the corner of the cross-section.

Fig. 13.27(c) illustrates the warping function. We simply change the sign in the above calculations in order to obtain the figures for the top flange and the right-hand web.

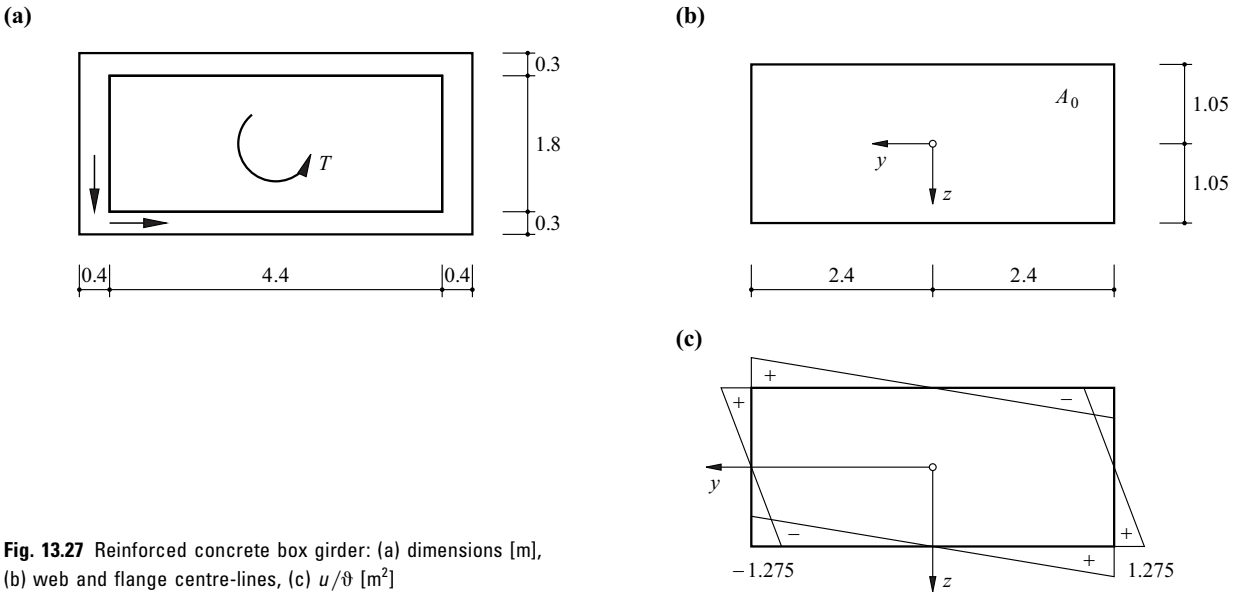

Fig. 13.27 Reinforced concrete box girder: (a) dimensions [m], (b) web and flange centre-lines, (c) u/ϑ [m^2]

Example 13.11 Twin-cell box girder

The box girder of example 13.10 is strengthened on one side with a further cell, see Fig. 13.28(a). How does this affect the torsion constant?

Different shear flows $S_1 = \Phi_1$ and $S_2 = \Phi_2$ ensue in the two cells. This gives rise to a shear flow $S_1 - S_2$ in the central web, in the direction shown in Fig. 13.28(b). Formulating (13.67) for each of the two cells results in

$$S_1\left(\frac{2\cdot 4.8}{0.3}+\frac{2.1}{0.4}\right)+(S_1-S_2)\frac{2.1}{0.4}=2G\cdot 4.8\ \text{m}\cdot 2.1\ \text{m}\cdot\vartheta$$

$$S_2\left(\frac{2\cdot 2.8}{0.3}+\frac{2.1}{0.4}\right)-(S_1-S_2)\frac{2.1}{0.4}=2G\cdot 2.8\ \text{m}\cdot 2.1\ \text{m}\cdot\vartheta$$

from which it follows that $S_1 = 0.536\,\text{m}^2 G\vartheta$, $S_2 = 0.500\,\text{m}^2 G\vartheta$. Consequently,

$$T = 2(0.536\cdot 4.8\cdot 2.1 + 0.500\cdot 2.8\cdot 2.1)\ \text{m}^4 G\vartheta = GI_x\vartheta$$

i. e. $I_x = 16.684\,\text{m}^4$. This value is only 0.16 % larger than the torsion constant

$$I_x=\frac{4\cdot(7.6\cdot 2.1)^2}{2\cdot\left(\frac{7.6}{0.3}+\frac{2.1}{0.4}\right)}=16.658\ \text{m}^4$$

of a box girder widened by a similar amount but without a central web.

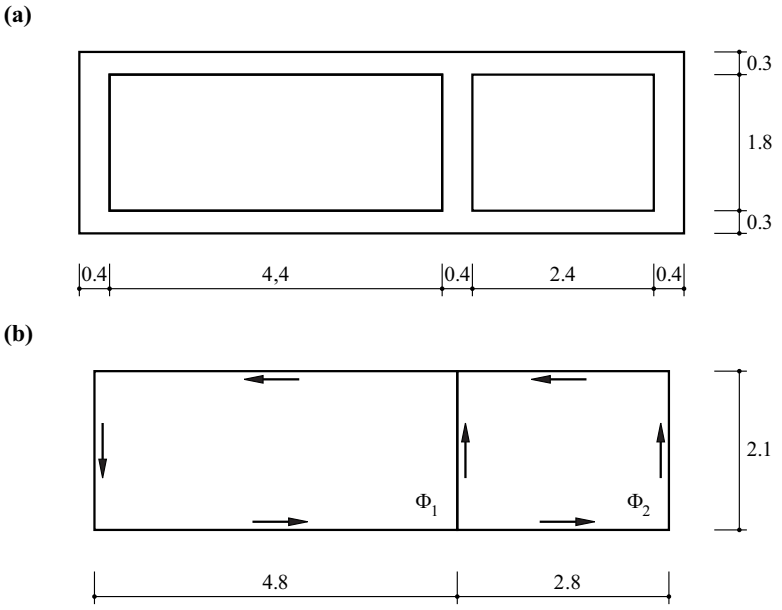

Fig. 13.28 Twin-cell box girder: (a) dimensions [m], (b) shear flows

To conclude this section on thin-wall hollow cross-sections, we need to look at a special instance that is particularly interesting in terms of construction technology. *Triangular cross-sections*, as shown in Fig. 13.29, are stable forms in themselves; they require no transverse bracing, plates or frames in order to maintain their cross-sectional form.

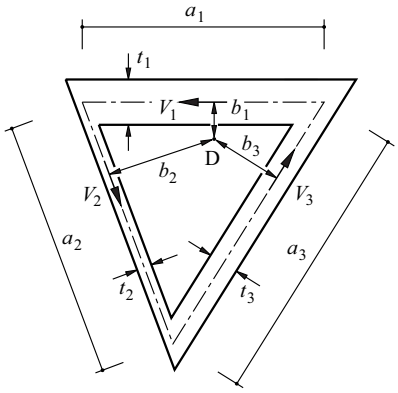

Fig. 13.29 Triangular cross-section subjected to torsion

The in-plane forces V_i must be proportional to the lengths of the sides a_i so that equilibrium of forces prevails in the section, i. e.

$$V_i = Sa_i \tag{13.69}$$

where S = const = shear flow. With distances b_i to the fulcrum D and a rotation φ_x, the plates displace by $b_i\,\varphi_x$. This leads to shear strains $\gamma_i = b_i\,\mathrm{d}\varphi_x/\mathrm{d}x$ which must be equal to $\tau_i/G = S/(t_iG)$. Therefore, it follows that

$$b_it_i = \text{const} \tag{13.70}$$

and hence the position of D is found.

The resulting torque is

$$T = \sum_{i=1}^{3} b_iV_i = \sum_{i=1}^{3} b_ia_it_i\tau_i = \vartheta G\sum_{i=1}^{3} a_ib_i^2t_i = GI_x\vartheta \tag{13.71}$$

For a triangular cross-section made up of three identical plates, where $a_i = a$ = const and $t_i = t$ = const, the result is, for example, $b_i = b = a\sqrt{3}/6$ and $I_x = a^3t/4$.

13.4.4 Warping torsion

13.4.4.1 Rotation of an I beam

If an I section is rotated by an amount φ_x as shown in Fig. 13.30(a), its two flanges are displaced by $v = \pm\varphi_x\,d/2$ in the y direction, which causes flange bending moments $M_f = -EI_f\,\mathrm{d}^2v/\mathrm{d}x^2$ (about the z axis) and corresponding flange shear forces $V_f = \mathrm{d}M_f/\mathrm{d}x$ (in the y direction). A very good approximation is to take the bending stiffness of the flange EI_f to be equal to half the bending stiffness EI_z of the section. Therefore,

$$V_f = -\frac{EI_zd}{4}\cdot\frac{\mathrm{d}^3\varphi_x}{\mathrm{d}x^3}$$

and the *warping torsional moment*

$$T_w = -\frac{EI_zd^2}{4}\cdot\frac{\mathrm{d}^3\varphi}{\mathrm{d}x^3} = -EI_\omega\frac{\mathrm{d}^3\varphi}{\mathrm{d}x^3} \tag{13.72}$$

corresponds to the couple $V_f\,d$. In addition, the *pure torsional moment*

$$T_s = GI_x\frac{\mathrm{d}\varphi_x}{\mathrm{d}x} \tag{13.73}$$

acts with the pure torsional stiffness GI_x determined according to (13.64). Where $T = T_w + T_s$ and $m_x = -\mathrm{d}T/\mathrm{d}x$, according to (8.30), the outcome is the differential equation

$$GI_x\cdot\frac{\mathrm{d}^2\varphi_x}{\mathrm{d}x^2} - EI_\omega\cdot\frac{\mathrm{d}^4\varphi_x}{\mathrm{d}x^4} + m_x = 0 \tag{13.74}$$

with the general solution

$$\varphi_x = c_1 + c_2x + c_3\cosh(\lambda x) + c_4\sinh(\lambda x) + \varphi_{\text{part}} \tag{13.75}$$

where

$$\lambda^2 = \frac{GI_x}{EI_\omega} \tag{13.76}$$

It should be noted that the stress distributions (apart from T) shown in Fig. 13.30(b) correspond to a residual stress state; $N = M_y = M_z = V_y = V_z = 0$ applies.

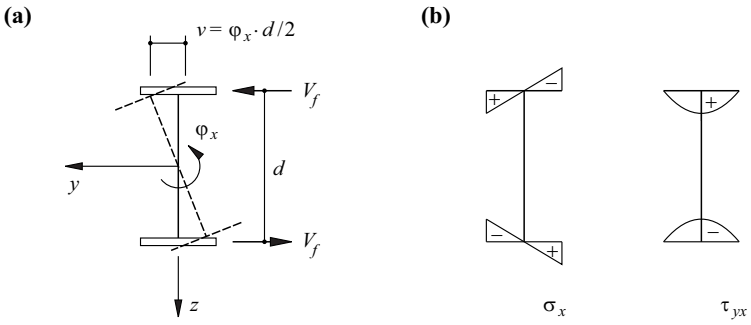

Fig. 13.30 Rotation of an I section: (a) designations, (b) stress distributions

Example 13.12 Twisted I beam – concentrated load

An I beam of length l is loaded at its centre by a couple Qd, see Fig. 13.31. The support at each end of the beam corresponds to a *fork support*, i. e. the flanges are restrained in the y direction, but the cross-section can warp without restraint in the x direction.

For reasons of symmetry, we can confine our investigation to one half of the beam ($0 \le x \le l/2$). Neither rotations nor flange bending moments can occur at the end of the beam, i. e. $\varphi_x = d^2\varphi_x/dx^2 = 0$ applies when $x = l/2$. At point $x = 0$, symmetry demands that $d\varphi_x/dx = 0$, and $T = T_w + T_s = -Qd/2$ applies for every point x, where T_w and T_s are in accord with (13.72) and (13.74) respectively. These conditions lead to $c_2 = -Qd/(2GI_x)$, $c_1 = -c_2 l/2$, $c_3 = (c_2/\lambda)\tanh(\lambda l/2)$, $c_4 = -c_2/\lambda$ and

$$T_w = -\frac{Qd}{2} \cdot \frac{\cosh\left[\lambda\left(\frac{l}{2} - x\right)\right]}{\cosh\left(\lambda\frac{l}{2}\right)}$$

see Fig. 13.31. In the middle of the beam, T is fully resisted by T_w, and depending on the magnitude of λ, a certain pure torsional moment T_s develops between here and the end of the beam.

If we ignore, for example, the roundings at the web-flange transitions of the rolled HEB 300 section examined in example 13.6 (Fig. 13.17), which are the outcome of the manufacturing process and reduce the shear stresses due to pure torsion, then the result is $I_z = 85.529 \cdot 10^6\,\text{mm}^4$, and using (13.64), then $I_x = 1.488 \cdot 10^6\,\text{mm}^4$. Where $\nu = 0.3$ and $d = 281\,\text{mm}$ and we consider (7.2), then (13.76) results in $\lambda^2 = 0.3390\,\text{m}^{-2}$. With a beam length $l = 3\,\text{m}$, we thus get a warping torsion component of $T_w/T = 1/\cosh(\lambda l/2) = 71.1\,\%$ at the end of the beam; with $l = 6\,\text{m}$ this is still 33.8 %.

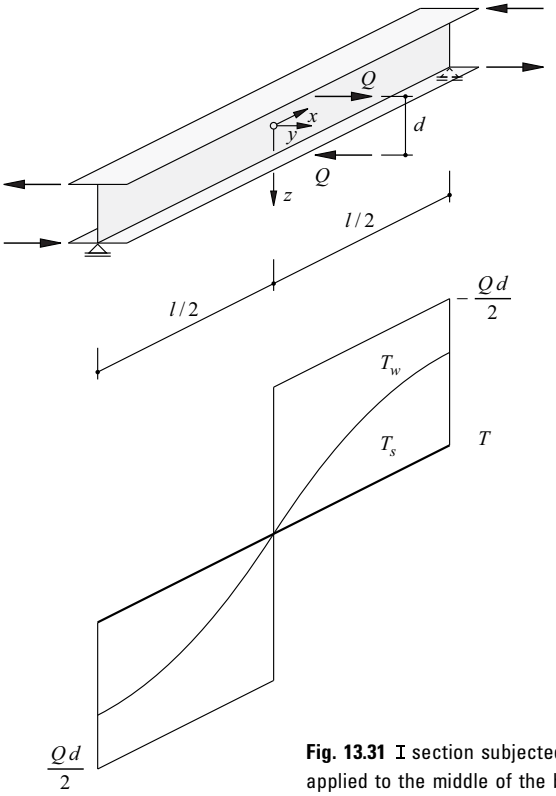

Fig. 13.31 I section subjected to a couple Qd applied to the middle of the beam

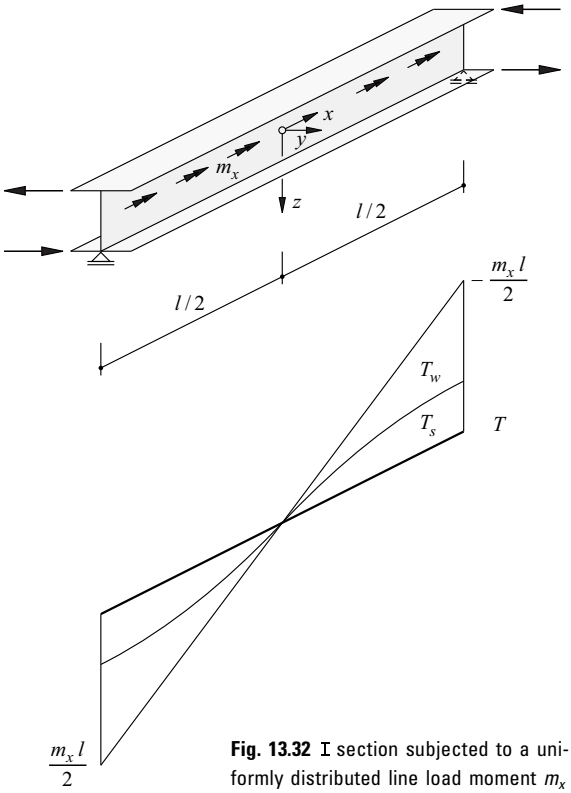

Fig. 13.32 I section subjected to a uniformly distributed line load moment m_x

Example 13.13 Twisted I beam – distributed load

If instead of a couple in the middle of the beam we apply a line load moment m_x uniformly distributed over the length of the beam of example 13.12 (see Fig. 13.32), the only condition that changes is $T_w + T_s = -x m_x$. We get

$$\varphi_x = \frac{m_x}{GI_x}\left[\left(\frac{\cosh(\lambda x)}{\cosh(\lambda l/2)} - 1\right) \cdot \lambda^{-2} - \frac{1}{2}\left(x^2 - \frac{l^2}{4}\right)\right]$$

and

$$T_w = -\frac{m_x}{\lambda} \cdot \frac{\sinh(\lambda x)}{\cosh(\lambda l/2)}$$

13.4.4.2 Bending and rotation of C sections

The C section already examined in section 13.3.4 will be analysed in more depth below.

Under bending M_y about the y axis, the C section shown in simplified form in Fig. 13.33(a) exhibits the distribution of normal stresses σ_x shown in Fig. 13.33(b), provided the associated shear force V_z passes through the shear centre M. At cross-section corner 2 the first moment of area $S = bcd/2$, i. e. the maximum shear stress occurring in the flange is $\tau_{yx,\max} = V_z bd/(2I_y)$ according to (13.37).

Consequently, $V_f = V_z b^2 cd/(4I_y)$, and (13.49) results in

$$a = \frac{b^2 c\, d^2}{4I_y} \tag{13.77}$$

where $I_y = d^3 e/12 + bcd^2/2$.

When a C section is subjected to a pure torque T, its flanges experience shear forces $V_f = T/d$ and associated bending moments M_f (about the z axis). If we imagine the section separated along edges 2 and 3, M_f in the flanges at 1 and 2 as well as 3 and 4 give rise to longitudinal stresses $\sigma_x = \mp 6M_f/(b^2 c)$.

In order to attain compatibility between the unstressed web and the two flanges, edge forces $\pm F$ acting on the web are introduced at 2 and 3, which act in the opposite direction on the adjoining flange. This results in the boundary stresses $\sigma_{x2w} = -\sigma_{x3w} = 6F/(de)$ in the web and boundary stresses $\sigma_{x2f} = -\sigma_{x3f} = -4F/(bc)$ and $\sigma_{x1f} = -\sigma_{x4f} = 2F/(bc)$ in the flanges. Compatibility at 2 or 3 requires

$$\frac{6M_f}{b^2 c} - \frac{4F}{bc} = \frac{6F}{de}$$

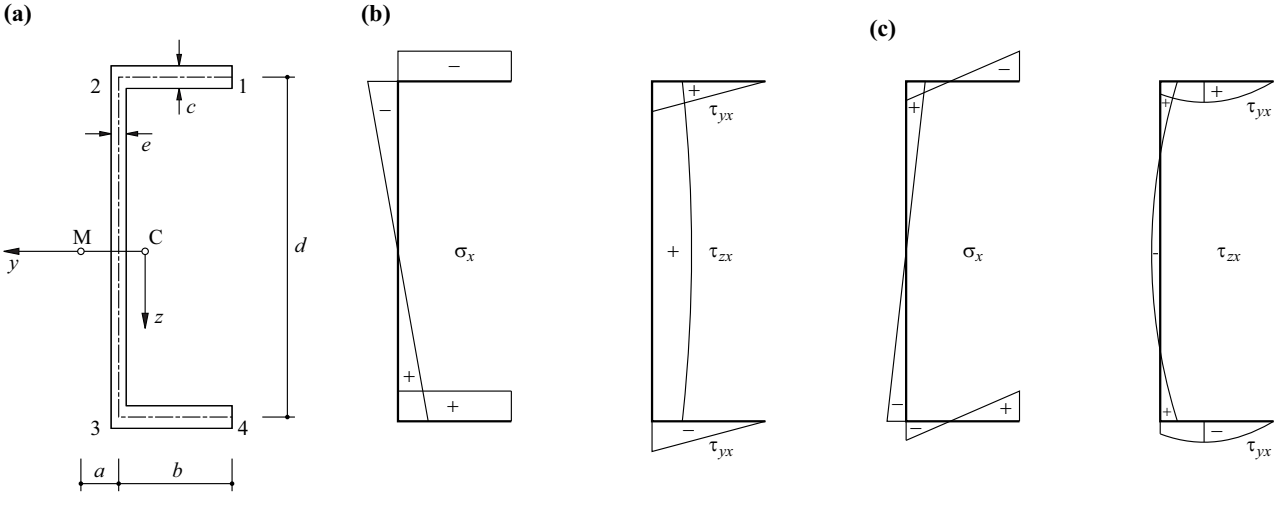

Fig. 13.33 C section: (a) notation, (b) stress distribution due to bending about the y axis, (c) stress distribution due to T_w

and therefore

$$F = \frac{3M_f de}{3b^2c + 2bde}$$

The boundary stresses are

$$\sigma_{x1} = -\sigma_{x4} = -\frac{6M_f}{b^2c} + \frac{2F}{bc} = -\frac{6M_f(3bc + de)}{b^2c(3bc + 2de)}$$

$$\sigma_{x2} = -\sigma_{x3} = \frac{6M_f}{b^2c} - \frac{4F}{bc} = \frac{18M_f bc}{b^2c(3bc + 2de)}$$

With a flange curvature of

$$\chi_f = \frac{\sigma_{x2} - \sigma_{x1}}{Eb} = -\frac{d}{2}\frac{\mathrm{d}^2\varphi_x}{\mathrm{d}x^2}$$

the result is

$$-\frac{\mathrm{d}^2\varphi_x}{\mathrm{d}x^2} = \frac{12M_f(6bc + de)}{Eb^3cd(3bc + 2de)}$$

and therefore owing to $V_f = \mathrm{d}M_f/\mathrm{d}x$ and $T_w = V_f d$,

$$T_w = -\frac{Eb^3cd^2(3bc + 2de)}{12(6bc + de)} \cdot \frac{\mathrm{d}^3\varphi_x}{\mathrm{d}x^3} = -EI_\omega \cdot \frac{\mathrm{d}^3\varphi_x}{\mathrm{d}x^3} \tag{13.78}$$

which is similar to (13.72).

The displacements v, w of the flange and the web in the y or z direction result from the rotation φ_x about the shear centre M at a distance a from the web on the y axis: $v = \pm d\varphi_x/2$, $w = -a\varphi_x$. However, these displacements are also proportional to the corresponding curvatures; we get

$$\frac{v}{w} = \frac{(\sigma_{x2} - \sigma_{x1})d}{(\sigma_{x3} - \sigma_{x2})b} = -\frac{d}{b}\left(1 + \frac{de}{6bc}\right) = -\frac{d}{2a}$$

for corner 2 of the cross-section, which confirms (13.77). The shear centre M is therefore not only the point of application of the shear force for bending without rotation, but also the fulcrum for rotation without bending. This reciprocity can be easily verified with MAXWELL's theorem (8.88) by applying a unit shear force through the shear centre or a unit torque; the associated rotation or the associated displacement of the shear centre are identical and both disappear.

The normal and shear stresses caused by T_w are shown in Fig. 13.33(c). Again, $N = M_y = M_z = V_y = V_z = 0$. We should also note that the zero points of the stresses σ_x (and hence the maxima of stresses τ_{yx}, too) in both flanges are at the same distance a from the web as the shear centre M.

13.4.4.3 General thin-wall cross-sections

Fig. 13.34(a) shows a general thin-wall cross-section with centroid C, principal axes y, z and shear centre M. The position along the centre-line of the cross-section and the thickness of the cross-section are denoted with s and $t(s)$ respectively. The following applies for the distances ρ and ρ_0 from the centroid or the shear centre respectively to the tangent to the centre-line of the cross-section at s:

$$\rho_0 = \rho + y_M \sin\alpha + z_M \cos\alpha \tag{13.79}$$

The shear strain $\gamma_{xs} = \partial u/\partial s + r\vartheta$ was used in deriving equation (13.67) for thin-wall hollow cross-sections. Here, r is replaced by ρ_0, and it is assumed that γ_{xs} is equal to zero, i. e.

$$\mathrm{d}u = -\frac{\rho_0\,\mathrm{d}\varphi_x}{\mathrm{d}x}\mathrm{d}s = -\rho_0\vartheta\,\mathrm{d}s$$

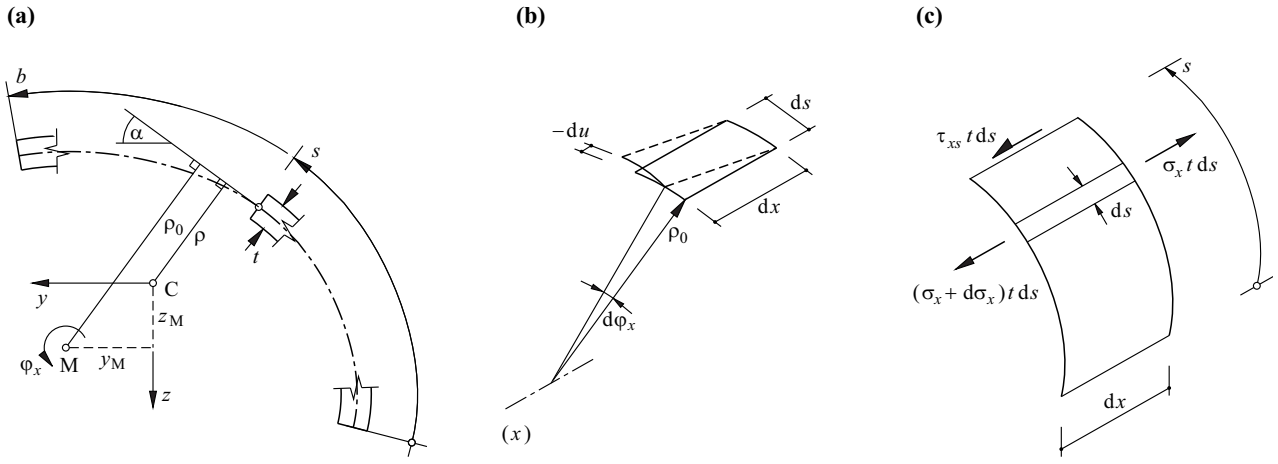

Fig. 13.34 Warping torsion of general thin-wall cross-sections: (a) notation, (b) $\gamma_{xs} \equiv 0$, (c) warping stresses and warping shear stresses

see Fig. 13.34(b). Therefore,

$$u = -\vartheta \int_0^s \rho_0 \, \mathrm{d}s + f(x) \tag{13.80}$$

applies. Using (13.79), $\mathrm{d}y = \mathrm{d}s\cos\alpha$ and $\mathrm{d}z = -\mathrm{d}s\sin\alpha$, we obtain the expression

$$\omega_0 = \int_0^s \rho_0 \, \mathrm{d}s = \int_0^s \rho \, \mathrm{d}s - y_\mathrm{M}(z - z_0) + z_\mathrm{M}(y - y_0) \tag{13.81}$$

for the integral in (13.80), the *warping* with respect to M, i. e. with the warping

$$\omega = \int_0^s \rho \, \mathrm{d}s \tag{13.82}$$

with respect to C

$$\omega_0 = \omega - y_\mathrm{M}(z - z_0) + z_\mathrm{M}(y - y_0) \tag{13.83}$$

The normal strains

$$\varepsilon_x = \frac{\partial u}{\partial x} = -\frac{\mathrm{d}\vartheta}{\mathrm{d}x}\omega_0 + \frac{\mathrm{d}f}{\mathrm{d}x}$$

result in the stresses

$$\sigma_x = E\varepsilon_x = E(f' - \omega_0\vartheta') \tag{13.84}$$

where here and from now on a superscript dash ($'$) indicates differentiation with respect to x.

The unknowns f, y_M, z_M follow from the residual stress condition $N = M_y = M_z = 0$:

$$N = \int_0^b \sigma_x t \, \mathrm{d}s = E(f' \int_0^b t \, ds - \vartheta' \int_0^b \omega_0 t \, \mathrm{d}s) = 0$$

$$M_y = \int_0^b \sigma_x z t \, \mathrm{d}s = E\,[f' \int_0^b z t \, \mathrm{d}s - \vartheta'(\int_0^b \omega z t \, \mathrm{d}s - y_\mathrm{M} \int_0^b z^2 t \, \mathrm{d}s + z_\mathrm{M} \int_0^b y z t \, \mathrm{d}s)] = 0$$

$$-M_z = \int_0^b \sigma_x y t \, \mathrm{d}s = E\,[f' \int_0^b y t \, \mathrm{d}s - \vartheta'(\int_0^b \omega y t \, \mathrm{d}s - y_\mathrm{M} \int_0^b y z t \, \mathrm{d}s + z_\mathrm{M} \int_0^b y^2 t \, \mathrm{d}s)] = 0$$

Owing to

$$A = \int_0^b t \, ds$$

the first of these equations together with (13.84) leads to

$$\sigma_x = E\vartheta' \left(\frac{1}{A} \int_0^b \omega_0 t \, ds - \omega_0 \right) = E\vartheta' \omega_n \tag{13.85}$$

where ω_n designates the *unit warping* with respect to M. Owing to

$$\int_0^b yt \, ds = \int_0^b zt \, ds = \int_0^b yzt \, ds = 0$$

the second and third equations are simplified to

$$y_M = \frac{\int_0^b \omega z t \, ds}{\int_0^b z^2 t \, ds} = \frac{I_{\omega z}}{I_y} \quad , \quad z_M = -\frac{\int_0^b \omega y t \, ds}{\int_0^b y^2 t \, ds} = -\frac{I_{\omega y}}{I_z} \tag{13.86}$$

The *warping shear stresses* $\tau_{xs} = \tau_{sx}$ correspond to the *warping stresses* σ_x according to (13.85). Equilibrium of forces in the x direction for the free body shown in Fig. 13.34(c) calls for

$$\tau_{xs} \cdot t(s) \, ds + \int_0^s d\sigma_x t \, ds = 0$$

Using (13.85) and the shortened form

$$S_\omega(s) = \int_0^s \omega_n t \, ds \tag{13.87}$$

this leads to

$$\tau_{xs} = -\frac{E S_\omega(s)}{t(s)} \vartheta'' \tag{13.88}$$

The warping torsional moment

$$T_w = -E\vartheta'' \int_0^b \rho_0 S_\omega \, ds$$

results from the shear flow $\tau_{sx} t = -ES_\omega \vartheta''$. According to (13.81) and (13.85), $\rho_0 = -d\omega_n / ds$. Further, according to (13.87), $dS_\omega / ds = \omega_n t$. Integration by parts of the equation for T_w thus results in

$$T_w = E\vartheta'' \left(\omega_n S_\omega \Big|_0^b - \int_0^b \omega_n^2 t \, ds \right)$$

The first term in the brackets disappears because $S_\omega(0) = S_\omega(b) = 0$. What remains is

$$T_w = -E\vartheta'' \int_0^b \omega_n^2 t \, ds = -EI_\omega \vartheta'' \tag{13.89}$$

where I_ω is the *warping constant*.

By introducing the *bimoment*

$$M_\omega = EI_\omega \vartheta' \tag{13.90}$$

eq. (13.89) then results in

$$T_w = -M_\omega' \tag{13.91}$$

and using (13.85) and (13.88), we get the equations

$$\sigma_w = \frac{M_\omega \omega_n}{I_\omega} \quad , \quad \tau_w = \frac{T_w S_\omega}{t I_\omega} \tag{13.92}$$

which are similar to (13.16) and (13.37).

Example 13.14 Reinforced concrete beam

The reinforced concrete beam shown in section in Fig. 13.35(a) has a span of $l = 30\,\text{m}$ and like the I beam examined in example 13.13 is subjected to a constant line load moment $m_x = 4.8\,\text{m} \cdot 20\,\text{kN/m} = 96$ kNm/m. The lower ends of web plates 1 and 3 are restrained in the z direction at the ends of the beam. We shall not look at the loads and support force variables in the x and y directions here, nor the static indeterminacy as a result of the redundant fourth support in the z direction. Furthermore, we shall work with the concrete cross-sectional values only and assume that $E = 30\,\text{kN/mm}^2$ and $\nu = 0.2$, i. e. $G = 12.5\,\text{kN/mm}^2$, see (7.2).

Fig. 13.35(b) shows the position of centroid C and shear centre M with $a = 0.9\,\text{m}$ according to (13.77). Instead of continuing directly with (13.78) and the corresponding equations for the boundary stresses in the plates etc. for C sections, we shall in this case use the equations derived above for general thin-wall cross-sections.

Eq. (13.82) initially results in the ω distribution shown in Fig. 13.35(c). Eq. $(13.86)_2$ gives us $I_{\omega y} = 16.5888\,\text{m}^5$, and using $I_z = 11.0592\,\text{m}^4$, it follows from $(13.86)_1$ that $z_M = -1.5\,\text{m}$, which means that ω_0 is determined according to (13.83). Eq. (13.85) provides ω_n and thus S_ω is given according to (13.87). Finally, we apply (13.89) to obtain the warping constant $I_\omega = 6.9673\,\text{m}^6$; eq. (13.78) can be used to reach the same figure.

Fig. 13.35(e) shows the diagrams of the functions φ_x, $T = T_s + T_w$ and M_ω for the beam half of Fig. 13.35(d), which result from example 13.13. Apart from the variables E, G, I_ω, l and m_x already given, we also use $I_x = (2 \cdot 2.4 + 4.8)(0.3)^3/3 = 0.0864\,\text{m}^4$ according to (13.64) here. Eq. (13.76) leads to $\lambda^{-1} = 13.912\,\text{m}$. We get

$$\varphi_x(0) = \frac{0.096}{12.5 \cdot 10^3 \cdot 0.0864} \cdot \left[\left(\frac{1}{\cosh\left(\frac{15}{13.912}\right)} - 1 \right) 13.912^2 + \frac{30^2}{8} \right] = 3.3 \text{ mrad}$$

for the rotation at $x = 0$ and

$$T_w(15\text{ m}) = -96 \cdot 13.912 \cdot \tanh\left(\frac{15}{13.912}\right) = -1058 \text{ kNm}$$

for the warping torsional moment at $x = l/2$. Finally, the result for the bimoment at mid-span is

$$M_\omega(0) = (13.912)^2 \cdot 0.096 \left[\frac{1}{\cosh\left(\frac{15}{13.912}\right)} - 1 \right] = -7.25 \text{ MNm}^2$$

Using the values given here, we apply (13.92) to obtain the warping stresses at mid-span, see Fig. 13.35(f), and the warping shear stresses at the end of the beam $x = l/2$, see Fig. 13.35(g). The rotation $\varphi_x(0)$ results in deflections of plates 2 and 3 at mid-span amounting to $\mp 3.3 \cdot 2.4 = \mp 7.9\,\text{mm}$. Fig. 13.35(h) shows free body diagrams for the beam half resolved into its individual plates. According to example 13.9, boundary shear stresses at the inner edge of the cross-section ($z = b/2$) amounting to

$$\frac{3 \cdot 0.382}{(2.4 + 4.8 + 2.4) \cdot 0.3^2} = 1.326 \text{ N/mm}^2$$

and hence according to $(5.16)_3$ twisting moments of

$$1326 \cdot \frac{(0.3)^2}{6} = 19.9 \text{ kNm/m}$$

which, as discussed in section 8.26, Fig. 8.8(c), can be replaced by statically equivalent corner forces of $2 \cdot 19.9 = 39.8\,\text{kN}$, correspond to the pure torsional moment $T_s = -1440 + 1058 = -382\,\text{kNm}$ at the end of the beam.

From T_w we get shear forces in plates 1 and 3 amounting to $1058/4.8 = 220.4\,\text{kN}$ at the end of the beam. The positive and negative shear flows in slab 2 cancel each other out, see Fig. 13.35(g).

The warping stresses illustrated in Fig. 13.35(f) lead to tensile and compressive forces at $x = 0$ amounting to $2.25 \cdot 0.3 \cdot 0.9/2 = 0.304\,\text{MN}$ and $3.75 \cdot 0.3 \cdot 1.5/2 = 0.844\,\text{MN}$ in webs 1 and 3 as well as $2.25 \cdot 0.3 \cdot 2.4/2 = 0.810\,\text{MN}$ in slab 2.

Longitudinal shear forces $s(x)$, shear forces $q(x)$ and transverse bending moments $r(x)$ are transferred between the webs and the slab.

The longitudinal shear forces s progress proportional to T_w, i. e. proportional to $\sinh(\lambda x)$. Their integral between $x = 0$ and $x = 15\,\text{m}$ is 540 kN. This, together with forces of 304 kN or 844 kN, leads to equilibrium of forces in the x direction in webs 1 and 3. In slab 2, we also get equilibrium of moments about the z axis together with the forces of 810 kN plus equilibrium of forces in the x direction.

The shear forces q progress proportional to T_w', i. e. proportional to $\cosh(\lambda x)$. Their integral is 220.4 kN and their centroid of forces occurs at $x = 8.15\,\text{m}$. This leads to equilibrium of forces in the z direction in webs 1 and 3 as well as equilibrium of moments about the y axis.

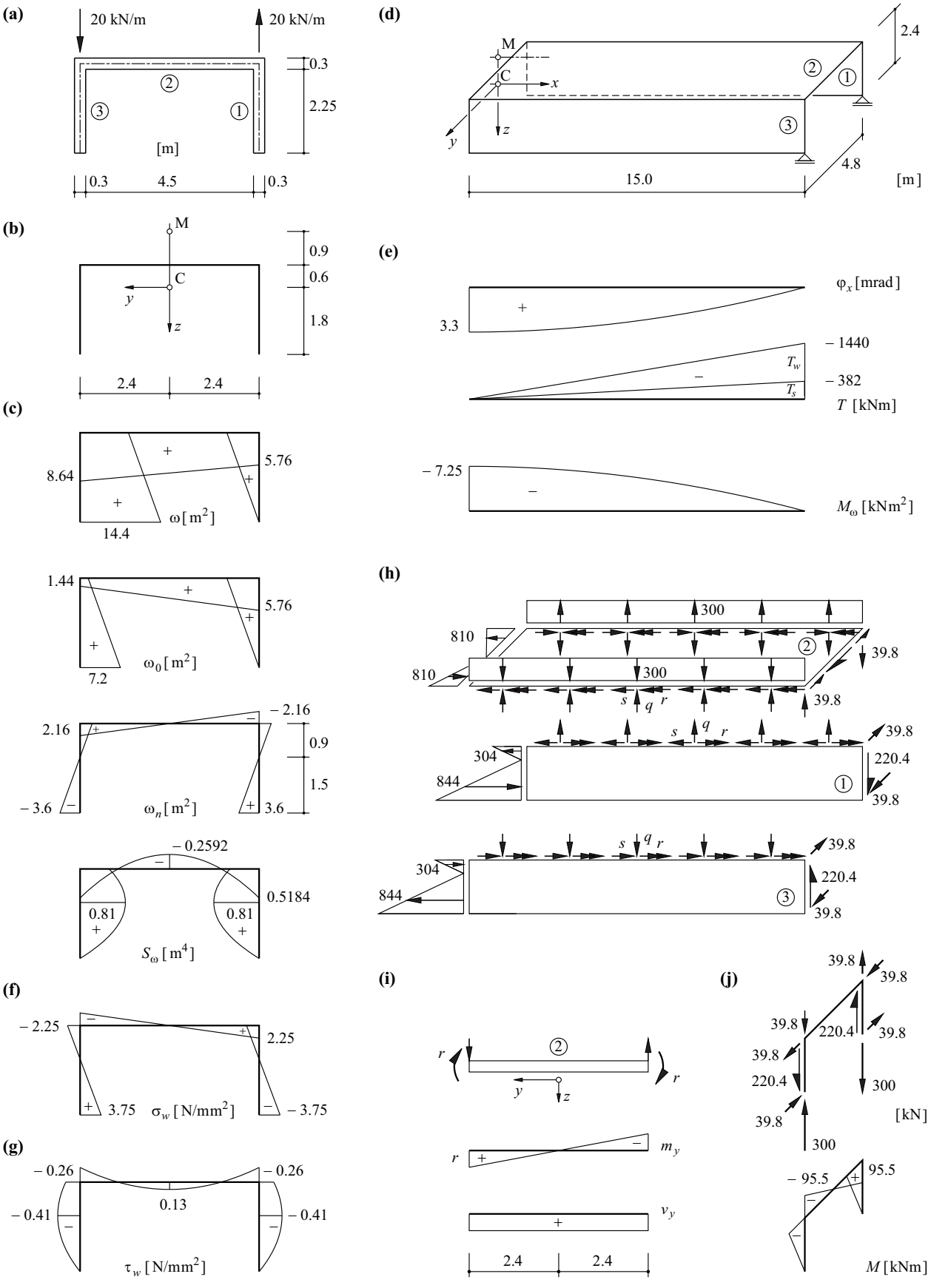

Fig. 13.35 Reinforced concrete beam subjected to a line load moment m_x = 96 kNm/m: (a) section, (b) centroid and shear centre, (c) basic values, (d) beam half, (e) rotation, torque and bimoment, (f) warping stresses at x = 0, (g) warping shear stresses at x = 15 m, (h) forces and moments acting on the plates of the cross-section, (i) transverse bending in slab, (j) stress resultants in transverse end frame

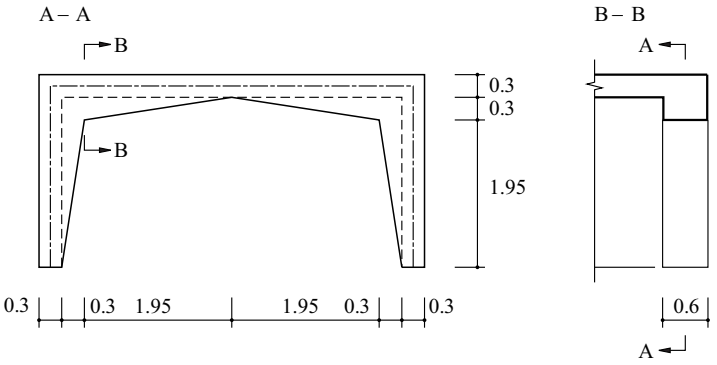

Fig. 13.36 Transverse end frame (dimensions in m)

The transverse bending moments r add up to $2.4 \cdot 39.8 = 95.5\,\text{kNm}$, i. e. webs 1 and 3 are in equilibrium with respect to moments about the x axis. In slab 2, the transverse bending moments r correspond to shear forces $v_y = r/(2.4\,\text{m})$ and moments $m_y = v_y \cdot y$, see Fig. 13.35(i); this slab loadbearing effect leads to part (39.8 kN in total) of the line loads of $15 \cdot 20 = 300\,\text{kN}$ applied to both edges of the slab being placed directly in equilibrium.
The transverse end frame is stressed according to Fig. 13.35(j). Corner moments amounting to $2.4 \cdot 39.8 = 95.5\,\text{kNm}$ ensue. Fig. 13.36 shows one possible constructional configuration for the transverse end frame.

Up until now we have only considered non-branched cross-sectional forms. If branchings are present, e. g. due to cantilevers, flanges or other attached cross-sectional parts, the considerations hitherto can be easily generalised, see Fig. 13.37. In the example, the ⊓ section on the left is modified by cantilevering slabs to form the ⊓⊓ section on the right. Both centroid C and shear centre M shift somewhat closer to the web. The ω diagram of the ⊓⊓ section is drawn in a similar way to the ⊓ section by continuing the drawing at the branching points accordingly for the cantilevers. The diagrams for ω_0, ω_n and S_ω can then be drawn without difficulty. The S_ω diagram shows us the magnitudes and directions of the shear flows that guarantee $V_y = V_z = 0$.

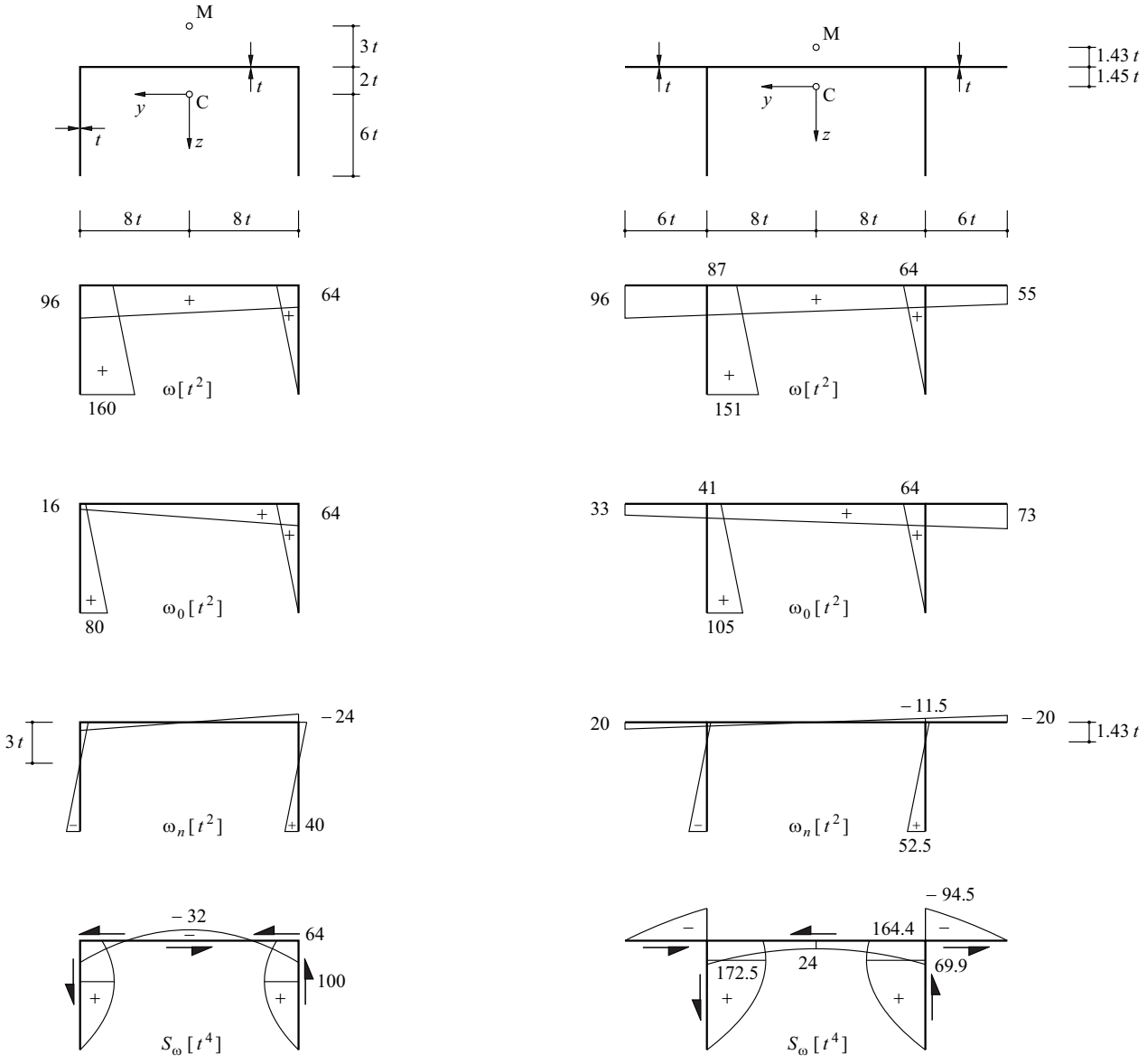

Fig. 13.37 How cantilevers affect the basic warping torsion values

13.5 Summary

1. The relationships between the stress resultants and the corresponding deformation variables of framed structures, already introduced in chapter 8, have been explored in detail. In doing so, it was assumed that the material behaviour is linear elastic and isotropic, and that first-order theory applies.
2. As an approximation, a uniaxial stress state plus bar cross-sections that remain plane and perpendicular to the deformed bar axis may be assumed for bars subjected to bending and normal force.
3. A cross-section generally has two principal axes at right-angles to each other which pass through the centroid of the section and have associated maximum or minimum moments of inertia. In the case of pure bending, the bending moment vector lies on a principal axis and the bar bends perpendicular to the direction of the bending moment vector. In the case of skew bending, the bending moment vector does not lie on a principal axis and the bar does not bend perpendicular to the direction of the bending moment vector. The principal moments of inertia

coincide for regular polygonal and circular cross-sections and every axis passing through the centroid is a principal axis.

4. The transformation of moments and products of inertia can be displayed graphically with the help of MOHR's circles in a similar way to stress and strain transformations.
5. When calculating the stresses for bending and normal forces, it is often expedient to assume an eccentric normal force statically equivalent to the stress resultants. If this force acts within the kern of the cross-section, the neutral axis of the normal stresses lies outside the cross-section, otherwise the neutral axis intersects the cross-section.
6. We use transformed section properties when composite cross-sections are involved, which means the area elements are multiplied by the associated modular ratios n (stiffnesses related to the basic material).
7. Deformations caused by temperature, shrinkage and swelling can be dealt with in a consistent way by considering the respective load-independent strains. In general, residual stress states over the cross-section are the result.
8. A number of computer programs and design tables are available for calculating the stresses and deformations of bar cross-sections subjected to bending and normal forces.
9. We can use (13.37) to approximate the shear stress distribution caused by shear forces in prismatic bars subjected to pure bending. The area shear factor $\alpha_v = A_v/A$ must be taken into account when calculating the shear stiffness GA_v (see appendix A4).
10. It is also possible to use (13.37) for calculating shear stresses due to shear forces in thin-wall sections provided the corresponding sections are perpendicular to the segments of the cross-section. In the case of asymmetric cross-sections, it is often better to work with axes parallel with the segments of the cross-section instead of the principal axes, and to use (13.47).
11. The normal stress distribution and deformation assumed for normal bending theory can only occur when the resulting shear force passes through the shear centre M of the cross-section. This is not only the point of application of the shear force for bending without rotation, but also the fulcrum for rotation without bending. The shear centre M can generally be obtained from the intersection of the resultants of the shear stresses for bending about the two principal axes.
12. The combined effect of pure torsion and warping torsion according to (13.74) must normally be considered when investigating torsion problems.
13. Pure torsion can generally be dealt with by using (13.61), with the associated shear stresses being obtained from (13.60). The stress function Φ can be displayed graphically with the help of the membrane analogy. This is done by considering an opening corresponding to the perimeter of the bar section with a membrane spanned across the opening with a small overpressure.
14. Eq. (13.64) results in a good approximation of the pure torsional stiffness of cross-sections that are made up of several narrow rectangles. BREDT's 2nd equation $(13.68)_2$ plays a similar role for thin-wall hollow cross-sections.
15. Box girders made up of three plates are stable in themselves. Their torsional stiffness is obtained from (13.71).
16. The rotation of I sections leads to flange bending moments and corresponding flange shear forces which correspond to a warping torsional moment. The rotation of C sections leads to similar, easily acquired relationships, although owing to the rotation about the shear centre lying outside the web, the web is bent as well as the two flanges. For general thin-wall cross-sections, we determine the shear centre (13.86) first of all, starting with the centroid and the principal axes and by introducing the warping (13.82), and then use (13.83) to obtain the unit warping (13.85) and the corresponding first (13.87) and second (13.89) moments. The warping stresses σ_w and the warping shear stresses τ_w then result – according to (13.92) – in a similar way to normal bending problems.

13.6 Exercises

13.1 Determine the centroid, principal axes y, z, principal moments of inertia I_y, I_z and kern of the cross-section shown in Fig. 13.38(a) (dimensions in mm).

13.2 The section shown in Fig. 13.38(b) (dimensions in mm) is used as a cantilever beam and loaded by the transverse force shown (components in kN). Determine the centroid, principal axes, principal moments of inertia and shear centre of the cross-section. Also determine the neutral axis for the normal stresses and the shear stress distribution over the cross-section.

13.3 Using a yield limit of $f_y = 235\,\mathrm{N/mm^2}$, calculate the bending moment M_η that leads to the onset of yielding of the idealised ⌜ cross-section shown in Fig. 13.38(c), which initially has no residual stresses.

13.4 Fig. 13.38(d) shows an I section (dimensions in mm) which initially has no residual stresses and is loaded by $N = -2\,\mathrm{MN}$, $V = 0.75\,\mathrm{MN}$ and $M = 0.75\,\mathrm{MNm}$. Calculate the stresses at A, B and C, and illustrate the corresponding stress states using MOHR's circles ($I_y = 1327 \cdot 10^6\,\mathrm{mm^4}$). When N, V and M are increased beyond the given values in proportion to each other, where is the yield limit reached and with which stress resultant (N, V, M)? Presume the VON MISES yield condition according to Fig. 7.8(c), with $f_y = 235\,\mathrm{N/mm^2}$

13.5 A 4 m long steel beam ($E = 210\,\mathrm{kN/mm^2}$, $\nu = 0.3$) with the square hollow cross-section shown in Fig. 13.38(e) (dimensions in mm) is subjected to a line load moment $m_x = 40\,\mathrm{kNm/m}$ constant over the length of the beam. Determine the rotation $\varphi_x(x)$. The transfer of the torques at the ends of the beam is via thin transverse end plates and does not need to be investigated further.

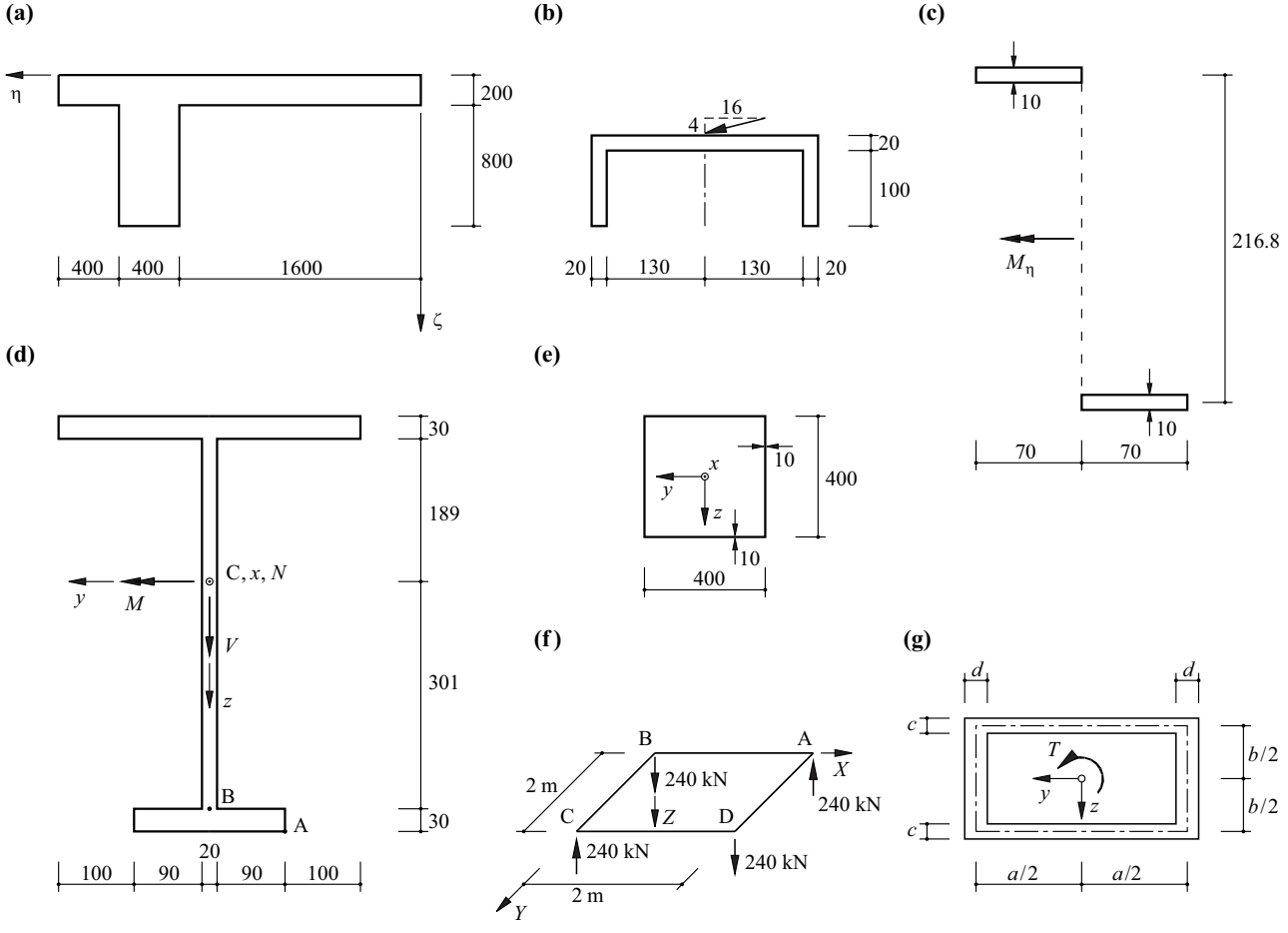

Fig. 13.38 Figures for section 13.6

13.6 The bottom flange of the section shown in Fig. 13.38(e) is sawn through in the $y = 0$ plane. Determine the shear centre as well as the values of ω_n, S_ω, I_ω and I_x.

13.7 Solve exercise 13.5 using the section of exercise 13.6. The transfer of the torques at the ends of the beam is similar to example 13.14 (via transverse end plates) and does not need to be investigated further.

13.8 The square frame ABCD in the XY plane shown in Fig. 13.38(f) is loaded by opposing forces of 240 kN applied at the corners and perpendicular to the plane of the frame. The frame is made up of four identical square hollow sections with a wall thickness of 6 mm and external dimensions of 106 mm ($E = 210\,\text{kN/mm}^2$, $\nu = 0.3$), which are welded together at the corners. Determine the positions, directions and magnitudes of the maximum principal stresses.

13.9 Show that the stress function

$$\Phi = \frac{8G\vartheta b^2}{\pi^3}\sum_{n=1}^{\infty}\frac{\sin(n\pi/2)\cos(n\pi z/b)}{n^3}\cdot\left[1-\frac{\cosh\left(\frac{n\pi y}{b}\right)}{\cosh\left(\frac{n\pi a}{2b}\right)}\right]$$

fulfils the boundary condition $\Phi = 0$ for a rectangular cross-section (side lengths a and b in y and z directions, $a \geq b$) and leads to

$$T = \frac{32G\vartheta b^3}{\pi^4}\sum_{n=1}^{\infty}\frac{\sin^2(n\pi/2)}{n^4}\cdot\left[a-\frac{2b}{n\pi}\tanh\left(\frac{n\pi a}{2b}\right)\right]$$

$$\approx \frac{G\vartheta a b^3}{3}\cdot\left[1-\frac{192b}{\pi^5 a}\tanh\left(\frac{\pi a}{2b}\right)\right]$$

and

$$\tau_{yx}(0,-b/2) = \frac{8G\vartheta b}{\pi^2}\sum_{n=1}^{\infty}\frac{\sin^2(n\pi/2)}{n^2}\cdot\left[1-\frac{1}{\cosh\left(\frac{n\pi a}{2b}\right)}\right]$$

$$\approx G\vartheta b\left[1-\frac{8}{\pi^2\cosh\left(\frac{\pi a}{2b}\right)}\right]$$

Note the identities

$$\sum_{n=1}^{\infty}\frac{\sin^2(n\pi/2)}{n^4} = \frac{\pi^4}{96} \quad , \quad \sum_{n=1}^{\infty}\frac{\sin^2(n\pi/2)}{n^2} = \frac{\pi^2}{8}$$

Determine an expression for the warping u as well.

13.10 Show that the (unrestrained) warping of the rectangular hollow section of Fig. 13.38(g) is given by

$$u = \frac{Tyz}{2Gab}\left(\frac{1}{ad}-\frac{1}{bc}\right)$$

for pairs of identical sidewalls, and thus verify Fig. 13.27(c).

14 SINGLE DEFORMATIONS

14.1 General

General work-associated force and deformation variables were first discussed in section 8.2.1. In this chapter, the aim is to determine single external deformation variables $\boldsymbol{u}$, $\boldsymbol{r}$ according to Fig. 8.3 and 8.4, especially displacements and rotations due to loads, thermal actions and other load-independent causes. In doing so, it will be assumed that first-order theory applies, see section 6.1.

The principle of virtual forces for determining external deformation variables for known stress resultants was used in example 8.2. This procedure is generalised and systematised below with the development and application of the *work theorem*.

Examples 8.8 and 8.9 were used to explain the application of ENGESSER's theorem for calculating external deformation variables. However, compared with the principle of virtual forces, the range of applications for ENGESSER's theorem is very limited. Actually, the latter is based on considering the active work of the force variables, the former, however, on the passive work of virtual force variables. Using ENGESSER's theorem, it is only possible to determine displacements or rotations acting in the same direction at the positions of single forces or single moments. If no force variable is present at a point of interest, a fictitious auxiliary force variable must be introduced which is set to zero after performing the differentiation (8.83) – a quite laborious process that is little suited to practical building applications. And the method cannot be used at all for thermal actions, shrinkage processes and other load-independent causes of deformations. For these reasons, the application of ENGESSER's theorem will not be pursued further.

The calculation of single deformations is vital in practical building situations, especially when considering serviceability limit states according to section 4.4, verifying serviceability according to (4.8), calculating prior deformations such as beam camber or presets for bearings and generally checking conditions during construction. Another important area of application is the so-called *observation method*, one possible method during the design, execution and use of structures when the basic design information is not sufficiently reliable, e. g. regarding the behaviour of the subsoil. In such cases, certain accepted risks are defined, the (deformation) behaviour is predicted and corresponding limit values plus all the associated monitoring and safety measures are specified. Finally, understanding the deformation behaviour for dealing with statically indeterminate systems is crucial; the equilibrium conditions must be supplemented by deformation conditions when analysing such systems.

Theory of Structures. First Edition. Peter Marti

14.2 The work theorem

14.2.1 Introductory example

The simply supported beam shown in Fig. 14.1(a) is loaded by the uniformly distributed line load q = const. Neither the beam's bending stiffness EI nor its shear stiffness GA_v are dependent on x. We require the deflection at mid-span w_m.

According to (8.23), the shear forces $V = -qx$ and the bending moments $M = q(l^2 - 4x^2)/8$ correspond to shear strains $\gamma = V/(GA_v)$ and curvatures $\chi = M/(EI)$ respectively. Together with the deflections w, these strain variables characterise the *deformation state* (compatibility set of deformation variables) present in this situation.

In order to calculate w_m by applying (8.64), we now introduce the virtual *force state* (equilibrium set of force variables) illustrated in Fig. 14.1(b), with the single force $Q_1 = 1$ at the position and in the direction of w_m. Using the corresponding stress resultants V_1 and M_1, (8.64) is therefore

$$1 \cdot w_m - \int_{-l/2}^{l/2} \left(V_1 \frac{V}{GA_v} + M_1 \frac{M}{EI} \right) \mathrm{d}x = 0 \tag{14.1}$$

Owing to the symmetry with respect to $x = 0$, this leads to

$$w_m = 2 \int_0^{l/2} \left[\frac{qx}{2GA_v} + \frac{l}{4}\left(1 - \frac{2x}{l}\right) \cdot \frac{ql^2}{8EI}\left(1 - \frac{4x^2}{l^2}\right) \right] \mathrm{d}x = \frac{ql^2}{8GA_v} + \frac{5ql^4}{384EI} \tag{14.2}$$

Taking into account (7.2), $(13.19)_1$ and $(13.40)_2$ results in

$$\frac{w_{mV}}{w_{mM}} = \frac{96(1+\nu)i^2}{5\alpha_v l^2} \tag{14.3}$$

for the ratio between the two terms w_{mV} and w_{mM} on the right in (14.2). Eq. (14.3) is a similar expression to (13.42). Taking a rather stocky rectangular cross-section with $l = 8h$, $\alpha_v = 5/6$ and $\nu = 0.2$, the result is $w_{mV}/w_{mM} = 3.6$ %, for example. As a rule, the amounts that the shear forces contribute to the deflections can obviously be ignored when compared with the contributions of the bending moments.

Eq. (14.1) assumes non-yielding supports. If, for example, one of the two supports in Fig. 14.1(a) were to be a translational spring according to Fig. 5.10(a), with a spring stiffness k_z, the deflection at this position in the deformation state would be $w_A = ql/(2k_z)$, see $(5.12)_2$. The support force acting in the opposite direction at this position in the force state, a value of 1/2, would do the passive work $(-1/2)\cdot w_A$ on w_A, and w_m would be increased by $w_A/2 = ql/(4k_z)$ compared with (14.2). Similarly, rotational springs or applied (imposed) support displacements or rotations can be taken into account by including the corresponding types of displacement.

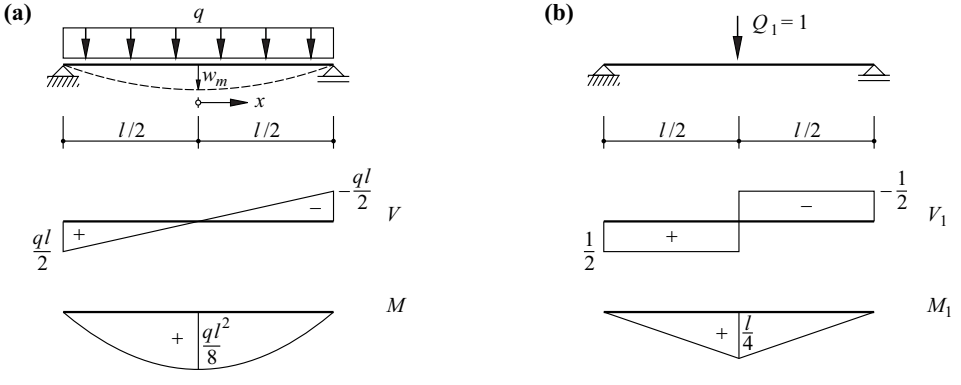

Fig. 14.1 Mid-span deflection of a simply supported beam subjected to a uniformly distributed line load: (a) deformation state, (b) force state

14.2.2 General formulation

Let us consider an arbitrary, compatible state of deformation for a spatial framed structure, which we shall denote with the index j. In order to calculate the single deformation δ_{ij} occurring at a certain position and in a certain direction i due to this deformation state, we shall introduce a force state, which we shall designate with the index i and which is characterised by a single force variable of magnitude 1 at the position and in the direction of δ_{ij}. Apart from the loads and the elastic deformations caused by such loads, we shall also consider thermal actions and support displacements. Using (8.28) and (7.53), eq. (8.64) results in

$$1 \cdot \delta_{ij} + \sum C_i c_j = \int \left[N_i \left(\frac{N_j}{EA} + \alpha_T T \right) + V_{yi} \frac{V_{yj}}{GA_{vy}} + V_{zi} \frac{V_{zj}}{GA_{vz}} + T_i \frac{T_j}{GI_x} + M_{yi} \left(\frac{M_{yj}}{EI_y} + \alpha_T \frac{\Delta T_z}{h} \right) + M_{zi} \left(\frac{M_{zj}}{EI_z} + \alpha_T \frac{\Delta T_y}{b} \right) \right] \mathrm{d}x \tag{14.4}$$

where C_i is a support force variable for the force state i, c_j is the corresponding (spring elastic or imposed) support displacement variable for the deformation state j. T is the uniform temperature change and ΔT_z or ΔT_y is the temperature difference over the depth of the cross-section h or the width of the cross-section b respectively (varying linearly with z or y respectively).

Shrinkage or swelling deformations can be dealt with by adding suitable terms to (14.4) in a similar way to thermal deformations. Creep deformations can be taken into account by increasing the terms for N_j, M_{xj}, M_{yj}, M_{zj} by the factor $(1 + \varphi)$, with the creep coefficient φ according to (7.42).

When applying (14.4) in practical situations, some of the terms can be omitted in most cases, and others may often be neglected for an approximate result. The sum on the left in (14.4) is to be applied over all the support force variables concerned and the integral on the right in (14.4) over the entire system or subsystem being examined.

The stress resultants corresponding to the force state i are often indicated with a horizontal line over the variable (e. g. $\overline{M}$), which renders the index i superfluous. This form of notation is used in examples 22.6 and 22.9 and also in Fig. 22.30.

14.2.3 Calculating the passive work integrals

The integrands on the right in (14.4) are each products of two functions which essentially progress arbitrarily and can also exhibit discontinuities. An analytic integration is only possible in exceptional cases. *Integration tables*, e. g. Fig. 14.2, are extremely useful for bar stiffnesses constant segment by segment. The values in the tables correspond to certain integrals (over length l) of the products of the functions shown; note that all parabolas are quadratic parabolas with the vertex in the middle or at one end of distance l.

Numerical integration methods can generally be used, e. g. the *trapezoidal rule* (n odd or even)

$$\int_l y \, \mathrm{d}x = \frac{\Delta}{2} (y_0 + 2y_1 + \ldots + 2y_{n-1} + y_n) \tag{14.5}$$

or SIMPSON*'s rule* (n even)

$$\int_l y \, \mathrm{d}x = \frac{\Delta}{3} (y_0 + 4y_1 + 2y_2 + 4y_3 + 2y_4 + \ldots + 4y_{n-1} + y_n) \tag{14.6}$$

where $\Delta = l/n$.

	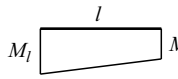	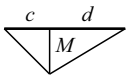	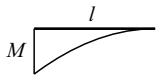	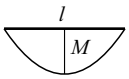	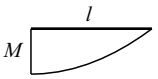
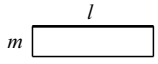	$\frac{1}{2}\, m\,(M_l + M_r)\, l$	$\frac{1}{2}\, m\, M\, l$	$\frac{1}{3}\, m\, M\, l$	$\frac{2}{3}\, m\, M\, l$	$\frac{2}{3}\, m\, M\, l$
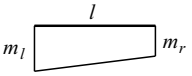	$\frac{l}{6}\left[m_l\,(2M_l + M_r) + m_r\,(M_l + 2M_r)\right]$	$\frac{Ml}{6}\left[m_l\left(1+\frac{d}{l}\right) + m_r\left(1+\frac{c}{l}\right)\right]$	$\frac{Ml}{12}\,(3m_l + m_r)$	$\frac{Ml}{3}\,(m_l + m_r)$	$\frac{Ml}{12}\,(5m_l + 3m_r)$
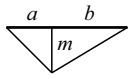	$\frac{ml}{6}\left[M_l\left(1+\frac{b}{l}\right) + M_r\left(1+\frac{a}{l}\right)\right]$	$\frac{l^2 - a^2 - d^2}{6bc}\, mMl$	$\frac{mMl}{12}\left(1+\frac{b}{l}+\frac{b^2}{l^2}\right)$	$\frac{mMl}{3}\left(1+\frac{ab}{l^2}\right)$	$\frac{mMl}{12}\left(5-\frac{a}{l}-\frac{a^2}{l^2}\right)$
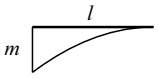	$\frac{ml}{12}\,(3M_l + M_r)$	$\frac{mMl}{12}\left(1+\frac{d}{l}+\frac{d^2}{l^2}\right)$	$\frac{1}{5}\, m\, M\, l$	$\frac{1}{5}\, m\, M\, l$	$\frac{3}{10}\, m\, M\, l$
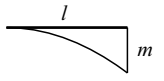	$\frac{ml}{12}\,(M_l + 3M_r)$	$\frac{mMl}{12}\left(1+\frac{c}{l}+\frac{c^2}{l^2}\right)$	$\frac{1}{30}\, m\, M\, l$	$\frac{1}{5}\, m\, M\, l$	$\frac{2}{15}\, m\, M\, l$
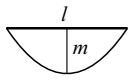	$\frac{ml}{3}\,(M_l + M_r)$	$\frac{mMl}{3}\left(1+\frac{cd}{l^2}\right)$	$\frac{1}{5}\, m\, M\, l$	$\frac{8}{15}\, m\, M\, l$	$\frac{7}{15}\, m\, M\, l$
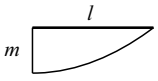	$\frac{ml}{12}\,(5M_l + 3M_r)$	$\frac{mMl}{12}\left(5-\frac{c}{l}-\frac{c^2}{l^2}\right)$	$\frac{3}{10}\, m\, M\, l$	$\frac{7}{15}\, m\, M\, l$	$\frac{8}{15}\, m\, M\, l$
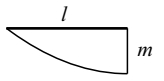	$\frac{ml}{12}\,(3M_l + 5M_r)$	$\frac{mMl}{12}\left(5-\frac{d}{l}-\frac{d^2}{l^2}\right)$	$\frac{2}{15}\, m\, M\, l$	$\frac{7}{15}\, m\, M\, l$	$\frac{11}{30}\, m\, M\, l$

Fig. 14.2 Integration table

Eq. (14.5) and (14.6) can be derived using theory of structures methods provided – in line with Fig. 14.3 – we interpret the given function $y(x)$ at the equidistant support points m with their support values y_m as a line load and replace it by the statically equivalent joint forces K_m.

The moment equilibrium conditions about m or $m-1$ result in the joint forces

$$K^r_{m-1} = \frac{\Delta}{6}(2y_{m-1} + y_m) \quad , \quad K^l_m = \frac{\Delta}{6}(y_{m-1} + 2y_m)$$

equivalent to the trapezium area ($m-1$, m, B, A) and, similarly, moment equilibrium conditions about $m+1$ or m result in the joint forces

$$K_m^r = \frac{\Delta}{6}(2y_m + y_{m+1}) \quad , \quad K_{m+1}^l = \frac{\Delta}{6}(y_m + 2y_{m+1})$$

equivalent to the trapezium area (m, $m+1$, C, B). Generally, the result for internal points is

$$K_m = \frac{\Delta}{6}(y_{m-1} + 4y_m + y_{m+1}) \tag{14.7}$$

and for start and end points

$$K_0 = \frac{\Delta}{6}(2y_0 + y_1) \quad , \quad K_n = \frac{\Delta}{6}(y_{n-1} + 2y_n) \tag{14.8}$$

Summating the joint forces K_0 to K_n according to (14.7) and (14.8) leads to (14.5).

If the shape of the function between the support points is approximated as a quadratic parabola, then according to Fig. 14.3, the following applies:

$$4f = y_m - \frac{y_{m-1} + y_{m+1}}{2}$$

The two small segments in Fig. 14.3 between the parabola and the trapezium have the area

$$\frac{2}{3}f\Delta = \frac{\Delta}{12}(-y_{m-1} + 2y_m - y_{m+1})$$

Adding this expression to (14.7) leads to the *parabolic rule*

$$K_m = \frac{\Delta}{12}(y_{m-1} + 10y_m + y_{m+1}) \tag{14.9}$$

and adding the corresponding half expressions to (14.8) results in the associated equations for the start and end points:

$$K_0 = \frac{\Delta}{24}(7y_0 + 6y_1 - y_2) \quad , \quad K_n = \frac{\Delta}{24}(-y_{n-2} + 6y_{n-1} + 7y_n) \tag{14.10}$$

When $m = 1$ and $n = 2$, adding together the expressions on the right in (14.9) and (14.10) gives us

$$\frac{\Delta}{3}(y_0 + 4y_1 + y_2)$$

If the distance 2Δ considered up to now is extended by further such distances, the result is (14.6).

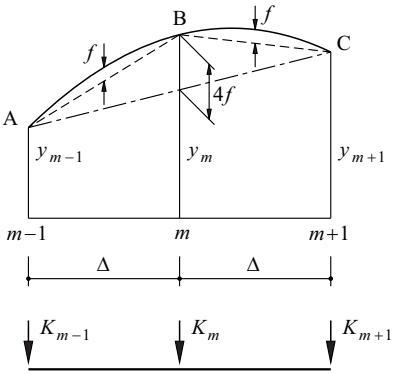

Fig. 14.3 Shape of the function and statically equivalent joint forces

Example 14.1 SIMPSON's rule

When $n = 2$, the integral

$$\int_0^{\pi/2} \sin x \cos x \, dx = \frac{1}{2}\sin^2 x \Big|_0^{\pi/2} = \frac{1}{2}$$

can be approximated according to SIMPSON's rule (14.6) with

$$\frac{1}{3}\cdot\frac{\pi}{4}\cdot 4\cdot\left(\frac{\sqrt{2}}{2}\right)^2 = \frac{\pi}{6} = 0.52360$$

i. e. a value that is 4.7 % too high. Putting $n = 4$ gives us the approximation

$$\frac{1}{3}\cdot\frac{\pi}{8}\cdot\left[4\cdot\frac{\sqrt{2}}{4} + 2\left(\frac{\sqrt{2}}{2}\right)^2 + 4\cdot\frac{\sqrt{2}}{4}\right] = \frac{\pi}{24}(2\sqrt{2}+1) = 0.50114$$

i. e. a value that deviates by only 0.23 % from the exact value of 1/2.

14.2.4 Systematic procedure

The following steps are necessary if we are to apply the work theorem (14.4):

1. Determine the stress resultants (N_j, V_{yj}, V_{zj}, M_{xj}, M_{yj}, M_{zj}), the support displacements (c_j) and the thermal deformations ($\alpha_T T$, $\alpha_T \Delta T_z/h$, $\alpha_T \Delta T_y/b$) of the deformation state j.
2. Choose a suitable force state i, characterised by a single force variable with magnitude 1 applied at the position and in the direction of the deformation variable δ_{ij} required.
3. Determine the stress resultants (N_i, V_{yi}, V_{zi}, M_{xi}, M_{yi}, M_{zi}) and the support force variables (C_i) of the force state i.
4. Set up and evaluate the work theorem (14.4) with the help of integration tables (e. g. Fig. 14.2) or numerical integration (e. g. SIMPSON's rule).

Clearly, potential simplifications as a result of terms that can be omitted or neglected should always be carried out at the start, in step 1. The force state i to be selected in step 2 is suitable when it leads to the simplest calculation for δ_{ij}; in particular, it is important to avoid the occurrence of support displacement variables c_j corresponding to the support force variables C_i which do not disappear or are unknown.

14.3 Applications

Example 14.2 Beam with one degree of static indeterminacy

Fig. 14.4(a) shows the beam with one degree of static indeterminacy already examined in example 8.5 (Fig. 8.13), which is subjected to a line load q uniformly distributed over length l. The deflection at mid-span w_m will be determined below. The only stress resultants are bending moments $M_y = M$ and shear forces $V_z = V$. We shall neglect shear force deformations and so the only term that remains on the right in (14.4) is the one containing the bending moments M_y.

Fig. 14.4(b) shows a first force state with the force $Q_1 = 1$ at the position and in the direction of w_m. In the deformation state, displacement variables equal to zero correspond to the moment $-l/2$ and the vertical force of magnitude 1 occurring due to the fixity; there is neither a rotation nor a vertical displacement at A in Fig. 14.4(a). By resolving M into trapezoidal (negative) and parabolic (positive) components over length $l/2$, using (14.4) and the integration table of Fig. 14.2 results in

$$1 \cdot w_m = \int_0^l M_{11} \frac{M}{EI}\,\mathrm{d}x = -\frac{l}{2} \cdot \frac{l}{2EI}\left[-\frac{1}{6} \cdot \left(2\frac{ql^2}{8} + \frac{ql^2}{16}\right) + \frac{1}{4}\frac{ql^2}{8}\right] = \frac{ql^4}{192EI}$$

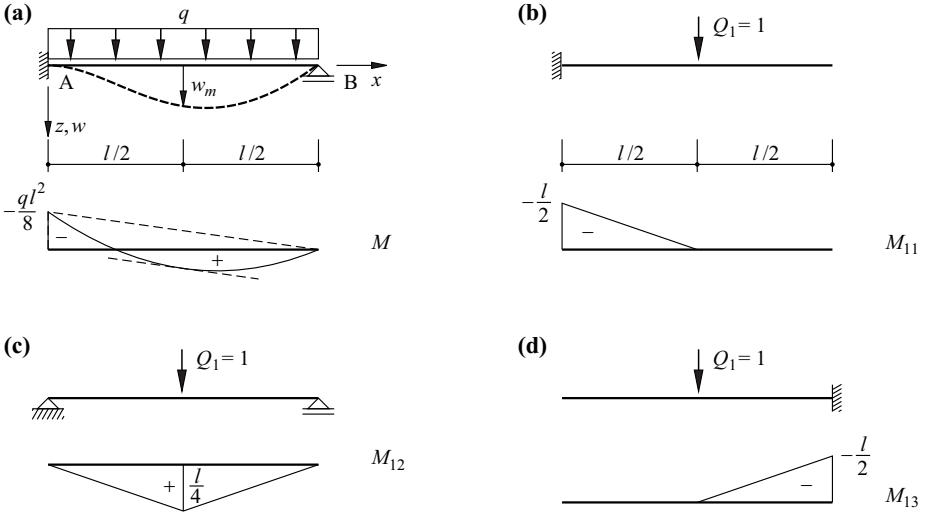

Fig. 14.4 Deflection at mid-span of a beam with one degree of static indeterminacy: (a) deformation state, (b) to (d) force states

The force state illustrated in Fig. 14.4(c) is also expedient. In a similar way to the above, we get

$$1 \cdot w_m = \int_0^l M_{12} \frac{M}{EI}\,\mathrm{d}x = \frac{l}{4} \cdot \frac{l}{EI} \cdot \left(\frac{5}{12} \frac{ql^2}{8} - \frac{1}{4} \cdot \frac{ql^2}{8} \right) = \frac{ql^4}{192EI}$$

On the other hand, the force state shown in Fig. 14.4(d) is unhelpful. In order to be able to use this state, the rotation in the deformation state of Fig. 14.4(a) corresponding to the fixity moment $-l/2$ at B would have to be known. The reader may like to show that this rotation is equal to $ql^3/(48EI)$. Eq. (14.4) is therefore

$$1 \cdot w_m - \frac{l}{2} \cdot \frac{ql^3}{48EI} = \int_0^{l/2} M_{13} \frac{M}{EI}\,\mathrm{d}x = -\frac{l}{2} \cdot \frac{l}{2EI} \left(-\frac{1}{6} \cdot \frac{ql^2}{16} + \frac{1}{4} \cdot \frac{ql^2}{8} \right) = -\frac{ql^4}{192EI}$$

from which it again follows that $w_m = ql^4/(192EI)$.

The remarkable thing in this example is that the deformation state refers to a statically indeterminate system, whereas all three of the force states considered assume statically determinate systems. If we were to introduce a sliding support at B in Fig. 14.4(b) and fixity at A in Fig. 14.4(c), the result would be the same system with one degree of static indeterminacy as that shown in Fig. 14.4(a). Restraint moments $X(1 - x/l)$ according to Fig. 8.13(b) would be superimposed on the moments M_{11} and M_{12} (with positive or negative X); where $M = -ql^2/8 + 5qlx/8 - qx^2/2$, it is easy to see that their contribution to the passive work integral becomes zero:

$$\int_0^l X\left(1 - \frac{x}{l}\right) \frac{\left(-\frac{ql^2}{8} + \frac{5qlx}{8} - \frac{qx^2}{2} \right)}{EI}\,\mathrm{d}x = \frac{ql^3 X}{8EI} \left[-\frac{x}{l} + 3\left(\frac{x}{l}\right)^2 - 3\left(\frac{x}{l}\right)^3 + \left(\frac{x}{l}\right)^4 \right]\Bigg|_0^l = 0$$

Calculating w_m with the help of the work theorem therefore remains unchanged; the restraint moment has no influence on w_m, i. e. it is possible to assume any statically determinate system when choosing the force state.

The disappearance of the passive work contribution of a restraint state can generally be obtained directly from the work equation (8.15) or (8.20) without further calculation. As the restraint state is free from loads, W_e equals zero and therefore W_i disappears on its own. When calculating single deformations in statically indeterminate systems with the help of the work theorem (14.4), we can therefore assume a force state i for any statically determinate basic system. This result is known as the *reduction theorem*.

Example 14.3 Hinged girder

The task is to calculate the rotation φ_G at hinge G for the hinged girder shown in Fig. 14.5(a), rigid in shear and with constant bending stiffness EI.

The only stress resultant relevant is the bending moment $M_y = M$. Using the force state illustrated in Fig. 14.5(b), we get the corresponding bending moment diagram M_1, and the support displacement variables c_j of the deformation state corresponding to the support force variables C_i of the force state disappear. Using Fig. 14.2, eq. (14.4) therefore results in

$$1 \cdot \varphi_G = \frac{1}{6}(1 + 2 \cdot 2) \cdot \left(-\frac{Ql}{2} \right) \cdot \frac{l}{2EI} + \frac{1}{3} \cdot 2 \cdot \left(-\frac{Ql}{2} \right) \cdot \frac{l}{EI} = -\frac{13Ql^2}{24EI}$$

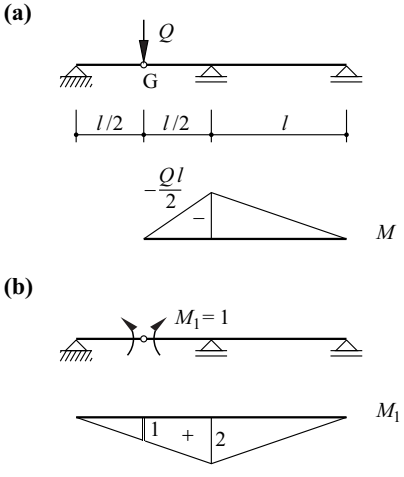

Fig. 14.5 Hinged girder: (a) deformation state, (b) force state

Example 14.4 Cantilever beam

The cranked cantilever beam shown in Fig. 14.6(a) is subjected to a temperature difference $\Delta T = T_u - T_o = 2T_u$ along AB. The average temperature change disappears, $T = (T_u + T_o)/2 = 0$. The task is to calculate the deflection w_C at C.

Using the force state illustrated in Fig. 14.6(b), eq. (14.4) then results in

$$1 \cdot w_C = \int M_1 \frac{\alpha_T \Delta T}{h}\, dx = -\frac{2l + l}{2} \cdot \frac{\alpha_T 2T_u}{h} \cdot \frac{l}{\cos\alpha} = -\frac{3\alpha_T T_u l^2}{h\ \cos\alpha}$$

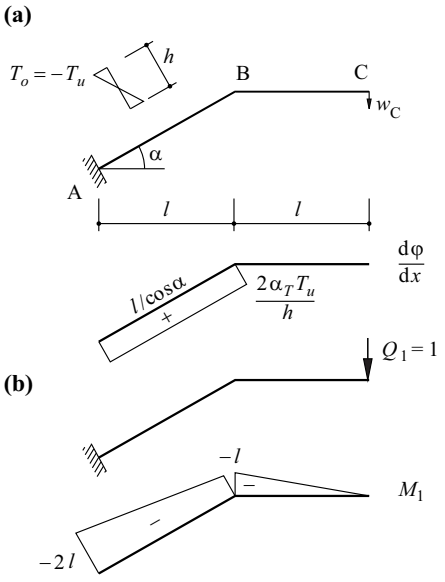

Fig. 14.6 Cantilever beam subjected to thermal action: (a) deformation state, (b) force state

Example 14.5 Cranked cantilever beam

The task is to calculate the rotation φ_B about the bar axis AB at B for the cranked cantilever beam shown in Fig. 14.7(a). The torsional stiffness GI_x of bar AB is constant.

Using the stress resultants of the deformation state of Fig. 14.7(b) and the force state of Fig. 14.7(c), eq. (14.4) then results in

$$1 \cdot \varphi_B = 1 \cdot \frac{Qa}{GI_x} \cdot l \quad , \quad \varphi_B = \frac{Qal}{GI_x}$$

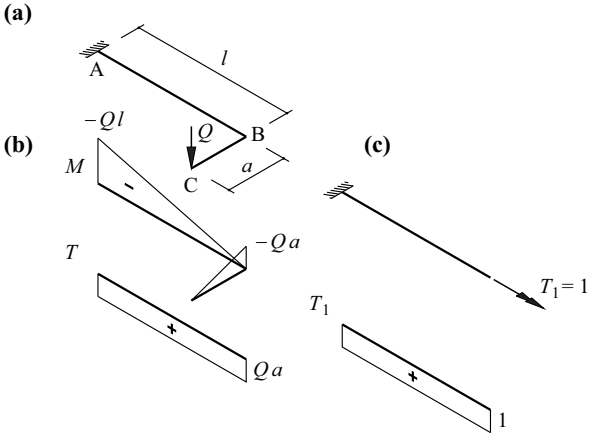

Fig. 14.7 Cranked cantilever beam subjected to a point load: (a) system and loads, (b) stress resultants of deformation state, (c) force state for calculating φ_B

Example 14.6 Plane truss

The temperature of bar DE in the statically determinate truss of Fig. 14.8(a) is raised by an amount T. The task is to calculate the associated deflection w_B.

Using one of the methods of calculation outlined in section 11.3, we can obtain a compressive force of magnitude 1 in bar DE for the force state of Fig. 14.8(b). Eq. (14.4) therefore results in

$$1 \cdot w_B = -1 \cdot \alpha_T T \cdot 2l \quad , \quad w_B = -2\alpha_T T\, l$$

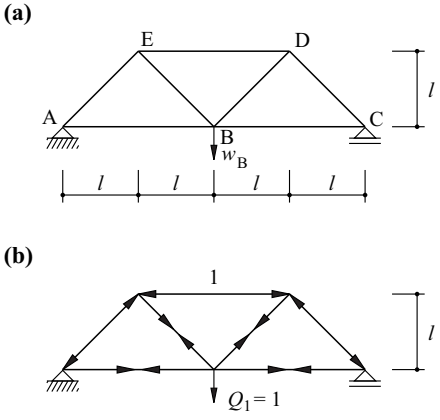

Fig. 14.8 Truss with temperature of bar DE raised by T: (a) system and notation, (b) force state

Example 14.7 Rectangular cross-section – area shear factor

The task is to use the work theorem to calculate the area shear factor α_v for the rectangular cross-section of example 13.5.

Fig. 14.9(a) shows the section through the bar and Fig. 14.9(b) illustrates the deformation state. We shall consider a bar element of length dx which undergoes a mean shear strain γ according to (8.23). Using $(7.3)_2$, the shear strains γ_{zx} result from the distribution of the shear stresses τ_{zx} determined in example 13.5:

$$\gamma_{zx} = \frac{\tau_{zx}}{G} = \frac{V_z}{Gbh}\left(\frac{3}{2} - \frac{6z^2}{h^2}\right)$$

Selecting the force state illustrated in Fig. 14.9(c) gives us the similar shear stress distribution

$$\tau_1 = \frac{1}{bh}\left(\frac{3}{2} - \frac{6z^2}{h^2}\right)$$

and (14.4) results in

$$1 \cdot \gamma\, \mathrm{d}x = \int_{-h/2}^{h/2} \tau_1 \cdot \gamma\, b\, \mathrm{d}x\, \mathrm{d}z = \int_{-h/2}^{h/2} \frac{V_z}{G(bh)^2}\left(\frac{3}{2} - \frac{6z^2}{h^2}\right)^2 b\, \mathrm{d}x\, \mathrm{d}z = \frac{V_z}{Gbh}\, \mathrm{d}x \cdot \frac{6}{5}$$

from which it follows that

$$\gamma = \frac{V_z}{G \cdot \left(\frac{5}{6} bh\right)} = \frac{V_z}{GA_v}$$

i. e. as $A = bh$ and $A_v = \alpha_v A$, then $\alpha_v = 5/6$, see section 13.3.1 and appendix A4.

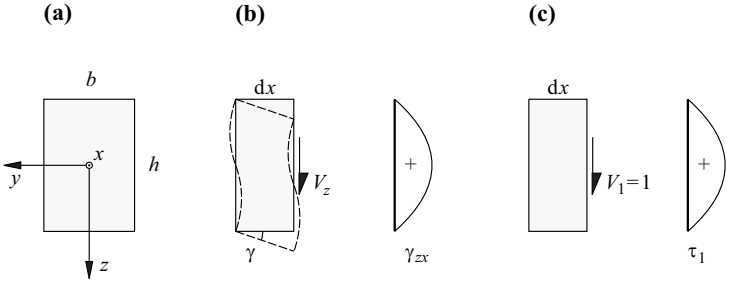

Fig. 14.9 Area shear factor α_v: (a) section, (b) deformation state, (c) force state

Example 14.8 Thin-wall hollow cross-section

The task is to use the work theorem to derive BREDT's 2nd equation $(13.68)_2$ for thin-wall hollow cross-sections.

Let us consider a bar segment of length dx with the cross-section shown in Fig. 14.10. According to (13.65), (13.66) and (7.3), the deformation state is characterised by the shear strains $\gamma_{sx} = \gamma = T/(2A_0Gt)$. Eq. (13.65) and (13.66) result in the shear stresses $\tau_1 = 1/(2A_0t)$ for the force state with a torque $T_1 = 1$. Consequently, according to (14.4), with the rotational increment $\mathrm{d}\varphi_x$ over element length dx, the following applies:

$$1 \cdot \mathrm{d}\varphi_x = \oint \tau_1 \cdot \gamma \,\mathrm{d}x \cdot t \,\mathrm{d}s = \frac{T \,\mathrm{d}x \oint (\mathrm{d}s/t)}{4A_0^2 G} = \frac{T \,\mathrm{d}x}{GI_x}$$

from which, with $\vartheta = \mathrm{d}\varphi_x/\mathrm{d}x$, the relationship $(13.68)_2$ follows.

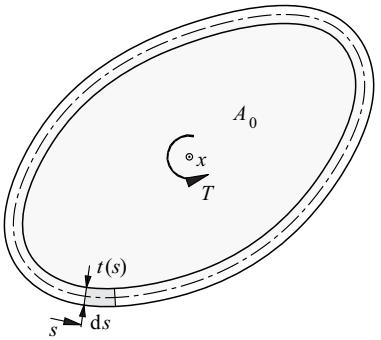

Fig. 14.10 Thin-wall hollow cross-section

Calculating single deformations using the work theorem is referred to again in different ways in the following chapters. Further examples are therefore unnecessary at this point.

14.4 MAXWELL's theorem

MAXWELL's *theorem* (8.88) regarding the reciprocity of displacements or the symmetry of the flexibility matrix for linear elastic systems was derived in section 8.4.3 and illustrated in Fig. 8.16(a). Fig. 14.11 contains a similar illustration for a simply supported beam; the notation of the work theorem (14.4) is used here. In Fig. 14.11(a), δ_{ji} is the displacement occurring at the position and in the direction of $Q_j = 1$ as a result of $Q_i = 1$. And vice versa, δ_{ij} in Fig. 14.11(b) is the displacement occurring at the position and in the direction of $Q_i = 1$ as a result of $Q_j = 1$. Obviously, the interchangeability of deformation and force states according to (14.4) means that

$$\delta_{ij} = \delta_{ji} \tag{14.11}$$

Fig. 14.12 is another illustration of MAXWELL's theorem; here, however, there is a rotation at point j and, accordingly, a moment $M_j = 1$ is considered as a force variable. The rotation δ_{ji} in Fig. 14.12(a) is negative and has the dimension 1/N because Q_i is dimensionless. And vice versa, the displacement δ_{ij} in Fig. 14.12(b) has the dimension m/(Nm) = 1/N because M_j is dimensionless, and δ_{ij} is negative as well.

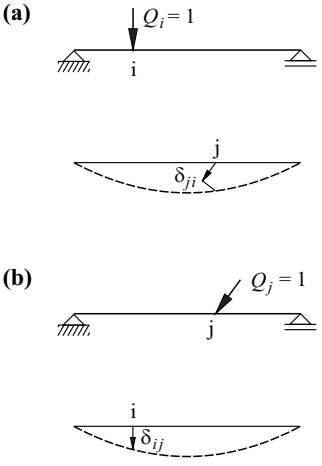

Fig. 14.11 MAXWELL's theorem: (a) deformation state *i*, force state *j*, (b) deformation state *j*, force state *i*

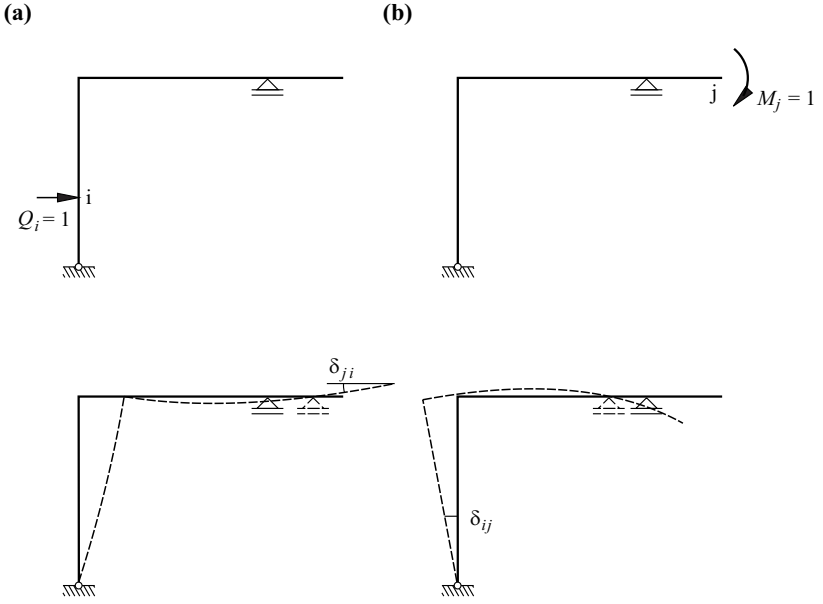

Fig. 14.12 MAXWELL's theorem: (a) deformations as a result of $Q_i = 1$, (b) deformations as a result of $M_j = 1$

14.5 Summary

1. External deformation variables can be calculated using the principle of virtual forces or ENGESSER's theorem. Compared with the principle of virtual forces, however, the range of applications for ENGESSER's theorem is very limited. In practice, therefore, the work theorem, which is based on the principle of virtual forces, is used almost exclusively.
2. The work theorem in its general formulation (14.4) permits the calculation of single deformations in any linear elastic framed structure according to first-order theory, taking into account loads, restraints and thermal, shrinkage, swelling or creep deformations. When we use the work theorem, it is usually possible to omit some of the terms given in (14.4), and others may often be neglected when an approximation is adequate.
3. In straightforward cases, the passive work integrals in the work theorem can be integrated analytically or with the help of integration tables, e. g. Fig. 14.2. Numerical integration methods should generally be used, e. g. SIMPSON's rule.
4. Restraint states in conjunction with compatible states of deformation result in zero passive work. Therefore, when calculating single deformations in statically indeterminate systems with the work theorem, the force state for any statically determinate basic system can be assumed (reduction theorem).
5. MAXWELL's theorem ($\delta_{ij} = \delta_{ji}$) follows from the work theorem (14.4) because of the interchangeability of deformation and force states.

14.6 Exercises

14.1 Consider the quarter-circle beam examined in exercise 5.7 and calculate the rotations about the radial axis at the torsional fixity and about the bar axis at the opposite end of the beam. Presume constant bending stiffness EI and torsional stiffness GI_x, and ignore the shear force deformations.

14.2 Calculate the displacement of sliding support 3 due to Q_X in the system of exercise 10.1. Presume a constant axial stiffness EA for all bars.

14.3 Calculate the horizontal displacement of sliding support 4 for the system of exercise 11.1. Only take into account bending deformations and assume $EI = 400\,\mathrm{MNm}^2 = \text{const.}$

14.4 Bar 123 of the system of exercise 14.3 experiences a temperature difference $\Delta T_z/h = 20°\mathrm{C/m}$. Calculate the corresponding rotation at hinge 1 and the displacement of sliding support 4 assuming a coefficient of thermal expansion $\alpha_T = 10^{-5}/°\mathrm{C}$.

14.5 Select appropriate steel sections for the bar forces calculated in exercise 11.2 and calculate the corresponding vertical displacement of the ridge hinge.

14.6 Calculate the relative displacement of the tops of the 8 m high vertical columns associated with the task of exercise 14.5.

14.7 Calculate the deflection of point D in exercise 13.8 when points A, B and C are restrained in the XY plane.

15 DEFORMATION DIAGRAMS

15.1 General

Every point on a bar axis generally undergoes certain displacements as a consequence of loads or restraints. The bar axis moves to a new, deformed position. *Deformation diagrams* describe the shape of the function of the displacement components along the bar axis (related to local coordinates). Deformation diagrams for the displacement components perpendicular to the bar axis are commonly called *deflection curves*.

Deformation diagrams can be approximated point by point with the help of the work theorem (section 14.2). But to determine the exact shape, it is necessary to integrate the corresponding differential equations that link the given loads with the deformations required. To do this, it is possible to rely on the analogy of the relationships, which are obtained from the link between the kinematic relations (8.27) and the constitutive equations (8.28), with the differential equations (8.26) for the equilibrium, and to apply normal theory of structures methods (MOHR*'s analogy*).

15.2 Differential equations for straight bar elements

15.2.1 In-plane loading

The relationship (5.57) for the radius of curvature ρ of a planar curve was used in example 5.6 without any further explanation. In preparation for the following observations, we shall consider an element of length

$$\mathrm{d}s = \rho\,\mathrm{d}\alpha \tag{15.1}$$

of a bar axis deformed in the xz plane with the radius of curvature ρ, see Fig. 15.1(a). There is a deflection $w = w(x)$ in the z direction and so

$$\tan\alpha = w' \quad , \quad \tan(\alpha - \mathrm{d}\alpha) = w' + w''dx$$

applies, where a superscript dash ($'$) denotes differentiation with respect to x. Therefore,

$$\tan(\mathrm{d}\alpha) = \frac{-\,w''\mathrm{d}x}{1 + w'(w' + w''\mathrm{d}x)}$$

from which, with the passage to the limit $\mathrm{d}x \to 0$, we get

$$\frac{\mathrm{d}\alpha}{\mathrm{d}x} = \frac{-\,w''}{1 + (w')^2} \tag{15.2}$$

Using

$$\mathrm{d}s = \mathrm{d}x\sqrt{1 + (w')^2} \tag{15.3}$$

eq. (15.1) and (15.2) give us the relationship for the *curvature*

$$\chi_y = \chi = \frac{1}{\rho} = \frac{-\,w''}{[1 + (w')^2]^{3/2}} \tag{15.4}$$

which is similar to (5.57), and because $w' \ll 1$ may be approximated by

$$\chi = -\,w'' \tag{15.5}$$

see (8.24) and (8.29).

Theory of Structures. First Edition. Peter Marti

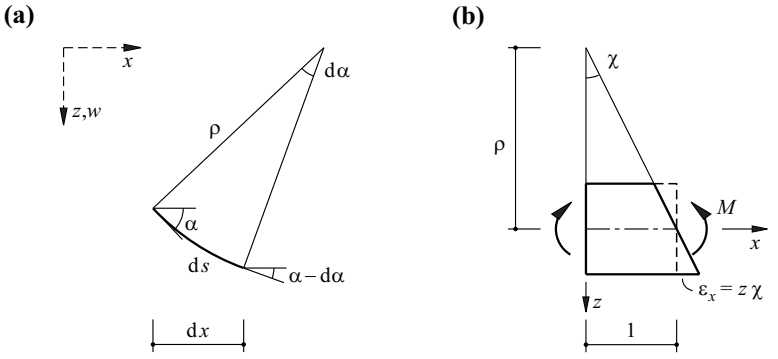

Fig. 15.1 Straight bar element: (a) deformed bar axis, (b) bending of an element of length 1

A negative (positive) second derivative w'' corresponds to a local downward (upward) convex deflection curve and hence a positive (negative) bending moment $M_y = M$. Fig. 15.1(b) shows a (positively) curved bar element of length 1 caused by a bending moment M, plus the associated variation of the normal strains ε_x over the depth of the element, see (13.3).

Boundary condition	u	u'	w	w'	w''	$(EIw'')'$
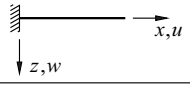	0		0	0		
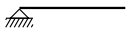	0		0		0	
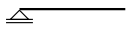		0	0		0	
		0			0	0
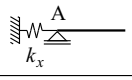	$-\frac{A_x}{k_x}$	$\left(-\frac{A_x}{EA}\right)$	0		0	
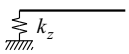		0	$-\frac{A_z}{k_z}$		0	(A_z)
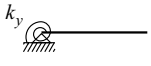	0		0	$\frac{M_A}{k_y}$	$\left(\frac{M_A}{EI}\right)$	
Continuity condition	$u]$		$w]$	$w']$	w''	$(EIw'')']$
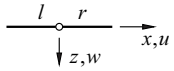	0		0		$w_l'' = 0$ $w_r'' = 0$	0
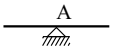	0		$w_l = 0$ $w_r = 0$	0	$EI_l\, w_l''$ $= EI_r\, w_r''$	A_z
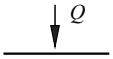	0		0	0	$EI_l\, w_l''$ $= EI_r\, w_r''$	Q

Fig. 15.2 Boundary and continuity conditions (flexible supports according to Fig. 5.10)

Assuming that $m_y = 0$, combining (8.21) or (8.25), (8.22) or (8.24) and (8.23) results in

$$(EA\,u')' = -q_x \quad , \quad (EIw'')'' = q_z \tag{15.6}$$

These relationships are valid for all static systems made up of straight bar elements, see chapter 9. The structural topography is taken into account here by way of *boundary* and *continuity conditions* at the ends of the elements (i. e. the joints of the structural model); one or two conditions have to be specified for u or w respectively for each end of the bar, see Fig. 15.2. We can see that

$$N = EA\,u' \quad , \quad M = -EIw'' \quad , \quad V = -(EIw'')' \tag{15.7}$$

A square bracket indicates an abrupt change in the corresponding function, e. g. $u] = u_r - u_l$.

15.2.2 General loading

In the case of general loading, we add the index y to I in $(15.6)_2$ (I_y). In addition to (15.6), combining (8.26) to (8.28) gives us the two similar differential equations

$$(GI_x\vartheta)' = -m_x \quad , \quad (EI_z v'')'' = q_y \tag{15.8}$$

where $m_z = 0$ is presumed. The integration methods outlined in section 15.3 for planar problems can be transferred to the situation of spatial problems without any difficulty, at least for straight bar elements.

15.2.3 The effect of shear forces

Eliminating φ from (8.22) gives us

$$w'' = -\chi + \gamma'$$

i. e. considering (8.23),

$$w'' = -\frac{M}{EI} + \left(\frac{V}{GA_v}\right)' \tag{15.9}$$

where according to (8.21),

$$M'' = -q_z - m_y' \quad , \quad V = M' + m_y \tag{15.10}$$

Compared with $(15.7)_2$, w'' is increased by $[V/(GA_v)]'$ according to (15.9). Owing to the equilibrium conditions (15.10), eq. (15.9) is generally integrated only numerically instead of analytically.

15.2.4 Creep, shrinkage and thermal deformations

Creep deformations can be considered in simplified form according to (7.48) by replacing the modulus of elasticity E by

$$E_a = \frac{E}{1+\varphi} \tag{15.11}$$

with the creep coefficient φ.

Shrinkage and thermal deformations can be considered as initial strains in accordance with (8.19). Taking the corresponding axial strains ε_s or ε_T and the curvatures χ_s or χ_T, we get

$$N = E_a A(u' - \varepsilon_s - \varepsilon_T) \quad , \quad M = E_a I(-w'' - \chi_s - \chi_T) \tag{15.12}$$

instead of $(15.7)_1$ and $(15.7)_2$.

15.2.5 Curved bar axes

Bars with curved axes (possibly curved in three dimensions and possibly with twisted principal axes) are generally approximated by polygons made up of straight bar elements. Consequently, the decoupled differential equations (15.6) and (15.8) apply to each bar element, and the coupling of the state variables (stress resultants, displacements and rotations) at the ends of the element must be taken into account.

Otherwise, the result is sets of simultaneous differential equations that normally can only be solved numerically.

15.3 Integration methods

15.3.1 Analytical integration

In the following we shall confine ourselves to stiffnesses that are constant for each bar.

Example 15.1 Simply supported beam

According to $(15.6)_2$, the differential equation

$$EIw'''' = q \tag{15.13}$$

applies to the simply supported beam shown in Fig. 15.3, which is subjected to a uniformly distributed line load $q_z = q$ = const and has $EI_y = EI$ = const. This has the general solution

$$w = w_{\text{part}} + c_1x^3 + c_2x^2 + c_3x + c_4 \tag{15.14}$$

The particular solution

$$w_{\text{part}} = \frac{qx^4}{24EI}$$

satisfies (15.13). The boundary conditions

$$w(0) = w''(0) = w(l) = w''(l) = 0$$

according to Fig. 15.2 lead to

$$c_1 = -\frac{ql}{12EI} \quad , \quad c_2 = 0 \quad , \quad c_3 = \frac{ql^3}{24EI} \quad , \quad c_4 = 0$$

and thus to

$$w = \frac{q}{24EI}(x^4 - 2lx^3 + l^3x)$$

where

$$w_{\max} = w\left(\frac{l}{2}\right) = \frac{5ql^4}{384EI}$$

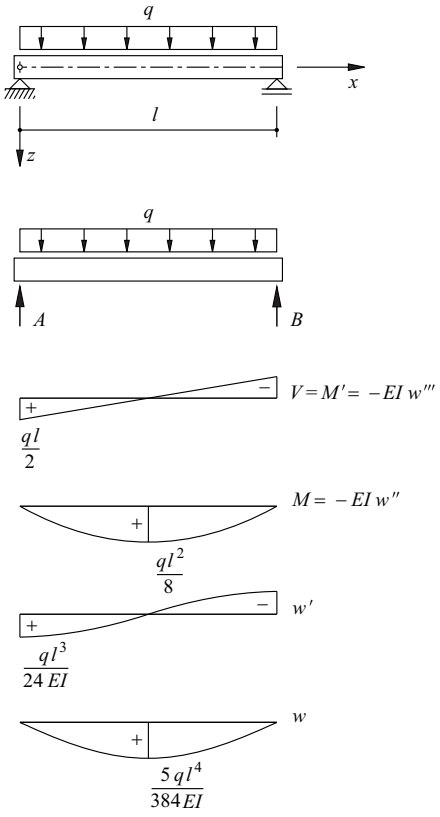

Fig. 15.3 Simply supported beam subjected to a load q = const

Example 15.2 Beam fixed at both ends

If the ends of the beam are fixed instead of simply supported as shown in example 15.1, and if the origin of the system of coordinates is placed in the centre of the beam, see Fig. 15.4, then the particular solution

$$w_{\text{part}} = \frac{qx^4}{24EI}$$

continues to apply, and owing to the symmetry of system and load, $c_1 = c_3 = 0$.

The boundary conditions

$$w\left(\frac{l}{2}\right) = w'\left(\frac{l}{2}\right) = 0$$

according to Fig. 15.2 lead to

$$c_2 = -\frac{ql^2}{48EI} \quad , \quad c_4 = \frac{ql^4}{384EI}$$

and therefore

$$w = \frac{q}{384EI}(16x^4 - 8l^2x^2 + l^4)$$

where

$$w_{\max} = w(0) = \frac{ql^4}{384EI}$$

Using $(15.7)_2$, it also follows that

$$M = \frac{ql^2}{24}\left(1 - \frac{12x^2}{l^2}\right)$$

As can be seen, in principle there is no difference between the way we treat this system with three degrees of static indeterminacy and the statically determinate system of example 15.1.

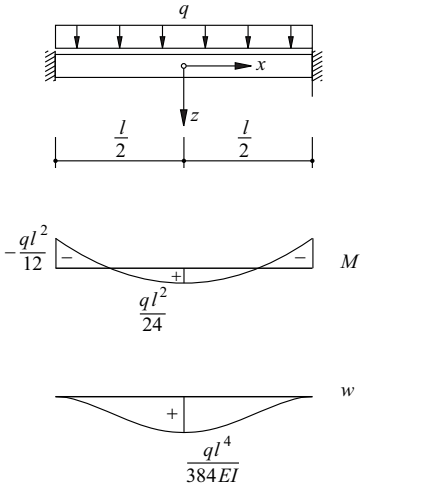

Fig. 15.4 Beam fixed at both ends subjected to a load q = const

Example 15.3 Beam with one degree of static indeterminacy

The beam with one degree of static indeterminacy shown in Fig. 15.5(a) is loaded by a point load Q only. Eq. (15.14) has to be formulated separately for each of the two parts of the beam to the left and right of the point of load application. As $q = 0$, then $w_{\text{part}} = 0$, and consequently

$$w = c_1x^3 + c_2x^2 + c_3x + c_4 \qquad (-a \le x \le 0)$$
$$w = c_5x^3 + c_6x^2 + c_7x + c_8 \qquad (0 \le x \le l - a)$$

In order to determine the eight coefficients c_1 to c_8, we have the boundary conditions

$$w(-a) = w'(-a) = w(l-a) = w''(l-a) = 0$$

and the continuity conditions

$$EI \cdot w'''(0)] = Q \quad , \quad w''(0)] = w'(0)] = w(0)] = 0$$

according to Fig. 15.2. We get

$$c_1 = -\frac{Q}{12EI}(2 - 3\alpha^2 + \alpha^3) \quad , \quad c_5 = \frac{Q\alpha^2}{12EI}(3 - \alpha)$$
$$c_2 = -\frac{Ql\alpha^2}{4EI}(3 - 4\alpha + \alpha^2) = c_6$$
$$c_3 = \frac{Ql^2\alpha^2}{4EI}(2 - 6\alpha + 5\alpha^2 - \alpha^3) = c_7$$
$$c_4 = \frac{Ql^3\alpha^3}{12EI}(4 - 9\alpha + 6\alpha^2 - \alpha^3) = c_8$$

where $\alpha = a/l$.

For example, with $\alpha = 1/2$, the result is

$$c_1 = -\frac{11Q}{96EI} \quad , \quad c_2 = c_6 = -\frac{5Q}{64EI} \quad , \quad c_3 = c_7 = \frac{Ql^2}{128EI} \quad , \quad c_4 = c_8 = \frac{7Ql^3}{768EI} \quad , \quad c_5 = \frac{5Q}{96EI}$$

Fig. 15.5(b) shows the corresponding state variables.

In the event of discontinuities in EI, we could proceed in a similar way, i. e. by integrating $(15.6)_2$ at intervals and taking into account the corresponding boundary and continuity conditions.

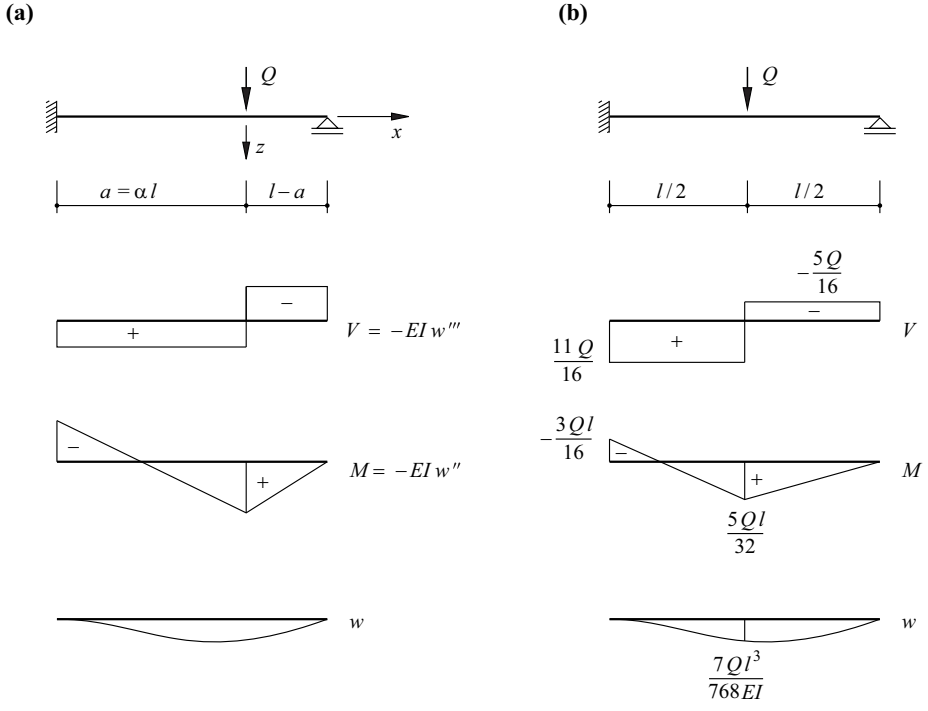

Fig. 15.5 Beam with one degree of static indeterminacy subjected to a point load Q: (a) general case, (b) $\alpha = 1/2$

15.3.2 MOHR's analogy

The differential equations (8.25)

$$N' = -q_x \quad , \quad M'' = -q_z \tag{15.15}$$

and the differential equations

$$u' = \frac{N}{EA} \quad , \quad w'' = -\frac{M}{EI} \tag{15.16}$$

resulting from combining (8.23) and (8.24) have similar forms. Deformation variables u and w can thus be calculated from $-N/(EA)$ or $M/(EI)$ with the same theory of structures methods as for calculating stress resultants N and M from line loads q_x and q_z. To do this, the real system is transformed into a *conjugate system* loaded by the *conjugate loads*

$$q_x^* = -\frac{N}{EA} \quad , \quad q_z^* = \frac{M}{EI} \tag{15.17}$$

The *conjugate stress resultants* N^*, V^* and M^* resulting from this are equal to the deformation variables u, $w' = -\varphi$ and w.

At the transition from the real to the conjugate system, it is important to consider the rules for the transformation of the boundary and continuity conditions summarised in Fig. 15.6. The notation of Fig. 5.10 and (5.12) applies here for the supports with translational and rotational springs.

Real system				Conjugate system			
u	w'	w	Condition	Condition	N^*	V^*	M^*
0	0	0	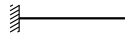		0	0	0
$\neq 0$	$\neq 0$	$\neq 0$			$\neq 0$	$\neq 0$	$\neq 0$
0	$\neq 0$	0	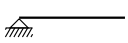	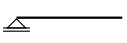	0	$\neq 0$	0
$\neq 0$	$\neq 0$	0	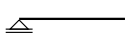	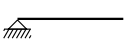	$\neq 0$	$\neq 0$	0
$\neq 0$	$w'] = 0$	0	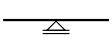		$\neq 0$	$V^*] = 0$	0
$\neq 0$	$w'] \neq 0$	$\neq 0$		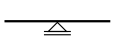	$\neq 0$	$V^*] \neq 0$	$\neq 0$
$-A_x/k_x$	$\neq 0$	0	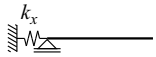	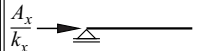	$-A_x/k_x$	$\neq 0$	0
0	M_A/k_y	0	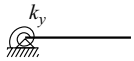	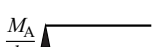	0	M_A/k_y	0
$\neq 0$	$\neq 0$	$-A_z/k_z$	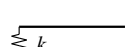	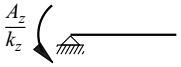	$\neq 0$	$\neq 0$	$-A_z/k_z$

Fig. 15.6 MOHR's analogy – transformation rules for boundary and continuity conditions

Example 15.4 Beam with spring restraint

The beam with length l shown in Fig. 15.7(a) is restrained by a spring at its left-hand end A and subjected to a line load q_x = const. Using the notation of Fig. 5.10 and equation (5.12), the support force is $A_x = -q_x l$ and the normal force N decreases linearly from $q_x l$ to zero between A and B.
In the conjugate system, Fig. 15.7(b), a force of magnitude $q_x l/k_x$ has to be imposed in the negative x direction at A according to Fig. 15.6 and the sliding support at B must be replaced by a hinged support. In addition, the (triangularly distributed) load q_x^* must be applied according to $(15.17)_1$. We therefore get the shape for $N^* = u$ shown in the bottom part of Fig. 15.7(b).

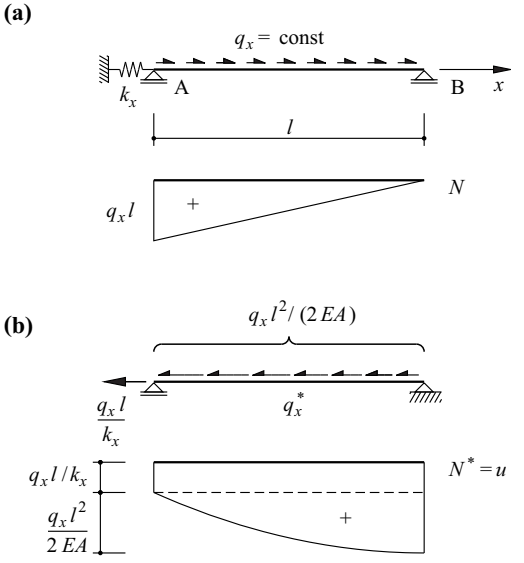

Fig. 15.7 Beam with spring restraint subjected to a load q_x = const: (a) real system, (b) conjugate system

Example 15.5 Cantilever beam

Fig. 15.8(a) shows a cantilever beam of length l loaded by a point load Q at its unsupported end plus the associated bending moment diagram.
In the conjugate system, Fig. 15.8(b), the roles of the fixed and free ends are reversed, see Fig. 15.6. According to $(15.17)_2$, the load q_z^* (triangularly distributed, acting in the negative z direction) gives rise to the bending moment diagram $M^* = w$ shown in the bottom part of Fig. 15.8(b).

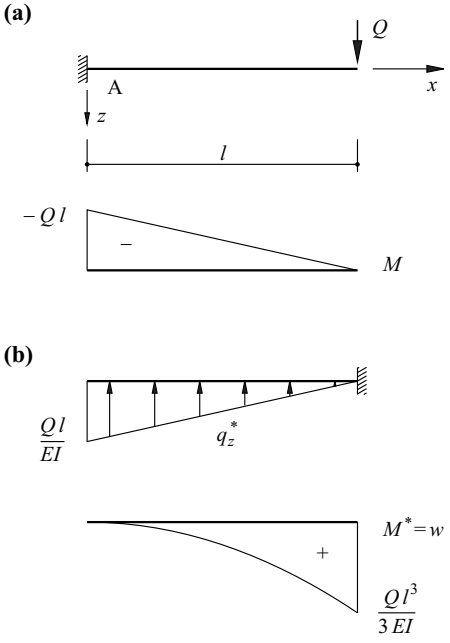

Fig. 15.8 Cantilever beam with point load at unsupported end: (a) real system, (b) conjugate system

Example 15.6 Beam with one degree of static indeterminacy

Fig. 15.9(a) again shows the beam with one degree of static indeterminacy already dealt with in example 8.5 (Fig. 8.13) and in example 14.2 (Fig. 14.4) subjected to a load $q_z = q$ = const, plus the associated bending moment distribution

$$M = \frac{ql^2}{8}\left(-1 + 5\frac{x}{l} - 4\frac{x^2}{l^2}\right)$$

The conjugate system, Fig. 15.9(b), has a free end at A and a hinged support at B according to Fig. 15.6, i. e. is kinematically unstable.

However, the conjugate load q_z^* forms an equilibrium system together with the conjugate support force B^*. Double integration of q_z^* between the limits 0 and x leads to

$$M^* = \frac{ql^4}{48EI}\left(3\frac{x^2}{l^2} - 5\frac{x^3}{l^3} + 2\frac{x^4}{l^4}\right) = w$$

where $w_{max} = ql^4/(184.6EI)$ at position $x = 0.5785l$. Further, we can confirm the value $w_m = ql^4/(192EI)$ found in example 14.2 for $x = l/2$.

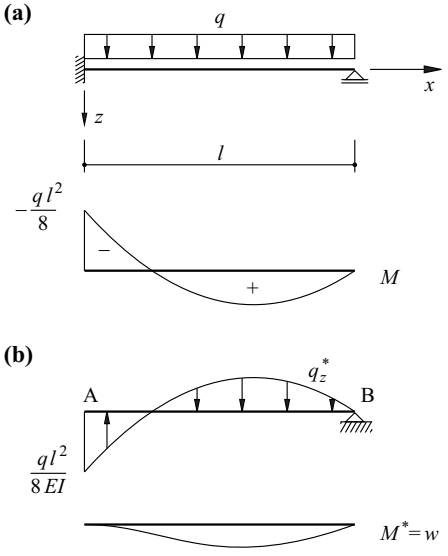

Fig. 15.9 Beam with one degree of static indeterminacy: (a) real system, (b) conjugate system

Example 15.7 Hinged girder

The hinged girder shown in Fig. 15.10(a) has support forces of 360, 1430 and 1180 kN at points 1, 7 and 13 respectively, see Fig. 15.10(b). With a spacing of $\Delta = 6$ m, according to (14.7) and (14.8), we first get the joint forces K and from them the shear forces V and finally the moments M by using the support forces, see Fig. 15.10(b) and Tab. 15.1.

For the conjugate system, Fig. 15.10(c), we use (14.9) and (14.10) to get the joint forces K^* as a result of q_z^* according to $(15.17)_2$, see Fig. 15.10(d) and Tab. 15.1. In order to be able to take into account the (small) influence of the shear force on the deformations, the differences $\Delta\gamma$ between the mean shear strains $\gamma = V/(GA_v)$ to the left and right of each joint are added to these joint forces according to (15.9). Using the final joint forces K^*, we get the variables V^* and $M^* = w$ by taking into account the conjugate support forces.

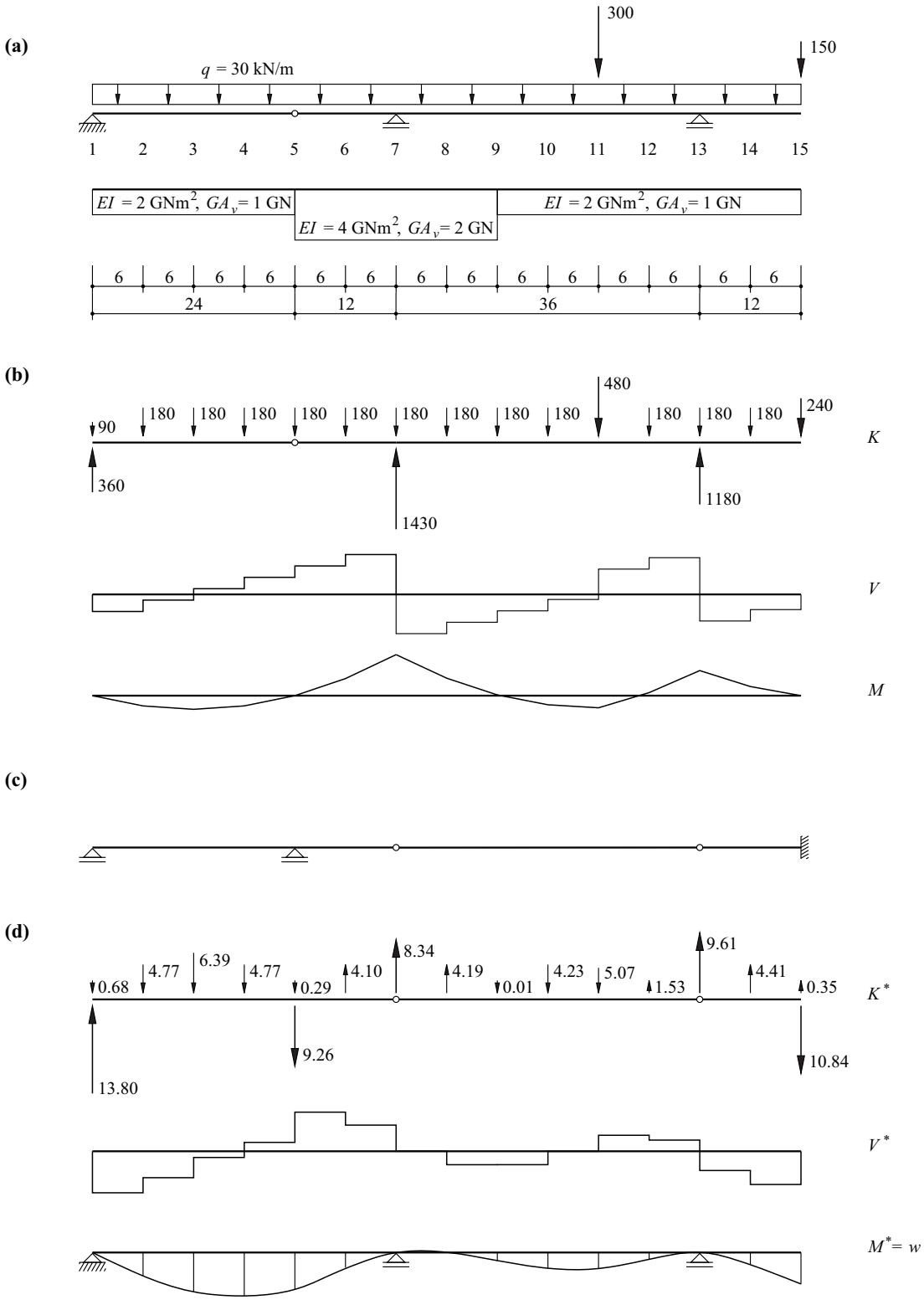

Fig. 15.10 Hinged girder: (a) diagram of static system [kN, m], (b) joint forces, shear forces, moments, (c) conjugate system, (d) conjugate joint forces, shear forces and moments

Tab. 15.1 Calculations for the hinged girder of Fig. 15.10.

i	K	V	M	q_z^*	$K^*(q_z^*)$	$V/(GA_y$	$\Delta\gamma$	K^*	V^*	$M^* = w$
		(360)							(13.80)	
1	90		0	0	0.95		– 0.27	0.68		0
		270				0.27			13.12	
2	180		1620	0.810	4.59		0.18	4.77		78.7
		90				0.09			8.35	
3	180		2160	1.080	6.21		0.18	6.39		128.8
		– 90				– 0.09			1.96	
4	180		1620	0.810	4.59		0.18	4.77		140.6
		– 270				– 0.27			– 2.81	
5	180		0	0	0.95 – 0.61		– 0.04	0.29		123.8
		– 450				– 0.23			– 12.36	
6	180		– 2700	– 0.675	– 4.19		0.09	– 4.10		49.6
		– 630				– 0.32			– 8.27	
7	180		– 6480	– 1.620	– 3.85 – 3.86		– 0.63	– 8.34		0
		620				0.31			0.07	
8	180		– 2760	– 0.690	– 4.28		0.09	– 4.19		0.4
		440				0.22			4.26	
9	180		– 120	– 0.03 /– 0.06	– 0.68 0.74		– 0.04	0.01		26.0
		260				0.26			4.24	
10	180		1440	0.720	4.05		0.18	4.23		51.4
		80				0.08			0.01	
11	480		1920	0.960	2.78 1.82		0.48	5.07		51.5
		– 400				– 0.40			– 5.06	
12	180		– 480	– 0.240	– 1.71		0.18	– 1.53		21.2
		– 580				– 0.58			– 3.53	
13	180		– 3960	– 1.980	– 4.07 – 4.55		– 1.00	– 9.61		0
		420				0.42			6.08	
14	180		– 1440	– 0.720	– 4.59		0.18	– 4.41		36.5
		240				0.24			10.49	
15	240		0	0			0.24	– 0.35		99.5
		(0)							(10.84)	
	kN	kN	kNm	mrad/m	‰	‰	‰	‰	‰	mm

15.4 Summary

1. Deformation diagrams describe the shape of the function of the displacement components along the bar axis related to local coordinates.
2. Deformation diagrams can be approximated by calculating single deformations with the help of the work theorem.
3. The exact shapes of the deformation diagrams for straight bar elements result from the integration of differential equations (15.6) and (15.8) while taking into account the boundary and continuity conditions summarised in Fig. 15.2.
4. The influence of shear force deformations can be taken into account by increasing the second derivatives of the deflections according to (15.9) by the derivatives of the mean shear strains.
5. Shrinkage and thermal deformations can be considered as initial strains, creep deformations by using a modulus of elasticity modified according to (15.11).
6. In contrast to straight bar elements, coupled sets of differential equations ensue when curved bar axes are involved. Instead of having to solve these, it is best to approximate the bar axis with straight elements; in doing so, the coupling of the state variables at the ends of the elements must be taken into account.
7. Instead of integrating the differential equations for the deformation diagrams analytically, MOHR's analogy allows normal theory of structures integration methods to be used. To do this, we use the transformation rules summarised in Fig. 15.6 to change from the real to the conjugate system, which is subjected to the conjugate loads (15.17). The associated conjugate stress resultants N^*, V^* and M^* are equal to the deformation variables u, w' and w required.

15.5 Exercises

15.1 Determine the deflection curve of the system examined in exercises 11.1 and 14.3.

15.2 Solve exercise 15.1 taking into account normal force deformations (EA = 1600 MN) and shear force deformations (GA_v = 100 MN).

15.3 Determine the deflection curve of the bottom chord of the system examined in exercise 10.5. Assume a constant axial stiffness EA for all bars.

15.4 Solve exercise 15.3 ignoring the deformations of the truss diagonals.

15.5 Solve exercise 15.3 assuming that the bar cross-sections A are adapted in such a way that the magnitudes of the stresses and strains in all bars are the same as in the bar with the highest normal force. Stability problems are ruled out.

16 THE FORCE METHOD

16.1 General

Examples 6.1, 8.5, 8.9, 14.2, 15.2 and 15.3 have already provided the reader with insights into the structural behaviour of statically indeterminate systems. Distinguishing between statically determinate and indeterminate systems was first looked at in section 5.1.3. The counting schemes for determining the degree n of static indeterminacy were formulated in section 9.3.3. Section 8.1.2 explained the basic idea of the force method, how the column deficit in the static transformation matrix $\boldsymbol{b}$ could be overcome by introducing a statically determinate basic system and a corresponding number of redundant variables X so that the solution to a statically indeterminate problem could be achieved via the compatibility conditions. Lastly, examples 6.1 and 8.5 introduced the concept of zero-load, so-called restraint, states, and section 14.3 made use of the work equation (8.15) to show that restraint states do not make any contribution to passive work. Consequently, with respect to the force state, an arbitrary statically determinate basic system can be assumed when applying the work theorem (14.4) to statically indeterminate systems (reduction theorem).

In this chapter we shall first discuss the structural behaviour of statically indeterminate systems by means of a simple example. Apart from elastic behaviour, the plastic behaviour dealt with in more detail in chapters 20 and 21 will also be looked at. After that, the force method will be developed in general in its classic form and illustrated by way of various practical examples. A presentation of the force method in matrix form follows in chapter 19.

16.2 Structural behaviour of statically indeterminate systems

16.2.1 Overview

Fig. 16.1(a) shows the plane frame already examined in examples 10.2 and 10.4. The load is confined to the point load $Q_5 = Q$, and in terms of deformations, we shall confine ourselves to calculating the variable $V_5 = V$ that corresponds to Q, see Fig. 10.8. Apart from the statically determinate system, statically indeterminate systems with one and two degrees of static indeterminacy will be analysed by introducing a hinge and fixity respectively at joint 4. The linear elastic-perfectly plastic moment-curvature diagram shown in Fig. 16.1(b) describes the behaviour of the bars. For simplicity, deformations as a consequence of shear and normal forces plus the interactions of these stress resultants with the bending moments are ignored.

The load-deflection diagrams of Fig. 16.1(c) summarise the structural behaviour of the three systems for a monotonic load increase. The plastic phase AB with (unconstrained) additional deformation V follows the elastic increase OA of the statically determinate system due to the formation of a *plastic hinge* at joint 2 for a load Q remaining at the *limit load* $0.476M_y/\text{m}$. In the system with one degree of static indeterminacy (hinged support at joint 4), a first plastic hinge forms at joint 3 (elastic-plastic phase CD) after the elastic phase OC and subsequently a second plastic hinge at joint 2, which leads to the plastic phase DE for the limit load $0.952M_y/\text{m}$. In the system with two degrees of static indeterminacy (fixity at joint 4), the successive formation of plastic hinges at joints 4, 3 and 2 after the elastic phase OF results in the two

Theory of Structures. First Edition. Peter Marti

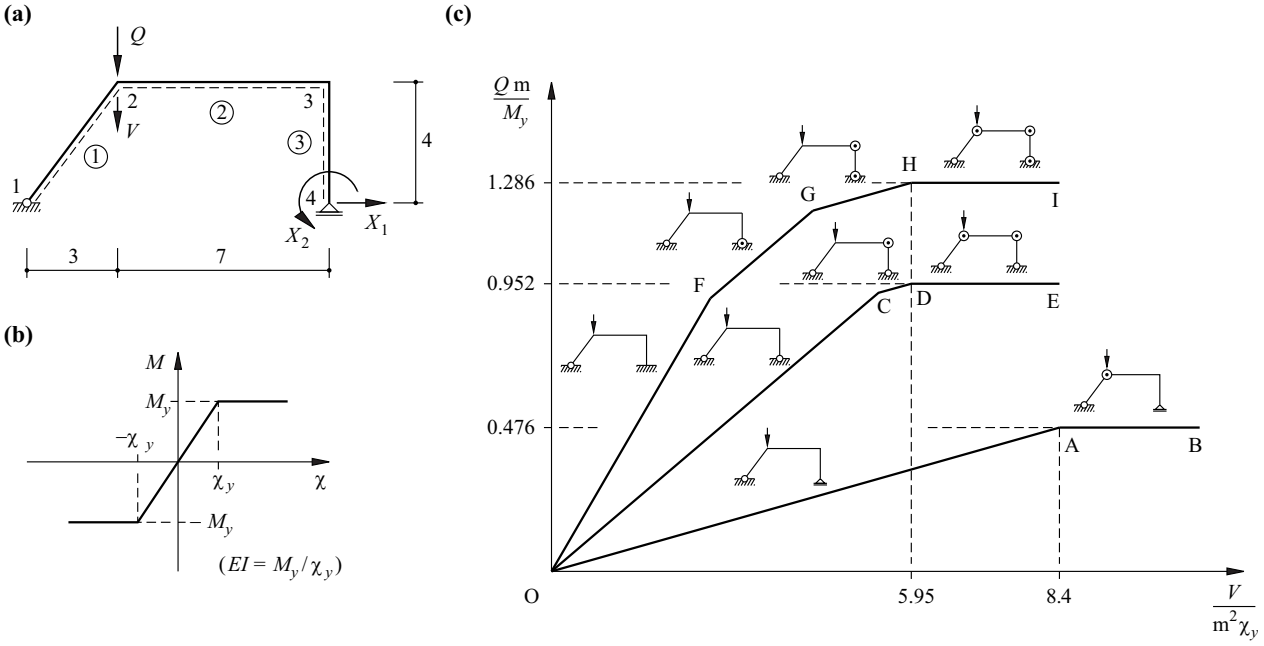

Fig. 16.1 Plane frame: (a) system and notation [m], (b) moment-curvature diagram, (c) load-deflection diagrams and development of plastic hinges

elastic-plastic phases FG and GH as well as the plastic phase HI for the limit load $1.286 M_y/\text{m}$.

The degree of static indeterminacy is reduced by one with the formation of each new plastic hinge. The final plastic hinge that forms (that at joint 2 in all three systems here) transforms the formerly statically determinate system into a *mechanism*.

In order to distinguish between plastic hinges and real (frictionless) hinges, the latter will continue to be indicated by a small circle, the former, however, by a circle around a dot.

As we can see, as the degree of static indeterminacy increases, there is not only an increase in the limit load and the ultimate resistance, but also an increase in the stiffness of the system being examined. In addition, with static indeterminacy, the decrease in stiffness associated with the successive formation of plastic hinges warns of the impending failure, i. e. that the limit load will be reached, or rather, that a mechanism will be formed.

It was assumed that the two statically indeterminate systems here are initially free from restraints (i. e. for $Q = 0$). If that were not the case, the result would be shorter or longer elastic and other elastic-plastic phases. However, the limit loads, i. e. the levels of the plastic phases in Fig. 16.1(c), are not affected by this.

Finally, it should be noted that the straight lines OA, CD and GH in Fig. 16.1(c) are parallel; likewise, the straight lines OC and FG.

16.2.2 Statically determinate system

The stress resultants of the statically determinate system are represented by the third column of the matrix on the right in (10.9). Fig. 16.2(a) shows the corresponding moment diagram with a moment of $Q \cdot 2.1\,\text{m}$ at joint 2. Should this moment reach the value M_y, the resistance of the system is exhausted, i. e. the limit load $M_y/(2.1\,\text{m}) = 0.476 M_y/\text{m}$ corresponding to line AB in Fig. 16.1(c) has been reached.

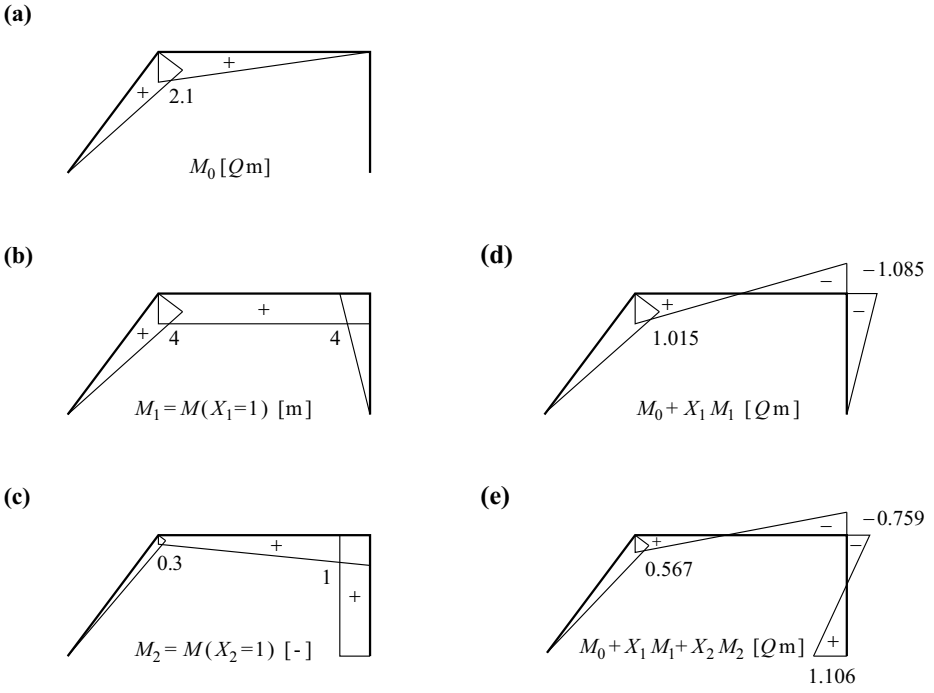

Fig. 16.2 Bending moments: (a) due to Q acting on the basic system, (b), (c) due to unit force variables, (d) system with one degree of static indeterminacy – hinged support at joint 4, (e) system with two degrees of static indeterminacy – fixity at joint 4

The distribution of the curvatures χ upon reaching the limit load is affine with the moment diagram Fig. 16.2(a), which results in the value χ_y at joint 2. The work theorem (14.4) will be applied to calculate the associated deflection V. A moment diagram affine with Fig. 16.2(a) and with a value of 2.1 m at joint 2 corresponds to the force state with the point load of magnitude 1 at the position and in the direction of V. Consequently, with the help of Fig. 14.2, the result is

$$V = \frac{1}{3} \cdot 2.1\,m \cdot \chi_y \cdot (5\,\mathrm{m} + 7\,\mathrm{m}) = 8.4\,\mathrm{m}^2 \chi_y$$

see point A in Fig. 16.1(c).

16.2.3 System with one degree of static indeterminacy

With a hinged support at joint 4, both V_{11} and degree of freedom V_{10} are passive according to Fig. 10.8(a). If we release this constraint by changing from the system shown in Fig. 16.1(a) to the statically determinate *basic system* examined in section 16.2.2 and introduce the *redundant variable* X_1 at the position of the released constraint, then according to the work theorem (14.4), combining the moment diagrams shown in Fig. 16.2(a) and (b) with $EI = M_y/\chi_y$ results in the displacement

$$\delta_{10} = \frac{1}{3} \cdot 4\,\mathrm{m} \cdot 2.1\,\mathrm{m} \cdot Q \cdot 5\,\mathrm{m} \cdot \chi_y/M_y + \frac{1}{2} \cdot 4\,\mathrm{m} \cdot 2.1\,\mathrm{m} \cdot Q \cdot 7\,\mathrm{m} \cdot \chi_y/M_y = 43.4\,\mathrm{m}^3 Q\,\chi_y/M_y$$

as a consequence of Q at the position and in the direction of X_1. On the other hand, a unit force variable $X_1 = 1$ causes the displacement

$$\delta_{11} = (4\,\mathrm{m})^2 \cdot \left(\frac{1}{3} \cdot 5\,\mathrm{m} + 7\,\mathrm{m} + \frac{1}{3} \cdot 4\,\mathrm{m} \right) \cdot \chi_y/M_y = 160\,\mathrm{m}^3 \chi_y/M_y$$

in the same direction. Effectively, V_{10} must disappear, i. e. the following *compatibility condition* applies:

$$\delta_1 = \delta_{10} + X_1 \delta_{11} = 0 \qquad (16.1)$$

from which we get $X_1 = -0.27125\,Q$.

The final moments are then obtained according to Fig. 16.2(d) from the superposition

$$M = M_0 + X_1 M_1 \tag{16.2}$$

of the moment components illustrated in Fig. 16.2(a) und (b).

If the moment at joint 3 reaches the value $-M_y$, a first plastic hinge forms at this position; the associated load amounts to $M_y/(1.085\,\mathrm{m}) = 0.922 M_y/\mathrm{m}$, corresponding to point C in Fig. 16.1(c). According to the work theorem, the deflection at the onset of yield results from combining the moment diagrams of Fig. 16.2(a) with $Q = 1$ and Fig. 16.2(d):

$$V = \frac{1}{3}\cdot 2.1\,\mathrm{m}\cdot\frac{1.015}{1.085}\chi_y\cdot 5\,\mathrm{m} + \frac{1}{6}\cdot 2.1\,\mathrm{m}\cdot\left(2\cdot\frac{1.015}{1.085}-1\right)\chi_y\cdot 7\,\mathrm{m} = 5.408\,\mathrm{m}^2\chi_y$$

During the elastic-plastic phase that follows the elastic phase OC in Fig. 16.1(c), the moment at joint 3 according to Fig. 16.1(b) remains at the value $-M_y$. The system has become statically determinate, and thanks to the plastic rotation at joint 3, load Q can continue to increase until the moment at joint 2 reaches the value M_y and a second plastic hinge forms at this position.

Fig. 16.3 illustrates the static and kinematic relationships corresponding to reaching the limit load at point D in Fig. 16.1(c). The limit load amounts to $20M_y/(21\,\mathrm{m}) = 0.952M_y/\mathrm{m}$, and the associated deflection is found by applying the work theorem:

$$V = \frac{1}{3}\cdot 2.1\,\mathrm{m}\cdot\chi_y\cdot 5\,\mathrm{m} + \frac{1}{6}\cdot 2.1\,\mathrm{m}\cdot\chi_y\cdot 7\,\mathrm{m} = 5.95\,\mathrm{m}^2\chi_y$$

As expected, lines CD and OA in Fig. 16.1(c) are parallel:

$$(0.952 - 0.922)/(5.95 - 5.408) \approx 0.476/8.4$$

The formation of the plastic hinge at joint 3 causes frame beam 2 to lose its fixity at column 3, and for loads that exceed the load at the onset of yield, the statically indeterminate system behaves in the same way as the statically determinate basic system with column 3 not restrained horizontally at its base (joint 4).

The plastic rotation at joint 3 upon reaching the limit load can be determined according to Fig. 16.4 by applying the work theorem:

$$\theta_{3p} = \left[\frac{1}{3}\cdot 0.3\cdot 5\,\mathrm{m} + \frac{1}{6}\cdot(2\cdot 0.3+1)\cdot 7\,\mathrm{m}\right]\cdot\left(1-\frac{1.015}{1.085}\right)\chi_y = 0.1527\,\mathrm{m}\,\chi_y$$

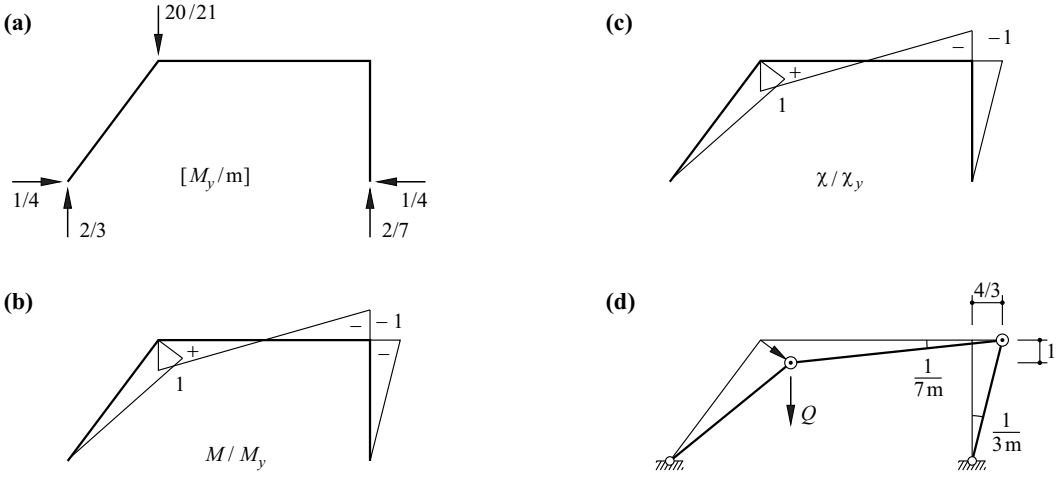

Fig. 16.3 System with one degree of static indeterminacy subjected to limit load: (a) free body diagram, (b) bending moments, (c) curvatures, (d) mechanism

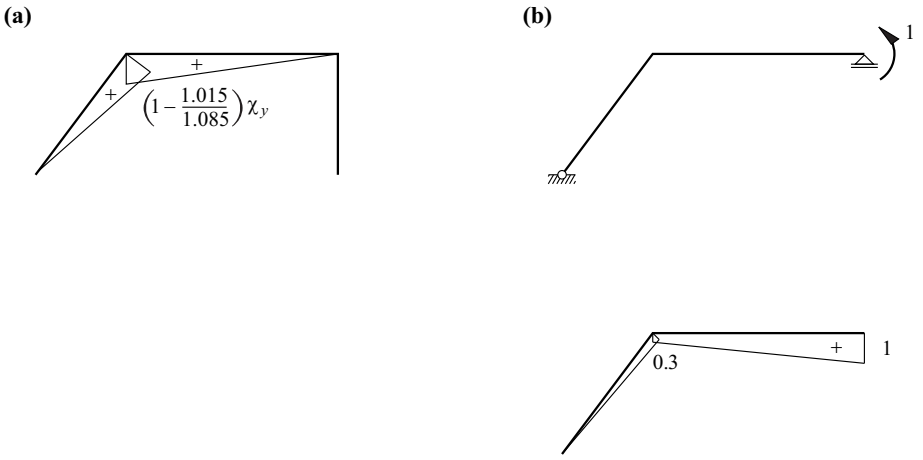

Fig. 16.4 Plastic rotation at joint 3 upon reaching the limit load for the system with one degree of static indeterminacy:
(a) deformation state – increase in curvature during elastic-plastic phase, (b) force state

Fig. 16.3(d) shows the mechanism with a virtual deflection of 1 at the point of application of load Q, which leads to a horizontal displacement of the frame beam corresponding to 4/3 and to plastic rotations of $1/(3\,\mathrm{m}) + 1/(7\,\mathrm{m}) = 10/(21\,\mathrm{m})$ at each of the two plastic hinges at joints 2 and 3. According to the work equation (8.15), the work $W_e = Q \cdot 1$ done by load Q is equal to the dissipation work $D = -W_i = 2M_y \cdot 10/(21\,\mathrm{m}) = 0.952 M_y/\mathrm{m}$ at the two plastic hinges. The three elastically deformed bars do not deform any further upon reaching the limit load; they can be treated like rigid bars when considering the mechanism and are therefore shown as straight lines in Fig. 16.3(d).

16.2.4 System with two degrees of static indeterminacy

With fixity at joint 4, V_{11} as well as the two degrees of freedom V_{10} and V_{12} are passive according to Fig. 10.8(a). If we introduce a second redundant variable X_2 as shown in Fig. 16.1(a), we get the moment diagram of Fig. 16.2(c), and applying the work theorem gives us the values

$$\delta_{20} = \left[\frac{1}{3}\cdot 0.3\cdot 5\,\mathrm{m} + \frac{1}{6}\cdot(2\cdot 0.3+1)\cdot 7\,\mathrm{m}\right]\cdot 2.1\,\mathrm{m}\cdot Q\cdot\chi_y/M_y = 4.97\,\mathrm{m}^2\,Q\,\chi_y/M_y$$

$$\delta_{12} = \delta_{21} = \left[\frac{1}{3}\cdot 0.3\cdot 5\,\mathrm{m} + \frac{1}{2}\cdot(0.3+1)\cdot 7\,\mathrm{m} + \frac{1}{2}\cdot 4\,\mathrm{m}\right]\cdot 4\,\mathrm{m}\cdot\chi_y/M_y = 28.2\,\mathrm{m}^2\chi_y/M_y$$

$$\delta_{22} = \left[\frac{1}{3}\cdot(0.3)^2\cdot 5\,\mathrm{m} + \frac{1}{6}\cdot(0.3\cdot 1.6 + 1\cdot 2.3)\cdot 7\,\mathrm{m} + 1\cdot 4\,\mathrm{m}\right]\chi_y/M_y = 7.393\,\mathrm{m}\,\chi_y/M_y$$

Together with the values δ_{10} and δ_{11} calculated in section 16.2.3, the result is the compatibility conditions

$$\delta_1 = \delta_{10} + X_1\delta_{11} + X_2\delta_{12} = 0 \quad , \quad \delta_2 = \delta_{20} + X_1\delta_{21} + X_2\delta_{22} = 0 \tag{16.3}$$

i. e.

$$\begin{Bmatrix}\delta_1\\ \delta_2\end{Bmatrix} = \begin{bmatrix}160\,\mathrm{m}^2 & 28.2\,\mathrm{m}\\ 28.2\,\mathrm{m} & 7.393\end{bmatrix}\begin{Bmatrix}X_1\\ X_2\end{Bmatrix} + \begin{Bmatrix}43.4\,\mathrm{m}^2\cdot Q\\ 4.97\,\mathrm{m}\cdot Q\end{Bmatrix} = \begin{Bmatrix}0\\ 0\end{Bmatrix}$$

from which we get

$$X_1 = -0.46613\,Q \quad , \quad X_2 = 1.10572\,\mathrm{m}\,Q$$

Fig. 16.2(e) shows the final moments resulting from the superposition

$$M = M_0 + X_1M_1 + X_2M_2 \tag{16.4}$$

Should the moment X_2 reach the value M_y at joint 4, see Fig. 16.5(a), a first plastic hinge forms at this position; the associated load amounts to $M_y/(1.10\,572\,\mathrm{m}) = 0.904 M_y/\mathrm{m}$, corresponding to point F in Fig. 16.1(c). According to

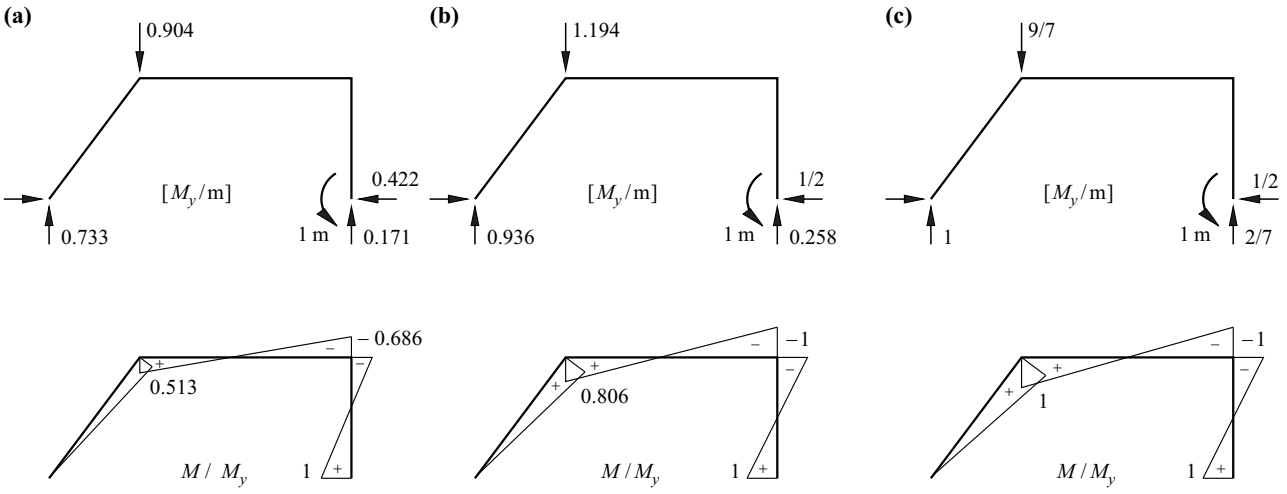

Fig. 16.5 System with two degrees of static indeterminacy: (a) onset of yield, (b) conclusion of first elastic-plastic phase, (c) conclusion of second elastic-plastic phase

the work theorem, the deflection at the onset of yield is given by combining the moment diagrams of Fig. 16.2(a) with $Q = 1$ and Fig. 16.2(e):

$$V = \left[\frac{1}{3} \cdot 0.567 \cdot 5\ \text{m} + \frac{1}{6} \cdot (2 \cdot 0.567 - 0.759) \cdot 7\ \text{m}\right] \cdot \frac{2.1\ \text{m}\,\chi_y}{1.106} = 2.628\ \text{m}^2\chi_y$$

After the elastic phase OF shown in Fig. 16.1(c), then $X_2 = M_y$ during the first elastic-plastic phase FG. The system has only one degree of static indeterminacy and behaves like the system examined in section 16.2.3 for loads that exceed the load at onset of yield. Fig. 16.5(b) illustrates the relationships that prevail at the end of this phase, i. e. point G in Fig. 16.1(c). We get a value of $1.194 M_y/\text{m}$ for the load Q, and the deflection V amounts to $4.324\,\text{m}^2\chi_y$.

During the second elastic-plastic phase GH in Fig. 16.1(c), the system is statically determinate owing to the two plastic hinges at joints 3 and 4, and behaves like the system examined in section 16.2.2 when additional loads are applied. Fig. 16.5(c) illustrates the conclusion of this phase, i. e. the relationships that prevail upon reaching the limit load. The limit load amounts to $27 M_y/(21\,\text{m}) = 1.286 M_y/\text{m}$, and the deflection upon reaching the limit load has the same value $V = 5.95\,\text{m}^2\chi_y$ as that in the system with one degree of static indeterminacy.

16.2.5 In-depth analysis of system with one degree of static indeterminacy

16.2.5.1 Choice of basic system

So far, the system with one degree of static indeterminacy (hinged support at joint 4) was transformed into a statically determinate basic system by introducing a sliding support or shear hinge at this position. The choice is arbitrary – introducing a sliding support at joint 1 or a flexural hinge somewhere in the frame, for example, would have been equally good. The only condition is that the system does not become unstable.

Taking the case shown in Fig. 16.6(a) with a flexural joint in column 34, the M_0 diagram is identical with Fig. 16.2(b), and the M_1 diagram only differs from Fig. 16.2(b) by the factor $1/a$. If a tends towards zero, the system becomes unusable.

Fig. 16.6(b) illustrates the similar case with a flexural hinge in column 12 ($4\,\text{m} \geq b > 0$), and Fig. 16.6(c) shows a general case with a flexural hinge in frame beam 23. Fig. 16.6(d) to (f) show systems with a sliding support at joint 1 which are similar to the three systems with flexural hinges; if α tends towards $\pi/2$, the system of Fig. 16.6(f) becomes unusable.

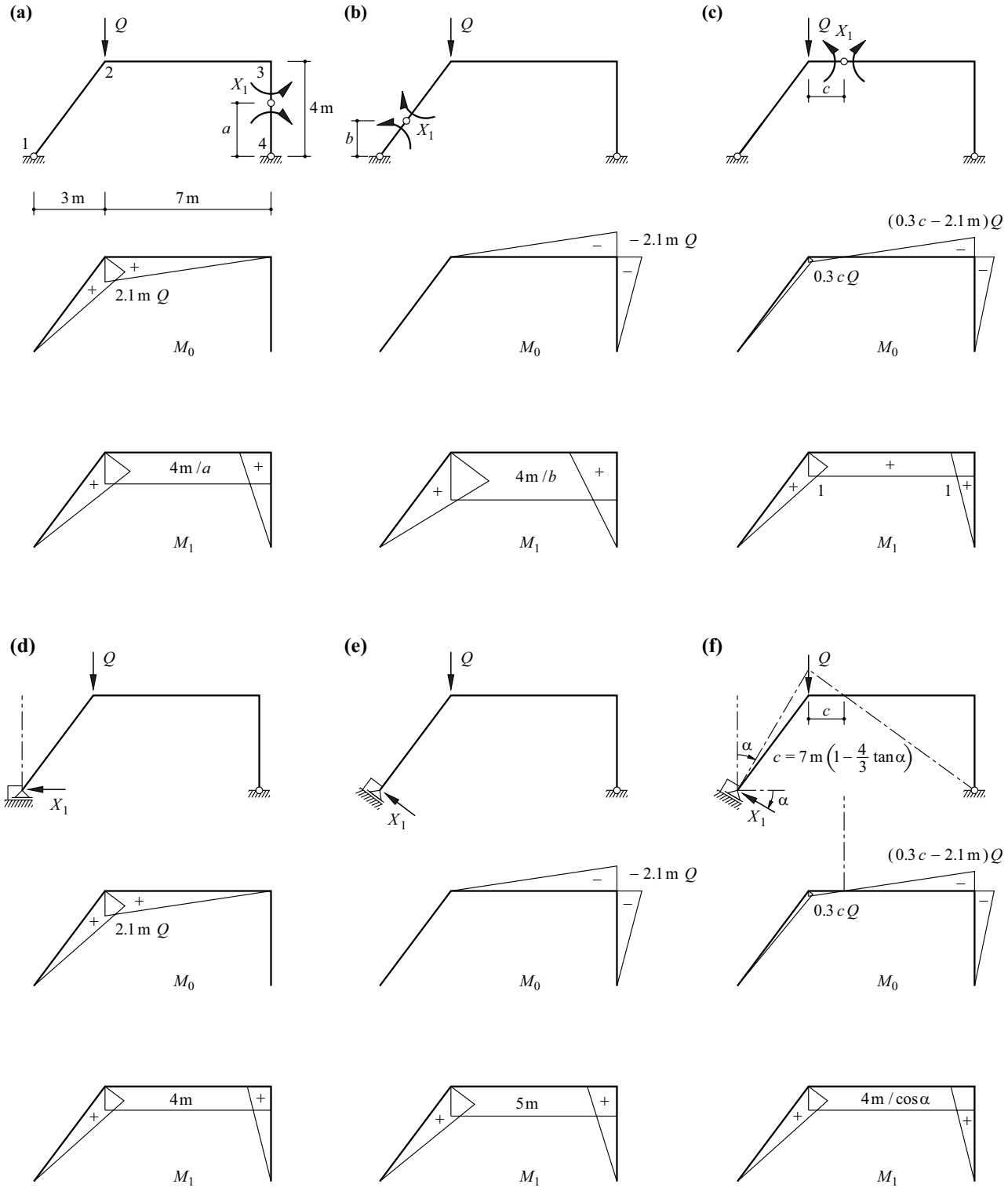

Fig. 16.6 Statically determinate basic systems: (a), (b) flexural hinges in columns, (c) flexural hinge in beam, (d) to (f) sliding support at joint 1

In order to distinguish between Fig. 16.2 and the variables associated with Fig. 16.6, a superscript asterisk (*) will be used below. Generally, the moments M_1^* in Fig. 16.6 result from M_1 in Fig. 16.2(b) by multiplying by a factor k_1, and the moments M_0^* in Fig. 16.6 follow from M_0 in Fig. 16.2(a) by adding a term $k_0 M_1$. Consequently, we get

$$\delta_{10}^* = (\delta_{10} + k_0\delta_{11})k_1 \quad , \quad \delta_{11}^* = \delta_{11}k_1^2 \tag{16.5}$$

i. e. according to (16.1),

$$X_1^* = -\frac{\delta_{10}^*}{\delta_{11}^*} = \frac{X_1 - k_0}{k_1} \tag{16.6}$$

and according to (16.2),

$$M^* = M_0^* + X_1^* M_1^* = M_0 + k_0 M_1 + \frac{X_1 - k_0}{k_1} \cdot M_1 k_1 = M_0 + X_1 M_1 = M \tag{16.7}$$

The choice of the basic system has no influence on the resulting force and deformation variables.

16.2.5.2 Yield limits – load and restraint

In the system considered here, plastic hinges can only form at joints 2 and 3 with the given load because constant flexural resistances are assumed. Further, $-M_y \le M_{2,3} \le M_y$ applies, see Fig. 16.7 with yield limit ABCD.

The solution to the one degree of static indeterminacy problem developed in section 16.2.3 for the system initially free from restraint corresponds to points on the straight lines OME or OF with the ratio $M_3/M_2 = -1.085/1.015 = -31/29$ for the moments at the corners of the frame. Points K and L correspond to, for example, the basic systems and M_0 diagrams shown in Fig. 16.6(a) and (b) respectively, and the lines KM and LM parallel with the diagonal AC correspond to the associated second term on the right in (16.2).

As we can see, specifying the two moments M_2 and M_3 is sufficient for the complete description of the potential stress states in the system under consideration, i. e. every point on the M_2M_3 plane describes a certain stress state. Zero-load, pure restraint states correspond to moments $M_2 = M_3$, i. e. points on the straight line OGA or OIC.

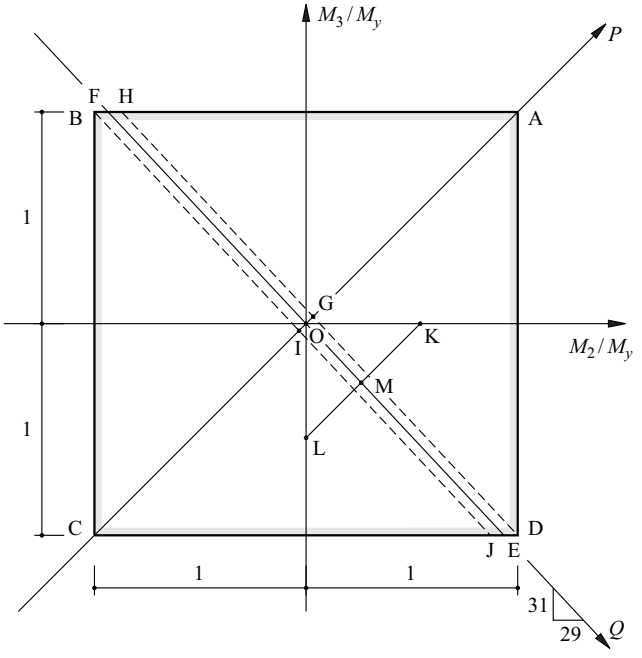

Fig. 16.7 Yield limits of the system with one degree of static indeterminacy

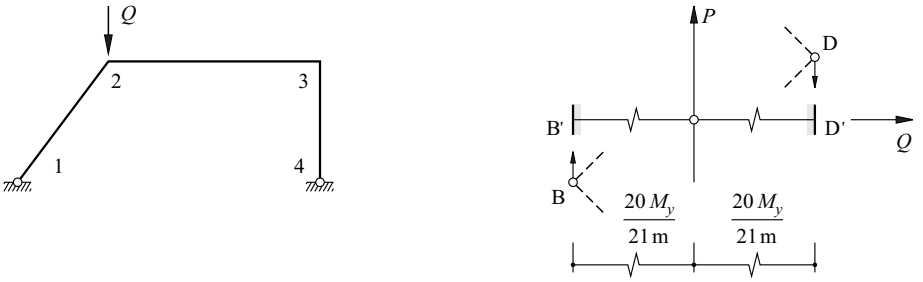

Fig. 16.8 Non-plastic domain B′D′ of rigid-plastic frame 1234

Applying a monotonic load to the initially restraint-free system causes the stress point in Fig. 16.7 to travel from O along the Q axis to point E, which corresponds to point C in Fig. 16.1(c). Afterwards, the stress point travels along the yield limit $M_3 = -M_y$ to point D, where $M_2 = M_y$ and hence the (positive) limit load characterised by plateau DE in Fig. 16.1(c) is reached. Subsequently relieving the load completely (purely elastically) causes the stress point to travel parallel with the Q axis along DG to point G on the P axis; the coordinates of G describe the restraint state remaining after relieving the load.

Subsequently loading in the opposite direction results in the stress path GH, where H indicates the formation of a (positive) plastic hinge at joint 3. During the following elastic-plastic phase, the stress point travels along HFB to the (negative) limit load point B, where $-M_2 = M_3 = M_y$, and fully relieving the load from this state causes the stress point to move along BI to point I on the P axis, a state that is opposite to the previous restraint state G.

Any loading-restraint histories in the skewed QP system of coordinates can be described in a similar way. Generally, an infinite number of stress points on lines parallel with the P axis, e. g. LMK, within the yield limits correspond to a certain level of loading Q. Apart from points D and B, for which the limit load is reached, the stress state therefore depends on the loading-restraint history.

In principle, the considerations made with the help of Fig. 16.7 can be readily transferred to multi-parameter loads (*m load parameters* Q_i) and systems with multiple degrees of indeterminacy (*n restraint parameters* P_j). The individual yield limits correspond to hyperplanes in the $(m+n)$-dimensional space of Q_i, P_j which enclose the *non-plastic domain* of the elastic-plastic system. The n-fold projection of this domain into the m-dimensional subspace of Q_i results in the yield limit or the non-plastic domain of the rigid-plastic system. For example, projecting points B and D parallel with the P axis onto the Q axis in Fig. 16.7 results in the non-plastic domain B′D′ of the rigid-plastic frame 1234 shown in Fig. 16.8. At the same time, the limit load $20M_y/(21\text{m})$ shown in Fig. 16.8 results in the Q axis scaling required in Fig. 16.7.

16.2.6 In-depth analysis of system with two degrees of static indeterminacy

Fig. 16.9 contains a diagram similar to Fig. 16.7 for the system with two degrees of static indeterminacy (fixed column base at joint 4). The non-plastic domain of the elastic-plastic system is a cube with sides of length $2M_y$. Points G, H and I in Fig. 16.9 correspond to Fig. 16.5(a), (b) and (c) or points F and G as well as line HI in Fig. 16.1(c). With a monotonic load increase, the stress point in Fig. 16.9 travels along line OGHI to point I, where the limit load $9M_y/(7\,\text{m})$ is reached.

Pure restraint states correspond to points on plane ABCDEF with the equation $M_2 - M_3 + 0.7M_4 = 0$. This plane is defined by vectors **OA** and **OB** (axes P_1, P_2), which are proportional to the unit force variable states shown in Fig. 16.2(b) and (c).

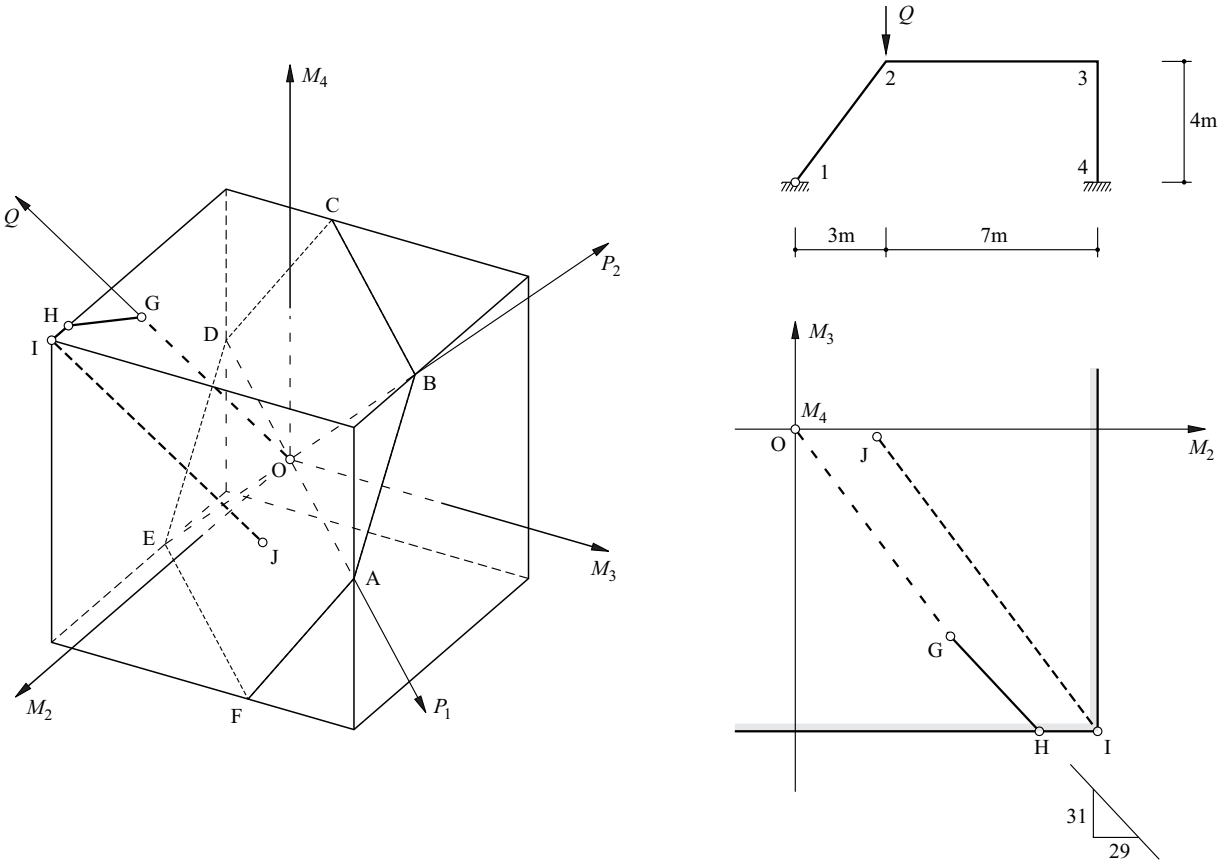

Fig. 16.9 System with two degrees of static indeterminacy

In the event of the load being completely relieved, the stress point travels back from I parallel with the Q axis until it reaches plane ABCDEF at point J with the coordinates $(0.271, -0.025, -0.422)M_y$.

16.3 Classic presentation of the force method

16.3.1 General procedure

The procedure explained in sections 16.2.3 and 16.2.4 with the help of statically indeterminate systems with one and two degrees of indeterminacy can be generalised as follows:

1. Determine the degree n of static indeterminacy.
2. Select a stable, statically determinate *basic system* by releasing n constraints and introducing corresponding *redundant variables* X_i.
3. Determine the support force variables and stress resultants C_0, S_0 and C_i, S_i for the basic system as a result of loads or as a result of unit force variables $X_i = 1$.
4. Determine the deformations (incompatibilities) δ_{i0} or δ_{ij} at the position and in the direction of X_i as a result of the external actions (loads and imposed deformations) or as a result of the unit force variables $X_j = 1$.
5. Set up and solve the following *compatibility conditions*:

$$\delta_i = \delta_{i0} + \sum_{j=1}^{n} \delta_{ij} X_j = 0 \qquad (i = 1, 2, \ldots, n) \tag{16.8}$$

6. Determine the support force variables and stress resultants for the statically indeterminate system by *superposing* the corresponding variables on the basic system:

$$C = C_0 + \sum_{i=1}^{n} C_i X_i \quad , \quad S = S_0 + \sum_{i=1}^{n} S_i X_i \tag{16.9}$$

16.3.2 Commentary

The methods discussed in section 9.3.3 are available for determining the degree n of static indeterminacy.

As outlined in section 16.2.5, apart from the requirement regarding kinematic stability, the choice of basic system is unimportant. Fig. 16.10 illustrates this requirement by way of systems with two degrees of static indeterminacy.

In order to achieve a set of equations (16.8) with minimal susceptibility to errors, the structural behaviour of the basic system should differ as little as possible from that of the statically indeterminate system. For example, for the system shown in Fig. 16.11, that is the case for the basic system of Fig. 16.11(c), but not for the basic system of Fig. 16.11(b). According to Fig. 16.11(b), neither of the components δ_{i0} and δ_{ij} in (16.8) is equal to zero, whereas according to Fig. 16.11(c), both δ_{30} and $\delta_{13} = \delta_{31}$ are equal to zero. When superposing M according to $(16.9)_2$, small differences result in large figures as shown at the bottom of Fig. 16.11(b); the associated set of equations (16.8) is *ill-conditioned*, i. e. even just small errors in δ_{i0} can lead to large errors in X_j. By contrast, the set of equations (16.8) belonging to Fig. 16.11(c) is *well conditioned*; the scopes of the redundant variables are limited, and therefore the elements not lying on the main diagonals of the *flexibility matrix* $\boldsymbol{\delta}$ with the coefficients δ_{ij} are only small or disappear completely, like $\delta_{13} = \delta_{31}$.

Instead of a statically determinate basic system, in some instances it can be worthwhile using a statically indeterminate basic system. Fig. 16.12 illustrates such a case. We get the expressions $Ql^3/(192EI)$ or $ql^4/(384EI)$ respectively for the deflection at mid-span of a beam of length l with infinite shear stiffness fixed at both ends and subjected to a central point load Q or a uniformly distributed line load q, where the bending stiffness EI is constant over the length of the beam. The statically indeterminate system with seven degrees of static indeterminacy shown in Fig. 16.12(a) can therefore be dealt with according to Fig. 16.12(b) by introducing a single redundant variable. The following applies:

$$\delta_{10} = \frac{ql_1^4}{384EI_1} \quad , \quad \delta_{11} = \frac{l_1^3}{192EI_1} + \frac{l_2^3}{192EI_2} + \frac{h}{EA}$$

from which X_1 follows from (16.1).

We shall refer to chapters 10 and 11 to calculate the support force variables and stress resultants using the statically determinate basic system, and the deformation variables δ_{i0} and δ_{ij} will be calculated with the help of the work theorem (14.4). The coefficients δ_{i0} combined in a column vector $\boldsymbol{\delta}_0$ are known as a *load vector.*

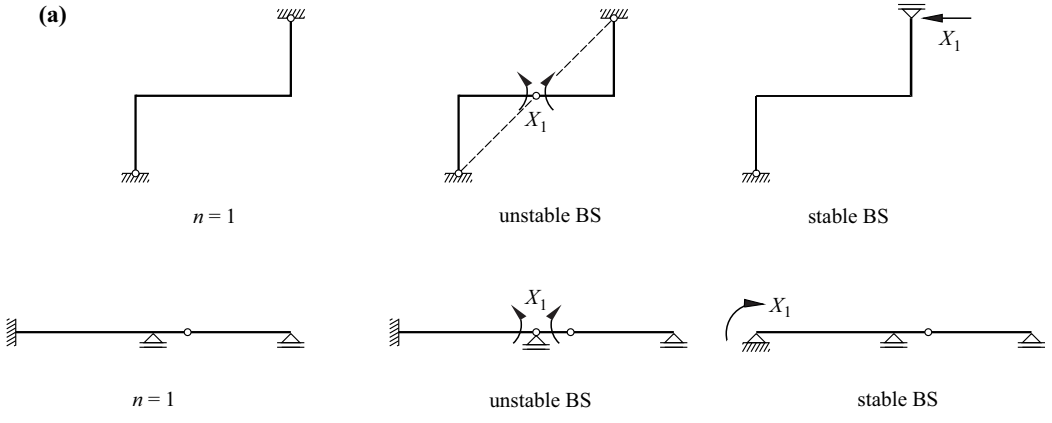

Fig. 16.10 Stability of basic system (BS): (a) staggered two-hinged frame, (b) cantilever beam with fixity at one end and propped beam at the other

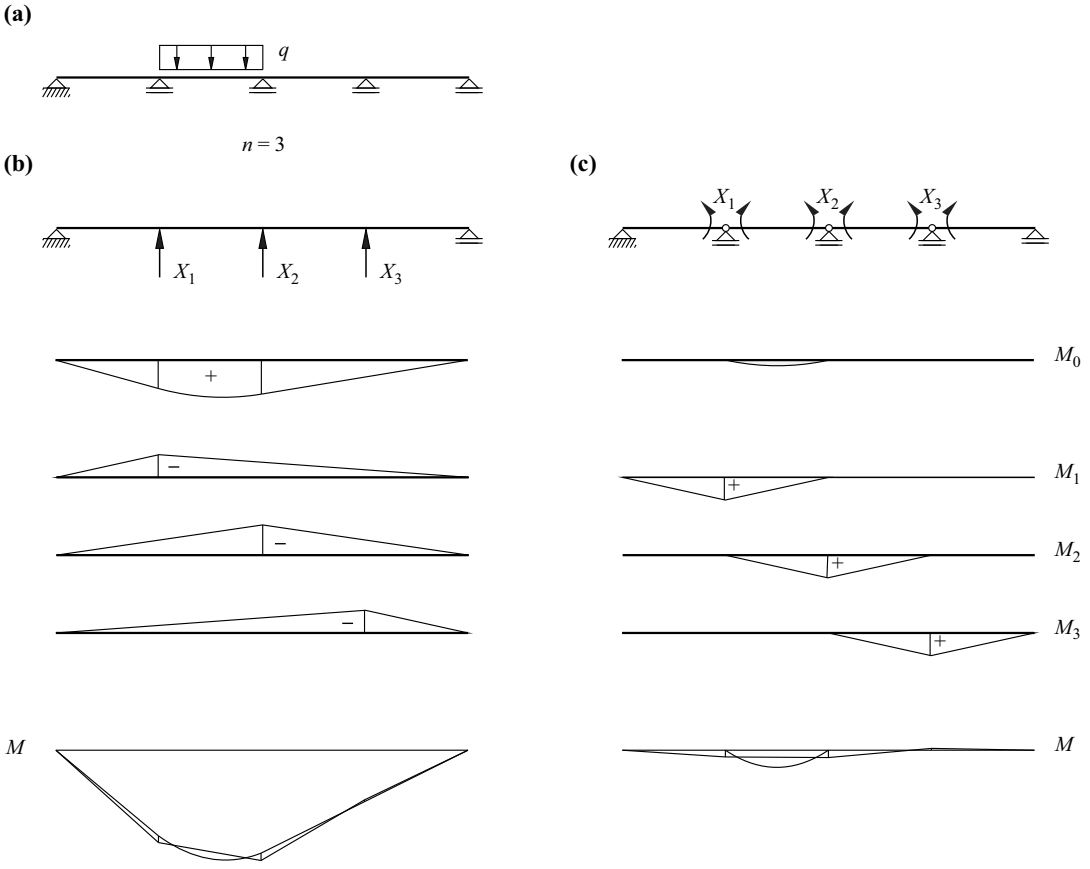

Fig. 16.11 Continuous beam with three degrees of static indeterminacy: (a) system and loads, (b) unsuitable basic system, (c) suitable basic system

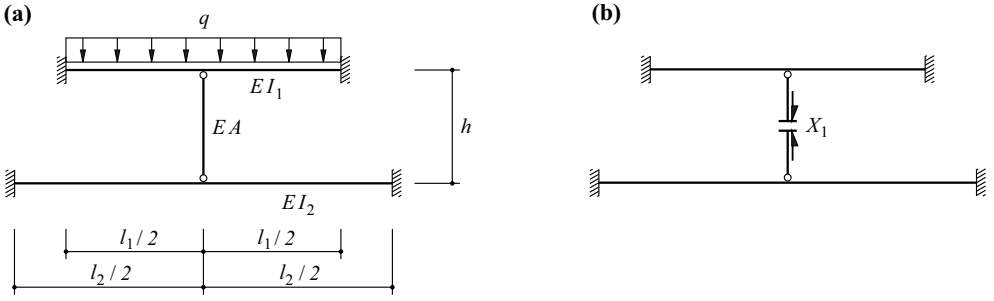

Fig. 16.12 Statically indeterminate basic system: (a) system and loads, (b) basic system and redundant variable

The *flexibility matrix* $\boldsymbol{\delta}$ with the coefficients δ_{ij} is square ($n \times n$), and symmetrical according to MAXWELL's theorem (8.88), and its main diagonal elements are positive:

$$\delta_{ii} = \int M_i \frac{M_i}{EI}\,\mathrm{d}x + \ \ldots = \int \frac{(M_i)^2}{EI}\,\mathrm{d}x + \ \ldots > 0 \tag{16.10}$$

Here, the ellipses (...) stand for the contributions of the other stress resultants according to the work theorem (14.4), which are often neglected. Further, owing to the linear independency of the compatibility conditions (16.8), $\boldsymbol{\delta}$ is invertible ($\det \boldsymbol{\delta} \neq 0$) and positive definite ($\boldsymbol{X}^{\mathrm{T}} \bullet \boldsymbol{\delta} \bullet \boldsymbol{X} > 0$).

According to ENGESSER's theorem (8.83), the deformation variables $\delta_j = \partial\Pi_i^*/\partial X_j$ corresponding to the redundant variables X_j must be equal to zero, i. e. using the complementary internal potential

$$\Pi_i^* = \int \left(\frac{M^2}{2EI} + \ ...\right) \mathrm{d}x = \int \left\{\frac{1}{EI} \cdot \left[\frac{M_0^2}{2} + M_0 \sum_{j=1}^{n} M_j X_j + \frac{(M_1 X_1)^2}{2} + M_1 X_1 \sum_{k=2}^{n} M_k X_k + \ ...\right] + \ ...\right\} \mathrm{d}x$$

resulting from the application of $(16.9)_2$, it follows that

$$\frac{\partial \Pi_i^*}{\partial X_j} = \int \left[\frac{1}{EI}\,(M_0 M_j + \sum_{k=1}^{n} M_j M_k X_k) + \ ...\right] \mathrm{d}x = \delta_{j0} + \sum_{k=1}^{n} \delta_{jk} X_k = 0$$

The compatibility conditions (16.8) thus correspond to maximum or minimum conditions of the function $\Pi_i^*(\boldsymbol{X})$; taking into account (16.10), we see that the effective (elastic, compatible) redundant variables $\boldsymbol{X}$ make the complementary internal potential Π_i^* a minimum.

The compatibility conditions (16.8) allow a further interpretation already known because of the reduction theorem mentioned in section 14.3. The unit force variable states are orthogonal to the effective (elastic, compatible) stress state, i. e. the internal displacement works

$$W_{ii} = \int M_i \frac{M}{EI}\,\mathrm{d}x + \ ... = \int M_i \frac{M_0 + \sum_{j=1}^{n} M_j X_j}{EI}\,\mathrm{d}x + \ ... = \delta_{i0} + \sum_{j=1}^{n} \delta_{ij} X_j$$

that they do on the deformations of the effective stress state are equal to zero because $W_{ei} = 0$ on its own. In addition to allowing the equilibrium to be easily checked (for the whole system or subsystems), these *orthogonality conditions* also permit an effective check of the results of calculations for statically indeterminate systems.

16.3.3 Deformations

16.3.3.1 Reduction theorem

If we initially confine ourselves to bending moment contributions $M_y = M$ when using the work theorem (14.4), then the theorem is reduced to

$$\delta_{ij} = \int M_i \frac{M_j}{EI}\,\mathrm{d}x \tag{16.11}$$

where the integral has to be applied over the entire statically indeterminate system or subsystem and the bending moments M_i and M_j according to $(16.9)_2$ are made up of components of generally dissimilar basic systems:

$$M_i = M_{i0} + \sum_{k=1}^{n} M_{ik} X_k \quad , \quad M_j = M_{j0} + \sum_{k=1}^{n} M_{jk} X_k \tag{16.12}$$

Owing to the fact that the unit force variable states M_{ik} are orthogonal to the elastic, compatible stress state M_j, or M_{jk} is orthogonal to M_i, as discussed in section 16.3.2, eq. (16.11) leads to the *reduction theorem*

$$\delta_{ij} = \int M_{i0} \frac{M_j}{EI}\,\mathrm{d}x = \int M_i \frac{M_{j0}}{EI}\,\mathrm{d}x \tag{16.13}$$

In order to calculate δ_{ij}, one of the two force states may be determined using any statically determinate basic system.

Example 16.1 Plane frame

The deflection V of the system with one degree of static indeterminacy due to load $Q = 0.922 M_y/\mathrm{m}$ was found to be $5.408\ \mathrm{m}^2\chi_y$ in section 16.2.3. In that section, Fig. 16.2(a) with $Q = 1$ played the role of M_{i0} in (16.13) and Fig. 16.2(d) that of M_j.

Applying Fig. 16.6(b) instead of Fig. 16.2(a) results in

$$V = \frac{1}{6} \cdot 2.1\,\mathrm{m} \cdot \left(2 \cdot 1 - \frac{1.015}{1.085}\right) \cdot \chi_y \cdot 7\,\mathrm{m} + \frac{1}{3} \cdot 2.1\,\mathrm{m} \cdot \chi_y \cdot 4\,\mathrm{m} = 5.408\,\mathrm{m}^2\chi_y$$

i. e. as expected, the same answer.

16.3.3.2 Thermal actions

Next, we shall investigate the effect of thermal actions and in doing so confine ourselves to uniform temperature changes T. Eq. (14.4) becomes

$$\delta_{ij} = \int N_i \left(\frac{N_j}{EA} + \alpha_T T \right) \mathrm{d}x = \int N_i \alpha_T T \, \mathrm{d}x \tag{16.14}$$

because N_j is a pure restraint state orthogonal to N_i. We can see that N_i in (16.14) refers to the statically indeterminate system.

Example 16.2 Bar fixed at both ends

The bar of length l shown in Fig. 16.13, which is fixed at both ends and has a constant axial stiffness EA = const and α_T = const, is subjected to a rise in temperature T = const along CD. The task is to calculate the displacement u_B of point B.

If point D can be displaced in the x direction, then $u_{D0} = \alpha_T T l/3$. A redundant variable $N_j = 1$ applied at D results in $u_{D1} = l/(EA)$, and from the compatibility condition $u_D = u_{D0} + N_j u_{D1} = 0$ it follows that $N_j = -EA\alpha_T T/3$. The expression in brackets in the integrand on the right in (16.14) corresponds to the normal strain $\varepsilon_x = \mathrm{d}u/\mathrm{d}x$ constant over each segment, which when considering the boundary conditions $u_A = u_D = 0$ results in a linear progression of u for each segment with $u_B = -\alpha_T T l/9$.

Instead of determining the displacement u via N_j und ε_x, the value of u_B can be obtained directly via $(16.14)_2$ from the force state N_i (for the statically indeterminate system) corresponding to a single force of magnitude 1 at B: $u_B = (-1/3)\alpha_T T l/3 = -\alpha_T T l/9$.

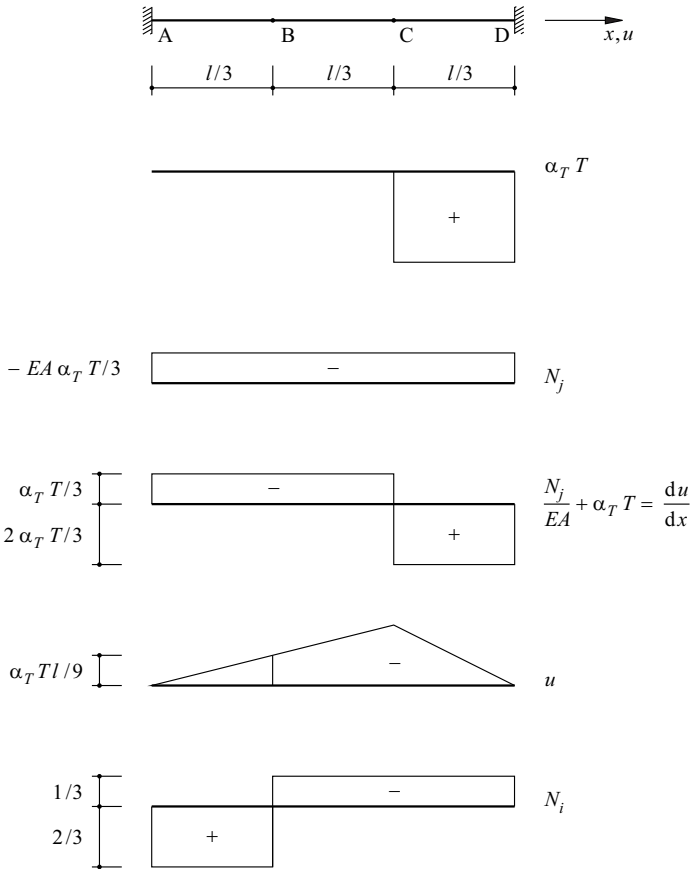

Fig. 16.13 Displacement u_B due to thermal action

16.3.3.3 Support displacements

To conclude this section, the influence of support displacements c_j will be investigated according to (14.4). The corresponding variables N_j etc. on the right in (14.4) may relate to the basic system according to (16.13), i. e. we may use N_{j0} etc. in the calcula-

tions. However, all these variables disappear in the statically determinate basic system; support displacements take place without restraint. Therefore,

$$\delta_{ij} = -\sum C_i c_j \tag{16.15}$$

applies, where C_i relates to the statically indeterminate system.

Example 16.3 Beam with one degree of static indeterminacy

Support C of the beam in Fig. 16.14(a), rigid in shear and with constant bending stiffness EI = const, is displaced downwards by an amount c. The task is to calculate the deflection w_B of point B. We get $\delta_{10} = 5l^3/(48EI)$ and $\delta_{11} = l^3/(3EI)$ for the force state shown in Fig. 16.14(b), from which, according to (16.1), it follows that $X_1 = C = -5/16$. Eq. (16.15) therefore results in $w_B = 5c/16$. As a check, we consider the cantilever beam examined in example 15.4 subjected to a point load Q at its unsupported end which causes a deflection of $Ql^3/(3EI)$ at this position. Putting this value equal to c results in a curvature $q_z^* = -3c/l^2$ at the unsupported end of the conjugate beam and therefore a moment $M_B^* = w_B = 5c/16$ at point B, see Fig. 16.14(c) and Fig. 15.8.

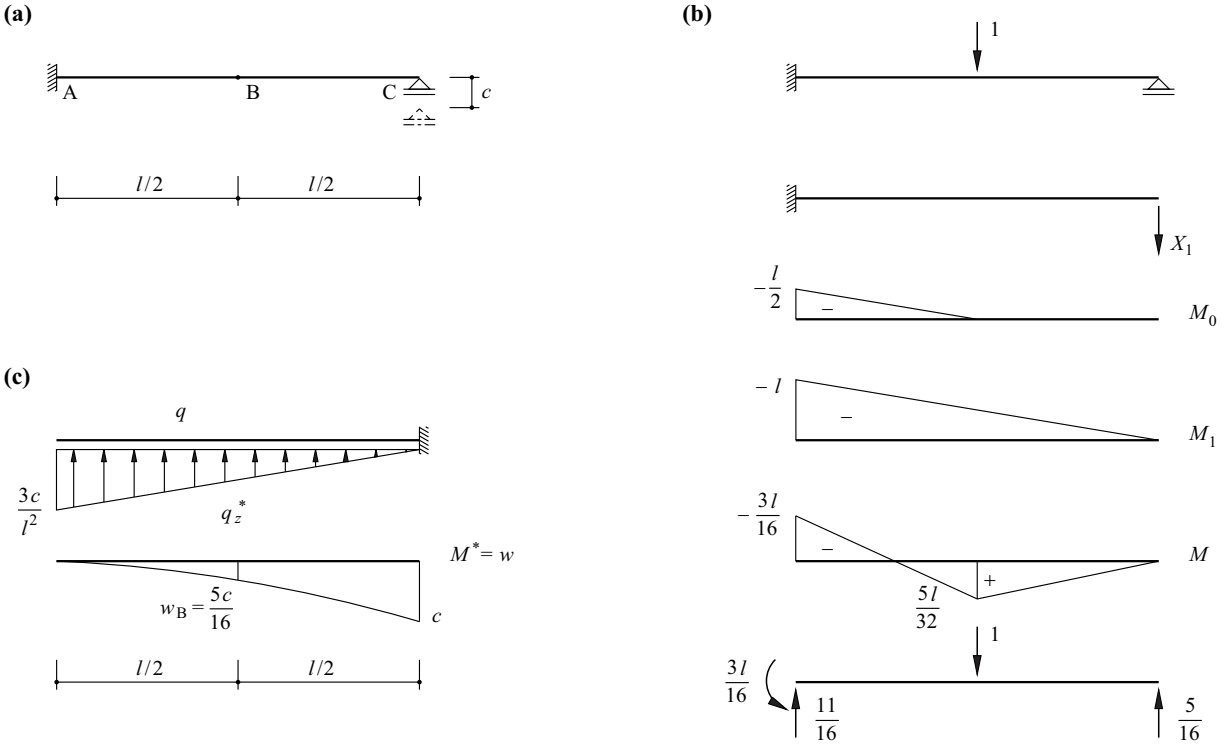

Fig. 16.14 Support displacement c: (a) system and notation, (b) force state, (c) conjugate system and deflection curve

16.3.3.4 Deformation diagrams

Deformation diagrams for statically indeterminate systems can be calculated in exactly the same way as for statically determinate cases: either point by point with the help of the work or reduction theorems, or as a whole by considering the exact shape of the function between individual joints. All the procedures outlined in chapter 15 can be applied similarly.

16.3.4 Influence lines

16.3.4.1 Influence lines for deformation variables

The relationship (12.3) applies irrespective of the degree n of static indeterminacy. The influence line of a deformation variable for a system with n degrees of static in-

determinacy is a deformation diagram that ensues when a corresponding unit force variable is applied to the system with n degrees of static indeterminacy at the position and in the direction of the deformation variable of interest.

Example 16.4 Continuous beam

In order to determine the influence line $\eta_{\varphi 2}$ for the rotation φ_2 at joint 2 of the system statically indeterminate to the second degree shown in Fig. 16.15(a), which is rigid in shear and has a constant bending stiffness EI, we introduce flexural hinges and corresponding redundant variables X_1 and X_2 at joints 1 and 2, see Fig. 16.15(b).

The moment of magnitude 1 at the position and in the direction of φ_2 can be applied to either bar 12 or bar 23 of the basic system, or to both bars proportionately. Considering the moments M_0, M_1 and M_2 due to the unit force variables, which are entered in Fig. 16.15(b), then according to (16.8), we get the following set of equations:

$$\begin{Bmatrix} 1/6 \\ 1/3 \end{Bmatrix} + \begin{bmatrix} 1/3 & 1/6 \\ 1/6 & 3/5 \end{bmatrix} \begin{Bmatrix} X_1 \\ X_2 \end{Bmatrix} = \begin{Bmatrix} 0 \\ 0 \end{Bmatrix}$$

where the factor $l/(EI)$ has been omitted from both terms on the left of the equation.

With the solution $X_1 = -8/31$, $X_2 = -15/31$, the result according to $(16.9)_2$ gives us the M diagram shown in Fig. 16.15(c). The curvature

$$\frac{M}{EI} = -w'' = \frac{-8 + 24x/l}{31EI}$$

of bar 12 is subjected to double integration, taking into account the boundary conditions $w(0) = w'(0) = 0$, to give us its deflection

$$w = \frac{4x^2(1 - x/l)}{31EI} \qquad (0 \le x \le l)$$

which is equal to the influence line between points 1 and 2 which we require, see Fig. 16.15(d). Similarly, the following applies between points 2 and 3:

$$-w'' = \frac{15(x - 1.8\,l)}{31EI \cdot 0.8\,l}$$

from which, by considering $w(l) = w(1.8l) = 0$, we get the deflection

$$w = \left(-0.1008\frac{x^3}{l^3} + 0.5444\frac{x^2}{l^2} - 0.9153\frac{x}{l} + 0.4718 \right) \frac{l^2}{EI} \qquad (l \le x \le 1.8l)$$

The unit of measurement for the "deflections" calculated here is $[m^2/(kNm^2)] = [1/kN]$. As expected, multiplying a coefficient of influence by a load [kN] results in a dimensionless value [kN/kN] = [-] or a rotation in rad or mrad.

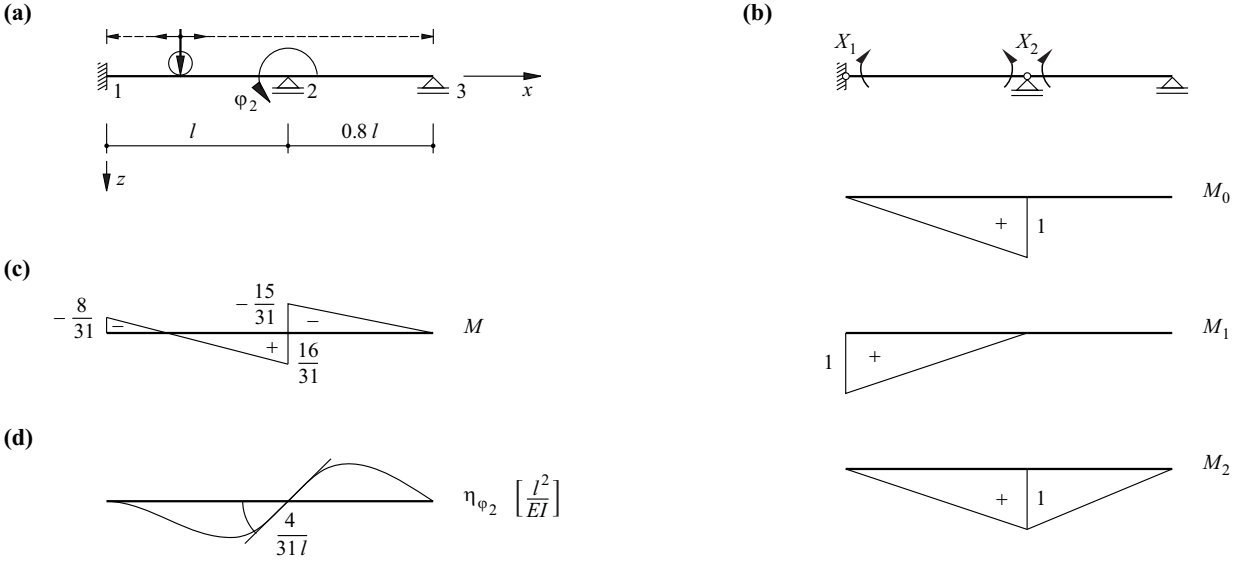

Fig. 16.15 Influence line for rotation φ_2: (a) system and notation, (b) basic system, redundant variables and unit force variable states, (c) bending moment due to unit force variable at the position and in the direction of φ_2, (d) influence line for φ_2

16.3.4.2 Influence lines for force variables

We shall make use of the system known from example 16.4 (see Fig. 16.16) in order to discuss influence lines for force variables. It was emphasized in section 12.3 that the kinematic method of determining influence lines retains its validity for statically indeterminate systems. However, the virtual deformation variable –1 must be imposed on the system with $n-1$ degrees of static indeterminacy, which means the individual system components are deformed. Bearing this in mind, the influence lines for the redundant variables X_1, X_2 and the moment M_4 shown in Fig. 16.16(d) to (f) can be immediately understood as deflection curves with a "kink –1" at the respective reference point. Generally, freehand sketching of such influence lines does not present any particular difficulties, and with a little practice they can be used not only qualitatively, e. g. for determining critical load positions, but also quantitatively, for estimating force variables.

The influence line of moment M_{40} shown in Fig. 16.16(c) for the statically determinate basic system of Fig. 16.16(b) ensues as a result of imposing a virtual rotation of –1 on the mechanism created by introducing a flexural hinge at point 4. This results in (positive) rotations of $1/2$ at the position of the redundant variables X_1, X_2, which are precisely equal to the moments M_{41} and M_{42} entered in Fig. 16.16(b), i. e. the moments occurring at point 4 as a result of $X_1 = 1$ and $X_2 = 1$ respectively.

Generally, the relationship

$$v_j = S_{ij} \tag{16.16}$$

applies for the deformation variable v_j at the position and in the direction of a redundant variable X_j according to the influence line for a force variable S_i in the basic system, where S_{ij} denotes the force variable S_i occurring in the basic system as a result of $X_j = 1$.

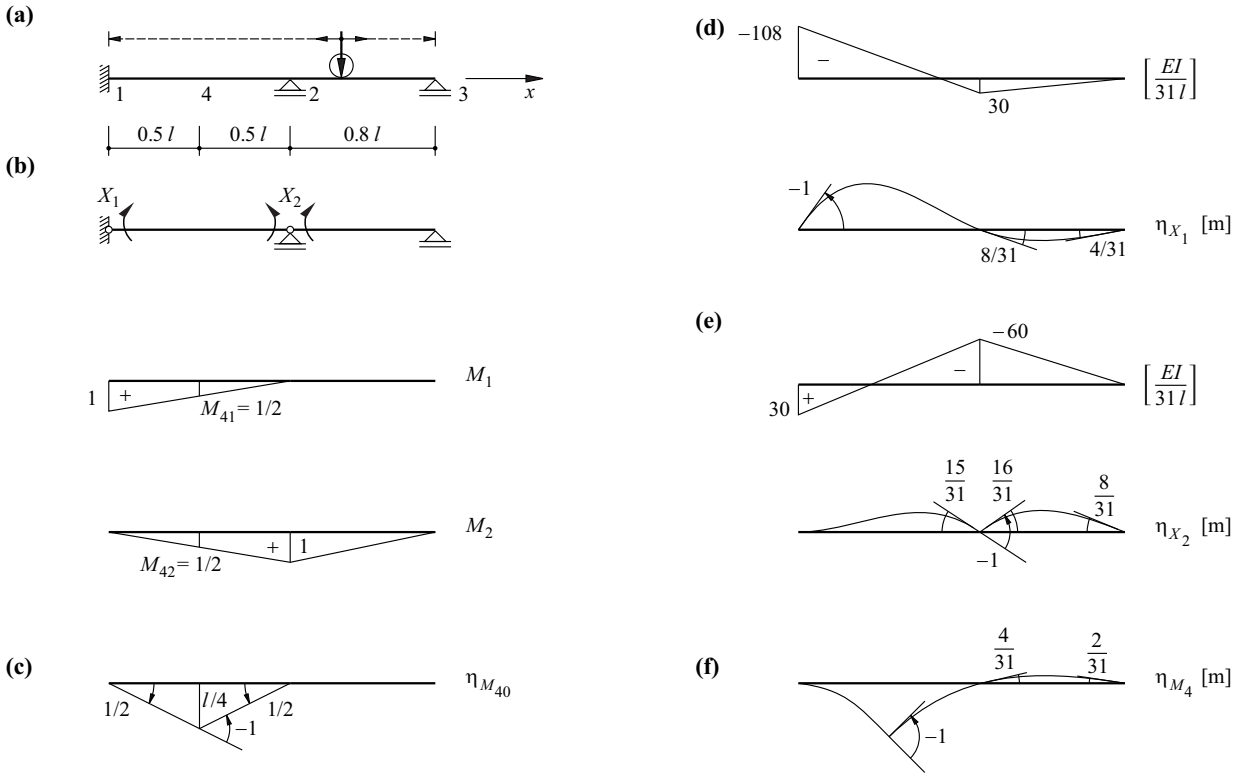

Fig. 16.16 Influence line for moment M_4: (a) system and notation, (b) basic system, redundant variables and unit force variable states, (c) influence line for basic system, (d) and (e) influence lines for redundant variables, (f) influence line for M_4

In order to verify (16.16), we combine the force state constituted by $X_j = 1$ with the virtual deformation state given by the influence line for S_i in the basic system. According to the work equation (8.14) or (8.15), only X_j and S_{ij} do work, i. e.

$$(X_j = 1) \cdot v_j + S_{ij} \cdot (-1) = 0$$

which verifies (16.16).

Eliminating the deformation variables v_j occurring on the influence line η_{Si0} for S_i in the basic system obviously requires the superposition of corresponding variables

$$v_j \cdot \eta_{X_j} = S_{ij} \cdot \eta_{X_j}$$

where η_{Xj} designates the influence line for X_j in the statically indeterminate system, i. e.

$$\eta_{S_i} = \eta_{S_{i0}} + \sum_{j=1}^{n} S_{ij} \cdot \eta_{X_j} \tag{16.17}$$

Owing to the discontinuities -1 occurring in η_{Xj} at positions j, the incompatibilities v_j in η_{Si0} are actually made to disappear:

$$v_j + S_{ij} \cdot (-1) = v_j + v_j \cdot (-1) = 0$$

The influence lines η_{Xj} for the redundant variables in the statically indeterminate system are obtained by imposing a (single) deformation variable $\delta_{j0} = 1$. According to (16.8), the following generally applies:

$$\boldsymbol{X} = -\boldsymbol{\delta}^{-1} \bullet \boldsymbol{\delta}_0 \tag{16.18}$$

The redundant variables ensuing as a result of $\delta_{j0} = 1$ are therefore specified by the jth column of the negative inverse of the flexibility matrix $\boldsymbol{\delta}$.

The matrix $\boldsymbol{\delta}$ already given in example 16.4 and its negative inverse are as follows:

$$\boldsymbol{\delta} = \frac{l}{EI}\begin{bmatrix} 1/3 & 1/6 \\ 1/6 & 3/5 \end{bmatrix} \quad , \quad -\boldsymbol{\delta}^{-1} = \frac{EI}{31l}\begin{bmatrix} -108 & 30 \\ 30 & -60 \end{bmatrix}$$

The moment diagrams shown in Fig. 16.16(d) and (e) are determined by the two columns of $-\boldsymbol{\delta}^{-1}$. Dividing by EI results in the corresponding curvatures, and double integration leads to η_{X1} and η_{X2}. Ultimately, (16.17) results in the influence line η_{M4} shown in Fig. 16.16(f).

Summing up, influence lines η_{Si} for force variables S_i for statically indeterminate systems according to (16.17) can be obtained by superposing the corresponding influence lines η_{Si0} for the statically determinate basic system and the weighted influence lines η_{Xj} for the redundant variables X_j for the statically indeterminate system. The latter appear as deformation lines by applying the redundant variables specified in the corresponding column of $-\boldsymbol{\delta}^{-1}$, and their weighting factors S_{ij} are equal to the force variables S_i for the basic system as a result of $X_j = 1$.

16.4 Applications

Example 16.5 Beam fixed at both ends

Fig. 16.17(a) shows once again the beam fixed at both ends which was examined in example 15.2, rigid in shear and with a constant bending stiffness EI. No loads or restraints in the x direction are to be considered and so we can confine ourselves to investigating the two redundant variables X_1 and X_2 of the basic system shown in Fig. 16.17(b).

According to (16.11), the unit force variable states shown in Fig. 16.17(b) result in the flexibility matrix

$$\boldsymbol{\delta} = \frac{l}{EI}\begin{bmatrix} 1/3 & 1/6 \\ 1/6 & 1/3 \end{bmatrix}$$

with the negative inverse

$$-\boldsymbol{\delta}^{-1} = \frac{EI}{l}\begin{bmatrix} -4 & 2 \\ 2 & -4 \end{bmatrix}$$

Using the M_0 diagram shown in Fig. 16.17(c), the load vector for the uniformly distributed line load q already considered in example 15.2 is

$$\boldsymbol{\delta}_0 = \frac{ql^3}{EI}\begin{Bmatrix} 1/24 \\ 1/24 \end{Bmatrix}$$

and therefore the solution to the compatibility conditions (16.8) leads to the redundant variables

$$\boldsymbol{X} = ql^2\begin{Bmatrix} -1/12 \\ -1/12 \end{Bmatrix}$$

Consequently, the result is the M diagram shown at the bottom of Fig. 16.17(c) and already known from Fig. 15.4.

We shall now consider a rotation of magnitude 1 at fixed end 2, as shown in Fig. 16.17(d). Using

$$\boldsymbol{\delta}_0 = \begin{Bmatrix} 0 \\ -1 \end{Bmatrix}$$

and solving (16.8) results in

$$\boldsymbol{X} = \frac{EI}{l}\begin{Bmatrix} -2 \\ 4 \end{Bmatrix}$$

So we get the linear shape to the bending moment (restraint moment) diagram shown in Fig. 16.17(d) (lower diagram), which corresponds to a constant shear force $V = 6\,EI/l^2$.

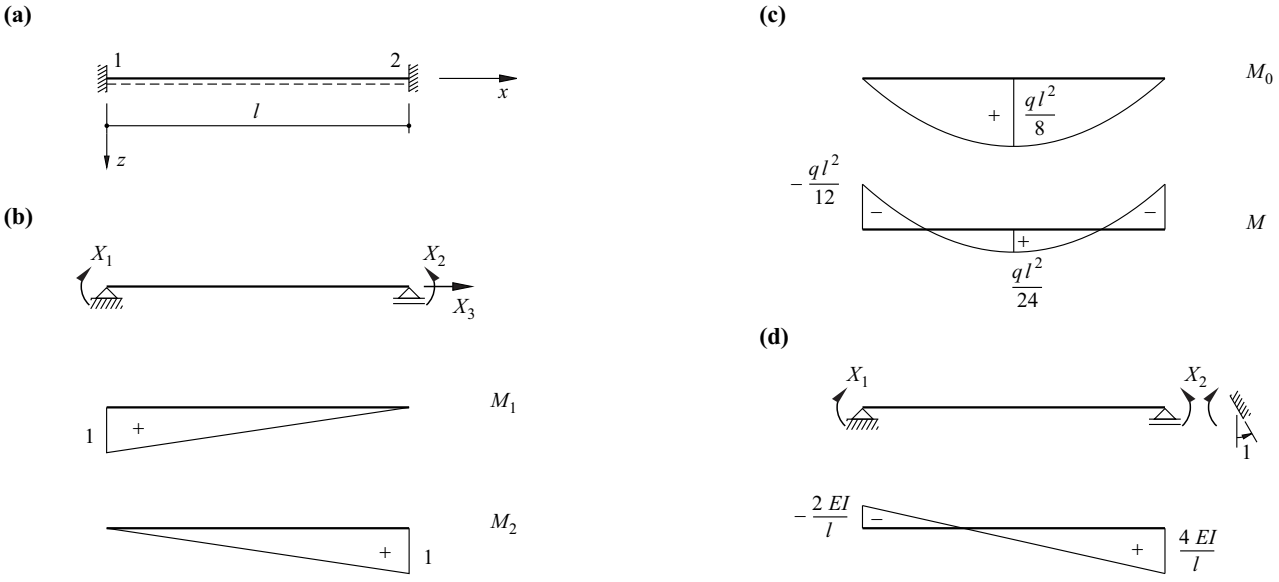

Fig. 16.17 Beam rigid in shear and fixed at both ends: (a) diagram of static system, (b) basic system, redundant variables and unit force variable states, (c) uniformly distributed line load, (d) support rotation

Example 16.6 Continuous beam of infinite length

The continuous beam shown in Fig. 16.18(a) has an infinite number of spans of length l, a constant bending stiffness EI and is rigid in shear. Subjected to uniformly distributed permanent loads g, the result according to example 16.5 is the bending moment diagram in Fig. 16.18(a) (lower diagram). The positive moments due to imposed loads q become a maximum when every second span is loaded, see Fig. 16.18(b). This is easy to see when we draw an influence line for the bending moment in the middle of a span, for instance. As is known from the rearrangement of the load in example 5.7, load q can be divided into a symmetric, uniformly distributed load $q_1 = q/2$ and an antisymmetric load $q_2 = \pm q/2$. Moment $M(q_1)$ results in a similar way to $M(g)$, and $M(q_2)$ is statically determinate. Altogether, the result for $M(q)$ is maximum values of $ql^2/12$ in the loaded spans and minimum vales of $-ql^2/24$ in the unloaded spans.

Fig. 16.18(c) shows the imposed load required to produce maximum support forces and moments (at A). We again use the procedure for rearranging the loads and introduce a flexural hinge at A for $M(q_2)$. According to the reduction theorem, the rotation φ_{A0} as a consequence of q_2 results from the introduction of the force state shown in Fig. 16.18(d). Applying Fig. 14.2, we get

$$\varphi_{A0} = -\frac{1}{3}\cdot 1 \cdot \frac{ql^2}{16}\cdot\frac{l}{EI} = -\frac{ql^3}{48EI}$$

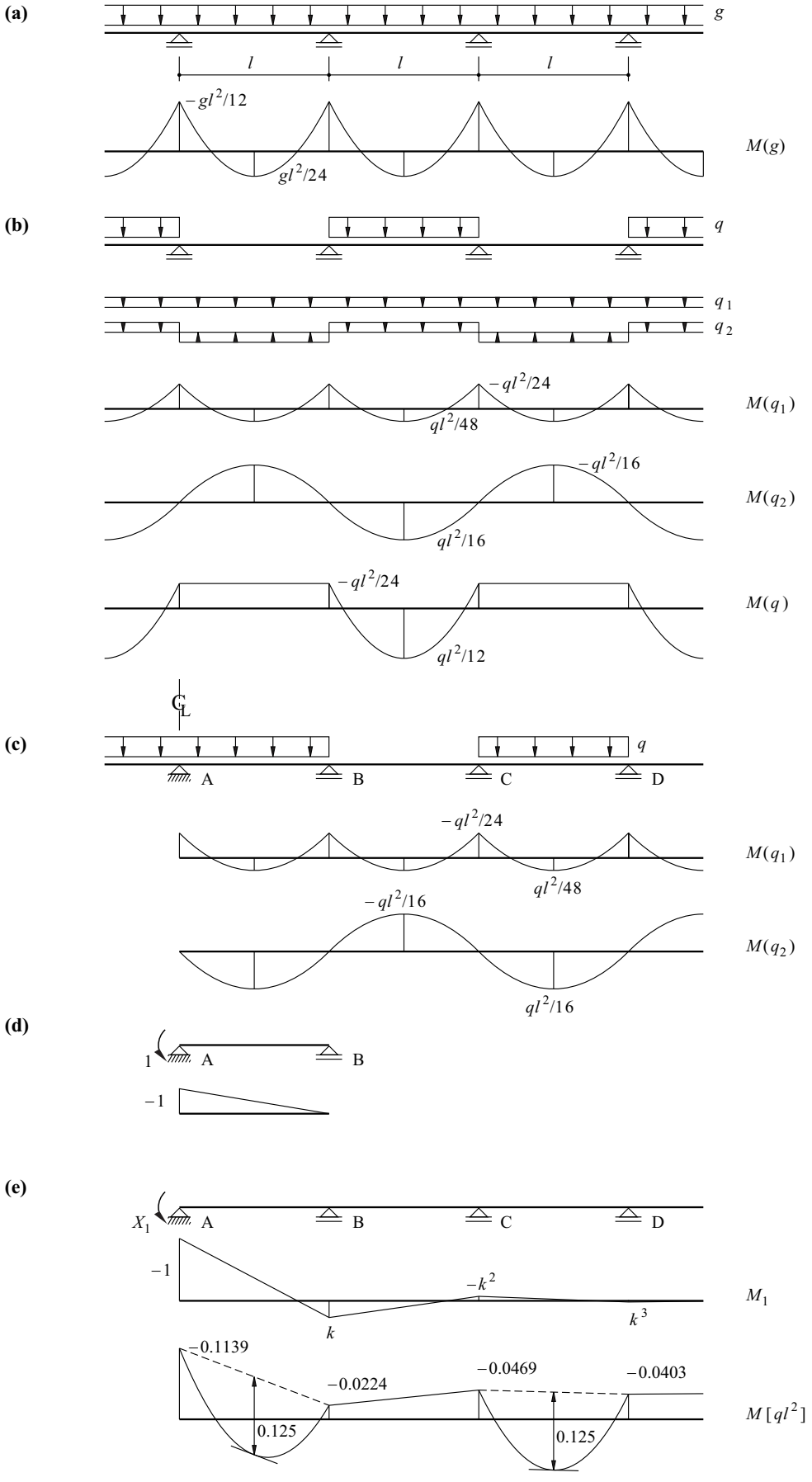

Fig. 16.18 Continuous beam of infinite length: (a) permanent loads, (b) arrangement of imposed loads for maximum span moments, (c) arrangement of loads for maximum support forces and moments (at A), (d) force state for calculating φ_{A0}, (e) influence of a redundant variable X_1 at A and resulting moments

A moment $X_1 = 1$ introduced at A causes moments of $k, -k^2, k^3$, ... at B, C, D, ... because owing to the infinite number of identical spans, there must be the same ratio $-k$ between the end moments in every span, see Fig. 16.18(e).

In order to determine the factor k, we calculate φ_B according to the reduction theorem by considering, on the one hand, a simply supported beam AB with a moment of magnitude 1 applied at B and, on the other, a similar simply supported beam BC. Using Fig. 14.2, it follows that

$$\varphi_B = \frac{l}{6EI}(-1 + 2k) = \frac{l}{6EI}(-2k + k^2)$$

from which it follows that $k = 2 \; -k = 2 - \sqrt{3}$.

Using the force state shown in Fig. 16.18(d) again, we get

$$\varphi_{A1} = \frac{l}{6EI}(2 - 2 + \sqrt{3}) = \frac{\sqrt{3}\,l}{6EI}$$

which according to (16.1) can be used to obtain

$$X_1 = -\frac{-\varphi_{A0}}{\varphi_{A1}} = \frac{\sqrt{3}\,ql^2}{24}$$

The moments $M(q)$ resulting from the superposition of $M(q_1)$, $M(q_2)$ and $X_1 M_1$ according to (16.2) are shown in the lower diagram of Fig. 16.18(e).

Fig. 16.19 summarises the various possible moment diagrams in one span for a numerical example ($l = 6$ m, $g = 8$ kN/m, $q = 5$ kN/m). The dotted lines in Fig. 16.19(c) and (d) indicate the moments when the span adjacent to the one being considered is loaded with the imposed load q. We can also see that the moment $M = 22.2$ kNm at mid-span in Fig. 16.19(d) does not correspond to the maximum positive moment, which is 22.5 kNm and occurs 211 mm from the middle of the span.

Fig. 16.20 shows all the moments for a half span. The envelopes enclosing all these lines for both positive and negative moments are called moment *envelopes*. For the positive moments, the envelope is made up of the solid line in Fig. 16.19(c) and the solid line on the right in Fig. 16.19(d); for the negative moments it is made up of the solid and dotted lines on the left in Fig. 16.19(d) plus the dotted line in Fig. 16.19(c). Quite remarkable is the fact that negative moments can occur over almost one-third of the span on either side of the support. To cope with such moments, a reinforced concrete beam, for example, will require reinforcement in the top face because the tensile strength of concrete is negligible.

Fig. 16.21 shows the maximum span and support moments (M^+ and M^-) caused by various load cases. Here, points A to D correspond to the solid lines in Fig. 16.19(a) to (d). The combination of the maximum positive and negative moments of 27.0 and -44.5 kNm corresponds to point E in Fig. 16.21. It is quite obvious that a safe design is one in which the resistance of all the cross-sections of the beam is designed for these moments. Actually, however, the resistance along the beam may be graduated to suit the envelopes, e. g. in a reinforced concrete beam by successively curtailing the amount of bottom reinforcement near mid-span or the top reinforcement near the supports.

All the moments drawn in Fig. 16.20 were calculated assuming an initially restraint-free system. A constant (positive or negative) restraint moment would cause an upward or downward displacement of the x axis in Fig. 16.20, and a displacement of the design point E in Fig. 16.21 along the straight line EF ($M^+ - M^- = 71.5$ kNm) downward to the right or upward to the left. Such a superposition of a restraint state (identical for all load cases and including load factors γ_F according to section 4.6.2) corresponds to a procedure according to the *shakedown theorem* discussed in sections 20.2.1.4 and 21.5.

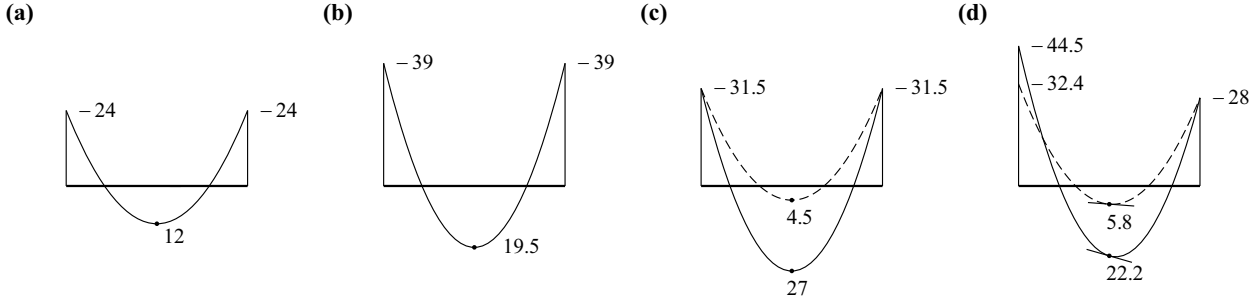

Fig. 16.19 Continuous beam of infinite length ($l = 6$ m, $g = 8$ kN/m, $q = 5$ kN/m) – moments [kNm] as a result of: (a) permanent load g, (b) total load $g + q$, (c) permanent and imposed loads for maximum span moments $g + q^+$, (d) permanent and imposed loads for maximum support moments $g + q^-$

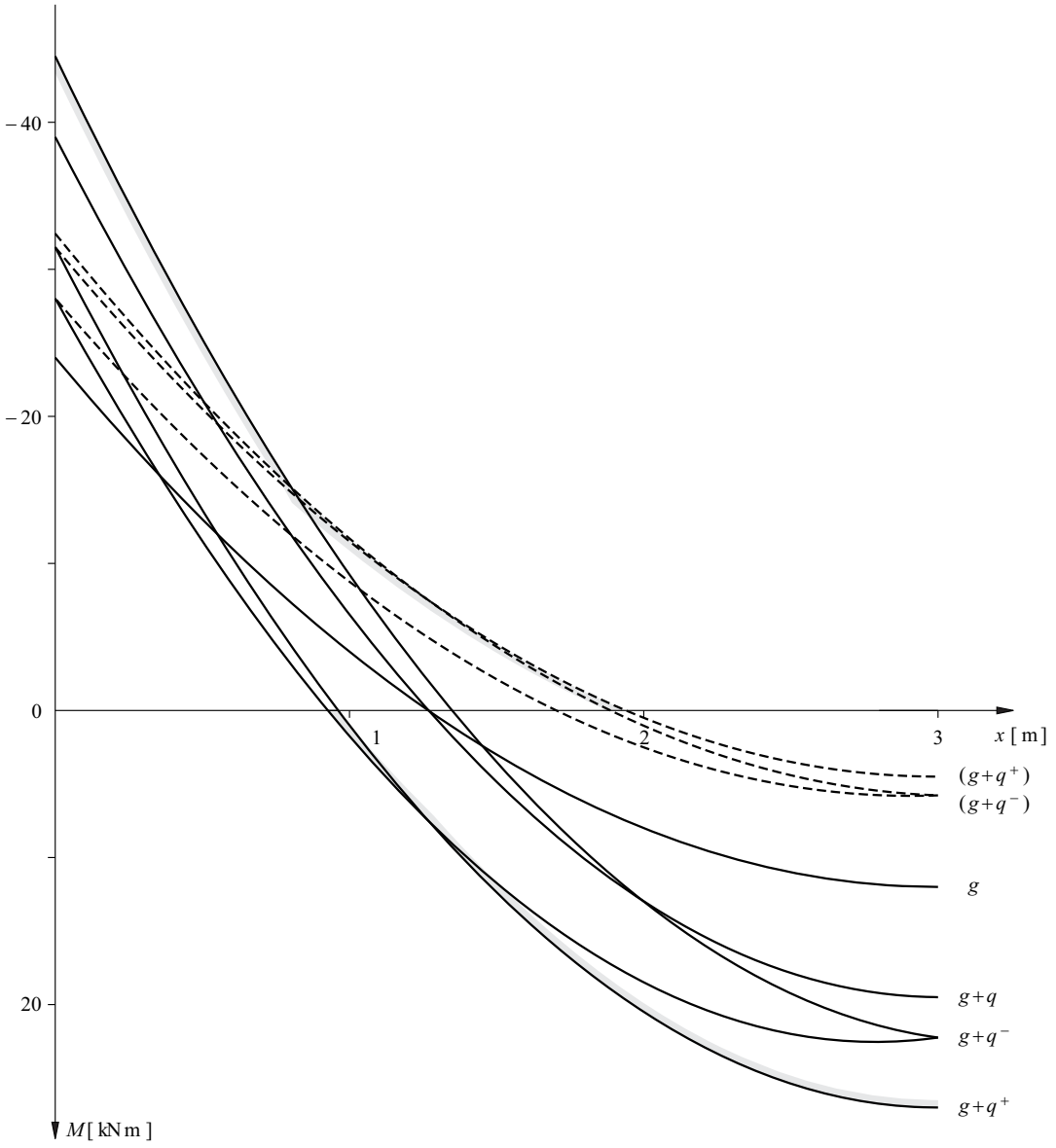

Fig. 16.20 Envelopes for the bending moments of a continuous beam of infinite length

Superposing a specific optimum restraint state for each load case causes a movement along straight line BCG ($M^+ - M^- = 58.5\,\text{kNm}$) in Fig. 16.21. In contrast to dimensioning according to the shakedown theorem, in which following an initial plastification, a purely elastic behaviour of a linear elastic - perfectly plastic system is guaranteed, such dimensioning can exhaust the *deformation capacity* of the system through *alternating* or *progressive plastification*. The risk of such a failure depends on the loading history, and it is up to the engineer to decide whether to compare the plastic *deformation demand* with the plastic deformation capacity and weigh up the situation. In principle, there is no objection to performing the dimensioning based on a rigid - perfectly plastic idealisation of the system, provided the necessary deformation capacity is guaranteed. Depending on the circumstances, considerably smaller resistances will have to be provided compared with dimensioning according to the shakedown theorem (line BCG instead of EF in Fig. 16.21), which results in much more economic solutions.

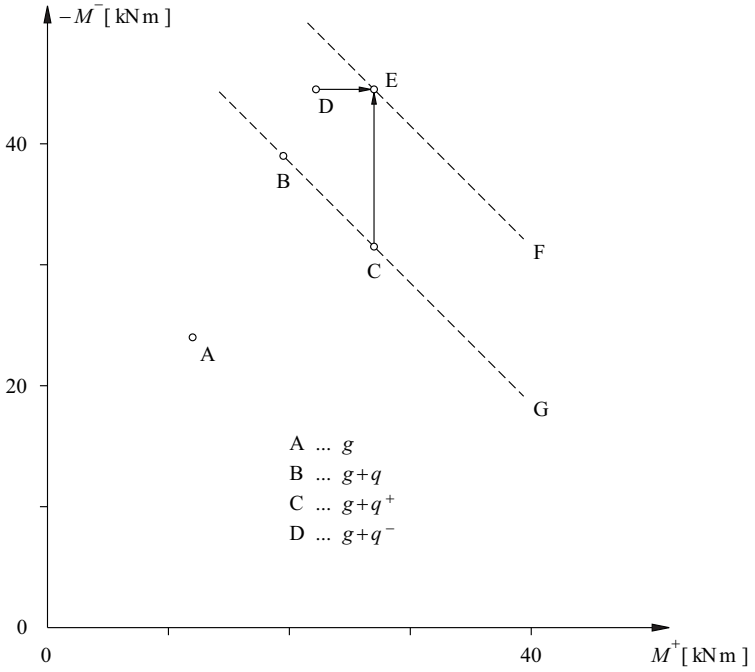

Fig. 16.21 Span and support moments for a continuous beam of infinite length – elastic-plastic (EF) or rigid-plastic (BCG) dimensioning

Example 16.7 Continuous beam – support settlement

Support B of the system shown in Fig. 16.22(a) undergoes a settlement δ_B. The basic system shown in Fig. 16.22(b) results in the load vector

$$\boldsymbol{\delta}_0 = \begin{Bmatrix} -l_2/l_1 - 1 \\ 1 \end{Bmatrix} \delta_B / l_2$$

and therefore X_1 and X_2 can be readily determined according to (16.8).

Fig. 16.22(c) shows an alternative basic system. In this case the compatibility conditions are

$$\begin{Bmatrix} \delta_1 \\ \delta_2 \end{Bmatrix} = \begin{bmatrix} \delta_{11} & \delta_{12} \\ \delta_{21} & \delta_{22} \end{bmatrix} \begin{Bmatrix} X_1 \\ X_2 \end{Bmatrix} = \begin{Bmatrix} -\delta_B \\ 0 \end{Bmatrix}$$

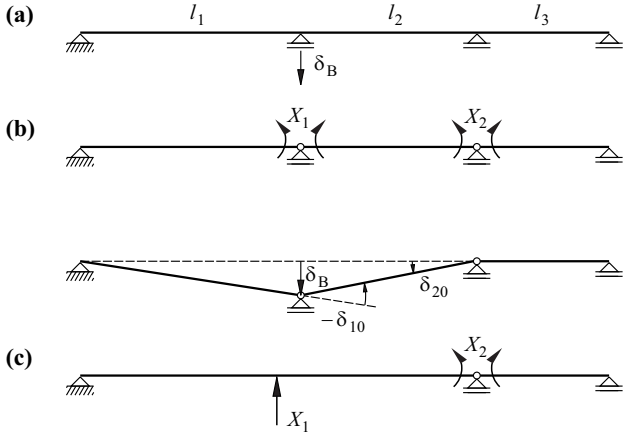

Fig. 16.22 Support settlement δ_B: (a) diagram of static system, (b) basic system, redundant variables and determining the load vector, (c) alternative basic system

Example 16.8 Arch fixed at both ends

The arch shown in Fig. 16.23(a) is subjected to an antisymmetric load $\pm q/2$; it is assumed to be inextensible and rigid in shear, and is in the form of a quadratic parabola. The bending stiffness is $EI = EI_S/\cos\varphi$, where EI_S designates the bending stiffness at the crown. Using the basic system and the redundant variables according to Fig. 16.23(b) results in the moment diagrams shown in Fig. 16.23(c). Considering $\mathrm{d}x = \mathrm{d}s\cos\varphi$, the elements of the load vector and the flexibility matrix are given by

$$\delta_{i0} = \int M_i \frac{M_0}{EI}\,\mathrm{d}s = \frac{1}{EI_S}\int M_i M_0\,\mathrm{d}x \quad , \quad \delta_{ik} = \int M_i \frac{M_k}{EI}\,\mathrm{d}s = \frac{1}{EI_S}\int M_i M_k\,\mathrm{d}x$$

Therefore, the compatibility conditions (16.8) are

$$\begin{Bmatrix}\delta_1\\ \delta_2\\ \delta_3\end{Bmatrix} = \frac{ql^3}{384EI_S}\begin{Bmatrix}1\\ -1\\ 0\end{Bmatrix} + \frac{l}{EI_S}\begin{bmatrix}1/3 & 1/6 & -f/3\\ 1/6 & 1/3 & -f/3\\ -f/3 & -f/3 & 8f^2/15\end{bmatrix}\begin{Bmatrix}X_1\\ X_2\\ X_3\end{Bmatrix} = \begin{Bmatrix}0\\ 0\\ 0\end{Bmatrix}$$

from which it follows that

$$\boldsymbol{X} = \frac{ql^2}{64}\begin{Bmatrix}1\\ -1\\ 0\end{Bmatrix}$$

Fig. 16.23(d) shows the ensuing bending moment and shear force diagrams, where V refers to vertical sections and not sections perpendicular to the bar axis. The maximum bending moments at the points of fixity are $\pm\, ql^2/64$, those in the span are $\pm\, 9ql^2/1024$, and occur at a distance of $3l/16$ on either side of the crown. Obviously, the flow of forces illustrated in Fig. 16.23(e) corresponds to that of the equivalent beam with one degree of static indeterminacy, see Fig. 16.23(f) and example 8.5.

Let us consider the arch with $f = 40\,\mathrm{m}$, $l = 200\,\mathrm{m}$ as a practical example, see Fig. 16.24(a), which is loaded with uniformly distributed permanent loads $g = 1\,\mathrm{MN/m}$ and an asymmetric imposed load $q = 0.1\,\mathrm{MN/m}$. The 8 m wide solid cross-section of the arch is 3 m deep at the springings and 2.76 m deep at the crown. Subjected to the uniformly distributed loads $g + q/2$, the beam with three degrees of static indeterminacy and fixed at both ends behaves in the same way as the statically determinate three-hinged arch of example 5.6. That gives rise to purely normal

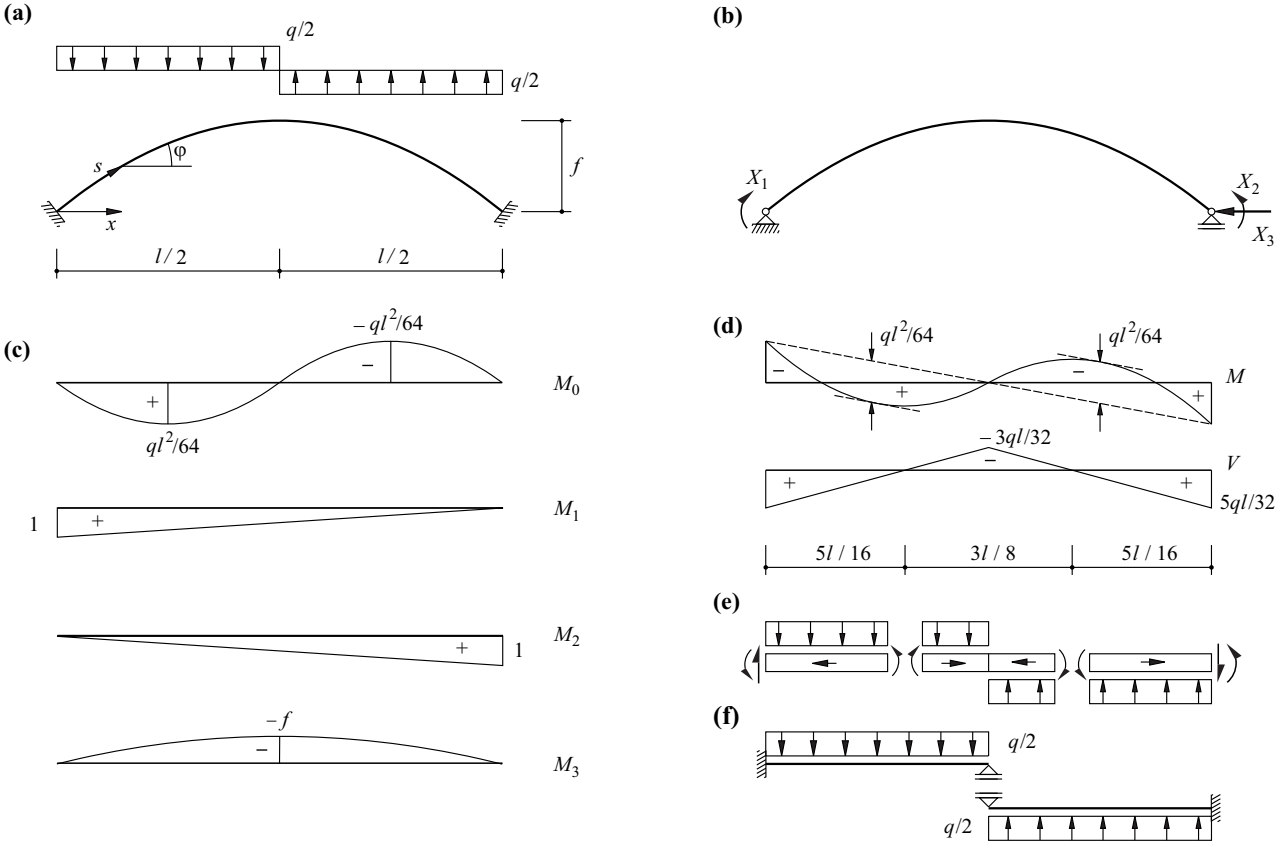

Fig. 16.23 Parabolic arch fixed at both ends and subjected to an antisymmetric load: (a) diagram of static system, (b) basic system and redundant variables, (c) moments for the basic system, (d) moments and shear forces for the statically indeterminate system, (e) free body diagrams and flow of forces, (f) equivalent beam

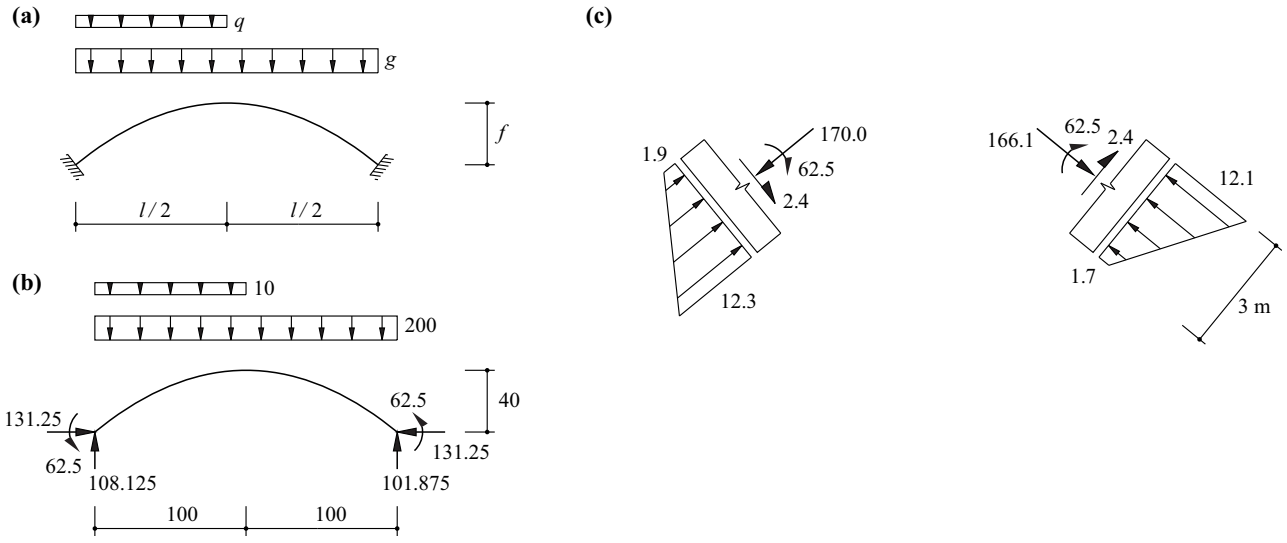

Fig. 16.24 Parabolic arch fixed at both ends: (a) diagram of static system, (b) free body diagram [m, MN], (c) stress resultants [MN, MNm] and normal stresses [N/mm^2] at the springings

forces (compressive forces) with a constant horizontal component $H = (g + q/2)l^2/(8f) = 1.05 \cdot 200^2/(8 \cdot 40) = 131.25$ MN. The antisymmetric imposed load $\pm q/2$ causes fixity moments amounting to $ql^2/64 = 0.1 \cdot 200^2/64 = 62.5$ MNm. The vertical support forces are $(g + q/2)l/2 \pm 5ql/32 = 1.05 \cdot 100 \pm 5 \cdot 0.1 \cdot 200/32 = 108.125$ and 101.875 MN, see Fig. 16.24(b). Fig. 16.24(c) shows the stress resultants converted to sections perpendicular to the axis of the arch at the two springings and the normal stress distributions resulting from bending and normal force according to (13.16).

Example 16.9 Beam on skew supports

Fig. 16.25(a) shows a beam of length l "skewed to the left", rigid in shear and with constant bending stiffness EI and constant torsional stiffness GK. The beam is supported on rigid transverse beams at A and B and loaded with q = const. The expression "skewed to the left" (or "skewed to the right") refers to the change in the direction of the beam axis from the normal to the transverse beam axis at the end. The basic system shown in Fig. 16.25(b) plus the resulting state diagrams of Fig. 16.25(c) result in

$$\delta_{10} = \frac{ql^3}{24EI}(\cos\beta + \sin\beta\cot\alpha) \quad , \quad \delta_{11} = \frac{l\cos^2\beta}{3EI}(\tan^2\beta\cot^2\alpha + \tan\beta\cot\alpha + 1) + \frac{l\sin^2\beta}{GI_x}$$

and therefore $X_1 = -\delta_{10}/\delta_{11}$ according to (16.1). As we can see, the skew to the left ($0 < \alpha, \beta < \pi/2$) leads to a negative X_1 value and therefore also negative torques $T = X_1 \sin\beta$. The result for a skew support to the right ($\pi/2 < \alpha, \beta < \pi$) is positive X_1 and T values.

Let us consider the case of $\alpha = \beta = \pi/4$ as a practical example, see Fig. 16.26. We get

$$X_1 = \frac{-\sqrt{2}ql^2}{12\left(1 + \dfrac{EI}{GI_x}\right)}$$

and support forces

$$A_{1,2} = B_{2,1} = \frac{ql}{4} \mp \frac{ql^2}{24a\left(1 + \dfrac{EI}{GI_x}\right)}$$

Presuming $l = 8a$ and $3EI = 5GI_x$ results in $A_1 = B_2 = ql/8$, $A_2 = B_1 = 3ql/8$ and $T = -ql^2/32$. The skew supports function like fixity at the ends of the beam. Supports A_2 and B_1 close to the load experience larger support forces than the supports A_1 and B_2 remote from the load.

Bridges are often executed in the form of skew slabs. Such structures can be approximated with the bar models shown here. It is clear that such slabs "span across the obtuse corners". Fig. 16.27 illustrates this for the case of a slab skewed to the left. With an extreme skew, the acute-angled corners can experience uplift and may need to be held down.

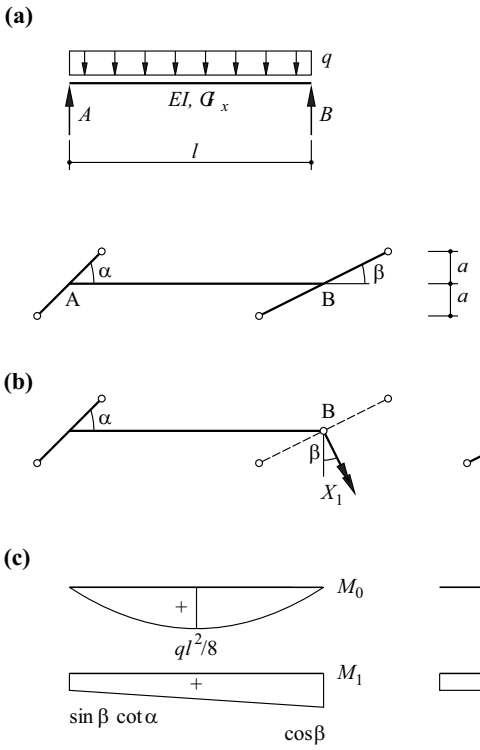

Fig. 16.25 Beam on skew supports: (a) diagram of static system (elevation and plan), (b) basic system and redundant variable, (c) state diagrams

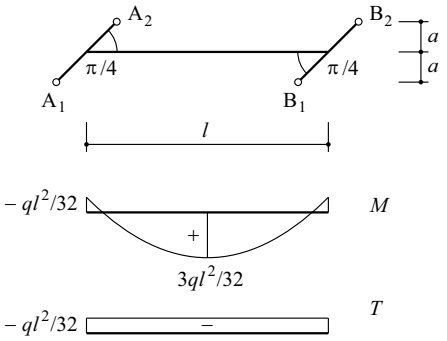

Fig. 16.26 Beam on skew supports ($\alpha = \beta = \pi/4$, $l = 8a$, $EI/(GI_x) = 5/3$) subjected to q = const

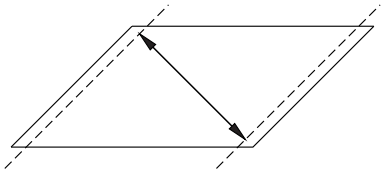

Fig. 16.27 Main direction of load transfer in a skew slab

Example 16.10 Beam as circular arc

Fig. 16.28 shows a curved beam statically indeterminate to the second degree plus its basic system and redundant variables. For the basic states shown in Fig. 16.28(b) equilibrium requires

$$\begin{Bmatrix} A \\ B \\ T_A \end{Bmatrix} = \begin{bmatrix} 1 - \dfrac{\sin\varphi_1}{\sin\varphi_0} & \dfrac{\cot\varphi_0}{r} & -\dfrac{1}{r} \\ \dfrac{\sin\varphi_1}{\sin\varphi_0} & -\dfrac{\cot\varphi_0}{r} & \dfrac{1}{r} \\ r(1-\cos\varphi_0)\dfrac{\sin\varphi_1}{\sin\varphi_0} - r(1-\cos\varphi_1) & \dfrac{(1-\cos\varphi_0)}{\sin\varphi_0} & 1 \end{bmatrix} \begin{Bmatrix} Q \\ X_1 \\ X_2 \end{Bmatrix}$$

and therefore

$$M_0 = \frac{Qr\sin\varphi_1}{\sin\varphi_0}\sin(\varphi_0-\varphi) - Qr\sin(\varphi_1-\varphi) \quad , \quad T_0 = \frac{Qr\sin\varphi_1}{\sin\varphi_0}[1-\cos(\varphi_0-\varphi)] - Qr[1-\cos(\varphi_1-\varphi)] \qquad (\varphi < \varphi_1)$$

$$M_0 = \frac{Qr\sin\varphi_1}{\sin\varphi_0}\sin(\varphi_0-\varphi) \quad , \quad T_0 = \frac{Qr\sin\varphi_1}{\sin\varphi_0}[1-\cos(\varphi_0-\varphi)] \qquad (\varphi > \varphi_1)$$

and

$$M_1 = -\cot\varphi_0\sin(\varphi_0-\varphi) + \cos(\varphi_0-\varphi) \quad , \quad T_1 = -\cot\varphi_0[1-\cos(\varphi_0-\varphi)] + \sin(\varphi_0-\varphi)$$

and

$$M_2 = 0 \quad , \quad T_2 = 1$$

For small values of φ_0, the calculation may be carried out on the developed beam of length $l = r\varphi_0$ as an approximation (as in example 5.8). Where $x = r\varphi$ and $x_1 = r\varphi_1$, we get the following:

$$M_0 = Qx\left(1-\frac{x_1}{l}\right) \quad , \quad T_0 = \int_x^l \frac{M_0}{r}\,dx \qquad (x < x_1)$$

$$M_0 = Qx_1\left(1-\frac{x}{l}\right) \quad , \quad T_0 = \int_x^l \frac{M_0}{r}\,dx \qquad (x > x_1)$$

instead of the above relationships, and

$$M_1 = \frac{x}{l} \quad , \quad T_1 = \frac{l^2-x^2}{2rl}$$

$$M_2 = 0 \quad , \quad T_2 = 1$$

Fig. 16.28(c) shows these relationships for the case $\varphi_1 = \varphi_0/2$.

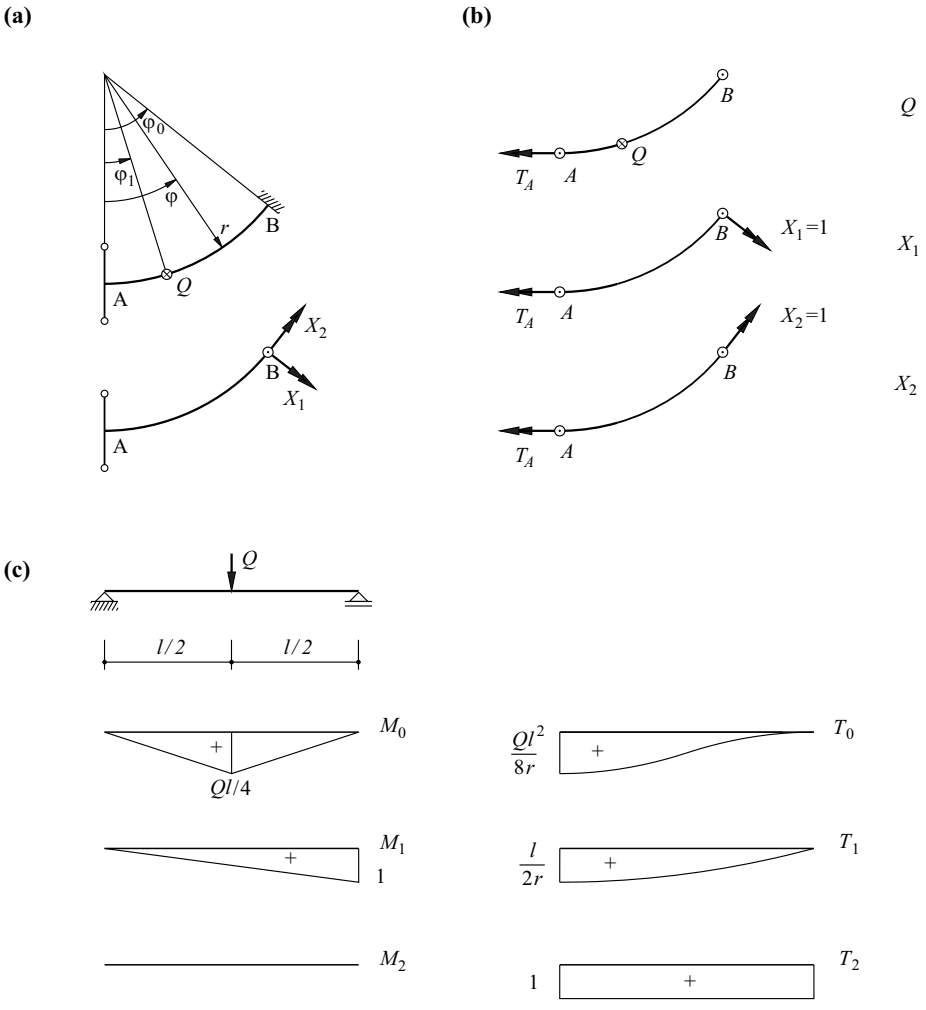

Fig. 16.28 Beam as circular arc subjected to point load Q: (a) diagram of static system, basic system and redundant variables, (b) basic states, (c) linearisation for small values of φ_0 and $\varphi_1 = \varphi_0/2$

Example 16.11 Considering subsystems

It is often worthwhile splitting complex systems into subsystems; considering the effects of the parts of the system that have been separated by way of translational and rotational springs according to Fig. 5.10 und (5.12). For example, the central beam of the system shown in Fig. 16.29(a) can be considered separately according to Fig. 16.29(b). The beam of length l has a constant bending stiffness EI and is idealised as rigid in shear. Using the uniformly distributed load q, we first find

$$\delta_{10} = \delta_{20} = \frac{ql^3}{24EI}$$

as in example 16.5.

In order to determine the stiffnesses k_{yl} and k_{yr} of the rotational springs, or rather their inverses $1/k_{yl}$ and $1/k_{yr}$ (their flexibilities), we apply moments of magnitude 1 to the separated parts of the system according to Fig. 16.29(c) and (d). According to $(5.12)_3$, the resulting rotations φ_l and φ_r are at the same time the flexibilities required. The flexibilities of bars 1 and 2 are obtained in a similar way to the diagonal elements of matrix $\boldsymbol{\delta}$ in example 16.5, i. e.

$$\varphi_l = \frac{M_1 l_1}{3EI_1} = \frac{M_2 l_2}{3EI_2}$$

and as $M_1 + M_2 = 1$, it follows that

$$\varphi_l = \frac{1}{k_{yl}} = \frac{1}{\dfrac{3EI_1}{l_1} + \dfrac{3EI_2}{l_2}}$$

Bar 4 corresponds to a yielding support for bar 3 with a translational spring stiffness of $48EI_4/l_4^3$. The moment of magnitude 1 causes a load $1/l_3$ acting on bar 4 and consequently a deflection of $l_4^3/(48EI_4 l_3)$. The corresponding rotation $l_4^3/(48EI_4 l_3^2)$ is added to the flexibility $l_3/(3EI_3)$ of bar 3, i. e.

$$\varphi_r = \frac{1}{k_{yr}} = \frac{l_3}{3EI_3} + \frac{l_4^3}{48 l_3^2 EI_4}$$

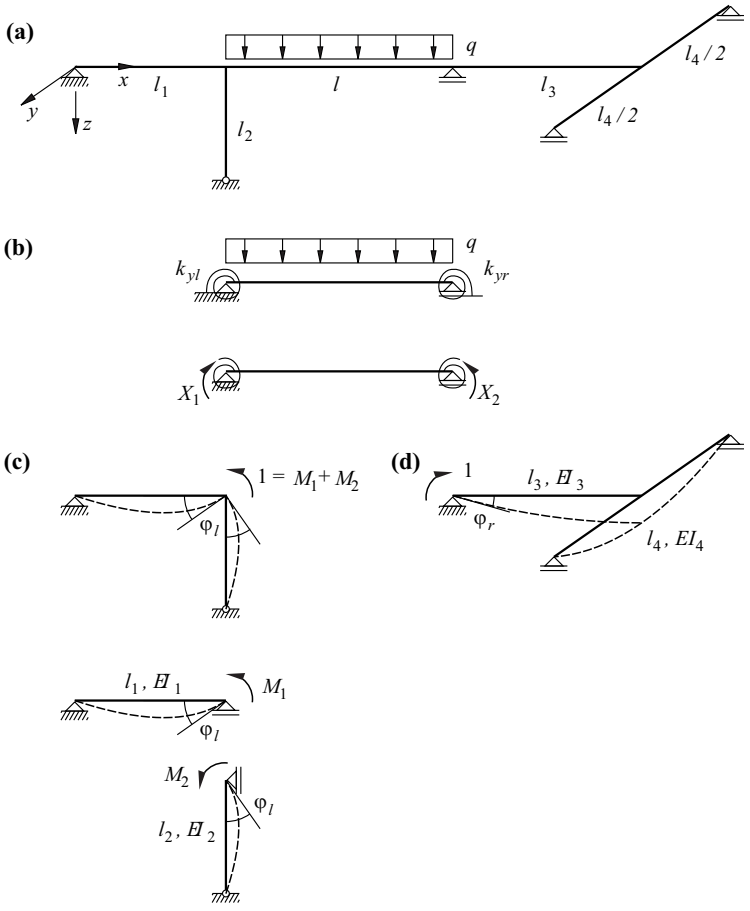

Fig. 16.29 Considering subsystems: (a) total system, (b) subsystem with redundant variables, (c) and (d) calculating the stiffnesses of the rotational springs

The flexibilities of the rotational springs add up to the diagonal elements of the flexibility matrix $\boldsymbol{\delta}$ for the subsystem of Fig. 16.29(b), i. e.

$$\boldsymbol{\delta} = \begin{bmatrix} \dfrac{l}{3EI} + \dfrac{1}{k_{yl}} & \dfrac{l}{6EI} \\ \dfrac{l}{6EI} & \dfrac{l}{3EI} + \dfrac{1}{k_{yr}} \end{bmatrix}$$

and therefore X_1, X_2 can be calculated from the solution to the set of equations (16.8).

16.5 Summary

1. When the load on a statically indeterminate, linear elastic - perfectly plastic system increases monotonically, plastic hinges form successively until the limit load is reached. The degree of static indeterminacy is reduced by one with each new plastic hinge, and the stiffness of the system decreases. The final plastic hinge converts the formerly statically determinate system into a mechanism.
2. The structural behaviour of an elastic-plastic system generally depends on the loading-restraint history. Only the limit loads and the associated mechanisms are not dependent on this; and here it is presumed that the plastic deformation capacity is sufficient to form the mechanisms and no stability problems occur.
3. A system with n degrees of static indeterminacy has n restraint states (i. e. zero-load stress states) associated with it which are independent of each other. When using the force method, these restraint states correspond to the redundant variables X_i (i = 1, 2, ... , n).

4. The force method can be used to investigate linear elastic framed structures with n degrees of static indeterminacy. The general algorithm of the force method is given in section 16.3.1.
5. Any basic system may be chosen when applying the force method, provided the requirement for kinematic stability is satisfied. However, the designer is recommended to select a basic system whose structural behaviour differs as little as possible from that of the statically indeterminate system.
6. The flexibility matrix $\boldsymbol{\delta}$ is square, symmetric, invertible and positive definite.
7. The compatibility conditions (16.8) correspond to minimum conditions for the complementary internal potential Π_i^*. The elastic, compatible redundant variables $\boldsymbol{X}$ make Π_i^* a minimum.
8. The unit force variable states (restraint states) associated with the redundant variables $\boldsymbol{X}$ are orthogonal to the elastic, compatible stress state.
9. The coefficients δ_{ij} of the flexibility matrix $\boldsymbol{\delta}$ may be calculated with one of the two force variable states occurring according to the work theorem (14.4) using any statically determinate basic system (reduction theorem).
10. Deformation diagrams for statically indeterminate systems can be determined in a similar way to those for statically determinate systems (chapter 15).
11. The influence line of a deformation variable is the deformation diagram of the system that ensues when a corresponding unit force variable is applied at the position and in the direction of the deformation variable of interest.
12. The influence line of a force variable S_i is the deformation diagram that ensues when a virtual deformation -1 is imposed on the system at the position and in the direction of the force variable of interest. Quantitatively, we get the influence lines for force variables for statically indeterminate systems through the superposition of the corresponding influence lines for the statically determinate basic systems and the weighted influence lines for the redundant variables X_j; the weighting factors S_{ij} of the latter are equal to the force variables S_i for the basic system as a result of $X_j = 1$.
13. When dealing with symmetrical statically indeterminate systems, rearranging the loads (dividing loads into symmetric and antisymmetric components) can often lead to considerable simplifications.
14. The envelopes, i. e. the lines enclosing the stress resultant diagrams of all load cases, are critical for the dimensioning. According to the shakedown theorem, any restraint state may be superposed on the elastic, compatible stress states; a linear elastic - perfectly plastic system then behaves purely elastically apart from any initial plastification. If on the other hand, a separate, optimally chosen restraint state is superposed for each load case, there is a risk of exhausting the deformation capacity as a result of alternating or progressive plastification of individual parts of the system. Although this approach can often achieve considerable savings in the dimensioning, the plastic deformation demand should, however, always be compared with the plastic deformation capacity and assessed accordingly.
15. A skew support acts like a fixed support at the end of a beam. The support forces become concentrated in the obtuse angles at the ends of the beam. With a large skew, the acute angles can lift and may need to be held down.
16. It is often worthwhile dividing complex systems into subsystems. The contributions of the separated parts of the system can be taken into account in such situations by way of equivalent translational and rotational springs.

16.6 Exercises

16.1 Rework exercise 11.1 presuming the system shown in Fig. 9.9(a), i. e. with fixity at 1 and a hinge at 4. Assume a constant bending stiffness EI, and neglect the deformations as a result of shear and normal forces.

16.2 The underslung beam 1234 shown in Fig. 9.9(e) has a constant bending stiffness EI. Shear deformations and deformations due to normal forces in beam 1234 and in struts 25 and 36 can be ignored. The tie 1564 has a constant axial stiffness EA and is prestressed to P_0 in segment 56. Calculate the forces in the struts for $b = a/4$ and $P_0 = 0$ when vertical point loads G are applied at 2 and 3. How large must P_0 be in order that joints 2 and 3 do not exhibit any deflection when subjected to G? What are the stress resultants in the system prestressed and loaded in this way when an additional point load $Q = G/2$ is applied at 2?

16.3 The system shown in Fig. 9.9(f) consists of two identical bars ($l = 2.5\,\text{m}$, $EI = 38.35\,\text{MNm}^2$) welded together at joint 2. Bar 12 experiences a temperature difference $\Delta T_z/h = -69°\text{C/m}$. Presuming $\alpha_T = 10^{-5}/°\text{C}$, determine the resulting restraint state (bending moments and shear forces) and the rotation φ_X at support 4.

16.4 Fig. 16.30(a) shows a continuous beam with constant bending stiffness EI. Show that the support forces are given by

$$A = \frac{3gl}{8} + Q\left(1 - \frac{5\alpha}{4} + \frac{\alpha^3}{4}\right)$$

$$B = \frac{5gl}{4} + Q\left(\frac{3\alpha}{2} - \frac{\alpha^3}{2}\right)$$

$$C = \frac{3gl}{8} + Q\left(-\frac{\alpha}{4} + \frac{\alpha^3}{4}\right)$$

and the moment envelopes by

$$M_{\max} = gl^2\left(\frac{3\xi}{8} - \frac{\xi^2}{2}\right) + Ql\left(\xi - \frac{5\xi^2}{4} + \frac{\xi^4}{4}\right)$$

$$M_{\min} = gl^2\left(\frac{3\xi}{8} - \frac{\xi^2}{2}\right) - \frac{Ql\xi}{6\sqrt{3}} \qquad (0 \le \xi \le 1)$$

16.5 Fig. 16.30(b) shows a continuous beam with constant bending stiffness EI. Determine the stress resultants due to q_1 and q_2.

16.6 Calculate the bending moment at 2 and the displacement at 3 as a function of k for the system shown in Fig. 16.30(c). Discuss the special cases $k \to \infty$, $k = 1$ and $k \to 0$.

16.7 Solve exercise 16.6 for the case of settlement Δ of support 3.

16.8 Calculate the displacement of the point of load application 3 in Fig. 16.30(d).

16.9 Compare the structural behaviour of the two systems shown in Fig. 16.30(e). Bars 12 and 34 lying in the XY plane are fixed at 1 and 4 respectively and connected by bar 23 at right-angles. Line load $q = \text{const}$ acts in the Z direction. All the bars have a constant bending stiffness EI and a constant torsional stiffness $GI_x = 3EI/5$.

16.10 Mast 245 in Fig. 16.30(f) has a thin-wall hollow cross-section ($EI = 51.79\,\text{MNm}^2$), and the two guy cables 14 and 34 ($EA = 29.25\,\text{MN}$) are prestressed to 50 kN. Work out an expression for the horizontal displacement of the top of the mast 5 due to Q. Compare the result with the behaviour of the unguyed mast.

16.11 A semicircular curved beam (radius r, bending stiffness EI_y = const, torsional stiffness GI_x = const) is fixed at both ends and loaded at mid-span by a point load Q acting perpendicular to the plane of the circle. Draw the diagrams of the stress resultants and determine the deflection and rotation of the beam at mid-span.

16.12 The base 1 of the system shown in Fig. 16.30(g) can be moved horizontally by a hydraulic cylinder. The load Q should not experience any deflection when moving from 2 to 3. How should point 1 be moved and what is the magnitude of the force needed to do this?

16.13 How should the hydraulic cylinder of the system in exercise 16.12 be controlled if the deflection curve at the position of Q must be horizontal?

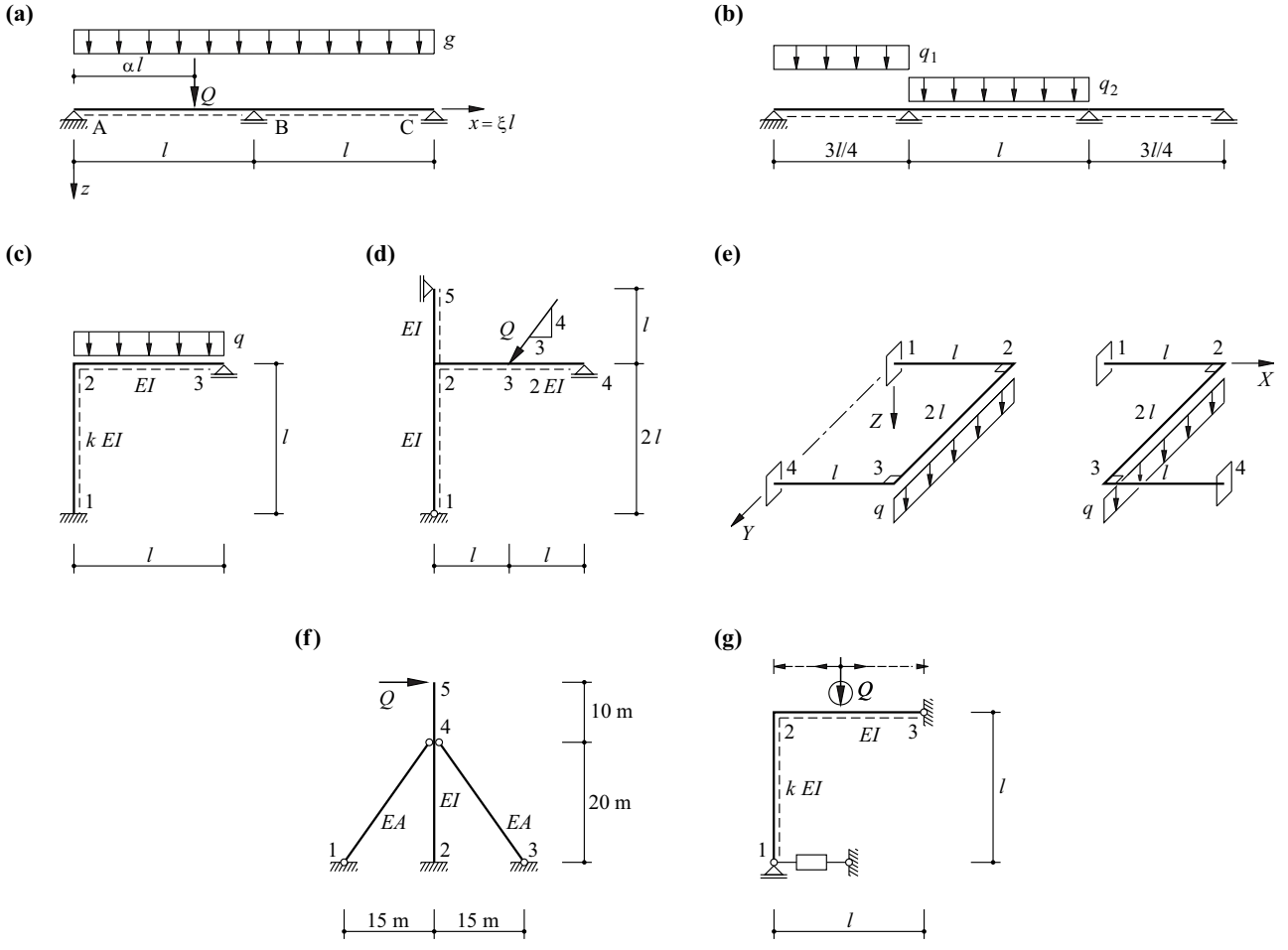

Fig. 16.30 Diagrams of static systems for section 16.6

17 THE DISPLACEMENT METHOD

17.1 Independent bar end variables

17.1.1 General

The basic idea of the displacement method has already been explained in section 8.1.2. Using the example of an ideal truss, it was possible to obtain the *global stiffness matrix* $\boldsymbol{K} = \boldsymbol{a}^{\mathrm{T}} \bullet \boldsymbol{k} \bullet \boldsymbol{a}$ by setting up the kinematic transformation matrix $\boldsymbol{a}$ and the diagonal matrix $\boldsymbol{k}$ for the bar stiffnesses $k_i = (EA/l)_i$. Inverting $\boldsymbol{K}$ resulted in the external deformation variables $\boldsymbol{V} = \boldsymbol{K}^{-1} \bullet \boldsymbol{Q}$ corresponding with the loads $\boldsymbol{Q}$, and hence the internal deformation variables $\boldsymbol{v} = \boldsymbol{a} \bullet \boldsymbol{V}$ plus the corresponding internal force variables $\boldsymbol{s} = \boldsymbol{k} \bullet \boldsymbol{v}$.

These deliberations will be transferred to general plane frameworks in the following with the help of the discretised structural model first seen in section 9.3. In doing so, the corresponding independent bar end variables $\boldsymbol{s}_{\mathrm{e}} = \{N_r, M_l, M_r\}^{\mathrm{T}}$ and $\boldsymbol{v}_{\mathrm{e}} = \{\Delta, \lambda, \rho\}^{\mathrm{T}}$ according to (9.7) will be used for each bar element e.

17.1.2 Member stiffness relationship

The beam of example 16.5, fixed at both ends, rigid in shear and with a constant bending stiffness EI, has this flexibility matrix $\boldsymbol{\delta}$

$$\boldsymbol{\delta} = \begin{bmatrix} \dfrac{l}{3EI} & \dfrac{l}{6EI} \\ \dfrac{l}{6EI} & \dfrac{l}{3EI} \end{bmatrix}$$

By adding relationship $(13.8)_1$ and assuming constant axial stiffness EA, we therefore get the relationship similar to $(8.5)_2$

$$\begin{Bmatrix} \Delta \\ \lambda \\ \rho \end{Bmatrix} = \begin{bmatrix} \dfrac{l}{EA} & 0 & 0 \\ 0 & \dfrac{l}{3EI} & \dfrac{l}{6EI} \\ 0 & \dfrac{l}{6EI} & \dfrac{l}{3EI} \end{bmatrix} \begin{Bmatrix} N_r \\ M_l \\ M_r \end{Bmatrix} \tag{17.1}$$

and inversion gives us the relationship similar to $(8.5)_1$

$$\begin{Bmatrix} N_r \\ M_l \\ M_r \end{Bmatrix} = \frac{EI}{l} \begin{bmatrix} A/I & 0 & 0 \\ 0 & 4 & -2 \\ 0 & -2 & 4 \end{bmatrix} \begin{Bmatrix} \Delta \\ \lambda \\ \rho \end{Bmatrix} \tag{17.2}$$

The *member stiffness matrix* $\boldsymbol{k}_{\mathrm{e}}$ on the right in (17.2) is square, symmetrical, invertible and positive definite. If we use sign convention II defined in Fig. 9.7 instead of sign convention I defined in Fig. 9.6, then the following applies:

$$\boldsymbol{s}_{\mathrm{e}} = \begin{Bmatrix} N_r \\ M_l \\ M_r \end{Bmatrix} = \frac{EI}{l} \begin{bmatrix} A/I & 0 & 0 \\ 0 & 4 & 2 \\ 0 & 2 & 4 \end{bmatrix} \begin{Bmatrix} \Delta \\ \lambda \\ \rho \end{Bmatrix} = \boldsymbol{k}_{\mathrm{e}} \bullet \boldsymbol{v}_{\mathrm{e}} \tag{17.3}$$

If we abandon the idea of rigidity in shear, i. e. we work with a finite shear stiffness GA_v according to (8.23), then the *member flexibility matrix* $\boldsymbol{f}_{\mathrm{e}} = \boldsymbol{k}_{\mathrm{e}}^{-1}$ has to take into account additional terms $\pm 1/(GA_v l)$. Instead of (17.1) we get

Theory of Structures. First Edition. Peter Marti

$$\begin{Bmatrix} \Delta \\ \lambda \\ \rho \end{Bmatrix} = \begin{bmatrix} \frac{l}{EA} & 0 & 0 \\ 0 & \frac{l}{3EI} + \frac{1}{GA_v l} & \frac{l}{6EI} - \frac{1}{GA_v l} \\ 0 & \frac{l}{6EI} - \frac{1}{GA_v l} & \frac{l}{3EI} + \frac{1}{GA_v l} \end{bmatrix} \begin{Bmatrix} N_r \\ M_l \\ M_r \end{Bmatrix} \tag{17.4}$$

and using the shortened form

$$\beta = \frac{12EI}{GA_v l^2} \tag{17.5}$$

and inverting and changing to sign convention II results in

$$\begin{Bmatrix} N_r \\ M_l \\ M_r \end{Bmatrix} = \frac{EI}{l} \begin{bmatrix} \frac{A}{I} & 0 & 0 \\ 0 & \frac{4+\beta}{1+\beta} & \frac{2-\beta}{1+\beta} \\ 0 & \frac{2-\beta}{1+\beta} & \frac{4+\beta}{1+\beta} \end{bmatrix} \begin{Bmatrix} \Delta \\ \lambda \\ \rho \end{Bmatrix} \tag{17.6}$$

With the member stiffness matrices $\boldsymbol{k}_e$ of all the elements of a structure arranged on the main diagonals of a hypermatrix $\boldsymbol{k}$, and the correspondingly structured columns $\boldsymbol{s}$ and $\boldsymbol{v}$ for all bar end variables $\boldsymbol{s}_e$ and $\boldsymbol{v}_e$, the following relationship, similar to $(8.5)_1$, applies

$$\boldsymbol{s} = \boldsymbol{k} \bullet \boldsymbol{v} \tag{17.7}$$

The *reduced stiffness matrix* $\boldsymbol{k}$ is, like its submatrices $\boldsymbol{k}_e$, square, symmetric, invertible and positive definite.

Where bars that are rigid in shear have cross-sectional properties that vary along the bar axis, e. g. haunched beams, the member flexibility matrix $\boldsymbol{f}_e$ in (17.1) has to be replaced by

$$\boldsymbol{f}_e = \begin{bmatrix} \int_0^l \frac{dx}{EA} & 0 & 0 \\ 0 & \int_0^l \frac{(l-x)^2}{EI\,l^2}\,dx & \int_0^l \frac{x(l-x)}{EI\,l^2}\,dx \\ 0 & \int_0^l \frac{x(l-x)}{EI\,l^2}\,dx & \int_0^l \frac{x^2}{EI\,l^2}\,dx \end{bmatrix} \tag{17.8}$$

according to (14.4), where inversion results in $\boldsymbol{k}_e = \boldsymbol{f}_e^{-1}$. As an approximation, the calculation can be performed with cross-sectional properties that are constant segment by segment, which presumes a suitably fine subdivision of the structure into individual bar elements.

17.1.3 Actions on bars

In order to take into account actions on individual bars, these are considered to be fully fixed at the joints at both ends and the reactions to the *fixed-end forces* entered at the appropriate points in the load vector $\boldsymbol{Q}$. Fig. 17.1 contains the complete fixed-end forces for a series of load cases; further cases can be obtained by specialisation or superposition.

Using independent bar end variables means that only the variables N_r, M_l and M_r in Fig. 17.1 are relevant; using complete bar end variables according to section 17.2 means that N_l, V_l and V_r are relevant, too.

$\alpha = a/l$ $\beta = b/l$ $\gamma = c/l$	N_l	V_l	M_l	N_r	V_r	M_r
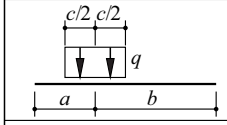		$-qc\left[\beta+\left(\alpha\beta-\frac{\gamma^2}{4}\right)(\beta-\alpha)\right]$	$qc\left[a\beta^2+\frac{\gamma^2}{12}(l-3b)\right]$		$-qc\left[\alpha+\left(\alpha\beta-\frac{\gamma^2}{4}\right)(\alpha-\beta)\right]$	$-qc\left[b\alpha^2+\frac{\gamma^2}{12}(l-3a)\right]$
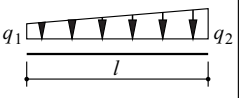		$-\frac{l}{20}(7q_1+3q_2)$	$\frac{l^2}{60}(3q_1+2q_2)$		$-\frac{l}{20}(3q_1+7q_2)$	$-\frac{l^2}{60}(2q_1+3q_2)$
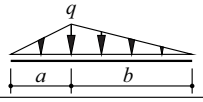		$-\frac{ql}{20}(3+3\beta+3\beta^2-2\beta^3)$	$\frac{ql^2}{30}(1+\beta+\beta^2-\frac{3}{2}\beta^3)$		$-\frac{ql}{20}(3+3\alpha+3\alpha^2-2\alpha^3)$	$-\frac{ql^2}{30}(1+\alpha+\alpha^2-\frac{3}{2}\alpha^3)$
parabolic 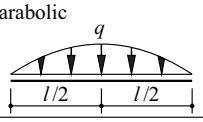		$-\frac{ql}{3}$	$\frac{ql^2}{15}$		$-\frac{ql}{3}$	$-\frac{ql^2}{15}$
sinusoidal 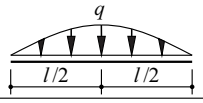		$-\frac{ql}{\pi}$	$\frac{2ql^2}{\pi^3}$		$-\frac{ql}{\pi}$	$-\frac{2ql^2}{\pi^3}$
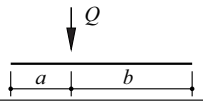		$-Q\beta^2(3-2\beta)$	$Qa\beta^2$		$-Q\alpha^2(3-2\alpha)$	$-Qb\alpha^2$
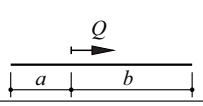	$-Q\beta$			$-Q\alpha$		
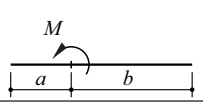		$-\frac{6M\alpha\beta}{l}$	$M\beta(3\alpha-1)$		$\frac{6M\alpha\beta}{l}$	$M\alpha(3\beta-1)$
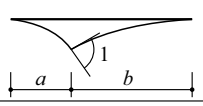		$\frac{6EI(\alpha-\beta)}{l^2}$	$\frac{2EI}{l}(3\beta-1)$		$-\frac{6EI(\alpha-\beta)}{l^2}$	$-\frac{2EI}{l}(3\alpha-1)$
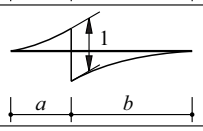		$\frac{12EI}{l^3}$	$-\frac{6EI}{l^2}$		$-\frac{12EI}{l^3}$	$-\frac{6EI}{l^2}$
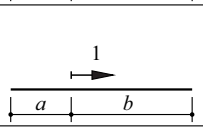	$-\frac{EA}{l}$			$-\frac{EA}{l}$		
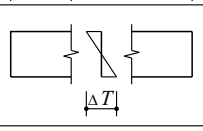			$EI\alpha_T\frac{\Delta T}{h}$			$-EI\alpha_T\frac{\Delta T}{h}$
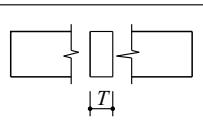	$EA\alpha_T T$			$-EA\alpha_T T$		

Fig. 17.1 Fixed-end forces due to actions on bars (sign convention II)

17.1.4 Algorithm for the displacement method

Based on the observations of sections 8.1.2, 9.3.4 and 10.3 as well as those of this chapter, it is possible to summarise the general approach of the displacement method as follows:

1. Determine the reduced stiffness matrix $\boldsymbol{k}$ and the load vector $\boldsymbol{Q}$.
2. Set up the kinematic transformation matrix $\boldsymbol{a}$ for the kinematically determinate basic system.
3. Calculate the global stiffness matrix
   $$\boldsymbol{K} = \boldsymbol{a}^{\mathrm{T}} \bullet \boldsymbol{k} \bullet \boldsymbol{a} \tag{17.9}$$
4. Invert $\boldsymbol{K}$ and calculate the degrees of freedom at the joints
   $$\boldsymbol{V} = \boldsymbol{K}^{-1} \bullet \boldsymbol{Q} \tag{17.10}$$
5. Calculate the bar end forces
   $$\boldsymbol{s} = \boldsymbol{k} \bullet \boldsymbol{v} + \boldsymbol{s}_0 \tag{17.11}$$
   from the internal deformation variables
   $$\boldsymbol{v} = \boldsymbol{a} \bullet \boldsymbol{V} \tag{17.12}$$
   taking into account the fixed-end forces $\boldsymbol{s}_0$.
6. Calculate the support force variables $\boldsymbol{C}$ by considering equilibrium at the joints.

Example 17.1 Cantilever beam rigid in shear

The cantilever beam with constant bending stiffness EI shown in Fig. 17.2(a) is loaded over its length l by a uniformly distributed line load q. A single bar element with the variables

$$\boldsymbol{v} = \begin{Bmatrix} \lambda \\ \rho \end{Bmatrix} \quad , \quad \boldsymbol{s} = \begin{Bmatrix} M_l \\ M_r \end{Bmatrix}$$

is adequate for modelling the beam. As there are no loads in the x direction, N_r, Δ and the corresponding degree of freedom V_4 at joint 2 may be eliminated; only the active degrees of freedom shown in Fig. 17.2(b) remain:

$$\boldsymbol{V} = \begin{Bmatrix} V_5 \\ V_6 \end{Bmatrix}$$

Eq. (17.3) supplies the reduced stiffness matrix

$$\boldsymbol{k} = \frac{EI}{l} \begin{bmatrix} 4 & 2 \\ 2 & 4 \end{bmatrix}$$

and Fig. 17.1 gives us the fixed-end forces

$$\boldsymbol{s}_0 = \begin{Bmatrix} M_{l0} \\ M_{r0} \end{Bmatrix} = \frac{ql^2}{12} \begin{Bmatrix} 1 \\ -1 \end{Bmatrix}$$

along with shear forces of $-ql/2$ at the ends of the bar, from which we get the load vector

$$\boldsymbol{Q} = \begin{Bmatrix} Q_5 \\ Q_6 \end{Bmatrix} = \begin{Bmatrix} ql/2 \\ ql^2/12 \end{Bmatrix}$$

From Fig. 17.2(c), it follows that

$$\boldsymbol{a} = \begin{bmatrix} 1/l & 0 \\ 1/l & 1 \end{bmatrix}$$

and hence according to (17.9),

$$\boldsymbol{K} = \frac{EI}{l} \begin{bmatrix} 12/l^2 & 6/l \\ 6/l & 4 \end{bmatrix}$$

Inverting $\boldsymbol{K}$ results in

$$\boldsymbol{K}^{-1} = \frac{l}{EI} \begin{bmatrix} l^2/3 & -l/2 \\ -l/2 & 1 \end{bmatrix}$$

from which, by using (17.10), we get

$$\boldsymbol{V} = \frac{ql^3}{EI} \begin{Bmatrix} l/8 \\ -1/6 \end{Bmatrix}$$

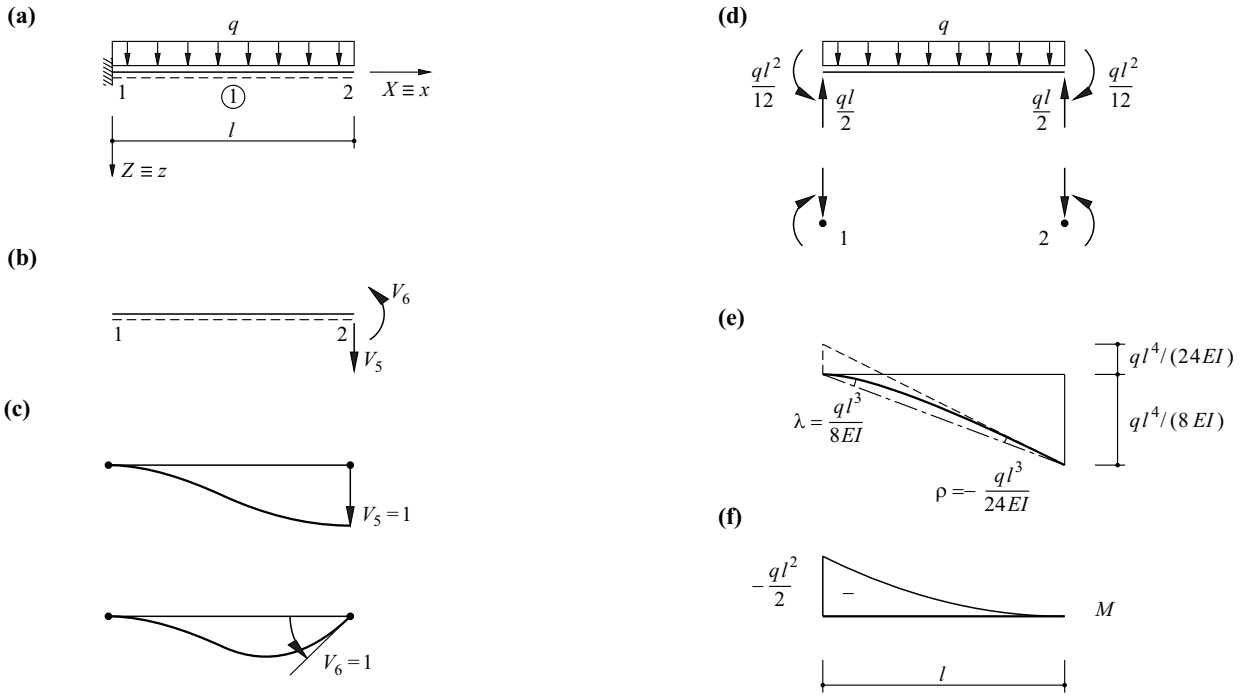

Fig. 17.2 Cantilever beam rigid in shear: (a) static system, (b) active degrees of freedom, (c) unit deformation states, (d) fixed-end forces, (e) deflection curve, (f) bending moments

and by using (17.12), we get

$$\boldsymbol{v} = \frac{ql^3}{EI}\begin{Bmatrix} 1/8 \\ -1/24 \end{Bmatrix}$$

Applying (17.11) in the end results in

$$\boldsymbol{s} = \begin{Bmatrix} ql^2/2 \\ 0 \end{Bmatrix}$$

and equilibrium at joint 1 calls for

$$\boldsymbol{C} = \begin{Bmatrix} -ql \\ ql^2/2 \end{Bmatrix}$$

Fig. 17.2(d) shows the fixed-end forces imposed at the ends of the bar and their reactions imposed at the joints. Fig. 17.2(e) illustrates the relationships for $\boldsymbol{V}$ and $\boldsymbol{v}$, and the resulting bending moment diagram is shown in Fig. 17.2(f).

17.2 Complete bar end variables

17.2.1 General

Applying the independent bar end variables used in section 17.1 keeps the matrices as small as possible. However, the *complete bar end forces*, like the stress resultant diagrams and the support force variables, must be calculated in a further step by considering the equilibrium. In order to overcome this disadvantage, we introduce the *complete bar end variables*

$$\overline{\boldsymbol{s}}_{\mathrm{e}} = \begin{Bmatrix} N_l \\ V_l \\ M_l \\ N_r \\ V_r \\ M_r \end{Bmatrix} \quad , \quad \overline{\boldsymbol{v}}_{\mathrm{e}} = \begin{Bmatrix} u_l \\ w_l \\ \varphi_l \\ u_r \\ w_r \\ \varphi_r \end{Bmatrix} \tag{17.13}$$

according to Fig. 17.3. These and the independent bar end variables $\boldsymbol{s}_{\mathrm{e}} = \{N_r, M_l, M_r\}^{\mathrm{T}}$ and $\boldsymbol{v}_{\mathrm{e}} = \{\Delta, \lambda, \rho\}^{\mathrm{T}}$ used previously are linked by the relationships

$$\overline{\boldsymbol{s}}_e = \boldsymbol{e}_e^T \bullet \boldsymbol{s}_e \quad , \quad \boldsymbol{v}_e = \boldsymbol{e}_e \bullet \overline{\boldsymbol{v}}_e \tag{17.14}$$

with the transformation matrix

$$\boldsymbol{e}_e = \begin{bmatrix} -1 & 0 & 0 & 1 & 0 & 0 \\ 0 & -1/l & 1 & 0 & 1/l & 0 \\ 0 & -1/l & 0 & 0 & 1/l & 1 \end{bmatrix} \tag{17.15}$$

Relationship $(17.14)_1$ has already been illustrated in Fig. 9.4(b) with the help of sign convention I.

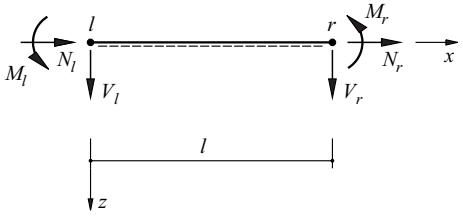

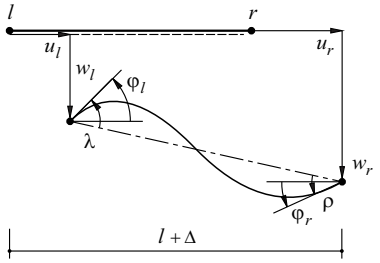

Fig. 17.3 Complete and independent bar end variables

17.2.2 Member stiffness relationship

Combining (17.3) and (17.14) results in

$$\overline{\boldsymbol{s}}_e = \boldsymbol{e}_e^T \bullet \boldsymbol{k}_e \bullet \boldsymbol{e}_e \bullet \overline{\boldsymbol{v}}_e = \overline{\boldsymbol{k}}_e \bullet \overline{\boldsymbol{v}}_e \tag{17.16}$$

where

$$\overline{\boldsymbol{k}}_e = \begin{bmatrix} \frac{EA}{l} & 0 & 0 & -\frac{EA}{l} & 0 & 0 \\ 0 & \frac{12EI}{l^3} & -\frac{6EI}{l^2} & 0 & -\frac{12EI}{l^3} & -\frac{6EI}{l^2} \\ 0 & -\frac{6EI}{l^2} & \frac{4EI}{l} & 0 & \frac{6EI}{l^2} & \frac{2EI}{l} \\ -\frac{EA}{l} & 0 & 0 & \frac{EA}{l} & 0 & 0 \\ 0 & -\frac{12EI}{l^3} & \frac{6EI}{l^2} & 0 & \frac{12EI}{l^3} & \frac{6EI}{l^2} \\ 0 & -\frac{6EI}{l^2} & \frac{2EI}{l} & 0 & \frac{6EI}{l^2} & \frac{4EI}{l} \end{bmatrix} \tag{17.17}$$

The *complete member stiffness matrix* $\overline{\boldsymbol{k}}_e$ is square and symmetrical, and its main diagonal elements are positive. However, $\overline{\boldsymbol{k}}_e$ is singular ($\det \overline{\boldsymbol{k}}_e = 0$); the nullity is equal to half the number of variables in $\overline{\boldsymbol{s}}_e$ or $\overline{\boldsymbol{v}}_e$. The fourth or fifth row results from the first or second row respectively by multiplying by –1, and the sixth row is reached by subtracting the third row from the fifth row. Further, the following applies:

$$Q = \overline{\boldsymbol{v}}_e^T \bullet \overline{\boldsymbol{k}}_e \bullet \overline{\boldsymbol{v}}_e \geq 0 \tag{17.18}$$

see (A5.25), i. e. $\overline{\boldsymbol{k}}_e$ is positive semi-definite.

The elements of the individual columns in $\overline{\boldsymbol{k}}_e$ correspond to the bar end forces that result when the bar end deformation variables $\overline{v}_{ei} = 1$ are imposed successively on the bar element.

In a similar way to (17.6), using (17.5) for bars with finite shear stiffness, we get

$$\overline{\boldsymbol{k}}_e = \begin{bmatrix} \frac{EA}{l} & 0 & 0 & -\frac{EA}{l} & 0 & 0 \\ 0 & \frac{12EI}{l^3(1+\beta)} & -\frac{6EI}{l^2(1+\beta)} & 0 & -\frac{12EI}{l^3(1+\beta)} & -\frac{6EI}{l^2(1+\beta)} \\ 0 & -\frac{6EI}{l^2(1+\beta)} & \frac{EI(4+\beta)}{l(1+\beta)} & 0 & \frac{6EI}{l^2(1+\beta)} & \frac{EI(2-\beta)}{l(1+\beta)} \\ -\frac{EA}{l} & 0 & 0 & \frac{EA}{l} & 0 & 0 \\ 0 & -\frac{12EI}{l^3(1+\beta)} & \frac{6EI}{l^2(1+\beta)} & 0 & \frac{12EI}{l^3(1+\beta)} & \frac{6EI}{l^2(1+\beta)} \\ 0 & -\frac{6EI}{l^2(1+\beta)} & \frac{EI(2-\beta)}{l(1+\beta)} & 0 & \frac{6EI}{l^2(1+\beta)} & \frac{EI(4+\beta)}{l(1+\beta)} \end{bmatrix} \tag{17.19}$$

instead of (17.17).

17.2.3 Actions on bars

In a similar way to (17.11), generalising (17.16) means that the following applies:

$$\overline{\boldsymbol{s}}_{\mathrm{e}} = \overline{\boldsymbol{k}}_{\mathrm{e}} \bullet \overline{\boldsymbol{v}}_{\mathrm{e}} + \overline{\boldsymbol{s}}_{\mathrm{e}0} \tag{17.20}$$

where $\overline{\boldsymbol{s}}_{\mathrm{e}0}$ stands for the complete fixed-end forces of the element, see Fig. 17.1.

17.2.4 Support force variables

Taking into account both the active degrees of freedom $\boldsymbol{V}$ and the passive degrees of freedom $\boldsymbol{V}_{\boldsymbol{C}}$ due to the support conditions, we get

$$\overline{\boldsymbol{v}} = \overline{\boldsymbol{a}} \bullet \boldsymbol{V} + \overline{\boldsymbol{a}}_{\boldsymbol{C}} \bullet \boldsymbol{V}_{\boldsymbol{C}} \tag{17.21}$$

instead of (8.1), where $\overline{\boldsymbol{a}}$ and $\overline{\boldsymbol{a}}_{\boldsymbol{C}}$ are obtained in the usual way column by column by imposing the individual degrees of freedom on the kinematically determinate basic system. Combining all the relationships (17.20) leads to

$$\overline{\boldsymbol{s}} = \overline{\boldsymbol{k}} \bullet \overline{\boldsymbol{v}} + \overline{\boldsymbol{s}}_0 \tag{17.22}$$

and therefore

$$\left\{ \begin{matrix} \boldsymbol{Q} \\ \boldsymbol{C} \end{matrix} \right\} = \begin{bmatrix} \boldsymbol{K} & \boldsymbol{K}_{\boldsymbol{C}}^{\mathrm{T}} \\ \boldsymbol{K}_{\boldsymbol{C}} & \boldsymbol{K}_{\boldsymbol{CC}} \end{bmatrix} \bullet \left\{ \begin{matrix} \boldsymbol{V} \\ \boldsymbol{V}_{\boldsymbol{C}} \end{matrix} \right\} + \left\{ \begin{matrix} \overline{\boldsymbol{a}}^{\mathrm{T}} \bullet \overline{\boldsymbol{s}}_0 \\ \overline{\boldsymbol{a}}_{\boldsymbol{C}}^{\mathrm{T}} \bullet \overline{\boldsymbol{s}}_0 \end{matrix} \right\} \tag{17.23}$$

instead of (8.2), where $\boldsymbol{Q}$ and $\boldsymbol{C}$ denote the loads and support force variables corresponding to $\boldsymbol{V}$ and $\boldsymbol{V}_{\boldsymbol{C}}$ respectively, and the variables

$$\boldsymbol{K} = \overline{\boldsymbol{a}}^{\mathrm{T}} \bullet \overline{\boldsymbol{k}} \bullet \overline{\boldsymbol{a}} \quad , \quad \boldsymbol{K}_{\boldsymbol{C}} = \overline{\boldsymbol{a}}_{\boldsymbol{C}}^{\mathrm{T}} \bullet \overline{\boldsymbol{k}} \bullet \overline{\boldsymbol{a}} \quad , \quad \boldsymbol{K}_{\boldsymbol{CC}} = \overline{\boldsymbol{a}}_{\boldsymbol{C}}^{\mathrm{T}} \bullet \overline{\boldsymbol{k}} \bullet \overline{\boldsymbol{a}}_{\boldsymbol{C}} \tag{17.24}$$

have been introduced.

With a rigid support, $\boldsymbol{V}_{\boldsymbol{C}} \equiv \boldsymbol{0}$, and therefore according to (17.23), the following applies:

$$\boldsymbol{V} = \boldsymbol{K}^{-1} \bullet (\boldsymbol{Q} - \overline{\boldsymbol{a}}^{\mathrm{T}} \bullet \overline{\boldsymbol{s}}_0) \quad , \quad \boldsymbol{C} = \boldsymbol{K}_{\boldsymbol{C}} \bullet \boldsymbol{V} + \overline{\boldsymbol{a}}_{\boldsymbol{C}}^{\mathrm{T}} \bullet \overline{\boldsymbol{s}}_0 \tag{17.25}$$

If support displacements $\boldsymbol{V}_{\boldsymbol{C}0}$ have been specified, then the following applies:

$$\boldsymbol{V} = \boldsymbol{K}^{-1} \bullet (\boldsymbol{Q} - \boldsymbol{K}_{\boldsymbol{C}}^{\mathrm{T}} \bullet \boldsymbol{V}_{\boldsymbol{C}0} - \overline{\boldsymbol{a}}^{\mathrm{T}} \bullet \overline{\boldsymbol{s}}_0) \quad , \quad \boldsymbol{C} = \boldsymbol{K}_{\boldsymbol{C}} \bullet \boldsymbol{V} + \boldsymbol{K}_{\boldsymbol{CC}} \bullet \boldsymbol{V}_{\boldsymbol{C}0} + \overline{\boldsymbol{a}}_{\boldsymbol{C}}^{\mathrm{T}} \bullet \overline{\boldsymbol{s}}_0 \tag{17.26}$$

Example 17.2 Cantilever beam rigid in shear

The variables corresponding to degrees of freedom V_1 and V_4 according to Fig. 17.4 can be eliminated in all relationships for the cantilever beam examined in example 17.1. Using the active degrees of freedom V_5, V_6 and the passive degrees of freedom V_2, V_3, eq. (17.21) is then

$$\begin{Bmatrix} w_{1l} \\ \varphi_{1l} \\ w_{1r} \\ \varphi_{1r} \end{Bmatrix} = \begin{bmatrix} 0 & 0 & 1 & 0 \\ 0 & 0 & 0 & 1 \\ 1 & 0 & 0 & 0 \\ 0 & 1 & 0 & 0 \end{bmatrix} \begin{Bmatrix} V_5 \\ V_6 \\ V_2 \\ V_3 \end{Bmatrix}$$

i. e.

$$\overline{\boldsymbol{a}} = \begin{bmatrix} 0 & 0 \\ 0 & 0 \\ 1 & 0 \\ 0 & 1 \end{bmatrix} \quad , \quad \overline{\boldsymbol{a}}_{\boldsymbol{C}} = \begin{bmatrix} 1 & 0 \\ 0 & 1 \\ 0 & 0 \\ 0 & 0 \end{bmatrix}$$

Eq. (17.17) results in

$$\overline{\boldsymbol{k}} = \frac{EI}{l^3} \begin{bmatrix} 12 & -6l & -12 & -6l \\ -6l & 4l^2 & 6l & 2l^2 \\ -12 & 6l & 12 & 6l \\ -6l & 2l^2 & 6l & 4l^2 \end{bmatrix}$$

and (17.24) therefore gives us

$$\boldsymbol{K} = \frac{EI}{l^3} \begin{bmatrix} 12 & 6l \\ 6l & 4l^2 \end{bmatrix} \quad , \quad \boldsymbol{K}_{\boldsymbol{C}} = \frac{EI}{l^3} \begin{bmatrix} -12 & -6l \\ 6l & 2l^2 \end{bmatrix} \quad , \quad \boldsymbol{K}_{\boldsymbol{CC}} = \frac{EI}{l^3} \begin{bmatrix} 12 & -6l \\ -6l & 4l^2 \end{bmatrix}$$

Using

$$\overline{\boldsymbol{s}}_0 = \begin{Bmatrix} V_{1l0} \\ M_{1l0} \\ V_{1r0} \\ M_{1r0} \end{Bmatrix} = ql \begin{Bmatrix} -1/2 \\ l/12 \\ -1/2 \\ -l/12 \end{Bmatrix}$$

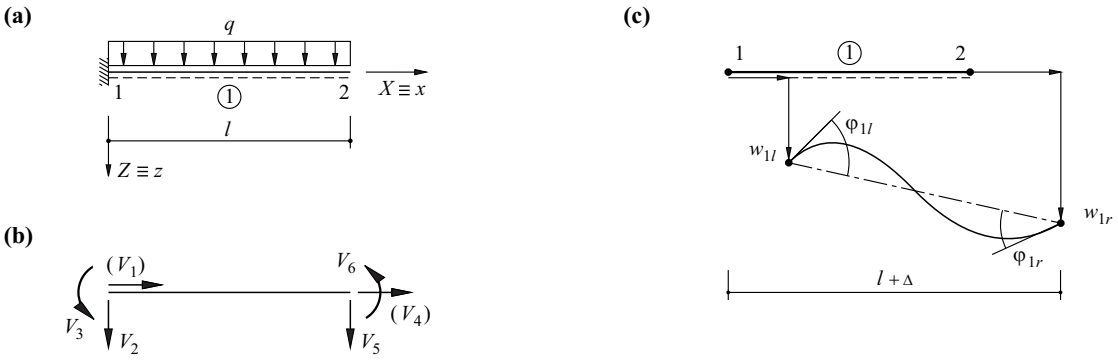

Fig. 17.4 Cantilever beam rigid in shear: (a) static system, (b) degrees of freedom, (c) complete kinematic bar end variables

according to Fig. 17.1 and

$$\boldsymbol{F} = \boldsymbol{K}^{-1} = \frac{l}{EI}\begin{bmatrix} l^2/3 & -l/2 \\ -l/2 & 1 \end{bmatrix}$$

as well as $\boldsymbol{Q} \equiv \boldsymbol{0}$, eq. $(17.25)_1$ then results in

$$\boldsymbol{V} = \begin{Bmatrix} V_5 \\ V_6 \end{Bmatrix} = \frac{ql^3}{EI}\begin{Bmatrix} l/8 \\ -1/6 \end{Bmatrix}$$

and therefore $(17.25)_2$ results in

$$\boldsymbol{C} = \begin{Bmatrix} C_2 \\ C_3 \end{Bmatrix} = ql\begin{Bmatrix} -1 \\ l/2 \end{Bmatrix}$$

The matrices $\boldsymbol{K}$, $\boldsymbol{K_C}$ and $\boldsymbol{K_{CC}}$ calculated above are identical with the (2×2) submatrices at bottom right, top right and top left in the (4×4) matrix $\overline{\boldsymbol{k}}$. It would have been possible to determine these directly from $\overline{\boldsymbol{k}}$ without carrying out the transformations (17.24). Actually, we get an identity matrix $\mathbf{I}$ for the kinematic transformation matrix describing the transition from the external to the internal deformation variables when the external deformation variables are not rearranged into the active and passive degrees of freedom $\boldsymbol{V}$ and $\boldsymbol{V_C}$ right at the start, but rather arranged in one column according to their numbering. The rearrangement in this case causes the first two rows and columns of $\overline{\boldsymbol{k}}$ to be exchanged with the last two.

17.3 The direct stiffness method

17.3.1 Incidence transformation

By using the complete bar end variables $(17.13)_2$ for the two-element frame shown in Fig. 17.5, eq. (8.1) is then

$$\begin{Bmatrix} \overline{\boldsymbol{v}}_{1l} \\ \overline{\boldsymbol{v}}_{1r} \\ \overline{\boldsymbol{v}}_{2l} \\ \overline{\boldsymbol{v}}_{2r} \end{Bmatrix} = \begin{bmatrix} \mathbf{I} & \mathbf{0} & \mathbf{0} \\ \mathbf{0} & \mathbf{I} & \mathbf{0} \\ \mathbf{0} & \mathbf{I} & \mathbf{0} \\ \mathbf{0} & \mathbf{0} & \mathbf{I} \end{bmatrix} \cdot \begin{Bmatrix} \boldsymbol{V}_1 \\ \boldsymbol{V}_2 \\ \boldsymbol{V}_3 \end{Bmatrix} \tag{17.27}$$

where $\overline{\boldsymbol{v}}_{1l} = \{u_{1l}, w_{1l}, \varphi_{1l}\}^{\mathrm{T}}$, ... and $\boldsymbol{V}_1 = \{V_1, V_2, V_3\}^{\mathrm{T}}$, ... The kinematic transformation matrix $\overline{\boldsymbol{a}}$ on the right in (17.27) turns out to be a pure *incidence matrix* that only contains the elements 0 and 1.

Using

$$\overline{\boldsymbol{k}}_{\mathrm{e}} = \begin{bmatrix} \overline{\boldsymbol{k}}_{\mathrm{e}ll} & \overline{\boldsymbol{k}}_{\mathrm{e}lr} \\ \overline{\boldsymbol{k}}_{\mathrm{e}rl} & \overline{\boldsymbol{k}}_{\mathrm{e}rr} \end{bmatrix}$$

according to (17.17) or (17.19), we get

$$\boldsymbol{K} = \overline{\boldsymbol{a}}^{\mathrm{T}} \cdot \overline{\boldsymbol{k}} \cdot \overline{\boldsymbol{a}} = \begin{bmatrix} \mathbf{I} & \mathbf{0} & \mathbf{0} & \mathbf{0} \\ \mathbf{0} & \mathbf{I} & \mathbf{I} & \mathbf{0} \\ \mathbf{0} & \mathbf{0} & \mathbf{0} & \mathbf{I} \end{bmatrix} \cdot \begin{bmatrix} \boldsymbol{k}_{1ll} & \boldsymbol{k}_{1lr} & \mathbf{0} & \mathbf{0} \\ \boldsymbol{k}_{1rl} & \boldsymbol{k}_{1rr} & \mathbf{0} & \mathbf{0} \\ \mathbf{0} & \mathbf{0} & \boldsymbol{k}_{2ll} & \boldsymbol{k}_{2lr} \\ \mathbf{0} & \mathbf{0} & \boldsymbol{k}_{2rl} & \boldsymbol{k}_{2rr} \end{bmatrix} \cdot \begin{bmatrix} \mathbf{I} & \mathbf{0} & \mathbf{0} \\ \mathbf{0} & \mathbf{I} & \mathbf{0} \\ \mathbf{0} & \mathbf{I} & \mathbf{0} \\ \mathbf{0} & \mathbf{0} & \mathbf{I} \end{bmatrix} = \begin{bmatrix} \boldsymbol{k}_{1ll} & \boldsymbol{k}_{1lr} & \mathbf{0} \\ \boldsymbol{k}_{1rl} & \boldsymbol{k}_{1rr} + \boldsymbol{k}_{2ll} & \boldsymbol{k}_{2lr} \\ \mathbf{0} & \boldsymbol{k}_{2rl} & \boldsymbol{k}_{2rr} \end{bmatrix} \tag{17.28}$$

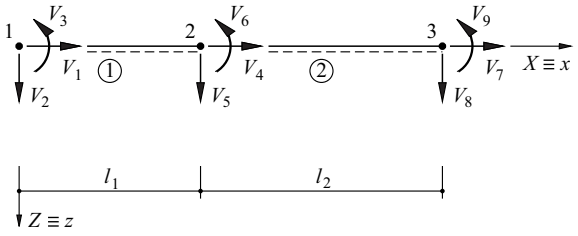

Fig. 17.5 Plane frame with degrees of freedom

Accordingly, the global stiffness matrix $\boldsymbol{K}$ can be obtained directly through superposition of the member stiffness matrices by entering the member stiffness values at the corresponding global positions. We can use the same procedure to set up the global load vector $\boldsymbol{Q}$.

17.3.2 Rotational transformation

According to Fig. 17.6, the following transformation relationships between the *local* and *global bar end variables* are valid:

$$\overline{\boldsymbol{s}}_{\mathrm{e}} = \boldsymbol{c}_{\mathrm{e}} \bullet \overline{\boldsymbol{s}}_{\mathrm{e}g} \quad , \quad \overline{\boldsymbol{v}}_{\mathrm{e}} = \boldsymbol{c}_{\mathrm{e}} \bullet \overline{\boldsymbol{v}}_{\mathrm{e}g} \tag{17.29}$$

and

$$\overline{\boldsymbol{s}}_{\mathrm{e}g} = \boldsymbol{c}_{\mathrm{e}}^{\mathrm{T}} \bullet \overline{\boldsymbol{s}}_{\mathrm{e}} \quad , \quad \overline{\boldsymbol{v}}_{\mathrm{e}g} = \boldsymbol{c}_{\mathrm{e}}^{\mathrm{T}} \bullet \overline{\boldsymbol{v}}_{\mathrm{e}} \tag{17.30}$$

where

$$\boldsymbol{c}_{\mathrm{e}} = \begin{bmatrix} \boldsymbol{c} & \boldsymbol{0} \\ \boldsymbol{0} & \boldsymbol{c} \end{bmatrix} \tag{17.31}$$

using the orthogonal rotation matrix

$$\boldsymbol{c} = \begin{bmatrix} \cos\alpha & -\sin\alpha & 0 \\ \sin\alpha & \cos\alpha & 0 \\ 0 & 0 & 1 \end{bmatrix} \tag{17.32}$$

see (A5.14).

Instead of (17.20), in terms of global variables we get

$$\overline{\boldsymbol{s}}_{\mathrm{e}g} = \overline{\boldsymbol{k}}_{\mathrm{e}g} \bullet \overline{\boldsymbol{v}}_{\mathrm{e}g} + \overline{\boldsymbol{s}}_{\mathrm{e}0g} \tag{17.33}$$

where

$$\overline{\boldsymbol{k}}_{\mathrm{e}g} = \boldsymbol{c}_{\mathrm{e}}^{\mathrm{T}} \bullet \overline{\boldsymbol{k}}_{\mathrm{e}} \bullet \boldsymbol{c}_{\mathrm{e}} \quad , \quad \overline{\boldsymbol{s}}_{\mathrm{e}0g} = \boldsymbol{c}_{\mathrm{e}}^{\mathrm{T}} \bullet \overline{\boldsymbol{s}}_{\mathrm{e}0} \tag{17.34}$$

In the case of spatial bar elements where $\overline{\boldsymbol{s}}_{\mathrm{e}} = \{N_l, V_{yl}, V_{zl}, M_{xl}, M_{yl}, M_{zl}; N_r, V_{yr}, V_{zr}, M_{xr}, M_{yr}, M_{zr}\}^{\mathrm{T}}$ and $\overline{\boldsymbol{v}}_{\mathrm{e}} = \{u_{xl}, u_{yl}, u_{zl}, \varphi_{xl}, \varphi_{yl}, \varphi_{zl}; u_{xr}, u_{yr}, u_{zr}, \varphi_{xr}, \varphi_{yr}, \varphi_{zr}\}^{\mathrm{T}}$, eq. (17.29) and (17.30) continue to apply. However,

$$\boldsymbol{c}_{\mathrm{e}} = \begin{bmatrix} \boldsymbol{c} & \boldsymbol{0} & \boldsymbol{0} & \boldsymbol{0} \\ \boldsymbol{0} & \boldsymbol{c} & \boldsymbol{0} & \boldsymbol{0} \\ \boldsymbol{0} & \boldsymbol{0} & \boldsymbol{c} & \boldsymbol{0} \\ \boldsymbol{0} & \boldsymbol{0} & \boldsymbol{0} & \boldsymbol{c} \end{bmatrix} \tag{17.35}$$

where the matrix

$$\boldsymbol{c} = \begin{bmatrix} \cos(x,X) & \cos(x,Y) & \cos(x,Z) \\ \cos(y,X) & \cos(y,Y) & \cos(y,Z) \\ \cos(z,X) & \cos(z,Y) & \cos(z,Z) \end{bmatrix} \tag{17.36}$$

of the direction cosine, i. e. the cosine of the angle between the local and global axes, has to be used.

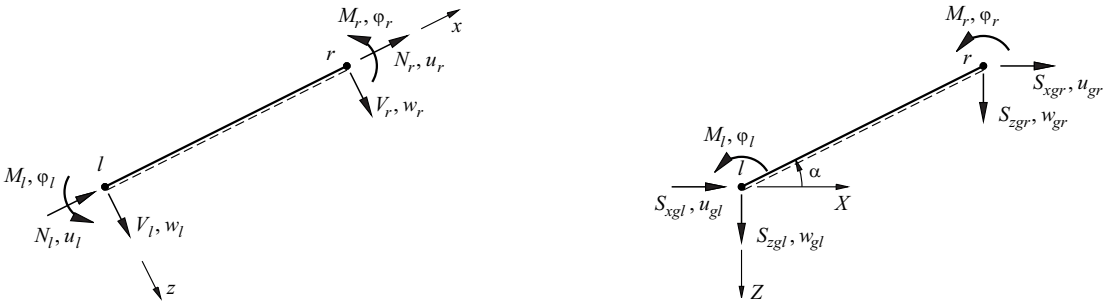

$$\bar{\boldsymbol{s}}_{\mathrm{e}} = \{N_l, V_l, M_l, N_r, V_r, M_r\}^{\mathrm{T}} \qquad \bar{\boldsymbol{s}}_{\mathrm{eg}} = \{S_{xgl}, S_{zgl}, M_l, S_{xgr}, S_{zgr}, M_r\}^{\mathrm{T}}$$

$$\bar{\boldsymbol{v}}_{\mathrm{e}} = \{u_l, w_l, \varphi_l, u_r, w_r, \varphi_r\}^{\mathrm{T}} \qquad \bar{\boldsymbol{v}}_{\mathrm{eg}} = \{u_{gl}, w_{gl}, \varphi_l, u_{gr}, w_{gr}, \varphi_r\}^{\mathrm{T}}$$

Fig. 17.6 Local and global bar end variables

17.3.3 Algorithm for the direct stiffness method

17.3.3.1 Basic concepts

Combining the relationships (17.33) for all elements results in

$$\bar{\boldsymbol{s}}_g = \begin{Bmatrix} \cdot \\ \cdot \\ \bar{\boldsymbol{s}}_{\mathrm{eg}} \\ \cdot \\ \cdot \\ \cdot \end{Bmatrix} = \begin{bmatrix} \cdot & & & & & \\ & \cdot & & & & \\ & & \bar{\boldsymbol{k}}_{\mathrm{eg}} & & & \\ & & & \cdot & & \\ & & & & \cdot & \\ & & & & & \cdot \end{bmatrix} \bullet \begin{Bmatrix} \cdot \\ \cdot \\ \bar{\boldsymbol{v}}_{\mathrm{eg}} \\ \cdot \\ \cdot \\ \cdot \end{Bmatrix} + \begin{Bmatrix} \cdot \\ \cdot \\ \bar{\boldsymbol{s}}_{\mathrm{e}0g} \\ \cdot \\ \cdot \\ \cdot \end{Bmatrix} = \bar{\boldsymbol{k}}_g \bullet \bar{\boldsymbol{v}}_g + \bar{\boldsymbol{s}}_{0g} \quad (17.37)$$

where $\bar{\boldsymbol{k}}_g$ = global stiffness matrix for all elements and $\bar{\boldsymbol{s}}_{0g}$ = vector for global fixed-end forces. Further, if we arrange the matrices $\boldsymbol{c}_{\mathrm{e}}$ according to (17.31) or (17.35) along the main diagonals of a square hypermatrix

$$\bar{\boldsymbol{c}} = \begin{bmatrix} \cdot & & & & & \\ & \cdot & & & & \\ & & \boldsymbol{c}_{\mathrm{e}} & & & \\ & & & \cdot & & \\ & & & & \cdot & \\ & & & & & \cdot \end{bmatrix} \quad (17.38)$$

then instead of (17.29) and (17.30), we get

$$\bar{\boldsymbol{s}} = \bar{\boldsymbol{c}} \bullet \bar{\boldsymbol{s}}_g \quad , \quad \bar{\boldsymbol{v}} = \bar{\boldsymbol{c}} \bullet \bar{\boldsymbol{v}}_g \quad (17.39)$$

or rather

$$\bar{\boldsymbol{s}}_g = \bar{\boldsymbol{c}}^{\mathrm{T}} \bullet \bar{\boldsymbol{s}} \quad , \quad \bar{\boldsymbol{v}}_g = \bar{\boldsymbol{c}}^{\mathrm{T}} \bullet \bar{\boldsymbol{v}} \quad (17.40)$$

Combining $(17.40)_2$ and (8.1) leads to

$$\bar{\boldsymbol{v}}_g = \bar{\boldsymbol{c}}^{\mathrm{T}} \bullet \bar{\boldsymbol{a}} \bullet \boldsymbol{V} = \bar{\boldsymbol{a}}_g \bullet \boldsymbol{V} \quad (17.41)$$

and combining (8.2) and $(17.39)_1$ results in

$$\boldsymbol{Q} = \bar{\boldsymbol{a}}^{\mathrm{T}} \bullet \bar{\boldsymbol{c}} \bullet \bar{\boldsymbol{s}}_g = \bar{\boldsymbol{a}}_g^{\mathrm{T}} \bullet \bar{\boldsymbol{s}}_g \quad (17.42)$$

Substituting (17.37) in (17.42) and taking into account (17.41) results in

$$\boldsymbol{Q} = \bar{\boldsymbol{a}}_g^{\mathrm{T}} \bullet \bar{\boldsymbol{k}}_g \bullet \bar{\boldsymbol{a}}_g \bullet \boldsymbol{V} + \bar{\boldsymbol{a}}_g^{\mathrm{T}} \bullet \bar{\boldsymbol{s}}_{0g} = \boldsymbol{K} \bullet \boldsymbol{V} + \boldsymbol{Q}_0 \quad (17.43)$$

According to (17.41), the kinematic transformation matrix $\bar{\boldsymbol{a}}_g$ links the degrees of freedom $\boldsymbol{V}$ at the joints defined in terms of global coordinates with the bar end deformation variables $\bar{\boldsymbol{v}}_g$ transformed into global coordinates. This is a pure incidence matrix that only contains the elements 0 and 1. The global stiffness matrix $\boldsymbol{K}$ can therefore be determined by the superposition of the values of the globally based member stiffness matrices $\bar{\boldsymbol{k}}_{\mathrm{eg}}$ described in section 17.3.1. Likewise, the component $\boldsymbol{Q}_0$ of the global load vector $\boldsymbol{Q}$ resulting from the bar loads is obtained by superposing the corresponding values of the globally based fixed-end force vectors $\bar{\boldsymbol{s}}_{0g}$.

17.3.3.2 Application

Structural analyses based on the direct stiffness method can be divided into the input, computation and output phases.

The *input phase* involves systematically ascertaining all the relevant joint- and member-related data in a similar way to Tab. 9.1, i. e.

- the joint and member types (nature and number of degrees of freedom)
- the member-joint relationships (bar elements with end joints, and in spatial systems reference joints for orientating the principal axes of the cross-section)
- the support conditions (passive degrees of freedom and, if applicable, given support displacements)
- the joint coordinates
- the member stiffness data
- the actions, i. e. loads on joints and members (bar loads).

The lengths and direction cosines of the individual bar elements can be determined geometrically using the joint coordinates, and the allocation of the degrees of freedom for members and joints follows from the member-joint relationships (incidence matrix $\overline{\boldsymbol{a}}_g$).

The *computation phase* involves

- forming the matrices $\boldsymbol{c}_e$ for all members and therefore determining the corresponding global variables $\overline{\boldsymbol{k}}_{eg}$ and $\overline{\boldsymbol{s}}_{e0g}$ from the local variables $\overline{\boldsymbol{k}}_e$ and $\overline{\boldsymbol{s}}_{e0}$ according to (17.34)
- setting up the global stiffness matrix $\boldsymbol{K}$ and the bar load component $\boldsymbol{Q}_0$ according to (17.43) and rearranging according to (17.23)
- determining the degrees of freedom $\boldsymbol{V}$ as well as the support force variables according to (17.25) and (17.26) respectively
- selecting the global bar end variables $\overline{\boldsymbol{v}}_{eg}$ from $\boldsymbol{V}$ to calculate the local bar end forces $\overline{\boldsymbol{s}}_e$ using $(17.29)_2$ and (17.20).

The results are further processed in a suitable way (e. g. by determining state variables between the joints, calculating envelopes, etc.) and presented (numerically or graphically) during the *output phase*.

Example 17.3 Plane frame

The plane frame shown in Fig. 17.7(a) consists of two reinforced concrete slabs 0.2 m deep in the z direction and 1 m wide in the y direction. For simplicity, the calculation is performed with the cross-sectional values of the concrete only: $E_c = E = 30\,\text{kN/mm}^2$. The result for the bending stiffness is $EI = 30 \cdot 10^3 \cdot (0.2)^3/12 = 20\ \text{MNm}^2$. The axial stiffness is $EA = 30 \cdot 10^3 \cdot 0.2 = 6000$ MN, and using $\nu_c = \nu = 0.2$ and $\alpha_v = 5/6$ (see appendix A4) and taking into account (7.2), the shear stiffness is $GA_v = \{30 \cdot 10^3/[2(1 + 0.2)]\} \cdot 0.2 \cdot 5/6 = 2083.3\,\text{MN}$.

Of the degrees of freedom shown in Fig. 17.7(a), those at joint 2 (V_4, V_5 and V_6) are active. The other degrees of freedom are passive because of the fixity at joints 1 and 3.

The action in this case is a uniformly distributed line load $q = 10\,\text{kN/m}$ in the Z direction applied to bar 2.

We shall ignore shear deformations at first, i. e. we shall calculate according to (17.5) using $\beta = 0$, and that means with $l_1 = 4\,\text{m}$ and $l_2 = 6\,\text{m}$ according to (17.17), we get the following complete member stiffness matrices:

$$\overline{\boldsymbol{k}}_1 = \begin{bmatrix} 1500 & 0 & 0 & -1500 & 0 & 0 \\ 0 & 3.75 & -7.5\,\text{m} & 0 & -3.75 & -7.5\,\text{m} \\ 0 & -7.5\,\text{m} & 20\,\text{m}^2 & 0 & 7.5\,\text{m} & 10\,\text{m}^2 \\ -1500 & 0 & 0 & 1500 & 0 & 0 \\ 0 & -3.75 & 7.5\,\text{m} & 0 & 3.75 & 7.5\,\text{m} \\ 0 & -7.5\,\text{m} & 10\,\text{m}^2 & 0 & 7.5\,\text{m} & 20\,\text{m}^2 \end{bmatrix} \frac{\text{MN}}{\text{m}}$$

and

$$\bar{k}_2 = \begin{bmatrix} 1000 & 0 & 0 & -1000 & 0 & 0 \\ 0 & 1.111 & -3.333\,\mathrm{m} & 0 & -1.111 & -3.333\,\mathrm{m} \\ 0 & -3.333\,\mathrm{m} & 13.333\,\mathrm{m}^2 & 0 & 3.333\,\mathrm{m} & 6.667\,\mathrm{m}^2 \\ -1000 & 0 & 0 & 1000 & 0 & 0 \\ 0 & -1.111 & 3.333\,\mathrm{m} & 0 & 1.111 & 3.333\,\mathrm{m} \\ 0 & -3.333\,\mathrm{m} & 6.667\,\mathrm{m}^2 & 0 & 3.333\,\mathrm{m} & 13.333\,\mathrm{m}^2 \end{bmatrix} \frac{\mathrm{MN}}{\mathrm{m}}$$

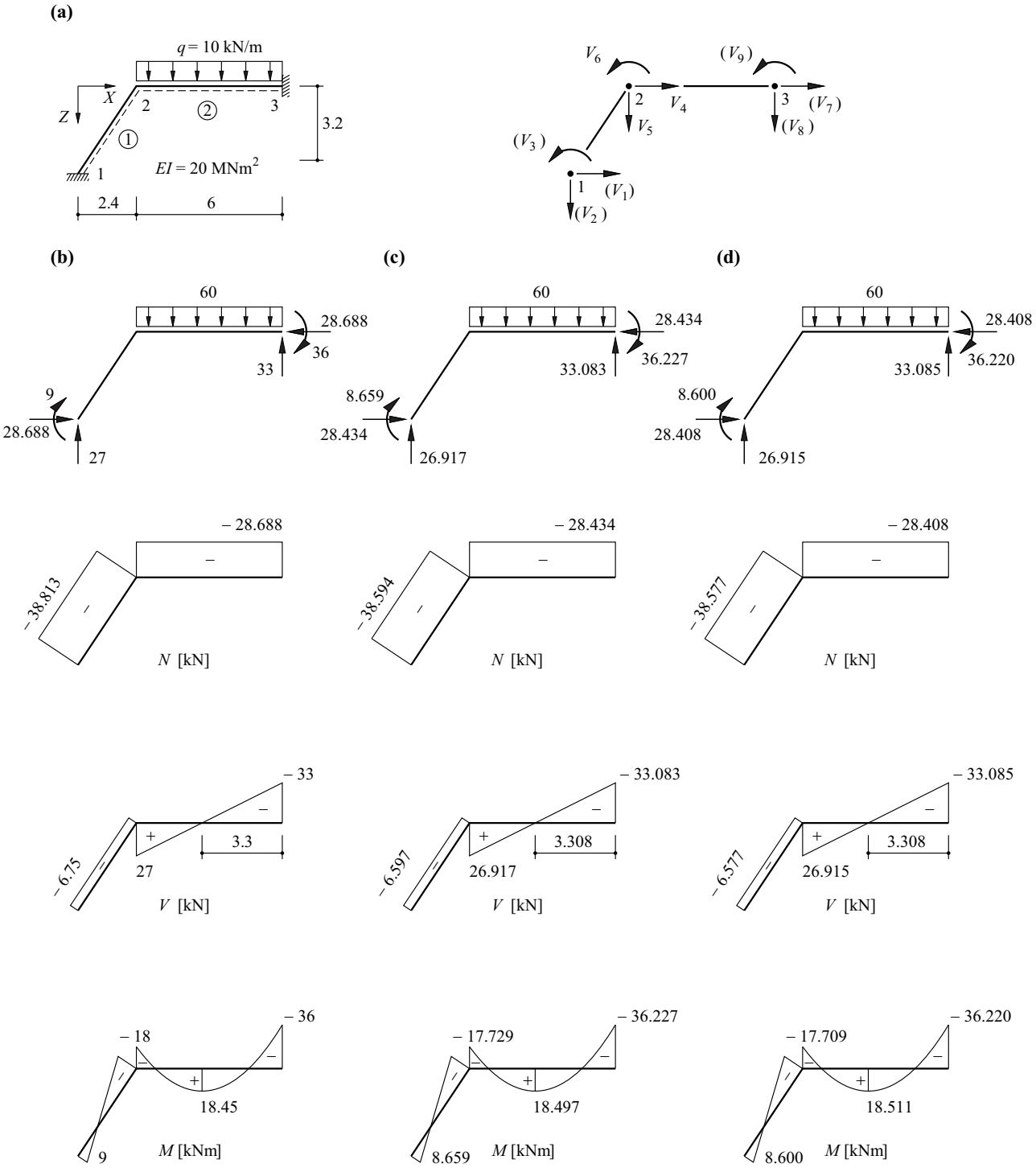

Fig. 17.7 Plane frame: (a) diagram of static system and degrees of freedom (dimensions in m), (b) diagrams of free bodies and stress resultants for inextensible bars rigid in shear (forces in kN, moments in kNm), (c) EA = 6000 MN, (d) EA = 6000 MN, GA_v = 2083.3 MN

Using the rotation matrix

$$\boldsymbol{c} = \begin{bmatrix} 0.6 & -0.8 & 0 \\ 0.8 & 0.6 & 0 \\ 0 & 0 & 1 \end{bmatrix}$$

according to (17.32), eq. $(17.34)_1$ results in the following for bar 1:

$$\overline{\boldsymbol{k}}_{1g} = \begin{bmatrix} 542.4 & -718.2 & -6\,\mathrm{m} & -542.4 & 718.2 & -6\,\mathrm{m} \\ -718.2 & 961.35 & -4.5\,\mathrm{m} & 718.2 & -961.35 & -4.5\,\mathrm{m} \\ -6\,\mathrm{m} & -4.5\,\mathrm{m} & 20\,\mathrm{m}^2 & 6\,\mathrm{m} & 4.5\,\mathrm{m} & 10\,\mathrm{m}^2 \\ -542.4 & 718.2 & 6\,\mathrm{m} & 542.4 & -718.2 & 6\,\mathrm{m} \\ 718.2 & -961.35 & 4.5\,\mathrm{m} & -718.2 & 961.35 & 4.5\,\mathrm{m} \\ -6\,\mathrm{m} & -4.5\,\mathrm{m} & 10\,\mathrm{m}^2 & 6\,\mathrm{m} & 4.5\,\mathrm{m} & 20\,\mathrm{m}^2 \end{bmatrix} \frac{\mathrm{MN}}{\mathrm{m}}$$

Furthermore, $\overline{\boldsymbol{k}}_{2g} = \overline{\boldsymbol{k}}_2$.

Using

$$\overline{\boldsymbol{s}}_{20} = \overline{\boldsymbol{s}}_{20g} = \begin{Bmatrix} 0 \\ -30 \\ 30\,\mathrm{m} \\ 0 \\ -30 \\ -30\,\mathrm{m} \end{Bmatrix} \mathrm{kN}$$

according to Fig. 17.1 and $\boldsymbol{Q} \equiv \boldsymbol{0}$, eq. (17.43) then results in

$$\begin{bmatrix} 542.4 & -718.2 & -6\,\mathrm{m} & -542.4 & 718.2 & -6\,\mathrm{m} & 0 & 0 & 0 \\ -718.2 & 961.35 & -4.5\,\mathrm{m} & 718.2 & -961.35 & -4.5\,\mathrm{m} & 0 & 0 & 0 \\ -6\,\mathrm{m} & -4.5\,\mathrm{m} & 20\,\mathrm{m}^2 & 6\,\mathrm{m} & 4.5\,\mathrm{m} & 10\,\mathrm{m}^2 & 0 & 0 & 0 \\ -542.4 & 718.2 & 6\,\mathrm{m} & 1542.4 & -718.2 & 6\,\mathrm{m} & -1000 & 0 & 0 \\ 718.2 & -961.35 & 4.5\,\mathrm{m} & -718.2 & 962.461 & 1.167\,\mathrm{m} & 0 & -1.111 & -3.333\,\mathrm{m} \\ -6\,\mathrm{m} & -4.5\,\mathrm{m} & 10\,\mathrm{m}^2 & 6\,\mathrm{m} & 1.167\,\mathrm{m} & 33.333\,\mathrm{m}^2 & 0 & 3.333\,\mathrm{m} & 6.667\,\mathrm{m}^2 \\ 0 & 0 & 0 & -1000 & 0 & 0 & 1000 & 0 & 0 \\ 0 & 0 & 0 & 0 & -1.111 & 3.333\,\mathrm{m} & 0 & 1.111 & 3.333\,\mathrm{m} \\ 0 & 0 & 0 & 0 & -3.333\,\mathrm{m} & 6.667\,\mathrm{m}^2 & 0 & 3.333\,\mathrm{m} & 13.333\,\mathrm{m}^2 \end{bmatrix} \begin{Bmatrix} 0 \\ 0 \\ 0 \\ V_4 \\ V_5 \\ V_6 \\ 0 \\ 0 \\ 0 \end{Bmatrix} = \begin{Bmatrix} 0 \\ 0 \\ 0 \\ 0 \\ 30 \\ -30\,\mathrm{m} \\ 0 \\ 30 \\ 30\,\mathrm{m} \end{Bmatrix} \mathrm{mm}$$

from which, making use of (17.25), the result is

$$V_4 = 28.434\,\mu\mathrm{m} \quad , \quad V_5 = 53.487\,\mu\mathrm{m} \quad , \quad V_6 = -906.990\,\mu\mathrm{rad}$$

$$C_1 = 28.434\,\mathrm{kN} \quad , \quad C_2 = -26.917\,\mathrm{kN} \quad , \quad C_3 = -8.659\,\mathrm{kNm}$$

$$C_7 = -28.434\,\mathrm{kN} \quad , \quad C_8 = -33.083\,\mathrm{kN} \quad , \quad C_9 = -36.227\,\mathrm{kNm}$$

Applying $(17.29)_2$ and (17.20) ultimately leads to

$$\overline{\boldsymbol{s}}_1 = \begin{Bmatrix} 38.594\,\mathrm{kN} \\ 6.597\,\mathrm{kN} \\ -8.659\,\mathrm{kNm} \\ -38.594\,\mathrm{kN} \\ -6.597\,\mathrm{kN} \\ -17.729\,\mathrm{kNm} \end{Bmatrix} \quad , \quad \overline{\boldsymbol{s}}_2 = \begin{Bmatrix} 28.434\,\mathrm{kN} \\ -26.917\,\mathrm{kN} \\ 17.729\,\mathrm{kNm} \\ -28.434\,\mathrm{kN} \\ -33.083\,\mathrm{kN} \\ -36.227\,\mathrm{kNm} \end{Bmatrix}$$

with which the diagrams of stress resultants shown in Fig. 17.7(c) are determined.

If we assume that both bars are inextensible, then $V_4 = V_5 = 0$, and we get

$$V_6 = \frac{-30\,\mathrm{m} \cdot \mathrm{mm}}{33.333\,\mathrm{m}^2} = -0.9\,\mathrm{mrad}$$

Fig. 17.7(b) shows the corresponding support force variables and stress resultants. Compared with the system with finite axial stiffness, Fig. 17.7(c), the normal forces (compressive forces) are slightly larger, and bar 1 is subjected to slightly greater bending; and vice versa, the finite axial stiffness leads to the fixity at joint 3 having a somewhat greater effect compared with the inextensible system.

Applying (17.5), the finite shear stiffness $GA_v = 2083.3\,\mathrm{MN}$ gives us the factors

$$\beta_1 = \frac{12 \cdot 20}{2083.3 \cdot 4^2} = 0.0072 \quad , \quad \beta_2 = \frac{12 \cdot 20}{2083.3 \cdot 6^2} = 0.0032$$

and therefore according to (17.19),

$$\overline{\boldsymbol{k}}_1 = \begin{bmatrix} 1500 & 0 & 0 & -1500 & 0 & 0 \\ 0 & 3.723193 & -7.446386\,\mathrm{m} & 0 & -3.723193 & -7.446386\,\mathrm{m} \\ 0 & -7.446386\,\mathrm{m} & 19.892772\,\mathrm{m}^2 & 0 & 7.446386\,\mathrm{m} & 9.892772\,\mathrm{m}^2 \\ -1500 & 0 & 0 & 1500 & 0 & 0 \\ 0 & -3.723193 & 7.446386\,\mathrm{m} & 0 & 3.723193 & 7.446386\,\mathrm{m} \\ 0 & -7.446386\,\mathrm{m} & 9.892772\,\mathrm{m}^2 & 0 & 7.446386\,\mathrm{m} & 19.892772\,\mathrm{m}^2 \end{bmatrix} \frac{\mathrm{MN}}{\mathrm{m}}$$

and

$$\bar{k}_2 = \begin{bmatrix} 1000 & 0 & 0 & -1000 & 0 & 0 \\ 0 & 1.107567 & -3.322701\,\mathrm{m} & 0 & -1.107567 & -3.322701\,\mathrm{m} \\ 0 & -3.322701\,\mathrm{m} & 13.301435\,\mathrm{m}^2 & 0 & 3.322701\,\mathrm{m} & 6.634769\,\mathrm{m}^2 \\ -1000 & 0 & 0 & 1000 & 0 & 0 \\ 0 & -1.107567 & 3.322701\,\mathrm{m} & 0 & 1.107567 & 3.322701\,\mathrm{m} \\ 0 & -3.322701\,\mathrm{m} & 6.634769\,\mathrm{m}^2 & 0 & 3.322701\,\mathrm{m} & 13.301435\,\mathrm{m}^2 \end{bmatrix} \frac{\mathrm{MN}}{\mathrm{m}}$$

Applying $(17.34)_1$ results in

$$\bar{k}_{1g} = \begin{bmatrix} 542.382843 & -718.212867 & -5.957109\,\mathrm{m} & -542.382843 & 718.212867 & -5.957109\,\mathrm{m} \\ -718.212867 & 961.340350 & -4.467832\,\mathrm{m} & 718.212867 & -961.340350 & -4.467832\,\mathrm{m} \\ -5.957109\,\mathrm{m} & -4.467832\,\mathrm{m} & 19.892772\,\mathrm{m}^2 & 5.957109\,\mathrm{m} & 4.467832\,\mathrm{m} & 9.892772\,\mathrm{m}^2 \\ -542.382843 & 718.212867 & 5.957109\,\mathrm{m} & 542.382843 & -718.212867 & 5.957109\,\mathrm{m} \\ 718.212867 & -961.340350 & 4.467832\,\mathrm{m} & -718.212867 & 961.340350 & 4.467832\,\mathrm{m} \\ -5.957109\,\mathrm{m} & -4.467832\,\mathrm{m} & 9.892772\,\mathrm{m}^2 & 5.957109\,\mathrm{m} & 4.467832\,\mathrm{m} & 19.892772\,\mathrm{m}^2 \end{bmatrix} \frac{\mathrm{MN}}{\mathrm{m}}$$

and $\bar{k}_{2g} = \bar{k}_2$.

The set of equations

$$\begin{bmatrix} 1542.382843 & -718.212867 & 5.957109\,\mathrm{m} \\ -718.212867 & 962.447917 & 1.145131\,\mathrm{m} \\ 5.957109\,\mathrm{m} & 1.145131\,\mathrm{m} & 33.194207\,\mathrm{m}^2 \end{bmatrix} \begin{Bmatrix} V_4 \\ V_5 \\ V_6 \end{Bmatrix} = \begin{Bmatrix} 0 \\ 30 \\ -30\,\mathrm{m} \end{Bmatrix} \mathrm{mm}$$

resulting from the superposition of the (3×3) submatrices bottom right in $\bar{k}_{1g}$ and top left in $\bar{k}_{2g}$ supplies the active degrees of freedom

$V_4 = 28.408\,\mu\mathrm{m}$, $V_5 = 53.453\,\mu\mathrm{m}$, $\mathrm{V}_6 = -\ 910.715\,\mu\mathrm{rad}$

in a similar way to the above, and applying $(17.25)_2$ gives us the following support force variables:

$C_1 = 28.408\,\mathrm{kN}$, $C_2 = -26.915\,\mathrm{kN}$, $C_3 = -8.600\,\mathrm{kNm}$

$C_7 = -28.408\,\mathrm{kN}$, $C_8 = -33.085\,\mathrm{kN}$, $C_9 = -36.220\,\mathrm{kNm}$

Fig. 17.7(d) shows the associated diagrams of the stress resultants. Compared with the system rigid in shear with finite axial stiffness, Fig. 17.7(c), bar 1 is marginally relieved, the compressive force in bar 2 is somewhat lower and the values of the negative moments in bar 2 decrease slightly at the expense of the positive moment. On the whole, the influence of the shear stiffness in this slender system is very small, as expected.

17.4 The slope-deflection method

17.4.1 General

As the direct stiffness method, explained in section 17.3, and the computer programs based on it have become more popular, so the *slope-deflection method*, which was developed for the manual calculation of plane frame systems, has essentially lost the significance it once had for practical applications. However, in teaching, the slope-deflection method is still very helpful because of its clarity. It opens up an alternative approach to understanding the structural behaviour of statically indeterminate framed structures and is particularly suitable for imparting that feel for statics so indispensable for engineers.

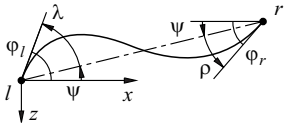

Fig. 17.8 Rotation of bars and joints

In the slope-deflection method, bars are assumed to be inextensible and rigid in shear. The member flexibility matrix (17.8) is therefore singular and can only be inverted for the bending components. After calculating the bending moments, the normal forces must be calculated from the joint equilibrium conditions.

The primary unknowns used in the slope-deflection method are the *joint rotations* φ and the *bar rotations* ψ. Sign convention II, described in section 9.3.4, is generally used here, i. e. moments acting in the anticlockwise direction, or rather about the positive y axis, and the corresponding rotations are positive. According to Fig. 17.8, the following therefore applies:

$$\lambda = \varphi_l - \psi \quad , \quad \rho = \varphi_r - \psi \tag{17.44}$$

In *non-sway systems* (systems with a braced network of joints), the only unknowns are the joint rotations, which are calculated from the equilibrium conditions of the moments at the joints. In *sway systems* (systems with an unbraced network of joints), the unknown joint rotations are supplemented by bar rotations; in this case, applying

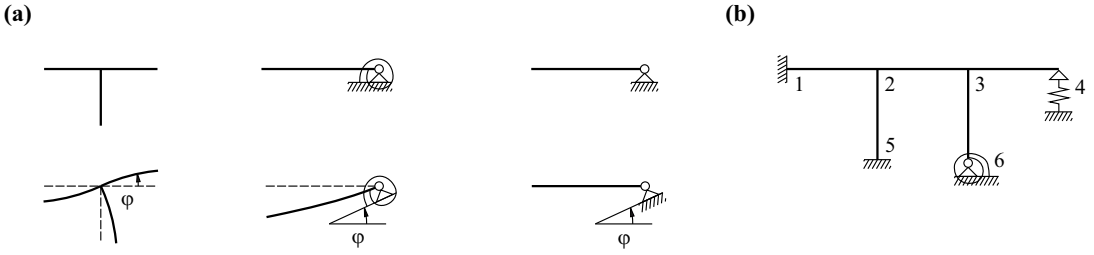

Fig. 17.9 Joint rotation: (a) individual joints, (b) example – φ_2 and φ_3 unknown

the principle of virtual deformations allows us to set up a number of displacement equilibrium conditions corresponding to the number of bar rotations to supplement the moment equilibrium conditions at the joints.

In principle, an unknown joint rotation has to be introduced at each joint, and springs and hinges must be considered as part of the bar, see Fig. 17.9(a). At the ends of the system, the joint rotations are equal to zero or are given; for example, in the system shown in Fig. 17.9(b), only φ_2 and φ_3 are not known.

The number of linear, independent bar rotations can be calculated from the fact that we introduce fictitious flexural hinges at all joints and count the restraining forces required to stabilise the system. Fig. 17.10(a) explains this procedure for a multi-storey frame that has three degrees of static indeterminacy both internally and externally. The mechanism created by introducing seven flexural hinges is, for example, stabilised by a restraining force at each of joints 4, 5 and 6, as shown; ψ_{12}, ψ_{23} and ψ_{25} could be chosen as independent bar rotations, for example, to which we add five further unknown joint rotations at joints 2 to 6. The inclined leg frame with five degrees of static indeterminacy shown in Fig. 17.10(b) requires only one restraining force to stabilise the mechanism that ensues after introducing the four flexural hinges at joints 2, 3, 5 and 6. The relationships between the bar rotations are $\psi_{12} = \psi_{43} = \psi_{52} \cdot c/a$, $\psi_{23} = -\psi_{52} \cdot c/(b/2)$ and $\psi_{63} = \psi_{52}$. The unknown independent bar rotation ψ_{52} is joined by the two unknown joint rotations φ_2 and φ_3.

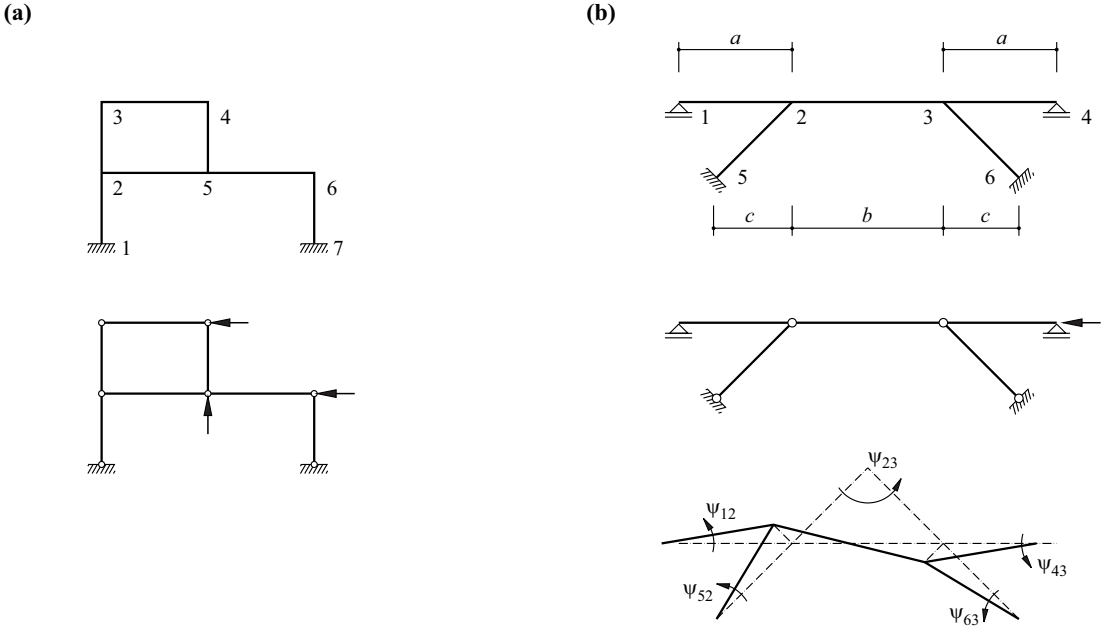

Fig. 17.10 Bar rotation: (a) multi-storey frame, (b) inclined leg frame

17.4.2 Basic states and member end moments

17.4.2.1 Standard bar

We shall first consider a standard bar of length l fixed at the adjacent joints i and k, see Fig. 17.11. The external load q causes *fixed-end moments* M_{ik}^0 and M_{ki}^0. The moments $M_{ik} = s_{ik}$ and $M_{ki} = t_{ki}$ correspond to the unit joint rotation $\varphi_i = 1$, and similarly, the moments $M_{ki} = s_{ki}$ and $M_{ik} = t_{ik}$ correspond to $\varphi_k = 1$. The values s_{ik} and s_{ki} are called *near-end bar stiffnesses*, and $t_{ki} = t_{ik}$ is the *far-end bar stiffness*. According to (17.44), a unit bar rotation $\psi_{ik} = 1$ has the same effect on the end tangent angles λ and ρ as simultaneous joint rotations $\varphi_i = \varphi_k = -1$, and accordingly, the member end moments are $M_{ik} = -(s_{ik} + t_{ik})$ and $M_{ki} = -(s_{ki} + t_{ki})$.

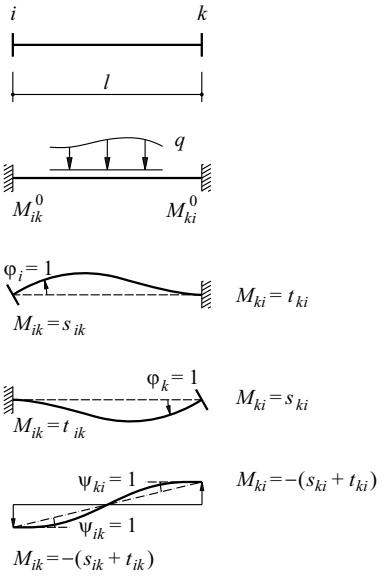

Fig. 17.11 Basic states with associated member end moments

We shall use the force method to calculate the fixed-end moments and the near- and far-end bar stiffnesses. Releasing the fixity and introducing the redundant variables M_{ik} and M_{ki} (anticlockwise = positive) creates the simply supported beam corresponding to the fixed-end bar as a basic system and gives us the joint rotations

$$\varphi_{i0} = -\int_0^l \frac{M(q)}{EI}\left(1 - \frac{x}{l}\right)\mathrm{d}x \quad , \quad \varphi_{k0} = \int_0^l \frac{M(q)}{EI}\cdot\frac{x}{l}\mathrm{d}x \tag{17.45}$$

as a result of external load q and

$$\varphi_{ii} = \int_0^l \frac{(l-x)^2}{EI\,l^2}\mathrm{d}x \quad , \quad \varphi_{ik} = \varphi_{ki} = -\int_0^l \frac{x(l-x)}{EI\,l^2}\mathrm{d}x \quad , \quad \varphi_{kk} = \int_0^l \frac{x^2}{EI\,l^2}\mathrm{d}x \tag{17.46}$$

as a result of unit force variables $M_{ik} = 1$ or $M_{ki} = 1$, see (17.8).

The set of equations

$$\begin{aligned} \varphi_i &= \varphi_{i0} + \varphi_{ii}M_{ik} + \varphi_{ik}M_{ki} \\ \varphi_k &= \varphi_{k0} + \varphi_{ki}M_{ik} + \varphi_{kk}M_{ki} \end{aligned} \tag{17.47}$$

with $\varphi_i = \varphi_k = 0$ gives us the fixed-end moments

$$M_{ik}^0 = \frac{\varphi_{ik}\varphi_{k0} - \varphi_{kk}\varphi_{i0}}{\varphi_{ii}\varphi_{kk} - \varphi_{ik}^2} \quad , \quad M_{ki}^0 = \frac{\varphi_{ki}\varphi_{i0} - \varphi_{ii}\varphi_{k0}}{\varphi_{ii}\varphi_{kk} - \varphi_{ik}^2} \tag{17.48}$$

Using $\varphi_i = 1$ and $\varphi_k = \varphi_{i0} = \varphi_{k0} = 0$, we get

$$s_{ik} = \frac{\varphi_{kk}}{\varphi_{ii}\varphi_{kk} - \varphi_{ik}^2} \quad , \quad t_{ki} = \frac{-\varphi_{ki}}{\varphi_{ii}\varphi_{kk} - \varphi_{ik}^2} \tag{17.49}$$

and with $\varphi_k = 1$ and $\varphi_i = \varphi_{i0} = \varphi_{k0} = 0$

$$s_{ki} = \frac{\varphi_{ii}}{\varphi_{ii}\varphi_{kk} - \varphi_{ik}^2} \quad , \quad t_{ik} = \frac{-\varphi_{ik}}{\varphi_{ii}\varphi_{kk} - \varphi_{ik}^2} \tag{17.50}$$

Superposition of all contributions results in the total member end moments

$$\begin{aligned} M_{ik} &= M_{ik}^0 + s_{ik}\varphi_i + t_{ik}\varphi_k - (s_{ik} + t_{ik})\,\psi_{ik} \\ M_{ki} &= M_{ki}^0 + t_{ki}\varphi_i + s_{ki}\varphi_k - (s_{ki} + t_{ki})\,\psi_{ik} \end{aligned} \tag{17.51}$$

For bars with a constant bending stiffness EI, (17.46) results in

$$\varphi_{ii} = \varphi_{kk} = \frac{l}{3EI} \quad , \quad \varphi_{ik} = \varphi_{ki} = -\frac{l}{6EI}$$

and therefore

$$s_{ik} = s_{ki} = \frac{4EI}{l} \quad , \quad t_{ik} = t_{ki} = \frac{2EI}{l} \tag{17.52}$$

follows from (17.49) and (17.50), see (17.3).

17.4.2.2 Special cases

If bar end k is fixed elastically as shown in Fig. 17.12(a), the amount $1/k_{yk}$ due to $M_{ki} = 1$ is added to the expression φ_{kk} in $(17.46)_3$, and instead of (17.49) and (17.50), we get

$$s_{ik} = \frac{\varphi_{kk} + 1/k_{yk}}{\varphi_{ii}(\varphi_{kk} + 1/k_{yk}) - \varphi_{ik}^2} \quad , \quad t_{ik} = t_{ki} = \frac{-\varphi_{ik}}{\varphi_{ii}(\varphi_{kk} + 1/k_{yk}) - \varphi_{ik}^2}$$
$$s_{ki} = \frac{\varphi_{ii}}{\varphi_{ii}(\varphi_{kk} + 1/k_{yk}) - \varphi_{ik}^2} \tag{17.53}$$

With a constant bending stiffness EI, these expressions are reduced to

$$s_{ik} = \frac{4EI}{l} \cdot \frac{3EI + k_{yk}l}{4EI + k_{yk}l} \quad , \quad t_{ik} = t_{ki} = \frac{2EI}{l} \cdot \frac{k_{yk}l}{4EI + k_{yk}l} \quad , \quad s_{ki} = \frac{4EI}{l} \cdot \frac{k_{yk}l}{4EI + k_{yk}l} \tag{17.54}$$

If the bar has a hinge at end k, see Fig. 17.12(b), then $k_{yk} = 0$ and

$$s_{ik} = \frac{1}{\varphi_{ii}} \quad , \quad t_{ik} = t_{ki} = s_{ki} = 0 \tag{17.55}$$

i. e. with constant EI

$$s_{ik} = \frac{3EI}{l} \quad , \quad t_{ik} = t_{ki} = s_{ki} = 0 \tag{17.56}$$

If the bar is given an intermediate hinge, see Fig. 17.12(c), the result is

$$s_{ik} = \frac{3EI}{l_i[1 + (l_k/l_i)^3]} \quad , \quad t_{ik} = t_{ki} = \frac{3EI\, l_i l_k}{l_i^3 + l_k^3} \quad , \quad s_{ki} = \frac{3EI}{l_k[1 + (l_i/l_k)^3]} \tag{17.57}$$

for a constant EI. When $l_k = 0$ and $l_i = l$, this leads back to (17.56), and when $l_i = 2l_k = 2l/3$ or $l_k = 2l_i = 2l/3$, we get (17.52) again.

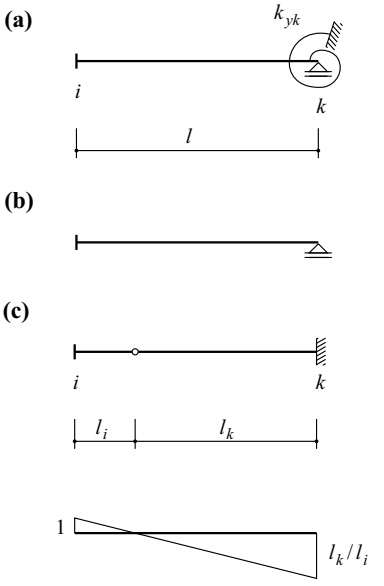

Fig. 17.12 Special cases: (a) elastic fixity at one end of a bar, (b) hinge at one end of a bar, (c) intermediate hinge

17.4.3 Equilibrium conditions

17.4.3.1 Joint equilibrium

According to Fig. 17.13, it is possible to formulate a moment-balance equation

$$M_i - \sum_{k=1}^{n} M_{ik} = 0 \tag{17.58}$$

at any joint with an unknown joint rotation φ, where M_i is an external moment applied at the joint.

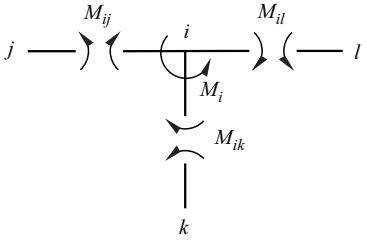

Fig. 17.13 Moment equilibrium at joint i

17.4.3.2 Displacement equilibrium

A displacement equilibrium condition is obtained for each degree of displacement freedom ψ by applying the principle of virtual deformations. To do this, we introduce flexural hinges at the ends of the bars until the system becomes a sway system with zero rotation at the joints.

We get the dependent rotations $\omega_{12} = \omega_{21} = -\omega\, a/b$ and $\omega_{25} = \omega_{52} = \omega\, h_1/h_2$ for the example shown in Fig. 17.14(a) with the independent rotation $\omega = \omega_{14}$ according to Fig. 17.14(b); moreover, $\omega_{23} = 0$. The principle of virtual deformations results in

$$qb\omega_{12}b/2 + M_{14}\omega_{14} + M_{12}\omega_{12} + M_{21}\omega_{21} + M_{25}\omega_{25} + M_{52}\omega_{52} = 0$$

and therefore

$$M_{14} - (M_{12} + M_{21})a/b + (M_{25} + M_{52})h_1/h_2 = qab/2$$

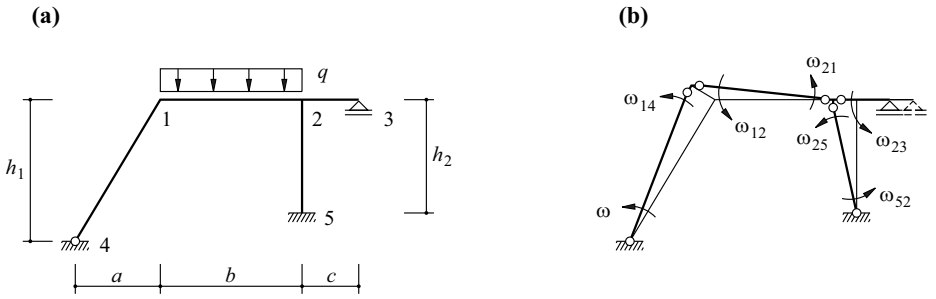

Fig. 17.14 Displacement equilibrium: (a) diagram of static system, (b) displaced system

17.4.4 Applications

Example 17.4 Non-sway frame

Only the joint rotation φ_2 is unknown in the non-sway frame shown in Fig. 17.15(a). Putting $M_{23}^{\,0} = ql^2/8$, $s_{21} = s_{24} = 4EI/l$ and $s_{23} = 3EI/l$ as well as $M_2 = 0$, then eq. (17.58) and the application of (17.51) results in

$$\frac{ql^2}{8} + 11\frac{EI}{l}\varphi_2 = 0$$

i. e.

$$\varphi_2 = -\frac{ql^3}{88EI}$$

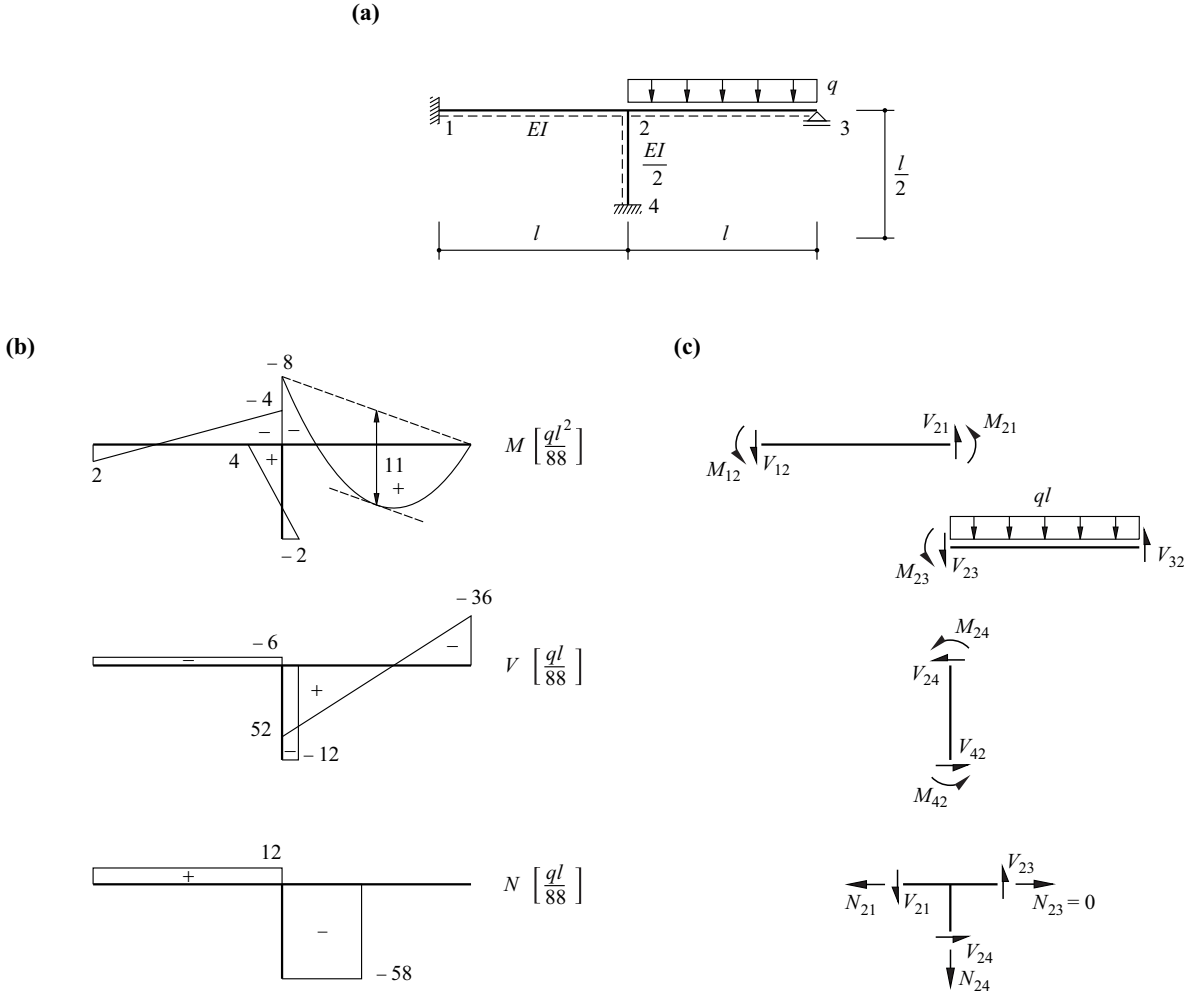

Fig. 17.15 Non-sway frame: (a) diagram of static system, (b) stress resultants, (c) free body diagrams for determining normal and shear forces

Substituting this value in (17.51) and considering $t_{12} = t_{42} = 2EI/l$ as well as $t_{32} = 0$ results in

$M_{12} = -2\,ql^2/88$, $M_{21} = M_{24} = -4\,ql^2/88$, $M_{23} = 8\,ql^2/88$, $M_{32} = 0$, $M_{42} = -2\,ql^2/88$,

see Fig. 17.15(b). Equilibrium of the free bodies shown in Fig. 17.15(c) calls for

$V_{12} = V_{21} = -(M_{12} + M_{21})/l = 6\,ql/88$, $V_{23} = -M_{23}/l - ql/2 = -52\,ql/88$

$V_{32} = ql + V_{23} = 36\,ql/88$, $V_{24} = V_{42} = -(M_{24} + M_{42}) \cdot 2/l = 12\,ql/88$

and

$N_{21} = V_{24} = 12\,ql/88$, $N_{24} = -V_{21} + V_{23} = -58\,ql/88$

We can see here that N_{23} must be equal to zero. Sign convention I is employed in Fig. 17.15(b), as is usual for diagrams of stress resultants.

Example 17.5 Grandstand frame

The load on the grandstand frame shown in Fig. 17.16(a) can be replaced by the equivalent loads at joint 3 according to Fig. 17.16(b). The joint rotations φ_2 and φ_3 as well as the bar rotation ψ_{12} are unknown. The bar rotations ψ_{23} and ψ_{34} result from the displacement diagram Fig. 17.16(a):

$\psi_{23} = \psi_{12} \cdot 0.2/2 = 0.1 \cdot \psi_{12}$, $\psi_{34} = \psi_{23} \cdot 2.4/0.6 = 0.4 \cdot \psi_{12}$

The member end moments are

$$\begin{Bmatrix} M_{12} \\ M_{21} \\ M_{23} \\ M_{32} \\ M_{34} \\ M_{43} \end{Bmatrix} = \begin{bmatrix} t_{12} & & -(s_{12} + t_{12}) \\ s_{21} & & -(s_{21} + t_{21}) \\ s_{23} & t_{23} & -0.1(s_{23} + t_{23}) \\ t_{32} & s_{32} & -0.1(s_{32} + t_{32}) \\ & s_{34} & -0.4(s_{34} + t_{34}) \\ & t_{43} & -0.4(s_{43} + t_{43}) \end{bmatrix} \begin{Bmatrix} \varphi_2 \\ \varphi_3 \\ \psi_{12} \end{Bmatrix}$$

and when assuming a constant bending stiffness EI, the values are

$s_{12} = s_{21} = 20\,EI/l$, $t_{12} = t_{21} = 10\,EI/l$; $s_{23} = s_{32} = 3.71\,EI/l$, $t_{23} = t_{32} = 1.86\,EI/l$

$s_{34} = s_{43} = 6.15\,EI/l$, $t_{34} = t_{43} = 3.08\,EI/l$

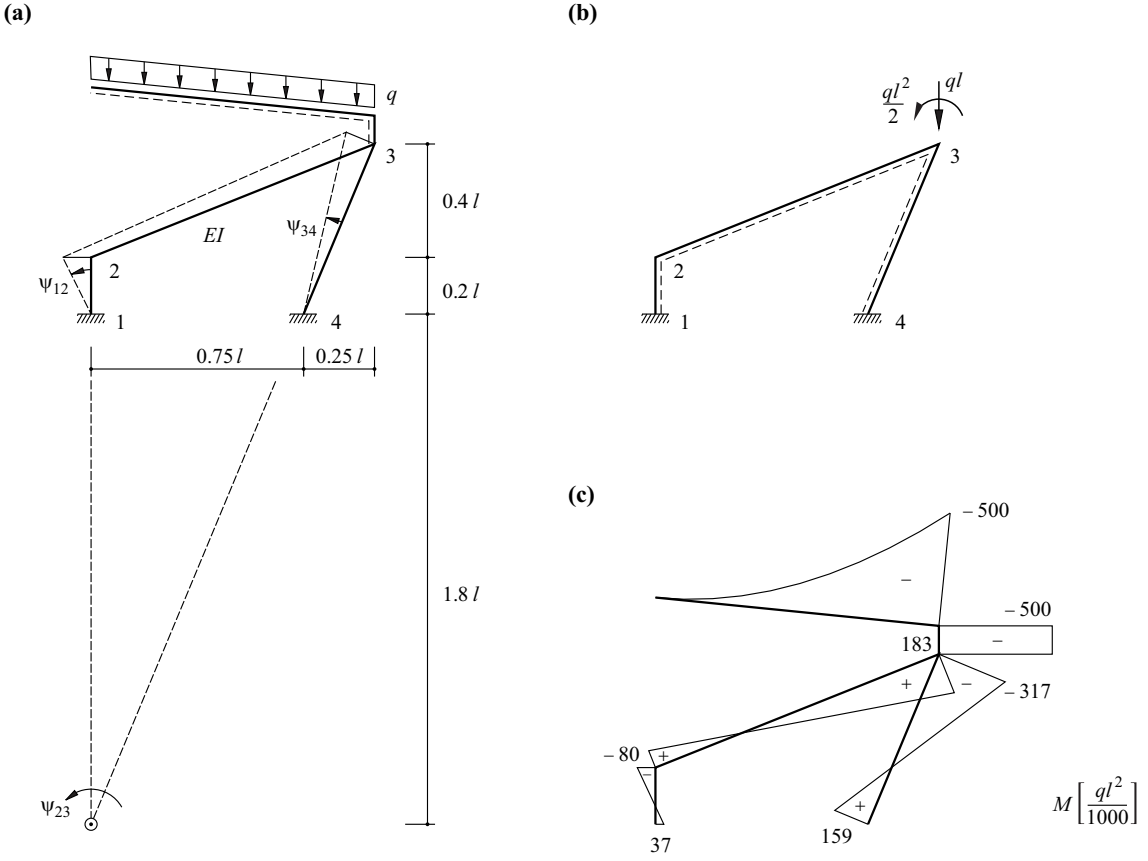

Fig. 17.16 Grandstand frame: (a) diagrams of static system and displacements, (b) equivalent reduced system, (c) bending moment diagram

Moment equilibrium at joints 2 and 3 calls for

$$-(s_{21}+s_{23})\cdot\varphi_2 - t_{23}\cdot\varphi_3 + (s_{21}+t_{21}+0.1\,s_{23}+0.1\,t_{23})\cdot\psi_{12} = 0$$

$$-t_{32}\cdot\varphi_2 - (s_{32}+s_{34})\cdot\varphi_3 + (0.1\,s_{32}+0.1\,t_{32}+0.4\,s_{34}+0.4\,t_{34})\cdot\psi_{12} + ql^2/2 = 0$$

and the principle of virtual deformations, with $\omega = \psi_{12}$, results in

$$(M_{12}+M_{21})\cdot\omega + (M_{23}+M_{32})\cdot 0.1\omega + (M_{34}+M_{43})\cdot 0.4\omega - ql\cdot 0.25l\cdot 0.4\omega = 0$$

We therefore get the set of equations

$$\begin{bmatrix} -23.71 & -1.86 & 30.56 \\ -1.86 & -9.86 & 4.25 \\ 30.56 & 4.25 & -63.06 \end{bmatrix} \begin{Bmatrix} \varphi_2 \\ \varphi_3 \\ \psi_{12} \end{Bmatrix} = \begin{Bmatrix} 0 \\ -0.5 \\ 0.1 \end{Bmatrix} \frac{ql^3}{EI}$$

with the solution

$$\begin{Bmatrix} \varphi_2 \\ \varphi_3 \\ \psi_{12} \end{Bmatrix} = \begin{Bmatrix} -0.0043 \\ 0.0514 \\ -0.0002 \end{Bmatrix} \frac{ql^3}{EI}$$

Substituting back into the relationships for the member end moments results in the values given in Fig. 17.16(c).

Example 17.6 Multi-storey sway frame

Fig. 17.17(a) shows a multi-storey sway frame in which the joint rotations $\varphi_2, \varphi_3, \varphi_4$ and φ_5 as well as the bar rotations $\psi_{12} = \psi_{56}$ and $\psi_{23} = \psi_{45}$ are unknown. Formulating the moment equilibrium conditions for joints 2, 3, 4 and 5 and applying the principle of virtual deformations to the mechanisms characterised by $\omega = \psi_{12}$ or $\omega = \psi_{23}$ while taking into account (17.52) and the fixed-end moments shown in Fig. 17.17(b) results in the set of equations

$$\begin{bmatrix} 28 & 2 & 0 & 8 & -12 & -6 \\ 2 & 12 & 4 & 0 & 0 & -6 \\ 0 & 4 & 12 & 2 & 0 & -6 \\ 8 & 0 & 2 & 28 & -12 & -6 \\ -12 & 0 & 0 & -12 & 48 & 0 \\ -6 & -6 & -6 & -6 & 0 & 24 \end{bmatrix} \begin{Bmatrix} \varphi_2 \\ \varphi_3 \\ \varphi_4 \\ \varphi_5 \\ \psi_{12} \\ \psi_{23} \end{Bmatrix} = \begin{Bmatrix} -1 \\ -1 \\ 0 \\ 0 \\ 0 \\ 6 \end{Bmatrix} \frac{M_Q l}{4EI}$$

with the solution

$$\begin{Bmatrix} \varphi_2 \\ \varphi_3 \\ \varphi_4 \\ \varphi_5 \\ \psi_{12} \\ \psi_{23} \end{Bmatrix} = \begin{Bmatrix} 5.192 \\ 5.577 \\ 34.423 \\ 14.808 \\ 5.000 \\ 77.500 \end{Bmatrix} \frac{M_Q l}{10^3 EI}$$

Substituting back into the relationships (not illustrated here) for the member end moments results in the values given in Fig. 17.17(c).

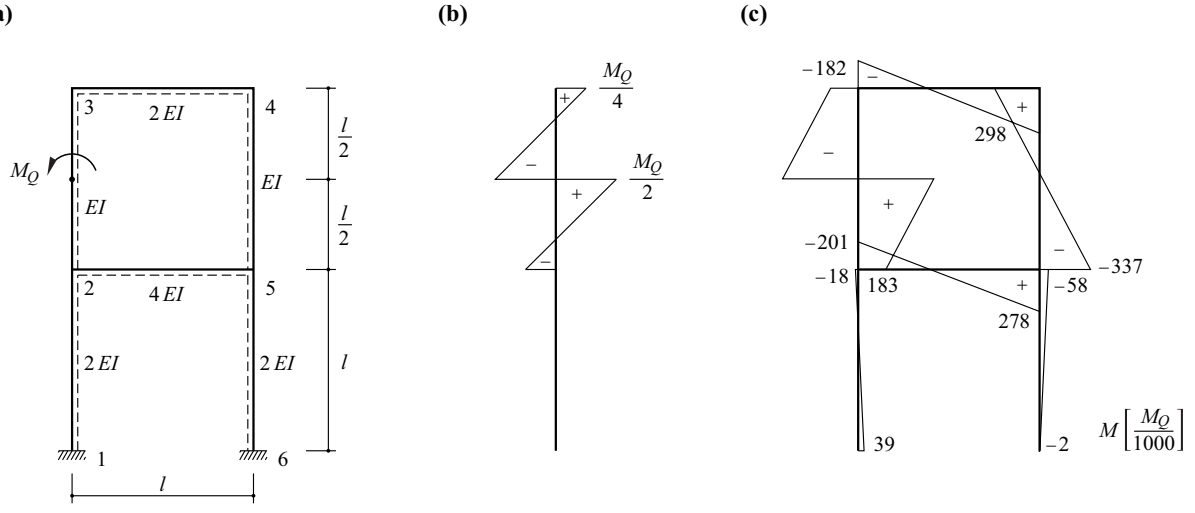

Fig. 17.17 Multi-storey frame: (a) diagram of static system, (b) fixed-end moments; (c) bending moment diagram

Example 17.7 Multi-storey non-sway frame

Fig. 17.18 shows a multi-storey non-sway frame. Owing to the symmetry of the system and the loading, the only unknowns are the joint rotations $\varphi_2 = -\varphi_5$ and $\varphi_3 = -\varphi_4$. With a fixed-end moment $M_{34}{}^0 = 30 \cdot 12^2/12 = 360\,\text{kNm}$, then according to (17.51) and (17.52), the member end moments are

$$M_{32} = \varphi_3 \cdot EI/(4\,\text{m}) + \varphi_2 \cdot EI/(8\,\text{m}) \quad , \quad M_{34} = 360\,\text{kNm} + \varphi_3 \cdot 4EI/(12\,\text{m}) + (-\varphi_3) \cdot 2EI/(12\,\text{m})$$

and

$$M_{21} = \varphi_2 \cdot EI/(4\,\text{m}) \quad , \quad M_{25} = \varphi_2 \cdot 4EI/(12\,\text{m}) + (-\varphi_2) \cdot 2EI/(12\,\text{m}) \quad , \quad M_{23} = \varphi_2 \cdot EI/(4\,\text{m}) + \varphi_3 \cdot EI/(8\,\text{m})$$

Accordingly, moment equilibrium at joints 3 and 2 calls for

$$\begin{bmatrix} 3 & 10 \\ 16 & 3 \end{bmatrix} \begin{Bmatrix} \varphi_2 \\ \varphi_3 \end{Bmatrix} = \begin{Bmatrix} -8640 \\ 0 \end{Bmatrix} \frac{\text{kNm}^2}{EI}$$

from which it follows that

$$\begin{Bmatrix} \varphi_2 \\ \varphi_3 \end{Bmatrix} = \begin{Bmatrix} 171.656 \\ -915.497 \end{Bmatrix} \frac{\text{kNm}^2}{EI}$$

Substituting back into the relationships for the member end moments results in the values given in Fig. 17.18(b), and therefore we get

$$V_{12} = -(21.5 + 42.9)/4 = -16.1\,\text{kN} \quad , \quad V_{23} = (71.5 + 207.4)/4 = 69.7\,\text{kN}$$

and

$$N_{25} = 16.1 + 69.7 = 85.8\,\text{kN} \quad , \quad N_{34} = -69.7\,\text{kN}$$

see Fig. 17.18(c) and Fig. 17.18(d).

Fig. 17.19(a) shows the resultant thrust line for this problem, see section 5.3.2.1. Points A and C at the ends of column 12 exhibit eccentricities of $21.5/180 = 0.119\,\text{m}$ and $42.9/180 = 0.238\,\text{m}$ respectively. Point D at the level of frame beam 25 has an eccentricity of $71.5/180 = 0.397\,\text{m}$ with respect to the column axis. The points of contraflexure in column 23 and frame beam 34 correspond to points E and F at distances of $4 \cdot 207.4/(207.4 + 71.5) = 207.4/69.7 = 2.975\,\text{m}$ and $6 \cdot (1 - \sqrt{332.6/540}) = 1.291\,\text{m}$ respectively from joint 3. The thrust line has an eccentricity of $332.6/69.7 = 4.772\,\text{m}$ in the middle of frame beam 34 (point G). An eccentricity of $28.6/85.8 = 0.333\,\text{m}$ of the tensile force of 85.8 kN corresponds to the moment of −28.6 kNm in frame beam 25; the eccentric tensile force intersects straight line DE at point H, and the extension

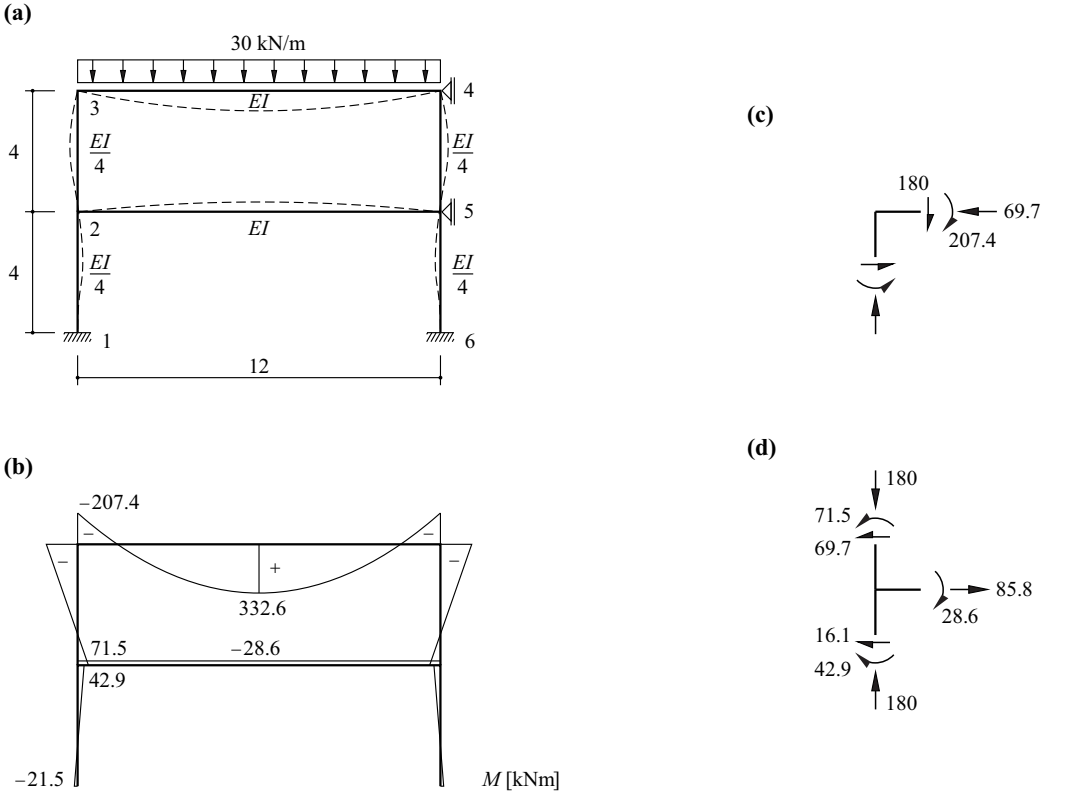

Fig. 17.18 Multi-storey frame: (a) diagram of static system (dimensions in m), (b) bending moment diagram, (c) joint 3 (forces in kN, moments in kNm), (d) joint 2

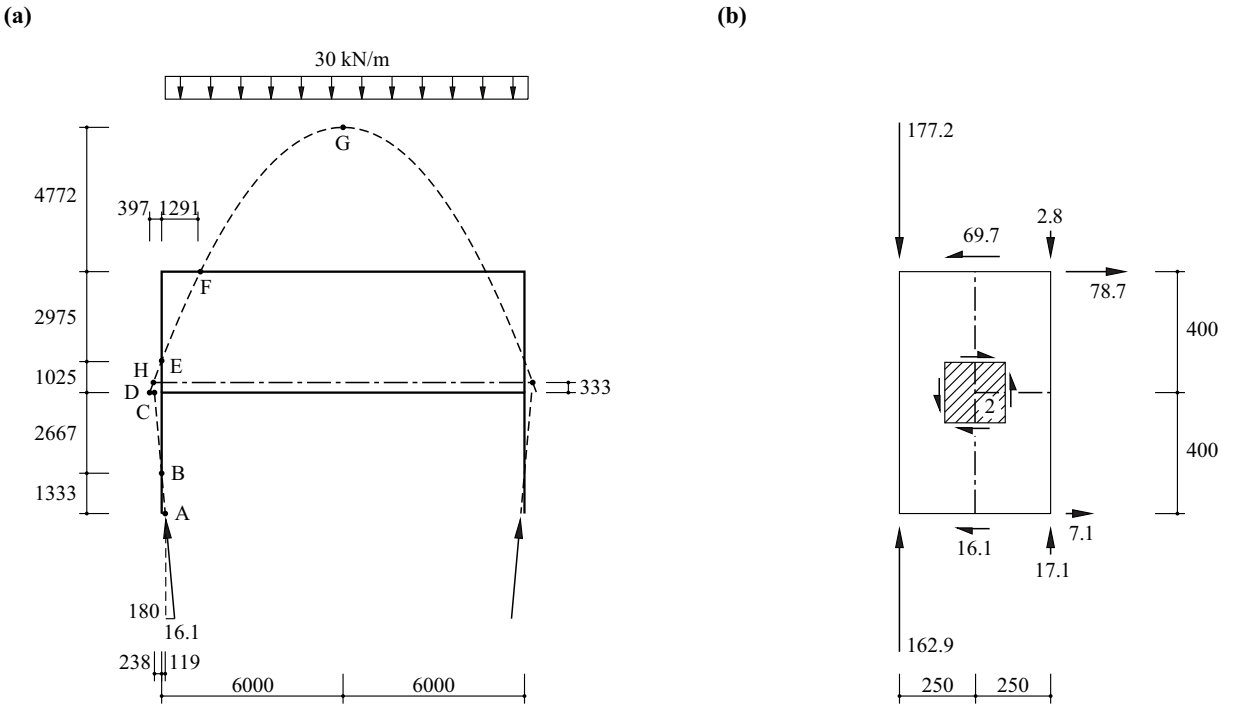

Fig. 17.19 Multi-storey frame: (a) thrust line (dimensions in mm), (b) joint region 2 (forces in kN, dimensions in mm)

of straight line ABC also passes through this point. The final result is thrust line ABCHEFG with straight segments ABCH and HE as well as parabolic segment EFG. The kink at H corresponds to the transfer of the eccentric tensile force in frame beam 25.

Fig. 17.19(b) shows a free body diagram for the region around joint 2. It is assumed that the columns and the frame beam have flanges at a spacing of 500 and 800 mm respectively to which the bending moments and normal forces are allocated – the webs between the flanges carry shear forces only. The moment acting at the top edge of the joint region amounts to $71.5 - 69.7 \cdot 0.4 = 43.6$ kNm, and that produces flange forces of $180/2 \pm 43.6/0.5 = 177.2$ and 2.8 kN. The moment acting at the bottom edge is $42.9 - 16.1 \cdot 0.4 = 36.5$ kNm, which leads to flange forces of $180/2 \pm 36.5/0.5 = 162.9$ and 17.1 kN. In the frame beam, the resulting flange forces are $85.8/2 \pm 28.6/0.8 = 78.7$ and 7.1 kN. There is a state of pure shear with membrane forces amounting to $(16.1 - 7.1)/0.5 \approx (17.1 - 2.8)/0.8 \approx (78.7 - 69.7)/0.5 \approx (177.2 - 162.9)/0.8 \approx 17.9$ kN/m in the web region of the joint.

This example is a good illustration of how the results of the structural analysis have to be further processed for the dimensioning, e. g. for structural steelwork or reinforced concrete, in order to specify or check the dimensions of the individual structural members. In the example, a joint region 0.5 m wide and 0.8 m deep corresponds to joint 2 (just a point in the structural analysis). The member end moments calculated in the structural analysis do not occur in reality; they are purely auxiliary variables that are employed to calculate the forces at the boundaries of the joint region. Within the joint region, the one-dimensional modelling as a framed structure fails; two-dimensional (three-dimensional) modelling is necessary in the case of a plane (spatial) frame.

17.4.5 Restraints

17.4.5.1 Non-sway systems

Restraints in non-sway systems can be treated by introducing fixed-end moments that occur at the fixed joints as a result of the restraint.

Example 17.8 Non-sway frame – settlement of supports

Column 24 of the frame shown in Fig. 17.20(a) settles by the amount c_4. With joint 2 fixed, this leads to the fixed-end moments

$$M_{12}^0 = M_{21}^0 = \frac{6EIc_4}{l^2} \quad , \quad M_{23}^0 = -\frac{3EIc_4}{(3l/4)^2} = -\frac{16EIc_4}{3l^2}$$

in the displaced state. The member end moments

$$M_{21} = M_{21}^0 + \frac{4EI}{l}\varphi_2 \quad , \quad M_{23} = M_{23}^0 + \frac{3EI}{3l/4}\varphi_2 \quad , \quad M_{24} = \frac{4EI/2}{l/2}\varphi_2$$

are in equilibrium with each other, and therefore

$$\varphi_2 = \frac{(-6 + 16/3)EIc_4/l^2}{12EI/l} = -\frac{c_4}{18l}$$

and

$$M_{12} = \left(6 - \frac{2}{18}\right)\frac{EIc_4}{l^2} \quad , \quad M_{21} = \left(6 - \frac{4}{18}\right)\frac{EIc_4}{l^2} \quad , \quad M_{23} = \left(-\frac{16}{3} - \frac{4}{18}\right)\frac{EIc_4}{l^2} \quad , \quad M_{24} = 2M_{42} = -\frac{4}{18}\frac{EIc_4}{l^2}$$

see Fig. 17.20(b).

Alternatively, we can consider the system in its non-displaced state with fixed-end moments equal to zero and imposed bar rotations of

$$\psi_{12} = -c_4/l \quad , \quad \psi_{23} = 4c_4/(3l)$$

The member end moments

$$M_{21} = \frac{4EI}{l}\varphi_2 + \frac{c_4}{l}\cdot\frac{6EI}{l} \quad , \quad M_{23} = \frac{3EI}{3l/4}\varphi_2 - \frac{4c_4}{3l}\cdot\frac{3EI}{3l/4} \quad , \quad M_{24} = \frac{4EI/2}{l/2}\varphi_2$$

agree with the values calculated above and the answer is the same.

(a)

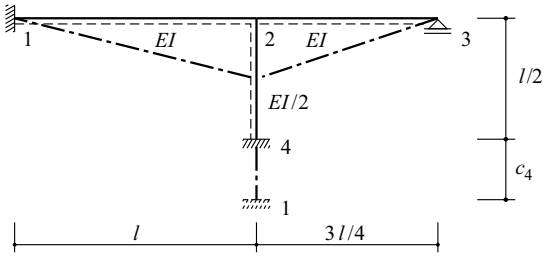

(b)

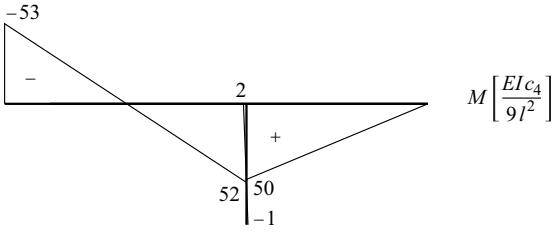

Fig. 17.20 Non-sway frame: (a) diagram of static system, (b) bending moments due to settlement c_4

Example 17.9 Non-sway frame – uniform rise in temperature

The frame considered in example 17.8 is subjected to a uniform rise in temperature T, which leads to elongations of bars 12 and 24 amounting to $\alpha_T Tl$ and $\alpha_T Tl/2$ respectively, see (14.4). The ensuing displacements of joint 2 shown in Fig. 17.21(a) correspond to the fixed-end moments

$$M_{12}^0 = M_{21}^0 = -\frac{6EI\alpha_T Tl/2}{l^2} \quad , \quad M_{23}^0 = \frac{3EI\alpha_T Tl/2}{(3l/4)^2} \quad , \quad M_{24}^0 = M_{42}^0 = \frac{6(EI/2)\alpha_T Tl}{(l/2)^2}$$

The moment-balance equation

$$\left(-3 + \frac{8}{3} + 12\right)\frac{EI\alpha_T T}{l} + 3\cdot\frac{4EI}{l}\cdot\varphi_2 = 0$$

for joint 2 leads to $\varphi_2 = -35\alpha_T T/36$, and hence to the member end moments

$$M_{12} = \left(-3 - \frac{35}{18}\right)\frac{EI\alpha_T T}{l} \quad , \quad M_{21} = \left(-3 - \frac{35}{9}\right)\frac{EI\alpha_T T}{l} \quad , \quad M_{23} = \left(\frac{8}{3} - \frac{35}{9}\right)\frac{EI\alpha_T T}{l} \quad , \quad M_{24} = \left(12 - \frac{35}{9}\right)\frac{EI\alpha_T T}{l} \quad , \quad M_{42} = \left(12 - \frac{35}{18}\right)\frac{EI\alpha_T T}{l}$$

see Fig. 17.21(b).

(a)

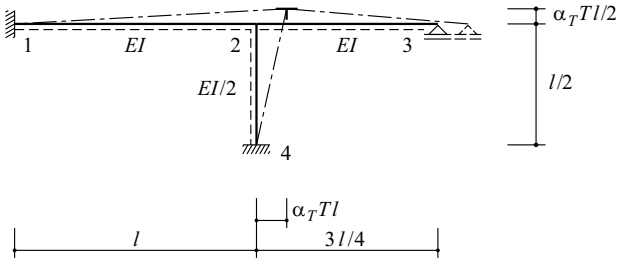

(b)

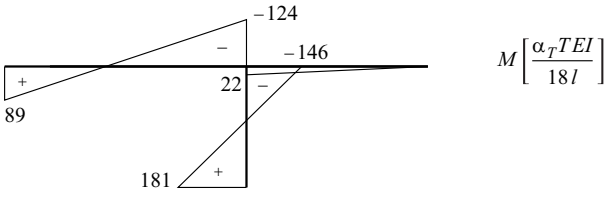

Fig. 17.21 Non-sway frame: (a) diagram of static system, (b) bending moments as a result of uniform rise in temperature T

(a)

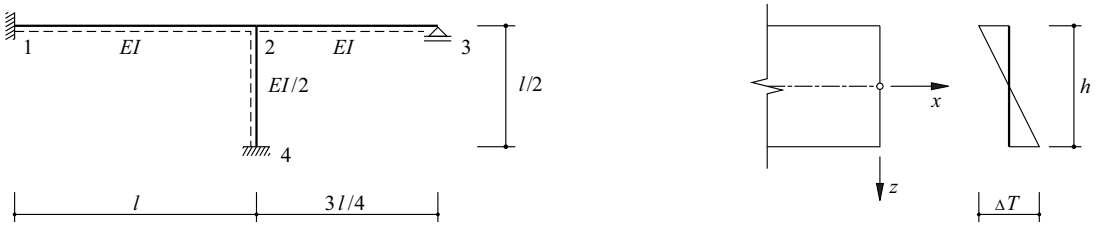

(b)

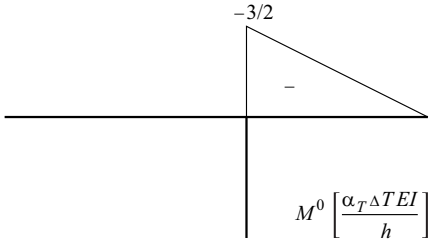

(c)

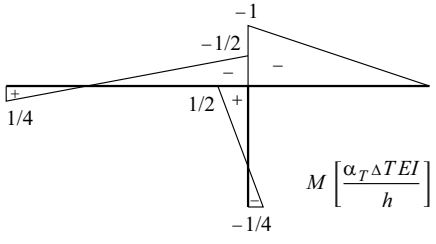

Fig. 17.22 Non-sway frame: (a) diagram of static system and temperature distribution in bar 23, (b) fixed-end moments, (c) resulting restraint moments

Example 17.10 Non-sway frame – temperature difference

Bar 23 of the frame examined in examples 17.8 and 17.9 is subjected to a linearly distributed temperature difference ΔT over its depth h, see Fig. 17.22(a), which would cause an unrestricted curvature $\alpha_T \Delta T/h$, see (14.4). If bar 23 were to be connected via a hinge at joint 2, a rotation of $(\alpha_T \Delta T/h) \cdot l_{23}/2$ would occur at that point. As $s_{23} = 3EI/l_{23}$, we require a fixed-end moment of $3EI\alpha_T \Delta T/(2h)$ at joint 2 in order to prevent this rotation, see Fig. 17.22(b). The moment-balance equation

$$-3EI\alpha_T \Delta T/(2h) - 3 \cdot (4EI/l) \cdot \varphi_2 = 0$$

for joint 2 leads to $\varphi_2 = -(\alpha_T \Delta T/h) \cdot l/8$, and hence to the restraint moments given in Fig. 17.22(c).

17.4.5.2 Sway systems

In sway systems we assume a system displaced in some arbitrary way according to the restraint and calculate the fixed-end moments for fixed joints. Different bar rotations result depending on the displacement initially selected.

Example 17.11 Sway frame – uniform rise in temperature

The frame shown in Fig. 17.23(a) is subjected to a uniform rise in temperature T that causes elongations $\alpha_T T$ in all three bars. The initial displacement assumed in Fig. 17.23(a) results in the fixed-end moments given in Fig. 17.23(b). The joint rotations φ_2 and φ_3 as well as the bar rotation ψ_{12} ($\psi_{34} = 3\psi_{12}/4$, $\psi_{23} = 0$) follow from two joint and one displacement equilibrium condition in the usual way:

$$\begin{bmatrix} 10.667 & 2 & -10 \\ 2 & 9 & -5.625 \\ -10 & -5.625 & 28.4375 \end{bmatrix} \begin{Bmatrix} \varphi_2 \\ \varphi_3 \\ \psi_{12} \end{Bmatrix} = \begin{Bmatrix} 1.2 \\ -8.175 \\ 14.0625 \end{Bmatrix}$$

This set of equations gives rise to

$$\{\varphi_2, \varphi_3, \psi_{12}\} = \{0.861535\ ,\ -0.686204\ ,\ 0.661730\}\alpha_T T$$

and hence the member end moments are

$$\{M_{12}\ ,\ M_{21} = -M_{23}\ ,\ M_{32} = -M_{34}\ ,\ M_{43}\} = \{-3.746\ ,\ -0.874\ ,\ -2.222\ ,\ 3.937\}\frac{\alpha_T TEI}{l}$$

see Fig. 17.23(c).

If we had initially chosen the displacement figure shown in Fig. 17.23(d), we would have arrived at the fixed-end moments shown in Fig. 17.23(e) and the following set of equations:

$$\begin{bmatrix} 10.667 & 2 & -10 \\ 2 & 9 & -5.625 \\ -10 & -5.625 & 28.4375 \end{bmatrix} \begin{Bmatrix} \varphi_2 \\ \varphi_3 \\ \psi_{12} \end{Bmatrix} = \begin{Bmatrix} 17.867 \\ 1.2 \\ -33.333 \end{Bmatrix}$$

The only difference between the solution resulting from this set of equations and the previous one is ψ_{12}; the new value is $-1.004936\,\alpha_T T$. Both solutions result in the displacements shown in Fig.17.23(f).

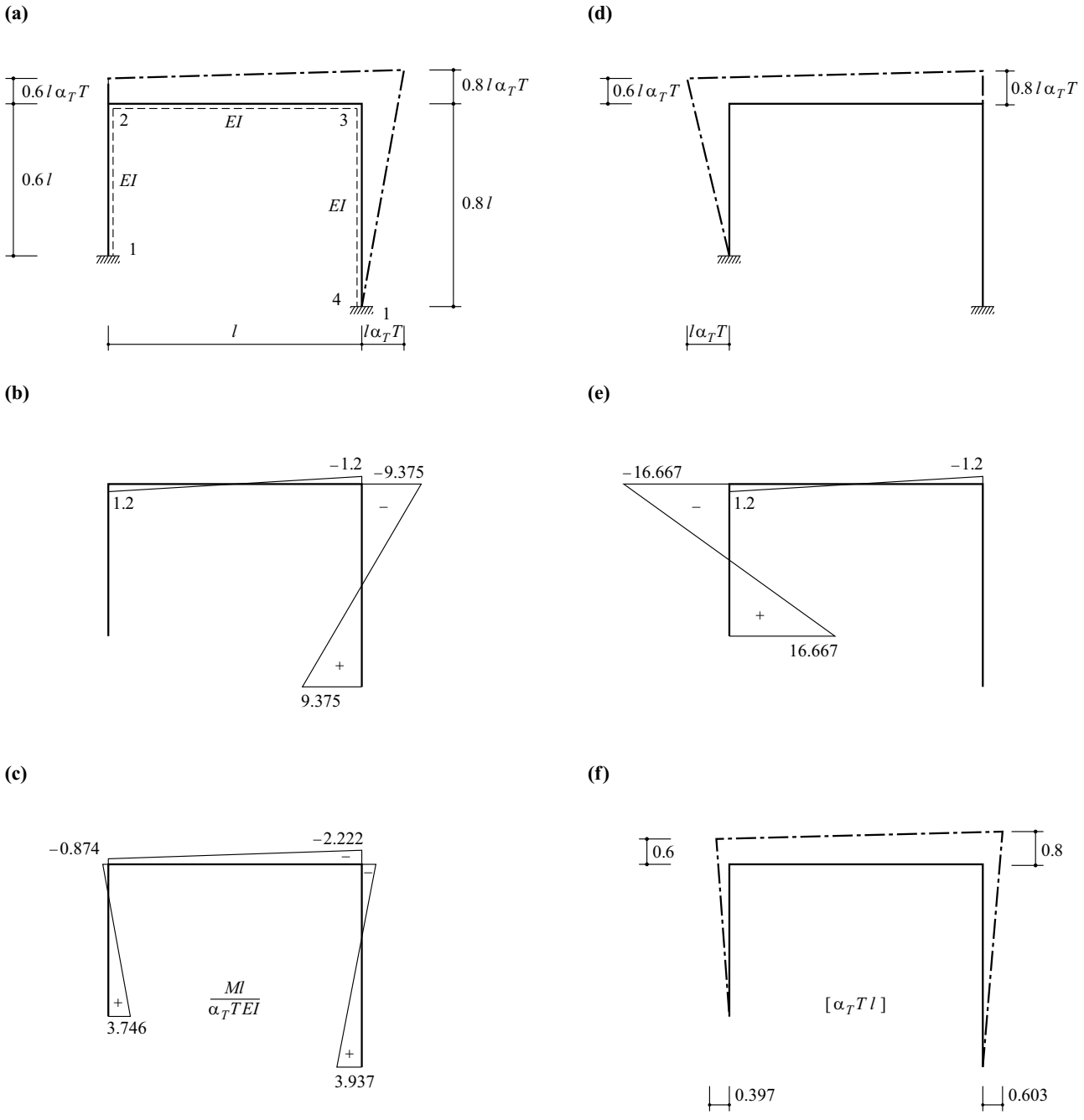

Fig. 17.23 Sway frame: (a) diagram of static system, (b) fixed-end moments, (c) restraint moments, (d) alternative initial displacement, (e) associated fixed-end moments, (f) displacements

17.4.6 Influence lines

The kinematic method for determining influence lines after LAND was introduced in section 12.3. Its application to statically indeterminate systems with the help of the force method was explained in section 16.3.4. According to the slope-deflection method, the moments are calculated directly as a result of the virtual deformation variable –1, and the associated deflections calculated from this using one of the methods outlined in chapter 15.

Fig. 17.24(a) illustrates the calculation of the fixed-end moments for a standard bar of length l with constant bending stiffness EI as a result of a virtual rotation –1 at ξ. Employing sign convention II, the following applies:

$$\delta_{i0} = \xi - 1 \quad , \quad \delta_{k0} = \xi$$

and

$$\delta_{ii} = \delta_{kk} = \frac{l}{3EI} \quad , \quad \delta_{ik} = \delta_{ki} = -\frac{l}{6EI}$$

The compatibility conditions

$$\begin{Bmatrix} \delta_i \\ \delta_k \end{Bmatrix} = \begin{bmatrix} \delta_{ii} & \delta_{ik} \\ \delta_{ki} & \delta_{kk} \end{bmatrix} \begin{Bmatrix} M_{ik}^0 \\ M_{ki}^0 \end{Bmatrix} + \begin{Bmatrix} \delta_{i0} \\ \delta_{k0} \end{Bmatrix} = \begin{Bmatrix} 0 \\ 0 \end{Bmatrix}$$

result in

$$M_{ik}^0 = \frac{EI}{l}(4 - 6\xi) \quad , \quad M_{ki}^0 = \frac{EI}{l}(2 - 6\xi) \tag{17.59}$$

Compare these with the variables M_l and M_r in the appropriate line in Fig. 17.1.

The example examined in Fig. 16.16 is considered again in Fig. 17.24(b). First of all, (17.59), with $\xi = 0.5$, results in the fixed-end moments $M_{12}{}^0 = -M_{21}{}^0 = EI/l$. Putting $s_{21} = 4EI/l$ and $s_{23} = 3EI/(0.8l) = 3.75EI/l$, the moment-balance equation $(s_{21} + s_{23})\varphi_2 + M_{21}{}^0 = 0$ at joint 2 gives us the rotation $\varphi_2 = 4/31$ and hence the bending moments M shown in the figure. Ultimately, the curvatures $M/(EI)$ allow the deflections to be determined, which are equal to the influence ordinates η_{M4} we require. Any of the methods described in chapter 15 may be used for this, especially MOHR's analogy, or the influence line can be determined point for point with the help of the

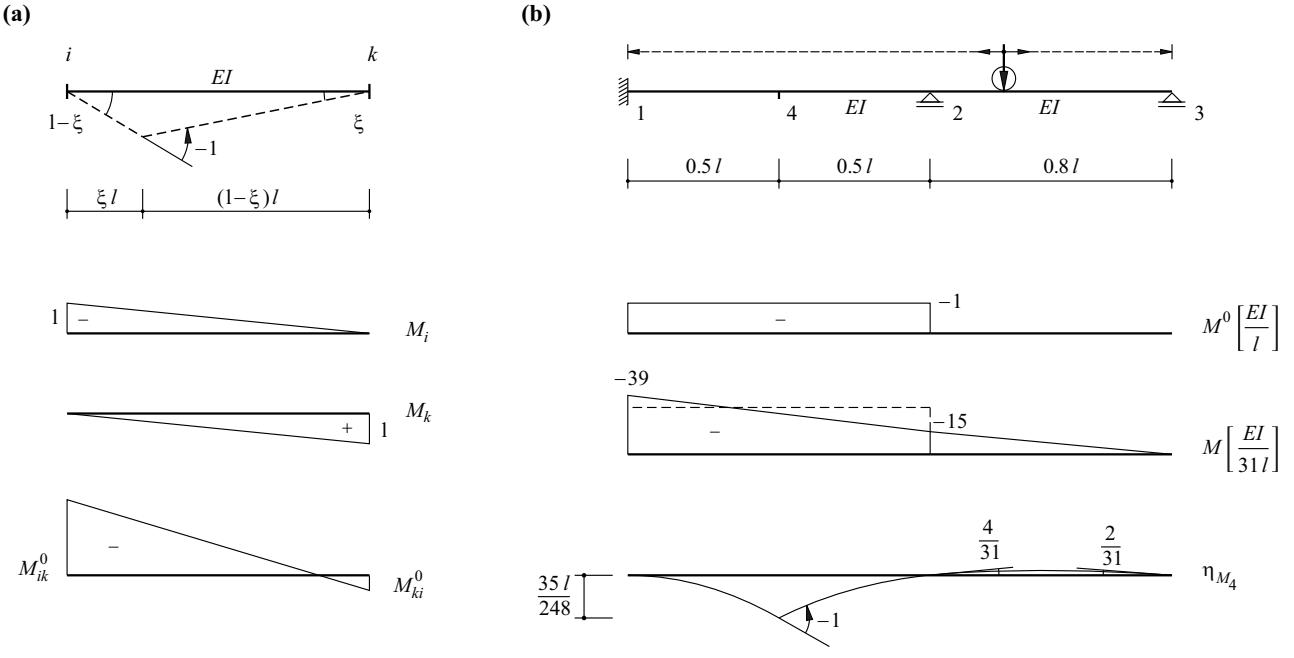

Fig. 17.24 Influence lines: (a) fixed-end moments due to a virtual deformation –1 applied to the standard bar, (b) application to the example of Fig. 16.16

work theorem (section 14.2), possibly using the reduction theorem. In order to illustrate the latter procedure, we shall calculate the influence ordinate η_{M4} at point 4 as an example by introducing a cantilever beam fixed at 1. The cantilever is loaded by a point load of magnitude 1 at its unsupported end 4. Using the integration table of Fig. 14.2 gives us the deflection

$$\frac{1}{6}\cdot 0.5\,l\cdot\left(2\cdot 39+\frac{39+15}{2}\right)\cdot\frac{EI}{31\,l}\cdot\frac{0.5\,l}{EI}=\frac{35\,l}{248}$$

see Fig. 17.24(b).

Example 17.12 Three-span frame

The task is to calculate the influence line η_{V23} for the shear force V_{23} to the right of joint 2 of the frame shown in Fig. 17.25. The fixed-end moments $M_{23}^{\ 0}=M_{32}^{\ 0}=-6EI/l^2$ correspond to the virtual deformation –1 (vertical displacement of magnitude 1 in bar 23 at edge of joint 2), see (17.17). Using

$s_{21}=s_{34}=3\,EI/l\quad,\quad s_{23}=s_{32}=2t_{23}=2t_{32}=4\,EI/l\quad,\quad s_{25}=2t_{52}=EI/l,$

the moment-balance equations for joints 2 and 3 result in

$$\begin{bmatrix}8 & 2\\ 2 & 7\end{bmatrix}\begin{Bmatrix}\varphi_2\\ \varphi_3\end{Bmatrix}=\begin{Bmatrix}6\\ 6\end{Bmatrix}\frac{1}{l}$$

and from that we get the joint rotations

$$\begin{Bmatrix}\varphi_2\\ \varphi_3\end{Bmatrix}=\begin{Bmatrix}15\\ 18\end{Bmatrix}\frac{1}{26l}$$

and the member end moments

$$\{M_{21}\,,M_{23}\,,M_{32}\,,M_{34}\,,M_{25}\,,M_{52}\}=\{45\,,-60\,,-54\,,54\,,15\,,7.5\}\frac{EI}{26\,l^2}$$

In the end, the shape of the bending moment M or curvature $M/(EI)$ diagram can be used to determine the associated deflections, i. e. the influence line η_{V23}, see Fig. 17.25.

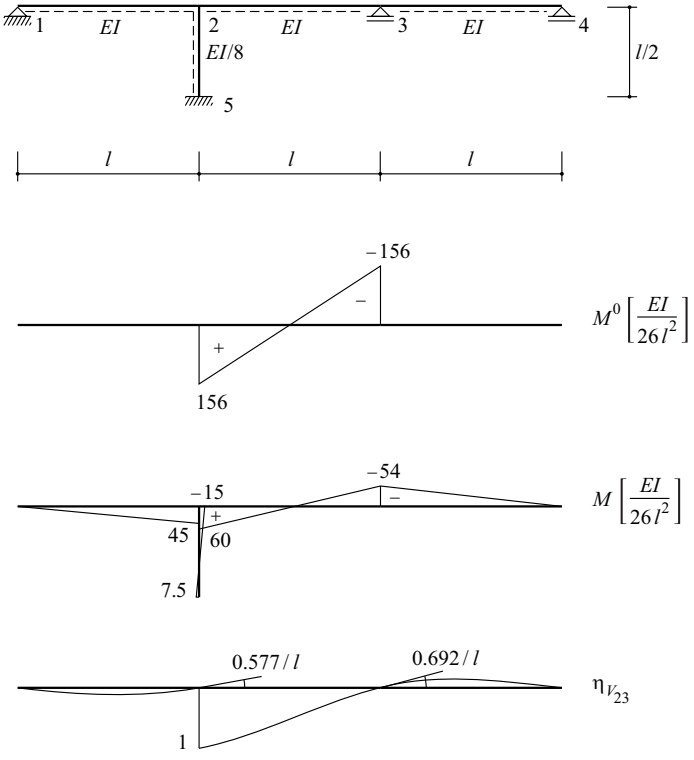

Fig. 17.25 Three-span frame – influence line for shear force V_{23}

17.4.7 CROSS method of moment distribution

17.4.7.1 General

The CROSS method of moment distribution solves the joint equilibrium conditions for a non-sway system iteratively. The advantage of this moment distribution method is that it is not necessary to determine joint rotation explicitly; the iteration is carried out directly for the joint moments, which leads to a very straightforward procedure.

A separate moment distribution has to be carried out for each load case and so the CROSS method is unsuitable when many load cases have to be considered. On the other hand, it is suitable for estimating the critical stress resultants from a few load cases during the conceptual design stage.

The CROSS method of moment distribution can be used for sway systems as well. To do that, we first distribute the moments on the non-sway (restrained) system and determine the corresponding restraining forces. In a second step, the restraining forces are cancelled out by imposing suitable displacement states (a unit displacement state for each restraining force) and by superposing the corresponding restraining forces.

The CROSS method of moment distribution is closely related to other iteration methods, e. g. that of KANI. Essentially, these methods correspond to an iteration technique introduced by GAUSS and SEIDEL for solving sets of linear equations.

17.4.7.2 Non-sway systems

The first step is to calculate the fixed-end moments $M_{ik}^{\,0}$ for the kinematically determinate basic system (all joints fixed, see section 9.3.4). After that, one joint is released and moment equilibrium at this joint achieved in accordance with the stiffnesses of the adjoining bars; the moments corresponding to the joint rotation carried over to the neighbouring joints are considered as surcharges on the moments already existing there. The joint moments are therefore successively improved. The iteration procedure is halted when the corrective moments are sufficiently small; at this point small moment values are no longer carried over to the neighbouring joints, but each joint must be balanced in itself.

As $\varphi_k = \psi_{ik} = 0$, the equilibrium condition (17.58) in conjunction with $(17.51)_1$ leads to

$$\varphi_i = \frac{M_i - \sum M_{ik}^0}{\sum s_{ik}} = -\frac{M_i^0}{\sum s_{ik}} \tag{17.60}$$

(where $M_i^{\,0}$ = *out-of-balance moment*) and hence to

$$\begin{aligned} M_{ik} &= M_{ik}^0 - \frac{s_{ik}}{\sum s_{ik}} M_i^0 = M_{ik}^0 - \kappa_{ik} M_i^0 \\ M_{ki} &= M_{ki}^0 - \frac{t_{ki}}{s_{ik}} \kappa_{ik} M_i^0 = M_{ki}^0 - \mu_{ik} \kappa_{ik} M_i^0 \end{aligned} \tag{17.61}$$

The ratios

$$\kappa_{ik} = \frac{s_{ik}}{\sum s_{ik}} \quad , \quad \mu_{ik} = \frac{t_{ki}}{s_{ik}} \tag{17.62}$$

are called *moment distribution* and *moment carry-over factors*.

The practical calculation is carried out in the following steps with the help of a table:

1. Clarify the sway condition of the system, introduce restraining forces if necessary.
2. Calculate moment distribution and carry-over factors as well as out-of-balance moments.
3. Release the joint with the maximum out-of-balance moment and apply (17.61).
4. Repeat step 3 until the iteration can be halted.

Example 17.13 Continuous beam

According to the findings of section 17.4.1, only the joint rotations φ_2 and φ_3 are unknown in the continuous beam of Fig. 17.26(a). Fig. 17.26(b) shows the fixed-end moments ($M_{23}^0 = -M_{32}^0 = 7.5 \cdot 4^2/12 = 10\,\text{kNm}$, $M_{34}^0 = -7.5 \cdot 1.33^2/4 = -3.33\,\text{kNm}$) corresponding to the applied load. Using $\{s_{21}, s_{23} = s_{32}, s_{34}\} = \{0.8, 1.0, 0.75\}EI/\text{m}$, the result according to $(17.62)_1$ is the moment distribution factors κ_{ik} shown in Fig. 17.26(c), and $\{t_{12}, t_{23} = t_{32}, t_{34} = t_{43}\} = \{0.4, 0.5, 0\}EI/\text{m}$ gives us the moment carry-over factors μ_{ik}.

Moment distribution begins by releasing joint 3 and distributing the out-of-balance moment $M_3^0 = -13.3\,\text{kNm}$; the line beneath the figures $7.6\,\text{kNm} = -\kappa_{32}M_3^0$ and $5.7\,\text{kNm} = -\kappa_{34}M_3^0$ means that moment equilibrium has been reached at joint 3, i.e. $M_{32} = (-10.0 + 7.6)\,\text{kNm} = -2.4\,\text{kNm} = -M_{34} = (3.3 - 5.7)\,\text{kNm}$.

The proportion $\mu_{23} \cdot 7.6\,\text{kNm} = 3.8\,\text{kNm}$ of the correction of 7.6 kNm at M_{32} is carried over to joint 2, where it increases the out-of-balance moment M_2^0 from 10.0 to 13.8 kNm. Moment distribution at joint 2 brings about corrections to M_{21} and M_{23} of – 6.1 and – 7.7 kNm respectively, and the moments of – 3.0 and 3.8 kNm carried over to joints 1 and 3 respectively.

After this step-by-step description, the four further iteration steps of Fig. 17.26(c) need no further explanation. The moments M_{ik} added together in each column are finally entered on the bending moment diagram, see Fig. 17.26(d).

(a)

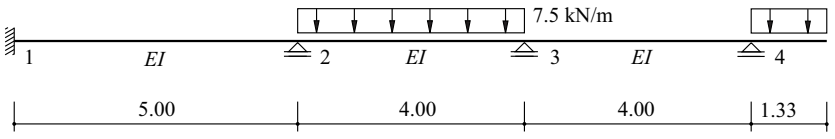

(b)

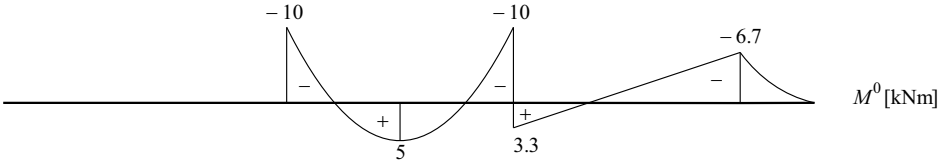

(c)

	0.44	0.56	0.57	0.43			κ_{ik}
0.5 ←		0.5 ← → 0.5					μ_{ik}
		10.0	– 10.0	– 3.3			M_{ik}^0
		3.8	7.6	5.7			
– 3.0	– 6.1	– 7.7	– 3.8				
		1.1	2.2	1.6			
– 0.2	– 0.5	– 0.6	– 0.3				
		0.1	0.2	0.1			
		– 0.1					
– 3.2	– 6.6	6.6	– 4.1	4.1			M_{ik}

(d)

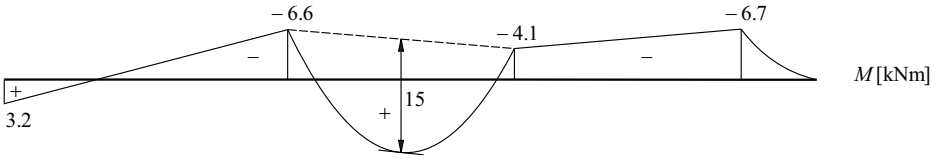

Fig. 17.26 Continuous beam: (a) diagram of static system, (b) fixed-end moments, (c) moment distribution table, (d) bending moment diagram

17.4.7.3 Sway systems

The sway frame shown in Fig. 17.27(a) is first considered as a non-sway system by introducing a horizontal restraining force F_0 at joint 3. Fig. 17.27(b) to (e) illustrate the moment distribution and the resulting moments.

In order to determine the restraining force, the displaced state shown in Fig. 17.27(f) is considered with $\psi_{12} = -2\psi_{23} = \psi_{34} = \psi$ and zero joint rotations. Applying the principle of virtual deformations results in

$$\psi \cdot [-102 - 205 - (205 - 231)/2 + 231 + 115]\,\text{kNm} + 600\,\text{kN} \cdot 3\,\text{m} \cdot (-\psi/2) + F_0 \cdot 4\,\text{m} \cdot \psi = 0$$

and consequently $F_0 = 212\,\text{kN}$.

Fig. 17.27(g) shows the fixed-end moments as a result of $\psi = 1$, and Fig. 17.27(h) shows the corresponding moment distribution. Applying the principle of virtual deformations once more results in

$$\psi \cdot [-1.058 - 0.915 - (0.915 + 0.968)/2 - 0.968 - 1.234]\,EI/\text{m} + F_1 \cdot 4\,\text{m} \cdot \psi = 0$$

and consequently a restraining force of $F_1 = 1.2791\,EI/\text{m}^2$.

The condition

$$F_0 + k\,F_1 = 0$$

leads to the proportionality factor

$$k = -\frac{212\,\text{kNm}^2}{1.2791\,EI} = -165.74\,\text{kNm} \cdot \frac{\text{m}}{EI}$$

with which the moments calculated in Fig. 17.27(h) are multiplied and superposed on those of Fig. 17.27(e). Fig. 17.27(i) shows the outcome of this superposition. Compared with the non-sway system, Fig. 17.27(e), the values of the moments at joints 3 and 4 are significantly larger and those at joints 1 and 2 significantly smaller.

(a)

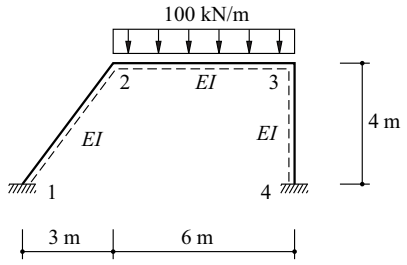

(b)

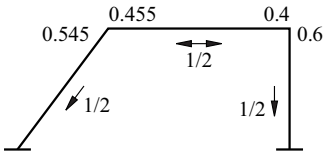

(c)

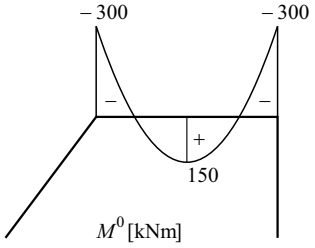

(d)

	300	– 300	
–164	–136	– 68	
	74	147	221
– 41	– 33	– 16	
– 205	205	– 6	10
		– 231	231

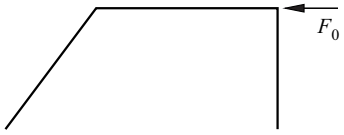

– 82	110
– 20	5
– 102	115

(e)

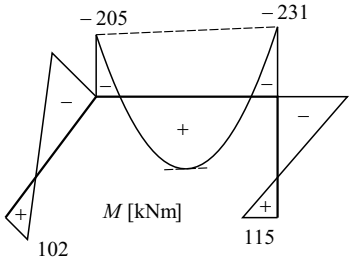

(f)

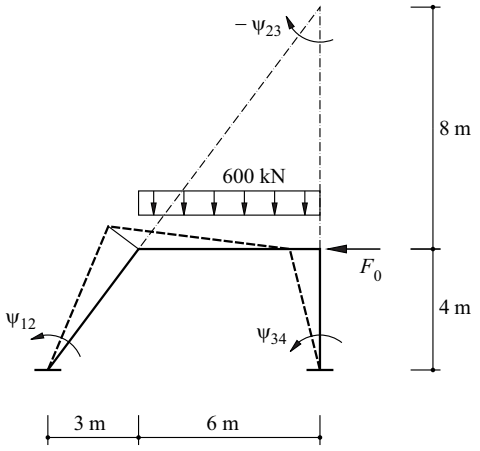

(g)

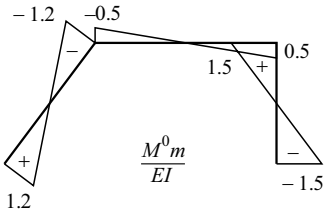

(h)

– 1.200	0.500	0.500	– 1.500
	0.200	0.400	0.600
0.272	0.228	0.114	
	– 0.023	– 0.046	– 0.068
0.013	0.010	0.968	– 0.968
– 0.915	0.915		

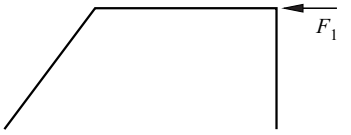

– 1.200	– 1.500
0.136	0.300
0.006	– 0.034
– 1.058	– 1.234

(i)

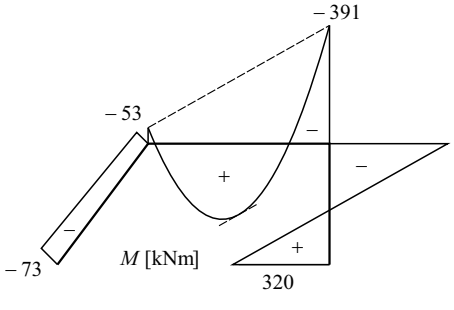

Fig. 17.27 Sway frame: (a) diagram of static system, (b) moment distribution and carry-over factors, (c) fixed-end moments, (d) moment distribution, (e) moments for the non-sway system, (f) displaced state, (g) fixed-end moments due to unit displacement, (h) moment distribution, (i) moments for the sway system

17.5 Summary

1. The basic idea of the displacement method introduced in section 8.1.2 is transferred to general plane frameworks by applying the discretised structural model introduced in section 9.3. Sign convention II is used throughout in this method.
2. The member stiffness matrices $\boldsymbol{k}_e$ linking the independent bar end variables N_r, M_l, M_r and Δ, λ, ρ as well as the reduced stiffness matrices $\boldsymbol{k}$ formulated from all these matrices are square, symmetrical, invertible and positive definite.
3. Actions on the individual bars are taken into account in accordance with Fig. 17.1 by way of fixed-end forces at the joints.
4. The heart of the displacement method is the formulation of the kinematic transformation matrix $\boldsymbol{a}$ for the kinematically determinate basic system as well as the calculation of the global stiffness matrix $\boldsymbol{K}$ according to (17.9) plus its inversion and further usage according to (17.10) to (17.12).
5. All matrices remain as small as possible when using independent bar end variables. However, the complete bar end variables and the support force variables must be calculated by considering the equilibrium subsequently. This disadvantage is avoided when using complete bar end variables. The complete member stiffness matrices $\overline{\boldsymbol{k}}_e$ are, however, singular and positive semi-definite.
6. The support force variables can be calculated directly by taking into account all degrees of freedom and by rearranging accordingly in line with (17.25) or (17.26).
7. According to the direct stiffness method, the global stiffness matrix $\boldsymbol{K}$ can be calculated by superposing the values of the member stiffness matrices $\overline{\boldsymbol{k}}_{eg}$ related via a rotational transformation to the global system of coordinates; the corresponding kinematic transformation matrix $\overline{\boldsymbol{a}}_g$ is a pure incidence matrix. Likewise, the component $\boldsymbol{Q}_0$ of the global load vector $\boldsymbol{Q}$ corresponding to the bar loads is found by superposing the fixed-end force variables $\overline{\boldsymbol{s}}_{0g}$ related to the global system of coordinates.
8. The slope-deflection method is a variation on the general displacement method which was developed for the manual calculation of plane frame systems. Bars are assumed to be inextensible and rigid in shear. The bar end moments are expressed according to (17.51) depending on the external load or restraint as well as the unknown joint and bar rotations φ and ψ respectively, and φ and ψ are determined via joint and displacement equilibrium conditions.
9. Restraints are taken into account in the slope-deflection method via fixed-end moments that occur at fixed joints as a result of the restraint. In doing this, we can assume any initial displacement figure when dealing with sway systems.
10. When determining influence lines according to the slope-deflection method, the moments as a result of a virtual deformation variable -1 are determined directly and the deflections associated with those calculated with the help of one of the methods described in chapter 15.
11. The CROSS method of moment distribution, which is based on the slope-deflection method, solves the joint equilibrium conditions of a non-sway system iteratively. To do this, the negative out-of-balance moment is distributed to the adjoining bars at each joint in turn and carried over to the neighbouring joints. The iteration is halted as soon as the corrective moments are sufficiently small.
12. When using the CROSS method to solve sway systems, we eliminate the restraining forces required for the non-sway system by considering suitable unit displacement states and superposing the corresponding restraining forces.

17.6 Exercises

17.1 Set up the global stiffness matrix for the system shown in Fig. 9.9(a). Use the cross-sectional values given in example 13.6 plus $E = 210\,\mathrm{kN/mm^2}$ and $\nu = 0.3$.

17.2 Examine the system shown in Fig. 9.9(g) using the slope-deflection method. Presume constant bending stiffnesses EI_b (beam 1234) and EI_c (columns 25 and 36) with the ratio $EI_b/EI_c = 10$. Determine the stress resultants due to a uniformly distributed load on end span 12 or interior span 23.

17.3 Investigate how a settlement c_5 influences the system examined in exercise 17.2.

17.4 The base 1 of the system shown in Fig. 17.28(a) experiences a settlement c_1 and a rotation $\varphi_1 = c_1/(4l)$. Calculate the corresponding restraint stress resultants and the deflection curve.

17.5 The bending stiffness of column 24 in Fig. 17.28(b) is three times smaller than that of frame beam 12 and column 23. Calculate the stress resultants due to the given load.

17.6 Calculate the stress resultants for the system shown in Fig. 17.28(c) subjected to the actions q and $Q = ql$.

17.7 Solve exercise 17.6 assuming a rigid connection between frame beam 123 and column 35.

17.8 Discuss the flow of the forces in joint region 3 of the system shown in Fig. 17.18(a) in a similar way to Fig. 17.19(b).

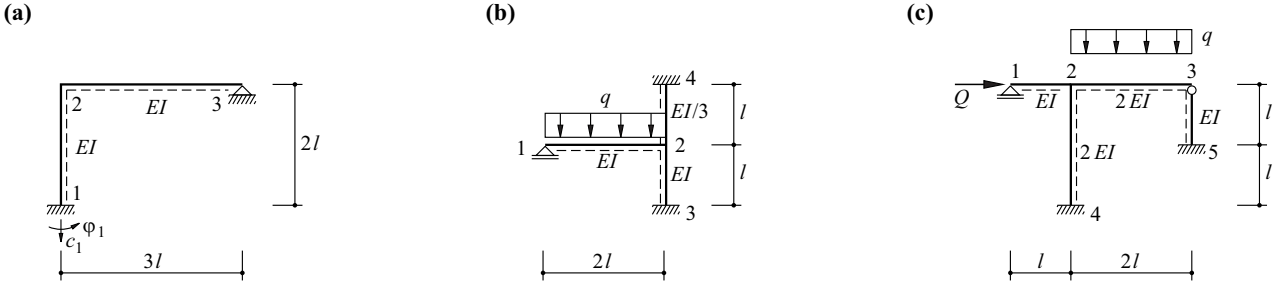

Fig. 17.28 Diagrams of static systems for section 17.6.

18 CONTINUOUS MODELS

18.1 General

Many problems in everyday construction practice can be analysed with the help of idealisation as one-dimensional continua according to section 8.2.1 (Introduction), 8.2.2 (Plane framed structures) and 8.2.3 (Spatial framed structures). Combining the equilibrium conditions (8.21) or (8.26) with the kinematic relations (8.22) or (8.27) plus the linear elastic constitutive equations (8.23) or (8.28) produces ordinary differential equations for the displacement variables relevant to the particular problem. Those variables in turn lead to the internal deformation and force variables we wish to find depending on the position on the bar axis.

This chapter looks at such problems. We have to find the diverse relationships and analogies between the different problems. Such relationships and analogies are suitable for improving our understanding of the structural behaviour of different types of construction.

To help the reader, each main section in this chapter has its own summary (instead of just one summary at the end as in the other chapters).

18.2 Bar extension

18.2.1 Practical examples

Fig. 18.1 shows a few typical practical examples of the analytical model dealt with below. The internal and external deformation and force variables are confined to the bar extension ε, the normal force N and the displacement u plus the line load q in the direction of the bar x. The applications range from columns (a) to piles with end bearing and skin friction (b) to the idealisation of beam flanges (c) or shell edge beams (d) in the form of *stringers*. Other examples concern the friction losses that occur with prestressing tendons (e) and similar phenomena in prestressed raft foundations (f) and rails subjected to thermal restraints (g). It is also possible to treat *bond* problems in concrete construction, e. g. pull-out of reinforcing steel (h), the anchorage of pretensioned steel in concrete (i), the tension-stiffening action of the concrete between adjacent cracks, which relieves the reinforcing steel (j), and the composite action of reinforcing laminates bonded to existing concrete beams (k). Further, joints between bars achieved with adhesives, rivets, dowels, keys and other connectors can be dealt with in a similar way.

Theory of Structures. First Edition. Peter Marti

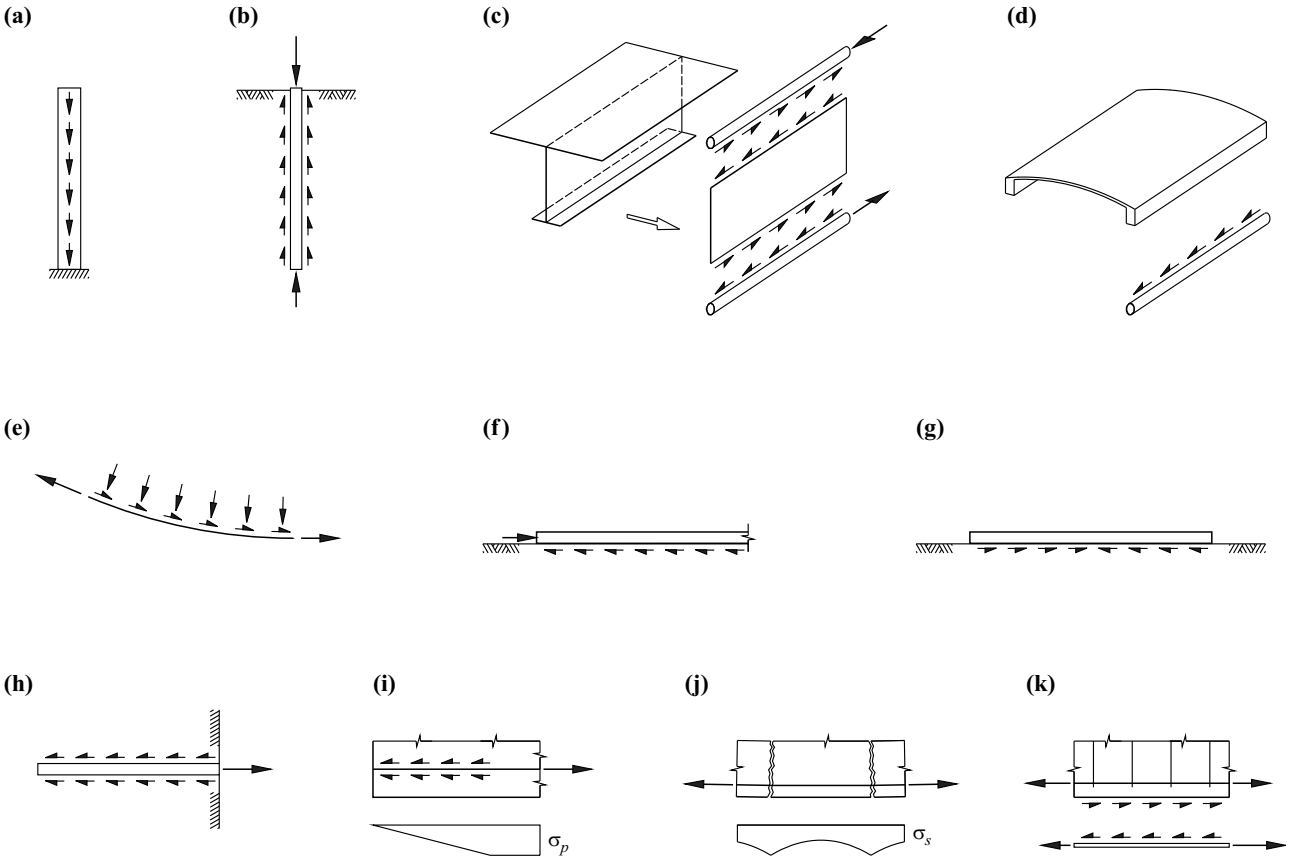

Fig. 18.1 Bar extension – examples: (a) column, (b) pile, (c) beam flange (stringer), (d) shell edge beam, (e) loss of prestress due to friction, (f) friction on prestressed raft foundation, (g) rail subjected to thermal restraint, (h) pull-out test, (i) anchorage of pretensioned reinforcement in concrete, (j) tension stiffening in cracked reinforced concrete, (k) reinforced concrete beam strengthened with bonded laminate

18.2.2 Analytical model

Using the abbreviated forms $' = \mathrm{d}/\mathrm{d}x$ and $q_x = q$, the relationships (8.21) and (8.22) are reduced to

$$q = -N' \quad , \quad \varepsilon = u' \tag{18.1}$$

for the case of a pure bar extension, see Fig. 18.2. By adding the *initial normal strains* ε_0, e. g. due to shrinkage or swelling (see section 7.4) or as a result of thermal actions (see section 7.5), the relationship $(13.8)_1$ is generalised to

$$\varepsilon = \frac{N}{EA} + \varepsilon_0 \tag{18.2}$$

and combining (18.1) and (18.2) results in

$$q + [(u' - \varepsilon_0)EA]' = 0 \tag{18.3}$$

When $\varepsilon_0 = 0$ and EA = const, (18.3) can be simplified to

$$q = -EA\,u'' \tag{18.4}$$

The appropriate boundary conditions according to Fig. 18.3 should be taken into account when integrating (18.3) or (18.4). A spring restraint (a) with the translational spring stiffness k[kN/m] means that $N = -ku$ applies, see $(5.12)_1$. At a free end (b), $N = 0$, which corresponds to $k = 0$. At a fixed end (c), $u = 0$, which corresponds to $k \to \infty$. In addition, all continuity conditions according to Fig. 18.4 have to be taken into account, e. g. abrupt changes in q or EA, singularities in q and at intermediate supports.

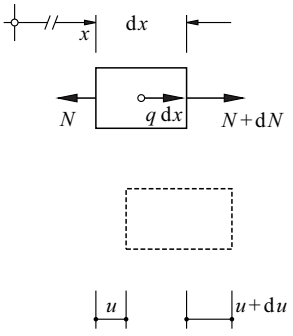

Fig. 18.2 Undeformed and deformed states of a differential bar element

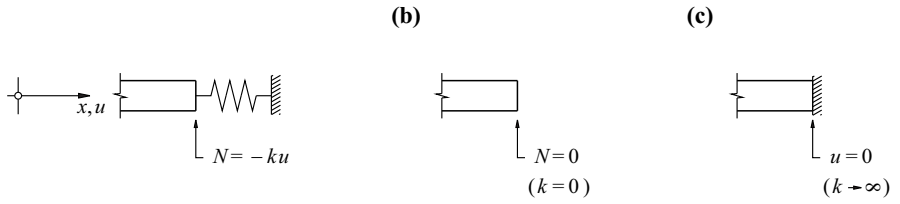

Fig. 18.3 Boundary conditions: (a) spring restraint, (b) free end, (c) fixed end

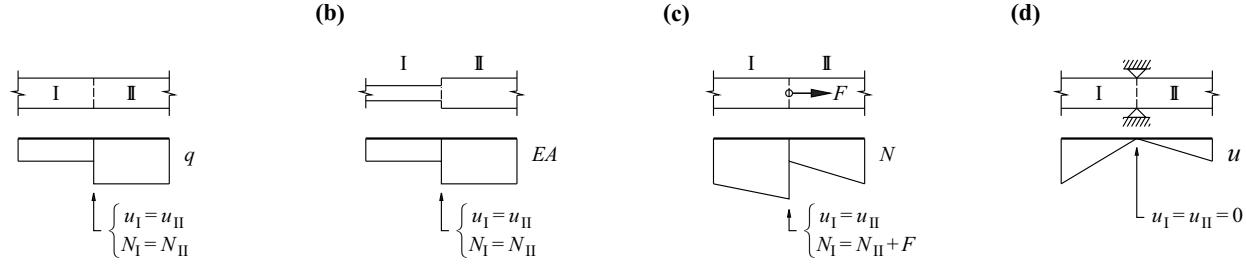

Fig. 18.4 Continuity conditions: (a) abrupt change in q, (b) abrupt change in EA, (c) singularity in q, (d) intermediate support

Example 18.1 Bar restrained at both ends

The bar of length l shown in Fig. 18.5 is restrained at both ends and loaded by the line load

$$q = q_0 \cos\left(\frac{\pi x}{l}\right)$$

It is assumed that $\varepsilon_0 = 0$ and EA = const. Integrating (18.4) twice results in

$$EAu = \frac{q_0 l^2}{\pi^2} \cos\left(\frac{\pi x}{l}\right) + c_1 x + c_2$$

for this load. The integration constants c_1 and c_2 follow from the boundary conditions $u(0) = u(l) = 0$:

$$c_1 = \frac{2q_0 l}{\pi^2} \quad , \quad c_2 = -\frac{q_0 l^2}{\pi^2}$$

and the following applies:

$$u = \frac{q_0 l^2}{\pi^2 EA}\left[\cos\left(\frac{\pi x}{l}\right) + \frac{2x}{l} - 1\right] \quad , \quad N = \frac{q_0 l}{\pi}\left[\frac{2}{\pi} - \sin\left(\frac{\pi x}{l}\right)\right]$$

The point of zero N at $x = (l/\pi)\arcsin(2/\pi) \approx 0.22\,l$ corresponds to the maximum displacement u.

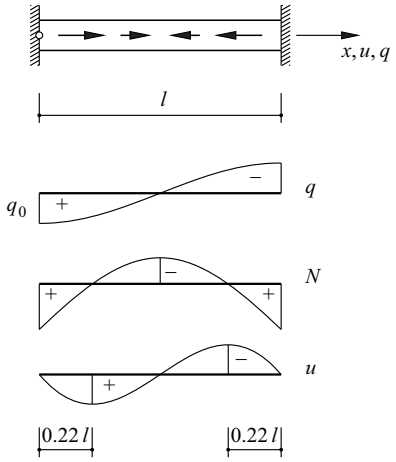

Fig. 18.5 Bar restrained at both ends ($\varepsilon_0 = 0$, EA = const)

Example 18.2 Bar with spring restraint at one end

The bar shown in Fig. 18.6, otherwise the same bar as that used for example 18.1, is restrained by a spring at its right-hand end ($k = EA/l$) and loaded by a single force F in the middle. As $q = 0$, it follows from (18.4) that

$$\text{I:} \quad EAu = c_1 x + c_2 \quad , \quad \text{II:} \quad EAu = c_3 x + c_4$$

for bar segments I and II, where $N_\text{I} = c_1$ and $N_\text{II} = c_3$. The boundary and continuity conditions result in

$$\left\{\begin{array}{ll} u_\text{I}(0) = 0 & : \; c_2 = 0 \\ u_\text{I}(l/2) = u_\text{II}(l/2) & : \; c_1 \cdot l/2 + c_2 = c_3 \cdot l/2 + c_4 \\ N_\text{I}(l/2) = N_\text{II}(l/2) + F & : \; c_1 = c_3 + F \\ N_\text{II}(l) = -ku_\text{II}(l) & : \; c_3 = -(1/l)\cdot(c_3 l + c_4) \end{array}\right\} \rightarrow \left\{\begin{array}{l} c_1 = 3F/4 \\ c_2 = 0 \\ c_3 = -F/4 \\ c_4 = Fl/2 \end{array}\right\}$$

and therefore we get the diagrams for N and u shown in Fig. 18.6.

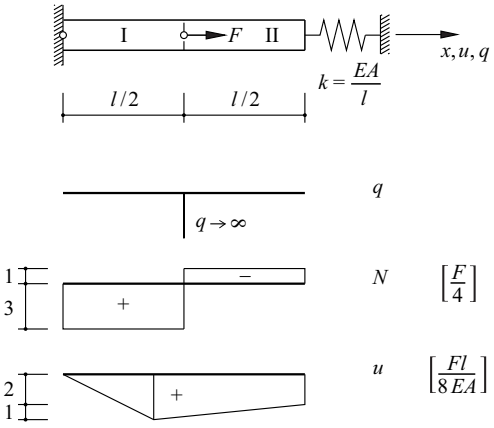

Fig. 18.6 Bar with spring restraint at one end ($\varepsilon_0 = 0$, EA = const)

18.2.3 Residual stresses

Let us consider a cross-section made up of two materials (e. g. concrete and reinforcing steel) according to Fig. 18.7. The parts of the cross-section have axial stiffnesses E_1A_1 and E_2A_2 and coefficients of thermal expansion α_{T1} and α_{T2}. Applying (7.53), a change in temperature T results in the initial normal strains

$$\varepsilon_{01} = \alpha_{T1}T \quad , \quad \varepsilon_{02} = \alpha_{T2}T$$

and therefore (18.2) – with $\varepsilon_1 = \varepsilon_2$ (cross-sections remain plane) and $N_1 + N_2 = 0$ (no external loads) – results in the relationships

$$N_1 = -N_2 = \frac{E_1A_1E_2A_2(\alpha_{T2} - \alpha_{T1})T}{E_1A_1 + E_2A_2} \quad , \quad \varepsilon_1 = \varepsilon_2 = \frac{(\alpha_{T1}E_1A_1 + \alpha_{T2}E_2A_2)T}{E_1A_1 + E_2A_2} \tag{18.5}$$

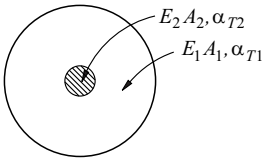

Fig. 18.7 Composite cross-section

Normally, changes in temperature occur simultaneously with shrinkage or swelling processes, and external loads have to be considered as well. Including the corresponding initial normal strains ε_0 means it is possible to deal with any problem with the help of (18.1) and (18.2).

Example 18.3 Reinforced concrete column – change in temperature

Let us consider a reinforced concrete column with a relatively high geometric reinforcement ratio of $A_2/(A_1 + A_2) = 8\,\%$ as well as $E_1 = 33.6\,\text{kN/mm}^2$, $\alpha_{T1} = 6 \cdot 10^{-6}/°\text{C}$, $E_2 = 205\,\text{kN/mm}^2$, $\alpha_{T2} = 10 \cdot 10^{-6}/°\text{C}$ and $T = 30°\text{C}$. Eq. (18.5) then gives us

$$\sigma_c = \frac{N_1}{A_1} = 1.4\,\text{N/mm}^2 \quad , \quad \sigma_s = \frac{N_2}{A_2} = -16.1\,\text{N/mm}^2 \quad , \quad \varepsilon = 0.222\,‰$$

The tensile stress in the concrete σ_c is only about half of the (albeit highly scattered) tensile strength of the concrete and so cracking of the concrete is unlikely.

Example 18.4 Reinforced concrete column – shrinkage

The task is to calculate the shrinkage strain ε_{cs} of the column examined in example 18.3, which causes a tensile stress of $f_{ctm} = 2.9\,\text{N/mm}^2$ (f_{ctm} = assumed mean concrete tensile strength). To do this, we replace $\alpha_{T1}T$ by ε_{cs} and put $\alpha_{T2} = 0$ and $N_1 = A_1 f_{ctm}$ in $(18.5)_1$. From the corresponding relationship

$$\varepsilon_{cs} = -\frac{f_{ctm}(E_1A_1 + E_2A_2)}{E_1E_2A_2}$$

we get $\varepsilon_{cs} = -0.25\,‰$, i. e. a shrinkage strain that can certainly occur, see section 7.4.1. Accordingly, heavily reinforced members can suffer from shrinkage cracks even when deformation is not inhibited.

18.2.4 Restraints

18.2.4.1 Homogeneous bar between rigid abutments subjected to change in temperature

The bar shown in Fig. 18.8 is restrained at both ends and subjected to an arbitrary change in temperature $T = T(x)$. The axial stiffness EA and the coefficient of thermal expansion α_T are both presumed to be constant. Putting $\varepsilon_0 = \alpha_T T$ and $q = 0$, and taking into account the boundary conditions $u(0) = u(l) = 0$, eq. (18.1) and (18.2) result in

$$N = -\frac{EA\alpha_T}{l}\int_0^l T\,\mathrm{d}x \quad , \quad u = \alpha_T\left(\int_0^x T\,\mathrm{d}x - \frac{x}{l}\int_0^l T\,\mathrm{d}x\right) \tag{18.6}$$

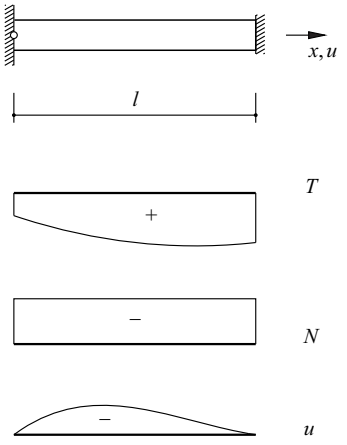

Fig. 18.8 Bar restrained at both ends subjected to arbitrary change in temperature

18.2.4.2 Homogeneous rail subjected to constant change in temperature

A homogeneous rail of length $2l$ (axial stiffness EA, coefficient of thermal expansion α_T) is subjected to a change in temperature $T = \text{const}$. The displacements u between the rail and the ground underneath cause forces $q = -ku$, see Fig. 18.9. Eq. (18.4) results in the homogeneous differential equation

$$EAu'' - ku = 0 \tag{18.7}$$

with the solution

$$u = c_1 e^{\omega x} + c_2 e^{-\omega x} \quad \left(\omega^2 = \frac{k}{EA}\right) \tag{18.8}$$

and (18.2) results in

$$N = EA(u' - \alpha_T T) = EA(c_1\omega e^{\omega x} - c_2\omega e^{-\omega x} - \alpha_T T)$$

With the boundary conditions $u(0) = 0$ and $N(l) = 0$, it follows that

$$c_1 = -c_2 = \frac{\alpha_T T}{2\omega\cosh(\omega l)}$$

which gives us

$$N = EA\alpha_T T\left[\frac{\cosh(\omega x)}{\cosh(\omega l)} - 1\right] \quad , \quad u = \frac{\alpha_T T \sinh(\omega x)}{\omega\cdot\cosh(\omega l)} \tag{18.9}$$

When $l \to \infty$, the stress N/A in the rail tends to $-E\alpha_T T$, i. e. with, for example, $E = 205\,\mathrm{kN/mm^2}$, $\alpha_T = 10\cdot 10^{-6}/°\mathrm{C}$ and $T = 40°\mathrm{C}$, it tends to $-82\,\mathrm{N/mm^2}$.

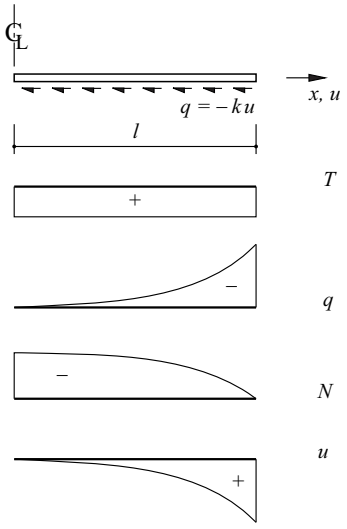

Fig. 18.9 Homogeneous rail subjected to constant change in temperature

18.2.4.3 Inhibited shrinkage of a reinforced concrete member

A reinforced concrete member of length l is restrained by a spring at one end as shown in Fig. 18.10 (spring stiffness k). The axial stiffnesses of the concrete (E_cA_c) and the reinforcing steel (E_sA_s) are presumed to be constant, and the shrinkage strain of the concrete is assumed to have a value $\varepsilon_{cs} = \text{const}$. Eq. (18.2) gives us the normal force components

$$N_c = E_cA_c(\varepsilon - \varepsilon_{cs}) \quad , \quad N_s = E_sA_s\varepsilon$$

in the concrete and the reinforcing steel. As $q = 0$, it follows from $(18.1)_1$ that $N = N_c + N_s$ is constant, and therefore both $\varepsilon = (N + E_cA_c\varepsilon_{cs})/(E_cA_c + E_sA_s)$ as well as N_c and N_s are constant, too. Taking into account the boundary condition $u(0) = 0$, eq. $(18.1)_2$ results in the relationship $u = \varepsilon x$, and taking the boundary condition $N_c + N_s + k\varepsilon l = 0$ at point $x = l$ results in

$$\varepsilon = \frac{\varepsilon_{cs}}{1 + \dfrac{E_sA_s + kl}{E_cA_c}} \tag{18.10}$$

When $k = 0$, this relationship is reduced to $(18.5)_2$ if we put $\alpha_{T2} = 0$ and replace E_1A_1 by E_cA_c, E_2A_2 by E_sA_s and $\alpha_{T1}T$ by ε_{cs} in that equation.

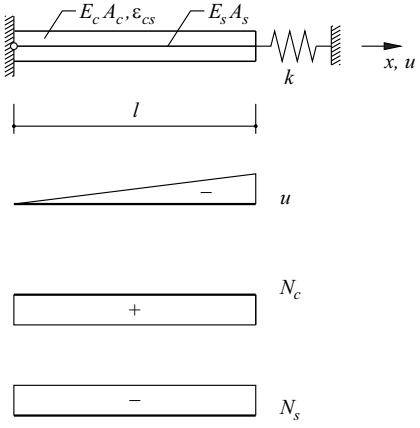

Fig. 18.10 Inhibited shrinkage of a reinforced concrete member

The stress in the concrete is

$$\sigma_c = \frac{N_c}{A_c} = \frac{-E_c\varepsilon_{cs}}{1 + \dfrac{E_cA_c}{E_sA_s + kl}}$$

which for k = 0 is reduced to the relationship for ε_{cs} derived in example 18.4 when σ_c is replaced by f_{ctm}, E_cA_c by E_1A_1 and E_sA_s by E_2A_2.

18.2.5 Bond

18.2.5.1 Pull-out test

A cylindrical bar with diameter Ø, modulus of elasticity E and length l is pulled out of a solid body (idealised as rigid) as shown in Fig. 18.11(a). The relative displacements u between the points on the surface of the bar and the points of contact with the solid body correspond to bond forces $\tau_b Ø\pi$ per unit length, i. e. a line load $q = -\tau_b Ø\pi$ acts on the bar. With $A = Ø^2\pi/4$, eq. (18.4) therefore gives us the differential equation

$$u'' - \frac{4\tau_b}{E\,Ø} = 0 \tag{18.11}$$

Provided the dependence of τ_b on u is known, (18.11) can be solved. Numerical integration methods must generally be used.

The three special cases of the bilinear bond shear stress-slip relationship

$$\tau_b = k_1 + k_2 u \tag{18.12}$$

shown in Fig. 18.11(b) are discussed below, see Fig. 18.11(c). Using the corresponding analytical solutions (see Fig. 18.12), it is possible to approximate the behaviour for general τ_b-u relationships.

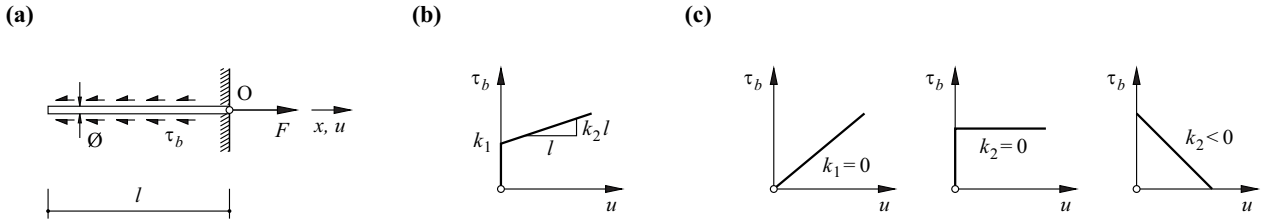

Fig. 18.11 Pull-out test: (a) diagram of static system, (b) bilinear bond shear stress-slip relationship, (c) special cases

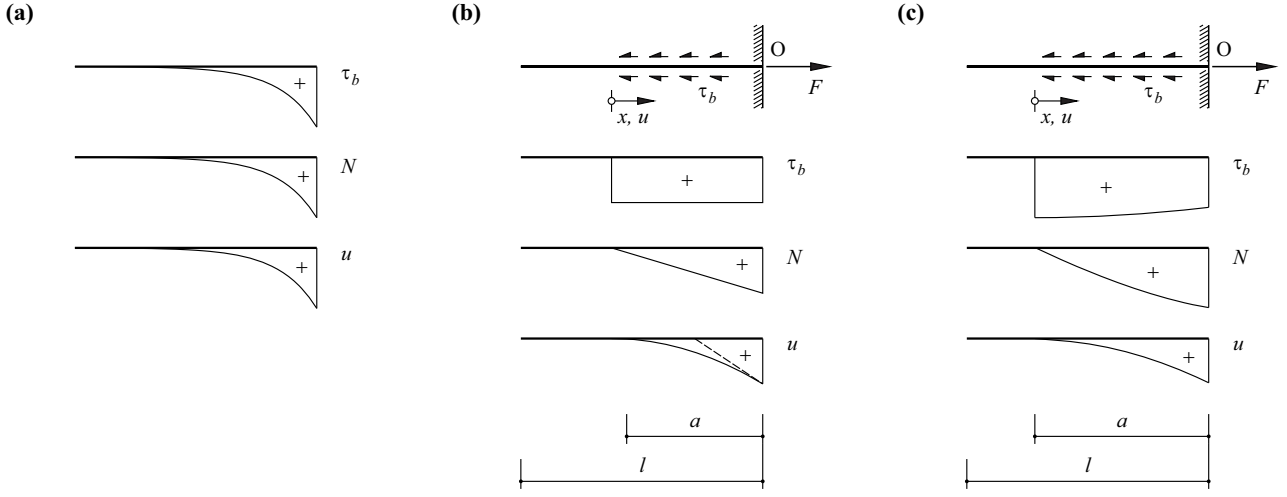

Fig. 18.12 Solutions for the special cases of Fig. 18.11(c): (a) $k_1 = 0$, $k_2 > 0$, (b) $k_1 > 0$, $k_2 = 0$, (c) $k_1 > 0$, $k_2 < 0$

When $k_1 = 0$, $k_2 > 0$, then (18.11) becomes similar to (18.7) and leads to

$$u = c_1 e^{\omega x} + c_2 e^{-\omega x} \qquad \left(\omega^2 = \frac{4k_2}{E\varnothing}\right)$$

and

$$N = k_2 \varnothing\pi \cdot \omega^{-1}(c_1 e^{\omega x} - c_2 e^{-\omega x})$$

Applying the boundary conditions $N(-l) = 0$ and $N(0) = F$, it follows that

$$c_1 = c_2 e^{2\omega l} \quad , \quad c_2(e^{2\omega l} - 1)k_2 \varnothing\pi\omega^{-1} = F$$

and therefore

$$N = \frac{F(e^{2\omega l}e^{\omega x} - e^{-\omega x})}{e^{2\omega l} - 1} \quad , \quad u = \frac{F\omega(e^{2\omega l}e^{\omega x} + e^{-\omega x})}{k_2 \varnothing\pi(e^{2\omega l} - 1)} \tag{18.13}$$

The case of $k_1 > 0$, $k_2 = 0$ leads to the general solution

$$u = \frac{2k_1}{E\varnothing}x^2 + c_1 x + c_2$$

and

$$N = \varnothing\pi k_1 x + c_1 E\varnothing^2\pi/4$$

Putting the origin of the x axis at the point at which $N = u = 0$, we get $c_1 = c_2 = 0$ and therefore

$$N = k_1 \varnothing\pi x \quad , \quad u = \frac{2k_1}{E\varnothing}x^2 \tag{18.14}$$

and from $N(a) = F$ it follows that

$$a = \frac{F}{k_1 \varnothing\pi} \tag{18.15}$$

When $k_1 > 0$, $k_2 < 0$, we get

$$u = c_1 \sin(\omega x) + c_2 \cos(\omega x) - \frac{k_1}{k_2} \qquad \left(\omega^2 = -\frac{4k_2}{E\varnothing}\right)$$

and

$$N = \frac{E\varnothing^2\pi\omega}{4}[c_1 \cos(\omega x) - c_2 \sin(\omega x)]$$

Putting the origin of the x axis at the point where $N = u = 0$, we get $c_1 = 0$ and $c_2 = k_1/k_2$. From $N(a) = F$, it follows that

$$\sin(\omega a) = -\frac{4k_2 F}{k_1 E\omega\varnothing^2\pi} \tag{18.16}$$

and the following applies:

$$N = F \cdot \frac{\sin(\omega x)}{\sin(\omega a)} \quad , \quad u = -\frac{k_1}{k_2}[1 - \cos(\omega x)] \tag{18.17}$$

Example 18.5 Pulling out a reinforcing bar

With $\varnothing = 20\,\text{mm}$, $l = 1000\,\text{mm}$ and $E = 205\,\text{kN/mm}^2$, the results for the case of $k_1 = 0$, $k_2 = 100\,\text{N/mm}^3$ are the values $\omega^{-1} = 101.2\,\text{mm}$ and $e^{2\omega l} = 379.6 \cdot 10^6 \gg 1$. Assuming a stress of $N/(\varnothing^2\pi/4) = 500\,\text{N/mm}^2$ at the end being pulled ($x = 0$), eq. (18.13) results in a slip of $u(0) = 0.25\,\text{mm}$, see Fig. 18.13(a). However, the corresponding bond shear stress $\tau_b(0) = k_2 \cdot u(0) \approx 25\,\text{N/mm}^2$ is very large and may well be impossible to accommodate; the validity of the solution would then be infringed.

When $k_1 = 5\,\text{N/mm}^2$, $k_2 = 0$, eq. (18.15) results in a value of $a = 500\,\text{mm}$ (assuming the aforementioned stress of $500\,\text{N/mm}^2$ at the pulled end), and $(18.14)_2$ results in $u(a) = 0.61\,\text{mm}$.

If in the end we assume $k_1 = 5\,\text{N/mm}^2$, $k_2 = -2.5\,\text{N/mm}^3$, it follows that $\omega^{-1} = 640.3\,\text{mm}$, and (18.16) and (18.17) result in $a = 573.8\,\text{mm}$ and $u(a) = 0.75\,\text{mm}$. Fig. 18.13(b) shows the corresponding τ_b-u diagram.

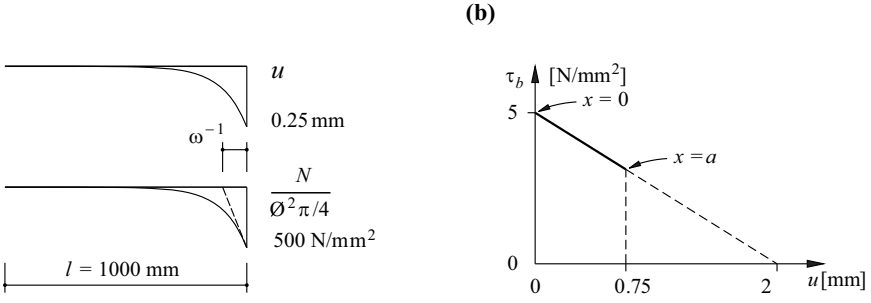

Fig. 18.13 Bar, Ø 20 mm: (a) bond shear stress increasing linearly with slip, (b) bond shear stress decreasing linearly with slip

18.2.5.2 Anchorage of pretensioned steel in concrete

During the *transfer* procedure, the prestressing steel pretensioned in a prestressing bed has to be released from its anchorage with the bed and re-anchored in the ends of the concrete member. During this process, the prestressing steel slips into the concrete a little. Eq. (18.11) and (18.12) can be used to deal with this phenomenon. The simplest approach, and usually adequate in practice, is to apply the case of $k_1 > 0$, $k_2 = 0$.

If we place the origin of the x axis at the point where $u = 0$, and assume $N = P$ (P = prestressing force), then according to (18.14) and (18.15),

$$N = P + k_1 \varnothing \pi x \quad , \quad u = \frac{2k_1 x^2}{E\varnothing} \quad (-a \le x \le 0) \tag{18.18}$$

and

$$a = \frac{P}{k_1 \varnothing \pi} \tag{18.19}$$

see Fig. 18.14.

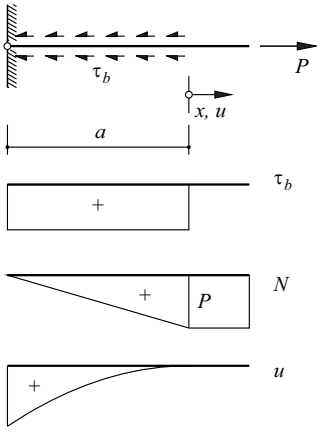

Fig. 18.14 Anchorage of pretensioned steel in concrete

It is often necessary to cut through prestressing tendons for a change of use or the deconstruction of prestressed concrete structures. The relationships that occur can be dealt with in a similar way.

18.2.5.3 Reinforced concrete tie

Let us consider a reinforced concrete tie with a cross-section according to Fig. 18.7. We shall replace indexes 1 and 2 by c (concrete) and s (reinforcing steel) and introduce the shortened forms $\rho = A_s/(A_c + A_s)$ for the geometric reinforcement ratio and $n = E_s/E_c$ for the modular ratio of the reinforcing steel (see section 13.2.4). Fig. 18.15(a) shows the diagrams for the normal forces N_c and N_s in the concrete and reinforcing steel respectively between two adjacent cracks separated by a distance s. In this case it is assumed that a constant bond shear stress $\tau_b = k_1$ acts at the surface of the reinforcing bar with diameter Ø. We often assume that k_1 is proportional to the concrete tensile strength f_{ct}, e. g. $k_1 = 2f_{ct}$.

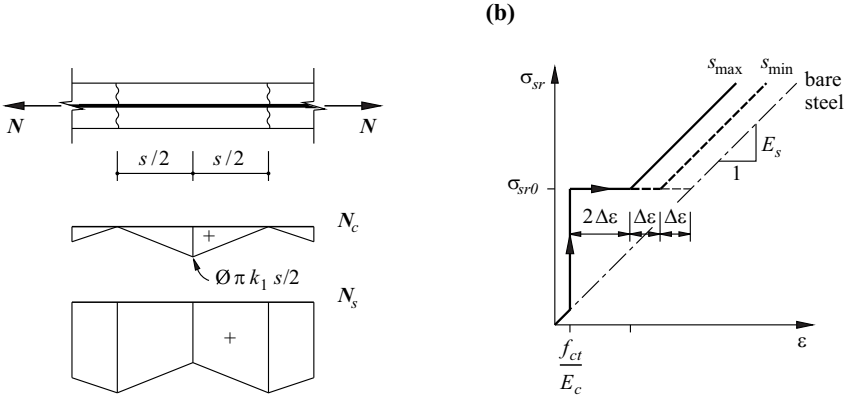

Fig. 18.15 Reinforced concrete tie: (a) diagrams of normal forces in concrete and steel in crack element, (b) steel stress at crack depending on mean normal strain

A further crack could appear in the middle of the crack element of length s as soon as the tensile force $N_c = Ø\pi k_1 s/2$ reaches the value $A_c f_{ct}$ ($Ø\pi k_1 s_{max}/2 = A_c f_{ct}$). This consideration, and putting $A_s = Ø^2\pi/4$, leads to the maximum or minimum *crack spacing* for the final crack pattern:

$$s_{max} = \frac{(1-\rho)Ø f_{ct}}{2\rho k_1} = 2s_{min} \quad , \quad s_{min} \le s \le s_{max} \tag{18.20}$$

The tensile force $N = N_c + N_s$ as the concrete cracks is $(A_c + A_s n)f_{ct}$. Upon cracking, the steel stress σ_{sr} at the crack changes abruptly from the value nf_{ct} to

$$\sigma_{sr0} = \frac{(A_c + A_s n)f_{ct}}{A_s} = \frac{f_{ct}(1 - \rho + \rho n)}{\rho} \tag{18.21}$$

The contribution of the concrete's tensile strength between the cracks reduces the mean normal strain at a maximum crack spacing $s = s_{max}$ by

$$\frac{Ø\pi k_1 s_{max}/2}{A_s E_s} \cdot \frac{1}{2} = 2\frac{f_{ct}(1-\rho)}{4\rho E_s} = 2\Delta\varepsilon \tag{18.22}$$

and by $\Delta\varepsilon$ for $s = s_{min}$, see Fig. 18.15(b). We can see that

$$\frac{\sigma_{sr0}}{E_s} = \frac{f_{ct}(1 - \rho + \rho n)}{\rho E_s} = \frac{f_{ct}(1-\rho)}{\rho E_s} + \frac{f_{ct}}{E_c} = 4\Delta\varepsilon + \frac{f_{ct}}{E_c}$$

After the concrete has cracked, the point in Fig. 18.15(b) for a monotonic load increase ($\sigma_{sr} > \sigma_{sr0}$) moves parallel with the characteristic line for the bare steel. The parallel displacement has a value between $\Delta\varepsilon$ and $2\Delta\varepsilon$ depending on the crack spacing. Compared with the behaviour of the bare steel, the contribution of the concrete's tensile strength between the cracks corresponds to a *tension stiffening*.

The *crack width* w results from the difference between the mean normal strains ε_{sm} and ε_{cm} of the reinforcing steel and the concrete respectively:

$$w = s(\varepsilon_{sm} - \varepsilon_{cm}) \quad , \quad \varepsilon_{sm} = \frac{\sigma_{sr}}{E_s} - 2\Delta\varepsilon\frac{s}{s_{max}} \quad , \quad \varepsilon_{cm} = \frac{f_{ct}}{2E_c} \cdot \frac{s}{s_{max}}$$

i. e. for $\sigma_{sr} \ge \sigma_{sr0}$, the following applies:

$$w = \frac{s}{E_s}\left(\sigma_{sr} - \frac{\sigma_{sr0} s}{2 s_{max}}\right) \tag{18.23}$$

18.2.5.4 Bar splices

Two bars are joined together over a length l according to Fig. 18.16(a). It is presumed here that the bond force per unit length $N_1' = -N_2'$ is proportional to the slip $\delta = u_1 - u_2$:

$$N_1' = -N_2' = k\delta$$

Equilibrium requires that $N_1 + N_2 = F$. According to $(18.1)_1$ and (18.2),

$$N_1 = E_1 A_1 u_1' \quad , \quad N_2 = E_2 A_2 u_2'$$

and therefore the following differential equation – similar to (18.7) – applies:

$$\delta'' - \left(\frac{1}{E_1 A_1} + \frac{1}{E_2 A_2}\right)k\delta = 0 \tag{18.24}$$

with the solution

$$\delta = c_1 e^{\omega x} + c_2 e^{-\omega x} \qquad \left(\omega^2 = \frac{k(E_1 A_1 + E_2 A_2)}{E_1 A_1 E_2 A_2}\right) \tag{18.25}$$

The boundary conditions $N_1(0) = 0$ and $N_2(0) = F$ lead to $\delta'(0) = -F/(E_2 A_2)$, and $N_1(l) = F$ as well as $N_2(l) = 0$ result in $\delta'(l) = F/(E_1 A_1)$. Applying (18.25) results in the set of equations

$$\begin{bmatrix} \omega & -\omega \\ \omega e^{\omega l} & -\omega e^{-\omega l} \end{bmatrix} \begin{Bmatrix} c_1 \\ c_2 \end{Bmatrix} = \begin{Bmatrix} -F/(E_2 A_2) \\ F/(E_1 A_1) \end{Bmatrix}$$

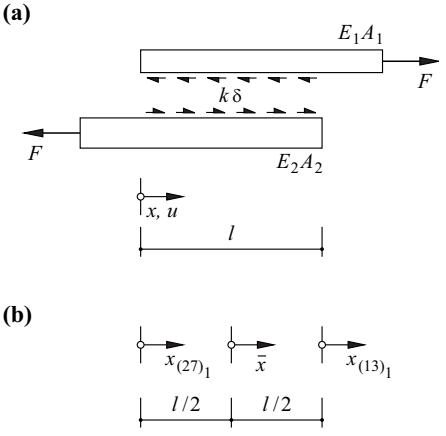

Fig. 18.16 Bar splice: (a) diagram of static system, (b) definitions of various coordinates

with the solution

$$c_1 = \frac{F(E_1A_1e^{-\omega l} + E_2A_2)}{\omega E_1A_1E_2A_2(e^{\omega l} - e^{-\omega l})} \quad , \quad c_2 = \frac{F(E_1A_1e^{\omega l} + E_2A_2)}{\omega E_1A_1E_2A_2(e^{\omega l} - e^{-\omega l})} \tag{18.26}$$

The normal forces are then

$$\begin{aligned} N_1 &= \frac{FE_1A_1}{E_1A_1 + E_2A_2}\left[1 + \frac{E_2A_2}{E_1A_1}\cdot\frac{e^{\omega x} - e^{-\omega x}}{e^{\omega l} - e^{-\omega l}} - \frac{e^{\omega(l-x)} - e^{-\omega(l-x)}}{e^{\omega l} - e^{-\omega l}}\right] \\ N_2 &= \frac{FE_2A_2}{E_1A_1 + E_2A_2}\left[1 - \frac{e^{\omega x} - e^{-\omega x}}{e^{\omega l} - e^{-\omega l}} + \frac{E_1A_1}{E_2A_2}\cdot\frac{e^{\omega(l-x)} - e^{-\omega(l-x)}}{e^{\omega l} - e^{-\omega l}}\right] \end{aligned} \tag{18.27}$$

For the case of $E_2A_2 \to \infty$, eq. (18.27) results in

$$N_1 = \frac{F\sinh(\omega x)}{\sinh(\omega l)} \tag{18.28}$$

This equation is identical with $(18.13)_1$ if we consider that there the origin of the x axis lies at the pulled end of the bar. Multiplying the numerators and denominators of the expression on the right in $(18.13)_1$ by $e^{-\omega l}$ results in

$$N = \frac{F(e^{\omega l}e^{\omega x} - e^{-\omega l}e^{-\omega x})}{e^{\omega l} - e^{-\omega l}} = \frac{F\sinh[\omega(x + l)]}{\sinh(\omega l)}$$

The expression $x+l$ according to $(18.13)_1$ corresponds to the x used in (18.27), see Fig. 18.16(b).

Using the coordinates $\overline{x} = x - l/2$ for the special case of $E_1A_1 = E_2A_2$, as shown in Fig. 18.16(b), then (18.27) results in

$$N_{1,2} = \frac{F}{2}\left[1 \pm \frac{\sinh(\omega\overline{x})}{\sinh(\omega l/2)}\right] \tag{18.29}$$

18.2.6 Summary

1. Extension problems in elastic bars lead to the differential equations (18.3) and (18.4). These must be integrated taking into account the respective boundary and continuity conditions.
2. Bars with an inhomogeneous cross-section develop residual stresses even when deformation is not inhibited. Restraints ensue when the deformation is inhibited.
3. Numerical methods for solving the basic differential equation (18.11) must be used for general bond shear stress-slip relationships. Linear elastic, perfectly plastic and linear softening τ_b-u relationships can be dealt with analytically and lead to hyperbolic, parabolic and harmonic functions $u(x)$.
4. Anchorage problems and issues concerning crack spacings, crack widths, tension stiffening, etc. in reinforced and prestressed concrete construction can be dealt with easily by using perfectly plastic τ_b-u relationships, which result in a good approximation.
5. It is expedient to introduce the slip $\delta = u_1 - u_2$ as the primary unknown for bar splices. If the bond forces are assumed to be proportional to δ, the result is hyperbolic functions for the $\delta(x)$ function and its derivatives.

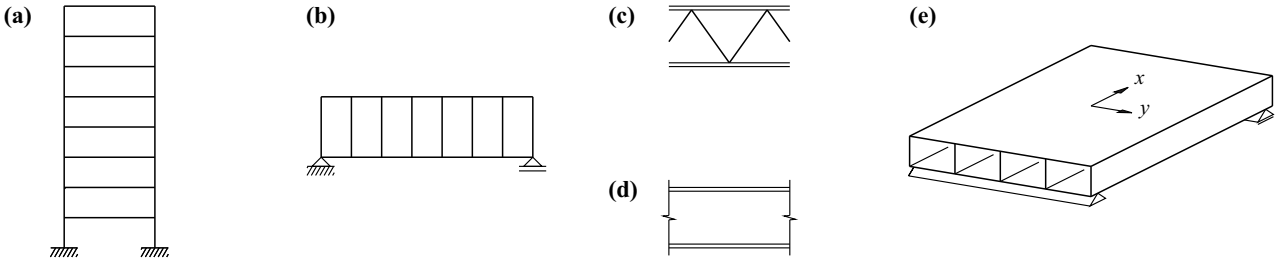

Fig. 18.17 Beams in shear – examples: (a) multi-storey frame, (b) VIERENDEEL girder, (c) trussed girder, (d) sandwich panel, (e) hollow slab

18.3 Beams in shear

18.3.1 Practical examples

The deformations of beams as a result of bending moments and shear forces can have different orders of magnitude. The shear deformations can often be neglected when compared with the bending deformations, especially in the case of slender beams with solid cross-sections. In such instances, the bars may be idealised as being rigid in shear, as shown in sections 8.2.2 and 8.2.3 and explained in more detail in section 13.3.1. However in the case of stocky beams, resolved cross-sections, frames and sandwich forms of construction, the shear deformations can be significant, may even dominate.

Fig. 18.17 shows a number of typical practical examples of the analytical model described below. The internal and external deformation and force variables of this model are limited to the shear strain γ, the shear force V, the deflection w and the line load q in the z direction. The applications range from multi-storey frames (a) to VIERENDEEL girders (b) and trussed girders (c) to sandwich panels (d) and the behaviour of hollow slabs (e) in the transverse direction (y direction).

18.3.2 Analytical model

When $q_z = q$, then (8.21) and (8.22) for a beam in shear only (see Fig. 18.18) are reduced to

$$q = -V' \quad , \quad \gamma = w' + \varphi \tag{18.30}$$

where because $\chi = \varphi' = 0$, the rotation φ about the y axis is constant (equal to zero in many cases). Using

$$V = GA_v\gamma \tag{18.31}$$

according to (8.23) and (13.39), eq. (18.30) then leads to the differential equation

$$q = -GA_v w'' \tag{18.32}$$

which is similar to (18.4).

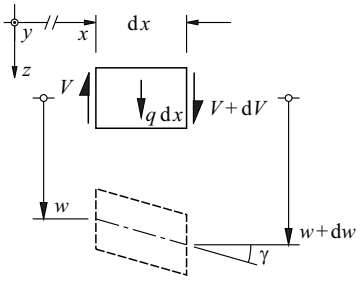

Fig. 18.18 Undeformed and deformed states of a differential bar element ($\varphi = 0$)

18.3.3 Multi-storey frame

Fig. 18.19(a) shows a four-storey frame supported as a simply supported beam plus its deformed shape as a result of a horizontal force applied to the top of the frame. The frame beams are initially assumed to be rigid ($EI_b \to \infty$). Fig. 18.19(b) shows the corresponding free body diagram, moment diagram and deflection curve for a single column of height h. With a constant bending stiffness for the column EI_c, applying the work theorem (14.4) results in a storey drift amounting to $\Delta = V_c h^3/(12EI_c)$, see (17.17), and from that, with $\gamma = \Delta/h$, $V = 2V_c$ and (18.31), we get the expression

$$GA_v = \frac{24EI_c}{h^2} \tag{18.33}$$

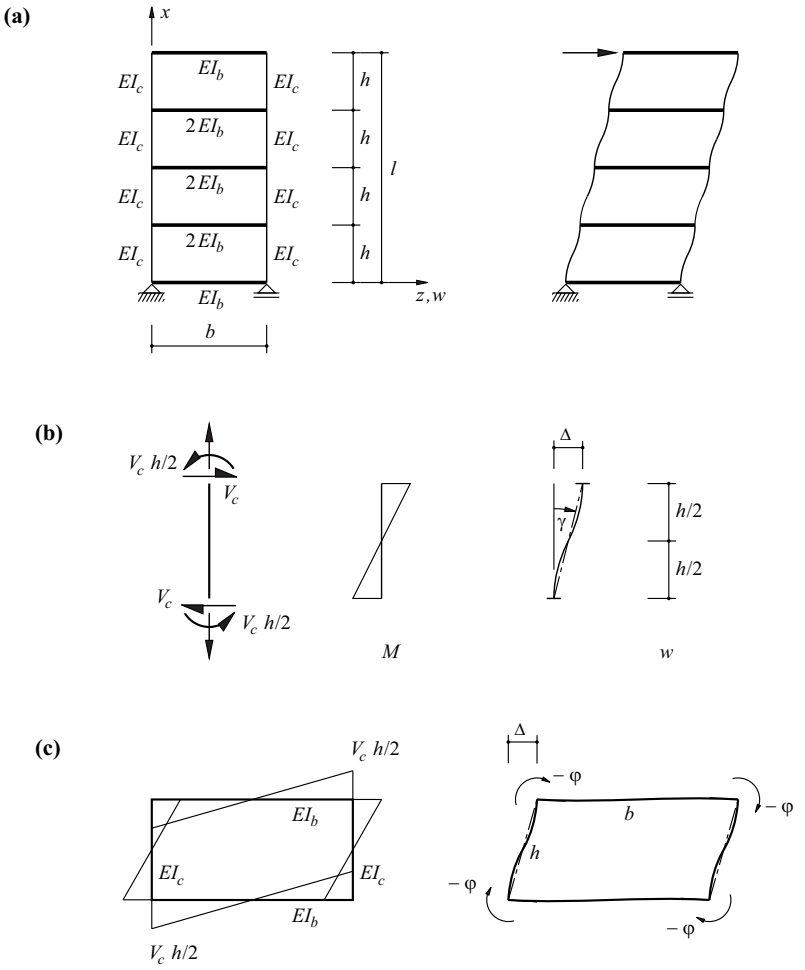

Fig. 18.19 Multi-storey frame: (a) notation and deformations, (b) single column, (c) frame element

Assuming a finite stiffness for the frame beams EI_b = const, the frame joints rotate by $\varphi = -V_c\,hb/(12EI_b)$ about the y axis, see Fig. 18.19(c), and Δ is increased by the amount $-\varphi \cdot h$. We thus get

$$GA_v = \frac{24}{h\left(\dfrac{h}{EI_c} + \dfrac{b}{EI_b}\right)} \tag{18.34}$$

instead of (18.33).

Example 18.6 Multi-storey frame

Fig. 18.20 shows the behaviour of a multi-storey frame subjected to a constant line load $q = q_0$ or a point load H. The diagrams for q, V and w illustrate the application of $(18.30)_1$ and (18.32) and are easily understood without further explanation.

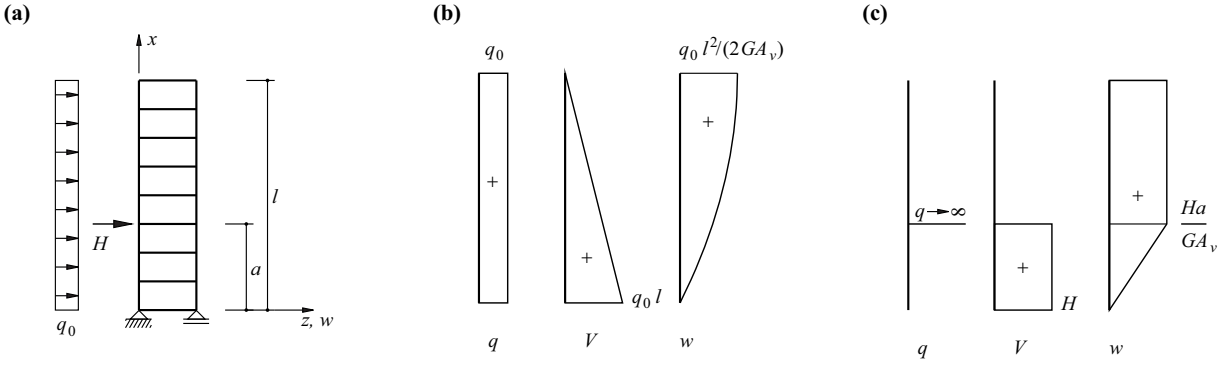

Fig. 18.20 Multi-storey frame: (a) diagram of static system, (b) and (c) behaviour when subjected to $q = q_0$ and H respectively

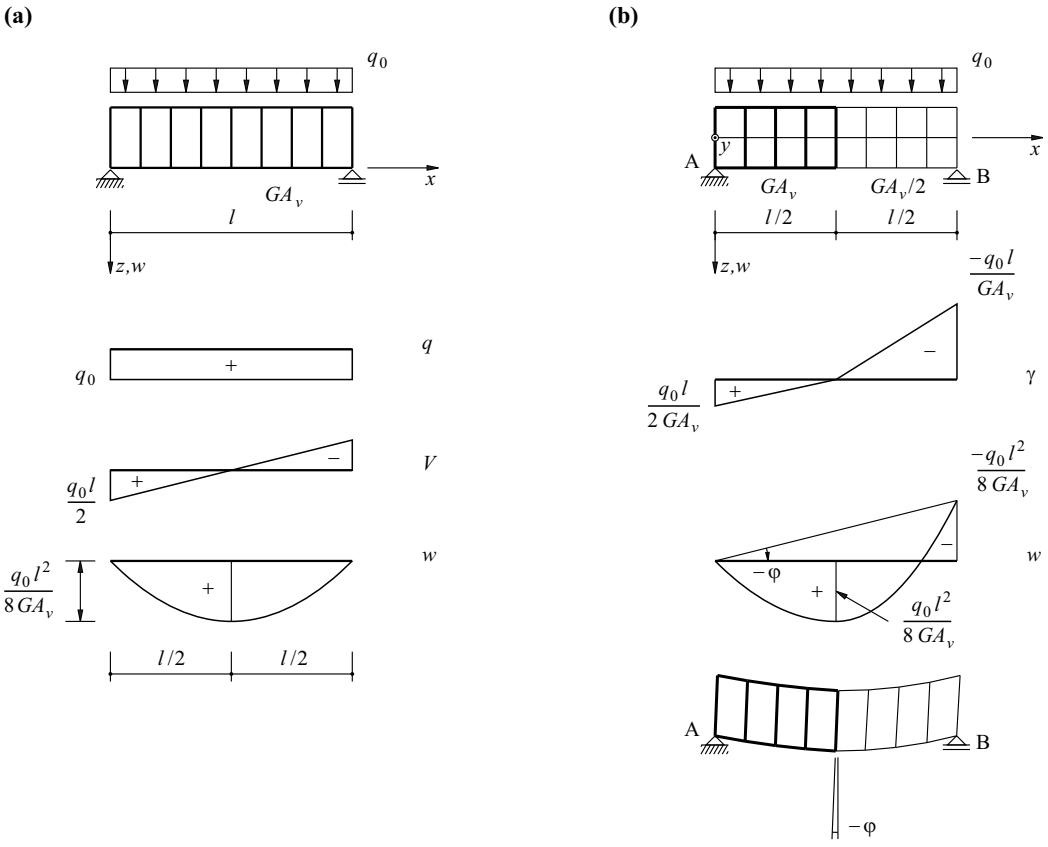

Fig. 18.21 Simply supported VIERENDEEL girder subjected to constant line load: (a) GA_v = const, (b) abrupt change in GA_v

18.3.4 VIERENDEEL girder

VIERENDEEL girders can be dealt with in the same way as multi-storey frames. For example, each half of the beam shown in Fig. 18.21(a) is identical to the system examined in Fig. 18.20 subjected to $q = q_0$.

If GA_v exhibits an abrupt change, as shown in Fig. 18.21(b), then γ exhibits a kink at the position of the abrupt change, and the integration of γ results in a deflection of $-q_0 l^2/(8GA_v)$ at support B, which is eliminated by a rotation $\varphi = -q_0 l/(8GA_v)$ about A, see $(18.30)_2$. As $\chi = \varphi' = 0$, all cross-sections rotate through the same angle, as indicated in the bottommost diagram of Fig. 18.21(b).

Example 18.7 Externally statically indeterminate VIERENDEEL girder

The rotation φ occurring in the system of Fig. 18.21(b) is prevented by fixity at A, see Fig. 18.22(a). The positive moment M_A about the positive y axis causes the deformations in the system released from support B as shown in Fig. 18.22(b). The compatibility condition $-q_0 l^2/(8GA_v) + 3M_A/(2GA_v) = 0$ results in $M_A = q_0 l^2/12$, and thus the deformations shown in Fig. 18.22(c). The point of zero shear in the system with one degree of external static indeterminacy occurs at $x = 7l/12$, and the deflection curve w has a kink at $x = l/2$.

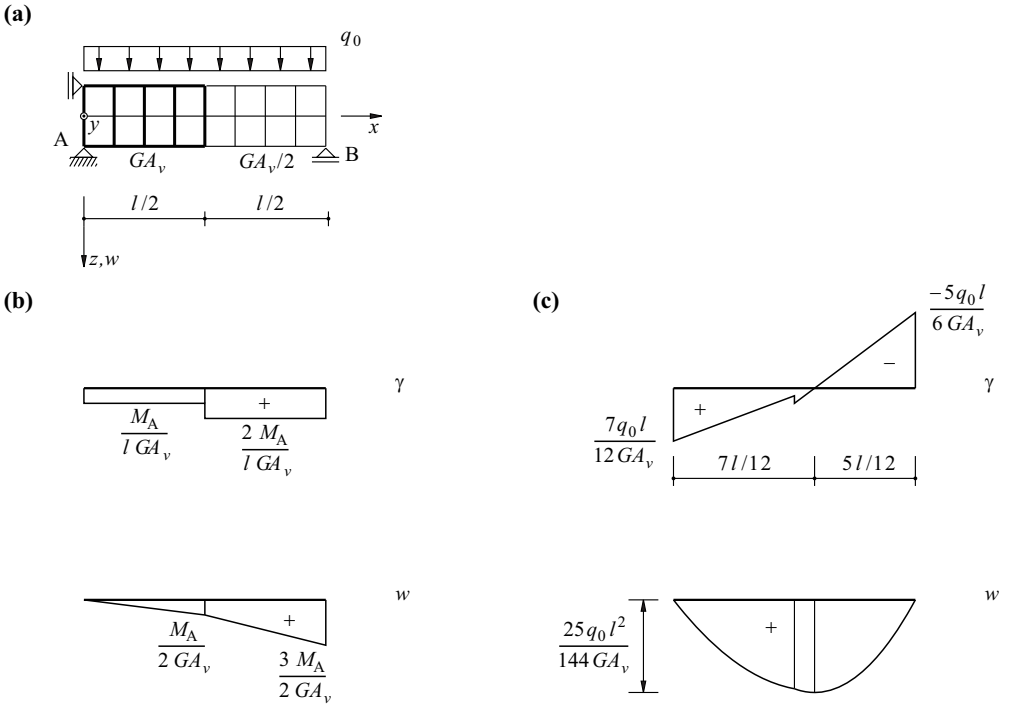

Fig. 18.22 Externally statically indeterminate beam: (a) diagram of static system, (b) deformations due to M_A, (c) resultant deformations

18.3.5 Sandwich panels

The sandwich panel shown in Fig. 18.23 consists of two thin, stiff outer faces (thickness t, modulus of elasticity E) either side of a soft core (thickness $h - 2t$, shear modulus G); $t \ll h$ and $G \ll E$ apply. The outer faces carry the normal stresses σ as a result of the bending moment m per unit length [kNm/m]. The bending stiffness per unit length is approximately

$$Ei = Et(h-t)^2/2 \tag{18.35}$$

The shear stresses τ as a result of the shear force v [kN/m] are constant over the depth of the core and decrease linearly to zero in the outer faces. The shear stiffness per unit length is approximately

$$Ga_v = G(h-t) \tag{18.36}$$

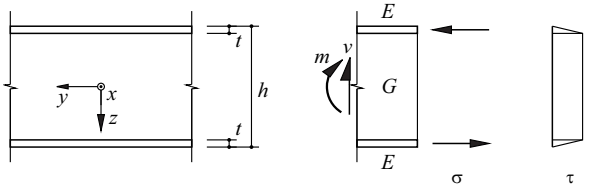

Fig. 18.23 Sandwich panel

Example 18.8 Plastic panel with bonded sheet steel outer faces

The plastic panel with bonded sheet steel outer faces shown in Fig. 18.24 ($h = 11\,\text{mm}$, $t = 1\,\text{mm}$, $G = 0.5\,\text{kN/mm}^2$, $E = 205\,\text{kN/mm}^2$) spans a distance of $l = 160\,\text{mm}$ in the x direction as a simply supported beam. The panel width b in the y direction is 100 mm. The longitudinal edges of the rectangular panel are unsupported. The panel carries a uniformly distributed load of 10 kN, which corresponds to $q = 625\,\text{kN/m}^2$.

The normal stresses in the outer faces due to the bending moment $m_x = ql^2/8$ at mid-span ($x = 0$) amount to

$$\sigma = \frac{ql^2}{8(h-t)t} = 200\,\text{N/mm}^2$$

and the shear stresses in the core at the supports ($x = \pm 80\,\text{mm}$) are equal to

$$\tau = \frac{ql}{2(h-t)} = 5\,\text{N/mm}^2$$

which corresponds to shear strains in the core of $\gamma = \tau/G = 1\,\%$.

The deflection at mid-span is

$$w_m = \frac{ql^2}{8Ga_v} + \frac{5ql^4}{384Ei} = \frac{0.625 \cdot 160^2}{8 \cdot 500 \cdot 10} + \frac{5 \cdot 0.625 \cdot 160^4 \cdot 2}{384 \cdot 205000 \cdot 10^2} = 0.4 + 0.52 = 0.92\,\text{mm}$$

Some 43 % of w_m is due to the shear deformations.

In order to investigate the influence of fixity at $x = -80\,\text{mm}$, we shall consider the system shown in Fig. 18.25(a), with

$$w_B = \frac{ql^4}{8Ei} + \frac{ql^2}{2Ga_v}$$

and the system of Fig. 18.25(b), with

$$w_B = \frac{Bl^3}{3Ei} + \frac{Bl}{Ga_v}$$

from which it follows that

$$B = ql\frac{3 + \dfrac{12Ei}{Ga_v l^2}}{8 + \dfrac{24Ei}{Ga_v l^2}} \qquad (18.37)$$

Assuming a rigid behaviour in shear ($E/G \to 0$), eq. (18.37) gives us the value $B = 3ql/8$ already known from example 8.5. Substituting the values of the previous example, we get $B = 0.3992ql$. The fixed-end moment is reduced by 19.4 %, from $ql^2/8$ to $0.1008ql^2$, i. e. compared with a rigid behaviour in shear, the fixity effect is lower.

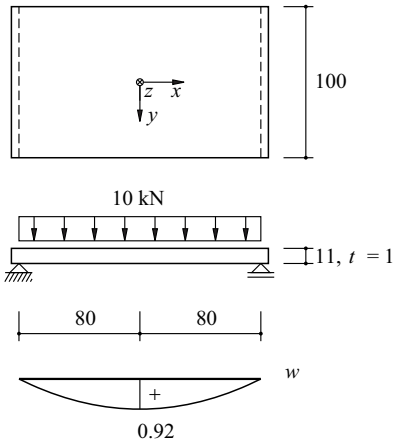

Fig. 18.24 Sandwich panel (dimensions in mm)

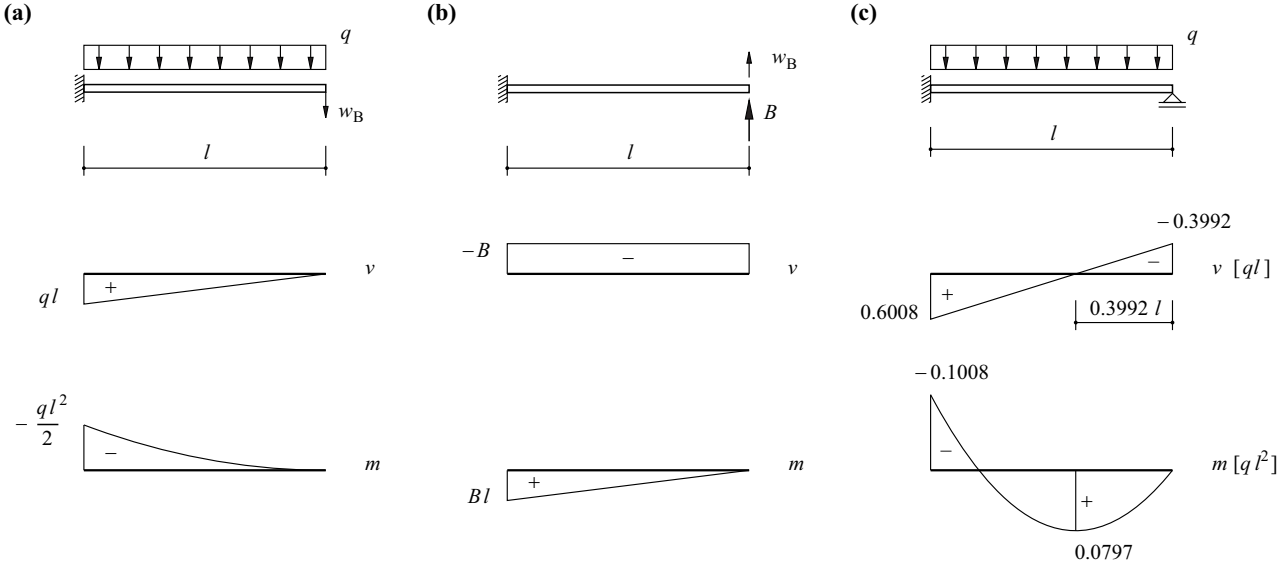

Fig. 18.25 Influence of edge fixity: (a) and (b) individual effects, (c) ensuing stress resultants

18.3.6 Summary

1. The differential equation (18.32) for a beam in shear is similar to the differential equation (18.4) for a bar extension problem. A solution to one problem can be transferred directly to the other.
2. The shear stiffness of a multi-storey frame can be estimated with (18.34).
3. VIERENDEEL girders can be treated in the same way as multi-storey frames.
4. The bending and shear stiffnesses of sandwich panels can be assessed using (18.35) and (18.36). Provided the panels are not too slender, the order of magnitude of the shear deformations is similar to that of the bending deformations. This also has an influence on the support force variables in the case of statically indeterminate systems.

18.4 Beams in bending

18.4.1 General

Bending problems are extremely important in structural design. We usually assume a rigid behaviour in shear according to sections 8.2.2 or 8.2.3. Behaviour commensurate with a finite shear stiffness is assumed below. The deliberations regarding the influence of restraints discussed in section 18.2.4 are broadened from bar extensions to the general case of extension and bending.

Many practical problems can be treated using the model of *beams on elastic foundation*. Fig. 18.26 shows a number of typical examples, which range from railway tracks (a) to laterally supported piles (b), pontoons, docks, pipes or tunnel segments floating on water (c) and grillages (d) to pressurised pipes with stiffening rings (e) and tanks or silos whose expansion at the top or bottom is inhibited (f).

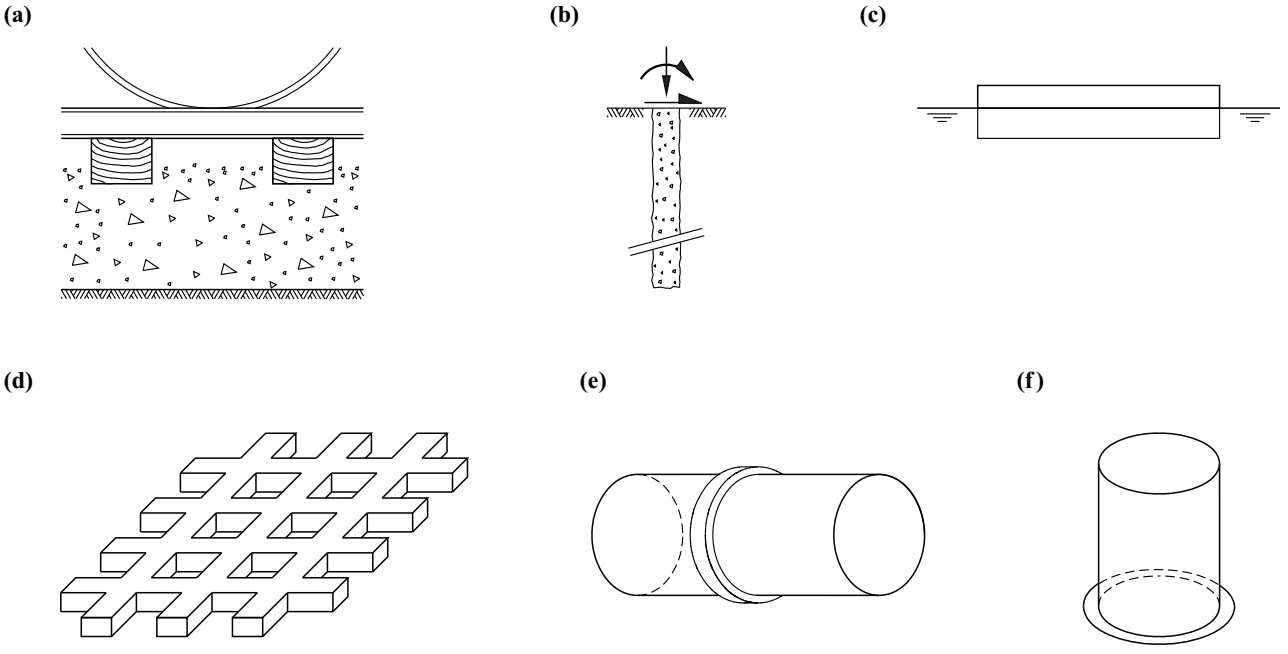

Fig. 18.26 Beams on elastic foundation: (a) railway track, (b) laterally supported piles, (c) pontoons, etc. floating on water, (d) grillages, (e) pressurised pipes with stiffening rings, (f) tanks, silos, etc.

18.4.2 Analytical model

Fig. 18.27, with $q_z = q$ and $m_y = m$, summarises the relevant variables that occur in (8.21) to (8.23). The following relationships apply:

$$q = -V' \quad , \quad m = V - M' \quad ; \quad \gamma = w' + \varphi \quad , \quad \chi = \varphi'$$
$$V = GA_v\gamma \quad , \quad M = EI\chi \tag{18.38}$$

Considering a beam in pure shear ($EI \to \infty$), eq. (18.38) is reduced to (18.32).

On the other hand, we get

$$M = -EIw'' \tag{18.39}$$

for a beam in bending only ($GA_v \to \infty$), see $(15.7)_1$. If EI = const and $m = 0$, then

$$q = EIw'''' \tag{18.40}$$

applies, and when $V = 0$, the result is

$$m = -EI\varphi'' \tag{18.41}$$

In the case of beams in shear and bending with GA_v = const and EI = const, the result is

$$q = -GA_v(w' + \varphi)' \quad , \quad m = GA_v(w' + \varphi) - EI\varphi'' \tag{18.42}$$

According to Fig. 18.28, the static or kinematic continuity conditions

$$V_I = V_{II} + Q \quad , \quad M_I = M_{II} + R \quad ; \quad w_I = w_{II} \quad , \quad \varphi_I = \varphi_{II} \tag{18.43}$$

apply for points within the beam, and the boundary conditions given in Fig. 18.29 must be considered for points at the end of the beam, see Fig. 15.2.

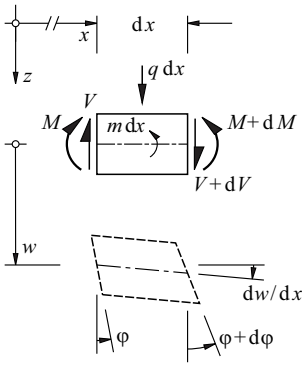

Fig. 18.27 Undeformed and deformed states of a differential bar element

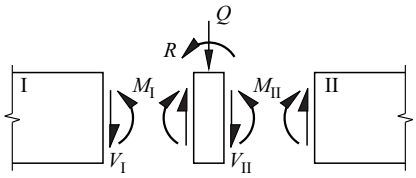

Fig. 18.28 Points within the beam

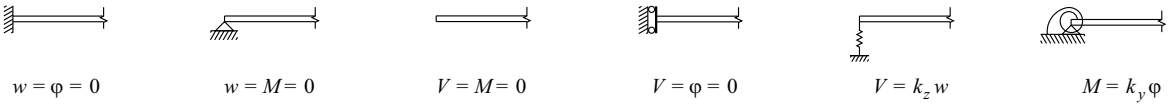

Fig. 18.29 Boundary conditions

Example 18.9 Simply supported beam – sinusoidal line load

Fig. 18.30 shows a simply supported beam (EI = const, GA_v = const) subjected to a line load $q = q_0\sin(n\pi x/l)$. According to (18.38) and taking into account the boundary conditions $M = w = 0$ at $x = 0$ and $x = l$, this causes the following variables:

$$V = \frac{q_0 l}{n\pi}\cos\left(\frac{n\pi x}{l}\right) \quad , \quad M = \frac{q_0 l^2}{n^2\pi^2}\sin\left(\frac{n\pi x}{l}\right) \quad , \quad w = \left(\frac{q_0 l^2}{n^2\pi^2 GA_v} + \frac{q_0 l^4}{n^4\pi^4 EI}\right)\sin\left(\frac{n\pi x}{l}\right)$$

The ratio of the shear to bending deformation components in w amounts to $(n\pi/l)^2 \cdot (EI/GA_v)$, i. e. the influence of the shear deformations increases while the bending stiffness EI remains constant and the wavelength $2l/n$ and shear stiffness GA_v decrease.

The sinusoidal load q, for example, can be part of a FOURIER series for approximating any line load, see (18.55).

The statement regarding the ratio of shear to bending deformations applies in general. Similar relationships have already been found in example 18.8.

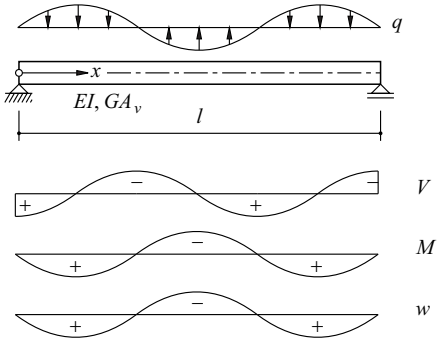

Fig. 18.30 Simply supported beam subjected to sinusoidal line load

18.4.3 Restraints

Initial normal strains ε_0 (constant over the cross-section) as a result of thermal or shrinkage actions were presumed in section 18.2.4. This restrictive assumption is now abandoned, but we shall still assume that $\chi_z = 0$. Putting $\chi_y = \chi$, we can use (13.3) and (13.4) to get

$$\varepsilon_x = \varepsilon + \chi z = \frac{\sigma_x}{E} + \varepsilon_0 \tag{18.44}$$

which is similar to (18.2), although ε now designates the normal strain on the bar axis.

Residual stresses generally ensue even in the case of uninhibited deformation, see section 13.2.5. We shall not explore this aspect further here, but rather confine ourselves to restraints as a result of inhibited deformation.

Example 18.10 Bar fixed at both ends – linear temperature gradient

The homogeneous bar (E = const, α_T = const) shown in Fig. 18.31(a) is fixed at both ends and has a length l and depth h. It is subjected to a temperature gradient presumed to be linear over x and z:

$$T(x,z) = \left(T_0 + \frac{\Delta T_0}{h} \cdot z\right) \frac{x}{l}$$

The solution for the bar extension problem is given by (18.6), see Fig. 18.31(b). The result is a compressive force amounting to $EA\alpha_T T_0/2$ and a displacement u varying in a parabolic form and having a maximum value of $\alpha_T T_0 l/8$ at $x = l/2$.

We shall solve the bending problem with the help of the force method, see Fig. 18.31(c). Using

$$\delta_{10} = -\frac{\alpha_T \Delta T_0 l}{2h} \quad , \quad \delta_{20} = \frac{\alpha_T \Delta T_0 l^2}{6h} \quad ; \quad \delta_{11} = \frac{l}{EI} \quad , \quad \delta_{12} = -\frac{l^2}{2EI} \quad , \quad \delta_{22} = \frac{l^3}{3EI} + \frac{l}{GA_v}$$

we get the set of equations

$$\begin{bmatrix} 1 & -\frac{l}{2} \\ -\frac{l}{2} & \frac{l^2}{3} + \frac{EI}{GA_v} \end{bmatrix} \begin{Bmatrix} X_1 \\ X_2 \end{Bmatrix} = \begin{Bmatrix} \frac{1}{2} \\ -\frac{l}{6} \end{Bmatrix} \frac{\alpha_T \Delta T_0 EI}{h}$$

with the solution

$$X_1 = \frac{\alpha_T \Delta T_0 EI}{h} \cdot \frac{GA_v l^2 + 6EI}{GA_v l^2 + 12EI} \quad , \quad X_2 = \frac{\alpha_T \Delta T_0 EI}{h} \cdot \frac{GA_v l}{GA_v l^2 + 12EI}$$

and the corresponding restraint stress resultants

$$V = -\frac{\frac{\alpha_T \Delta T_0 EI}{lh}}{1 + \frac{12EI}{GA_v l^2}} \quad , \quad M = -\frac{\frac{\alpha_T \Delta T_0 EI}{h}\left(\frac{x}{l} + \frac{6EI}{GA_v l^2}\right)}{1 + \frac{12EI}{GA_v l^2}}$$

Fig. 18.31(d) shows the diagrams for M and V for the case of $GA_v \to \infty$. In this case, the curvatures M/EI are opposed to those of the thermal action, i. e. the bar remains straight, $w \equiv 0$.

With finite shear stiffness GA_v, eq. (18.38) gives us the deflection

$$w = \frac{V}{GA_v} \cdot x \cdot \left(1 - \frac{x}{l}\right) \cdot \left[3 + \frac{GA_v l^2}{6EI}\left(1 + \frac{x}{l}\right)\right]$$

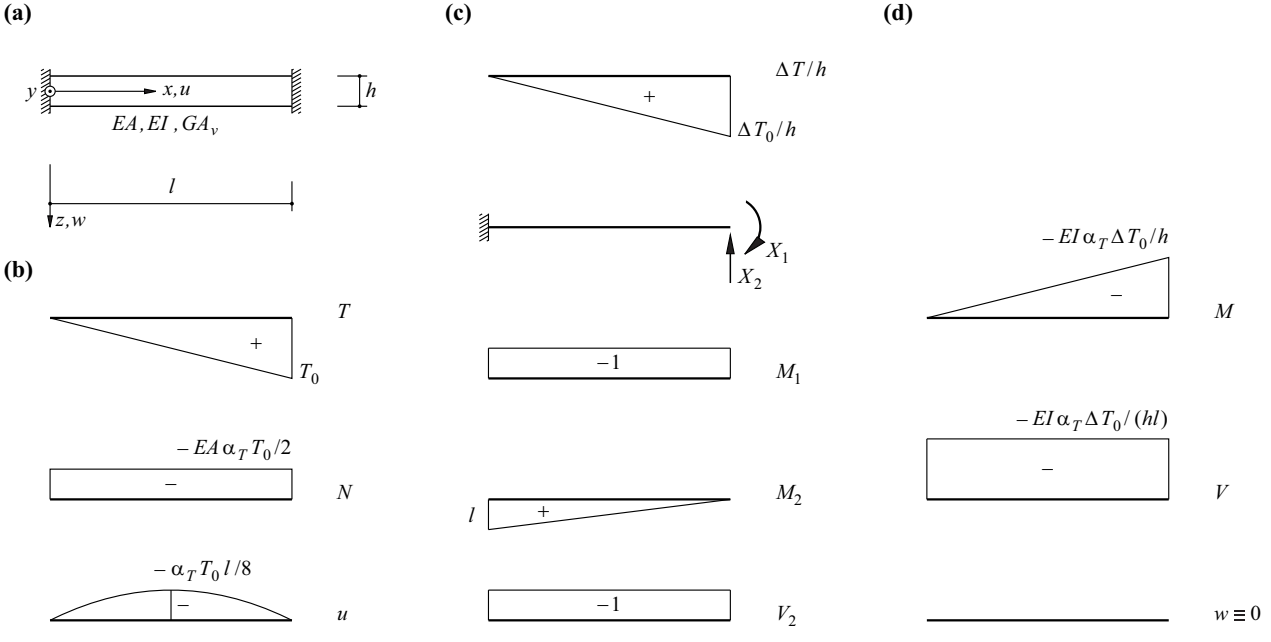

Fig. 18.31 Restraint due to temperature varying linearly with x and z: (a) system and notation, (b) bar extension, (c) bar bending, (d) $GA_v \to \infty$

18.4.4 Elastic foundation

18.4.4.1 Differential equation and foundation modulus

We often make use of a proposal by WINKLER when dimensioning foundations and dealing with similar problems, i. e. a bearing pressure

$$p = kw \tag{18.45}$$

proportional to the deflection w, where k [MN/m^2] is the *foundation modulus*, see Fig. 18.32(a). Taking the beam width b and the *modulus of subgrade reaction* c [MN/m^3], then $k \approx bc$ applies. Depending on the compactness of the soil, the modulus of subgrade reaction can lie between about 10 and 100 MN/m^3 for sands, or 100 and 300 MN/m^3 for gravels. In the case of bodies floating on a fluid, e. g. a covering of ice floating on water, according to ARCHIMEDES' work on hydrostatic buoyancy, the modulus of subgrade reaction corresponds to the specific weight of the fluid, so about 10 kN/m^3 for water.

Ignoring shear deformations ($GA_v \to \infty$) and assuming constant bending stiffness EI, we get

$$EIw'''' + kw = q \tag{18.46}$$

instead of (18.40).

The beam would be rigid for the limiting case of $EI \to \infty$, and therefore w – and according to (18.45) with constant k, then p as well – could at best vary linearly with x. We thus arrive at the *trapezoidal stress distribution method* already used in Fig. 5.4(e), according to which the bearing pressures are calculated from the equilibrium conditions. If, as in Fig. 18.32(b), we use R to designate the resultant of the line loads q acting on a bar of length l, and e to designate its eccentricity with respect to the middle of the bar, then the following applies:

$$R = (p_1 + p_2)l/2 \quad , \quad e = \frac{(p_1 - p_2)l}{6(p_1 + p_2)} \tag{18.47}$$

(a)

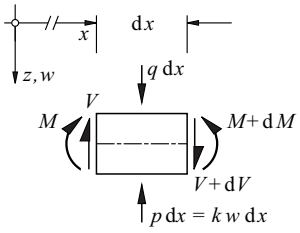

(b)

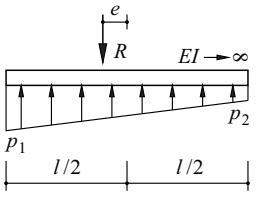

Fig. 18.32 Elastic foundation: (a) bar element, (b) trapezoidal stress distribution method as limiting case

18.4.4.2 Solution to the homogeneous differential equation

Using the shortened form

$$\frac{k}{EI} = 4\beta^4 \tag{18.48}$$

and $q = 0$, then (18.46) becomes

$$w'''' + 4\beta^4 w = 0$$

The general solution to this differential equation is

$$w = e^{\beta x}[c_1 \cos(\beta x) + c_2 \sin(\beta x)] + e^{-\beta x}[c_3 \cos(\beta x) + c_4 \sin(\beta x)] \tag{18.49}$$

The function w and its derivatives have the character of damped vibrations. Setting

$$w = c_0 e^{-\beta x} \sin(\beta x)$$

we get the derivative

$$w' = -\beta\sqrt{2}c_0 e^{-\beta x} \sin(\beta x - \pi/4)$$

i. e. the amplitude is multiplied by $-\beta\sqrt{2}$ and the phase angle reduced by $\pi/4$. This finding also applies to all other derivatives, i. e.

$$w'' = \beta^2 2c_0 e^{-\beta x} \sin(\beta x - \pi/2) \quad , \quad w''' = -\beta^3 2\sqrt{2}c_0 e^{-\beta x} \sin(\beta x - 3\pi/4) \quad , \text{ etc.}$$

Putting $c_0 = -2\beta^2 R/k$ results in $M(0) = -EIw''(0) = -R$. We have therefore obviously found the solution for a beam infinitely long on either side of a moment $2R$ applied at the middle of the beam. If $x \geq 0$, then

$$\begin{aligned} w &= -\frac{2\beta^2 R}{k} e^{-\beta x} \sin(\beta x) \quad , \quad w' = \frac{2\sqrt{2}\beta^3 R}{k} e^{-\beta x} \sin(\beta x - \pi/4) \\ M &= R e^{-\beta x} \sin(\beta x - \pi/2) \quad , \quad V = -\sqrt{2}\beta R e^{-\beta x} \sin(\beta x - 3\pi/4) \end{aligned} \tag{18.50}$$

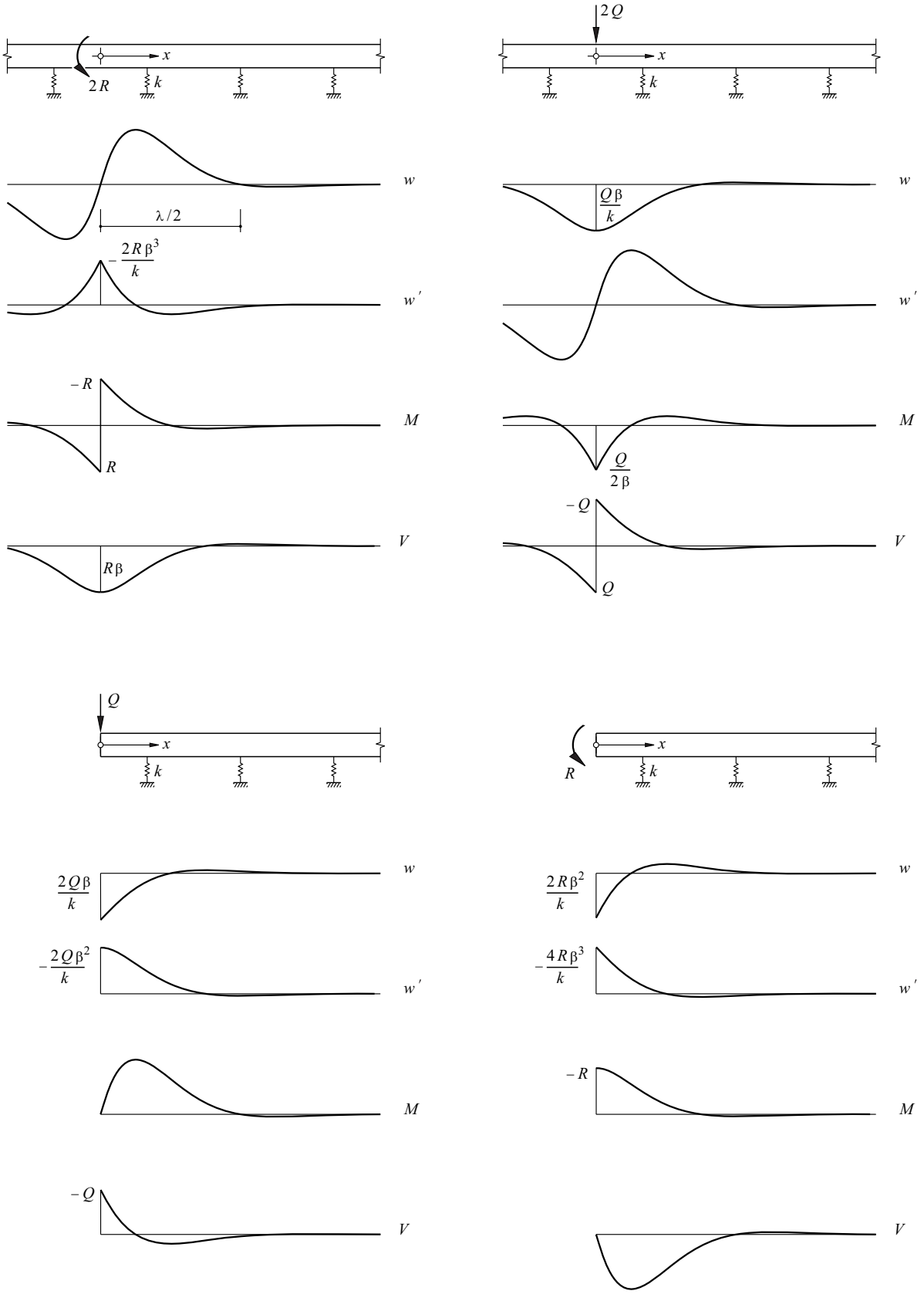

Fig. 18.33 Basic cases for a beam infinitely long on one or both sides on an elastic foundation

Similarly, setting

$$w' = c_0 e^{-\beta x} \sin(\beta x)$$

with $c_0 = -2\beta^2 Q/k$ leads to the solution for a beam infinitely long on either side of a point load $2Q$ applied at the middle of the beam. If $x \geq 0$, then

$$\begin{aligned} w &= \frac{\sqrt{2}\beta Q}{k} e^{-\beta x} \sin(\beta x + \pi/4) \quad , \quad w' = -\frac{2\beta^2 Q}{k} e^{-\beta x} \sin(\beta x) \\ M &= -\frac{Q}{\sqrt{2}\beta} e^{-\beta x} \sin(\beta x - \pi/4) \quad , \quad V = Q e^{-\beta x} \sin(\beta x - \pi/2) \end{aligned} \tag{18.51}$$

Using

$$w'' = c_0 e^{-\beta x} \sin(\beta x)$$

with $c_0 = 4\beta^3 Q/k$, we get the solution for a beam infinitely long on one side which is loaded at end $x = 0$ by a point load Q:

$$\begin{aligned} w &= \frac{2\beta Q}{k} e^{-\beta x} \sin(\beta x + \pi/2) \quad , \quad w' = -\frac{2\sqrt{2}\beta^2 Q}{k} e^{-\beta x} \sin(\beta x + \pi/4) \\ M &= -\frac{Q}{\beta} e^{-\beta x} \sin(\beta x) \quad , \quad V = Q\sqrt{2} e^{-\beta x} \sin(\beta x - \pi/4) \end{aligned} \tag{18.52}$$

Finally,

$$w''' = c_0 e^{-\beta x} \sin(\beta x)$$

with $c_0 = 8\beta^5 R/k$ leads to the solution for a beam infinitely long on one side which is subjected to a moment R at $x = 0$:

$$\begin{aligned} w &= \frac{2\sqrt{2}\beta^2 R}{k} e^{-\beta x} \sin(\beta x + 3\pi/4) \quad , \quad w' = -\frac{4\beta^3 R}{k} e^{-\beta x} \sin(\beta x + \pi/2) \\ M &= -\sqrt{2} R e^{-\beta x} \sin(\beta x + \pi/4) \quad , \quad V = 2\beta R e^{-\beta x} \sin(\beta x) \end{aligned} \tag{18.53}$$

The relationships (18.50) to (18.53) are illustrated in Fig. 18.33 (basic cases $2R$, $2Q$, Q and R). The length

$$\lambda = \frac{2\pi}{\beta} \tag{18.54}$$

is called the *natural wavelength*. The zero points in the functions shown in Fig. 18.33 are each offset by $\lambda/8$ according to the reduction in the phase angle of $\pi/4$ per derivative.

18.4.4.3 Particular solutions to the differential equation

If the line load can be expressed as a third-order polynomial

$$q = a_0 + a_1 x + a_2 x^2 + a_3 x^3$$

then q/k is a particular solution to (18.46).

When $q = q_1 \sin(\pi x/l)$, we get the following particular solution

$$w = \frac{q_1}{\frac{\pi^4 EI}{l^4} + k} \cdot \sin\left(\frac{\pi x}{l}\right)$$

Any line loads can be presented by means of a FOURIER series

$$q = \sum_{n=1}^{\infty} q_n \sin\left(\frac{n\pi x}{l}\right)$$

and we get

$$w = \sum_{n=1}^{\infty} \frac{q_n}{\frac{n^4\pi^4 EI}{l^4} + k} \cdot \sin\left(\frac{n\pi x}{l}\right)$$

e. g. for $q = q_0 = \text{const}$:

$$q = \sum_{n=1,3,\ldots}^{\infty} \frac{4q_0}{n\pi} \cdot \sin\left(\frac{n\pi x}{l}\right) \quad , \quad w = \sum_{n=1,3,\ldots}^{\infty} \frac{4q_0}{n\pi\left(\frac{n^4\pi^4 EI}{l^4} + k\right)} \cdot \sin\left(\frac{n\pi x}{l}\right) \tag{18.55}$$

18.4.4.4 Practical application

Many practical problems can be solved through the superposition of known particular solutions and the basic cases of Fig. 18.33.

For example, considering the case shown in Fig. 18.34(a), the particular solution q_0/k combined with the basic case Q gives us the answer we are looking for; in doing so, $w(0)$ must disappear, i. e. $q_0/k = -2Q\beta/k$:

$$w = \frac{q_0}{k}\left[1 - e^{-\beta x}\sin(\beta x + \pi/2)\right]$$

Similarly, particular solution q_0/k combined with basic case $2Q$ supplies the solution to the example shown in Fig. 18.34(b):

$$w = \frac{q_0}{k}\left[1 - \sqrt{2}e^{-\beta x}\sin(\beta x + \pi/4)\right]$$

Turning to Fig. 18.34(c), we consider the two halves of the beam with the particular solutions $w = 0$ or q_0/k for negative or positive x and superpose the positive or negative basic case Q and $q_0/(2k) = 2Q\beta/k$. When $x > 0$, this results in

$$w = \frac{q_0}{k}\left[1 - \frac{1}{2}e^{-\beta x}\sin(\beta x + \pi/2)\right]$$

The case shown in Fig. 18.34(d) can be solved with the help of the example of Fig. 18.34(c) by determining the stress resultants $M(a)$ and $V(a)$ for that case and eliminating them by superposing the corresponding variables R and Q. This procedure can also be used for beams of finite length.

18.4.5 Summary

1. Bending problems generally lead to the set of equations (18.38) for the deflection $w(x)$ and rotation of the cross-section $\varphi(x)$. Four boundary or continuity conditions have to be formulated per beam segment in order to solve such problems.
2. Residual stresses (in the case of uninhibited deformation) and restraints (in the case of inhibited deformation) can be determined on the basis of (18.44).
3. Many practical problems can be likened to the beam (bending stiffness EI in MNm^2) on an elastic foundation (foundation modulus k in MN/m^2). The solution to the corresponding inhomogeneous fourth-order differential equation (18.46) can often be found by combining simple particular solutions and the four basic cases for the solution to the homogeneous differential equation (Fig. 18.33). The solutions $w(x)$ to the homogeneous differential equation have the character of damped vibrations; deriving once involves multiplying the amplitude by $-[k/(EI)]^{1/4}$ and reducing the phase angle by $\pi/4$.

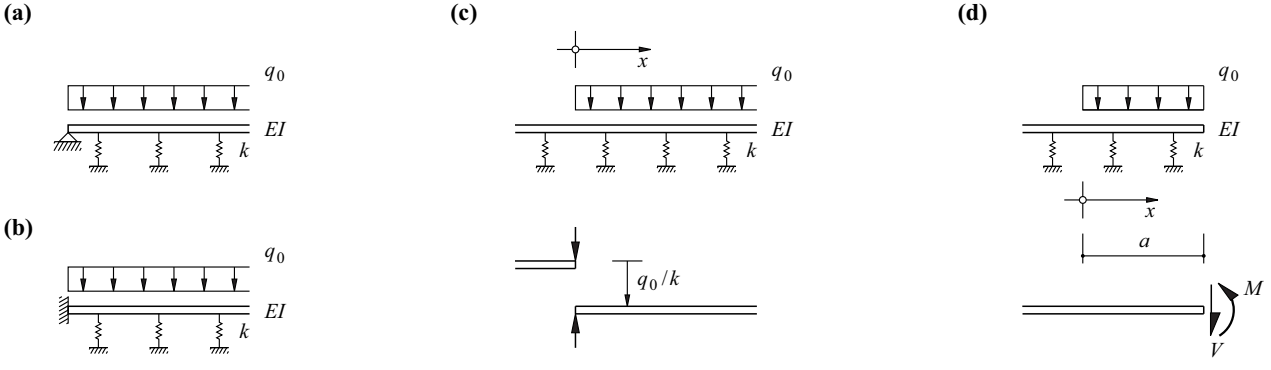

Fig. 18.34 Examples of the superposition of known particular solutions and the basic cases of Fig. 18.33

18.5 Combined shear and bending response

18.5.1 General

Frameworks in buildings are mostly combined with elements stiff in flexure such as stair shafts, lift shafts or walls, see Fig. 18.35(a). Horizontal forces, e. g. due to wind or seismic effects, are then carried by combined shear and bending response, see Fig. 18.35(b).

Connecting systems in shear and bending with horizontal stiffening beams, called *outriggers*, e. g. on plant floors, can bring about a considerable stiffening of the whole system, see Fig. 18.35(c).

When walls are resolved into truss-type constructions, it is generally necessary to consider the shear deformations as well as the bending deformations, also the axial stiffnesses of the columns in the case of very tall frames.

Walls broken up by door and window openings, Fig. 18.36(a), as well as walls connected via joints, Fig. 18.36(b), function in a similar way to *dowelled beams*; the *shear wall coupling beams* between the openings and the *coupling joints* correspond to the dowels of a dowelled beam. When the shear wall coupling beams are stiff, and especially in the case of coupling joints, it is generally necessary to take the axial stiffnesses of the walls into account as well.

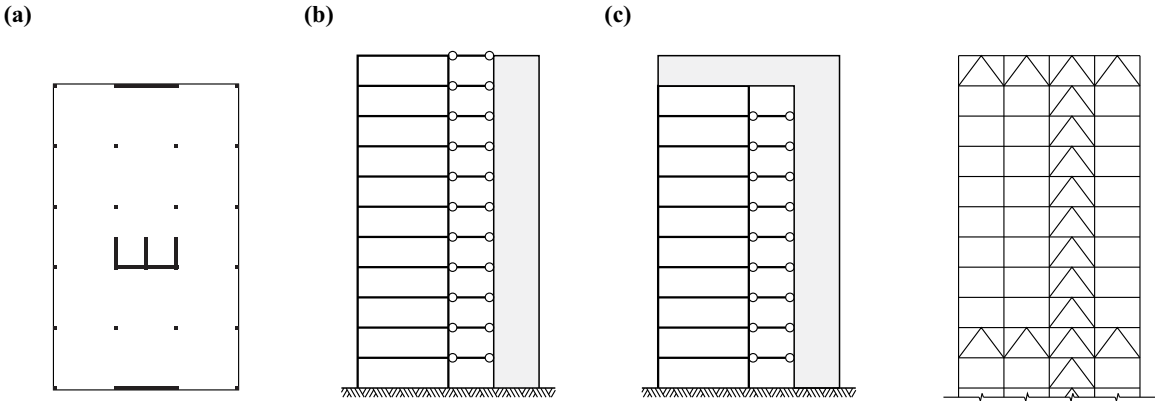

Fig. 18.35 Building structures: (a) typical plan form, (b) systems in shear and bending, (c) systems with outriggers

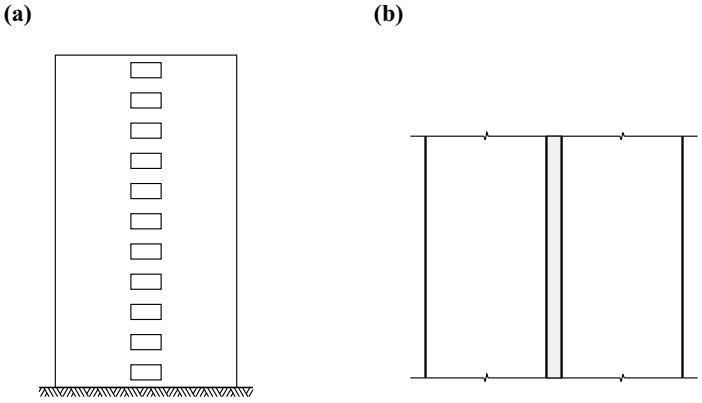

Fig. 18.36 Shear wall connection: (a) wall with openings, (b) coupling joint

The analytical models and solutions presented below are suitable for ascertaining the fundamental structural behaviour and for the rough calculations necessary during the conceptual design or when checking structures. It is expedient to employ computer programs for the structural analysis during the tender and detail design phases. The methods presented here are suitable for checking such calculations.

18.5.2 Shear wall - frame systems

18.5.2.1 Basis concepts

Let us consider the coupled shear wall - frame system of Fig. 18.37, with EI = const and GA_v = const. Applying (18.32) and (18.40), we get the differential equation

$$EIw'''' - GA_v w'' = q \tag{18.56}$$

which is similar to (13.74) and has the solution

$$w = c_1 + c_2 x + c_3 \cosh(\lambda x) + c_4 \sinh(\lambda x) + w_{\text{part}} \quad \left(\lambda^2 = \frac{GA_v}{EI}\right) \tag{18.57}$$

see (13.75) and (13.76). A uniformly distributed load $q = q_0$ = const or a triangular load $q = q_1 x/l$ result in the following particular solutions

$$w_{\text{part}} = -\frac{q_0 x^2}{2GA_v} \quad , \quad w_{\text{part}} = -\frac{q_1 x^3}{6GA_v l} \tag{18.58}$$

The integration constants in (18.57) follow from the boundary conditions $w(0) = w'(0) = w''(l) = 0$ plus $GA_v w'(l) - EIw'''(l) = 0$. A concentrated force is transferred between the shear wall and the frame at the top of the system ($x = l$).

18.5.2.2 Systems without outriggers

The result for a uniformly distributed load $q = q_0$ is

$$w = \frac{q_0 l^2}{GA_v}\left\{\frac{x}{l} - \frac{x^2}{2l^2} + \frac{\cosh(\lambda x) + \lambda l \sinh[\lambda(l-x)] - 1 - \lambda l \sinh(\lambda l)}{(\lambda l)^2 \cosh(\lambda l)}\right\} \tag{18.59}$$

We get the known solutions

$$GA_v w = q_0(lx - x^2/2) \quad , \quad EIw = q_0(x^4/24 - lx^3/6 + l^2x^2/4) \tag{18.60}$$

for the limiting cases $EI \to 0$ or $GA_v \to 0$, see Fig. 18.20(b) and (A7.45).

The result for a triangular load $q = q_1 x/l$ is

$$w = \frac{q_1 l^2}{GA_v}\left\{\kappa\frac{x}{l} - \frac{x^3}{3l^3} + \frac{2\cosh(\lambda x) + \kappa\lambda l \sinh[\lambda(l-x)] - 2 - \kappa\lambda l \sinh(\lambda l)}{(\lambda l)^2 \cosh(\lambda l)}\right\} \quad \left(\kappa = 1 - \frac{2}{\lambda^2 l^2}\right) \tag{18.61}$$

We get

$$GA_v w = q_1[lx/2 - x^3/(6l)] \quad , \quad EIw = \frac{q_1}{120l}(x^5 - 10l^2x^3 + 20l^3x^2) \tag{18.62}$$

for the limiting cases $EI \to 0$ or $GA_v \to 0$.

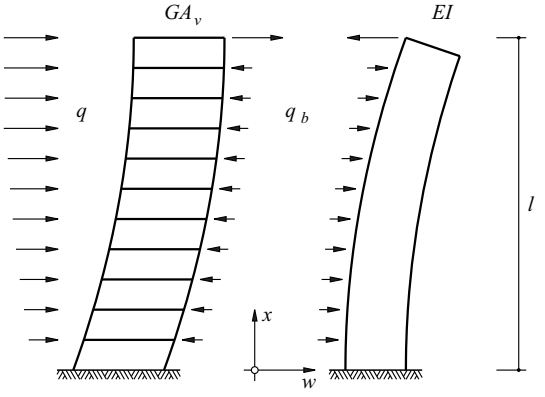

Fig. 18.37 Shear wall-frame system

Example 18.11 High-rise building

A system with $l = 90\,\text{m}$, $GA_v = 2593\,\text{MN}$ and $EI = 2.4 \cdot 10^6\,\text{MNm}^2$ is loaded by a uniformly distributed load $q_0 = 90\,\text{kN/m}$ and a triangular load $q_1 = 180\,\text{kN/m}$. Fig. 18.38 illustrates the corresponding structural behaviour, in which the stress resultants of the shear wall system subjected to the uniformly distributed load are given by

$$q_b = q_0 \cdot \frac{\cosh(\lambda x) + \lambda l \sinh[\lambda(l-x)]}{\cosh(\lambda l)} \quad , \quad V_b = \frac{q_0}{\lambda} \cdot \frac{-\sinh(\lambda x) + \lambda l \cosh[\lambda(l-x)]}{\cosh(\lambda l)}$$

$$M_b = \frac{q_0}{\lambda^2} \cdot \left\{ 1 - \frac{\cosh(\lambda x) + \lambda l \sinh[\lambda(l-x)]}{\cosh(\lambda l)} \right\} \tag{18.63}$$

and those for the triangular load by

$$q_b = q_1 \cdot \frac{2\cosh(\lambda x) + \kappa\lambda l \sinh[\lambda(l-x)]}{2\cosh(\lambda l)} \quad , \quad V_b = \frac{q_1}{2\lambda} \cdot \left\{ \frac{2}{\lambda l} - \frac{2\sinh(\lambda x) - \kappa\lambda l \cosh[\lambda(l-x)]}{\cosh(\lambda l)} \right\}$$

$$M_b = \frac{q_1}{2\lambda^2} \cdot \left\{ \frac{2x}{l} - \frac{2\cosh(\lambda x) + \kappa\lambda l \sinh[\lambda(l-x)]}{\cosh(\lambda l)} \right\} \tag{18.64}$$

According to (18.39) and (18.40), eq. (18.63) and (18.64) follow from the second to fourth derivatives of functions (18.59) and (18.61). The stress resultants for the frame system are given by

$$q_s = q - q_b \quad , \quad V_s = V - V_b \quad , \quad q_s = M - M_b \tag{18.65}$$

where

$$V = q_0(l-x) \quad , \quad M = -q_0(l-x)^2/2 \tag{18.66}$$

or rather

$$V = q_1 \frac{(l^2 - x^2)}{2l} \quad , \quad M = -\frac{q_1(2l^3 - 3l^2x + x^3)}{6l} \tag{18.67}$$

Subjected to the uniformly distributed load q_0, the combined system undergoes a deflection at the top amounting to 74.8 mm, see Fig. 18.38(a) and Tab. 18.1. At the top, the frame system exerts a restraining force of 1.885 MN on the shear wall system. In addition, above the point of inflection of the deflection curve ($x = 38.6\,\text{m}$), the frame system contributes to resisting q_0; in the lower part of the system it places a load on the shear wall system. The deflections at the top of the building clearly reveal the effectiveness of the combined system; according to (18.60), the value is 140.6 mm for the frame system, and 307.5 mm for the wall system, which compares with the value of 74.8 mm for the combined system.

Considering the triangular load, the situation is similar in principle, see Fig. 18.38(b) and Tab. 18.2. According to (18.62), the result is deflections at the top of 187.4 and 451.1 mm for the frame and wall systems respectively, whereas the combined system undergoes a deflection at the top of 107.9 mm.

Tab. 18.1 System without outriggers subjected to uniformly distributed load

X	q_b	V_b	M_b	w
90	90.0	– 1885	0	74.8
80	74.2	– 1071	14.6	67.5
70	66.4	– 374	21.8	59.5
60	65.9	282	22.3	50.6
50	72.6	968	16.1	40.9
40	87.2	1761	2.6	30.5
30	111.4	2745	– 19.8	20.0
20	147.6	4028	– 53.3	10.4
10	200.0	5751	– 101.8	3.0
0	274.1	8100	– 170.4	0
M	kN/m	kN	MNm	mm

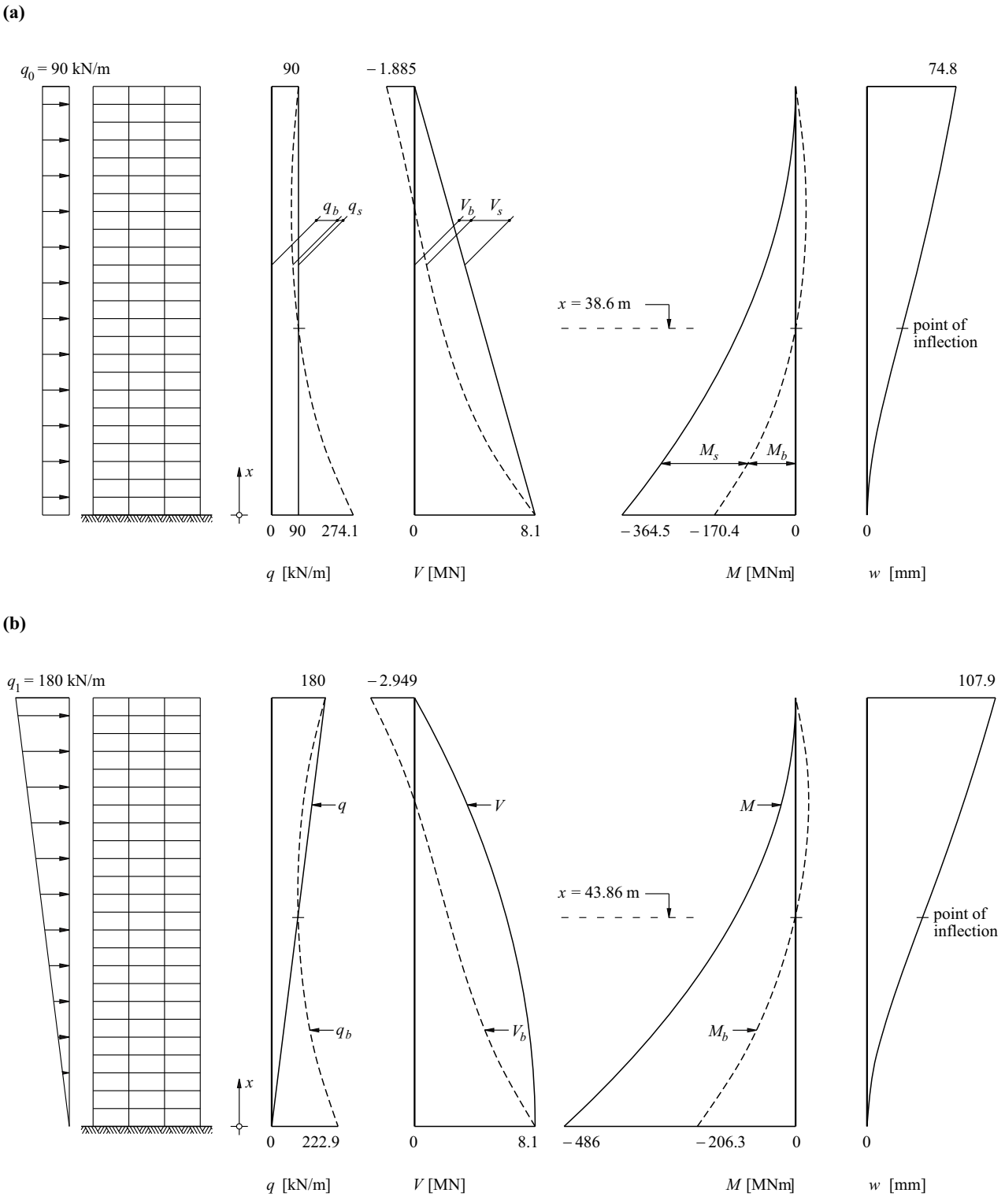

Fig. 18.38 Structural behaviour of a 90 m tall high-rise building system: (a) uniformly distributed load, (b) triangular load

Tab. 18.2 System without outriggers subjected to triangular load

X	q_b	V_b	M_b	w
90	180.0	– 2949	0	107.9
80	137.0	– 1378	21.3	96.3
70	109.0	– 159	28.7	83.9
60	92.8	841	25.2	70.4
50	86.7	1731	12.3	55.8
40	90.2	2608	– 9.4	40.8
30	103.4	3567	– 40.2	26.2
20	127.9	4713	– 81.4	13.2
10	166.3	6171	– 135.5	3.8
0	222.9	8100	– 206.3	0
M	kN/m	kN	MNm	mm

18.5.2.3 Systems with outriggers

If the bending deformations of an outrigger situated at the top of a system are – like the column extensions – ignored, then (18.57) continues to apply. However, the inextensible columns together with the outrigger prevent rotation at the top, i. e. $w'(l) = 0$, and therefore as $GA_v w'(l) = EIw'''(l)$, then $w'''(l) = 0$, too. When $q = q_0$, we get the relationships

$$
\begin{aligned}
w &= \frac{q_0 l^2}{GA_v}\left\{\frac{x}{l} - \frac{x^2}{2l^2} + \frac{\cosh[\lambda(l-x)] - \cosh(\lambda l)}{\lambda l \sinh(\lambda l)}\right\} \\
q_b &= q_0 \cdot \frac{\lambda l \cosh[\lambda(l-x)]}{\sinh(\lambda l)} \\
V_b &= q_0 l \cdot \frac{\sinh[\lambda(l-x)]}{\sinh(\lambda l)} \\
M_b &= q_0 l^2 \cdot \left\{\frac{1}{2(\lambda l)^2} - \frac{\cosh[\lambda(l-x)]}{\lambda l \sinh(\lambda l)}\right\}
\end{aligned}
\tag{18.68}
$$

instead of (18.59) and (18.63).

Example 18.12 High-rise building with outrigger

Fig. 18.39 and Tab. 18.3 illustrate the behaviour of the system examined in example 18.11 when an outrigger is positioned at the top of the system. Compared with Fig. 18.38(a), the deflection at the top is reduced by 27 % to 54.9 mm. The point of inflection of the deflection curve shifts from $x = 38.6$ m to $x = 57.6$ m. The upper part of the frame system contributes more to resisting q. There is no shear force between the frame and shear wall systems at the top. The fixity of the shear wall system at the top is relatively low. In the lower part of the wall, M_b and V_b are slightly larger than in the system without outrigger.

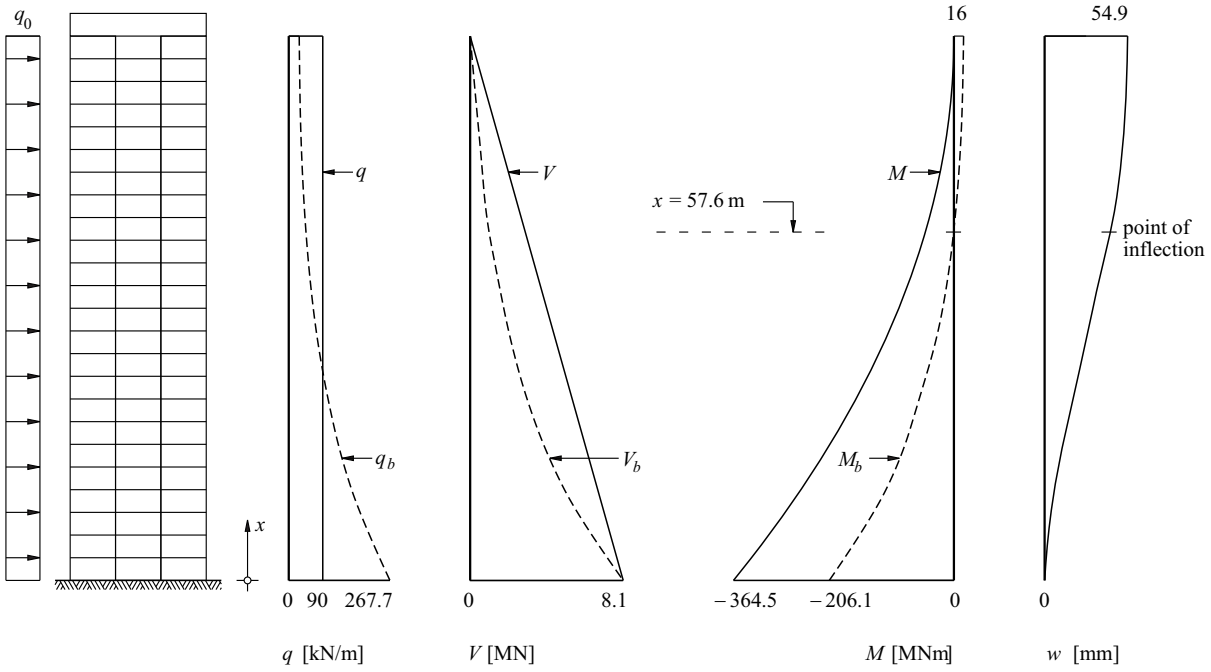

Fig. 18.39 System with outrigger subjected to uniformly distributed load

Tab. 18.3 System with outrigger subjected to uniformly distributed load

x	q_b	V_b	M_b	w
90	27.7	0	16.0	54.9
80	29.2	282	14.6	53.7
70	33.9	595	10.3	50.2
60	42.3	973	2.5	44.5
50	55.3	1457	– 9.6	37.0
40	74.4	2099	– 27.2	28.2
30	101.5	2971	– 52.3	18.8
20	139.7	4167	– 87.7	9.9
10	193.2	5816	– 137.1	2.9
0	267.7	8100	– 206.1	0
m	kN/m	kN	MNm	mm

18.5.3 Shear wall connection

18.5.3.1 Basis concepts

Wall 1 (width a_1, bending stiffness EI_1) and wall 2 (width a_2, bending stiffness EI_2) in Fig. 18.40 are connected with shear wall coupling beams (length b, bending stiffness EI) at the spacing of the storeys h and exhibit the same deflections w and rotations φ, i. e. $w_1 = w_2 = w$ and $\varphi_1 = \varphi_2 = \varphi = -w'$. A point of inflection in the deflection curve ensues in the middle of the shear wall coupling beam, and the ends of the beam undergo a relative displacement $\Delta = aw'$, where $a = b + (a_1 + a_2)/2$ = spacing of wall axes. The associated shear forces of $12EI\Delta/b^3$ result in a shear flow

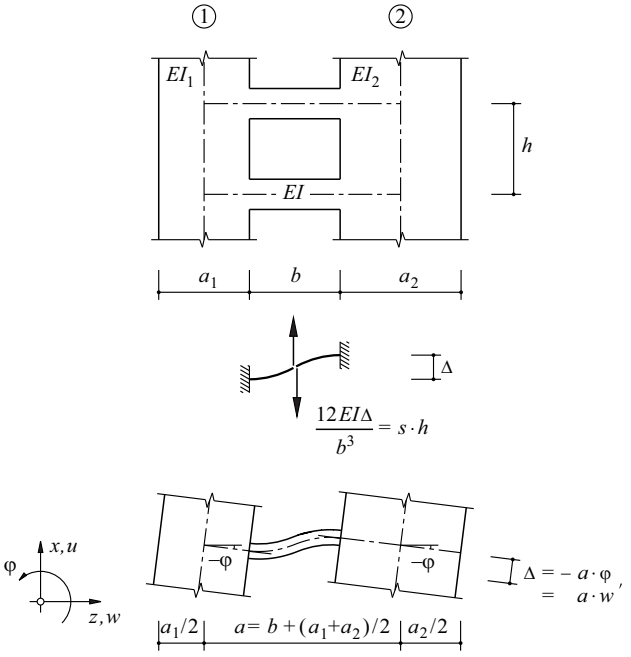

Fig. 18.40 Shear wall connection

$$s = \frac{12EI\Delta}{b^3 h} = k_s a w' \qquad \left(k_s = \frac{12EI}{b^3 h}\right) \tag{18.69}$$

and this corresponds to a shear force

$$V_s = as = k_s a^2 w' \tag{18.70}$$

in the beam in shear of width a. In a similar way to (18.56),

$$(EI_1 + EI_2)w'''' - k_s a^2 w'' = q \tag{18.71}$$

therefore applies, where the terms $q_b = (EI_1 + EI_2)w''''$ and $q_s = -k_s a^2 \mathrm{w}''$ denote the bending and shear components of q respectively.

The axial stiffnesses of the walls must be taken into account when considering stiff shear wall coupling beams and, in particular, coupling joints ($k_s = Gt/b$, where b = joint thickness and t = joint width perpendicular to plane of wall). Then $\Delta = aw' - u_1 + u_2$ applies instead of $\Delta = aw'$, where u_1 and u_2 denote the wall displacements in a certain cross-section in the in x direction. Using

$$\varphi_s = \frac{u_2 - u_1}{a} \tag{18.72}$$

we get

$$V_s = k_s a^2(w' + \varphi_s) \quad , \quad (EI_1 + EI_2)w'''' - k_s a^2(w'' + \varphi_s') = q \tag{18.73}$$

instead of $(18.70)_2$ and (18.71). The derivatives $N_1' = -N_2' = -V_s/a$ correspond to the normal forces $N_1 = EA_1 u_1'$ and $N_2 = EA_2 u_2'$; therefore, using $N_1' = EA_1 u_1''$ and $N_2' = EA_2 u_2''$ and (18.72), the following applies:

$$\varphi_s'' = \frac{V_s}{EI_s} \qquad \left(EI_s = \frac{a^2}{\dfrac{1}{EA_1} + \dfrac{1}{EA_2}}\right) \tag{18.74}$$

thus (18.73) becomes

$$EI_s \varphi_s'' = k_s a^2(w' + \varphi_s) \tag{18.75}$$

Finding the third derivative of this relationship and considering (18.74) leads to

$$w'''' = \frac{V_s'''}{k_s a^2} - \frac{V_s'}{EI_s}$$

and hence, by considering (18.73),

$$V_s''' - (\lambda\mu)^2 V_s' = q\lambda^2 \qquad \left(\lambda^2 = \frac{k_s a^2}{EI_1 + EI_2},\ \mu^2 = 1 + \frac{EI_1 + EI_2}{EI_s}\right) \tag{18.76}$$

18.5.3.2 Neglecting the wall extensions

Eq. (18.71) is similar to (18.56), and the corresponding solutions, with adjusted coefficients, can be applied directly. For example, (18.59) can be used to find the deflection w due to a uniformly distributed load $q = q_0$ by replacing GA_v by $k_s a^2$ and putting $\lambda^2 = k_s a^2/(EI_1 + EI_2)$; the shear flow s is then

$$s = k_s a w' = \frac{q_0 l}{a}\left\{1 - \frac{x}{l} + \frac{\sinh(\lambda x) - \lambda l \cosh[\lambda(l-x)]}{\lambda l \cosh(\lambda l)}\right\} \tag{18.77}$$

and the relationships (18.63) apply for M_b, V_b and q_b.

Example 18.13 Shear wall

The shear wall shown in Fig. 18.41 ($l = 25h = 90\,\text{m}$, $E = 30\,\text{kN/mm}^2$, $a = 10\,\text{m}$, $I = 0.3 \cdot 1^3/12 = 0.025\,\text{m}^4$, $b = 4\,\text{m}$, $I_1 = I_2 = 0.3 \cdot 6^3/12 = 5.4\,\text{m}^4$) is loaded by the uniformly distributed load $q_0 = 40\,\text{kN/m}$. Using

$$k_s = \frac{12 \cdot 30 \cdot 10^3 \cdot 0.025}{4^3 \cdot 3.6} = 39.0625\,\text{MN/m}^2 \quad , \quad \lambda = \sqrt{\frac{39.0625 \cdot 10^2}{2 \cdot 30 \cdot 10^3 \cdot 5.4}} = 0.1098\,\text{m}^{-1}$$

the procedure described above results in the values listed in Tab. 18.4.

The point of inflection of the deflection curve w is located at $x = 20.867\,\text{m}$; at this point, the maximum shear flow is $s_{\max} = 240.1\,\text{kN/m}$, and $M_b = 0$ applies. A maximum shear force of $s_{\max} \cdot h = 240.1 \cdot 3.6 = 864.5\,\text{kN}$ in the shear wall coupling beam between the 5th and 6th storeys corresponds to the maximum shear flow.

The system essentially responds like a beam in shear. The shear flows s add up over l to form the normal forces $\pm k_s a \cdot w(l) = \pm 13.253\,\text{MN}$ in walls 1 and 2 at the base of the wall $x = 0$. Moment equilibrium at the base of the wall is satisfied: $-29.469\,\text{MNm} - 10\,\text{m} \cdot 13.253\,\text{MN} = -162\,\text{MNm} = -q_0 l^2/2$.

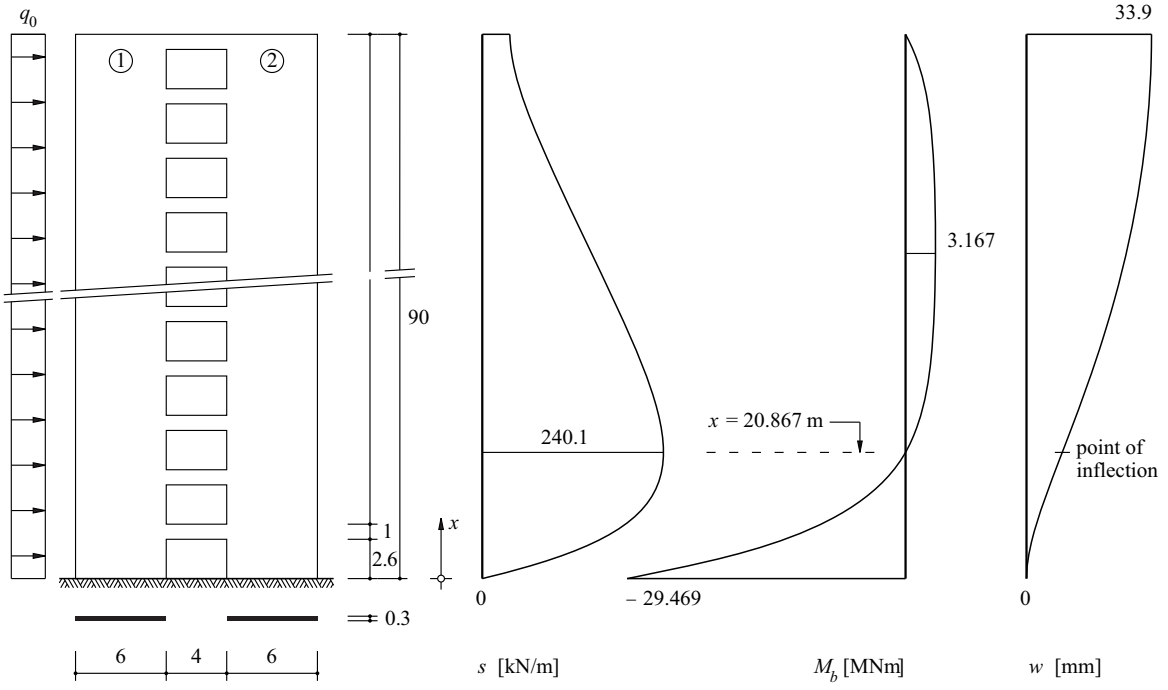

Fig. 18.41 A 25-storey shear wall with openings (dimensions in m, $q_0 = 40$ kN/m)

Tab. 18.4 Values of the functions for the shear wall of Fig. 18.41

x	w	s	M_b
90	33.9	36.4	0
72	31.5	76.9	2.846
54	26.5	143.7	3.167
36	18.3	209.2	2.680
18	7.7	238.1	– 1.226
0	0	0	– 29.469
m	mm	kN/m	MNm

18.5.3.3 Considering the wall extensions

We shall confine ourselves to the case of a uniformly distributed load $q = q_0$, for which (18.76) has the general solution

$$V_s = c_1 \sinh(\lambda\mu x) + c_2 \cosh(\lambda\mu x) + c_3 - \frac{q_0 x}{\mu^2} \tag{18.78}$$

At the base of the wall ($x = 0$), $w' = \varphi_s = 0$, and therefore according to $(18.73)_1$: $V_s(0) = 0$. At the top of the wall, $(x = l)$, $M_b = N_1 = N_2 = 0$, and therefore $w'' = u_1' = u_2' = 0$, i. e. according to (18.72) and $(18.73)_1$: $V_s'(l) = 0$. Finally, as $V = V_s + V_b = V_s - (EI_1 + EI_2)w'''$ and $V(l) = 0$ for $x = l$: $V_s = (EI_1 + EI_2)w'''$, i. e. taking into account $(18.73)_1$ and (18.74): $V_s''(l) = (\lambda\mu)^2 \cdot V_s(l)$. These boundary conditions result in

$$V_s = \frac{q_0 l}{\mu^2}\left\{1 - \frac{x}{l} + \frac{\sinh(\lambda\mu x) - \lambda\mu l \cosh[\lambda\mu(l-x)]}{\lambda\mu l \cosh(\lambda\mu l)}\right\} \tag{18.79}_1$$

and from that as $V = q_0(l - x)$ and $M_b' = V - V_s$, taking into account the boundary condition $M_b(l) = 0$, we get

$$M_b = \frac{q_0 l^2}{\mu^2}\left\{(\mu^2 - 1)\left(\frac{x}{l} - \frac{x^2}{2l^2} - \frac{1}{2}\right) + \frac{1}{(\lambda\mu l)^2} - \frac{\cosh(\lambda\mu x) + \lambda\mu l \sinh[\lambda\mu(l-x)]}{(\lambda\mu l)^2 \cosh(\lambda\mu l)}\right\} \tag{18.79}_2$$

Finally, as $M_b = -(EI_1 + EI_2)w''$, taking into account the boundary conditions $w(0) = w'(0) = 0$ it follows that

$$w = \frac{q_0 l^2}{\mu^2 k_s a^2}\left\{(\mu^2 - 1)(\lambda l)^2\left(\frac{x^2}{4l^2} - \frac{x^3}{6l^3} + \frac{x^4}{24l^4}\right) + \frac{1}{\mu^2}\left(\frac{x}{l} - \frac{x^2}{2l^2}\right) + \frac{\cosh(\lambda\mu x) + \lambda\mu l \sinh[\lambda\mu(l-x)] - 1 - \lambda\mu l \sinh(\lambda\mu l)}{\lambda^2\mu^4 l^2 \cosh(\lambda\mu l)}\right\} \tag{18.79}_3$$

Putting $\mu = 1$, the equations (18.79) are reduced to (18.77), $(18.63)_3$ and (18.59) when $V_s = sa$ is taken into account and $k_s a^2$ is replaced by GA_v.

Example 18.14 Shear wall – influence of wall extensions

Consider the shear wall of example 18.13; eq. (18.79) with

$$EI_s = \frac{a^2 EA_1 EA_2}{EA_1 + EA_2} = \frac{a^2 EA_1}{2} = \frac{10^2 \cdot 30 \cdot 10^3 \cdot 6 \cdot 0.3}{2} = 2.7 \cdot 10^6\ \text{MNm}^2$$

and

$$\mu^2 = 1 + \frac{2EI_1}{EI_s} = 1 + \frac{2 \cdot 30 \cdot 10^3 \cdot 5.4}{2.7 \cdot 10^6} = 1.12$$

results in the values given in Tab. 18.5.

Compared with Tab. 18.4, the wall extensions have a significant influence here. The deflection at the top increases four-fold, the point of inflection of the deflection curve is much higher, and the bending response in the lower part of the wall is much greater.

Tab. 18.5 Values of the functions for the shear wall of Fig. 18.41 taking into account the wall extensions

x	w	$s = V_s/a$	M_b
90	135.8	30.7	0
72	105.1	68.0	1.618
54	73.0	128.4	– 0.225
36	41.3	188.0	– 4.030
18	13.9	217.5	– 11.880
0	0	0	– 42.373
m	mm	kN/m	MNm

The inclusion of an outrigger keeps the cross-sections at the top of the wall in one plane, i. e. $\Delta(l) = 0$. Consequently, the second boundary condition $V_s'(l) = 0$ derived above for the system without outriggers is replaced by $V_s(l) = 0$, and the third boundary condition is simplified to $V_s''(l) = 0$. It can be shown that each third term in the curly brackets on the right in the equations (18.79) can be replaced by the following expressions:

$$-\frac{\sinh[\lambda\mu(l-x)]}{\sinh(\lambda\mu l)} \quad , \quad -\frac{\cosh[\lambda\mu(l-x)]}{\lambda\mu l \sinh(\lambda\mu l)} \quad , \quad \frac{\cosh[\lambda\mu(l-x)] - \cosh(\lambda\mu l)}{\lambda\mu^3 l \sinh(\lambda\mu l)} \tag{18.80}$$

The stiffening effect of the outrigger is essentially confined to the upper part of the wall, but remains comparatively small, which is easy to show with the help of example 18.14, for instance.

18.5.4 Dowelled beams

Dowelled beams can be dealt with in a similar way to shear walls connected via coupling joints. The dowelled timber beam shown in Fig. 18.42(a), with the cross-section shown in Fig. 18.42(b), is in the form of a simply supported beam with a span of $l = 8\,\text{m}$ loaded at mid-span by a point load of 20 kN. If the two identical single beams were not dowelled together, there would be boundary stresses amounting to

$$\frac{1}{2} \cdot 20 \cdot 10^3 \cdot \frac{8000}{4} \cdot \frac{6}{180 \cdot 240^2} = 11.57\,\text{N/mm}^2$$

at mid-span, and the deflection at mid-span, assuming a modulus of elasticity of $10\,\text{kN/mm}^2$, would be

$$\frac{20 \cdot 10^3 \cdot (8000)^3 \cdot 12}{48 \cdot 10^4 \cdot 2 \cdot 180 \cdot 240^3} = 51.44\,\text{mm}$$

It is assumed that the two single beams are connected together with dowels every 1 m. The stiffness of the dowels is 50 kN/mm. Therefore, when assuming continuous dowelling, $k_s = 50\,000/1000 = 50\,\text{N/mm}^2$. Putting $a = 240$ mm, then according to (18.76),

$$\lambda = \sqrt{\frac{50 \cdot 240^2 \cdot 12}{2 \cdot 10^4 \cdot 180 \cdot 240^3}} = \frac{5}{6}\,\text{m}^{-1}$$

and with

$$EI_s = \frac{1}{2} \cdot 240^2 \cdot 10^4 \cdot 180 \cdot 240 = 12.4416 \cdot 10^{12}\,\text{Nmm}^2$$

and

$$EI_b = EI_1 + EI_2 = 2EI = 2 \cdot 10^4 \cdot \frac{180 \cdot 240^3}{12} = 4.1472 \cdot 10^{12}\,\text{Nmm}^2$$

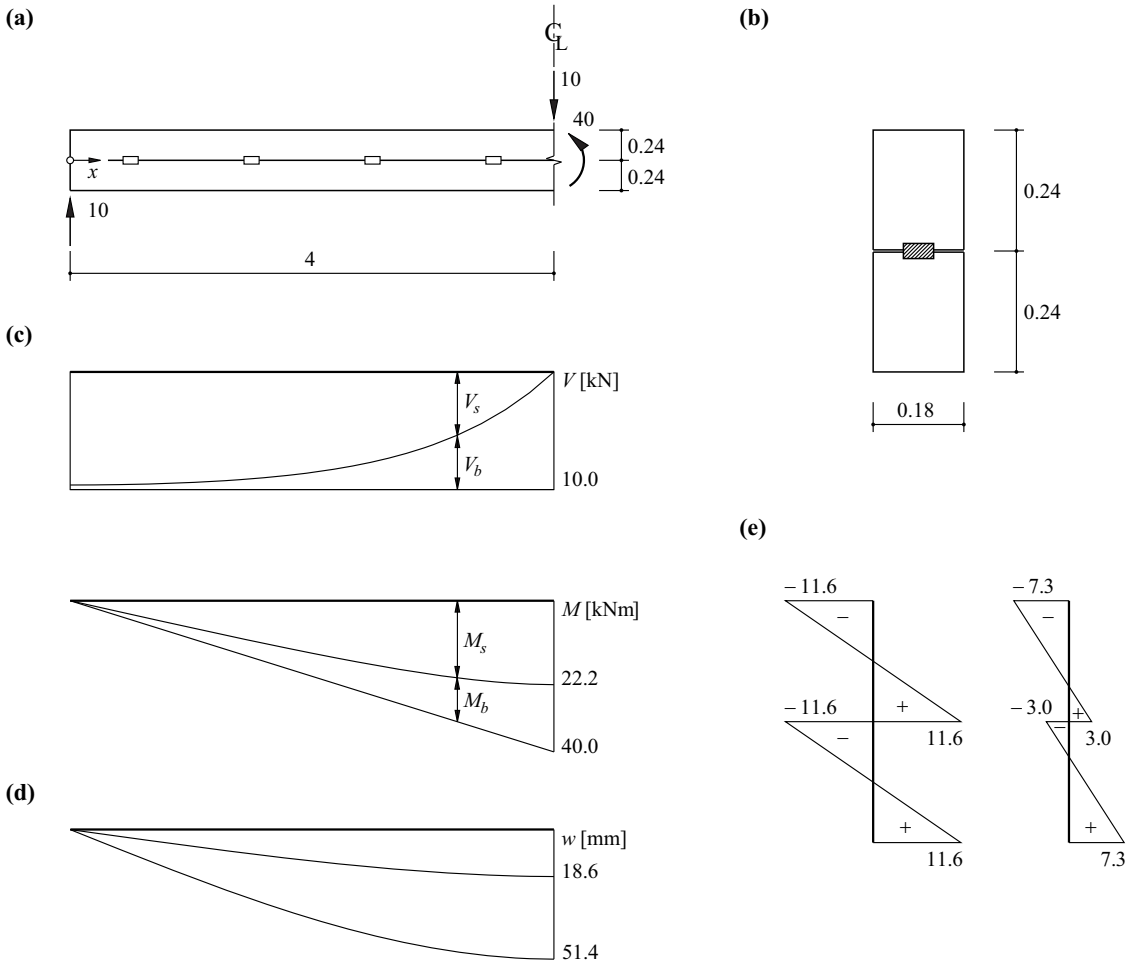

Fig. 18.42 Dowelled timber beam: (a) diagram of static system (forces in kN, dimensions in m), (b) cross-section, (c) stress resultants, (d) deflections, (e) stress distribution [N/mm^2] at mid-span without and with dowelling

the result is

$$\mu^2 = \frac{4}{3}$$

At point $x = 0$, $M_b = N_1 = N_2 = 0$ and therefore $V_s'(0) = 0$. At $x = l/2$, $w' = \varphi_s = 0$ applies and therefore $V_s(l/2) = 0$. When $q_0 = 0$, eq. (18.78) then gives us

$$V_s = c[\cosh(\lambda\mu x) - \cosh(\lambda\mu l/2)]$$

As $V_s = V - V_b = V + EI_b w'''$, and taking into account $(18.73)_1$ and (18.74), the constant c is

$$c = -\frac{V}{\mu^2 \cosh(\lambda\mu l/2)}$$

i. e.

$$V_s = \frac{V}{\mu^2}\left[1 - \frac{\cosh(\lambda\mu x)}{\cosh(\lambda\mu l/2)}\right]$$

and consequently, considering the fact that $M_s(0) = 0$,

$$M_s = \frac{V}{\mu^2}\left[x - \frac{\sinh(\lambda\mu x)}{\lambda\mu \cosh(\lambda\mu l/2)}\right] \quad , \quad M_b = M - M_s = -EI_b w''$$

Taking into account $w'(l/2) = 0$ and $w(0) = 0$, in the end we get

$$w = \frac{V}{\mu^2 EI_b}\left[(\mu^2 - 1)\left(\frac{l^2 x}{8} - \frac{x^3}{6}\right) + \frac{x}{\lambda^2\mu^2} - \frac{\sinh(\lambda\mu x)}{\lambda^3\mu^3 \cosh(\lambda\mu l/2)}\right]$$

Tab. 18.6 Values of the functions for the dowelled beam of Fig. 18.42

x	$s = V_s/a$	M_s	w
0	29.92	0	0
1	29.25	7.13	6.58
2	26.59	13.89	12.46
3	19.28	19.53	16.84
4	0	22.21	18.64
m	kN/m	kNm	mm

The corresponding values $s = V_s/a$, M_s and w are specified in Tab. 18.6 for a number of values of x, see also Fig. 18.42(c) and (d). The shear flows s add up from the end of the beam to mid-span to form normal forces $-N_1 = N_2 = M_s(l/2)/a = 92.55\,\text{kN}$. When $M_b(l/2) = 17.79\,\text{kNm}$, the boundary stresses in beam 2 at mid-span are $92\,550/(180 \cdot 240) \pm 1/2 \cdot 17.79 \cdot 10^6 \cdot 6/(180 \cdot 240^2) = 7.3$ and $-3.0\,\text{N/mm}^2$, see Fig. 18.42(e).

As we can see, the dowelling reduces the boundary stresses at mid-span by $(11.6 - 7.3)/11.6 = 37\,\%$, the deflections by $(51.4 - 18.6)/51.4 = 64\,\%$.

18.5.5 Summary

1. The structural behaviour of shear wall-frame systems is described by the differential equation (18.56) with the general solution (18.57). The solutions given for uniformly distributed and triangular loads enable general trapezoidal loads to be dealt with through superposition.
2. Outriggers can be used to achieve an effective stiffening of shear wall frame systems. The shear force at the top between the frame and shear wall systems, which characterises systems without outriggers, is eliminated in this case.
3. The influence of the wall extensions is generally considerable in the case of shear walls connected via coupling beams or coupling joints. By contrast, the stiffening influence of additional outriggers is generally small.
4. Dowelled beams can be dealt with in a similar way to shear walls connected via coupling joints.
5. The analytical models and solutions presented here are suitable for assessing the fundamental structural behaviour and for the rough calculations necessary during the conceptual design or when checking structures. In addition, they enable suitably refined computer analyses to be checked for plausibility.

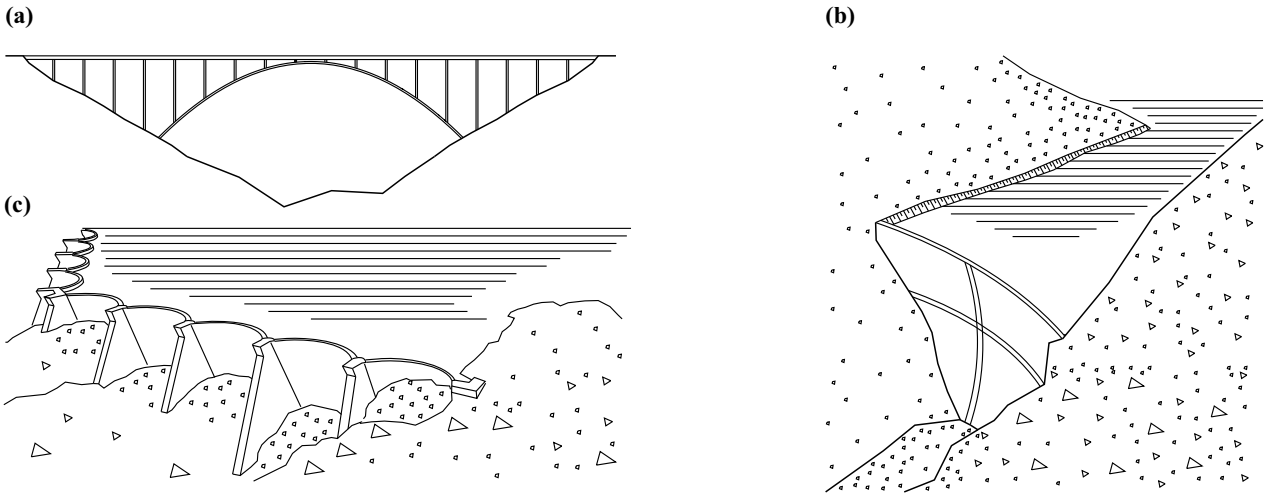

Fig. 18.43 Arches: (a) bridge, (b) dam, (c) retaining wall, weir

18.6 Arches

18.6.1 General

People have been building masonry arches for millennia. And over the last 200 years or so, arches of iron, steel and concrete have been erected as well, which has enabled the spans to be increased from a few dozen to several hundred metres.

It is primarily the form of an arch that gives it its load-carrying capacity and enables to resist large loads or forces. Fig. 18.43 shows three typical examples.

Arches are generally loaded by compressive forces in the direction of the bar. For general load cases, the arch axis deviates to some extent from the thrust line (section 5.3.2) and therefore it is always necessary to take a certain amount of bending into account. It is for this reason, and to rule out the risk of buckling, that arches require adequate bending stiffness, or must be stiffened in some other way.

Various aspects of arch structures have already been discussed with the help of examples 5.6, 5.7, 10.5, 12.2 and 16.8.

18.6.2 Analytical model

We shall confine ourselves to vertical loads ($q_x = 0$, $q_z = q$) and consider an arch (bending stiffness EI_a) connected via inextensible pin-ended struts to a beam in bending (bending stiffness EI_b) as shown in Fig. 18.44(a). The beam in bending and the arch are presumed to be rigid in shear ($GA_v \to \infty$), and the arch has a shallow curvature, i. e. $\mathrm{d}s \approx \mathrm{d}x$ or $(z')^2/2 \ll 1$, see Fig. 18.44(b).

Equilibrium at the deformed arch element in Fig. 18.44(b) calls for

$$H = \text{ const} \quad , \quad V' + q = 0 \quad , \quad -H(z+w)' + M' - V = 0 \tag{18.81}$$

where, as usual, $' = \mathrm{d}/\mathrm{d}x$. Using (18.39) and putting $EI_a + EI_b = EI = \text{const}$, we get the following differential equation:

$$EIw'''' + H(z+w)'' = q \tag{18.82}$$

Assuming that the arch is inextensible ($EA \to \infty$), we can read off the relation $\mathrm{d}u = -\mathrm{d}w \cdot z'$ from Fig. 18.44(b), i. e. $u' = -w'z'$. Accordingly, with a finite axial stiffness the result is

$$u' = -w'z' - \frac{H}{EA} \tag{18.83}$$

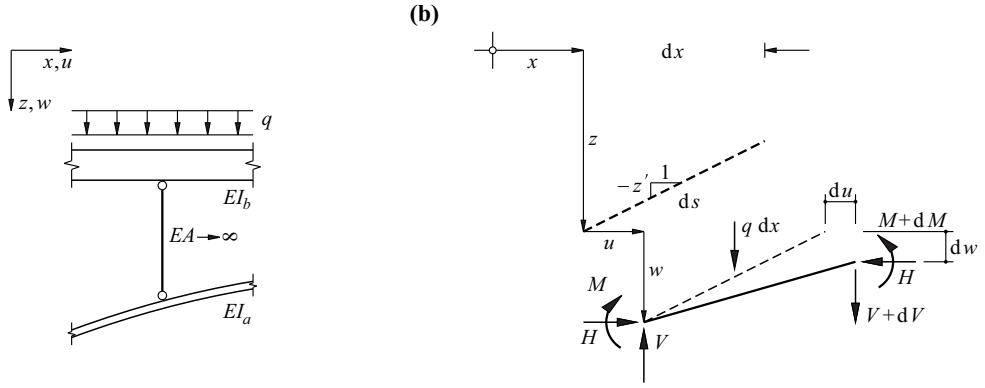

Fig. 18.44 Arch: (a) diagram of static system, (b) static and kinematic variables for the differential arch element

18.6.3 Applications

Eq. (18.82) is fulfilled for the two-hinged arch shown in Fig. 18.45(a) with the parabolic form $z = -4fx(l-x)/l^2$, where $w \equiv 0$ and $H = ql^2/(8f)$ and load q = const, see (5.59) and (5.60). The arch axis coincides with the thrust line.

As (18.83) shows, this solution with mutually braced supports is only valid when the arch is inextensible. With a finite axial stiffness, the distance between the two supports would have to be shortened by $Hl/(EA) = ql^3/(8fEA)$ in order for the solution to remain true.

According to (18.83), the following applies for mutually braced supports:

$$\frac{Hl}{EA} = -\int_0^l w'z'\,\mathrm{d}x$$

Integration by parts and taking into account $z(0) = z(l) = 0$ and $w'' = -M/(EI)$ results in the following relationship:

$$\frac{Hl}{EA} = -\left.w'z\right|_0^l + \int_0^l w''z\,\mathrm{d}x = -\int_0^l \frac{Mz}{EI}\,\mathrm{d}x$$

i. e. when $M = Hz + M_0$

$$\int_0^l \frac{M_0 z}{EI}\,\mathrm{d}x + H\left(\frac{l}{EA} + \int_0^l \frac{z^2}{EI}\mathrm{d}x\right) = 0 \qquad (18.84)$$

Relationship (18.84) corresponds to the compatibility condition

$$\delta_1 = \delta_{10} + H\delta_{11} = 0$$

where

$$\delta_{10} = \int_0^l \frac{M_0 z}{EI}\,\mathrm{d}s \approx \int_0^l \frac{M_0 z}{EI}\,\mathrm{d}x = -\frac{ql^3 f}{15EI} \quad , \quad \delta_{11} = \int_0^l \frac{z^2}{EI}\,\mathrm{d}s + \int_0^l \frac{\cos^2\varphi}{EA}\,\mathrm{d}s \approx \int_0^l \frac{z^2}{EI}\,\mathrm{d}x + \frac{l}{EA} = \frac{8f^2 l}{15EI} + \frac{l}{EA}$$

according to the force method, see Fig. 18.45(b). We get the following for H

$$H = -\frac{\delta_{10}}{\delta_{11}} = \frac{\dfrac{ql^2}{8f}}{1 + \dfrac{15i^2}{8f^2}} \qquad (18.85)$$

where $i^2 = I/A$, see (13.19). Normally, $i \ll f$, which means that, as a result of assuming a finite axial stiffness, H is reduced by only a small amount compared with the inextensible system.

If we swap the roles of w' and z' in the integration by parts leading to (18.84), the result when taking into account $w(0) = w(l) = 0$ and $z'' = 8f/l^2$ is

$$\frac{Hl}{EA} = -\left. z'w\right|_0^l + \int_0^l z''w\,dx = \frac{8f}{l^2}\int_0^l w\,dx$$

i. e. for $EA \to \infty$

$$\int_0^l w\,dx = 0 \tag{18.86}$$

The deflections of the inextensible arch disappear on average; settlement at one point is compensated for by heaving at another point.

Let us return to the problem of Fig. 18.45 and place the origin of coordinates at the crown of the arch, as shown in Fig. 5.30(a). Putting $z = 4fx^2/l^2$, eq. (18.82) – taking into account the symmetry condition $w'(0) = 0$ and the boundary conditions $w(l/2) = w''(l/2) = 0$ – gives us the deflection

$$w = f\left(\frac{ql^2}{8fH} - 1\right)\left\{\frac{4x^2}{l^2} - 1 + \frac{2}{\kappa^2}\left[\frac{\cos(2\kappa x/l)}{\cos\kappa} - 1\right]\right\} \qquad \left(\kappa^2 = \frac{Hl^2}{4EI}\right) \tag{18.87}$$

and the condition

$$\int_0^{l/2} u'\,dx = 0$$

used with (18.83) leads to the conditional equation

$$H = EA\left(\frac{4f}{l}\right)^2\left(\frac{ql^2}{8fH} - 1\right)\left(\frac{\tan\kappa}{\kappa^3} - \frac{1}{\kappa^2} - \frac{1}{3}\right) \qquad \left(\kappa^2 = \frac{Hl^2}{4EI}\right) \tag{18.88}$$

for the thrust H in the arch.

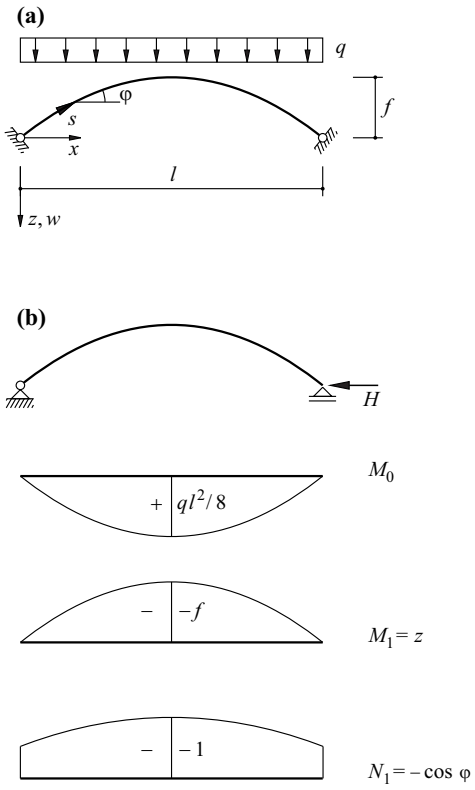

Fig. 18.45 Two-hinged arch: (a) diagram of static system, (b) basic system and basic states according to the force method

Example 18.15 Two-hinged arch – uniformly distributed load

Applying (18.88) to the two-hinged arch of Fig. 18.46, with $l = 200\,\text{m}$, $f = 40\,\text{m}$, $EA = 720\,\text{GN}$, $EI = 540\,\text{GNm}^2$ and $q = 1\,\text{MN/m}$, results in the values $\kappa = 1.521410$ and $H = 124.9932\,\text{MN}$. Substituting in (18.87) results in a settlement of $w(0) = 34\,\text{mm}$ at the crown. Eq. (18.87) gives us

$$M = -EIw'' = \frac{8EIf}{l^2}\left(\frac{ql^2}{8fH} - 1\right)\left[\frac{\cos(2\kappa x/l)}{\cos\kappa} - 1\right]$$

for the bending moments, with a value of $M(0) = 4.526\,\text{MNm}$ at the crown.

Assuming that the arch is inextensible, we get a thrust in the arch of $H = ql^2/(8f) = 125\,\text{MN}$. On the other hand, the approximation (18.85), where $i^2 = EI/EA = 0.75\,\text{m}^2$, results in a value of $H = 124.8902\,\text{MN}$. Although the approximation for H is very good, if this value were to be used to determine κ and entered into (18.87), the result would be large errors. The reason for this becomes clear when we develop the last factor on the right in (18.88) into a TAYLOR series. We get the expression

$$\frac{2}{15}\kappa^2 + \frac{17}{315}\kappa^4 + \frac{62}{2835}\kappa^6 + \ldots$$

and can see that (18.88) gives us the approximation (18.85) when only the first term in this series is considered.

The dimensions of the two-hinged arch investigated here are identical with those of example 16.8, so it is possible to compare the results directly.

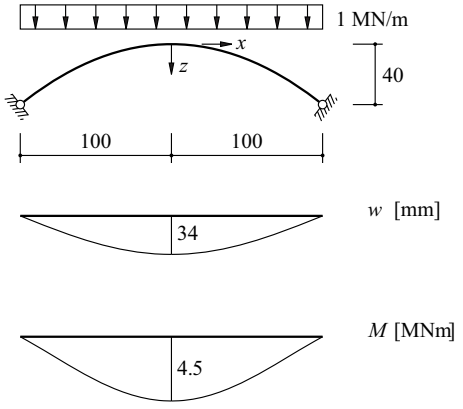

Fig. 18.46 Two-hinged arch subjected to uniformly distributed load (dimensions in m)

The inextensible two-hinged arch shown in Fig. 18.47(a), with the form $z = -4fx(l - x)/l^2$, is loaded by the uniformly distributed load q_0 and also the asymmetric load $q = q_1 \cdot \sin(2\pi x/l)$. The uniformly distributed load causes a thrust in the arch $H = q_0/z'' = q_0 l^2/(8f)$, and (18.82) is reduced to

$$EIw'''' + Hw'' = q_1 \cdot \sin\left(\frac{2\pi x}{l}\right)$$

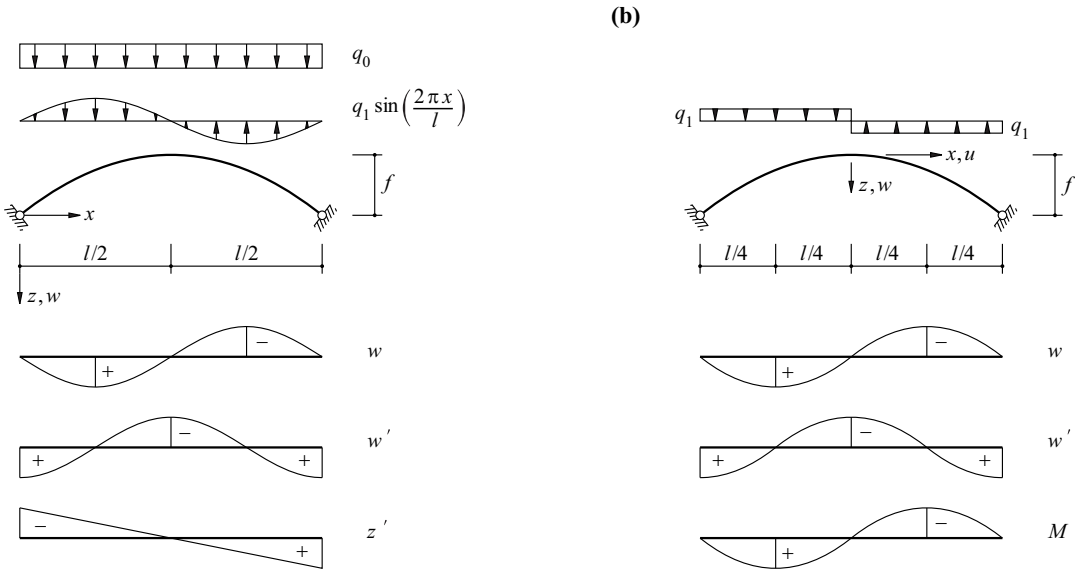

Fig. 18.47 Two-hinged arch subjected to asymmetric load: (a) sinusoidal load, (b) constant load segment by segment

Setting $w = c \cdot \sin(2\pi x/l)$, which satisfies the boundary conditions $w(0) = w''(0) = w(l) = w''(l) = 0$, results in the following deflections

$$w = \frac{\dfrac{q_1 l^4}{16\pi^4 EI} \sin\left(\dfrac{2\pi x}{l}\right)}{1 - \dfrac{Hl^2}{4\pi^2 EI}} \tag{18.89}$$

and bending moments

$$M = -EIw'' = \frac{\dfrac{q_1 l^2}{4\pi^2} \sin\left(\dfrac{2\pi x}{l}\right)}{1 - \dfrac{Hl^2}{4\pi^2 EI}} \tag{18.90}$$

We should also note that because of (18.83) and

$$\int_0^l w'z' \, dx = 0$$

the thrust H in the arch is not affected by the asymmetric load. This assumption implied above is therefore confirmed.

The equations (18.89) and (18.90) show that the deflections and the bending moments obtained without considering H have to be multiplied by the *amplification factor*

$$\mu = \frac{1}{1 - \alpha} \qquad \left(\alpha = \frac{H}{H_E}, \quad H_E = \frac{\pi^2 EI}{l_E^2}\right) \tag{18.91}$$

already known from the expression for w in example 8.16, although in this case $l_E = l/2$, see (22.12).

Example 18.16 Two-hinged arch – sinusoidal load

Let us consider the case examined in example 18.15. Here, putting $H = 125\,\text{MN}$ in (18.91) gives us the value $\mu = 1.3064$. Therefore, (18.89) and (18.90), with $q_1 = 50\,\text{kN/m}$, result in a maximum deflection $w_{max} = w(l/4) = 124.2\,\text{mm}$ and a maximum bending moment $M_{max} = M(l/4) = 66.2\,\text{MNm}$.

Turning to Fig. 18.47(b) and the case of an asymmetric load $\pm q_1$ constant segment by segment, (18.82) is reduced to

$$EIw'''' + Hw'' = -q_1 \qquad (x \geq 0)$$

Taking into account the boundary conditions $w(0) = w''(0) = w(l/2) = w''(l/2) = 0$, the result is

$$w = \frac{q_1 l^2}{4H}\left\{\frac{\cos(\kappa/2) - \cos[\kappa(2x/l - 1/2)]}{\kappa^2 \cos(\kappa/2)} + \frac{x}{l}\left(1 - \frac{2x}{l}\right)\right\} \qquad \left(x \geq 0, \quad \kappa^2 = \frac{Hl^2}{4EI}\right) \tag{18.92}$$

For negative values of x, the function w and its even derivatives must be continued antisymmetrically, the odd ones symmetrically.

As

$$\int_{-l/2}^{l/2} w'z'\,\mathrm{d}x = 0$$

H does not change as a result of the asymmetric load. However, the points on the arch between the supports undergo displacements u in the x direction. In particular, the crown of the arch is displaced by

$$u(0) = \int_{-l/2}^{0} w'z'\,\mathrm{d}x = \frac{2flq_1}{H}\left[\frac{\tan(\kappa/2) - (\kappa/2)}{\kappa^3} - \frac{1}{24}\right] \tag{18.93}$$

to the right. Using the coordinates of Fig. 18.47(b) we get the expression

$$u(0) = \frac{2fl^3 q_1}{4\pi^5 EI - \pi^3 Hl^2} \tag{18.94}$$

for the case shown in Fig. 18.47(a).

Example 18.17 Two-hinged arch – constant load segment by segment

If we replace the sinusoidal load of example 18.16 by the circumscribed rectangular load distribution, where $q_1 = 50\,\mathrm{kN/m}$, eq. (18.92) gives us a maximum deflection $w_{\max} = w(-l/4) = -w(l/4) = 157.6\,\mathrm{mm}$ and the second derivative gives us a maximum bending moment $M_{\max} = M(-l/4) = -M(l/4) = 82.2\,\mathrm{MNm}$. Compared with the corresponding values

$$\frac{5q_1 l^4}{6144EI} = \frac{5 \cdot 0.05 \cdot 200^4}{6144 \cdot 540000} = 0.1206\,\mathrm{m} \quad , \quad \frac{q_1 l^2}{32} = \frac{0.05 \cdot 200^2}{32} = 62.5\,\mathrm{MNm}$$

without the influence of H, this corresponds to amplification factors of 1.3075 and 1.3153. As w and M are only approximately sinusoidal functions, the result is small deviations from the value $\mu = 1.3064$ calculated in example 18.16. As we can see, the use of (18.91) would lead to excellent approximations.

The displacement at the crown according to (18.93) is 80.6 mm. Using (18.94), the result for the inscribed sinusoidal load according to example 18.16 is 63.2 mm.

Shallow arches are very sensitive to horizontal relative displacements of their abutments. For example, increasing the span l by Δ for an arch with the form $z = -f\sin(\pi x/l)$ and assuming a deflection $w = c\sin(\pi x/l)$, eq. (18.83) gives us the approximation

$$\Delta = \frac{\pi^2 cf}{2l}$$

At $x = l/2$, we get the maximum curvature

$$\chi_{\max} = -w''(l/2) = \frac{\pi^2 c}{l^2} = \frac{2\Delta}{fl}$$

which, for example, for a rectangular cross-section with depth h and modulus of elasticity E leads to boundary stresses amounting to

$$\chi_{\max} \cdot \frac{h}{2} \cdot E = \frac{\Delta hE}{fl} \tag{18.95}$$

Example 18.18 Displacement of the abutments to a concrete arch

A concrete arch ($E = 30\,\mathrm{kN/mm^2}$, span $l = 100\,\mathrm{m}$, rise $f = 10\,\mathrm{m}$, depth $h = 1.5\,\mathrm{m}$) with hinged supports at the abutments undergoes a relative displacement of the abutments amounting to $\Delta = 60\,\mathrm{mm}$ and hence a settlement at the crown of $2 \cdot 100 \cdot 0.06/(\pi^2 \cdot 10) = 0.1216\,\mathrm{m}$. According to (18.95), the corresponding boundary stresses at the crown of the arch are about

$$\frac{60 \cdot 1.5 \cdot 30}{10 \cdot 100} = 2.7\,\mathrm{N/mm^2}$$

The dependence on time (see example 7.2), which should generally be considered with such restraint problems, has been ignored here for simplicity.

18.6.4 Summary

1. It is primarily the form of an arch that gives it its load-carrying capacity. Besides the dominant compressive normal force, the associated bending moment must always be considered.
2. In structural systems comprising an arch and (deck) beams, the necessary bending stiffness can, in principle, be apportioned to the arch and the beams as required.
3. The deflections of an inextensible arch disappear on average; settlement at one point is compensated for by heaving at another point.
4. How the thrust in the arch influences the deflections and the stress resultants can be ascertained by way of amplification factors in a similar way to columns.
5. Apart from deflections, it is also necessary to consider horizontal displacements for arches, especially with asymmetric loads.
6. Arches are sensitive to displacements of their abutments.

18.7 Annular structures

18.7.1 General

Cylindrical shells are used in many practical applications, e. g. pipes, tunnels, silos, chimneys, reservoirs, see Fig. 18.48. The main aspects of their structural behaviour can be ascertained by considering them as thin-wall rings (the basic concepts have already been laid down in sections 5.3.2 and 13.2.6). In this section we shall confine ourselves to circular rings rigid in shear (radius of curvature $\rho = r = \mathrm{const}$, $GA_v \to \infty$) and use polar coordinates with the apex angle $\theta = s/r$ as independent variable.

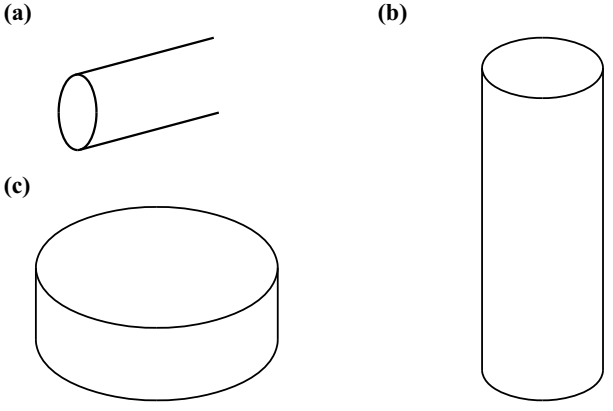

Fig. 18.48 Annular structures: (a) pipes, tunnels, (b) silos, chimneys, (c) reservoirs

18.7.2 Analytical model

Using the notation given in Fig. 18.49(a), we get the equilibrium conditions

$$\mathrm{d}N + V\mathrm{d}\theta + q_t r\mathrm{d}\theta = 0 \quad , \quad -N\mathrm{d}\theta + \mathrm{d}V + q_r r\mathrm{d}\theta = 0 \quad , \quad \mathrm{d}M - Vr\mathrm{d}\theta = 0$$

for the free body diagram of Fig. 18.49(b). Eliminating V from these relationships leads to

$$\boldsymbol{q} = \begin{Bmatrix} q_t \\ q_r \end{Bmatrix} = \begin{bmatrix} -\frac{1}{r}\mathrm{d}_\theta & -\frac{1}{r^2}\mathrm{d}_\theta \\ \frac{1}{r} & -\frac{1}{r^2}\mathrm{d}_\theta^2 \end{bmatrix} \begin{Bmatrix} N \\ M \end{Bmatrix} = \boldsymbol{D}_s \bullet \boldsymbol{\sigma} \tag{18.96}$$

where $\mathrm{d}_\theta = \mathrm{d}/\mathrm{d}\theta$, see (8.21).

On the other hand, using the displacement components v, w and the rotation φ defined in Fig. 18.49(c), the following applies:

$$\varepsilon r\mathrm{d}\theta = \mathrm{d}v + w\mathrm{d}\theta \quad , \quad \varphi = \frac{v}{r} - \frac{\mathrm{d}w}{r\mathrm{d}\theta} \quad , \quad \chi = \frac{\mathrm{d}\varphi}{r\mathrm{d}\theta}$$

where ε = extension of bar axis and χ = curvature. The second of these three relationships already allows for the fact that the shear strain γ is equal to zero, see (8.22). Eliminating φ results in

$$\boldsymbol{\varepsilon} = \begin{Bmatrix} \varepsilon \\ \chi \end{Bmatrix} = \begin{bmatrix} \frac{1}{r}\mathrm{d}_\theta & \frac{1}{r} \\ \frac{1}{r^2}\mathrm{d}_\theta & -\frac{1}{r^2}\mathrm{d}_\theta^2 \end{bmatrix} \begin{Bmatrix} v \\ w \end{Bmatrix} = \boldsymbol{D}_k \bullet \boldsymbol{u} \tag{18.97}$$

The even and odd differential operators, as elements of $\boldsymbol{D}_s$ and $\boldsymbol{D}_k$, are $\boldsymbol{D}_k = \boldsymbol{D}_s^{\mathrm{T}}$ and $\boldsymbol{D}_k = -\boldsymbol{D}_s^{\mathrm{T}}$ respectively, see section 8.2.2.3.

The relationship between the internal force and deformation variables is

$$\boldsymbol{\sigma} = \begin{Bmatrix} N \\ M \end{Bmatrix} = \begin{bmatrix} EA & -\frac{EI}{r} \\ -\frac{EI}{r} & EI \end{bmatrix} \begin{Bmatrix} \varepsilon \\ \chi \end{Bmatrix} = \boldsymbol{E} \bullet \boldsymbol{\varepsilon} \tag{18.98}$$

see (8.23).

The $-EI/r$ terms in the elasticity matrix $\boldsymbol{E}$ result from the hyperbolic distribution of the strains over the depth of the cross-section h, see (13.30):

$$\varepsilon_s\left(1 + \frac{z}{r}\right) = \varepsilon + z\chi$$

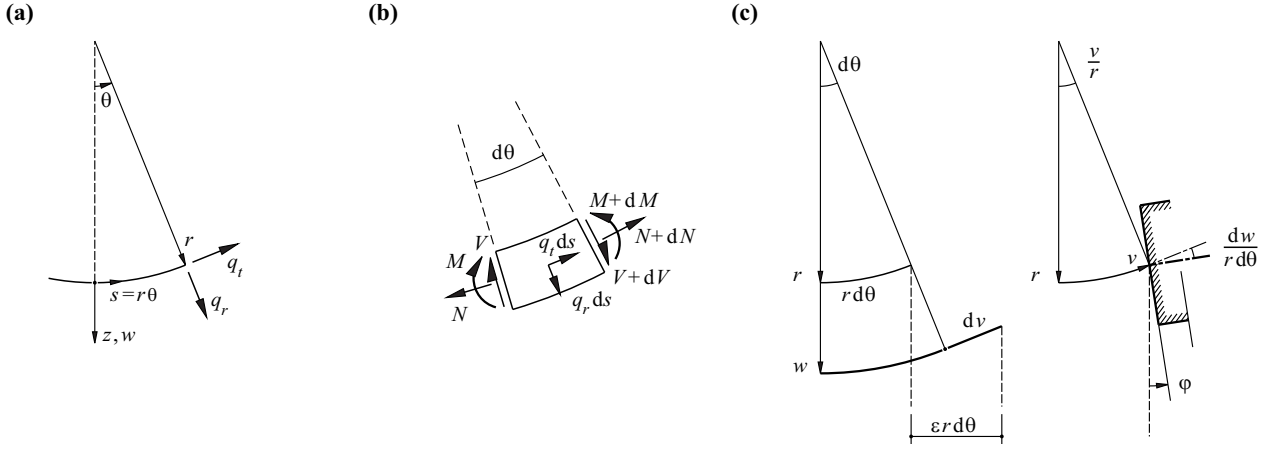

Fig. 18.49 Circular ring: (a) notation, (b) free body diagram, (c) displacement variables

Thus, for a rectangular cross-section of width b, the result for $\chi = 0$ is the bending moment

$$M = \int_{-h/2}^{h/2} E\varepsilon_s b z \mathrm{d}z = Eb\varepsilon \int_{-h/2}^{h/2} \frac{z}{1+z/r}\,\mathrm{d}z = Eb\varepsilon\left[rz - r^2\ln\left(1+\frac{z}{r}\right)\right]\Big|_{-h/2}^{h/2}$$
$$= Eb\varepsilon\left[rh - r\left(\frac{h}{2} - \frac{h^2}{8r} + \frac{h^3}{24r^2} - \ldots\right) - r\left(\frac{h}{2} + \frac{h^2}{8r} + \frac{h^3}{24r^2} + \ldots\right)\right]$$
$$= -E\frac{bh^3}{12r}\varepsilon = -\frac{EI}{r}\varepsilon$$

and for $\varepsilon = 0$ the normal force

$$N = \int_{-h/2}^{h/2} E\varepsilon_s b \mathrm{d}z = Eb\chi \int_{-h/2}^{h/2} \frac{z}{1+z/r}\,\mathrm{d}z = -\frac{EI}{r}\chi$$

18.7.3 Applications

18.7.3.1 Radial uniformly distributed load

The case $q_r = q_0 = \text{const}$, $q_t \equiv 0$ has already been examined for the static situation in example 5.5. Using (18.96) to (18.98) results in

$$N = q_0 r \quad , \quad M = -q_0 i^2 \quad ; \quad \varepsilon = \frac{w}{r} = \frac{q_0 r}{EA} \quad , \quad \chi = 0 \quad ; \quad v = 0 \quad , \quad w = \frac{q_0 r^2}{EA} \tag{18.99}$$

where $i^2 = I/A$. Eq. $(18.99)_1$ corresponds to the hoop stress formula, see (5.52).

The boundary bending stresses $\pm M/W$, where $W = bh^2/6 = Ah/6$, behave in proportion to $i^2/(hr) \sim h/r$ with regard to the average stresses N/A, i. e. are relatively small for thin rings ($h \ll r$).

18.7.3.2 Harmonic radial load $q_r = q_n\cos(n\theta)$, $n \geq 2$

With this type of load (see Fig. 18.50), the external forces are in equilibrium in themselves, as for a radial uniformly distributed load. Eq. (18.96) leads to the differential equation $N'' + N = rq_r$ (where $' = \mathrm{d}/\mathrm{d}\theta$), which is satisfied by the particular solution

$$N_n = \frac{rq_n\cos(n\theta)}{1-n^2}$$

The coefficients c_1 and c_2 for the general solution $c_1\cos\theta + c_2\sin\theta$ of the homogeneous part of the differential equation must disappear because $\cos\theta$ and $\sin\theta$ each have only one axis of symmetry, but q_r,on the other hand, at least two. Further, as q_r has at least two axes of antisymmetry, using (18.96) it must be that $M_n = -rN_n$; eq. (18.98) therefore results in the relationships $\varepsilon = 0$ and $M = EI\chi$, and (18.97) in the end results in $v' = -w$ and $\chi r^2 = -w - w''$. In total, the result is

$$N = \frac{rq_n\cos(n\theta)}{1-n^2} \quad , \quad M = -rN \quad ; \quad \varepsilon = 0 \quad , \quad \chi = \frac{M}{EI}$$
$$v = -\frac{r^4 q_n \sin(n\theta)}{n(n^2-1)^2 EI} \quad , \quad w = \frac{r^4 q_n\cos(n\theta)}{(n^2-1)^2 EI} \tag{18.100}$$

Superposing a radial uniformly distributed load $q_r = q_0 = \text{const}$ and the case $q_r = q_2\cos(2\theta)$, e. g. with $q_2 = q_0/3$, is one way of dealing with, for example, a pipe laid in the ground ($q_0 < 0$).

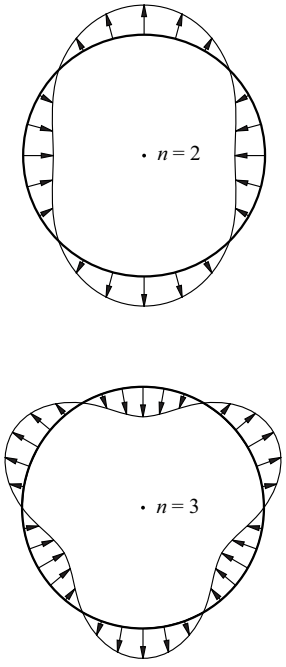

Fig. 18.50 Harmonic radial load

18.7.3.3 Radial load $q_1\cos\theta$

Such a load (see Fig. 18.51) has a vertical resultant

$$R = 2\int_0^{\pi} r q_1 \cos^2\theta \, d\theta = \pi r q_1$$

which, for example, can be brought into equilibrium by applying an appropriate support force at the crown. The FOURIER series

$$q_r(R) = \frac{R}{2\pi r} + \frac{R}{\pi r}[-\cos\theta + \cos(2\theta) - \cos(3\theta) + \ ...]$$

for the support force together with $q_1\cos\theta$ results in

$$q_r(R) = \frac{q_1}{2} + q_1[\cos(2\theta) - \cos(3\theta) + \ ...]$$

According to $(18.100)_2$, the second term on the right in this equation leads to

$$M = q_1 r^2 \left[\frac{1}{3}\cos(2\theta) - \frac{1}{8}\cos(3\theta) + \frac{1}{15}\cos(4\theta) - ...\right] \qquad (18.101)_1$$

Applying $(18.99)_1$ and $(18.100)_1$, the following applies:

$$N = \frac{q_1 r}{2} - \frac{M}{r} \qquad (18.101)_2$$

and from $(18.100)_6$ it follows that

$$w = \frac{q_1 r^4}{EI}\left[\frac{1}{9}\cos(2\theta) - \frac{1}{64}\cos(3\theta) + \frac{1}{225}\cos(4\theta) - ...\right] \qquad (18.101)_3$$

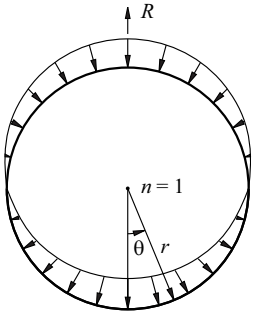

Fig. 18.51 Radial load $q_1\cos\theta$

18.7.3.4 Opposing point loads

This case has already been examined in example 8.9 but with different notation, see Fig. 18.52. In a similar way to the series development of R as a result of $q_1\cos\theta$, the following applies:

$$q_r(\pm Q) = \frac{Q}{\pi r} + \frac{2Q}{\pi r}[\cos(2\theta) + \cos(4\theta) + \ ...]$$

and we get

$$M = \frac{2Qr}{\pi}\left[\frac{1}{3}\cos(2\theta) + \frac{1}{15}\cos(4\theta) + \ ...\right] \quad , \quad N = \frac{Q}{\pi} - \frac{M}{r}$$

$$w = \frac{2Qr^3}{\pi EI}\left[\frac{1}{9}\cos(2\theta) + \frac{1}{225}\cos(4\theta) + \ ...\right] \qquad (18.102)$$

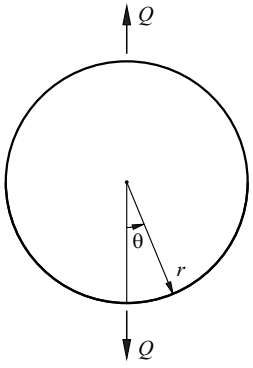

Fig. 18.52 Opposing point loads

18.7.4 Edge disturbances in cylindrical shells

The expansion of pipes, silos or tanks is often inhibited, e. g. by stiffening rings or the ground, or the roof in the case of a reservoir. This has already been pointed out in section 18.4.1. Such problems bring us back to the theory of the beam on elastic foundation.

Let us consider the cylindrical shell of Fig. 18.53 (radius r, wall thickness h). Unrestricted deformation as a consequence of the internal pressure q_0 [kN/m^2] according to (18.99) causes membrane forces $n = q_0 r$ [kN/m] and radial displacements $w = q_0 r^2/(Eh)$ in the radial direction at a certain point x. On the other hand, each strip of the shell with unit width acts as a beam in bending in the x direction with stiffness $D = Eh^3/[12(1 - \nu^2)]$ according to (8.48). The load $q_r = q$ is therefore carried by a bending component Dw'''' according to (18.40) and a membrane force component Ehw/r^2, i. e.

$$Dw'''' + \frac{Eh}{r^2}w = q \qquad (18.103)$$

The differential equation (18.103) is similar to (18.46). Using

$$4\beta^4 = \frac{Eh}{Dr^2} = \frac{12(1-\nu^2)}{r^2h^2}$$

enables all the considerations of section 18.4.4 to be adopted.

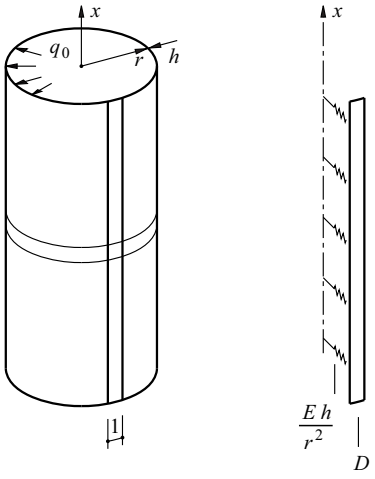

Fig. 18.53 Cylindrical shell subjected to internal pressure

Example 18.19 Stiffened pipe subjected to internal pressure

The case of a pipe stiffened with rigid stiffening rings and subjected to an internal pressure q_0 leads back to the basic case $2Q$ according to Fig. 18.33. The minimum moment [kNm/m] in the shell occurs beneath the stiffening ring and is equal to

$$m = -\frac{q_0}{2\beta^2} = -\frac{q_0 rh}{\sqrt{12(1-\nu^2)}}$$

The corresponding boundary stresses are

$$\frac{6|m|}{h^2} = q_0 \frac{r}{h}\sqrt{\frac{3}{(1-\nu^2)}}$$

and the stiffening ring has to accommodate a hoop tension of $2q_0 r/\beta$.

18.7.5 Summary

1. The structural behaviour of circular rings is described generally by the relationships (18.96) to (18.98).
2. The important limiting case of a radial uniformly distributed load leads to (18.99).
3. It is often easier to calculate the stress resultants and deformations of annular structures with the help of FOURIER series than by solving the differential equations directly.
4. Edge disturbance problems in cylindrical shells can be dealt with by using the theory of the beam on elastic foundation.

18.8 Cables

18.8.1 General

Cables (the general term for wire ropes) are used for diverse applications in bridges, roofs, guyed towers, aerial ropeways, overhead lines, etc., see Fig. 18.54.

A *spiral cable* is made up of one or more layers of wires wound around a core wire. Such cables consist of round wires (open cables), or a combination of round and wedge-shaped wires (semi-locked cables), or round and Z-shaped wires (fully locked cables). *Parallel-wire cables* are made up of bundles of round wires in a parallel arrangement. A *strand* is a spiral cable with just one layer; a *stranded cable* is a cable made up of several such strands.

Owing to the make-up of their cross-sections, the stress-strain behaviour of cables is not linear. Upon being loaded for the first time, a strain hardening takes place as the voids close; the axial stiffness increases and a certain elongation remains, the *cable stretch*, which is only established completely after a number of loading cycles (the

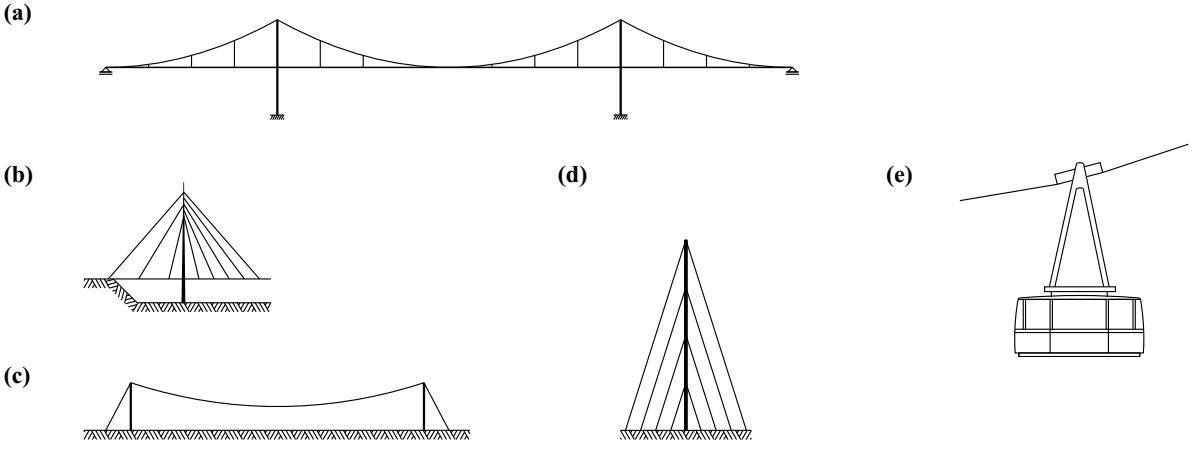

Fig. 18.54 Typical applications for cables: (a) suspension bridge, (b) cable-stayed bridge, (c) suspended roof, (d) guyed tower, (e) aerial ropeway

number depends on the cable configuration). Accordingly, the modulus of a cable is generally specified as the secant modulus between two stress values after a certain number of loading cycles. For steel cables this figure is about 100 kN/mm^2 for round stranded cables, 150 and 170 kN/mm^2 for open and fully locked spiral cables respectively, and 190 and 200 kN/mm^2 for parallel-strand and parallel-wire bundles respectively.

18.8.2 Analytical model

When dealing with cables, it is not primarily their strength that concerns us, but rather their stiffness, or rather their deformations. The equilibrium conditions must be formulated for the deformed system. We must therefore depart from the realm of linear statics. However, cable problems are related to other problems in this chapter and so will be investigated here and not in part IV of this book (Non-linear analysis of framed structures).

18.8.2.1 Vertical loads

Let us consider a flexible cable spanning between points O and A as shown in Fig. 18.55(a) The cable has a constant axial stiffness ($EI \longrightarrow 0$, EA = const), an *initial length* L, and carries a vertical line load q.

From Fig. 18.55(b) it follows that with

$$\mathrm{d}s = \sqrt{\mathrm{d}x^2 + \mathrm{d}z^2} = \mathrm{d}x\sqrt{1 + z'^2}$$

and the equilibrium conditions

$$\mathrm{d}H = 0 \quad , \quad q\mathrm{d}x + \mathrm{d}V = 0 \quad , \quad H\mathrm{d}z - V\mathrm{d}x = 0$$

we get the conditions

$$H = \text{ const} \quad , \quad V = Hz' \quad , \quad -Hz'' = q \tag{18.104}$$

and the *cable force* is

$$S = \sqrt{H^2 + V^2} = H\sqrt{1 + z'^2} \tag{18.105}$$

The length of the cable in the deformed state is given by the *cable equation*

$$\int_0^l \sqrt{1 + z'^2}\mathrm{d}x = L\left(1 + \alpha_T T - \frac{\sigma_0}{E}\right) + \int_0^l \frac{S\sqrt{1 + z'^2}}{EA}\mathrm{d}x \tag{18.106}$$

which apart from the elastic strains $S/(EA)$ generally also includes thermal deformations and a prestress σ_0 of the cable in the calculation.

The following applies for the second term on the right in (18.106):

$$\int_0^l \frac{S\sqrt{1 + z'^2}}{EA}\mathrm{d}x = \frac{H}{EA}\int_0^l (1 + z'^2)\mathrm{d}x = \frac{Hl}{EA} + \frac{H}{EA}\int_0^l (\tan\alpha + \overline{V}/H)^2\mathrm{d}x \tag{18.107}$$

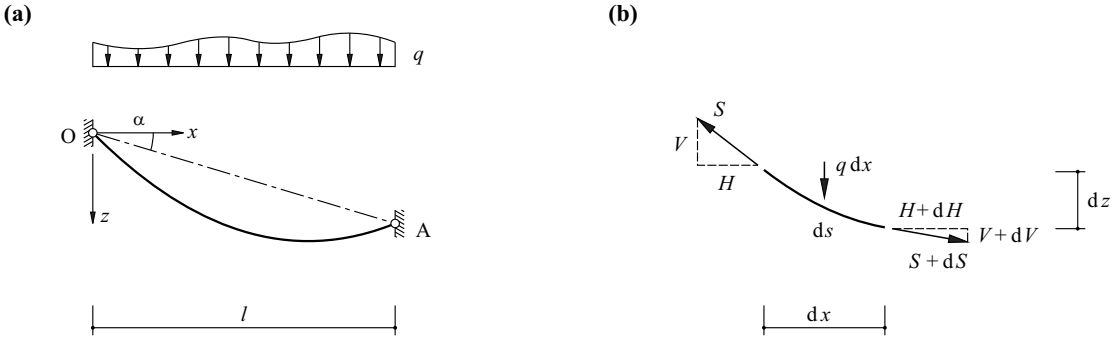

Fig. 18.55 Cables: (a) diagram of static system, (b) cable element

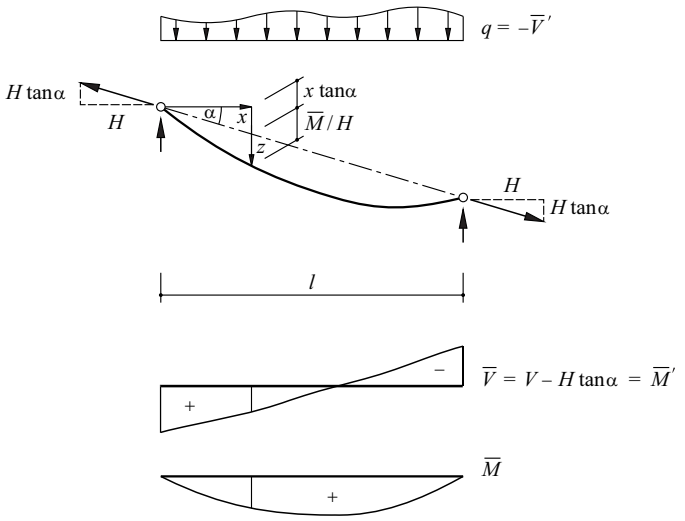

Fig. 18.56 Equivalent stress resultants for a simply supported beam

where $\overline{V}$ designates the shear force occurring in a simply supported beam of length l as a result of q, see Fig. 18.56. Applying the associated moments $\overline{M}$, it follows that

$$z = \frac{\overline{M}}{H} + x\tan\alpha \quad , \quad z' = \frac{\overline{V}}{H} + \tan\alpha \quad , \quad z'' = -\frac{q}{H} \tag{18.108}$$

Numerical values for the *horizontal tension* H and the *cable curve* $z(x)$ can be calculated iteratively from (18.106) and $(18.108)_1$. Starting with an estimate for H, it is possible to determine z and z' according to (18.108), and we can use (18.107) to check whether condition (18.106) has been satisfied. If the result does not achieve the required accuracy, we repeat the calculation with a better initial estimate for H.

The initial length L is often not given, instead, for example, has to be determined in such a way that a certain *cable sag* (maximum sag with respect to the chord of the cable) is not exceeded for given actions. These problems, too, can be solved iteratively on the basis of equations (18.106) and (18.108). In doing so, we vary L and σ_0 until the required cable sag has been reached.

18.8.2.2 Vertical and horizontal loads

The two cable force components V and H vary for combined vertical and horizontal loads. Eq. $(18.105)_1$ and (18.106) continue to apply, but the following is new

$$H = -\overline{\overline{V}} + S_s\cos\alpha \quad , \quad V = \overline{V} + S_s\sin\alpha \tag{18.109}$$

where S_s = force in direction of cable chord, see Fig. 18.57. Instead of $(18.108)_1$, the following applies:

$$\overline{M} + \overline{\overline{M}} - S_s(z\cos\alpha - x\sin\alpha) = 0 \tag{18.110}$$

The iteration begins with an initial value for S_s, and we use (18.110) to get the associated cable curve. Therefore, we can use $(18.105)_1$ and (18.109) to check that the cable equation (18.106) has been satisfied. By correcting S_s and repeating the calculation until we stop the iteration, we get the final value of S_s. Applying (18.109) gives us the cable force components H and V, (18.110) gives us the cable curve and $(18.105)_1$ the cable force diagram.

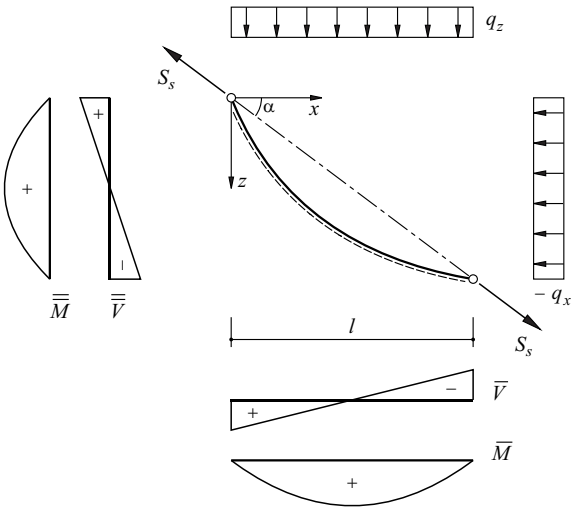

Fig. 18.57 Combined loading

18.8.3 Inextensible cables

It is often sufficient to consider inextensible cables that are tensioned in their chord direction by a force $S_s = H/\cos\alpha$. Subjected to vertical loads, such cables take on the form described by $(18.108)_1$. The cable equation (18.106) is unnecessary.

Fig. 18.58 shows three simple examples. The cable sags given in the figure correspond to the maximum moments $\overline{M}$ of $q_0 l^2/8$, $9q_0 l^2/128$ and $Qa(1 - a/l)$.

Subjected to its self-weight, the cable takes on the form of a *catenary*. When γ_s designates the unit weight of the cable, then

$$q = \frac{\gamma_s A \, \mathrm{d}s}{\mathrm{d}x} = \gamma_s A \sqrt{1 + z'^2}$$

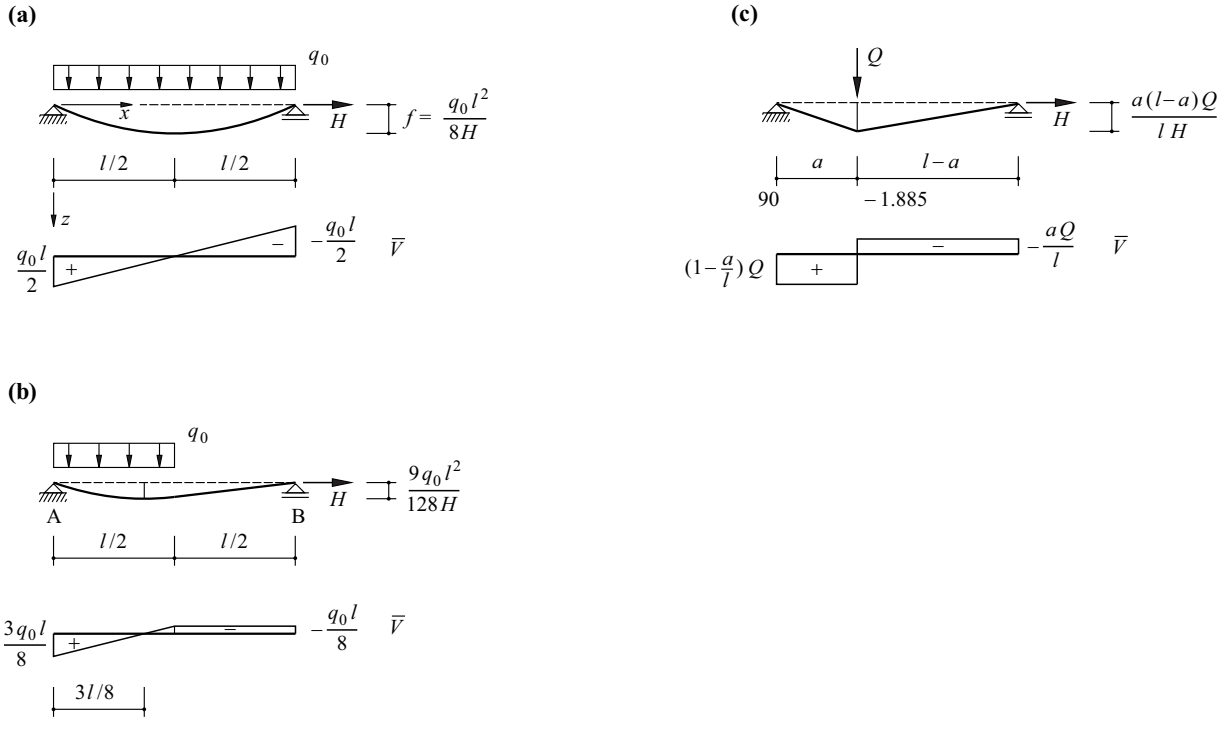

Fig. 18.58 Inextensible cables: (a) uniformly distributed load, (b) asymmetric line load, (c) point load

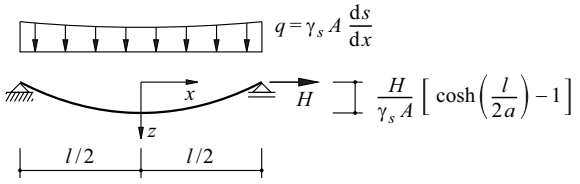

Fig. 18.59 Cable subjected to self-weight

and we get the coordinates

$$z = a\left[\cosh\left(\frac{l}{2a}\right) - \cosh\left(\frac{x}{a}\right)\right] \qquad \left(a = \frac{H}{\gamma_s A}\right)$$

entered in Fig. 18.59.

With a relatively small sag, the catenary deviates only marginally from a quadratic parabola. Putting $q_0 = \gamma_s A$ and $f = l/8$ results in, for example, according to Fig. 18.58(a), a horizontal tension $H = \gamma_s Al$. This horizontal tension, with the catenary ($a = l$), results in a cable sag of

$$l\,[\cosh(1/2) - 1] = 0.1276\,l \approx l/8$$

In an aerial ropeway system, the track cable often passes around a pulley at one end and is loaded with a weight G, see Fig. 18.60. Taking a cable force $S = G$ and a vertical component $V = -q_0 l/2$ at the pulley, the result according to $(18.105)_1$ is

$$H = \sqrt{G^2 - (q_0 l/2)^2}$$

and therefore

$$f = \frac{q_0 l^2}{8G\sqrt{1 - \left(\frac{q_0 l}{2G}\right)^2}}$$

In the case of taut cables with $f \ll l$, a valid approximation is $H \approx S \approx G = \text{const.}$

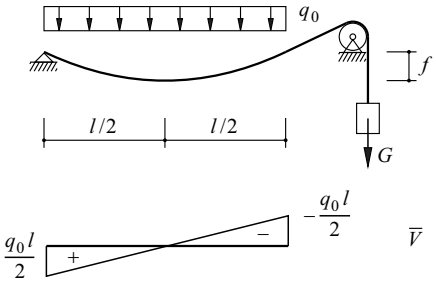

Fig. 18.60 Track cable for aerial ropeway

18.8.4 Extensible cables

Generally, $L > l/\cos\alpha$ applies for the initial lengths of cables and their axial stiffness is finite. The cable equation (18.106) must be used to analyse their structural behaviour.

18.8.4.1 Uniformly distributed load

The integrals in (18.106) can be expressed analytically for vertical loads q constant segment by segment. For example, the cable equation for a horizontal cable subjected to a uniformly distributed load $q = q_0$ is

$$\frac{l}{2}\left[\sqrt{1+\beta^2} + \frac{\ln\left(\beta + \sqrt{1+\beta^2}\right)}{\beta}\right] = L\left(1 + \alpha_T T - \frac{\sigma_0}{E}\right) + \frac{q_0 l^2}{2EA\beta}\left(1 + \frac{\beta^2}{3}\right) \tag{18.111}$$

where $\beta = 4f/l$ and f is the cable sag. The cable curve is a quadratic parabola and the horizontal tension is given by $H = q_0 l^2/(8f)$.

It is often convenient to express the term on the left in (18.111) with the power series

$$l\left(1 + \frac{\beta^2}{6} - \frac{\beta^4}{40} + \frac{\beta^6}{112} - \frac{5\beta^8}{1152} + \ldots\right)$$

Example 18.20 Single strand – uniformly distributed load
A single strand ($A = 100\,\text{mm}^2$, $E = 195\,\text{kN/mm}^2$, $L = 40.5\,\text{m}$) spans horizontally over a distance $l = 40\,\text{m}$ and is loaded by the uniformly distributed load $q_0 = 1.5\,\text{kN/m}$. Eq. (18.111) results in $f = 3.255\,\text{m}$ and therefore we get $H = 92.2\,\text{kN}$.

Example 18.21 Single strand – thermal action
The task is to calculate the initial length L of the single strand ($\alpha_T = 10^{-5}/°\text{C}$) considered in example 18.20 such that when subjected to a load $q_0 = 1\,\text{kN/m}$ and $T = 40\,°\text{C}$, a cable sag of $f = 3\,\text{m}$ is achieved. We can use (18.111) to find $L = 40.435\,\text{m}$.

Example 18.22 Single strand – prestress
The single strand of example 18.20 should exhibit a cable sag of $f = 1\,\text{m}$ when subjected to a load $q_0 = 0.2\,\text{kN/m}$. Taking $\beta = 0.1$ and $L = l$, it is possible to achieve this by using (18.111) when the strand is prestressed to $\sigma_0 = 76.8\,\text{N/mm}^2$ (i. e. a force of 7.68 kN):

$$40.0666 = 40 \cdot \left(1 - \frac{76.8}{195000}\right) + \frac{0.2 \cdot 40^2 \left(1 + \dfrac{0.01}{3}\right)}{2 \cdot 195 \cdot 100 \cdot 0.1}$$

Subjected to q_0, a horizontal tension $H = 40\,\text{kN}$ is established.

18.8.4.2 Constant loads on both halves of the span

Fig. 18.61(a) shows a cable carrying loads of q_1 and κq_1 on the two halves of its span ($0 < \kappa \leq 1$). For this case we get the cable equation

$$\sum_{i=1}^{4} a_i \left[\sqrt{1+\beta_i^2} + \frac{1}{\beta_i} \ln\left(\beta_i + \sqrt{1+\beta_i^2}\right)\right] = L\left(1 + \alpha_T T - \frac{\sigma_0}{E}\right) + \frac{Hl}{EA} + \frac{q_1^2 l^3}{192EAH}(5 + 6\kappa + 5\kappa^2) \tag{18.112}$$

which is similar to (18.111), where

$$a_1 = (3+\kappa)l/16 \quad , \quad a_2 = (1-\kappa)l/16 \quad , \quad a_3 = (3+1/\kappa)l/16 \quad , \quad a_4 = (1-1/\kappa)l/16$$

$$\beta_1 = (3+\kappa)\frac{q_1 l}{8H} \quad , \quad \beta_2 = (1-\kappa)\frac{q_1 l}{8H} \quad , \quad \beta_3 = (1+3\kappa)\frac{q_1 l}{8H} \quad , \quad \beta_4 = (1-\kappa)\frac{q_1 l}{8H}$$

The cable sag

$$f = \frac{(3+\kappa)^2 q_1 l^2}{128H}$$

occurs at a distance of $l(1 - \kappa)/8$ from the middle of the cable.

Owing to the greater load on the left half of the span, the points on the cable between the ends of the cable shift to the left. This can be prevented, for example, by providing a guy cable DBE, see Fig. 18.61(b), which is connected to the middle of cable ABC at point B and prestressed with a certain force P_0. With respect to the asymmetric load, point B functions like a fixed point. Differential forces $\pm \Delta P$ build up in the guy cable and a kink forms in the cable curve at B.

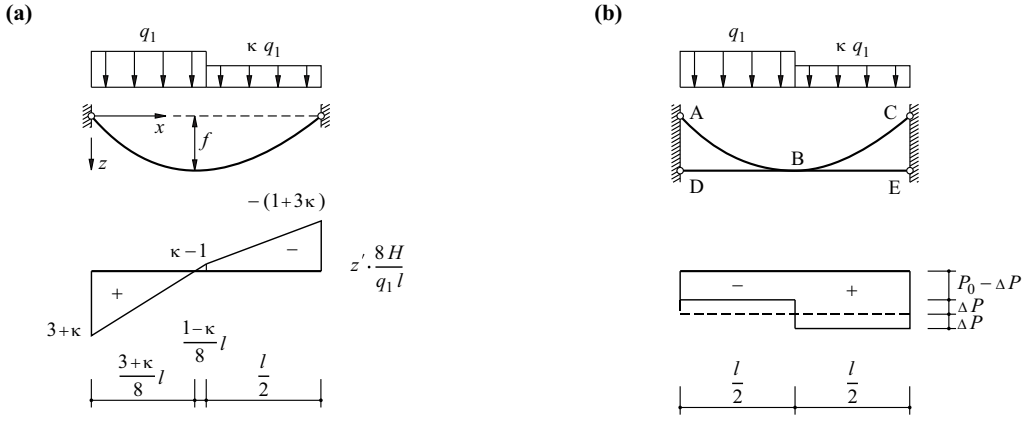

Fig. 18.61 Cable with constant loads on the two halves of its span (a) uninhibited deformation, (b) effect of a guy cable

Example 18.22 Single strand – constant loads on both halves of the span

The single strand examined in example 18.20 is loaded by $q_1 = 2\,\text{kN/m}$ and $\kappa q_1 = 1\,\text{kN/m}$ on the two halves of its span. Eq. (18.112) results in a horizontal tension of $H = 93.2\,\text{kN}$, and therefore the resulting cable sag is $f = 3.286\,\text{m}$ at a distance of 2.5 m from the middle of the cable.

Compared with example 18.20 with the same (albeit uniformly distributed) total load of 60 kN, the result is slightly higher values for f and H.

18.8.5 Axial stiffness of laterally loaded cables

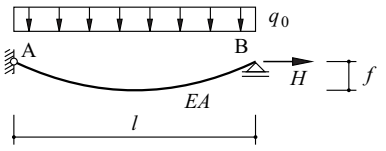

Fig. 18.62 How a lateral load affects the axial stiffness

If the cable shown in Fig. 18.62, which carries no lateral load ($q_0 = 0$), is subjected to an increase in horizontal tension H amounting to dH, the sliding support B is displaced by d$Hl/(EA)$ to the right. Loading the cable with the uniformly distributed load q_0 causes a cable sag of $f = q_0 l^2/(8H)$, see Fig. 18.58(a). The support displacement now established for an increment dH can be estimated with the help of the cable equation (18.111). If in the power series of the expression on the left in this equation we confine ourselves to the first two terms and neglect the term $\beta^2/3$ in the brackets in the second term on the right, which is generally small compared with 1, then differentiating with respect to H for the resulting expressions results in the displacement

$$\mathrm{d}H\left(\frac{l}{EA} + \frac{q_0^2 l^3}{12H^3}\right)$$

Accordingly, compared with the value EA without the effect of the lateral loading, the axial stiffness is reduced to the value

$$\frac{EA}{1 + \dfrac{q_0^2 l^2 EA}{12H^3}} \qquad (18.113)_1$$

In the case of a cable at an angle α to the horizontal with total weight G, eq. $(18.113)_1$ must be replaced by

$$\frac{EA}{1 + \dfrac{G^2 \cos^2\alpha EA}{12S_s^3}} \qquad (18.113)_2$$

where S_s = force in direction of cable chord.

The relationship $(18.113)_1$ can also be obtained through an energy approach. The cable sag changes as a result of dH by an amount $\mathrm{d}f = -q_0 l^2 \mathrm{d}H/(8H^2)$, i. e. the loads q_0 are raised on average by 2/3 of the amount of this value because of the parabolic cable curve, and the potential energy is increased by

$$q_0 l \cdot \frac{2}{3} \cdot \frac{q_0 l^2 \mathrm{d}H}{8H^2} = \frac{q_0^2 l^3 \mathrm{d}H}{12H^2}$$

By contrast, the energy stored elastically in the cable is increased by

$$H \cdot \frac{\mathrm{d}H\, l}{EA}$$

The sum of these two terms is equal to the work done by forc H on the displacement of support B, which brings us back to $(18.113)_1$ again.

18.8.6 Summary

1. This section is limited to flexible cables with a constant axial stiffness lying in one plane.
2. The cable curve is generally calculated iteratively from the cable equation (18.106) and – for vertical, or rather general loads – from the moment-balance equations $(18.108)_1$ or (18.110).
3. It is often sufficient to consider an inextensible cable. The cable curve then results from the pure equilibrium conditions.
4. The integral expressions in the cable equation (18.106) can be specified analytically for vertical loads constant segment by segment.

5. The cable equations for horizontal cables subjected to uniformly distributed loads or loads constant over half the span are (18.111) or (18.112) respectively.
6. A lateral load reduces the axial stiffness of a cable. This is particularly the case with long cables and cables that are not pulled especially taut, see (18.113).

18.9 Combined cable-type and bending response

18.9.1 Analytical model

In a similar way to the differential equation (18.82) for an arch, combining (18.39) and $(18.104)_3$ gives us the differential equation

$$EIw'''' - (H + \Delta H)(z + w)'' = g + q \tag{18.114}$$

where z is the cable curve and H the horizontal tension due to permanent loads g, and w and ΔH, on the other hand, the deflections and the change in the horizontal tension respectively as a result of the variable loads q. If we assume that the permanent loads are carried solely by a cable-type response, i. e. $g = -Hz''$, we get the differential equation

$$EIw'''' - (H + \Delta H)w'' = q - g\frac{\Delta H}{H} \tag{18.115}$$

which is similar to (18.56) and has the general solution

$$w = c_1 + c_2 x + c_3 \cosh(\lambda x) + c_4 \sinh(\lambda x) + w_{\text{part}} \qquad \left(\lambda^2 = \frac{H + \Delta H}{EI}\right) \tag{18.116}_1$$

or

$$w = C_1 + C_2 x + C_3 e^{\lambda x} + C_4 e^{-\lambda x} + w_{\text{part}} \qquad \left(\lambda^2 = \frac{H + \Delta H}{EI}\right) \tag{18.116}_2$$

In order to determine ΔH, we consider (18.83) again (not forgetting to change the sign of H, or rather ΔH) and stipulate

$$\int_0^l w'z' \,\mathrm{d}x = \frac{\Delta H l}{EA}$$

Integration by parts when considering $w(0) = w(l) = 0$ and $z'' = -8f/l^2$ results in

$$\int_0^l w'z' \,\mathrm{d}x = w\,z'\Big|_0^l - \int_0^l w\,z'' \,\mathrm{d}x = \frac{8f}{l^2}\int_0^l w \,\mathrm{d}x$$

and therefore

$$\Delta H = \frac{8fEA}{l^3}\int_0^l w \,\mathrm{d}x \tag{18.117}$$

see (18.86). The assumption $z'' = -8f/l^2$ corresponds to a parabolic cable curve with a cable sag f when subjected to g = const.

The values of w and ΔH can be determined with (18.115) and (18.117). We generally proceed iteratively by estimating ΔH first of all and then improving it with the solution to (18.115) and the help of (18.117).

Differential equation (18.115) covers the entire spectrum from a bending response only ($\lambda = 0$) to beam in bending with tensile force and bending-resistant ties right up to a cable-type response ($\lambda \to \infty$).

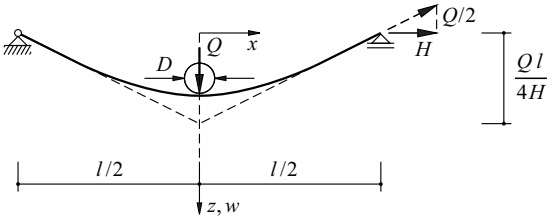

Fig. 18.63 Cable with wheel load

18.9.2 Bending-resistant ties

18.9.2.1 Cable with wheel load

Using $(18.116)_2$ for the case shown in Fig. 18.63, with $\Delta H = 0$ and the conditions

$$w(l/2) = 0 \quad , \quad w'(0) = 0 \quad , \quad -EIw''(l/2) = 0 \quad , \quad -EIw'''(0) = -Q/2$$

results in the relationships

$$w = \frac{Ql}{4H}\left(1 - \frac{2x}{l}\right) - \frac{Q(e^{-\lambda x} - e^{-\lambda l}\cdot e^{\lambda x})}{2H\lambda(1 + e^{-\lambda l})} \quad , \quad M = \frac{Q(e^{-\lambda x} - e^{-\lambda l}\cdot e^{\lambda x})}{2\lambda(1 + e^{-\lambda l})} \qquad \left(\lambda^2 = \frac{H}{EI}\right) \tag{18.118}$$

The first term on the right in $(18.118)_1$ describes the deflection of the cable without bending stiffness. The second term is approximated very well with $-Qe^{-\lambda x}/(2H\lambda)$. The maximum bending moment at $x = 0$ according to $(18.118)_2$ is approximated very well by $Q/(2\lambda)$. The radius of curvature of the cable at $x = 0$ is roughly

$$R = \frac{2\lambda EI}{Q} = \frac{2H}{\lambda Q} \tag{18.119}$$

We shall assume that the diameter of the wheel is $D < 2R$.

Example 18.24 Cable with wheel load

A cable with a circular solid section (diameter $d = 30\,\text{mm}$, $l = 120\,\text{m}$, $E = 200\,\text{kN/mm}^2$) is tensioned with $H = 300\,\text{kN}$ and loaded with $Q = 10\,\text{kN}$. Putting $I = d^4\pi/64 = 39\,761\,\text{mm}^4$ results in $\lambda^{-1} = 162.81\,\text{mm}$ and therefore (18.119) gives us $R = 9.77\,\text{m}$, and (18.118) the values $w(0) = 997\,\text{mm}$ and $M(0) = 814\,\text{Nm}$. The normal stresses of $300\,000/(30^2 \cdot \pi/4) = 424\,\text{N/mm}^2$ as a result of H are joined by extreme fibre stresses of $(814\,000/39\,761)\cdot 15 = 307\,\text{N/mm}^2$ due to bending under the wheel load Q.

18.9.2.2 Bending of stay cables

A stay cable at an angle α to the horizontal has the inclined length b and is loaded by the normal force N, see Fig. 18.64(a). The anchorage at A (rotated through φ_0 with respect to the chord x) acts as a fixed support. The self-weight g [kN/m] of the cable

(a)

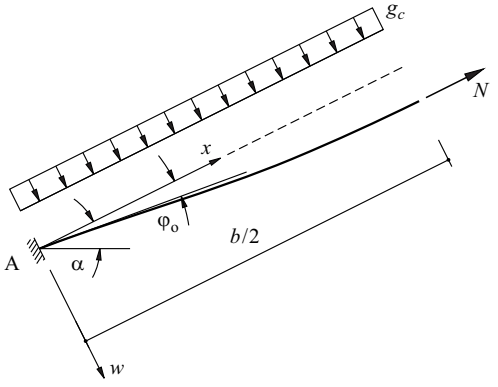

(b)

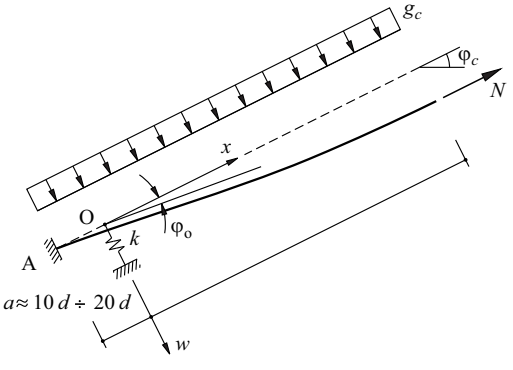

Fig. 18.64 Stay cable: (a) diagram of static system, (b) elastic support

corresponds to line loads $g_c = g\cos\alpha$ transverse to the direction of the cable, which can lead to considerable bending stresses in the region of the anchorage.

Taking the boundary conditions $w(0) = 0$, $w'(0) = \varphi_0$, $w'(b/2) = 0$ and $w'''(b/2) = 0$, eq. $(18.116)_1$ gives us

$$w = \frac{g_c x(b-x)}{2N} + \left(\frac{\varphi_0}{\lambda} - \frac{g_c b}{2N\lambda}\right) \cdot \left[\sinh(\lambda x) - \frac{\cosh(\lambda x) - 1}{\tanh(\lambda b/2)}\right] \qquad \left(\lambda^2 = \frac{N}{EI}\right) \tag{18.120}$$

and therefore

$$M = -EIw'' = \frac{g_c}{\lambda^2} + \left(\varphi_0 - \frac{g_c b}{2N}\right)\sqrt{NEI} \cdot \frac{\cosh[\lambda(b/2 - x)]}{\sinh(\lambda b/2)} \tag{18.121}$$

The first term on the right in (18.121) can be neglected with respect to the second because $\lambda b/2 \gg 1$. With a cable of diameter d ($A = d^2\pi/4$, $I = d^4\pi/64$), the extreme fibre bending stresses at $x = 0$ are therefore

$$\left|\varphi_0 - \frac{g_c b}{2N}\right| \cdot \sqrt{\frac{NE}{I}} \cdot \frac{d}{2} = 2\sqrt{E\sigma} \cdot \left|\varphi_0 - \frac{g_c b}{2N}\right| \tag{18.122}$$

where $\sigma = N/A$.

It is expedient to select the prior rotation φ_0 in such a way that the bending stresses due to permanent actions G disappear, i. e. $\varphi_0 = g_c b/(2A\sigma_G)$, where σ_G = normal stress in cable due to G. Variable actions Q together with G lead to normal stresses σ_{G+Q} and therefore to bending stress differences of

$$\Delta\sigma_b = \frac{g_c b\sqrt{E\sigma_{G+Q}}}{A}\left(\frac{1}{\sigma_G} - \frac{1}{\sigma_{G+Q}}\right) \tag{18.123}$$

Example 18.25 Stresses in stay cable

Taking a stay cable with $b = 200\,\text{m}$, $g_c/A = 90\,\text{kN/m}^3$, $E = 200\,\text{kN/mm}^2$, $\sigma_G = 540\,\text{N/mm}^2$ and $\sigma_{G+Q} = 720\,\text{kN/mm}^2$, the result with a prior rotation of $\varphi_0 = 90 \cdot 200/(2 \cdot 540) = 16.7\,\text{mrad}$ when using (18.123) is $\Delta\sigma_b = 100\,\text{N/mm}^2$. The stress difference $\sigma_{G+Q} - \sigma_G = 180\,\text{N/mm}^2$ is increased by $\Delta\sigma_b$ to $280\,\text{N/mm}^2$.

Apart from the variation in the normal force N, the effects of wind on the cable plus rotations of the beam to which the cable is connected at A lead to bending stresses in the cable. Such effects can be taken into account by way of an additional rotation in the expression between the absolute value signs in (18.122). On the whole, the stress differences that occur can have a considerable fatigue effect. To reduce this effect, it is possible to arrange an elastic support for the cable at a distance a = approx. $10d$ to $20d$ from the anchorage, for instance, see Fig. 18.64(b). The stiffness k of the translational spring in such an arrangement should lie in the region of about $Ed/1000$ to $Ed/10\,000$.

18.9.3 Suspended roofs and stress ribbons

18.9.3.1 Uniformly distributed load

Applying $(18.116)_1$ to the case shown in Fig. 18.65, with the continuity and boundary conditions $w'(0) = w'''(0) = w(l/2) = w''(l/2) = 0$, results in the following deflection:

$$w = \frac{q - g\dfrac{\Delta H}{H}}{2(H + \Delta H)} \cdot \left[\frac{l^2}{4} - \frac{2}{\lambda^2} + \frac{2\cosh(\lambda x)}{\lambda^2\cosh(\lambda l/2)} - x^2\right] \tag{18.124}$$

and from (18.117) it follows that

$$\Delta H = \frac{q - g\dfrac{\Delta H}{H}}{2(H + \Delta H)} \cdot 16 f EA \cdot \left[\frac{1}{12} - \frac{1}{(\lambda l)^2} + \frac{2\tanh(\lambda l/2)}{(\lambda l)^3}\right] \tag{18.125}$$

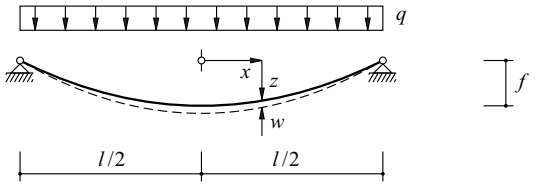

Fig. 18.65 Suspended roof subjected to uniformly distributed load

Example 18.26 Suspended roof – uniformly distributed load

A 200 mm deep concrete roof (g = 5 kN/m, EA = 6 GN and EI = 20 MNm^2 per metre width of roof) spans a distance of l = 100 m as a suspended roof with a sag of f = 10 m. The horizontal tension as a result of g amounts to $H = 5 \cdot 100^2/(8 \cdot 10) = 625$ kN per metre width of roof.

With q = 2 kN/m, eq. (18.125) results in ΔH = 249.3 kN and $\lambda = 0.209\,082\,\mathrm{m}^{-1}$. Eq. (18.124) leads to a deflection at mid-span of $w(0)$ = 7.8 mm.

If for simplicity we were to take $\Delta H = (q/g) \cdot H$ = 250 kN, then the result according to (18.124) would be $w \equiv 0$. The combination with (18.117) is more interesting. Assuming a parabolic deflection curve, then

$$\Delta H = \frac{8fEA}{l^3} \cdot \frac{2}{3} w(0) \cdot l$$

applies and therefore we get

$$w(0) = \frac{3\Delta H l^2}{16fEA} = \frac{3 \cdot 0.25 \cdot 100^2}{16 \cdot 10 \cdot 6 \cdot 10^3} = 0.0078\,\mathrm{m}$$

18.9.3.2 Asymmetric imposed load

The expressions

$$w_1 = c_1 + c_2 x + c_3 \cosh(\lambda x) + c_4 \sinh(\lambda x) - \frac{q - g\dfrac{\Delta H}{H}}{2(H + \Delta H)} x^2 \quad (-l/2 \le x \le 0)$$

$$w_2 = c_5 + c_6 x + c_7 \cosh(\lambda x) + c_8 \sinh(\lambda x) + \frac{g\dfrac{\Delta H}{H}}{2(H + \Delta H)} x^2 \quad (0 \le x \le l/2) \tag{18.126}$$

for the case shown in Fig. 18.66, with the boundary conditions

$$w_1(-l/2) = w_1''(-l/2) = w_2(l/2) = w_2''(l/2) = 0$$

and the continuity conditions

$$w_1(0) = w_2(0) \quad , \quad w_1'(0) = w_2'(0) \quad , \quad w_1''(0) = w_2''(0) \quad , \quad w_1'''(0) = w_2'''(0)$$

lead to

$$c_1 = \frac{\left(q - g\dfrac{\Delta H}{H}\right)\left(\dfrac{l^2}{8} - \dfrac{2}{\lambda^2}\right) - \dfrac{l^2}{8} g \dfrac{\Delta H}{H}}{2(H + \Delta H)} \quad , \quad c_2 = c_6 = \frac{-ql}{8(H + \Delta H)}$$

$$c_3 = \frac{q[\cosh(\lambda l/2) + 1] - 2g\dfrac{\Delta H}{H}}{2(H + \Delta H)\lambda^2 \cosh(\lambda l/2)} \quad , \quad c_4 = c_8 = \frac{q[\cosh(\lambda l/2) - 1]}{2(H + \Delta H)\lambda^2 \sinh(\lambda l/2)}$$

$$c_5 = \frac{\left(q - 2g\dfrac{\Delta H}{H}\right)\dfrac{l^2}{8} + \dfrac{2}{\lambda^2} g \dfrac{\Delta H}{H}}{2(H + \Delta H)} \quad , \quad c_7 = \frac{-q[\cosh(\lambda l/2) - 1] - 2g\dfrac{\Delta H}{H}}{2(H + \Delta H)\lambda^2 \cosh(\lambda l/2)}$$

and (18.117) gives us

$$\Delta H = \frac{\left(q - 2g\dfrac{\Delta H}{H}\right) fEA}{(H + \Delta H)} \cdot \left[\frac{1}{3} - \frac{4}{(\lambda l)^2} + \frac{8\tanh(\lambda l/2)}{(\lambda l)^3}\right] \tag{18.127}$$

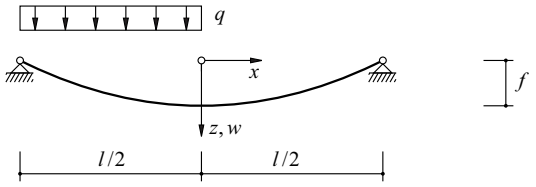

Fig. 18.66 Suspended roof subjected to an asymmetric imposed load

Example 18.27 Suspended roof – asymmetric imposed load

Loading the suspended roof shown in example 18.26 with $q = 2\,\text{kN/m}$ on one side only and using (18.127) results in $\Delta H = 124.7\,\text{kN}$ and $\lambda = 0.193\,610\,\text{m}^{-1}$. Applying (18.126) results in the deflection and bending moment diagrams shown in Fig. 18.67(a).

If we were to use the approximation $\Delta H = (q/g)\cdot H/2 = 125$ kN, then the result of (18.115) would be an asymmetric parabolic diagram for w with maximum/minimum values of

$$\pm\frac{ql^2}{64(H+\Delta H)} = \pm\frac{2\cdot 100^2}{64\cdot(625+125)} = \pm 0.4167\,\text{m}$$

and (18.127) would result in $\Delta H = 0$. The radius of curvature $1/\chi$ of $25^2/(2\cdot 0.4167) = 750\,\text{m}$ would then correspond to constant moments of $EI\chi = 20\,000/750 = 26.7\,\text{kNm/m}$, see Fig. 18.67(b).

According to the approximate solution, the bending moments due to an asymmetric imposed load already analysed in example 5.7 (maximum/minimum values of $ql^2/64$ at the quarter-points of the span l) are resisted by a corresponding deformation of the roof entirely by way of a cable-type response. The constant moments are a side-effect; they infringe the static boundary and continuity conditions, but agree well with the maximum/minimum values of the moments according to the exact solution.

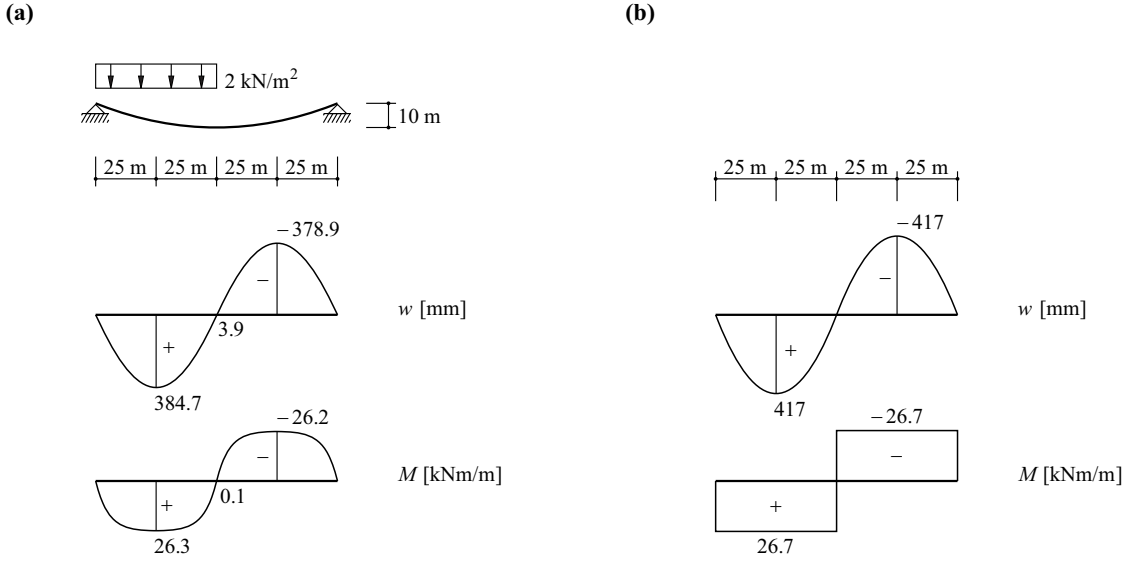

Fig. 18.67 Suspended roof subjected to an asymmetric imposed load: (a) exact solution, (b) approximate solution

Example 18.28 Stress ribbon – asymmetric imposed load

The approximate solution discussed in example 18.27 is less accurate for shallow stress ribbons. To illustrate this fact, let us consider the 300 mm thick stress ribbon of Fig. 18.68 ($g = 7.5\,\text{kN/m}$, $EA = 9\,\text{GN}$, $EI = 67.5\,\text{MNm}^2$ per metre width of ribbon), which spans a distance of $l = 50\,\text{m}$ with a sag of $f = 0.75\,\text{m}$ and has to carry an asymmetric load $q = 4\,\text{kN/m}$. The horizontal tension as a result of g amounts to $H = 7.5\cdot 50^2/(8\cdot 0.75) = 3125\,\text{kN}$ per metre width of ribbon.

The approximation $\Delta H = (4/7.5)\cdot 3125/2 = 833.3\,\text{kN}$ results in deflections at the quarter-points amounting to $\pm 4\cdot 50^2/[64(3125 + 833.3)] = \pm 39.5\,\text{mm}$. The corresponding moments are $\pm 67\,500\cdot 2\cdot 0.0395/(12.5)^2 = \pm 34.1\,\text{kNm/m}$.

Eq. (18.127) results in $\Delta H = 607.2\,\text{kN}$ and $\lambda = 0.235\,142\,\text{m}^{-1}$. The w and M diagrams resulting from (18.126) are shown in Fig. 18.68.

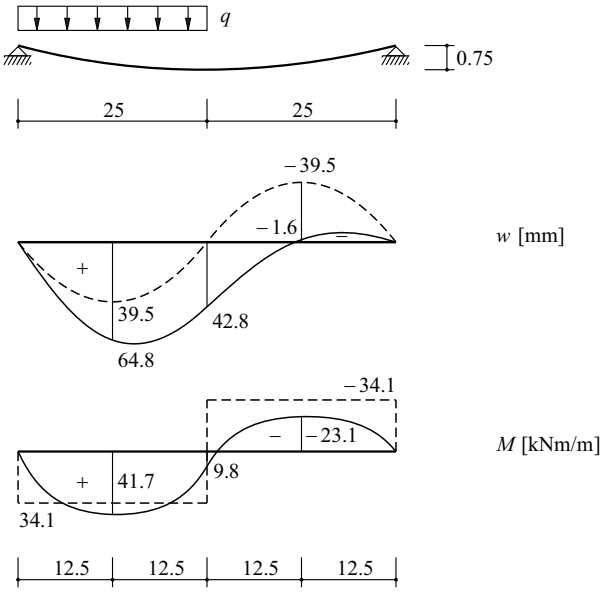

Fig. 18.68 Stress ribbon subjected to an asymmetric imposed load

18.9.3.3 Central point load

Eq. $(18.116)_1$ with the particular solution

$$w_{\text{part}} = \frac{\Delta H g x^2}{2H(H + \Delta H)} \tag{18.128}$$

applies for the case of a central point load Q as shown in Fig. 18.69(a). Using the boundary and continuity conditions

$$w(l/2) = w''(l/2) = w'(0) = 0 \quad , \quad -EIw'''(0) = -Q/2$$

(a)

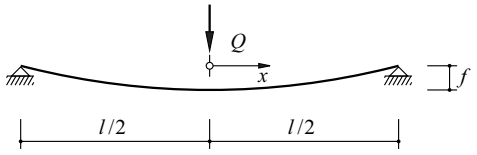

(b)

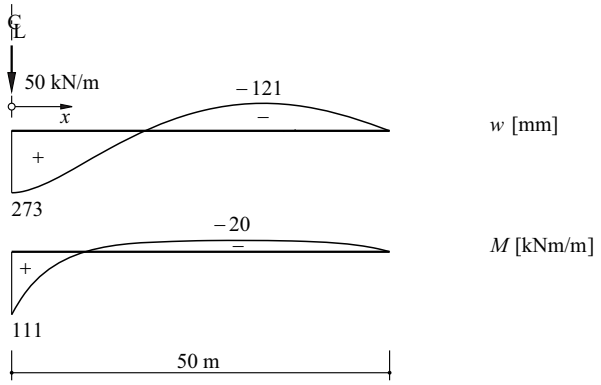

Fig. 18.69 Suspended roof with central point load: (a) diagram of static system, (b) deflections and bending moments for example 18.29

we get the constants

$$c_1 = \frac{\frac{Ql}{4} - g\frac{\Delta H}{H}\left(\frac{l^2}{8} - \frac{1}{\lambda^2}\right)}{2(H + \Delta H)} \quad , \quad c_2 = \frac{-Q}{2(H + \Delta H)}$$

$$c_3 = -\frac{\frac{Q}{2\lambda}\sinh(\lambda l/2) + \frac{g}{\lambda^2}\frac{\Delta H}{H}}{(H + \Delta H)\cosh(\lambda l/2)} \quad , \quad c_4 = \frac{Q}{2\lambda(H + \Delta H)}$$

and from (18.117) it follows that

$$\Delta H = \frac{16 f EA}{(H + \Delta H)} \cdot \left\{ \frac{Q}{l}\left[\frac{1}{16} - \frac{1}{2(\lambda l)^2} + \frac{1}{2(\lambda l)^2\cosh(\lambda l/2)}\right] - g\frac{\Delta H}{H}\left[\frac{1}{24} - \frac{1}{2(\lambda l)^2} + \frac{\tanh(\lambda l/2)}{(\lambda l)^3}\right]\right\} \tag{18.129}$$

Example 18.29 Suspended roof – central point load

Applying (18.129) to the suspended roof of example 18.26, with $H = 625\,\text{kN}$ and a central point load $Q = 50\,\text{kN}$ per metre width of roof, results in $\Delta H = 94.3\,\text{kN}$ and $\lambda = 0.1668\,\text{m}^{-1}$. The deflections and associated bending moments calculated with $(18.116)_1$ and (18.128) are shown in Fig. 18.69(b). The peak moment occurring beneath Q has a parabolic rounding when Q is introduced distributed over a finite width.

According to the FOURIER series development for the expression on the left in (18.111), a relative displacement of the two ends of the cable amounting to about $16f\delta/(3l)$ corresponds to a virtual increase δ in the sag f for an unstressed cable. According to the principle of virtual deformations, the following applies for the individual actions g and Q:

$$gl \cdot \frac{2\delta}{3} - H \cdot \frac{16 f\,\delta}{3l} = 0 \quad , \quad Q \cdot \delta - \Delta H \cdot \frac{16 f\,\delta}{3l} = 0$$

and therefore we get the approximation

$$\Delta H \approx H \cdot \frac{3Q}{2gl} = \frac{3Ql}{16f} = \frac{3 \cdot 50 \cdot 100}{16 \cdot 10} = 93.75\,\text{kN}$$

18.9.3.4 Thermal action and prestress

We can see from the series development for the expression on the left in (18.111) that the cable sag as a result of thermal action and prestress changes approximately by the amount

$$\mathrm{d}f \approx \frac{3l^2}{16f}\left(\alpha_T T - \frac{\sigma_0}{E}\right) \tag{18.130}$$

Example 18.30 Stress ribbon – thermal action

The stress ribbon examined in example 18.28 reacts very sensitively to changes in temperature. Putting $l = 50\,\text{m}$, $f = 0.75\,\text{m}$, $\alpha_T = 10^{-5}/°\text{C}$ and $T = 20\,°\text{C}$, then (18.130) results in $\mathrm{d}f = 125\,\text{mm}$. In the suspended roof of example 18.26 ($l = 100\,\text{m}$, $f = 10\,\text{m}$), the same thermal action would cause a change in the cable sag of only 37.5 mm.

The prestress as well as the creep and shrinkage of the concrete reduce the sag of the stress ribbon according to (18.130). The corresponding deformations must be considered carefully for the construction stage in order to achieve the desired final situation. If this stress ribbon were to be built on falsework, this would need to have, for example, a sag at mid-span amounting to about 1 m (assuming a strain of 0.4‰) in order to achieve the desired value of $f = 0.75\,\text{m}$ in the final condition.

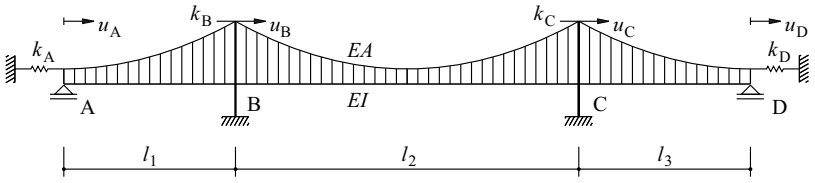

Fig. 18.70 Suspension bridge

18.9.4 Suspension bridges

We should generally assume the cable equation (18.106) and also (18.114) for suspension bridges. The horizontal tension in the central span differs from that in the side spans depending on the stiffness of the pylons. In addition, the flexibility of the abutments must be considered. Using the notation of Fig. 18.70 and

$$u_A = \frac{\Delta H_1}{k_A} \quad , \quad u_B = \frac{\Delta H_2 - \Delta H_1}{k_B} \quad , \quad u_C = \frac{\Delta H_3 - \Delta H_2}{k_C} \quad , \quad u_D = -\frac{\Delta H_3}{k_D} \tag{18.131}$$

plus the changes Δl_i in the span lengths determined according to (18.106), the compatibility conditions are

$$\Delta l_1 + u_A - u_B = 0 \quad , \quad \Delta l_2 + u_B - u_C = 0 \quad , \quad \Delta l_3 + u_C - u_D = 0 \tag{18.132}$$

The calculation is carried out iteratively by successively improving ΔH_i, preferably by using existing spreadsheet programs or mathematics software.

Suspension bridges are normally built with vertical suspenders. Such bridges behave in a similar way to suspended roofs when carrying an asymmetric imposed load. Deflections and bending moments in the stiffening girder (deck beam) can be estimated with the approximate method discussed in example 18.27.

Suspension cable and deck beam are often connected together at mid-span, which achieves a similar stiffening effect to that of a guy cable, see Fig. 18.61(b).

Connecting the deck beam to the suspension cable via inclined suspenders, in a similar way to a WARREN truss without posts or a BROWN truss, can bring about a considerable stiffening effect. Provided no suspenders are relieved, the system functions like a trussed girder. Apart from the danger of suspenders being relieved, which can be dealt with by providing and prestressing an upward-curving guy cable if necessary, it is primarily the fatigue effects in the suspenders that must be considered.

18.9.5 Summary

1. The structural behaviour of systems with combined cable-type and bending response can generally be assessed with the differential equation (18.114) and the cable equation (18.106). As in section 18.8 (Cables), the non-linear behaviour means that the superposition law does not apply.
2. If permanent loads g are carried purely by cable action, (18.114) leads to the differential equation (18.115) for the deflections w due to the variable loads q. When g = const, the relationship (18.117) can be used instead of the cable equation (18.106).
3. Wheel loads Q on horizontal cables with a circular cross-section and a horizontal tension $H = A\sigma$ give rise to extreme fibre bending stresses amounting to $(Q/A)\sqrt{E/\sigma}$.
4. Considerable bending stresses can build up around the anchorages of stay cables. Providing an elastic support to the cable can reduce these stresses and hence improve the structural safety with respect to fatigue.
5. Closed solutions are given for various load cases on suspended roofs and stress ribbons.

6. The flexibilities of the abutments and the pylons influence the horizontal tension in the spans of a suspension bridge. Connecting suspension cables and deck beams at mid-span and providing inclined suspenders can make suspension bridge systems much stiffer; however, the fatigue effects associated with such a design must be given special attention.

18.10 Exercises

18.1 Two outer timber members (120×200 mm) are connected via 16 split-ring timber connectors Ø65 mm and 8 bolts Ø12 mm to a central timber member (180×200 mm) as shown in Fig. 18.71(a). Each connector has a stiffness of 12 kN/mm, and the modulus of elasticity of the timber is 11 kN/mm^2. Assume a continuous connection over a length $l = 600$ mm and determine the diagrams for the normal forces plus the displacements assuming a maximum slip of 1 mm.

18.2 Discuss the influence of lengthening the row of connectors in exercise 18.1 ($l = n \cdot 150$ mm) assuming all other factors remain unchanged.

18.3 Examine the behaviour of the system of Fig. 18.20(a) subjected to a trapezoidal distributed line load q.

18.4 A circular cast-in-place concrete pile (Ø = 1 m, $E_c = 32$ kN/mm^2) is loaded at the top by shear forces and moments as shown in Fig. 18.26(b). Using Fig. 18.33, calculate the corresponding translational and rotational spring stiffnesses at the level of the top of the pile. Vary the foundation modulus between 10 and 400 MN/m^2, and draw the diagrams for w, w', M and V along the axis of the pile.

18.5 Verify (18.80) and apply these expressions to example 18.14.

18.6 The arch of example 18.15 assumes a solid rectangular concrete cross-section (width $b = 8$ m, depth $h = 3$ m, $E = 30$ kN/mm^2, $\gamma_c = 25$ kN/m^3). Replace this cross-section by a resolved cross-section (e. g. hollow cross-section), take into account the saving in weight in q and H and repeat the considerations of example 18.17. Draw the stress profiles at the quarter-points of the span.

18.7 Replace the hinges at the springings in example 18.16 by fixed supports and discuss how this change to the structural system affects the structural response.

18.8 The pressurised steel water pipe ($E = 210$ kN/mm^2, $\nu = 0.3$) shown in Fig. 18.71(b) is made from 8 m long segments, riveted together via splices. Assuming a pressure head of 160 m, calculate the radial displacements and the bending moments along the axis of the pipe. What are the maximum stresses as a result of membrane and bending behaviour?

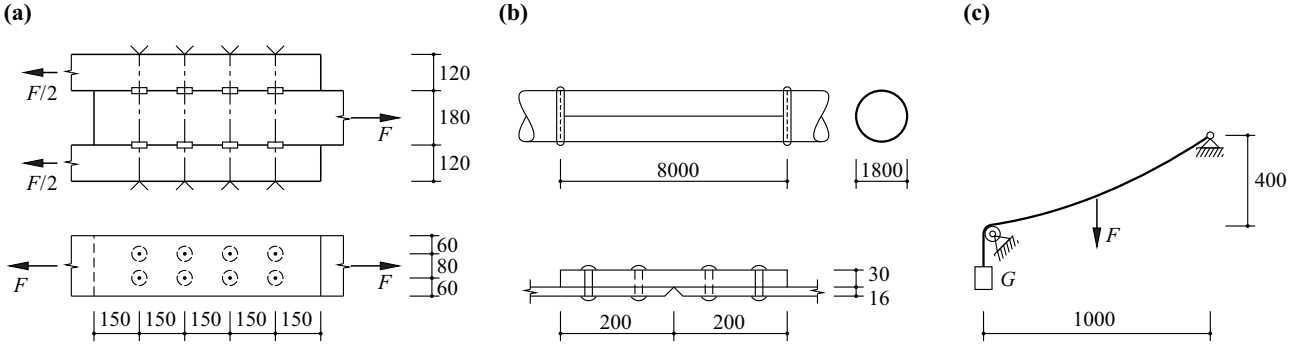

Fig. 18.71 Figures for section 18.10

18.9 An aerial ropeway according to Fig. 18.71(c) rises a vertical distance of 400 m and bridges a horizontal distance of 1000 m. The track cable (cross-sectional area $A = 2100\,\text{mm}^2$, self-weight $g = 0.162\,\text{kN/m}$, $E = 165\,\text{kN/mm}^2$) is tensioned in the lower station with a counterweight $G = 1.1\,\text{MN}$. Calculate the maximum sag of the track cable due to self-weight and the weight of the cabin $F = 200\,\text{kN}$. How is the counterweight displaced as the cabin travels? If displacement of the counterweight is prevented, what are the maximum sag values and the stress differences in the track cable during movement of the cabin?

18.10 Verify (18.111) and (18.112).

18.11 Select a suitable prestress for example 18.27 according to Fig. 18.61 and discuss its effect.

18.12 Use an existing example to select approximate dimensions for a suspension bridge and discuss the effect of inclined instead of vertical suspenders for an asymmetric imposed load. Ensure an adequate distance between suspension cable and deck beam at mid-span, compare the structural behaviour and discuss the consequences for the execution.

19 DISCRETISED MODELS

19.1 General

A basic scheme for discretised structural models (section 9.3) was introduced in Fig. 8.2. That scheme summarises the internal and external force and deformation variables plus the relationships between them.

The emphasis in the lower part of that figure, which corresponds to the displacement method, is that statically indeterminate and statically determinate systems are both dealt with in the same way. The kinematic transformation matrix $\boldsymbol{a}$ and the stiffness matrix $\boldsymbol{k}$ for all bar elements gives us the global stiffness matrix $\boldsymbol{K} = \boldsymbol{a}^{\mathrm{T}} \bullet \boldsymbol{k} \bullet \boldsymbol{a}$. And therefore we get the displacements $\boldsymbol{V} = \boldsymbol{K}^{-1} \bullet \boldsymbol{Q}$ corresponding to the loads $\boldsymbol{Q}$ plus the internal deformation and force variables $\boldsymbol{v} = \boldsymbol{a} \bullet \boldsymbol{V}$ and $\boldsymbol{s} = \boldsymbol{k} \bullet \boldsymbol{v}$.

This procedure was generalised in sections 17.1 to 17.3 by considering actions on bars (Fig. 17.1) and by using complete bar end variables and global coordinates. The actions on bars not contained in (8.6) cause the additional term $\boldsymbol{Q}_0$ on the right in (17.43). This and the global stiffness matrix $\boldsymbol{K}$ can be determined from the superposition of the fixed-end force vectors, or rather member stiffness matrices, related to the global coordinates.

According to the force method corresponding to the upper part of Fig. 8.2, statically determinate and statically indeterminate systems are approached in different ways. Determining the forces for statically determinate systems has been explained in sections 9.3 and 10.3. On the one hand, $\boldsymbol{g} = \boldsymbol{a}^{\mathrm{T}}$ applies for the equilibrium matrix $\boldsymbol{g}$ occurring in (9.2) with $\boldsymbol{Q} = \boldsymbol{g} \bullet \boldsymbol{s}$, i. e. it can be obtained from the kinematic transformation matrix $\boldsymbol{a}$ through transposition; on the other hand, $\boldsymbol{g}$ is the inverse of the static transformation matrix $\boldsymbol{b}$: $\boldsymbol{b} = \boldsymbol{g}^{-1}$.

In systems with n degrees of static indeterminacy, $\boldsymbol{g}$ is not square, but rather rectangular, with a row deficit of n according to (9.3) or (9.4). Although $\boldsymbol{g} \bullet \boldsymbol{b} = \mathbf{I}$ still applies, $\boldsymbol{g}$ cannot be inverted, and $\boldsymbol{b}$ has a column deficit of n. In order to eliminate this deficit, n constraints are released at the joints, which therefore introduces corresponding additional degrees of freedom V_i and corresponding external joint force variables X_i. The relationships (8.8) to (8.12) then allow the problems without actions on bars to be solved.

The classic approach to the force method was developed and illustrated in chapter 16. In the following, the force method will be generalised and supplemented in a similar way to the presentation of the displacement method in sections 17.1 to 17.3. In addition, chapter 17 will be rounded off with an introduction to the finite element method.

Theory of Structures. First Edition. Peter Marti

19.2 The force method

19.2.1 Complete and global bar end forces

If we use complete bar end forces according to $(17.13)_1$ and Fig. 17.3 plus the associated sign convention II, we get

$$\left\{ \begin{matrix} \boldsymbol{Q} \\ \boldsymbol{C} \end{matrix} \right\} = \left[\begin{matrix} \overline{\boldsymbol{g}} \\ \overline{\boldsymbol{g}}_{\boldsymbol{sC}} \end{matrix} \right] \bullet \{\overline{\boldsymbol{s}}\} \tag{19.1}$$

instead of (9.2), where $\overline{\boldsymbol{g}}$ and $\overline{\boldsymbol{g}}_{\boldsymbol{sC}}$ are pure incidence matrices containing the elements 0 and 1 only. We get

$$\begin{Bmatrix} Q_3 \\ Q_4 \\ Q_6 \\ C_1 \\ C_2 \\ C_5 \end{Bmatrix} = \begin{bmatrix} 0 & 0 & 1 & 0 & 0 & 0 \\ 0 & 0 & 0 & 1 & 0 & 0 \\ 0 & 0 & 0 & 0 & 0 & 1 \\ 1 & 0 & 0 & 0 & 0 & 0 \\ 0 & 1 & 0 & 0 & 0 & 0 \\ 0 & 0 & 0 & 0 & 1 & 0 \end{bmatrix} \begin{Bmatrix} N_l \\ V_l \\ M_l \\ N_r \\ V_r \\ M_r \end{Bmatrix}$$

for the case illustrated in Fig. 9.5(d), for example. The complete bar end forces are related to the independent bar end forces according to $(17.14)_1$, i. e.

$$\overline{\boldsymbol{s}} = \boldsymbol{e}^{\mathrm{T}} \bullet \boldsymbol{s} \tag{19.2}$$

and therefore (9.2) becomes

$$\boldsymbol{Q} = \boldsymbol{g} \bullet \boldsymbol{s} \qquad (\boldsymbol{g} = \overline{\boldsymbol{g}} \bullet \boldsymbol{e}^{\mathrm{T}}) \quad , \quad \boldsymbol{C} = -\boldsymbol{g}_{\boldsymbol{sC}} \bullet \boldsymbol{s} \qquad (\boldsymbol{g}_{\boldsymbol{sC}} = -\overline{\boldsymbol{g}}_{\boldsymbol{sC}} \bullet \boldsymbol{e}^{\mathrm{T}}) \tag{19.3}$$

The bars are generally skewed with respect to the global coordinates. Therefore, we initially use complete, global bar end forces $\overline{\boldsymbol{s}}_g$ in the joint equilibrium conditions. In a first step according to $(17.39)_1$, we transform these into complete, local bar end forces $\overline{\boldsymbol{s}}$, which is followed by the transformation (19.2) into independent bar end forces $\boldsymbol{s}$.

19.2.2 Member flexibility relation

According to (9.8), the internal deformation variables associated with the independent bar end forces N_r, M_l, M_r are the bar extension Δ and the bar end rotations λ and ρ. Eq. $(17.14)_2$ shows that the complete kinematic bar end variables $\overline{\boldsymbol{v}}_{\mathrm{e}}$ include an additional rigid body deformation compared with the independent variables $\boldsymbol{v}_{\mathrm{e}}$, i. e. the latter follow from the former by eliminating this rigid body deformation.

There is a relationship between the variables $\boldsymbol{v}_{\mathrm{e}}$ and the independent bar end forces $\boldsymbol{s}_{\mathrm{e}}$ which is the inverse of (17.3):

$$\boldsymbol{v}_{\mathrm{e}} = \boldsymbol{f}_{\mathrm{e}} \bullet \boldsymbol{s}_{\mathrm{e}} \tag{19.4}$$

see (17.1) or (17.4) and (17.8). We normally get the coefficients of the member flexibility matrix $\boldsymbol{f}_{\mathrm{e}}$ from the work theorem (14.4), i. e.

$$f_{eij} = \int_0^l \left(\frac{N_i N_j}{EA} + \frac{V_i V_j}{GA_v} + \frac{M_i M_j}{EI} \right) \mathrm{d}x \tag{19.5}_1$$

for planar and

$$f_{eij} = \int_0^l \left(\frac{N_i N_j}{EA} + \frac{V_{yi} V_{yj}}{GA_{vy}} + \frac{V_{zi} V_{zj}}{GA_{vz}} + \frac{T_i T_j}{GI_x} + \frac{M_{yi} M_{yj}}{EI_y} + \frac{M_{zi} M_{zj}}{EI_z} \right) \mathrm{d}x \tag{19.5}_2$$

for spatial systems, see (16.11). From this derivation it follows that $\boldsymbol{f}_{\mathrm{e}}$ is square, symmetric, invertible and positive definite.

By arranging all the $\boldsymbol{f}_{\mathrm{e}}$ values on the main diagonals of a hypermatrix $\boldsymbol{f}$, the *flexibility matrix for all members*, with the appropriately configured columns $\boldsymbol{v}$ and $\boldsymbol{s}$ for all bar end variables $\boldsymbol{v}_{\mathrm{e}}$ and $\boldsymbol{s}_{\mathrm{e}}$, we get the relationship

$$\boldsymbol{v} = \boldsymbol{f} \bullet \boldsymbol{s} \tag{19.6}$$

which is similar to $(8.5)_2$, see (17.7).

$\alpha = a/l$ $\beta = b/l$ $\gamma = c/l$	$-N_l$	$-V_l$	$-V_r$	$EA\,\Delta$	$-EI\,\lambda$	$EI\,\rho$
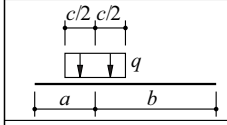		$ql\,\beta\gamma$	$ql\,\alpha\gamma$		$\frac{ql\,\beta\gamma\,(1-\beta-\gamma^2/4)}{6}$	$\frac{ql\,\alpha\gamma(1-\alpha-\gamma^2/4)}{6}$
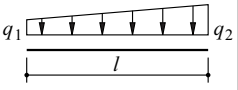		$\frac{l\,(2q_1+q_2)}{6}$	$\frac{l\,(q_1+2q_2)}{6}$		$\frac{l^3(8q_1+7q_2)}{360}$	$\frac{l^3(7q_1+8q_2)}{360}$
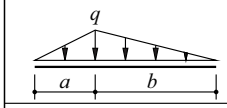		$\frac{ql\,(1+\beta)}{6}$	$\frac{ql\,(1+\alpha)}{6}$		$\frac{ql^3(1+\beta)(7-3\beta^2)}{360}$	$\frac{ql^3(1+\alpha)(7-3\alpha^2)}{360}$
parabolic 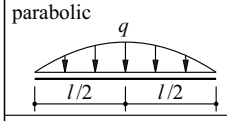		$\frac{ql}{3}$	$\frac{ql}{3}$		$\frac{ql^3}{30}$	$\frac{ql^3}{30}$
sinusoidal 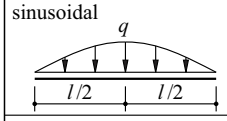		$\frac{ql}{\pi}$	$\frac{ql}{\pi}$		$\frac{ql^3}{\pi^3}$	$\frac{ql^3}{\pi^3}$
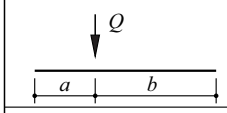		$Q\beta$	$Q\alpha$		$\frac{Ql^2\alpha\,\beta(1+\beta)}{6}$	$\frac{Ql^2\alpha\,\beta(1+\alpha)}{6}$
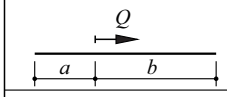	Q			Qa		
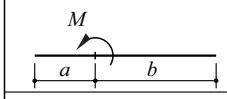		$\frac{M}{l}$	$-\frac{M}{l}$		$\frac{Ml(1-3\beta^2)}{6}$	$-\frac{Ml(1-3\alpha^2)}{6}$
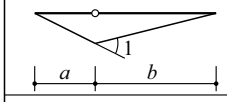					$EI\,\beta$	$EI\,\alpha$
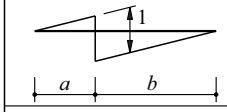					$-\frac{EI}{l}$	$\frac{EI}{l}$
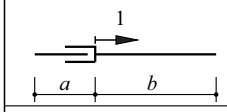				EA		
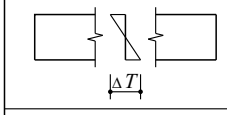					$\frac{EI\alpha_T\,\Delta T\,l}{2h}$	$\frac{EI\alpha_T\,\Delta T\,l}{2h}$
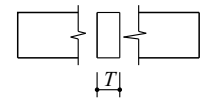				$EA\alpha_T\,T\,l$		

Fig. 19.1 Additional joint loads and bar end deformation variables due to actions on bars (sign convention II)

19.2.3 Actions on bars

Actions on bars cause additional terms for the joint loads and bar end deformation variables. These can be determined by calculating the support force variables for a fictitious simply supported beam of length l or by applying the work theorem (14.4). Fig. 19.1 contains such variables for coplanar bars with constant axial and bending stiffnesses for a number of load cases, see Fig. 17.1.

The variables $-N_l$, $-V_l$, $-V_r$ given in Fig. 19.1 must be considered in the joint load vector $\boldsymbol{Q}$. The additional bar end deformation variables Δ, λ, ρ lead to corresponding additions to (19.4) and (19.6), i. e.

$$\boldsymbol{v}_e = \boldsymbol{f}_e \bullet \boldsymbol{s}_e + \boldsymbol{v}_{e0} \quad , \quad \boldsymbol{v} = \boldsymbol{f} \bullet \boldsymbol{s} + \boldsymbol{v}_0 \tag{19.7}$$

see (17.11) or (17.20) and (17.22).

The calculation using the discretised structural model supplies the state variables at the joints and ends of the bars. In the subsequent calculation of the state variables between the nodes, the force and deformation variables for the fictitious simply supported beam must be superposed on the corresponding variables for the system loaded by joint loads only.

19.2.4 Algorithm for the force method

Eq. (8.4) and $(19.7)_2$, taking into account (8.8) and the submatrices

$$\boldsymbol{F}_{00} = \boldsymbol{b}_0^T \bullet \boldsymbol{f} \bullet \boldsymbol{b}_0 \quad , \quad \boldsymbol{F}_{10} = \boldsymbol{b}_1^T \bullet \boldsymbol{f} \bullet \boldsymbol{b}_0 \quad , \quad \boldsymbol{F}_{11} = \boldsymbol{b}_1^T \bullet \boldsymbol{f} \bullet \boldsymbol{b}_1$$

already defined in (8.10) und (8.12), result in the following relationship for the global flexibility matrix for the statically determinate basic system:

$$\begin{Bmatrix} \boldsymbol{V} \\ \boldsymbol{0} \end{Bmatrix} = \begin{bmatrix} \boldsymbol{F}_{00} & \boldsymbol{F}_{10}^T \\ \boldsymbol{F}_{10} & \boldsymbol{F}_{11} \end{bmatrix} \bullet \begin{Bmatrix} \boldsymbol{Q} \\ \boldsymbol{X} \end{Bmatrix} + \begin{Bmatrix} \boldsymbol{b}_0^T \bullet \boldsymbol{v}_0 \\ \boldsymbol{b}_1^T \bullet \boldsymbol{v}_0 \end{Bmatrix} \tag{19.8}$$

from which it follows that

$$\boldsymbol{X} = -\boldsymbol{F}_{11}^{-1} \bullet (\boldsymbol{F}_{10} \bullet \boldsymbol{Q} + \boldsymbol{b}_1^T \bullet \boldsymbol{v}_0) \tag{19.9}$$

Substituting in (8.8) results in

$$\boldsymbol{s} = \boldsymbol{b} \bullet \boldsymbol{Q} - \boldsymbol{k}_1 \bullet \boldsymbol{v}_0 \qquad (\boldsymbol{b} = \boldsymbol{b}_0 - \boldsymbol{b}_1 \bullet \boldsymbol{F}_{11}^{-1} \bullet \boldsymbol{F}_{10} \quad , \quad \boldsymbol{k}_1 = \boldsymbol{b}_1 \bullet \boldsymbol{F}_{11}^{-1} \bullet \boldsymbol{b}_1^T) \tag{19.10}$$

and substituting in the upper part of (19.8) we get

$$\boldsymbol{V} = \boldsymbol{F} \bullet \boldsymbol{Q} + \boldsymbol{V}_0 \qquad (\boldsymbol{F} = \boldsymbol{F}_{00} - \boldsymbol{F}_{10}^T \bullet \boldsymbol{F}_{11}^{-1} \bullet \boldsymbol{F}_{10} \quad , \quad \boldsymbol{V}_0 = \boldsymbol{b}^T \bullet \boldsymbol{v}_0) \tag{19.11}$$

see (17.43).

Example 19.1 Plane frame

Fig. 19.2 shows the basic system selected for the plane frame (Fig. 17.7) examined in example 17.3, together with the redundant variables X_1, X_2, X_3. The loads applied at joint 2, Q_1, Q_2, Q_3, are also shown. The units MN and m are used for force and length respectively in the following calculations. The independent bar end variables are used directly.

The following applies for the flexibility matrix for all members using sign convention II according to (17.1):

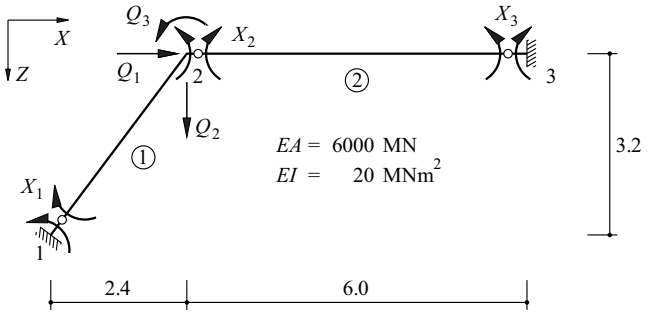

Fig. 19.2 Basic system, redundant variables and joint loads for the frame of Fig. 17.7 (dimensions in m)

$$\boldsymbol{f} = \begin{bmatrix} 1/1500 & 0 & 0 & 0 & 0 & 0 \\ 0 & 1/15 & -1/30 & 0 & 0 & 0 \\ 0 & -1/30 & 1/15 & 0 & 0 & 0 \\ 0 & 0 & 0 & 1/1000 & 0 & 0 \\ 0 & 0 & 0 & 0 & 1/10 & -1/20 \\ 0 & 0 & 0 & 0 & -1/20 & 1/10 \end{bmatrix}$$

and it is possible to set up relationship (8.8) on the basis of simple equilibrium considerations:

$$\begin{Bmatrix} N_{1r} \\ M_{1l} \\ M_{1r} \\ N_{2r} \\ M_{2l} \\ M_{2r} \end{Bmatrix} = \begin{bmatrix} 0 & -5/4 & 3/16 & -3/16 & 19/48 & -5/24 \\ 0 & 0 & 0 & -1 & 0 & 0 \\ 0 & 0 & 1 & 0 & 1 & 0 \\ -1 & -3/4 & 5/16 & -5/16 & 7/16 & -1/8 \\ 0 & 0 & 0 & 0 & -1 & 0 \\ 0 & 0 & 0 & 0 & 0 & 1 \end{bmatrix} \begin{Bmatrix} Q_1 \\ Q_2 \\ Q_3 \\ X_1 \\ X_2 \\ X_3 \end{Bmatrix}$$

These variables enable us to obtain

$$\begin{Bmatrix} V_1 \\ V_2 \\ V_3 \\ 0 \\ 0 \\ 0 \end{Bmatrix} = \frac{1}{6912000} \begin{bmatrix} 6912 & 5184 & -2160 & 2160 & -3024 & 864 \\ 5184 & 11088 & -2700 & 2700 & -4548 & 1848 \\ -2160 & -2700 & 461637 & 229563 & 462087 & -450 \\ 2160 & 2700 & 229563 & 461637 & 229113 & 450 \\ -3024 & -4548 & 462087 & 229113 & 1154045 & 344842 \\ 864 & 1848 & -450 & 450 & 344842 & 691508 \end{bmatrix} \begin{Bmatrix} Q_1 \\ Q_2 \\ Q_3 \\ X_1 \\ X_2 \\ X_3 \end{Bmatrix}$$

according to (19.8), if for the time being we work without actions on bars.

Inverting $\boldsymbol{F}_{11}$ results in

$$\boldsymbol{F}_{11}^{-1} = \begin{bmatrix} 16.9291 & -3.9456 & 1.9566 \\ -3.9456 & 7.9577 & -3.9658 \\ 1.9566 & -3.9658 & 11.9719 \end{bmatrix}$$

and therefore we also get

$$\boldsymbol{F} = \begin{bmatrix} 0.9950 & 0.7427 & -0.2051 \\ 0.7427 & 1.5935 & -0.1894 \\ -0.2051 & -0.1894 & 30.0437 \end{bmatrix} \cdot 10^{-3} \quad , \quad \boldsymbol{b} = \begin{bmatrix} 0.0042 & -1.2437 & 0.0428 \\ 0.0073 & 0.0097 & 0.2984 \\ 0.0052 & 0.0078 & 0.5988 \\ -0.9950 & -0.7427 & 0.2051 \\ -0.0052 & -0.0078 & 0.4012 \\ -0.0038 & -0.0066 & 0.2009 \end{bmatrix}$$

and

$$\boldsymbol{k}_1 = \begin{bmatrix} 3.7542 & 5.1436 & 4.7159 & 4.2245 & -4.7159 & -4.4308 \\ 5.1436 & 16.9291 & 3.9456 & 7.2611 & -3.9456 & -1.9566 \\ 4.7159 & 3.9456 & 7.9577 & 5.2102 & -7.9577 & -3.9658 \\ 4.2245 & 7.2611 & 5.2102 & 5.0289 & -5.2102 & -3.8430 \\ -4.7159 & -3.9456 & -7.9577 & -5.2102 & 7.9577 & 3.9658 \\ -4.4308 & -1.9566 & -3.9658 & -3.8430 & 3.9658 & 11.9719 \end{bmatrix}$$

With a uniformly distributed load $q = 0.01\,\mathrm{MN/m}$ applied to bar 2 as shown in Fig. 17.7(a), then according to Fig. 19.1 we get

$$\boldsymbol{v}_0 = \begin{Bmatrix} \Delta_1 \\ \lambda_1 \\ \rho_1 \\ \Delta_2 \\ \lambda_2 \\ \rho_2 \end{Bmatrix} = \begin{Bmatrix} 0 \\ 0 \\ 0 \\ 0 \\ -0.0045 \\ 0.0045 \end{Bmatrix}$$

and, in addition, $-V_{2l} = 0.03\,\mathrm{MN}$ has to be considered in Q_2. Eq. (19.10) and (19.11) then result in

$$\begin{Bmatrix} N_{1r} \\ M_{1l} \\ M_{1r} \\ N_{2r} \\ M_{2l} \\ M_{2r} \end{Bmatrix} = \boldsymbol{s} = \boldsymbol{b} \bullet \boldsymbol{Q} - \boldsymbol{k}_1 \bullet \boldsymbol{v}_0 = \begin{Bmatrix} -0.0373 \\ 0.0003 \\ 0.0002 \\ -0.0223 \\ -0.0002 \\ -0.0002 \end{Bmatrix} - \begin{Bmatrix} 0.0013 \\ 0.0090 \\ 0.0180 \\ 0.0062 \\ -0.0180 \\ 0.0360 \end{Bmatrix} = \begin{Bmatrix} -0.0386 \\ -0.0087 \\ -0.0178 \\ -0.0285 \\ 0.0178 \\ -0.0362 \end{Bmatrix}$$

or rather

$$\begin{Bmatrix} V_1 \\ V_2 \\ V_3 \end{Bmatrix} = \boldsymbol{V} = \boldsymbol{F} \bullet \boldsymbol{Q} + \boldsymbol{V}_0 = \begin{Bmatrix} 0.0223 \\ 0.0478 \\ -0.0057 \end{Bmatrix} \cdot 10^{-3} + \begin{Bmatrix} 0.0063 \\ 0.0054 \\ -0.9014 \end{Bmatrix} \cdot 10^{-3} = \begin{Bmatrix} 0.0286 \\ 0.0532 \\ -0.9071 \end{Bmatrix} \cdot 10^{-3}$$

The global stiffness matrix $\boldsymbol{K}$ for this problem is equal to the central (3×3) submatrix of the (9×9) matrix given in example 17.3. The global flexibility matrix $\boldsymbol{F}$ given above is the inverse of this matrix $\boldsymbol{K}$, a fact that is easily checked.

The bar end force and displacement variables calculated above agree with the values given in Fig. 17.7(c) and example 17.3 apart from small rounding-off errors, which have been left in to illustrate the effect of the accuracy of the calculation.

19.2.5 Comparison with the classic force method

According to the classic force method summarised in section 16.3.1, only one load case $\boldsymbol{Q}^*$ is considered each time, i. e. one very specific combination of the joint loads Q_i generally possible.

Comparing $(16.9)_2$ with (8.8) reveals that merely the product $\boldsymbol{b}_0 \bullet \boldsymbol{Q}$ is ascertained with S_0, $\boldsymbol{b}_0$ is not calculated. On the other hand, the coefficients S_i correspond to the matrix $\boldsymbol{b}_1$.

Comparing the compatibility conditions (16.8) and (8.9) reveals that matrix δ_{ij} is equal to $\boldsymbol{F}_{11} = \boldsymbol{b}_1^{\mathrm{T}} \bullet \boldsymbol{f} \bullet \boldsymbol{b}_1$, and that vector δ_{i0} corresponds to the expression $\boldsymbol{b}_1^{\mathrm{T}} \bullet \boldsymbol{f} \bullet \boldsymbol{b}_0 \bullet \boldsymbol{Q} + \boldsymbol{b}_1^{\mathrm{T}} \bullet \boldsymbol{v}_0$ when the general formulation in the lower part of (19.8) is used with the bar end deformation variables $\boldsymbol{v}_0$ resulting from the actions on bars.

As $\boldsymbol{b}_0$ is not calculated when employing the classic approach, both the global flexibility matrix $\boldsymbol{F}$ and the static transformation matrix $\boldsymbol{b}$ occurring in (19.10) and (19.11) remain unknown. So although far fewer calculations are required, the results are much more limited – support force variables and stress resultants only according to (16.9). Extra work is required to determine the influence lines and deformation variables.

19.2.6 Practical application

According to (19.10) and (19.11), the columns j of the static transformation matrix $\boldsymbol{b}$ and the global flexibility matrix $\boldsymbol{F}$ contain the state variables s_i and V_i respectively due to the joint load $Q_j = 1$. And vice versa, the rows i of these matrices reveal how all joint loads Q_j have an influence on a certain variable s_i or V_i. Accordingly, the two matrices contain a wealth of information relevant to the state diagrams and influence lines. This fact has already been pointed out in conjunction with (10.9).

State diagrams for stress resultants can be obtained from the columns of matrix $\boldsymbol{b}$ by considering the rules outlined in chapter 11. And vice versa, the coefficients of one row in $\boldsymbol{b}$ correspond to individual points on the associated influence lines for the forces. These influence lines are curved for statically indeterminate systems (see sections 12.3, 16.3.4 and 17.4.6) and so the general recommendation is to choose a joint spacing that is so close that a linear approximation between the joints is sufficiently accurate.

Similar remarks apply to the calculation of state diagrams and influence lines for deformation variables from the columns and rows respectively of matrix $\boldsymbol{F}$.

19.2.7 Reduced degrees of freedom

To reduce the amount of calculation work, internal degrees of freedom are often suppressed, e. g. by assuming inextensible bars. This means that the member flexibility matrices $\boldsymbol{f}_{\mathrm{e}}$, as given in section 17.4.1, are singular and can be inverted for the bending components only. The normal forces must be determined from equilibrium conditions after calculating the bending moments.

The singularity of the member flexibility matrices $\boldsymbol{f}_{\mathrm{e}}$ would be carried over into the flexibility matrix $\boldsymbol{f}$ of all bars and into the global flexibility matrix $\boldsymbol{F}$ and render a solution impossible. To prevent this, certain external degrees of freedom and joint loads must be suppressed or combined.

For example, in the frame (see Fig. 17.27) shown in Fig. 19.3(a), assuming inextensible bars ($\Delta_1 = \Delta_2 = \Delta_3 = 0$) eliminates degree of freedom V_5 and combines degrees of freedom V_1, V_2 und V_4 :

$$V_2 = \frac{3}{4} V_1 \quad , \quad V_4 = V_1$$

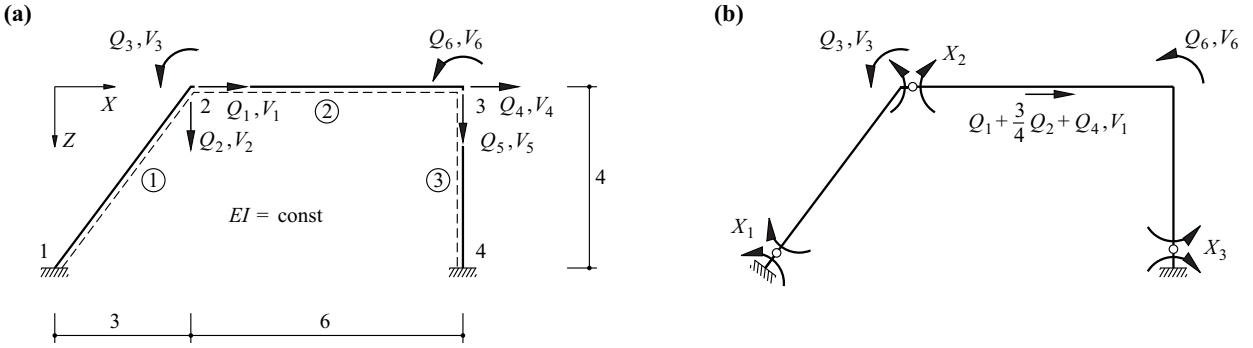

Fig. 19.3 Plane frame: (a) diagram of static system (dimensions in m), (b) basic system, redundant variables and reduced degrees of freedom

Consequently, joint loads Q_1, Q_2 and Q_4 are combined to form a total action $Q_1 + 3Q_2/4 + Q_4$, and since $V_5 \equiv 0$, joint load Q_5 is not included in the flexibility calculation because it does no work.

The joint equilibrium conditions

$$\begin{Bmatrix} Q_1 \\ Q_2 \\ Q_3 \\ Q_4 \\ Q_5 \\ Q_6 \end{Bmatrix} = \begin{bmatrix} 3/5 & 4/25 & 4/25 & -1 & & & & & & \\ -4/5 & 3/25 & 3/25 & & & -1/6 & -1/6 & & & \\ & & 1 & & & 1 & & & & \\ & & & 1 & & & & & 1/4 & 1/4 \\ & & & & & 1/6 & 1/6 & -1 & & \\ & & & & & & 1 & & 1 & \end{bmatrix} \begin{Bmatrix} N_{1r} \\ M_{1l} \\ M_{1r} \\ N_{2r} \\ M_{2l} \\ M_{2r} \\ N_{3r} \\ M_{3l} \\ M_{3r} \end{Bmatrix} \tag{19.12}$$

are therefore rearranged:

$$\begin{Bmatrix} Q_1 + \frac{3}{4}Q_2 + Q_4 \\ Q_3 \\ Q_6 \\ Q_2 \\ Q_4 \\ Q_5 \end{Bmatrix} = \begin{bmatrix} 1/4 & 1/4 & -1/8 & -1/8 & 1/4 & 1/4 & & & \\ & 1 & 1 & & & & & & \\ & & & & 1 & 1 & & & \\ 3/25 & 3/25 & -1/6 & -1/6 & & & -4/5 & & \\ & & & & 1/4 & 1/4 & & 1 & \\ & & 1/6 & 1/6 & & 1 & & & -1 \end{bmatrix} \begin{Bmatrix} M_{1l} \\ M_{1r} \\ M_{2l} \\ M_{2r} \\ M_{3l} \\ M_{3r} \\ N_{1r} \\ N_{2r} \\ N_{3r} \end{Bmatrix} \tag{19.13}$$

Empty places in matrices (19.12) and (19.13) are filled with zeros.

The (3×6) matrix $\boldsymbol{g}_{rr}$ at top left in (19.13) links the joint loads $\boldsymbol{Q}_r$ corresponding to the reduced external degrees of freedom $\boldsymbol{V}_r = \{V_1, V_3, V_6\}^{\mathrm{T}}$ with the bar end moments $\boldsymbol{s}_r$ corresponding to the reduced internal degrees of freedom $\boldsymbol{v}_r = \{\lambda_1, \rho_1, \lambda_2, \rho_2, \lambda_3, \rho_3\}^{\mathrm{T}}$. The coefficients in the first row of this matrix correspond to the displacement equilibrium condition introduced in section 17.4.3, those of the second and third rows correspond to the joint moment equilibrium condition (17.58). Generally, the following applies:

$$\boldsymbol{Q}_r = \boldsymbol{g}_{rr} \bullet \boldsymbol{s}_r \tag{19.14}$$

The (3×6) matrix $\boldsymbol{g}_{ur}$ at bottom left and the (3×3) matrix $\boldsymbol{g}_{uu}$ at bottom right in (19.13) link the remaining joint loads $\boldsymbol{Q}_u$ with $\boldsymbol{s}_r$ or the bar end normal forces $\boldsymbol{s}_u$ corresponding to the suppressed internal degrees of freedom $\boldsymbol{v}_u = \{\Delta_1, \Delta_2, \Delta_3\}^{\mathrm{T}} = \boldsymbol{0}$:

$$\boldsymbol{Q}_u = \boldsymbol{g}_{ur} \bullet \boldsymbol{s}_r + \boldsymbol{g}_{uu} \bullet \boldsymbol{s}_u \tag{19.15}$$

Further calculation leads to

$$\boldsymbol{s}_r = \boldsymbol{b}_{rr} \bullet \boldsymbol{Q}_r \quad , \quad \boldsymbol{V}_r = \boldsymbol{F}_{rr} \bullet \boldsymbol{Q}_r \qquad (\boldsymbol{F}_{rr} = \boldsymbol{b}_{rr}^{\mathrm{T}} \bullet \boldsymbol{f}_{rr} \bullet \boldsymbol{b}_{rr}) \tag{19.16}$$

and

$$\boldsymbol{s}_u = \boldsymbol{b}_{ur} \bullet \boldsymbol{Q}_r + \boldsymbol{b}_{uu} \bullet \boldsymbol{Q}_u \qquad (\boldsymbol{b}_{ur} = -\boldsymbol{g}_{uu}^{-1} \bullet \boldsymbol{g}_{ur} \bullet \boldsymbol{b}_{rr} \quad , \quad \boldsymbol{b}_{uu} = \boldsymbol{g}_{uu}^{-1}) \tag{19.17}$$

Using the basic system and the redundant variables according to Fig. 19.3(b) plus

$$\boldsymbol{f}_{rr} = \frac{\mathrm{m}}{6EI} \begin{bmatrix} 10 & -5 & 0 & 0 & 0 & 0 \\ -5 & 10 & 0 & 0 & 0 & 0 \\ 0 & 0 & 12 & -6 & 0 & 0 \\ 0 & 0 & -6 & 12 & 0 & 0 \\ 0 & 0 & 0 & 0 & 8 & -4 \\ 0 & 0 & 0 & 0 & -4 & 8 \end{bmatrix} \tag{19.18}$$

initially gives us

$$\begin{Bmatrix} M_{1l} \\ M_{1r} \\ M_{2l} \\ M_{2r} \\ M_{3l} \\ M_{3r} \end{Bmatrix} = \frac{1}{3} \begin{bmatrix} 0 & 0 & 0 & -3 & 0 & 0 \\ 0 & 3 & 0 & 0 & 3 & 0 \\ 0 & 0 & 0 & 0 & -3 & 0 \\ -8\,\mathrm{m} & 2 & 2 & -2 & 3 & 2 \\ 8\,\mathrm{m} & -2 & 1 & 2 & -3 & -2 \\ 0 & 0 & 0 & 0 & 0 & 3 \end{bmatrix} \begin{Bmatrix} Q_1 + \frac{3}{4}Q_2 + Q_4 \\ Q_3 \\ Q_6 \\ X_1 \\ X_2 \\ X_3 \end{Bmatrix} \tag{19.19}$$

for this example, and therefore according to (19.8),

$$\begin{Bmatrix} V_1 \\ V_3 \\ V_6 \\ 0 \\ 0 \\ 0 \end{Bmatrix} = \frac{\mathrm{m}}{54EI} \begin{bmatrix} 1280\,\mathrm{m}^2 & -320\,\mathrm{m} & -128\,\mathrm{m} & 320\,\mathrm{m} & -624\,\mathrm{m} & -416\,\mathrm{m} \\ -320\,\mathrm{m} & 170 & 32 & -35 & 246 & 104 \\ -128\,\mathrm{m} & 32 & 56 & -32 & 84 & 20 \\ 320\,\mathrm{m} & -35 & -32 & 170 & -111 & -104 \\ -624\,\mathrm{m} & 246 & 84 & -111 & 486 & 192 \\ -416\,\mathrm{m} & 104 & 20 & -104 & 192 & 200 \end{bmatrix} \begin{Bmatrix} Q_1 + \frac{3}{4}Q_2 + Q_4 \\ Q_3 \\ Q_6 \\ X_1 \\ X_2 \\ X_3 \end{Bmatrix} \tag{19.20}$$

from which it follows that

$$\boldsymbol{F}_{11}^{-1} = \begin{bmatrix} 0.467503 & 0.017294 & 0.226499 \\ 0.017294 & 0.179637 & -0.163459 \\ 0.226499 & -0.163459 & 0.544700 \end{bmatrix} \frac{EI}{\mathrm{m}} \tag{19.21}$$

and therefore

$$\boldsymbol{b}_{rr} = \begin{bmatrix} 0.8257\,\mathrm{m} & 0.2120 & -0.1662 \\ 0.7141\,\mathrm{m} & 0.5077 & -0.2086 \\ -0.7141\,\mathrm{m} & 0.4923 & 0.2086 \\ -0.7588\,\mathrm{m} & 0.2106 & 0.4717 \\ 0.7588\,\mathrm{m} & -0.2106 & 0.5283 \\ 0.9651\,\mathrm{m} & -0.1576 & 0.1868 \end{bmatrix} \quad , \quad \boldsymbol{F}_{rr} = \begin{bmatrix} 3.1242\,\mathrm{m}^3 & -0.2789\,\mathrm{m}^2 & -0.4129\,\mathrm{m}^2 \\ -0.2789\,\mathrm{m}^2 & 0.7392\,\mathrm{m} & -0.1060\,\mathrm{m} \\ -0.4129\,\mathrm{m}^2 & -0.1060\,\mathrm{m} & 0.6831\,\mathrm{m} \end{bmatrix} \frac{1}{EI} \tag{19.22}$$

Eq. (19.17) thus results in

$$\begin{Bmatrix} N_{1r} \\ N_{2r} \\ N_{3r} \end{Bmatrix} = \begin{bmatrix} 0.5379 & -0.0385 \cdot \frac{1}{\mathrm{m}} & -0.1980 \cdot \frac{1}{\mathrm{m}} \\ -0.4310 & 0.0921 \cdot \frac{1}{\mathrm{m}} & -0.1788 \cdot \frac{1}{\mathrm{m}} \\ -0.2455 & 0.1172 \cdot \frac{1}{\mathrm{m}} & 0.1134 \cdot \frac{1}{\mathrm{m}} \end{bmatrix} \begin{Bmatrix} Q_1 + \frac{3}{4}Q_2 + Q_4 \\ Q_3 \\ Q_6 \end{Bmatrix} + \begin{bmatrix} -\frac{5}{4} & 0 & 0 \\ 0 & 1 & 0 \\ 0 & 0 & -1 \end{bmatrix} \begin{Bmatrix} Q_2 \\ Q_4 \\ Q_5 \end{Bmatrix}$$

or rather, rearranged with respect to joint loads,

$$\begin{Bmatrix} N_{1r} \\ N_{2r} \\ N_{3r} \end{Bmatrix} = \begin{bmatrix} 0.5379 & -0.8466 & -0.0385 \cdot \frac{1}{\mathrm{m}} & 0.5379 & 0 & -0.1980 \cdot \frac{1}{\mathrm{m}} \\ -0.4310 & -0.3233 & 0.0921 \cdot \frac{1}{\mathrm{m}} & 0.5690 & 0 & -0.1788 \cdot \frac{1}{\mathrm{m}} \\ -0.2455 & -0.1841 & 0.1172 \cdot \frac{1}{\mathrm{m}} & -0.2455 & -1 & 0.1134 \cdot \frac{1}{\mathrm{m}} \end{bmatrix} \begin{Bmatrix} Q_1 \\ Q_2 \\ Q_3 \\ Q_4 \\ Q_5 \\ Q_6 \end{Bmatrix} \tag{19.23}$$

19.2.8 Supplementary remarks

Fig. 16.9 illustrated the static structural behaviour of an elastic-plastic frame with two degrees of static indeterminacy ($n = 2$) subjected to a single joint load ($m = 1$). Specifying the three moments M_2, M_3, M_4, or rather a corresponding vector $\boldsymbol{s}$, in the $(m+n)$-dimensional space, enabled the stress state to be described completely. Alternatively, the stress state can be also described in the system with the axes Q, P_1, P_2. The transformation between the two systems is described by the relationship (8.8) fundamental to the force method.

Pure restraint states without any loads are characterised in Fig. 16.9 by points on the plane ABCDEF defined by the axes P_1, P_2 (or X_1, X_2). Obviously, the choice of the redundant variables is completely arbitrary, and we can generally assume any combination of n linear restraint states that are independent of each other. Further, the fact that the straight lines OG and JI are parallel shows that nothing has essentially changed with respect to the calculation of the elastic system when the zero-load system already exhibits a restraint state; such a state is simply superposed on the elastic, load-dependent stress state.

Choosing suitable redundant variables enables matrix $\boldsymbol{F}_{11}$ to be diagonalised. This leads to the specific eigenvalue problem

$$\boldsymbol{F}_{11} \bullet \boldsymbol{X} = \lambda \boldsymbol{X} \tag{19.24}$$

see section A5.5. The eigenvalues λ_i follow from the characteristic equation

$$\det(\boldsymbol{F}_{11} - \lambda \mathbf{I}) = 0 \tag{19.25}$$

The directions of the associated eigenvectors $\boldsymbol{X}_i$ can be determined, but not their values; the vectors define the principal axes of the restraints in the n-dimensional subspace of the $(m+n)$-dimensional space of the internal static variables $\boldsymbol{s}$. The $n(n+1)/2$ data of the symmetrical $(n \times n)$ matrix $\boldsymbol{F}_{11}$ is transferred to the n eigenvalues and $n(n-1)/2$ data of the modal matrix $\boldsymbol{X}_o$ for the orthonormalised eigenvectors.

The global flexibility matrix $\boldsymbol{F}$ can be diagonalised in exactly the same way, too. In this case, the m columns of the resulting modal matrix describe load groups that are orthogonal to each other. The original static system is replaced by an equivalent system with m individual springs.

Example 19.2 Orthogonalised restraint states

Applying (19.25) to the (3×3) matrix $\boldsymbol{F}_{11}$ at bottom right in the matrix on the right in (19.20) gives us the characteristic equation

$$\lambda^3 - 15.\overline{851}\,\frac{\mathrm{m}}{EI}\lambda^2 + 52.75\left(\frac{\mathrm{m}}{EI}\right)^2\lambda - 44.\overline{259}\left(\frac{\mathrm{m}}{EI}\right)^3 = 0$$

with the eigenvalues

$$\lambda_1 = 1.316880\,\frac{\mathrm{m}}{EI} \quad , \quad \lambda_2 = 2.884888\,\frac{\mathrm{m}}{EI} \quad , \quad \lambda_3 = 11.650084\,\frac{\mathrm{m}}{EI}$$

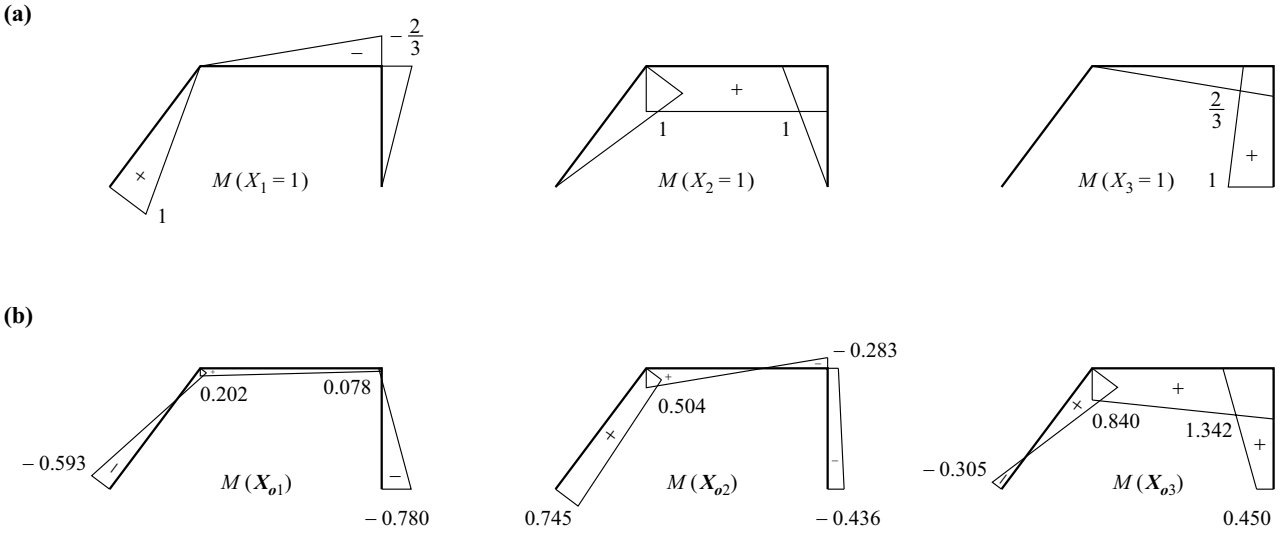

Fig. 19.4 Orthogonal unit states: (a) initial restraint states, (b) orthogonalised restraint states

as roots. The associated orthonormalised eigenvectors $\boldsymbol{X}_{oi}$ are summarised in the columns of the modal matrix

$$\boldsymbol{X}_o = \begin{bmatrix} -0.592931 & 0.745323 & -0.304839 \\ 0.202091 & 0.504177 & 0.839622 \\ -0.779482 & -0.436232 & 0.449565 \end{bmatrix}$$

Fig. 19.4 shows the corresponding moment diagrams orthogonal to each other together with the non-orthogonal initial restraint states.

To conclude this section, Fig. 19.5 shows a modified form of the scheme known from Fig. 8.2. Static, kinematic and constitutive relationships are arranged along the axes S, K, W. The lower (right-hand) part of the figure corresponds to the force method, the upper (left-hand) part the displacement method.

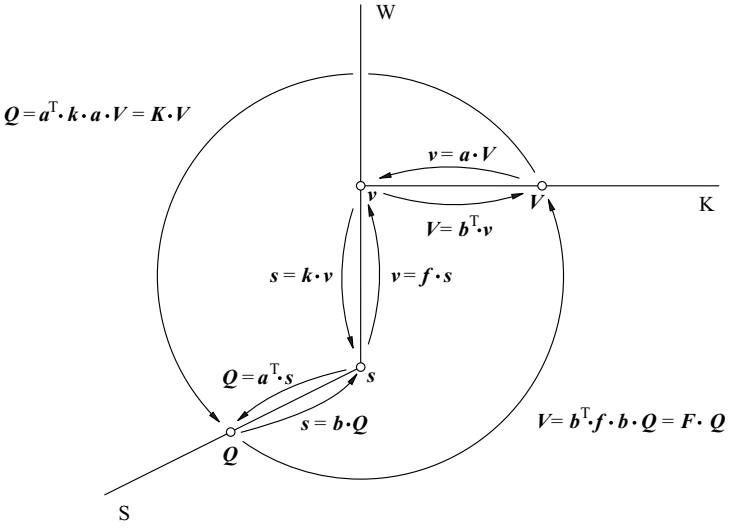

Fig. 19.5 Static and kinematic variables and their relationships

19.3 Introduction to the finite element method

19.3.1 Basic concepts

According to (8.63), the principle of virtual deformations (8.62) corresponds to a global (weak) or averaged formulation of the equilibrium:

$$\delta W = \int_V \delta \boldsymbol{u}^{\mathrm{T}} \bullet \boldsymbol{q}\, \mathrm{d}V + \int_{S_t} \delta \boldsymbol{r}^{\mathrm{T}} \bullet \boldsymbol{t}_0\, \mathrm{d}S - \int_V \delta \boldsymbol{\varepsilon}^{\mathrm{T}} \bullet \boldsymbol{\sigma}\, \mathrm{d}V = 0 \tag{19.26}$$

Here, the virtual deformation variables must satisfy the compatibility conditions (8.18) in V or on S_r:

$$\delta \boldsymbol{\varepsilon} = \boldsymbol{D_k} \bullet \delta \boldsymbol{u} \quad , \quad \delta \boldsymbol{r} = \boldsymbol{R} \bullet \delta \boldsymbol{u} \tag{19.27}$$

The fundamental thinking behind the finite element method (FEM) is to divide the model space V into a finite number of discrete elements and to approximate the displacements $\boldsymbol{u}_\mathrm{e}$ occurring within the elements in a similar way to the RITZ method (section 8.5.2) depending on the degrees of freedom at the joints $\boldsymbol{v}_\mathrm{e}$:

$$\boldsymbol{u}_\mathrm{e} = \boldsymbol{\Omega}_\mathrm{e} \bullet \boldsymbol{v}_\mathrm{e} \tag{19.28}$$

Matrix $\boldsymbol{\Omega}_\mathrm{e}$ contains the *shape functions*, or RITZ functions, and the degrees of freedom at the joints play the role of the RITZ coefficients c_i in (8.92).

19.3.2 Element matrices

From (19.28) we get the variation

$$\delta \boldsymbol{u}_\mathrm{e} = \boldsymbol{\Omega}_\mathrm{e} \bullet \delta \boldsymbol{v}_\mathrm{e} \tag{19.29}$$

and thus, by substituting in (19.27),

$$\delta \boldsymbol{\varepsilon}_\mathrm{e} = \boldsymbol{D_k} \bullet \boldsymbol{\Omega}_\mathrm{e} \bullet \delta \boldsymbol{v}_\mathrm{e} = \boldsymbol{H}_\mathrm{e} \bullet \delta \boldsymbol{v}_\mathrm{e} \quad , \quad \delta \boldsymbol{r}_\mathrm{e} = \boldsymbol{R} \bullet \boldsymbol{\Omega}_\mathrm{e} \bullet \delta \boldsymbol{v}_\mathrm{e} \tag{19.30}$$

where $\boldsymbol{H}_\mathrm{e}$ stands for the *strain interpolation matrix*. Using

$$\boldsymbol{\sigma}_\mathrm{e} = \boldsymbol{E} \bullet (\boldsymbol{\varepsilon}_\mathrm{e} - \boldsymbol{\varepsilon}_{\mathrm{e}0}) = \boldsymbol{E} \bullet \boldsymbol{H}_\mathrm{e} \bullet \boldsymbol{v}_\mathrm{e} - \boldsymbol{E} \bullet \boldsymbol{\varepsilon}_{\mathrm{e}0} \tag{19.31}$$

according to (8.19) and $(19.30)_1$, then applying (19.26) to the element leads to

$$\delta W_\mathrm{e} = \delta \boldsymbol{v}_\mathrm{e}^{\mathrm{T}} \bullet \Big(\int_V \boldsymbol{\Omega}_\mathrm{e}^{\mathrm{T}} \bullet \boldsymbol{q}\, \mathrm{d}V + \int_{S_t} \boldsymbol{\Omega}_\mathrm{e}^{\mathrm{T}} \bullet \boldsymbol{R}^{\mathrm{T}} \bullet \boldsymbol{t}_0\, \mathrm{d}S - \int_V \boldsymbol{H}_\mathrm{e}^{\mathrm{T}} \bullet \boldsymbol{E} \bullet \boldsymbol{H}_\mathrm{e}\, \mathrm{d}V \bullet \boldsymbol{v}_\mathrm{e} + \int_V \boldsymbol{H}_\mathrm{e}^{\mathrm{T}} \bullet \boldsymbol{E} \bullet \boldsymbol{\varepsilon}_{\mathrm{e}0}\, \mathrm{d}V \Big) = 0 \tag{19.32}$$

The expression in brackets in this relationship, which must disappear because of the randomness of $\delta \boldsymbol{v}_\mathrm{e}$, represents the joint force vector $\boldsymbol{s}$ corresponding to $\delta \boldsymbol{v}_\mathrm{e}$. Using

$$\boldsymbol{s}_\mathrm{e} = \int_{S_t} \boldsymbol{\Omega}_\mathrm{e}^{\mathrm{T}} \bullet \boldsymbol{R}^{\mathrm{T}} \bullet \boldsymbol{t}_0\, \mathrm{d}S \quad , \quad \boldsymbol{k}_\mathrm{e} = \int_V \boldsymbol{H}_\mathrm{e}^{\mathrm{T}} \bullet \boldsymbol{E} \bullet \boldsymbol{H}_\mathrm{e}\, \mathrm{d}V \quad , \quad \boldsymbol{s}_{\mathrm{e}0} = -\int_V (\boldsymbol{\Omega}_\mathrm{e}^{\mathrm{T}} \bullet \boldsymbol{q} + \boldsymbol{H}_\mathrm{e}^{\mathrm{T}} \bullet \boldsymbol{E} \bullet \boldsymbol{\varepsilon}_{\mathrm{e}0})\, \mathrm{d}V \tag{19.33}$$

the following relationship applies:

$$\boldsymbol{s}_\mathrm{e} = \boldsymbol{k}_\mathrm{e} \bullet \boldsymbol{v}_\mathrm{e} + \boldsymbol{s}_{\mathrm{e}0} \tag{19.34}$$

see (17.20).

19.3.3 Bar element rigid in shear

In the following, a bar element rigid in shear is investigated in the form of independent bar end variables (Fig. 19.6) and complete bar end variables (Fig. 19.7). The element index e is suppressed, as is the superscript horizontal line ($\bar{}$) introduced in section 17.2 for indicating complete bar end variables; this corresponds to the standard presentation used in the finite element method and does not need to be specially indicated.

In the form of independent variables, Fig. 19.6, the following RITZ formulation

$$\boldsymbol{u} = \begin{Bmatrix} u \\ w \end{Bmatrix} = \boldsymbol{\Omega} \bullet \boldsymbol{v} = \begin{bmatrix} \xi & 0 & 0 \\ 0 & (-\xi + 2\xi^2 - \xi^3)l & (\xi^2 - \xi^3)l \end{bmatrix} \begin{Bmatrix} \Delta \\ \lambda \\ \rho \end{Bmatrix} \tag{19.35}$$

(a)

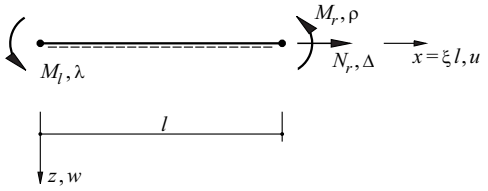

(b)

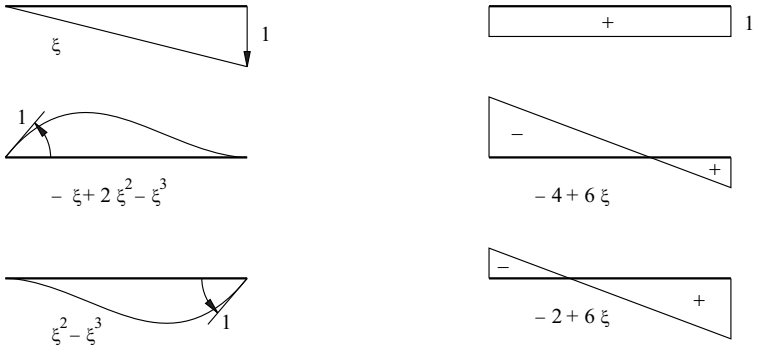

Fig. 19.6 Bar element rigid in shear (independent bar end variables): (a) notation, (b) shape functions for displacements and strains

according to (19.28) corresponds to the exact solutions to the homogeneous differential equations $EAu'' = 0$ and $EIw'''' = 0$. With $\boldsymbol{D_k}$ according to (8.24), eq. $(19.30)_1$ results in

$$\boldsymbol{H} = \begin{bmatrix} \mathrm{d}_x & 0 \\ 0 & -\mathrm{d}_x^2 \end{bmatrix} \begin{bmatrix} \xi & 0 & 0 \\ 0 & (-\xi + 2\xi^2 - \xi^3)l & (\xi^2 - \xi^3)l \end{bmatrix} = \begin{bmatrix} 1 & 0 & 0 \\ 0 & -4 + 6\xi & -2 + 6\xi \end{bmatrix} \cdot \frac{1}{l} \tag{19.36}$$

see Fig. 19.6(b), and using

$$\boldsymbol{E} = \begin{bmatrix} EA & 0 \\ 0 & EI \end{bmatrix}$$

according to (8.23), we get

$$\boldsymbol{H}^{\mathrm{T}} \bullet \boldsymbol{E} \bullet \boldsymbol{H} = \begin{bmatrix} A/I & 0 & 0 \\ 0 & (4 - 6\xi)^2 & (4 - 6\xi)(2 - 6\xi) \\ 0 & (2 - 6\xi)(4 - 6\xi) & (2 - 6\xi)^2 \end{bmatrix} \frac{EI}{l^2} \tag{19.37}$$

for the integrand in $(19.33)_2$. By performing the integration (e. g. with help of the integration table of Fig. 14.2), we get the stiffness matrix given in (17.3).

Uniformly distributed line loads q_x and q_z result in the integrand

$$\boldsymbol{\Omega}^{\mathrm{T}} \bullet \boldsymbol{q} = \begin{bmatrix} \xi & 0 \\ 0 & (-\xi + 2\xi^2 - \xi^3)l \\ 0 & (\xi^2 - \xi^3)l \end{bmatrix} \begin{Bmatrix} q_x \\ q_z \end{Bmatrix} = \begin{Bmatrix} q_x \xi \\ q_z l(-\xi + 2\xi^2 - \xi^3) \\ q_z l(\xi^2 - \xi^3) \end{Bmatrix}$$

in $(19.33)_3$, and therefore we get the fixed-end forces

$$\boldsymbol{s}_0 = \begin{Bmatrix} -q_x l/2 \\ q_z l^2/12 \\ -q_z l^2/12 \end{Bmatrix} \tag{19.38}$$

see example 17.1.

(a)

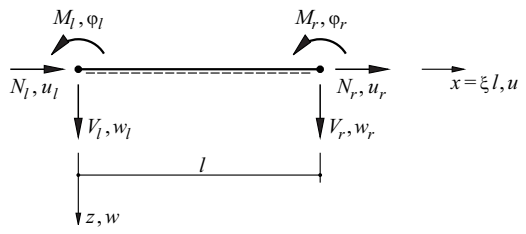

(b)

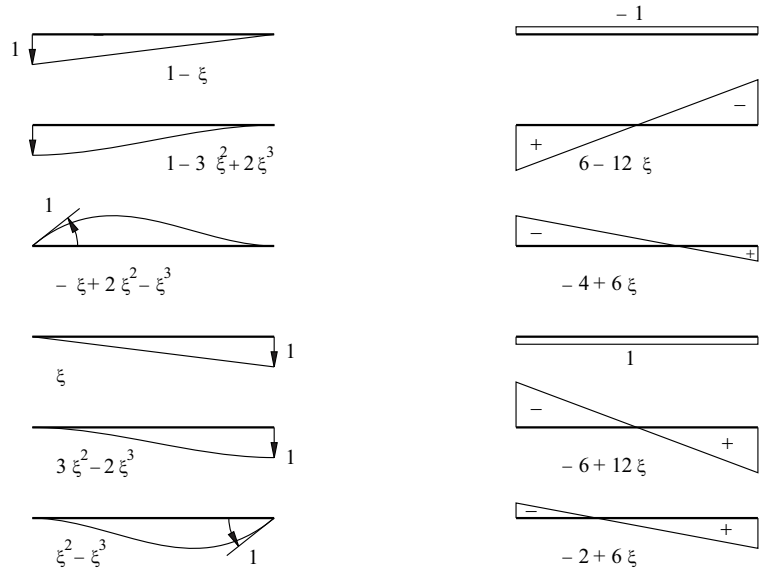

Fig. 19.7 Bar element rigid in shear (complete bar end variables): (a) notation, (b) shape functions for displacements and strains

The formulation similar to (19.35)

$$\boldsymbol{u} = \begin{Bmatrix} u \\ w \end{Bmatrix} = \boldsymbol{\Omega} \bullet \boldsymbol{v} = \begin{bmatrix} 1-\xi & 0 & 0 & \xi & 0 & 0 \\ 0 & 1-3\xi^2+2\xi^3 & (-\xi+2\xi^2-\xi^3)l & 0 & 3\xi^2-2\xi^3 & (\xi^2-\xi^3)l \end{bmatrix} \begin{Bmatrix} u_l \\ w_l \\ \varphi_l \\ u_r \\ w_r \\ \varphi_r \end{Bmatrix} \tag{19.39}$$

in the form of complete bar end variables leads to

$$\boldsymbol{\varepsilon} = \begin{Bmatrix} \varepsilon \\ \chi \end{Bmatrix} = \boldsymbol{H} \bullet \boldsymbol{v} = \begin{bmatrix} -1 & 0 & 0 & 1 & 0 & 0 \\ 0 & (6-12\xi)/l & -4+6\xi & 0 & (-6+12\xi)/l & -2+6\xi \end{bmatrix} \begin{Bmatrix} u_l \\ w_l \\ \varphi_l \\ u_r \\ w_r \\ \varphi_r \end{Bmatrix} \tag{19.40}$$

see Fig. 19.7(b). The integrand $\boldsymbol{H}^{\mathrm{T}} \bullet \boldsymbol{E} \bullet \boldsymbol{H}$ of the element stiffness matrix $(19.33)_2$ is then

$$\begin{bmatrix} A/I & 0 & 0 & -A/I & 0 & 0 \\ 0 & (6-12\xi)^2/l^2 & -(6-12\xi)(4-6\xi)/l & 0 & -(6-12\xi)^2/l^2 & -(6-12\xi)(42-6\xi)/l \\ 0 & -(4-6\xi)(6-12\xi)/l & (4-6\xi)^2 & 0 & (4-6\xi)(6-12\xi)/l & (4-6\xi)(2-6\xi) \\ -A/I & 0 & 0 & A/I & 0 & 0 \\ 0 & -(6-12\xi)^2/l^2 & (6-12\xi)(4-6\xi)/l & 0 & (6-12\xi)^2/l^2 & (6-12\xi)(2-6\xi)/l \\ 0 & -(2-6\xi)(6-12\xi)/l & (2-6\xi)(4-6\xi) & 0 & (2-6\xi)(6-12\xi)/l & (2-6\xi)^2 \end{bmatrix} \frac{EI}{l^2} \tag{19.41}$$

and performing the integration results in (17.17).

With uniformly distributed line loads q_x and q_z, eq. $(19.33)_3$ results in the fixed-end forces

$$\boldsymbol{s}_0 = -\int_x \boldsymbol{\Omega} \cdot \boldsymbol{q}\, \mathrm{d}x = \begin{Bmatrix} -q_x l/2 \\ -q_z l/2 \\ q_z l^2/12 \\ -q_x l/2 \\ -q_z l/2 \\ -q_z l^2/12 \end{Bmatrix} \tag{19.42}$$

The shape functions in (19.35) and (19.39) correspond to the influence functions for the bar end forces of the prismatic bar fixed at both ends. Thus, for prismatic bars subjected to the action of arbitrary bar loads $\boldsymbol{q}$, eq. $(19.33)_3$ provides us with the statically equivalent joint forces and hence the exact joint displacements within the scope of the assumptions made.

Example 19.3 Beam with one degree of static indeterminacy

Let us consider the beam of example 15.6 once again, see Fig. 19.8(a). Using the notation selected here, the deflection function given in example 15.6 is

$$w = \frac{q}{24EI}(24x^2l^2 - 10x^3l + x^4)$$

and from that we get the rotations of the cross-section

$$\varphi = -\frac{\mathrm{d}w}{\mathrm{d}x} = \frac{q}{12EI}(-24xl^2 + 15x^2l - 2x^3)$$

The four bar elements are identical and have the following element stiffness matrices:

$$\boldsymbol{k} = \frac{EI}{l}\begin{bmatrix} 12/l^2 & -6/l & -12/l^2 & -6/l \\ -6/l & 4 & 6/l & 2 \\ -12/l^2 & 6/l & 12/l^2 & 6/l \\ -6/l & 2 & 6/l & 4 \end{bmatrix}$$

The first and fourth rows and columns in (17.17) are omitted because there are no loads in the x direction and no normal forces occur. Fig. 19.8(b) shows the corresponding, reduced degrees of freedom, of which V_1, V_2 and V_9 are passive.

According to the direct stiffness method, it is now possible to specify the global stiffness matrix:

$$\boldsymbol{K} = \frac{EI}{l}\begin{bmatrix} 24/l^2 & 0 & -12/l^2 & -6/l & 0 & 0 & 0 \\ 0 & 8 & 6/l & 2 & 0 & 0 & 0 \\ -12/l^2 & 6/l & 24/l^2 & 0 & -12/l^2 & -6/l & 0 \\ -6/l & 2 & 0 & 8 & 6/l & 2 & 0 \\ 0 & 0 & -12/l^2 & 6/l & 24/l^2 & 0 & -6/l \\ 0 & 0 & -6/l & 2 & 0 & 8 & 2 \\ 0 & 0 & 0 & 0 & -6/l & 2 & 4 \end{bmatrix}$$

We can see that this matrix contains only the rows and columns corresponding to the active degrees of freedom. Inversion leads to the global flexibility matrix

$$\boldsymbol{F} = \frac{l}{768EI}\begin{bmatrix} 135l^2 & -153l & 200l^2 & 12l & 133l^2 & 111l & 144l \\ -153l & 327 & -312l & 12 & -219l & -177 & -240 \\ 200l^2 & -312l & 448l^2 & -96l & 344l^2 & 264l & 384l \\ 12l & 12 & -96l & 240 & -156l & -84 & -192 \\ 133l^2 & -219l & 344l^2 & -156l & 351l^2 & 189l & 432l \\ 111l & -177 & 264l & -84 & 189l & 279 & 144 \\ 144l & -240 & 384l & -192 & 432l & 144 & 768 \end{bmatrix}$$

Using the load vector

$$\boldsymbol{Q} = ql\{1, 0, 1, 0, 1, 0, l/12\}^{\mathrm{T}}$$

results in the external deformation variables

$$\boldsymbol{V} = \begin{Bmatrix} w_2 \\ \varphi_2 \\ w_3 \\ \varphi_3 \\ w_4 \\ \varphi_4 \\ \varphi_5 \end{Bmatrix} = \boldsymbol{F} \cdot \boldsymbol{Q} = \frac{ql^3}{24EI}\begin{Bmatrix} 15l \\ -22 \\ 32l \\ -8 \\ 27l \\ 18 \\ 32 \end{Bmatrix}$$

which agree with the initially analytically specified values for w and φ at the quarter-points and the simply supported end of the beam, see Fig. 19.8(c).

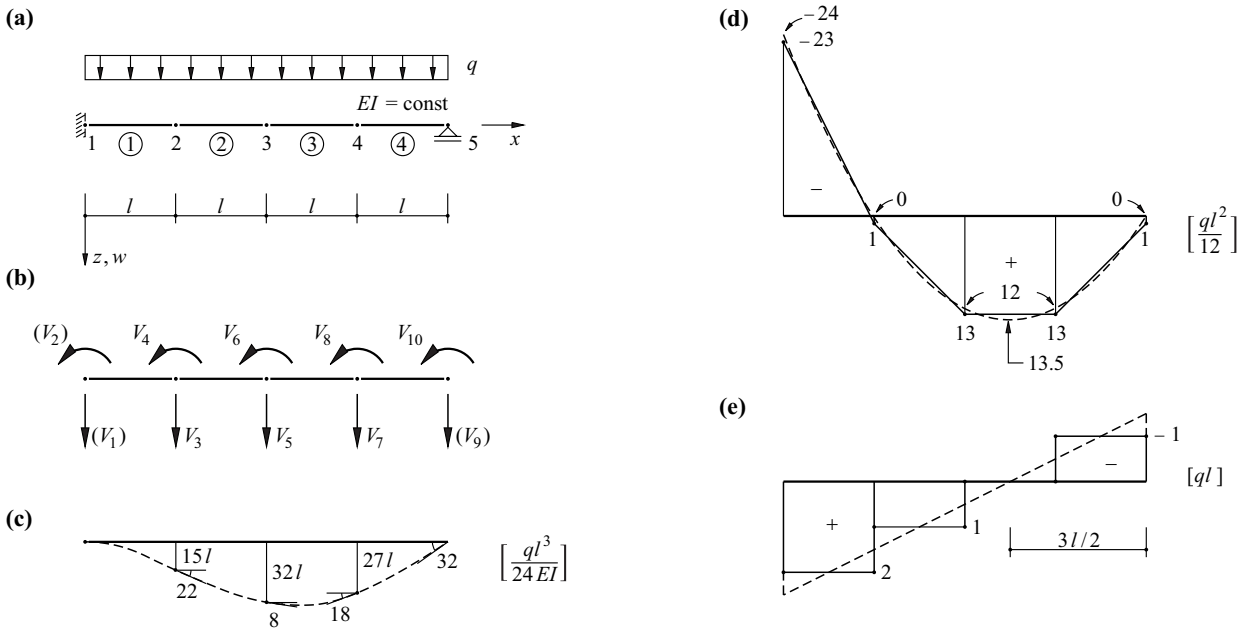

Fig. 19.8 Beam with one degree of static indeterminacy: (a) diagram of static system, (b) degrees of freedom, (c) deflection curve, (d) bending moments, (e) shear forces

Finally, (19.34) can be used to obtain the bending moments and shear forces shown in Fig. 19.8(d) and (e). The solid line in each diagram corresponds to the linear connection between the $\boldsymbol{k} \cdot \boldsymbol{v}$ values at the joints. The difference between this and the exact solution, which is indicated by the dotted line, is given by the fixed-end forces $\boldsymbol{s}_0$, see (19.42).

19.3.4 Shape functions

The main feature of the kinematic approach to the finite element method is that shape functions are introduced within the individual elements according to (19.28). The components of the displacement vector $\boldsymbol{u}$ are therefore presented as functions of the unknown joint displacement parameters $\boldsymbol{v}$. A coefficient Ω_{ij} in matrix $\boldsymbol{\Omega}$ specifies the value of displacement component u_i due to $v_j = 1$. Simple polynomial functions are mostly used for this.

The parametric displacement field formed with the shape functions Ω_{ij} should be continuous at the joints. This means that the parameters $\boldsymbol{v}$ must agree with the joint values for the displacements $\boldsymbol{u}$. Obviously, the shape functions play the role of *interpolating functions* for the components of the displacement vector $\boldsymbol{u}$.

The finite element method generally supplies approximate solutions that should converge to the exact solution as the element mesh is increasingly refined. To guarantee this, certain *convergence requirements* must be satisfied:

1. If the joint displacements $\boldsymbol{v}$ correspond to a rigid body deformation, then the strains $\boldsymbol{\varepsilon} = \boldsymbol{H} \cdot \boldsymbol{v}$ within the element must disappear, $\boldsymbol{\varepsilon} \equiv \boldsymbol{0}$.
2. If the joint displacements $\boldsymbol{v}$ correspond to a state of constant strains, then the strains must take on this value throughout the element, $\boldsymbol{\varepsilon} \equiv$ const.
3. If n stands for the highest order of the derivatives occurring in the kinematic operator $\boldsymbol{D}_k$, then the shape functions must satisfy the boundary conditions for $\boldsymbol{u}$ and its derivatives up to the order $n-1$ at the boundary of the element (essential boundary conditions, see section A7.2).

No exceptions are permitted to requirements 1 and 2, which concern the *completeness* of the formulation. Requirement 3 is not a problem for bar elements because the joints at the ends of each bar are the only boundary points of the element; however, in the case of two- and three-dimensional elements, this requirement regarding the *conformity* of the formulation can lead to difficulties and is not absolutely necessary in every case.

Formulations (19.35) and (19.39) satisfy all convergence requirements, a fact that is easily checked. In addition, all equilibrium conditions are fulfilled exactly (and not just approximately) for the case of prismatic bars (the only exception within the scope of the finite element method).

19.3.5 Commentary

The observations of sections 19.3.1, 19.3.2 and 19.3.4 generally apply to the kinematic approach to the finite element method. The treatment of bars rigid in shear in section 19.3.3 corresponds to one simple illustration of this method adapted to this introduction to FEM.

Most of the structural analysis programs that utilise the finite element method work according to the direct stiffness method described in section 17.3. The reader should refer to appropriate specialist publications for further information.

19.4 Summary

1. In contrast to the classic presentation of the force method (chapter 16), the matrix approach according to section 19.2 supplies both the global flexibility matrix $\boldsymbol{F}$ and the static transformation matrix $\boldsymbol{b}$. Although much more calculation work is necessary, the results are, however, much more general.
2. The columns j of matrices $\boldsymbol{b}$ and $\boldsymbol{F}$ contain the state variables s_i and V_i due to unit load $Q_j = 1$. However, the rows i of these matrices reveal how all Q_j values influence a certain state variable s_i or V_i.
3. The calculations are often carried out with a reduced number of degrees of freedom, e. g. owing to the assumption of inextensible bars. In doing so, certain external degrees of freedom are suppressed or combined.
4. In the $(m+n)$-dimensional space of the internal static variables $\boldsymbol{s}$, the m load and the n restraint states can be specified as required apart from the requirement regarding linear independence. In particular, it may be worthwhile considering orthogonal load or restraint states.
5. The heart of the kinematic approach to the finite element method is that shape functions are used to form a parametric displacement field within the individual finite elements. The joint displacement parameters $\boldsymbol{v}$ agree with the joint values for displacement $\boldsymbol{u}$, and the shape functions play the role of interpolating functions for the components of $\boldsymbol{u}$.
6. To guarantee the convergence of the solution, the shape functions must be complete and generally also conformal.
7. The element stiffness matrices are generally calculated with $(19.33)_2$, and the global stiffness matrix $\boldsymbol{K}$ is obtained by applying the direct stiffness method (section 17.3).

19.5 Exercises

19.1 Work through the frame with two degrees of static indeterminacy examined in section 16.2.4 in a similar way to example 19.1. Use the algorithm from section 19.2.4 ($EI = 46.875\,\mathrm{MNm}^2$, $EA = 9000\,\mathrm{MN}$, $GA_v \to \infty$) and compare the results with those of section 16.2.4.

19.2 Starting with (8.14) and using (8.8) and (8.9), prove the reduction theorem formulated in section 14.3 in the form $V_i = \boldsymbol{b}_{0i}{}^{\mathrm{T}} \bullet \boldsymbol{v}$. To this end, consider the deformation state $\boldsymbol{V}$, $\boldsymbol{v}$ of the statically indeterminate system as well as the force state in which the load vector $\boldsymbol{Q}$ contains only $Q_i = 1$.

19.3 Solve exercise 19.1 assuming inextensible bars (reduced degrees of freedom).

19.4 Determine the orthogonalised restraint states associated with exercise 19.3 in a similar way to example 19.2 and discuss the result.

19.5 Check some of the coefficients of the global flexibility matrix given in example 19.3. To do this, determine the bending moments occurring in the statically indeterminate system as a result of a unit force or a unit moment applied at any arbitrary point (see example 15.3) and apply the reduction theorem.

19.6 Determine the global stiffness matrix for the frame examined in exercise 19.3. Invert this and verify the results given in section 16.2.4.

20 ELASTIC-PLASTIC SYSTEMS

20.1 General

The linear elastic - perfectly plastic material behaviour for uniaxial loading, characterised by the two parameters E (modulus of elasticity) and f_y (yield limit) was introduced in section 7.1, see Fig. 7.3(c). A similar linear elastic - perfectly plastic moment-curvature diagram for analysing the structural behaviour of a frame with two degrees of static indeterminacy was presumed for Fig. 16.1(b) in section 16.2, but without any further explanation. The terms "plastic hinge", "limit load" and "mechanism" were used, but not investigated in depth. The analysis led to the depiction of the stress state in a system as a point in the $(m+n)$-dimensional space of the m load parameters Q_i and the n restraint parameters P_j (Fig. 16.7 and 16.9). The individual yield limits corresponded to hyperplanes that limit the non-plastic domain of the elastic-plastic system in the $(m+n)$-dimensional space, and the n-fold projection into the m-dimensional space of Q_i resulted in the non-plastic domain of the rigid-plastic system.

These deliberations will now be investigated in further detail with the help of a truss with one degree of static indeterminacy and a number of beam bending problems. One aim of this is to ease the transition to the rigid - perfectly plastic systems discussed in chapter 21, a form of structural behaviour that is not immediately accessible. The other aim is to demonstrate how deformations can be estimated in order to check the applicability of plastic methods of calculation in particular (first-order theory, adequate plastic deformation capacity).

20.2 Truss with one degree of static indeterminacy

20.2.1 Single-parameter loading

20.2.1.1 Monotonic loading

The three bars of the ideal truss shown in Fig. 20.1(a) are prismatic and homogeneous; they have a cross-sectional area A and are made from a material that behaves according to the linear elastic - perfectly plastic stress-strain diagram shown in Fig. 20.1(b). The load Q increases monotonically from zero to the limit load Q_u. The task is to find the associated vertical displacement $V_4 = V$ at joint 4, which corresponds to Q. To do this, it is first assumed that the system is initially free from restraints, i. e. we presume that the bar forces N_i of the unloaded system disappear: $N_i(Q = 0) \equiv 0$ (virgin system).

Equilibrium at joint 4, shown as a free body on the left of Fig. 20.1(c), calls for

$$(-N_1 + N_3)\frac{\sqrt{2}}{2} = 0 \quad , \quad N_2 + (N_1 + N_3)\frac{\sqrt{2}}{2} - Q = 0 \tag{20.1}$$

According to the displacement diagram shown on the right of Fig. 20.1(c), the following compatibility condition applies for elastic behaviour of the bars:

$$V = \frac{N_2 l}{EA} = \frac{2N_1 l}{EA} \tag{20.2}$$

Theory of Structures. First Edition. Peter Marti

Combining relationships (20.1) and (20.2) results in

$$N_1 = N_3 = \frac{N_2}{2} = \frac{Q}{2+\sqrt{2}} \quad , \quad V = \frac{Ql}{\left(1+\frac{\sqrt{2}}{2}\right)EA} \tag{20.3}$$

for the *elastic phase* OA in Fig. 20.1(d). The *onset of yield* ($N_2 = Af_y$) is then characterised by

$$Q_y = Af_y\left(1+\frac{\sqrt{2}}{2}\right) \quad , \quad V_y = \frac{f_y l}{E} \tag{20.4}$$

During the *elastic-plastic phase* AB according to Fig. 20.1(d), $N_2 = Af_y$. The system has become statically determinate. Eq. $(20.2)_1$ no longer applies, but nevertheless, $V = 2N_1 l/(EA)$. Together with (20.1), we get

$$N_1 = N_3 = \frac{Q - Af_y}{\sqrt{2}} \quad , \quad N_2 = Af_y \quad , \quad V = \frac{(Q - Af_y)\, l\sqrt{2}}{EA} \tag{20.5}$$

Point B ($N_1 = N_3 = Af_y$) marks the end of the elastic-plastic phase and the point at which the *limit load* is reached. Load and displacement here are

$$Q_u = Af_y(1+\sqrt{2}) \quad , \quad V_u = \frac{2f_y l}{E} \tag{20.6}$$

During the *plastic phase* BC according to Fig. 20.1(d), $N_1 = N_2 = N_3 = Af_y$ and $Q = Q_u$. There is no limit to how much V can increase beyond V_u; the system is kinematically unstable to the first degree, i. e. it has become a *mechanism*.

The elastic-plastic phase AB in Fig. 20.1(d), in which only bar 2 yields, is also called the phase of *contained plastic deformation*. Once the limit load Q_u has been reached at B, phase BC begins, the phase of *uncontained plastic deformation*.

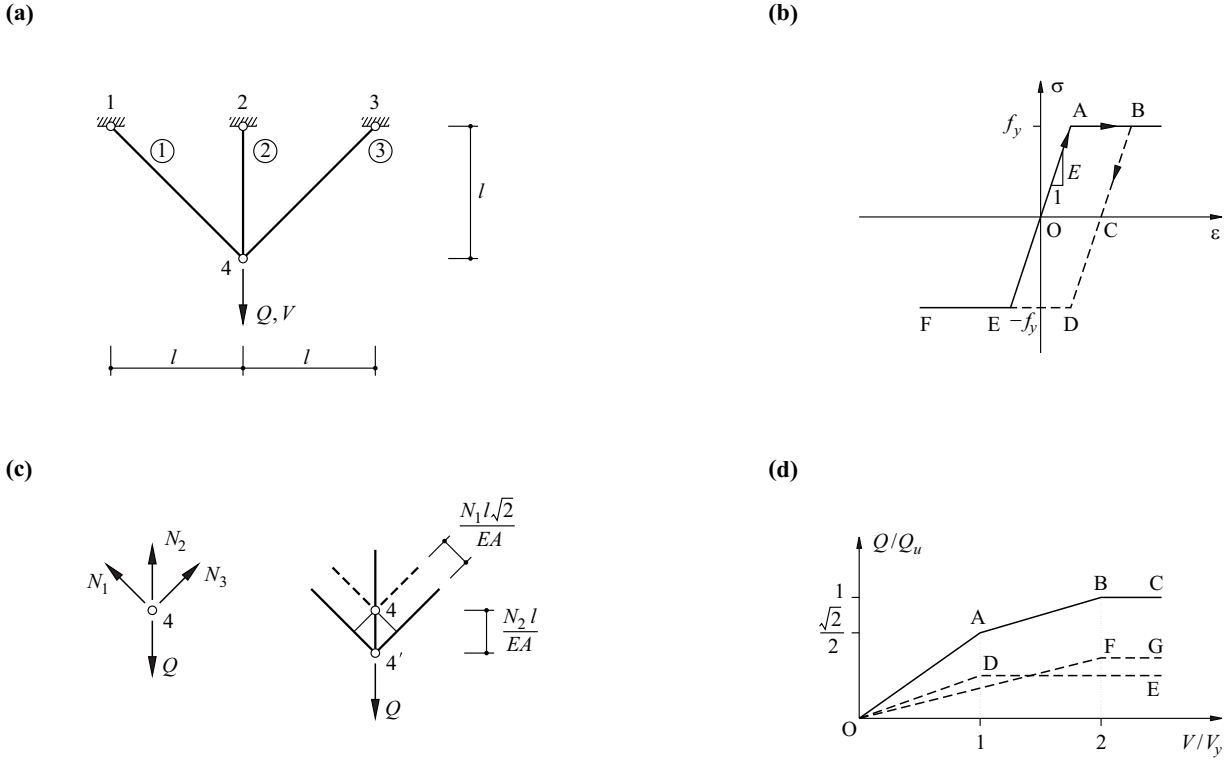

Fig. 20.1 Ideal truss: (a) diagram of static system, (b) stress-strain diagram, (c) equilibrium and compatibility at joint 4, (d) load-displacement diagram

We also note that a *geometric hardening* takes place during the plastic phase because of the increasing inclination α of bars 1 and 3, which is characterised by

$$Q = Af_y(1 + 2\sin\alpha) = Af_y\left[1 + \frac{2(l+V)}{\sqrt{l^2 + (l+V)^2}}\right] \tag{20.7}$$

Such second-order effects will not be considered below – we shall work according to first-order theory, see section 6.1 and example 8.3.

Lines ODE and OFG in Fig. 20.1(d) illustrate the behaviour of the single bar 2 and the pair of bars 1 and 3. Line OABC of the system made up of these individual systems results from adding together the appropriate ordinates $Q(V)$. The individual systems correspond to two non-linear springs working in parallel. Lines AB and OF are parallel; during the elastic-plastic phase, only bars 1 and 3 contribute to the stiffness.

20.2.1.2 Arbitrary loading processes

Line OABC in Fig. 20.2(a) corresponds to line OABC in Fig. 20.1(d). If we relieve the system starting at C, the point moves along CD, parallel with OA, to point D.

Fig. 20.2(b) illustrates how the bar forces change depending on Q. The lines OA or OB in Fig. 20.2(b) correspond to the elastic phase OA in Fig. 20.2(a). The lines AC or BC in Fig. 20.2(b) are allocated to the elastic-plastic phase AB in Fig. 20.2(a), and the plastic phase BC in Fig. 20.2(a) corresponds to point C in Fig. 20.2(b). Upon relieving the load starting at C, the point in Fig. 20.2(b) moves along CD or CE, parallel with lines OA or OB. Points D and E characterise the restraint state

$$N_1 = N_3 = -\frac{N_2}{\sqrt{2}} = Af_y\left(1 - \frac{\sqrt{2}}{2}\right) \tag{20.8}$$

If after relieving the system completely the loading is continued in the opposite direction, the point in Fig. 20.2(b) moves along DF or EG, and the point in Fig. 20.2(a) along DE. Point F in Fig. 20.2(b) is where bar 2 reaches the yield limit $-f_y$; the load associated with this is $Q = Q_u - 2Q_y = -Af_y = (1 - \sqrt{2})Q_u$. The lines FH or GH in Fig. 20.2(b) correspond to the subsequent elastic-plastic phase EF in Fig. 20.2(a). Once the yield limit $-f_y$ has been reached in bars 1 and 3, point H in Fig. 20.2(b), the result is the plastic phase FHI with $Q = -Q_u$ in Fig. 20.2(a). Buckling of the bars in compression is ruled out here.

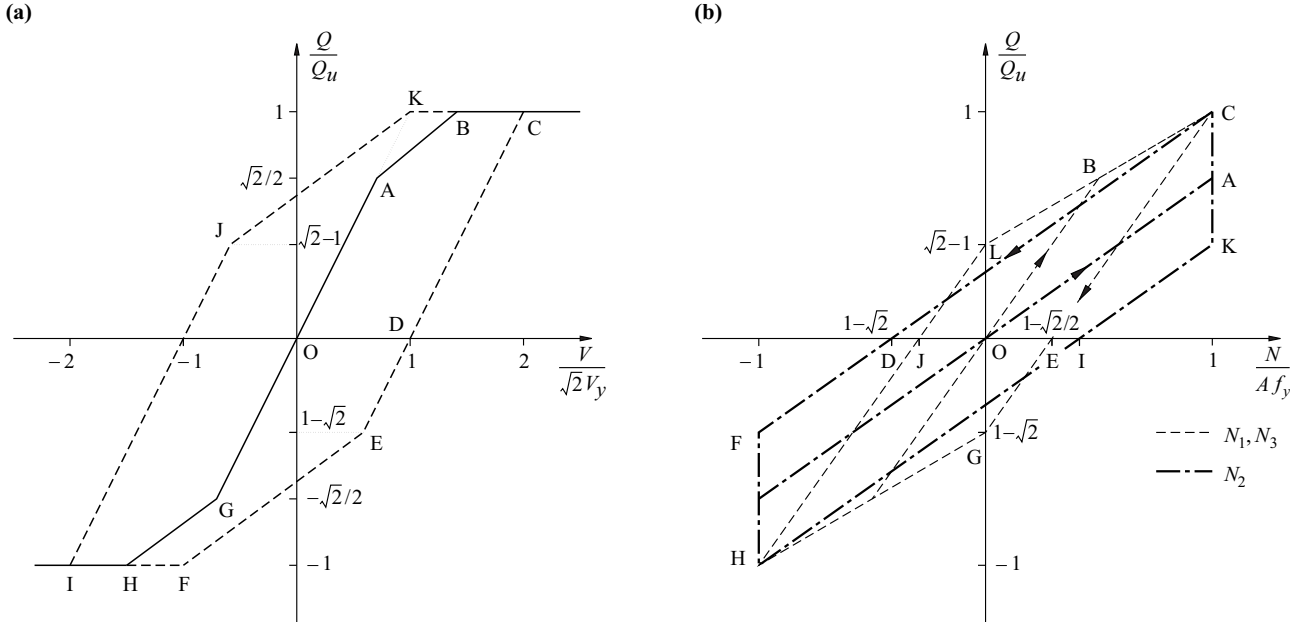

Fig. 20.2 The influence of loading processes on: (a) displacements, (b) bar forces

Upon reapplying the load, the point in Fig. 20.2(a) moves from I along line IJK, and in Fig. 20.2(b) along HIKC or HJLC. The restraint state characterised by points I and J in Fig. 20.2(b) is just the opposite of the restraint state D,E described by (20.8), i. e. a tensile force of $(\sqrt{2}-1)Af_y$ prevails in bar 2, which is balanced by the compressive forces of $(1-\sqrt{2}/2)Af_y$ in each of the bars 1 and 3.

If the system is relieved starting at point K in Fig. 20.2(a), the point returns to the origin O. The remaining restraint state is once again described by points D and E in Fig. 20.2(b) or by (20.8). In the event of a subsequent reloading, the points would move purely elastically along OAK in Fig. 20.2(a) or DC and EC in Fig. 20.2(b). In this case, the restraint state corresponds to a favourable *prestressing* of the system which postpones the onset of yield until the limit load is reached.

The yield limit of the system previously plastically deformed in tension is reached at point E in Fig. 20.2(a) with a compressive force Q amounting to $(\sqrt{2}-1)Q_u$. If the system had not been plastically deformed in tension first of all, the onset of yield would have taken place at point G in Fig. 20.2(a), i. e. at a compressive force Q amounting to $Q_u/\sqrt{2}$. The drop in the yield limit as a result of a prior plastic deformation in the opposite direction is named after BAUSCHINGER. The decrease in stiffness linked with the BAUSCHINGER *effect* is mainly important in second-order problems.

20.2.1.3 Yield loci

The yield conditions

$$|N_i| \leq Af_y \qquad (i = 1, 2, 3) \tag{20.9}$$

restrict the location of potential points in Fig. 20.3(a) to strip-like zones that intersect to form the weakly convex square ABCD. According to the thinking so far, superposing a *restraint state*

$$P\boldsymbol{N_r} = P\begin{Bmatrix} -\sqrt{2}/2 \\ 1 \\ -\sqrt{2}/2 \end{Bmatrix}$$

and an elastically compatible *loading stress state*

$$Q\boldsymbol{N_e} = \frac{Q}{2+\sqrt{2}}\begin{Bmatrix} 1 \\ 2 \\ 1 \end{Bmatrix}$$

can represent any stress state

$$\boldsymbol{N} = Q\boldsymbol{N_e} + P\boldsymbol{N_r} \tag{20.10}$$

where $\boldsymbol{N_e}$ and $\boldsymbol{N_r}$ denote the load-dependent elastic and zero-load or residual (i. e. remaining after relieving the system completely) unit stress states respectively.

If instead of N_2 and $N_{1,3}$ we choose the load parameter Q and the restraint parameter P as our coordinates, the square ABCD of Fig. 20.3(a) transforms into the parallelogram ABCD of Fig. 20.3(b). Here, N_2 and $N_{1,3}$ form a skewed system of coordinates that is orthogonal to the corresponding yield limits in tension (2^+ and $1^+, 3^+$) or compression (2^- and $1^-, 3^-$).

Upon loading the initially restraint-free (virgin) system for the first time, the point in Fig. 20.3(b) moves along OEA to point A, where the limit load Q_u is reached. Subsequently relieving the load takes place purely elastically, i. e. the point moves along AF parallel with the Q axis. Loading in the opposite direction and reloading leads to the form FGCHIEA etc. Applying this loading cycle several times carries with it the risk of exhausting the deformation capacity as a result of the *alternating plasticity* of bar 2 in compression or tension corresponding to lines GC and IEA. In more general cases, *progressive plastification* of a sufficient number of areas of a system can lead to its failure.

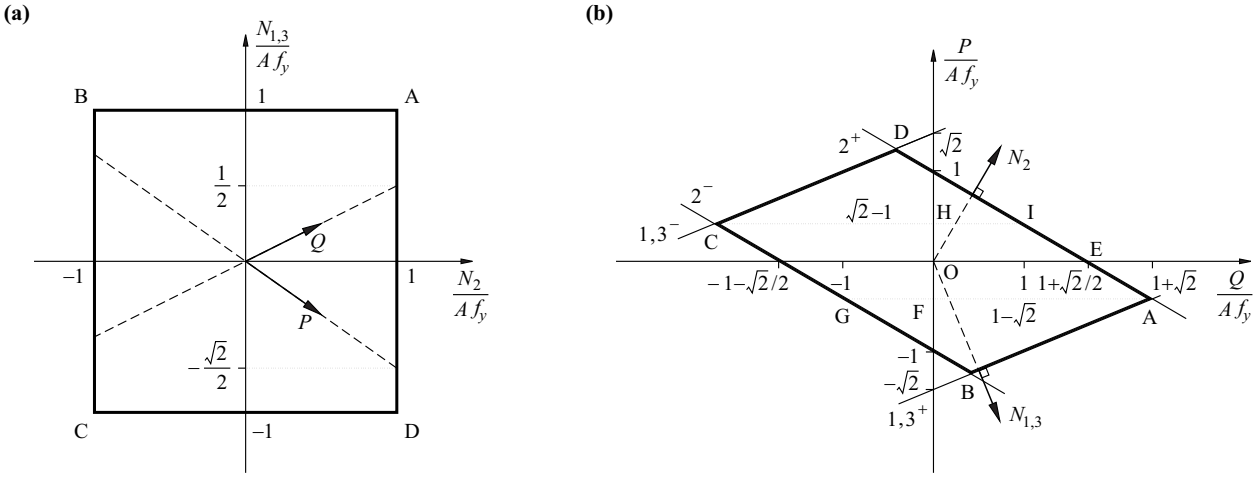

Fig. 20.3 Yield loci: (a) bar forces, (b) load and restraint

20.2.1.4 Initial restraints and general loading histories

Presuming that a system is initially free from restraints, point O in Fig. 20.3(b), is a – mostly implicit – assumption made during structural analysis, but is in no way trivial. If, for example, during the erection of the truss bar 2 turned out to be too short, this inaccurate fit could be corrected with a corresponding restraint, which would result in an initial tensile force P in bar 2 and an initial compressive force of $P/\sqrt{2}$ in each of the bars 1 and 3. Compared with the initially zero-restraint system, the elastic phase would be shortened (e. g. HI instead of OE) but the limit load would remain unaffected (point A).

Initial restraint states can also ensue as a result of thermal deformations as well as settlement, slip at connections, shrinkage or swelling and similar effects. For example, a temperature change T with a constant α_T corresponds to the restraint $P = EA\alpha_T T/(1 + \sqrt{2})$. As we can see, with the help of Fig. 20.3(b), any restraint cycles and hence general loading histories can basically be discussed in a similar way to the loading cycles. However, in practice it is in most cases far harder to estimate the initial restraint states (and possibly later restraint cycles) than the potential loading cycles. The significance of Fig. 20.3(b) is therefore primarily qualitative. It shows that apart from points A and C, where the limit load is reached, the stress state is dependent on the loading history, but can only be determined roughly because it is difficult to quantify the restraints. In particular, it is clear that the loading stress state occurring in the virgin system cannot be guaranteed to be the priority case when compared with other statically admissible force states. The statically admissible force states for a certain loading differ only in terms of their restraint components. In Fig. 20.3(b) they correspond to points on so-called *equilibrium lines* parallel with the P axis.

Obviously, the resistance of the system is not exhausted when it is possible to specify a statically admissible force state in which the yield limit is not reached anywhere. In Fig. 20.3(b), such a state of equilibrium corresponds to a point on the equilibrium line belonging to the respective loading Q within the yield locus ABCD. This finding is generalised in section 21.2 using the static or *lower-bound theorem*.

If, conversely, a kinematically admissible deformation state can be specified which turns the system into a mechanism, the resistance must have been exhausted; this is the case for points A and C in Fig. 20.3(b). This finding is generalised in section 21.2 using the kinematic or *upper-bound theorem*.

Varying the loading Q between given limiting values and specifying a restraint state P such that the ensuing limiting values for stress do not exceed the yield limit anywhere causes the system to behave purely elastically, possibly following initial plastification.

The system adapts to the given loading, it undergoes shakedown as we say, i. e. the risk of failure due to alternating plasticity or progressive plastification is averted. For example, if Q is varied between the limiting values corresponding to points A and G in Fig. 20.3(b), the system experiences shakedown; the associated restraint state P corresponds to point F. We can generalise this result as the *shakedown theorem*: given loading limit values lie within the *adaptability* of a system if a restraint state can be specified in such a way that the resulting limiting values for stress do not exceed the yield limit anywhere.

The limit load that can be contained by the upper- and lower-bound theorems relates to the failure of a system subjected to a one-off loading. By comparison, the shakedown theorem relates to a loading that can be accommodated elastically any number of times; an *incremental plastic failure* may occur at the limit of adaptability, which is characterised by the successive increase in plastic deformations as a result of the cyclic loading. The relationship between the limit load and the shakedown load, which cannot be greater than the limit load, is discussed further in section 21.5.

20.2.1.5 Complementary internal total potential

The theorem of least complementary (internal) total potential Π_i^* was formulated in section 8.4.2. According to the theorem, in a conservative system subjected to rigid constraints $\boldsymbol{r}_0 \equiv \mathbf{0}$, the real statically admissible stress state is the one for which Π_i^* is a minimum. And according to ENGESSER's theorem, the partial derivative of Π_i^* with respect to a force variable Q supplies the corresponding deformation variable V.

Owing to the plastic deformability, the current system is not conservative. The expression

$$\Pi_i^* = \sum_{j=1}^{3} \frac{N_j^2 l_j}{2EA}$$

therefore generally corresponds to a fictitious potential. Taking into account (20.9) results in

$$\Pi_i^* = Q^2 \sum_{j=1}^{3} \frac{N_{ej}^2 l_j}{2EA} + QP \sum_{j=1}^{3} \frac{N_{ej} N_{rj} l_j}{EA} + P^2 \sum_{j=1}^{3} \frac{N_{rj}^2 l_j}{2EA} \tag{20.11}$$

As the restraint state $\boldsymbol{N}_r$ does no work on the deformations of the elastically compatible stress state $\boldsymbol{N}_e$, the second term on the right in (20.11) disappears, and the outcome is (exercise 20.1)

$$\Pi_i^* = Q^2 \frac{l}{(2+\sqrt{2})EA} + P^2 \frac{(1+\sqrt{2})l}{2EA} \tag{20.12}$$

According to (20.12), the equipotential lines Π_i^* = const in the QP plane are ellipses, and the terms on the right in (20.12) correspond to the triangular areas Π_e^* and Π_r^* in the Q-V diagram, see Fig. 20.4(a) and (b).

Points O, E and A in Fig. 20.4(a) correspond to points O and A and line GH in Fig. 20.4(b) and, vice versa, point B in Fig. 20.4(b) corresponds to a point on line EA in Fig. 20.4(a). With a monotonic rise in the load from O to B, the stress state changes in such a way that Π_i^* is minimised each time without the yield limit being exceeded anywhere. The point in Fig. 20.4(a) moves from O to E and then along EA – points below this line would correspond to larger Π_i^* values. Differentiating Π_e^* with respect to Q results in the elastic deformation

$$V_e = \frac{\mathrm{d}\Pi_e^*}{\mathrm{d}Q} = \frac{2Ql}{(2+\sqrt{2})EA} \tag{20.13}$$

see $(20.3)_4$, and taking into account the relationship

$$P + \frac{2Q}{2+\sqrt{2}} = Af_y \tag{20.14}$$

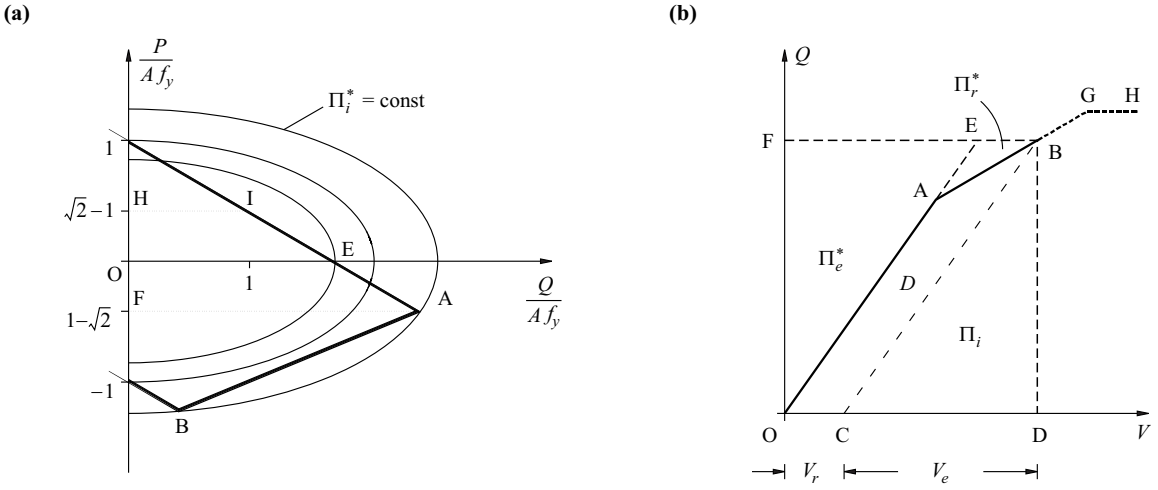

Fig. 20.4 Complementary internal potential: (a) yield locus and equipotential lines, (b) elastic-plastic deformation $V = V_e + V_r$, internal potential Π_i, dissipation D and complementary internal potential $\Pi_i^* = \Pi_e^* + \Pi_r^*$

for the yield limit IEA in Fig. 20.4(a) results in

$$\frac{\mathrm{d}\Pi_r^*}{\mathrm{d}Q} = \frac{P(1+\sqrt{2})l}{EA} \cdot \frac{-2}{2+\sqrt{2}} = \frac{-\sqrt{2}Pl}{EA} \tag{20.15}$$

If point B coincides with A or G in Fig. 20.4(b), eq. (20.15) gives us the values 0 or $(2-\sqrt{2})lf_y/E$, and between these the result is a linear variation with Q. Clearly, these values correspond precisely to the respective plastic deformation, i. e. the deformation remaining after relieving the load completely:

$$V_r = \frac{\mathrm{d}\Pi_r^*}{\mathrm{d}Q} \tag{20.16}$$

The following generally applies for the *elastic-plastic deformation*:

$$V = V_e + V_r \tag{20.17}$$

Apart from Π_e^* and Π_r^* (triangles OEF and ABE), Fig. 20.4(b) also identifies the internal potential Π_i (triangle CDB) belonging to B and the corresponding dissipation energy D (OABC). As the load is relieved (BC), the energy Π_i stored elastically is retrieved. By contrast, D is dissipated during phase AB (contained plastic deformation), i. e. is converted into heat. We can read off the relationship

$$QV_r = D + \Pi_r^* = \int_{\mathrm{O}}^{\mathrm{C}} Q\,\mathrm{d}V_r + \int_{\mathrm{A}}^{\mathrm{E}} V_r\,\mathrm{d}Q \tag{20.18}$$

for parallelogram OCBE and, similarly,

$$QV_e = \Pi_i + \Pi_e^* \tag{20.19}$$

applies.

20.2.2 Dual-parameter loading and generalisation

Applying an arbitrary loading $\boldsymbol{Q}$ to joint 4 in Fig. 20.5(a), with vertical and horizontal components Q_1 and Q_2, results in

$$\boldsymbol{N} = \begin{Bmatrix} N_1 \\ N_2 \\ N_3 \end{Bmatrix} = \frac{Q_1}{2+\sqrt{2}} \begin{Bmatrix} 1 \\ 2 \\ 1 \end{Bmatrix} + \frac{Q_2}{\sqrt{2}} \begin{Bmatrix} 1 \\ 0 \\ -1 \end{Bmatrix} + P \begin{Bmatrix} -\sqrt{2}/2 \\ 1 \\ -\sqrt{2}/2 \end{Bmatrix} \tag{20.20}$$

instead of (20.10). The yield conditions (20.9) in conjunction with (20.20) result in areas in space Q_1, Q_2, P which are bounded by parallel planes and whose intersection forms the parallelepiped of Fig. 20.6. Fig. 20.5(b) shows, on the one hand, the intersection IJKLMN of the parallelepiped with plane $P = 0$ and, on the other, the projec-

tion ABCDEF of the parallelepiped onto this plane. Parallelogram AGDH in plane $Q_2 = 0$ in Fig. 20.6 corresponds to parallelogram ADCB in Fig. 20.3(b).

The intersection IJKLMN of the parallelepiped with plane $P = 0$ corresponds to the yield locus, or rather the non-plastic domain, of the initially restraint-free elastic-plastic system. The side faces ABGF and HCDE of the parallelepiped ($N_2 = \pm Af_y$) give rise to lines of intersection NI and KL, faces ABCH and DEFG ($N_1 = \pm Af_y$) to lines of intersection IJ and LM, and faces AHEF and BCDG ($N_3 = \pm Af_y$) to lines of intersection MN and JK.

The projection of the parallelepiped onto plane $P = 0$ corresponds to the yield locus, or rather the non-plastic domain, of the rigid-plastic system. Hexagon ABCDEF in Fig. 20.5(b) is identical with A′B′C′D′E′F′ in Fig. 20.6. At the limit load, two bars yield in tension or compression, and the third bar remains elastic. In Fig. 20.5(b), the bars that remain elastic are indicated by double lines, the ones yielding in tension or compression by a single solid or dotted line respectively. The bars that remain elastic do not undergo any additional deformations due to the mechanisms that become established at the limit load. They behave like rigid bars, and the displacement increments $\dot{\boldsymbol{V}}$ for joint 4 must be orthogonal to these bars. As we can see, the vectors $\dot{\boldsymbol{V}}$ for yield locus ABCDEF are orthogonal, outward vectors, see (7.12). At the corners of the yield locus, $\dot{\boldsymbol{V}}$ generally lies between the orthogonal vectors of the adjoining sides of the yield locus, see (7.13).

Let us consider an arbitrary vector $\boldsymbol{Q}$ with an end-point at the yield limit of the rigid-plastic system and the displacement increment $\dot{\boldsymbol{V}}$ compatible with this plus an arbitrary vector $\boldsymbol{Q}^*$ with an end-point within the yield limit. In this situation

$$(\boldsymbol{Q} - \boldsymbol{Q}^*) \cdot \dot{\boldsymbol{V}} \geq 0 \tag{20.21}$$

applies, see (7.18). The *principle of maximum dissipation energy* discussed in section 7.3.2 applies not only in the space of the stresses $\boldsymbol{\sigma}$ but also in the space of

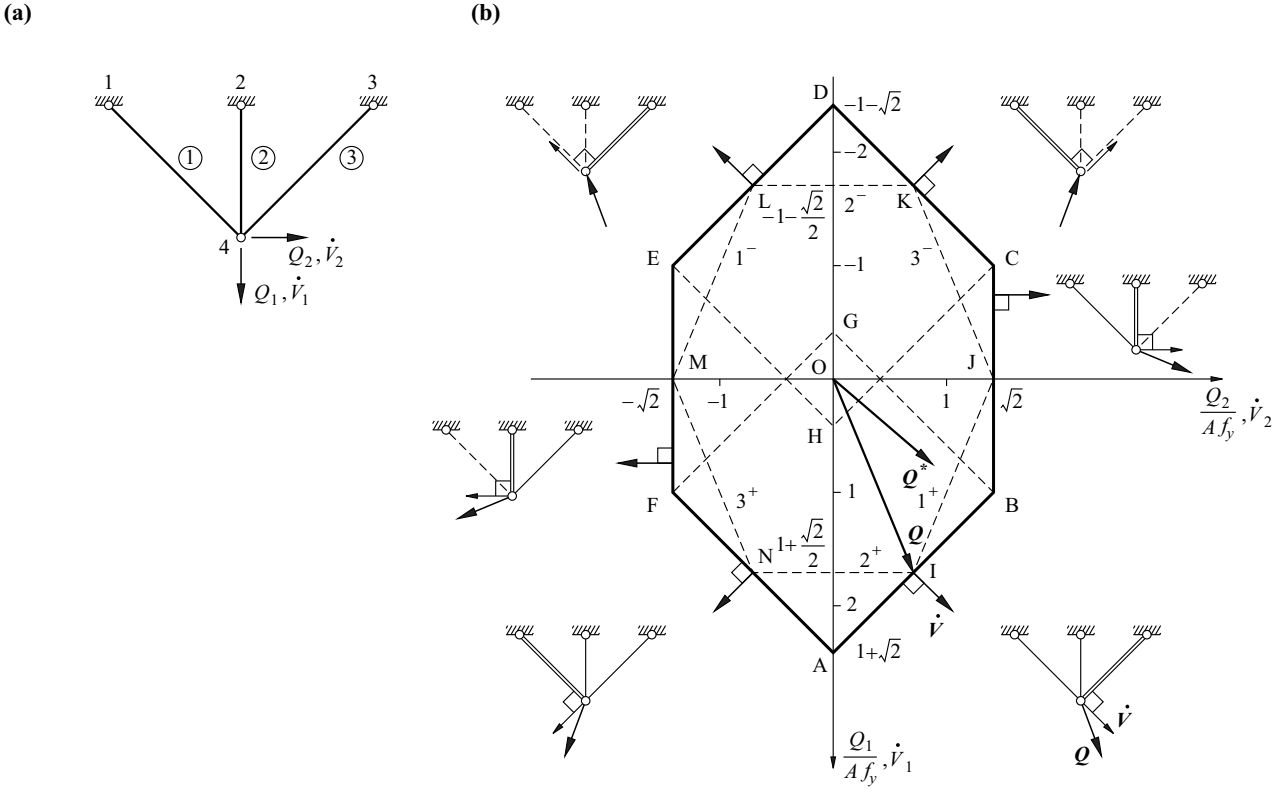

Fig. 20.5 Dual-parameter loading: (a) diagram of static system, (b) yield loci ABCDEF (rigid-plastic) and IJKLMN (elastic-plastic) plus mechanisms

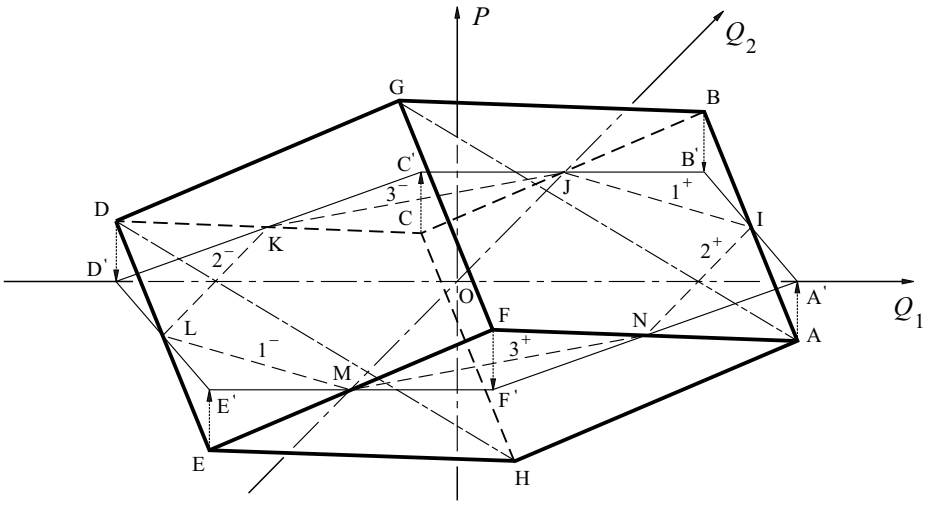

Fig. 20.6 Yield surface of the elastic-plastic system – intersection IJKLMN with plane Q_1-Q_2 and projection A′B′C′D′E′F′ onto plane Q_1-Q_2

the loads $\boldsymbol{Q}$. Convex yield surfaces ensue within this space, and the outward orthogonal vectors $\dot{\boldsymbol{V}}$ describe the associated mechanisms for points on the yield surface.

During the phase of contained plastic deformation, the non-plastic domain of the elastic-plastic system changes successively with the loading. This corresponds to intersections P = const of the parallelepiped shown in Fig. 20.6. For example, the transformation of the plastic zone from hexagon IJKLMN to triangle ACE in Fig. 20.5(b) corresponds to the transition from point E to point A in Fig. 20.3(b). By contrast, the triangular non-plastic domain BDF in Fig. 20.5(b) corresponds to the opposite limiting case, i. e. point C in Fig. 20.3(b).

Axes N_1, N_2, N_3 forming a skewed system of coordinates orthogonal to the side faces of the parallelepiped could be introduced in Fig. 20.6 in a similar way to Fig. 20.3(b). On the other hand, the yield conditions (20.9) in the Cartesian space with the coordinates N_1, N_2, N_3 as a non-plastic domain result in a cube, and the axes Q_1, Q_2, P form a skewed system of coordinates within this, similar to axes Q, P_1, P_2 in Fig. 16.9. The normal forcesN_i are – like the moments M_i in Fig. 16.9 – *generalised stresses* $\boldsymbol{s}$, i. e. internal force variables that correspond to the external force variables $\boldsymbol{Q}$. The corresponding internal deformation variables, which correspond to the external deformation variables $\dot{\boldsymbol{V}}$, are *generalised deformation increments* $\dot{\boldsymbol{v}}$, i. e. bar extension increments in the case of N_i and rotation increments in the case of M_i. Obviously, the relationship

$$(\boldsymbol{s} - \boldsymbol{s}^*) \bullet \dot{\boldsymbol{v}} \geq 0 \tag{20.22}$$

which is similar to (20.21), applies for vectors $\boldsymbol{s}$ with an end-point on the yield surface, the deformation increments $\dot{\boldsymbol{v}}$ corresponding to that and arbitrary vectors $\boldsymbol{s}^*$ with an end-point within the yield surface; i. e. the principle of maximum dissipation also applies in the space of the generalised stresses.

We also note that for a mechanism to form, a sufficient expansion of the yielding areas of the system is necessary. According to Fig. 20.6, this is the case for the edges AB, BC, CD, DE, EF and FA of the parallelepiped where the yield surfaces of two bars coincide each time, and which are mapped during the projection onto plane $P = 0$ in Fig. 20.5(b). According to Fig. 16.9, this is the case for point I (where the yield surfaces $M_2 = -M_3 = M_4 = M_y$ meet), which is projected onto the Q axis parallel with plane P_1P_2.

20.3 Beams in bending

20.3.1 Moment-curvature diagrams

20.3.1.1 Rectangular cross-section

The rectangular cross-section shown in Fig. 20.7(a) is subjected to a bending moment M about the y axis. All the fibres of the cross-section exhibit a linear elastic - perfectly plastic behaviour according to the stress-strain diagram shown in Fig. 20.1(b) and it is assumed that all cross-sections remain plane according to (13.3), i. e. $\varepsilon = z\chi$, see Fig. 20.7(b).

The elastic behaviour is characterised by $\sigma = E\varepsilon$ and $M = EI\chi$, with $I = bh^3/12$, see $(13.8)_2$ and $(13.9)_2$. With a monotonic rise in M, this phase is concluded by the onset of yield, where

$$\chi_y = \frac{2f_y}{Eh} \quad , \quad M_y = \frac{bh^2 f_y}{6} = Wf_y \tag{20.23}$$

and $W = bh^2/6 = I/(h/2)$ is the *elastic section modulus* of the cross-section, see Fig. 20.7(c).

The following applies in the subsequent elastic-plastic phase:

$$\chi = \frac{f_y}{E\zeta h} \quad , \quad M = \left(\frac{bh^2}{4} - \frac{b\zeta^2 h^2}{3}\right) f_y \tag{20.24}$$

where $1/2 \geq \zeta > 0$, i. e. when using (20.23)

$$\frac{M}{M_y} = \frac{3}{2} - \frac{\chi_y^2}{2\chi^2} \tag{20.25}$$

So when $\chi \to \infty$, the resistance of the cross-section

$$M_u = \frac{bh^2 f_y}{4} = Zf_y = fM_y \tag{20.26}$$

is reached; Z is the *plastic section modulus* of the cross-section and the quotient $f = Z/W = 1.5$ is called the *shape factor* of the cross-section.

Fully relieving the elastic-plastic cross-section subjected to M according to $(20.24)_2$ leaves behind the extreme fibre stresses at top and bottom

$$\mp \sigma_{r1} = \pm \left(f_y - \frac{M}{W}\right) = \pm f_y \left(2\zeta^2 - \frac{1}{2}\right) \tag{20.27}$$

as well as the stresses

$$\pm \sigma_{r2} = \pm \left(f_y - 2\zeta \frac{M}{W}\right) = \pm f_y (1 - 3\zeta + 4\zeta^3) \tag{20.28}$$

at the extreme fibres $z = \pm \zeta h$ of the elastic core of the cross-section, see Fig. 20.7(d).

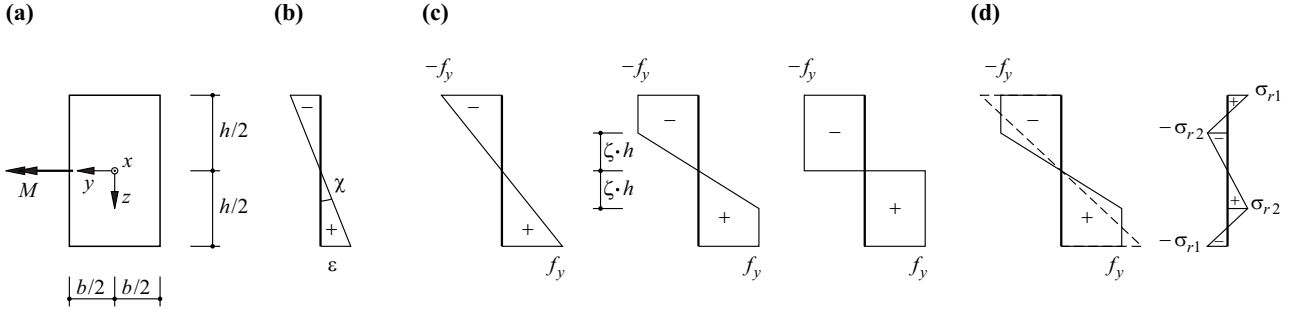

Fig. 20.7 Rectangular cross-section: (a) notation, (b) strains, (c) stress distribution at onset of yield, in elastic-plastic phase and upon reaching the resistance of the cross-section, (d) relieving the load and distribution of residual stresses

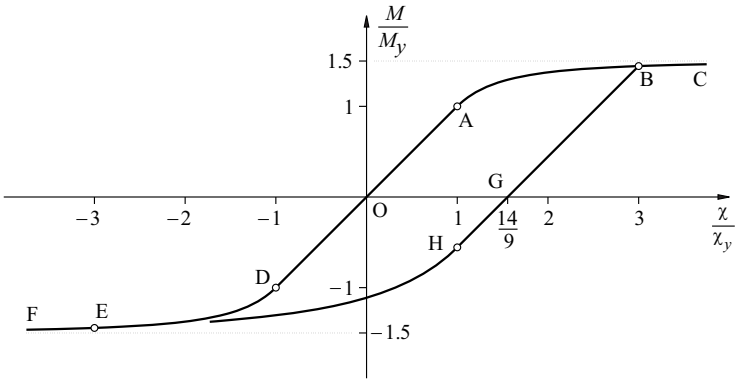

Fig. 20.8 Moment-curvature diagram for the rectangular cross-section of Fig. 20.7

Fig. 20.8 summarises the moment-curvature behaviour of the cross-section. The elastic-plastic phase ABC follows the elastic phase OA. Upon relieving the load, e. g. starting at B ($\chi = 3\chi_y$, $M = 13M_y/9$), a curvature of $14\chi_y/9$ remains, corresponding to point G. With $\zeta = 1/6$, eq. (20.27) and (20.28) give us the values $\sigma_{r1} = 4f_y/9$ and $\sigma_{r2} = 14f_y/27$, which characterise the residual stress state.

Continuing the loading in the opposite direction starting from point G in Fig. 20.8 brings us to point H ($\chi = \chi_y$, $M = -5M_y/9$), the onset of yield for the extreme fibres at top and bottom in tension and compression. Comparing this with the onset of yield at D ($M = -M_y$) in the virgin system, we notice once again the BAUSCHINGER effect discussed in section 20.2.1.

20.3.1.2 General cross-sections and stress resultants

As described in section 13.2.1, the planar distribution (13.3) of the strains ε_x allows us to determine the stress resultants belonging to a set of deformation variables ε, χ_y, χ_z for cross-sections of any shape and composition from the stress-strain relationships $\sigma_x = \sigma_x(\varepsilon_x)$ of the individual fibres by means of integration. However, calculating the deformation variables ε, χ_y, χ_z belonging to a set of stress resultants N, M_y, M_z generally calls for an iterative procedure. Such an approach enables us, for example, to work out a set of M_y-χ_y diagrams point by point for various normal forces N = const for a column cross-section where $M_z = 0$.

Profiled beam sections have much smaller shape factors f than beams with a solid cross-section, e. g. f for HEA-type beams varies between about 1.10 and 1.15. In practice, therefore, we often neglect the small difference between M_u and M_y in deformation calculations and work with a linear elastic - perfectly plastic moment-curvature diagram, see Fig. 16.1(b). By assuming a shape factor of 1, the expansion of the plastified zones is neglected, which results in ideal *plastic hinges* in the most heavily stressed sections. This means the stiffness is somewhat overestimated. But as the strain hardening is also ignored, this effect is practically compensated for.

20.3.2 Simply supported beams

20.3.2.1 Simply supported beam with central point load

The simply supported beam with a rectangular cross-section shown in Fig. 20.9(a) is loaded at mid-span by a monotonically increasing point load Q. The task is to find the associated deflection w_m at mid-span. We shall assume that the beam is initially free from residual stresses, i. e. we shall work with the moment-curvature diagram OABC according to Fig. 20.8.

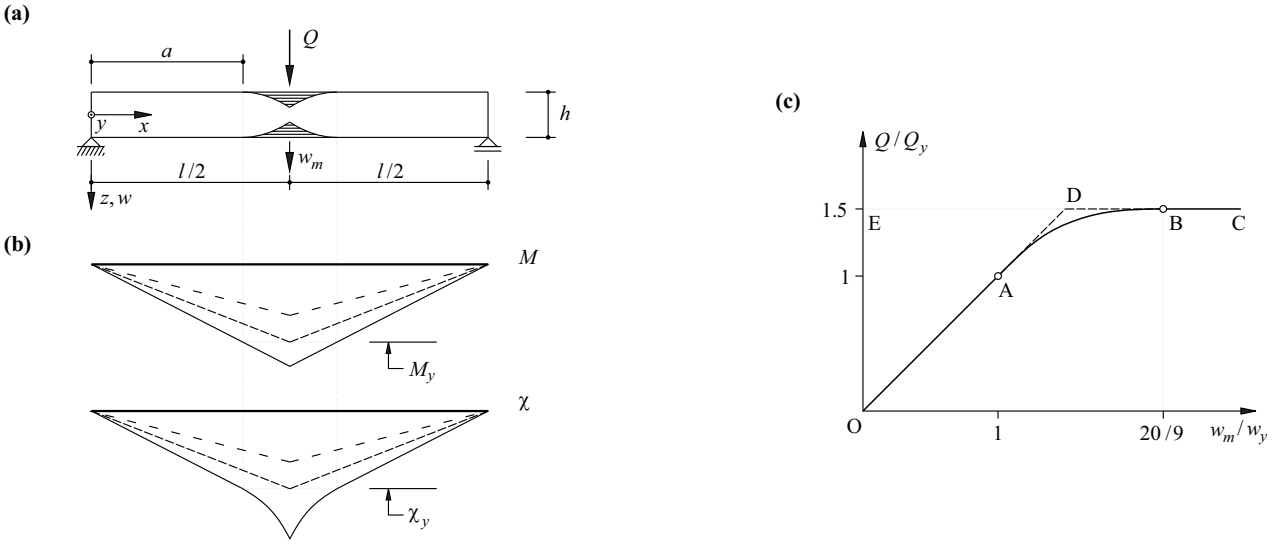

Fig. 20.9 Simply supported beam with rectangular cross-section: (a) diagram of static system, (b) moments and curvatures, (c) load-deflection diagram (mid-span)

Fig. 20.9(b) illustrates the bending moments M and the associated curvatures χ. When loaded with

$$Q_y = \frac{4M_y}{l} \tag{20.29}$$

the onset of yield is established at mid-span. The associated deflection at mid-span is

$$w_y = \frac{\chi_y l^2}{12} = \frac{Q_y l^3}{48EI} \tag{20.30}$$

When $Q > Q_y$, the onset of yield takes place at the edges of the cross-section at a distance of

$$a = \frac{l\,Q_y}{2Q} \tag{20.31}$$

from the support. The shading in Fig. 20.9(a) indicates the plastified zones that form in the region of the load. The following applies in the remaining elastic zone $0 \le x < a$:

$$\chi = -w'' = \chi_y\, x/a$$

and therefore

$$w = -\frac{\chi_y\, x^3}{6a} + c_1 x + c_2$$

In the partially plastified zone $a \le x \le l/2$, as $M = M_y x/a$ and (20.25), then

$$\chi = \frac{\chi_y}{\sqrt{3 - 2x/a}}$$

and therefore

$$w = -\chi_y (3 - 2x/a)^{3/2} \cdot a^2/3 + c_3 x + c_4$$

Using the boundary condition $w(0) = 0$, the symmetry condition $w'(l/2) = 0$ and the fact that w and w' must be continuous for $x = a$, we get

$$c_1 = \chi_y a\left[3/2 - (3 - l/a)^{1/2}\right] \quad , \quad c_2 = 0 \quad , \quad c_3 = -\chi_y a\,(3 - l/a)^{1/2} \quad , \quad c_4 = 5\chi_y a^2/3$$

and hence (exercise 20.4), taking into account (20.29), (20.30) and (20.31),

$$w_m = w_y \left(\frac{Q_y}{Q}\right)^2 \left[5 - \left(3 + \frac{Q}{Q_y}\right)\left(3 - \frac{2Q}{Q_y}\right)^{1/2}\right] \tag{20.32}$$

In Fig. 20.9(c), eq. (20.32) describes the arc AB. Upon reaching the limit load $Q_u = 1.5Q_y = fQ_y$, the final deflection at mid-span for point B is $w_m = 20w_y/9$, although the curvature χ at $x = l/2$ when subjected to Q_u is infinitely large. The extreme fibres are plastified over a length of $l - 2a = l/3$ upon reaching the limit load Q_u.

A bilinear moment-curvature diagram (shape factor = 1) would give the approximation OADBC in Fig. 20.9(c). If the elastic deformations were to be ignored, the result would be the rigid - perfectly plastic behaviour OEDBC. In both cases, the plastic deformation would be confined to the cross-section beneath the load Q, i. e. an ideal plastic hinge would form at this point.

20.3.2.2 Simply supported beam with uniformly distributed load

Loading the simply supported beam, which is initially free from residual stresses, with a monotonically increasing uniformly distributed load q instead of a central point load Q results in the onset of yield at mid-span at a load of $q_y = 8M_y/l^2$. The limit load is $q_u = 12M_y/l^2 = fq_y$ when the moment-curvature diagram of Fig. 20.8 is used. In contrast to the case with the central point load, the limit load is, theoretically, not reached at a finite, but rather at an infinite mid-span deflection when, as before, second-order effects are ignored (exercise 20.5). However, owing to the strain hardening of the material which normally takes place and the influence of second-order effects, this cannot happen in reality.

The ratio between limit load and load at onset of yield is known as the *plastic reserve*. In statically determinate systems this is obviously equal to the shape factor of the cross-section in which the plastic hinge needed to create the mechanism is formed.

20.3.2.3 Fixed beam with uniformly distributed load

The beam with a rectangular cross-section shown in Fig. 20.10(a) initially has no residual stresses and no restraints. Therefore,

$$q_y = \frac{12M_y}{l^2} \quad , \quad w_y = \frac{q_y l^4}{384EI} = \frac{\chi_y l^2}{32} \tag{20.33}$$

applies for the onset of yield at the fixed supports, see example 15.2.

Subjected to a limit load q_u, a mechanism becomes established with plastic hinges at the fixed supports and mid-span. The following applies:

$$q_u = \frac{16M_u}{l^2} = \frac{16fM_y}{l^2} = 2q_y \tag{20.34}$$

i. e. there is a plastic reserve of $q_u/q_y = 4f/3 = 2$.

The dotted lines in Fig. 20.10(b) indicate the bending moments and curvatures for the onset of yield at the fixed supports. Point A corresponds to this state in the load-deflection diagram of Fig. 20.10(c). In order to approximate the load-deflection line between this point and the limit load level CD, we assume a simplified bilinear moment-curvature diagram (shape factor = 1). The "onset of yield" at the fixed supports therefore shifts from point A to point B, i. e. ideal plastic hinges appear there for a load of $3q_y/2$. The system then behaves like a simply supported beam until the limit load is reached. We get the following deflection for point C:

$$w_u = \frac{3w_y}{2} + \frac{5(q_u - 3q_y/2)l^4}{384EI} = 4w_y \tag{20.35}$$

and the associated rotation of the plastic hinges at the fixed supports is

$$\theta = \frac{(q_u - 3q_y/2)l^3}{24EI} = \frac{M_u l}{6EI} = \frac{f_y l}{2Eh} = \frac{\chi_y l}{4} \tag{20.36}$$

Using the non-linear moment-curvature diagram OABC or ODEF in Fig. 20.8 enables the problem to be solved numerically; it should be remembered that the deflection curve must exhibit horizontal tangents at the fixed supports and at mid-span.

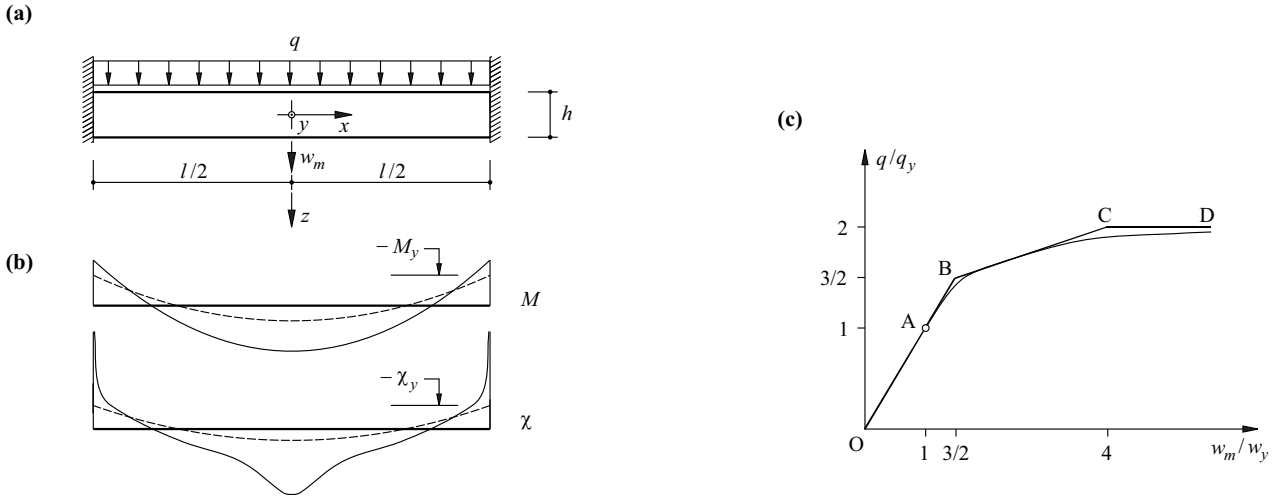

Fig. 20.10 Fixed beam: (a) diagram of static system, (b) moments and curvatures, (c) load-deflection diagram (mid-span)

Tab. 20.1 lists the results of a corresponding calculation, which are drawn in Fig. 20.10(c) (arc AD). There is a redistribution of the internal forces beyond point A in Fig. 20.10(c). This is characterised by the fact that the span moments ($x = 0$) increase successively to a greater extent than according to the elastic solution, whereas the fixed-end moments ($x = \pm\, l/2$) increase successively to a lesser extent. As in the case of the simply supported beam subjected to a uniformly distributed load, the limit load is, theoretically, only reached with an infinitely large deflection at mid-span. It is remarkable that arc AD in Fig. 20.10(c) lies above straight-line BC – with the equation $w_m = (5q/q_y - 6)w_y$ – in the range of about $q = 1.6q_y$ to $q = 1.7q_y$. In addition, we note that individual cross-sections in the region of the fixed supports are relieved elastically in a certain load range as the load increases; however, this effect has only a very small influence on the development of the deflection curve.

Tab. 20.1 Results of calculations corresponding to arc AD in Fig. 20.10(c)

q	$M(x = 0)$	$M(x = \pm\, l/2)$	w_m
1.0	0.5000	– 1.0000	1.000
1.1	0.5502	– 1.0998	1.101
1.2	0.6015	– 1.1985	1.206
1.3	0.6555	– 1.2945	1.321
1.4	0.7149	– 1.3851	1.457
1.5	0.7862	– 1.4638	1.639
1.6	0.9007	– 1.4993	1.993
1.7	1.0501	– 1.4999	2.496
1.8	1.2000	– 1.4999..	3.085
1.9	1.3500	– 1.4999..	4.034
1.99	1.4850	– 1.4999..	7.363
2.0	1.5000	– 1.5000	∞
q_y	M_y	M_y	w_y

20.3.3 Continuous beams

The continuous beam shown in Fig. 20.11(a) has two equal spans l, a constant bending stiffness EI, constant bending resistances $\pm M_u$ and line loads q_1 and q_2 constant within each span. We can derive the support forces and bending moments for the elastic, initially restraint-free system shown in Fig. 20.11(b) from example 8.5, and Fig. 20.11(c) is characteristic of a general restraint state for the system with one degree of static indeterminacy. Fig. 20.11(d) shows the linear elastic - perfectly plastic moment-curvature diagram on which the analysis is based.

For reasons of symmetry, it is sufficient to consider one quadrant in the interaction diagram of Fig. 20.11(e). Line DEC represents the yield limit, or rather the non-plastic domain, of the elastic, initially restraint-free system; $M_B = -(q_1 + q_2)l^2/16 = -M_u$ applies along line DE, and $C^2/(2q_2) = M_u$ along EC, where $C = (7q_2 - q_1)l/16$. Line AEBC corresponds to the yield limit, or rather the non-plastic domain, of the rigid - perfectly plastic system, and the intervening space between this and line DEC indicates the plastic reserve in the system, see section 20.3.5. Along line AEB, one plastic hinge forms at intermediate support B and another in span BC:

$$P - (q_1 + q_2)l^2/16 = -M_u \quad ; \quad C^2/(2q_2) = M_u \quad , \quad C = P/l + (7q_2 - q_1)l/16$$

Eliminating P removes q_1 from the calculation and we get

$$q_2 = \frac{2M_u}{l^2(\sqrt{2}-1)^2} \tag{20.37}$$

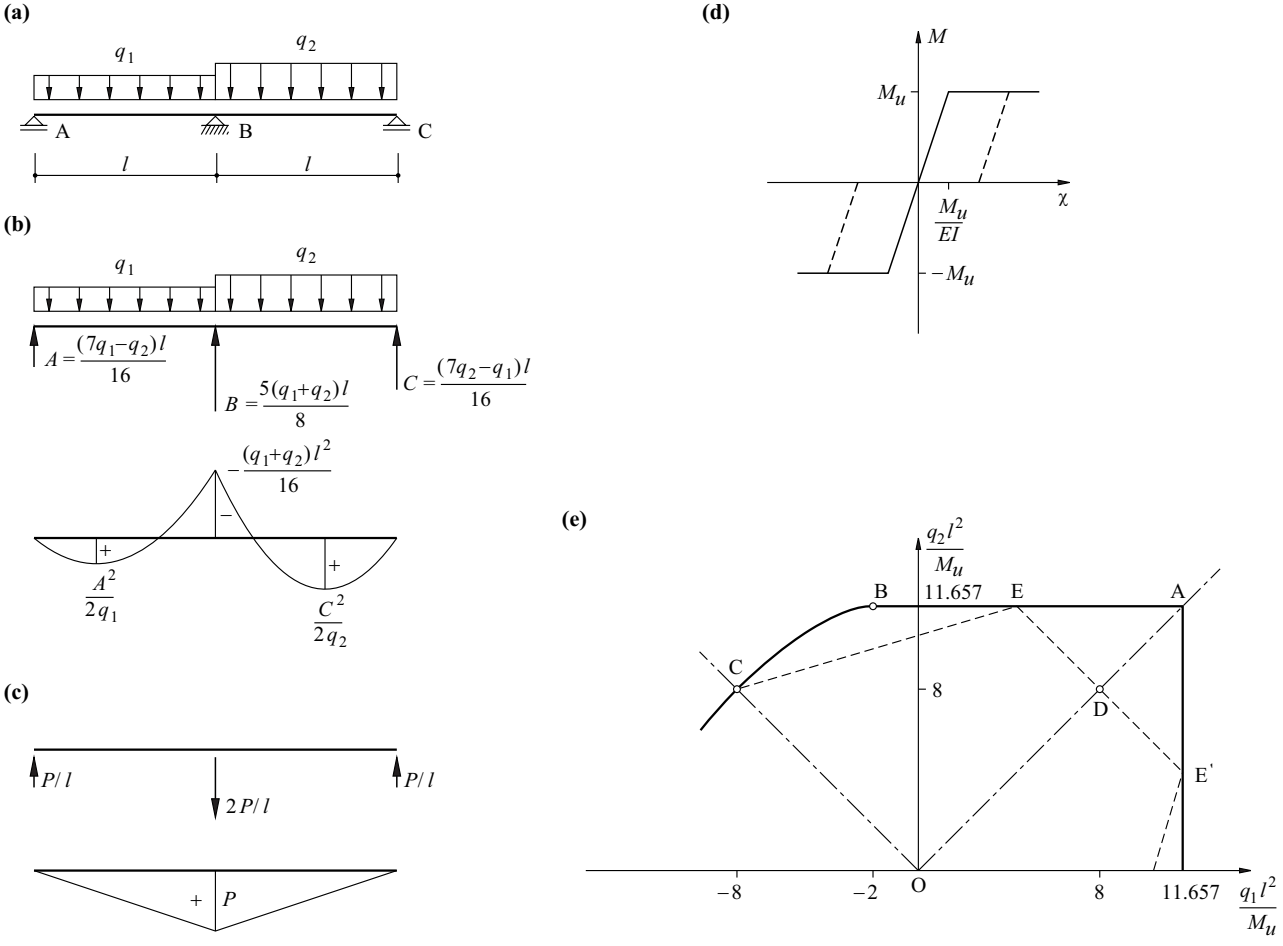

Fig. 20.11 Continuous beam: (a) diagram of static system, (b) elastic, restraint-free system, (c) restraint state, (d) moment-curvature diagram, (e) interaction diagram

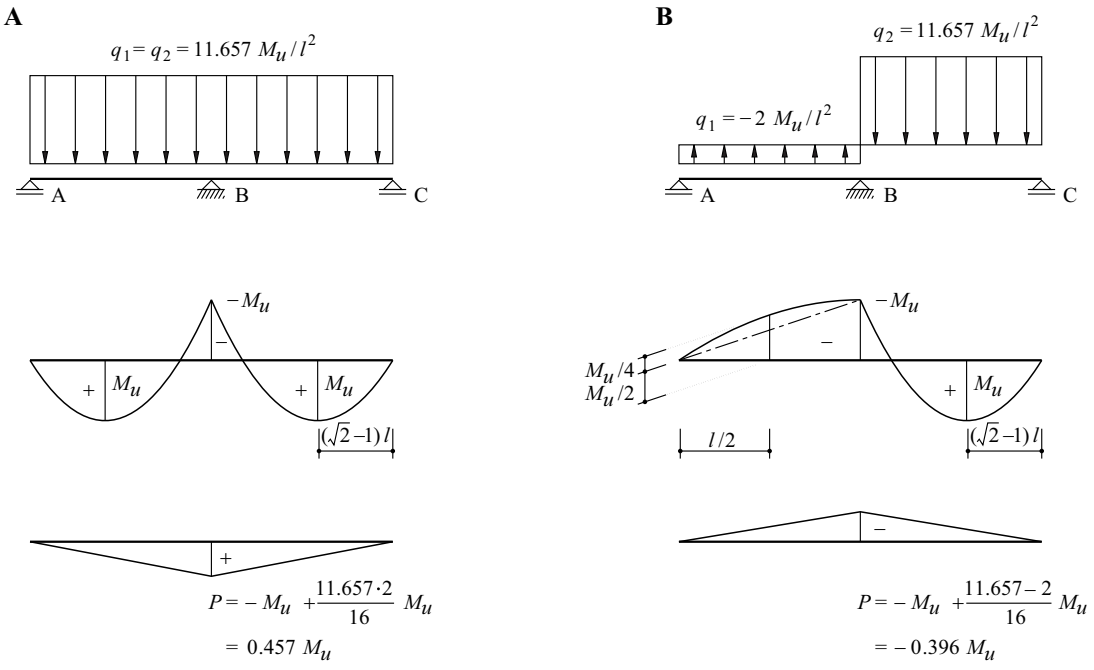

Fig. 20.12 Details of points A and B in Fig. 20.11(e)

Along line BC, a negative plastic hinge forms in span AB and a positive plastic hinge in span BC:

$$A^2/(2q_1) = -M_u \quad , \quad A = P/l + (7q_1 - q_2)l/16 \quad ; \quad C^2/(2q_2) = M_u \quad , \quad C = P/l + (7q_2 - q_1)l/16$$

Eliminating P results in

$$\sqrt{2M_u}\left(\sqrt{-q_1} + \sqrt{q_2}\right) + (q_1 - q_2)l/2 = 0 \tag{20.38}$$

At B and C in Fig. 20.11(e), the tangents to arc BC described by (20.38) are horizontal and at an angle of $\pi/4$ with respect to axes q_1 and q_2 respectively.

Fig. 20.12 shows the loads, moments and restraint states corresponding to points A and B in Fig. 20.11(e).

20.3.4 Frames

Fig. 20.13(a) shows once again the frame with two degrees of static indeterminacy investigated in section 16.2. This is to be analysed in a similar way to section 20.2.1.5 with reference to the complementary internal total potential.

Fig. 20.13(b) corresponds to Fig. 16.2(e) and shows the elastic moment distribution of the initially restraint-free system. The associated potential is

$$\Pi_e^* = \int \frac{M_e^2}{2EI}\,\mathrm{d}x = 1.453\ \frac{Q^2\mathrm{m}^3}{EI} \tag{20.39}$$

This is represented by triangular areas in Fig. 20.13(d) bounded at the sides by legs OFK and OL and at the top by Q = const. For example, when $Q = Q_\mathrm{H} = Q_u$, the outcome is triangle OKL.

According to section 16.2.4, plastic hinges form successively at joints 4, 3 and 2 as a result of a monotonic loading on the system. Points F, G and H in Fig. 20.13(d), or Fig. 16.1(c), correspond to these states. Fig. 20.13(c) illustrates the bending moments that ensue in the system with one degree of static indeterminacy as a result of imposing P_1 at joint 4, and in the statically determinate system by imposing P_2 at joint 3. The associated potentials amount to

$$\Pi_{r1}^* = \int \frac{M_{r1}^2}{2EI}\,\mathrm{d}x = 1.212\ \frac{P_1^2\mathrm{m}}{EI} \quad , \quad \Pi_{r2}^* = \int \frac{M_{r2}^2}{2EI}\,\mathrm{d}x = 5\ \frac{P_2^2\mathrm{m}}{EI} \tag{20.40}$$

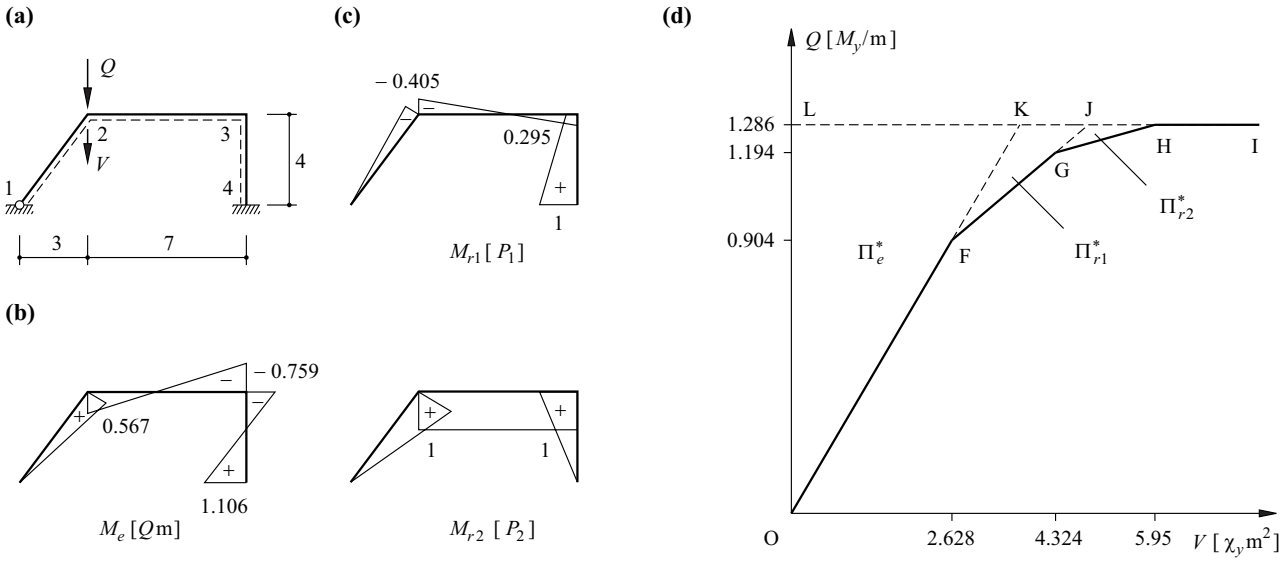

Fig. 20.13 Frame from Fig. 16.1: (a) diagram of static system, (b) elastic moment distribution, (c) restraint states corresponding to plastic hinges at joints 4 and 3, (d) load-deflection diagram and complementary internal potential

The complementary internal total potential generally amounts to

$$\Pi_i^* = \Pi_e^* + \sum_{j=1}^{k} \Pi_{rj}^* \qquad (k \le n) \tag{20.41}$$

where n is the degree of static indeterminacy and the summation includes all the k potential components involved depending on Q. The relationships (20.17) and $(20.13)_1$ for V and V_e respectively continue to apply, and (20.16) is used to determine V_r in the sense of (20.41). For example, when $Q = Q_H = Q_u = 1.286 M_y/\text{m}$, we get

$$V/(\chi_y \text{m}^2) = 2 \cdot 1.453 \cdot 1.286 + 2 \cdot 1.212 \cdot (-0.422) \cdot (-1.106) + 2 \cdot 5 \cdot 0.100 \cdot (0.759 + 0.295 \cdot 1.106) = 5.95$$

where $P_1 = (-1.106 \cdot 1.286 + 1)M_y = -0.422 M_y$ and $P_2 = (0.759 \cdot 1.286 + 0.295 \cdot 0.422 - 1)M_y = 0.100 M_y$, and the chain rule is used to take into account the derivatives with respect to Q. Note that the designations of the restraint states deviate from those of Fig. 16.9. After relieving the load at point H in Fig. 20.13(d), the restraint state $M_2 = -0.405 \cdot (-0.422 M_y) + 0.100 M_y = 0.271 M_y$, $M_3 = 0.295 \cdot (-0.422 M_y) + 0.100 M_y = -0.025 M_y$, $M_4 = -0.422 M_y$ remains, i. e. the result is the values corresponding to point J in Fig. 16.9.

20.3.5 Commentary

In statically determinate systems like the one examined in section 20.3.2.2, the plastic reserve is equal to the shape factor f of the cross-section in which the plastic hinge occurs. By comparison, in statically indeterminate systems there is usually an additional *plastic reserve in the system*. For example, this reserve is 4/3 for the beam with fixed ends carrying a uniformly distributed load examined in section 20.3.2.3. Generally, the plastic reserve is represented by the intervening space between the non-plastic domains of the virgin elastic-plastic and the rigid-plastic systems.

The plastified regions of the beam can extend over considerable lengths in cross-sections with large shape factors, especially with low shear forces. For example, the extreme fibres of the simply supported beam with rectangular cross-section and central point load examined in section 20.3.2.1 are plastified over a length of $l/3$ upon reaching the limit load; this length increases to $l/\sqrt{3}$ with a uniformly distributed load and otherwise identical conditions (section 20.3.2.2). In such cases the concept of an ideal plastic hinge confined to one cross-section (shape factor = 1) supplies only a rough

approximation of the actual behaviour. However, the behaviour is also influenced by the strain hardening of the material and second-order effects, and assuming plastic hinges leads to an easily managed, practical approach that supplies an approximation that is mostly adequate for deformation calculations.

It is usually necessary to consider the interaction of the bending moments with the other stress resultants (normal force, shear force and torque). This aspect is investigated further in section 21.4.

In steel structures, for example, plastic deformations are often already found in the serviceability state. Apart from the aforementioned restraints, such deformations are often caused by peak stresses (e. g. at the tips of notches, around holes or at points of load transfer) and fabrication-related residual stresses (e. g. as a result of cold-forming or uneven cooling after rolling or welding).

20.4 Summary

1. Subjected to a monotonic loading, an elastic-plastic system exhibits elastic-plastic behaviour (contained plastic deformation) with a successive decrease in stiffness after the elastic phase until a mechanism is established (uncontained plastic deformation) at the limit load.
2. Upon relieving the load, an elastic-plastic system behaves purely elastically provided no yield limit has been reached. In statically indeterminate systems, a restraint state generally remains after relieving the load fully.
3. Plastic deformation generally changes the restraint state.
4. In principle, a system can be prestressed for certain types of loading in such a way that it behaves purely elastically.
5. In the case of an opposite prior plastic deformation, the onset of yield is generally established at a lower load than that of the virgin system (BAUSCHINGER effect).
6. With m load parameters, the stress state of a system with n degrees of static indeterminacy can be depicted by superposing m elastically compatible loading stress states and n restraint states.
7. Inaccurate fits during erection, thermal deformations, settlement, slip at connections, shrinkage, swelling and similar effects generally result in initial restraint stresses in real systems which, however, are difficult to assess accurately. Although the initial restraints have an influence on the structural behaviour up to the limit load, they do not affect the limit load itself provided no second-order effects occur and the plastic deformation capacity of the system is adequate for the redistribution of the internal forces which is necessary.
8. The deformations of elastic-plastic systems can be split into elastic and plastic components according to (20.17). These components follow from the corresponding components of the complementary internal total potential (20.41) in line with ENGESSER's theorem according to $(20.13)_1$ and (20.16).
9. The principle of maximum dissipation is transferred from the space of the local stresses $\boldsymbol{\sigma}$ to the spaces of the loads $\boldsymbol{Q}$ and the generalised stresses $\boldsymbol{s}$. Convex yield surfaces result in these spaces and the outward orthogonal vectors $\dot{\boldsymbol{V}}$ and $\dot{\boldsymbol{v}}$ describe the associated mechanisms, or rather the corresponding generalised deformations increments, for points on the yield surface.
10. In statically determinate systems, the plastic reserve is equal to the shape factor of the cross-section in which the plastic hinge occurs. In statically indeterminate systems there is usually an additional plastic reserve in the system.
11. Owing to the assumption that the bar cross-sections remain plane and perpendicular to the bar axis, it is possible to determine the deformation variables ε, χ_y, χ_z belonging to a set of stress resultants N, M_y, M_z for cross-sections of any shape and composition. Based on this, non-linear deformation calculations can be performed for any systems, any loads.

12. A bilinear linear elastic - perfectly plastic idealisation of the moment-curvature behaviour (shape factor = 1) usually leads to sufficiently accurate results for bars with low shape factors, e. g. profiled beam sections. In this situation the plastic deformations are concentrated at ideal plastic hinges in individual cross-sections, and the associated plastic rotations can be calculated by applying the work theorem, for instance.

20.5 Exercises

20.1 Verify (20.12).

20.2 The three pin-jointed bars of the system shown in Fig. 20.14(a) have a cross-sectional area A and are made from a material that behaves according to Fig. 20.1(b). Beam 246 is rigid. Discuss the structural behaviour for the case of $Q_4 = 2Q_6$ in a similar way to Fig. 20.2 and Fig. 20.3.

20.3 Draw a Q_4-Q_6 interaction diagram which is similar to Fig. 20.5(b) for the task of exercise 20.2 and discuss the behaviour, also in the space of the generalised stresses (i. e. the normal forces in the pin-jointed members).

20.4 Verify (20.32).

20.5 Develop an expression similar to (20.32) for the simply supported beam with rectangular cross-section and monotonically increasing uniformly distributed load examined in section 20.3.2.2.

20.6 Draw the Q-V diagram for the beam shown in Fig. 20.14(b) subjected to a monotonically increasing load Q. The system is initially free from restraint and the beam cross-sections behave according to the moment-curvature diagram shown in Fig. 20.11(d). Calculate the plastic hinge rotations occurring in the elastic-plastic phase and discuss the behaviour in a similar way to Fig. 20.4(b) and Fig. 20.13(d).

20.7 Discuss the structural behaviour of the continuous beam of Fig. 20.14(c) in a similar way to exercise 20.6. Show that upon onset of yield

$$Q_y = \frac{8M_u}{l} \cdot \frac{3+2\alpha}{3+4\alpha} \quad , \quad V_y = \frac{M_u l^2}{24EI} \cdot \frac{3+8\alpha}{3+4\alpha}$$

and that upon reaching the limit load

$$Q_u = \frac{8M_u}{l} \quad , \quad V_u = \frac{M_u l^2}{24EI} \cdot (1+4\alpha)$$

In particular, consider the limiting cases $\alpha \to 0$ and $\alpha \to \infty$.

20.8 Discuss the structural behaviour of the frame shown in Fig. 20.14(d) for the case of $Q_1 = Q_2$ in a similar way to exercise 20.6.

20.9 Assuming Fig. 20.11(d), determine a yield surface similar to Fig. 20.6 for the system shown in Fig. 20.14(e); see also example 21.2.

20.10 With the help of Fig. 20.5 and Fig. 20.6, discuss for which value of Q_0 the system can just shake down when subjected to loads $0 \le Q_1 \le Q_0$, $0 \le |Q_2| \le Q_0/2$, and determine the associated restraint state.

20.11 Show that the system examined in exercise 20.9, with a restraint moment $-M_u/19$ at the intermediate support, can undergo shakedown when Q_1 and Q_2 vary between 0 and $96M_u/(19l)$. Interpret the result with the help of the answer worked out in exercise 20.9 and discuss the difference between shakedown load and limit load.

20.12 Show that a beam of span l fixed at both ends, whose cross-sections behave according to Fig. 20.11(d), can accommodate – purely elastically – a point load of $432M_u/(59l)$ travelling backwards and forwards any number of times between the ends of the beam. To do this, use the influence functions for the fixed-end moments in (19.39).

20.13 Two identical bars in a vertical plane, rigid in shear and with length l, form a bipod standing on a horizontal plane. The bars are joined together rigidly at the top at a right-angle and fixed at their bases. Discuss the behaviour of the bipod subjected to a monotonically increasing horizontal force applied at the top and acting in the plane of the bipod. Assume pure stringer cross-sections (cross-sectional area of each $A/2$ at spacing h) and a linear elastic - perfectly plastic behaviour (modulus of elasticity E, yield limit f_y). What conclusions can be drawn with respect to the secondary stresses in trusses mentioned in section 11.3.1?

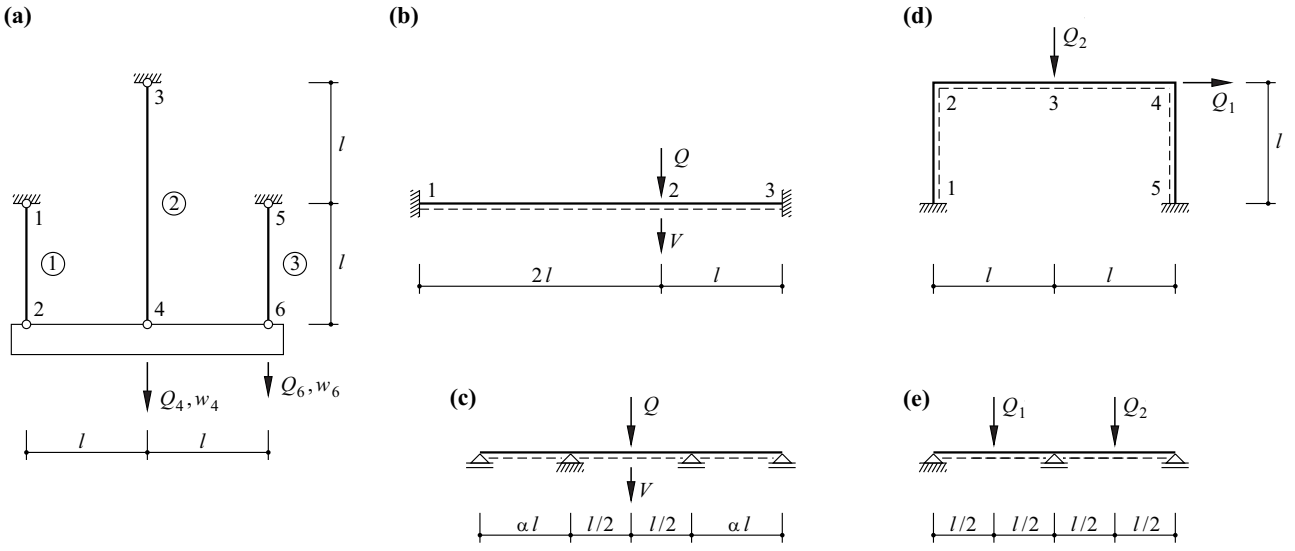

Fig. 20.14 Diagrams of static systems for section 20.5

21 LIMIT ANALYSIS

21.1 General

Limit analysis methods are used to calculate the limit loads of rigid - perfectly plastic systems. They are based on the upper- and lower-bound theorems, which in turn are based on the principle of virtual work and the principle of maximum dissipation and, for a single-parameter loading, permit the limit load to be contained from above or below. Limit analysis enables the structural safety to be assessed when dimensioning or checking structures (see chapter 4). The application of limit analysis to framed structures is presented in this chapter, and extended to cover plate and shell structures in chapters 23 to 26.

According to the classic concept of dimensioning based on *permissible stresses*, discussed in section 4.7, a certain safety margin with respect to the onset of yield was desirable at every point in a structure. The structural members were therefore dimensioned for the stress resultants obtained from a linear elastic analysis of the system that was assumed (mostly implicitly) to be initially free from residual stresses and restraints. Based on the observations of chapter 20, such a procedure is inherently questionable – the aforementioned assumption is in no way fulfilled; partial plastification is usually already present in the serviceability state and the structural behaviour upon collapse of a structure is not ascertained directly.

An *elastic-plastic* analysis should generally be carried out in order to ascertain the structural behaviour of a system as accurately as possible; second-order effects plus the way circumstances change over time may need to be considered, too. However, such an analysis, as shown in chapter 20, can become very involved, even for simple systems. The non-plastic domain of an elastic-plastic system changes successively with the loading process and this must be investigated step by step. In addition, this type of analysis presumes knowledge of the initial stress and deformation states. But the necessary variables can only be estimated approximately at best. For these reasons, the use of elastic-plastic analyses is severely restricted in practice.

By assuming *rigid - perfectly plastic* instead of elastic-plastic behaviour, we can work with a fixed non-plastic domain that can be investigated from inside or outside using the static and kinematic methods of limit analysis. The limit loads corresponding to the boundaries of the non-plastic domain and the associated mechanisms are not dependent on the initial stress or deformation states nor the subsequent loading-restraint history. In this approach it is presumed that first-order theory can be applied and the plastic deformation capacity is sufficiently large, which may have to be checked with the help of an elastic-plastic analysis.

Theory of Structures. First Edition. Peter Marti

21.2 Upper- and lower-bound theorems

21.2.1 Basic concepts

The *theory of plastic potential* for a volume element was presented in section 7.3.2. In chapter 20 it became apparent that the *principle of maximum dissipation energy*, which characterises this theory, is transferred from the space of the local stresses $\boldsymbol{\sigma}$ to the space of the loads $\boldsymbol{Q}$ and the space of the generalised stresses $\boldsymbol{s}$, see (7.18), (20.21) and (20.22). Convex (or at least not concave, i. e. weakly convex) yield surfaces ensue in these spaces. Further, for points on the yield surface, the outward orthogonal vectors correspond to the generalised displacement increments $\dot{\boldsymbol{V}}$ or the generalised deformation increments $\dot{\boldsymbol{v}}$.

The following proofs of the upper- and lower-bound theorems are based on the *principle of virtual work*, which is expressed here in the following form:

$$\boldsymbol{Q}_1 \bullet \dot{\boldsymbol{V}}_2 - \boldsymbol{s}_1 \bullet \dot{\boldsymbol{v}}_2 = 0 \tag{21.1}$$

according to (8.14). The static variables $\boldsymbol{Q}_1$, $\boldsymbol{s}_1$ form a force state in equilibrium, and the kinematic variables $\dot{\boldsymbol{V}}_2$, $\dot{\boldsymbol{v}}_2$ form a compatible deformation state. The two states need not be related to each other.

The two states in (21.1) are *compatible* when they are linked with each other via the flow rule

$$\begin{aligned} &\dot{\boldsymbol{v}}_2 = \kappa \,\mathrm{grad}\, Y(\boldsymbol{s}_1) \qquad (Y = 0\,,\ \kappa \geq 0) \\ &\dot{\boldsymbol{v}}_2 = 0 \qquad\qquad\qquad\quad (Y < 0) \end{aligned} \tag{21.2}$$

see (7.12). According to (21.2), we can distinguish between three regions of the structure: in region I, the stress state is at the yield limit, and plastic deformations occur ($\kappa > 0$); in region II, the stress state is also at the yield limit, but there are no plastic deformations ($\kappa = 0$), i. e. the region remains rigid; region III is also rigid and the stress state lies below the yield limit here ($Y < 0$).

The limit load $\lambda_u \boldsymbol{Q}$ for a certain direction $\boldsymbol{Q}$ in the space of the loads, the associated stress state $\boldsymbol{s}$ and the deformation state $\dot{\boldsymbol{v}}$, $\dot{\boldsymbol{V}}$ compatible with this are considered below. We shall also look at a statically admissible stress state $\boldsymbol{s}_s$ according to (8.61), which is in equilibrium with the load $\lambda_s \boldsymbol{Q}$, and a kinematically admissible deformation state $\dot{\boldsymbol{v}}_k$, $\dot{\boldsymbol{V}}_k$ according to (8.59).

21.2.2 Lower-bound theorem

Every loading for which it is possible to specify a statically admissible stress state that does not infringe the yield condition is not greater than the limit load.

To prove this theorem we shall use the variables $\dot{\boldsymbol{v}}$, $\dot{\boldsymbol{V}}$ associated with the limit load as our deformation state in (21.1) as well as, on the one hand, the variables $\boldsymbol{s}$, $\lambda_u \boldsymbol{Q}$ compatible with this and, on the other, the variables $\boldsymbol{s}_s$, $\lambda_s \boldsymbol{Q}$ as our force state:

$$\lambda_u \boldsymbol{Q} \bullet \dot{\boldsymbol{V}} - \boldsymbol{s} \bullet \dot{\boldsymbol{v}} = 0 \quad , \quad \lambda_s \boldsymbol{Q} \bullet \dot{\boldsymbol{V}} - \boldsymbol{s}_s \bullet \dot{\boldsymbol{v}} = 0$$

This results in the following:

$$(\lambda_u - \lambda_s)\, \boldsymbol{Q} \bullet \dot{\boldsymbol{V}} = (\boldsymbol{s} - \boldsymbol{s}_s) \bullet \dot{\boldsymbol{v}} \tag{21.3}$$

As the scalar product $\boldsymbol{Q} \bullet \dot{\boldsymbol{V}}$ is positive and the expression on the right in (21.3) is – according to (20.22) – not negative, the result is, as asserted,

$$\lambda_s \leq \lambda_u \tag{21.4}$$

21.2.3 Upper-bound theorem

Every loading that results from equating the work of the external forces for a kinematically admissible deformation state with the associated dissipation work is not less than the limit load.

In order to prove this theorem, we shall formulate (21.1) using the force state $\lambda_u \boldsymbol{Q}$, $\boldsymbol{s}$ associated with the limit load and the kinematically admissible deformation state $\dot{\boldsymbol{v}}_k$, $\dot{\boldsymbol{V}}_k$:

$$\lambda_u \boldsymbol{Q} \bullet \dot{\boldsymbol{V}}_k - \boldsymbol{s} \bullet \dot{\boldsymbol{v}}_k = 0$$

According to (7.14), the dissipation work is a single-valued function of the generalised deformation increments $\dot{\boldsymbol{v}}_k$, i. e.

$$\dot{D} = \dot{D}(\dot{\boldsymbol{v}}_k)$$

and according to (20.22), then

$$\dot{D}(\dot{\boldsymbol{v}}_k) \geq \boldsymbol{s} \bullet \dot{\boldsymbol{v}}_k$$

i. e.

$$\lambda_u \boldsymbol{Q} \bullet \dot{\boldsymbol{V}}_k \leq \dot{D}(\dot{\boldsymbol{v}}_k) \tag{21.5}$$

or, as asserted,

$$\lambda_u \leq \frac{\dot{D}(\dot{\boldsymbol{v}}_k)}{\boldsymbol{Q} \bullet \dot{\boldsymbol{V}}_k} = \lambda_k \tag{21.6}$$

21.2.4 Compatibility theorem

A load is a limit load when a statically admissible stress state that does not infringe the yield condition and a compatible kinematically admissible state of deformation can be specified for that load.

The force and deformation states linked by this theorem constitute a *complete solution* to the respective problem.

It is worth noting that the calculation according to (21.6) does not need to be performed; instead, it is only necessary to verify the compatibility of the two states according to (21.2).

21.2.5 Consequences of the upper- and lower-bound theorems

The lower-bound theorem expresses the ability of a system to adapt to a given loading provided this is somehow possible. By contrast, the upper-bound theorem states that a system cannot withstand a loading when a collapse mechanism exists.

The upper- and lower-bound theorems can be formulated as follows for general (multiparameter) loadings:

- Collapse cannot occur when – for any possible loading – it is possible to specify statically admissible stress states that do not infringe the yield conditions at any point.
- Collapse must occur when a kinematically admissible collapse mechanism exists for some loading.

Relationships (21.4) and (21.6) lead to the following bounds:

$$\lambda_s \leq \lambda_u \leq \lambda_k \tag{21.7}$$

for the limit load factor λ_u. The *static method* described in section 21.3 is used to make the static load factor λ_s as large as possible. And vice versa, the *kinematic method* is used to find a kinematic load factor λ_k that is as small as possible.

The upper- and lower-bound theorems also lead to other consequences often useful in practical situations:

- Adding (subtracting) weightless material cannot decrease (increase) the limit load.
- Raising (lowering) the yield limit of the material in any region of a system cannot decrease (increase) its limit load.
- The limit load that can be calculated with a yield surface circumscribing (inscribing) the effective yield surface forms an upper (lower) bound to the effective limit load.

In order to reach a decision regarding the uniqueness of complete solutions, we shall consider two complete solutions belonging to a certain limit load which are characterised by $\boldsymbol{s}_1$, $\dot{\boldsymbol{v}}_1$, $\dot{\boldsymbol{V}}_1$ and $\boldsymbol{s}_2$, $\dot{\boldsymbol{v}}_2$, $\dot{\boldsymbol{V}}_2$. Applying the principle of virtual work to the differential stress state $\boldsymbol{s}_1 - \boldsymbol{s}_2$ while using the deformation state $\dot{\boldsymbol{v}}_1 - \dot{\boldsymbol{v}}_2$, $\dot{\boldsymbol{V}}_1 - \dot{\boldsymbol{V}}_2$ shows that the following must be true for every point in the system:

$$(\boldsymbol{s}_1 - \boldsymbol{s}_2) \bullet (\dot{\boldsymbol{v}}_1 - \dot{\boldsymbol{v}}_2) = 0 \tag{21.8}$$

This is because $\boldsymbol{s}_1 - \boldsymbol{s}_2$ represents a restraint state, and according to (20.22), neither $(\boldsymbol{s}_1 - \boldsymbol{s}_2) \bullet \dot{\boldsymbol{v}}_1$ nor $(\boldsymbol{s}_2 - \boldsymbol{s}_1) \bullet \dot{\boldsymbol{v}}_2$ can be negative. From this, we can derive the following:

- In regions that remain rigid for both solutions ($\dot{\boldsymbol{v}}_1 = \dot{\boldsymbol{v}}_2 = \boldsymbol{0}$), it is possible to have different statically admissible stress states that do not infringe the yield condition ($\boldsymbol{s}_1 \neq \boldsymbol{s}_2$).
- In regions in which plastic deformations occur with one solution at least ($\dot{\boldsymbol{v}}_1 \neq \boldsymbol{0}$ or $\dot{\boldsymbol{v}}_2 \neq \boldsymbol{0}$), the end-points of the vectors $\boldsymbol{s}_1$ and $\boldsymbol{s}_2$ plus the entire straight line connecting them belong to the yield surface $Y(\boldsymbol{s}) = 0$. When strongly convex yield surfaces are present, the stress state in such regions is therefore unique ($\boldsymbol{s}_1 = \boldsymbol{s}_2$).

21.3 Static and kinematic methods

21.3.1 General

Limit analysis is based on defining bounds (21.7) for the limit load.

In the *static method*, possible equilibrium states are investigated irrespective of kinematic considerations. The method supplies assertions regarding the ultimate resistances required at every point in a system and is therefore particularly suitable for dimensioning. The flow of the forces can be followed right down to the details, and appropriate detailing is thus possible.

In the *kinematic method*, possible mechanisms are investigated irrespective of considerations regarding the flow of the forces. The difference between this and the static method is that the ultimate resistances are considered at the points of plastic deformation only. Therefore, in terms of dimensioning, the kinematic method does not supply any information that can be regarded as equivalent to that provided by the static method. However, applying the kinematic method generally involves less effort. The kinematic method is therefore primarily suited to checking existing or conceptual designs, but in simple cases it can be useful for dimensioning purposes, too. Ultimately, applying the kinematic method systematically, which is then also correspondingly involved, we get a procedure that can rank alongside the static method in every respect.

The skill in applying the two methods lies in using them in such a way that they complement each other and lead to a reasonable solution to the respective problem with the minimum effort.

21.3.2 Simply supported beams

21.3.2.1 Simply supported beam with overhang at one end

The beam shown in Fig. 21.1(a) carries a uniformly distributed load q_1 between the supports and another load q_2 on the cantilever. These loads can vary between the limit values $q_{1\min}$ and $q_{1\max}$, or $q_{2\min}$ and $q_{2\max}$. Determining the bending moments drawn in Fig. 21.1(b) presents no difficulties in this statically determinate case and appropriate dimensioning could be carried out without any further problems.

Fig. 21.1(c) shows four possible mechanisms each with one plastic hinge. Mechanism 3 represents the limiting case between mechanisms 2 ($\eta = 1$) and 4 ($\zeta = 1$). The work equations to be set up according to the upper-bound theorem are

$$\begin{aligned}
\frac{q_1 l_1}{2} - \frac{q_2 l_2^2}{2l_1(1-\xi)} &= M_{u1}\left[\frac{1}{\xi l_1} + \frac{1}{l_1(1-\xi)}\right] \\
-\frac{q_1 l_1}{2} + \frac{q_2 l_2^2}{2l_1(1-\eta)} &= M_{u2}\left[\frac{1}{\eta l_1} + \frac{1}{l_1(1-\eta)}\right] \\
\frac{q_2 l_2}{2} &= M_{u3}\cdot\frac{1}{l_2} \\
\frac{q_2 \zeta l_2}{2} &= M_{u4}\cdot\frac{1}{\zeta l_2}
\end{aligned} \tag{21.9}$$

We can see that the absolute magnitudes of the deformations (which are assumed to be infinitesimal) play no role. Only the relative deformations of the individual parts of the system are relevant.

The bending moment envelopes shown in Fig. 21.1(b) can be determined by varying the parameters ξ, η, ζ and substituting the corresponding maximum/minimum values of q_1 and q_2 in (21.9):

$$M_{u1} = q_{1\max} l_1^2 \xi(1-\xi)/2 - q_{2\min} l_2^2 \xi/2 \quad , \quad M_{u2} = q_{1\min} l_1^2 \eta(1-\eta)/2 + q_{2\max} l_2^2 \eta/2 \quad , \quad M_{u4} = q_{2\max} l_2^2 \zeta^2/2 \tag{21.10}$$

The systematic application of the kinematic method therefore supplies the same result as the static procedure, which would be much simpler in this case.

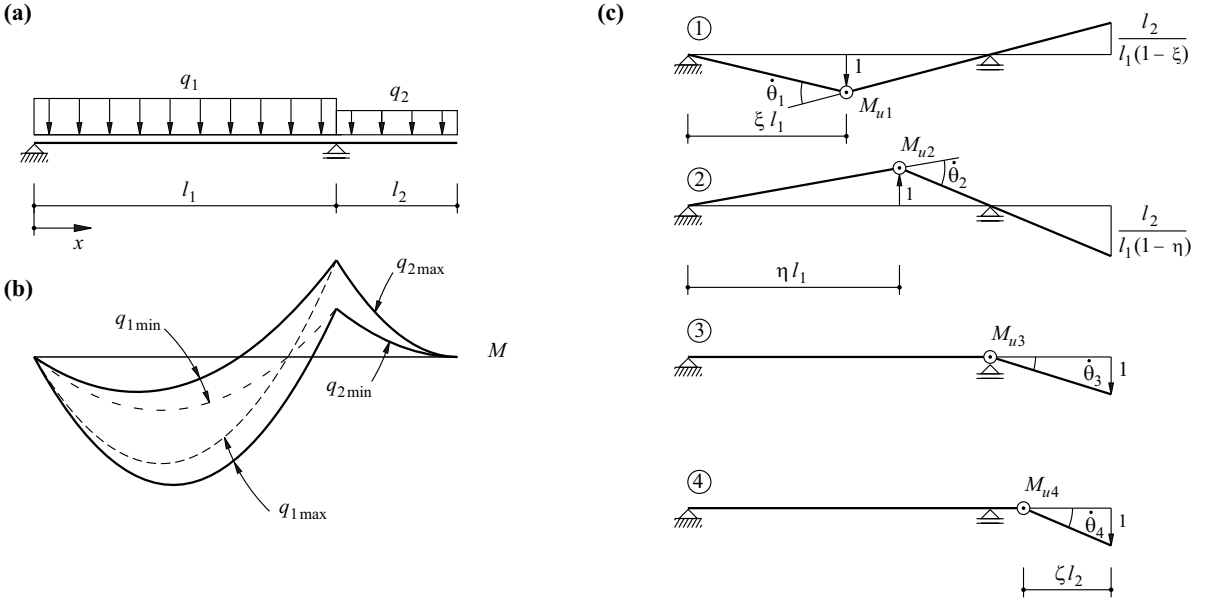

Fig. 21.1 Simply supported beam with overhang at one end: (a) diagram of static system, (b) bending moments, (c) mechanisms

21.3.2.2 Beam with one degree of static indeterminacy

The beam shown in Fig. 21.2(a) has constant bending resistances $\pm M_u$ and is loaded at its third-points by monotonically increasing loads Q. The task is to find the limit load Q_u.

Fig. 21.2(b) shows three possible mechanisms and illustrates the *plasticity check* using free body and moment diagrams. The work equation for the first mechanism is $Q \cdot 1 = M_u \cdot (3/l + 6/l)$. Therefore, according to the upper-bound theorem, we get the condition $Q_u \leq 9M_u/l$ for the limit load. The loads and moments known at joints 2 and 3 enable us to determine the free body diagram and the associated moments shown in the figure. We can see that the yield condition between joints 1 and 2 is infringed. In this area, the beam would have to be strengthened for the moments shaded in grey in order to be able to carry the loads of $9M_u/l$. The plasticity check is not satisfied and therefore $Q_u < 9M_u/l$.

The work equation for the second mechanism is $Q \cdot 3/2 = M_u \cdot [3/l + 9/(2l)]$, from which it follows that $Q_u \leq 5M_u/l$. The loads and moments known at joints 1 and 2 enable us to determine the free body diagram and the associated moments shown in the figure. The yield condition is infringed for the positive moments in the area $l/3 < x < 3l/4$. The plasticity check is not satisfied and therefore $Q_u < 5M_u/l$.

The work equation for the third mechanism is $Q \cdot 3/2 = M_u \cdot [3/(2l) + 9/(2l)]$, from which it follows that $Q_u \leq 4M_u/l$. The plasticity check is satisfied and therefore $Q_u = 4M_u/l$.

The static method allows the limit load to be determined according to Fig. 21.2(c) in a very simple way. With a simple support at joint 1, the moment diagram would be ABCD. If we now add a closing line DE to the moment diagram in such a way that the moments at 1 and 3 amount to M_u, then $M_u + M_u/3 = Ql/3$, i. e. $Q_u \geq 4M_u/l$. The third mechanism in Fig. 21.2(b) is compatible with this stress state; the plastic hinges at joints 1 and 3 agree with the moments and produce a mechanism. Consequently, we have found the complete solution to the problem, and the limit load is $Q_u = 4M_u/l$.

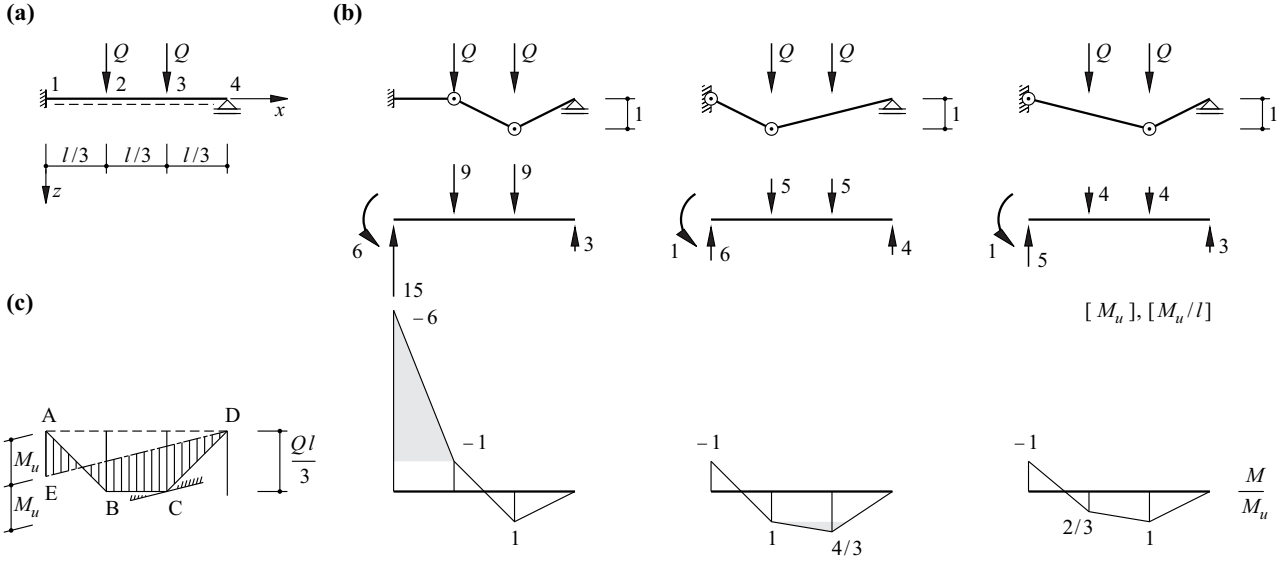

Fig. 21.2 Beam with one degree of static indeterminacy: (a) diagram of static system, (b) mechanisms and plasticity checks, (c) static method

21.3.3 Continuous beams

We normally use a linear elastic analysis to find the bending moments of continuous beams. Certain restraint moments can then be superimposed for each individual load case (or for all load cases together) during the dimensioning, which is equivalent to shifting the closing line of the bending moment diagrams. This is illustrated in Fig. 21.3 for end and interior spans. We get the final moments M from the moments M_0 initially calculated by superimposing the restraint moments ΔM varying linearly between the supports.

Fig. 21.3 also shows various potential mechanisms that can be analysed in a similar way to Fig. 21.1(c). Apart from the "usual" mechanisms 1 with plastic hinges at the intermediate supports and around mid-span, it is mechanisms 2 to 4 with plastic hinges near the points of contraflexure that need to be considered, especially with concrete structures. Working with reinforced concrete allows us to adjust the bending resistance to match bending moments practically at will. So there is often only little longitudinal reinforcement around the points of contraflexure, and there is a risk that this reinforcement is curtailed too soon. The influence of the shear force aggravates this effect because additional longitudinal reinforcement is needed to withstand the shear, see (23.36), for example.

On the whole, the restraint moments ΔM do no work on the mechanisms. The restraint state corresponds to a load-free state of equilibrium. As the work of the external forces is equal to zero, the work of the internal forces must also be zero for every virtual deformation state. Therefore, as already noted in chapter 20, the limit loads – assuming adequate plastic deformation capacity plus the applicability of first-order theory – are not dependent on restraints.

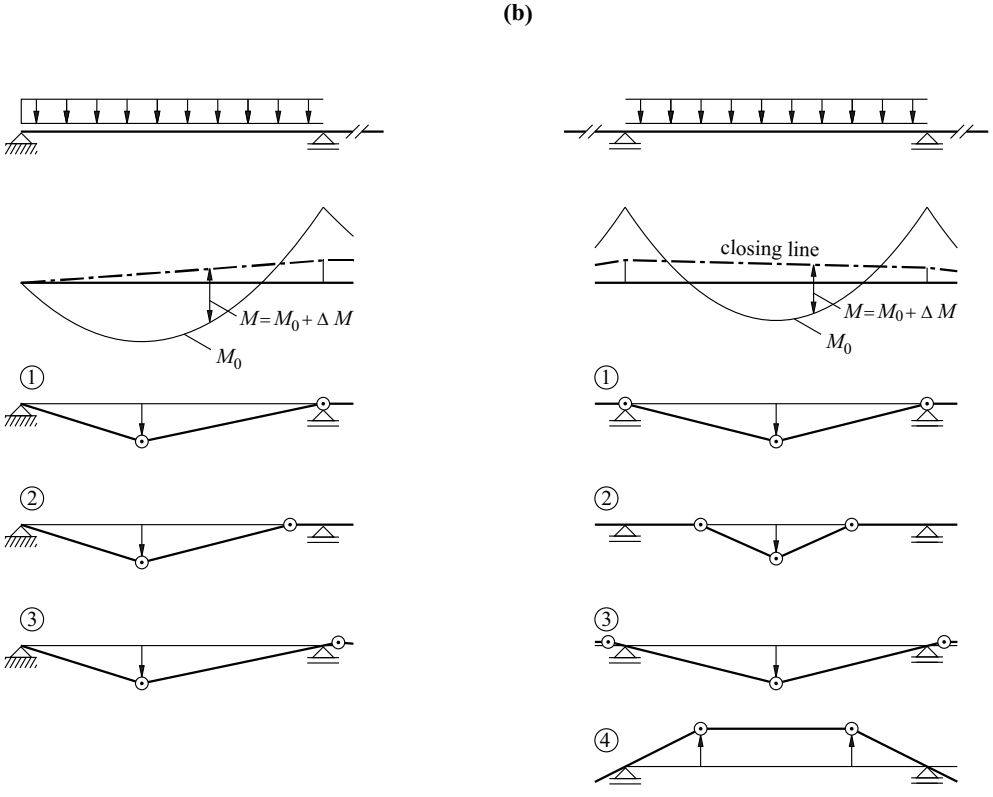

Fig. 21.3 Continuous beam: (a) end span, (b) interior span

In a system with n degrees of static indeterminacy, the limit load is reached, at the latest, when $n+1$ plastic hinges have formed. Partial mechanisms with fewer than $n+1$ plastic hinges govern in most instances. This is obvious in the case of continuous beams with three or more spans ($n \geq 2$), see Fig. 21.3.

We can arrive at quite different answers to our dimensioning depending on whether redistribution of moments is carried out for each individual load case or for all load cases together. This matter has already been mentioned in example 16.6, and will be addressed again in sections 21.5 and 21.7.3.

21.3.4 Plane frames

21.3.4.1 Introductory example

The frame with three degrees of static indeterminacy shown in Fig. 21.4(a) is loaded by the monotonically increasing loads $Q_1 = 3Q$ and $Q_2 = Q$. The bending resistances of columns 12 and 56 are $\pm M_u$, and the bending resistance of frame beam 2345 is $\pm 2M_u$. The task is to find the limit load Q_u.

Owing to the linear progression of the moments segment by segment and the constant bending resistances, plastic hinges can only form at points 1 to 6. Fig. 21.4(b) shows a *beam mechanism*, a *sway mechanism* and a *combined mechanism* plus all the plasticity checks in a similar way to Fig. 21.2(b). The work equations for the three mechanisms and the resulting upper bounds for Q_u are

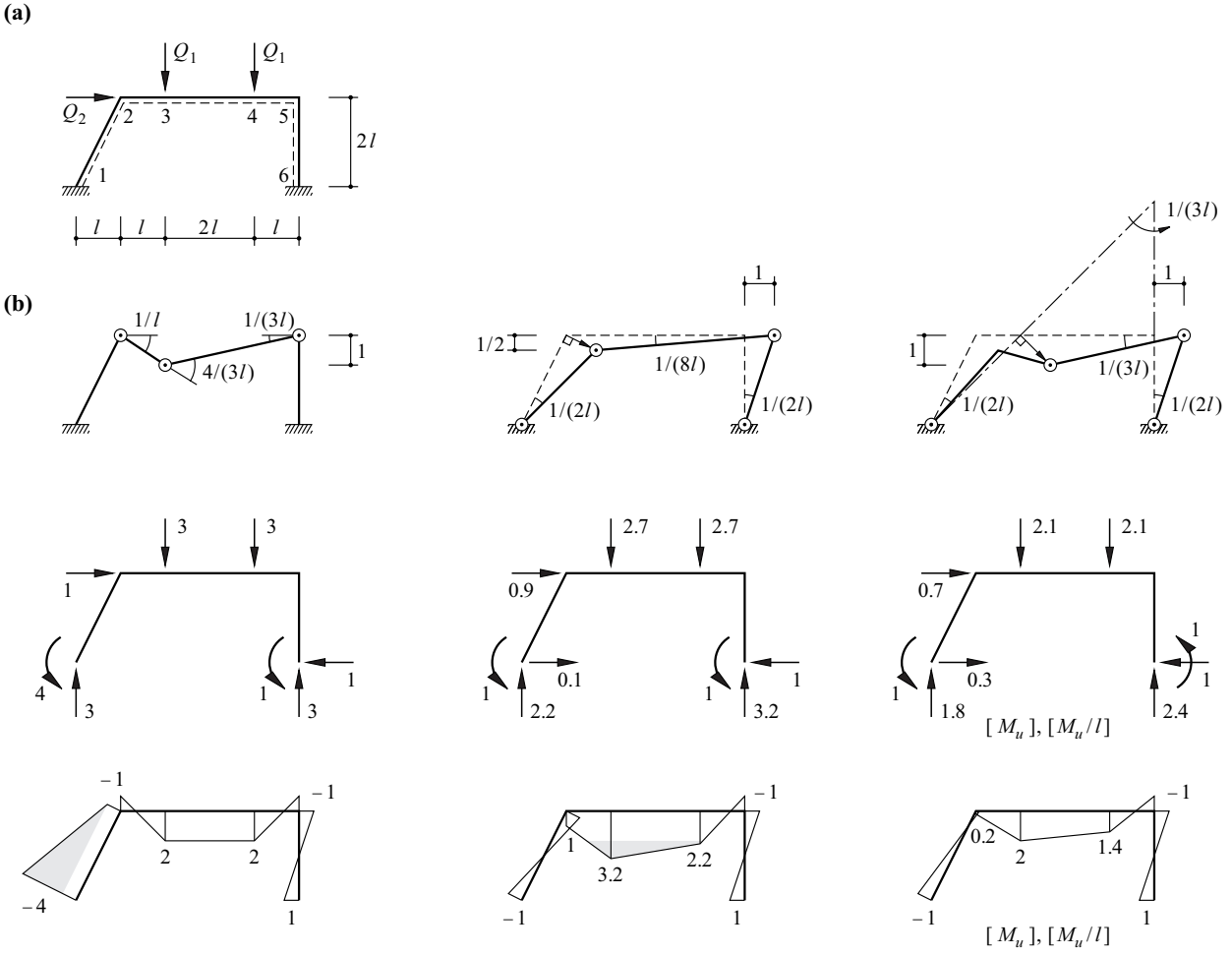

Fig. 21.4 Plane frame: (a) diagram of static system, (b) mechanisms and plasticity checks

$$3Q \cdot \left(1 + \frac{1}{3}\right) = M_u \left(\frac{1}{l} + 2 \cdot \frac{4}{3l} + \frac{1}{3l}\right) \quad \ldots \quad Q_u \leq M_u/l$$

$$Q \cdot 1 + 3Q \cdot \left(\frac{3}{8} + \frac{1}{8}\right) = M_u \left(4 \cdot \frac{1}{2l} + 2 \cdot \frac{1}{8l}\right) \quad \ldots \quad Q_u \leq 0.9 M_u/l$$

$$Q \cdot 1 + 3Q \cdot \left(1 + \frac{1}{3}\right) = M_u \left[3 \cdot \frac{1}{2l} + \frac{1}{3l} + 2 \cdot \left(\frac{1}{2l} + \frac{1}{3l}\right)\right] \quad \ldots \quad Q_u \leq 0.7 M_u/l$$

In the beam and sway mechanisms, the yield condition is infringed in column 12 and frame beam 2345 respectively. On the other hand, the plasticity check for the combined mechanism is satisfied, and the limit load is $Q_u = 0.7 M_u/l$.

The combined mechanism is a linear combination of the beam and sway mechanisms. The corresponding combination factors are 5/8 and 1. Finally, it should be mentioned that the plastic hinges at points 2 and 5 occur at the tops of the columns (bending resistance M_u) and not in the frame beam ($2M_u$).

21.3.4.2 Elementary, combined and partial mechanisms

When the bending moments remain linear segment by segment and the bending resistances are constant for each segment, then plastic hinges can form at the points of fixity, at the points of load application, at corners and at changes of cross-section. If k denotes the number of these *joints*, then for a system with n degrees of static indeterminacy we can formulate

$$m = k - n \tag{21.11}$$

linear, independent equilibrium conditions for the k unknown moments or generalised stresses. These can be obtained as work equations from m *elementary mechanisms*. According to (8.2), the following applies:

$$\boldsymbol{Q} = \boldsymbol{a}^{\mathrm{T}} \bullet \boldsymbol{s} \tag{21.12}$$

where a_{ij} designates the rotation increment at point i as a result of the jth elementary mechanism ($\dot{V}_k = 1$ for $k = j$ and $\dot{V}_k = 0$ for $k \neq j$), and the vectors $\boldsymbol{Q}$ and $\boldsymbol{s}$ include the m generalised loads and the k generalised stresses.

For the frame of Fig. 21.4(a), $k = 6$ and $n = 3$, i. e. $m = 3$ according to (21.11). The beam mechanism shown in Fig. 21.4(b), a similar beam mechanism with a settlement of 1 at joint 4 and the sway mechanism, also shown in Fig. 21.4(b), can be identified as elementary mechanisms. According to (8.1), we get the relationship

$$\dot{\boldsymbol{v}} = \boldsymbol{a} \bullet \dot{\boldsymbol{V}} \tag{21.13}$$

for the generalised deformation increments $\dot{\boldsymbol{v}}$ and the generalised displacement increments $\dot{\boldsymbol{V}}$, i. e.

$$\dot{\boldsymbol{v}} = \begin{Bmatrix} \dot{\theta}_1 \\ \dot{\theta}_2 \\ \dot{\theta}_3 \\ \dot{\theta}_4 \\ \dot{\theta}_5 \\ \dot{\theta}_6 \end{Bmatrix} = \frac{1}{l} \begin{bmatrix} 0 & 0 & -1/2 \\ -1 & -1/3 & 5/8 \\ 4/3 & 0 & 0 \\ 0 & 4/3 & 0 \\ -1/3 & -1 & -5/8 \\ 0 & 0 & 1/2 \end{bmatrix} \begin{Bmatrix} \dot{V}_1 \\ \dot{V}_2 \\ \dot{V}_3 \end{Bmatrix} = \boldsymbol{a} \bullet \dot{\boldsymbol{V}}$$

and (21.12) is

$$\boldsymbol{Q} = \begin{Bmatrix} 4Q_1/3 \\ 4Q_1/3 \\ Q_1/2 + Q_2 \end{Bmatrix} = \frac{1}{l} \begin{bmatrix} 0 & -1 & 4/3 & 0 & -1/3 & 0 \\ 0 & -1/3 & 0 & 4/3 & -1 & 0 \\ -1/2 & 5/8 & 0 & 0 & -5/8 & 1/2 \end{bmatrix} \begin{Bmatrix} M_1 \\ M_2 \\ M_3 \\ M_4 \\ M_5 \\ M_6 \end{Bmatrix} = \boldsymbol{a}^{\mathrm{T}} \bullet \boldsymbol{s}$$

Turning to the combined mechanism of Fig. 21.4(b), then $\dot{V}_1 = 5/8$, $\dot{V}_2 = 0$, $\dot{V}_3 = 1$, and consequently, according to (21.13), $\dot{\theta}_1 = -1/(2l)$, $\dot{\theta}_2 = 0$, $\dot{\theta}_3 = 5/(6l)$, $\dot{\theta}_4 = 0$, $\dot{\theta}_5 = -5/(6l)$, $\dot{\theta}_6 = 1/(2l)$.

Elementary mechanisms can also include *joint mechanisms* as well as beam and sway mechanisms. Fig. 21.5 shows an example where $k = 9$, $n = 4$ and therefore $m = 5$. Three beam, one sway and one joint mechanism can be identified here as elementary mechanisms. The joint mechanism can occur, for instance, in conjunction with the sway mechanism if the bending resistance of the column at 5 is greater than the sum of the bending resistances of the frame beams at 4 and 6; the plastic hinge at the top of the column (5) in the sway mechanism is closed, and therefore we get plastic hinges at the junctions with the frame beams (4 and 6).

Fig. 21.4(b) and Fig. 21.5 show that, as with continuous beams, frames also often have *partial mechanisms* in which fewer than $n+1$ plastic hinges occur. With p plastic hinges, the distribution of the moments at the limit load still has $(n+1-p)$ degrees of static indeterminacy. Fig. 21.6 illustrates this for a frame with a constant bending resistance $\pm M_u$, $k = 5$ and $n = 3$. With the given loading, the result is the beam mechanism shown ($p = 3$), and the distribution of the moments in frame beam 234 is known. However, any statically admissible continuation of the moments into columns 12 and 45 is possible provided this does not infringe the yield condition $|M| \leq M_u$. Equilibrium at the structural members illustrated as free bodies calls for

$$M_1 + 3lV_2 + M_u = 0 \quad , \quad V_2 + V_4 = 0 \quad , \quad M_5 - lV_4 + M_u = 0$$

and therefore the following relationship applies for the moments at the bases of the columns:

$$M_1 - 3M_5 = 2M_u$$

Permissible points along straight line AB result in the M_1-M_5 interaction diagram, and corresponding progressions between the limiting cases A and B are possible in the bending moment diagram. All these bending moments are compatible with the beam mechanism. Further statements regarding the column moments could only be made with the help of an elastic-plastic analysis. As described in section 21.4.3, additional conditions result (e. g. in reinforced concrete frames) if in addition to the bending moments the normal forces are considered as generalised stresses, too.

Sometimes, apparently hyperstatic mechanisms with $p > n+1$ hinges occur. Fig. 21.7(a) shows a frame with constant bending resistance $\pm M_u$, $k = 7$ and $n = 3$. The symmetric mechanism of Fig. 21.7(b) with $p = 5$ plastic hinges is compatible with the bending moment diagram of Fig. 21.7(c) and results in the limit load $Q_u = 2M_u/l$. However, this bending moment diagram is also compatible with the mechanism with $p = 4$ plastic hinges shown in Fig. 21.7(d). Small imperfections

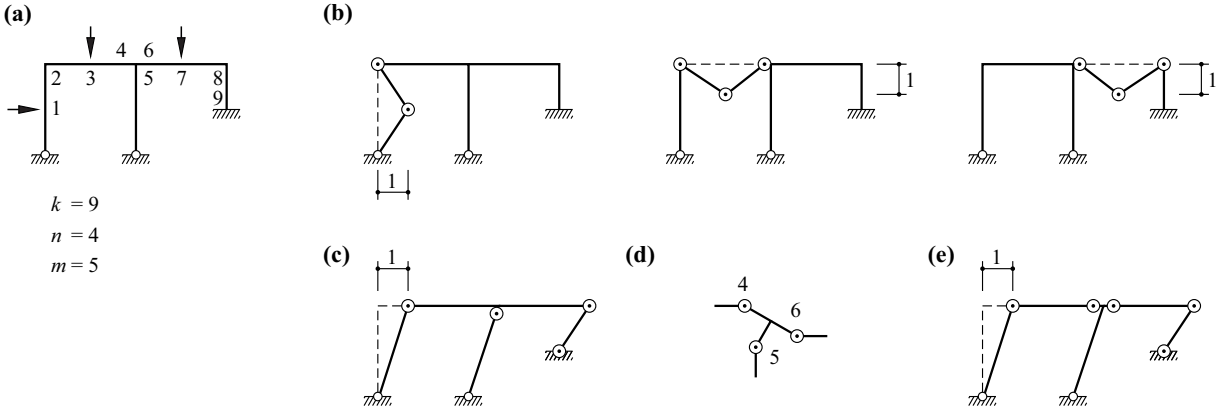

Fig. 21.5 Mechanisms: (a) diagram of static system, (b) beam mechanisms, (c) sway mechanism, (d) joint mechanism, (e) combined mechanism

are always present and so the asymmetric mechanism is to be expected in reality or during a test. The symmetric mechanism corresponds to a theoretical limit case, i. e. the combination of the two asymmetric mechanisms possible. These can occur in any (non-negative) linear combination. Incidentally, Fig. 21.7(e) shows the thrust line corresponding to the structural response of the frame.

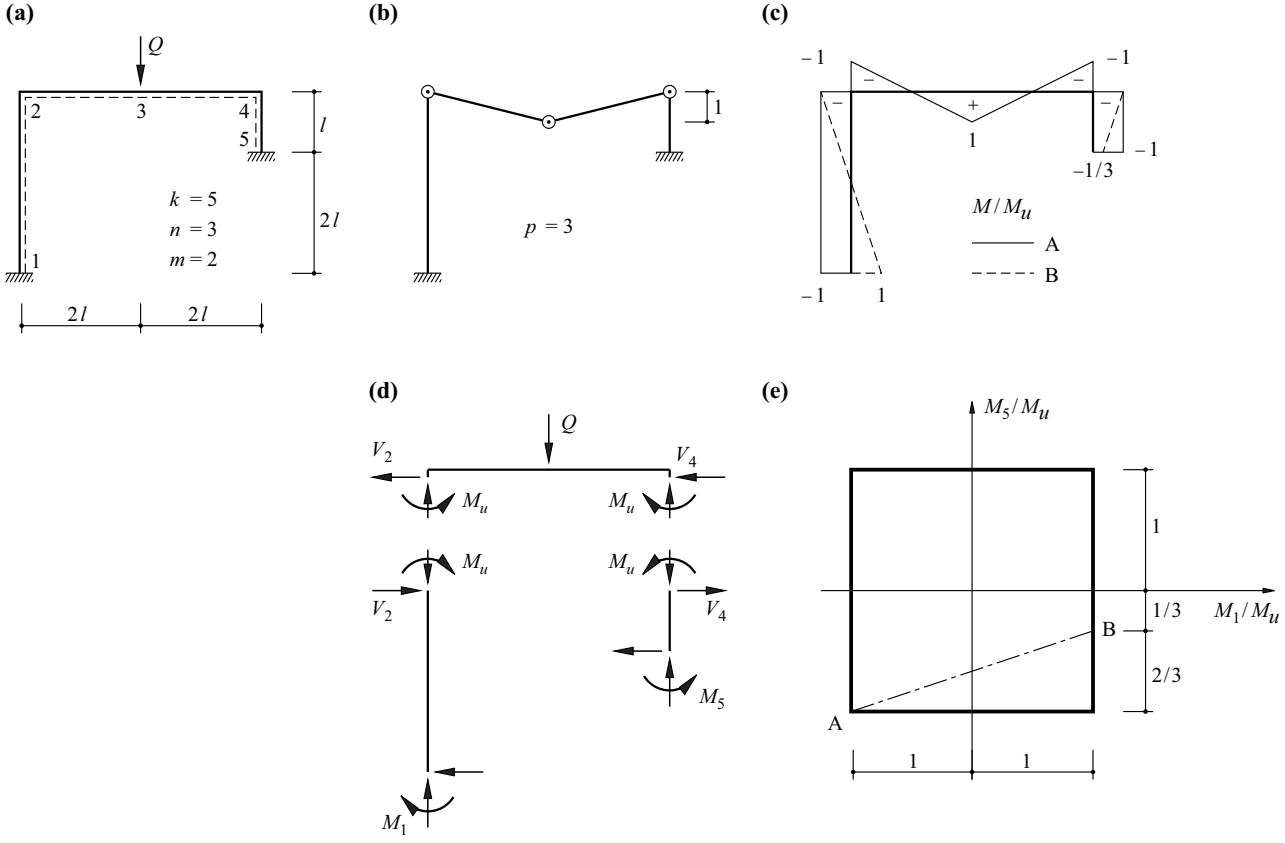

Fig. 21.6 Partial mechanism: (a) diagram of static system, (b) beam mechanism, (c) distribution of moments, (d) free body diagrams (e) M_1-M_5 interaction diagram

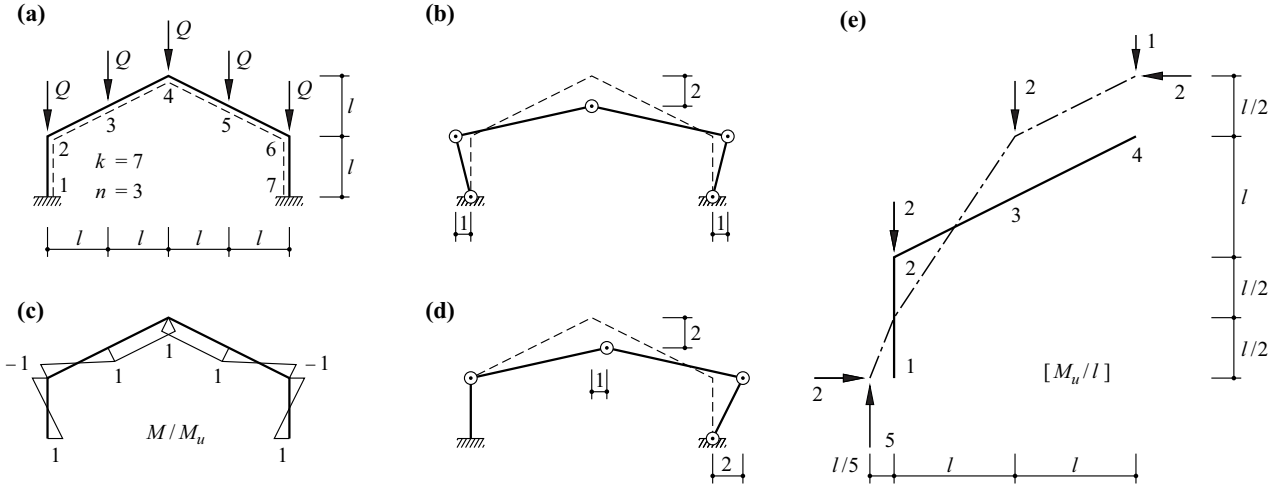

Fig. 21.7 Symmetric frame: (a) diagram of static system, (b) symmetric mechanism, (c) bending moments, (d) asymmetric mechanism, (e) thrust line for half the system

21.3.4.3 Method of inequalities

The elementary mechanisms for the frame shown in Fig. 21.8, with constant bending resistance $\pm M_u$, are two beam mechanisms and one sway mechanism. According to (21.12), we therefore get

$$\begin{Bmatrix} Q_2 \\ Q_1 \\ Q_2/2 \end{Bmatrix} = \frac{1}{l}\begin{bmatrix} 4 & -2 & 0 & 0 & 0 \\ 0 & -2 & 4 & -2 & 0 \\ 0 & 1 & 0 & -1 & 1 \end{bmatrix}\begin{Bmatrix} M_1 \\ M_2 \\ M_3 \\ M_4 \\ M_5 \end{Bmatrix}$$

By solving these relationships for M_1, M_3 and M_5 in conjunction with the yield conditions

$$|M_i| \le M_u \tag{21.14}$$

we get the relations

$$\begin{aligned} -4M_u &\le \quad Q_2 l + 2M_2 \quad\quad\; \le 4M_u \\ -4M_u &\le Q_1 l \quad\; + 2M_2 + 2M_4 \le 4M_u \\ -2M_u &\le \quad Q_2 l - 2M_2 + 2M_4 \le 2M_u \end{aligned} \tag{21.15}$$

with the unknown frame corner moments M_2 and M_4. Moment M_4 can be eliminated from $(21.15)_2$ and $(21.15)_3$ together with (21.14). We get

$$\begin{aligned} -M_u \quad\quad\quad\quad\quad\quad &\le M_4 \le M_u \\ -2M_u - \frac{Q_1 l}{2} \quad\quad - M_2 &\le M_4 \le 2M_u - \frac{Q_1 l}{2} \quad\quad - M_2 \\ -M_u \quad\quad - \frac{Q_2 l}{2} + M_2 &\le M_4 \le M_u \quad\quad - \frac{Q_2 l}{2} + M_2 \end{aligned}$$

from which it follows that

$$\left\{\begin{aligned} -M_u &\le 2M_u - \frac{Q_1 l}{2} - M_2 \\ -M_u &\le M_u - \frac{Q_2 l}{2} + M_2 \end{aligned}\right\} \quad \left\{\begin{aligned} -2M_u - \frac{Q_1 l}{2} - M_2 &\le M_u \\ -2M_u - \frac{Q_1 l}{2} - M_2 &\le M_u - \frac{Q_2 l}{2} + M_2 \end{aligned}\right\} \quad \left\{\begin{aligned} -M_u - \frac{Q_2 l}{2} + M_2 &\le M_u \\ -M_u - \frac{Q_2 l}{2} + M_2 &\le 2M_u - \frac{Q_1 l}{2} - M_2 \end{aligned}\right\}$$

Together with (21.14) and $(21.15)_1$, eliminating M_2 results in

$$\begin{aligned} -M_u \quad\quad\quad\quad\quad\quad &\le M_2 \le M_u \\ -3\,M_u - \frac{Q_1 l}{2} \quad\quad &\le M_2 \le 3\,M_u - \frac{Q_1 l}{2} \\ -2\,M_u \quad\quad + \frac{Q_2 l}{2} &\le M_2 \le 2\,M_u \quad\quad + \frac{Q_2 l}{2} \\ -\frac{3}{2}M_u - \frac{Q_1 l}{4} + \frac{Q_2 l}{4} &\le M_2 \le \frac{3}{2}M_u - \frac{Q_1 l}{4} + \frac{Q_2 l}{4} \\ -2\,M_u \quad\quad - \frac{Q_2 l}{2} &\le M_2 \le 2\,M_u \quad\quad - \frac{Q_2 l}{2} \end{aligned}$$

from which it follows that

$$\begin{aligned} -8M_u/l &\le \quad Q_1 \quad\quad\; \le 8M_u/l \\ -6M_u/l &\le \quad\quad\; Q_2 \le 6M_u/l \\ -10M_u/l &\le -Q_1 + Q_2 \le 10M_u/l \\ -10M_u/l &\le \quad Q_1 + Q_2 \le 10M_u/l \\ -18M_u/l &\le \quad Q_1 + Q_2 \le 18M_u/l \\ -10M_u/l &\le \quad Q_1 + Q_2 \le 10M_u/l \\ -14M_u/l &\le \quad Q_1 + Q_2 \le 14M_u/l \\ -4M_u/l &\le \quad\quad\; Q_2 \le 4M_u/l \\ -14M_u/l &\le \quad Q_1 - 3\,Q_2 \le 14M_u/l \end{aligned} \tag{21.16}$$

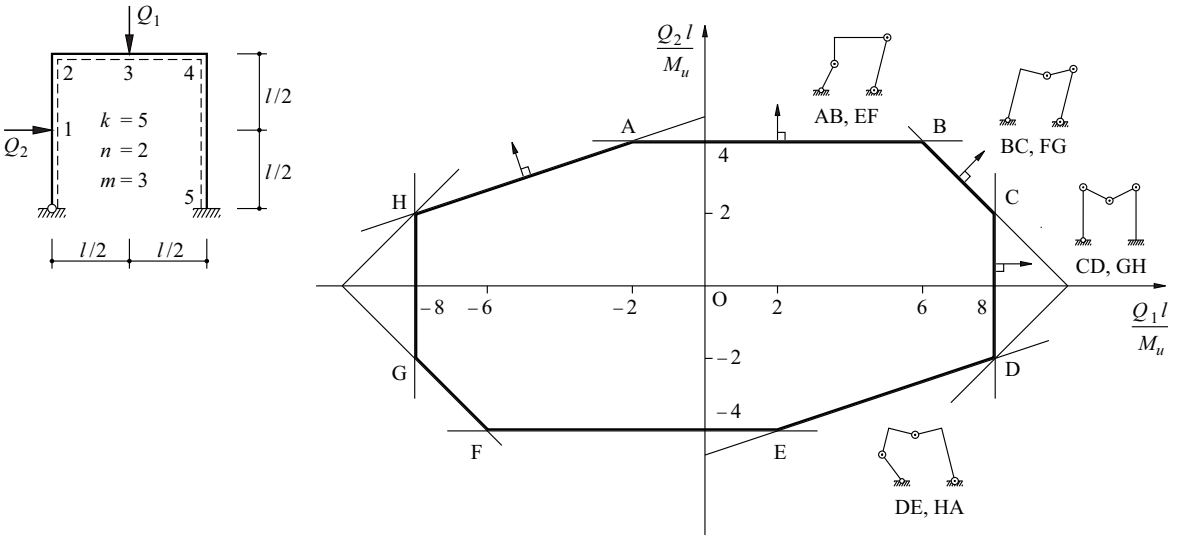

Fig. 21.8 Plane frame with dual-parameter loading

The relationships (21.16) define parallel strips in the Q_1Q_2 plane whose intersection forms the yield locus shown in Fig. 21.8. Regimes AB, EF correspond to $(21.16)_8$, i. e. a pure sway mechanism. On the other hand, regimes CD, GH correspond to $(21.16)_1$, i. e. a pure beam mechanism. Combined mechanisms corresponding to regimes BC, FG and DE, HA result from $(21.16)_4$ and $(21.16)_9$. The other relations of (21.16) are not critical.

21.3.5 Plane frames subjected to transverse loads

21.3.5.1 Torsionless cranked beam

The cranked beam in the XY plane shown in Fig. 21.9(a) is loaded in the Z direction at joint 2 by a monotonically increasing point load Q. Beams 12 and 23 with constant bending resistance $\pm M_u$ are torsionless, i. e. their torsional resistance T_u is zero. The resulting collapse mechanism is a rotation of both beams about axis 13, as shown in Fig. 21.9(b). The bending moments vary linearly between 0 at the point of load application 2 and $-M_u$ at the points of fixity 1 and 3. The limit load is $Q_u = 2M_u/l$.

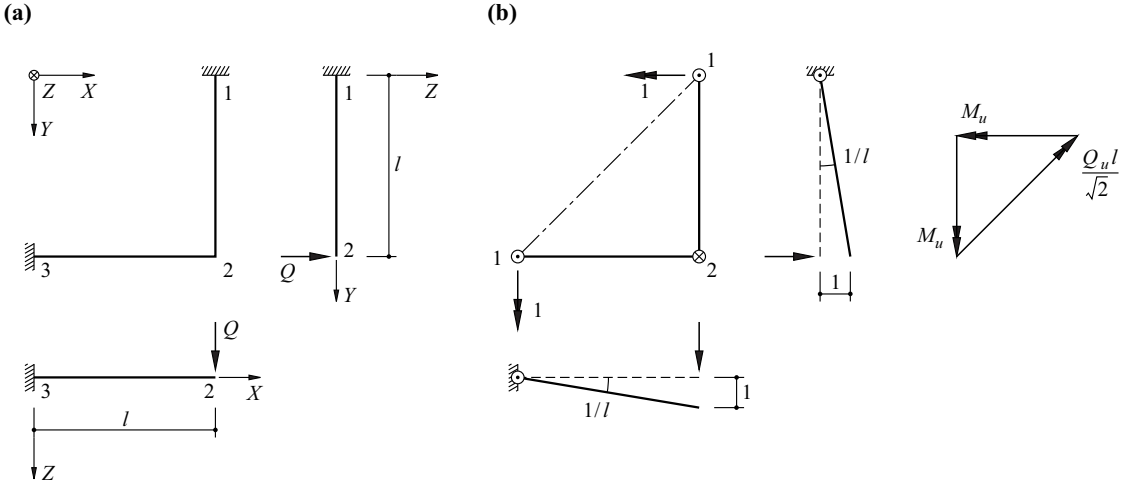

Fig. 21.9 Torsionless cranked beam: (a) diagram of static system, (b) free body diagram [M_u, M_u/l], mechanism and moment equilibrium about axis 13

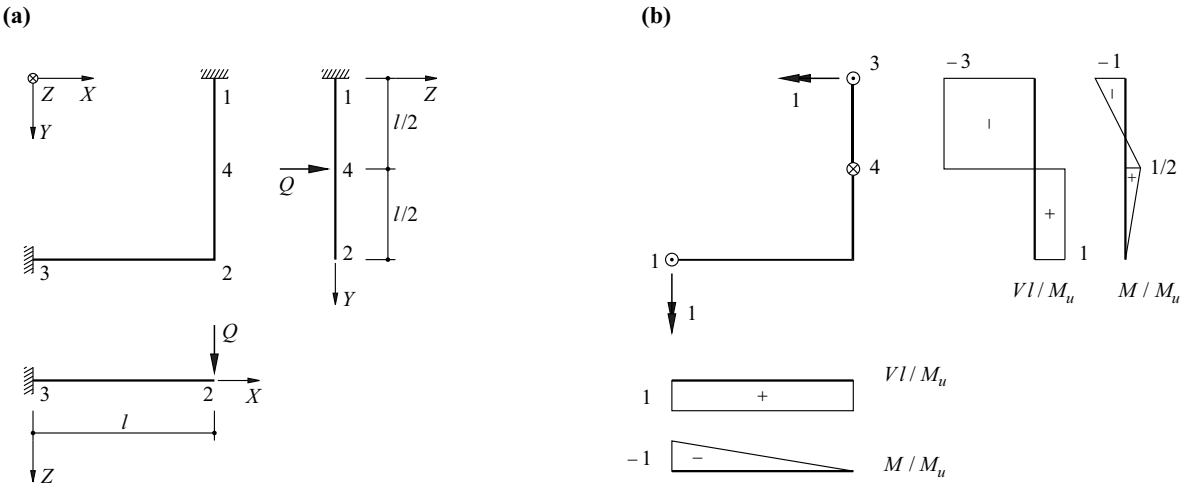

Fig. 21.10 Torsionless cranked beam: (a) diagram of static system, (b) free body diagram [M_u, M_u/l] and stress resultants at limit load

If we shift load Q to point 4 in the middle of beam 12, the result is that shown in Fig. 21.10. The limit load amounts to $Q_u = 4M_u/l$, and the mechanism remains the same as that shown in Fig. 21.9(b).

21.3.5.2 Torsion-resistant cranked beam

Rotation increments amounting to $1/l$ about the bar axis, also transverse to the bar axis, occur at the points of fixity of the mechanism of Fig. 21.9(b). They cause corresponding torques in torsion-resistant beams. To investigate this, we assume – based on section 21.4.4 – that the interaction between torques and bending moments is described by an elliptical yield locus with the equation

$$\left(\frac{M}{M_u}\right)^2 + \left(\frac{T}{T_u}\right)^2 = 1 \tag{21.17}$$

where M_u and T_u designate the pure bending and torsional resistances, see Fig. 21.11(a).

According to the flow rule (21.2), we get

$$\frac{\dot{\theta}_x}{\dot{\theta}_y} = \frac{T M_u^2}{M T_u^2} \tag{21.18}$$

for the relationship between the rotation increments, where x and y denote the local axes corresponding to the torques and bending moments, and T and M satisfy the relationship (21.17). When $|\dot{\theta}_x| = |\dot{\theta}_y|$, the result is $|T| = |M| \cdot (T_u/M_u)^2$, and substituting back into (21.17) results in

$$M = \frac{M_u^2}{\sqrt{M_u^2 + T_u^2}} \quad , \quad T = \frac{T_u^2}{\sqrt{M_u^2 + T_u^2}}$$

The moment-balance equation

$$Q_u l/\sqrt{2} - 2(M + T)/\sqrt{2} = 0$$

about axis 31 therefore leads to a limit load of

$$Q_u = \frac{2\sqrt{M_u^2 + T_u^2}}{l} \tag{21.19}$$

for the problem of Fig. 21.9(a), see Fig. 21.11(b). When $T_u = 0$, eq. (21.19) leads back to the value $Q_u = 2M_u/l$ given above, and when $T_u = M_u$, then $Q_u = 2\sqrt{2}M_u/l$, i. e. the limit load is increased by 41.4 % compared with the torsionless beam.

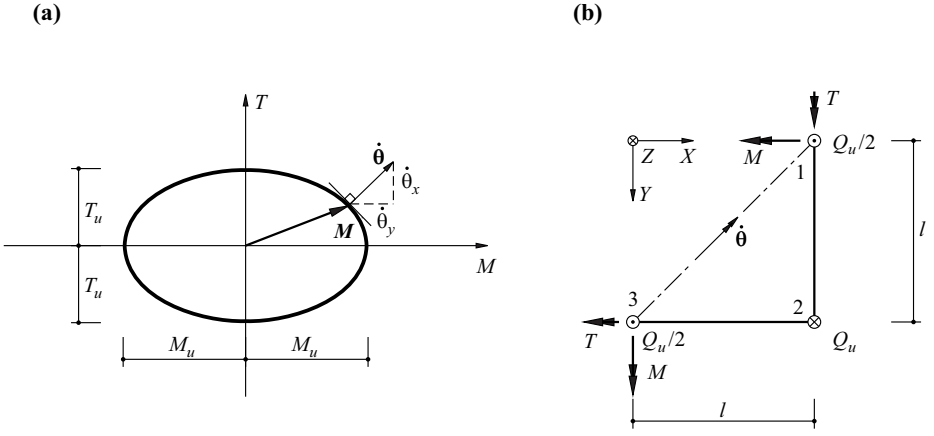

Fig. 21.11 Torsion-resistant cranked beam: (a) yield locus, (b) free body diagram

In order to find a solution to the problem of Fig. 21.10(a), too, while taking into account the torsional resistance, we shall restrict ourselves to the case of $T_u = M_u$, i. e. a circular yield locus. According to (21.18), the rotation increment vectors $\dot{\boldsymbol{\theta}}$ therefore have the same direction as the moment vectors $\boldsymbol{M}$, which have a value of M_u, see Fig. 21.12(a).

Assuming plastic hinges at points of fixity 1 and 3, we first realise that the corresponding moment vectors with a value of M_u must form the same angle α with axes X and Y in order to guarantee equilibrium of moments about axis 13. The moment vectors form an isosceles triangle, and the following applies:

$$Q_u = 4\sqrt{2}\left(\frac{M_u}{l}\right)\sin\left(\frac{\pi}{4}+\alpha\right) \tag{21.20}$$

see Fig. 21.12(b).

The rotation increments $\dot{\theta}_1$ and $\dot{\theta}_3$ are related to each other because they must lead to the same settlement at point 4:

$$\dot{\theta}_3 l \cdot \left(\cos\alpha - \frac{\sin\alpha}{2}\right) = \dot{\theta}_1 \cdot \frac{l\cos\alpha}{2} \tag{21.21}$$

A further plastic hinge develops at point 4. The mutual rotation of beam segments 14 and 324 at this hinge is described by the differential vector $\dot{\boldsymbol{\theta}}_4$ of vectors $\dot{\boldsymbol{\theta}}_1$ and $\dot{\boldsymbol{\theta}}_3$, see Fig. 21.12(c). The torque in beam 142 is constant and so according to the circular yield locus of Fig. 21.12(a), the positive bending moment at plastic hinge 4 must have the same magnitude as the negative bending moment at plastic hinge 1. Consequently, $\dot{\boldsymbol{\theta}}_4$ also forms an angle α with the X axis, and the following applies:

$$\frac{\dot{\theta}_3}{\cos\alpha} = 2\dot{\theta}_1 \sin\alpha \tag{21.22}$$

which together with (21.21) leads to

$$\tan\alpha = \frac{1}{3}$$

Substituting in (21.20) results in

$$Q_u = \frac{16 M_u}{\sqrt{10}\, l} \tag{21.23}$$

Compared with the torsionless cranked beam of Fig. 21.10, the limit load is increased by 26.5 %, but once again a quarter of the load is transferred to fixed support 3.

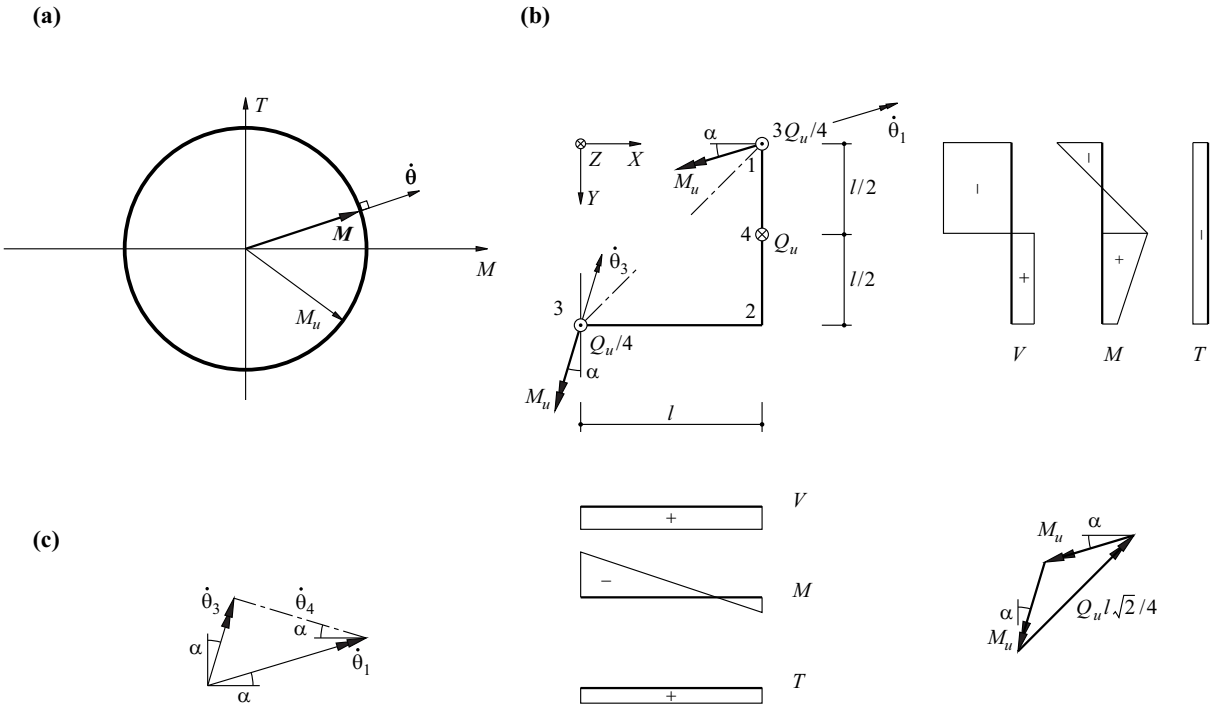

Fig. 21.12 Torsion-resistant cranked beam: (a) yield locus, (b) overview and static relationships, (c) rotation increments at plastic hinges

As can be easily recognised, the yield condition is just satisfied at points 1, 3 and 4 only, and not infringed at any other point. The stress state shown in Fig. 21.12(b) is compatible with the mechanism characterised by Fig. 21.12(c), i. e. the problem is solved completely.

21.3.5.3 Torsionless grillage

The grillage shown in Fig. 21.13(a) consists of eight identical firmly interconnected beams that can accommodate positive and negative bending moments up to a value of M_u or M_u'. A monotonically increasing point load Q is applied at each of the 16 intersections. For reasons of symmetry, we can confine our analysis to half an interior beam (123) and half an exterior beam (2′45), or rather one-eighth of the system.

Fig. 21.13(b) illustrates one possible mechanism. The associated work equation is

$$Q \cdot \left(4 \cdot 1 + 8 \cdot \frac{1}{3} + 4 \cdot \frac{1}{9}\right) = 8(M_u + M_u')\left(\frac{1}{3l} + \frac{1}{9l}\right)$$

from which it follows that $Q_u \leq (M_u + M_u')/(2l)$ according to the upper-bound theorem. The stress state shown in Fig. 21.13(c) is valid for interior and exterior beams and is compatible with the assumed mechanism. Consequently, the limit load amounts to

$$Q_u = \frac{M_u + M_u'}{2l} \tag{21.24}$$

This approach corresponds to the analysis of a uniformly loaded square slab according to the (simple) *strip method*, see section 24.4.3. Using the bending resistances related to the unit length $m_u = M_u/(2l)$ and $m_u' = M_u'/(2l)$, the total load applied to the slab is $16(m_u + m_u')$.

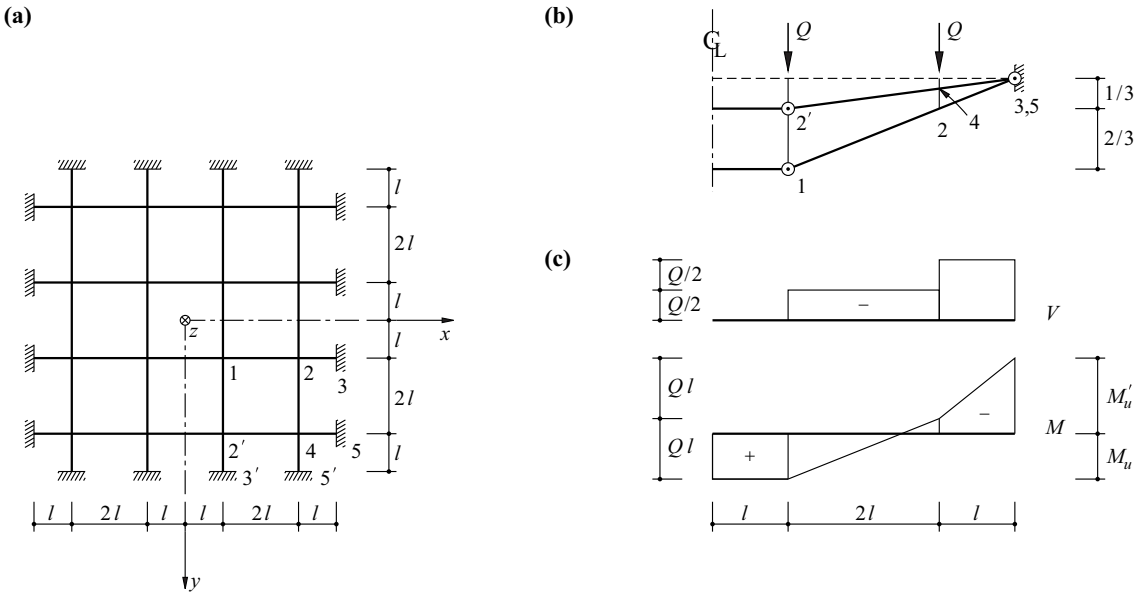

Fig. 21.13 Torsionless grillage: (a) plan, (b) mechanism, (c) stress resultants

21.3.5.4 Torsion-resistant grillage

In the following it will be assumed that the yield locus of Fig. 21.12(a) and the mechanism of Fig. 21.13(b) apply to the beams of the system shown in Fig. 21.13(a). Plastic flexural hinges, where $\dot{\theta}_y = 1/(3l)$, $\dot{\theta}_x = 0$, develop at points 1 and 3. A flexural-torsional hinge, where $\dot{\theta}_y = 1/(9l)$, $\dot{\theta}_x = 2/(9l)$, develops at $2'$, and one with $\dot{\theta}_y = \dot{\theta}_x = 1/(9l)$ at 5. Therefore, the work equation is

$$Q \cdot \left(4 \cdot 1 + 8 \cdot \frac{1}{3} + 4 \cdot \frac{1}{9}\right) = 8M_u \left[2 \cdot \frac{1}{3l} + \frac{1}{9l}(\sqrt{5} + \sqrt{2})\right]$$

from which, according to the upper-bound theorem, it follows that $Q_u \leq 1.206 M_u/l$.

Fig. 21.14 shows a distribution of stress resultants compatible with the assumed mechanism. The yield condition is satisfied at points 1, 3, $2'$ and 5, and not infringed at any other point. Consequently, the limit load amounts to $Q_u = 1.206 M_u/l$. Compared with the torsionless grillage where $M_u = M_u'$, the limit load is increased by 20.6 %.

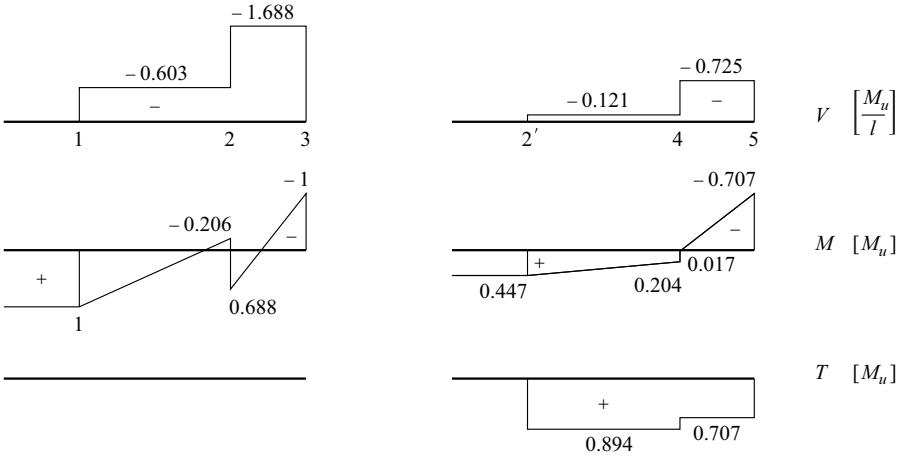

Fig. 21.14 Stress resultants for torsion-resistant grillage subjected to the limit load

21.3.5.5 More complex systems

The static analysis of more complex systems is usually very involved. On the other hand, applying the kinematic method enables good upper-bound values for the limit loads of grillages to be obtained relatively easily every time. In a similar way to the application of the yield line method for slabs (see section 24.5), we assume that the mechanism here is in the form of a deflected surface. The rotation increments at the plastic hinges are therefore easy to calculate and the work equation can be formulated.

21.4 Plastic strength of materials

21.4.1 General

Up until now we have mostly confined ourselves to simple cross-sections in pure bending. The procedure for calculating the deformation behaviour of general cross-sections subjected to any stress resultants caused by bending moments and normal forces was briefly explained in section 20.3.1. The following descriptions are concerned with the resistances and plastic deformations of bars subjected to combined stress resultants. This is intended to supplement chapter 13 in the meaning of a *plastic strength of materials*.

21.4.2 Skew bending

21.4.2.1 Rectangular cross-sections

Assuming equal yield limits in tension and compression ($f_{yt} = f_{yc} = f_y$, see Fig. 7.6), the neutral axis n - n inclined at an angle α to the y axis must pass through the centroid of the cross-section, see Fig. 21.15(a). When $\tan\alpha \le h/b$, we get

$$M_y = M_{yu} - \frac{b^3 f_y \tan^2\alpha}{12} \quad , \quad M_z = \frac{b^3 f_y \tan^2\alpha}{6} \tag{21.25}$$

where M_{yu} designates the bending resistance $bh^2 f_y/4$ for pure bending about the y axis as given by $(20.26)_1$. Eq. (21.25) results in arc AB in the interaction diagram of Fig. 21.15(b). At point B, $M_y = W_y f_y$ and $M_z = W_z f_y$, where $W_y = bh^2/6$ and $W_z = hb^2/6$, see $(20.23)_2$.

After eliminating α, eq. (21.25) results in

$$\frac{M_y}{M_{yu}} + \frac{3}{4}\left(\frac{M_z}{M_{zu}}\right)^2 = 1 \qquad \left(|M_z/M_y| \le h/b\right) \tag{21.26}_1$$

and swapping the indexes results in the similar expression

$$\frac{M_z}{M_{zu}} + \frac{3}{4}\left(\frac{M_y}{M_{yu}}\right)^2 = 1 \qquad \left(|M_z/M_y| \ge h/b\right) \tag{21.26}_2$$

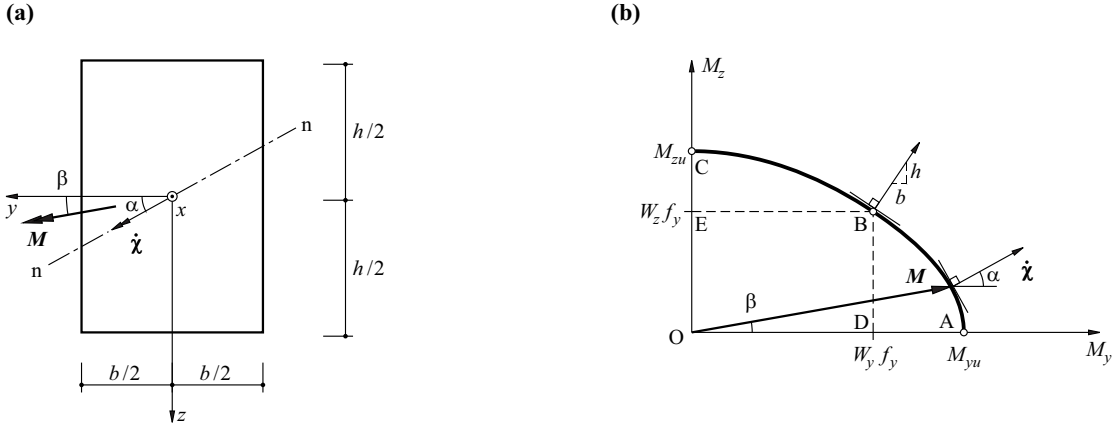

Fig. 21.15 Skew bending of a rectangular cross-section ($f_{yt} = f_{yc} = f_y$): (a) notation, (b) interaction diagram

for arc BC in Fig. 21.15(b), where

$$M_{yu} = b\,h^2 f_y/4 \quad , \quad M_{zu} = h\,b^2 f_y/4 \tag{21.27}$$

The parabolas AB and CB given by (21.26) can be approximated with the circumscribing ellipse described by the equation

$$\left(\frac{M_y}{M_{yu}}\right)^2 + \left(\frac{M_z}{M_{zu}}\right)^2 = 1 \tag{21.28}$$

In doing this, we overestimate the resistance at point B by 6 %. On the other hand, the bilinear approximation ABC results in an approximation that is on the safe side. A straight line AC provides an even rougher approximation – on the safe side, however.

Dimensioning based on permissible stresses restricts the allowable moments to a smaller region affine with triangle ODE, depending on the factor of safety used. Therefore, in a case of distinctly skew bending, the result is a clear overdesign compared with dimensioning according to plastic theory, i. e. uneconomic design.

Applying the flow rule (21.2) to (21.26) shows that vectors $\boldsymbol{M}$ and $\dot{\boldsymbol{\chi}}$ in Fig. 21.15(b) are collinear ($\alpha = \beta$) for pure bending only (points A and C), but with square cross-sections ($h = b$) they are collinear for the case of $M_y = M_z$ as well (point B, $\alpha = \beta = \pi/4$).

21.4.2.2 General cross-sections

As with the rectangular cross-section, the neutral axis does not generally coincide with the axis of the bending moment ($\alpha \neq \beta$). According to our assumptions, the normal force disappears and $f_{yt} = f_{yc} = f_y$, so the axis still halves the cross-sectional area. However, it does not pass through a fixed point, but rather shifts according to the loading.

Assuming an arbitrary yz system of coordinates in the plane of the cross-section results in a skew-symmetric interaction diagram for the M_y, M_z components of the bending moment; every point in the interaction diagram corresponds to a diametrically opposed point with opposite stresses. The result is generally two directions, the *principal plastic directions*, for which $\alpha = \beta$ or $\dot{\boldsymbol{\chi}} \sim \boldsymbol{M}$. These are not normally orthogonal, nor do they coincide with the principal elastic directions.

Example 21.1 Unequal leg angle

The angle shown in Fig. 21.16, with constant thickness t, has the moments

$$M_y = \left(\frac{a^2}{4} - ac - c^2\right) t f_y \quad , \quad M_z = \left(\frac{b^2}{4} + bc - c^2\right) t f_y \tag{21.29}$$

where c is the parameter defining the position of the neutral axis, $|c| \leq b/2$ and $t \ll b < a$. Eq. (21.29) results in arc AB in Fig. 21.16(b). For point A, where $c = -b/2$, the result is $M_y = (a^2 + 2ab - b^2)tf_y/4$ and $M_z = -b^2 t f_y/2$. For point B, where $c = b/2$, the result is $M_y = (a^2 - 2ab - b^2)tf_y/4$ and $M_z = b^2 t f_y/2$.

The skew-symmetric supplement to the interaction diagram leads to arc A′B′. The neutral axis lies in the long leg of the section for points on straight lines AB′ and A′B. The neutral axis passes through the point $y = 0$, $z = (b - a)/2$ for point A, and the angle formed by the neutral axis and the y axis can take on any value between arc tan $[(a - b)/(2b)]$ and $-\pi/2$.

The "strong" axis OA in Fig. 21.16(b) corresponds to the first principal plastic direction. The second principal plastic direction is obtained from the condition $(b/2 - c)/(a/2 + c) = M_y/M_z$ with the moment components according to (21.29). This leads to a cubic equation for c which has a real root. For example, the result for the case of $b/a = 2/3$ shown in the figure is the value $c = 0.2598\,b$, which corresponds to the "weak" axis OC.

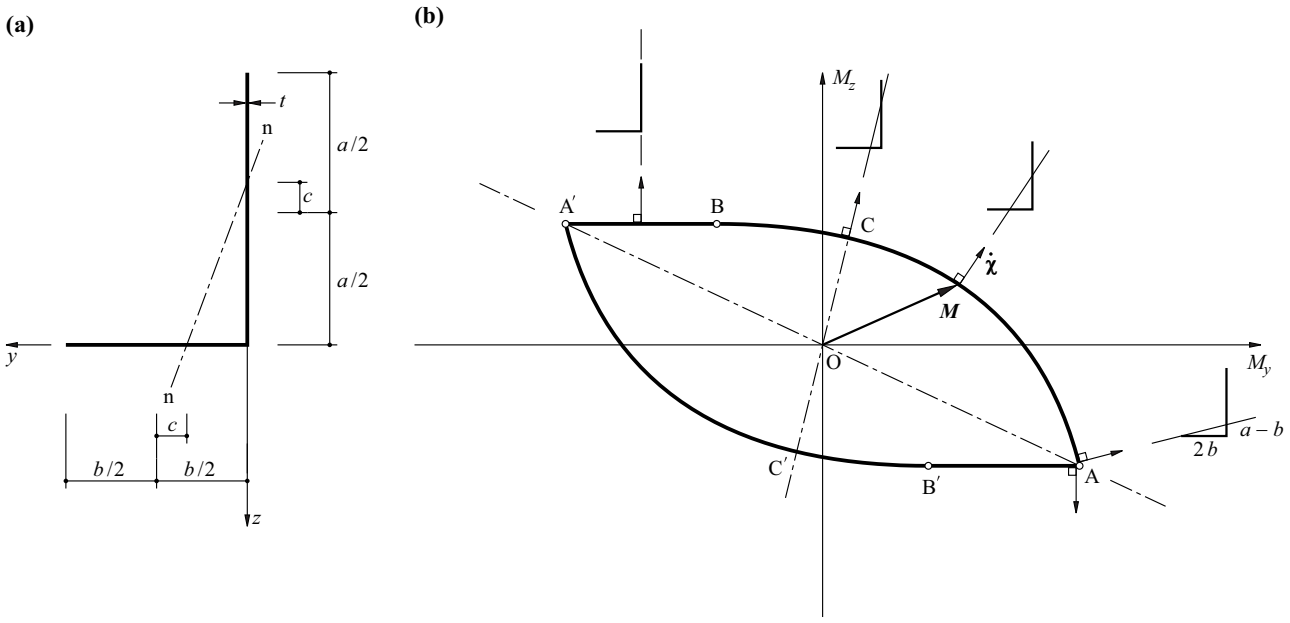

Fig. 21.16 Skew bending for an unequal leg angle: (a) notation, (b) interaction diagram

21.4.3 Bending and normal force

21.4.3.1 Rectangular cross-section

Fig. 21.17(a) is obtained from Fig. 21.15(a) through parallel translation of the neutral axis upwards by the amount c. The compression zone decreases in favour of the tension zone and a normal force $N = 2cbf_y$ develops. An amount c^2bf_y is deducted from M_y in $(21.25)_1$; eq. $(21.25)_2$ is not altered. When $N_u = bhf_y$, the result is therefore

$$\frac{M_y}{M_{yu}} + \frac{3}{4}\left(\frac{M_z}{M_{zu}}\right)^2 + \left(\frac{N}{N_u}\right)^2 = 1 \qquad (21.30)_1$$

and by swapping the indexes we get

$$\frac{M_z}{M_{zu}} + \frac{3}{4}\left(\frac{M_y}{M_{yu}}\right)^2 + \left(\frac{N}{N_u}\right)^2 = 1 \qquad (21.30)_2$$

for the position of the neutral axis shown in Fig. 21.17(b).

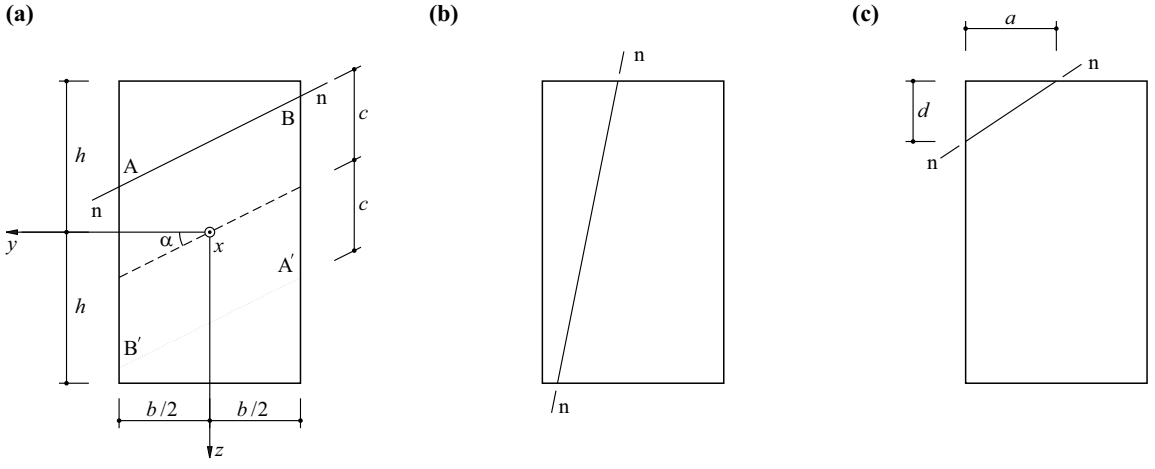

Fig. 21.17 Skew bending and normal force for a rectangular cross-section

The following applies for the situation shown in Fig. 21.17(c):

$$N = (bh - ad)f_y \quad , \quad M_y = adf_y\left(\frac{h}{2} - \frac{d}{3}\right) \quad , \quad M_z = adf_y\left(\frac{b}{2} - \frac{a}{3}\right)$$

from which, by eliminating parameters a and d and introducing reference values N_u, M_{yu}, M_{zu}, it follows that

$$\left[\frac{M_y}{M_{yu}} - 2\left(1 - \frac{N}{N_u}\right)\right]\left[\frac{M_z}{M_{zu}} - 2\left(1 - \frac{N}{N_u}\right)\right] - \frac{16}{9}\left(1 - \frac{N}{N_u}\right)^3 = 0 \qquad (21.30)_3$$

The equations (21.30) describe the yield surface in the first octant. As this surface is symmetrical with respect to axes N, M_y, M_z, this is adequate.

21.4.3.2 Reinforced concrete

Fig. 21.18(a) shows a composite cross-section made up of concrete (cross-sectional area $A_c = bh$) and reinforcing steel (cross-sectional area $A_s = \rho A_c$). The reinforcement is located symmetrically at the top and bottom faces of the cross-section. The concrete cover to the reinforcement is neglected.

The reinforcement is presumed to be perfectly plastic with yield limits $\pm f_y$ in tension and compression. It is assumed that the concrete behaves according to Fig. 7.6, where $f_{yt} = 0$ and $f_{yc} = f_c$, i. e. its tensile strength is neglected and it is treated as a perfectly plastic material from the point of view of compressive stresses. In order to take into account the difference between this and the true behaviour of the concrete (see Fig. 7.2), the "yield limit" f_c is taken to be equal to, for example, 60 % of the uniaxial compressive strength; f_c is often referred to as the *effective strength*.

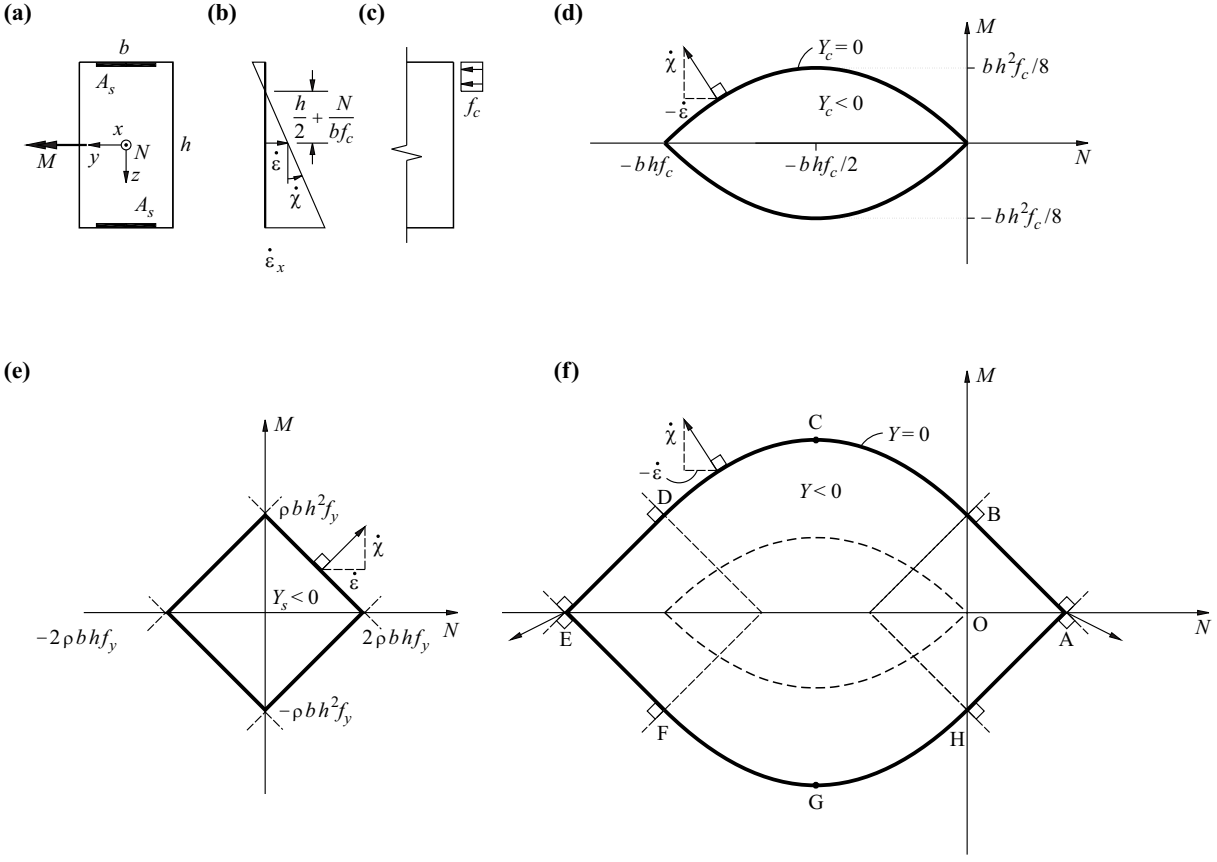

Fig. 21.18 Symmetrically reinforced rectangular cross-section without concrete cover: (a) notation, (b) strain increments, (c) stress distribution, (d) to (f) yield loci for concrete, reinforcement and reinforced concrete

Fig. 21.18(b) illustrates the strain increments

$$\dot{\varepsilon}_x = \dot{\varepsilon} + \dot{\chi} z \tag{21.31}$$

with the generalised deformation increments $\dot{\varepsilon}$ and $\dot{\chi}$, see (13.3), and Fig. 21.18(c) shows the corresponding stress distribution in the concrete. The neutral axis ($\dot{\varepsilon}_x = 0$) is located at a distance of $h/2 + N/(bf_c)$ from the y axis because the compressive stresses in the concrete f_c are distributed over a depth of $-N/(bf_c)$. With the stress resultant N and its lever arm $h/2 + N/(2bf_c)$, the moment about the y axis equals $-N[h/2 + N/(2bf_c)]$. Apart from the sign of M, the same expression applies for a negative $\dot{\chi}$. The following generally applies:

$$Y_c = |M| + N\left(\frac{h}{2} + \frac{N}{2bf_c}\right) = 0 \qquad (N \leq 0) \tag{21.32}$$

The yield function Y_c describes the yield locus made up of two parabolas forming the boundaries to the non-plastic domain of the concrete, see Fig. 21.18(d).

In a similar way to Fig. 21.18(d), we get the yield locus $Y_s = 0$ shown in Fig. 21.18(e) for the reinforcement.

The linear combination of the stress states $\boldsymbol{\sigma}_c$ and $\boldsymbol{\sigma}_s$ possible for the concrete and the reinforcement results in the yield locus $Y = 0$ for the reinforced concrete shown in Fig. 21.18(f). This yield locus can be thought of – for example, with a fixed yield locus for the reinforcement – as the yield locus of the concrete undergoing a pure translation such that its origin includes all positions on the yield locus of the reinforcement. The envelope enclosing all translated positions of the yield locus of the concrete is then the yield locus of the reinforced concrete cross-section we require.

Fig. 21.19(a) illustrates the effect of asymmetric reinforcement ($A_s' = A_s/2$). The yield locus is constructed in a similar way to that of Fig. 21.18(f).

In contrast to Fig. 21.18(f), a concrete cover c to the reinforcement has been assumed in Fig. 21.19(b). The two parabolic boundaries to the non-plastic domain of the concrete are therefore each divided into three in the yield locus for the reinforced concrete.

It is possible to generalise the findings for the rectangular cross-section for any cross-sections without any inherent difficulties. The principle behind such considerations was described in sections 13.2.1 and 20.3.1. Many cross-section design programs are now available to ease the practical calculation work. Most of these use the stress-strain diagrams and place limits on the strains. Compared with a rigid - perfectly plastic approach, the deviations are normally relatively small. However, limiting the strains can lead to partially concave interaction diagrams.

Considering *M-N* interaction diagrams generally leads to an iterative procedure when analysing frameworks. Starting with estimates of the bending resistances, working according to section 21.3.4 for a certain load case results in the mechanism associated with that case plus the normal forces present at the plastic hinges. Applying the interaction diagrams of the hinge cross-sections improves the bending resistances, and the calculation can be repeated until sufficient accuracy has been achieved. It is also necessary to check whether a mechanism other than the one assumed is critical, and then adapt the calculation if necessary.

The normal forces at the plastic hinges can remain indeterminate in partial mechanisms such as the one shown in Fig. 21.6. In the example, the compressive force in frame beam 234 can take on values between 0 and $2M_u/(3l)$. A more accurate analysis reveals that the neutral axes at points 2, 3, 4 lie at different levels because of the thin concrete compression zones, which causes an elongation of the frame beam and requires a further plastic hinge at the base 1 of the long column. As a result of this finding, the iterative calculation can be carried out as explained above using the bending resistances that are dependent on the normal forces.

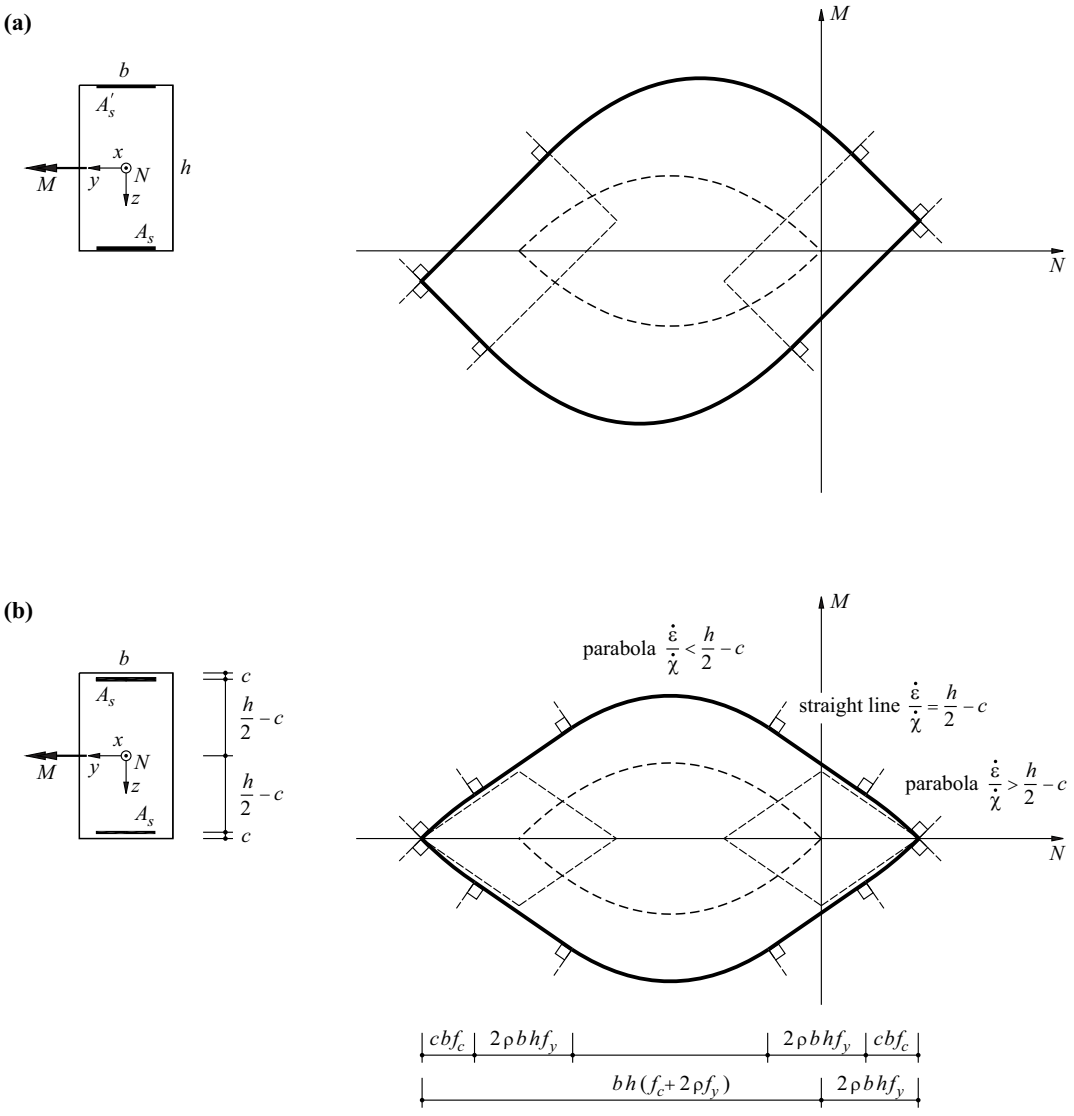

Fig. 21.19 Additional influences: (a) asymmetric reinforcement, (b) concrete cover

21.4.3.3 Masonry

As an approximation, masonry can be treated like plain (i. e. unreinforced) concrete. The compressive stresses in the masonry are in most instances so much lower than its compressive strength (e. g. 10 % or less) that the approximation of Fig. 21.20(a) can be used instead of the yield locus of Fig. 21.18(d), i. e.

$$Y_c = |M| + \frac{Nh}{2} = 0 \qquad (N \leq 0) \tag{21.33}$$

If we wish to consider the finite compressive strength of the masonry, then h can be reduced to, for example, 90 % of the effective depth of the cross-section. We calculate, so to speak, with what is outwardly a "shaved" cross-section.

A consequence of the assumptions made is that a masonry structure cannot fail if it is possible to specify a thrust line for a given load which lies entirely within the masonry. Fig. 21.20(b) illustrates this for an arch loaded by the point load Q. The mechanism shown, with hinges at A, B, C and D, can occur if the thrust line ABD touches the intrados at C.

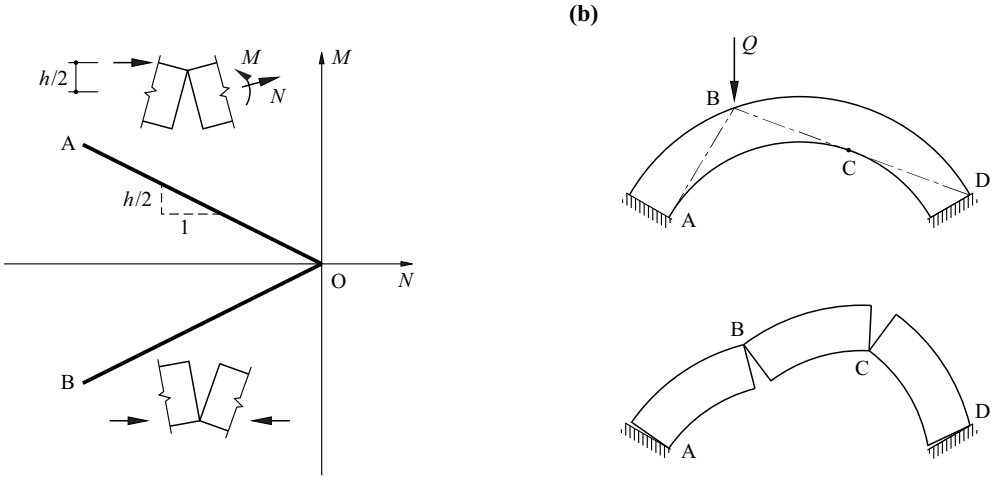

Fig. 21.20 Masonry: (a) interaction diagram, (b) thrust line and mechanism

It is best to use a graphic approach for the practical analysis of masonry structures. This involves first establishing a thrust line for the permanent actions, which should deviate as little as possible from the system axis of the structure. Based on this, it is possible to determine the extent to which the thrust line deviates sideways as a result of variable actions. The risk of collapse can then be estimated.

21.4.4 Bending and torsion

According to the VON MISES yield condition, see Fig. 7.8(c), the shear stresses $\tau_{\varphi x}$ in the thin-wall circular hollow section of Fig. 21.21(a) cannot exceed the value $\tau_y = f_y/\sqrt{3}$. According to (13.66), this results in a torsional resistance of

$$T_u = \frac{2\pi}{\sqrt{3}} r^2 t f_y \qquad (21.34)_1$$

where t is the wall thickness and r is the radius to the centre of the wall of the cross-section. On the other hand, we get the following for the bending resistance:

$$M_u = 4 \int_0^{\pi/2} t f_y r^2 \sin\varphi \, d\varphi = 4 r^2 t f_y \qquad (21.34)_2$$

In the case of combined bending and torsion, the normal stresses σ_x and the shear stresses $\tau_{\varphi x}$ according to (7.21) and $(5.40)_2$ satisfy the condition

$$\sigma_x^2 + 3\tau_{\varphi x}^2 = f_y^2 \qquad (21.35)$$

Using $M = 4r^2 t\sigma_x$, $T = 2\pi r^2 t\tau_{\varphi x}$ and (21.34), we therefore get the interaction relationship

$$\left(\frac{M}{M_u}\right)^2 + \left(\frac{T}{T_u}\right)^2 = 1 \qquad (21.36)$$

see (21.17).

Eq. (21.36) also applies for the rectangular hollow section shown in Fig. 21.21(b), where

$$M_u = \left(\frac{a}{b} + \frac{1}{2}\right) b^2 t f_y \quad , \quad T_u = \frac{2a}{\sqrt{3}b} b^2 t f_y \qquad (21.37)$$

If we use the TRESCA instead of the VON MISES yield condition, then the factor of $\sqrt{3}$ in $(21.34)_1$ and $(21.37)_2$ must be replaced by 2 ($\tau_y = f_y/2$), and the factor of 3 in (21.35) must be replaced by 4.

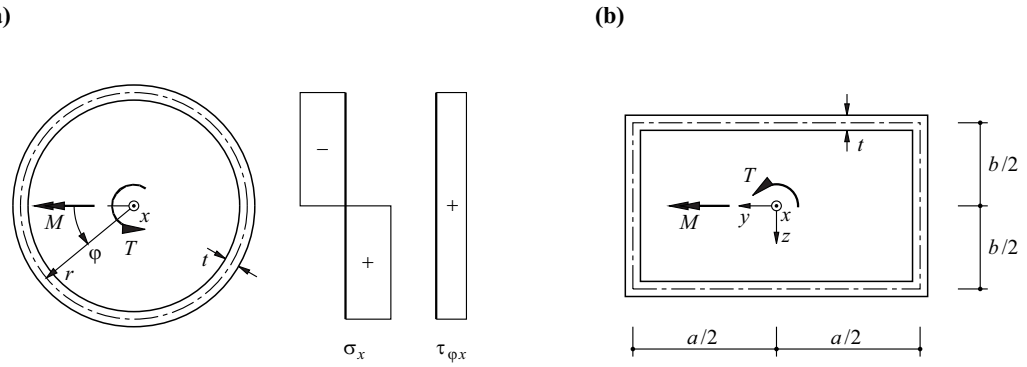

Fig. 21.21 Bending and torsion in thin-wall hollow cross-sections

According to (21.34) and (21.37), $M_u \approx T_u$. Therefore, for simplicity, we often work with $M_u = T_u$, see Fig. 21.11(a) and Fig. 21.12(a).

We get, on the one hand,

$$M_u = \frac{4r_0^3 f_y}{3} \qquad (21.38)_1$$

for the circular solid section shown in Fig. 21.22(a), and, on the other, using $\tau_{\varphi x} = \tau_y = \text{const}$, we get the torsional resistance

$$T_u = \int_0^{r_0} 2\pi r^2 \tau_y \mathrm{d}r = \frac{2\pi}{3} r_0^3 \tau_y \qquad (21.38)_2$$

Compared with this, the onset of yield at the edge of the cross-section according to (13.52) results in a torque of

$$T_y = \frac{\pi}{2} r_0^3 \tau_y \qquad (21.39)$$

i. e. the shape factor of the cross-section is $f = T_u/T_y = 4/3$.

The membrane analogy in the case of elastic behaviour (see section 13.4.2) has to be replaced by the *sand hill analogy* in the case of plastic behaviour, as shown in Fig. 21.22(a). Twice the volume covered by a membrane inclined at an angle τ_y at the edge of the cross-section amounts to

$$2\int_0^{r_0} 2\pi r \frac{\tau_y r_0}{2}\left[1 - \left(\frac{r}{r_0}\right)^2\right]\mathrm{d}r = \frac{\pi}{2} r_0^3 \tau_y = T_y$$

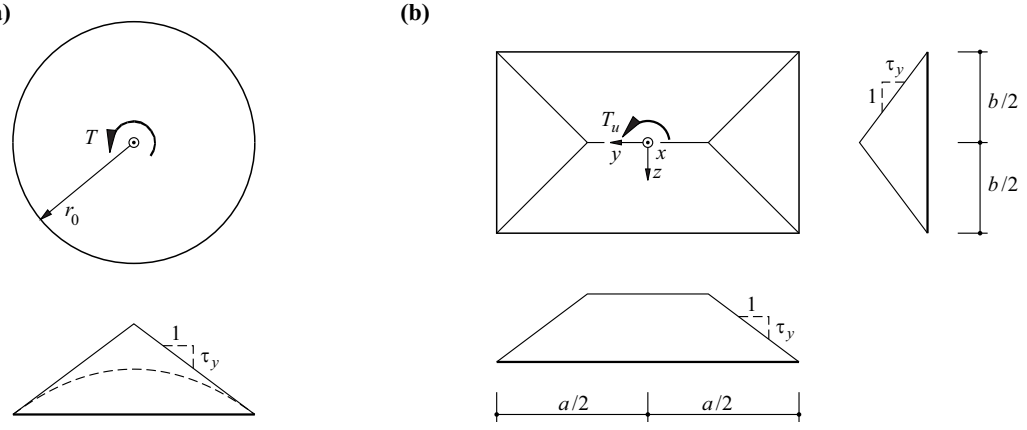

Fig. 21.22 Plastic torsion of solid cross-sections

A volume in the form of a circular cone corresponds to the plastic behaviour. The generator of the cone, like with a pile of sand, exhibits a constant slope of τ_y. Twice the volume of the cone amounts to $(2\pi/3)r_0^3\tau_y = T_u$.

Considering a rectangular cross-section, see Fig. 21.22(b), we get, on the one hand,

$$M_u = \frac{ab^2 f_y}{4} \qquad (21.40)_1$$

and, on the other, the sand hill analogy gives us the torsional resistance

$$T_u = 2\left(\frac{b}{3} + \frac{a-b}{2}\right)\frac{\tau_y b^2}{2} = \frac{b^2(3a-b)\tau_y}{6} \qquad (a \geq b) \qquad (21.40)_2$$

For the onset of yield in the middle of the long sides of the cross-section ($y = 0$, $z = \pm b/2$), a very good approximation is

$$T_y = \frac{ab^2\tau_y}{3} \cdot \frac{1 - \dfrac{192b}{\pi^5 a}\tanh\left(\dfrac{\pi a}{2b}\right)}{1 - \dfrac{8}{\pi^2 \cosh\left(\dfrac{\pi a}{2b}\right)}} \qquad (21.41)$$

see exercise 13.9. The shape factor $f = T_u/T_y$ for a square cross-section ($a = b$) is 1.594, and 1.5 for very wide cross-sections ($a \gg b$).

Eq. (21.36) applies for the interaction between bending and torsion in solid cross-sections, too.

21.4.5 Bending and shear force

Combinations of large bending moments and large shear forces can occur at fixed supports, the intermediate supports of continuous beams, frame corners and similar situations. It is advisable to introduce the *shear span*

$$c = \left|\frac{M_0}{V_0}\right| \qquad (21.42)$$

to enable uniform treatment of such cases. The shear span is the length of a fictitious cantilever that is loaded at its unsupported end by a point load that, at the section being examined, causes the same ratio between bending moment and shear force as the effective loading on the actual system, see Fig. 21.23; c is equal to the distance from the section being examined to the intersection of the tangent to the M line at the section being examined and the base line of the moment diagram.

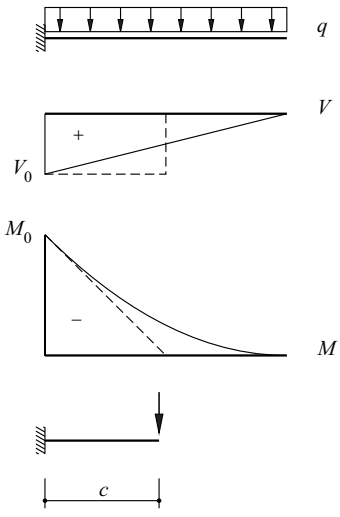

Fig. 21.23 Shear span c

In contrast to the cases of bending plus normal force and bending plus torsion, the case of bending plus shear force does not give rise to a true interaction between the stress resultants M_0 and V_0. In fact, these are linked via the shear span c. Just considering the cross-section alone is insufficient, i. e. the stress state at the section being examined and in the vicinity of that section must always be analysed as a whole. However, such an analysis is quite complicated and will not be explored any further here.

In order to estimate to what extent the shear forces influence the bending resistances of thin-wall I sections, the stress distribution shown in Fig. 21.24(a) gives us the relationship

$$M = a\,b\,t_f f_y + \frac{b_w^2 t_w f_y}{4}\sqrt{1 - \left(\frac{V}{V_u}\right)^2} \qquad (b_w = b - t_f\ ,\ V_u = b_w t_w f_y/\sqrt{3}) \qquad (21.43)_1$$

see Fig. 21.24(b). If we use the TRESCA instead of the VON MISES yield condition, the factor of $\sqrt{3}$ in the expression for V_u has to be replaced by 2. Point B in Fig. 21.24(b) generally lies on ellipse AC, and the decrease in the bending resistance is relatively small. Regime CD can become critical with very short shear spans and thin webs.

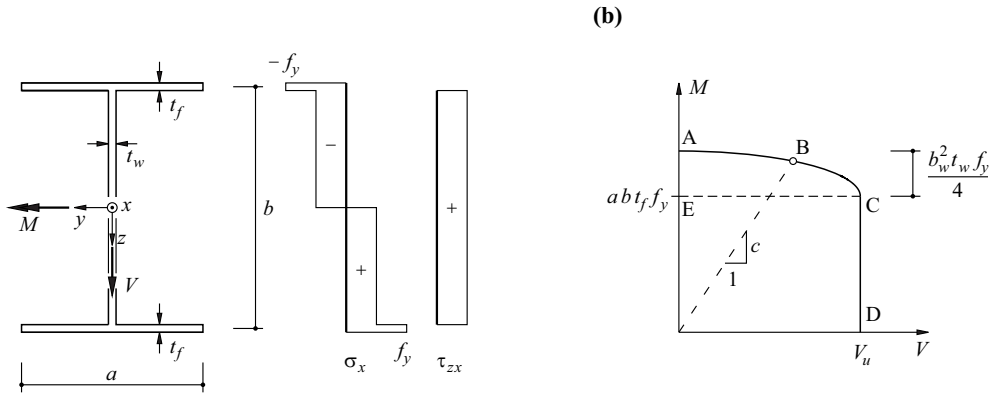

Fig. 21.24 Bending and shear force in I sections: (a) notation and assumed stress distribution, (b) interaction diagram

If a normal force N has to be considered as well as the shear force V, then the root expression in the second term on the right in $(21.43)_1$ has to be replaced by

$$\frac{1-\left(\frac{V}{V_u}\right)^2-\left(\frac{N}{N_{wu}}\right)^2}{\sqrt{1-\left(\frac{V}{V_u}\right)^2}} \qquad (N_{wu}=b_w t_w f_y) \qquad (21.43)_2$$

21.5 Shakedown and limit loads

The shakedown theorem was introduced in section 20.2.1. This theorem permits statements to be made about actions (loads and restraints) that can be accommodated elastically any number of times. The difference between dimensioning using elastic-plastic and rigid-plastic approaches has already been pointed out in example 16.6 (Fig. 16.21): in elastic-plastic dimensioning based on the shakedown theorem, a common restraint state is superposed on the stress resultants determined elastically for all load cases, whereas in rigid-plastic dimensioning based on the static method of limit analysis, a specific restraint state can be used for each load case.

Let $s_{ei,\max}$ and $s_{ei,\min}$ denote the limit values of the elastically compatible stress resultants at point i, and s_{ui} and s_{ui}' the magnitudes of the corresponding positive and negative resistances. The necessary and sufficient conditions for avoiding collapse as a result of *progressive plastification* are then

$$s_{ui} \geq s_{ei,\max} + s_{ri} \quad , \quad s_{ei,\min} + s_{ri} \geq -s_{ui}' \qquad (21.44)$$

where s_{ri} is the restraint at point i, which is superposed on the elastically compatible stress state. In order to avoid collapse as a result of *alternating plasticity*, we require

$$s_{ei,\max} - s_{ei,\min} \leq s_{yi} + s_{yi}' \qquad (21.45)$$

where s_{yi} and s_{yi}' stand for the values of the yield limits of the virgin system at point i with positive and negative stress resultants. Note that the variables $s_{ei,\max}$ and $s_{ei,\min}$ also contain restraint components as well as load components for general loading-restraint cycles.

The relationship between shakedown load and limit load is discussed further in the following and commented on with respect to the practical analysis and dimensioning of structures. A brief outline of a computational method for the elastic-plastic dimensioning of structures for minimum weight is given in section 21.7.3.

Example 21.2 Two-span beam – repeated variable actions

Fig. 21.25(a) shows by way of parallelogram EFGH the intersection of the yield surface obtained in exercise 20.9 with the plane $Q_1 = 5.4M_u/l$. Fig. 21.25(b) shows the bending moments for the two-span beam being examined as a result of four different loadings Q_2 when $Q_1 = 5.4M_u/l$ = const.

In the load range $-1/3 \leq Q_2/Q_1 \leq 1$, the resulting limit load for the system being considered is $Q_1 = 6M_u/l$. Similarly, for the load range $-1/3 \leq Q_1/Q_2 \leq 1$, the limit load is $Q_2 = 6M_u/l$. If Q_1 and Q_2 can vary between 0 and the maximum value Q_s, we get the shakedown load $Q_s = 96M_u/(19l)$, see exercise 20.11.

Applying a monotonically increasing load Q_1 to the initially restraint-free system establishes the onset of yield at point 1 ($M_1 = M_u$) when $Q_1 = 64M_u/(13l)$; we get $M_3 = -6M_u/13$ for the associated moment at intermediate support 3. Increasing the load further to $Q_1 = 5.4M_u/l$ results in moment diagram A in Fig. 21.25(b). Relieving the load completely at this stage would leave a moment $M_3 = P = -0.7M_u + (5.4M_u/l)\cdot(3l/32) = -31M_u/160$ at the intermediate support, corresponding to point A in Fig. 21.25(a).

Increasing Q_2 starting from 0 while Q_1 at $5.4M_u/l$ = const causes the point in Fig. 21.25(a) to trace the path AB until the moment $M_3 = -0.7M_u + (3.2M_u/l)\cdot(3l/32) = -M_u$ is reached at $Q_2 = 3.2M_u/l$. At the same time, the moment at point 1 is reduced to $M_1 = M_u - (3.2M_u/l)\cdot(3l/64) = 0.85M_u$. Increasing Q_2 further, up to $5.4M_u/l$, and subsequently relieving completely as far as $Q_2 = 0$ results in the path BCDA shown in Fig. 21.25(a). Segment BC corresponds to a negative plastic rotation at intermediate support 3, and segment DA corresponds to a positive plastic rotation at point 1. If the loading cycle is repeated several times, the plastic rotations at points 1 and 3 increase successively and there is a risk of exhausting the plastic deformation capacity.

According to the work theorem (14.4), the plastic rotation at point 3 amounts to $0.55M_u\cdot 1\cdot(1/4)\cdot l/(EI) = 11M_u l/(80EI)$ per cycle. We get a corresponding value of $11M_u l/(40EI)$ at point 1. The curvature $M_u/(EI)$ at the onset of yield is inversely proportional to the depth of the cross-section h. For a curvature of, for example, $1/(250h)$, where $l = 20h$, the plastic rotation increment is 22 mrad per cycle at point 1 and 11 mrad at point 3.

Restraint cycles can increase, or rather accelerate, progressive plastification. For example, a temperature difference ΔT over the depth of the cross-section h, constant over the full length of the beam, causes a restraint state characterised by $P = -3EI\Delta T\alpha_T/(2h)$. Putting $\Delta T = \pm 20°C$, $\alpha_T = 10^{-5}/°C$ and $EI = 250M_u h$ results in $P = \mp 0.075M_u$, for instance. We get the path AIJBCKLDA in Fig.

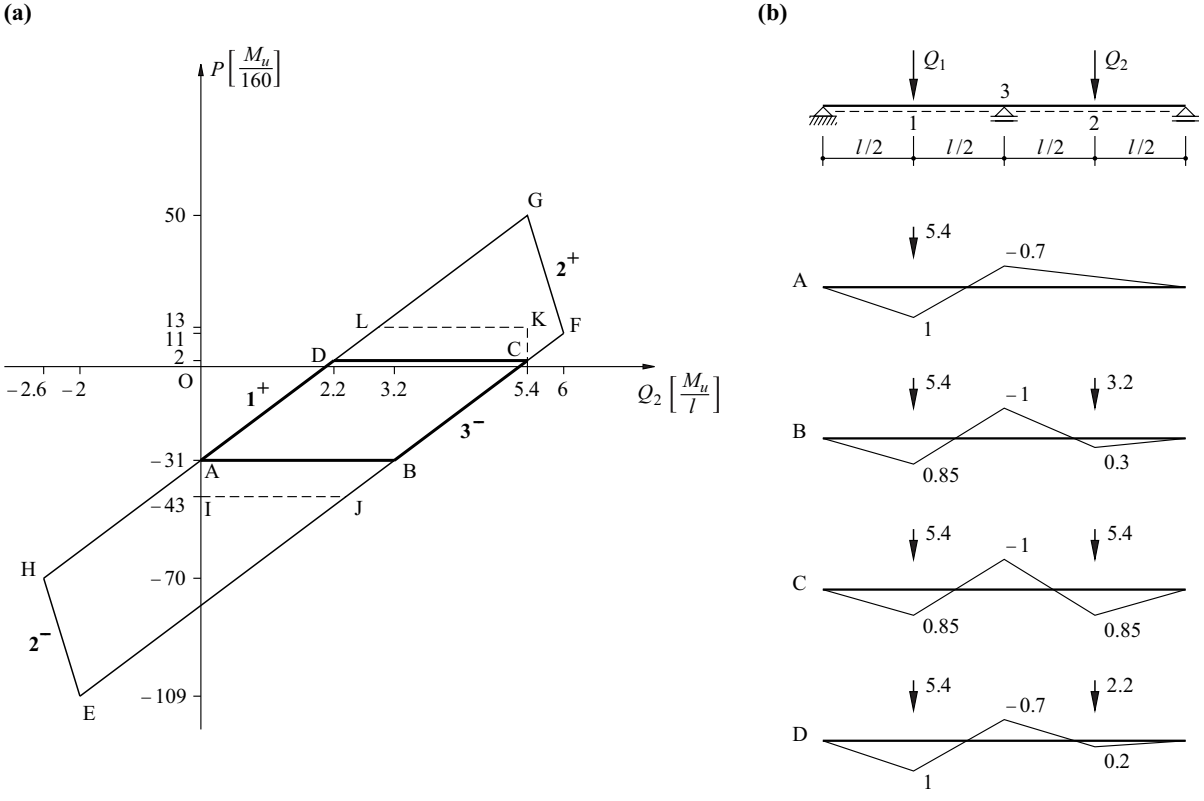

Fig. 21.25 Continuous beam subjected to $Q_1 = 5.4M_u/l$ = const: (a) yield locus, (b) loads $[M_u/l]$ and moments $[M_u]$

21.25(a) when $\Delta T = +20°C$ or $\Delta T = -20°C$ occurs at positions A or C and is kept constant during the subsequent variation in Q_2. The values of the plastic rotation increments at points 3 and 1 therefore increase from 11 to 15 and from 22 to 30 mrad per cycle respectively.
If Q_1 and Q_2 can vary between 0 and the same maximum value Q_s, eq. (21.44), taking into account $\Delta T = \pm 20°C$, provides us with the conditions

$$\frac{13}{64}Q_s l + 0.0375M_u + \frac{\Delta P}{2} = M_u \quad , \quad \frac{6}{32}Q_s l + 0.075M_u - \Delta P = M_u$$

for the moments at points 1 and 3. Consequently, $Q_s = 24M_u/(5l)$, i. e. a shakedown load reduced by 5 % compared with $96M_u/(19l)$. The variable $\Delta P = -M_u/40$ corresponds to the restraint state superposed on the elastic stresses due to load and thermal actions. The shakedown load $Q_s = 4.8M_u/l$ that comes about as a result of taking into account the loading and restraint cycles is equal to 80 % of the limit load $Q_u = 6M_u/l$ in this case.

The plastic deformations of a structure generally remain relatively small during a single loading-restraint cycle. The plastic deformation is restricted by the parts of the system that remain elastic. The incremental growth in plastic deformations during repeated cycles can certainly become substantial, but does lead to advance warning of collapse. In fact, a typical structure that has collapsed due to progressive plastification as a result of repeated variable actions is unknown in practice.

In practical dimensioning assignments, we generally confine ourselves – according to section 4.5 – to considering single load cases characterised by a leading action (e. g. wind forces) and one or more variable accompanying actions (e. g. imposed loads in buildings). Verification of structural safety is then carried out according to (4.5) and (4.6), like with a one-off static overload, with the reduced probability of the simultaneous occurrence of the most unfavourable values of several independent actions being taken into account by way of corresponding reduction factors. This procedure implies that collapse due to progressive plastification is also ruled out.

Knowledge regarding the various actions on structures varies greatly and is sometimes associated with major uncertainties. The scientific basis for assessing the practical significance of shakedown load calculations is therefore weak compared with limit load calculations. The conventional approach to dimensioning structures, based on the static method of limit analysis, does not seem to lead to any problems in normal cases. But for abnormal cases, e. g. large cyclic restraints as a result of thermal actions, the information given here enables additional checks to be carried out.

21.6 Dimensioning for minimum weight

21.6.1 General

Up until now it has been assumed that we know the geometry of and the loading on a system plus the ratios of the resistances of all the bars. Limit analysis was able to determine the ratio of limit load to reference resistance, or at least to define it within limits.

The resistances of all the bars have to be specified with dimensioning according to plastic theory. The customary practical approach is to estimate a possible first distribution of the resistances and then to try to improve this iteratively with respect to certain criteria with the help of appropriate modifications.

Many factors have an influence on the economy of a structure, as discussed in section 3.2. Apart from the qualities and quantities of the materials used, constructional restrictions such as maximum and minimum dimensions, fabrication, transport and erection conditions, etc. all play a key role. In the light of this, it is clear that dimensioning for minimum weight, as explained below, can only represent a reference value for designing structures. It in no way corresponds to "optimum design" – which owing to the complexity of the objective function and the secondary conditions is essentially an illusion – but does provide designers with valuable information regarding the

efficiency that can be achieved plus the consequences of their decisions during the conceptual design of a structure.

21.6.2 Linear objective function

The cross-sectional area A and the plastic section modulus Z of geometrically similar sections are proportional to the second or third power of the depth of the cross-section h. Therefore, with the same specific weight and yield limit, the dead load g of a bar per unit length is proportional to $M_u^{2/3}$, and the following applies for the dead load G of the total design:

$$G \sim \sum_{i=1}^{l} l_i M_{ui}^{2/3} \tag{21.46}$$

where l_i denotes the total length of all sections with resistance M_{ui}.

The linearisation

$$g = c_1 + c_2 M_u \quad , \quad G = c_1 \sum_{i=1}^{l} l_i + c_2 \sum_{i=1}^{l} l_i M_{ui} \tag{21.47}$$

is possible for a certain range of sections. With a given system geometry, the first term on the right in $(21.47)_2$ is constant, and G together with the sum in the second term is a minimum. Generally, therefore, the objective function

$$C = \sum_{i=1}^{l} l_i M_{ui} \quad \rightarrow \quad \text{Min!} \tag{21.48}$$

is assumed, a linear function of the l resistances M_{ui} relevant in the design.

21.6.3 FOULKES mechanisms

Sections with bending resistances of $\pm M_b$ or $\pm M_c$ are to be used for the beam and the two columns of the frame depicted in Fig. 21.26(a), which is statically indeterminate to the second degree. The problem corresponds to that of Fig. 21.8, where $Q_1 = 2Q_2 = 2Q$. But as the bending resistance can now change abruptly at the corner of the frame, two joints must be introduced at each corner (2, 3 and 5, 6). Including the points of load application (1, 4) and fixity (7) means $k = 7$, and when $n = 2$, then the result according to (21.11) is $m = 5$. We can identify the elementary mechanisms as two beam mechanisms, one sway mechanism and two joint mechanisms. Fig. 21.26(b) shows the two beam mechanisms, the sway mechanism and the two combined mechanisms, with the plastic hinges at the frame corners able to form in the columns or the frame beam in each case. The corresponding work equations are:

$$\begin{aligned}
&a \ldots\ 2Q = 8M_b/l && b \ldots\ 2Q = 4M_b/l + 4M_c/l \\
&c \ldots\ Q = 6M_c/l && d \ldots\ Q = 2M_b/l + 4M_c/l \\
&e \ldots\ Q = 4M_b/l + 2M_c/l && f \ldots\ Q = 6M_c/l \\
&g \ldots\ 3Q = 8M_b/l + 2M_c/l && h \ldots\ 3Q = 4M_b/l + 6M_c/l \\
&i \ldots\ Q = M_b/l + 3M_c/l && j \ldots\ Q = 4M_c/l
\end{aligned}$$

These are shown as straight lines in Fig. 21.26(c). The permissible region for M_b, M_c in this FOULKES *diagram* is bounded by the polygonal line ABCDE (which is convex with respect to the origin); Fig. 21.26(d) shows that the plasticity check is satisfied for points B, C and D.

The objective function (21.48) for the frame of Fig. 21.26(a) is $C = lM_b + 2lM_c$. Fig. 21.26(c) shows that, within the permissible region, this function is a minimum for point D ($M_b = 0.375Ql$, $M_c = 0.25Ql$). Taking the stress state for point D shown in Fig. 21.26(d), any non-negative linear combinations of mechanisms h and j according to Fig. 21.26(b) are compatible. A mechanism with two degrees of freedom, such that the straight line of the mechanism coincides with the straight line C = const, is only possible for solution point D, but not for the other two corners B and C in the

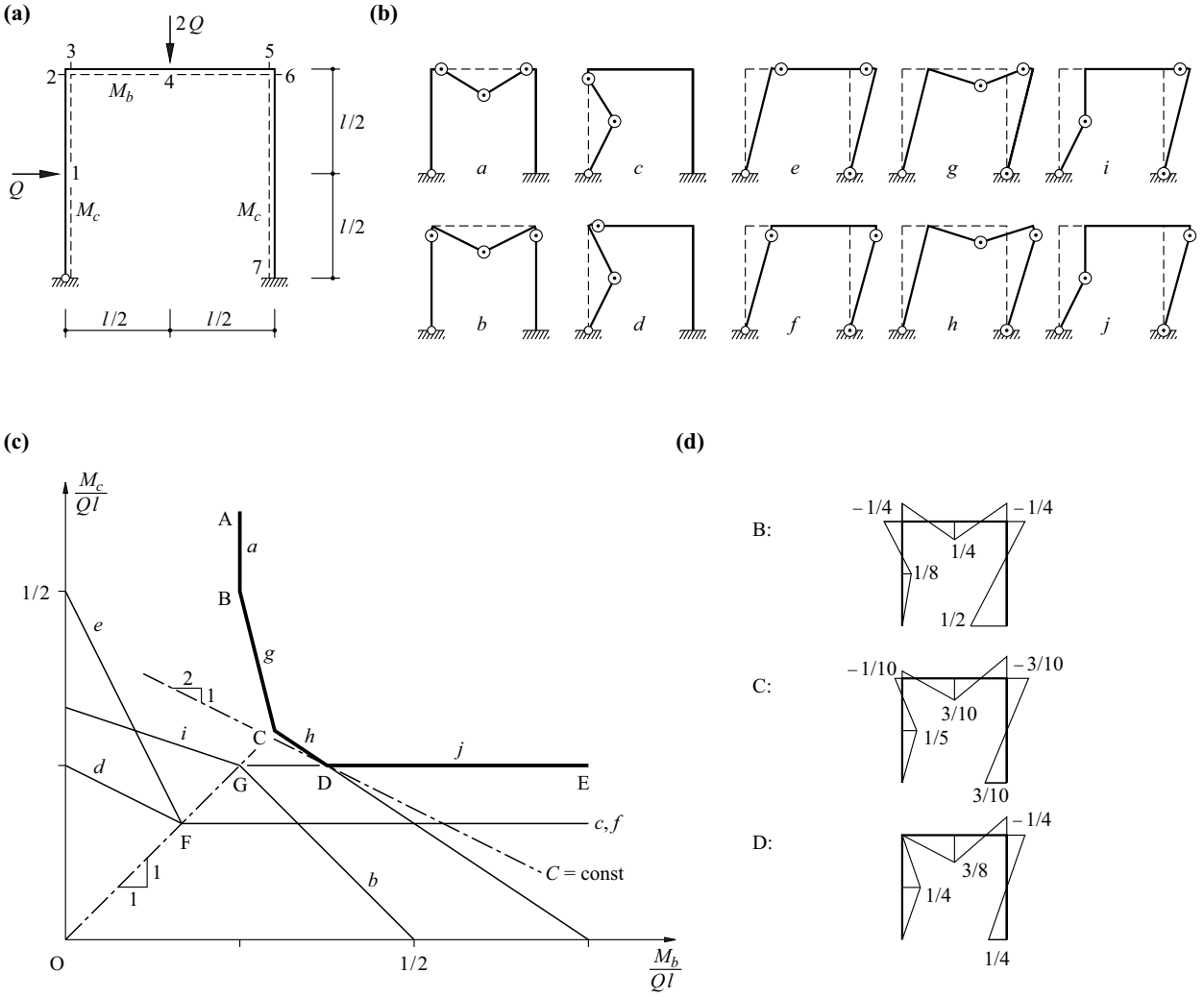

Fig. 21.26 Dimensioning for minimum weight: (a) diagram of static system, (b) mechanisms, (c) FOULKES diagram, (d) moments [Ql]

permissible region. Let $\dot{V}_h$ and $\dot{V}_j$ denote the corresponding generalised displacement increments. The work equation for this mechanism is then

$$3Q\dot{V}_h + Q\dot{V}_j = \frac{M_b}{l} \cdot 4\,\dot{V}_h + \frac{M_c}{l}(6\,\dot{V}_h + 4\,\dot{V}_j)$$

where

$$\frac{4\,\dot{V}_h}{6\,\dot{V}_h + 4\,\dot{V}_j} = \frac{1}{2} = \frac{l_b}{l_c} \qquad (l_b = l,\ l_c = 2l)$$

i. e. $\dot{V}_h = 2\dot{V}_j$. The sums of the magnitudes of the rotation increments occurring in the frame beam and in the columns are

$$\dot{\theta}_b = \frac{4\,\dot{V}_h}{l} \quad , \quad \dot{\theta}_c = \frac{6\,\dot{V}_h + 4\,\dot{V}_j}{l}$$

And we can see that $\dot{\theta}_b/l_b = \dot{\theta}_c/l_c$.

The following generally applies for a FOULKES *mechanism*:

$$\frac{\dot{\theta}_i}{l_i} = \text{const} \qquad (i = 1, 2, \ldots, l) \tag{21.49}$$

i. e. the values of the mean curvature increments in the individual parts of the system are constant. With l bending resistances M_{ui} determining the design, the work equations of the individual mechanisms correspond to hyperplanes in the l-dimensional space, which limit the permissible region (convex with respect to the origin). A hyperplane that touches the permissible region at the solution point corresponds to the objective function (21.48). The mechanism compatible with the stress state at the solution point generally turns out to be a non-negative linear combination of l mechanisms, and the constraints (21.49) apply for the corresponding FOULKES mechanism.

Summing up, dimensioning for minimum weight is achieved when it is possible to specify a FOULKES mechanism and a statically admissible stress state compatible with that mechanism. This is the case for point D in Fig. 21.26(c). Although a FOULKES mechanism exists for point F, there is no statically admissible stress state compatible with this; the dead load of the system must therefore lie below the minimum weight. And although collapse mechanisms and statically admissible stress states compatible with those mechanisms can be specified for all the points on the boundary of the permissible region, e. g. point C, apart from solution point D, there is no FOULKES mechanism present; thus, the dead load of the system cannot lie below the minimum weight. Finally, it should be noted that there are also points outside the permissible region for which it is not possible to specify a FOULKES mechanism, e. g. point G in Fig. 21.26(c).

21.6.4 Commentary

Several load cases normally have to be considered. The permissible region in the FOULKES diagram is then obtained by combining the permissible regions of all load cases. Dimensioning points in the common range of the permissible regions of the individual load cases are permitted.

Generally, secondary conditions restrict the choice of resistances. On the one hand, certain minimum resistances are necessary; these can result from, for example, minimum thicknesses, constructional conditions or stability aspects. On the other hand, maximum resistances will have to be considered as well for aesthetic and constructional reasons. Further, relative restrictions often have to be considered, e. g. it could be that one particular resistance may not be larger than another particular resistance. All such secondary conditions lead to corresponding constraints in the FOULKES diagram. In this situation it can turn out that the minimum resistances called for already correspond to one point within the permissible region of the FOULKES diagram; the solution to the problem of dimensioning for minimum weight is then unimportant. On the other hand, choosing maximum resistances that are unreasonably small can make it impossible to solve this problem. It is not possible to save very much if the prescribed minimum resistances are only marginally smaller than the resistances representing the dimensioning for minimum weight. And vice versa, very uneconomic solutions can result when the prescribed maximum resistances are small compared with the resistances representing the dimensioning for minimum weight.

In larger systems it is worthwhile adjusting the resistances along the bar axes to suit the stress resultants present. This can be done by varying the depth of the beam (haunches) and by varying the plate thicknesses of steel beams or curtailing the reinforcement in reinforced concrete beams. From (21.49) it follows that at the limiting case $l_i \rightarrow 0$, the corresponding FOULKES mechanisms must be characterised by deflection curves that are curved between the points of inflection and exhibit a constant radius. Accordingly, in the case of a beam fixed at both ends, see Fig. 21.27(a), the point of inflection must be at the quarter-points of the span irrespective of the loading; starting with the moment diagram of the associated simply supported beam, the closing line for the statically indeterminate system can be fitted to suit. Fig. 21.27(b) illustrates the similar procedure for a beam fixed at one end and simply supported at the other. The positions

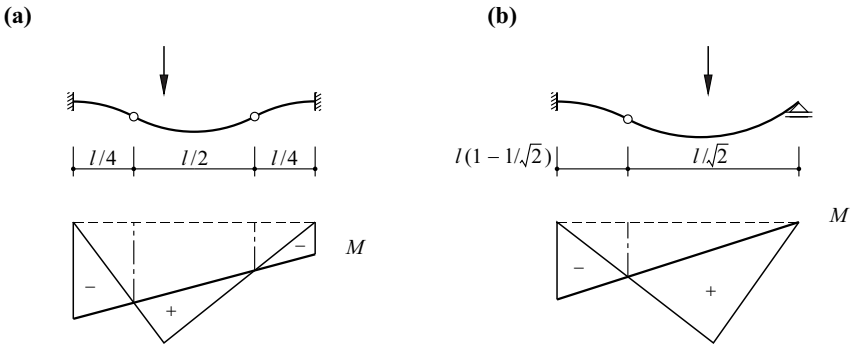

Fig. 21.27 Resistance matched perfectly to the stress resultant and compatible mechanisms

of the points of inflection of the deflection curve for continuous beams and frames are best calculated iteratively.

The assertion that the collapse mechanisms – when the resistance has been perfectly matched to the stress resultant – are characterised by deflection curves in the form of circular arcs with a constant radius for each segment can be verified as follows. The mechanism is described by the deflection increment $\dot{w}(s)$ and the curvature increment $\dot{\chi}(s)$, where either $\dot{\chi} = \dot{\chi}_0$ or $\dot{\chi} = -\dot{\chi}_0$ ($\dot{\chi}_0 = \text{const}$). According to (21.1), with the loads $q(s)$ and the perfectly matched moments $M(s)$ in equilibrium with those loads, then

$$\int q\dot{w}\,\mathrm{d}s = \int M\dot{\chi}\,\mathrm{d}s = \dot{\chi}_0 \int |M|\,\mathrm{d}s = \dot{\chi}_0 C_0 \tag{21.50}$$

Eq. $(21.50)_2$ results because M and $\dot{\chi}$ are compatible according to (21.2), and $(21.50)_3$ draws on (21.48); C_0 denotes the minimum of the objective function C. If we consider an arbitrary statically admissible stress state $M_s(s)$, which is in equilibrium with $q(s)$, then according to (21.1),

$$\int q\dot{w}\,\mathrm{d}s = \int M_s\dot{\chi}\,\mathrm{d}s$$

and the comparison with (21.50) results in

$$C_0 = \int M_s \frac{\dot{\chi}}{\dot{\chi}_0}\,\mathrm{d}s \le \int |M_s|\,\mathrm{d}s = C \tag{21.51}$$

i. e. C_0 is actually the minimum of C. Note that M_s is generally not compatible with $\dot{\chi}$, from which the relation $(21.51)_2$ follows taking into account $\dot{\chi}/\dot{\chi}_0 = \pm 1$.

Section 21.6.3 presumes that a continuous range of sections, or rather cross-section resistances, is available. However, rolled sections, for example, are produced in certain discrete steps. And even reinforced concrete cross-sections are subjected to similar restrictions owing to the discrete diameters of reinforcing bars with constant bar spacings for each area. When applying FOULKES mechanisms, it is practical to choose possible combinations of resistances within the permissible region which come as close as possible to the theoretical minimum. Alternatively, the minimum that can be achieved in practice could be found simply by trial and error.

Choosing a "more realistic" objective function – corresponding to the expression on the right in (21.46), for instance – instead of the linear objective function (21.48) usually results in only a small or indeed no change to the minimum weight of a design.

21.7 Numerical methods

21.7.1 The force method

Let us consider a system with n degrees of static indeterminacy and k joints according to section 21.3.4. The k generalised deformation increments $\dot{v}_i$ correspond to the k generalised stresses $\dot{s}_i$; the former are linked with the $m = k - n$ generalised displacement increments $\dot{V}_j$ via (21.13). And vice versa, the m generalised loads Q_j

are linked to the k generalised stresses s_i via (21.12). Splitting s_i into m statically determinate variables s_{0i} and n redundant variables X_i results in

$$\left\{\begin{matrix}\dot{\boldsymbol{v}}_0\\ \dot{\boldsymbol{v}}_1\end{matrix}\right\} = \begin{bmatrix}\boldsymbol{a}_0\\ \boldsymbol{a}_1\end{bmatrix}\{\dot{\boldsymbol{V}}\} \quad , \quad \{\boldsymbol{Q}\} = \begin{bmatrix}\boldsymbol{a}_0^{\mathrm{T}} & \boldsymbol{a}_1^{\mathrm{T}}\end{bmatrix}\left\{\begin{matrix}\boldsymbol{s}_0\\ \boldsymbol{X}\end{matrix}\right\} \tag{21.52}$$

where $\dot{v}_{0i}$ and $\dot{v}_{1i}$ denote the kinematic variables corresponding to s_{0i} and X_i.

Multiplying $(21.52)_2$ by $(\boldsymbol{a}_0^{\mathrm{T}})^{-1}$ first and considering the identity

$$\left(\boldsymbol{a}_0^{\mathrm{T}}\right)^{-1}\bullet\ \boldsymbol{a}_1^{\mathrm{T}} = \left(\boldsymbol{a}_1 \bullet \boldsymbol{a}_0^{-1}\right)^{\mathrm{T}}$$

leads to

$$\left\{\begin{matrix}\boldsymbol{s}_0\\ \boldsymbol{X}\end{matrix}\right\} = \begin{bmatrix}\left(\boldsymbol{a}_0^{\mathrm{T}}\right)^{-1} & -\left(\boldsymbol{a}_1 \bullet \boldsymbol{a}_0^{-1}\right)^{\mathrm{T}}\\ \mathbf{0} & \mathbf{I}\end{bmatrix}\left\{\begin{matrix}\boldsymbol{Q}\\ \boldsymbol{X}\end{matrix}\right\} \tag{21.53}$$

see (8.8). Eq. $(21.52)_1$ results in $\boldsymbol{a}_0^{-1}\bullet\dot{\boldsymbol{v}}_0 = \dot{\boldsymbol{V}}$ and therefore $\dot{\boldsymbol{v}}_1 = \boldsymbol{a}_1\bullet\boldsymbol{a}_0^{-1}\bullet\dot{\boldsymbol{v}}_0$, i. e.

$$\begin{bmatrix}-\boldsymbol{a}_1\bullet\boldsymbol{a}_0^{-1} & \mathbf{I}\end{bmatrix}\left\{\begin{matrix}\dot{\boldsymbol{v}}_0\\ \dot{\boldsymbol{v}}_1\end{matrix}\right\} = \{\mathbf{0}\} \tag{21.54}$$

see (8.9).

Example 21.3 Plane frame

Let us return to the problem of Fig. 21.8. We shall call $\dot{V}_1$ and $\dot{V}_2$ the displacement increments of the two beam mechanisms at points 1 and 3, and $\dot{V}_3$ the incremental displacement of frame beam 234 in the sway mechanism. Using the notation of Fig. 21.8, the generalised loads corresponding with this are Q_2, Q_1 and $Q_2/2$.

Eq. $(21.52)_1$ is then

$$\left\{\begin{matrix}\dot{\theta}_1\\ \dot{\theta}_2\\ \dot{\theta}_3\\ \dot{\theta}_4\\ \dot{\theta}_5\end{matrix}\right\} = \frac{1}{l}\begin{bmatrix}4 & 0 & 0\\ -2 & -2 & 1\\ 0 & 4 & 0\\ 0 & -2 & -1\\ 0 & 0 & 1\end{bmatrix}\left\{\begin{matrix}\dot{V}_1\\ \dot{V}_2\\ \dot{V}_3\end{matrix}\right\}$$

where the rotation increments $\dot{\theta}_i$ correspond to the moments M_i . Relationship $(21.52)_2$ has already been set up as the basis of the relations (21.15).

If we change over to a statically determinate three-hinged frame as our basic system by introducing hinges at joints 4 and 5, then (21.53) results in

$$\left\{\begin{matrix}M_1\\ M_2\\ M_3\\ M_4\\ M_5\end{matrix}\right\} = \begin{bmatrix}l/4 & 0 & l/2 & 1/2 & -1/2\\ 0 & 0 & l & 1 & -1\\ 0 & l/4 & l/2 & 1 & -1/2\\ 0 & 0 & 0 & 1 & 0\\ 0 & 0 & 0 & 0 & 1\end{bmatrix}\left\{\begin{matrix}Q_2\\ Q_1\\ Q_2/2\\ M_4\\ M_5\end{matrix}\right\}$$

From (21.54) it follows that

$$\begin{bmatrix}1/2 & 1 & 1 & 1 & 0\\ -1/2 & -1 & -1/2 & 0 & 1\end{bmatrix}\left\{\begin{matrix}\dot{\theta}_1\\ \dot{\theta}_2\\ \dot{\theta}_3\\ \dot{\theta}_4\\ \dot{\theta}_5\end{matrix}\right\} = \left\{\begin{matrix}0\\ 0\end{matrix}\right\}$$

The two rows of the matrix describe the moments for the basic system as a result of $M_4 = 1$ or $M_5 = 1$.

21.7.2 Limit load program

According to the lower-bound theorem, the intensity of the loading λ for a proportional loading $\lambda\boldsymbol{Q}/|\boldsymbol{Q}|$ taking into account the equilibrium conditions (21.53) and the yield conditions

$$-M_{ui}' \le M_i \le M_{ui} \qquad (i = 1, 2, \ldots, k) \tag{21.55}$$

must be a maximum. We therefore get the linear program

$$\begin{aligned}\lambda &= \lambda \quad \rightarrow \ \text{Max!}\\ \boldsymbol{x} &= \boldsymbol{M_u} - \boldsymbol{b}_1\bullet\boldsymbol{X} - \lambda\boldsymbol{M}_0\\ \boldsymbol{x}' &= \boldsymbol{M_u}' + \boldsymbol{b}_1\bullet\boldsymbol{X} + \lambda\boldsymbol{M}_0\end{aligned} \tag{21.56}$$

with the non-negative *control variables*

$$x_i = M_{ui} - M_i \quad , \quad x_i' = M_{ui}' + M_i \tag{21.57}$$

plus the $(k \times n)$ matrix

$$\boldsymbol{b}_1 = \begin{bmatrix} -(\boldsymbol{a}_1 \bullet \boldsymbol{a}_0^{-1})^{\mathrm{T}} \\ \mathbf{I} \end{bmatrix} \tag{21.58}$$

and the vector

$$\boldsymbol{M}_0 = \begin{Bmatrix} (\boldsymbol{a}_0^{\mathrm{T}})^{-1} \bullet \boldsymbol{Q}/|\boldsymbol{Q}| \\ \mathbf{0} \end{Bmatrix} \tag{21.59}$$

for the stress variables in the basic system as a result of $\boldsymbol{Q}/|\boldsymbol{Q}|$.

Example 21.4 Plane frame – static program

Putting $Q_1 = 2Q_2$ in example 21.3, then (21.58) and (21.59) result in

$$\boldsymbol{b}_1 = \begin{bmatrix} 1/2 & -1/2 \\ 1 & -1 \\ 1 & -1/2 \\ 1 & 0 \\ 0 & 1 \end{bmatrix} \quad , \quad \boldsymbol{M}_0 = \frac{l}{\sqrt{5}} \begin{Bmatrix} 1/2 \\ 1/2 \\ 3/4 \\ 0 \\ 0 \end{Bmatrix}$$

When $M_{ui} = M_{ui}' = M_u$ (i =1, 2, ... , 5), the result according to (21.56) is the linear program

$$\begin{Bmatrix} \lambda \\ x_1 \\ x_2 \\ x_3 \\ x_4 \\ x_5 \\ x_1' \\ x_2' \\ x_3' \\ x_4' \\ x_5' \end{Bmatrix} = \begin{bmatrix} 0 & 0 & 0 & \sqrt{5}/l \\ 1 & -1/2 & 1/2 & -1/2 \\ 1 & -1 & 1 & -1/2 \\ 1 & -1 & 1/2 & -3/4 \\ 1 & -1 & 0 & 0 \\ 1 & 0 & -1 & 0 \\ 1 & 1/2 & -1/2 & 1/2 \\ 1 & 1 & -1 & 1/2 \\ 1 & 1 & -1/2 & 3/4 \\ 1 & 1 & 0 & 0 \\ 1 & 0 & 1 & 0 \end{bmatrix} \begin{Bmatrix} M_u \\ M_4 \\ M_5 \\ \lambda l/\sqrt{5} \end{Bmatrix} \quad , \quad \lambda \rightarrow \text{Max!}$$

with the solution

$$-M_4 = M_5 = M_u \quad , \quad \lambda = \frac{10\sqrt{5}M_u}{3l}$$

The control variables x_3, x_4' and x_5 disappear, which means that corresponding plastic hinges occur at the associated points, see Fig. 21.8 (regime BC). We get the values $M_u/3$ and $4M_u/3$ for x_1 and x_2, i. e. $M_1 = 2M_u/3$ and $M_2 = -M_u/3$ according to $(21.57)_1$.

In line with the *duality theorem of linear programming*, the coefficient matrix of the dual program is equal to the negative transpose of the matrix of the original program, and the objective function is minimised instead of maximised, but has the same optimum value as that of the original program. We therefore get – first of all purely formally – the dual program with respect to (21.56)

$$\begin{aligned} \lambda = \quad & \boldsymbol{M}_{\boldsymbol{u}}^{\mathrm{T}} \bullet \dot{\boldsymbol{\theta}} + \boldsymbol{M}_{\boldsymbol{u}}'^{\mathrm{T}} \bullet \dot{\boldsymbol{\theta}}' \quad \rightarrow \text{Min!} \\ \mathbf{0} = \quad & \boldsymbol{b}_1^{\mathrm{T}} \bullet \dot{\boldsymbol{\theta}} - \boldsymbol{b}_1^{\mathrm{T}} \bullet \dot{\boldsymbol{\theta}}' \\ 0 = -1 + & \boldsymbol{M}_0^{\mathrm{T}} \bullet \dot{\boldsymbol{\theta}} - \boldsymbol{M}_0^{\mathrm{T}} \bullet \dot{\boldsymbol{\theta}}' \end{aligned} \tag{21.60}$$

where $\dot{\theta}_i$ and $\dot{\theta}_i'$ denote the values of the rotation increments at the positive and negative plastic hinges.

Eq. $(21.60)_3$ follows from (21.1) with $\boldsymbol{Q}_1 = \boldsymbol{Q}/|\boldsymbol{Q}|$, $\boldsymbol{s}_1 = \boldsymbol{M}_0$ and $\dot{V}_2 = 1$, $\dot{\boldsymbol{v}}_2 = \dot{\boldsymbol{\theta}}$ or $\dot{\boldsymbol{\theta}}'$. Eq. $(21.60)_2$ guarantees the compatibility, see (21.54), and $(21.60)_1$ – owing to the normalising contained in $(21.60)_3$ – corresponds to equating the work of the external forces with the dissipation work, i. e. (21.60) implements the upper-bound theorem.

Example 21.5 Plane frame – kinematic program
The kinematic program

$$\begin{Bmatrix} \lambda \\ 0 \\ 0 \\ 0 \end{Bmatrix} = \begin{bmatrix} 0 & M_u & M_u & M_u & M_u & M_u & M_u & M_u & M_u & M_u & M_u \\ 0 & 1/2 & 1 & 1 & 1 & 0 & -1/2 & -1 & -1 & -1 & 0 \\ 0 & -1/2 & -1 & -1/2 & 0 & 1 & 1/2 & 1 & 1/2 & 0 & -1 \\ -\sqrt{5}/l & 1/2 & 1/2 & 3/4 & 0 & 0 & -1/2 & -1/2 & -3/4 & 0 & 0 \end{bmatrix} \begin{Bmatrix} 1 \\ \dot{\theta}_1 \\ \dot{\theta}_2 \\ \dot{\theta}_3 \\ \dot{\theta}_4 \\ \dot{\theta}_5 \\ \dot{\theta}_1' \\ \dot{\theta}_2' \\ \dot{\theta}_3' \\ \dot{\theta}_4' \\ \dot{\theta}_5' \end{Bmatrix}, \quad \lambda \rightarrow \text{Min!}$$

with the solution

$$\dot{\theta}_3 = \dot{\theta}_4' = 2\dot{\theta}_5 = \frac{4\sqrt{5}}{3l} \quad , \quad \lambda = \frac{10\sqrt{5}M_u}{3l}$$

corresponds to the static program discussed in example 21.4. All other rotation increments are equal to zero. The generalised deformations are compatible with the generalised stresses determined in example 21.4 and together with them constitute the complete solution to the problem.

21.7.3 Optimum design

Despite the remarks of section 21.6.1, the term "optimum design" has been selected here because it has become established in the literature.

21.7.3.1 Rigid-plastic optimisation

When dimensioning for a certain load case characterised by the vector $\boldsymbol{Q}$, then $\lambda = |\boldsymbol{Q}|$ is known, and the resistances combined in the vectors $\boldsymbol{M_u}, \boldsymbol{M_u}'$ have to be determined in such a way that the objective function C is a minimum when generalising (21.48):

$$C = \boldsymbol{c}^{\mathrm{T}} \bullet \boldsymbol{M_u} + \boldsymbol{c}'^{\mathrm{T}} \bullet \boldsymbol{M_u}' \quad \rightarrow \quad \text{Min!} \tag{21.61}$$

The relationships $(21.56)_2$ and $(21.56)_3$ continue to be valid and therefore we get the linear program

$$\begin{aligned} C &= \boldsymbol{c}^{\mathrm{T}} \bullet \boldsymbol{M_u} + \boldsymbol{c}'^{\mathrm{T}} \bullet \boldsymbol{M_u}' && \rightarrow \quad \text{Min!} \\ \boldsymbol{x} &= -|\boldsymbol{Q}|\boldsymbol{M}_0 + \mathbf{I} \bullet \boldsymbol{M_u} - \boldsymbol{b}_1 \bullet \boldsymbol{X} \\ \boldsymbol{x}' &= |\boldsymbol{Q}|\boldsymbol{M}_0 + \mathbf{I} \bullet \boldsymbol{M_u}' + \boldsymbol{b}_1 \bullet \boldsymbol{X} \end{aligned} \tag{21.62}$$

and the dual program

$$\begin{aligned} C &= |\boldsymbol{Q}|\boldsymbol{M}_0^{\mathrm{T}} \bullet \dot{\boldsymbol{\theta}} - |\boldsymbol{Q}|\boldsymbol{M}_0^{\mathrm{T}} \bullet \dot{\boldsymbol{\theta}}' && \rightarrow \quad \text{Max!} \\ \boldsymbol{y} &= \boldsymbol{c} - \mathbf{I} \bullet \dot{\boldsymbol{\theta}} \\ \boldsymbol{y}' &= \boldsymbol{c}' - \mathbf{I} \bullet \dot{\boldsymbol{\theta}}' \\ \mathbf{0} &= \boldsymbol{b}_1^{\mathrm{T}} \bullet \dot{\boldsymbol{\theta}} - \boldsymbol{b}_1^{\mathrm{T}} \bullet \dot{\boldsymbol{\theta}}' \end{aligned} \tag{21.63}$$

Eq. $(21.63)_4$, like $(21.60)_2$, guarantees the compatibility. Using the non-negative control variables y_i and y_i', the constraints $(21.63)_2$ and $(21.63)_3$ require that the rotation increment $\dot{\theta}_i$ or $\dot{\theta}_i'$ should not exceed the limit values c_i and c_i'; at the solution point, these constraints – apart from an unimportant factor – correspond to the conditions (21.49) for a FOULKES mechanism. According to (21.1), the objective function C is equal to the work done by the external forces in the mechanism described by $\dot{\boldsymbol{\theta}}, \dot{\boldsymbol{\theta}}'$ because $\boldsymbol{s}_1 = |\boldsymbol{Q}|\boldsymbol{M}_0$ is in equilibrium with $\boldsymbol{Q}_1 = \boldsymbol{Q}$.

The optimum stress state must be determined for each load case if several load cases have to be considered, and combining all these states determines the resistances required for a minimum value of C. The linear program matrix increases in proportion to the square of the number of load cases, and the number of essential computational operations increases roughly by the power of five.

Generally, the dimensioning of a system is defined by $l < 2k$ relevant resistances. The columns in the linear program matrix (21.62) are reduced accordingly and the coefficients added.

Secondary conditions of the type

$$d_i = d_{i0} + \sum_{j=1}^{l} d_{ij}\, M_{uj} \geq 0 \qquad (i = 1, 2, \ldots, t) \tag{21.64}$$

lead to a corresponding enlargement of the linear program matrix.

Example 21.6 Plane frame – minimum weight

Eq. (21.62) results in the linear program

$$\begin{Bmatrix} C \\ x_1 \\ x_2 \\ x_3 \\ x_4 \\ x_5 \\ x_6 \\ x_7 \\ x_1' \\ x_2' \\ x_3' \\ x_4' \\ x_5' \\ x_6' \\ x_7' \end{Bmatrix} = \begin{bmatrix} 0 & 1 & 2 & 0 & 0 \\ -1/2 & 0 & 1 & -1/2 & 1/2 \\ -1/2 & 0 & 1 & -1 & 1 \\ -1/2 & 1 & 0 & -1 & 1 \\ -3/4 & 1 & 0 & -1 & 1/2 \\ 0 & 1 & 0 & -1 & 0 \\ 0 & 0 & 1 & -1 & 0 \\ 0 & 0 & 1 & 0 & -1 \\ 1/2 & 0 & 1 & 1/2 & -1/2 \\ 1/2 & 0 & 1 & 1 & -1 \\ 1/2 & 1 & 0 & 1 & -1 \\ 3/4 & 1 & 0 & 1 & -1/2 \\ 0 & 1 & 0 & 1 & 0 \\ 0 & 0 & 1 & 1 & 0 \\ 0 & 0 & 1 & 0 & 1 \end{bmatrix} \begin{Bmatrix} Ql \\ M_b \\ M_c \\ M_4 \\ M_5 \end{Bmatrix} \quad , \quad C \rightarrow \text{Min!}$$

for the frame (Fig. 21.26) examined in section 21.6.3, with the solution

$$C = \frac{7Ql}{8} \quad , \quad M_b = \frac{3Ql}{8} \quad , \quad M_c = \frac{Ql}{4} \quad , \quad M_4 = -\frac{Ql}{4} \quad , \quad M_5 = \frac{Ql}{4}$$

The control variables x_1, x_4, x_7 and x_6' disappear, which means that the corresponding yield limits are reached at these points. All the other control variables are positive, and bending moment diagram D in Fig. 21.26(d) is confirmed.

21.7.3.2 Elastic-plastic optimisation

If we work with the limit values $M_{i\,\max}$ and $M_{i\,\min}$ for the stress resultants determined elastically from a number of load cases, then we get

$$\begin{aligned} C &= \boldsymbol{c}^{\mathrm{T}} \bullet \boldsymbol{M_u} + \boldsymbol{c'}^{\mathrm{T}} \bullet \boldsymbol{M_u}' \rightarrow \text{Min!} \\ \boldsymbol{x} &= -\boldsymbol{M}_{\max} + \mathbf{I} \bullet \boldsymbol{M_u} - \boldsymbol{b}_1 \bullet \boldsymbol{X} \\ \boldsymbol{x}' &= \boldsymbol{M}_{\min} + \mathbf{I} \bullet \boldsymbol{M_u}' + \boldsymbol{b}_1 \bullet \boldsymbol{X} \end{aligned} \tag{21.65}$$

instead of (21.62). The relationships $(21.65)_2$ and $(21.65)_3$ correspond to (21.44). Compared with rigid-plastic optimisation, there is a considerable reduction in the linear program matrix when several load cases are considered. Secondary conditions can be taken into account in a similar way to rigid-plastic optimisation. Putting $\boldsymbol{X} = \mathbf{0}$ in (21.65) corresponds to a purely elastic, generally non-optimised dimensioning – a procedure that is widespread in practice but mostly applied without taking proper notice.

21.7.3.3 Elastic optimisation

The stress states for each load case can be chosen as required for rigid-plastic optimisation (21.62); they depend only on the n redundant variables X_i. In contrast to this, there is only one elastically compatible solution for each load case; the redundant variables $\boldsymbol{X}$ are not independent variables, but rather are dependent on the stiffness relationships of the entire structure, see (8.10). Mathematically, the result is generally a complex variational problem. Upon discretisation, the k elements of the diagonal flexibility matrix $\boldsymbol{f}$ become independent variables of the problem; however, the fundamental difficulties resulting from the non-linearity of the relationships (8.10) still remain.

21.8 Summary

1. The limit loads of rigid - perfectly plastic systems can be contained by the lower-bound (static) and upper-bound (kinematic) theorems.
2. The upper- and lower-bound theorems are based on the principle of virtual work and the principle of maximum dissipation.
3. A limit load problem is completely solved when it is possible to specify a statically admissible stress state that does not infringe the yield conditions at any point and a compatible kinematically admissible deformation state. The associated loading is equal to the limit load.
4. The static method of limit analysis based on the lower-bound theorem is especially suitable for dimensioning. Contrasting with this, the kinematic method based on the upper-bound theorem is primarily suited to checking existing or conceptual designs.
5. In a system with n degrees of static indeterminacy, the limit load is reached at the latest when $n+1$ plastic hinges have formed. Partial mechanisms with fewer than $n+1$ plastic hinges often govern.
6. With a bending moment diagram linear segment by segment and bending resistances constant for each segment, plastic hinges can occur at points of fixity, points of load application, corners and changes of cross-section. With k such points, we can distinguish between $k-n$ elementary mechanisms (beam, sway and joint mechanisms) in a system with n degrees of static indeterminacy.
7. The consideration of elementary mechanisms and combined mechanisms according to the kinematic method can be supplemented by the plasticity check in order to assess whether a complete solution or merely an upper bound to the limit load has been obtained.
8. It is generally necessary to consider the interaction of the stress resultants (bending moments, torques and normal forces) occurring at the plastic hinge sections. As a rule, this leads to an iterative procedure starting with estimates of the resistances and positions of the plastic hinges which are successively improved.
9. There is no real interaction between the stress resultants in the case of bending and shear. The stress state at the cross-section examined and in its immediate vicinity may need to be analysed as a whole.
10. When employing elastic-plastic dimensioning based on the shakedown theorem, one restraint state is superposed on the stress resultants determined elastically for all load cases. However, in the case of rigid-plastic dimensioning, a specific restraint state is used for each load case.
11. In practice, shakedown load calculations play a subsidiary role compared with limit load calculations. They enable supplementary checks to be carried out in situations with general loading-restraint cycles.
12. Dimensioning for minimum weight supplies valuable information about the potential efficiency and is therefore a helpful tool for the conception and design of structures. As an approximation, the sum of the products of the lengths and the bending resistances of the individual parts of a system can be used as an objective function that is to be minimised. The average curvature increments corresponding to the associated mechanism in all parts of the system have the same value in the optimum solution for a certain load case.
13. The limit load can be calculated statically or kinematically by way of the dual linear programs (21.56) and (21.60).
14. A rigid-plastic optimisation of the weight of the structure leads to the linear programs (21.62) and (21.63).
15. Using an elastic-plastic optimisation of the weight of the structure according to (21.65) corresponding to the shakedown theorem results in a considerable reduction in the linear program matrix compared with the rigid-plastic optimisation for several load cases.

21.9 Exercises

21.1 The frame shown in Fig. 21.28(a) can have different support conditions at A and B. Verify the limit loads given in the table. Draw the corresponding moment diagrams and mechanisms, also the force and funicular polygons for the respective loads and support force variables.

21.2 The frame shown in Fig. 21.28(b) has constant bending resistances of $\pm M_u$. Develop an interaction diagram similar to Fig. 21.8.

21.3 Replace Q_1 in exercise 21.2 by a uniformly distributed load q on frame beam 234 and solve the exercise again.

21.4 Fig. 21.12(a) describes the bending and torsional resistances of the two bars of the system shown in Fig. 21.28(c). Calculate the limit load Q_u.

21.5 How does the limit load for the system of exercise 21.4 change when Q is applied midway between 1 and 2 instead of at 2?

21.6 Using the same assumptions as for exercise 21.4, determine the limit loads q_u for the systems shown in Fig. 16.30(e).

21.7 The grillage shown in Fig. 9.9(h) consists of eight torsionless beams with a constant bending resistance $\pm M_u$. The load is made up of four identical point loads Q applied to the four joints in the middle. Determine the limit load.

21.8 How does the limit load of exercise 21.7 change when the group of loads is applied in one of the four corner areas of the grillage instead of in the middle?

21.9 Shift the group of loads in exercise 21.8 by 2 m in the X or Y direction to one of the four perimeter areas of the grillage and determine the limit load again.

21.10 Discuss the influence of a torsional resistance according to Fig. 21.12(a) for exercise 21.7. What changes when the beams are fixed at the edge as well?

21.11 A compressive force Q is applied to the middle of one leg of the equal angle shown in section in Fig. 21.28(d) (dimensions in mm). The cross-section of the angle initially free from residual stresses remains unchanged and there are no stability problems. Calculate the load Q_y at the onset of yield, the limit load Q_u and the associated stress distributions. Perform the calculation using a yield limit of $f_y = 235\,\mathrm{N/mm^2}$, and treat the legs as single lines ($12\,\mathrm{mm} \ll 200\,\mathrm{mm}$).

(a)

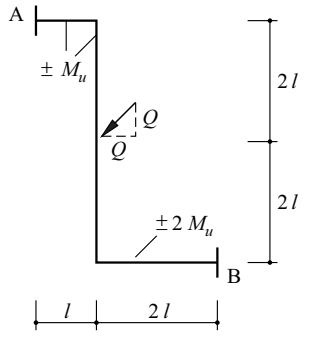

					A / B
18	14	12	12	6	
14	9	9	6		
12	8				
10	6	$\frac{12\,l\,Q_u}{M_u}$			
4					

(b)

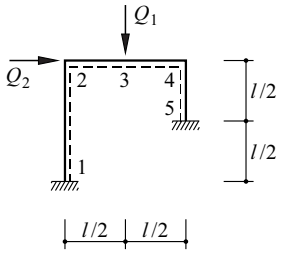

(c)

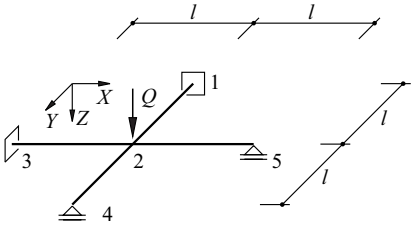

(d)

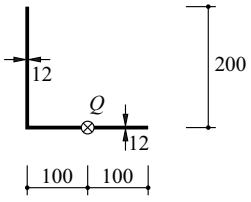

Fig. 21.28 Figures for section 21.9

22 STABILITY

22.1 General

We looked at problems regarding the *overall stability* of structures (limit state of structural safety type 1) in sections 4.4 and 4.6.3. To illustrate this, section 5.1.4 included two examples dealing with overall stability, and section 5.1.5 specified the conditions for braced systems in two or three dimensions. Such rigid body equilibrium problems are not the concern of this chapter.

Instead, this chapter investigates framed structure problems in which the equilibrium conditions have to be formulated for the deformed system according to *second-order theory*, see section 6.1. As described in section 8.3.4, we can use the principle of virtual deformations for this, which in contrast to the principle of virtual forces is also valid for geometric non-linear problems.

Sections 8.5.2 and 8.5.3 included examples of elastic ideal columns and columns subjected to transverse loads to illustrate the methods of RITZ and GALERKIN. The differential equation (18.82) for the equilibrium of deformed arches subjected to vertical loads was set up in section 18.6, and this was followed by a similar differential equation for combined cable-type and bending response in section 18.9. That work will be explored in more detail here.

Elastic and elastic-plastic buckling plus the flexural-torsional and lateral buckling of bars are the topics of this chapter. The buckling of plates and shells will be dealt with in sections 24.7.1 and 26.8.

22.2 Elastic buckling

22.2.1 Column deflection curve

22.2.1.1 Differential equation and boundary conditions

Fig. 22.1 shows a differential column element that bends in the xz plane. The column is initially straight ($w_0 \equiv 0$) and is loaded by line loads (q_x, q_z) in the longitudinal and transverse directions. The stress resultants, besides the moment M about the y axis, are the forces C and V_o acting in the x and z directions. Equilibrium calls for

$$C' = q_x \quad , \quad V_o' = -q_z \quad , \quad M' = V_o + Cw' \tag{22.1}$$

where the superscript dash ($'$) represents differentiation with respect to x. Using $(15.7)_2$ or (18.39), it follows that

$$(EIw'')'' + (Cw')' = q_z \tag{22.2}$$

where C has to be calculated from $(22.1)_1$. If bearing pressures and inertial forces have to be considered, too, then

$$(EIw'')'' + (Cw')' + kw + \rho A\ddot{w} = q_z \tag{22.3}$$

applies, where k = foundation modulus according to (18.45), ρ = density, A = cross-sectional area and $\ddot{w}$ = acceleration in the z direction.

Theory of Structures. First Edition. Peter Marti

Using the notation chosen here, (8.94) gives us the following total potential

$$\Pi = \int_0^l \left(\frac{EIw''^2}{2} - \frac{Cw'^2}{2} - q_z w \right) \mathrm{d}x \tag{22.4}$$

the first variation of which is zero according to the theorem of least total potential:

$$\begin{aligned}
\delta\Pi &= \int_0^l (EIw''\delta w'' - Cw'\delta w' - q_z\delta w)\,\mathrm{d}x \\
&= EIw''\delta w'\Big|_0^l - \int_0^l (EIw'')'\delta w'\,\mathrm{d}x - Cw'\delta w\Big|_0^l + \int_0^l (Cw')'\delta w\,\mathrm{d}x - \int_0^l q_z\delta w\,\mathrm{d}x \\
&= EIw''\delta w'\Big|_0^l - (EIw'')'\delta w\Big|_0^l + \int_0^l (EIw'')''\delta w\,\mathrm{d}x - Cw'\delta w\Big|_0^l + \int_0^l (Cw')'\delta w\,\mathrm{d}x - \int_0^l q_z\delta w\,\mathrm{d}x \\
&= \int_0^l [(EIw'')'' + (Cw')' - q_z]\delta w\,\mathrm{d}x + [EIw''\delta w' - Cw'\delta w - (EIw'')'\delta w]\Big|_0^l = 0
\end{aligned} \tag{22.5}$$

In accordance with the fundamental lemma of calculus of variations, the expression in square brackets in the integrand of the first term on the right in $(22.5)_4$ disappears, which takes us back to (22.2). On the other hand, $EIw''\delta w' = -M\delta w'$ and $Cw'\delta w + (EIw'')'\delta w = -V_o\delta w$, which means that because the second term on the right in $(22.5)_4$ has to disappear, then

$$-M\delta w'\Big|_0^l + V_o\delta w\Big|_0^l = 0 \tag{22.6}$$

The work-related derivation supplies not only differential equation (22.2), but also the boundary conditions (22.6). Fig. 22.2 shows that one of the factors in the two terms on the left in (22.6) disappears in every case.

Abandoning the assumption of inextensibility used hitherto results in the strain $\varepsilon = u' + w'^2/2$ for the bar axis, see Fig. 8.21(b), and therefore $(15.7)_1$ gives us $C = -N = -EA(u' + w'^2/2)$. Together with $(22.1)_1$ and (22.2), the result is the simultaneous differential equations

$$-[EA(u' + w'^2/2)]' = q_x \quad , \quad (EIw'')'' - [EA(u' + w'^2/2)w']' = q_z \tag{22.7}$$

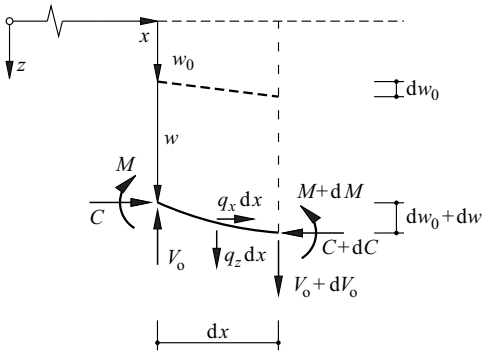

Fig. 22.1 Differential column element

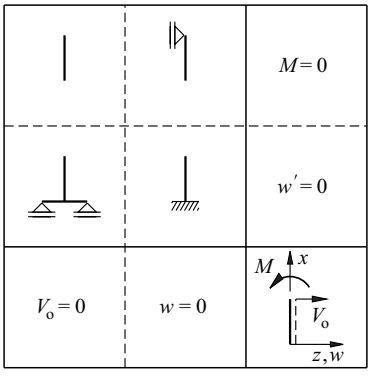

Fig. 22.2 Boundary conditions

22.2.1.2 Methods of solution

Only in certain cases is it possible to obtain an analytical solution to the inhomogeneous fourth-order differential equation with variable coefficients (22.2). Generally, approximation methods such as those of RITZ and GALERKIN must be used, or the differential equation is replaced by a difference equation by assuming that EI and C are constant segment for segment.

Where EI = const and C = const, then the general solution to the homogeneous differential equation is

$$w = c_1 \cos(\kappa x) + c_2 \sin(\kappa x) + c_3 x + c_4 \qquad \left(\kappa^2 = \frac{C}{EI}\right) \tag{22.8}$$

In addition to this we have a particular solution to the inhomogeneous differential equation (22.2) dependent on q_z.

If the normal force in the bar is not a compressive force but rather a tensile force $T = -C$, then (22.2) results in a differential equation similar to (18.56) and (13.74).

We should also note that structural analyses according to second-order theory generally require an iterative procedure. In the first step we can use the forces C in the individual bars of the system which are obtained according to first-order theory. Deformations of the system modify these forces to some extent, a fact that has to be taken into account in the subsequent second-order theory calculations. In most instances, one further calculation step according to second-order theory is sufficient for practical building applications. Normally, the compressive forces C lie well below the associated bifurcation loads and the influence of second-order theory on deformations and stresses is generally in the order of magnitude of 15 %.

Example 22.1 Beam column

For reasons of symmetry it is sufficient to consider just the bottom half ($0 \le x \le l/2$) of the column shown in Fig. 22.3(a), with EI = const, $C = Q_1$ = const and $M = -EIw'' = Cw + Q_2 x/2$. The result is the differential equation

$$w'' + \frac{Cw}{EI} = -\frac{Q_2 x}{2EI}$$

with the general solution

$$w = c_1 \cos(\kappa x) + c_2 \sin(\kappa x) - \frac{Q_2 x}{2C} \qquad \left(\kappa^2 = \frac{C}{EI}\right)$$

The boundary condition $w(0) = 0$ results in $c_1 = 0$, and the symmetry condition $w'(l/2) = 0$ gives us $c_2 = Q_2/[2C\kappa\cos(\kappa l/2)]$, i. e.

$$w = \frac{Q_2}{2C\kappa}\left[\frac{\sin(\kappa x)}{\cos(\kappa l/2)} - \kappa x\right]$$

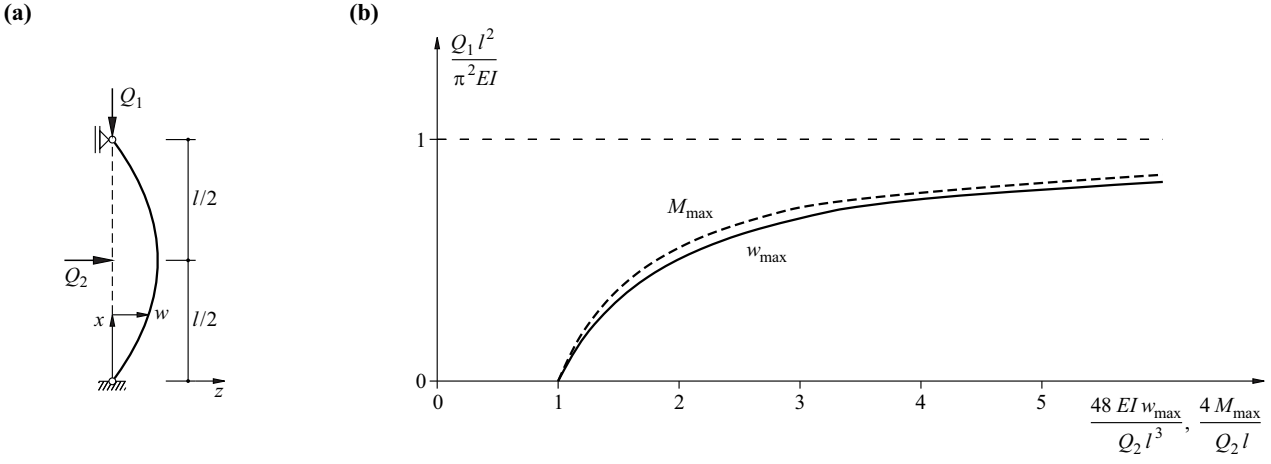

Fig. 22.3 Beam column: (a) diagram of static system, (b) maximum deflections and bending moments as a function of the loading (see Tab. 22.1)

Tab. 22.1 Results of calculations according to Fig. 22.3(b)

Q_1	w_{max}	M_{max}
0	1	1
1/8	1.1410	1.1173
1/4	1.3289	1.2732
3/8	1.5919	1.4910
1/2	1.9863	1.8168
5/8	2.6435	2.3589
3/4	3.9578	3.4413
7/8	7.9001	6.6854
1	$\to \infty$	$\to \infty$
$\frac{\pi^2 EI}{l^2}$	$\frac{Q_2 l^3}{48EI}$	$\frac{Q_2 l}{4}$

The deflection at point $x = l/2$ is

$$w(l/2) = w_{max} = \frac{Q_2 l^3}{48EI} \cdot \frac{3[\tan(\kappa l/2) - \kappa l/2]}{(\kappa l/2)^3} \approx \frac{Q_2 l^3}{48EI} \cdot \left(1 + \frac{\kappa^2 l^2}{10} + \frac{17\kappa^4 l^4}{1680} + ...\right)$$

and the bending moment at this point is

$$M(l/2) = M_{max} = \frac{Q_2 l}{4} \cdot \frac{\tan(\kappa l/2)}{\kappa l/2} \approx \frac{Q_2 l}{4} \cdot \left(1 + \frac{\kappa^2 l^2}{12} + \frac{\kappa^4 l^4}{120} + ...\right)$$

When $\kappa \to \pi/l$, i. e. $Q_1 \to \pi^2 EI/l^2$, both w_{max} and M_{max} approach infinity, see Fig. 22.3(b) and Tab. 22.1.

22.2.1.3 The influence of an initial deformation

If we have to consider an initial deformation w_0 according to Fig. 22.1, then w' in $(22.1)_3$ and (22.2) must be replaced by $(w_0 + w)'$, i. e. (22.2) becomes

$$(EIw'')'' + [C(w_0 + w)']' = q_z \tag{22.9}$$

When EI = const and C = const, the result is then

$$EIw'''' + Cw'' = q_z - Cw_0'' \tag{22.10}$$

i. e. via $-Cw_0''$, the initial deformation has an effect similar to that of the transverse load q_z.

The column with constant bending stiffness EI shown in Fig. 22.4 has the initial shape

$$w_0 = w_{0m} \sin\left(\frac{\pi x}{l}\right)$$

Together with the deflection $w(x)$, the bending moments are

$$M = -EIw'' = Q(w_0 + w)$$

i. e. we get the differential equation

$$EIw'' + Q(w_0 + w) = 0$$

Assuming $w = w_m \sin(\pi x/l)$ leads to $-EIw_m\pi^2/l^2 + Q(w_{0m} + w_m) = 0$. By introducing the EULER *buckling load* (bifurcation load)

$$Q_E = \frac{\pi^2 EI}{l^2} \tag{22.11}$$

and rearranging, we get

$$w_{0m} + w_m = \frac{w_{0m}}{1 - \frac{Q}{Q_E}}$$

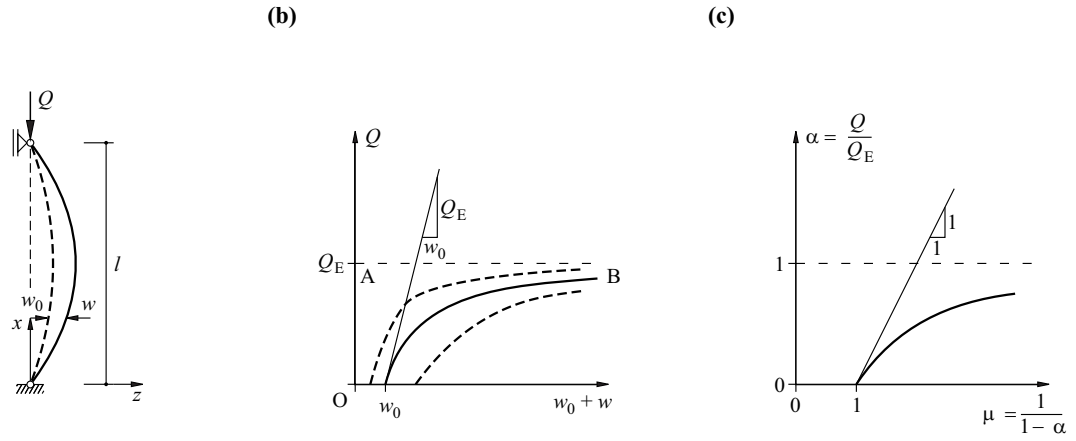

Fig. 22.4 Initial deformation: (a) notation, (b) bending as a function of the loading, (c) amplification factor μ

and therefore, owing to the affinity relationship $w/w_0 = w_m/w_{0m}$, the general solution is

$$\frac{w_0 + w}{w_0} = \frac{1}{1-\alpha} = \mu \qquad \left(\alpha = \frac{Q}{Q_E}\right) \tag{22.12}$$

The deflections w_0 at any point x as a result of Q are multiplied by the *amplification factor* μ.

Fig. 22.4(b) shows the function $w_0 + w$ plotted against Q. The relationship between Q and $w_0 + w$ is a one-to-one correspondence; Q_E is reached asymptotically at $w_m \to \infty$. The bar behaves more and more imperfectly as w_{0m} increases. Line OAB is the result for a perfect bar where $w_0 \equiv 0$. This situation is practically impossible and not desirable either because there would be no advance warning of buckling.

Fig. 22.4(c) shows the normalised diagram according to $(22.12)_2$. Owing to the affinity of the deflection curves, the amplification factor μ can be applied to the deflections and, in particular, the bending moments M, too. It follows from examples 8.15 and 22.1 (Tab. 22.1) that this is approximately the case for non-affine deflection curves as well.

The use of the amplification factor μ presumes that the EULER buckling load Q_E is known. This is obtained from the solution to the bifurcation problem for the ideal system corresponding to the imperfect system without initial deformation and without transverse loading.

22.2.2 Bifurcation problems

When $q_z = 0$, $w_0 = 0$, EI = const and C = const, the possible solutions to (22.2) – apart from the trivial solution $w \equiv 0$ – are those described by (22.8). The boundary conditions of a problem lead to four homogeneous linear equations for coefficients c_1 to c_4. For example, the case of Fig. 22.4 leads to the following set of equations:

$$\begin{Bmatrix} w(0) \\ w''(0) \\ w(l) \\ w''(l) \end{Bmatrix} = \begin{bmatrix} 1 & 0 & 0 & 1 \\ -\kappa^2 & 0 & 0 & 0 \\ \cos(\kappa l) & \sin(\kappa l) & l & 1 \\ -\kappa^2\cos(\kappa l) & -\kappa^2\sin(\kappa l) & 0 & 0 \end{bmatrix} \begin{Bmatrix} c_1 \\ c_2 \\ c_3 \\ c_4 \end{Bmatrix} = \begin{Bmatrix} 0 \\ 0 \\ 0 \\ 0 \end{Bmatrix}$$

From the first and second equations it follows that $c_1 = c_4 = 0$, and from the fourth equation we therefore get the relationship $-c_2\kappa^2\sin(\kappa l) = 0$, which is satisfied when $c_2 = 0$, $\kappa = 0$ or $\kappa l = n\pi$ ($n = 1, 2, ...$); in each of these cases, c_3 must be equal to zero because of the third equation. The case of $c_2 = 0$ corresponds to the trivial solution $w \equiv 0$, and $\kappa = 0$ means that $C = 0$. The *buckling modes* and *buckling loads*

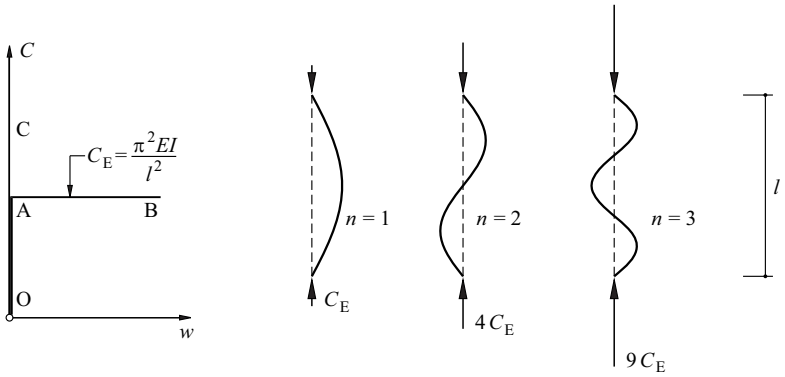

Fig. 22.5 Bifurcation point for equilibrium and buckling modes

$$w = c_2 \sin\left(\frac{n\pi x}{l}\right) \quad , \quad C = n^2 \frac{\pi^2 EI}{l^2} \tag{22.13}$$

correspond to the case of $\kappa l = n\pi$, see Fig. 22.5.

Subjected to a monotonically increasing compressive force C, the point in Fig. 22.5 moves along line OA. The "equilibrium bifurcates" at A. On the one hand, the point can continue along line AB, which means that c_2 remains indeterminate and the column buckles at $C = C_E = \pi^2 EI/l^2$ in the shape of a half sine wave. On the other hand, the point can continue along AC, whereupon the column can buckle at a higher buckling mode ($n > 1$). The column would have to be laterally supported at the points of inflection of the higher buckling modes in order for these modes to occur.

The distance l/n in (22.13) between the adjacent points of inflection of a buckling mode is known as the *buckling length*. According to $(22.13)_2$, the buckling load is inversely proportional to the square of the buckling length.

The system is *stable* for points on the C axis in Fig. 22.5 below A. Below $C_E = \pi^2 EI/l^2$, the system is *neutral*, and w remains indeterminate. And when $C > \pi^2 EI/l^2$, the system is *unstable*.

22.2.3 Approximation methods

22.2.3.1 RAYLEIGH quotient

In the case of the bifurcation problem for a bar without transverse load ($q_z = 0$), w remains indeterminate for C = const. The following must be true according to the theorem of least total potential and (22.4):

$$\Pi = \int_0^l \frac{EIw''^2}{2}\,\mathrm{d}x - C\int_0^l \frac{w'^2}{2}\,\mathrm{d}x \quad \rightarrow \quad \text{Min!}$$

A permissible function w satisfying the essential (kinematic) boundary conditions of a problem must remain permissible when it is multiplied by a constant, and so it is equally valid to demand that the RAYLEIGH *quotient*

$$R(w) = \frac{\int_0^l EIw''^2\,\mathrm{d}x}{\int_0^l w'^2\,\mathrm{d}x} \tag{22.14}$$

is a minimum. The minimum value of R corresponds to the buckling load C_E.

Example 22.2 Cantilever column

If we assume the following for the ideal column examined in example 8.14:

$w = 6\xi^2 - 4\xi^3 + \xi^4 \qquad (\xi = x/l)$

corresponding to the deflection curve (A7.45) for a cantilever rigid in shear where q_z = const, then (22.14) results in

$$R = \frac{EI}{l^2} \cdot \frac{\int_0^1 [12(1-\xi)^2]^2 d\xi}{\int_0^1 [4\xi(3 - 3\xi + \xi^2)]^2 d\xi} = 2.8\frac{EI}{l^2}$$

Compared with the exact value $C_E = \pi^2 EI/(2l)^2 = 2.4674\,EI/l^2$, this result is relatively poor. But this can be explained by the different bending moment diagrams for the buckling problem and the beam column shown in Fig. 8.22(c).

Assuming

$w = 20\xi^2 - 10\xi^3 + \xi^5$

corresponding to a line load q_z proportional to ξ, we get

$$R = \frac{EI}{l^2} \cdot \frac{\int_0^1 [20(2 - 3\xi + \xi^3)]^2 d\xi}{\int_0^1 [5\xi(8 - 6\xi + \xi^3)]^2 d\xi} = 2.6954\frac{EI}{l^2}$$

i. e. a better value, but one that is still 9.2 % higher than the exact value.

By assuming $w = \xi^2 + c\xi^3$, we get the RAYLEIGH quotient

$$R = \frac{EI}{l^2} \cdot \frac{60(1 + 3c + 3c^2)}{20 + 45c + 27c^2}$$

depending on the parameter c, which has the minimum value $2.4860\,EI/l^2$ when $c = -0.3018$. This is confirmed by the calculation carried out according to the RITZ method in example 8.14 with $n = 3$.

22.2.3.2 RITZ method

The RITZ method explained in sections 8.5.2 and A7.9 is illustrated here with a further example.

Example 22.3 Ideal column

In order to calculate the bifurcation load for the case shown in Fig. 22.4(a), we shall follow (8.92) and assume

$w = c_1\xi(1 - \xi) + c_2\xi^2(1 - \xi)^2 \qquad (\xi = x/l)$

Putting $\kappa = Ql^2/(EI)$, we get

$$\begin{bmatrix} 4 - \frac{\kappa}{3} & -\frac{\kappa}{15} \\ -\frac{\kappa}{15} & \frac{4}{5} - \frac{2\kappa}{105} \end{bmatrix} \begin{Bmatrix} c_1 \\ c_2 \end{Bmatrix} = \begin{Bmatrix} 0 \\ 0 \end{Bmatrix}$$

similar to example 8.14. The characteristic polynomial $\kappa^2 - 180\kappa + 1680 = 0$ leads to the eigenvalues

$\kappa_1 = 9.8751 \quad , \quad \kappa_2 = 170.1249$

and κ_1 lies only 0.056 % above the exact value π^2.

22.2.3.3 GALERKIN method

The GALERKIN method explained in section 8.5.3 is illustrated here with a further example.

Deflection curves according to first-order theory, with EI = const and certain loadings (e. g. constant or linearly varying line loads, or point loads) plus buckling mode shapes and vibration mode shapes with EI = const are particularly suitable as approximating functions for the GALERKIN method.

Example 22.4 Beam column

We assume the following for example 8.16:

$w = c(\xi - 2\xi^3 + \xi^4) \qquad (\xi = x/l)$

which corresponds to the deflection curve of a simply supported beam subjected to q_z = const. This assumption satisfies all boundary conditions, i. e. the kinematic (essential) and the static (natural): $w(0) = w(l) = 0$ and $w''(0) = w''(l) = 0$. We therefore have the conditions for applying the ordinary GALERKIN method. Eq. (8.97) results in

$$\int_0^1 \left[EI\frac{24c}{l^4} - Q\frac{c}{l^2}\cdot 12\xi(1-\xi) - q_z \right] c(\xi - 2\xi^3 + \xi^4) l \, \mathrm{d}\xi = 0$$

from which it follows that

$$c = \frac{7q_z l^4}{168EI - 17Ql^2}$$

For the pure transverse bending problem ($Q = 0$), we get the exact solution with the deflection $5q_z l^4/(384EI)$ at $x = l/2$. For the bifurcation problem ($q_z = 0$), we get the approximation $168EI/(17l^2) = 9.8824EI/l^2$, which lies 0.13 % above the exact buckling load $\pi^2 EI/l^2$.

22.2.3.4 Successive approximation of the column deflection curve

The deformations w_1 according to first-order theory in conjunction with the compressive forces C result in bending moments Cw_1 and hence additional curvatures $Cw_1/(EI)$, which correspond to additional deformations w_{21}. The latter for their part cause further curvatures $Cw_{21}/(EI)$, and corresponding further deformations w_{22}, and so on. Such a situation generally results in a very rapidly decreasing series w_{2i}, the sum of which is equal to the deformations w_2 according to second-order theory. By taking into account initial deformations w_0, we get the total deformation

$$w = w_0 + w_1 + w_2 \tag{22.15}$$

In the case of bifurcation problems, we can start by estimating the deflection curve w_{21} and arrive at w_{22} etc. by using

$$w_{2i+1}'' = -\frac{Cw_{2i}}{EI} \tag{22.16}$$

Integrating twice to get to w_{2i+1} is best carried out according to MOHR's analogy (section 15.3.2). Putting w_{2i+1} equal to w_{2i} at any point x results in an approximate value for the buckling load C_E, which can be greater or less than the actual C_E value. In contrast to this, estimates based on the RAYLEIGH, RITZ and GALERKIN methods do not lead to values less than C_E.

The approximation method named after ENGESSER and VIANELLO will be described below with the help of a number of examples of bifurcation and second-order problems.

Example 22.5 Ideal column

Let us consider the column shown in Fig. 22.4(a), with $w_0 \equiv 0$, EI = const and $C = Q$ = const, and assume that $w_{21} = 4f\xi(1 - \xi)$, where $\xi = x/l$ and f = deflection at point $x = l/2$. Considering the boundary conditions, then (22.16), with $i = 1$, results in

$$w_{22} = \frac{Ql^2 f(\xi - 2\xi^3 + \xi^4)}{3EI}$$

The quotient

$$\frac{w_{21}}{w_{22}} = \frac{12EI(1-\xi)}{Ql^2(1 - 2\xi^2 + \xi^3)}$$

is a maximum for $\xi = 0$ and a minimum for $\xi = 1/2$, i. e. $12EI/(Ql^2)$ and $9.6EI/(Ql^2)$; taking the mean of all ξ values results in a figure of $10EI/(Ql^2)$. Putting $w_{21} = w_{22}$ results in corresponding approximate values of 12, 9.6 and 10 for $Q_E l^2/(EI) = \pi^2 \approx 9.87$.

Applying (22.16) to w_{22} ($i = 2$) results in

$$w_{23} = \frac{Q^2 l^4 f(3\xi - 5\xi^3 + 3\xi^5 - \xi^6)}{90(EI)^2}$$

and equating w_{22} and w_{23} at points $\xi = 0$ and $\xi = 1/2$ results in approximate values of 10 and $600/61 = 9.836$ for $Q_E l^2/(EI)$; taking the mean of all ξ values results in the excellent approximate value 9.882.

As we can see, the method of ENGESSER and VIANELLO can be employed to estimate the buckling load with any degree of accuracy. Just the first step alone provides a usable approximation in most cases.

When we use the value $Q = 9.6EI/l^2$ in the expression for w_{22}, then

$$w_{22} = f(3.2\xi - 6.4\xi^3 + 3.2\xi^4)$$

And therefore it follows that

$$w_{23} = \frac{8Ql^2 f(3\xi - 5\xi^3 + 3\xi^5 - \xi^6)}{75EI}$$

or when using the value $Q = 600EI/(61l^2)$, then

$$w_{23} = f(3.1475\xi - 5.2459\xi^3 + 3.1475\xi^5 - 1.0492\xi^6)$$

This function is already a very good approximation of the exact buckled shape

$$w_{23} = f\sin(\pi\xi) = f(3.1416\xi - 5.1677\xi^3 + 2.5502\xi^5 - ...)$$

Example 22.6 Ideal column with one degree of static indeterminacy

Fig. 22.6 shows an estimate of the buckled shape w_{21} on the left and the bending moment diagram $\overline{M}$ on the right; these moments are the result of a virtual unit load applied at joint 5 of the statically indeterminate system. Applying SIMPSON's rule (14.6) and the reduction theorem (section 14.3) results in a deflection of $144.6Ql^2/(2916EI)$ according to the calculation carried out in Tab. 22.2. Equating this expression with the deflection of 1 assumed at joint 5 results in the approximation $Q_E \approx 20.17EI/l^2$.

In order to check the quality of the approximation, in accordance with (22.8) and using $\overline{x} = l - x$ we shall assume $w = c_2\sin(\kappa\overline{x}) + c_3\overline{x}$, which satisfies the boundary conditions $w = 0$ and $w'' = 0$ at joint 7. Taking the boundary conditions $w = 0$ and $w' = 0$ at joint 1 results in the condition $\kappa l = \tan(\kappa l)$, i. e. $\kappa l = 4.4934$ and therefore $Q_E = \kappa^2 EI \approx 20.19EI/l^2$.

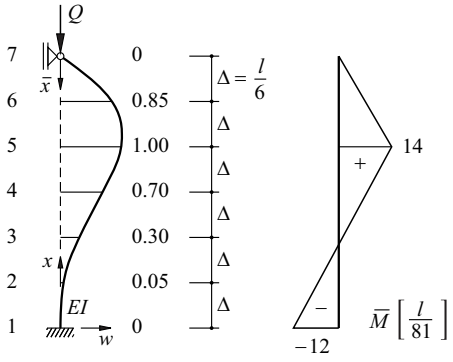

Fig. 22.6 Estimated buckled shape and virtual force state

Tab. 22.2 Calculations for Fig. 22.6

Joint	$\frac{Qw_{21}}{EI}$	$\overline{M}$	Factor	Product	Total
7	0	0	1	0	
6	0.85	14	4	47.6	
5	1.00	28	2	56	
4	0.70	15	4	42	144.6
3	0.30	2	2	1.2	
2	0.05	– 11	4	– 2.2	
1	0	– 24	1	0	
	$\frac{Q}{EI}$	$\frac{l}{162}$	$\frac{l}{18}$	$\frac{Ql^2}{2916EI}$	$\frac{Ql^2}{2916EI}$

Example 22.7 Column with abrupt change in stiffness

The column shown in Fig. 22.7 has an abrupt change of stiffness at the point at which load Q is applied. The bending moments are

$$M = Qw - \frac{Qw_Q x}{l} \qquad (0 \le x \le 0.6l) \quad , \quad M = Qw_Q\left(1 - \frac{x}{l}\right) \qquad (0.6l \le x \le l)$$

Tab. 22.3 contains corresponding calculations for the successive approximation of the buckled shape. We select the parabola $w_{21} = 4x(l - x)/l^2$ as our starting function and use the parabolic rule (14.9), (14.10) with $\Delta = l/10$.

Comparing w_{22} and w_{21} at point $x = l/2$ results in $Q_E \approx 1200EI/(37.7640l^2) = 31.78EI/l^2$, and comparing w_{23} and w_{22} results in $Q_E \approx 1200EI/(37.4411l^2) = 32.05EI/l^2$.

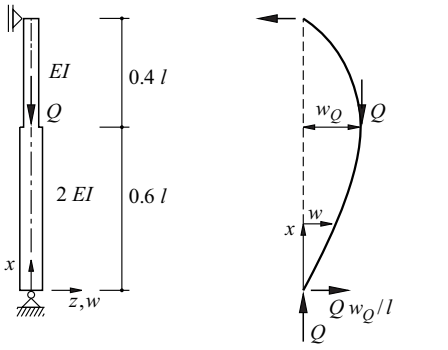

Fig. 22.7 Column with abrupt change in stiffness at point of load application

Tab. 22.3 Calculations for Fig. 22.7(b)

x	w_{21}	M	K_{i1}	V_{i1}	M_{i1}	w_{22}	M	K_{i2}	V_{i2}	M_{i2}	w_{23}
1.0	0	0	0.192	– 12.1152	0	0	0	0.1916	– 12.0416	0	0
0.9	0.36	0,096	1.152	– 11.9232	11.9232	0.3157	0.0958	1.1495	– 11.8500	11.8498	0.3165
0.8	0.64	0.192	2.304	– 10.7712	22.6944	0.6010	0.1916	2.2992	– 10.7005	22.5503	0.6023
0.7	0.84	0.288	3.456	– 8.4672	31.1616	0.8252	0.2874	3.4488	– 8.4013	30.9516	0.8267
0.6	0.96	0.384	2.112	– 5.0112	36.1728	0.9579	0.3832	2.1076	– 4.9525	35.9041	0.9589
			1.308					1.3079			
0.5	1.00	0.520	3.080	– 1.5912	37.7640	1.0	0.5211	3.0858	– 1.5370	37.4411	1.0
0.4	0.96	0.576	3.416	1.4888	36.2752	0.9606	0.5774	3.4192	1.5488	35.8923	0.9586
0.3	0.84	0.552	3.272	4.9048	31.3704	0.8307	0.5433	3.2165	4.9680	30.9243	0.8259
0.2	0.64	0,448	2.648	8.1768	23.1936	0.6142	0.4226	2.5005	8.1845	22.7398	0.6073
0.1	0.36	0.264	1.544	10.8248	12.3688	0.3275	0.2317	1.3698	10.6850	12.0548	0.3220
0	0	0	0,284	12.3688	0	0	0	0.2419	12.0548	0	0
l	-	Q	$\frac{Q\Delta}{12EI}$	$\frac{Q\Delta}{12EI}$	$\frac{Q\Delta^2}{12EI}$	-	Q	$\frac{Q\Delta}{12EI}$	$\frac{Q\Delta}{12EI}$	$\frac{Q\Delta^2}{12EI}$	-

Example 22.8 Load applied to top of cantilever column

The vertical cantilever shown in Fig. 22.8, with $l = 4$ m and $EI = 60\,\mathrm{MNm}^2 = \text{const}$, is loaded at the top by $Q_1 = 700$ kN and $Q_2 = 120$ kN. According to first-order theory, Q_2 causes a deflection f_1 of $Q_2 l^3/(3EI) = 42.67$ mm at the top of the column. If the deflection curve is approximated by a parabola, Q_1 causes an additional deflection of

$$f_{21} = \frac{5Q_1 f_1 l^2}{12EI} = 3.32\,\mathrm{mm}$$

and

$$f_{22} = \frac{5Q_1 f_{21} l^2}{12EI} = 0.26\,\mathrm{mm}$$

and

$$f_{23} = \frac{5Q_1 f_{22} l^2}{12EI} = 0.02\,\mathrm{mm}$$

In total, according to (22.15), we get a deflection at the top of 46.27 mm and a fixed-end moment at the base of the column amounting to $120 \cdot 4 + 700 \cdot 0.04\,627 = 512.4$ kNm.

With a buckling length of $2l = 8$ m, the buckling load is $Q_E = \pi^2 \cdot 60/8^2 = 9.253$ MN. According to $(22.12)_2$, putting $\alpha = 0.7/9.253 = 0.0757$ results in the amplification factor $\mu = 1.0818$ and hence a deflection at the top of $42.67 \cdot 1.0818 = 46.26$ mm, for instance, plus a fixed-end moment at the base of the column amounting to about $480 \cdot 1.0818 = 519.3$ kNm.

The quality of the two approximate solutions (according to ENGESSER-VIANELLO on the one hand and by applying the amplification factor on the other) can be checked with the help of the exact

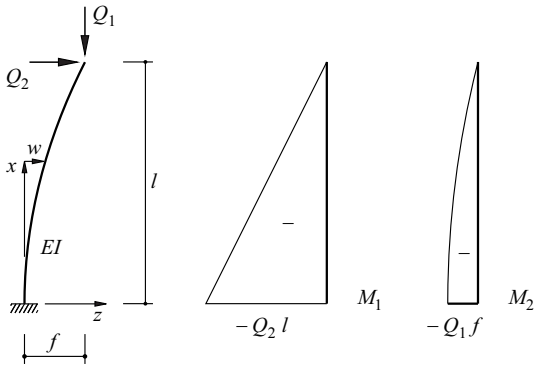

Fig. 22.8 Vertical cantilever loaded at the top

solution to differential equation (22.2) worked out in example 22.1. In fact, the vertical cantilever considered here corresponds to one half of the column shown in Fig. 22.3(a), where $l/2$ has to be replaced by l and Q_2 by $2Q_2$. Therefore, referring to Fig. 22.8, we get

$$w_{\max} = w(l) = \frac{Q_2}{Q_1}\left[\frac{\tan(\kappa l)}{\kappa} - l\right] \quad , \quad M_{\max} = |M(0)| = Q_2\,\frac{\tan(\kappa l)}{\kappa} \qquad \left(\kappa^2 = \frac{Q_1}{EI}\right)$$

i. e.

$$w_{\max} = \frac{120}{700}\cdot\left[\frac{\tan\left(4\cdot\sqrt{\frac{0.7}{60}}\right)}{\sqrt{\frac{0.7}{60}}} - 4\right] = 46.11\,\text{mm} \quad , \quad M_{\max} = 120\cdot\frac{\tan\left(4\cdot\sqrt{\frac{0.7}{60}}\right)}{\sqrt{\frac{0.7}{60}}} = 512.3\,\text{kNm}$$

Example 22.9 Statically determinate frame

According to first-order theory, we get the forces and moments given in Fig. 22.9(b) for the statically determinate frame of Fig. 22.9(a), and according to the work theorem, using $\overline{M}$ according to Fig. 22.9(c) results in the following frame beam displacement:

$$f_1 = \frac{1000\cdot 10\cdot 10}{3\cdot 200} + \frac{[1000(2\cdot 10+5)+6500(2\cdot 5+10)]\cdot 10}{6\cdot 3000} + \frac{6500\cdot 5\cdot 10}{3\cdot 3000} = 325\,\text{mm}$$

The vertical component of the pin-ended strut force is therefore increased to

$(100\cdot 10 + 1200\cdot 10.325)/20 = 669.5\,\text{kN}$

The bending moment in the middle of the frame beam is therefore now 6695 kNm and that at the corner of the frame is 1390 kNm.

If we continue to work with the approximation of bending moments linear over each segment, then the additional second-order moments cause a further displacement of the frame beam amounting to

$$f_{21} = \frac{390\cdot 10\cdot 10}{3\cdot 200} + \frac{390\cdot 10\cdot 20}{3\cdot 3000} = 73.67\,\text{mm}$$

and, accordingly, the bending moment at the corner of the frame is increased by $1200\cdot 0.07\,367 = 88.4$ kNm. Further iteration leads to a power series that adds up to

$$f_2 = f_{21} + f_{22} + f_{23} + \ldots = \frac{f_{21}}{1 - \frac{88.4}{390}} = 95.26\,\text{mm}$$

or rather

$$f = f_1 + f_2 = \frac{f_1}{1 - \frac{88.4}{390}} = 420.26\,\text{mm}$$

and the moment at the corner is

$$1000 + \frac{390}{1 - \frac{88.4}{390}} = 1504.3\,\text{kNm}$$

Fig. 22.9(d) shows the forces and moments resulting from second-order theory.

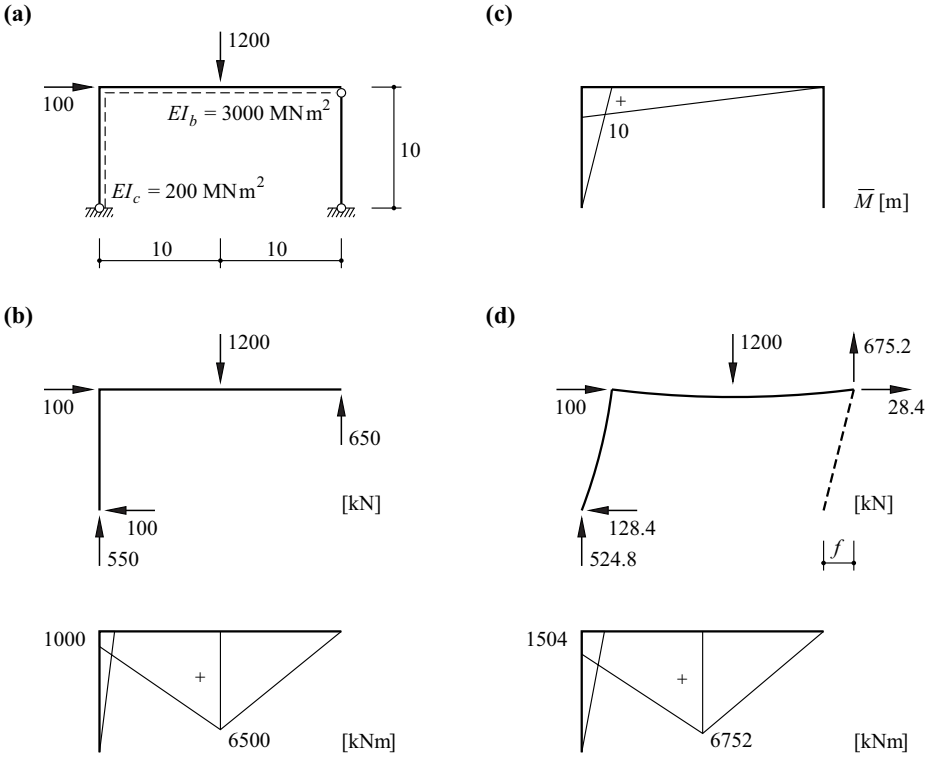

Fig. 22.9 Statically determinate frame (dimensions in m, forces in kN): (a) diagram of static system, (b) forces and moments according to first-order theory, (c) virtual force state, (d) forces and moments according to second-order theory

22.2.4 Further considerations

22.2.4.1 Variable-direction forces

The problem shown in Fig. 22.10(a) can be reduced to example 22.8. The rigid column 12 is loaded via the rigid pin-ended strut 23 that is connected via a hinge. In addition to the vertical force Q_1, the column is also subjected to a horizontal force $Q_2 = Q_1 w_{\max}/h$ applied at the top. Substituting this expression into the relationship for $w_{\max}$ derived in example 22.8 results in the equation

$$\tan(\kappa l) = \kappa l\left(1 + \frac{h}{l}\right) \qquad \left(\kappa^2 = \frac{Q_1}{EI}\right)$$

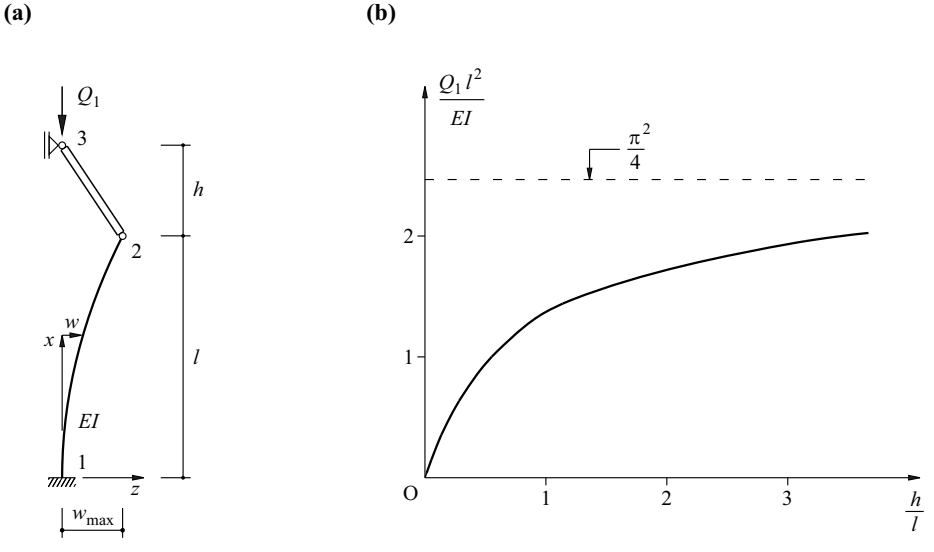

Fig. 22.10 Rigid pin-ended strut on top of vertical cantilever: (a) diagram of static system, (b) bifurcation load plotted against h/l

illustrated in Fig. 22.10(b). For small values of h/l, the bifurcation load is very much lower than the buckling load $Q_E = \pi^2 EI/(2l)^2$ for a column unsupported at its upper end. In practice, this can lead to extremely dangerous situations if, in scaffolding, for example, short elements are added to vertical members as extensions or to suit the geometry.

The problem discussed here belongs to a class of problems with variable-direction but nevertheless guided forces. Such problems are conservative, see section 8.4.2, and the customary methods of elastic stability theory can be applied.

22.2.4.2 The effect of shear deformations

When building with steel and lightweight metals, built-up columns are often used in order to save materials and minimise the dead load as well as the area of the structure exposed to the wind. The effect of shear deformations can be considerable for such structural members. And in the case of built-up columns in timber construction, the flexibility of the connections (e. g. split-ring, shear-plate, toothed-plate connectors, nails, etc.) must be considered as well.

Eq. (15.9) and $(15.10)_2$, with EI = const, GA_v = const and $m_y = 0$, initially result in

$$w'' = -\frac{M}{EI} + \frac{M''}{GA_v}$$

and $(22.1)_2$ and $(22.2)_3$, with $q_z = 0$ and C = const, result in the relationship $M'' = Cw''$. Substituting in the relationship for w'' and differentiating twice results in

$$EI\left(1 - \frac{C}{GA_v}\right)w'''' + Cw'' = 0 \tag{22.17}$$

When we assume $w = c\sin(\pi x/l)$ for a bar with hinged supports at both ends, we can see that, for example, the bifurcation load $C_E = \pi^2 EI/l^2$ of the bar rigid in shear, taking into account the shear deformations, is reduced to $C_E/[1 + C_E/(GA_v)]$.

Although the horizontal members of the built-up column shown in Fig. 22.11(a) halve the buckling length of each vertical member, they contribute nothing to the shear stiffness. The flexibility $1/(GA_v)$ is equal to the shear strain $\gamma = \Delta/h$ as a result of the shear force $V = 1$. This causes a compressive force amounting to $1/\sin\alpha$ in the diagonals with length $d = b/\sin\alpha$, which are shortened by the amount $d/(EA_d\sin\alpha) = \Delta\sin\alpha$. Putting $b/h = \tan\alpha$, this results in

$$\frac{1}{GA_v} = \frac{d^3}{EA_d b^2 h} \tag{22.18}_1$$

In the built-up column with X-bracing, see Fig. 22.11(b), there are two diagonals available for resisting $V = 1$, and therefore

$$\frac{1}{GA_v} = \frac{d^3}{2EA_d b^2 h} \tag{22.18}_2$$

The built-up column of Fig. 22.11(c) has parallel diagonals and $V = 1$ causes additional deformation in the horizontal members amounting to $b/(EA_h)$, i. e.

$$\frac{1}{GA_v} = \frac{d^3}{EA_d b^2 h} + \frac{b}{EA_h h} \tag{22.18}_3$$

and the situation for the K-truss of Fig. 22.11(d) is similar:

$$\frac{1}{GA_v} = \frac{d^3}{2EA_d b^2 h} + \frac{b}{4EA_h h} \tag{22.18}_4$$

Lastly, according to (18.34), the following applies for the built-up column with rigid joints shown in Fig. 22.11(e):

$$\frac{1}{GA_v} = \frac{h^2}{24EI_c} + \frac{bh}{12EI_b} \tag{22.19}$$

It should be noted here that the stiffness of the frame beam in Fig. 18.19 was given as $2EI_b$.

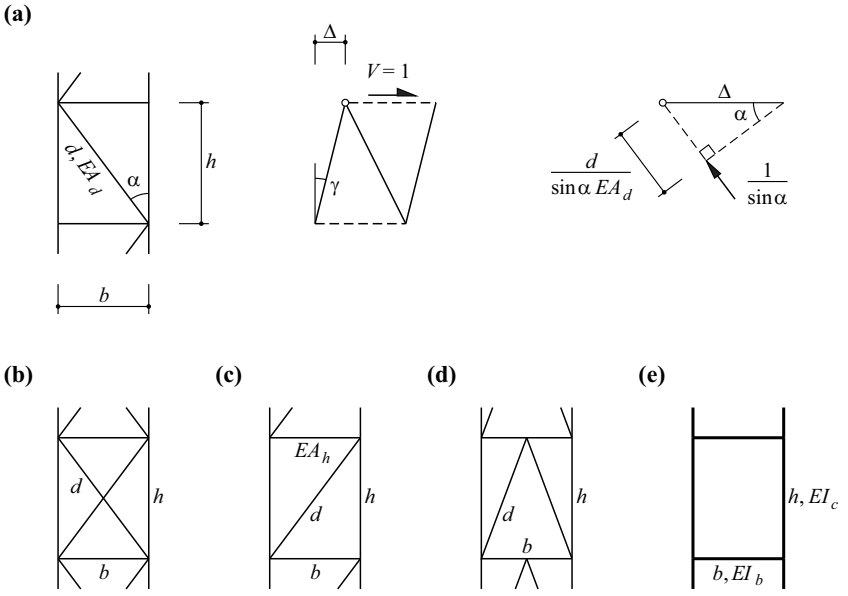

Fig. 22.11 Built-up columns: (a) with alternating diagonals, (b) with X-bracing, (c) with parallel diagonals, (d) with K-truss, (e) with rigid joints

22.2.4.3 Snap-through

Shallow arches and inclined leg frames, like those systems shown in Fig. 22.12(a) and Fig. 22.12(b), can snap through because of the axial compressive strain and the lateral flexibility at the abutments. At the *snap-through load*, the system is suddenly displaced into a new, stable equilibrium position. In contrast to bifurcation problems, the equilibrium position upon reaching the snap-through load is not neutral, but rather *divergent*.

A simple model of such structural behaviour is investigated in Fig. 22.12(c). The normal force $N = -Q/(2\sin\alpha)$ due to load Q causes a strain $\varepsilon = -Q/(2EA\sin\alpha)$ in the struts, and therefore we get a displacement of the support amounting to $l\{\cos\,[1 - Q/(2EA\sin\alpha)] - \cos\alpha_0\}$, where α_0 designates the inclination of the strut in the unloaded state. The horizontal component $Q\cot\alpha/2$ of the strut force corresponds, on the one hand, to a displacement $Q\cot\alpha/(2k)$ of the spring elastic abutment. This leads to the equation

$$\sin\alpha - \cos\alpha_0 \tan\alpha = \frac{Q}{2kl}\left(1 + \frac{kl}{EA}\right) \tag{22.20}$$

for the odd function $Q(\alpha)$. Differentiating the expression on the left in (22.20) with respect to α shows that Q is a maximum for

$$\alpha = \arccos\sqrt[3]{\cos\alpha_0} \tag{22.21}$$

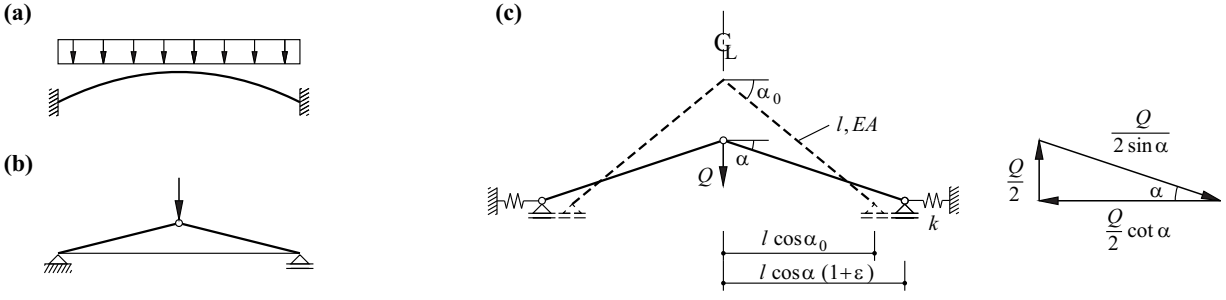

Fig. 22.12 Snap-through problems: (a) shallow arch, (b) inclined leg frame with tie, (c) inclined leg frame with elastic lateral support

Example 22.10 Elastically supported inclined leg frame

We get the values given in Tab. 22.4 for the system shown in Fig. 22.13(a), with $\sin\alpha_0 = 0.1$, $l = 10\,\text{m}$, $EA = 3000\,\text{MN}$ and $k = 100\,\text{MN/m}$. Here, $H = Q\cot\alpha/2$ is the horizontal thrust, $w = 1\,\text{m} + Ql/(2EA) - l\sin\alpha$ is equal to the deflection at the point of load application and $H(\alpha)$ is an even function.

In Fig. 22.13(b), the point traces the path OAEF for a monotonic loading provided vibrations about the equilibrium position E after snap-through are ignored. Path ABCDE can be achieved in a displacement-controlled test.

Fig. 22.13(c) illustrates the change in the horizontal thrust depending on the deflection. Its maximum value ($\alpha = 0$, point B) is $l(1 - \cos\alpha_0)/[1/k + l/(EA)] = 3759\,\text{kN}$.

Tab. 22.4 Calculations for Fig. 22.13(b) and Fig. 22.13(c)

α	Q	H	w	Remarks
0.1002	0	0	0	initial position (O)
0.0850	179	1052	151	
0.0700	270	1923	301	
0.0579	290	2504	422	snap-through (A)
0.0400	253	3160	601	
0.0200	144	3609	800	
0	0	3759	1000	maximum horizontal thrust (B)
– 0.1002	0	0	2000	(D)
– 0.1100	171	– 774	2098	
– 0.1200	394	– 1634	2200	
rad	kN	kN	mm	

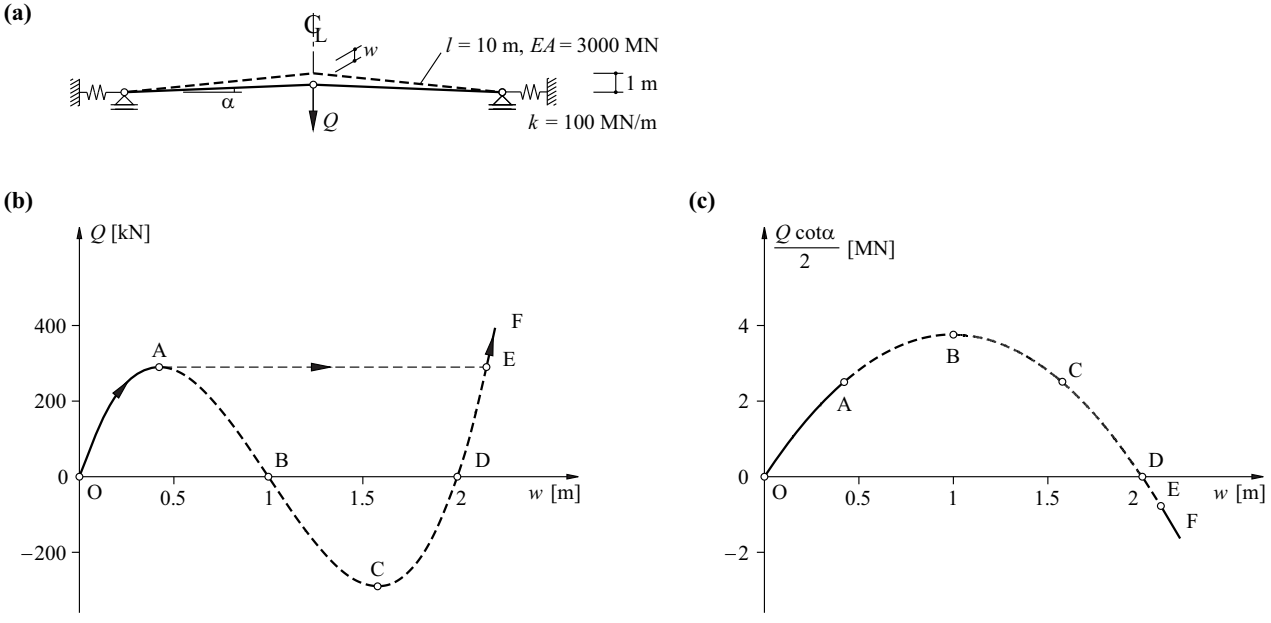

Fig. 22.13 Elastically supported inclined leg frame: (a) diagram of static system, (b) load-deflection diagram, (c) horizontal thrust-deflection diagram

22.2.4.4 Natural vibrations

Putting $k = 0$, $q_z = 0$, EI = const and C = const simplifies (22.3) to

$$EIw'''' + Cw'' + \rho A\ddot{w} = 0 \tag{22.22}$$

Separating the variables according to

$$w = w(x) \cdot \sin(\omega t) \tag{22.23}$$

transforms (22.22) into

$$EIw'''' + Cw'' - \rho A\omega^2 w = 0 \tag{22.24}$$

where ω is the angular frequency of a harmonic *natural vibration*. Using $\xi = x/l$, eq. (22.24) has the general solution

$$w = c_1 \cosh(\lambda_1\xi) + c_2 \sinh(\lambda_1\xi) + c_3 \cos(\lambda_2\xi) + c_4 \sin(\lambda_2\xi) \tag{22.25}$$

with the eigenvalues λ_1 and λ_2 given by

$$\lambda_{1,2}^2 = l^2 \left(\mp \frac{C}{2EI} + \sqrt{\left(\frac{C}{2EI}\right)^2 + \frac{\rho A\omega^2}{EI}} \right) \tag{22.26}$$

In the case of a bar with hinged supports at $x = 0$ and $x = l$, w and w'' must disappear for $\xi = 0$ and $\xi = 1$, i. e.

$$\begin{bmatrix} 1 & 0 & 1 & 0 \\ (\lambda_1/l)^2 & 0 & -(\lambda_2/l)^2 & 0 \\ \cosh\lambda_1 & \sinh\lambda_1 & \cos\lambda_2 & \sin\lambda_2 \\ (\lambda_1/l)^2 \cdot \cosh\lambda_1 & (\lambda_1/l)^2 \cdot \sinh\lambda_1 & -(\lambda_2/l)^2 \cdot \cos\lambda_2 & -(\lambda_2/l)^2 \cdot \sin\lambda_2 \end{bmatrix} \begin{Bmatrix} c_1 \\ c_2 \\ c_3 \\ c_4 \end{Bmatrix} = \begin{Bmatrix} 0 \\ 0 \\ 0 \\ 0 \end{Bmatrix}$$

Setting the determinant to zero results in the eigenvalue equation

$$\sinh\lambda_1 \cdot \sin\lambda_2 = 0 \tag{22.27}$$

with the general solution $\lambda_2 = n\pi$, i. e. using (22.26),

$$\left(\frac{n^2\pi^2}{l^2}\right)^2 = \frac{\rho A\omega^2}{EI} + \frac{n^2\pi^2}{l^2} \cdot \frac{C}{EI} \tag{22.28}$$

where n is a whole number. When $\omega = 0$, we get the *buckling loads*

$$C_n = n^2 \frac{\pi^2 EI}{l^2} \tag{22.29}$$

and when $C = 0$, we get the *fundamental angular frequencies*

$$\omega_n = n^2 \frac{\pi^2}{l^2} \sqrt{\frac{EI}{\rho A}} \tag{22.30}$$

Eq. (22.28) therefore becomes the interaction relationship

$$\frac{C}{C_n} + \left(\frac{\omega}{\omega_n}\right)^2 = 1 \tag{22.31}$$

see Fig. 22.14(a).

According to (22.31), buckling corresponds to an infinitely slow vibration ($\omega \to 0$).

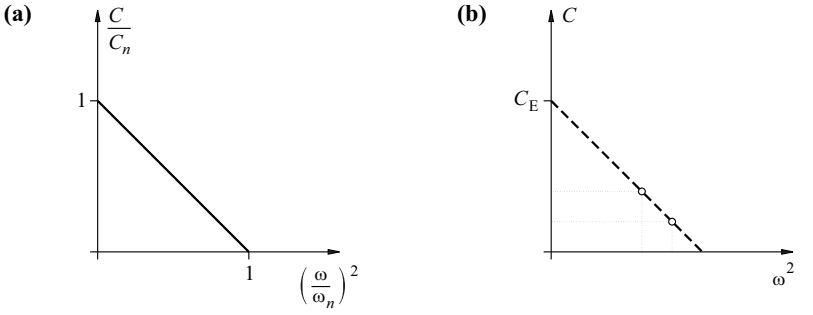

Fig. 22.14 Natural vibrations: (a) how the natural angular frequency ω depends on compressive force C, (b) C_E determined experimentally by measuring the natural angular frequency and extrapolating

In principle, if $n = 1$, then $C_1 = C_E$ can be determined experimentally according to Fig. 22.14(b) through extrapolation by measuring the natural frequencies for at least two values $C < C_E$. And vice versa: if the buckling load and fundamental angular frequency are known, it is possible, in principle, to deduce the loading by measuring the frequency.

Provided the eigenmodes of the buckling and vibration problems are not affine, the sum on the left in (22.31) is not less than 1.

22.2.5 Slope-deflection method

The slope-deflection method described in section 17.4 is generalised in the following by including second-order deformations. In doing so, it is presumed that bending stiffnesses EI and compressive forces C remain constant for each bar. The fundamental relationships (17.51) for the member end moments continue to apply, as do the relationships (17.49) and (17.50) for the near- and far-end bar stiffnesses as well as the relationships (17.48) for the fixed-end moments. However, the rotations $\varphi_{ii} = \varphi_{kk}$ and $\varphi_{ik} = \varphi_{ki}$ as well as φ_{i0} and φ_{k0} have to be calculated taking into account $C = \text{const}$.

Using (22.2) and (22.8) with $\xi = x/l$ and the *axial force parameter*

$$\lambda = \kappa l = l\sqrt{\frac{C}{EI}} \tag{22.32}$$

results in the following:

$$\begin{aligned}
w &= \frac{q_0 l^4}{EI\lambda^4}\left[\cos(\lambda\xi) + \frac{1-\cos\lambda}{\sin\lambda}\cdot\sin(\lambda\xi) - 1 - \frac{\lambda^2}{2}\cdot\xi(1-\xi)\right] \\
w &= \frac{q_1 l^4}{EI\lambda^4}\left[\frac{\sin(\lambda\xi)}{\sin\lambda} - \xi - \frac{\lambda^2}{6}\cdot\xi(1-\xi^2)\right] \\
w &= \frac{Ql^3}{EI\lambda^2}\left[\frac{\sin(\lambda-\lambda\alpha)}{\lambda\sin\lambda}\cdot\sin(\lambda\xi) - (1-\alpha)\xi\right] \qquad (0 \le \xi \le \alpha) \\
w &= \frac{Ql^3}{EI\lambda^2}\left[\frac{\sin(\lambda\alpha)}{\lambda\sin\lambda}\cdot\sin(\lambda-\lambda\xi) - \alpha(1-\xi)\right] \qquad (\alpha \le \xi \le 1) \\
w &= \frac{Ml^2}{EI\lambda^2}\left[-\frac{\cos(\lambda-\lambda\alpha)}{\sin\lambda}\cdot\sin(\lambda\xi) + \xi\right] \qquad (0 \le \xi \le \alpha) \\
w &= \frac{Ml^2}{EI\lambda^2}\left[\frac{\cos(\lambda\alpha)}{\sin\lambda}\cdot\sin(\lambda-\lambda\xi) - 1 + \xi\right] \qquad (\alpha \le \xi \le 1)
\end{aligned} \tag{22.33}$$

for a simply supported beam with the load cases shown in Fig. 22.15.

Where $M = -1$ and $\alpha = 0$, eq. $(22.33)_6$ results in

$$\varphi_{ii} = -w'(0) = \frac{1-\lambda\cot\lambda}{Cl} \quad , \quad \varphi_{ki} = -w'(l) = \frac{1-\lambda/\sin\lambda}{Cl} \tag{22.34}$$

when using (22.32), and therefore using (17.49) and (17.50) instead of (17.52) results in

$$\begin{aligned}
s_{ik} = s_{ki} &= \frac{EI}{l}\cdot\frac{\lambda(\sin\lambda - \lambda\cos\lambda)}{2(1-\cos\lambda) - \lambda\sin\lambda} = \frac{EI}{l}\cdot\overline{s}(\lambda) \\
t_{ki} = t_{ik} &= \frac{EI}{l}\cdot\frac{\lambda(\lambda - \sin\lambda)}{2(1-\cos\lambda) - \lambda\sin\lambda} = \frac{EI}{l}\cdot\overline{t}(\lambda)
\end{aligned} \tag{22.35}$$

for a standard bar. When $\lambda = 0$, the factors $\overline{s}$ and $\overline{t}$ in the products on the right in (22.35) take on the values 4 and 2 respectively.

Eq. (17.55) continues to apply for a bar with a hinged connection at one end. Eq. $(17.56)_1$ must be replaced by

$$r_{ik} = \frac{EI}{l}\cdot\frac{\lambda^2}{1-\lambda\cot\lambda} = \frac{EI}{l}\cdot\overline{r}(\lambda) \tag{22.36}$$

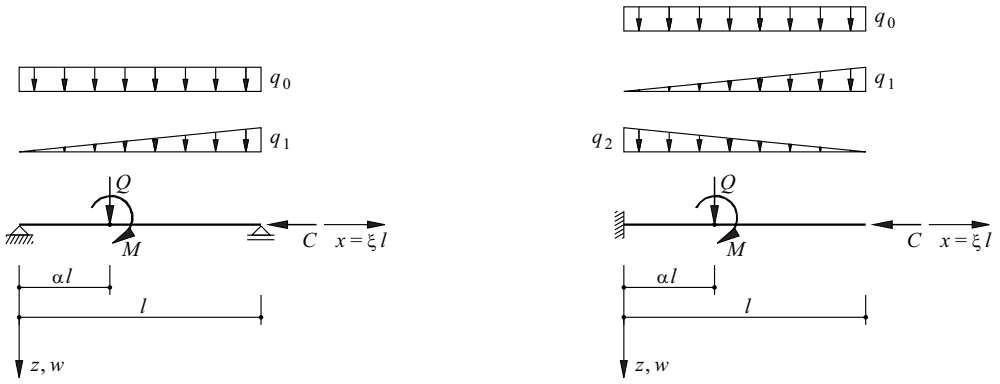

Fig. 22.15 Load cases for simply supported and cantilever beams

The relationships (22.33) can be applied to determine the fixed-end moments according to (17.48). For example, $(22.33)_1$ initially gives us

$$w' = \frac{q_0 l^3}{EI\lambda^4}\left[-\lambda\sin(\lambda\xi) + \frac{\lambda(1-\cos\lambda)}{\sin\lambda}\cdot\cos(\lambda\xi) - \frac{\lambda^2}{2}\cdot(1-2\xi)\right]$$

for a beam fixed at both ends and subjected to a uniformly distributed load q_0, i. e.

$$\varphi_{i0} = -w'(0) = -\varphi_{k0} = w'(l) = -\frac{q_0 l^3}{EI\lambda^2}\left[\frac{1-\cos\lambda}{\lambda\sin\lambda} - \frac{1}{2}\right]$$

and therefore

$$M_{ik}^0 = -M_{ki}^0 = q_0 l^2 \frac{2+\bar{t}-\bar{s}}{2\lambda^2} \tag{22.37}$$

In a similar way to (22.33), the following applies for cantilever beams with the load cases shown in Fig. 22.15:

$$w = \frac{q_0 l^4}{EI\lambda^4}\left\{\lambda\sin(\lambda\xi) - \frac{1-\sin\lambda}{\cos\lambda}[1-\cos(\lambda\xi)] - \lambda^2\cdot\left(\xi - \frac{\xi^2}{2}\right)\right\}$$

$$w = \frac{q_1 l^4}{EI\lambda^4}\left\{\frac{(2+\lambda^2)\sin\lambda - 2\lambda}{2\lambda\cos\lambda}[1-\cos(\lambda\xi)] + \frac{2+\lambda^2}{2\lambda}\sin(\lambda\xi) - \frac{1}{2}\left[(2+\lambda^2)\xi - \frac{\lambda^2\xi^3}{3}\right]\right\}$$

$$w = \frac{q_2 l^4}{EI\lambda^4}\left\{-\frac{(2-\lambda^2)\sin\lambda}{2\lambda\cos\lambda}[1-\cos(\lambda\xi)] - \frac{2-\lambda^2}{2\lambda}\sin(\lambda\xi) + \frac{1}{2}\left[(2-\lambda^2)\xi + \lambda^2\xi^2 - \frac{\lambda^2\xi^3}{3}\right]\right\}$$

$$w = \frac{Ql^3}{EI\lambda^3}\{[\tan\lambda(1-\cos(\lambda\alpha)) + \sin(\lambda\alpha)]\cdot[1-\cos(\lambda\xi)] + \sin(\lambda\xi) - \lambda\xi\} \qquad (0 \le \xi \le \alpha)$$

$$w = \frac{Ql^3}{EI\lambda^3}\{\tan\lambda[1-\cos(\lambda\alpha)][1-\cos(\lambda\xi)] + [1-\cos(\lambda\alpha)]\sin(\lambda\xi) + \sin(\lambda\alpha) - \lambda\alpha\} \qquad (\alpha \le \xi \le 1)$$

$$w = \frac{Ml^2}{EI\lambda^2}[\tan\lambda\cdot\sin(\lambda\alpha) + \cos(\lambda\alpha)][1-\cos(\lambda\xi)] \qquad (0 \le \xi \le \alpha)$$

$$w = \frac{Ml^2}{EI\lambda^2}\{\tan\lambda\cdot\sin(\lambda\alpha)[1-\cos(\lambda\xi)] + \sin(\lambda\alpha)\cdot\sin(\lambda\xi) - 1 + \cos(\lambda\alpha)\} \qquad (\alpha \le \xi \le 1)$$

(22.38)

This means that rotations, bending moments and shear forces can be calculated as required by differentiation.

With tensile instead of compressive normal forces in the bars, all the relationships given here can still be used provided λ is replaced by $i\cdot\lambda$ and the relations $(i\lambda)^2 = -\lambda^2$, $\cos(i\lambda) = \cosh\lambda$ and $\sin(i\lambda) = i\sinh\lambda$ are taken into account. The (stiffening) effect of tensile forces is often neglected for simplicity.

Example 22.11 Two-hinged frame

If the two-hinged frame shown in Fig. 22.16(a) is braced, it buckles symmetrically according to Fig. 22.16(b). When $\varphi_2 = -\varphi_3$, the moment equilibrium condition for joint 2 is

$$M_{21} + M_{23} = \left[\frac{EI_c}{h} \cdot \bar{r}_{21} + \frac{EI_b}{l} \cdot (4-2)\right] \cdot \varphi_2 = 0$$

i. e. we get the following equation

$$\lambda^2 = 2(\lambda \cot \lambda - 1)\frac{EI_b h}{EI_c l} \qquad \left(\lambda = h\sqrt{\frac{Q}{EI_c}}\right)$$

for the bifurcation load. We can see that no normal forces occur in frame beam 23, i. e. $\bar{s}_{23} = 2\bar{t}_{23} = 4$. If the frame beam is very stiff in relation to the columns, then $\lambda = \tan\lambda = 4.4934$, see example 22.6; the columns are fixed at the rigid frame beam and exhibit a buckling length of $h\pi/\lambda \approx 0.7h$. However, with a frame beam that is very flexible compared with the columns, then the latter act as if they are hinged at both ends and thus have a buckling length of h; $\lambda = \pi$ then applies

A sway system deforms antisymmetrically as shown in Fig. 22.16(c), where $\varphi_2 = \varphi_3$ and $\psi_{12} = \psi_{34}$. The moment equilibrium condition for joint 2 is

$$M_{21} + M_{23} = \left[\frac{EI_c}{h} \cdot \bar{r}_{21} + \frac{EI_b}{l} \cdot (4+2)\right] \cdot \varphi_2 - \frac{EI_c}{h} \cdot \bar{r}_{21} \cdot \psi_{12} = 0$$

and equilibrium of moments at column 12, considered as a free body, calls for

$$M_{21} + Qh \cdot \psi_{12} = \frac{EI_c}{h} \cdot \bar{r}_{21} \cdot \varphi_2 + \left[Qh - \frac{EI_c}{h} \cdot \bar{r}_{21}\right] \cdot \psi_{12} = 0$$

The resulting homogeneous set of equations is

$$\begin{bmatrix} \bar{r}_{21} + 6\dfrac{EI_b h}{EI_c l} & -\bar{r}_{21} \\ \bar{r}_{21} & \dfrac{Qh^2}{EI_c} - \bar{r}_{21} \end{bmatrix} \begin{Bmatrix} \varphi_2 \\ \psi_{12} \end{Bmatrix} = \begin{Bmatrix} 0 \\ 0 \end{Bmatrix}$$

Setting the determinant to zero results in the equation

$$\lambda \cdot \tan\lambda = 6 \cdot \frac{EI_b h}{EI_c l}$$

for the bifurcation load.

If the frame beam is very stiff in relation to the columns, then λ tends to $\pi/2$ and the result is a buckling length $h\pi/\lambda$ equal to $2h$. But where the frame beam is very flexible compared with the columns, the buckling length of the latter tends to infinity, and the system is unusable.

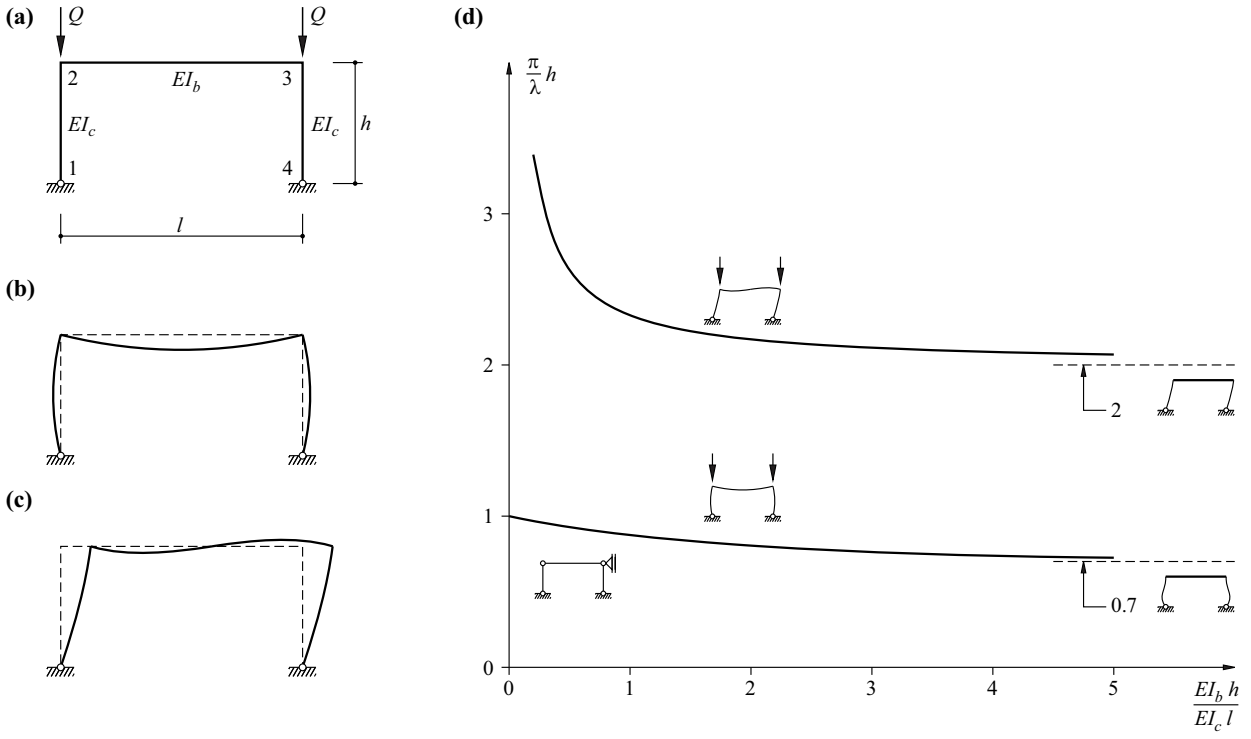

Fig. 22.16 Two-hinged frame: (a) diagram of static system, (b) symmetric buckling, (c) antisymmetric buckling, (d) buckling lengths plotted against stiffness ratios

Example 22.12 Non-sway frame

Let us consider the non-sway frame of Fig. 22.17. When $\varphi_2 = -\varphi_3$, the moment equilibrium condition is

$$M_{21} + M_{23} = \left[\frac{EI_c}{h} \cdot \bar{s}_{21} + \frac{EI_b}{l} \cdot (\bar{s}_{23} - \bar{t}_{23})\right] \cdot \varphi_2 + M_{23}^0 = 0$$

The compressive forces $C = Q + ql/2$ in the columns need to be taken into account. The ensuing compressive force in frame beam 23 is $-\varphi_2(\bar{s}_{21} + \bar{t}_{12})EI_c/h^2$

Initially ignoring the compressive force in the frame beam means that $\bar{s}_{23} = 2\bar{t}_{23} = 4$ and $M_{23}{}^0 = ql^2/12$, and so it is possible to determine an initial value for φ_2. We consider how the compressive force in the frame beam influences $\bar{s}_{23}$, $\bar{t}_{23}$ and $M_{23}{}^0$ in a second step. The result is an improved value for φ_2, and the accuracy of the calculation can be improved in further iteration steps if required.

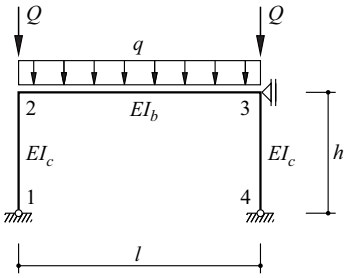

Fig. 22.17 Non-sway frame

Example 22.13 Sway frame

Equilibrium of moments at joint 2 of the sway frame shown in Fig. 22.18 calls for

$$M_{21} + M_{23} + M_{24} = \left[\frac{EI_c}{h} \cdot \bar{s}_{24} + \frac{EI_b}{l} \cdot (\bar{r}_{21} + \bar{r}_{23})\right] \cdot \varphi_2 - \frac{EI_c}{h} \cdot (\bar{s}_{24} + \bar{t}_{24}) \cdot \psi_{24} = 0$$

where $\bar{r}_{21} = \bar{r}_{23} = 3$. The compressive force $C = Q_1$ in column 24 has to be taken into account. Equilibrium of the horizontal forces at joint 2 requires $Q_2 - Q_1\psi_{24} - (M_{24} + M_{42})/h = 0$, i. e.

$$(\bar{s}_{24} + \bar{t}_{24}) \cdot \varphi_2 + (\lambda^2 - 2\bar{s}_{24} - 2\bar{t}_{24}) \cdot \psi_{24} = \frac{Q_2 h^2}{EI_c}$$

The resulting set of equations is

$$\begin{bmatrix} \bar{s}_{24} + 6\dfrac{EI_b h}{EI_c l} & -(\bar{s}_{24} + \bar{t}_{24}) \\ \bar{s}_{24} + \bar{t}_{24} & \lambda^2 - 2\bar{s}_{24} - 2\bar{t}_{24} \end{bmatrix} \begin{Bmatrix} \varphi_2 \\ \psi_{24} \end{Bmatrix} = \begin{Bmatrix} 0 \\ \dfrac{Q_2 h^2}{EI_c} \end{Bmatrix} \qquad \left(\lambda = h\sqrt{\frac{Q_1}{EI_c}}\right)$$

and when $Q_2 = 0$ we get the condition

$$\lambda^2\left(\bar{s}_{24} + 6\frac{EI_b h}{EI_c l}\right) = (\bar{s}_{24} + \bar{t}_{24})\left(\bar{s}_{24} - \bar{t}_{24} + 12\frac{EI_b h}{EI_c l}\right)$$

for the bifurcation load.

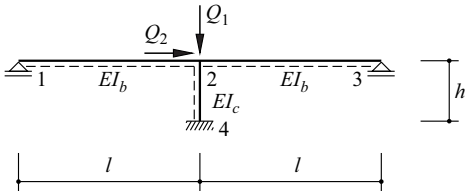

Fig. 22.18 Sway frame

Example 22.14 Elastically restrained vertical cantilever

The bar rotation ψ_{12} is unknown in the elastically restrained vertical cantilever of Fig. 22.19. Equilibrium of moments about the base of the column considered as a free body calls for

$$M_{12} + Q_1\psi_{12}l - M - Q_2 l - \psi_{12} l^2 k = 0$$

where

$$M_{12} = M_{12}^0 - s_{12}\psi_{12}$$

with s_{12} according to (22.36). Eq. $(22.33)_5$, with $\alpha = 1$, gives us the rotation

$$w'(0) = \frac{Ml}{EI\lambda^2}\left(1 - \frac{\lambda}{\sin\lambda}\right)$$

and therefore, using (22.36), the fixed-end moment

$$M_{12}^0 = s_{12}w'(0) = M\frac{\sin\lambda - \lambda}{\sin\lambda - \lambda\cos\lambda}$$

Substituting into the moment equilibrium condition results in

$$\psi_{12} = -\frac{Q_2 l + M\dfrac{\lambda(1 - \cos\lambda)}{\sin\lambda - \lambda\cos\lambda}}{kl^2 - Q_1 l + \dfrac{EI}{l} \cdot \dfrac{\lambda^2}{1 - \lambda\cot\lambda}}$$

We get the condition

$$\frac{kl^3}{EI}(\sin\lambda - \lambda\cos\lambda) + \lambda^3\cos\lambda = 0 \qquad \left(\lambda = l\sqrt{\frac{Q_1}{EI}}\right)$$

for the bifurcation problem ($Q_2 = M = 0$).

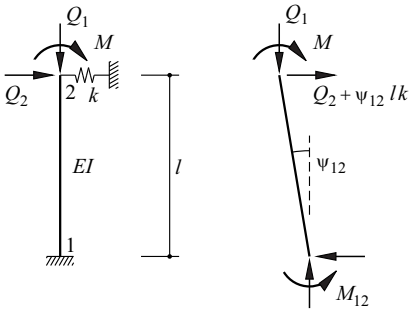

Fig. 22.19 Elastically restrained vertical cantilever

22.2.6 Stiffness matrices

22.2.6.1 Non-linear member matrices

The member stiffness matrix (17.17) – taking into account (22.35) and (22.32) – is generalised as follows:

$$\boldsymbol{k}_{\mathrm{e}}^{\mathrm{II}} = \frac{EI}{l}\begin{bmatrix} A/I & 0 & 0 & -A/I & 0 & 0 \\ 0 & \dfrac{2(\bar{s}+\bar{t})-\lambda^2}{l^2} & -\dfrac{\bar{s}+\bar{t}}{l} & 0 & -\dfrac{2(\bar{s}+\bar{t})-\lambda^2}{l^2} & -\dfrac{\bar{s}+\bar{t}}{l} \\ 0 & -\dfrac{\bar{s}+\bar{t}}{l} & \bar{s} & 0 & \dfrac{\bar{s}+\bar{t}}{l} & \bar{t} \\ -A/I & 0 & 0 & A/I & 0 & 0 \\ 0 & -\dfrac{2(\bar{s}+\bar{t})-\lambda^2}{l^2} & \dfrac{\bar{s}+\bar{t}}{l} & 0 & \dfrac{2(\bar{s}+\bar{t})-\lambda^2}{l^2} & \dfrac{\bar{s}+\bar{t}}{l} \\ 0 & -\dfrac{\bar{s}+\bar{t}}{l} & \bar{t} & 0 & \dfrac{\bar{s}+\bar{t}}{l} & \bar{s} \end{bmatrix} \tag{22.39}$$

The last two columns of this matrix are illustrated in Fig. 22.20.

If we consider the first three terms in the TAYLOR series for $\sin\lambda$ and $\cos\lambda$, then (22.35) leads to the approximation

$$\bar{s} \approx 4 \cdot \frac{1-\lambda^2/10}{1-\lambda^2/15} \quad , \quad \bar{t} \approx 2 \cdot \frac{1-\lambda^2/20}{1-\lambda^2/15} \tag{22.40}$$

Substituting these expressions into (22.39) and deducting the expression on the right in (17.17) – abbreviated to $\boldsymbol{k}_{\mathrm{e}}^{\mathrm{I}}$ – results in the approximation

$$\boldsymbol{k}_{\mathrm{e}}^{\mathrm{II}} - \boldsymbol{k}_{\mathrm{e}}^{\mathrm{I}} \approx -C\begin{bmatrix} 0 & 0 & 0 & 0 & 0 & 0 \\ 0 & \dfrac{6}{5l} & -\dfrac{1}{10} & 0 & -\dfrac{6}{5l} & -\dfrac{1}{10} \\ 0 & -\dfrac{1}{10} & \dfrac{2l}{15} & 0 & \dfrac{1}{10} & -\dfrac{l}{30} \\ 0 & 0 & 0 & 0 & 0 & 0 \\ 0 & -\dfrac{6}{5l} & \dfrac{1}{10} & 0 & \dfrac{6}{5l} & \dfrac{1}{10} \\ 0 & -\dfrac{1}{10} & -\dfrac{l}{30} & 0 & \dfrac{1}{10} & \dfrac{2l}{15} \end{bmatrix} = \boldsymbol{k}_{\mathrm{g}} \tag{22.41}$$

if $\lambda^2/15$ is ignored in comparison with 1 in the denominator of the differential expressions.

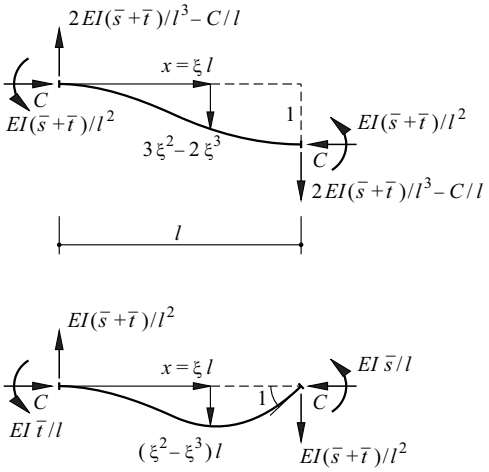

Fig. 22.20 Shape functions for the displacements and coefficients of the non-linear member matrix

22.2.6.2 Geometric stiffness matrix

The *geometric stiffness matrix* $\boldsymbol{k}_g$ on the right in (22.41) can be obtained in a similar way to $\boldsymbol{k}_e^I$. According to (22.4), the variable $-C$ is analogous with EI and w' analogous with w'' in the expression for the total potential Π. Accordingly, the coefficients

$$k_{gij} = -C\int_0^l \Omega_{2i}'\Omega_{2j}'\,dx \tag{22.42}$$

can be determined in a similar way to $(19.33)_2$ from the products of the derivatives of the cubic shape functions Ω_{2i} included for w in (19.39), i. e.

$$\begin{aligned}
k_{g55} &= -C\int_0^l [6\xi(1-\xi)/l]^2\,dx &&= -C\cdot\frac{6}{5l}\\
k_{g56} &= -C\int_0^l [6\xi(1-\xi)(2\xi-3\xi^2)/l]\,dx &&= -C\cdot\frac{1}{10}\\
k_{g63} &= -C\int_0^l (-1+4\xi-3\xi^2)(2\xi-3\xi^2)\,dx = &&\quad C\cdot\frac{l}{30}\\
k_{g66} &= -C\int_0^l (2\xi-3\xi^2)^2\,dx &&= -C\cdot\frac{2l}{15}
\end{aligned}$$

see (22.41). Fig. 22.21 illustrates the equilibrium corresponding to the four columns of $\boldsymbol{k}_g$ not equal to zero.

Often, $\boldsymbol{k}_g$ is simplified further by considering $k_{g22} = -k_{g25} = -k_{g52} = k_{g55} = -C/l$ as the only coefficients not equal to zero. This corresponds to assuming that both ends of each bar have hinged connections, or rather linear instead of cubic shape functions Ω_{2i}.

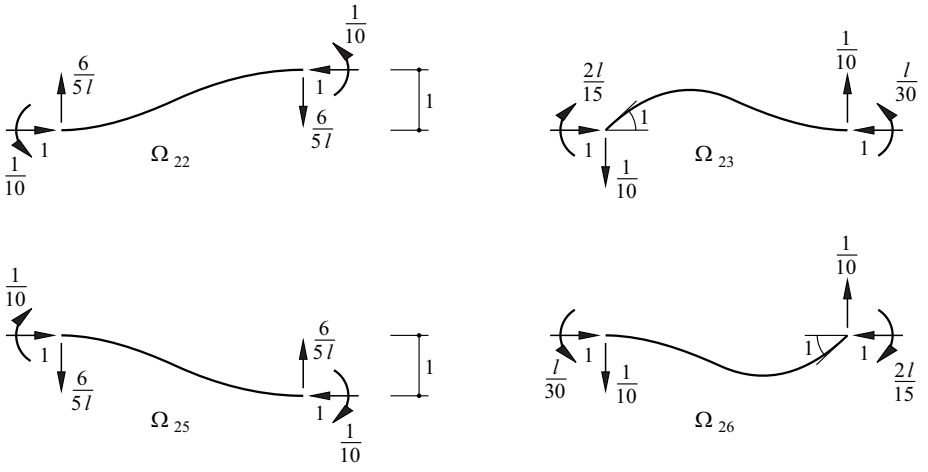

Fig. 22.21 Coefficients of the geometric stiffness matrix

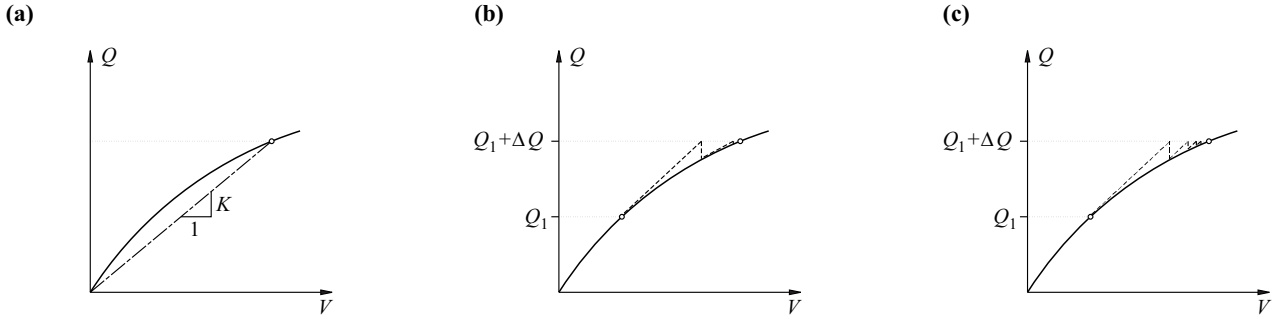

Fig. 22.22 Method of solving non-linear load-deformation problems: (a) total step with secant stiffness matrix, (b) NEWTON-RAPHSON method with updated tangential stiffness matrix, (c) modified method with constant stiffness within one load step

22.2.6.3 Commentary

The geometric stiffness matrices $\boldsymbol{k}_g$ are handled in the same way as stiffness matrices $\boldsymbol{k}_e^I$ according to first-order theory when setting up the global stiffness matrix $\boldsymbol{K}$ in accordance with section 17.3. The non-linear relationship between the loads $\boldsymbol{Q}$ and the associated displacements $\boldsymbol{V}$ is approximated with $\boldsymbol{K}$ as a *secant stiffness matrix*, see Fig. 22.22(a).

The compressive forces C are specified in the case of bifurcation problems apart from a constant factor. The factor is obtained from the solution to the associated linear eigenvalue problem by setting the determinant of the stiffness matrix to zero.

When analysing very flexible systems, e. g. cable-net structures, it may be necessary to perform calculations according to *third-order theory* taking into account large deformations. As a rule, this is carried out in several load steps by means of an incremental, iterative method. In this process, the global tangential stiffness matrix is updated each time with respect to the last deformation state, i. e. the elastic and non-linear geometric stiffness matrices are set up anew for the respective geometry. The iteration of the equilibrium necessary for each load step is carried out according to the NEWTON-RAPHSON method. In the standard method, Fig. 22.22(b), the tangential stiffness matrix is updated for every iteration step, whereas the modified method, Fig. 22.22(c), is based on a constant stiffness within one load step.

22.3 Elastic-plastic buckling

22.3.1 Concentrically loaded columns

22.3.1.1 Buckling stress curves

The column shown in Fig. 22.23(a) exhibits an initial deflection w_0 at $x = l/2$. Using the amplification factor μ according to (22.12) for a compressive force C results in extreme fibre stresses at $x = l/2$ amounting to

$$\frac{C}{A} + \frac{M}{W} = \frac{C}{A} + \frac{C(w_0 + w)}{W} = \frac{C}{A} + \frac{Cw_0\mu}{W} = \frac{C}{A}\left(1 + \frac{\dfrac{w_0 A}{W}}{1 - \dfrac{C}{C_E}}\right) \qquad \left(C_E = \frac{\pi^2 EI}{l^2}\right) \tag{22.43}$$

Equating this value to f_y and carrying out a little computation results in

$$\frac{C}{Af_y} = \frac{1}{\beta + \sqrt{\beta^2 - \lambda^2}} \qquad \left(2\beta = 1 + \bar{\lambda}^2 + \frac{w_0 A}{W} \quad , \quad \bar{\lambda} = \frac{l}{i} \cdot \frac{1}{\pi}\sqrt{\frac{f_y}{E}}\right) \tag{22.44}$$

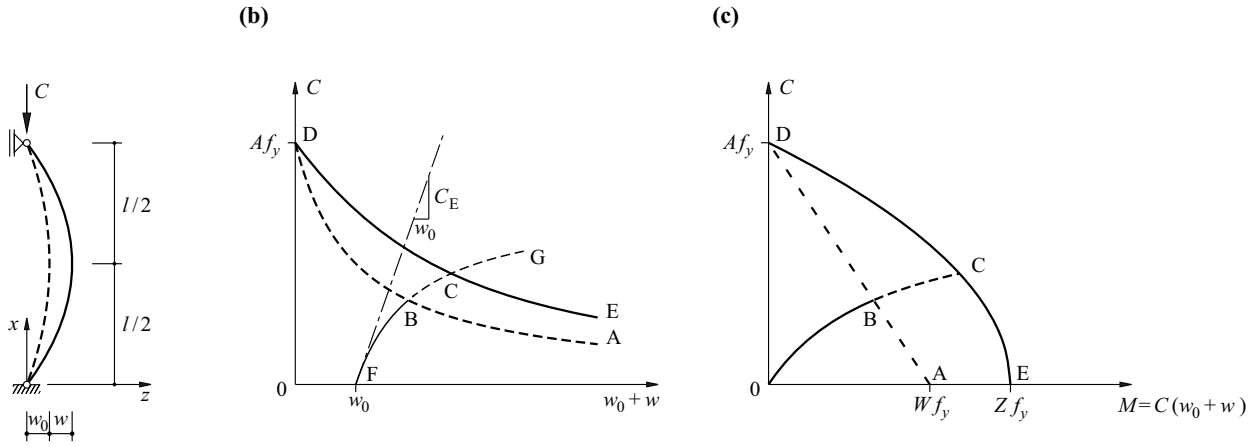

Fig. 22.23 Imperfect column: (a) notation, (b) load-deflection diagram, (c) bending and normal force at section $x = l/2$

where $i = \sqrt{I/A}$ is the radius of gyration according to (13.19) and $\bar{\lambda}$ is the buckling slenderness ratio related to the *yield slenderness ratio* $\lambda_E = \pi\sqrt{E/f_y}$.

In the load-deflection diagram, Fig. 22.23(b), the result for an increasing compressive force C is the line FBCG according to (22.12), with Q replaced by C, see Fig. 22.4(b). Restricting the boundary stresses to f_y corresponds to line ABD with the equation

$$\frac{C}{A} + \frac{C(w_0 + w)}{W} = f_y \tag{22.45}$$

In the interaction diagram, Fig. 22.23(c), this relationship corresponds to the straight line ABD.

The yield limit ECD in Fig. 22.23(c) describes the resistance of the most highly stressed cross-section at $x = l/2$; the yield limit is, for example, given by $(21.30)_1$, where $M_y = M$, $M_z = 0$, $M_{yu} = Zf_y$ and $N_u = Af_y$. We get the corresponding line ECD in Fig. 22.23(b). The amplification factor μ can no longer be used in the elastic-plastic zone between lines ABD and ECD. The actual load-deflection line must lie below arc BC because of the reduced stiffness due to the partial plastic deformation. This aspect will be investigated further in section 22.3.3.

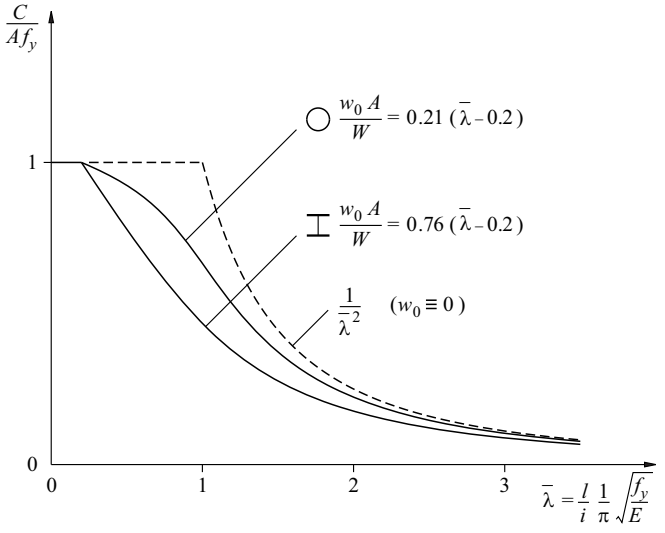

Fig. 22.24 Buckling stress curves according to (22.44)

When $w_0 = 0$, eq. (22.44) gives us the EULER buckling stress curve $C/(Af_y) = 1/\overline{\lambda}^2$ shown by the dotted line in Fig. 22.24. The buckling stress curves for imperfect columns lie below this hyperbola. The figure also shows the limiting cases for standard curves for steel sections (hot-rolled hollow sections and rolled sections with thick flanges), including the associated assumptions for w_0.

22.3.1.2 The influence of residual stresses

The model column shown in Fig. 22.25(a) consists of two flanges at a spacing h. The flange thickness t is small in comparison with the flange width b and the web is ignored. Consequently, $I_y = bth^2/2$ and $I_z = b^3t/6$.

For simplicity, a linear distribution of residual stresses is assumed in the flanges, see Fig. 22.25(b). The outer parts of the section, which cool more rapidly after rolling or welding, experience compressive residual stresses, but the inner parts, which cool at a slower rate, tensile residual stresses. Factor α is about 0.4 to 0.5.

An elastic-plastic stress distribution according to Fig. 22.25(c) is established for $\overline{\lambda} < 1/\sqrt{1-\alpha}$ at the buckling load. The elastic core is reduced to width βb. The mean compressive stress is $(1 - \alpha\beta)f_y$, and the second moments of area I_y and I_z are reduced to βI_y and $\beta^3 I_z$. Therefore, the result is a buckling stress

$$\frac{C}{Af_y} = 1 - \alpha\beta = \frac{\beta^k}{\overline{\lambda}^2} \qquad \left(\overline{\lambda} \le \frac{1}{\sqrt{1-\alpha}} \quad , \quad 0 \le \beta \le 1\right) \tag{22.46}$$

related to the yield limit f_y, where the exponent k takes on a value of 1 for buckling about the "strong" (y) axis, but a value of 3 for buckling about the "weak" (z) axis. Eliminating parameter β results in the buckling stress curves between points A and C shown in Fig. 22.25(d). EULER buckling stress curve (B)CD applies for $\overline{\lambda} > 1/\sqrt{1-\alpha}$ provided initial deformations are neglected.

22.3.1.3 Application of buckling stress curves

The combined effects of initial deformations and residual stresses are approximated in the standard curves for steel sections drawn in Fig. 22.24. In order to apply the buckling stress curves, it is necessary to estimate the relevant conditions and also make an estimate of the buckling length l depending on the boundary conditions of a given problem.

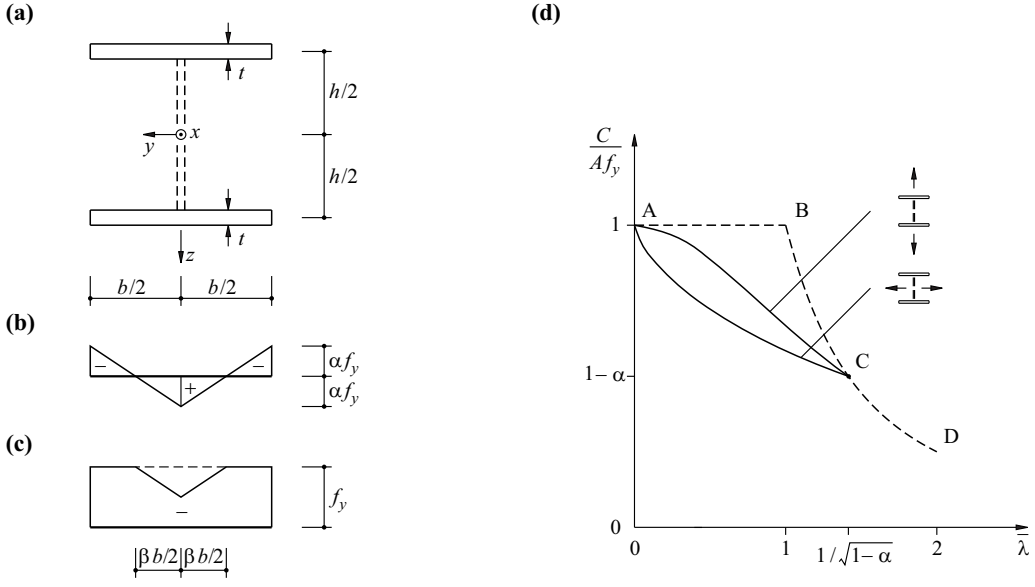

Fig. 22.25 How residual stresses affect the buckling load: (a) model column, (b) assumed distribution of residual stresses, (c) stress distribution at buckling load, (d) buckling stress curves

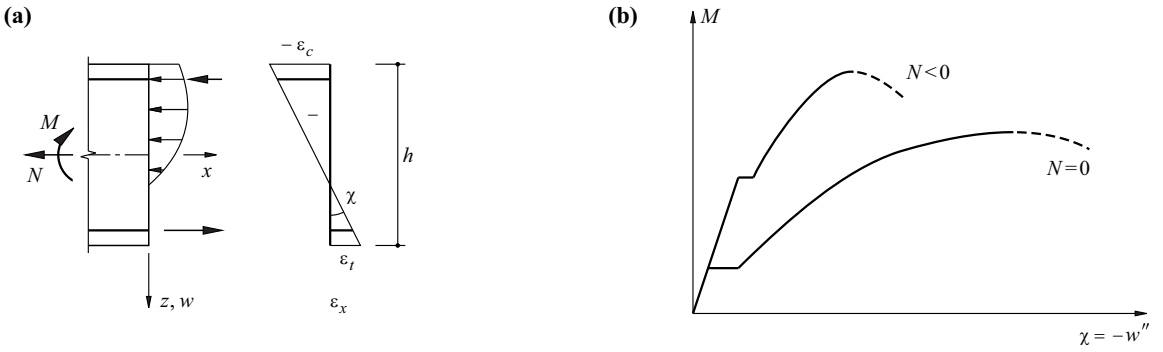

Fig. 22.26 Reinforced concrete cross-section subjected to N = const: (a) stress resultants, stresses and strains, (b) moment-curvature diagram

22.3.2 Eccentrically loaded columns

22.3.2.1 General procedure

Generally, the relationship between the bending moments M and the curvatures $\chi = -w''$ is not linear and depends on the normal force N. Fig. 22.26 illustrates this fact for the example of a typical reinforced concrete cross-section, (see the remarks in sections 13.2.1 and 20.3.1.2).

The relationships (22.1) continue to apply. The approximate relationship between internal force components C, V_o (related to the x or z direction) and internal force components N, V (related to the deformed bar axis) is

$$\begin{Bmatrix} N \\ V \end{Bmatrix} = \begin{bmatrix} -1 & w' \\ w' & 1 \end{bmatrix} \begin{Bmatrix} C \\ V_o \end{Bmatrix} \tag{22.47}$$

We therefore get the set of equations

$$C' = -q_x \quad , \quad V_o' = -q_z \quad , \quad N = -C + V_o w' \quad , \quad V_o' = M''(N, -w'') - (Cw')' \tag{22.48}$$

which can be solved numerically for a given problem – taking into account the corresponding boundary conditions – through discretisation and by applying an incremental, iterative procedure (as described in section 22.2.6.3). The basis for the solution lies in knowledge of the non-linear moment-curvature diagrams $M(N,-w'')$ for all cross-sections, or rather bar elements.

22.3.2.2 Column deflection curves

Fig. 22.27 shows a group of column deflection curves for C = const. To draw these, we assume an initial eccentricity e_0 and then, using $M_0 = Ce_0$, calculate the associated curvature χ_0 from the non-linear moment-curvature diagram presumed to be valid over the entire length of the bar. From this, taking a step of Δ, we get the rotation $e_1' = -\chi_0\Delta$ and the eccentricity $e_1 = e_0 - \chi_0\Delta^2/2$ at point 1. Putting $M_1 = Ce_1$, we can then use the moment-curvature diagram to find χ_1, and we get $e_2' = e_1' - \chi_1\Delta$ and $e_2 = e_1 + e_1'\Delta - \chi_1\Delta^2/2$. Repeating this procedure with the help of the recurrence relations

$$e_i' = e_{i-1}' - \chi_{i-1}\Delta \quad , \quad e_i = e_{i-1} + e_{i-1}'\Delta - \chi_{i-1}\Delta^2/2 \tag{22.49}$$

and calculating the curvatures χ_i via $M_i = Ce_i$ from the moment-curvature diagram finally leads to $e_n \approx 0$, which defines one curve of the group.

Applying the column deflection curves determined in this way requires picking out the curve that fits with the respective boundary conditions of a problem, as is illustrated in Fig. 22.28.

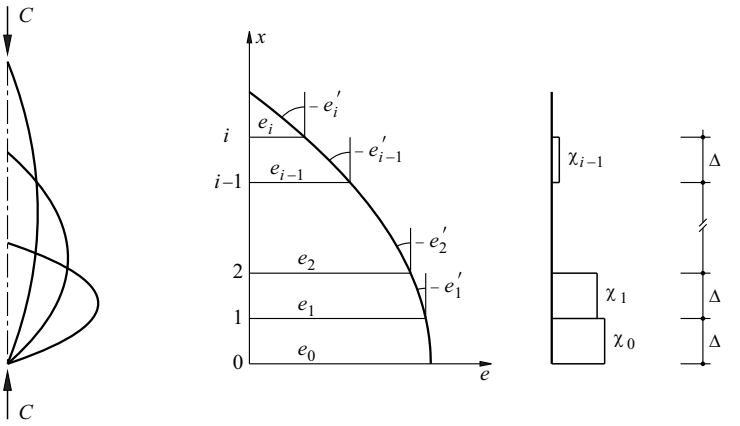

Fig. 22.27 Group of column deflection curves for C = const with variable initial eccentricity e_0

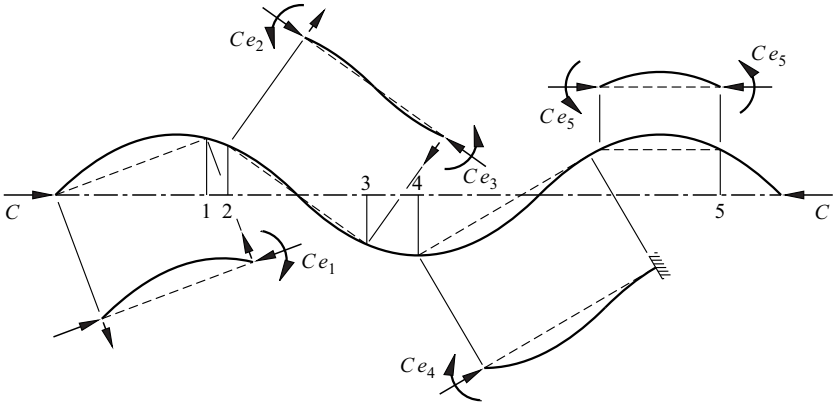

Fig. 22.28 Applying column deflection curves depending on the boundary conditions of a problem

22.3.2.3 Approximation methods

One practical approximation method involves using the *secant stiffness* M_m/χ_m resulting from the moment-curvature diagram for the stress resultants $N_m = -C$ and $M_m = Ce_m$ for the most highly stressed (critical) cross-section together with the amplification factor μ. According to Fig. 22.29(a), the following applies:

$$e_m = e_0 + e_1 + e_2 \tag{22.50}$$

where e_0 and e_1 represent the eccentricity due to geometric imperfections and the eccentricity due to actions calculated using first-order theory respectively. The eccentricity e_2 according to second-order theory is calculated from the buckling length l and the curvature χ_m as a result of N_m and M_m as follows:

$$e_2 = \frac{\chi_m l^2}{c} \tag{22.51}$$

The c factor is generally

$$c = \alpha\pi^2 + (1-\alpha)\frac{\sum_{i=1}^{n} M_{1i}}{\sum_{i=1}^{n} \frac{M_{1i}}{c_i}} \qquad \left(\alpha = \frac{C}{C_E}\,,\; C_E = \frac{\pi^2 M_m}{\chi_m l^2}\right) \tag{22.52}$$

where the sums must be applied over all n components to the first-order moments M_1 (including component Ce_0 due to imperfections). The individual c_i factors are calculated using the work theorem according to Fig. 22.30 depending on the loading

$$c_i = \frac{\chi_{mi} l^2}{e_{1i}} = \frac{M_{1i}\chi_m l^2/M_m}{\int_0^l \chi_i \overline{M}\,\mathrm{d}x} \tag{22.53}$$

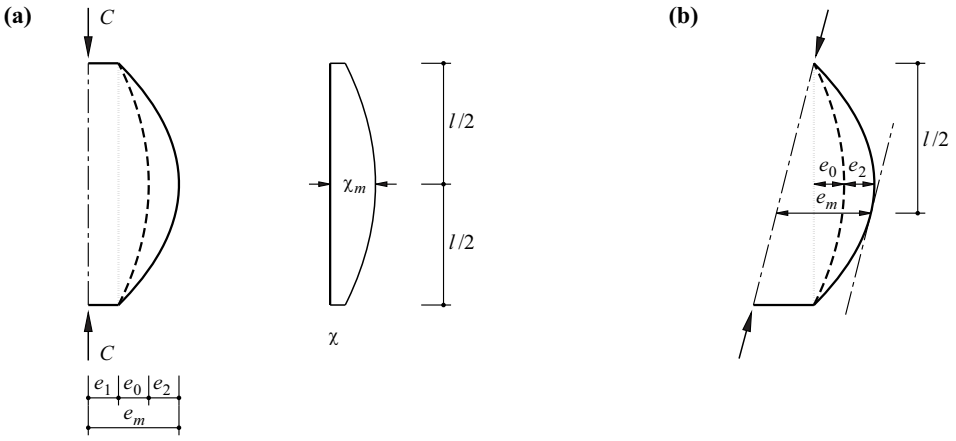

Fig. 22.29 Approximation method: (a) eccentricities and curvatures, (b) critical cross-section for unequal end eccentricities

We start from

$$M_m = Ce_2 + \sum_{i=1}^{n} M_{1i} \quad , \quad e_2 = \frac{\sum_{i=1}^{n} e_{1i}}{1-\alpha} \tag{22.54}$$

in order to prove (22.52). Substituting $(22.54)_2$ in (22.51) and taking into account (22.53), $(22.54)_1$ plus

$$(1-\alpha)Ce_2 = C\sum_{i=1}^{n} e_{1i} = C\sum_{i=1}^{n} \frac{M_{1i}\chi_m l^2}{c_i M_m} = \frac{C}{C_E}\cdot\pi^2\cdot\sum_{i=1}^{n}\frac{M_{1i}}{c_i}$$

results in, as asserted,

$$c = \frac{\chi_m l^2}{e_2} = \frac{(1-\alpha)\left(Ce_2 + \sum_{i=1}^{n} M_{1i}\right)}{\sum_{i=1}^{n}\frac{M_{1i}}{c_i}} = \alpha\pi^2 + (1-\alpha)\frac{\sum_{i=1}^{n} M_{1i}}{\sum_{i=1}^{n}\frac{M_{1i}}{c_i}} \tag{22.55}$$

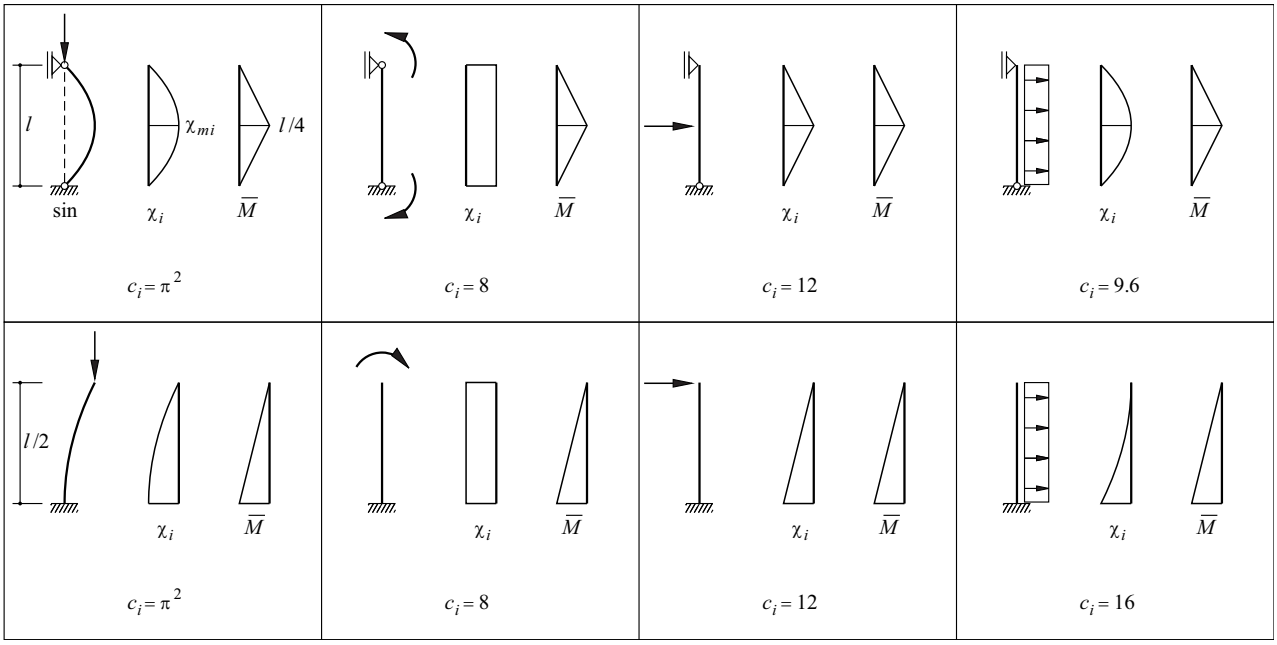

Fig. 22.30 The c_i factors according to (22.52)

Example 22.14 Vertical cantilever

The vertical cantilever shown in Fig. 22.31 has a buckling length of $l = 8\,\text{m}$ and a geometrical imperfection $e_0 = 14\,\text{mm}$. Subjected to a compressive force $C = 2000$ kN, its bending resistance is 305 kNm, and the associated strain distribution according to Fig. 22.26(a) results in a curvature of 12.4 mrad/m.

With a secant stiffness of $305/12.4 = 24.6\,\text{MNm}^2$, we initially get $C_E = \pi^2 \cdot 24.6/8^2 = 3793\,\text{kN}$ and $\alpha = 2000/3793 = 0.5273$, and from that, using $M_{11} = 2000 \cdot 0.014 = 28\,\text{kNm}$, $M_{12} = 32 \cdot 4 = 128\,\text{kNm}$, $c_1 = \pi^2$ and $c_2 = 12$, according to (22.52) we get

$$c = 0.5273 \cdot \pi^2 + 0.4727 \frac{28 + 128}{\frac{28}{\pi^2} + \frac{128}{12}} = 10.665$$

Eq. (22.51) results in $e_2 = 12.4 \cdot 8^2/10.665 = 74.4\,\text{mm}$. Putting $e_1 = M_{12}/C = 64\,\text{mm}$ and $e_0 = 14$ mm, the eccentricity at the critical cross-section at the base of the column according to (22.50) is therefore $e_m = 14 + 64 + 74.4 = 152.4$ mm. The moment at the base of the column is $2000 \cdot 0.1524 = 304.8\,\text{kNm}$, i. e. the bending resistance of 305 kNm is just adequate.

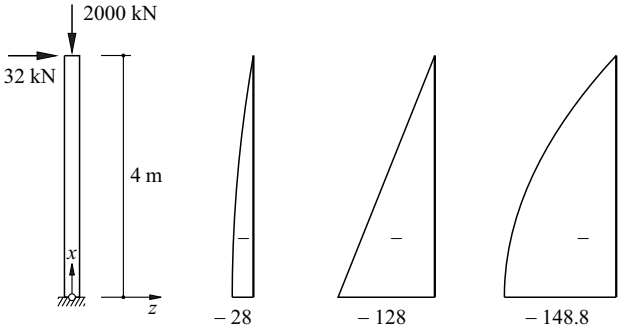

Fig. 22.31 Vertical cantilever with moments [kNm] due to imperfection, horizontal force and deformation

In the approximation method, the secant stiffness at the critical cross-section is used over the entire length of the column as an approximation in order to calculate the deformations. This approach underestimates the stiffness and the ensuing stress resultants are on the safe side.

The eccentricities must be reduced according to Fig. 22.29(b) if the critical cross-section is not at the position of the maximum values of e_0 and e_2. It can be assumed that the progression of e_2 over the length of the column is similar to the buckled shape.

If applicable, the effects of shrinkage and creep must be taken into account when calculating χ_m from the strain distribution according to Fig. 22.26(a).

22.3.3 Limit loads of frames according to second-order theory

22.3.3.1 General

The treatment of general geometric and material non-linear problems while taking into account geometric imperfections and restraints is very involved. Incremental, iterative methods of solution, as described in section 22.2.6.3, will normally be required.

One appropriate way of checking such calculations and providing rough treatments is to analyse the statically determinate deformed system immediately prior to reaching the limit load. The difference between this and calculating the limit load according to first-order theory is that it is necessary to know which plastic hinge forms last. Another difficulty is that the maximum load, taking into account the deformations, can even occur before the conclusion of the plastic hinge formation according to first-order theory.

This method is explained below with the help of a simple example.

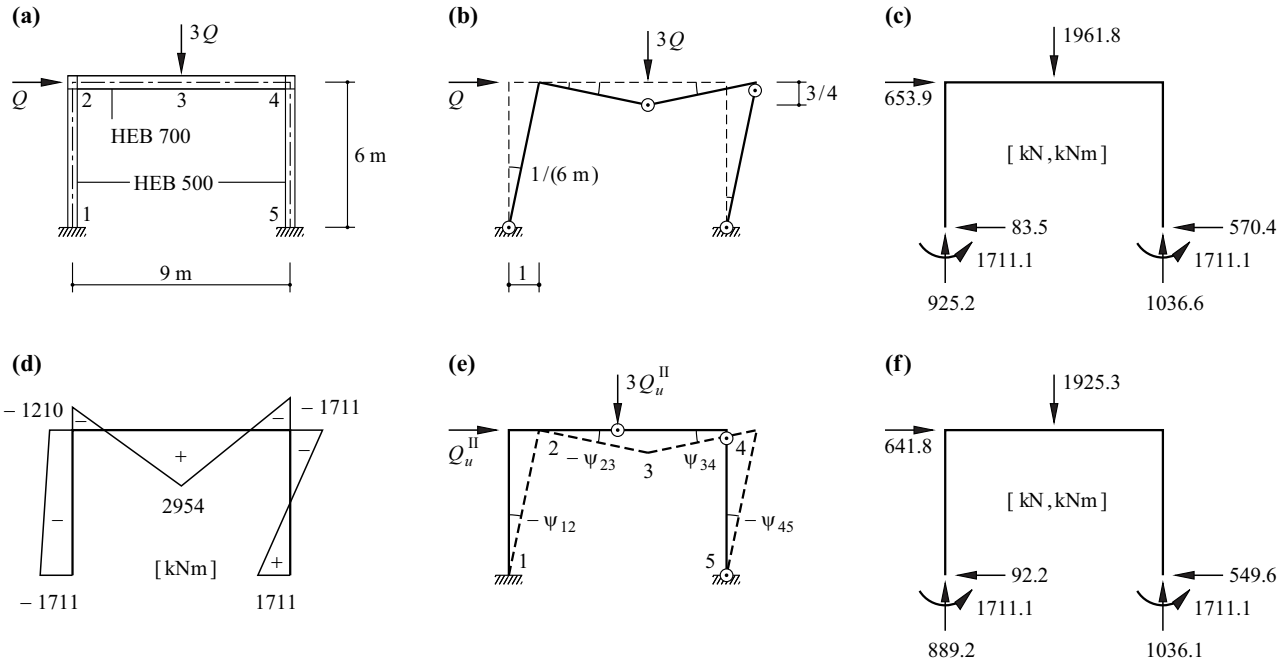

Fig. 22.32 Plane frame: (a) static system, (b) mechanism, (c) free body diagram for Q_u^{I}, (d) bending moments for Q_u^{I}, (e) statically determinate system immediately prior to reaching Q_u^{II}, (f) free body diagram for Q_u^{II}

22.3.3.2 Limit load according to first-order theory

The task is to calculate the limit load of the plane frame shown in Fig. 22.32(a), which is statically indeterminate to the third degree. Using the yield limit $f_y = 355\,\mathrm{N/mm^2}$ and the plastic section moduli $Z_b = 8.32 \cdot 10^6\,\mathrm{mm^3}$ and $Z_c = 4.82 \cdot 10^6\,\mathrm{mm^3}$, the frame beam and the two columns have bending resistances of $M_{ub} = Z_b f_y = 2953.6\,\mathrm{kNm}$ and $M_{uc} = Z_c f_y = 1711.1\,\mathrm{kNm}$. The mechanism of Fig. 22.32(b) supplies the work equation

$$Q \cdot \left(1 + 3 \cdot \frac{3}{4}\right) = (1711.1\,\mathrm{kNm} \cdot 4 + 2953.6\,\mathrm{kNm} \cdot 2)/(6\,\mathrm{m}) = 2125.3\,\mathrm{kN}$$

from which it follows that $Q = 653.9\,\mathrm{kN}$. The free body diagram, Fig. 22.32(c), and the bending moment diagram, Fig. 22.32(d), show that the plasticity check is satisfied, i. e. the limit load according to first-order theory is $Q_u^{\mathrm{I}} = 653.9\,\mathrm{kN}$.

22.3.3.3 Limit load according to second-order theory – approximation via mechanism

By assuming that the plastic hinge at 1 forms last, the displacement of the frame beam upon reaching the limit load – with $E = 210\,\mathrm{kN/mm^2}$ and $I_c = 1.072 \cdot 10^9\,\mathrm{mm^4}$ – according to the work theorem is

$$\frac{1}{6} \cdot 6\,\mathrm{m} \cdot (2 \cdot 1711\,\mathrm{kNm} + 1210\,\mathrm{kNm}) \cdot 6\,\mathrm{m}/(210 \cdot 1.072 \cdot 10^9\,\mathrm{kNmm^2}) = 123.4\,\mathrm{mm}$$

The influence of the inclination of the columns can be approximated by including an additional horizontal force of $3 \cdot 653.9\,\mathrm{kN} \cdot 123.4\,\mathrm{mm}/6000\,\mathrm{mm} = 40.3\,\mathrm{kN}$ in the above work equation:

$$Q_u^{\mathrm{II}} \cdot \left(1 + 3 \cdot \frac{3}{4}\right) + 40.3\,\mathrm{kN} \cdot 1 \approx 2125.3\,\mathrm{kN}$$

which results in $Q_u^{\mathrm{II}} \approx 641.5\,\mathrm{kN}$.

It is not necessary to carry out a full elastic-plastic analysis in order to check our assumption that the plastic hinge at 1 forms last; it is sufficient to calculate the displacements of the frame beam one by one assuming that one of the other plastic hinges

forms last. All of these displacements are smaller than the value of 123.4 mm calculated above and so it is clear that the plastic hinge at 1 is the last one to form.

22.3.3.4 Limit load according to second-order theory – slope-deflection method

The slope-deflection method explained in section 22.2.5 will be used to ascertain the structural behaviour of the statically determinate system immediately prior to the formation of the plastic hinge at 1 more accurately. We shall continue to use the full plastic bending resistances, i. e. we shall neglect the interaction with the normal and shear forces according to (21.43).

Fig. 22.32(e) shows the statically determinate deformed system immediately prior to reaching Q_u^{II}. The unknowns are Q_u^{II}, the joint rotation φ_2 and the two bar rotations $\psi_{12} = \psi_{45}$ and $\psi_{23} = -\psi_{34}$. In order to determine these four unknowns, we have at our disposal the moment equilibrium conditions at joints 1 and 2 as well as the equilibrium conditions for the horizontal and vertical forces applied to the frame beam, or rather at joint 3:

$$t_{12}\varphi_2 - (s_{12} + t_{12})\psi_{12} = M_{uc}$$
$$(s_{21} + r_{23})\varphi_2 - (s_{21} + t_{21})\psi_{12} - r_{23}\psi_{23} + M_{ub}t_{23}/s_{23} = 0$$
$$-(s_{21} + t_{12})\varphi_2/l_{12} + 2(s_{21} + t_{12})\psi_{12}/l_{12} - (C_{12} + C_{45})\psi_{12} - 2M_{uc}/l_{45} + Q_u^{II} = 0$$
$$-r_{23}\varphi_2/l_{23} + r_{23}\psi_{23}/l_{23} - (C_{23} + C_{34})\psi_{23} - M_{ub}(s_{23} + t_{23})/(s_{23}l_{23}) - (M_{ub} + M_{uc})/l_{34} + 3Q_u^{II} = 0$$

Using the basic values given in Tab. 22.5, we get the set of equations

$$\begin{bmatrix} 75.22 & -224.55 & 0 & 0 \\ 508.48 & -224.55 & -359.15 & 0 \\ -37.43 & 72.89 & 0 & 1 \\ -79.81 & 0 & 79.81 & 3 \end{bmatrix} \begin{Bmatrix} \varphi_2 \\ \psi_{12} \\ \psi_{23} \\ Q_u^{II} \end{Bmatrix} = \begin{Bmatrix} 1.7111 \\ -1.4784 \\ 0.5704 \\ 2.0215 \end{Bmatrix}$$

with the solution

$$\varphi_2 = -37.20\,\text{mrad} \quad , \quad \psi_{12} = -20.08\,\text{mrad} \quad , \quad \psi_{23} = -35.99\,\text{mrad} \quad , \quad Q_u^{II} = 641.8\,\text{kN}$$

The corresponding free body diagram is shown in Fig. 22.32(f) – compare this with Fig. 22.32(c). The displacement of the frame beam upon reaching the limit load is $20.08 \cdot 6 = 120.5$ mm, and therefore we get

$$C_{45} = \{641.8 \cdot [6 + (4.5 + 0.1205) \cdot 3] - 2 \cdot 1711.1\}/9 = 1036.1\,\text{kN}$$

and

$$C_{34} = (2 \cdot 1711.1 - 1036.1 \cdot 0.1205)/6 = 549.6\,\text{kN}$$

The compressive forces C given in Tab. 22.5 are based on calculations according to first-order theory. The next step could be to repeat the calculation according to second-order theory using the improved compressive forces $C_{12} = 889$ kN etc. and thus improve the accuracy. This avenue will not be pursued here any further.

Up until now we have ignored the influence of the normal and shear forces, but this is not inconsiderable. To the right of joint 3, with $b_w = 636$ mm, $t_w = 17$ mm, $V \approx 1037$ kN, $-N \approx 550$ kN and $f_y = 355\,\text{N/mm}^2$, the bending resistance is reduced by 85.1 kNm according to (21.43), i. e. it is reduced by 2.9 % to $0.971M_{ub} = 2868.5$ kNm. Similarly, at the ends of column 45, with $b_w = 444$ mm, $t_w = 14.5$ mm, $V \approx 550$ kN, $-N \approx 1037$ kN, we get a decrease of 80.5 kNm, i. e. the bending resistance is reduced by 4.7 % to $0.953M_{uc} = 1630.6$ kNm. Repeating the calculation with lower bending resistances will not be carried out here.

The negative influence of the normal and shear forces is balanced by the positive influence of the finite dimensions of nodal zones 2 and 4. The maximum bending resistances are not required at the theoretical joints, but rather at the boundaries of the nodal zones, where somewhat lower moments occur. The flow of the forces in the nodal zones can be investigated as shown in example 17.7 (Fig. 17.19).

Tab. 22.5 Basic values for using the slope-deflection method

Bar	l	EI	C	λ	$\bar{s}$	$\bar{t}$	$\bar{r}$	s	t	r
12	6	225.1	0.925	0.3846	3.9802	2.0050		149.33	75.22	
23	4.5	539.5	0.570	0.1463	3.9971	2.0007	2.9957	479.21	239.86	359.15
34	4.5	539.5	0.570	0.1463	3.9971	2.0007		479.21	239.86	
45	6	225.1	1.037	0.4072	3.9778	2.0056		149.24	75.24	
	m	MNm^2	MN	-	-	-	-	MNm	MNm	MNm

22.4 Flexural-torsional buckling and lateral buckling

22.4.1 Basic concepts

Let us consider a prismatic, linear elastic bar with any cross-section subjected to an eccentric compressive force C, see Fig. 22.33(a), where C is the centroid, M is the shear centre, x is the bar axis and y, z are the principal axes of the cross-section. We shall assume that deformations do not alter the form of the cross-section.

The shear centre M undergoes the displacements v, w in the directions of the initial axes y_0, z_0, and the cross-section rotates by an amount φ_x about the axis through the shear centre. The displacement components of the centroid C are therefore $v + z_M\varphi_x$ and $w - y_M\varphi_x$, see Fig. 22.33(b), where the eccentric compressive force is related to the origin of the system of coordinates y_0, z_0.

In Fig. 22.33(c) the eccentric compressive force is related to the system of coordinates y,z at any point on the deformed bar axis x. Owing to the inclination of the bar axis, the resulting shear forces in the y and z directions are Cv' and Cw' respectively. The bending moments about the principal axes of the cross-section (ignoring small variables) are

$$M_y = C(-z_A + w - y_M\varphi_x + y_A\varphi_x) \quad , \quad M_z = C(y_A - v - z_M\varphi_x + z_A\varphi_x) \qquad (22.56)$$

Stresses σ distributed over the cross-section and parallel with the x_0 axis correspond to the compressive force C. Owing to the relative rotation $d\varphi_x$ of infinitesimally remote neighbouring cross-sections, the inclination of the fibres amounts to $\rho\varphi_x'$ at a distance ρ from the shear centre, as is shown in Fig. 22.33(c) for a point P on the cross-section in the plane of the cross-section and perpendicular to the plane. Accordingly, besides an elementary normal force, there is also an elementary shear force $-\sigma\rho\varphi_x'dA$ (perpendicular to radius ρ) acting in the plane of the cross-section on a surface element dA connected with point P; the shear force causes an elementary torque of $-\sigma\rho^2\varphi_x'dA$ about the shear centre. In addition to this torque component, there are two other components we must consider:

$$C(y_A w' - z_A v')$$

because of the inclination of the bar axis, and

$$C(v' z_M - w' y_M)$$

because the shear forces Cv' and Cw' are shifted from the centroid to the shear centre. In total, the result is

$$T = C[v'(z_M - z_A) - w'(y_M - y_A)] - \int_A \sigma\rho^2\varphi_x' dA \qquad (22.57)$$

where

$$\rho^2 = (y - y_M)^2 + (z - z_M)^2 \qquad (22.58)$$

and according to (13.18),

$$-\sigma = \frac{C}{A}\left(1 + \frac{z\,z_A}{i_y^2} + \frac{y\,y_A}{i_z^2}\right) \qquad (22.59)$$

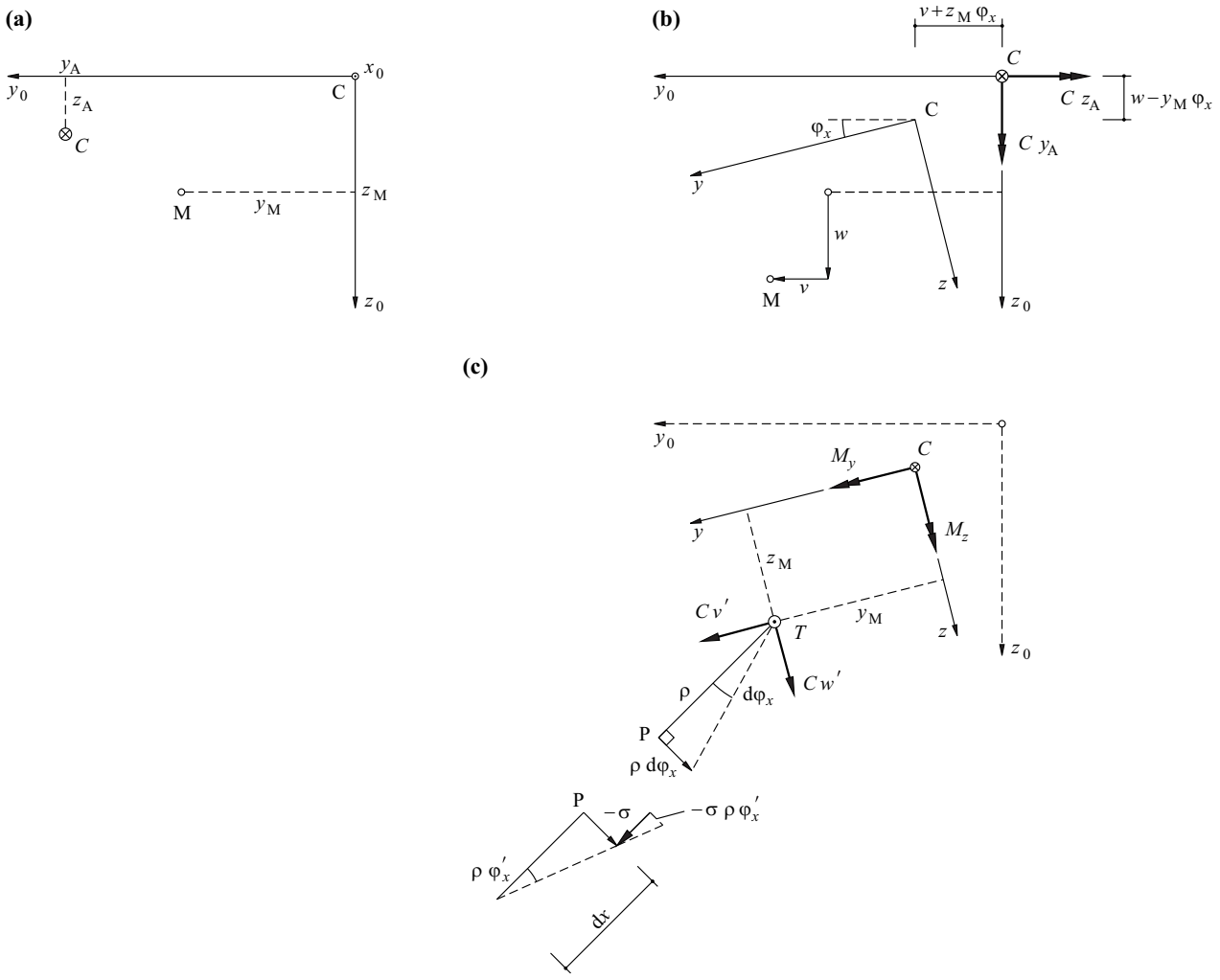

Fig. 22.33 Eccentrically compressed bar cross-section: (a) undeformed position, (b) deformed position (*C* related to y_0, z_0), (c) deformed position (*C* related to *y*, *z*)

Taking into account (13.7) and (13.9), eq. (22.57) therefore gives us

$$T = C\left[v'(z_M - z_A) - w'(y_M - y_A) + \varphi_x'(r_0^2 + s_z z_A + s_y y_A)\right] \tag{22.60}$$

with the shortened forms

$$r_0^2 = y_M^2 + z_M^2 + i_y^2 + i_z^2 \quad , \quad s_z = \frac{\int_A z^3 dA + \int_A y^2 z\, dA}{I_y} - 2z_M \quad , \quad s_y = \frac{\int_A y^3 dA + \int_A y z^2 dA}{I_z} - 2y_M \tag{22.61}$$

Combining (22.56) with (13.8) as well as (8.29) and (22.60) with (13.72) and (13.73) results in the set of differential equations

$$\begin{aligned} &EI_z v'' + C[v + \varphi_x(z_M - z_A)] = Cy_A \\ &EI_y w'' + C[w - \varphi_x(y_M - y_A)] = Cz_A \\ &EI_\omega \varphi_x''' - \varphi_x'\left[GI_x - C(r_0^2 + s_z z_A + s_y y_A)\right] + Cv'(z_M - z_A) - Cw'(y_M - y_A) = 0 \end{aligned} \tag{22.62}$$

22.4.2 Concentric loading

Putting $y_A = z_A = 0$ simplifies (22.62) to the form

$$v'' + \frac{C}{EI_z}(v + \varphi_x z_M) = 0 \quad , \quad w'' + \frac{C}{EI_y}(w - \varphi_x y_M) = 0 \quad , \quad \varphi_x''' - \varphi_x' \frac{GI_x - Cr_0^2}{EI_\omega} + \frac{C}{EI_\omega}(z_M v' - y_M w') = 0 \tag{22.63}$$

22.4.2.1 $y_M = z_M = 0$

Centroids and shear centres coincide in doubly symmetric I or cruciform sections, and in polar symmetric Z sections, too. As $y_M = z_M = 0$, eq. (22.63) results in the independent differential equations

$$v'' + \frac{C}{EI_z}v = 0 \quad , \quad w'' + \frac{C}{EI_y}w = 0 \quad , \quad \varphi_x''' - \varphi_x' \frac{GI_x - Cr_0^2}{EI_\omega} = 0 \tag{22.64}$$

for *flexural buckling* about the z or y axis and *torsional buckling* about the x axis.

By assuming

$$v = v_0 \sin\left(\frac{n\pi x}{l}\right) \quad , \quad w = w_0 \sin\left(\frac{n\pi x}{l}\right) \quad , \quad \varphi_x = \varphi_{x0} \sin\left(\frac{n\pi x}{l}\right)$$

for a simply supported bar of length l with disappearing values for v, v'', w, w'', φ_x and φ_x'' for $x = 0$ and $x = l$, and with $n = 1$ from (22.64), we get the bifurcation loads

$$C_v = \frac{\pi^2 EI_z}{l^2} \quad , \quad C_w = \frac{\pi^2 EI_y}{l^2} \quad , \quad C_\varphi = \frac{1}{r_0^2}\left(GI_x + \frac{\pi^2 EI_\omega}{l^2}\right) \tag{22.65}$$

where $r_0^2 = i_y^2 + i_z^2$.

The lowest value obtained from (22.65) is the critical one. Flexural buckling is always critical for I sections. Torsional buckling can be critical for angle and cruciform sections with $I_\omega = 0$ for small values of l.

22.4.2.2 $y_M \neq 0$ and $z_M \neq 0$

By assuming $v = v_0 \sin(\pi x/l)$, $w = w_0 \sin(\pi x/l)$ and $\varphi_x = \varphi_{x0} \sin(\pi x/l)$ and using (22.65), then (22.63) results in the set of homogeneous linear equations

$$\begin{bmatrix} C - C_v & 0 & Cz_M \\ 0 & C - C_w & -Cy_M \\ Cz_M & -Cy_M & r_0^2(C - C_\varphi) \end{bmatrix} \begin{Bmatrix} v_0 \\ w_0 \\ \varphi_{x0} \end{Bmatrix} = \begin{Bmatrix} 0 \\ 0 \\ 0 \end{Bmatrix} \tag{22.66}$$

for a bar simply supported at both ends. The determinant of this matrix

$$\begin{aligned} \text{Det} = {} & C^3(r_0^2 - y_M^2 - z_M^2) - C^2\left[r_0^2(C_v + C_w + C_\varphi) - y_M^2 C_v - z_M^2 C_w\right] \\ & + Cr_0^2(C_v C_w + C_w C_\varphi + C_\varphi C_v) - r_0^2 C_v C_w C_\varphi \end{aligned} \tag{22.67}$$

must be equal to zero for a non-trivial solution.

If we assume that $C_v < C_w < C_\varphi$, then (22.67) results in the value of the function Det being negative at positions 0, C_w, C_φ, and positive at position C_v; $C_1 < C_v$ applies for the critical, lowest zero point, see Fig. 22.34. The determinant can be examined in a similar way for other sequences of flexural and torsional buckling loads, and the eigenvalues C_i can be determined numerically in every case.

We can see from the first two equations (22.66) that the outcome is fixed relationships $v_0/\varphi_{x0} = v/\varphi_x = -z_M/(1 - C/C_v)$ and $w_0/\varphi_{x0} = w/\varphi_x = y_M/(1 - C/C_v)$, i. e. the bar buckles in a very particular way.

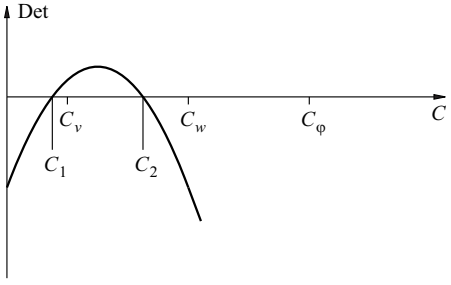

Fig. 22.34 Investigating the determinant (22.67)

22.4.2.3 $y_M = 0$

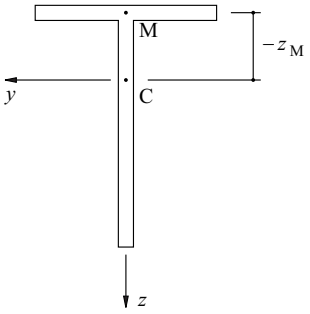

Fig. 22.35 shows two examples of singly symmetric sections with $y_M = 0$. In such cases $C_1 = C_w$ irrespective of the flexural-torsional buckling loads C_2 and C_3 determined by C_v and C_φ. Eq. (22.67) simplifies to

$$\text{Det} = r_0^2(C - C_v)(C - C_\varphi) - C^2 z_M^2 \tag{22.68}$$

and from Det = 0 we get

$$C_{2,3} = \frac{C_v + C_\varphi \mp \sqrt{(C_v + C_\varphi)^2 - 4C_v C_\varphi \left[1 - (z_M/r_0)^2\right]}}{2\left[1 - (z_M/r_0)^2\right]} \tag{22.69}$$

The smaller of the two values C_1 and C_2 governs.

22.4.3 Eccentric loading in the strong plane

22.4.3.1 General

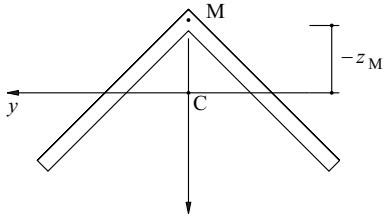

Fig. 22.35 Singly symmetric sections

If $I_y \gg I_z$ and $y_A = 0$, then (22.62) simplifies to

$$\begin{aligned} &v'' + \frac{C}{EI_z}[v + \varphi_x(z_M - z_A)] = 0 \\ &\varphi_x''' - \varphi_x' \left[\frac{GI_x}{EI_\omega} - \frac{C(r_0^2 + s_z z_A)}{EI_\omega}\right] + \frac{Cv'(z_M - z_A)}{EI_\omega} = 0 \end{aligned} \tag{22.70}$$

Displacement w is small in comparison with the deformations due to v und φ_x, and therefore $(22.62)_2$ can be ignored.

Fig. 22.36(a) illustrates a general case and Fig. 22.36(b) three special cases: $y_M = z_M = 0$, $r_0^2 = i_y^2 + i_z^2$ and $s_z = 0$ apply for the symmetrical I section; $y_M = 0$, $r_0^2 = z_M^2 + i_y^2 + i_z^2$ and $s_z \neq 0$ apply for the T section; $z_M = 0$, $r_0^2 = y_M^2 + i_y^2 + i_z^2$ and $s_z = 0$ apply for the channel section.

Sinusoidal formulations for v and φ_x lead to

$$\begin{bmatrix} C - C_v & C(z_M - z_A) \\ C(z_M - z_A) & r_0^2\left[C\left(1 + \dfrac{s_z z_A}{r_0^2}\right) - C_\varphi\right] \end{bmatrix} \begin{Bmatrix} v_0 \\ \varphi_{x0} \end{Bmatrix} = \begin{Bmatrix} 0 \\ 0 \end{Bmatrix} \tag{22.71}$$

for a bar simply supported at both ends, where

$$\text{Det} = r_0^2(C - C_v)\left[C\left(1 + \frac{s_z z_A}{r_0^2}\right) - C_\varphi\right] - C^2(z_M - z_A)^2 \tag{22.72}$$

Apart from the case of two positive roots to the characteristic equation Det = 0, as shown in Fig. 22.36(c), it is also possible to have the situation with one positive and one negative root, as shown in Fig. 22.36(d). The relationship $v/\varphi_x = -(z_M - z_A)/(1 - C/C_v)$ reveals how the bar deflects sideways in the event of flexural-torsional buckling; e. g. the cross-section of Fig. 22.36(d) rotates about a fulcrum beneath the beam as a result of the eccentric tensile force $-C_2$.

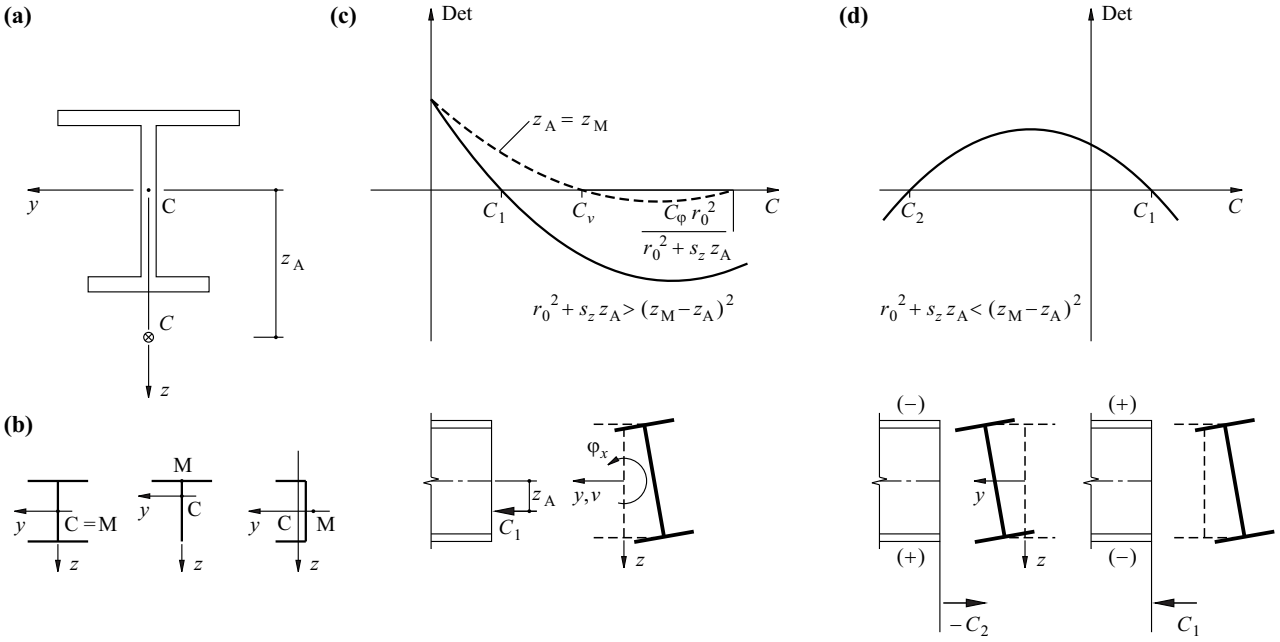

Fig. 22.36 Eccentric compression in the strong plane: (a) notation, (b) special cases, (c) and (d) examining the determinant (22.72) and buckling modes for $z_M = s_z = 0$

22.4.3.2 Special case $z_A = z_M$

Applying C at the shear centre results in the greatest possible bifurcation load compared with all possible loading positions, i. e. either C_v or $C_\varphi/(1 + s_z z_A/r_0^2)$, see Fig. 22.36(c).

22.4.3.3 Lateral buckling

If we allow the compressive force C to tend to zero for a constant moment $M_y = M = Cz_A$, then (22.72) results in the quadratic equation

$$M^2 + MC_v s_z - r_0^2 C_v C_\varphi = 0$$

with the solutions

$$M_{1,2} = \frac{1}{2}\left(-C_v s_z \pm \sqrt{C_v^2 s_z^2 + 4r_0^2 C_v C_\varphi}\right) \tag{22.73}$$

The result is positive and negative critical moments with different values when $s_z \neq 0$. And when $s_z = 0$, the result – making use of $(22.65)_1$ and $(22.65)_3$ – is the *overturning moments*

$$M_{cr} = \pm\, r_0 \sqrt{C_v C_\varphi} = \pm \frac{\pi}{l}\sqrt{EI_z\left(GI_x + \frac{\pi^2 EI_\omega}{l^2}\right)} \tag{22.74}$$

Using $(13.9)_2$, $(13.9)_3$, (13.64) and (13.72) for the model cross-section of an I section shown in Fig. 22.25(a) results in

$$I_y = \frac{b\,t\,h^2}{2} \quad , \quad I_z = \frac{b^3 t}{6} \quad , \quad I_x = \frac{2b\,t^3}{3} \quad , \quad I_\omega = \frac{I_z h^2}{4} = \frac{b^3 t\,h^2}{24}$$

and therefore according to (13.16), (22.74) and (7.2),

$$\sigma_{cr} = \frac{M_{cr}}{I_y}\cdot\frac{h}{2} = E\frac{b\,t}{h\,l}\cdot\sqrt{\frac{\pi^2}{18(1+\nu)}}\cdot\sqrt{1 + \frac{\pi^2(1+\nu)}{8}\cdot\left(\frac{b\,h}{l\,t}\right)^2} \tag{22.75}$$

By ignoring the first compared with the second term in the second root, the result is the approximation

$$\sigma_{cr} \approx \frac{\pi^2 E b^2}{12 l^2} = E\left(\frac{\pi\, i_z}{l}\right)^2 \tag{22.76}$$

which shows that the lateral buckling of a beam essentially corresponds to the lateral buckling of its compression flange, see Fig. 22.24 and (22.44).

22.4.3.4 Special case $y_M = z_M = s_z = 0$

In the case of doubly symmetric cross-sections, e. g. I sections, using $M = Cz_A$ from (22.72) with Det = 0 results in the relationship

$$M^2 = r_0^2(C - C_v)(C - C_\varphi)$$

which in conjunction with $(22.74)_1$ leads to the interaction relationship

$$\left(\frac{M}{M_{cr}}\right)^2 = \left(1 - \frac{C}{C_v}\right)\left(1 - \frac{C}{C_\varphi}\right) \tag{22.77}$$

between the bending moments M and the compressive forces C, as shown in Fig. 22.37. When we consider cross-sections with a very large torsional stiffness, e. g. hollow sections, then $C_\varphi \gg C_v$, and therefore the interaction relationship is parabolic. With a smaller torsional stiffness it can be the case, for instance, that $C_\varphi = C_v$, which corresponds to a linear interaction relationship.

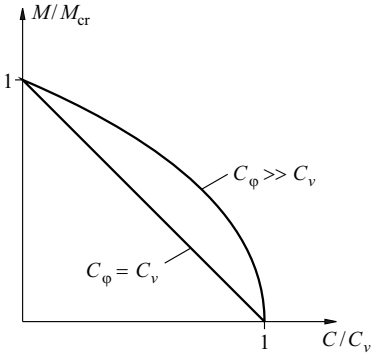

Fig. 22.37 Interaction between bending moments and compressive forces for doubly symmetric cross-sections

22.4.4 General loading

22.4.4.1 Basic concepts

Besides the eccentric compressive force C, which is still presumed to be constant over the length of the bar, it is also generally necessary to consider eccentric line loads q_y und q_z, see Fig. 22.38; the corresponding bending moments are designated with M_{yq}, M_{zq}. Eq. (22.62) is generalised as follows:

$$\begin{aligned}
&EI_z v'''' + Cv'' + C(z_M - z_A)\varphi_x'' + (M_{yq}\varphi_x)'' - M_{zq}'' = 0\\
&EI_y w'''' + Cw'' - C(y_M - y_A)\varphi_x'' + M_{yq}'' + (M_{zq}\varphi_x)'' = 0\\
&EI_\omega \varphi_x'''' - \left[GI_x - C(r_0^2 + s_z z_A + s_y y_A)\right]\varphi_x'' - s_z(M_{yq}\varphi_x')' + s_y(M_{zq}\varphi_x')'\\
&\qquad + \left[M_{yq} + C(z_M - z_A)\right]v'' + \left[M_{zq} - C(y_M - y_A)\right]w''\\
&\qquad + q_y(e_z + e_y\varphi_x) - q_z(e_y - e_z\varphi_x) = 0
\end{aligned} \tag{22.78}$$

Moments M_{yq} and M_{zq} result in the additional terms $M_{zq} - M_{yq}\varphi_x$ and $-M_{yq} - M_{zq}\varphi_x$ on the right-hand sides of $(22.62)_1$ and $(22.62)_2$; differentiating twice thus results in $(22.78)_1$ and $(22.78)_2$. Similarly to $s_z C z_A \varphi_x'$ and $s_y C y_A \varphi_x'$, we get the terms $-s_z M_{yq}\varphi_x'$ and $s_y M_{zq}\varphi_x'$ contributing to T in (22.60) and $(22.62)_3$; differentiating once results in the third and fourth terms on the left in $(22.78)_3$. The curvature of the bar corresponds to a contribution of $-(M_{yq}v'' + M_{zq}w'')$ to m_x according to (13.74), and considering Fig. 22.38 results in the other contribution $-q_y(e_z + e_y\varphi_x) + q_z(e_y - e_z\varphi_x)$ to m_x; therefore, $(22.78)_3$ is fully explained as well.

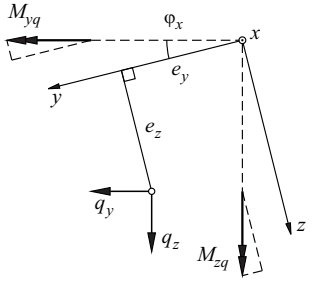

Fig. 22.38 Line loads and associated bending moments

22.4.4.2 Commentary

It is often necessary to consider the interaction of various structural members. For example, the roof covering generally guarantees a certain amount of support for the roof structure. This can be modelled as an elastic support with translational and rotational springs. Appropriate additional terms are necessary in (22.78).

The axis of twist is often not free, but rather constrained by some constructional means, e. g. some form of hinge. The kinematic constraint leads to a corresponding simplification of the set of differential equations (22.78); for example, v can be eliminated.

Solving general flexural-torsional and lateral buckling problems is difficult. Analytical solutions are successful in special cases only. Numerical approximation methods should normally be employed, see section 22.2.3.

Example 22.15 Lateral buckling of an I section

Fork supports at the ends of the doubly symmetric I section shown in Fig. 22.39 ($y_M = z_M = s_z = 0$) prevent the beam from rotating (see example 13.12). The point load Q at mid-span causes pure bending about the y axis, where

$$M_{yq} = \frac{Qx}{2} \qquad (0 \le x \le l/2)$$

Eq. $(22.78)_1$ and $(22.78)_2$ simplify to

$$EI_z v'' + M_{yq}\varphi_x = 0 \quad , \quad EI_\omega \varphi_x'''' - GI_x \varphi_x'' + M_{yq} v'' = 0$$

from which it follows that

$$EI_\omega \varphi_x'''' - GI_x \varphi_x'' - \frac{M_{yq}^2}{EI_z}\varphi_x = 0 \tag{22.79}$$

Setting

$$\varphi_x = c \, \sin\left(\frac{\pi x}{l}\right)$$

satisfies the boundary conditions $\varphi_x(0) = \varphi_x''(0) = \varphi_x(l) = \varphi_x''(l) = 0$, and therefore using the GALERKIN method and omitting the non-essential factor $2c^2$, we get the condition

$$\int_0^{l/2} \left[EI_\omega \left(\frac{\pi}{l}\right)^4 + GI_x \left(\frac{\pi}{l}\right)^2 - \frac{Q^2 x^2}{4EI_z} \right] \sin^2\left(\frac{\pi x}{l}\right) \mathrm{d}x = 0$$

for the bifurcation load, or rather the overturning moment. Using

$$\int_0^{l/2} \sin^2\left(\frac{\pi x}{l}\right) \mathrm{d}x = \frac{l}{4} \quad , \quad \int_0^{l/2} x^2 \sin^2\left(\frac{\pi x}{l}\right) \mathrm{d}x = \frac{l^3}{48} + \frac{l^3}{8\pi^2}$$

results in the approximation

$$\left(\frac{Ql}{4}\right)_{cr} \approx \frac{4.291}{l} \sqrt{EI_z \left(GI_x + \frac{\pi^2 EI_\omega}{l^2} \right)} \tag{22.80}$$

see (22.74). The factor 4.291 lies about 1.3 % above the known exact value of 4.234.

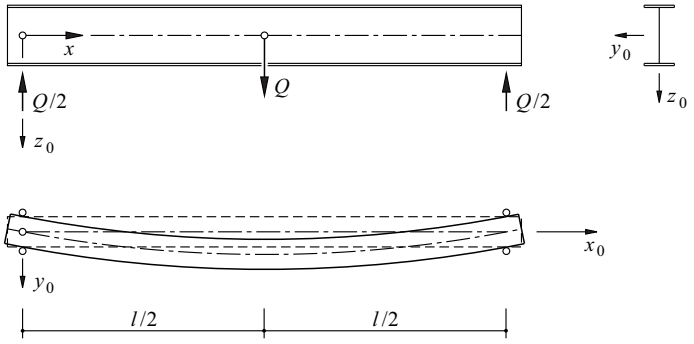

Fig. 22.39 Lateral buckling of a symmetrical I section subjected to a central point load

Example 22.16 Lateral buckling – shifting the point of load application

It was assumed in example 22.15 that Q is applied at the level of the bar axis. However, if the point of load application is above or below this, the result is a destabilising or stabilising influence. This effect increases as the pure torsional stiffness GI_x decreases in relation to the warping torsion stiffness EI_ω/l^2 related to the square of the span l.

Lateral buckling increases the internal potential by

$$\Delta\Pi_i = \frac{EI_z}{2}\int_0^l v''^2 \, \mathrm{d}x + \frac{GI_x}{2}\int_0^l \varphi_x'^2 \, \mathrm{d}x + \frac{EI_\omega}{2}\int_0^l \varphi_x''^2 \, \mathrm{d}x$$

The third term on the right in this relationship follows from integrating over the whole system with $\pi_i = \sigma_w^2/(2E)$ according to (13.92), (13.90) and (13.89) as well as $\vartheta = \varphi_x'$. According to Fig. 22.40, the point of application of Q rises with lateral buckling by the amount

$$z_Q(1 - \cos\varphi_{x0}) + \int_0^{l/2} \varphi_x x \, v'' \mathrm{d}x \approx \frac{z_Q \varphi_{x0}^2}{2} + \int_0^{l/2} \varphi_x x \, v'' \mathrm{d}x$$

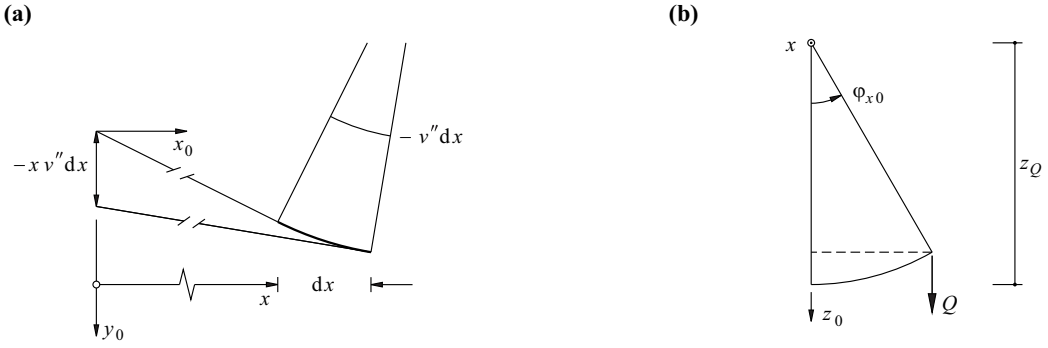

Fig. 22.40 Shifting the point of load application of Fig. 22.39: (a) plan, (b) rotation $\varphi_{x0} = \varphi_x(l/2)$

and therefore the external potential, taking into account $\varphi_x = -2EI_z v''/(Qx)$, increases by

$$\Delta\Pi_e = \frac{Qz_Q\varphi_{x0}^2}{2} + Q\int_0^{l/2}\varphi_x x\,v''\,dx = \frac{Qz_Q\varphi_{x0}^2}{2} - 2EI_z\int_0^{l/2}v''^2\,dx$$

According to the theorem of least total potential, $\Delta\Pi_e + \Delta\Pi_i = 0$, and therefore

$$-\frac{Qz_Q\varphi_{x0}^2}{2} + EI_z\int_0^{l/2}v''^2\,dx = GI_x\int_0^{l/2}\varphi_x'^2 x\,dx + EI_\omega\int_0^{l/2}\varphi_x''^2\,dx$$

or rather

$$-\frac{Qz_Q\varphi_{x0}^2}{2} + \frac{Q^2}{4EI_z}\int_0^{l/2}x^2\varphi_x^2\,dx = GI_x\int_0^{l/2}\varphi_x'^2 x\,dx + EI_\omega\int_0^{l/2}\varphi_x''^2\,dx$$

Assuming $\varphi_x = c\sin(\pi x/l)$, this leads to the quadratic equation

$$Q_{cr}^2\cdot\frac{l^2}{8EI_z}\left(\frac{1}{6}+\frac{1}{\pi^2}\right) - Q_{cr}\frac{2z_Q}{l} - \frac{\pi^2}{l^2}\left(GI_x + \frac{\pi^2 EI_\omega}{l^2}\right) = 0$$

for Q_{cr}. Applying $(13.72)_2$ results in

$$Q_{cr} = \frac{8\pi^2 EI_z d\left[\alpha + \sqrt{\alpha^2 + (1+\pi^2/6)(\beta+\pi^2)/8}\right]}{l^3(1+\pi^2/6)} \qquad \left(\alpha = \frac{z_Q}{d/2}\ ,\ \beta = \frac{4GI_x l^2}{EI_z d^2}\right) \tag{22.81}$$

where d = spacing of flanges.

Tab. 22.6 specifies the relationships $Q_{cr}(\alpha)/Q_{cr}(\alpha = 0)$ for a number of values of β depending on whether Q is applied to the top flange ($\alpha = -1$), at the centroid ($\alpha = 0$) or to the bottom flange ($\alpha = 1$).

Tab. 22.6 Relative overturning loads according to (22.81) depending on the position of the point of load application (α) and the stiffness ratio (β)

β	($\alpha = -1$)	($\alpha = 0$)	($\alpha = 1$)
0	0.589	1	1.697
5	0.646	1	1.548
10	0.683	1	1.464
20	0.731	1	1.368
40	0.784	1	1.276
80	0.833	1	1.200
160	0.875	1	1.142
320	0.909	1	1.100

22.5 Summary

1. This chapter deals with problems in framed structures in which the equilibrium conditions have to be formulated for the deformed system according to second-order theory.
2. Elastic deflection curves for inextensible columns are described by the differential equation (22.2) or (22.9) with the boundary conditions (22.6). Analytical solutions are confined to special cases.
3. An initial deformation in a column has an effect similar to that of a transverse load.
4. The second-order influences on the deformations and stress resultants of columns can be approximated by multiplying the values calculated according to first-order theory by the amplification factor (22.12). This procedure supplies exact results for the case of deflection curves affine with first- and second-order theory.
5. The application of the amplification factor presumes that the theoretical bifurcation load is known. The latter can be calculated with the help of the RAYLEIGH quotient (22.14), with the RITZ or GALERKIN methods, or with the method of successive approximation of the column deflection curve according to ENGESSER-VIANELLO; in contrast to the other methods, the ENGESSER-VIANELLO method can also supply approximate values that lie below the theoretically exact bifurcation load.
6. Structural analyses according to second-order theory generally require an iterative procedure. The normal forces initially estimated or calculated according to first-order theory for the individual columns of a system are improved in one or more steps by taking into account the deformation influences.
7. Problems with variable-direction, but nevertheless guided, forces are conservative and can be handled according to the customary methods of elastic stability theory. One particularly dangerous example of this type of problem relevant in practical construction situations ensues from connecting columns to short pin-jointed members (Fig. 22.10).
8. The influence of shear deformations can be considerable in the case of built-up columns. In addition, the flexibility of the connectors must be considered in built-up timber columns.
9. Shallow arches and inclined leg frames can experience snap-through. The equilibrium position upon reaching the snap-through load – in contrast to that upon reaching a bifurcation load – is not neutral, but rather divergent.
10. There is a linear relationship (22.31) between the compressive forces related to the bifurcation loads and the squares of the basic frequency-related frequencies of the bending vibrations of elastic columns.
11. The slope-deflection method can be applied in a similar way to first-order theory when dealing with second-order problems. The effect of the deformation is included in the near- and far-end bar stiffnesses by way of the axial force parameter (22.32). The stiffening influence of tensile forces is often neglected, but can be dealt with easily by changing from harmonic to hyperbolic functions.
12. The non-linear member stiffness matrix (22.39) according to second-order theory can be presented as the sum of the linear member stiffness matrix (17.17) according to first-order theory and the geometric stiffness matrix (22.41).
13. An analysis according to third-order theory may be necessary in the case of very flexible systems. Such an analysis is generally performed with an incremental, iterative procedure in which several load steps are employed to update the global tangential stiffness matrix related to the last deformation state by iterating the equilibrium.
14. Buckling stress curves plotted against the relative slenderness can be used to ascertain how geometric imperfections and residual stresses influence the buckling of concentrically loaded columns (Fig. 22.24).

15. With known non-linear moment-curvature diagrams, the deflection curves of eccentrically loaded columns can generally be determined through discretisation and by employing an incremental, iterative procedure. As an approximation, the secant stiffness in the most highly stressed cross-section can be used in conjunction with the amplification factor.
16. The limit loads of frames can be analysed according to second-order theory by considering the statically determinate deformed system immediately prior to the development of the final plastic hinge.
17. Flexural-torsional and lateral buckling problems of elastic bars are generally described by way of the differential equations (22.62) and (22.78). These are normally solved with the help of numerical approximation methods.

22.6 Exercises

22.1 Replace the point load Q_2 in example 22.1 by a uniformly distributed transverse load q. Conduct a similar discussion and compare the result with example 8.16.

22.2 Confirm the expression

$$\sqrt[3]{\frac{7.834EI}{A\rho g}}$$

for the critical length of a prismatic vertical cantilever that buckles under its self-weight (EI = bending stiffness, A = cross-sectional area, ρ = density of column material, g = acceleration due to gravity = $9.81\,\mathrm{m/s^2}$). Compare the corresponding critical lengths of columns made from steel ($\rho = 7850\,\mathrm{kg/m^3}$, $E = 210\,\mathrm{kN/mm^2}$) and timber ($\rho = 500\,\mathrm{kg/m^3}$, $E = 10\,\mathrm{kN/mm^2}$) with solid or hollow circular cross-sections.

22.3 Develop an expression for the bifurcation load of the system shown in Fig. 22.41(a). Discuss the limiting cases $k_y = 0$ or $k_y \to \infty$ and $k_z = 0$ or $k_z \to \infty$ and $EI \to \infty$.

22.4 Show that the buckling load of a prismatic column with hinged supports at both ends (bending stiffness EI = const, length l) is $18.67\,EI/l^2$ for an axial force acting at half height. Solve this task exactly first of all and then using the ENGESSER-VIANELLO method.

22.5 Calculate the bifurcation load of the system shown in Fig. 22.41(b) ($E = 210\,\mathrm{kN/mm^2}$, $I_{AB} = 21.86 \cdot 10^6\,\mathrm{mm^4}$, $I_{BC} = 14.99 \cdot 10^6\,\mathrm{mm^4}$) by means of the method according to ENGESSER-VIANELLO.

22.6 Discuss the behaviour of the system shown in Fig. 22.41(c) in a similar way to example 22.10. The two pin-jointed members of length l are initially inclined at an angle α_0 to the horizontal and may be regarded as rigid ($EA \to \infty$).

22.7 Add an equation to (22.33) for the case of a temperature gradient ΔT over the depth of the beam h (coefficient of thermal expansion α_T).

22.8 Add an equation to each of the equations $(22.38)_4$ and $(22.38)_6$ for the case $\alpha = 1$ assuming an elastic fixed support to the cantilever (rotational spring stiffness k_y).

22.9 Calculate the bifurcation load of the system shown in Fig. 22.41(d) as a function of parameter α.

22.10 Examine the buckling in the plane of the equilateral frame shown in Fig. 22.41(e). The stiffening influence of the tensile force in bar 12 may be neglected.

22.11 Rework exercise 22.5 using the slope-deflection method.

22.12 Select a suitable column for the problem of Fig. 22.41(f) and discuss its behaviour with the help of the slope-deflection method.

22.13 The intermediate supports in the system of Fig. 22.41(f) are elastically supported (translational spring stiffnesses k_{z2} and k_{z3}), but the column is fully fixed at its base 1. Set up the set of equations for the unknown deformations according to the slope-deflection method.

22.14 Discuss the behaviour of the system shown in Fig. 22.41(g). First of all, cables 14 and 34 are prestressed to the tensile force T_0. Afterwards, Q is increased monotonically. The normal force deformations of bar 24 may be neglected. Select suitable cross-sections for the case of $Q = 1\,\text{MN}$, $l = 10\,\text{m}$, $\alpha = 0.6$, $\beta = 30°$, specify a suitable prestress and analyse the structural behaviour for an increasing value of Q.

22.15 Calculate the limit load according to second-order theory for the frame shown in Fig. 22.41(h). Column 12 has a bending stiffness of $52.9\,\text{MNm}^2$ and a bending resistance of 663 kNm; the respective values for frame beam 23 are $359.1\,\text{MNm}^2$ and 2279 kNm.

22.16 Replace the pin-ended strut 34 in exercise 22.15 by a sliding support and work through the problem again.

22.17 Develop an equation similar to (22.80) for the overturning moment of a simply supported beam subjected to a uniformly distributed load. Compare the resulting numerical factor with the known exact value of 3.538.

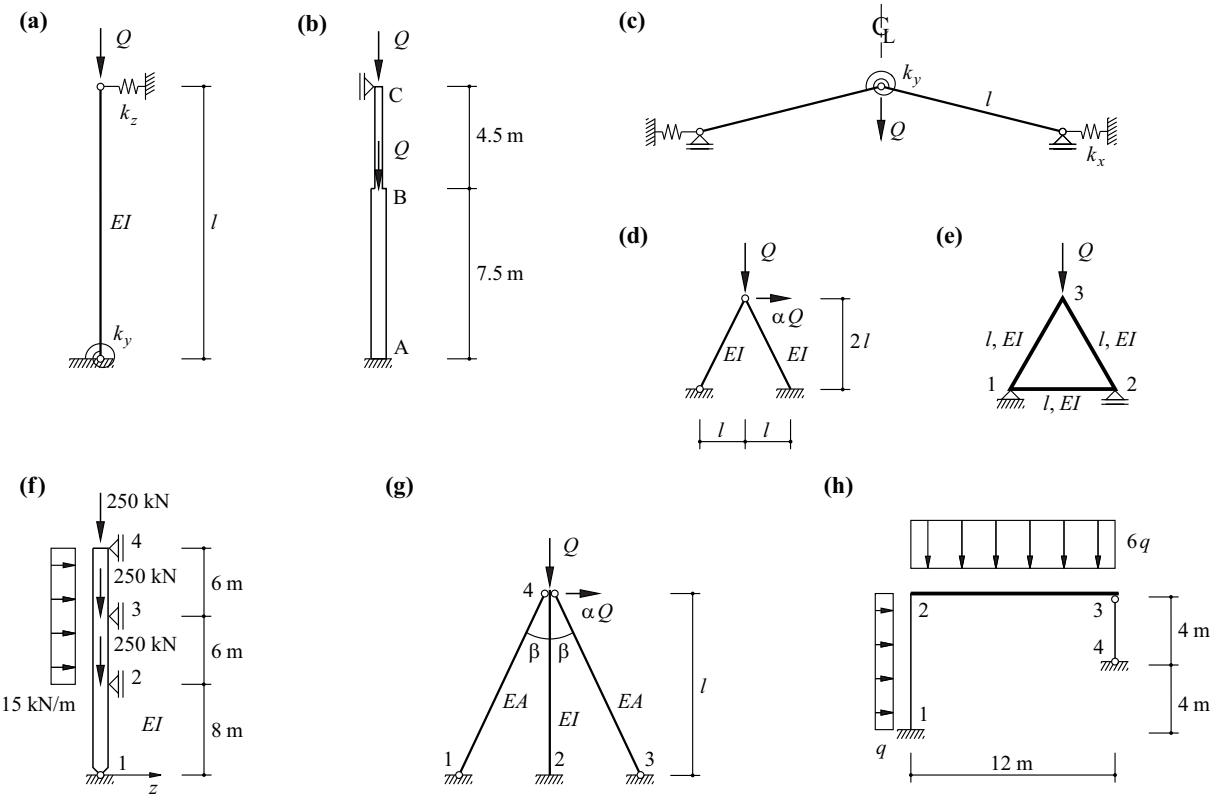

Fig. 22.41 Diagrams of static systems for section 22.6

23 PLATES

23.1 General

Plates (= in-plane-loaded elements) are very important in construction – as loadbearing walls and as parts of built-up sections (box girders, plate girders, folded plates). Furthermore, the structural response of slabs (= out-of-plane-loaded elements) can be reduced to the structural response of plates by applying sandwich models.

The equilibrium conditions (8.32) and the kinematic relations (8.33) for plates were set up in section 8.2.4. The result for homogenous and isotropic, linear elastic plates was (8.35). In addition, the yield loci according to VON MISES and TRESCA for the coplanar stress state were shown in Fig. 7.8(c) (see also exercise 7.8), and the COULOMB yield condition, the modified COULOMB yield condition and the square yield condition for the coplanar stress state were discussed with the help of Figs. 7.10(b), 7.11(b) and 7.12(b).

Linear elastic analyses of plate problems essentially make use of the finite element method. Analytical solutions, briefly explained in section 23.2, are still important for a basic understanding of the structural behaviour of plates. Moreover, such solutions supply valuable reference figures and render possible quick estimates of the stress resultants for practical situations, e. g. at points of load application or at geometric discontinuities such as corners and openings.

Modelling plates as linear elastic elements is applicable to only a limited extent in structural design. Plates made from reinforced concrete in particular exhibit a distinctly non-linear behaviour owing to the cracking of the concrete and the yielding of the reinforcement. Section 23.3 describes appropriate yield conditions for plate elements and sections 23.4 and 23.5 discuss the application of the static and kinematic methods of limit analysis to reinforced concrete plates and related problems in geotechnical engineering.

23.2 Elastic plates

23.2.1 Stress function

Differentiating the relationships (8.33) twice gives us the *compatibility condition*

$$\frac{\partial^2 \varepsilon_x}{\partial y^2} + \frac{\partial^2 \varepsilon_y}{\partial x^2} = \frac{\partial^2 \gamma_{xy}}{\partial x \partial y} \tag{23.1}$$

Using (8.34) and integrating the stresses over the thickness of the plate h leads to

$$\frac{\partial^2}{\partial y^2}(n_x - \nu n_y) + \frac{\partial^2}{\partial x^2}(n_y - \nu n_x) = 2(1+\nu)\frac{\partial^2 n_{xy}}{\partial x \partial y}$$

Differentiating $(8.32)_1$ and $(8.32)_2$ with respect to x or y and adding the two expressions results in

$$-\left(\frac{\partial q_x}{\partial x} + \frac{\partial q_y}{\partial y}\right) - \frac{\partial^2 n_x}{\partial x^2} - \frac{\partial^2 n_y}{\partial y^2} = 2\frac{\partial^2 n_{xy}}{\partial x \partial y}$$

Theory of Structures. First Edition. Peter Marti

and substituting in the previous relationship gives us

$$\Delta(n_x + n_y) = -(1+\nu)\left(\frac{\partial q_x}{\partial x} + \frac{\partial q_y}{\partial y}\right) \tag{23.2}$$

see also (24.28).

If we assume that the loads have a potential Π_e, i. e.

$$q_x = -\frac{\partial \Pi_e}{\partial x} \quad , \quad q_y = -\frac{\partial \Pi_e}{\partial y}$$

the equilibrium conditions (8.32) then become

$$\frac{\partial}{\partial x}(n_x - \Pi_e) + \frac{\partial n_{xy}}{\partial y} = 0 \quad , \quad \frac{\partial}{\partial y}(n_y - \Pi_e) + \frac{\partial n_{xy}}{\partial x} = 0$$

Introducing the AIRY *stress function F*, where

$$\frac{\partial^2 F}{\partial y^2} = n_x - \Pi_e \quad , \quad \frac{\partial^2 F}{\partial x^2} = n_y - \Pi_e \quad , \quad \frac{\partial^2 F}{\partial x \partial y} = -n_{xy} \tag{23.3}$$

satisfies the equilibrium conditions, and substituting (23.3) in (23.2) results in

$$\Delta\Delta F = -(1-\nu)\Delta\Pi_e \tag{23.4}$$

If q_y corresponds to the dead load $\rho g h$ (ρ = density, g = acceleration due to gravity), then $\Pi_e = -\rho g h y$, and the right-hand side of (23.4) equals zero. Generally, the bipotential equation

$$\Delta\Delta F = 0 \tag{23.5}$$

applies for $\boldsymbol{q}$ = **const**. Eq. (23.5) is satisfied by polynomials up to the third degree for x and y and x^3y and xy^3 with any coefficients. For higher-degree polynomials, the coefficients must comply with certain conditions in order to satisfy (23.5). Further solutions can be obtained, for example, by using FOURIER series with the following types of function:

$$F_n = \sin\left(\frac{n\pi x}{l}\right) \cdot \left[c_1 \cosh\left(\frac{n\pi y}{l}\right) + c_2 \sinh\left(\frac{n\pi y}{l}\right) + c_3 y \cosh\left(\frac{n\pi y}{l}\right) + c_4 y \sinh\left(\frac{n\pi y}{l}\right)\right] \tag{23.6}$$

Example 23.1 Cantilever beam

If we use the stress function

$F = Axy + Bxy^3$

for the plate shown in Fig. 23.1(a), then (23.3) results in

$n_x = 6Bxy \quad , \quad n_y = 0 \quad , \quad n_{xy} = n_{yx} = -A - 3By^2$

The boundary conditions $n_{xy} = 0$ for $y = \pm b/2$ call for $A = -3Bb^2/4$, and the following applies for the shear force:

$$Q = -\int_{-b/2}^{b/2} n_{yx}\,\mathrm{d}y = -3B\int_{-b/2}^{b/2}\left(\frac{b^2}{4} - y^2\right)\mathrm{d}y = -\frac{Bb^3}{2}$$

Consequently,

$$n_x = -\frac{Qxy}{b^3/12} \quad , \quad n_y = 0 \quad , \quad n_{xy} = -\frac{3Q}{2b}\left(1 - \frac{4y^2}{b^2}\right)$$

The stresses distributed uniformly over the thickness of the plate h – Fig. 23.1(b) – agree with those of beam theory, see (13.16) and example 13.5. However, n_{yx} must exhibit a parabolic distribution over depth b at the ends of the plate $x = 0$ and $x = a$.

Substituting the stress components in (8.35) and inverting – together with (8.33) and $I = hb^3/12$ – results in

$$\frac{\partial u}{\partial x} = -\frac{Qxy}{EI} \quad , \quad \frac{\partial v}{\partial y} = \frac{\nu Qxy}{EI} \quad , \quad \frac{\partial u}{\partial y} + \frac{\partial v}{\partial x} = -\frac{3Q(1+\nu)}{Ebh}\left(1 - \frac{4y^2}{b^2}\right)$$

The integration of these differential equations, taking into account the boundary conditions $u(a, 0) = v(a, 0) = 0$ and $u(a, \pm b/2) = 0$, results in the displacements

$$u = \frac{Q(a^2 - x^2)y}{2EI} + \frac{(2+\nu)Q(4y^3 - b^2 y)}{24EI}$$

$$v = \frac{Q(2a^3 - 3a^2 x + x^3)}{6EI} + \frac{(4+5\nu)Q(a-x)b^2}{24EI} + \frac{\nu Q x y^2}{2EI}$$

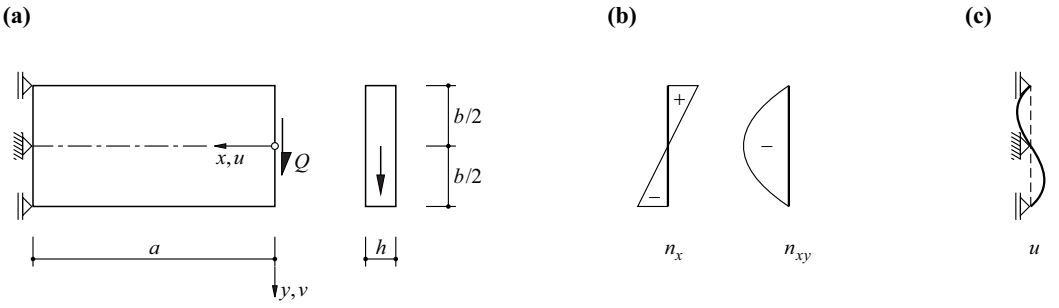

Fig. 23.1 Cantilever beam: (a) diagram of static system, (b) stress distribution, (c) displacements at "fixed support cross-section" $x = a$

Fig. 23.1(c) shows the displacements u at the "fixed support cross-section" $x = a$. Actually, u and v should be equal to zero at all points of the fixed support cross-section. However, this cannot be achieved with the very simple formulation for F.
The first term on the right in the expression for v corresponds to the bending deformation of a cantilever beam, see exercise 8.7. We get the expression $(0.5 + 0.625\nu)(b/a)^2$ for the ratio of the deflections as a result of shear and bending deformations at the free end of the cantilever $x = 0$; compared with this, beam theory, with $A_v = 5hb/6$, results in the expression $(0.6 + 0.6\nu)(b/a)^2$.

23.2.2 Polar coordinates

23.2.2.1 General relationships

Using the polar coordinates

$$r = \sqrt{x^2 + y^2} \quad , \quad \varphi = \arctan(y/x) \tag{23.7}$$

according to Fig. 23.2 means that

$$\frac{\partial r}{\partial x} = \cos\varphi \quad , \quad \frac{\partial r}{\partial y} = \sin\varphi \quad , \quad \frac{\partial \varphi}{\partial x} = -\frac{\sin\varphi}{r} \quad , \quad \frac{\partial \varphi}{\partial y} = \frac{\cos\varphi}{r}$$

applies, and thus for any functions $f(x,y) = f(r\cos\varphi, r\sin\varphi)$

$$\frac{\partial f}{\partial x} = \frac{\partial f}{\partial r}\cdot\frac{\partial r}{\partial x} + \frac{\partial f}{\partial \varphi}\cdot\frac{\partial \varphi}{\partial x} = \frac{\partial f}{\partial r}\cdot\cos\varphi - \frac{\partial f}{\partial \varphi}\cdot\frac{\sin\varphi}{r}$$

$$\frac{\partial f}{\partial y} = \frac{\partial f}{\partial r}\cdot\frac{\partial r}{\partial y} + \frac{\partial f}{\partial \varphi}\cdot\frac{\partial \varphi}{\partial y} = \frac{\partial f}{\partial r}\cdot\sin\varphi + \frac{\partial f}{\partial \varphi}\cdot\frac{\cos\varphi}{r}$$

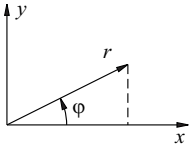

Fig. 23.2 Polar coordinates

Differentiating once more results in

$$\begin{Bmatrix} \dfrac{\partial^2 f}{\partial x^2} \\ \dfrac{\partial^2 f}{\partial y^2} \\ -\dfrac{\partial^2 f}{\partial x \partial y} \end{Bmatrix} = \begin{bmatrix} \cos^2\varphi & \sin^2\varphi & 2\sin\varphi\cos\varphi \\ \sin^2\varphi & \cos^2\varphi & -2\sin\varphi\cos\varphi \\ -\sin\varphi\cos\varphi & \sin\varphi\cos\varphi & \cos^2\varphi - \sin^2\varphi \end{bmatrix} \begin{Bmatrix} \dfrac{\partial^2 f}{\partial r^2} \\ \dfrac{1}{r}\cdot\dfrac{\partial f}{\partial r} + \dfrac{1}{r^2}\cdot\dfrac{\partial^2 f}{\partial \varphi^2} \\ -\dfrac{\partial}{\partial r}\left(\dfrac{1}{r}\cdot\dfrac{\partial f}{\partial \varphi}\right) \end{Bmatrix} \tag{23.8}$$

Inverting and rearranging (5.21) gives us, on the one hand (where $n \to r$, $t \to \varphi$),

$$\begin{Bmatrix} \sigma_y \\ \sigma_x \\ \tau_{xy} \end{Bmatrix} = \begin{bmatrix} \cos^2\varphi & \sin^2\varphi & 2\sin\varphi\cos\varphi \\ \sin^2\varphi & \cos^2\varphi & -2\sin\varphi\cos\varphi \\ -\sin\varphi\cos\varphi & \sin\varphi\cos\varphi & \cos^2\varphi - \sin^2\varphi \end{bmatrix} \begin{Bmatrix} \sigma_\varphi \\ \sigma_r \\ \tau_{r\varphi} \end{Bmatrix}$$

and the comparison with (23.3) shows that f can be interpreted as a stress function:

$$\sigma_r = \frac{1}{r}\cdot\frac{\partial f}{\partial r} + \frac{1}{r^2}\cdot\frac{\partial^2 f}{\partial \varphi^2} \quad , \quad \sigma_\varphi = \frac{\partial^2 f}{\partial r^2} \quad , \quad \tau_{r\varphi} = -\frac{\partial}{\partial r}\left(\frac{1}{r}\cdot\frac{\partial f}{\partial \varphi}\right) \tag{23.9}$$

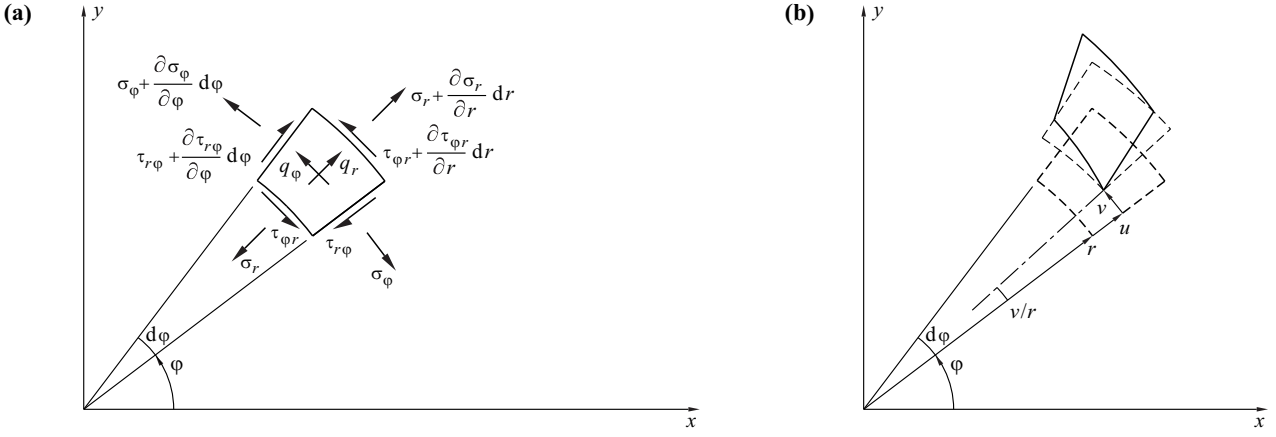

Fig. 23.3 Differential plate element: (a) statics, (b) kinematics

From the first two rows of (23.8) it follows that the LAPLACE operator is

$$\Delta = \frac{\partial^2}{\partial x^2} + \frac{\partial^2}{\partial y^2} = \frac{\partial^2}{\partial r^2} + \frac{1}{r}\cdot\frac{\partial}{\partial r} + \frac{1}{r^2}\cdot\frac{\partial^2}{\partial \varphi^2} \tag{23.10}$$

According to (23.2), the relationship $\Delta(\sigma_x + \sigma_y) = 0$ applies for disappearing loads, and therefore because of $\sigma_x + \sigma_y = \sigma_r + \sigma_\varphi$ and (23.9) as well as (23.10), in a similar way to (23.5),

$$\Delta\Delta f = 0 \tag{23.11}$$

We can read off the equilibrium conditions

$$\boldsymbol{q} = \begin{Bmatrix} q_r \\ q_\varphi \end{Bmatrix} = \begin{bmatrix} -\partial_r - 1/r & 1/r & -\partial_\varphi/r \\ 0 & -\partial_\varphi/r & -\partial_r - 2/r \end{bmatrix} \begin{Bmatrix} \sigma_r \\ \sigma_\varphi \\ \tau_{r\varphi} \end{Bmatrix} = \boldsymbol{D_s} \bullet \boldsymbol{\sigma} \tag{23.12}$$

from Fig. 23.3(a). When $q_r = q_\varphi = 0$, these relationships are satisfied by (23.9). Using Fig. 23.3(b), the kinematic relations are

$$\boldsymbol{\varepsilon} = \begin{Bmatrix} \varepsilon_r \\ \varepsilon_\varphi \\ \gamma_{r\varphi} \end{Bmatrix} = \begin{bmatrix} \partial_r & 0 \\ 1/r & \partial_\varphi/r \\ \partial_\varphi/r & \partial_r - 1/r \end{bmatrix} \begin{Bmatrix} u \\ v \end{Bmatrix} = \boldsymbol{D_k} \bullet \boldsymbol{u} \tag{23.13}$$

and according to (8.35),

$$\boldsymbol{\sigma} = \begin{Bmatrix} \sigma_r \\ \sigma_\varphi \\ \tau_{r\varphi} \end{Bmatrix} = \frac{E}{1-\nu^2} \begin{bmatrix} 1 & \nu & 0 \\ \nu & 1 & 0 \\ 0 & 0 & \dfrac{1-\nu}{2} \end{bmatrix} \begin{Bmatrix} \varepsilon_r \\ \varepsilon_\varphi \\ \gamma_{r\varphi} \end{Bmatrix} = \boldsymbol{E} \bullet \boldsymbol{\varepsilon} \tag{23.14}$$

23.2.2.2 Rotational symmetry

If the stress function f depends exclusively on r, then it follows that where $\Delta = d^2/dr^2 + (d/dr)/r$ according to (23.10), we get the differential equation

$$f'''' + 2f'''/r - f''/r^2 + f'/r^3 = 0 \qquad (' = d/dr) \tag{23.15}$$

from (23.11), with the general solution

$$f = c_1 + c_2 r^2 + c_3 \ln r + c_4 r^2 \ln r \tag{23.16}$$

which, applying (23.9), leads to the principal stresses

$$\sigma_r = 2c_2 + \frac{c_3}{r^2} + c_4(1 + 2\ln r) \quad , \quad \sigma_\varphi = 2c_2 - \frac{c_3}{r^2} + c_4(3 + 2\ln r) \tag{23.17}$$

Substituting (23.17) into (23.14) and subsequently inverting, then substituting in (23.13) and integrating, while considering $\gamma_{r\varphi} = 0$, results in

$$\begin{aligned} u &= [2(1-\nu)r(c_2 + c_4 \ln r) - (1+\nu)(c_3/r + c_4 r)]/E + c_5 \sin\varphi + c_6 \cos\varphi \\ v &= 4c_4 r\varphi/E + c_5 \cos\varphi - c_6 \sin\varphi + c_7 r \end{aligned} \tag{23.18}$$

Example 23.2 Cylindrical pipe

Let us consider the cylindrical pipe shown in Fig. 23.4. As $v(r, 0) = v(r, 2\pi)$, eq. $(23.18)_2$ initially gives us $c_4 = 0$ and therefore $(23.17)_1$ results in

$$2c_2 + \frac{c_3}{r_i^2} = -q_i \quad , \quad 2c_2 + \frac{c_3}{r_e^2} = -q_e$$

i. e.

$$c_2 = \frac{q_i r_i^2 - q_e r_e^2}{2(r_e^2 - r_i^2)} \quad , \quad c_3 = \frac{q_e - q_i}{r_e^2 - r_i^2} r_e^2 r_i^2$$

Substituting in (23.17) results in

$$\sigma_{r,\varphi} = \frac{q_i r_i^2 - q_e r_e^2}{r_e^2 - r_i^2} \pm \frac{q_e - q_i}{r_e^2 - r_i^2} \cdot \frac{r_e^2 r_i^2}{r^2}$$

As $\sigma_r + \sigma_\varphi$ is constant over the entire pipe cross-section, the result is a uniform strain of $(2\nu/E)(q_e r_e^2 - q_i r_i^2)/(r_e^2 - r_i^2)$ in the axial direction, i. e. pipe cross-sections remain plane.

In the case of $q_e = 0$, the result is

$$\sigma_{r,\varphi} = \frac{q_i r_i^2}{r_e^2 - r_i^2}\left(1 \mp \frac{r_e^2}{r^2}\right)$$

where σ_r is a compressive stress and σ_φ a tensile stress; σ_φ takes on a maximum for $r = r_i$, i. e. $q_i(r_e^2 + r_i^2)/(r_e^2 - r_i^2)$, see (5.52) and $(18.99)_1$.

When $q_e = 0$ and $r_e \to \infty$, the result is the limiting case of a perforated plate with the stresses $\sigma_\varphi = -\sigma_r = q_i r_i^2/r^2$. Superimposing a homogeneous tensile stress state $\sigma_r = \sigma_\varphi = q_i = \sigma$ on these stresses results in $\sigma_r = \sigma(1 - r_i^2/r^2)$ and $\sigma_\varphi = \sigma(1 + r_i^2/r^2)$. Further, $\sigma_r = 0$ and $\sigma_\varphi = 2\sigma$ applies at the edge of the hole $r = r_i$, i. e. for σ_φ, the result is a *stress concentration factor* $\sigma_{\varphi,\max}/\sigma = 2$.

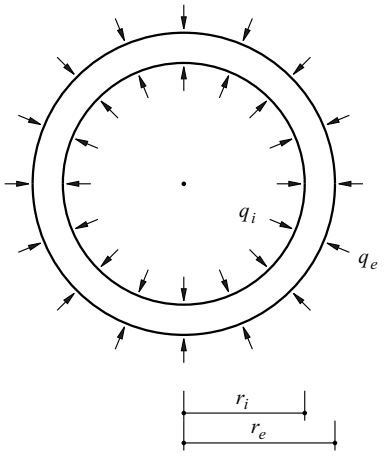

Fig. 23.4 Cylindrical pipe subjected to internal and external pressures

Example 23.3 Beam in the form of a circular arc

The following conditions apply for the curved beam shown in Fig. 23.5:

$$\sigma_r(r_i) = \sigma_r(r_e) = 0 \quad , \quad \int_{r_i}^{r_e} \sigma_\varphi b \, \mathrm{d}r = 0 \quad , \quad \int_{r_i}^{r_e} \sigma_\varphi b r \, \mathrm{d}r = M$$

Using (23.17), these conditions result in three linear equations for c_2, c_3 and c_4. Substituting back into (23.17) results in the stresses

$$\sigma_r = \frac{4M\left(r_e^2 \ln\frac{r}{r_e} - r_i^2 \ln\frac{r}{r_i} + \frac{r_e^2 r_i^2}{r^2}\ln\frac{r_e}{r_i}\right)}{b\left[(r_e^2 - r_i^2)^2 - 4r_e^2 r_i^2\left(\ln\frac{r_e}{r_i}\right)^2\right]} \quad , \quad \sigma_\varphi = \frac{4M\left(r_e^2 - r_i^2 + r_e^2 \ln\frac{r}{r_e} - r_i^2 \ln\frac{r}{r_i} - \frac{r_e^2 r_i^2}{r^2}\ln\frac{r_e}{r_i}\right)}{b\left[(r_e^2 - r_i^2)^2 - 4r_e^2 r_i^2\left(\ln\frac{r_e}{r_i}\right)^2\right]}$$

A bending moment M causing tensile stresses in the outer fibres and compressive stresses σ_φ in the inner fibres, as shown in Fig. 23.5, gives rise to transverse compressive stresses σ_r. In the opposite situation, the resulting transverse tensile stresses σ_r can lead to cracks in concrete beams, fissures in timber beams. Bolts or transverse reinforcement must then be provided in order to prevent failure.

Where $u = v = \mathrm{d}v/\mathrm{d}r = 0$ is required for $r = (r_e + r_i)/2$ and $\varphi = 0$, then (23.18) results in

$$\left[(1-\nu)(r_e + r_i)\left(c_2 + c_4 \ln\frac{r_e + r_i}{2}\right) - (1+\nu)\left(\frac{2c_3}{r_e + r_i} + c_4 \frac{r_e + r_i}{2}\right)\right]/E + c_6 = 0 \quad , \quad c_5 + c_7 \frac{r_e + r_i}{2} = 0 \quad , \quad c_7 = 0$$

from which it follows that $c_5 = c_7 = 0$ and

$$v = \frac{4c_4 r\varphi}{E} - c_6 \sin\varphi$$

It becomes clear from the last relationship that cross-sections remain plane.

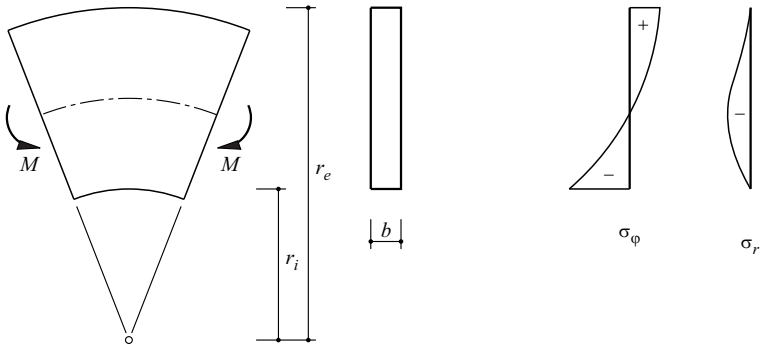

Fig. 23.5 Beam in the form of a circular arc subjected to pure bending

23.2.3 Approximating functions for displacement components

Combining (8.23), (8.33) and (8.35) shows that both $\Delta\Delta u = 0$ and $\Delta\Delta v = 0$ are valid when $\boldsymbol{q} = \textbf{const}$ (exercise 8.2). Accordingly, as an alternative to using stress functions, elastic plate problems can be solved in a similar way by using displacement components. As for the stress functions, third-degree polynomials for x and y, including x^3y and xy^3, and functions of the type (23.6) are suitable as approximating functions.

23.3 Reinforced concrete plate elements

23.3.1 Orthogonal reinforcement

23.3.1.1 Yield conditions and stress states

Fig. 23.6(a) shows a concrete element of thickness h reinforced in the x and z directions. The reinforcement is idealised as infinitely finely distributed (continuously distributed), rigid - perfectly plastic fibres rigidly bonded to the concrete The yield locus resulting from the cross-sectional areas a_{sx}, a_{sz} related to the unit length and the corresponding yield limits f_{yx}, f_{yz} for tension and f_{yx}', f_{yz}' for compression is the one shown in Fig. 23.6(b). We shall presume the "square yield condition" (7.37) for the concrete, which was introduced in section 7.3.3.5. Using (5.24), the result in the space n_x, n_z, n_{xz} is the elliptical cone surfaces shown in Fig. 23.6(c), which have the following equations:

$$Y_c = n_{xz}^2 - n_x n_z = 0 \quad , \quad Y_c' = n_{xz}^2 - (hf_c + n_x)(hf_c + n_z) = 0 \tag{23.19}$$

Similarly to the construction of Fig. 21.18(f), combining Fig. 23.6(b) and Fig. 23.6(c) leads to the yield surface shown in Fig. 23.6(d) for the reinforced concrete element.

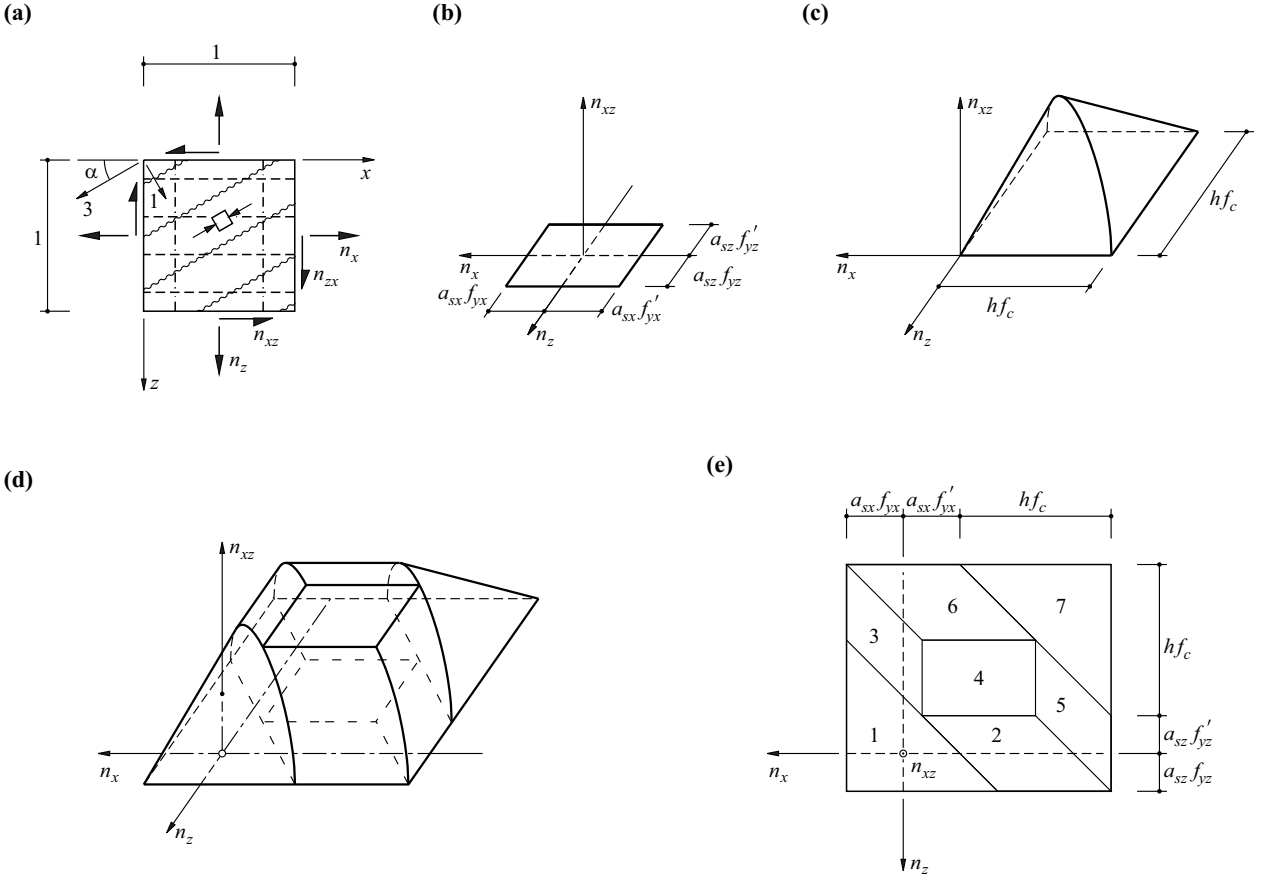

Fig. 23.6 Yield condition for reinforced concrete plate element with orthogonal reinforcement: (a) notation, (b) yield locus for reinforcement, (c) yield surface for concrete, (d) yield surface for reinforced concrete, (e) yield regimes

According to Fig. 23.6(e), this is divided into seven regimes that satisfy the conditions:

$$\begin{aligned}
Y_1 &= n_{xz}^2 - (a_{sx}f_{yx} - n_x)(a_{sz}f_{yz} - n_z) &&= 0\\
Y_2 &= n_{xz}^2 - (hf_c - a_{sz}f_{yz} + n_z)(a_{sz}f_{yz} - n_z) &&= 0\\
Y_3 &= n_{xz}^2 - (a_{sx}f_{yx} - n_x)(hf_c - a_{sx}f_{yx} + n_x) &&= 0\\
Y_4 &= n_{xz}^2 - (hf_c/2)^2 &&= 0\\
Y_5 &= n_{xz}^2 + (a_{sx}f_{yx}' + n_x)(hf_c + a_{sx}f_{yx}' + n_x) &&= 0\\
Y_6 &= n_{xz}^2 + (hf_c + a_{sz}f_{yz}' + n_z)(a_{sz}f_{yz}' + n_z) &&= 0\\
Y_7 &= n_{xz}^2 - (hf_c + a_{sx}f_{yx}' + n_x)(hf_c + a_{sz}f_{yz}' + n_z) &&= 0
\end{aligned} \tag{23.20}$$

In regime 1, the reinforcement in both directions yields in tension, $\sigma_{sx} = f_{yx}$ and $\sigma_{sz} = f_{yz}$, whereas $0 \geq \sigma_{c3} \geq -f_c$ applies for the principal compressive stress in the concrete. In regime 2, the z reinforcement yields in tension, $\sigma_{sz} = f_{yz}$, and $\sigma_{c3} = -f_c$ applies for the concrete, $-f_{yx}' \leq \sigma_{sx} \leq f_{yx}$ for the x reinforcement. Regime 3 is characterised in a similar way by $\sigma_{sx} = f_{yx}$, $\sigma_{c3} = -f_c$, $-f_{yz}' \leq \sigma_{sz} \leq f_{yz}$. In regime 5, $\sigma_{sx} = -f_{yx}'$, $\sigma_{c3} = -f_c$, $-f_{yz}' \leq \sigma_{sz} \leq f_{yz}$. Similarly, in regime 6, $\sigma_{sz} = -f_{yz}'$, $\sigma_{c3} = -f_c$, $-f_{yx}' \leq \sigma_{sx} \leq f_{yx}$. In regime 4, $\sigma_{c3} = -f_c$, $-f_{yx}' \leq \sigma_{sx} \leq f_{yx}$ and $-f_{yz}' \leq \sigma_{sz} \leq f_{yz}$. Finally, in regime 7, $\sigma_{c3} = -f_c$, $0 \geq \sigma_{c1} \geq -f_c$, $\sigma_{sx} = -f_{yx}'$ and $\sigma_{sz} = -f_{yz}'$. In regimes 1 to 6, $\sigma_{c1} = 0$, i. e. a uniaxial compressive stress state prevails in the concrete.

23.3.1.2 Strain increments and principal direction of compression

According to the flow rule (7.13), the (generalised) deformation increments $\dot{\boldsymbol{\nu}} = \{\dot{\varepsilon}_x, \dot{\varepsilon}_z, \dot{\gamma}_{xz}\}^T$ corresponding to the generalised stresses $\boldsymbol{s} = \{n_x, n_z, n_{xz}\}^T$ according to (20.22) give rise to external orthogonal vectors of the yield surfaces (23.20). Applying (6.14), we get

$$\cot(2\alpha) = \frac{\dot{\varepsilon}_z - \dot{\varepsilon}_x}{\dot{\gamma}_{xz}}$$

for the angle α between the x axis and the principal compression direction 3 shown in Fig. 23.6(a). Using

$$\cot\alpha = \frac{\cos\alpha}{\sin\alpha} = \frac{\cos^2\alpha - \sin^2\alpha + 1}{2\sin\alpha\cos\alpha} = \cot(2\alpha) + \sqrt{\frac{\cos^2(2\alpha) + \sin^2(2\alpha)}{\sin^2(2\alpha)}} = \cot(2\alpha) + \sqrt{\cot^2(2\alpha) + 1}$$

it follows that

$$\cot\alpha = \frac{\dot{\varepsilon}_z - \dot{\varepsilon}_x}{\dot{\gamma}_{xz}} + \sqrt{\left(\frac{\dot{\varepsilon}_z - \dot{\varepsilon}_x}{\dot{\gamma}_{xz}}\right)^2 + 1} \tag{23.21}$$

which leads to the expressions for the seven regimes:

$$\begin{aligned}
Y_1&: \quad \cot^2\alpha = (a_{sx}f_{yx} - n_x)/(a_{sz}f_{yz} - n_z)\\
Y_2&: \quad \cot^2\alpha = (hf_c - a_{sz}f_{yz} + n_z)/(a_{sz}f_{yz} - n_z)\\
Y_3&: \quad \cot^2\alpha = (a_{sx}f_{yx} - n_x)/(hf_c - a_{sx}f_{yx} + n_x)\\
Y_4&: \quad \cot^2\alpha = 1\\
Y_5&: \quad \cot^2\alpha = -(a_{sx}f_{yx}' + n_x)/(hf_c + a_{sx}f_{yx}' + n_x)\\
Y_6&: \quad \cot^2\alpha = -(hf_c + a_{sz}f_{yz}' + n_z)/(a_{sz}f_{yz}' + n_z)\\
Y_7&: \quad \cot^2\alpha = (hf_c + a_{sx}f_{yx}' + n_x)/(hf_c + a_{sz}f_{yz}' + n_z)
\end{aligned} \tag{23.22}$$

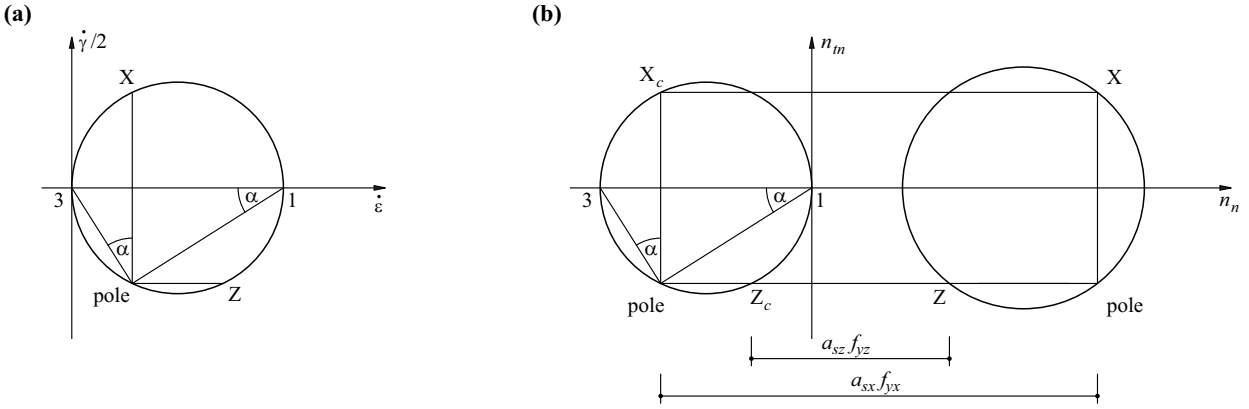

Fig. 23.7 Yield regime 1: (a) strain increments, (b) stresses

23.3.1.3 Regime 1

According to (7.12), eq. $(23.20)_1$, with $\kappa \geq 0$, results in

$$\dot{\varepsilon}_x = \kappa(a_{sz} f_{yz} - n_z) \quad , \quad \dot{\varepsilon}_z = \kappa(a_{sx} f_{yx} - n_x) \quad , \quad \dot{\gamma}_{xz} = \kappa 2 n_{xz}$$

and therefore by back-substitution into $(23.20)_1$ we get

$$\dot{\varepsilon}_x \dot{\varepsilon}_z = \left(\frac{\dot{\gamma}_{xz}}{2}\right)^2$$

which with (6.13) leads to

$$\dot{\varepsilon}_1 = \dot{\varepsilon}_x + \dot{\varepsilon}_z \geq 0 \quad , \quad \dot{\varepsilon}_3 = 0 \tag{23.23}$$

and also confirms $(23.22)_1$. Eq. $(23.23)_2$ means that the concrete remains rigid, i. e. is not crushed. Fig. 23.7(a) illustrates the corresponding kinematic relationships. When $\dot{\varepsilon}_x > 0$ and $\dot{\varepsilon}_z > 0$, the reinforcement in both directions yields in tension, and $\dot{\varepsilon}_1 > 0$ means that *collapse cracks* form in the concrete parallel with the principal compression direction 3. This corresponds to the case $\alpha = \pi/2$ in Fig. 7.12(b), and (7.38) shows that – because we presume $f_{ct} = 0$ – no energy is dissipated in the concrete.

Fig. 23.7(b) illustrates the static relationships corresponding with Fig. 23.7(a), where

$$n_x = h\sigma_{c3} \cos^2\alpha + a_{sx} f_{yx} \quad , \quad n_z = h\sigma_{c3} \sin^2\alpha + a_{sz} f_{yz} \quad , \quad n_{xz} = -h\sigma_{c3} \sin\alpha \cos\alpha \tag{23.24}$$

The condition $\sigma_{c3} \geq -f_c$ leads to the limit of validity

$$a_{sx} f_{yx} + a_{sz} f_{yz} - n_x - n_z \leq h f_c \tag{23.25}$$

Eq. (23.24), using the parameter $k = |\cot\alpha|$, gives us the relationships

$$a_{sx} f_{yx} \geq n_x + k|n_{xz}| \quad , \quad a_{sz} f_{yz} \geq n_z + \frac{1}{k}|n_{xz}| \tag{23.26}$$

for the dimensioning. In practice, $k = 1$ is often used, which corresponds to assuming $\alpha = \pm\pi/4$.

Example 23.4 Uniaxial tension

A 200 mm thick concrete plate is reinforced on both sides with Ø18 mm bars at a spacing of 150 mm in the x direction and with Ø12 mm bars at a spacing of 200 mm in the z direction. We shall assume $f_{yx} = f_{yz} = 500\,\text{N/mm}^2$ and $f_c = 15\,\text{N/mm}^2$. The task is to calculate the ultimate resistance for a uniaxial tension n_1 applied at any angle φ to the x axis, see Fig. 23.8(a).

Using (5.19), the following applies:

$$n_x = n_1 \cos^2\varphi \quad , \quad n_z = n_1 \sin^2\varphi \quad , \quad n_{xz} = n_1 \sin\varphi \cos\varphi$$

The resistances of the reinforcing bars are

$$a_{sx} f_{yx} = \frac{9^2 \cdot \pi \cdot 500}{150} \cdot 2 = 1696.5\,\text{kN/m} \quad , \quad a_{sz} f_{yz} = \frac{6^2 \cdot \pi \cdot 500}{200} \cdot 2 = 565.5\,\text{kN/m} = a_{sx} f_{yx}/3$$

Eq. $(23.20)_1$ results in

$$(a_{sx} f_{yx} - n_1 \cos^2\varphi)(a_{sx} f_{yx}/3 - n_1 \sin^2\varphi) = n_1^2 \sin^2\varphi \cos^2\varphi$$

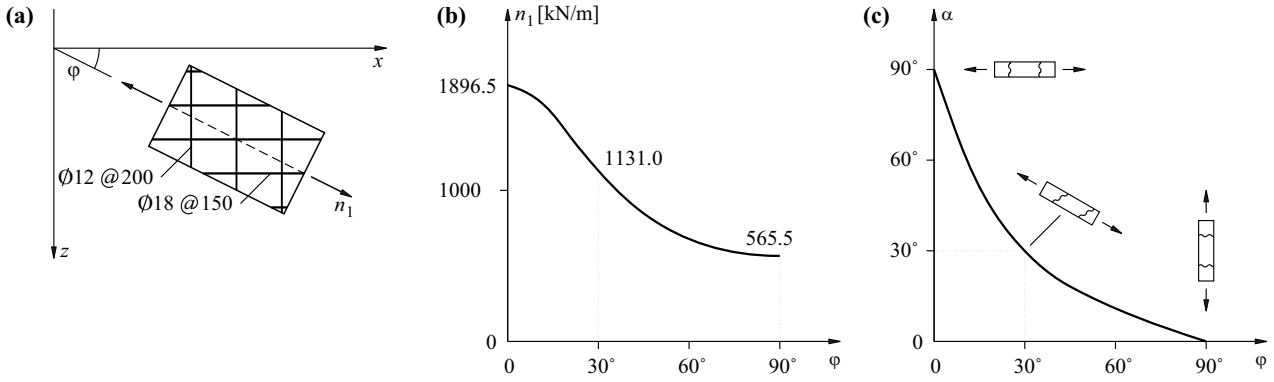

Fig. 23.8 Reinforced concrete plate subjected to uniaxial tension: (a) notation, (b) ultimate resistance, (c) direction of collapse cracks

from which it follows that

$$n_1 = \frac{a_{sx} f_{yx}}{3\sin^2\varphi + \cos^2\varphi}$$

see Fig. 23.8(b). Therefore, $(23.22)_1$ leads to

$$\cot\alpha = \sqrt{\frac{a_{sx}f_{yx} - \dfrac{a_{sx}f_{yx}\cos^2\varphi}{3\sin^2\varphi + \cos^2\varphi}}{\dfrac{a_{sx}f_{yx}}{3} - \dfrac{a_{sx}f_{yx}\sin^2\varphi}{3\sin^2\varphi + \cos^2\varphi}}} = \sqrt{\frac{3\sin^2\varphi + \cos^2\varphi - \cos^2\varphi}{\sin^2\varphi + \dfrac{\cos^2\varphi}{3} - \sin^2\varphi}} = 3\tan\varphi$$

see Fig. 23.8(c). As $n_x + n_z = n_1 \geq a_{sz} f_{yz}$, then (23.25) is satisfied, $a_{sx} f_{yx} < h f_c = 3000\,\text{kN/m}$, i. e. regime 1 is actually applicable.

For the limiting cases of $\varphi = 0$ and $\varphi = 90°$, the direction of the collapse cracks is orthogonal to the principal tension direction, $\alpha + \varphi = 90°$. For intermediate values, then $\alpha + \varphi < 90°$, i. e. the collapse cracks rotate from the direction perpendicular to the principal tension direction to the direction of the stronger reinforcement in the x direction. When $\varphi = 30°$, then, for example, $\alpha = 30°$ applies; compared with the initial direction of the cracks, which are approximately perpendicular to the principal tension direction, a redistribution of 30° can be expected by the time the ultimate resistance is reached.

23.3.1.4 Regime 2

According to (7.12), eq. $(23.20)_2$ results in

$$\dot\varepsilon_x = 0 \quad , \quad \dot\varepsilon_z = \kappa(h f_c - 2a_{sz} f_{yz} + 2n_z) \quad , \quad \dot\gamma_{xz} = \kappa 2 n_{xz}$$

The associated MOHR's circle for the strain increments shown in Fig. 23.9(a) reveals that the principal directions 1 and 3 bisect the angles $\pi - 2\alpha$ and 2α between *slip lines* I and II. The slip lines are inextensible, $\dot\varepsilon_I = \dot\varepsilon_{II} = 0$.

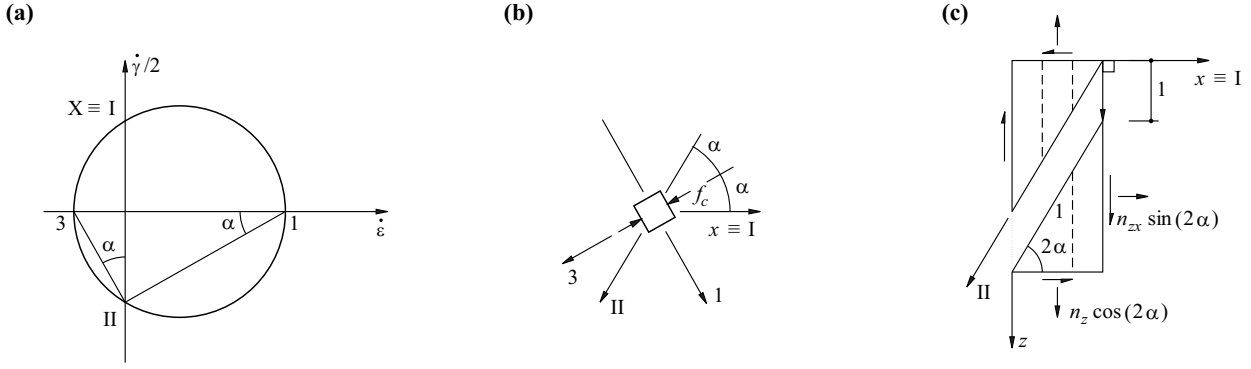

Fig. 23.9 Yield regime 2: (a) strain increments, (b) principal directions and slip lines, (c) collapse mechanism

The significance of the slip lines can be seen in the collapse mechanism shown in Fig. 23.9(c). According to (7.38), the unit displacement vector at an angle $\pi/2 - 2\alpha$ to the element of length 1 in the II direction results in dissipation work amounting to $hf_c[1 - \cos(2\alpha)]/2$ in the concrete. Added to this is an amount $a_{sz}f_{yz}\cos(2\alpha)$ for the yielding reinforcement in the z direction. The dissipation work is opposed by the work $n_z\cos(2\alpha) + n_{zx}\sin(2\alpha)$ of the external forces, i. e.

$$n_z\cos(2\alpha) + n_{zx}\sin(2\alpha) = \frac{hf_c}{2}[1 - \cos(2\alpha)] + a_{sz}f_{yz}\cos(2\alpha)$$

or rather

$$n_{zx} = (a_{sz}f_{yz} - n_z)\cot(2\alpha) + \frac{hf_c}{2}\tan\alpha \tag{23.27}$$

Differentiating this expression with respect to $\tan\alpha$ and equating to zero leads to $(23.22)_2$, and back-substituting into (23.27) results in $(23.20)_2$. The uniaxial compressive stress state at the yield limit of the concrete shown in Fig. 23.9(b) is therefore compatible with collapse mechanisms characterised by a displacement orthogonal to the first slip line along the second slip line.

Yield regime 2 applies, in particular, in beams with thin webs heavily reinforced or prestressed in the x direction. A *web crushing failure* can occur in such cases. Such a failure is characterised by yielding of the shear links (often called stirrups) in the z direction and crushing of the web concrete (which is compressed at an angle α to the x direction) along slip lines at an angle 2α to the x axis.

23.3.1.5 Regime 4

Regime 2 is transformed to regime 4 at the limiting case $\alpha \to \pi/4$. According to Fig. 23.9(c), the result is a pure slip parallel with the z axis. Eq. (23.27) is simplified to $n_{zx} = hf_c/2$, see $(23.20)_4$.

23.3.2 General reinforcement

The effect of reinforcement inclined at an angle β_i to the x axis can be ascertained through equivalent mean stresses

$$n_{xs} = a_{si}\sigma_{si}\cos^2\beta_i \quad , \quad n_{zs} = a_{si}\sigma_{si}\sin^2\beta_i \quad , \quad n_{xzs} = a_{si}\sigma_{si}\sin\beta_i\cos\beta_i \tag{23.28}$$

which are limited by

$$-f_{yi}' \le \sigma_{si} \le f_{yi} \tag{23.29}$$

see Fig. 23.10. Each reinforcement direction corresponds to a vector in the n_x, n_z, n_{xz} space. Combining two reinforcement directions results in a parallelogram, and combining three non-collinear reinforcement directions results in a parallelepiped. The yield surface of a concrete plate element reinforced in this way can be obtained in a similar way to Fig. 23.6(d).

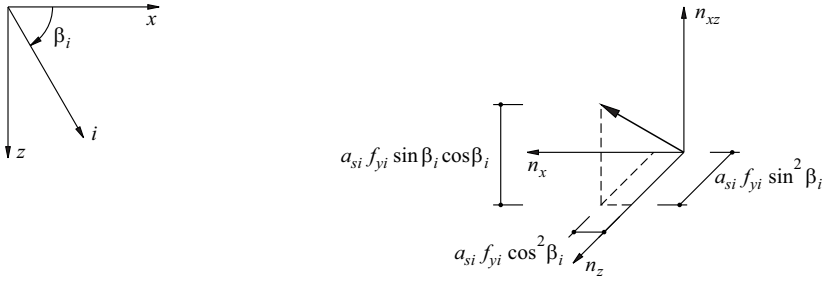

Fig. 23.10 Skew reinforcement

23.4 Static method

23.4.1 General

This section deals with the application of the static method (chapter 21.3.1) to reinforced concrete plates. Related problems in geotechnical engineering, which generally correspond to a coplanar strain state and can be dealt with in a similar way, are also mentioned.

Linear elastic analyses have very limited applicability for reinforced concrete plates because of the cracking of the concrete and the yielding of the reinforcement. Such analyses permit the structural behaviour in the uncracked state to be ascertained, also an estimate of the position and direction of the first cracks and the associated loads. They also supply a statically admissible stress state which, in conjunction with (23.26), for example, can form the starting point for dimensioning. This approach, popular in practice, essentially corresponds to applying the static method. However, the practical application is often fraught with considerable difficulties. Stress concentrations can demand reinforcement layouts that are impractical, maybe even impossible. On the other hand, the minimum reinforcement distributed over the plate, which is required anyway, is frequently exploited to only a moderate degree, which compromises the economy.

In order to overcome these problems and enable a consistent procedure based on the lower-bound theorem, alternative methods must be found for achieving statically admissible stress states. From observations of the crack patterns and deformations of reinforced concrete plates and beams, it is possible to visualise and follow the internal forces rigorously with the help of *truss models*. Expanding the truss bars and joints to finite plate areas enables us to reach *discontinuous stress fields*. Finally, *stringer-panel models* with an orthogonal mesh of tension and compression members plus intermediate panels in shear is another practical way of idealising plates with orthogonal reinforcement.

23.4.2 Truss models

23.4.2.1 Introductory example

Fig. 23.11(a) shows one half of a simply supported plate subjected to a uniformly distributed load applied along CD. Only a bending moment acts at section BC. As illustrated, the moment can be replaced by the couple formed by the resulting tensile and compressive forces in the cracked bottom part and compressed upper part of the plate. It is assumed below that these forces can be transferred within the plate in the same way as a parallel-chord truss.

In the model shown on the left of Fig. 23.11(b), tension chord AB and compression chord CD are connected together via strut AD. A point load equivalent to the uniformly distributed load of Fig. 23.11(a) acts at joint D. The tensile force at B is transferred by the tension chord to support joint A and must be anchored there. On the right of Fig. 23.11(b), the strut is replaced by the fan ACD centred on A. In the fan, radial compressive stresses – the magnitude of which is inversely proportional to the distance from A – act in the direction of A. Owing to the uniformly distributed vertical load and the successively increasing inclination of the fan forces, the horizontal forces along DC transferred to the compression chord vary linearly, which leads to a parabolic variation in the force in the compression chord. Area ABC between the tension chord and the fan remains stress-free.

In Fig. 23.11(c), the uniformly distributed load in the left-hand diagram is replaced by two statically equivalent point loads at D and E carried via the polygonal strut CDEA. The figure on the right shows the polygonal strut replaced by the continuous parabolic arc CA. A homogeneous uniaxial compressive stress state in the vertical direction prevails in area ACD, as shown, and area ABC remains stress-free. The lateral extent of

the parabolic arc is ignored and so the compressive stresses in the arc are infinitely large.

The effect of including vertical shear links is examined in Fig. 23.11(d). On the left, the load is replaced by two statically equivalent point loads, as in Fig. 23.11(c). The vertical force transferred via strut EB to joint B is suspended from joint F by tie BF and transferred from there, together with the second point load, via strut FA to support A. At B the tensile force in the bottom chord is reduced by the horizontal component of the force in strut BE. Accordingly, at support A it is no longer necessary to anchor the full tensile force occurring at C, which means the reinforcement in the tension chord can be curtailed. The two struts AF and BE in the left half of the figure correspond to the fan AEF and the parallelogram-shaped panel ABDE shown on the right of the figure. A homogeneous uniaxial compressive stress state in the concrete prevails in panel ABDE, and uniformly distributed vertical shear link forces in area ABEF. The force in the compression chord exhibits a parabolic variation along FE and a linear variation along ED. Likewise, the variation in the tension chord force along AB is linear. The stresses in area BCD remain equal to zero.

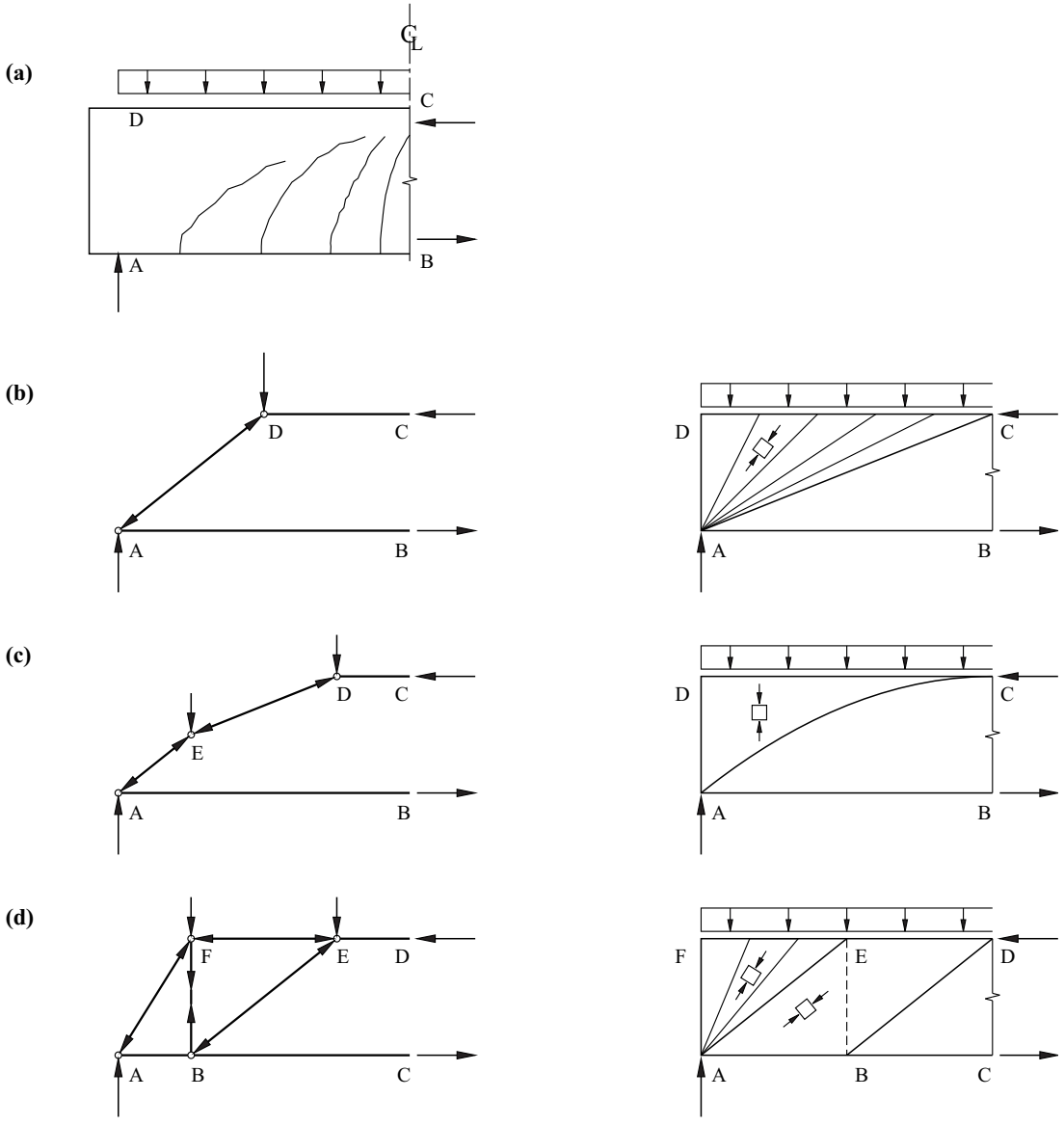

Fig. 23.11 Development of truss models and stress fields: (a) free body and crack pattern, (b) strut action and fan action, (c) arch action, (d) considering the shear links

23.4.2.2 Commentary

The introductory example reveals clearly different fundamental structural responses: *strut action*, *fan action* and *arch action*. It also illustrates the effect of regularly spaced shear links. On the whole, it shows how truss models can be employed plausibly to find internal force states that are in equilibrium with given external forces.

However, the introductory example also throws up various questions that need to be investigated. The first problem area concerns the infinitely large compressive stresses that theoretically occur at the origin of the fan in Fig. 23.11(b) and (d) as well as the arch in Fig. 23.11(c). The second question concerns the effect of distributed horizontal reinforcement. Thirdly, in the light of the varying chord forces, the assumption of parallel chords requires further discussion. And finally, a general discussion is necessary regarding how the ideal truss joints can be replaced by finite nodal zones – in which statically admissible stress states occur that do not infringe the yield conditions – when presuming finite material stiffnesses. All these questions are looked at in section 23.4.3.

Another question that often causes irritation can be illustrated, for example, by the left part of Fig. 23.11(b). The figure corresponds to a funicular polygon of the forces. In order to achieve a stably supported truss that is stable in itself, a hinged support at A plus a strut BD must be introduced, for example, and the other half of the system modified accordingly. Strut BD and its symmetrical counterpart would then be identified as zero-force members for the given loading, and the horizontal component of the support force at A would also be zero because of the absence of horizontal loads. As we can see, strictly speaking, the term *truss model* only applies when Fig. 23.11(b) is modified in this way. Notwithstanding, we shall continue to use this term for figures that – like Fig. 23.11(b) – are reduced to the essentials.

23.4.2.3 Practical application of truss models

An iterative procedure is generally necessary when developing truss models. Trial and error leads to an initial truss geometry that is then successively improved. In doing so, it is important to check that the plate areas corresponding to the compression members in the truss, taking into account the effective compressive stress of the concrete, fit into the given geometry of the structural member and that the forces corresponding to the tension members in the truss can be accommodated and properly transferred by the reinforcement.

It is often advantageous to consider only the effect of the (concentrated) main reinforcement in the first step. The effect of distributed (minimum) reinforcement can then be taken into account in a fine-tuning, second step.

The development of truss models is a skill that needs to be practised. Helpful here is the fact that certain basic themes often recur, see Fig. 23.12. Further examples are shown in Fig. 23.13.

Fig. 23.14 shows a truss model with $\tan\alpha = 3/4$ and $n_x = n_z = 0$ which corresponds to Fig. 23.6(a). Equilibrium at the perimeter joints (assuming yielding reinforcement) calls for

$$(n_{zx}/4) \cdot 4/3 = a_{sx} f_{yx}/4 \quad , \quad (n_{xz}/3) \cdot 3/4 = a_{sz} f_{yz}/3$$

which confirms both $(23.20)_1$ and $(23.22)_1$. Additional forces n_x and n_z would have to be accommodated by additional reinforcement and transferred through the element. The truss model illustrates in a very graphic way how yield regime 1 functions in plate elements with orthogonal reinforcement. The further relationships (23.20) and (23.22) can be verified by employing similar approaches.

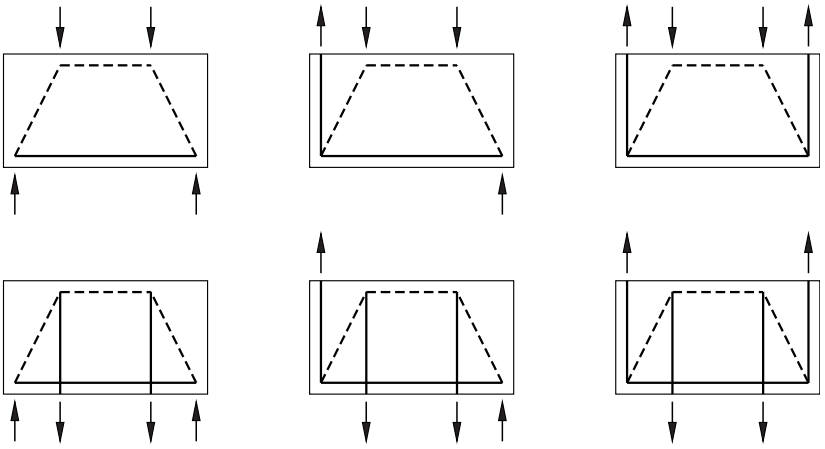

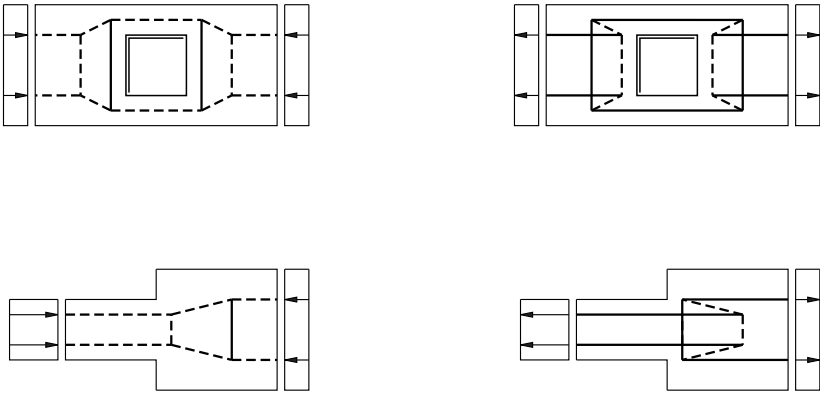

Fig. 23.12 Variations on a basic theme

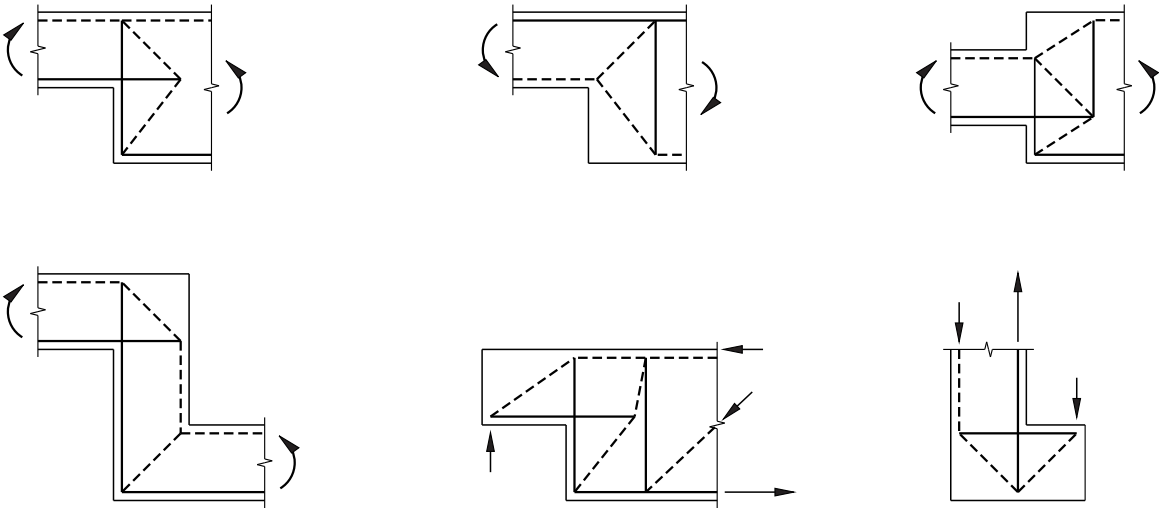

Fig. 23.13 Further examples of truss models

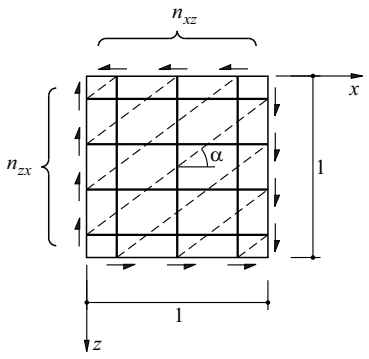

Fig. 23.14 Plate element subjected to pure shear stresses

At positions of *force transfer*, a good recommendation is to consider the stresses occurring according to the elastic strength of materials at a spacing equal to about the width of the plate and develop a truss model based on that. For example, the concentrated force applied to the top edge of the plate in Fig. 23.15 spreads out while activating the distributed horizontal reinforcement in the upper part of the plate GDEF in such a way that it is distributed uniformly in the middle part of the plate HCDG; it is then transferred to the supports at A and B through the activation of the distributed horizontal reinforcement in the bottom part of the plate ABCH. Fig. 23.16 shows a similar problem with a force that is applied eccentrically, e. g. as a result of anchoring a prestressing tendon.

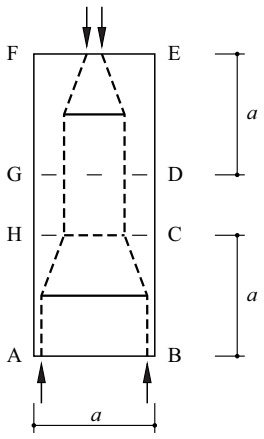

Fig. 23.15 Force transfer in a deep plate

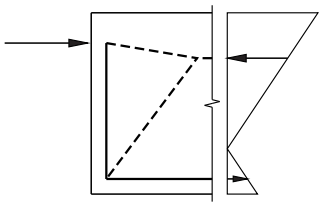

Fig. 23.16 Transferring an eccentric force

23.4.3 Discontinuous stress fields

23.4.3.1 Stress discontinuity lines

For reasons of equilibrium, the normal and shear stresses at every line element with direction t must be continuous:

$$\sigma_n^{I} = \sigma_n^{II} \quad , \quad \tau_{tn}^{I} = \tau_{tn}^{II} \tag{23.30}$$

see Fig. 23.17, whereas the normal stress components parallel with t may be discontinuous:

$$\sigma_t^{I} = \sigma_t^{II} \quad \text{or} \quad \sigma_t^{I} \neq \sigma_t^{II} \tag{23.31}$$

Once $(23.31)_2$ is satisfied, we speak of a *stress discontinuity line*. The poles of the MOHR's circles for stress states I and II on both sides of a stress discontinuity line lie together with the common stress point N on a line parallel with t.

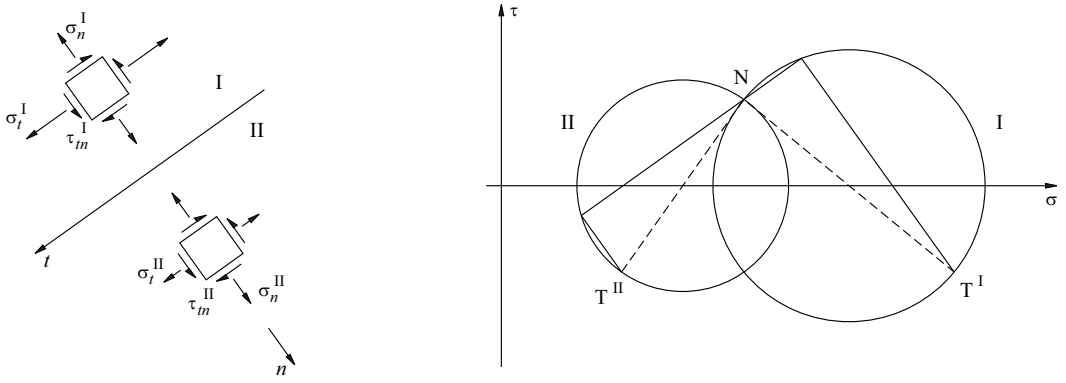

Fig. 23.17 Stress discontinuity line

Example 23.5 Vertical embankment

Fig. 23.18 shows a vertical embankment of height h. It is presumed that the material is homogeneous, satisfies the COULOMB yield condition and exhibits a body load q. The yield condition for $\varphi > 0$ along line $z = h$ is just satisfied by the stress state shown in the figure and not infringed at any other point. Using $(7.30)_1$, it follows that according to (21.4),

$$h \geq \frac{2c}{q} \tan\left(\frac{\pi}{4} + \frac{\varphi}{2}\right) = \frac{2c\cos\varphi}{q(1 - \sin\varphi)} \tag{23.32}$$

When $\varphi = 0$, the (TRESCA) yield condition in the range $x \geq 0$, $z \geq h$ is satisfied and not infringed at any other point; $h \geq 2c/q$ applies.

When $z > h$, the z axis plays the role of a stress discontinuity line; σ_z increases abruptly by the amount qh.

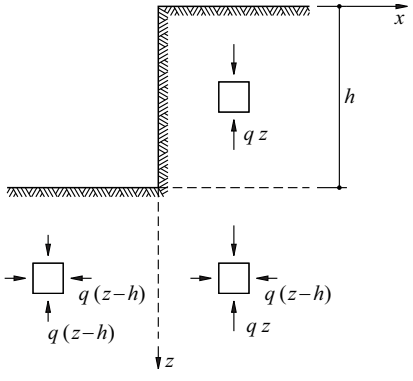

Fig. 23.18 Statically admissible stress state in the region of a vertical embankment

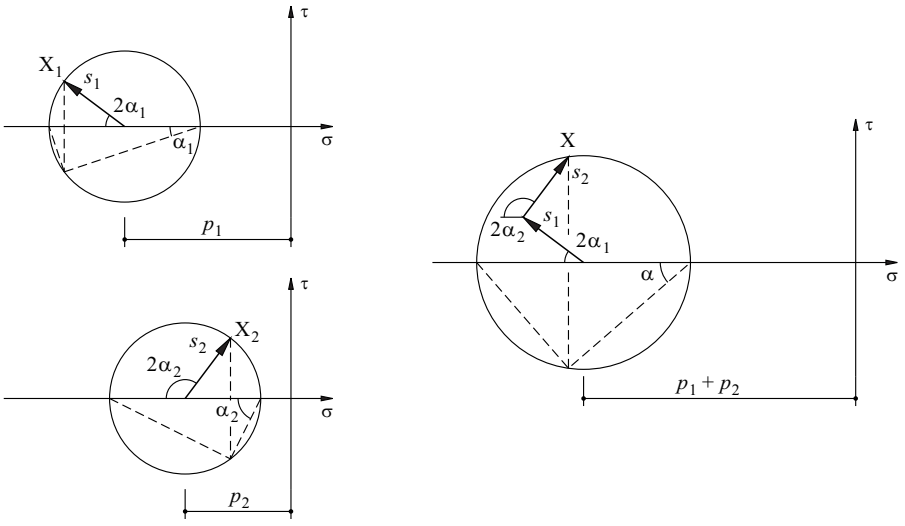

Fig. 23.19 Two overlapping stress fields

23.4.3.2 Overlapping stress fields

With two overlapping stress fields, the associated stress vectors for surface elements in the same direction are added together as vectors. Fig. 23.19 shows a corresponding diagram with MOHR's circles for elements with normal direction x. The hydrostatic pressures p_1 and p_2 are added together algebraically, the deviatoric components s_1 and s_2 vectorially.

Example 23.6 Strip foundation on TRESCA half-space

Fig. 23.20 shows the overlap between two stress fields 5 inclined at $\pi/3$ to the horizontal, a vertical stress field 6 and a horizontal stress field 7, all of which are loaded uniaxially by compressive stresses with a magnitude of $2c$. Principal compressive stresses with a magnitude of $-3c$ and $-c$ inclined at $\pi/6$ and $\pi/3$ to the horizontal ensue in the overlap area 3 of fields 5 and 7. A hydrostatic compressive stress state with a magnitude of $2c$ ensues in the overlap area 4 of fields 6 and 7. Principal compressive stresses of $-4c$ and $-2c$ inclined at $\pi/3$ and $\pi/6$ to the horizontal ensue in area 2, horizontal and vertical principal compressive stresses of $-3c$ and $-5c$ in area 1. All partial stress states comply with the TRESCA yield condition. Consequently, the uniform bearing pressure applied by a strip foundation to a weightless half-space of TRESCA material upon reaching the limit load cannot be less than $5c$. In reality, we have the exact solution $(2 + \pi)c$ for this problem named after PRANDTL, see example 23.10.

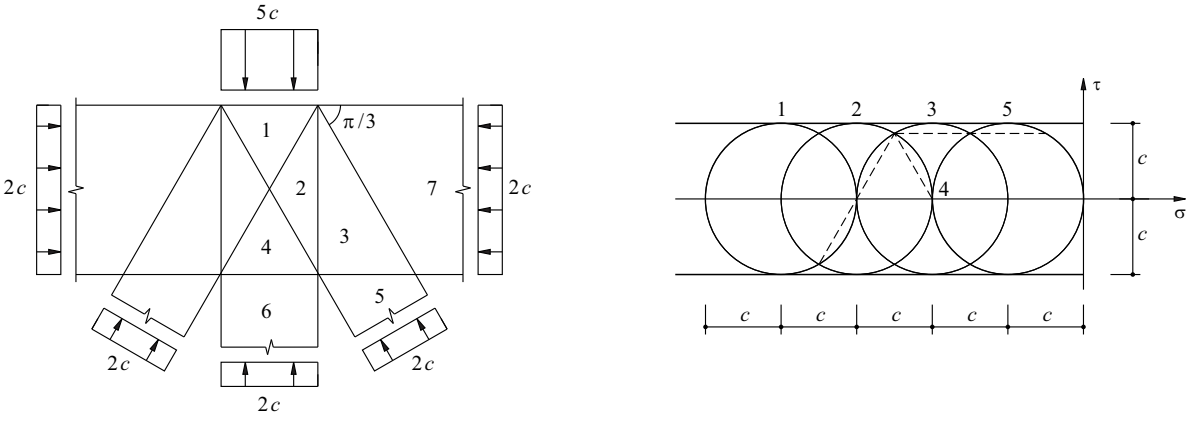

Fig. 23.20 Strip foundation on weightless TRESCA half-space

23.4.3.3 Nodal zones

By choosing the stresses $-\sigma_A, -\sigma_B$ and $-\sigma_C$ in the truss diagonals, the resulting widths of those diagonals are $t_A = -A/(h\sigma_A)$, $t_B = -B/(h\sigma_B)$, $t_C = -C/(h\sigma_C)$ for forces ***A***, ***B*** and ***C*** in equilibrium according to Fig. 23.21(a) and Fig. 23.21(b), where h = plate thickness. The intersections A, B, C, of the boundary lines of the truss diagonals define a triangular nodal zone, see Fig. 23.21(b). The MOHR's circles with their poles a, b and c corresponding to the three diagonals are shown in Fig. 23.21(c). The lines parallel with the boundary lines of the joint passing through poles a, b, c intersect with the corresponding circles at points A, B and C. Two of these three points define the MOHR's circle for the stresses in the nodal zone, which is centred on the σ axis. The third point must likewise lie on this circle with the principal stresses σ_1 and σ_2. Another control mechanism is that straight lines Aa, Bb, Cc must intersect at pole d of this circle.

If we choose $\sigma_A = \sigma_B = \sigma_C = \sigma_0$, then the MOHR's circles for the three truss diagonals coincide, and the MOHR's circle for the nodal zone degenerates to the point $\sigma_1 = \sigma_2 = \sigma_0$ on the σ axis. The boundaries of the joint are orthogonal to the directions of the diagonals and a (biaxial) hydrostatic stress state ensues in the nodal zone, see Fig. 23.22(a).

When one of the three forces acting on the nodal zone is a tensile force, the situation that ensues is, for example, that shown in Fig. 23.22(b). In the left part of the figure it is assumed that ***C*** is anchored to a rigid plate beneath the joint and acts on the joint via this and a short uniaxial compression field. An anchorage for ***C*** in the form of uniformly distributed bond forces along the line of intersection of the two struts is presumed in the right part of the figure.

Fig. 23.22(c) shows analogous stress fields for the case of two tensile forces acting on the nodal zone. Forces ***A*** and ***B*** are transferred along AO and BO via uniformly

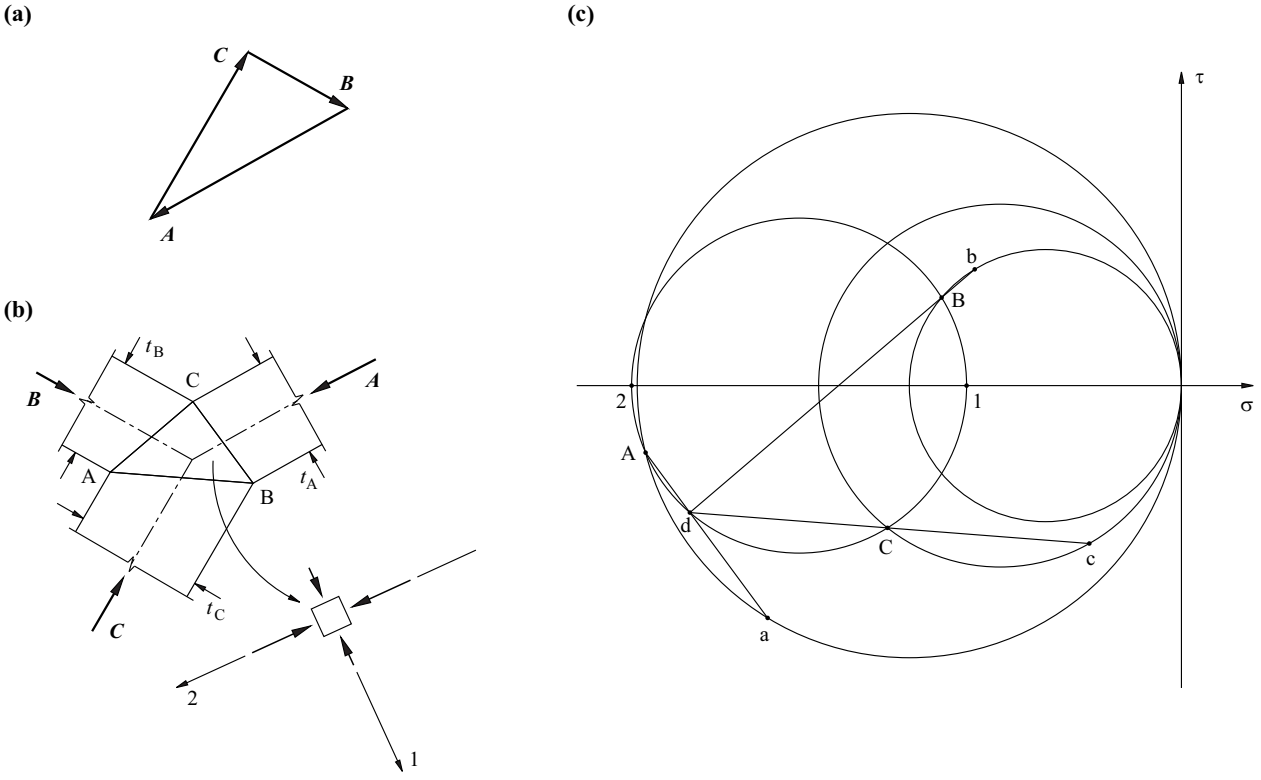

Fig. 23.21 Joint: (a) force polygon, (b) funicular polygon with truss diagonals and nodal zone ABC, (c) MOHR's circles

distributed bond forces in the right part of the figure. A uniaxial compressive stress state parallel with AB is established in area OAB, see Fig. 23.22(d).

Anchoring ties via end plates as presumed on the left of Fig. 23.22(b) and Fig. 23.22(c) is rarely possible in practice. Fig. 23.23(a) shows a similar detail for the support joint of a plate. Fig. 23.23(b) shows an equivalent solution suitable for reinforced concrete which has four horizontal U-bars and two heavy-duty vertical dowel bars in the corners. The effect of this reinforcement can be analysed using the truss models drawn in Fig. 23.23(c). The horizontal compressive stresses in the concrete arising behind the nodal zone are transferred locally to the bends of the U-bars via arch or shell action in the concrete as well as via the dowel action of the vertical bars. This means that the middle part of each U-bar running orthogonal to the plane of the plate is stressed in tension. Activating the concrete in the concrete cover to the U-bars on both sides causes tensile stresses in the concrete orthogonal to the plane of the plate between

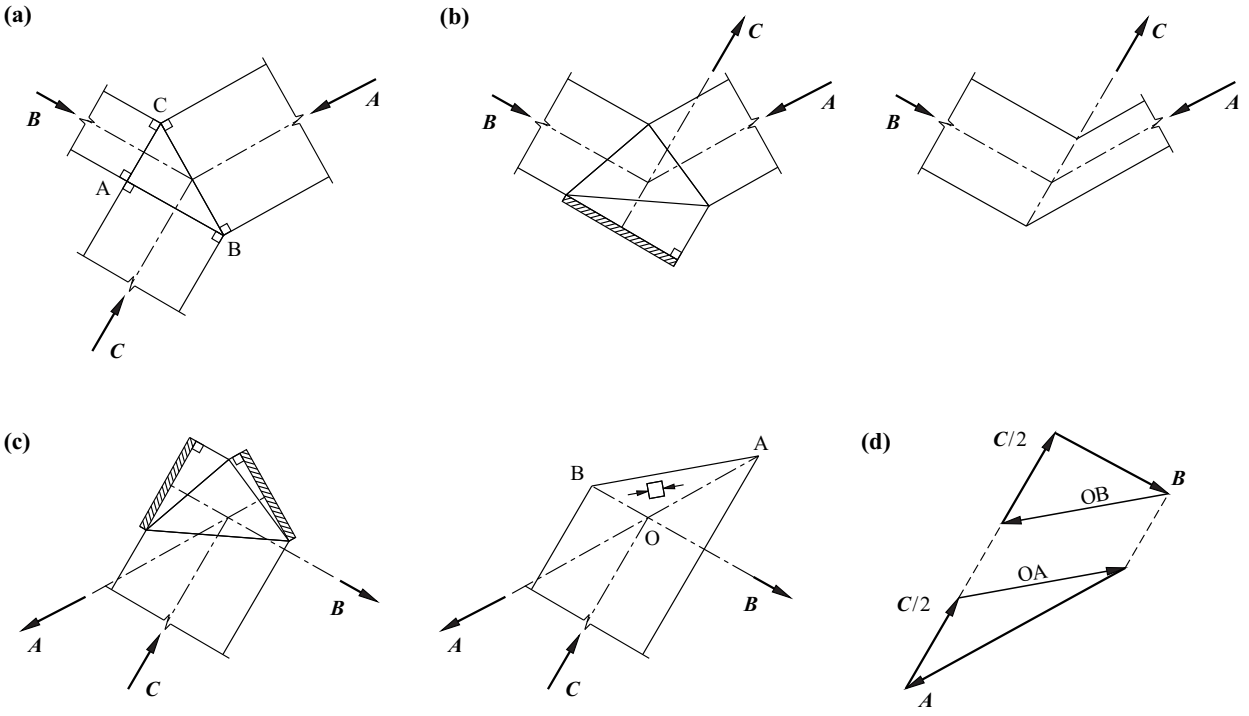

Fig. 23.22 Nodal zones: (a) uniform stresses in all truss diagonals, (b) compression – tension – compression, (c) tension – compression – tension, (d) force polygon for the diagram on the right of (c)

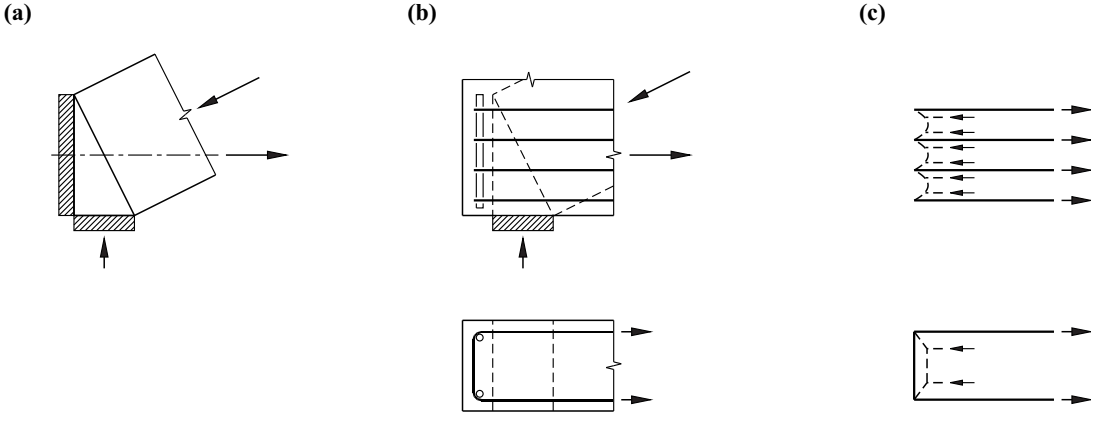

Fig. 23.23 Support joint: (a) longitudinal reinforcement with end plate, (b) U-bars and dowel bars, (c) truss model, elevation (top) and plan (bottom)

the individual longitudinal legs of the U-bars, which could lead to spalling of the concrete cover.

23.4.3.4 Homogeneous partial stress fields

The reinforcement in concrete plates is generally in the form of a distributed minimum reinforcement and concentrations of additional reinforcing bars. The minimum reinforcement limits cracking (see Fig. 18.15 and associated discussion) and guarantees adequate deformation capacity. In most cases it also makes a significant contribution to the ultimate resistance. Discontinuous stress fields can be used to describe very graphically how it does this.

Fig. 23.24(a) shows one half of a plate with span a which is loaded along its top edge by a load Q uniformly distributed over the width $2c$. There is *indirect support* along edge AJGF, i. e. the plate is connected to a second plate here which transfers the load further. The plate with depth b and thickness h is reinforced horizontally and vertically with finely distributed reinforcement having a geometric reinforcement ratio $\rho = a_s/h = \text{const}$. The yield limit of the reinforcement is f_y, the effective compressive strength of the concrete f_c. Compressive stresses in the reinforcement are neglected.

The stress distribution given in the figure ensues at section BCD. There is no normal force present and so the expression for the depth of the zone in flexural compression is $b/[f_c/(\rho f_y) + 1]$, and equilibrium of moments results in

$$Q = \frac{2b^2 h f_c}{(a-c)\left(\dfrac{f_c}{\rho f_y} + 1\right)} \tag{23.33}$$

It is easy to draw the discontinuous stress field if we assume a truss model with strut IJ and tie JK. Point K lies in the middle of distance BC, and point I halves distance CE. A biaxial compressive stress state – given by the stresses indicated at the top and to the side – prevails in area 1 (CDE). In area 2 (CEG), whose boundary EG is parallel with IJ, the outcome is a uniaxial compressive stress state parallel with that boundary. A uniaxial, horizontal tensile stress state prevails in area 4 (ABC), and a biaxial tensile-compressive stress state is the result in area 3 (ACG) between areas 2 and 4. The MOHR's circles and their poles corresponding to the four partial stress fields are easily

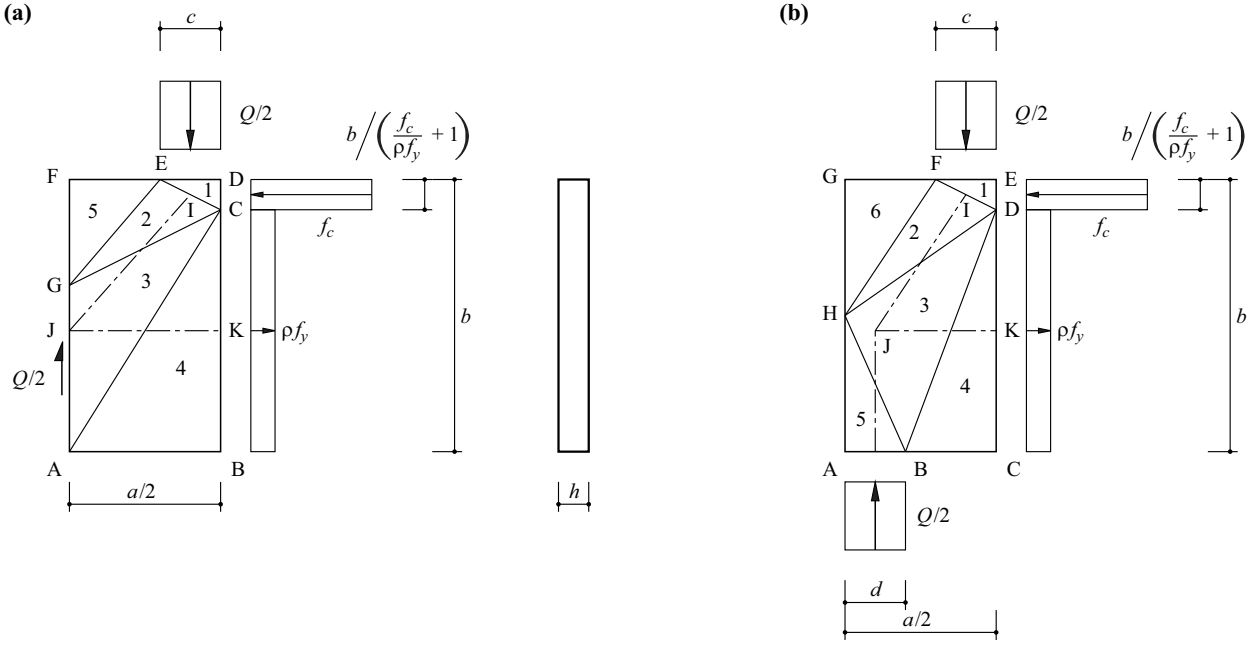

Fig. 23.24 Homogeneous partial stress fields: (a) indirect support, (b) direct support

constructed from the known boundary stresses and the known stress discontinuity lines (exercise 23.15). The stress in area 5 (EFG) is zero.

In Fig. 23.24(b), the indirect support is replaced by a *direct support* of width d. In a similar way to (23.33), we get

$$Q = \frac{2b^2 h f_c}{(a - c - d)\left(\frac{f_c}{\rho f_y} + 1\right)} \tag{23.34}$$

In the truss model, the support force is directed vertically upwards towards joint J, where it is balanced by the forces from strut IJ and tie KJ. Boundary FH to area 2 is parallel with IJ. The partial stress fields 1 to 4 are similar to those in Fig. 23.24(a). There is also the vertical, uniaxially compressed area 5 (ABH). The stress in area 6 (FGH) is zero.

23.4.3.5 Supplementary remarks

Any loadings can be dealt with according to Fig. 23.25 by first replacing them by their resultant Q and carrying this with an equivalent diagonal ACDE. In the subsequent fanning-out of the truss diagonal, it is only the form of the boundary of joint AC that changes; points A and C are not displaced. It is presumed here that a coplanar hydrostatic compressive stress state according to Fig. 23.22(a) prevails in the nodal zone.

A further development of the stress field shown on the right of Fig. 23.11(d) is shown in Fig. 23.26. Nodal zone ABEF has finite dimensions and compression zone LMNJK varies in depth. Bond forces are transferred to the longitudinal reinforcement along GH, and shear link forces are activated in area GHNM. The loading on area LM is carried directly via fan AFML. Fan FGNM carries the shear link forces and the loads applied over area MN. The parallel concrete compressive stress field ABDE in Fig. 23.11(d) becomes area GHJN, which carries the loads over area NJ and transfers these to the bottom ends of the shear links. The lines of action of the individual stress resultants are indicated by chain-dot lines.

Complete stress fields such as those of Fig. 23.26 are rarely required. It is mostly sufficient to examine just a few important details in depth with the help of the methods explained here.

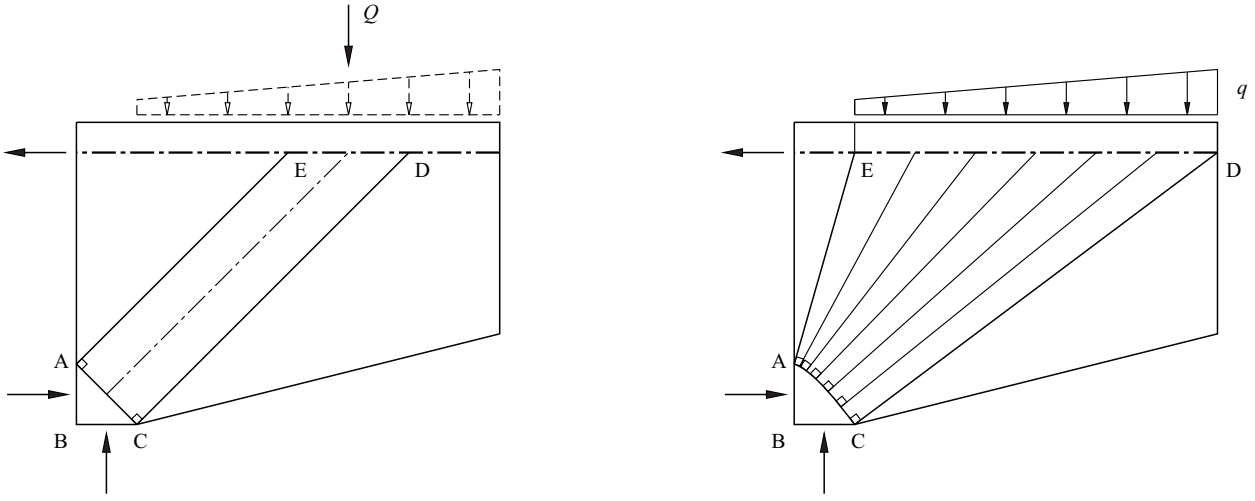

Fig. 23.25 Equivalent diagonal and fanning-out for any loading

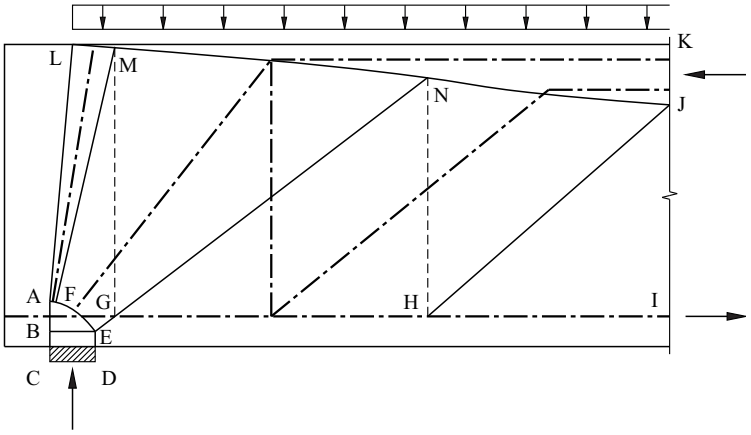

Fig. 23.26 Further development of Fig. 23.11(d)

Suitable "suspension reinforcement" should be provided in a beam or plate carrying suspended loads. Such reinforcement enables the load to be carried either concentrated on the opposite edge or distributed over the depth of the structural member.

23.4.4 Stringer-panel model

One notion that is often helpful is to model a reinforced concrete plate replaced by an orthogonal network of stringers and shear-resistant infill panels. External forces can be applied either concentrated at the joints of the network or distributed along the stringers.

We shall consider a 250 mm thick plate subjected to a shear flow of 750 kN/m in order to explain this model. The plate serves as the bottom plate of a hollow box girder with side webs at a spacing of 2 m. There is a square access opening measuring 0.7×0.7 m in the centre of the plate. Fig. 23.27 shows a corresponding stringer-panel model with four transverse stringers (1 to 4) at a spacing of 800 mm and two longitudinal stringers (B, C) which are 800 mm apart and 600 mm from the side webs (A, D).

Assuming symmetrical behaviour, the shear flows in the four panels adjoining the opening are statically determinate, and therefore we can also calculate the shear flows in the four panels in the corners of the model plus the forces in the stringers as well. The maximum shear flow of 1250 kN/m occurs in the two panels between the opening

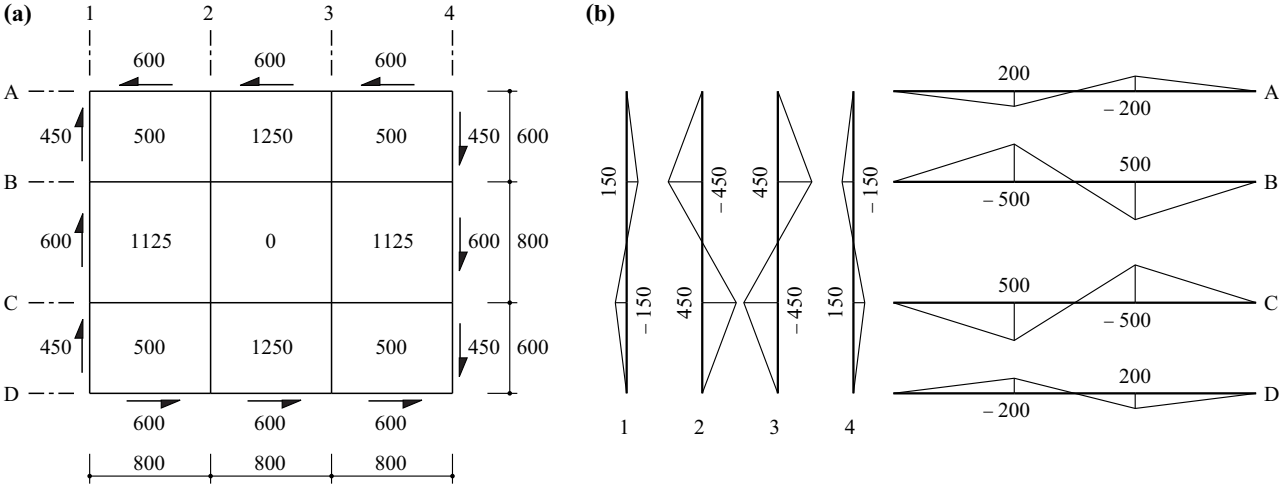

Fig. 23.27 Stringer-panel model: (a) overview (forces in kN, dimensions in mm, shear flows in kN/m), (b) stringer forces (kN)

and the web, and the maximum forces of ± 500 kN in the longitudinal stringers occur at the corners of the opening.

The relationships (23.26) can be used to dimension the panels. If the stringer forces cannot be accommodated locally by concentrations of reinforcement or compression zones, then they must be transferred to the panels at the side, which must then be able to handle such forces. This approach requires additional transverse reinforcement, for which it is expedient to employ truss models for the dimensioning, in a similar way to the bursting reinforcement required at the anchorages of prestressing tendons.

As with the development of truss models and discontinuous stress fields within the scope of the equilibrium conditions, there is plenty of leeway when developing stringer-panel models. With more and more practice, this freedom can be utilised better and better, and the outcome is an individual procedure that enables the flow of the forces – on both a large and a small scale – in a structure to be ascertained with an accuracy that is adequate for the respective purpose.

23.5 Kinematic method

23.5.1 Applications in reinforced concrete

23.5.1.1 Overview

Fig. 23.28(a) illustrates the typical collapse mechanism of an under-reinforced beam subjected to bending moments and shear forces. Theoretically, a collapse crack opens up (see regime 1 discussion in section 23.3.1), which is intersected by yielding longitudinal reinforcing bars and shear links.

When the longitudinal reinforcement is strong enough, it does not yield, and a web crushing failure according to Fig. 23.28(b) can occur (regime 2 in section 23.3.1.3). The failure is characterised by yielding of the shear links and crushing of the web concrete in a parallelogram-shaped region; in this situation, the lines parallel with the inclined boundary lines within the area are active slip lines II according to Fig. 23.9(c).

Similar translation mechanisms with a discrete slip line are possible in corbels, for example, see Fig. 23.28(c). The result for pure strut action is generally rotation mechanisms with hyperbolic slip lines, see Fig. 23.28(d).

In the case of continuous beams and statically indeterminate frames, the areas in which plastic deformations occur (region I according to section 21.2.1), must be sufficiently extended in order that collapse mechanisms can actually become established. It is possible to use Fig. 21.3 as a guide here and replace the plastic hinges that occur by discontinuities of the type shown in Fig. 23.28, see Fig. 23.29. In doing so, it is important

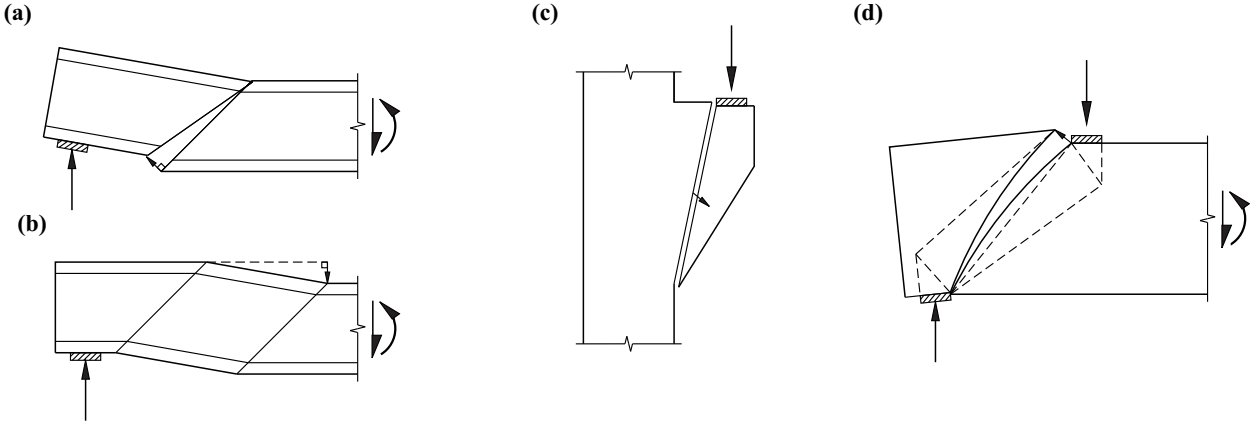

Fig. 23.28 Applying the kinematic method to plates: (a) flexural-shear failure, (b) web crushing failure, (c) corbel failure, (d) hyperbolic slip line corresponding to pure strut action

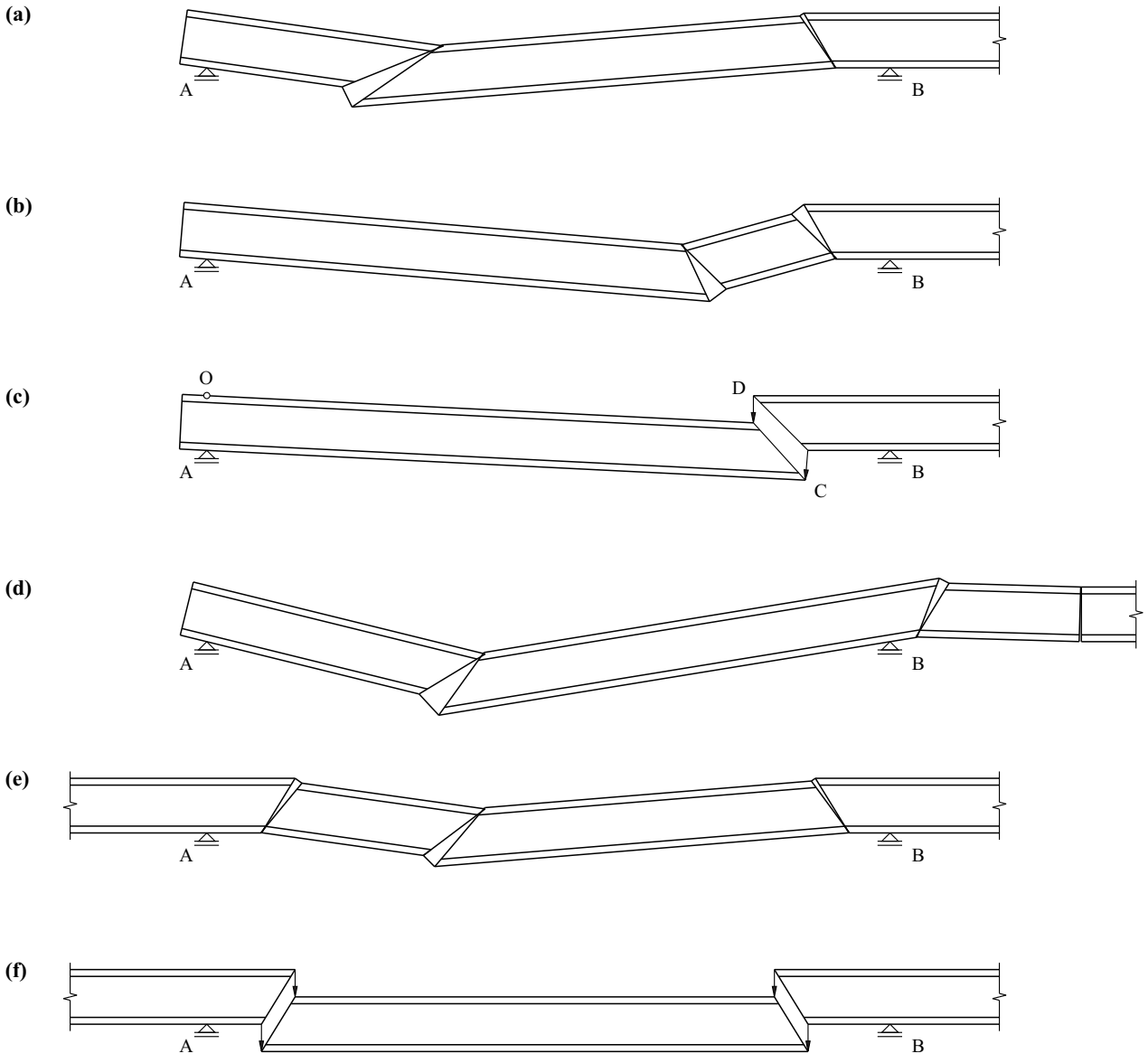

Fig. 23.29 Collapse mechanisms for continuous beams

to realise that, for example, a rotation mechanism with a slip line according to Fig. 23.29(c) in an end span of a continuous beam is already enough to cause collapse. Likewise, a translation mechanism with two slip lines according to Fig. 23.29(f) can lead to failure of an interior span in a continuous beam.

23.5.1.2 Flexural failure

Simple flexural failure mechanisms are often compatible with discontinuous stress fields, see (21.2) and section 21.2.4. For example, the stress field shown in Fig. 23.24(a) is compatible with a collapse mechanism that exhibits a collapse crack that starts at C and has an open end at B, and in which the concrete is crushed along CD. The two halves of the plate rotate with respect to each other about point C; $\alpha = \pi/2$ and $\alpha = -\pi/2$ apply along BC and CD according to Fig. 7.12(b). Points C, D and E in the stress field shown in Fig. 23.24(b) play the roles of B, C and D in Fig. 23.24(a).

A collapse mechanism compatible with the stress field of Fig. 23.25 is one in which there is a collapse crack along AE and a crushing zone along AC.

The collapse mechanisms compatible with Fig. 23.26 are those with centre of rotation J and crushing zone JK and one or more collapse cracks in area IJH running towards J.

We can see that the crushing of the concrete compression zones considered here is only possible in a coplanar stress state. The strain increments perpendicular to the plane of the plate are uninhibited in this case, see the remark following (7.38).

23.5.1.3 Flexural-shear failure

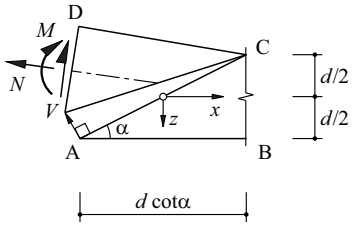

Fig. 23.30 Flexural-shear failure

Fig. 23.30 shows an element of a beam with parallel chords AB and CD at a spacing d; N, V and M are the stress resultants in cross-section AD at the open end A of a collapse crack and A_s denotes the cross-sectional area of the reinforcement in the tension chord at point A. There is also reinforcement distributed uniformly over the plate in the x and z directions, the cross-sectional areas of which related to the unit width are a_{sx} and a_{sz} respectively. All the reinforcement has a yield limit f_y.

A unit rotation about C gives us the work equation

$$M + N\frac{d}{2} + Vd\cot\alpha = A_s f_y\, d + a_{sx} f_y \frac{d^2}{2} + a_{sz} f_y \frac{(d\cot\alpha)^2}{2}$$

or rather

$$\frac{M}{d} + \frac{N}{2} - A_s f_y - a_{sx} f_y \frac{d}{2} = -V\cot\alpha + a_{sz} f_y \frac{d}{2}\cot^2\alpha$$

Differentiating the expression on the right with respect to cotα and equating to zero results in

$$V = a_{sz} f_y d\cot\alpha \tag{23.35}$$

and therefore

$$\frac{M}{d} + \frac{1}{2}(N - a_{sx} f_y d) + \frac{V\cot\alpha}{2} = A_s f_y \tag{23.36}$$

applies.

Example 23.7 Curtailed reinforcement in tension chord

The tension chord reinforcement in the beam shown in Fig. 23.31, with d = 1.11 m, is curtailed from eight to four Ø30 mm bars at A. The Ø10 mm two-leg shear links at a spacing of 200 mm provide $a_{sz} = 5^2 \cdot \pi \cdot 2/0.2 = 785\,\text{mm}^2/\text{m}$. The structural longitudinal reinforcement distributed over the depth of the beam is neglected, $a_{sx} = 0$. The task is to check the admissibility of curtailing A_s for the given forces and assuming $f_y = 435\,\text{N/mm}^2$.

We introduce a collapse crack AC with centre of rotation C and assume that the first and last shear links in the critical zone are located at sections AD and BC, but do not intersect the collapse crack and thus remain rigid. We therefore get the expressions

$$\dot{W} = 655 \cdot (1.5 + n \cdot 0.2) - 87 \cdot 1.5 \cdot (0.75 + n \cdot 0.2) - 13.5 \cdot (n \cdot 0.2)^2/2$$

$$\dot{D} = 4 \cdot 15^2 \cdot \pi \cdot 435 \cdot 1.11 + (n-1) \cdot 2 \cdot 5^2 \cdot \pi \cdot 435 \cdot n \cdot 0.2/2$$

for the work of the external forces, or rather the dissipation work. When n = 8, we get the minimum ratio $\dot{D}/\dot{W}$ = 1747.9 kNm/1706.5 kNm = 1.024 > 1. So the curtailment is permissible, albeit only just.

Assuming continuously dristibuted instead of individual shear links, then (23.35) results in cotα = (655 – 87·1.5)/(785·435· 1.11) = 1.383. The left side of (23.36) then equals [655·1.5 – 87·(1.5)^2/2]/1.11 + (655 – 87·1.5)·1.383/2 = 1159.7 kN, which is 1.061 times smaller than the resistance $A_s f_y = 4 \cdot 15^2 \cdot \pi \cdot 435 = 1229.9$ kN.

This example shows that it is not safe to assume continuously distributed reinforcement. Taking into account reinforcing bars at discrete spacings leads to lower limit loads. This effect can be considerable if the spacing of the bars is large compared with the depth of the beam and must be taken into account.

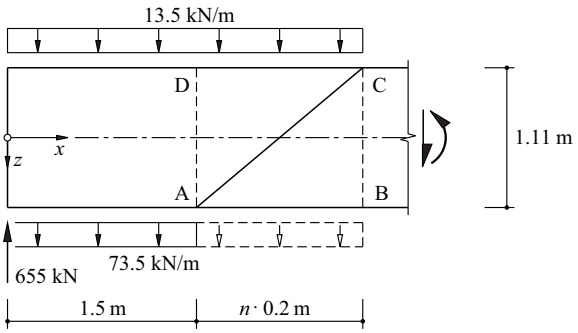

Fig. 23.31 End of beam with open end A of collapse crack and curtailed tension chord reinforcement

23.5.1.4 Web crushing failure

The parallel-chord beam shown in Fig. 23.32 (chord spacing d, web thickness h) is reinforced with vertical shear links at a spacing s, each of which has a cross-sectional area A_{sz} and a yield limit f_y. The effective concrete compressive strength is f_c. As in Fig. 23.31, discrete slip lines between the ends of the shear links are considered in such a way that the first and last shear links are not activated.

If a translation mechanism is assumed, then the following applies for the work of the external forces:

$$\dot{W} = V + \int_0^{ns} q_{\text{inf}} \mathrm{d}x \tag{23.37}$$

and using (7.38), the result for the dissipation work is

$$\dot{D} = (n-1)A_{sz}f_y + \frac{f_c h}{2}\left(\sqrt{d^2 + (ns)^2} - ns\right) \tag{23.38}$$

Varying n allows us to determine the most critical (smallest) ratio $\dot{D}/\dot{W}$ from (23.37) and (23.38).

Assuming continuously distributed shear links with $a_{sz}f_{yz} = A_{sz}f_y/s$, it follows from $(23.20)_2$ and $(23.22)_2$ (assuming $n_z = 0$ and $V = dn_{xz}$) that

$$V = hdf_c\sqrt{\frac{A_{sz}f_y}{shf_c}\left(1 - \frac{A_{sz}f_y}{shf_c}\right)} \quad , \quad \cot\alpha = \sqrt{\frac{shf_c}{A_{sz}f_y} - 1} \tag{23.39}$$

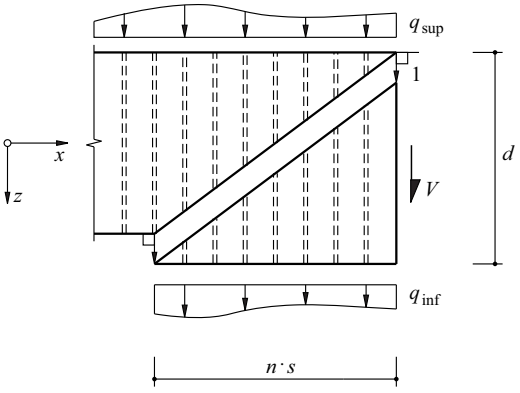

Fig. 23.32 Web crushing failure along slip line between ends of shear links

Differentiating the expression on the right in (23.38) with respect to n and equating to zero results in

$$A_{sz}f_y + \frac{f_c h}{2}\left(\frac{ns^2}{\sqrt{d^2+(ns)^2}} - s\right) = 0$$

i. e.

$$\frac{ns}{\sqrt{d^2+(ns)^2}} = 1 - 2\frac{A_{sz}f_y}{shf_c}$$

Using $(23.39)_2$, we therefore get

$$\frac{ns}{\sqrt{d^2+(ns)^2}} = \cos(2\alpha)$$

i. e. the inclination of the slip line with respect to the x axis is twice as large as the inclination α of the principal compressive stresses in the concrete, which amount to f_c. When considering the limiting case $s \to 0$ and neglecting q_{inf}, then (23.37) and (23.38) therefore lead to (23.39) – see the discussion regarding regime 2 in section 23.3.1.4.

Example 23.8 Web crushing failure

A beam with $d = 2\,\text{m}$, $h = 0.3\,\text{m}$ and $f_c = 12\,\text{N/mm}^2$ is reinforced with Ø14 mm two-leg shear links at a spacing $s = 250\,\text{mm}$ ($f_y = 435\,\text{N/mm}^2$). Putting $A_{sz} = 2 \cdot 7^2 \cdot \pi = 308\,\text{mm}^2$, eq. (23.39) gives us $V = 2562\,\text{kN}$ and $\alpha = 22.7°$. However, putting $q_{\text{inf}} = 0$, we get, the minimum value $V = 2429\,\text{kN}$ for $n = 8$ by equating (23.37) and (23.38), i. e. compared with assuming continuously distributed shear links, a resistance that is 5.2 % lower.

23.5.1.5 Rotation mechanism with hyperbolic slip line

The rectangular area ABCD in Fig. 23.33 – like in a prism compression test – is loaded by homogeneous compressive stresses of magnitude f_c. The task is to find the most general rotation mechanism with a discontinuity line between points A and C. To do this we shall assume a system of Cartesian coordinates parallel with the principal directions 1, 3 of the stress state with centre of rotation O and consider any random point P on the discontinuity line with the coordinates x and z. The principal directions 1 and 3 bisect the angles between slip lines I and II at P and therefore the differential equation

$$\frac{\mathrm{d}x}{-\mathrm{d}z} = \frac{x}{z}$$

applies, which has the solution

$$xz = \text{const} \tag{23.40}$$

i. e. slip line AC is a hyperbola. As $x_A = x_D$, $z_A = z_B$, $x_C = x_B$, $z_C = z_D$ and $x_A z_A = x_C z_C$, then $x_D z_B = x_B z_D$ or $x_B/z_B = x_D/z_D$, i. e. the centre of rotation O lies on the continuation of diagonal BD.

The rotation mechanism becomes a translation mechanism with the straight discontinuity line AC if O migrates to infinity. If, on the other hand, O coincides with D, a collapse crack opens along DC, and the concrete is crushed along DA; the hyperbola degenerates to the right-angle ADC.

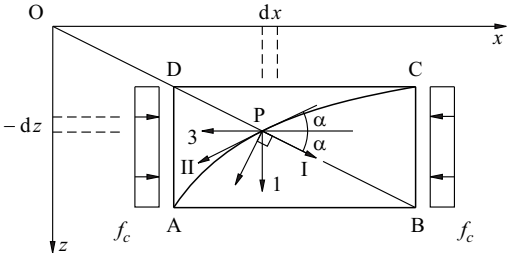

Fig. 23.33 Rotation mechanism compatible with strut action

Example 23.9 Dissipation at hyperbolic slip line

Fig. 23.34 corresponds to the rotation mechanism illustrated in Fig. 23.29(c), which has a hyperbolic slip line CD in the end span AB of a continuous beam whose web has a cross-sectional area dh. The task is to find an expression for the energy $\dot{D}_c$ dissipated in the concrete for a unit rotation about O. The following applies for the end C of the slip line:

$\xi_C = x_C \cos\alpha + d \sin\alpha \quad , \quad \eta_C = x_C \sin\alpha - d \cos\alpha$

As $\xi\eta$ = const, $\xi_D = x_D \cos\alpha$ and $\eta_D = x_D \sin\alpha$, we obtain

$x_D^2 = x_C^2 - d^2 - 2 x_C d \cot(2\alpha)$

which means that strut CFDE is known with respect to C and α. Instead of using (7.38) to determine $\dot{D}_c$ by integrating along CD, it is easier to calculate the work (with the same magnitude) of the compressive stresses (which are uniformly distributed over DE and amount to f_c) at the mean displacement $(\eta_D + \eta_C)/2$:

$$\dot{D}_c = (\eta_D - \eta_C) f_c h (\eta_D + \eta_C)/2 = (\eta_D^2 - \eta_C^2) f_c h/2 = \frac{f_c dh}{2} (x_C \tan\alpha - d)$$

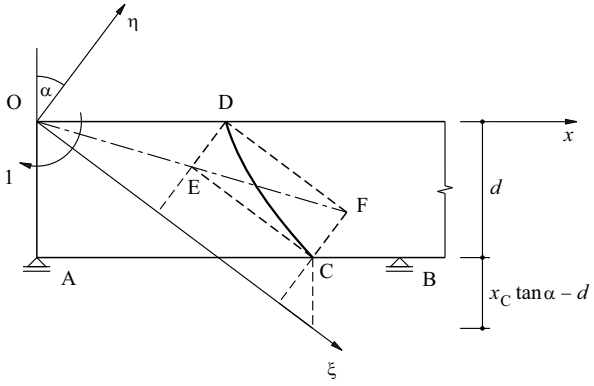

Fig. 23.34 Rotation mechanism with hyperbolic slip line in the end span of a continuous beam

23.5.2 Applications in geotechnical engineering

23.5.2.1 Overview

Methods for dealing with geotechnical engineering problems have been developed and used since the second half of the 18th century. However, the theory behind those methods did not become fully available until the formulation of the upper- and lower-bound theorems of plastic theory around the middle of the 20th century. Most of the methods involve applications of the kinematic method and corresponding approximation methods. Fig. 23.35 provides an overview.

Fig. 23.35(a) shows the COULOMB. yield condition in the stress plane, see Fig. 7.10(a). Fig. 23.35(b) specifies orders of magnitude for cohesion c and angle of internal friction φ for soil, rock, concrete and steel. As the reader can see, the COULOMB yield condition (possibly modified by limiting or neglecting the tensile strength) allows diverse construction materials and subsoil types to be handled in the same way

Fig. 23.35(c) and (d) illustrate the slip line fields and collapse mechanisms associated with problems of active and passive earth pressure. The slip lines intersect at angles of $\pi/2 \pm \varphi$ and do not undergo any change in length upon failure. At failure, a relative displacement of the bodies separated by the slip line takes place along a slip line acting as a kinematic discontinuity line. As the relative displacement is inclined at an angle φ to the slip line, there is a dilatation for $\varphi > 0$. The obtuse (acute) angles formed by the slip lines are decreased (increased) in corresponding homogeneous deformation states, which again causes a dilatation for $\varphi > 0$.

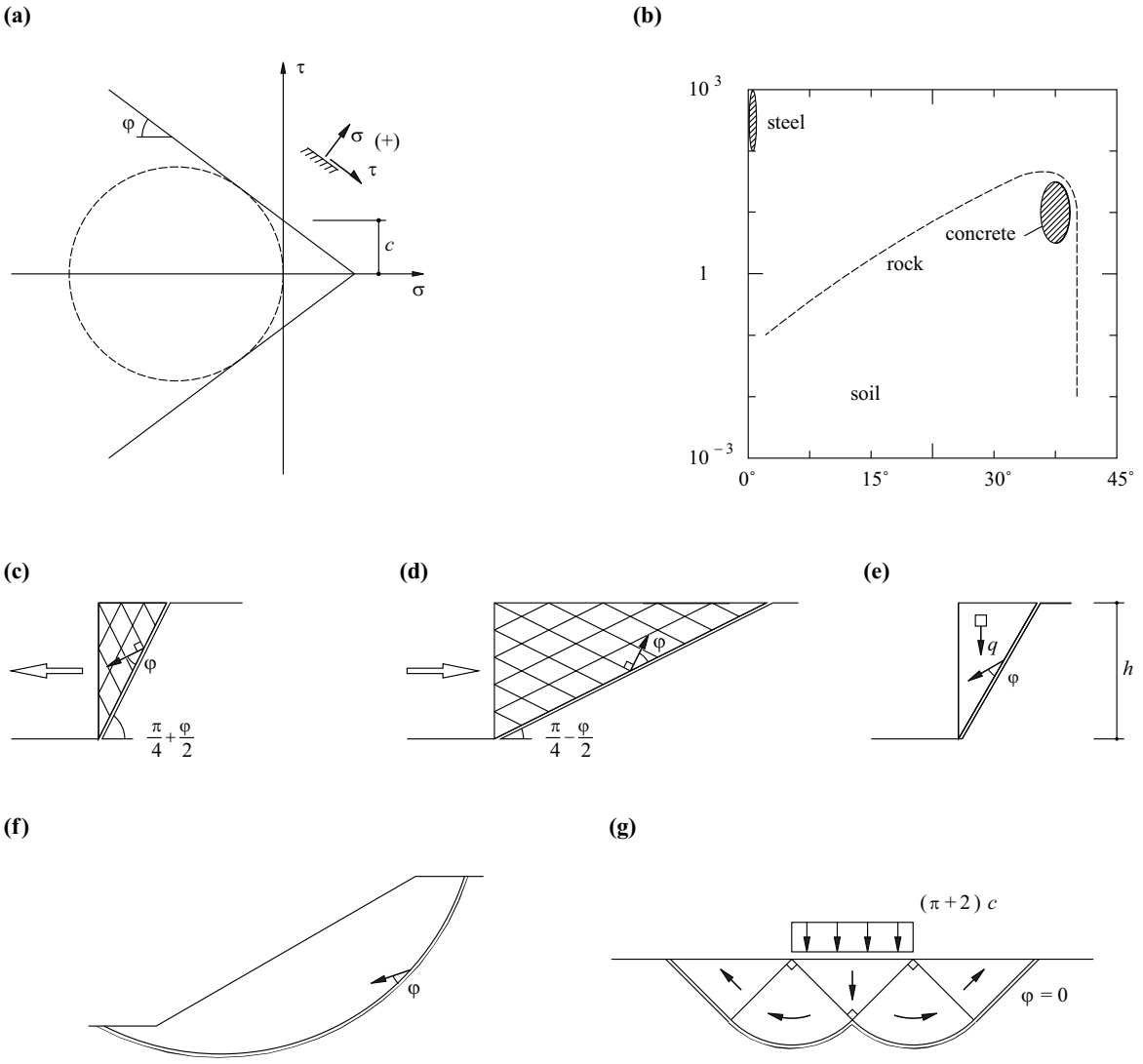

Fig. 23.35 Application of limit analysis to geotechnical engineering problems: (a) COULOMB yield condition, (b) orders of magnitude of cohesion c [N/mm^2] and angle of internal friction φ, (c) active earth pressure, (d) passive earth pressure, (e) unsupported height of vertical embankment, (f) rotational slip failure, (g) load-carrying capacity of strip foundation

If we apply a mechanism analogous with Fig. 23.35(c) to the problem of the unsupported height of a vertical embankment shown in Fig. 23.35(e), we get the following bound (exercise 23.19):

$$h \leq \frac{4c\cos\varphi}{q(1-\sin\varphi)} \tag{23.41}$$

where q is the body load of the soil, which is assumed to be constant, see (23.32). Potential rotational slip failures generally require an analysis of mechanisms with slip lines in the form of logarithmic spirals according to Fig. 23.35(f). However, for simplicity, and because of the inhomogeneity of the subsoil, appropriate approximation methods are used in most situations.

Finally, Fig. 23.35(g) illustrates the problem of the load-carrying capacity of a strip foundation on a TRESCA half-space ($\varphi = 0$). Using the mechanism shown in the figure and additional considerations, it is possible to show that the limit load amounts to $(\pi + 2)c$, see example 23.10.

It is obvious from Fig. 23.35 that in geotechnical engineering, in contrast to reinforced concrete construction, the kinematic method of plastic theory or corresponding approximation methods are the most popular approaches. However, static methods are becoming ever more important as construction in built-up areas becomes increasingly complex. Following the flow of the forces, i. e. ascertaining the equilibrium on the small scale, is the aspect that characterises the static method, and this method occurs more and more alongside investigating the equilibrium on the large scale which is possible with the kinematic method. The need for an in-depth examination of local force variables results from the growing use of all kinds of reinforcement, anchorages and injection methods. In a similar way to reinforced concrete construction, this leads to composite forms of construction, and the properties of the subsoil and the construction materials are exploited in a very specific way.

The application of plastic theory to reinforced concrete benefited enormously from corresponding earlier developments in geotechnical engineering. It seems possible that now some developments in concrete construction could be transferred to geotechnical applications, with similar benefits.

23.5.2.2 Logarithmic spirals as slip lines

Consider the differential element of a slip line in COULOMB material shown in Fig. 23.36, where $\mathrm{d}r = r\mathrm{d}\theta\tan\varphi$. Integrating results in

$$r = r_0 \mathrm{e}^{\theta\tan\varphi} \tag{23.42}$$

i. e. the equation for a logarithmic spiral. Using (7.36) with $\alpha = \varphi$ and $0 \le \theta \le \beta$ and a unit rotation about the fulcrum O results in the incremental dissipation work

$$\dot{D} = \int_0^\beta c\cos\varphi \cdot r\frac{\mathrm{d}\theta}{\cos\varphi} = \int_0^\beta cr^2\mathrm{d}\theta = \frac{cr_0^2}{2\tan\varphi}(\mathrm{e}^{2\beta\tan\varphi} - 1) \tag{23.43}$$

In TRESCA material ($\varphi = 0$) the logarithmic spiral (23.42) degenerates to the circle $r = r_0 = \text{const}$, and we get the expression $\dot{D} = cr_0{}^2\beta$ instead of (23.43).

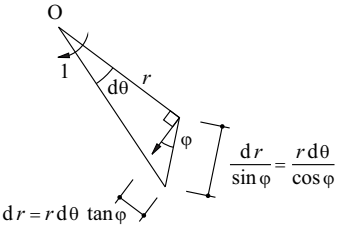

Fig. 23.36 Element of a slip line in the form of a logarithmic spiral

Example 23.10 Strip foundation on TRESCA half-space

The problem shown in Fig. 23.37 has already been investigated statically in example 23.6 (Fig. 23.20). In the following, the lower bound $5c$ for the bearing pressure q beneath the strip foundation derived in that example is supplemented by corresponding upper bounds.

For the mechanism of Fig. 23.37(a) it is assumed that BB′A (a rigid body) is displaced vertically downwards by the amount 1. The rigid bodies ABC, AB′C′ and BCD, B′C′D′ to the sides are thus displaced by 1 or $\sqrt{2}$ as indicated by the arrows. Relative displacements of $\sqrt{2}$ ensue along AB, AB′ and CD, C′D′, and relative displacements of 1 along AC, AC′ and BC, B′C′. The work equation is

$$qb \cdot 1 = 2 \cdot (b/2) \cdot c \cdot (2 \cdot \sqrt{2} \cdot \sqrt{2} + 2 \cdot 1 \cdot 1) = 6bc$$

from which it follows that the upper bound for q is $6c$.

A slip line AC in the form of a circular arc with centre at O is assumed in the mechanism of Fig. 23.37(b). A rotation of 1 about O gives us the work equation

$$\frac{qb^2}{2} \cdot 1 = c\frac{b^2}{\sin^2\beta}2\beta$$

Differentiating this relationship for q with respect to β and equating to zero, we find that the minimum point of q is given by $\tan\beta = 2\beta$, from which it follows that $\beta = 66.782°$ and $q \le 5.52c$.

In the mechanism of Fig. 23.37(c), rigid body BB′A is displaced by 1 vertically downwards, and the rigid bodies BCD, B′C′D′ to the sides are displaced by $1/\sqrt{2}$ in the direction of the arrows. Quadrant ABC rotates, on the one hand, by an amount $1/b$ about B in the anticlockwise direction; on the other, it undergoes a shear deformation that is characterised by the fact that boundaries AB and CB rotate clockwise by the amount $1/b$ about the displaced points A and C respectively. Opposite displacements ensue for area AB′C′. There are no relative displacements along BC and B′C′.

In quadrant ABC, the radii r originating from B and the concentric circles orthogonal to these do not experience any strains ($\dot{\varepsilon}_r = \dot{\varepsilon}_\varphi = 0$); they form the slip line field. We use (23.13) to obtain the shear strain increment $\dot{\gamma}_{r\varphi} = 1/(\sqrt{2}r)$ from the displacement $r/b - 1/\sqrt{2}$ in the tangential direction and consequently the incremental dissipation work

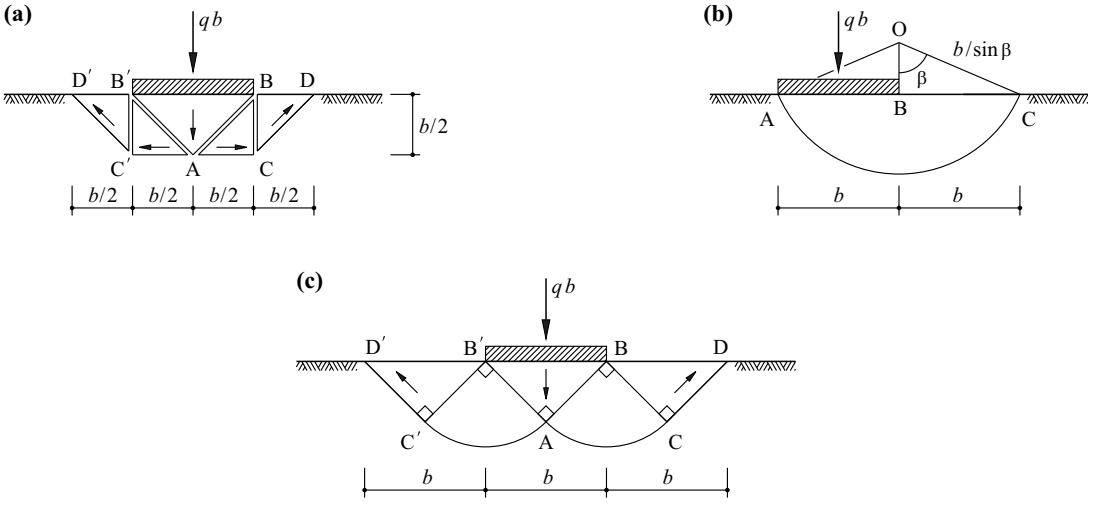

Fig. 23.37 Failure mechanisms for a strip foundation on a weightless TRESCA half-space

$$\dot{D}_{ABC} = \int_0^{b/\sqrt{2}} \int_0^{\pi/2} \frac{c}{\sqrt{2}r} r \, d\varphi dr = \frac{cb\pi}{4}$$

by applying (7.32) in area ABC. The corresponding expressions for slip lines AC, AB and CD are

$$\dot{D}_{AC} = c \cdot \frac{1}{\sqrt{2}} \cdot \frac{b}{\sqrt{2}} \cdot \frac{\pi}{2} = \frac{cb\pi}{4} \quad , \quad \dot{D}_{AB} = \dot{D}_{CD} = c \cdot \frac{1}{\sqrt{2}} \cdot \frac{b}{\sqrt{2}} = \frac{cb}{2}$$

In total, the result is

$$\dot{D} = 2 \cdot \left(2 \cdot \frac{cb}{2} + 2 \cdot \frac{cb\pi}{4} \right) = cb(2 + \pi)$$

and by equating this with the external work qb we get

$q \leq c(2 + \pi)$

according to the upper-bound theorem.

The stress state compatible with the deformation state in ABC described here is given by $\sigma_r = \sigma_\varphi = -c(1 + 2\varphi)$ and $\tau_{r\varphi} = c$, with φ being measured from BC. A compressive stress state with horizontal and vertical principal stresses of πc and $(2 + \pi)c$ respectively prevails in area ABB′. Outside of BC und B′C′, the result is horizontal compressive stresses of $2c$. The continuation of the stress state beneath quadrants AC and AC′ can be achieved without infringing the TRESCA yield condition, but will not be pursued further here [4]. As we have a statically admissible stress state and a state of deformation compatible with this, we are dealing with a complete solution, and the following applies:

$q = c(2 + \pi)$

23.6 Summary

1. Following a brief look at the theory of elastic plates, this chapter is devoted to applying limit analysis to reinforced concrete plates and related problems in geotechnical engineering.
2. For constant loads, the AIRY stress function defined in (23.3) generally satisfies the bipotential equation (23.5).
3. A formulation with polar coordinates using the stress components (23.9) and the LAPLACE operator (23.10) is often worthwhile. In the case of rotationally symmetric problems, the bipotential equation (23.11) is simplified to the homogeneous ordinary fourth-order different differential equation (23.15) with the general solution (23.16).
4. In order to solve elastic plate problems, an alternative approach is to assume approximations for the displacement components instead of using stress functions. With constant loads, the result is analogous homogeneous bipotential equations, as for the stress functions.

5. The ultimate resistance of reinforced concrete plate elements with orthogonal reinforcement can be described by the yield conditions (23.20). In doing so, it is presumed that the square yield condition (7.37) is valid for the concrete in the coplanar stress state, and that the reinforcement consists of finely distributed, rigid - perfectly plastic fibres rigidly bonded to the concrete.
6. When both layers of reinforcement yield in tension (regime 1), collapse cracks open up parallel with the principal compression direction in the concrete. The dimensioning of the reinforcement can be carried out by presuming (23.25) based on the relationships (23.26).
7. If only one of the two layers of reinforcement yields in tension (regime 2), the concrete is crushed along a slip line. The principal compression direction in the concrete then bisects the angle between the slip line and the direction of the reinforcement that is not yielding.
8. The considerations for orthogonal reinforcement layouts can be transferred to skew and multi-layer reinforcement layouts without any fundamental difficulties.
9. Truss models, discontinuous stress fields and stringer-panel models enable a consistent treatment of (cracked) reinforced concrete plates on the basis of the lower-bound theorem.
10. An iterative procedure is generally necessary when developing truss models. Any distributed forces can be replaced by statically equivalent forces. The plate areas corresponding to the truss members and joints must fit into the given geometry and the forces to be carried by the reinforcing bars must be transferred correctly.
11. The normal stress components parallel with a stress discontinuity line may change abruptly. The poles of the MOHR's circles for the stress states on either side lie together with the common stress point on a straight line parallel with the discontinuity line.
12. When stress fields overlap, the stress vectors for surface elements in the same direction must be added vectorially.
13. The intersections of the boundary lines of three struts in equilibrium with each other define a triangular nodal zone. The stress state in the nodal zone results from the stress discontinuities at its boundaries.
14. If the same compressive stress prevails in all struts, then each adjoins the nodal zone at a right-angle and there is a (biaxial) hydrostatic stress state in the zone.
15. Discontinuous stress fields made up of homogeneous partial stress fields are especially suitable for considering the resistance of the (generally uniformly distributed) minimum reinforcement.
16. It is often helpful to use the notion of an orthogonal network of stringers with shear-resistant infill panels as a model. External forces can thus be applied as point loads at the joints of this network or as loads distributed along the stringers.
17. Flexural and flexural-shear failure mechanisms are characterised by collapse cracks that open up orthogonal to their direction. Reinforcement crossing the collapse cracks yields in tension.
18. In web crushing failures, the concrete is crushed along a slip line or in an area with parallel slip lines. The reinforcement orthogonal to the relative displacement vector at the slip line remains rigid.
19. Collapse cracks and slip lines generally begin and end at the ends of the discretely spaced reinforcing bars. The outermost reinforcing bars are not activated in this situation and compared with the assumption of continuously distributed reinforcement, there is a certain reduction in the ultimate resistance.
20. When there is a strut-type uniaxial compressive stress state at the yield limit, a rotation mechanism is compatible with a hyperbolic slip line in the most general case. The origin of the system of coordinates – in which hyperbola equation (23.40) applies – parallel with the boundaries of the strut lies on a continuation of the strut diagonal in the opposite direction to the slip line.

21. The COULOMB yield condition (possibly modified by limiting or neglecting the tensile strength) permits a uniform treatment of diverse problems in structures and geotechnics.
22. Assuming the COULOMB yield condition, the slip lines intersect at angles of $\pi/2 \pm \varphi$, e. g. in the form of radii and logarithmic spirals. The logarithmic spirals become circles at the TRESCA limiting case $\varphi = 0$.

23.7 Exercises

23.1 Show that the relationship

$$\Delta\Delta F = -\frac{1-2\nu}{1-\nu}\Delta\Pi_e$$

similar to (23.4) applies for the coplanar strain state (see section 8.2.5).

23.2 Show that the functions $f_1 + xf_2, f_1 + yf_2$ and $f_1 + (x^2 + y^2)f_2$ are bipotential functions, i. e. satisfy (23.5) when f_1 and f_2 are potential functions, i. e. satisfy $\Delta f_1 = 0$ and $\Delta f_2 = 0$.

23.3 Show that (23.6) is a stress function, i. e. satisfies (23.5).

23.4 The dam shown in Fig. 23.38(a) is subjected to dead load (density ρ_c) and hydrostatic pressure (density of water = ρ_w). Show that the stress components

$$\sigma_x = -\rho_c g(x - ya/b) + \rho_w g(x - 2ya/b)(a/b)^2\ ,\ \sigma_y = -\rho_w g x\ ,\ \tau_{xy} = -\rho_w g y(a/b)^2$$

satisfy the equilibrium conditions within the dam and the static boundary conditions along the water side OA and the air side OB. Discuss the stress distribution at the underside of the dam AB. What would happen if hydrostatic pressure were to act at the underside of the dam AB and how can this be avoided?

23.5 The area $0 \le x \le a,\ 0 \le y \le b$ has the stress components

$$\sigma_x = \sigma_0(3b - 6y)(a - x)^2/b^3\ ,\ \sigma_y = \sigma_0(3y^2b - 2y^3 - b^3)/b^3\ ,\ \tau_{xy} = \sigma_0 \cdot 6(b - y)y(a - x)/b^3$$

Discuss the internal equilibrium and the static boundary conditions at the boundary of the area. Determine the principal stress trajectories.

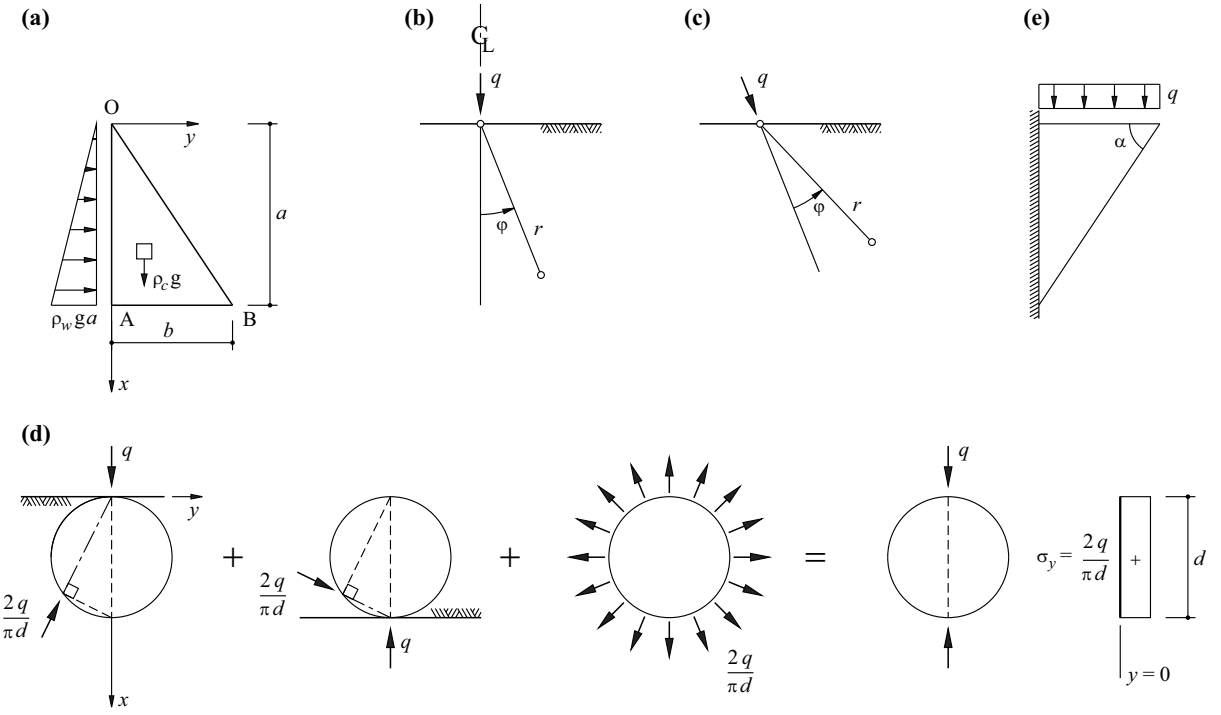

Fig. 23.38 Figures for section 23.7

23.6 Treat the stress state

$\sigma_x = \tau_0(3y - b)(a - x)^2/(ab^2)$, $\sigma_y = -\tau_0 y^2(b - y)/(ab^2)$, $\tau_{xy} = \tau_0 y(3y - 2b)(a - x)/(ab^2)$

in a similar way to exercise 23.5.

23.7 a) Show that the stress function

$$f = \tau\left(r_i^2 - \frac{r^2}{2} - \frac{r_i^4}{2r^2}\right)\cos(2\varphi)$$

describes the stress state in an infinitely large plate that is subjected to a state of pure shear $\sigma_x = -\sigma_y = \tau$ and has a circular hole of radius r_i in its centre. Verify the stress concentration factor $\sigma_{\varphi,\max}/\tau = 4$ at the edge of the hole.

b) Combine the stress state from part a) with the stress state discussed at the end of example 23.2 in such a way that a uniaxial stress state ensues, and show that the corresponding stress concentration factor is 3.

23.8 Compare the solution developed in example 23.3 for the case of $r_e = 2r_i$ with (13.33).

23.9 a) Show that the stress function $f = -qr\sin\varphi \cdot (\varphi/\pi)$ describes the case of a line load q acting on a half-space as shown in Fig. 23.38(b), and compare the stress state with that of exercise 7.4.

b) Show that the stress state from part a) is valid according to Fig. 23.38(c) for forces q in any direction when φ is measured from the direction of the force.

c) Show that superposing two stress states according to part a) and a homogeneous stress state as shown in Fig. 23.38(d) describes the stress state in a cylindrical specimen of diameter d which is loaded by two diametrically opposed line loads q (split-cylinder test). Verify that a constant transverse tensile stress of $2q/(\pi d)$ ensues in the plane of the load.

23.10 Develop an expression similar to $(23.20)_2$ for the pure shear resistance ($n_x = n_z = 0$) of a reinforced concrete plate element that has reinforcement inclined at an angle β to the x axis, and whose reinforcement in the x direction is so strong that it does not yield ($\dot{\varepsilon}_x = 0$). Compare the result for the case $\beta = 45°$ with the case of vertical shear links ($\beta = 90°$).

23.11 Replace the fan area AEF in Fig. 23.11(d) by an arc and discuss the associated flow of the forces in comparison with Fig. 23.11(d).

23.12 Use Fig. 23.14 to expand the considerations to yield regime 2.

23.13 Examine the stress discontinuity lines occurring in Fig. 23.20 with the help of the corresponding MOHR's circles and their poles.

23.14 Discuss the force transfer via bond forces according to the figures on the right of Fig. 23.22(b) or Fig. 23.22(c). In a similar way to Fig. 23.23(b), assume that the forces $\boldsymbol{C}$ or $\boldsymbol{A}$ and $\boldsymbol{B}$ are carried by a finite number of bars and discuss the effect of including confining reinforcement in the form of bars transverse to the plane of the plate.

23.15 Draw the MOHR's circles belonging to the partial stress fields of Fig. 23.24.

23.16 Develop stringer-panel models for a number of the problems shown in the lower half of Fig. 23.12 and Fig. 23.13.

23.17 Develop a discontinuous stress field for the problem of Fig. 23.27.

23.18 The same assumptions apply to the corbel of thickness 1 shown in Fig. 23.38(e) as for Fig. 23.24. Develop a stress field made up of homogeneous partial stress fields and discuss the collapse mechanism compatible with this. Ignore the compressive stresses in the reinforcement and show that the limit load is $\rho f_y \sin^2\alpha/(\cos^2\alpha + \rho f_y/f_c)$.

23.19 Verify (23.41).

23.20 Show that by assuming a logarithmic spiral as a slip line, the factor of 4 occurring in (23.41) can be reduced to 3.83. Note that the centre of rotation is determined by two parameters.

23.21 Replace the right-angles at A and C in Fig. 23.37(c) by $\pi/2 - \varphi$ and $\pi/2 + \varphi$ and quadrant AC by the corresponding logarithmic spirals. Show that the relationship

$$q = c\cot\varphi\left[e^{\pi\tan\varphi}\tan^2\left(\frac{\pi}{4}+\frac{\varphi}{2}\right)-1\right]$$

applies for a weightless COLOUMB material and that it is simplified to $q = c(2 + \pi)$ for the limiting case $\varphi = 0$.

24 SLABS

24.1 Basic concepts

24.1.1 General

The stress resultants connected with plate and shell structures were introduced in section 5.1.7, see Fig. 5.16, as well as relationships (5.14), (5.15) and (5.16). Bending moments, twisting moments and shear forces are our prime concern when looking at slabs (= out-of-plane-loaded elements). Membrane forces are relevant, for example, when slabs function as parts of folded plate structures, also in inhomogeneous cross-sections such as reinforced concrete slabs whose deformations in the plane of the slab are inhibited. In addition, membrane forces generally have to be considered when the deflections of a slab in relation to its thickness can no longer be regarded as small (second-order problems).

The basic static, kinematic and constitutive relationships for homogeneous, linear elastic slabs with small deflections were presented in section 8.2.6. In doing so, a distinction was made between slabs rigid in shear and slabs with finite shear stiffness, in a similar way to framed structures (sections 8.2.2 and 8.2.3).

The first pages of this chapter are devoted to a detailed examination of the static and kinematic relationships (sections 24.1.2 and 24.1.3); second-order effects are also taken into account in this discussion. Section 24.2 contains an outline of the theory of linear elastic slabs rigid in shear with small deflections. Sections 24.3 to 24.5 are concerned with the application of limit analysis to slabs, with the emphasis here on reinforced concrete slabs. Sections 24.6 and 24.7 explain the influence of shear and membrane forces.

24.1.2 Static relationships

24.1.2.1 Equilibrium conditions

According to Fig. 8.8(a) and eq. (8.38), using Cartesian coordinates results in the relationships

$$v_{x,x} + v_{y,y} + q = 0 \quad , \quad v_x = m_{x,x} + m_{xy,y} \quad , \quad v_y = m_{yx,x} + m_{y,y} \tag{24.1}$$

and combining these results in

$$m_{x,xx} + 2m_{xy,xy} + m_{y,yy} + q = 0 \tag{24.2}$$

see (8.47).

We get similar results when using cylindrical coordinates (Fig. 24.1):

$$(rv_r)_{,r} + v_{\varphi,\varphi} + qr = 0 \quad , \quad rv_r = (rm_r)_{,r} - m_\varphi + m_{r\varphi,\varphi} \quad , \quad rv_\varphi = 2m_{r\varphi} + rm_{r\varphi,r} + m_{\varphi,\varphi} \tag{24.3}$$

and combining these results in

$$r \cdot (rm_r)_{,rr} + m_{\varphi,\varphi\varphi} - r \cdot m_{\varphi,r} + 2(rm_{r\varphi})_{,r\varphi} + qr^2 = 0 \tag{24.4}$$

In cases where loading and supports are rotationally symmetric, then $m_{r\varphi}$ and v_φ disappear, and m_r, m_φ and v_r only depend on r. From (24.4) it follows that

$$(rm_r)_{,r} - m_\varphi + \int_0^r qr\mathrm{d}r = 0 \tag{24.5}$$

Theory of Structures. First Edition. Peter Marti

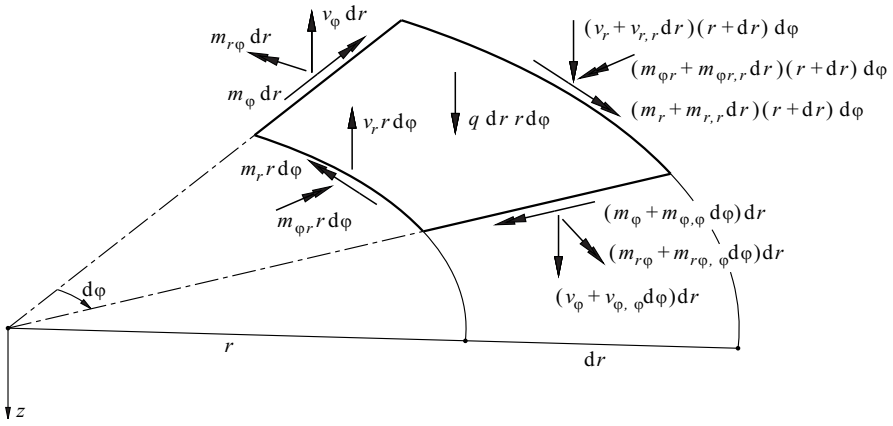

Fig. 24.1 Differential slab element in cylindrical coordinates system

24.1.2.2 Stress transformation

We can read off

$$\overline{\boldsymbol{v}} = \begin{Bmatrix} v_n \\ v_t \end{Bmatrix} = \begin{bmatrix} \cos\varphi & \sin\varphi \\ -\sin\varphi & \cos\varphi \end{bmatrix} \begin{Bmatrix} v_x \\ v_y \end{Bmatrix} = \boldsymbol{c}^{\mathrm{T}} \bullet \boldsymbol{v} \tag{24.6}$$

from Fig. 24.2. Where $m_{ij} = m_{ji}$, it also follows that

$$\begin{Bmatrix} m_n \\ m_t \\ m_{nt} \end{Bmatrix} = \begin{bmatrix} \cos^2\varphi & \sin^2\varphi & \sin(2\varphi) \\ \sin^2\varphi & \cos^2\varphi & -\sin(2\varphi) \\ -\sin\varphi\cos\varphi & \sin\varphi\cos\varphi & \cos(2\varphi) \end{bmatrix} \begin{Bmatrix} m_x \\ m_y \\ m_{xy} \end{Bmatrix} \tag{24.7}_1$$

or rather

$$\overline{\boldsymbol{m}} = \boldsymbol{c}^T \bullet \boldsymbol{m} \bullet \boldsymbol{c} \tag{24.7}_2$$

where

$$\boldsymbol{c} = \begin{bmatrix} \cos\varphi & -\sin\varphi \\ \sin\varphi & \cos\varphi \end{bmatrix}$$

denotes the rotation matrix introduced in (A6.1), see $(6.7)_3$.

According to (24.6) and (24.7), the shear force components constitute a vector $\boldsymbol{v}$ and the moment components a symmetric tensor

$$\boldsymbol{m} = \begin{bmatrix} m_x & m_{xy} \\ m_{yx} & m_y \end{bmatrix} \tag{24.8}$$

Eq. $(24.7)_1$ and (24.8) are similar to (5.21) and (5.27). If we replace σ and τ in Fig. 5.20 by m_n and m_{tn}, then the MOHR's circle approach can be used in a similar way. The principal moments and their directions are

$$m_{1,2} = \frac{m_x + m_y}{2} \pm \sqrt{\left(\frac{m_x - m_y}{2}\right)^2 + m_{xy}^2} \quad , \quad \tan(2\varphi_1) = \frac{2m_{xy}}{m_x - m_y} \tag{24.9}$$

and these variables

$$m_{\mathrm{I}} = m_1 + m_2 = m_x + m_y = m_n + m_t \quad , \quad m_{\mathrm{II}} = -m_1 m_2 = m_{xy}^2 - m_x m_y \tag{24.10}$$

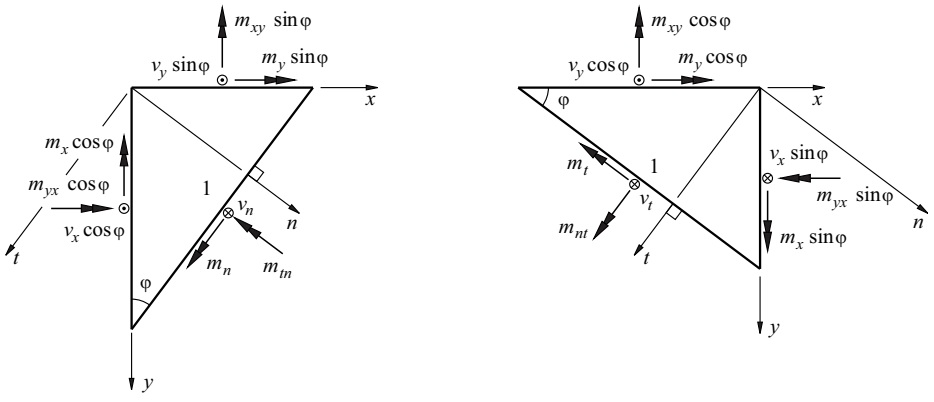

Fig. 24.2 Free body diagrams

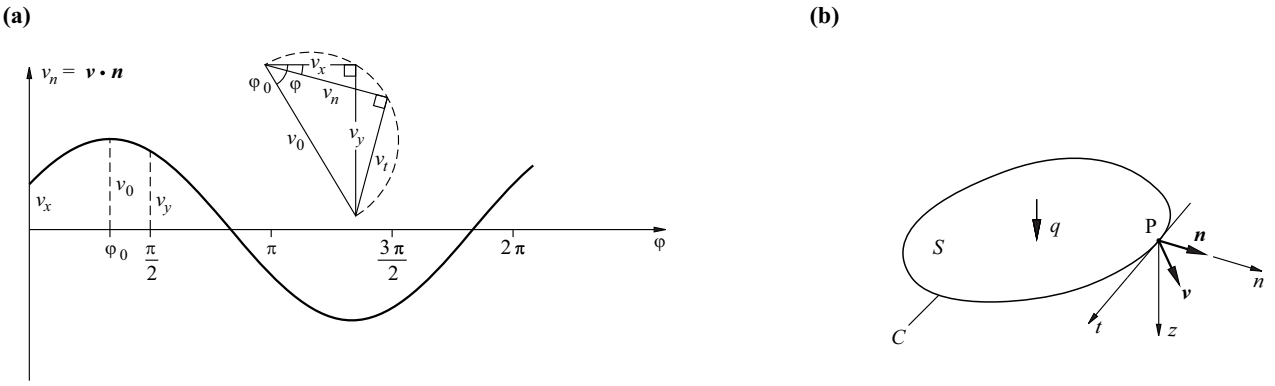

Fig. 24.3 Shear flow: (a) directional dependence at one point, (b) simply-connected slab area

are invariant.

24.1.2.3 Shear flow

The magnitude and direction of the shear force vector $\boldsymbol{v}$ is given by

$$|\boldsymbol{v}| = v_0 = \sqrt{v_x^2 + v_y^2} = \sqrt{v_n^2 + v_t^2} \quad , \quad \tan\varphi_0 = \frac{v_y}{v_x} \tag{24.11}$$

see Fig. 24.3(a); v_0 is known as the *principal shear force*, and $v_n = 0$ in the direction $\varphi_0 + \pi/2$. The principal directions of the shear forces and the moments coincide in special cases only; generally, $\varphi_0 \neq \varphi_1$.

Eq. $(24.1)_1$ can be expressed in the form

$$\operatorname{div} \boldsymbol{v} + q = 0 \tag{24.12}$$

Let us consider a point P according to Fig. 24.3(b) and a simply-connected slab area S bounded by the (arbitrary) closed curve C which passes through P. In this case, according to GAUSS' theorem (A6.30),

$$\oint_C \boldsymbol{v} \cdot \boldsymbol{n} \, \mathrm{d}t = \int_S \operatorname{div} \boldsymbol{v} \, \mathrm{d}S \tag{24.13}$$

the relationship

$$\oint_C v_n \mathrm{d}t + \int_S q \, \mathrm{d}S = 0 \tag{24.14}$$

applies, where $\boldsymbol{n}$ is the outward unit normal vector and $v_n = \boldsymbol{v} \cdot \boldsymbol{n}$ is equal to the flow of the shear force, or rather the *shear flow* at any point along C.

Eq. (24.14) corresponds to an integral formulation of the equilibrium of the forces in the z direction.

24.1.2.4 Static discontinuity lines

Fig. 24.4 shows – in a similar way to Fig. 23.17 – a differential element of the separating line between slab areas I and II, e. g. at an abrupt change in the thickness of the slab or at the edge of a slab. Equilibrium demands

$$m_n^{\mathrm{I}} = m_n^{\mathrm{II}} \quad , \quad V_t = m_{tn}^{\mathrm{II}} - m_{tn}^{\mathrm{I}} \quad , \quad v_n^{\mathrm{I}} + m_{tn,t}^{\mathrm{I}} = v_n^{\mathrm{II}} + m_{tn,t}^{\mathrm{II}} \tag{24.15}$$

where V_t is a shear force [kN] transferred along the discontinuity line. The bending moment m_t can exhibit an abrupt change in value at the discontinuity line. Further, v_n and m_{tn} may also be discontinuous, but must comply with constraint $(24.15)_3$. We can see that the relationship $V_{t,t} = m_{tn,t}^{\mathrm{II}} - m_{tn,t}^{\mathrm{I}}$, which follows from $(24.15)_2$, has been incorporated in $(24.15)_3$.

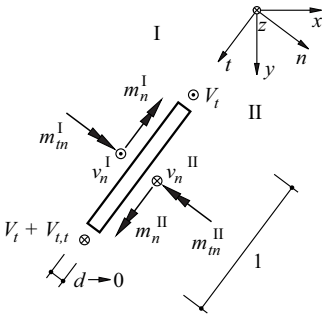

Fig. 24.4 Differential element of a static discontinuity line

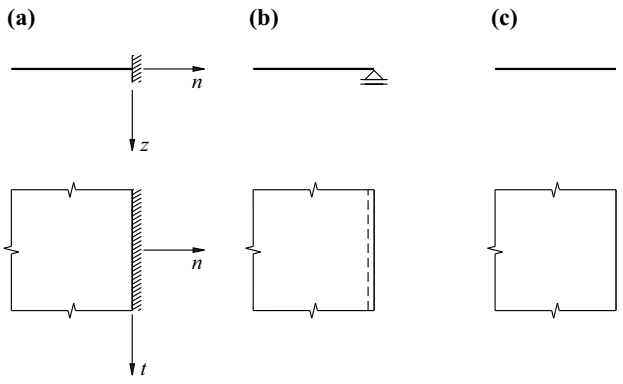

Fig. 24.5 Boundary conditions: (a) fixed, (b) simply supported, (c) free (unsupported)

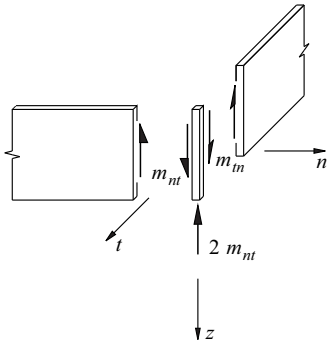

Fig. 24.6 Corner force

24.1.2.5 Static boundary conditions

Any shear forces v_n, bending moments m_n and twisting moments m_{tn} can be transferred at a fixed slab edge, see Fig. 24.5(a).

Simply supported and free slab edges are static discontinuity lines. The bending moment m_n at a simply supported edge, Fig. 24.5(b), must be equal to zero, and the support force [kN/m] considered to be positive in the positive z direction according to section 9.3.1 is equal to the *edge shear force* $v_n + m_{tn,t}$, see $(24.15)_3$. And both the bending moment m_n and the edge shear force $v_n + m_{tn,t}$ must disappear at a free edge, Fig. 24.5(c).

According to $(24.15)_2$, the fact that $m_{tn}^{\text{II}} = 0$ means that a shear force $V_t = -m_{tn}^{\text{I}} = -m_{tn}$ is transferred along simply supported and free slab edges. *Corner forces* amounting to $-2m_{nt}$ in the positive z direction, or rather $2m_{nt}$ in the negative z direction, ensue at right-angled slab corners because $m_{tn} = m_{nt}$, see Fig. 24.6.

We can also see that special measures may need to be taken in order to deal with corner forces (e. g. anchorages in the z direction). Unsecured corners can experience uplift, and therefore it is not possible to use moment fields, which exhibit negative twisting moments m_{nt} at the corners.

Example 24.1 Square slab supported at the corners

The formulation

$$m_x = m_0\left(1 - \frac{4x^2}{l^2}\right) \quad , \quad m_y = m_0\left(1 - \frac{4y^2}{l^2}\right) \quad , \quad m_{xy} = m_0\frac{4xy}{l^2}$$

for the square slab shown in Fig. 24.7(a) leads – according to $(24.1)_2$ and $(24.1)_3$ – to

$$v_x = -\frac{4m_0x}{l^2} \quad , \quad v_y = -\frac{4m_0y}{l^2}$$

and therefore according to $(24.1)_1$, to $q = 8m_0/l^2 = \text{const}$.

Eq. $(24.9)_1$ results in

$$m_1 = m_0 \quad , \quad m_2 = m_0\left(1 - \frac{4x^2}{l^2} - \frac{4y^2}{l^2}\right)$$

and using $(24.9)_2$ gives us $\tan\varphi_1 = x/y$. The principal moment trajectories shown in Fig. 24.7(b) are hyperbolas ($x^2 - y^2 = \text{const}$ and $xy = \text{const}$).

Eq. $(24.11)_1$ results in $v_0 = 4m_0r/l^2$, where $r = (x^2 + y^2)^{1/2}$, and $(24.11)_2$ results in $\tan\varphi_0 = y/x$. The shear force vectors are radial and directed away from the origin, and $v_0 = \text{const}$ along concentric circles, see Fig. 24.7(c).

At the edge of the slab $x = l/2$, both m_x and the edge shear force $v_x + m_{yx,y} = m_{x,x} + 2m_{yx,y}$ disappear, i. e. the edge is free. A corner force amounting to $2m_0$ in the negative z direction acts on the slab at corner $x = y = l/2$.

Fig. 24.7(d) summarises the result. The assumed moments correspond to a square slab supported at the corners subjected to a uniformly distributed load of $8m_0$. If we reverse the sign of m_{xy}, then we get the solution for a square slab simply supported on all sides and subjected to a uniformly distributed load of $24m_0$, which is in equilibrium with edge shear forces of $-8m_0/l$ and corner forces of $2m_0$ acting in the positive z direction (exercise 24.1).

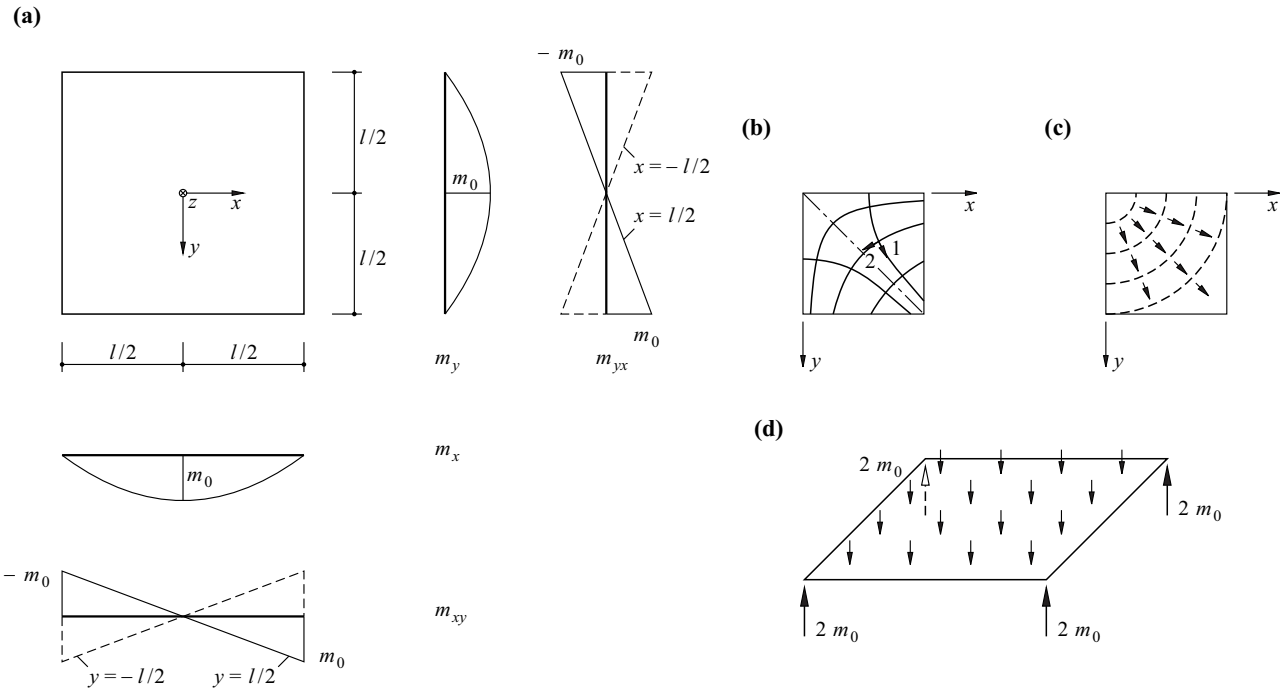

Fig. 24.7 Square slab supported at the corners and subjected to a uniformly distributed load: (a) moments, (b) principal moment trajectories, (c) shear flow, (d) free body diagram

Example 24.2 Square slab supported in the centre

Let us use the following formulation for octant OAB ($0 \le y \le x \le l/2$) of the square slab shown in Fig. 24.8 [17]:

$$m_x = 0 \quad , \quad m_y = m_0\left(\frac{y^2}{x^2} - 1\right) \quad , \quad m_{xy} = m_0\left(\frac{y}{x} - \frac{4xy}{l^2}\right)$$

which according to (24.1) leads to

$$v_x = \frac{m_0}{x}\left(1 - \frac{4x^2}{l^2}\right) \quad , \quad v_y = v_x \cdot \frac{y}{x} \quad , \quad q = 8\frac{m_0}{l^2} = \text{const}$$

Eq. $(24.11)_2$ shows that the shear force vectors are radial and directed towards the origin O. The edge is free because $m_x = 0$ and $v_x + m_{yx,y} = 2m_{yx,y} = 0$ along AB ($x = l/2$). At B ($x = y = l/2$), $m_{xy} = 0$ and therefore there is no corner force.

As the slab is symmetrical, the stress states in the other octants are easily worked out. The principal moments lie between m_0 (at O) and $-m_0$ (along the x and y axes), see exercise 24.3. The shear forces are infinitely large at the point support at the centre O.

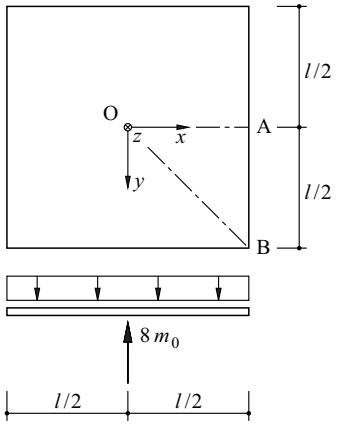

Fig. 24.8 Square slab supported in the centre and subjected to a uniformly distributed load

Example 24.3 Rectangular slab supported at the corners

The rectangular slab shown in Fig. 24.9 is supported at corners A, B, C, D and loaded in the centre O by a point load Q. Introducing uniaxial moment fields $m_y = (Q/4)\tan\alpha$ in areas OAB, OCD, but $m_x = (Q/4)\cot\alpha$ in areas OAD, OBC, leads to the relationships illustrated by the two MOHR's circles. For reasons of symmetry, we can confine our examination to areas OAB (= I) and OAD (= II).

First of all, $m_n = (Q/4)\sin\alpha\cos\alpha$ along OA. Further, $m_{tn}^{\text{I}} = -(Q/4)\sin^2\alpha$ and $m_{tn}^{\text{II}} = (Q/4)\cos^2\alpha$. Therefore, according to $(24.15)_2$, a shear force $V_t = Q/4$ is transferred along OA. In accordance with (24.1), $v_x = v_y = q = 0$ applies over the whole slab, and as the moment fields are parallel with edges AB, AD, these are free.

Summing up, the slab diagonals function as static discontinuity lines. One-quarter of load Q is carried along each of these to the corners of the slab. Points N^{I} and N^{II} on the MOHR's circles illustrate the corresponding abrupt change in the twisting moment, which amounts to $(Q/4)(\cos^2\alpha + \sin^2\alpha) = Q/4$.

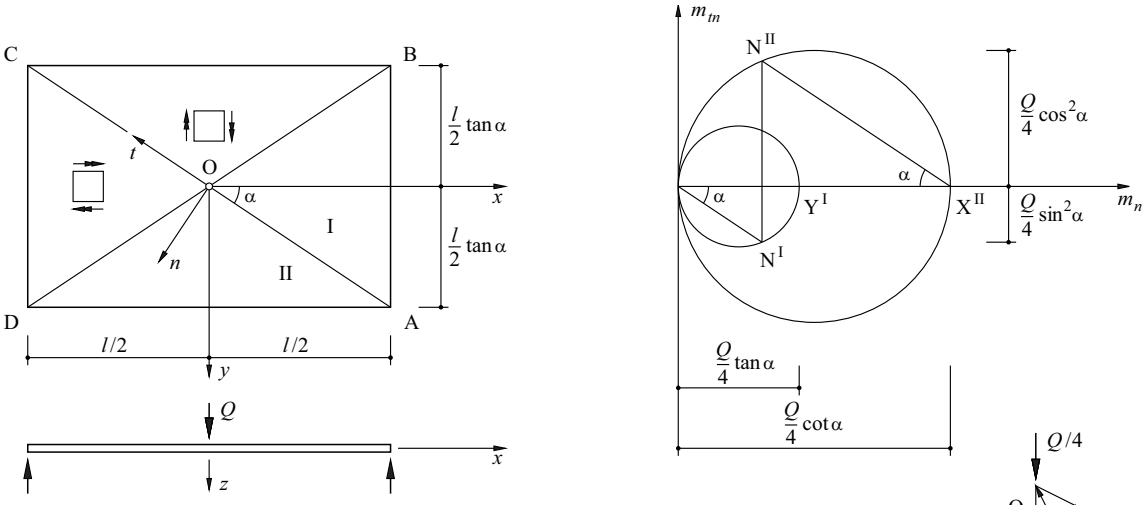

Fig. 24.9 Rectangular slab supported at the corners and subjected to a central point load

In order that the diagonals do function as described, it is important to form these appropriately, e. g. in a reinforced concrete slab. Fig. 24.10 shows a truss model for diagonal OA in Fig. 24.9. The load component $Q/4$ is transferred from O to A via diagonal struts and vertical ties. As indicated, equilibrium of the horizontal forces at the joints of the truss is guaranteed by the flexural tension and compression forces. The reinforcement for the vertical ties can be achieved with shear rails, for instance, and the flexural tension reinforcement must be fully anchored at the joints of the truss.

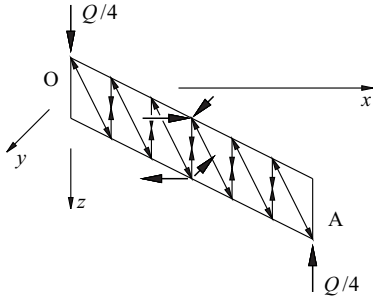

Fig. 24.10 Truss model for diagonal OA in Fig. 24.9

24.1.2.6 Influence of membrane forces

By introducing membrane forces n_x, n_y, $n_{xy} = n_{yx}$ as shown in Fig. 24.11 and specifying that $q_x = q_y = 0$, then according to (8.32),

$$n_{x,x} + n_{xy,y} = 0 \quad , \quad n_{yx,x} + n_{y,y} = 0 \tag{24.16}$$

applies. Projecting the forces n_x and their increments onto the z axis results in

$$[(n_x + n_{x,x}\mathrm{d}x)(w_{,x} + w_{,xx}\mathrm{d}x) - n_x w_{,x}]\mathrm{d}y = (n_x w_{,xx} + n_{x,x} w_{,x})\mathrm{d}x\mathrm{d}y$$

if we ignore small terms of higher order. Similarly, the projection of n_y results in the expression

$$(n_y w_{,yy} + n_{y,y} w_{,y})\mathrm{d}y\mathrm{d}x$$

and by projecting n_{xy} and n_{yx} we get

$$(n_{xy} w_{,xy} + n_{xy,y} w_{,x})\mathrm{d}y\mathrm{d}x$$

or rather

$$(n_{yx} w_{,yx} + n_{yx,x} w_{,y})\mathrm{d}x\mathrm{d}y$$

On the whole, the influence of the membrane forces, taking into account (24.16), increases the loading in the z direction from $q_z = q$ to

$$q + n_x w_{,xx} + n_y w_{,yy} + 2n_{xy} w_{,xy} \tag{24.17}$$

If q_x and q_y are not equal to zero, then applying (8.32) results in the similar expression

$$q_z + n_x w_{,xx} + n_y w_{,yy} + 2n_{xy} w_{,xy} - q_x w_{,x} - q_y w_{,y} \tag{24.18}$$

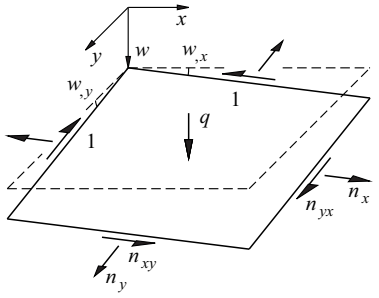

Fig. 24.11 Membrane forces acting on a slab element

24.1.3 Kinematic relationships

24.1.3.1 Deflection, curvature and twist

Let us consider an arbitrary point on the *middle plane of a slab* that undergoes a *deflection* $w = w(x, y)$, see Fig. 24.12(a). The slopes of the deformed *middle surface of the slab* in the x and y directions amount to $w_{,x}$ and $w_{,y}$ respectively. The slope in any direction n is

$$\frac{\mathrm{d}w}{\mathrm{d}n} = \frac{\partial w}{\partial x}\cdot\frac{\mathrm{d}x}{\mathrm{d}n} + \frac{\partial w}{\partial y}\cdot\frac{\mathrm{d}y}{\mathrm{d}n} = w_{,x}\cos\varphi + w_{,y}\sin\varphi$$

and for the direction t perpendicular to that we get

$$\frac{\mathrm{d}w}{\mathrm{d}t} = \frac{\partial w}{\partial x}\cdot\frac{\mathrm{d}x}{\mathrm{d}t} + \frac{\partial w}{\partial y}\cdot\frac{\mathrm{d}y}{\mathrm{d}t} = -w_{,x}\sin\varphi + w_{,y}\cos\varphi$$

These transformations are similar to (24.6). The maximum slope

$$(w_{,n})_{\max} = \sqrt{w_{,x}^2 + w_{,y}^2}$$

occurs in the direction $\varphi = \arctan(w_{,y}/w_{,x})$ and the slope of the slab perpendicular to that disappears, see (24.11). The slab slopes $w_{,i}$ correspond to a vector field $\mathrm{grad}\, w$. Apart from its sign, the associated vector gradient $w_{,ij}$ is equal to the *curvature tensor* considered below.

We can use

$$\frac{\partial}{\partial n} = \frac{\partial}{\partial x}\cos\varphi + \frac{\partial}{\partial y}\sin\varphi$$

to get the following expression for the curvature $\chi_n = -w_{,nn}$:

$$\chi_n = -\left(\frac{\partial}{\partial x}\cos\varphi + \frac{\partial}{\partial y}\sin\varphi\right)\left(\frac{\partial w}{\partial x}\cos\varphi + \frac{\partial w}{\partial y}\sin\varphi\right) = -\frac{\partial^2 w}{\partial x^2}\cos^2\varphi - \frac{\partial^2 w}{\partial y^2}\sin^2\varphi - 2\frac{\partial^2 w}{\partial x \partial y}\sin\varphi\cos\varphi$$
$$= \chi_x\cos^2\varphi + \chi_y\sin^2\varphi + 2\chi_{xy}\sin\varphi\cos\varphi$$

where χ_x, χ_y and χ_{xy} are the variables defined in (8.46). Similarly, using

$$\frac{\partial}{\partial t} = -\frac{\partial}{\partial x}\sin\varphi + \frac{\partial}{\partial y}\cos\varphi$$

results in the relationship

$$\chi_t = -w_{,tt} = \chi_x\sin^2\varphi + \chi_y\cos^2\varphi - 2\chi_{xy}\sin\varphi\cos\varphi$$

and also

$$\chi_{nt} = -w_{,nt} = -\chi_x\sin\varphi\cos\varphi + \chi_y\sin\varphi\cos\varphi + \chi_{xy}(\cos^2\varphi - \sin^2\varphi)$$

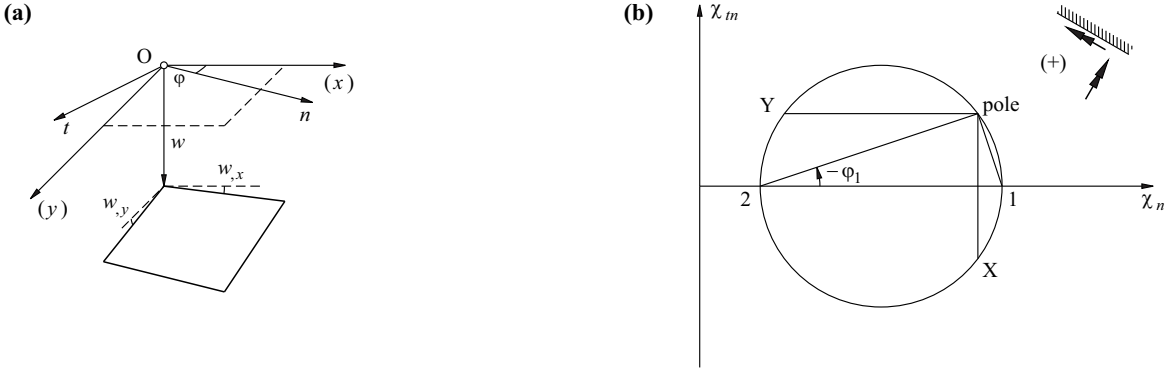

Fig. 24.12 Deformation of the middle plane of a slab: (a) deflection and slab slopes, (b) curvatures and twists

These transformations are similar to (24.7). Accordingly, the *curvatures* and *twists* form the symmetric tensor $-w_{,ij}$, or rather

$$\boldsymbol{\chi} = \begin{bmatrix} \chi_x & \chi_{xy} \\ \chi_{yx} & \chi_y \end{bmatrix} = \begin{bmatrix} -w_{,xx} & -w_{,xy} \\ -w_{,yx} & -w_{,yy} \end{bmatrix} \tag{24.19}$$

with the principal values χ_1, χ_2 and the principal direction φ_1 :

$$\chi_{1,2} = \frac{\chi_x + \chi_y}{2} \pm \sqrt{\left(\frac{\chi_x - \chi_y}{2}\right)^2 + \chi_{xy}^2} \quad , \quad \tan(2\varphi_1) = \frac{2\chi_{xy}}{\chi_x - \chi_y} \tag{24.20}$$

The variables

$$\chi_{\mathrm{I}} = \chi_1 + \chi_2 = \chi_x + \chi_y = -\Delta w \quad , \quad \chi_{\mathrm{II}} = -\chi_1\chi_2 = \chi_{xy}^2 - \chi_x\chi_y \tag{24.21}$$

are invariant, and it is possible to use the MOHR's circle as shown in Fig. 24.12(b).

The $\chi_{\mathrm{I}}/2$ value is equal to the *mean curvature*. If χ_{I} equals zero at all points on a surface, the surface is a *minimal surface*.

The expression $\chi_1\chi_2 = -\chi_{\mathrm{II}}$ denotes the GAUSS*ian curvature* or the *total curvature* at the point on the deformed middle surface of the slab under consideration. When χ_{II} is negative, the point is *elliptical*, and when $\chi_{\mathrm{II}} > 0$, it is *hyperbolic* (e. g. a point on a saddle surface), and when $\chi_{\mathrm{II}} = 0$, the corresponding point is *parabolic*. If all points on a surface are parabolic, it is *developable* on a flat plane (e. g. a cylindrical or conical surface).

Ruled surfaces can be generated by moving straight lines in space. Not all ruled surfaces are developable. For example, although hyperboloids of one sheet and hyperbolic paraboloids are ruled surfaces, they are not developable.

Note that according to GAUSS' theorem (A6.30), the following applies for a slab fixed at edge C:

$$\int_S w_{,ii}\,\mathrm{d}S = \int_S \Delta w\,\mathrm{d}S = \oint_C w_{,n}\,\mathrm{d}t = 0$$

because $w_{,n} = 0$ along C. This means that $\chi_{\mathrm{I}} = -\Delta w$, or rather the mean curvature $\chi_{\mathrm{I}}/2$ for a fixed slab is equal to zero on average.

The variable χ_{II}, or rather the total curvature, also disappears on average in the case of slabs fixed at the edge and slabs with polygonal forms, where either w or $w_{,n}$ is zero at their edges. In fact,

$$\chi_{\mathrm{II}} = \frac{1}{2}\left(w_{,ij}^2 - w_{,jj}w_{,ii}\right) = \frac{1}{2}\left(w_{,ij}w_{,j} - w_{,jj}w_{,i}\right)_{,i}$$

and therefore according to GAUSS' theorem (A6.30),

$$\int_S \chi_{\mathrm{II}}\,\mathrm{d}S = \frac{1}{2}\oint_C \left(\frac{\partial^2 w}{\partial n \partial t} \cdot \frac{\partial w}{\partial t} - \frac{\partial^2 w}{\partial^2 t} \cdot \frac{\partial w}{\partial n}\right)\mathrm{d}t$$

The integrand for a fixed edge ($w_{,n} = 0$) as well as for straight edges that are either simply supported ($w_{,t} = w_{,tt} = 0$), or have $w_{,n} = 0$ and hence also $w_{,nt} = 0$, disappears in the curvilinear integral; the latter case ($w_{,nt} = 0$) occurs, for instance, in one bay of a uniformly loaded, infinitely large flat slab with identical bays, e. g. along the support axes $x = \pm a/2$ or $y = \pm b/2$ in Fig. 24.20(a).

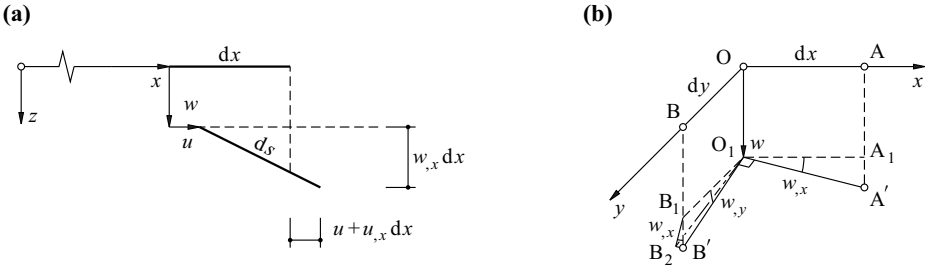

Fig. 24.13 Strains in the middle plane of a slab due to deflection

24.1.3.2 Strains in the middle plane of a slab

Where membrane forces have to be considered, then the corresponding terms due to the deflection w have to be added to the strain components

$$\varepsilon_x = u_{,x} \quad , \quad \varepsilon_y = v_{,y} \quad , \quad \gamma_{xy} = u_{,y} + v_{,x}$$

given by (6.4) and (6.5) in a similar way to (22.7). We get

$$ds^2 = dx^2(1 + u_{,x})^2 + dx^2 w_{,x}^2$$

from Fig. 24.13(a), i. e.

$$\varepsilon_x = \frac{ds}{dx} - 1 \approx u_{,x} + \frac{1}{2} w_{,x}^2 \qquad (24.22)_1$$

and similarly,

$$\varepsilon_y \approx v_{,y} + \frac{1}{2} w_{,y}^2 \qquad (24.22)_2$$

Points A, B in Fig. 24.13(b) are displaced to positions A′, B′. Right-angle $A_1O_1B_1$ decreases because of slopes $w_{,x}$ and $w_{,y}$. Angle $B'B_1B_2$ is equal to $w_{,x}$. Using length $w_{,y}dy$ of distance B_1B' results in the expression $w_{,x} \cdot w_{,y}dy$ for distance B_2B', and hence the product $w_{,x} \cdot w_y$ for the differential angle B_2O_1B', i. e. using (6.5),

$$\gamma_{xy} \approx u_{,y} + v_{,x} + w_{,x} \cdot w_{,y} \qquad (24.22)_3$$

Adding together the second derivatives of the expressions (24.22) and applying $(24.21)_2$ results in

$$\varepsilon_{x,yy} + \varepsilon_{y,xx} - \gamma_{xy,xy} = \left(\frac{\partial^2 w}{\partial x \partial y}\right)^2 - \frac{\partial^2 w}{\partial x^2} \cdot \frac{\partial^2 w}{\partial y^2} = \chi_{II} \qquad (24.23)$$

instead of the compatibility condition (23.1).

24.2 Linear elastic slabs rigid in shear with small deflections

24.2.1 Fundamental relationships

24.2.1.1 Stress resultants

Using (8.43) and (8.46) as well as the definition for slab stiffness D in (8.48), we get the moments

$$m_x = -D(w_{,xx} + \nu w_{,yy}) \quad , \quad m_y = -D(w_{,yy} + \nu w_{,xx}) \quad , \quad m_{xy} = m_{yx} = -(1 - \nu)Dw_{,xy} \qquad (24.24)$$

And applying $(24.1)_2$ and $(24.1)_3$, we therefore obtain the shear forces

$$v_x = -D(\Delta w)_{,x} \quad , \quad v_y = -D(\Delta w)_{,y} \qquad (24.25)$$

We also note here that the invariants (24.10) and (24.21) are linked with each other via

$$m_I = D(1 + \nu)\chi_I \quad , \quad m_{II} = D^2\left[(1 - \nu)^2 \chi_{II} - \nu\chi_I^2\right]$$

24.2.1.2 Shear force potential

From (24.25) it follows that $v_{x,y} = v_{y,x}$, i. e. the shear force field $\boldsymbol{v}$ is irrotational, $\operatorname{curl}\boldsymbol{v} \equiv 0$. Therefore, the expression $-D\Delta w$ corresponds to a *shear force potential* Φ_v ($\boldsymbol{v} = \operatorname{grad}\Phi_v$), and the comparison with $(24.24)_1$ and $(24.24)_2$ as well as $(24.21)_1$ reveals that

$$\Phi_v = -D\Delta w = \frac{m_x + m_y}{1+\nu} = \frac{m_\mathrm{I}}{1+\nu} = D\chi_\mathrm{I} \tag{24.26}$$

We get

$$\operatorname{div}\boldsymbol{v} = \frac{\Delta m_\mathrm{I}}{1+\nu} \tag{24.27}$$

for the expression $\operatorname{div}\boldsymbol{v} = \operatorname{div}\operatorname{grad}\Phi_v = \Delta\Phi_v = -q_z$ in (24.12). This relationship is similar to the one for elastic plates (23.2), which can be expressed in the form

$$\operatorname{div}\boldsymbol{q} = -\frac{\Delta n_\mathrm{I}}{1+\nu} \tag{24.28}$$

where $\boldsymbol{q} = \{q_x, q_y\}^\mathrm{T}$.

Irrotationality of the shear force field is a consequence of presuming the slab to be linear elastic and rigid in shear. Generally, the shear force gradient $v_{i,j}$ is not symmetrical, and

$$\boldsymbol{v} = \operatorname{grad}\Phi_v + \operatorname{grad}\Phi_r + \operatorname{rot}\boldsymbol{\psi} \tag{24.29}$$

applies, where Φ_v satisfies the POISSON differential equation

$$\Delta\Phi_v = -q_z \tag{24.30}$$

On the other hand, the potential Φ_r, which like the vector potential $\boldsymbol{\psi} = (0, 0, \psi)$ describes a restraint state, satisfies the LAPLACE differential equation

$$\Delta\Phi_r = 0 \tag{24.31}$$

The potential Φ_v is either equal to the elastic shear force potential (24.26) or may be made up of this plus a superposed potential that corresponds to a restraint state, i. e. satisfies (24.31).

Section 24.6.1 shows that the relationship $\Delta\psi = 10\psi/h^2$ applies for linear elastic slabs with a thickness h and finite shear stiffness, see (24.112).

24.2.1.3 Boundary conditions

The two kinematic boundary conditions

$$w = 0 \quad , \quad w_{,n} = 0 \tag{24.32}$$

apply at a fixed edge with normal n. Along a straight fixed edge $w_{,nt}$ and therefore m_{nt} disappear; further, $w_{,t} = 0$ and $m_t = \nu m_n$.

The following must be satisfied at a simply supported edge:

$$w = 0 \quad , \quad m_n = 0 \tag{24.33}$$

As explained in section 24.1.2, the shear forces v_n and the derivatives $m_{tn,t}$ of the twisting moments are added together to form the edge shear forces $v_n + m_{tn,t} = m_{n,n} + 2m_{tn,t}$. Along a straight edge $w_{,tt} = 0$ applies, and therefore as $m_n = -D(w_{,nn} + \nu w_{,tt}) = 0$, then $w_{,nn} = 0$ or $\Delta w = 0$ and $m_t = -D(w_{,tt} + \nu w_{,nn}) = 0$ as well.

The following applies at a free edge:

$$m_n = 0 \quad , \quad v_n + m_{tn,t} = 0 \tag{24.34}$$

24.2.1.4 Cylindrical coordinates

Making use of (23.8) results in the curvatures

$$\chi_r = -w_{,rr} \quad , \quad \chi_\varphi = -\frac{w_{,\varphi\varphi}}{r^2} - \frac{w_{,r}}{r} \tag{24.35}$$

and the twist

$$\chi_{r\varphi} = -\left(\frac{w_{,\varphi}}{r}\right)_{,r} = \frac{w_{,\varphi}}{r^2} - \frac{w_{,r\varphi}}{r} \tag{24.36}$$

The following applies in the rotationally symmetric case (where $' = \mathrm{d}/\mathrm{d}r$):

$$\chi_r = -w'' \quad , \quad \chi_\varphi = -\frac{w'}{r} \quad , \quad \chi_{r\varphi} = 0 \tag{24.37}$$

Using (23.10), we get

$$\Delta\Delta w = \left(\frac{\partial^2}{\partial r^2} + \frac{1}{r}\cdot\frac{\partial}{\partial r} + \frac{1}{r^2}\cdot\frac{\partial^2}{\partial\varphi^2}\right)\left(\frac{\partial^2 w}{\partial r^2} + \frac{1}{r}\cdot\frac{\partial w}{\partial r} + \frac{1}{r^2}\cdot\frac{\partial^2 w}{\partial\varphi^2}\right) = \frac{q}{D} \tag{24.38}$$

instead of (8.48), and (24.24) – applying (24.35) and (24.36) – becomes

$$m_r = -D\left[w_{,rr} + \nu\left(\frac{w_{,r}}{r} + \frac{w_{,\varphi\varphi}}{r^2}\right)\right] \quad , \quad m_\varphi = -D\left(\frac{w_{,r}}{r} + \frac{w_{,\varphi\varphi}}{r^2} + \nu w_{,rr}\right) \quad , \quad m_{r\varphi} = -(1-\nu)D\left(\frac{w_{,r\varphi}}{r} - \frac{w_{,\varphi}}{r^2}\right) \tag{24.39}$$

and instead of (24.25), the result is

$$v_r = -D(\Delta w)_{,r} \quad , \quad v_\varphi = -\frac{D(\Delta w)_{,\varphi}}{r} \tag{24.40}$$

As $w_{,r} = 0$, $w_{,r\varphi} = 0$ and $w_{,\varphi\varphi} = 0$ along a fixed edge in the form of a circular arc, then $m_{r\varphi} = 0$ and $m_\varphi = \nu m_r$ along that edge.

In the rotationally symmetric case (where $' = \mathrm{d}/\mathrm{d}r$), then

$$m_r = -D\left(w'' + \nu\frac{w'}{r}\right) \quad , \quad m_\varphi = -D\left(\frac{w'}{r} + \nu w''\right) \quad , \quad m_{r\varphi} = 0 \tag{24.41}$$

and

$$v_r = -D\left(w''' + \frac{w''}{r} - \frac{w'}{r^2}\right) = -D\left[\frac{1}{r}(rw')'\right]' \quad , \quad v_\varphi = 0 \tag{24.42}$$

apply, and instead of (24.38), the result of using $(24.3)_1$ and (24.42) is the simply integrable differential equation

$$\frac{1}{r}\left\{r\left[\frac{1}{r}(rw')'\right]'\right\}' = \frac{q}{D} \tag{24.43}$$

24.2.2 Methods of solution

The slab equation (24.43) for rotationally symmetric problems can be solved directly (section 24.2.3). For example, FOURIER series approaches are suitable for rectangular slabs (section 24.2.4) and flat slabs (section 24.2.5); many of the design tables for slabs with different boundary conditions and loading arrangements are based on such an approach. Energy methods (section 24.2.6) render possible approximate solutions to the slab equation (8.48) or (24.38).

These days, the finite element method (FEM) is the most popular approach in practice. FEM can be employed to solve slabs with any boundary conditions, any loading arrangements.

However, many of the solutions explained in the literature for relatively simple boundary conditions and loading arrangements are still extremely valuable when it comes to estimating the orders of magnitude of moments, shear forces and deflections. Indeed, such solutions are excellent choices when applying the plausibility check (which is always necessary) to results obtained from, for example, the finite element method.

24.2.3 Rotationally symmetric problems

24.2.3.1 Uniform loading

The general solution to the inhomogeneous differential equation (24.43) with q = const is

$$w = \frac{qr^4}{64D} + c_1 + c_2 r^2 + c_3 \ln r + c_4 r^2 \ln r \tag{24.44}$$

For reasons of symmetry, the slope w' in the centre of the slab $r = 0$ must disappear, and the curvature $\chi_r = -w''$ must be finite. From this it follows that $c_3 = c_4 = 0$.

Considering a circular slab of radius r_0 and fixed at its outer edge, see Fig. 24.14(a), the boundary conditions $w(r_0) = w'(r_0) = 0$ result in

$$c_1 = \frac{qr_0^4}{64D} \quad , \quad c_2 = -\frac{qr_0^2}{32D}$$

and therefore by employing the shortened form $\rho = r/r_0$ we get

$$w = \frac{qr_0^4}{64D}(1-\rho^2)^2 \quad , \quad m_r = \frac{qr_0^2}{16}[1+\nu-\rho^2(3+\nu)] \quad , \quad m_\varphi = \frac{qr_0^2}{16}[1+\nu-\rho^2(1+3\nu)] \tag{24.45}$$

If the outer edge is simply supported, see Fig. 24.14(b), then $w(r_0) = m_r(r_0) = 0$ results in

$$c_1 = \frac{qr_0^4}{64D}\cdot\frac{5+\nu}{1+\nu} \quad , \quad c_2 = -\frac{qr_0^2}{32D}\cdot\frac{3+\nu}{1+\nu}$$

and therefore

$$w = \frac{qr_0^4}{64D}(1-\rho^2)\left(\frac{5+\nu}{1+\nu}-\rho^2\right) \quad , \quad m_r = \frac{qr_0^2}{16}(3+\nu)(1-\rho^2) \quad , \quad m_\varphi = \frac{qr_0^2}{16}[3+\nu-\rho^2(1+3\nu)] \tag{24.46}$$

Comparing the deflection $qr_0^4/(64D)$ in the centre of the fixed slab with the deflection $ql^4/(384EI)$ at mid-span of a beam fixed at both ends (see example 15.2) and putting $l = 2r_0$ and $EI = D$, then the result is a ratio of 3/8.

The moments according to (24.45) and (24.46) differ by the constant amount $qr_0^2/8$.

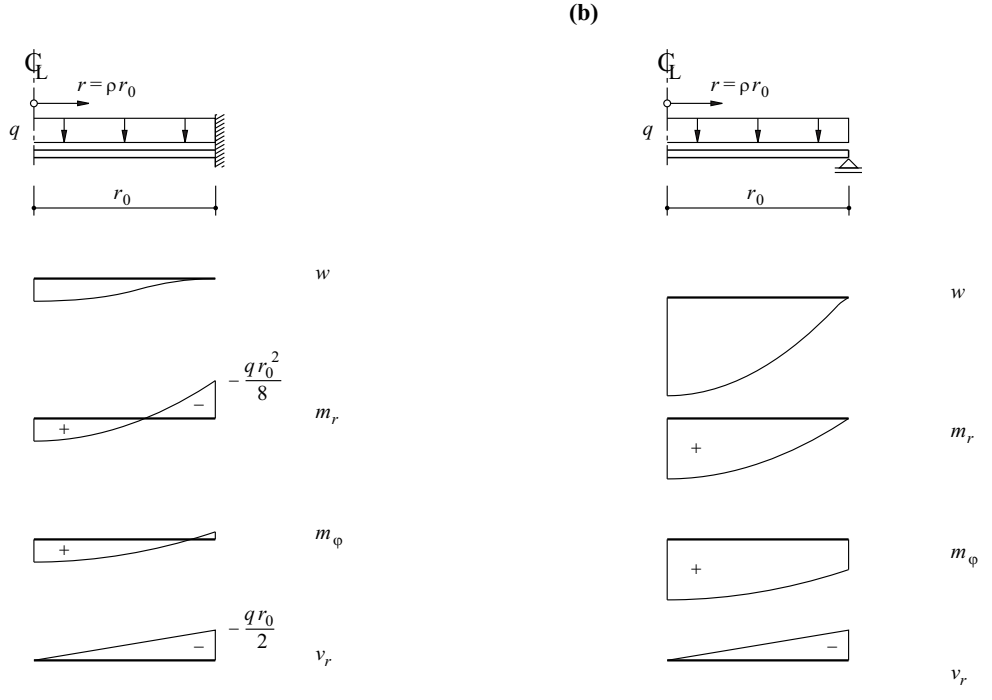

Fig. 24.14 Uniformly loaded circular slabs

The easiest way to obtain the shear forces $v_r = -qr/2$ is to use (24.14) and consider the circle C with radius r, i. e. $v_r 2\pi r + qr^2\pi = 0$. They can also be calculated using (24.29) with $\Phi_v = (m_r + m_\varphi)/(1 + \nu)$, i. e. $v_r = \Phi_v' = -qr/2$.

24.2.3.2 Annular slabs

Three further boundary conditions $w(r_0) = m_r(r_0) = 0$ and $v_r(r_1) = 0$ apply for the case shown in Fig. 24.15(a), which is an annular slab simply supported at its outer edge and loaded on its inner edge by a line load moment $m_r(r_1) = m = \text{const}$. When $q = 0$, the latter of these three conditions in conjunction with (24.44) and $(24.42)_1$ leads to $c_4 = 0$, and together with the other conditions the result is

$$w = \frac{mr_1^2}{D(1-\rho_1^2)}\left[\frac{\ln\rho}{1-\nu} - \frac{1-\rho^2}{2(1+\nu)}\right] \tag{24.47}$$

The case shown in Fig. 24.15(b) has a shear force $v_r = -Q/(2\pi r)$. Using this and the boundary conditions $w(r_0) = m_r(r_0) = m_r(r_1) = 0$, we can use (24.44) to obtain

$$w = \frac{Qr_0^2}{8\pi D}\left\{\rho^2\ln\rho + \frac{3+\nu}{2(1+\nu)}(1-\rho^2) - \frac{\rho_1^2\ln\rho_1}{1-\rho_1^2}\left[1-\rho^2-\frac{2(1+\nu)}{1-\nu}\ln\rho\right]\right\} \tag{24.48}$$

The third term in the curly brackets on the right in (24.48) disappears when $\rho_1 = 0$. We therefore arrive at the expression

$$\frac{Qr_0^2(3+\nu)}{16\pi(1+\nu)D}$$

for the deflection $w(0)$ of a simply supported circular slab subjected to a central point load Q. The deflection at the centre is larger by a factor of $4(3 + \nu)/(5 + \nu)$ when compared with that calculated using $(24.46)_1$ for the case of a load of the same magnitude but uniformly distributed, e. g. when $\nu = 0.2$, the factor is $32/13 \approx 2.46$.

The case shown in Fig. 24.15(c) can be solved through the superposition of (24.47) and (24.48) in such a way that $w'(r_1) = 0$. We get

$$m = m_r(r_1) = \frac{Q[(1-\nu)(1-\rho_1^2) - 2(1+\nu)\ln\rho_1]}{4\pi[(1-\nu)\rho_1^2 + 1 + \nu]} \tag{24.49}$$

for the fixed-end moment. Substituting this expression in (24.47) and superposition with (24.48) gives us the deflection w.

In the case of Fig. 24.15(d), we superpose $(24.46)_1$, (24.47) with $m = -qr_0^2(3 + \nu)(1 - \rho_1^2)/16$ and (24.48) with $Q = -qr_1/2$.

Cases with other boundary conditions can be solved in a similar way, see exercises 24.8 and 24.9.

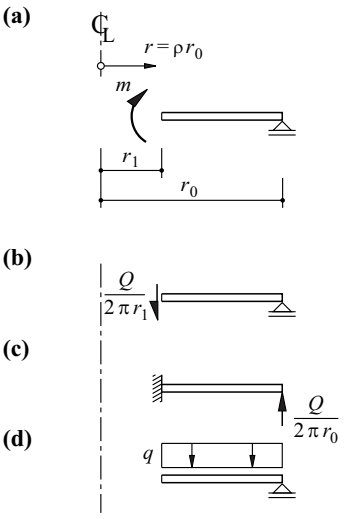

Fig. 24.15 Annular slabs

24.2.3.3 Concentric loading

Fig. 24.16(a) shows a circular slab simply supported at its outer edge and carrying a uniformly distributed load Q applied via a concentric annulus of radius r_1. The superposition of (24.48) and (24.47) gives us the solution in the region $r_1 \le r \le r_0$ in such a way that $w'(r_1)$ is continuous. According to (24.44), $w = c_1 + c_2 r^2$ applies in the region $0 \le r \le r_1$; therefore, $w' = 2c_2 r$ and $w'' = 2c_2$. The result of (24.41) is $m_r = m_\varphi = -2c_2(1 + \nu)D = m$, and thus

$$w'(r_1) = -\frac{mr_1}{(1+\nu)D}$$

applies. By equating this expression with the sum of the derivatives of (24.47) and (24.48) at point r_1, it follows that

$$m = \frac{Q}{8\pi}[(1-\nu)(1-\rho_1^2) - 2(1+\nu)\ln\rho_1]$$

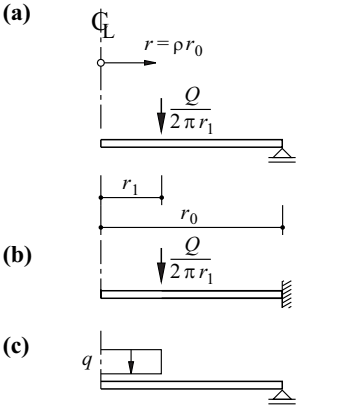

Fig. 24.16 Circular slabs with concentric loading

Substituting in (24.47) and adding (24.48) results in

$$w = \frac{Qr_0^2}{8\pi D}\left\{(1-\rho^2)\left[1+\frac{(1-\nu)(1-\rho_1^2)}{2(1+\nu)}\right]+(\rho_1^2+\rho^2)\ln\rho\right\} \qquad (r_1 \le r \le r_0) \tag{24.50}_1$$

The outcome for the inner part of the slab is

$$w = \frac{Qr_0^2}{8\pi D}\left[(1-\rho_1^2)\frac{3+\nu-(1-\nu)\rho^2}{2(1+\nu)}+(\rho_1^2+\rho^2)\ln\rho_1\right] \qquad (0 \le r \le r_1) \tag{24.50}_2$$

Considering the limiting case of a central point load, then $(24.50)_1$ with $\rho_1 \to 0$ results in

$$w = \frac{Qr_0^2}{8\pi D}\left[\frac{3+\nu}{2(1+\nu)}(1-\rho^2)+\rho^2\ln\rho\right] \tag{24.51}$$

and (24.41) results in

$$m_r = -\frac{Q}{4\pi}(1+\nu)\ln\rho \quad , \quad m_\varphi = \frac{Q}{4\pi}[1-\nu-(1+\nu)\ln\rho] \tag{24.52}$$

When $\rho \to 0$, the moments (24.52) tend to infinity, but on the other hand, $w(0) = w_{\max}$ remains finite:

$$w_{\max} = \frac{Qr_0^2(3+\nu)}{16\pi(1+\nu)D} \tag{24.53}$$

Fixing the outer edge of the slab according to Fig. 24.16(b) means that the solution is obtained from (24.50) by superposing the case of a slab loaded on its outer edge by line load moments $m_r(r_0) = m$ in such a way that $w'(r_0)$ disappears. It follows from $(24.50)_1$ that

$$w'(r_0) = -\frac{Qr_0(1-\rho_1^2)}{4\pi(1+\nu)D}$$

and similarly to the expression derived above for the rotation due to m, we get

$$w'(r_0) = -\frac{mr_0}{(1+\nu)D}$$

The sum of these two expressions must be equal to zero, and therefore

$$m = -\frac{Q(1-\rho_1^2)}{4\pi}$$

This moment at the edge causes the deflections

$$w = \frac{mr_0^2(1-\rho^2)}{2(1+\nu)D} \tag{24.53}$$

which together with (24.50) leads to

$$\begin{aligned} w &= \frac{Qr_0^2}{8\pi D}\left[(1-\rho^2)\frac{1+\rho_1^2}{2}+(\rho_1^2+\rho^2)\ln\rho\right] \qquad (r_1 \le r \le r_0) \\ w &= \frac{Qr_0^2}{8\pi D}\left[(1+\rho^2)\frac{1-\rho_1^2}{2}+(\rho_1^2+\rho^2)\ln\rho_1\right] \qquad (0 \le r \le r_1) \end{aligned} \tag{24.54}$$

Eq. $(24.54)_1$ for $\rho_1 \to 0$ results in

$$w = \frac{Qr_0^2}{8\pi D}\left(\frac{1-\rho^2}{2}+\rho^2\ln\rho\right) \tag{24.55}$$

for the limiting case of a central point load, and (24.41) results in

$$m_r = -\frac{Q}{4\pi}[1+(1+\nu)\ln\rho] \quad , \quad m_\varphi = -\frac{Q}{4\pi}[\nu+(1+\nu)\ln\rho] \tag{24.56}$$

These moments and the values of (24.52) differ by the amount of $Q/(4\pi)$. The deflection

$$w_{\max} = \frac{Qr_0^2}{16\pi D} \tag{24.57}$$

at the centre of the slab is $(3+\nu)/(1+\nu)$ times smaller than that at the edge of a simply supported slab, see (24.53).

With a uniform loading on the central area of the slab $0 \le r \le r_1$, as shown in Fig. 24.16(c), the solution can be obtained by superposing individual annular loads $q\mathrm{d}r$ according to Fig. 24.16(a). Applying $(24.50)_1$ and integrating from 0 to r_1, with the total load $Q = q\pi {r_1}^2$, results in the deflections

$$w = \frac{Qr_0^2}{16\pi D}\left\{\frac{3+\nu}{1+\nu}(1-\rho^2) + 2\rho^2 \ln\rho + \rho_1^2\left[\ln\rho - \frac{1-\nu}{2(1+\nu)}(1-\rho^2)\right]\right\} \qquad (r_1 \le r \le r_0) \tag{24.58}$$

in the unloaded outer part of the slab. The deflection in the centre of the slab is obtained from $(24.50)_2$ plus a corresponding integration:

$$w_{\max} = \frac{Qr_0^2}{16\pi D}\left[\frac{3+\nu}{1+\nu} + \rho_1^2 \ln\rho_1 - \frac{7+3\nu}{4(1+\nu)}\rho_1^2\right] \tag{24.59}$$

The maximum bending moment occurs in the centre of the slab and amounts to

$$m_{\max} = \frac{Q}{4\pi}\left[1 - \frac{(1-\nu)\rho_1^2}{4} - (1+\nu)\ln\rho_1\right] \tag{24.60}$$

24.2.4 Rectangular slabs

24.2.4.1 Sinusoidal loading

Eq. (8.48) for the problem illustrated in Fig. 24.17 is

$$\Delta\Delta w = \frac{q_0}{D}\sin\left(\frac{\pi x}{a}\right)\sin\left(\frac{\pi y}{b}\right)$$

Setting

$$w = c\sin\left(\frac{\pi x}{a}\right)\sin\left(\frac{\pi y}{b}\right)$$

gives us

$$c = \frac{q_0}{\pi^4 D\left(\frac{1}{a^2}+\frac{1}{b^2}\right)^2}$$

and therefore

$$w = \frac{q_0 \sin\left(\frac{\pi x}{a}\right)\sin\left(\frac{\pi y}{b}\right)}{\pi^4 D\left(\frac{1}{a^2}+\frac{1}{b^2}\right)^2} \tag{24.61}$$

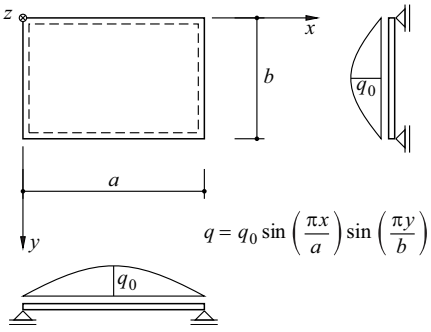

Fig. 24.17 Simply supported rectangular slab subjected to a load with a sinusoidal distribution

Eq. (24.24) provides the moments

$$m_x = \frac{q_0\left(\frac{1}{a^2}+\frac{\nu}{b^2}\right)\sin\left(\frac{\pi x}{a}\right)\sin\left(\frac{\pi y}{b}\right)}{\pi^2\left(\frac{1}{a^2}+\frac{1}{b^2}\right)^2} \quad , \quad m_y = \frac{q_0\left(\frac{\nu}{a^2}+\frac{1}{b^2}\right)\sin\left(\frac{\pi x}{a}\right)\sin\left(\frac{\pi y}{b}\right)}{\pi^2\left(\frac{1}{a^2}+\frac{1}{b^2}\right)^2} \quad , \quad m_{xy} = -\frac{q_0(1-\nu)\cos\left(\frac{\pi x}{a}\right)\cos\left(\frac{\pi y}{b}\right)}{\pi^2\left(\frac{1}{a^2}+\frac{1}{b^2}\right)^2 ab} \tag{24.62}$$

and (24.25) the shear forces

$$v_x = \frac{q_0\cos\left(\frac{\pi x}{a}\right)\sin\left(\frac{\pi y}{b}\right)}{\pi a\left(\frac{1}{a^2}+\frac{1}{b^2}\right)} \quad , \quad v_y = \frac{q_0\sin\left(\frac{\pi x}{a}\right)\cos\left(\frac{\pi y}{b}\right)}{\pi b\left(\frac{1}{a^2}+\frac{1}{b^2}\right)} \tag{24.63}$$

The edge shear forces are

$$v_x + m_{yx,x}\Big|_{x=a} = -\frac{q_0\left(\frac{1}{a^2}+\frac{2-\nu}{b^2}\right)\sin\left(\frac{\pi y}{b}\right)}{\pi a\left(\frac{1}{a^2}+\frac{1}{b^2}\right)^2} \quad , \quad v_y + m_{xy,x}\Big|_{y=b} = -\frac{q_0\left(\frac{2-\nu}{a^2}+\frac{1}{b^2}\right)\sin\left(\frac{\pi x}{a}\right)}{\pi b\left(\frac{1}{a^2}+\frac{1}{b^2}\right)^2} \tag{24.64}_1$$

and the corner forces acting at the corners of the slab are

$$\frac{2q_0(1-\nu)}{\pi^2 ab\left(\frac{1}{a^2}+\frac{1}{b^2}\right)^2} \qquad (24.64)_2$$

in the positive z direction.

For a square slab with $a = b = l$, the maximum values

$$w_{\max} = \frac{q_0 l^4}{4\pi^4 D} \quad , \quad m_{\max} = \frac{q_0 l^2(1+\nu)}{4\pi^2} \qquad (24.65)$$

occur in the centre of the slab.

24.2.4.2 General loading

In a similar way to (24.61), the loading

$$q = q_0 \sin\left(\frac{m\pi x}{a}\right)\sin\left(\frac{n\pi y}{b}\right) \qquad (m,n = 1,2,3,\ldots)$$

results in

$$w = \frac{q_0 \sin\left(\frac{m\pi x}{a}\right)\sin\left(\frac{n\pi y}{b}\right)}{\pi^4 D\left(\frac{m^2}{a^2}+\frac{n^2}{b^2}\right)^2}$$

A general loading $q(x,y)$ can be represented by a double FOURIER series:

$$q(x,y) = \sum_{m=1}^{\infty}\sum_{n=1}^{\infty} a_{mn}\sin\left(\frac{m\pi x}{a}\right)\sin\left(\frac{n\pi y}{b}\right)$$

When determining the coefficients a_{mn}, we first realise that

$$\int_0^b q\sin\left(\frac{n'\pi y}{b}\right)\mathrm{d}y = \frac{b}{2}\sum_{m=1}^{\infty} a_{mn'}\sin\left(\frac{m\pi x}{a}\right)$$

because the integral

$$\int_0^b \sin\left(\frac{n\pi y}{b}\right)\sin\left(\frac{n'\pi y}{b}\right)\mathrm{d}y$$

disappears provided $n \neq n'$, and is equal to $b/2$ if $n = n'$. Moreover,

$$\int_0^a\int_0^b q\sin\left(\frac{m'\pi x}{a}\right)\sin\left(\frac{n'\pi y}{b}\right)\mathrm{d}y\,\mathrm{d}x = \frac{ab}{4}a_{m'n'}$$

and therefore

$$a_{mn} = \frac{4}{ab}\int_0^a\int_0^b q\sin\left(\frac{m\pi x}{a}\right)\sin\left(\frac{n\pi y}{b}\right)\mathrm{d}y\,\mathrm{d}x \qquad (24.66)$$

and

$$w = \frac{1}{\pi^4 D}\sum_{m=1}^{\infty}\sum_{n=1}^{\infty}\frac{a_{mn}\sin\left(\frac{m\pi x}{a}\right)\sin\left(\frac{n\pi y}{b}\right)}{\left(\frac{m^2}{a^2}+\frac{n^2}{b^2}\right)^2} \qquad (24.67)$$

Using (24.66) for a uniformly distributed loading q = const results in

$$a_{mn} = \frac{16q}{\pi^2 mn} \qquad (m,n = 1,3,\ldots)$$

and hence according to (24.67),

$$w = \frac{16q}{\pi^6 D} \sum_{m=1,3,\ldots}^{\infty} \sum_{n=1,3,\ldots}^{\infty} \frac{\sin\left(\frac{m\pi x}{a}\right) \sin\left(\frac{n\pi y}{b}\right)}{mn\left(\frac{m^2}{a^2} + \frac{n^2}{b^2}\right)^2} \tag{24.68}$$

Note that the coefficients a_{mn} disappear for even values of m and n.

Turning to the deflection w, it is sufficient to terminate the series (24.68) after just one or a few terms. On the other hand, higher terms in the series must also be considered for the moments and shear forces obtained according to (24.24) or (24.25) from the second or third derivatives of w in order to achieve adequate accuracy. For example, considering a square slab where $a = b = l$, then we get

$$\begin{aligned}
w\left(\frac{l}{2},\frac{l}{2}\right) = w_{\max} &= \frac{16ql^4}{\pi^6 D}\left(\frac{1}{4} - \frac{2\cdot 1}{3\cdot 1\cdot 10^2} + \frac{1}{3\cdot 3\cdot 18^2} + \ldots\right) \\
&= \frac{4ql^4}{\pi^6 D}\left(1 - \frac{2}{75} + \frac{1}{729} + \ldots\right) \approx 0.00406\frac{ql^4}{D} \\
m_x\left(\frac{l}{2},\frac{l}{2}\right) = m_{\max} &= \frac{16ql^2}{\pi^4}\left(\frac{1+\nu}{4} - \frac{1+9\nu}{300} - \frac{9+\nu}{300} + \frac{1+\nu}{9\cdot 324} + \frac{1+25\nu}{5\cdot 26^2} + \frac{25+\nu}{5\cdot 26^2} - \ldots\right) \\
&= \frac{4ql^2(1+\nu)}{\pi^4}\left(1 - \frac{2}{15} + \frac{1}{729} + \frac{2}{65} - \ldots\right) \approx 0.0369(1+\nu)ql^2 \\
v_x\left(0,\frac{l}{2}\right) = v_{x\max} &= \frac{16ql}{\pi^3}\left(\frac{1}{2} + \frac{1}{10} - \frac{1}{30} - \frac{1}{54} + \frac{1}{130} + \frac{1}{26} - \ldots\right) \\
&= \frac{8ql}{\pi^3}\left(1 + \frac{1}{5} - \frac{1}{15} - \frac{1}{27} + \frac{1}{65} + \frac{1}{13} - \ldots\right) \approx 0.307ql
\end{aligned}$$

According to the exact solution, the values of the three numerical coefficients are (in order) 0.00406, 0.0368 and 0.338.

24.2.4.3 Superposition of load and restraint states

The convergence of the series obtained from (24.68) through differentiation is not particularly good. We get a better solution from the superposition

$$w = w_1 + w_2 \tag{24.69}$$

of the deflections of a loading stress state 1 and those of a restraint state 2.

We use the notation of Fig. 24.18 and set

$$w_1 = \frac{q}{24D}(x^4 - 2ax^3 + a^3x) \tag{24.70}$$

for a strip of slab in the x direction loaded by the constant uniformly distributed load q, see example 15.1. This formulation satisfies (8.48) and the boundary conditions along $x = 0$ and $x = a$.

The restraint state deflections

$$w_2 = \sum_{m=1,3,\ldots}^{\infty} Y_m \sin\left(\frac{m\pi x}{a}\right) \tag{24.71}$$

with the Y_m functions dependent on y only must satisfy

$$\Delta\Delta w_2 = 0 \tag{24.72}$$

on the one hand and, on the other, enable the boundary conditions (24.33), i. e. $w = 0$ and $w_{,yy} = 0$ along $y = \pm b/2$, to be satisfied as well. Using (24.72) together with (24.71), it follows that

$$\sum_{m=1,3,\ldots}^{\infty} \left(Y_m'''' - 2\frac{m^2\pi^2}{a^2}Y_m'' + \frac{m^4\pi^4}{a^4}Y_m\right) \sin\left(\frac{m\pi x}{a}\right) = 0$$

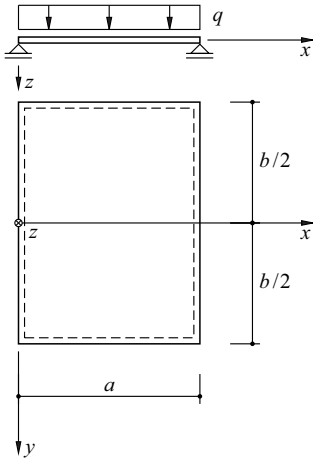

Fig. 24.18 Simply supported rectangular slab subjected to a uniformly distributed load

This relationship can only be satisfied when the first factor after the summation symbol disappears. This leads to the general solution

$$Y_m = \frac{qa^4}{D}\left[A_m \cosh\left(\frac{m\pi y}{a}\right) + B_m \frac{m\pi y}{a}\sinh\left(\frac{m\pi y}{a}\right) + C_m \sinh\left(\frac{m\pi y}{a}\right) + D_m \frac{m\pi y}{a}\cosh\left(\frac{m\pi y}{a}\right)\right] \tag{24.73}$$

Owing to the symmetry with respect to the x axis, the odd functions are dropped, i. e. $C_m = D_m = 0$.

Eq. (24.70) can be developed into the series

$$w_1 = \frac{4qa^4}{\pi^5 D}\sum_{m=1,3,\ldots}^{\infty} \frac{\sin\left(\frac{m\pi x}{a}\right)}{m^5}$$

Consequently, (24.69) is

$$w = \frac{qa^4}{D}\sum_{m=1,3,\ldots}^{\infty}\left[\frac{4}{\pi^5 m^5} + A_m \cosh\left(\frac{m\pi y}{a}\right) + B_m \frac{m\pi y}{a}\sinh\left(\frac{m\pi y}{a}\right)\right]\sin\left(\frac{m\pi x}{a}\right)$$

and (24.33), where $\alpha_m = m\pi b/(2a)$, calls for

$$\frac{4}{\pi^5 m^5} + A_m \cosh\alpha_m + B_m \alpha_m \sinh\alpha_m = 0$$

$$(A_m + 2B_m)\cosh\alpha_m + B_m \alpha_m \sinh\alpha_m = 0$$

from which it follows that

$$A_m = -\frac{2\alpha_m \tanh\alpha_m + 4}{\pi^5 m^5 \cosh\alpha_m} \quad , \quad B_m = \frac{2}{\pi^5 m^5 \cosh\alpha_m}$$

Substituting in the expression for w results in

$$w = \frac{4qa^4}{\pi^5 D}\sum_{m=1,3,\ldots}^{\infty}\frac{1}{m^5}\left[1 - \frac{\alpha_m \tanh\alpha_m + 2}{2\cosh\alpha_m}\cosh\left(\frac{m\pi y}{a}\right) + \frac{\alpha_m y}{b\cosh\alpha_m}\sinh\left(\frac{m\pi y}{a}\right)\right]\sin\left(\frac{m\pi x}{a}\right) \tag{24.74}$$

If we consider only the first term in the series (24.74) when dealing with a square slab ($a = b = l$), the result is $w(l/2, 0) = w_{\max} \approx 0.00411 ql^4/D$, i. e. compared with the exact value of $0.00406 ql^4/D$, this is an excellent approximation.

24.2.4.4 Continuous slabs

Continuous slabs with rectangular bays and linear supports in the form of walls or beams can be analysed approximately by examining the individual bays such that a continuous edge is treated like a fixed one. We can thus make use of the solutions given in design tables for the cases shown in Fig. 24.19.

The resulting fixed-end moments for the continuous edges are generally different, and it might be possible to compensate for this by applying a correct moment distribution. For simplicity, we often take the average of the fixed-end moments, mostly without fully analysing the consequences for the span moments. Usable approximations can be obtained when the spans and stiffnesses of adjacent bays are roughly the same and the loads are not too different. However, calculations based on the finite element method are generally to be preferred. FEM allows us to consider, in particular, fixed supports at walls and columns as well as the beam stiffnesses, and leads to a complete stress state which is in itself consistent.

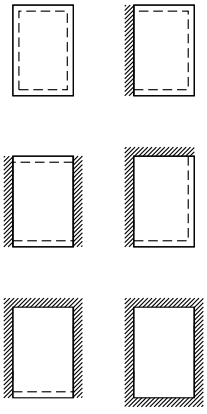

Fig. 24.19 Rectangular slabs with various boundary conditions

24.2.5 Flat slabs

24.2.5.1 Slabs with point supports on a rectangular grid

Let us use (24.69) with

$$w_1 = \frac{qb^4(1-4y^2/b^2)^2}{384D} \tag{24.75}$$

for the case of an infinitely large slab with regularly spaced columns which carries a uniformly distributed load q, as shown in Fig. 24.20(a). This deflection function corresponds to a strip of slab fixed at both ends according to example 15.2 and satisfies the boundary conditions $w_{,x} = 0$ and $v_x = -D(\Delta w)_{,x} = 0$ along $x = \pm a/2$.

Considering w_2, the formulation

$$w_2 = A_0 + \sum_{m=2,4,\ldots}^{\infty} \left[Y_m \cos\left(\frac{m\pi x}{a}\right) \right]$$

similar to (24.71), which satisfies the boundary conditions mentioned along $x = \pm a/2$, and taking into account (24.72) plus symmetry with respect to the x axis leads to

$$w_2 = A_0 + \sum_{m=2,4,\ldots}^{\infty} \left[A_m \cosh\left(\frac{m\pi y}{a}\right) + B_m \frac{m\pi y}{a} \sinh\left(\frac{m\pi y}{a}\right) \right] \cos\left(\frac{m\pi x}{a}\right) \tag{24.76}$$

The boundary condition $w_{,y} = 0$ along $y = b/2$ results in

$$B_m = -\frac{A_m \tanh\alpha_m}{\alpha_m + \tanh\alpha_m} \qquad \left(\alpha_m = \frac{m\pi b}{2a}\right)$$

The shear force v_y along $y = b/2$ must disappear for $0 \le x \le a/2 - c$ and take on the value $-qab/(4c)$ over the infinitesimal width c. As shown in Fig. 24.20(b), we can specify the FOURIER series

$$v_y\Big|_{y=b/2} = -\frac{qb}{2} + qb\left[\cos\left(\frac{2\pi x}{a}\right) - \cos\left(\frac{4\pi x}{a}\right) + \cos\left(\frac{6\pi x}{a}\right) - \ldots\right]$$

for this. However, the boundary condition $w_{,y} = 0$ means that $v_y = -Dw_{,yyy}$ applies along $y = b/2$, and therefore, considering (24.75),

$$-Dw_{2,yyy}\Big|_{y=b/2} = -qb \sum_{m=2,4,\ldots}^{\infty} (-1)^{m/2} \cos\left(\frac{m\pi x}{a}\right)$$

Using (24.76), this leads to

$$\frac{Dm^3\pi^3}{a^3}\left[(A_m + 3B_m)\sinh\alpha_m + B_m\alpha_m\cosh\alpha_m\right] = qb(-1)^{m/2} \qquad \left(\alpha_m = \frac{m\pi b}{2a}\right)$$

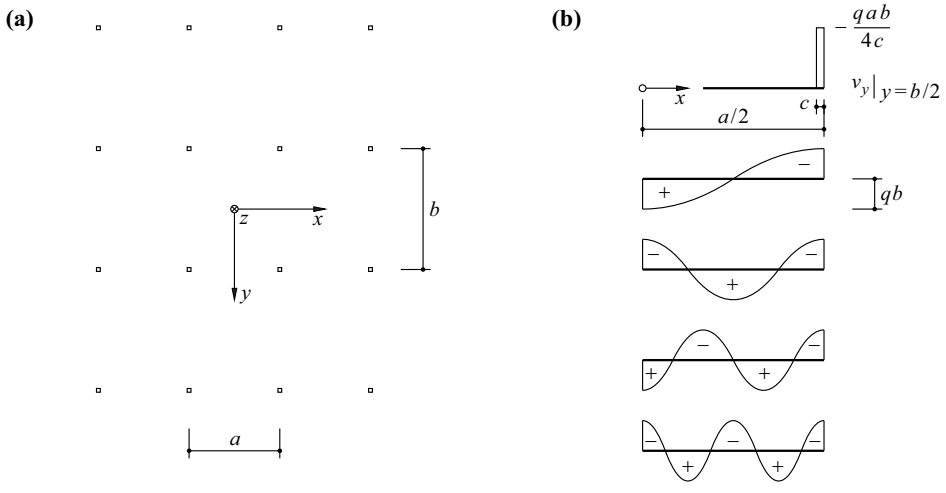

Fig. 24.20 Flat slab supported by columns on a rectangular grid: (a) plan, (b) diagram of v_y along support axis $y = b/2$

and together with the relationship between A_m and B_m derived above, in turn to

$$A_m = -\frac{qa^3b(-1)^{m/2}}{2m^3\pi^3D}\cdot\frac{\alpha_m + \tanh\alpha_m}{\sinh\alpha_m\tanh\alpha_m} \quad , \quad B_m = \frac{qa^3b(-1)^{m/2}}{2m^3\pi^3D}\cdot\frac{1}{\sinh\alpha_m}$$

The condition $w = 0$ for $x = a/2$, $y = b/2$ means that (24.69), (24.75) and (24.76) give us

$$A_0 = \frac{qa^3b}{2\pi^3D}\sum_{m=2,4,\ldots}^{\infty}\frac{\alpha_m + \tanh\alpha_m - \alpha_m\tanh^2\alpha_m}{m^3\tanh^2\alpha_m}$$

The final result for the deflection w is

$$w = \frac{qb^4\left(1-\frac{4y^2}{b^2}\right)^2}{384D} + \frac{qa^3b}{2\pi^3D}\sum_{m=2,4,\ldots}^{\infty}\frac{1}{m^3}\left\{\frac{\alpha_m + \tanh\alpha_m - \alpha_m\tanh^2\alpha_m}{\tanh^2\alpha_m}\right.$$
$$\left. + \frac{(-1)^{m/2}\cos\left(\frac{m\pi x}{a}\right)}{\sinh\alpha_m\tanh\alpha_m}\left[\tanh\alpha_m\frac{m\pi y}{a}\sinh\left(\frac{m\pi y}{a}\right) - (\alpha_m + \tanh\alpha_m)\cosh\left(\frac{m\pi y}{a}\right)\right]\right\} \tag{24.77}$$

With a square grid ($a = b$), the deflection at mid-span ($x = y = 0$) is $0.00581qb^4/D$, but still $0.00337qb^4/D$ for $a = 2b/3$, and we get a value of $0.00292qb^4/D$ for $a = b/2$. Putting $\nu = 0.2$ results in bending moments $m_x = m_y = 0.0331qb^2$ at mid-span for the case $a = b$ according to (24.24); we get $m_x = 0.0131qb^2$ and $m_y = 0.0387qb^2$ for $a = 2b/3$, and $m_x = 0.0092qb^2$ and $m_y = 0.0411qb^2$ for $a = b/2$. The value w_2 disappears for the case $a/b \to 0$, and the result is the mid-span values $qb^4/(384D) = 0.00260qb^4/D$, $m_y = qb^2/24 = 0.0417qb^2$ known from example 15.2 as well as $m_x = \nu m_y = 0.0083qb^2$. Further, we get the moments $m_x = -0.0185qb^2$, $m_y = 0.0512qb^2$ at point $x = a/2$, $y = 0$ for the case $a = b$.

24.2.5.2 Singularity of the moments over the columns

The (negative) moments tend to infinity over the point supports. If we assume that the column reactions are transferred uniformly distributed as line loads over a circle with radius c, then it is possible to estimate the minimum moments for the case $a = b$ based on $(24.54)_2$ and $(24.45)_2$ or $(24.45)_3$. We replace one bay by a circular slab with radius $r_0 = a/\sqrt{\pi}$, which has the same area and is fixed at its edge, and allow the vertical load q to act from above and the opposing equal annular load from below. Putting $\rho_1 = c/r_0$, the resulting moment in the centre of the slab over the support is

$$\frac{Q}{4\pi}(1+\nu)\left(\ln\rho_1 + \frac{1}{2} - \frac{\rho_1^2}{2} + \frac{1}{4}\right) \approx \frac{Q(1+\nu)}{4\pi}\left(\ln\rho_1 + \frac{3}{4}\right) \tag{24.78}$$

For example: putting $\nu = 0.2$ and $\rho_1 = 0.05$ results in a value of $-0.214Q$, and with $\rho_1 = 0.1$ the outcome is $-0.148Q$, and when $\rho_1 = 0.025$ we get $-0.281Q$. With customary dimensions, the minimum moments lie between about $-Q/6$ and $-Q/4$. But the distribution of the moment in the region of the column is more important than the respective peak value. The peak values do not have to be covered in flat slabs of reinforced concrete. Instead, it is sufficient to accommodate the average moment over a width defined by the width of the column and strips of slab on both sides with a width equal to about twice the thickness of the slab; averaging over one-fifth of the span is carried out in the equivalent frames method, see Fig. 24.22(b).

24.2.5.3 Placing the imposed load in the most unfavourable position

As with continuous beams, the imposed loads on flat slabs should always be placed in the most unfavourable position. For example, the strip-type loading according to Fig. 24.21(a) for the case $a = b$ leads to maximum deflections and moments m_x in the middle of bay A amounting to $(0.00581 + 5/384)\cdot qb^4/(2D) = 0.00942qb^4/D$ and

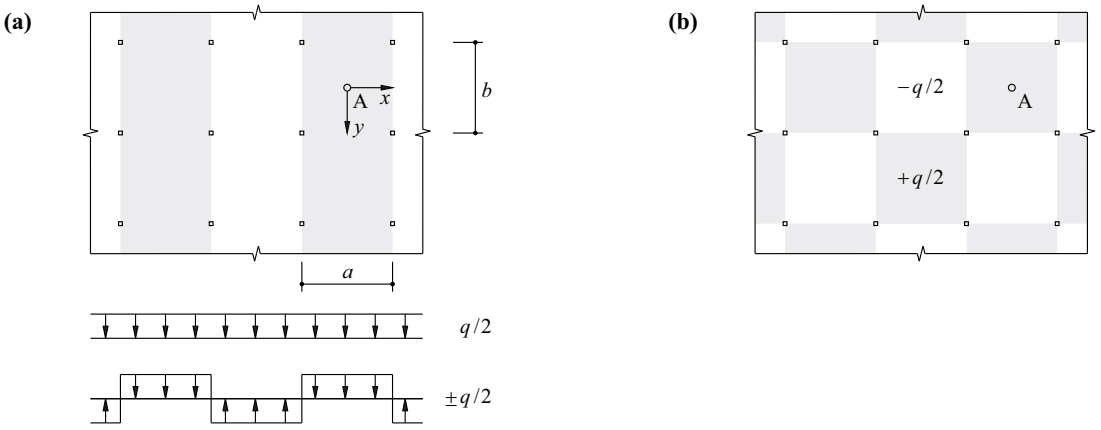

Fig. 24.21 Flat slab with strip- or chessboard-type loading

$(0.0331 + 1/8)\cdot qb^2/2 = 0.0791qb^2$ assuming hinged connections at the point supports. And the moments m_x at point $x = 0$, $y = b/2$ are $(0.0512 + 1/8)\cdot qb^2/2 = 0.0881qb^2$.

The chessboard-type loading arrangement shown in Fig. 24.21(b) results in deflections of $(0.00581 + 0.00406)\cdot qb^4/(2D) = 0.00494qb^4/D$ at A when we apply (24.68). The moments $m_x = m_y$ at A are $(0.0331 + 0.0369\cdot 1.2)\cdot qb^2/2 = 0.0387qb^2$ when $\nu = 0.2$.

24.2.5.4 Equivalent frames method

Fig. 24.22(a) illustrates an approximation method frequently used in practice. It involves making cuts halfway between adjacent rows of columns to form *equivalent frames* in the x and y directions. The frames are analysed for permanent and variable actions in the most unfavourable positions. This produces envelopes for the bending moments which have typical values of M_x^-, M_x^+ or M_y^-, M_y^+ over the columns and in the spans. Afterwards, these moments are apportioned to the *column strips* (width = 40 % of frame width) and the intervening *middle strips* transverse to the frame direction, as shown in Fig. 24.22(b).

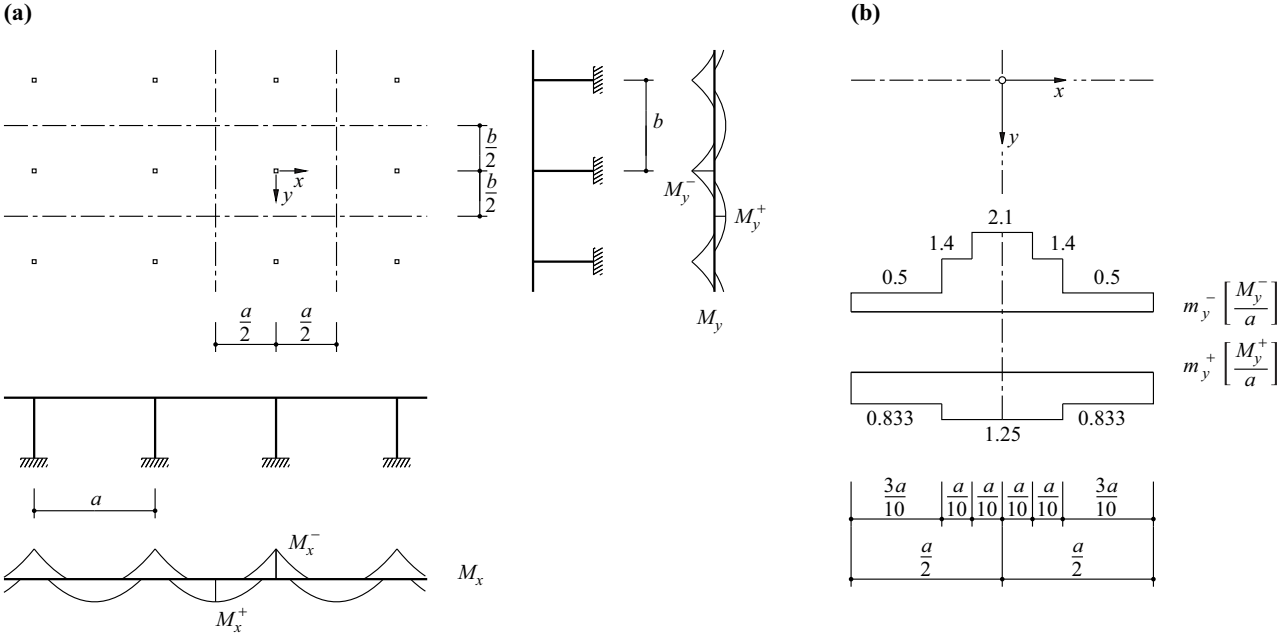

Fig. 24.22 Equivalent frames method: (a) plan, sections and bending moments, (b) apportioning moments to column and middle strips

The equivalent frames method represents a highly graphic approach that can be applied to a huge variety of column and load configurations. It is easy to take into account fixed-end moments at the columns due to bending and, if necessary, fixed-end moments due to torsion in downstand beams etc. The method supplies a global equilibrium state. The apportionment of the moments in the transverse direction is carried out based on elastic slab theory. Local equilibrium is not investigated further and so there is no statically admissible stress state (which is required when applying the lower-bound theorem of limit analysis in a strict sense).

The average moment of $2.1M_y^-/a$ which has to be accommodated in the column strip over the column over a width of one-fifth of span a, see Fig. 24.22(b), corresponds to a value of $-2.1qab^2/(12a) = -0.175qb^2$ in the case of an infinitely large flat slab subjected to a uniform loading q and supported by columns on a square grid ($a = b$). Similarly, the value $0.833M_y^+/a$ at mid-span corresponds to a value of $0.833qab^2/(24a) = 0.0347qb^2$, and the value for $1.25M_y^+/a$ in the column strip is $0.0521qb^2$; by way of comparison, we get practically identical values of $0.0331qb^2$ and $0.0512qb^2$ when using (24.77). However, the value of $0.5M_y^-/a = -0.0417qb^2$ at the column section of the middle strip deviates quite considerably from the value $-0.0185qb^2$ in the middle of the middle strip on the column axis obtained from (24.77); it should be remembered here that the latter value is the lowest negative moment along the column axis, but the value of $-0.0417qb^2$ is the average negative moment in the middle strip along the column axis.

24.2.6 Energy methods

We can use (8.46) and (8.47) to obtain the specific strain energy

$$\pi_i = \frac{1}{2}(m_x\chi_x + m_y\chi_y + 2m_{xy}\chi_{xy})$$

according to (8.67), and applying (24.21) and (24.24) results in

$$\pi_i = D\left[\frac{\chi_I^2}{2} + (1-\nu)\chi_{II}\right]$$

Using the specific external potential $-qw$ therefore results in the total potential

$$\Pi = \int_A \left\{D\left[\frac{\chi_I^2}{2} + (1-\nu)\chi_{II}\right] - qw\right\} dA \tag{24.79}$$

according to (8.73), which according to the theorem of least total potential is a minimum for the true deformation state.

The RITZ and GALERKIN methods can be used as described in section 8.5. It should be noted that concerning the integral on the right in (24.79), the relationship

$$\int_A \chi_{II} dA = 0 \tag{24.80}$$

applies for fixed slabs according to section 24.1.3; this relationship – as shown in section 24.1.3 – is also valid for slabs with straight boundaries and the boundary condition $w = 0$ or $w_{,n} = 0$ (n = edge normal) as well as generally for slabs with a combination of the three aforementioned boundary conditions.

Example 24.4 Simply supported square slab

Setting

$$w = w_0 \sin\left(\frac{\pi x}{l}\right) \sin\left(\frac{\pi y}{l}\right)$$

for a simply supported square slab (side length l, D = const) uniformly loaded with q, where

$$\chi_x = w_0 \frac{\pi^2}{l^2} \sin\left(\frac{\pi x}{l}\right) \sin\left(\frac{\pi y}{l}\right) = \chi_y = \chi_I/2$$

and taking into account (24.80) according to (24.79) results in

$$\Pi = \frac{D w_0^2 \pi^4}{2l^2} - \frac{4ql^2 w_0}{\pi^2}$$

Differentiating with respect to w_0 and equating to zero then results in

$$w_0 = \frac{4ql^4}{\pi^6 D} = 0.00416 \frac{ql^4}{D}$$

i. e. the first term in the series discussed following (24.68).

Example 24.5 Fixed square slab

Let us fix the edges of the square plate of example 24.4 and shift the origin of the system of coordinates from the corner of the slab to its centre (notation as given in exercise 24.5). Setting

$$w = w_0(1 - \xi^2)^2(1 - \eta^2)^2 \qquad (\xi = 2x/l\,,\ \eta = 2y/l)$$

based on example 15.2, we get

$$\chi_x = \frac{16 w_0}{l^2}(3\xi^2 - 1)(1 - \eta^2)^2 \quad , \quad \chi_y = \frac{16 w_0}{l^2}(3\eta^2 - 1)(1 - \xi^2)^2$$

and (24.79) – taking into account (24.80) – then results in

$$\Pi = \frac{128 D w_0^2}{l^2}\left[2 \cdot \frac{4}{5} \cdot \frac{128}{315} + 2 \cdot \left(\frac{32}{105}\right)^2\right] - \left(\frac{8}{15}\right)^2 ql^2 w_0$$

Differentiating with respect to w_0 and equating to zero then gives us

$$w_0 = \frac{49ql^4}{36864D} = 0.001329 \frac{ql^4}{D}$$

Putting $\nu = 0.2$ gives us a bending moment

$$m_x = m_y = \frac{49ql^2}{1920} = 0.0255\, ql^2$$

in the centre of the slab ($\xi = \eta = 0$), and the fixed-end moment in the middle of the edge of the slab ($\xi = 1$, $\eta = 0$) is then

$$m_x = -\frac{49ql^2}{1152} = -0.0425\, ql^2$$

24.3 Yield conditions

24.3.1 VON MISES and TRESCA yield conditions

24.3.1.1 General

Let us consider homogeneous slabs of depth h which satisfy the condition (7.21) or (7.24). Using the generalised deformation increments $\dot{\boldsymbol{\nu}} = \dot{\boldsymbol{\chi}} = \{\dot{\chi}_x, \dot{\chi}_y, 2\dot{\chi}_{xy}\}^T$ according to (8.46), we can use (8.40) – with z instead of ζ – to obtain the strain increments $\dot{\boldsymbol{\varepsilon}} = \{\dot{\varepsilon}_x, \dot{\varepsilon}_y, \dot{\gamma}_{xy}\}^T = z\dot{\boldsymbol{\chi}}$, i. e. the vectors $\dot{\boldsymbol{\varepsilon}}$ are in the same direction for all points on one side of the middle plane of the slab, and their sign changes when we change sides.

We shall assume a coplanar stress state $\boldsymbol{\sigma} = \{\sigma_x, \sigma_y, \tau_{xy}\}^T$ for all values of z and require that the membrane forces (5.14) disappear, i. e. only bending and twisting moments (5.16) occur.

The VON MISES yield condition (7.25) in the coplanar stress state can be expressed in the form

$$Y = \sigma_x^2 - \sigma_x\sigma_y + \sigma_y^2 + 3\tau_{xy}^2 - f_y^2 = 0$$

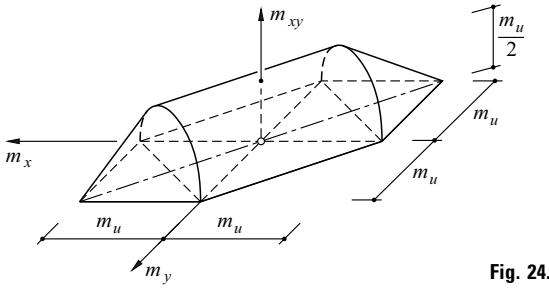

Fig. 24.23 TRESCA yield condition

(exercise 7.8) and corresponds to a (strictly convex) ellipsoid in the space σ_x, σ_y, τ_{xy}. Each $\dot{\boldsymbol{\chi}}$ is assigned a vector $\boldsymbol{\sigma}$ for $z > 0$ and $-\boldsymbol{\sigma}$ for $z < 0$ in a one-to-one correspondence. The membrane forces therefore disappear automatically, and using the reference value

$$m_u = \frac{h^2 f_y}{4} \tag{24.81}$$

according to (20.26), the plastic moment related to the unit width $b = 1$, we get the yield condition

$$Y = m_x^2 - m_x m_y + m_y^2 + 3m_{xy}^2 - m_u^2 = 0 \tag{24.82}$$

for the generalised stresses $\boldsymbol{s} = \{m_x, m_y, m_{xy}\}^{\mathrm{T}}$.

The TRESCA yield condition in the coplanar stress state can be expressed in the form

$$\mathrm{Max}(|\sigma_1|,|\sigma_2|,|\sigma_1 - \sigma_2|) - f_y = 0$$

see Fig. 7.8(c). The yield locus exhibits weak convexity and that means there is no unique distribution of the local stresses $\boldsymbol{\sigma}$. However, owing to the fact that the membrane forces must be equal to zero, the result is a condition similar to the VON MISES yield condition:

$$\mathrm{Max}(|m_1|,|m_2|,|m_1 - m_2|) - m_u = 0$$

or rather

$$\begin{aligned} Y_1 &= m_{xy}^2 - (m_u - m_x)(m_u - m_y) = 0 \\ Y_2 &= 4m_{xy}^2 + (m_x - m_y)^2 - m_u^2 = 0 \\ Y_3 &= m_{xy}^2 - (m_u + m_x)(m_u + m_y) = 0 \end{aligned} \tag{24.83}$$

see exercise 7.8. The conditions $(24.83)_1$ and $(24.83)_3$ correspond to elliptical cones in the space m_x, m_y, m_{xy}, but $(24.83)_2$ corresponds to an elliptical cylinder. Fig. 24.23 illustrates (24.83) confined to positive twisting moments m_{xy}. Eq. $(24.83)_1$ and $(24.83)_3$ are similar to $(23.20)_1$ and $(23.20)_7$.

The ellipsoid (24.82) circumscribes the TRESCA yield surface consisting of the three regimes (24.83). The two conditions coincide when $m_x + m_y = \pm m_u$ and $m_x = m_y$, $m_{xy} = 0$. When $m_y = m_u/\sqrt{3}$ and $m_{xy} = 0$, we get $m_{x\max} = 2m_u/\sqrt{3}$, and therefore the ellipsoid of VON MISES can be circumscribed by a TRESCA yield surface with a plastic moment increased by $2/\sqrt{3} - 1 = 15.4\,\%$. This means that the limit loads calculated according to the VON MISES yield condition cannot lie more than 15.4 % higher than the corresponding limit loads calculated on the basis of the TRESCA yield condition for the same plastic moment.

Tab. 24.1 General relationships for rotationally symmetric TRESCA slabs

Regime	$\dot{\chi}_r$	$\dot{\chi}_\varphi$	$\dot{w}$	m_r/m_u	m_φ/m_u
A, D	$\geq 0, \leq 0$		$\dot{w}'] \neq 0$	± 1	0
AB, DE	$\leq 0, \leq 0$	0	const	± 1	$\mu \pm 1$
B, E	$\geq 0, \leq 0$	$\geq 0, \leq 0$	$\dot{w}'] \neq 0$	± 1	± 1
BC, EF	0	$\geq 0, \leq 0$	$a_1 r + b_1$	$\pm 1 + c_1/r - (1/r)\int \mu \mathrm{d}r$	± 1
C, F		$\geq 0, \leq 0$	$\dot{w}'] = 0$	0	± 1
CD, FA	$-\dot{\chi}_\varphi$	$-\dot{\chi}_r$	$a_2 \ln\rho + b_2$	$\pm \ln\rho + c_2 - \int(\mu/r)\mathrm{d}r$	$\pm \ln\rho + c_2 \pm 1 - \int(\mu/r)\mathrm{d}r$

24.3.1.2 Rotationally symmetric TRESCA slabs

Rotational symmetry means that $m_{r\varphi} = 0$ applies. The moments m_r and m_φ are principal moments and limited by the yield locus shown in Fig. 24.24. According to (24.37), the principal curvature increments are

$$\dot{\chi}_r = -\dot{w}'' \quad , \quad \dot{\chi}_\varphi = -\frac{\dot{w}'}{r} \qquad (' = \mathrm{d}/\mathrm{d}r) \tag{24.84}$$

Using this it is possible to specify the deflection increments $\dot{w}$ for the individual regimes in general form, and applying (24.5) plus the shortened forms

$$\mu = \frac{\int_0^r qr\,\mathrm{d}r}{m_u} \quad , \quad \rho = \frac{r}{r_0} \tag{24.85}$$

gives us general expressions for the moments as well, see Tab. 24.1.

The outcome for regimes A, D and B, E is *yield lines* with an abrupt change in $\dot{w}'$. Contrasting with this, $\dot{w}'$ must be continuous for regimes C, F, i. e. smooth transitions from the linear profiles of the deflection increments of regimes BC, EF to the logarithmic profiles of regimes CD, FA.

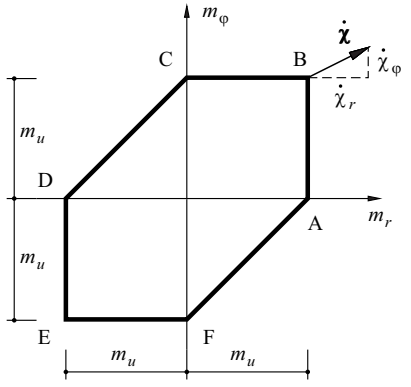

Fig. 24.24 Yield locus for rotationally symmetric TRESCA slabs

Example 24.6 Simply supported circular slab

Fig. 24.25 shows a circular slab uniformly loaded in the centre and simply supported at the edge. At the centre $r = 0$, it must be the case that $m_r = m_\varphi = m_u$ at the limit load; at the edge $r = r_0$, then $m_r = 0$ applies, and at $r = r_1$, then m_r must be continuous. Assuming regime BC, we read off $m_\varphi = m_u = \text{const}$ from Tab. 24.1, and

$$m_r = m_u + \frac{C_1}{r} - \frac{qr^2}{6} \qquad (0 \leq r \leq r_1)$$

$$m_r = m_u + \frac{C_2}{r} - \frac{qr_1^2}{2} \qquad (r_1 \leq r \leq r_0)$$

As $m_r(0) = m_u$, it follows that $C_1 = 0$, the continuity condition for m_r at point $r = r_1$ gives us $C_2 = qr_1^3/3$ and the boundary condition $m_r(r_0) = 0$ leads to

$$qr_1^2\pi = \frac{2\pi m_u}{1 - \frac{2\rho_1}{3}}$$

The given moments are compatible with the deflection increments $\dot{w} = \dot{w}_0(1 - \rho)$, i. e. the problem is solved completely. The limiting cases of $\rho_1 = 0$ and $\rho_1 = 1$ give rise to limit loads of $2\pi m_u$ and $6\pi m_u$.

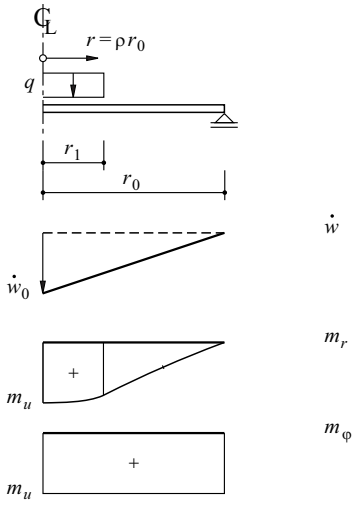

Fig. 24.25 TRESCA circular slab uniformly loaded in the centre and simply supported at the edge

Example 24.7 Fixed circular slab

Fig. 24.26 shows a uniformly loaded circular slab fixed at its edge. We shall assume regime BC for region $0 \le r \le r_1$, but regime CD for region $r_1 \le r \le r_0$, i. e.

$$m_r = m_u - \frac{qr^2}{6} \qquad (0 \le r \le r_1)$$

$$m_r = m_u \ln \rho + C_2 - \frac{qr^2}{4} \qquad (r_1 \le r \le r_0)$$

It follows from $m_r(r_1) = 0$ that $qr_1^{\,2} = 6m_u$, and applying $m_r(r_0) = -m_u$ gives us $C_2 = -m_u + qr_0^{\,2}/4$. Finally, the continuity condition for m_r at point $r = r_1$ results in the relationship

$$\ln \rho_1 - 1 + \frac{3}{2}\left(\frac{1}{\rho_1^2} - 1\right) = 0$$

i. e. $\rho_1 \approx 0.73$ and $qr_0^{\,2}\pi = 35.37 m_u$.

The resulting moments and deflection increments are

$$m_r = m_u\left(1 - \frac{\rho^2}{\rho_1^2}\right) \quad , \quad m_\varphi = m_u \quad , \quad \dot{w} = \dot{w}_0\left(1 - \frac{\rho/\rho_1}{1 - \ln \rho_1}\right) \qquad (0 \le r \le r_1)$$

$$m_r = m_u\left(-1 + \ln \rho + \frac{3}{2} \cdot \frac{1 - \rho^2}{\rho_1^2}\right) \quad , \quad m_\varphi = m_u + m_r \quad , \quad \dot{w} = \dot{w}_0 \frac{\ln \rho}{\ln \rho_1 - 1} \qquad (r_1 \le r \le r_0)$$

At the fixed support there is a yield line with a rotation increment amounting to $0.76\dot{w}_0/r_0$.

The comparison with $(24.45)_2$ reveals that the moment m_r at the fixed support for a loading of $qr_0^{\,2}\pi = 16\pi m_u/3$ reaches the value $-m_y = -h^2 f_y/6$ according to $(20.23)_2$ upon onset of yield in the outermost fibres of the slab, i. e. presuming a system initially free from residual stresses, the onset of yield is established for a load equal to 47.4 % of the limit load.

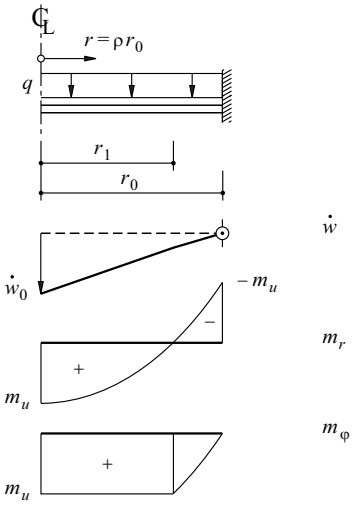

Fig. 24.26 Fixed TRESCA circular slab subjected to uniform loading

24.3.1.3 Commentary

Any rotationally symmetric problems concerning TRESCA slabs can be dealt with in a similar way to examples 24.6 and 24.7. Complete solutions can certainly be provided (exercise 24.17).

The limit load for a point load applied to simply supported or fixed TRESCA slabs with any form is $2\pi m_u$ [27]. The limit load for simply supported TRESCA slabs with any form and subjected to a uniformly distributed loading is at least $6\pi m_u$ [30].

In contrast to TRESCA slabs, slabs that satisfy the VON MISES yield condition give rise to non-linear differential equations that generally have to be solved numerically. Further, compared with TRESCA slabs, there are significant differences in the collapse mechanisms [27]. However, the limit loads cannot be more than 15.4 % higher for the same plastic moment m_u, as already mentioned above.

24.3.2 Reinforced concrete slabs

24.3.2.1 Normal moment yield condition

Fig. 24.27(a) illustrates the stress distribution as a result of the plastic moments m_{xu}, m_{yu} in a slab reinforced in the x and y directions. The cross-sectional areas of the reinforcement related to the unit width are designated with a_x, a_y (bottom reinforcement) and a_x', a_y' (top reinforcement). The yield limit for the reinforcement in tension and compression is presumed to be f_y. The square yield condition ODEF will be assumed for the coplanar stress state according to Fig. 7.11(b).

The depths of the compression zones c_x, c_y follow from the condition that the membrane forces n_x, n_y disappear. The two layers of top reinforcement yield in compression when they lie within the compression zone, see Fig. 24.27(a). The compression zone can lie within the concrete cover if this is very deep and the bottom reinforcement is relatively light; the top reinforcement then yields in tension according to the rigid - perfectly plastic idealisation. The top reinforcement remains rigid if it coincides exactly with the neutral axis, i. e. its stresses can lie anywhere between the limit values f_y and $-f_y$. We should also note that, strictly speaking, when the reinforcement lies within the compression zone, a stress of $-f_y + f_c$ should be assumed instead of $-f_y$ (or a force of $a_x' f_c$ or $a_y' f_c$ deducted) because there is no concrete available at this par-

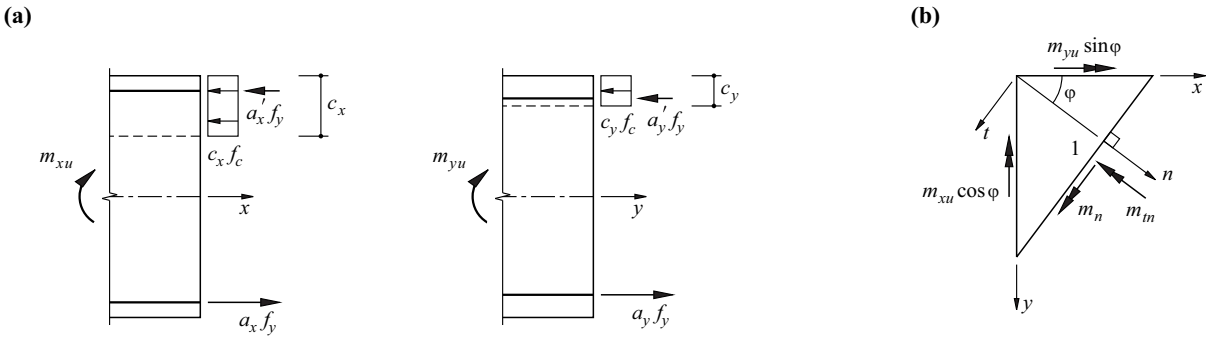

Fig. 24.27 Reinforced concrete slab with orthogonal reinforcement: (a) plastic moments in reinforcement directions, (b) superposition of the two stress states

ticular location in the cross-section. The influence on the plastic moment is marginal and so this effect is usually neglected.

Superposing the two stress states of Fig. 24.27(a) results in a statically admissible stress state. The values that apply at any section according to Fig. 24.27(b) are $n_n = n_{tn} = 0$, $m_n = m_{xu}\cos^2\varphi + m_{yu}\sin^2\varphi$ and $m_{tn} = (m_{yu} - m_{xu})\sin\varphi\cos\varphi$. The depths of the compression zones c_x and c_y are generally different and so no compatible yield line mechanism can be associated with the stress state. Therefore, the following applies for the plastic moment in the n direction according to the lower-bound theorem:

$$m_{nu} \geq m_{xu}\cos^2\varphi + m_{yu}\sin^2\varphi \tag{24.86}$$

When $c_x = c_y$, then the equal sign is valid in (24.86), and even for the general case of $c_x \neq c_y$, the right-hand side of (24.86) results in a very good approximation for m_{nu}.

We shall omit the inequality sign in (24.86) in the following and supplement the relationship with a similar relationship for the magnitudes of the negative plastic moments, i. e.

$$m_{nu} = m_{xu}\cos^2\varphi + m_{yu}\sin^2\varphi \quad , \quad m_{nu}' = m_{xu}'\cos^2\varphi + m_{yu}'\sin^2\varphi \tag{24.87}$$

The moments m_n according to $(24.7)_1$ must lie between the corresponding resistances for all directions n. This leads to the *normal moment yield condition*

$$-m_{nu}' \leq m_n \leq m_{nu} \tag{24.88}$$

see Fig. 24.28(a).

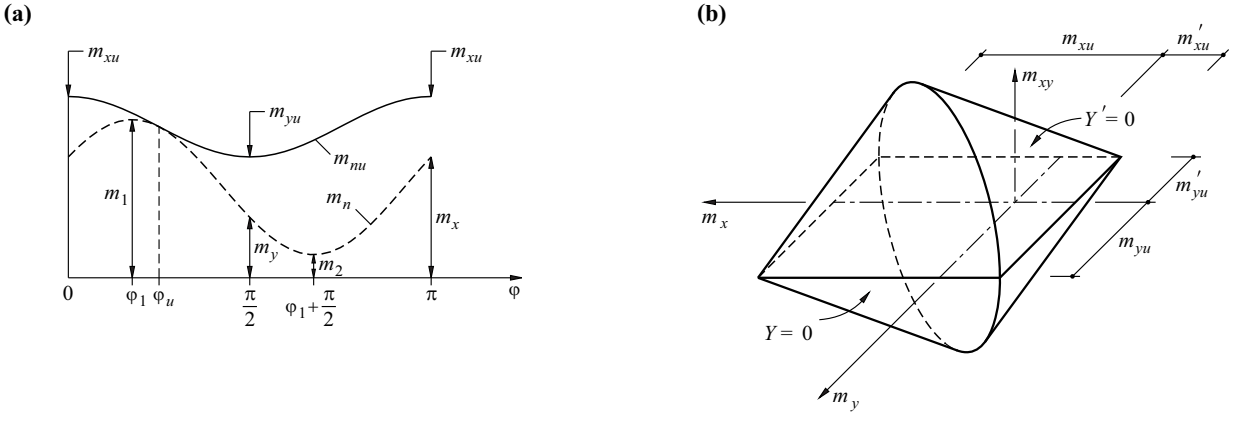

Fig. 24.28 Normal moment yield condition: (a) normal moments and resistances, (b) yield surface

Considering the yield line direction φ_u, then $m_n = m_{nu}$ applies on the one hand and $dm_n/d\varphi = dm_{nu}/d\varphi$ on the other, i. e.

$$\begin{aligned} &(m_{xu} - m_x)\cos^2\varphi_u + (m_{yu} - m_y)\sin^2\varphi_u - 2m_{xy}\sin\varphi_u\cos\varphi_u = 0 \\ -&(m_{xu} - m_x) \qquad + (m_{yu} - m_y) \qquad - 2m_{xy}\cot(2\varphi_u) \quad = 0 \end{aligned}$$

where the second equation has been divided by $\sin(2\varphi_u)$. Dividing the first equation by $\sin^2\varphi_u$ or $\cos^2\varphi_u$ and subtracting or adding the second equation results in

$$m_{xu} = m_x + m_{xy}\tan\varphi_u \quad , \quad m_{yu} = m_y + m_{xy}\cot\varphi_u \qquad (24.89)_1$$

Similarly, we get

$$m_{xu}' = -m_x - m_{xy}\tan\varphi_u' \quad , \quad m_{yu}' = -m_y - m_{xy}\cot\varphi_u' \qquad (24.89)_2$$

Eliminating φ_u or φ_u' results in the yield conditions

$$Y = m_{xy}^2 - (m_{xu} - m_x)(m_{yu} - m_y) = 0 \quad , \quad Y' = m_{xy}^2 - (m_{xu}' + m_x)(m_{yu}' + m_y) = 0 \qquad (24.90)$$

(and note that the expressions in brackets may not be negative). The following applies for the yield line directions:

$$\tan\varphi_u = \frac{m_{xu} - m_x}{m_{xy}} = \frac{m_{xy}}{m_{yu} - m_y} = \sqrt{\frac{m_{xu} - m_x}{m_{yu} - m_y}} \quad , \quad \tan\varphi_u' = -\frac{m_{xu}' + m_x}{m_{xy}} = -\frac{m_{xy}}{m_{yu}' + m_y} = \sqrt{\frac{m_{xu}' + m_x}{m_{yu}' + m_y}} \qquad (24.91)$$

We can see that the yield line direction does not generally coincide with a principal moment direction, i. e. as a rule $\varphi_u \neq \varphi_1$, see (24.8).

The yield conditions (24.90) are similar to $(23.20)_1$. Putting $k = |\tan\varphi_u|$ and $k' = |\tan\varphi_u'|$ results in the relationships

$$\begin{aligned} m_{xu} &\geq m_x + k|m_{xy}| \quad , \quad m_{yu} \geq m_y + \frac{1}{k}|m_{xy}| \\ m_{xu}' &\geq -m_x + k'|m_{xy}| \quad , \quad m_{yu}' \geq -m_y + \frac{1}{k'}|m_{xy}| \end{aligned} \qquad (24.92)$$

for the dimensioning, which are similar to (23.26). The parameters k and k' are often taken to be equal to 1 in practice.

In the space m_x, m_y, m_{xy}, the yield conditions (24.90) correspond to the two elliptical cone surfaces shown in Fig. 24.28(b). According to the flow rule (7.12) or $(21.2)_1$, the following applies for points on the cone surface $(24.90)_1$ apart from the apex of the cone and the ellipse at the intersection of the two cones:

$$\dot\chi_x = \kappa(m_{yu} - m_y) \quad , \quad \dot\chi_y = \kappa(m_{xu} - m_x) \quad , \quad 2\dot\chi_{xy} = \kappa \cdot 2m_{xy} \qquad (\kappa \geq 0)$$

and similarly for the cone surface $(24.90)_2$:

$$\dot\chi_x = -\kappa(m_{yu}' + m_y) \quad , \quad \dot\chi_y = -\kappa(m_{xu}' + m_x) \quad , \quad 2\dot\chi_{xy} = \kappa \cdot 2m_{xy} \qquad (\kappa \geq 0)$$

Taking into account (24.90) and $(24.21)_2$, it follows that

$$\dot\chi_{xy}^2 - \dot\chi_x\dot\chi_y = -\dot\chi_1\dot\chi_2 = \dot\chi_{II} = 0$$

see $(23.23)_1$, i. e. we get developable surfaces for the deflection increments $\dot w$; the corresponding points on the slab are parabolic.

According to (7.13), the following applies for points on the ellipse at the intersection of the two cone surfaces:

$$\begin{aligned} \dot\chi_x &= \kappa_1(m_{yu} - m_y) - \kappa_2(m_{yu}' + m_y) \\ \dot\chi_y &= \kappa_1(m_{xu} - m_x) - \kappa_2(m_{xu}' + m_x) \qquad (\kappa_1 \geq 0,\ \kappa_2 \geq 0) \\ \dot\chi_{xy} &= (\kappa_1 + \kappa_2)m_{xy} \end{aligned}$$

and therefore $\dot\chi_{II} \geq 0$. Stress states with points on the ellipse at the intersection therefore correspond – in terms of the deflection increments $\dot w$ – to parabolic or hyperbolic points with negligible or negative total curvature.

Finally, the apexes of the cones correspond to parabolic or elliptical points with negligible or positive total curvature, i. e. $\dot\chi_{II} \leq 0$ and either $\dot\chi_x \geq 0$ or $\dot\chi_x \leq 0$.

Example 24.8 Reinforced concrete slab – dimensioning for bending

The task is to determine the bending resistances required in the x and y directions for the moments $m_x = 30\,\text{kNm/m}$, $m_y = 0$, $m_{xy} = 20\,\text{kNm/m}$ given in Fig. 24.29(a).

According to (24.92), the result is the areas bounded by hyperbolas shown in Fig. 24.29(b). Permissible dimensioning points m_{xu}, m_{yu} or m_{xu}', m_{yu}' lie within the shaded areas.

The hyperbolas in the displaced system of coordinates $m_{xu} - m_x$, $m_{yu} - m_y$ or $m_{xu}' + m_x$, $m_{yu}' + m_y$ shown in Fig. 24.29(b) correspond to the intersections of the two elliptical cones of Fig. 24.28(b) with the plane $m_{xy} = \text{const}$.

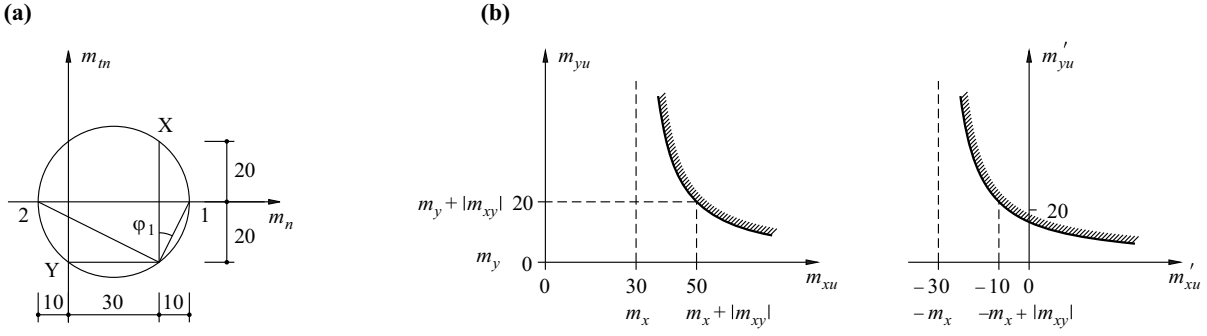

Fig. 24.29 Dimensioning a reinforced concrete slab for bending: (a) stress resultants, (b) permissible ranges for bending resistances (moments in kNm/m = kN)

24.3.2.2 Theory of thin plastic slabs

The middle plane of a reinforced concrete slab generally experiences strain increments which we shall designate $\dot{\varepsilon}_{xm}$, $\dot{\varepsilon}_{ym}$, $\dot{\gamma}_{xym}$. These are added to the variables $\dot{\chi}_x$, $\dot{\chi}_y$, $2\dot{\chi}_{xy}$ in the form of generalised deformation increments, and

$$\dot{\varepsilon}_x = \dot{\varepsilon}_{xm} + \dot{\chi}_x z \quad , \quad \dot{\varepsilon}_y = \dot{\varepsilon}_{ym} + \dot{\chi}_y z \quad , \quad \dot{\gamma}_{xy} = \dot{\gamma}_{xym} + 2\dot{\chi}_{xy} z \tag{24.93}$$

applies, see Fig. 24.30. The relationships (24.93) correspond to kinematic constraints that constitute the theory of thin plastic slabs (rigid in shear). The principal values

$$\dot{\varepsilon}_{1,2} = \frac{\dot{\varepsilon}_x + \dot{\varepsilon}_y}{2} \pm \sqrt{\left(\frac{\dot{\varepsilon}_x - \dot{\varepsilon}_y}{2}\right) + \frac{\dot{\gamma}_{xy}^2}{4}}$$

of the strain increments generally exhibit a hyperbolic variation over the slab depth h, and the principal directions vary according to

$$\tan(2\varphi_1) = \frac{\dot{\gamma}_{xy}}{\dot{\varepsilon}_x - \dot{\varepsilon}_y}$$

see (6.13) and (6.14).

The condition

$$\dot{\varepsilon}_{\text{II}} = -\dot{\varepsilon}_x \dot{\varepsilon}_y + \frac{\dot{\gamma}_{xy}^2}{4} = -\dot{\varepsilon}_1 \dot{\varepsilon}_2 = 0$$

for equating $\dot{\varepsilon}_1$ and $\dot{\varepsilon}_2$ to zero results in the quadratic equation

$$z^2 \dot{\chi}_{\text{II}} - z(\dot{\varepsilon}_{xm}\dot{\chi}_y + \dot{\varepsilon}_{ym}\dot{\chi}_x - \dot{\gamma}_{xym}\dot{\chi}_{xy}) + \dot{\varepsilon}_{\text{II}m} = 0$$

from which we generally get a maximum of two levels z_1 and z_2 within the slab depth h. If we assume the square yield condition according to Fig. 24.31 for the concrete, see Fig. 7.11(b), then it is possible to distinguish various zones over the depth of the slab which correspond to regimes O, A and B. For example, in the case shown in Fig. 24.30, $\dot{\varepsilon}_1$ and $\dot{\varepsilon}_2$ bottommost in the slab are both positive (regime O) and topmost both negative (regime B), whereas in between $\dot{\varepsilon}_1$ is positive and $\dot{\varepsilon}_2$ is negative (regime A).

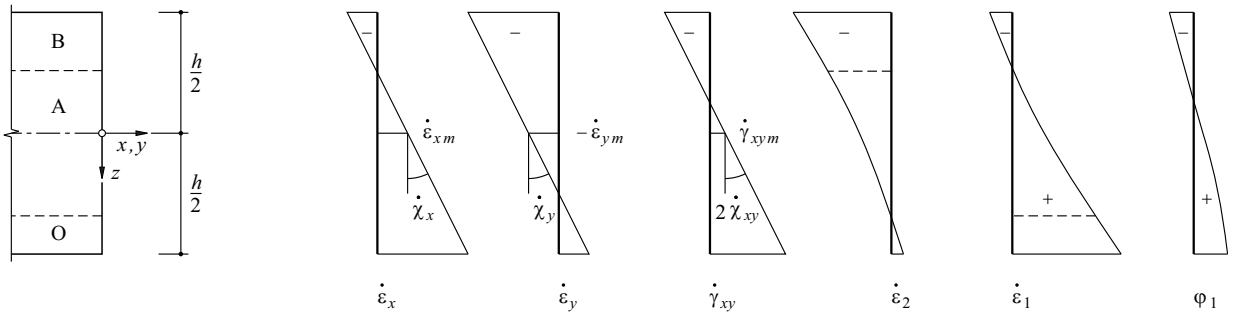

Fig. 24.30 How the strain increments and principal directions vary over the depth of a slab

Calculating the stresses $n_x, \ldots, m_x, \ldots$ belonging to a set of generalised deformation increments $\dot{\varepsilon}_{xm}, \ldots, \dot{\chi}_x, \ldots$ does not present any particular difficulties. With the given yield conditions for all layers in a slab, it is possible to calculate the specific dissipation energy $\dot{D} = \dot{D}(\dot{\varepsilon}_{xm}, \ldots, \dot{\chi}_x, \ldots)$ on the basis of (24.93), and the associated generalised stresses follow according to (7.17), i. e.

$$n_x = \frac{\partial \dot{D}}{\partial \dot{\varepsilon}_{xm}} \quad , \quad \ldots \quad , \quad m_x = \frac{\partial \dot{D}}{\partial \dot{\chi}_x}$$

The reverse of this problem, i. e. calculating the generalised deformation increments belonging to a set of generalised stresses, generally calls for an iterative numerical procedure; please refer to the comments at the end of section 13.2.1. For example, the yield surface in the space m_x, m_y, m_{xy} can be determined point for point by varying the variables $\dot{\varepsilon}_{xm}$, $\dot{\varepsilon}_{ym}$, $\dot{\gamma}_{xym}$ for each assumed set $\dot{\chi}_x$, $\dot{\chi}_y$, $2\dot{\chi}_{xy}$ until $n_x = n_y = n_{xy} = 0$. Analytical solutions are also possible in some circumstances.

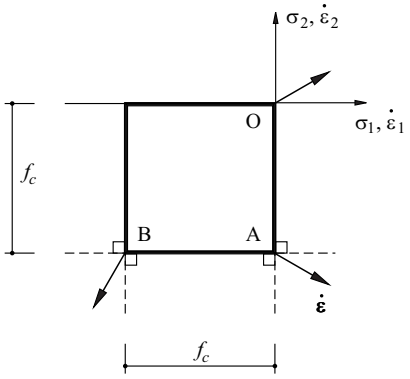

Fig. 24.31 Square yield condition for concrete

Example 24.9 Slab element subjected to pure twist

The slab element shown in Fig. 24.32 is reinforced symmetrically about the middle plane. The reinforcement cross-sections in the four layers are identical ($a_x = a_y = a_x' = a_y'$) and the yield limit for the reinforcement is f_y. The square yield condition, see Fig. 24.31, is presumed for the concrete. For reasons of symmetry, a pure twist stress resultant ($m_{xy} = m_{yx} > 0$, $m_x = m_y = 0$) has $\dot{\chi}_x = \dot{\chi}_y = \dot{\gamma}_{xym} = 0$ and $\dot{\varepsilon}_x = \dot{\varepsilon}_y = \text{const}$. The principal values $\dot{\varepsilon}_1$ and $\dot{\varepsilon}_2$ vary linearly with z on both sides of the middle plane, and $\dot{\varepsilon}_2$ is zero at the points $z = \pm z_0 = \dot{\varepsilon}_x/\dot{\chi}_{xy}$. The value of φ_1 is constant ($\pi/4$ or $3\pi/4$) on both sides of the middle plane; an abrupt change in φ_1 ensues at the middle plane. Regime O applies for the concrete in the inner area $0 \le |z| < z_0$, and regime A in the outer areas $z_0 \le |z| \le h/2$. Taking the corresponding stresses $-\sigma_{cx} = -\sigma_{cy} = |\tau_{cxy}| = f_c/2$ in the concrete in the outer areas, then

$$n_x = n_y = 2\left[-\frac{f_c}{2}\left(\frac{h}{2} - z_0\right) + a_x f_y\right] = 0 \quad , \quad m_{xy} = \frac{f_c}{2}\left(\frac{h}{2} - z_0\right)\left(\frac{h}{2} + z_0\right)$$

applies, i. e. using the mechanical reinforcement ratio $\omega = a_x f_y/(h f_c)$, then $z_0 = h(1/2 - 2\omega)$, and the result for the twisting resistance m_{xyu} is

$$m_{xyu} = f_c h^2 \omega(1 - 2\omega)$$

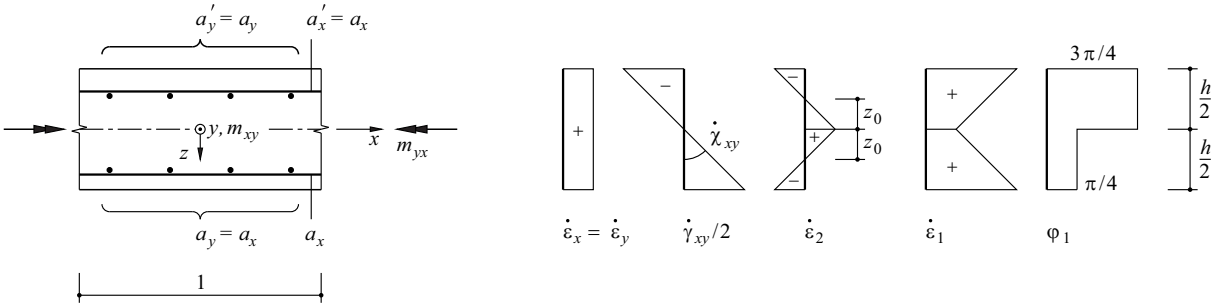

Fig. 24.32 Symmetrically reinforced slab element subjected to pure twist

This relationship applies for $\omega \leq 1/4$. If $\omega > 1/4$, then $m_{xyu} = f_c h^2/8$ and $\dot{\varepsilon}_x = 0$, i. e. the reinforcement does not yield, and as $z_0 = 0$, there is no inner area in which the concrete is stress-free (regime O).

Provided the entire reinforcement is placed in the inner area, i. e. for the case that the effective depth of the (outer) reinforcement in the x direction does not exceed the value $h/2 + z_0 = h(1 - 2\omega)$, then (24.90) also results in a twisting resistance of $f_c h^2 \omega(1 - 2\omega)$. This is the case for small reinforcement ratios, but not for moderate and heavy reinforcement. As ω increases, so the twisting resistance becomes increasingly overestimated by the normal moment yield condition (24.90).

24.3.2.3 Sandwich model

One model [18] that is suitable for dimensioning reinforced concrete slabs subjected to general stress resultants results from splitting a slab into two outer faces reinforced in the x and y directions and an intermediate core, see Fig. 24.33(a). The shear forces are assigned to the core, membrane forces as well as bending and twisting moments assigned to the outer faces. The thicknesses of the outer faces depend on the average effective depths d_m and d_m' of the reinforcement a_x, a_y and a_x', a_y', i. e. are equal to $2(h - d_m)$ and $2d_m'$, where h = slab depth. Thus, the thickness of the core is $d_v = d_m - d_m'$. We shall presume that the core is reinforced in the z direction according to a geometric reinforcement ratio ρ_z.

The principal shear force v_0 according to $(24.11)_1$ is carried as shown in Fig. 24.33(b) via a compressive stress field in the concrete core inclined at an angle α to the xy plane. In a similar way to $(23.26)_2$ or (23.35), the reinforcement required in the z direction is

$$\rho_z f_y \geq \frac{v_0 \tan\alpha}{d_v} \tag{24.94}$$

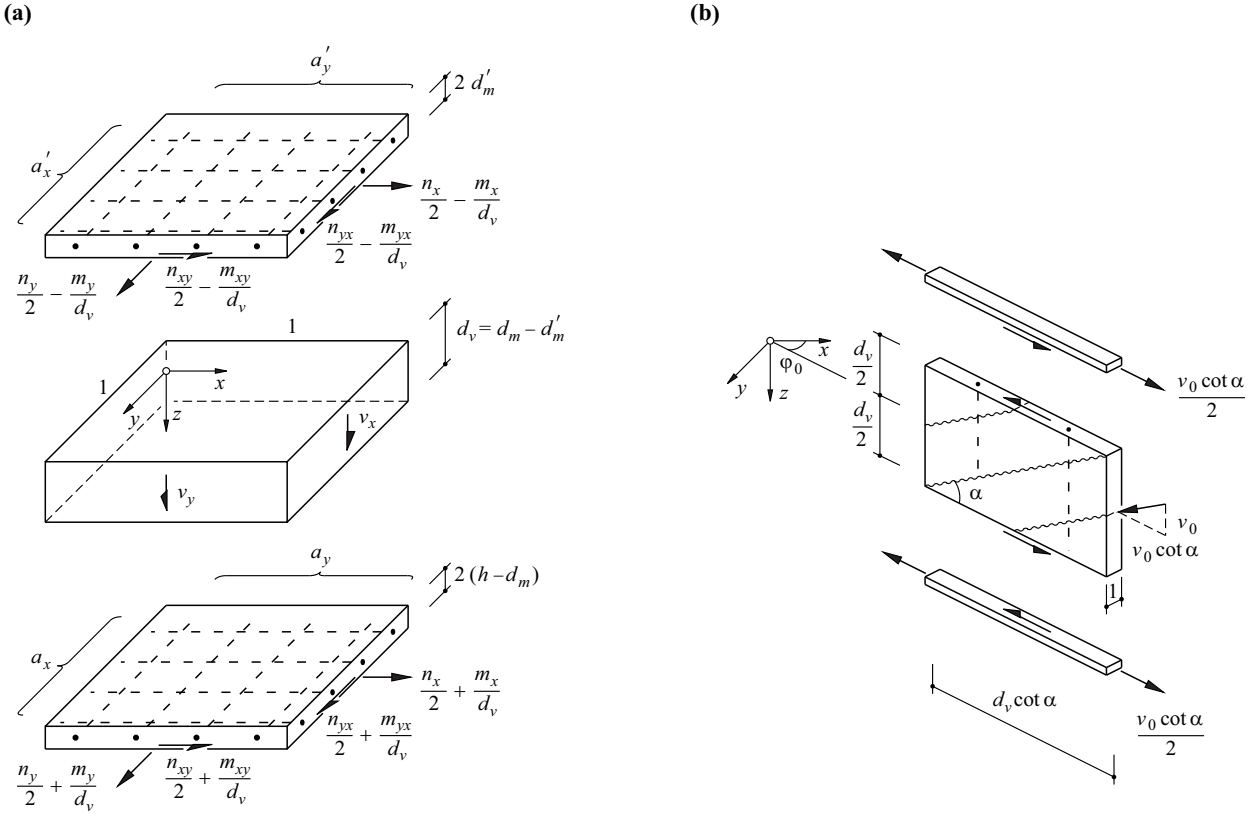

Fig. 24.33 Sandwich model: (a) core and outer faces, (b) compressive stress field in core

The tensile forces $v_0\cot\alpha/2$ required to compensate for the compressive force $v_0\cot\alpha$ in the φ_0 direction – taking into account (24.11) – lead to additional membrane forces

$$n_{xv} = \frac{v_0}{2}\cot\alpha\cos^2\varphi_0 = \frac{v_x^2\cot\alpha}{2v_0} \quad , \quad n_{yv} = \frac{v_0}{2}\cot\alpha\sin^2\varphi_0 = \frac{v_y^2\cot\alpha}{2v_0} \quad , \quad n_{xyv} = \frac{v_0}{2}\cot\alpha\sin\varphi_0\cos\varphi_0 = \frac{v_x v_y\cot\alpha}{2v_0}$$

in the outer faces of the sandwich.

Compression stress fields in the concrete at angles of β and β' to the x axis are assumed in the outer faces of the sandwich. Putting $k = |\cot\beta|$ and $k' = |\cot\beta'|$ and using (23.26) results in the requirements

$$\begin{aligned}
a_x f_y &\geq \frac{n_x}{2} + \frac{m_x}{d_v} + \frac{v_x^2\cot\alpha}{2v_0} + k\left|\frac{n_{xy}}{2} + \frac{m_{xy}}{d_v} + \frac{v_x v_y\cot\alpha}{2v_0}\right| \\
a_y f_y &\geq \frac{n_y}{2} + \frac{m_y}{d_v} + \frac{v_y^2\cot\alpha}{2v_0} + \frac{1}{k}\left|\frac{n_{xy}}{2} + \frac{m_{xy}}{d_v} + \frac{v_x v_y\cot\alpha}{2v_0}\right| \\
a_x' f_y &\geq \frac{n_x}{2} - \frac{m_x}{d_v} + \frac{v_x^2\cot\alpha}{2v_0} + k'\left|\frac{n_{xy}}{2} - \frac{m_{xy}}{d_v} + \frac{v_x v_y\cot\alpha}{2v_0}\right| \\
a_y' f_y &\geq \frac{n_y}{2} - \frac{m_y}{d_v} + \frac{v_y^2\cot\alpha}{2v_0} + \frac{1}{k'}\left|\frac{n_{xy}}{2} - \frac{m_{xy}}{d_v} + \frac{v_x v_y\cot\alpha}{2v_0}\right|
\end{aligned} \tag{24.95}$$

The bending and twisting moments here are related to the x, y axes that lie in the middle plane of the core.

Eq. (24.94) and (24.95) can be used for sizing the reinforcement for given stress resultants. The choice of α, k and k' is left to the designer, who is recommended to remain within the following limits: $0.5 \leq \tan\alpha \leq 1$, $0.5 \leq k \leq 2$, $0.5 \leq k' \leq 2$. Similarly to (23.25), checking the concrete compressive stresses in the outer faces of the sandwich calls for

$$\begin{aligned}
\left|\frac{n_{xy}}{2} + \frac{m_{xy}}{d_v} + \frac{v_x v_y\cot\alpha}{2v_0}\right| \cdot \left(k + \frac{1}{k}\right) &\leq 2(h - d_m)f_c \\
\left|\frac{n_{xy}}{2} - \frac{m_{xy}}{d_v} + \frac{v_x v_y\cot\alpha}{2v_0}\right| \cdot \left(k' + \frac{1}{k'}\right) &\leq 2d_m' f_c
\end{aligned} \tag{24.96}$$

24.3.2.4 Commentary

This presentation of yield conditions for reinforced concrete slabs is confined to elements with orthogonal reinforcement. However, as with reinforced concrete plates (section 23.3.2), the observations can be extended to skew reinforcement.

Compared with (24.93), assuming yield lines corresponds to a more severe kinematic constraint. Therefore, apart from special cases, which can be attributed to omitting the inequality sign in (24.86), the normal moment yield condition cannot supply any resistances that lie below those calculated in accordance with the theory of thin plastic slabs.

The bending resistance m_{nu} at a yield line in the t direction is generally determined in such a way that $n_n = 0$. As a rule, this leads to a membrane shear force n_{tn} and to a twisting moment m_m. Like the shear forces, these stress resultants are not generalised stresses; their associated strain increments disappear, and so they do not contribute to dissipation.

Assuming $n_n = 0$ at a yield line presumes that the associated extension of the middle plane of the slab is not inhibited. Depending on the boundary conditions of a problem, it may be that this assumption cannot be fulfilled, and the result is corresponding membrane effects.

In contrast to the normal moment yield condition and the theory of thin plastic slabs, the sandwich model is not based on a kinematic constraint, but rather on a pure static treatment. No kinematic variables can be directly assigned to the static variables and

so the sandwich model is a dimensioning procedure and not really a way of assessing yield conditions for slab elements. Furthermore, it should be noted that, on the one hand, the simplified assumption regarding the depth of the outer faces of the sandwich infringes the moment equilibrium conditions to a certain extent because the position of the reinforcement effectively deviates slightly from the middle of the face; on the other hand, the available resistance of the concrete is in most cases not fully exploited. In addition, allocating all the membrane forces to the outer faces of the sandwich can prove to be a disadvantage. The influence of all these shortcomings is quickly assessed in each individual case thanks to the simplicity of this type of model, and the designer can decide whether a more detailed treatment according to the theory of plastic slabs is preferable.

24.4 Static method

24.4.1 Rotationally symmetric problems

24.4.1.1 "Isotropic" reinforcement

When $m_{xu} = m_{yu} = m_u$, $m_{xu}' = m_{yu}' = \lambda m_u$, then according to (24.87), $m_{nu} = m_u$ or $m_{nu}' = \lambda m_u$ for all directions n. Comparing (24.9) with (24.91) reveals that in such cases taking into account (24.90) means $\varphi_1 = \varphi_u$ or $\varphi_1 = \varphi_u'$, i. e. the yield line direction coincides with a principal moment direction. Such slabs are referred to as having "isotropic" reinforcement or, more correctly, as slabs with an isotropic bending resistance.

Referring to the yield locus shown in Fig. 24.34(a), we get the relationships shown in Tab. 24.2 (which is similar to Tab. 24.1). In contrast to the TRESCA yield condition, yield lines can ensue for the stress states at all corners of the yield locus.

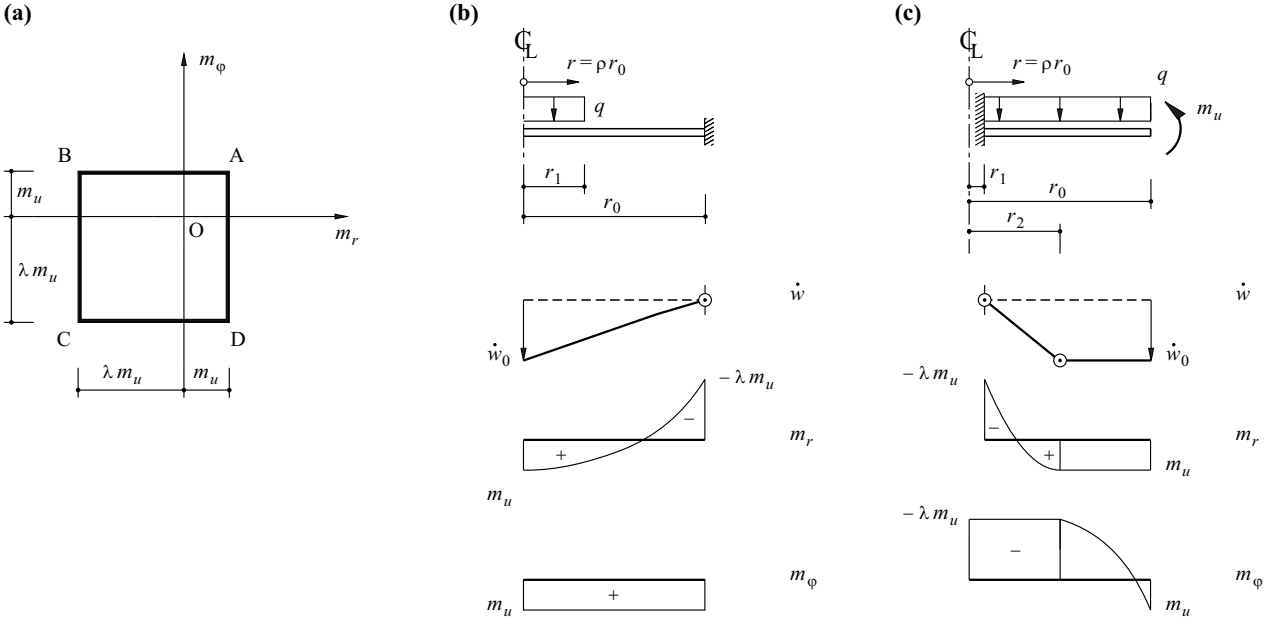

Fig. 24.34 Rotationally symmetric slabs with "isotropic" reinforcement: (a) yield locus, (b) fixed slab with uniformly distributed central load, (c) uniformly loaded annular slab with fixed support on the inside and $m_r = m_u$ loading on the outside

Tab. 24.2 General relationships for rotationally symmetric slabs with "isotropic" reinforcement

Regime	$\dot{\chi}_r$	$\dot{\chi}_\varphi$	$\dot{w}$	m_r/m_u	m_φ/m_u
DA, BC	$\geq 0, \leq 0$	0	const	$1\ ,-\lambda$	$\mu+1\ ,\mu-\lambda$
C	$\geq 0, \leq 0$	$\geq 0, \leq 0$	$\dot{w}'] \neq 0$	$1\ ,-\lambda$	$1\ ,-\lambda$
AB, CD	0	$\geq 0, \leq 0$	$ar+b$	$1+c/r-(1/r)\int\mu dr\ ,-\lambda+c/r-(1/r)\int\mu dr$	$1\ ,-\lambda$
C	$\leq 0, \geq 0$	$\geq 0, \leq 0$	$\dot{w}'] \neq 0$	$-\lambda\ ,1$	$1\ ,-\lambda$

Example 24.10 Fixed circular slab

Assuming regime AB for the slab shown in Fig. 24.34(b), as in example 24.6, then $m_\varphi = m_u = \text{const}$ and

$$m_r = m_u + \frac{C_1}{r} - \frac{qr^2}{6} \qquad (0 \leq r \leq r_1)$$

$$m_r = m_u + \frac{C_2}{r} - \frac{qr_1^2}{2} \qquad (r_1 \leq r \leq r_0)$$

It follows from $m_r(0) = m_u$ that $C_1 = 0$, the continuity condition for m_r at the point $r = r_1$ requires $C_2 = qr_1{}^3/3$, and the condition $m_r(r_0) = -\lambda m_u$ results in the limit load

$$qr_1^2\pi = \frac{2\pi m_u(1+\lambda)}{1-\frac{2\rho_1}{3}}$$

A yield line (regime B) becomes established at the edge of the slab and a collapse mechanism (regime AB) in the form of a circular cone is set up within the slab.

When $\lambda = 0$, the solution is identical with that of example 24.6.

Putting $\rho_1 = 1$ results in the same moment distribution as for a simply supported square plate subjected to a uniformity distributed load q (side length $l = 2r_0$, $m_0 \to m_u$, corners restrained), see exercise 24.1 and $(24.7)_1$ with $\tan\varphi = y/x$, $r^2 = x^2 + y^2$: $m_r/m_u = 1 - (r/r_0)^2$, $m_\varphi = m_u$, $m_{r\varphi} = 0$. This formulation is not only suitable for square slabs; it also generally applies to slabs in the form of regular polygons that are simply supported and carry uniformly distributed loads. With n corners, the total load applied to the slab upon reaching the limit load is $6nm_u\tan(\pi/n)$. When $n \to \infty$, we get the limiting case of a circular slab with a limit load of $6\pi m_u$. Top reinforcement is required outside the slab's inscribed circle. The moment field is compatible with a mechanism in which (positive) yield lines run from the centre of the slab to its corners.

Example 24.11 Annular slab fixed at its inner edge and loaded on its outer edge by m_u

As an approximation, the annular slab shown in Fig. 24.34(c) can be considered as representing the interior bays of the area $r_0{}^2\pi$ of uniformly loaded flat slabs [17]. By assuming regimes CD and DA in the regions $r_1 \leq r \leq r_2$ and $r_2 \leq r \leq r_0$, we get

$$m_r = -\lambda m_u + \frac{C_1}{r} - \frac{qr^2}{6} + \frac{qr_0^2}{2} \qquad (r_1 \leq r \leq r_2)$$

$$m_\varphi = m_u + \frac{qr^2}{2} - \frac{qr_0^2}{2} \qquad (r_2 \leq r \leq r_0)$$

From $m_r(r_1) = -\lambda m_u$ it follows that

$$C_1 = \frac{qr_1^3}{6} - \frac{qr_0^2 r_1}{2}$$

and therefore $m_r(r_2) = m_u$ results in

$$(1+\lambda)m_u = \frac{qr_0^2}{2} - \frac{qr_2^2}{6} + \frac{q}{r_2}\left(\frac{r_1^3}{6} - \frac{r_0^2 r_1}{2}\right)$$

Owing to the fact that $m_\varphi(r_2) = -\lambda m_u$, it is also the case that

$$(1+\lambda)m_u = \frac{qr_0^2}{2} - \frac{qr_2^2}{2}$$

Consequently,

$$\rho_2 = \sqrt[3]{\frac{3}{2}\rho_1 - \frac{1}{2}\rho_1^3}$$

and the limit load is

$$q(r_0^2 - r_1^2)\pi = \frac{2\pi m_u(1+\lambda)(1-\rho_1^2)}{1-\rho_2^2}$$

24.4.1.2 Variable bending resistances

In many large circular slabs, only the central area contains orthogonal reinforcement, and the outer areas are reinforced with radial and curved bars, see Fig. 24.35(a). The bar diameter remains constant but the spacing of the radial bars increases with the radius r and so the corresponding bending resistance m_{ru} is approximately proportional to $1/r$. In order that the spacing of the radial bars does not become too large near the outer edge of the slab, intermediate bars may be required. In such a case, m_{ru} is approximately proportional to $1/r$ for each particular area; $m_{ru}(r)$ then progresses in sawtooth fashion.

In order to discuss the effect of the variable bending resistance $m_{ru}(r)$, we shall make use of the relationship (24.5), which will be written in the form

$$m_\varphi = \frac{\mathrm{d}}{\mathrm{d}r}(rm_r) + \int_0^r qr\,\mathrm{d}r \tag{24.97}$$

If we substitute the resistance $m_{ru}(r)$ for m_r in this relationship, then the result for any loading $q(r)$ is the required resistance $m_{\varphi u}(r)$. The spacing of the curved reinforcing bars can be easily varied and so it is not difficult to adapt $m_{\varphi u}$ to suit the static requirements.

Eq. (24.97) leads to another interesting finding. The total mass of the (bottom) reinforcement in a circular slab simply supported at its outer edge $r = r_0$ and subjected to any loading $q(r) \geq 0$ is proportional to the "moment volume"

$$M = 2\pi \int_0^{r_0} (m_{ru} + m_{\varphi u}) r\,\mathrm{d}r$$

provided we assume the same yield limits, densities and lever arms for all the reinforcing bars. If we presume that the bending resistances for a certain load case are just reached for all values of r, then we can replace m_{ru} and $m_{\varphi u}$ by m_r and m_φ, and use (24.97). Making use of $(24.85)_1$ results in

$$M = 2\pi \int_0^{r_0} \left[rm_r + r \cdot \frac{\mathrm{d}}{\mathrm{d}r}(rm_r) + m_u \mu r \right] \mathrm{d}r = 2\pi \left(r^2 m_r \Big|_0^{r_0} + m_u \int_0^{r_0} \mu r \mathrm{d}r \right)$$

The first term in brackets on the right disappears because one of its factors is zero at each limit of integration. Consequently, we are left with the following:

$$M = 2\pi \int_0^{r_0} r \int_0^r qr \mathrm{d}r \mathrm{d}r \tag{24.98}$$

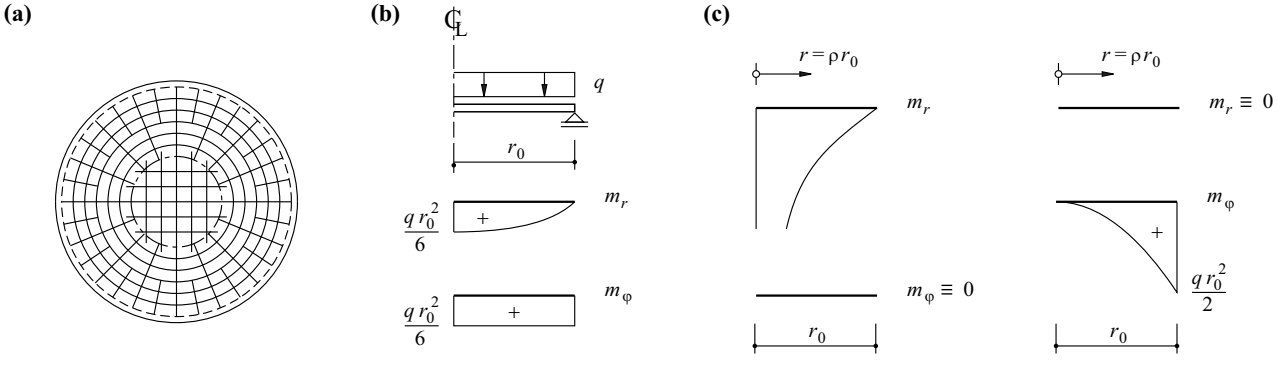

Fig. 24.35 Radial and curved reinforcing bars: (a) reinforcement layout, (b) bending moment diagram according to example 24.10 ($\rho_1 = 1$), (c) extreme bending moment diagrams

According to this, all the reinforcement in a circular slab simply supported at its outer edge with ideally curtailed reinforcement is dependent on the respective load case only and not on the apportionment of the bending resistances chosen in the radial and circular directions.

When q = const, then (24.98) results in, for example, $M = \pi q r_0^4/4$. The limiting case of $\rho_1 = 1$ in example 24.10 leads to the bending moment diagrams shown in Fig. 24.35(b) with the integral

$$M = 2\pi \cdot \frac{q r_0^2}{6} \int_0^{r_0} r \left[1 - \left(\frac{r}{r_0} \right)^2 + 1 \right] \mathrm{d}r = \frac{\pi q r_0^2}{3} \cdot \left(r_0^2 - \frac{r_0^2}{4} \right) = \frac{\pi q r_0^4}{4}$$

We get the same integral for the potential extreme bending moment diagrams

$$m_r = \frac{q}{6} \left(\frac{r_0^3}{r} - r^2 \right) \quad , \quad m_\varphi \equiv 0$$

shown in Fig. 24.35(c) according to (24.97), or rather

$$m_r \equiv 0 \quad , \quad m_\varphi = \frac{q r^2}{2}$$

and likewise for the elastic moment distribution $(24.46)_2$ and $(24.46)_3$, see exercise 24.19.

The case shown on the left of Fig. 24.35(c) is impossible because m_r for $r \to 0$ tends to infinity. On the other hand, any deflection profiles $\dot{w}(r)$ in which the relationship $\mathrm{d}\dot{w}/\mathrm{d}r \leq 0$ is satisfied for all values of r are compatible with the bending moment diagram shown on the right of Fig. 24.35(c) because $m_r = m_{ru} = 0$, e. g. $\dot{w} = \dot{w}_0(1 - \rho^2)$, which leads to $\dot{\chi}_r = \dot{\chi}_\varphi = -2\dot{w}_0/r_0^2$.

24.4.1.3 Commentary

As with rotationally symmetric TRESCA slabs, complete solutions can be worked out for any rotationally symmetric problems connected with reinforced concrete slabs.

When we specify m_r or m_φ on the basis of an existing resistance, for example, it follows that m_φ or m_r can be obtained from (24.97) for a given loading $q(r)$.

Eq. (24.98) is only valid for a circular slab simply supported at its outer edge and having non-negative moments. In the case of a slab uniformly loaded and fixed at its outer edge, the result with $m_r = -qr^2/6$ and $m_\varphi = 0$, for example, is the minimum reinforcement (exercise 24.20).

24.4.2 Moment fields for rectangular slabs

The examples 24.1, 24.2 and 24.3 were used to show how a skilfully chosen moment field for a given problem can satisfy the equilibrium condition (24.2) on the one hand, and the static boundary conditions on the other. This procedure is examined in more depth with the help of exercises 24.1, 24.2 and 24.5.

Polynomial formulations are generally suitable for the moments. The equilibrium conditions, the static boundary conditions and, where applicable, symmetry conditions provide certain relationships between the coefficients of the polynomial terms. The remaining free coefficients can be specified, for example, by considering the most rational arrangement of the reinforcement.

Further examples are given below.

Example 24.12 Simply supported rectangular slab

The slab shown in Fig. 24.36 is simply supported on all sides and carries a uniformly distributed load. Employing the shortened forms $\xi = 2x/a$, $\eta = 2y/b$, we use the moment field

$$m_x = m_u(1-\xi^2) \quad , \quad m_y = m_u(1-\eta^2) \quad , \quad m_{xy} = -m_u\xi\eta$$

Eq. (24.2) results in

$$qab = 8\left(\frac{b}{a} + \frac{a}{b} + 1\right)m_u$$

and $(24.9)_1$ gives us

$$m_1 = m_u \quad , \quad m_2 = m_u(1-\xi^2-\eta^2)$$

The moment field corresponds to a generalisation of that of exercise 24.1. The constant principal moment m_1 can be accommodated by an isotropic bending resistance m_u constant over the entire slab. Outside the inscribing ellipse to the slab, m_2 is negative. At the corners of the slab, $m_2 = -m_u$, and corner forces with a magnitude of $2m_u$ build up and act on the slab in the positive z direction. Theoretically, the top reinforcement can be confined to the corner regions ($\xi^2 + \eta^2 \geq 1$).

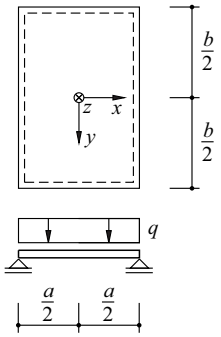

Fig. 24.36 Simply supported rectangular slab

Example 24.13 Square slab simply supported along two adjacent edges

The moment field

$$m_x = \frac{3}{2}m_u\xi(1-\xi) \quad , \quad m_y = \frac{3}{2}m_u\eta(1-\eta) \quad , \quad m_{xy} = -\frac{3}{4}m_u(\xi+\eta-\xi\eta)$$

for the square slab [22] shown in Fig. 24.37 – using $(24.1)_2$ and $(24.1)_3$ – leads to

$$v_x = \frac{3m_u}{4l}(1-3\xi) \quad , \quad v_y = \frac{3m_u}{4l}(1-3\eta)$$

and using (24.2) leads to

$$ql^2 = \frac{9m_u}{2}$$

According to (24.11), the principal shear forces are directed away from point D ($\xi = \eta = 1/3$) – as indicated by the arrows in Fig. 24.37. The bending moments and edge shear forces disappear along OA and OC, i. e. these edges are free (unsupported). The bending moments disappear along AB and BC, and the result is constant edge shear forces amounting to $-3m_u/(2l)$. Corner forces of $3m_u/2$ act on the slab in the negative z direction at corners A and C, and at corner B there is an equally large corner force in the positive z direction.

Assuming an isotropic bending resistance $m_{xu} = m_{yu} = m_u$, then $(24.90)_1$ gives us

$$Y = m_u^2\left[\frac{9}{16}(\xi+\eta-\xi\eta)^2 - \left(1-\frac{3}{2}\xi+\frac{3}{2}\xi^2\right)\left(1-\frac{3}{2}\eta+\frac{3}{2}\eta^2\right)\right]$$

$$= -m_u^2\left\{\left[1-\frac{3}{4}(\xi+\eta)\right]^2 + \frac{3}{8}\xi^2\left(1-\frac{3}{2}\eta\right)^2 + \frac{3}{8}\eta^2\left(1-\frac{3}{2}\xi\right)^2\right\}$$

The yield condition $Y = 0$ is only satisfied for point E ($\xi = \eta = 2/3$); $Y < 0$ at all other points on the slab, i. e. the available resistance is not fully utilised.

The maximum negative moment occurs at point B, where $m_1 = -m_2 = 3m_u/4$ applies.

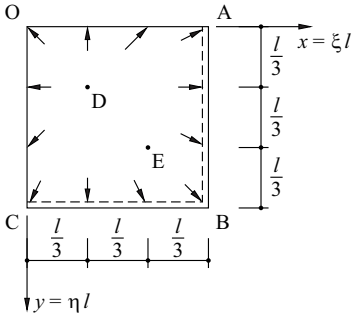

Fig. 24.37 Square slab simply supported along two adjacent edges and subjected to q = const

Example 24.14 Simply supported regular polygonal slabs

Fig. 24.38 shows two alternative stress states for simply supported regular polygonal slabs with n sides and subjected to a central point load Q. For reasons of symmetry, it is sufficient to consider just one triangular segment OAB with the apex angle π/n.

Fig. 24.38(a) assumes – like example 24.3 – uniaxial moment fields parallel with the edge. The line OB separating areas I and II is a static discontinuity line along which a shear force of $m_u\sin(2\pi/n)$ is transferred. Consequently, we get

$$Q = nm_u\sin\left(\frac{2\pi}{n}\right)$$

The slab only has to be supported at its corners, the edges can be free. The MOHR's circle on the right of Fig. 24.38(a) contains points O and P, which are the poles of areas I and II. Mechanisms in which the static discontinuity lines are also (positive) yield lines are compatible with the stress state considered here. When $n \to \infty$, we get the limit load $2\pi m_u$ known from example 24.10 ($\rho_1 = 0$, $\lambda = 0$), when $n = 12$, we get $6m_u$, and when $n = 6$, 4 and 3, the results are $5.196m_u$, $4m_u$ and $2.598m_u$ respectively.

The moments

$$m_x = 0 \quad , \quad m_y = m_u\left(1-\frac{y^2}{x^2}\right) \quad , \quad m_{xy} = -m_u\frac{y}{x}$$

correspond to

$m_\varphi = m_1 = m_u \quad , \quad m_r = m_2 = -m_u \tan^2\varphi$

according to Fig. 24.38(b). Eq. (24.2) provides $q = 0$ and we can use $(24.1)_2$ and $(24.1)_3$ to get $v_x = -m_u/x = v_y x/y$, i. e. using $(24.11)_2$, $\tan\varphi_0 = y/x$. We get edge shear forces $v_x + m_{yx,y}$ of $-2m_u/a$ along AB, and a corner force of $2m_u\tan(\pi/n)$ (acting on the slab in the positive z direction) develops at corner B. Accordingly, a force

$$Q = 2nm_u \tan\left(\frac{\pi}{n}\right)$$

acts in the centre of the slab which is carried away radially towards the edges. The principal shear force $(24.11)_1$ amounts to $v_0 = m_u r/x^2$. There are mechanisms compatible with the stress state considered in which (positive) yield lines run from the centre of the slab to all its corners. When $n \to \infty$, we again get the limit load $Q_u = 2\pi m_u$, when $n = 12$, the result is $6.431m_u$, and when $n = 6$, 4 and 3, the results are $6.928m_u$, $8m_u$ and $10.3923m_u$ respectively.

The difference between the limit loads of the two alternative stress states is based on the fact that according to Fig. 24.38(a), only positive bending resistances are required, whereas according to Fig. 24.38(b), besides the yield lines for $m_\varphi = m_u$, ever larger negative moments have to be accommodated in the radial direction as n decreases. In the limiting case $n = 3$, the result for $\varphi = \pi/3$ according to Fig. 24.38(b) is $m_r = -3m_u$, and when $n = 4$ and $\varphi = \pi/4$, then $m_r = -m_u$ applies.

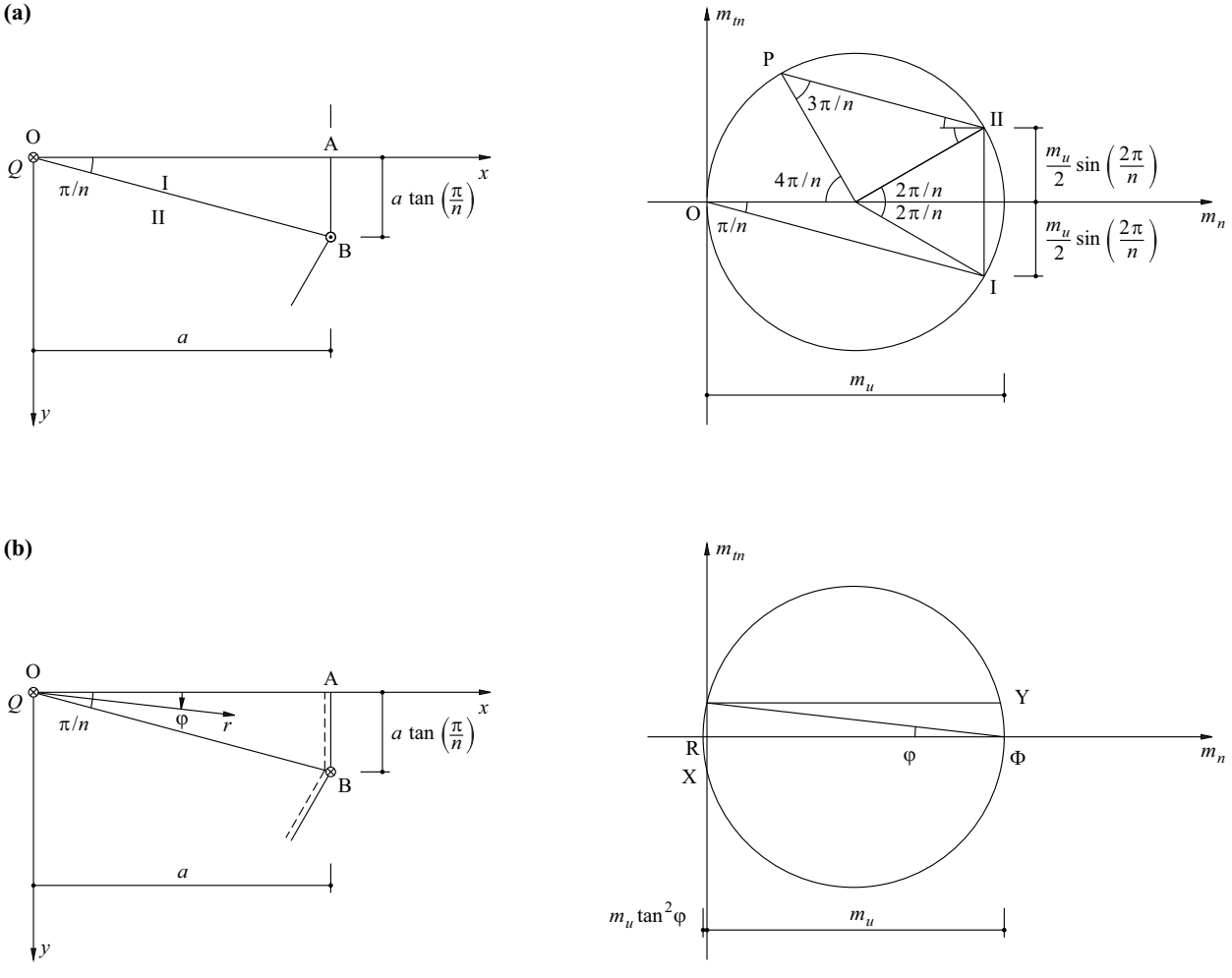

Fig. 24.38 Simply supported regular polygonal slab subjected to a central point load

Example 24.15 Cantilever slab with point load on edge

Fig. 24.39(a) shows a cantilever slab of width a which is infinitely long in the y direction and loaded on its edge at A by the point load Q. Assuming $m_\varphi = -m_r = m_u$ for area OAB and $m_x = m_y = 0$, $m_{xy} = m_u$ for area ABCD, then $(24.3)_2$ gives us the shear force $v_r = -2m_u/r$ in OAB, and according to $(24.15)_2$, the shear force $V_y = -m_u$ is carried away along AD. Consequently, the result, considering the symmetry about the x axis, is

$$Q = 2\left(\frac{2m_u}{r} \cdot r\frac{\pi}{4} + m_u\right) = (2+\pi)m_u$$

Fig. 24.39(b) shows a short cantilever slab with $\alpha \geq \pi/4$. In this case we shall assume $m_x = -m_u$, $m_y = m_u\cot^2\varphi$, $m_{xy} = 0$ for area OAB, whereas area ABC is assumed to be free from stresses. Therefore, a twisting moment with a magnitude of $m_u\cot\alpha$ acts along AB, and according to $(24.15)_2$, a corresponding shear force is carried away along this line. According to (24.1), the result for area OAB is $v_x = v_y = 0$. Therefore, considering the symmetry about the x axis, the result is

$$Q = 2m_u\cot\alpha$$

Area ABC is assumed to be stress-free in the long cantilever slab of Fig. 24.39(c), where $\alpha \leq \pi/4$. A state of pure twist $m_1 = -m_2 = m_u$ with respect to axes 1 and 2 perpendicular to or parallel with AD is presumed in area ABD. According to Fig. 24.39(a), we assume $m_\varphi = -m_r = m_u$ for area OAD. A shear force $-m_u$ acts along discontinuity line AB and a force of $2m_u(\pi/4 - \alpha)$ is carried away in the radial direction in area OAD. In total, considering the symmetry about the x axis, the result is

$$Q = (2 + \pi - 4\alpha)m_u \qquad (0 \leq \alpha \leq \pi/4)$$

The limiting cases $\alpha = 0$ and $\alpha = \pi/4$ have the values $(2+\pi)m_u$ and $2m_u$, i. e. the same values as those obtained with the solutions already discussed for the infinitely long or short slab.

By assuming an isotropic bending resistance $\pm m_u$, the solutions for the infinitely long and the short cantilever slabs ($\alpha = 0$ or $\pi/4 \leq \alpha \leq \pi/2$) are complete, i. e. there are collapse mechanisms compatible with the stress states considered, see example 24.20. On the other hand, the solution for the long cantilever slab ($0 < \alpha < \pi/4$) only corresponds to a lower bound of the limit load.

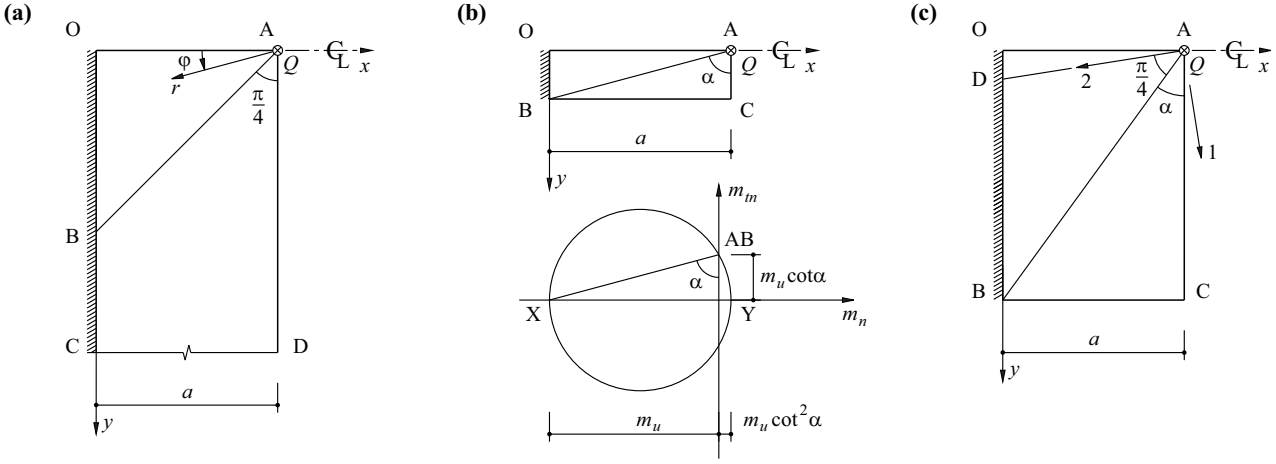

Fig. 24.39 Cantilever slab with point load on edge: (a) infinitely long, (b) short ($\alpha \geq \pi/4$), (c) long ($\alpha \leq \pi/4$)

24.4.3 Strip method

24.4.3.1 Introductory example

In order to introduce the *strip method* [11], we shall consider the square plate shown in Fig. 24.40(a) subjected to a uniformly distributed load q. We shall replace the slab by adjacent strips of slab with a width of 1 in the x and y directions acting as simply supported beams and assign a line load of $q/2$ to each strip. Taking a span l, this leads to maximum moments of $(q/2)\cdot l^2/8 = ql^2/16$ at mid-span.

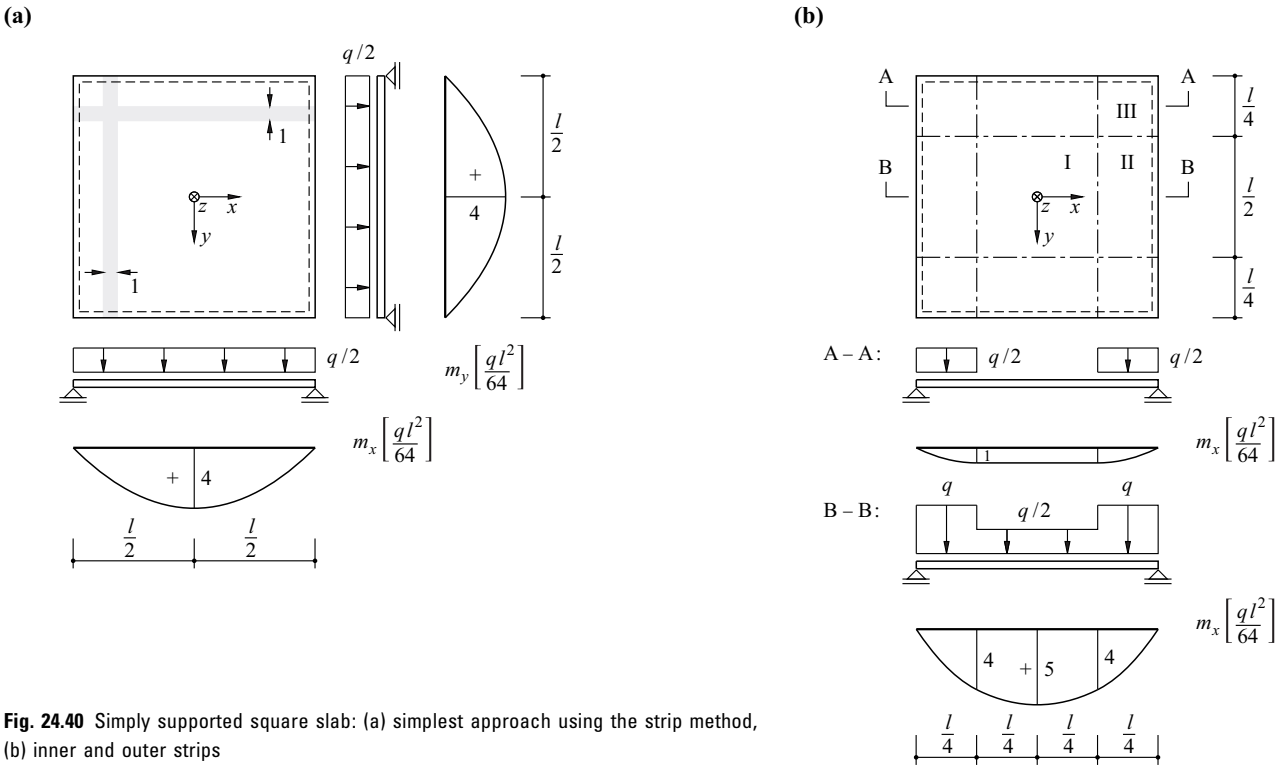

Fig. 24.40 Simply supported square slab: (a) simplest approach using the strip method, (b) inner and outer strips

Generally, applying (24.2) allows us to assume a load apportionment of

$$q = q_x + q_y + q_{xy} \qquad \left(q_x = -\frac{\partial^2 m_x}{\partial x^2}\,,\; q_y = -\frac{\partial^2 m_y}{\partial y^2}\,,\; q_{xy} = -2\frac{\partial^2 m_{xy}}{\partial x \partial y}\right) \tag{24.99}$$

and specifying $m_{xy} \equiv 0$ allows us to confine our examination to the bending moments m_x und m_y.

Fig. 24.40(b) shows the slab divided into inner strips of width $l/2$ and outer strips of width $l/4$, which results in the inner area I plus four perimeter areas II and four corner areas III. We shall assume $q_x = q_y = q/2$ for the inner and corner areas, whereas the load in the perimeter areas is transferred directly to the associated edge ($q_x = q$ or $q_y = q$). Sections A-A and B-B illustrate the corresponding moments resulting in the perimeter and inner strips.

As in (24.98), it is interesting to compare the "moment volumes"

$$M = \int_{-l/2}^{l/2}\int_{-l/2}^{l/2} (m_x + m_y)\,\mathrm{d}x\,\mathrm{d}y$$

of the two bending moment diagrams. We get $M = 2\cdot(ql^2/16)\cdot(2/3)\cdot l^2 = ql^4/12$ for Fig. 24.40(a), and $M = 2\cdot(ql^2/64)\cdot(1 + 2/3)/2\cdot l^2 + ql^4/24 = 13ql^4/192$ for Fig. 24.40(b), i. e. a value that is about 19 % less.

The moment field of exercise 24.1 corresponds to the load apportionment $q_x = q_y = q_{xy} = q/3$ according to (24.99). Eq. $(24.90)_1$ shows that to accommodate this, constant bottom reinforcement with a bending resistance of $m_{xu} = m_{yu} = ql^2/24$ is required over the entire slab, which itself leads to a "moment volume" of $ql^4/12$. In addition, according to $(24.90)_2$, there is also top reinforcement in the corner areas outside the slab's inscribed circle. Compared with the mass of the (ideally curtailed) reinforcement according to the simplest possible approach of Fig. 24.40(a), the more complicated approach of exercise 24.1 results in more reinforcement. The comparison with Fig. 24.40(b) shows the strip method to be even more favourable.

24.4.3.2 Rectangular slabs

Fig. 24.41(a) illustrates one possible load apportionment for simply supported rectangular slabs ($a > b$) carrying uniformly distributed loads. Area I has $q_y = q$, but perimeter areas II have $q_x = q$, and the corner areas III have $q_x = q_y = q/2$.

If two neighbouring edges are fixed as shown in Fig. 24.41(b), then the boundaries to the areas are shifted by choosing parameter α in such a way that the magnitude of the fixed-end moments is about 1.5 to 2.5 times greater than that of the maximum positive moments. This leads to α values between 0.35 and 0.39.

Fig. 24.42 shows one possible way of dealing with a rectangular slab which is subjected to a uniformly distributed load and has one free and three simply supported edges. A so-called strong band is introduced in area II over a width βb. Applying the load apportionment $q_x = (1 - \gamma)q$, $q_y = \gamma q$ in area I results in the strong band carrying the load q_s in addition to the uniformly distributed load q. Fig. 24.42 shows the corresponding bending moment diagrams.

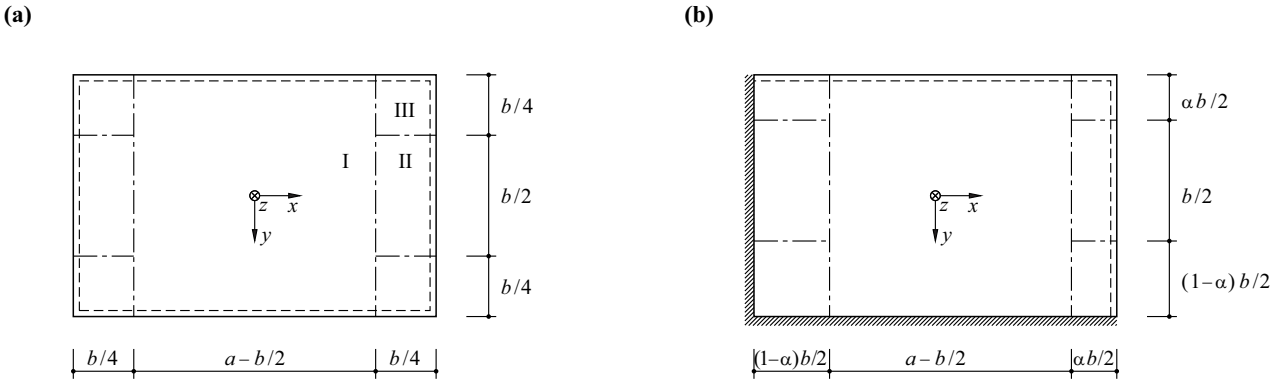

Fig. 24.41 Using the strip method to analyse rectangular slabs with different boundary conditions

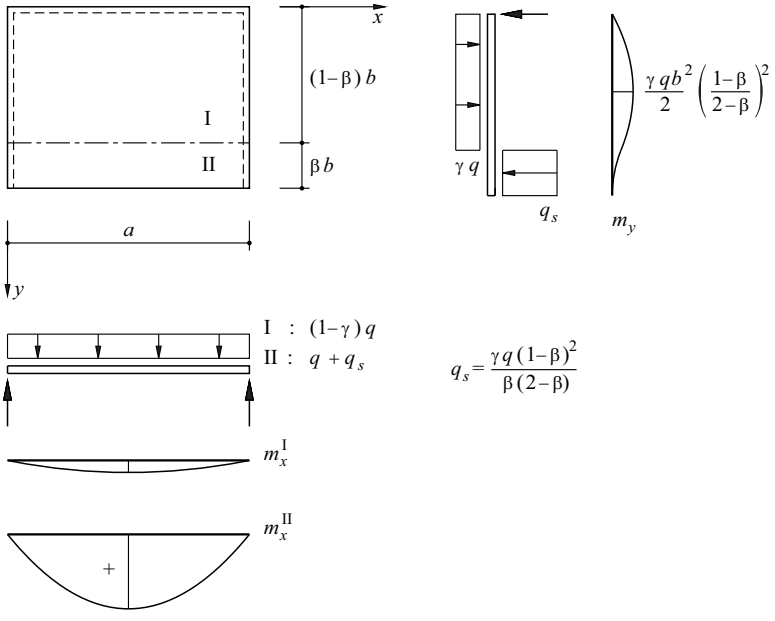

Fig. 24.42 Strong band along unsupported edge of slab

24.4.3.3 Concentrated forces

The strip method is not directly suited to dealing with concentrated loads or reactions. Such forces can be balanced by uniformly distributed forces, e. g. by means of the load distribution elements shown in Fig. 24.43. The uniformly distributed forces are then applied in the reverse sense to strips of width $2a$ or a.

We get the moments

$$m_x = 0 \quad , \quad m_y = m\left(1 - \frac{\eta^2}{\xi^2}\right) \quad , \quad m_{xy} = m\left(\xi\eta - \frac{\eta}{\xi}\right) \tag{24.100}$$

for the element shown on the left in Fig. 24.43 with a central point force $8m$ based on example 24.2 for area OAB.

If we cut the element along the x axis, superposing $m_y = -m$ results in

$$m_x = 0 \quad , \quad m_y = -m\frac{\eta^2}{\xi^2} \quad , \quad m_{xy} = m\left(\xi\eta - \frac{\eta}{\xi}\right) \tag{24.101}$$

for area OAB and

$$m_x = m\left(1 - \frac{\xi^2}{\eta^2}\right) \quad , \quad m_y = -m \quad , \quad m_{xy} = m\left(\xi\eta - \frac{\xi}{\eta}\right) \tag{24.102}$$

for area OBC. These moments correspond to the element shown in the middle of Fig. 24.43, which is acted on by a force $4m$ on its edge (exercise 24.22). The edge moment $m_y = -m$ along $y = a$ must be considered in the continuation of the moment field in the adjoining strip of width $2a$.

Based on example 24.1, we get the moments

$$m_x = m\xi(\xi - 2) \quad , \quad m_y = m\eta(\eta - 2) \quad , \quad m_{xy} = m(\xi + \eta - \xi\eta - 1) \tag{24.103}$$

for the element shown on the right in Fig. 24.43. The edge moments $m_x = -m$ along $x = a$ as well as $m_y = -m$ along $y = a$ must be considered in the continuation of the moment field in the adjoining strips of width a.

Fig. 24.44 shows an example of applying load distribution elements in conjunction with strips in the x and y directions. Slab ABCD carries a uniformly distributed load, has a fixed support along AB and point supports at corners C and D. The corner areas CHLG and DJKI correspond to the element shown on the right of Fig. 24.43. They carry the actual loads on those areas plus the loads transferred from area IKLH via strip DJGC. The perimeter strips GLFB and KJAE, likewise the intermediate strip LKEF, also transfer the loads applied to them to the fixed support. The arrows indicate the directions of the flow of the forces, and the moments m_x or m_y are given for three sections.

The generalisation of the strip method by incorporating load distribution elements to deal with concentrated forces is known as the *advanced strip method*. As long as we can manage without load distribution elements, we are working with the *simple strip method*.

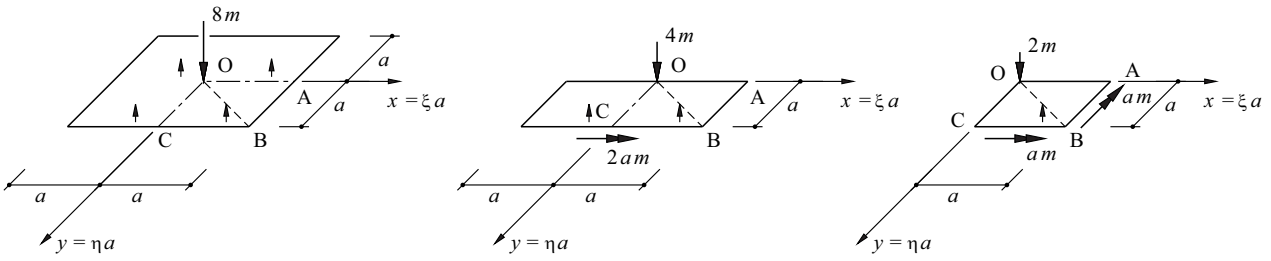

Fig. 24.43 Load distribution elements

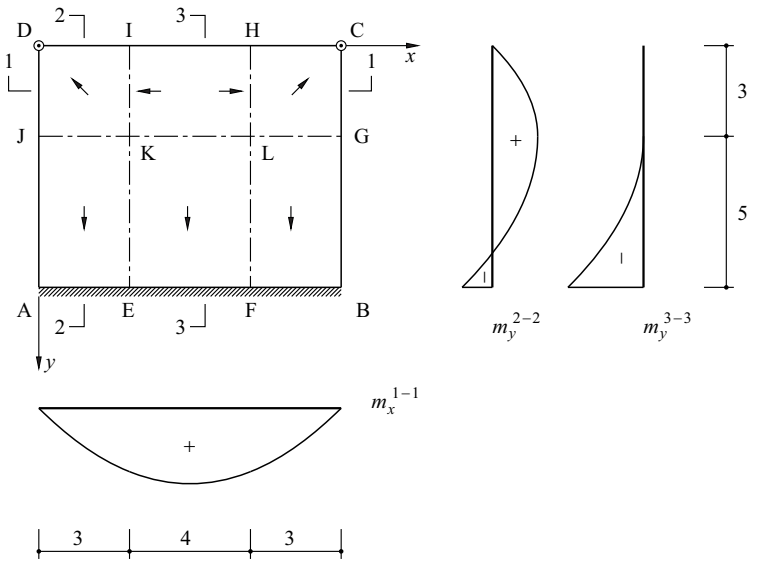

Fig. 24.44 Example of the application of the advanced strip method

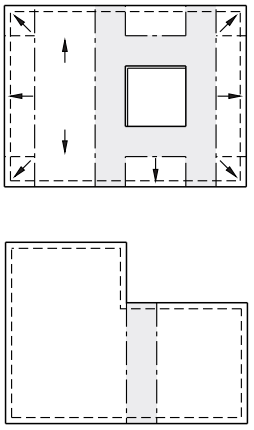

Fig. 24.45 Strong bands

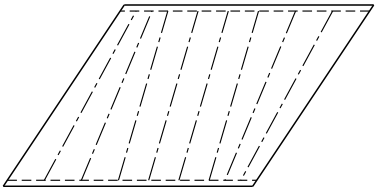

Fig. 24.46 Strips with varying widths

24.4.3.4 Commentary

Strong bands are not only useful modelling notions in the case of unsupported slab edges (Fig. 24.42), but also at openings and re-entrant corners, for example, see Fig. 24.45. They can be used to convert complex geometric problems into a series of simpler geometric problems.

Assuming strips with varying widths can be worthwhile in the case of skew slabs, see Fig. 24.46 and Fig. 16.27.

In the case of the load distribution elements shown on the left and right of Fig. 24.43, the principal moments lie between $-m$ and m. However, the load distribution element shown in the middle of Fig. 24.43 results in a maximum moment of $m(1 + \sqrt{5})/2$ (exercise 24.22).

24.5 Kinematic method

24.5.1 Introductory example

The *yield line method* for reinforced concrete slabs is discussed in this section [12]. This method involves introducing yield lines into slabs of any geometry to divide them into rigid parts in such a way that a mechanism is formed. We shall presume (24.87) for the bending resistances at the yield lines, and therefore upper bounds for the limit load can be determined according to (21.6).

The slab shown in Fig. 24.47, which has a fixed support along AB and point supports at C and D, will serve as our introductory example. Slab areas ABJHI, CKHJ and DIHK rotate about the axes EF, FG and GE respectively. For reasons of compatibility, the continuations of the positive yield lines HI, HJ and HK must pass through the intersections E, F and G of the axes of rotation of the slab areas joined by the yield lines. A negative yield line results along the fixed support AB.

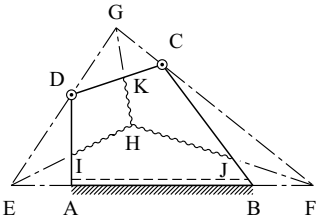

Fig. 24.47 Yield lines and axes of rotation

The yield line mechanism shown in Fig. 24.47 contains four free parameters, e. g. distances EA and BF plus the coordinates of point H. Defining EA and BF allows us to define the axes of rotation and point G, and choosing the position of H fixes the yield lines. Selecting a deflection of 1 at point H defines the rotations of the three parts of the slab, and the relative rotations along the yield lines result from the (vectorial) difference between the rotations of the adjoining parts of the slab. The

calculation according to (21.6) can thus be performed and the limit load minimised with respect to the free parameters.

Unlike with framed structures, the high degree of static indeterminacy of the slab sections, which are presumed to be rigid, means it is not possible to carry out a plasticity check.

24.5.2 Calculating the dissipation work

24.5.2.1 Discrete yield lines

Fig. 24.48(a) shows a differential element of a yield line in the t direction. Using the relative rotation $\dot{\omega}_n$ and the bending resistance m_{nu} according to $(24.87)_1$, we get the elementary dissipation work for that element:

$$\mathrm{d}\dot{D} = m_{nu}\dot{\omega}_n \mathrm{d}t = (m_{xu}\cos^2\varphi + m_{yu}\sin^2\varphi)\omega_n \mathrm{d}t$$

The rotation components $\dot{\omega}_x = \dot{\omega}_n\cos\varphi$, $\dot{\omega}_y = \dot{\omega}_n\sin\varphi$ and $\mathrm{d}y = \mathrm{d}t\cos\varphi$, $\mathrm{d}x = \mathrm{d}t\sin\varphi$ allow us to write

$$\mathrm{d}\dot{D} = m_{xu}\dot{\omega}_x \mathrm{d}y + m_{yu}\dot{\omega}_y \mathrm{d}x \tag{24.104}$$

i. e. $\mathrm{d}\dot{D}$ can be calculated directly from the bending resistances and rotations in the directions of the reinforcement.

24.5.2.2 Fan mechanisms

Fig. 24.48(b) shows a differential element of a circular fan mechanism with radius r_0. The deflection $\dot{w} = 1$ of the centre of the slab corresponds to a slope $\dot{w}_{,r} = -1/r_0$ and therefore a curvature increment $\dot{\chi}_\varphi = 1/(rr_0)$ according to $(24.35)_2$. We thus get the elementary dissipation work

$$\mathrm{d}\dot{D} = m_{\varphi u}\mathrm{d}r\,\dot{\chi}_\varphi r\mathrm{d}\varphi = \frac{m_{\varphi u}}{r_0}\mathrm{d}r\,\mathrm{d}\varphi \tag{24.105}$$

When we consider a fan with an apex angle β and $m_{\varphi u} = \text{const}$, integrating (24.105) results in the expression $\dot{D} = m_{\varphi u}\beta$. If in addition a bending resistance $m_{ru}' = \text{const}$ is activated at the outer edge $r = r_0$, the result is

$$\dot{D} = \beta(m_{\varphi u} + m_{ru}') \tag{24.106}$$

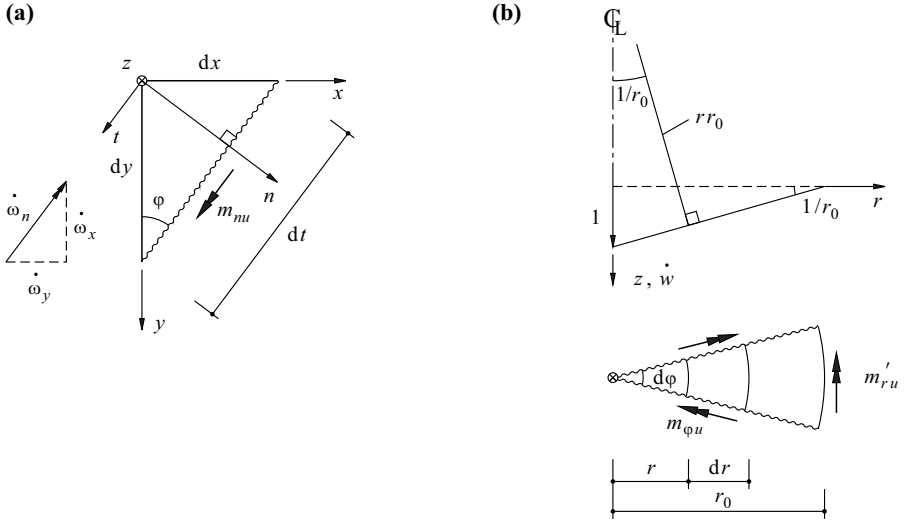

Fig. 24.48 Calculating the dissipation work: (a) discrete yield line, (b) fan mechanism

24.5.3 Applications

Example 24.16 Fixed rectangular slab

The yield line mechanism shown in Fig. 24.49 contains the free parameter c. Assuming isotropic bending resistances m_u and $-\lambda m_u$, the result for a uniformly distributed loading q is the work equation

$$qb\left(\frac{a}{2}-\frac{c}{3}\right)=m_u(1+\lambda)\left(4\frac{a}{b}+2\frac{b}{c}\right)$$

Differentiating the corresponding expression for q with respect to c, equating to zero and using $\beta = b/a \leq 1$ results in

$$c=\frac{b}{2}\left(\sqrt{3+\beta^2}-\beta\right)$$

According to the upper-bound theorem, the limit load q_u is therefore

$$q_u \leq \frac{24(1+\lambda)m_u}{b^2\left(\sqrt{3+\beta^2}-\beta\right)^2}$$

If the slab is not fixed at the edge, but rather simply supported, we lose the λ term in the work equation and in the expression for q_u.

Together with the relationship derived in example 24.12, we get the bounds

$$8(1+\beta+\beta^2)\leq\frac{q_u b^2}{m_u}\leq\frac{24}{\left(\sqrt{3+\beta^2}-\beta\right)^2}$$

for simply supported rectangular slabs. The agreement is excellent. When $\beta = 1$ and $\beta = 0$, the upper and lower bounds coincide, and in between they deviate from each other by no more than about 1.5 %. The reader should note that the lower bound presumes $\lambda = 1$ according to example 24.12.

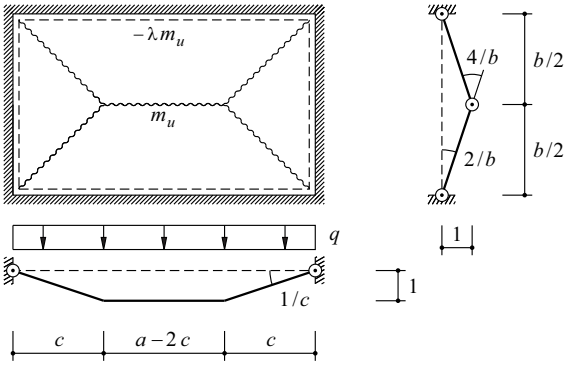

Fig. 24.49 Yield line mechanism for a rectangular slab carrying a uniformly distributed load

Example 24.17 Square slab simply supported along two adjacent edges

We get the work equation

$$\frac{qla}{3}+\frac{ql(l-a)}{2}=m_u\left(\frac{l}{a}+\frac{a}{l}\right)$$

for the problem of example 24.13 with the mechanism shown in Fig. 24.50. The derivative with respect to a of the corresponding expression for q is equated to zero and results in the quadratic equation

$$3a^2+2al-3l^2=0$$

which has the solution

$$a=\frac{\sqrt{10}-1}{3}l$$

and therefore

$$q_u l^2 \leq 5.55\, m_u$$

The lower bound of $9m_u/2$ for $q_u l^2$ determined in example 24.13 amounts to 81 % of the upper bound calculated here.

Introducing a second yield line BD′, which is symmetrical with respect to yield line BD when mirrored in axis OB, does not change the upper bound value of $5.55m_u$ for $q_u l^2$.

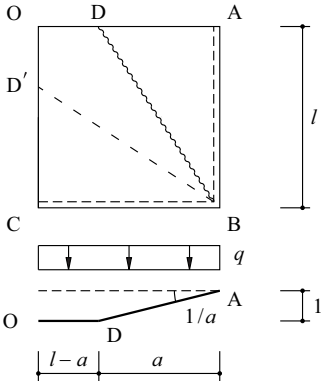

Fig. 24.50 Yield line mechanism for the problem of Fig. 24.37

Example 24.18 Fixed square slab

Fig. 24.51 shows a square slab fixed on all sides and subjected to a uniformly distributed load. For reasons of symmetry, it is sufficient to consider just one octant. With circular fans having an apex angle of 2α between the centre of the slab and its corners, the work equation for a deflection of 1 at the centre of the slab is

$$\frac{ql^2}{3}\left[\tan\left(\frac{\pi}{4}-\alpha\right)+\frac{\alpha}{\cos^2\left(\frac{\pi}{4}-\alpha\right)}\right]=8m_u(1+\lambda)\left[\tan\left(\frac{\pi}{4}-\alpha\right)+\alpha\right]$$

Minimising the expression for q with respect to α results in α = 14.3° and

$q_u l^2 \leq 21.75(1+\lambda)m_u$

The lower bound of $37.96m_u$ (λ = 1) examined in exercise 24.5 amounts to 87 % of the upper bound calculated here. A complete solution is known for this problem [7]; $q_u l^2 = 42.85m_u$ applies.

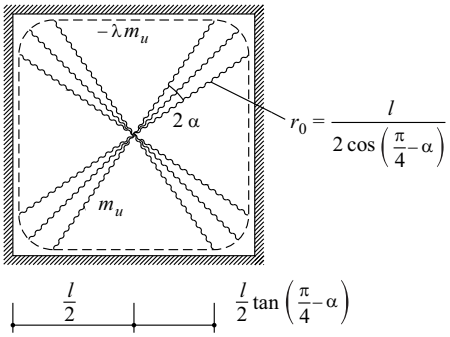

Fig. 24.51 Fixed square slab subjected to a uniformly distributed load

Example 24.19 Slab strip subjected to a central point load

For a deflection of 1 due to the point load Q in the centre of the slab strip illustrated in Fig. 24.52, the work equation is

$Q = m_u(1+\lambda_i)\,4\alpha + m_u(1+\lambda_e)\,4\cot\alpha$

When $\lambda_i = \lambda_e = 0$ or 1, we get the minimum value for Q when α = π/2, i. e. $2\pi m_u$ or $4\pi m_u$. When $\lambda_e = 0$, we get the minimum value for Q when

$\cot\alpha = \sqrt{\lambda_i}$

and the following applies:

$$Q_u \leq 4m_u\left[\sqrt{\lambda_i}+(1+\lambda_i)\operatorname{arc\,tan}\left(\frac{1}{\sqrt{\lambda_i}}\right)\right]$$

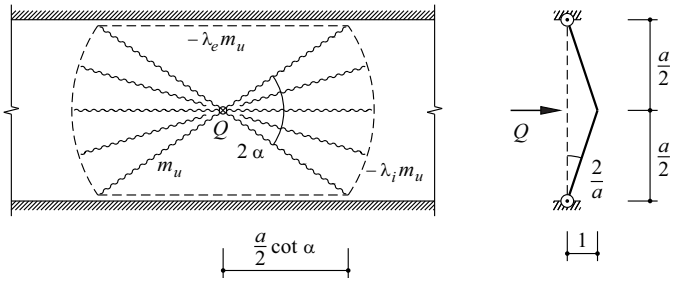

Fig. 24.52 Slab strip subjected to a central point load

Example 24.20 Cantilever slab with point load on edge

In a similar way to example 24.19, the work equation for the problem shown in Fig. 24.53 is

$Q = m_u(1+\lambda)\,2\alpha + 2\lambda m_u\cot\alpha$

and minimising Q with respect to α results in $\tan^2\alpha = \lambda$.

When λ = 1, we get α = π/4 and therefore the limit load $Q_u = (2+\pi)m_u$ known from example 24.15.

We should also note that the short cantilever slabs with a central point load dealt with in example 24.15 can fail with a yield line along the fixed support. Such a mechanism is compatible with Fig. 24.39(b) and therefore the limit load is $Q_u = 2m_u\cot\alpha$.

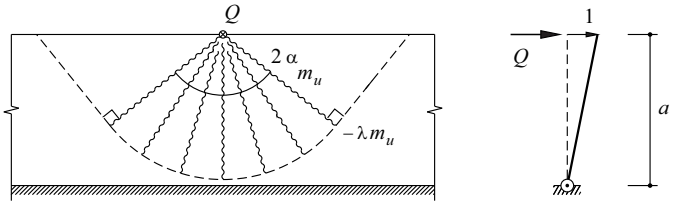

Fig. 24.53 Edge load on cantilever slab

Example 24.21 Flat slab

The mechanism shown in Fig. 24.54 corresponds to the problem already investigated in example 24.11, but with the round columns replaced by square ones. The work equation is

$$q\left(ab - \alpha^2 a^2 - 4\frac{\alpha\gamma a^2}{2} - \frac{\gamma^2 a^2 \pi}{3}\right) = 4m_u(1+\lambda)\left(\frac{\pi}{2} + \frac{\alpha a}{\gamma a}\right)$$

Putting $\beta = b/a$ and minimising q results in the cubic equation

$$\frac{\pi}{3}\gamma^3 + 2\pi\alpha\gamma^2 + 4\alpha^2\gamma - \alpha(\beta - \alpha^2) = 0$$

for the free parameter γ, and we get the condition

$$\frac{q_u a^2}{m_u(1+\lambda)} \leq \frac{2\left(\pi + \frac{2\alpha}{\gamma}\right)}{\beta - \alpha^2 - 2\alpha\gamma - \frac{\pi}{3}\gamma^2}$$

for the limit load q_u.

Tab. 24.3 contains the corresponding values γ and q_u for $\beta = 1$ and some values of α.

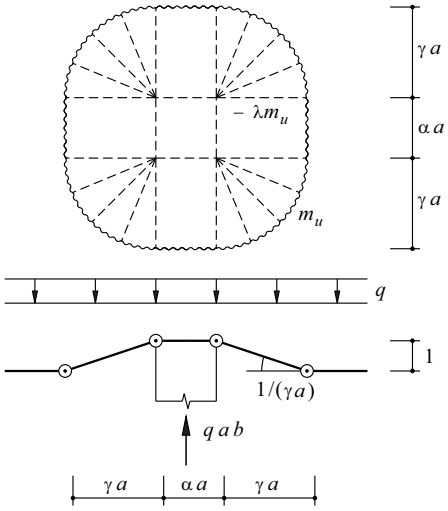

Fig. 24.54 Yield line mechanism around an interior column of a uniformly loaded flat slab supported on a rectangular grid

Tab. 24.3 Numerical values for example 24.21

α	γ	$q_u a^2/[m_u(1+\lambda)] \leq$
0	0	6.28
0.04	0.2045	7.53
0.08	0.2387	8.51
0.12	0.2550	9.54

24.5.3.1 Commentary

The concept of yield lines was first introduced for rotationally symmetric TRESCA slabs (Tab. 24.1, regimes A, D, B, E). Complete solutions to such problems are always possible. It is easy to specify the mechanisms compatible with the respective moment fields, and the calculation according to (21.6) is superfluous. The same is true for rotationally symmetric problems with reinforced concrete slabs.

The moment fields discussed in examples 24.1, 24.2 and 24.3 are compatible with yield lines along the x and y axes. Mechanisms compatible with the moment fields considered have already been pointed out in example 24.14. The same applies to the short and infinitely long cantilever slabs of example 24.15 (compare with example 24.20). All these examples correspond to complete solutions.

Putting $\lambda = 0$ means that example 24.18 provides the upper bound $21.75m_u$ for the limit load $q_u l^2$ for a uniformly loaded, simply supported square slab that has only bottom reinforcement with an isotropic bending resistance m_u. On the other hand, the strip method according to Fig. 24.40(a) provides the lower bound $16m_u$. Compared with that, including top reinforcement in the corners of slabs and securing the corners against uplift results in a limit load of $q_u l^2 = 24m_u$ according to exercise 24.1.

In practice, the reinforcement is generally curtailed in each segment in order to avoid uneconomic reinforcement layouts. The curtailment process must ensure, on the one hand, that the required bending resistances are provided, e. g. according to (24.92), and, on the other, that the requirements regarding adequate minimum reinforcement are taken into account in order to avoid sudden brittle fractures and to guarantee good crack distribution. The bending resistances along the individual yield lines are therefore not normally constant, which somewhat complicates the process of setting up the work equation, but does not lead to any fundamental problems.

Optimising a mechanism with respect to its free parameters can be carried out analytically or numerically, as demonstrated in the examples. Small deviations from the optimum parameter combination have only a minor influence on the corresponding upper bounds to the limit load. In most cases the optimum range is quite easy to find by way of trial and error.

Instead of making a great effort trying to optimise a particular mechanism, the designer is recommended to search for alternative, possibly more risky, mechanisms. With flat slabs, for example, simple line mechanisms with negative yield lines tangential to the edges of neighbouring columns and positive yield lines in the intervening span may lead to lower upper bounds for the limit load than the mechanism shown in Fig. 24.54 (example 24.21) because of the curtailment of the reinforcement.

24.6 The influence of shear forces

24.6.1 Elastic slabs

The theory of linear elastic slabs with infinite shear stiffness and small deflections, which was presented in section 24.2, reduces the number of boundary conditions from three to two, as described in section 8.2.6. This greatly simplifies the analysis of the stresses. Some fine-tuning is sometimes necessary, e. g. in order to ascertain the relationships at the edges of slabs or around holes whose diameter is small compared with the thickness of the slab.

We shall presume a parabolic distribution of the shear stresses τ_{zx} and τ_{zy} over the slab depth h and take into account an area shear factor $\alpha_v = 5/6$ in (8.45). Taking the boundary conditions $\sigma_z(h/2) = 0$, $\sigma_z(-h/2) = -q$, eq. (5.29) or (8.49) – with $i = z$ – because of the parabolic variation in the shear stresses gives us the cubic variation

$$\sigma_z = q\left(-\frac{1}{2} + \frac{3z}{2h} - \frac{2z^3}{h^3}\right)$$

of the normal stresses in the z direction, see Fig. 24.55. According to (8.34), these stresses correspond to restraint stresses $\Delta\sigma_x$ and $\Delta\sigma_y$. Putting $E\Delta\varepsilon_x = \Delta\sigma_x - \nu(\Delta\sigma_y + \sigma_z) = 0$ and $E\Delta\varepsilon_y = \Delta\sigma_y - \nu(\Delta\sigma_x + \sigma_z) = 0$ results in $\Delta\sigma_x = \Delta\sigma_y = \sigma_z\nu/(1 - \nu)$, and therefore we get the moments

$$\Delta m_x = \Delta m_y = \int_{-h/2}^{h/2} \Delta\sigma_x z \, dz = \frac{\nu q h^2}{10(1-\nu)}$$

Eq. (8.41) gives us

$$\chi_x = \varphi_{x,x} = \gamma_{x,x} - w_{,xx} \quad , \quad \chi_y = \varphi_{y,y} = \gamma_{y,y} - w_{,yy} \quad , \quad 2\chi_{xy} = -2w_{,xy} + \gamma_{x,y} + \gamma_{y,x}$$

and (8.45) – taking into account $\alpha_v = 5/6$ – results in

$$\gamma_x = 2.4(1+\nu)\frac{v_x}{Eh} \quad , \quad \gamma_y = 2.4(1+\nu)\frac{v_y}{Eh}$$

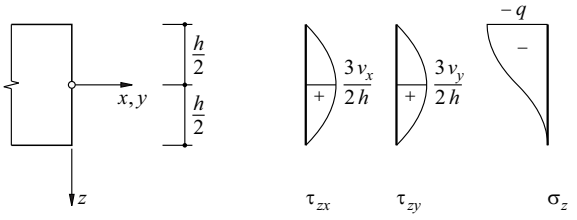

Fig. 24.55 Stress variations perpendicular to the plane of the slab

Therefore, eq. (8.43), taking into account $(24.1)_1$ and the definition of the slab stiffness D in (8.48) and incorporating $\Delta m_x = \Delta m_y$, results in the moments

$$\begin{aligned} m_x &= -D(w_{,xx} + \nu w_{,yy}) + \frac{h^2}{5} v_{x,x} - \frac{\nu q h^2}{10(1-\nu)} \\ m_y &= -D(w_{,yy} + \nu w_{,xx}) + \frac{h^2}{5} v_{y,y} - \frac{\nu q h^2}{10(1-\nu)} \\ m_{xy} &= -(1-\nu) D\, w_{,xy} + \frac{h^2}{10}(v_{x,y} + v_{y,x}) \end{aligned} \tag{24.107}$$

Substituting in $(24.1)_2$ and $(24.1)_3$ and taking into account $(24.1)_1$ gives us the shear forces

$$\begin{aligned} v_x &= -D(\Delta w)_{,x} + \frac{h^2}{10}\left(\Delta v_x - \frac{q_{,x}}{1-\nu}\right) \\ v_y &= -D(\Delta w)_{,y} + \frac{h^2}{10}\left(\Delta v_y - \frac{q_{,y}}{1-\nu}\right) \end{aligned} \tag{24.108}$$

When $h \to 0$, eq. (24.107) and (24.108) simplify to (24.24) and (24.25).

Eq. (24.108), together with $(24.1)_1$, leads to

$$D\Delta\Delta w = q - \frac{(2-\nu)h^2}{10(1-\nu)}\Delta q \tag{24.109}$$

see (8.48). This relationship is satisfied by

$$w = w_1 + w_2 \tag{24.110}$$

where w_1 designates a particular solution to the inhomogeneous differential equation (24.109), but w_2 the general solution to the homogeneous bipotential equation $\Delta\Delta w = 0$. According to (24.29), we can set

$$v_x = v_{x1} - D(\Delta w_2)_{,x} + \psi_{,y} \quad , \quad v_y = v_{y1} - D(\Delta w_2)_{,y} - \psi_{,x} \tag{24.111}$$

where $\boldsymbol{v}_1$ satisfies the relationships

$$v_{x1} = -D(\Delta w_1)_{,x} + \frac{h^2}{10}\left(\Delta v_{x1} - \frac{q_{,x}}{1-\nu}\right) \quad , \quad v_{y1} = -D(\Delta w_1)_{,y} + \frac{h^2}{10}\left(\Delta v_{y1} - \frac{q_{,y}}{1-\nu}\right)$$

Comparing (24.111) and (24.108) reveals that

$$\left(\psi - \frac{h^2}{10}\Delta\psi\right)_{,y} = -\left(\psi - \frac{h^2}{10}\Delta\psi\right)_{,x} = 0$$

i. e. the expression in brackets is constant. The constant can be equated to zero, and therefore

$$\Delta\psi = \frac{10\psi}{h^2} \tag{24.112}$$

Eq. (24.109) und (24.112) are fourth-order and second-order differential equations respectively which enable us to satisfy three boundary conditions. The deflection w and the rotations φ_n and φ_t or the shear force v_n as well as the bending moment m_n and the twisting moment m_{tn} can be specified with the coordinates n and t perpendicular to and parallel with the edge. The following applies for a simply supported edge: $w = m_n = m_{tn} = 0$, and there are no concentrated corner forces.

Example 24.22 Semi-infinite rectangular slab subjected to edge loads

The slab shown in Fig. 24.56 is loaded along edge $x = 0$ by

$$m_x = m_0 \sin\left(\frac{n\pi y}{a}\right) \quad , \quad m_{yx} = t_0 \cos\left(\frac{n\pi y}{a}\right) \quad , \quad v_x = v_0 \sin\left(\frac{n\pi y}{a}\right) \qquad (n = 1, 2, \ldots)$$

As $q = 0$, then $w_1 = 0$ and we can use the formulation

$$w_2 D = \left(A + \frac{n\pi x}{a} B\right) e^{-n\pi x/a} \sin\left(\frac{n\pi y}{a}\right)$$

for w_2, which satisfies the conditions $\Delta\Delta w_2 = 0$ and $w = 0$ for $x \to \infty$. The formulation $\psi = f(x) \cdot \cos(n\pi y/a)$ in conjunction with (24.112) leads to

$$\psi = C e^{-\kappa x} \cos\left(\frac{n\pi y}{a}\right) \qquad \left[\kappa^2 = \left(\frac{n\pi}{a}\right)^2 + \frac{10}{h^2}\right]$$

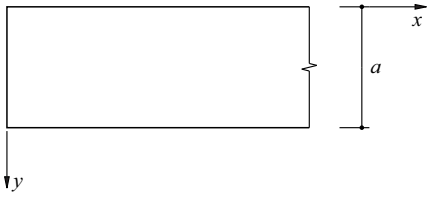

Fig. 24.56 Semi-infinite rectangular slab

Putting $v_{x1} = v_{y1} = 0$ and using (24.111) gives us

$$v_x = -\left[2B\left(\frac{n\pi}{a}\right)^3 e^{-n\pi x/a} + C\frac{n\pi}{a}e^{-\kappa x}\right] \cdot \sin\left(\frac{n\pi y}{a}\right)$$

$$v_y = \left[2B\left(\frac{n\pi}{a}\right)^3 e^{-n\pi x/a} + C\kappa e^{-\kappa x}\right] \cdot \cos\left(\frac{n\pi y}{a}\right)$$

and therefore

$$v_x\Big|_{x=0} = -\left[2B\left(\frac{n\pi}{a}\right)^3 + C\frac{n\pi}{a}\right] \cdot \sin\left(\frac{n\pi y}{a}\right)$$

Applying (24.107) results in the two further relationships

$$m_x\Big|_{x=0} = \left[-A(1-\nu) + 2B\left(1 + \frac{n^2\pi^2h^2}{5a^2}\right) + C\frac{\kappa a h^2}{5n\pi}\right]\frac{n^2\pi^2}{a^2}\sin\left(\frac{n\pi y}{a}\right)$$

$$m_{yx}\Big|_{x=0} = \left[A(1-\nu) - B\left(1-\nu+\frac{2n^2\pi^2h^2}{5a^2}\right) - C\left(\frac{a^2}{n^2\pi^2} + \frac{h^2}{5}\right)\right]\frac{n^2\pi^2}{a^2}\cos\left(\frac{n\pi y}{a}\right)$$

and therefore we can determine the constants A, B, C depending on m_0, t_0, v_0.

24.6.2 Rotationally symmetric VON MISES slabs

Assuming $\sigma_z = 0$ means that the VON MISES yield condition (7.21) takes on the form

$$\sigma_r^2 - \sigma_r\sigma_\varphi + \sigma_\varphi^2 + 3\tau^2 = f_y^2$$

where $\tau = \tau_{zr}$. Applying (7.12) results in

$$\dot\varepsilon_r = \kappa(2\sigma_r - \sigma_\varphi) \quad , \quad \dot\varepsilon_\varphi = \kappa(2\sigma_\varphi - \sigma_r) \quad , \quad \dot\gamma_{zr} = \dot\gamma = 6\kappa\tau$$

and therefore using $\dot\varepsilon_r = \dot\chi_r z$ and $\dot\varepsilon_\varphi = \dot\chi_\varphi z$

$$\sigma_r = \frac{2(2\alpha+\beta)zf_y}{\sqrt{3}A} \quad , \quad \sigma_\varphi = \frac{2(2\beta+\alpha)zf_y}{\sqrt{3}A} \quad , \quad \tau = \frac{f_y}{\sqrt{3}A}$$

where

$$\alpha = \frac{\dot\chi_r}{\dot\gamma} \quad , \quad \beta = \frac{\dot\chi_\varphi}{\dot\gamma} \quad , \quad A^2 = 1 + 4z^2(\alpha^2 + \alpha\beta + \beta^2) = 1 + 4z^2B^2$$

We therefore get the stress resultants

$$m_r = \int_{-h/2}^{h/2} \sigma_r z\,dz = \frac{(2\alpha+\beta)f_y}{4\sqrt{3}B^2}\left[h\sqrt{1+h^2B^2} - \frac{1}{B}\operatorname{Arsh}(hB)\right]$$

$$m_\varphi = \int_{-h/2}^{h/2} \sigma_\varphi z\,dz = \frac{(2\beta+\alpha)f_y}{4\sqrt{3}B^2}\left[h\sqrt{1+h^2B^2} - \frac{1}{B}\operatorname{Arsh}(hB)\right]$$

$$v_r = \int_{-h/2}^{h/2} \tau\,dz = \frac{f_y}{\sqrt{3}B}\operatorname{Arsh}(hB)$$

depending on the parameters α and β. Putting $v_u = f_y h/\sqrt{3}$ and $m_u = f_y h^2/4$ results in the relationships

$$v_r = v_u\frac{\ln\left(b+\sqrt{1+b^2}\right)}{b} \quad , \quad m_r^2 - m_r m_\varphi + m_\varphi^2 = m_u^2\left(\frac{\sqrt{1+b^2} - v_r/v_u}{b}\right)^2$$

which are only dependent on the parameter $b = hB$. This describes the yield surface in the space m_r, m_φ, v_r, which exhibits elliptical contour lines $v_r = \text{const}$. When $b \to \infty$, then $v_r = 0$ and $m_r^2 - m_r m_\varphi + m_\varphi^2 = m_u^2$, and when $b \to 0$, the result is $v_r = v_u$ and $m_r = m_\varphi = 0$.

In order to apply the yield surface, a suitable linearisation is recommended, e. g. according to [27]. In a similar way to beams (section 21.4.5), the shear forces only have a significant influence on the limit load in the case of very stocky slabs or high shear forces.

24.6.3 Reinforced concrete slabs

According to the sandwich model presented in section 24.3.2, the core is responsible for the nominal shear stresses v_0/d_v resulting from the principal shear force v_0. These stresses are normally low apart from in the vicinity of concentrated forces. The compression field shown in Fig. 24.33(b) can be replaced by the notion of a state of pure shear with principal compressive and tensile stresses amounting to v_0/d_v at an angle of 45° to the plane of the slab. In this approach, v_0/d_v should be limited to a carefully chosen fraction of the mean tensile strength of the concrete f_{ctm}, e. g. about $0.17 f_{ctm}$ at the serviceability level, see section 4.7. The reinforcement in the z direction may be omitted in such cases, and no additional reinforcement is required in the x and y directions in order to cope with v_0.

High shear stresses generally occur at points of force application or transfer, especially around columns supporting flat slabs, and there is a risk of a brittle *punching failure*. This risk can be dealt with by choosing suitable dimensions (slab depth and column diameter), providing column heads and punching reinforcement, and including prestressing tendons over the columns. Three-dimensional truss models are recommended for investigating the flow of the forces.

The risk of brittle shear failure in slabs reinforced only in their plane rises as the depth of the slab increases. This *scale effect*, which can be explained with the help of fracture mechanics, limits the actually considerable deformation capacity of reinforced concrete slabs quite significantly. Therefore, in a similar way to beams, a minimum amount of reinforcement transverse to the plane of the slab should normally be provided, particularly in deep slabs. Such reinforcement improves the deformation capacity significantly, is practical because it can be used to support the top reinforcement and in conjunction with appropriate curtailing of the bending reinforcement on the whole leads to economic solutions.

24.7 Membrane action

24.7.1 Elastic slabs

24.7.1.1 Slab equation taking into account membrane forces – buckling

Taking into account (24.17) or (24.18), the slab equation (8.48) becomes

$$D\Delta\Delta w = q + n_x w_{,xx} + n_y w_{,yy} + 2n_{xy} w_{,xy} \qquad (24.113)_1$$

or rather

$$D\Delta\Delta w = q_z + n_x w_{,xx} + n_y w_{,yy} + 2n_{xy} w_{,xy} - q_x w_{,x} - q_y w_{,y} \qquad (24.113)_2$$

Example 24.23 Buckling of simply supported rectangular slabs

According to (24.66), the load q = const applied to the rectangular slab of Fig. 24.57 can be expressed as a FOURIER series

$$\frac{16q}{\pi^2} \sum_{m=1,3,\ldots}^{\infty} \sum_{n=1,3,\ldots}^{\infty} \frac{\sin\left(\frac{m\pi x}{a}\right) \sin\left(\frac{n\pi y}{b}\right)}{mn}$$

Eq. $(24.113)_1$ results in

$$\Delta\Delta w - \frac{n_x}{D} w_{,xx} = \frac{16q}{\pi^2 D} \sum_{m=1,3,\ldots}^{\infty} \sum_{n=1,3,\ldots}^{\infty} \frac{\sin\left(\frac{m\pi x}{a}\right) \sin\left(\frac{n\pi y}{b}\right)}{mn}$$

and similarly to (24.68), we get

$$w = \frac{16q}{\pi^6 D} \sum_{m=1,3,\ldots}^{\infty} \sum_{n=1,3,\ldots}^{\infty} \frac{\sin\left(\frac{m\pi x}{a}\right) \sin\left(\frac{n\pi y}{b}\right)}{mn\left[\left(\frac{m^2}{a^2} + \frac{n^2}{b^2}\right)^2 + \frac{m^2 n_x}{\pi^2 D a^2}\right]}$$

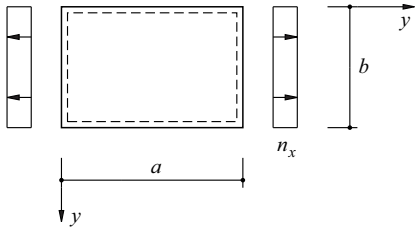

Fig. 24.57 Simply supported rectangular slab subjected to q = const and n_x = const

When n_x is positive (tension), w is decreased somewhat compared with (24.68) because of the term $m^2 n_x/(\pi^2 D a^2)$, and when n_x is negative (compression), it is increased. Provided $n = 1$ and

$$-n_x = \frac{\pi^2 D}{b^2}\left(\frac{mb}{a} + \frac{a}{mb}\right)^2$$

then w can tend to infinity for $q = 0$, i. e. the slab buckles. Putting $a = mb$ gives us the minimum *buckling load* of $-n_x = 4\pi^2 D/b^2$.

24.7.1.2 Initial deformation

When a slab with an initial deflection w_0 (presumed to be small) is loaded by q, it undergoes additional deflections w_1. Eq. $(24.113)_1$ is generalised to

$$D\Delta\Delta w_1 = q + n_x(w_0 + w_1)_{,xx} + n_y(w_0 + w_1)_{,yy} + 2n_{xy}(w_0 + w_1)_{,xy} \qquad (24.114)$$

i. e. the initial deformation corresponds to an additional load of

$$n_x w_{0,xx} + n_y w_{0,yy} + 2n_{xy} w_{0,xy}$$

Example 24.24 Rectangular slab with initial deformation

Presuming the initial deformation

$$w_0 = c \sin\left(\frac{\pi x}{a}\right) \sin\left(\frac{\pi y}{b}\right)$$

for the slab examined in example 24.23, then (24.114) results in

$$D\Delta\Delta w_1 = n_x\left[w_{1,xx} - \frac{c\pi^2}{a^2} \sin\left(\frac{\pi x}{a}\right) \sin\left(\frac{\pi y}{b}\right)\right]$$

Setting

$$w_1 = A \sin\left(\frac{\pi x}{a}\right) \sin\left(\frac{\pi y}{b}\right)$$

leads to

$$A = \frac{-cn_x}{\frac{\pi^2 D}{a^2}\left(1 + \frac{a^2}{b^2}\right)^2 + n_x}$$

and therefore to

$$w = w_0 + w_1 = \frac{w_0}{1 - \alpha}$$

where

$$\alpha = \frac{-n_x}{\frac{\pi^2 D}{a^2}\left(1 + \frac{a^2}{b^2}\right)^2}$$

see (22.12).

24.7.1.3 Large deflections

Expressing the membrane forces in $(24.113)_1$ by means of (23.3) ($\Pi_e = 0$), then the resulting equilibrium condition is

$$D\Delta\Delta w = q + F_{,yy} w_{,xx} + F_{,xx} w_{,yy} - 2F_{,xy} w_{,xy} \qquad (24.115)_1$$

and taking into account (24.23), we get the compatibility condition

$$\Delta\Delta F = Eh\chi_{II} \qquad (24.115)_2$$

instead of (23.5). When $h \longrightarrow 0$, then $D = 0$, and (24.115) describes the deflection of a flexible membrane.

The examination of elastic slabs with large deflections leads to the solution of the non-linear differential equations (24.115) named after VON KÁRMÁN. A direct solution is not generally possible, and the designer will have to resort to approximations based on energy methods. The specific strain energy

$$\pi_i = \frac{Eh}{1 - \nu^2}\left[\frac{\varepsilon_I^2}{2} + (1 - \nu)\varepsilon_{II}\right]$$

corresponds to the strains (24.22) in the middle plane of the slab, and that energy is added to the specific strain energy due to bending which was introduced in section 24.2.6. Accordingly, (24.79) is supplemented as follows:

$$\Pi = \int_A \left\{ \frac{Eh}{1-\nu^2}\left[\frac{\varepsilon_I^2}{2} + (1-\nu)\varepsilon_{II}\right] + D\left[\frac{\chi_I^2}{2} + (1-\nu)\chi_{II}\right] - qw \right\} dA \qquad (24.116)$$

Example 24.25 Square membrane

We set

$$u = c\sin\left(\frac{\pi x}{a}\right)\cos\left(\frac{\pi y}{2a}\right) \quad , \quad v = c\sin\left(\frac{\pi y}{a}\right)\cos\left(\frac{\pi x}{2a}\right) \quad , \quad w = w_0\cos\left(\frac{\pi x}{2a}\right)\cos\left(\frac{\pi y}{2a}\right)$$

for the square membrane ($D = 0$) shown in Fig. 24.58, which is subjected to q = const. This displacement field satisfies the boundary conditions $u = v = w = 0$. Using

$$\varepsilon_x = \frac{\pi c}{a}\cos\left(\frac{\pi x}{a}\right)\cos\left(\frac{\pi y}{2a}\right) + \frac{\pi^2 w_0^2}{8a^2}\sin^2\left(\frac{\pi x}{2a}\right)\cos^2\left(\frac{\pi y}{2a}\right)$$

$$\varepsilon_y = \frac{\pi c}{a}\cos\left(\frac{\pi y}{a}\right)\cos\left(\frac{\pi x}{2a}\right) + \frac{\pi^2 w_0^2}{8a^2}\sin^2\left(\frac{\pi y}{2a}\right)\cos^2\left(\frac{\pi x}{2a}\right)$$

$$\gamma_{xy} = -\frac{\pi c}{2a}\left[\sin\left(\frac{\pi x}{a}\right)\sin\left(\frac{\pi y}{2a}\right) + \sin\left(\frac{\pi y}{a}\right)\sin\left(\frac{\pi x}{2a}\right)\right] + \frac{\pi^2 w_0^2}{4a^2}\sin\left(\frac{\pi x}{2a}\right)\sin\left(\frac{\pi y}{2a}\right)$$

and (6.15) plus (6.16), then (24.116) results in

$$\Pi = \frac{Eh}{1-\nu^2}\left\{c^2\left[\frac{\pi^2(9-\nu)}{8} + \frac{8(1+\nu)}{9}\right] - \frac{cw_0^2}{a}\cdot\frac{\pi^2(11-10\nu)}{24} + \frac{w_0^4}{a^2}\cdot\frac{\pi^4(25-15\nu)}{1024}\right\} - \int_{-a}^{a}\int_{-a}^{a} qw_0\cos\left(\frac{\pi x}{2a}\right)\cos\left(\frac{\pi y}{2a}\right)dx\,dy$$

It follows from $\partial\Pi/\partial c = 0$ that for $\nu = 0.3$

$$c = 0.1384\frac{w_0^2}{a}$$

and putting $d\Pi/dw_0 = 0$, we get

$$w_0 = 0.598\,a\sqrt[3]{\frac{qa}{Eh}}$$

The strains are $\varepsilon_x = \varepsilon_y = \pi c/a = 0.435(w_0/a)^2$ in the centre of the slab $x = y = 0$ and therefore the stresses are $\sigma_x = \sigma_y = E\varepsilon_x/(1-\nu) = 0.621E(w_0/a)^2$.

The linear elastic membrane exhibits a geometric non-linear behaviour similar to the system of example 8.3. The loading increases by the cube of the deflection and the stresses are proportional to the square of the deflection.

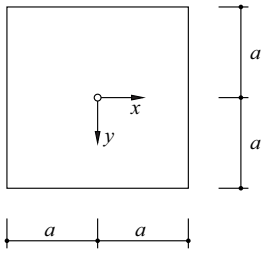

Fig. 24.58 Uniformly loaded square membrane

24.7.2 Perfectly plastic slab strip

The slab strip of width 1 shown in Fig. 24.59(a) is fixed at both ends; it is presumed that the strip exhibits a perfectly plastic behaviour with yield limits $\pm f_y$ in tension and compression. The normal force n and the bending moment m are treated as generalised stresses in the meaning of (20.22).

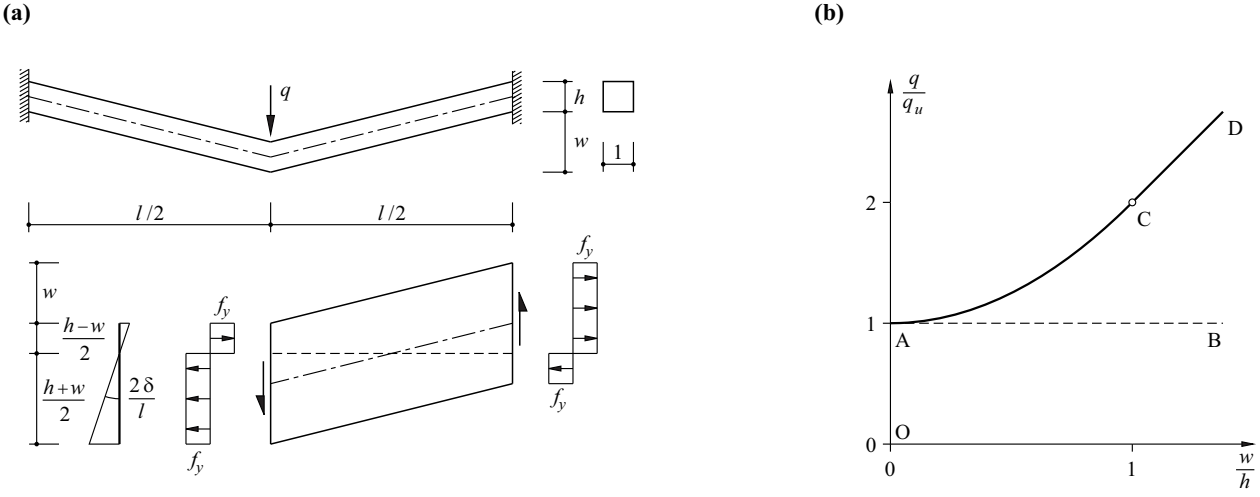

Fig. 24.59 Membrane action in a perfectly plastic slab strip: (a) deformed system, (b) load-deflection diagram

With yield lines at the fixed supports and below the line load q at mid-span, putting $m_u = f_y h^2/4$ results in the limit load $q_u = 8m_u/l$ for $w = 0$. A tensile membrane action occurs when $w > 0$. The axes of rotation at the plastic hinges are displaced from the middle plane, but must lie on a horizontal plane for reasons of symmetry. Applying the principle of virtual deformations to the deformed system for a virtual additional deflection δ at the point of load application results in

$$q\delta - \frac{2\delta}{l}\left[\left(\frac{h+w}{2}\right)^2\frac{f_y}{2} + \left(\frac{h-w}{2}\right)^2\frac{f_y}{2}\right]\cdot 4 = 0$$

and therefore

$$\frac{q}{q_u} = 1 + \left(\frac{w}{h}\right)^2 \qquad (w \le h) \qquad (24.117)_1$$

When $w > h$, the result is a pure tensile membrane action with $q = f_y h \cdot (2w/l)\cdot 2$, i. e.

$$\frac{q}{q_u} = 2\frac{w}{h} \qquad (w > h) \qquad (24.117)_2$$

We get the line ACD in the load-deflection diagram of Fig. 24.59(b).

Eq. (24.117) can also be derived via the yield condition

$$\frac{m}{m_u} + \left(\frac{n}{n_u}\right)^2 = 1 \qquad \left(m_u = \frac{f_y h^2}{4}\ ,\ n_u = f_y h\right)$$

shown in Fig. 24.60 and the associated flow rule. The deflection δ causes the curvature increment $\dot{\chi} = 2\delta/l$ plus the strain increment $\dot{\varepsilon} = (2\delta/l)\cdot w/2 = \delta w/l$ in the middle plane. Using the ratio $\dot{\varepsilon}/\dot{\chi} = w/2$ means that m and n are known according to (7.17), and q follows from the equilibrium condition

$$\frac{ql}{4} - 2m - wn = 0$$

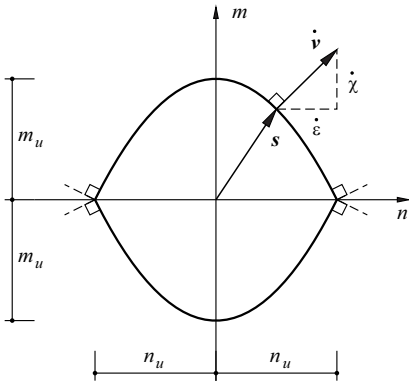

Fig. 24.60 Yield locus for the perfectly plastic slab strip

24.7.3 Reinforced concrete slabs

Let us consider a reinforced concrete slab of depth h which has bottom reinforcement only, see Fig. 24.61(a). The cover to the reinforcement is neglected, as shown in Fig. 21.19(a). Using the effective concrete compressive strength f_c and the mechanical reinforcement ratio ω plus the generalised deformation increments $\dot{\varepsilon}$ and $\dot{\chi}$ and taking into account $\zeta h = \dot{\varepsilon}/\dot{\chi}$ results in the incremental dissipation energy

$$\dot{D} = \dot{\varepsilon}\omega h f_c + f_c(h - \dot{\varepsilon}/\dot{\chi})^2\dot{\chi}/2$$

and therefore according to (7.17),

$$n = \frac{\partial \dot{D}}{\partial \dot{\varepsilon}} = h f_c(\omega - 1 + \zeta) \quad , \quad m = \frac{\partial \dot{D}}{\partial \dot{\chi}} = \frac{h^2 f_c}{2}(1 - \zeta^2)$$

Eliminating ζ results in the interaction relationship

$$\frac{m}{m_u} + \frac{2(1-\omega)}{2-\omega}\cdot\frac{n}{n_u} + \frac{\omega}{2-\omega}\left(\frac{n}{n_u}\right)^2 = 1 \qquad \left[n_u = \omega h f_c\ ,\ m_u = h^2 f_c \omega\left(1 - \frac{\omega}{2}\right)\right]$$

for arc AB in Fig. 24.61(b).

The square slab shown in Fig. 24.61(c) is subjected to a uniformly distributed load q and its lateral displacement at the edge is uninhibited. We shall assume a pyramid-shaped mechanism with yield lines along the diagonals. The level ηh of the instantaneous centre of rotation M of each of the four triangular slab areas joined by the yield lines depends on the deflection w of the centre of the slab, see Fig. 24.61(d). The principle of virtual deformations results in the following equation for an additional deflection δ at the centre of the slab:

$$\frac{ql^3\delta}{3} - 8\int_0^{l/2}\left\{\frac{2\delta}{l}\left(\frac{2xw}{l} + \eta h\right)\omega h f_c + \frac{2\delta}{l}\left[(1-\eta)h - \frac{2xw}{l}\right]^2\cdot\frac{f_c}{2}\right\}\mathrm{d}x = 0$$

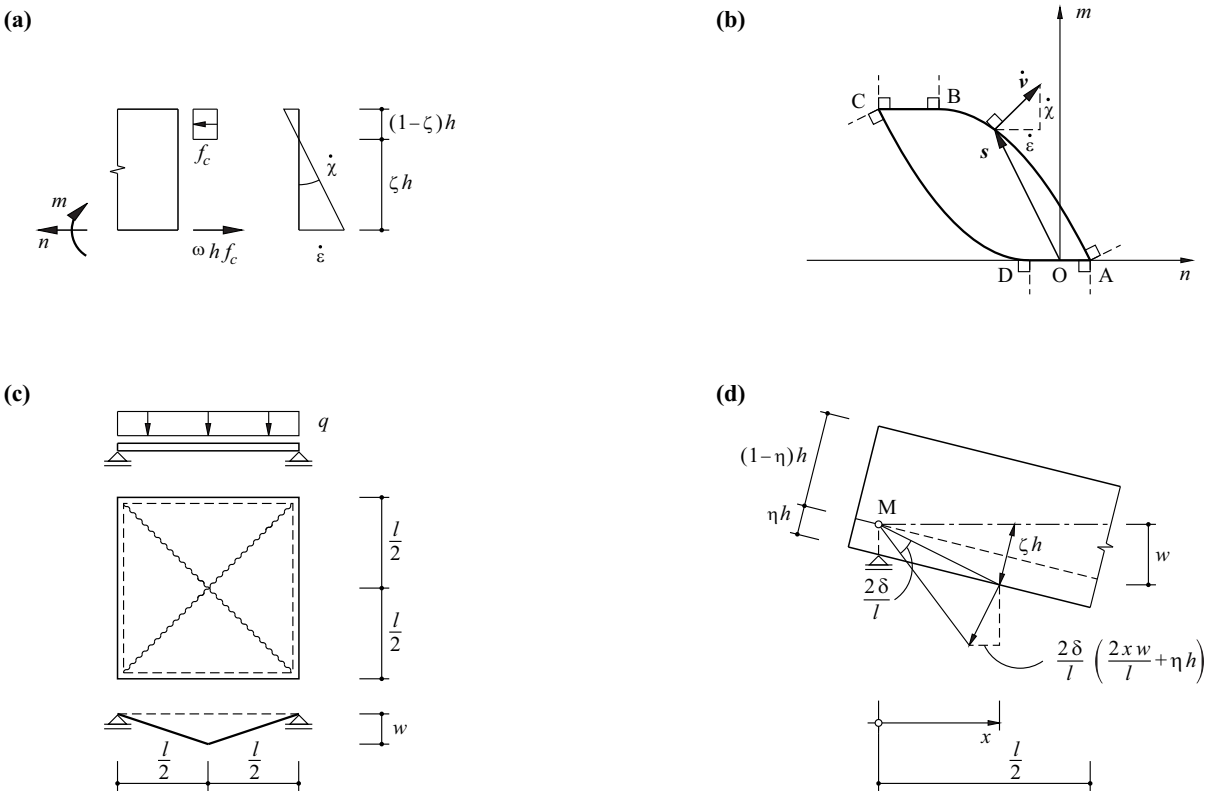

Fig. 24.61 Membrane action in a simply supported reinforced concrete slab: (a) stresses and deformations, (b) *m-n* interaction, (c) mechanism, (d) kinematics

Parameter η is obtained by differentiating the integral and equating to zero and is then $\eta = 1 - \omega - w/(2h)$. The condition $\eta h + w \leq h$ means that the solution is only valid for $w \leq 2\omega h$. Substituting η back into the expression for q and using the limit load $q_u = 24m_u/l^2$ known from exercise 24.1 and example 24.10 results in the relationship

$$\frac{q}{q_u} = 1 + \frac{w^2}{12\omega(2-\omega)h^2} \qquad (w \leq 2\omega h) \qquad (24.118)_1$$

When $w > 2\omega h$, a tensile membrane action develops in the middle part $(1-\eta)lh/(2w) = x_0 \leq x \leq l/2$. Only in the part $0 \leq x \leq x_0$ do we get a contribution to $\dot{D}$ as a result of m:

$$\dot{D} = 8\left\{\frac{2\delta}{l}\omega h f_c\left(\frac{w}{l}\cdot\frac{l}{4} + \eta h\frac{l}{2}\right) + \frac{f_c\delta}{l}\left[(1-\eta)^2h^2x_0 - 4(1-\eta)\frac{hwx_0^2}{2l} + \frac{4w^2x_0^3}{3l^2}\right]\right\}$$

$$= 8\delta h^2 f_c\left[\omega\left(\frac{w}{2h}+1\right) - \omega(1-\eta) + (1-\eta)^3\cdot\frac{h}{6w}\right]$$

Differentiating this expression with respect to $(1-\eta)$ and equating to zero results in $\eta = 1 - (2\omega w/h)^{1/2}$ and therefore

$$\frac{q}{q_u} = 1 + \frac{\frac{w}{h} + \omega - \frac{4}{3}\sqrt{\frac{2\omega w}{h}}}{(2-\omega)} \qquad (w > 2\omega h) \qquad (24.118)_2$$

Restraining the slab along the edges in its plane at the level of the reinforcement means that $\eta \equiv 0$. For $w = 0$, a mechanism is only possible if the stress state corresponds to point B in Fig. 24.61(b), i. e. $\dot{\varepsilon} = 0$, $\dot{\chi} > 0$. The loading required for this amounts to $q_u/[\omega(2-\omega)]$. Substituting $\eta = 0$ in all the above relationships results in

$$\frac{q}{q_u} = \frac{1-(1-\omega)\dfrac{w}{h}+\dfrac{w^2}{3h^2}}{\omega(2-\omega)} \qquad (w \le h)$$

$$\frac{q}{q_u} = \frac{\omega\dfrac{w}{h}+\dfrac{h}{3w}}{\omega(2-\omega)} \qquad (w > h) \qquad (24.119)$$

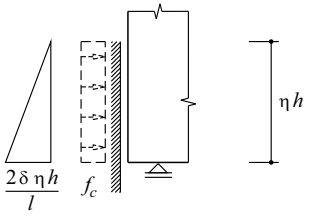

Fig. 24.62 Conditions at the edge of the slab

The lateral restraint calls for large compressive membrane forces which can lead to damage to the concrete at the edge of the slab. According to Fig. 24.62, this can be taken into account by including the additional dissipation energy

$$4l\eta h \cdot \frac{2\delta}{l} \cdot \frac{\eta h f_c}{2} = 8\delta h^2 f_c \cdot \eta^2/2$$

where η is again free. Using the relationships that led to $(24.118)_1$, we get $\eta = (1-\omega)/2 - w/(4h)$, and the requirement $\eta h + w \le h$ is satisfied by $w \le 2(1+\omega)h/3$. We get

$$\frac{q}{q_u} = \frac{1}{2} + \frac{\dfrac{1}{2}\left(1-\dfrac{w}{2h}\right)^2 + \dfrac{w^2}{12h^2} + \dfrac{\omega w}{2h}}{\omega(2-\omega)} \qquad \left[w \le \frac{2(1+\omega)h}{3}\right] \qquad (24.120)_1$$

Similarly, for a large w – via

$$\dot{D} = 8\delta h^2 f_c\left[\omega\frac{2w}{h} + \omega\eta + \frac{\eta^2}{2} + \frac{(1-\eta)^3 h}{6w}\right]$$

and $\mathrm{d}\dot{D}/\mathrm{d}\eta = 0$ – we get the relationship

$$\eta = 1 + \frac{w}{h} - \sqrt{\frac{2w}{h} + \frac{w^2}{h^2} + \frac{2\omega w}{h}}$$

and therefore

$$\frac{q}{q_u} = \frac{\left(1+\dfrac{w}{h}\right)^2 - \dfrac{w^2}{3h^2} + \omega\left(2+3\dfrac{w}{h}\right) - \dfrac{2}{3}\sqrt{\dfrac{w}{h}}\left(2+2\omega+\dfrac{w}{h}\right)^{3/2}}{\omega(2-\omega)} \qquad \left[w > \frac{2(1+\omega)h}{3}\right] \qquad (24.120)_2$$

Fig. 24.63 illustrates the relationships (24.118) to (24.120) for $\omega = 0.2$. Uninhibited lateral movement results in a stable tensile membrane effect according to (24.118). With restraint, according to $(24.119)_1$, large values of q/q_u and large compressive membrane action occur for small deflections w, especially for small reinforcement ratios ω; following an initial elastic rise, we get a snap-through to the branch described by $(24.119)_2$ in the load-deflection diagram. Taking into account the crushing in the support zone, according to (24.120), the compressive membrane action is reduced when compared with that of (24.119).

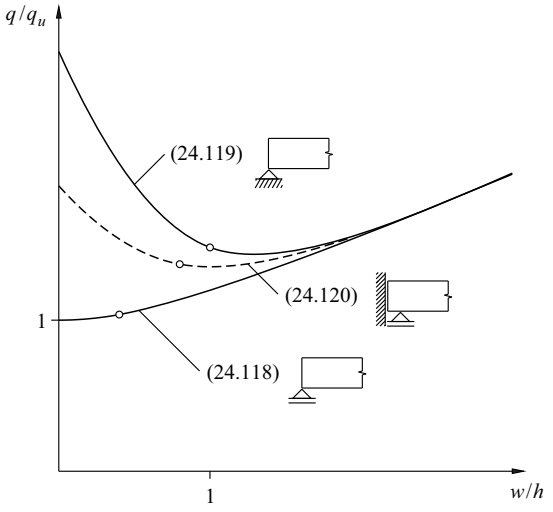

Fig. 24.63 Load-deflection diagrams for various boundary conditions ($\omega = 0.2$)

The structural behaviour of reinforced concrete slabs is already quite complex because of the material non-linearity due to the cracking of the concrete and the yielding of the reinforcement. Including the (geometric non-linear) membrane action leads to further complications, as the example discussed here indicates. However, the example also reveals the considerable reserves of loadbearing capacity that ensue in some circumstances and which are not utilised in normal dimensioning situations, but can prove useful when checking existing structures.

24.8 Summary

1. The moment and shear force components – constituting a symmetric tensor and a vector respectively – are the most important stress resultants for slabs.
2. The differential relationship $(24.1)_1$ or (24.12) for the equilibrium of forces perpendicular to the plane of the slab corresponds to the integral formulation (24.14). According to this, the total load applied to a simply-connected slab area and the sum of the shear flows at the boundary of the area are in equilibrium.
3. The variables m_t, v_n and m_{tn} can be discontinuous at a static discontinuity line in the t direction. An abrupt change in the twisting moment m_{tn} corresponds to a shear force V_t transferred along the discontinuity line.
4. Simply supported and free (unsupported) slab edges are static discontinuity lines. At a free edge, m_n and the edge shear force $v_n + m_{tn,t}$ disappear. At a simply supported edge, $m_n = 0$. Corner forces amounting to $-2m_{nt}$ ensue at right-angled slab corners.
5. Membrane forces, in conjunction with the curvatures and twists of a slab, lead to an additional loading according to (24.17).
6. The curvatures and twists $-w_{,ij}$ corresponding to the deflection w form a symmetric tensor.
7. The integral of the mean curvature is zero in a slab that is fixed at the edge. The integral of the GAUSSian curvature is zero in slabs fixed at the edge and also in polygonal slabs in which, at the edges, either the deflection w or the slope $w_{,n}$ of the deflected surface perpendicular to the edge is equal to zero.
8. The kinematic relations (6.4), (6.5) and the compatibility condition (23.1) for plates should be replaced by (24.22) or (24.23) in the case of additional slab action.
9. The inhomogeneous bipotential equations (8.48) or (24.38) describe the behaviour of linear elastic slabs with infinite shear stiffness and small deflections. The simply integrable ordinary differential equation (24.43) applies in the case of rotational symmetry.
10. Eq. (24.29) generally applies for the shear forces. Presuming a linear elastic behaviour and infinite shear stiffness, the shear force field is irrotational and specified by the shear force potential (24.26).
11. The slab equation (24.43) for rotationally symmetric problems can be solved directly. FOURIER series approaches and the energy methods of RITZ and GALERKIN are suitable for more general problems. With this as our basis, it is possible to deal with a whole variety of problems with relatively simple boundary conditions and loading arrangements, some of which are presented here. Such solutions enable the relevant force and deformation variables to be quickly estimated for a particular problem. In particular, they enable the designer to check results obtained with, for example, the finite element method. FEM, which enables any boundary conditions and loading arrangements to be considered, is widely used in practice, but is not investigated any further here.
12. The VON MISES and TRESCA yield conditions for the coplanar stress state are transferred directly to the space m_x, m_y, m_{xy} according to (24.82) and (24.83). The limit loads of VON MISES slabs cannot lie more than 15.4 % higher than those of the corresponding TRESCA slabs for the same plastic moment.

13. Complete solutions are always possible for rotationally symmetric problems of TRESCA slabs. Non-linear differential equations result for VON MISES slabs and the collapse mechanisms are substantially different to those of TRESCA slabs.
14. The normal moment yield condition (24.90) is generally used for reinforced concrete slabs and leads to the dimensioning relationships (24.92). Regular points on the yield surface, see Fig. 24.28(b), correspond to developable areas in the collapse mechanism, but points on the ellipse at the intersection or at the apexes of the two cones correspond to areas with negative or positive GAUSSian curvature.
15. According to the theory of thin plastic slabs, the strain increments of the middle plane are added to the curvature and twist increments as generalised deformation increments. The principal strain increments generally vary hyperbolically over the depth of the slab and can have a maximum of two zero points.
16. The normal moment yield condition contains a more severe kinematic constraint than the theory of thin plastic slabs. The twisting resistance at higher reinforcement ratios can be considerably overestimated according to the normal moment yield condition.
17. For general stress resultants due to moments, shear forces and membrane forces, the sandwich model, see Fig. 24.33, leads to relationships (24.94) and (24.95) for sizing the reinforcement.
18. Complete solutions can be worked out for any rotationally symmetric problems connected with reinforced concrete slabs. When dimensioning for a certain load case, it is possible to specify the bending resistances in the radial and circular directions (which generally vary with the radius) on the basis of the equilibrium condition (24.97).
19. Moment fields can be used to work out lower-bound solutions according to the static method of limit analysis by considering the equilibrium conditions, the static boundary conditions and, if applicable, symmetry conditions. One variation of this method that is particularly useful in practice is the simple strip method in which only the bending moments are considered in groups of criss-crossing strips of slab, if necessary in the form of strong bands. The strip method can be expanded to deal with concentrated forces by introducing load distribution elements.
20. The application of the kinematic method by means of yield line mechanisms generally leads to an optimisation of a number of free parameters that describe the respective mechanism. This is relatively simple, like setting up the work equation, even in the event of complex slab geometries and a complicated distribution of the resistance. In contrast to framed structures, a plasticity check is impossible and so special care must be exercised when searching for alternative, possibly more critical, mechanisms.
21. The behaviour of linear elastic slabs with finite shear stiffness can be ascertained with the two differential equations (24.109) and (24.112). Compliance with three boundary conditions is thus assured. In contrast to linear elastic slabs with infinite shear stiffness, the shear force field is not irrotational.
22. The nominal shear stresses in reinforced concrete slabs without reinforcement transverse to the plane of the slab should be limited to a carefully chosen fraction of the concrete's tensile strength. Owing to the risk of punching, special measures are necessary in the vicinity of force application and transfer points.
23. The slab equation (24.113), generalised by including membrane forces, enables the designer to investigate the buckling of slabs. How membrane forces affect the deflection of slabs with prior deformation can be ascertained via amplification factors in a similar way to bars in compression.
24. Examining elastic slabs with large deflections leads to the solution of the VON KÁRMÁN differential equations (24.115). Energy methods should generally be used in this situation.

25. In certain circumstances, membrane forces in slabs lead to reserves of loadbearing capacity that are considerable when compared with determining the limit load according to first-order theory. Such reserves are not normally utilised in dimensioning practice, but can prove helpful when investigating existing structures. However, the discussion surrounding the effective stiffnesses and the boundary conditions with respect to displacements in the plane of the slab must be approached with great care.

24.9 Exercises

24.1 Reverse the sign of m_{xy} in the moment field of example 24.1 and carry out a similar discussion, see also example 24.10.

24.2 Discuss the following moment fields in a similar way to exercise 24.1:

a) $m_x = 0$, $m_y = m_0(1 - 4y^2/l^2)$, $m_{xy} = m_0 \cdot 4xy/l^2$

b) $m_x = m_0(1/2 - 2x^2/l^2)$, $m_y = m_0(1/2 - 2y^2/l^2)$, $m_{xy} = m_0 \cdot 4xy/l^2$

c) $m_x = 0$, $m_y = m_0(1 - y^2/x^2)$, $m_{xy} = -m_0 \cdot y/x$

d) $m_x = m_0[4x^2/(3l^2) - 1/3]$, $m_y = m_0[2y^2/(3x^2) + 4y^2/(3l^2) - 1]$, $m_{xy} = m_0[2y/(3x) - 8xy/(3l^2)]$

The moment fields defined in c) and d) for $0 \leq y \leq x \leq l/2$ have to be supplemented in the other octants in accordance with the symmetry.

24.3 Calculate the principal moments and principal moment trajectories for example 24.2.

24.4 Show that the shear force field $\boldsymbol{v}$ in example 24.2 follows from

$$\Phi_v = -2m_0(x^2 + y^2)/l^2 \quad , \quad \Phi_r = 0 \quad , \quad \psi = m_0 y/x$$

according to (24.29).

24.5 Discuss the moment field

$$m_x = m_0(1 - \xi^2\alpha - \xi^4\beta + \xi^2\eta^2) \quad , \quad m_y = m_0(1 - \eta^2\alpha - \eta^4\beta + \xi^2\eta^2) \quad , \quad m_{xy} = m_0[-\xi\eta\alpha + \xi\eta(\xi^2 + \eta^2)\gamma]$$

where

$$\alpha = \frac{4}{3} + \frac{\sqrt{5}}{9} \quad , \quad \beta = \frac{2}{3} - \frac{\sqrt{5}}{9} \quad , \quad \gamma = 1 - \frac{2\sqrt{5}}{9}$$

for the square slab fixed on all sides and subjected to a uniformly distributed load as shown in Fig. 24.64(a). Show that the associated shear force field $\boldsymbol{v}$ is irrotational ($\psi = 0$) and that the potentials occurring in (24.29) are given by

$$\Phi_v = -\frac{12 + \sqrt{5}}{6}(\xi^2 + \eta^2)m_0 \quad , \quad \Phi_r = \frac{2\sqrt{5} - 15}{36}(\xi^4 + \eta^4 - 6\xi^2\eta^2)m_0$$

24.6 Swap the boundary conditions in Fig. 24.15(a) and solve the corresponding problem of an annular slab simply supported at the inner edge and loaded on the outer edge by a constant line load moment.

24.7 Verify (24.48).

24.8 Swap the boundary conditions in Fig. 24.15(d) and solve the corresponding problem.

24.9 Replace the simple supports in Fig. 24.15(d) and exercise 24.8 by fixed supports and solve the corresponding problems.

24.10 Verify (24.58), (24.59) and (24.60).

24.11 Compare the moments, shear forces, edge shear forces and corner forces associated with the elastic solution (24.68) for the case of $a = b = l$ with those of exercise 24.1 for the same load.

24.12 A square slab ($a = b = l$, slab stiffness D) is loaded uniformly with q and supported at its edges by four identical, torsionless simply supported beams (span l, bending stiffness $EI = Dl/2$). Show that the twisting moments m_{xy} parallel with the edges of the slab disappear everywhere in the slab and compare the force and deformation variables with those of exercise 24.11.

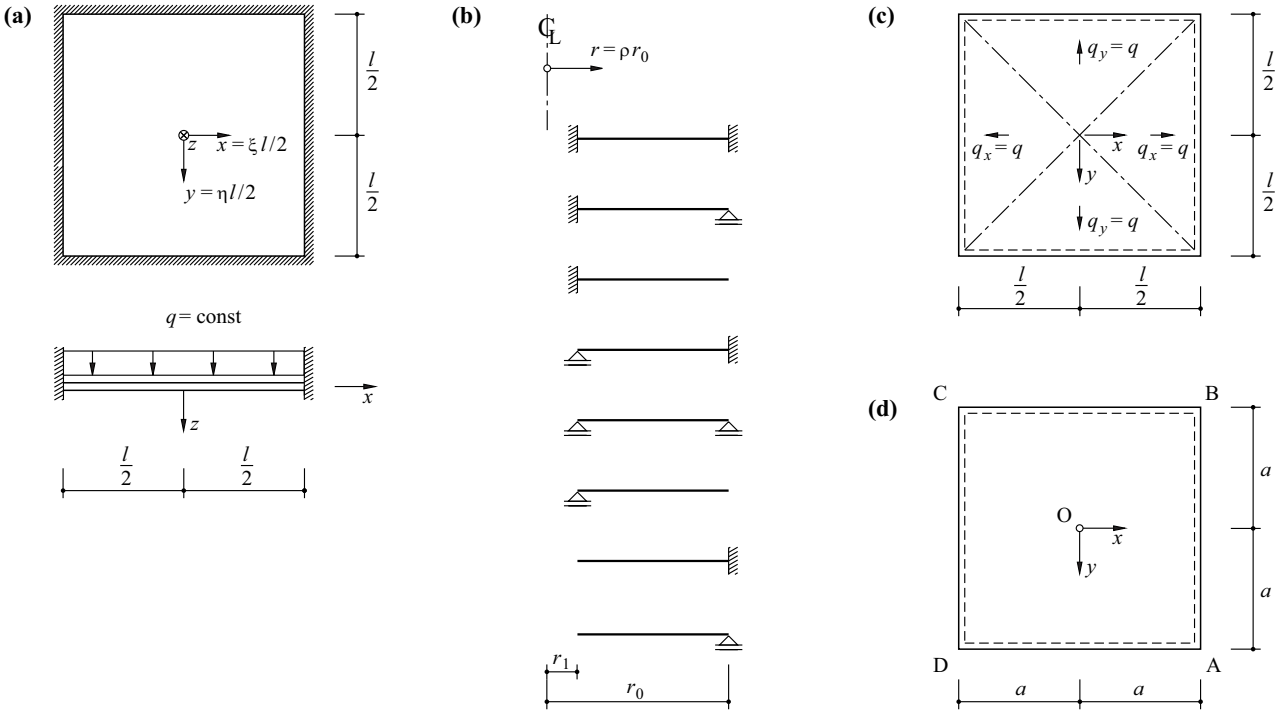

Fig. 24.64 Figures for section 24.9

24.13 A rectangular slab with side lengths a and b in the x and y directions is simply supported along $x = 0$ and $x = a$, and free along $y = \pm b/2$. A line load $q = q_0 \sin(\pi x/a)$ is applied along the slab edge $y = b/2$. Use (24.71) with (24.73) as well as $m = 1$ and discuss the behaviour of the slab for $a \gg b$, $a = b$ and $a \ll b$.

24.14 Verify (24.78) and present the deflection w plus the associated stress resultants m_r, m_φ, v_r for the case of $a = b$, $\nu = 0.2$, $\rho_1 = 0.05$ as functions of r. Compare the results at sections $x = y$ and $x = a/2$ according to Fig. 24.20 with those obtained using (24.77).

24.15 Replace the deflection field in example 24.5 by

$$w = (1 - \xi^2)^2(1 - \eta^2)^2[c_1 + c_2(\xi^2 + \eta^2) + c_3\xi^2\eta^2]$$

Apply the theorem of least total potential and calculate the coefficients c_1, c_2 and c_3. Compare the deflections, moments and shear forces with those obtained in example 24.5. In doing so, consider sections $\eta = 0$ and $\xi = \eta$ at least.

24.16 Verify the figures given in Tab. 24.1.

24.17 Subject some of the TRESCA annular slabs shown in Fig. 24.64(b) to a treatment similar to that of examples 24.6 and 24.7. Consider concentric annular loads and uniformly distributed loads.

24.18 Example 24.9 is modified in such a way that $a_x = a_x' \geq a_y = a_y'$. Show that when $\omega_x = a_x f_y/(h f_c)$, $\omega_y = a_y f_y/(h f_c)$, the lower bound for the twisting resistance m_{xyu} is

$$f_c h^2 \sqrt{\omega_x \omega_y}(1 - \omega_x - \omega_y)$$

where $\omega_y \leq \omega_x \leq (1 - \omega_y)/3$. In doing so, consider uniaxial concrete compressive stress fields (regime A according to Fig. 24.31) with thickness $h(\omega_x + \omega_y)$ top and bottom in the slab at angles of

$$\pm \arctan\sqrt{\omega_y/\omega_x}$$

to the x axis.

24.19 Compare the bending moment diagrams for the case of $\rho_1 = 1$ in example 24.10 with $(24.46)_2$ and $(24.46)_3$. Calculate M according to (24.98) from the elastic moments and from the moment diagrams given in Fig. 24.35(c).

24.20 Use (24.97) to discuss the theoretical reinforcement required for a circular slab fixed at its outer edge $r = r_0$ and loaded by q = const. In what way does the optimum theoretical solution change when minimum reinforcement in the circular direction with a resistance $m_{\varphi u} = m_0$ = const is specified in the bottom of the slab in order to limit cracking? How would you curtail the top radial reinforcement and how does that affect the effective reinforcement?

24.21 As an alternative to Fig. 24.40(b), investigate the load apportionment shown in Fig. 24.64(c) according to the simple strip method and calculate the associated "moment volume". Compare the resulting reinforcement layout with that according to Fig. 24.40(b) and discuss the practicability of the solutions.

24.22 Discuss the moment field described by (24.101) and (24.102). Show that the maximum moment amounts to $m(1 + \sqrt{5})/2$ and that the principal shear forces are radial to the origin of coordinates.

24.23 Replace the free slab edge BC in Fig. 24.44 by a simple support and work out an appropriate way to carry a uniformly distributed load using the advanced strip method.

24.24 The slab shown in Fig. 24.64(d) has a point support at the centre O in addition to being simply supported along the edges. Develop a suitable load-carrying system for a uniformly distributed load and draw the corresponding moment diagrams.

24.25 Apply the advanced strip method to the flat slab problem of Fig. 24.20. Choose a width of $2a/5$ or $2b/5$ for the column strips and compare the bending resistances required at mid-span and on the column axes with those resulting from the application of the equivalent frames method (Fig. 24.22).

24.26 Vary the boundary conditions for the slab shown in Fig. 24.47 (fixed, simply supported or free edges plus corner columns) and discuss the corresponding yield line mechanisms (axes of rotation, free parameters).

24.27 Show that m_y disappears for $y = 0$ and $y = a$ in example 24.22 and discuss the distribution of m_{xy} along these edges.

24.28 Draw the yield surface discussed in section 24.6.2 and compare the stress distributions over the depth of the slab h for the cases $\alpha = \beta = 1/h$, $\alpha = -\beta = \sqrt{3}/h$ and $\alpha = \sqrt{3}/h$, $\beta = 0$.

24.29 Use (24.36) and (24.37) to express (24.115) in cylindrical coordinates.

24.30 Verify the expression for the total potential Π in example 24.25.

25 FOLDED PLATES

25.1 General

Folded plates consist of thin slabs positioned at various angles which are connected together such that they can transfer forces across their lines of intersection, their *edges*. The slabs provide mutual support for each other along those edges. The forces occurring at the slab edges are transferred via membrane forces, i. e. the slabs are activated as plates. The structural response of a folded plate structure is therefore characterised by the interplay between the "stiff" *plate action* in the plane of its elements and the "flexible" *slab action* transverse to that plane. The support provided to the slabs meeting at an edge is either practically rigid or flexible depending on the slenderness ratios and boundary conditions of the plates.

Folded plates can be constructed in a huge diversity of forms and therefore offer corresponding architectural design options. Fig. 25.1 illustrates a number of typical examples. Fig. 25.1(a) shows a barrel vault in which the membrane forces at the ends of the five longitudinal plates are transferred to the two *end plates* in the planes of the columns; the end plates can be solid or resolved into trusses or frames. Fig. 25.1(b) and Fig. 25.1 (c) show sawtooth roofs made up of rectangular or triangular plates, and

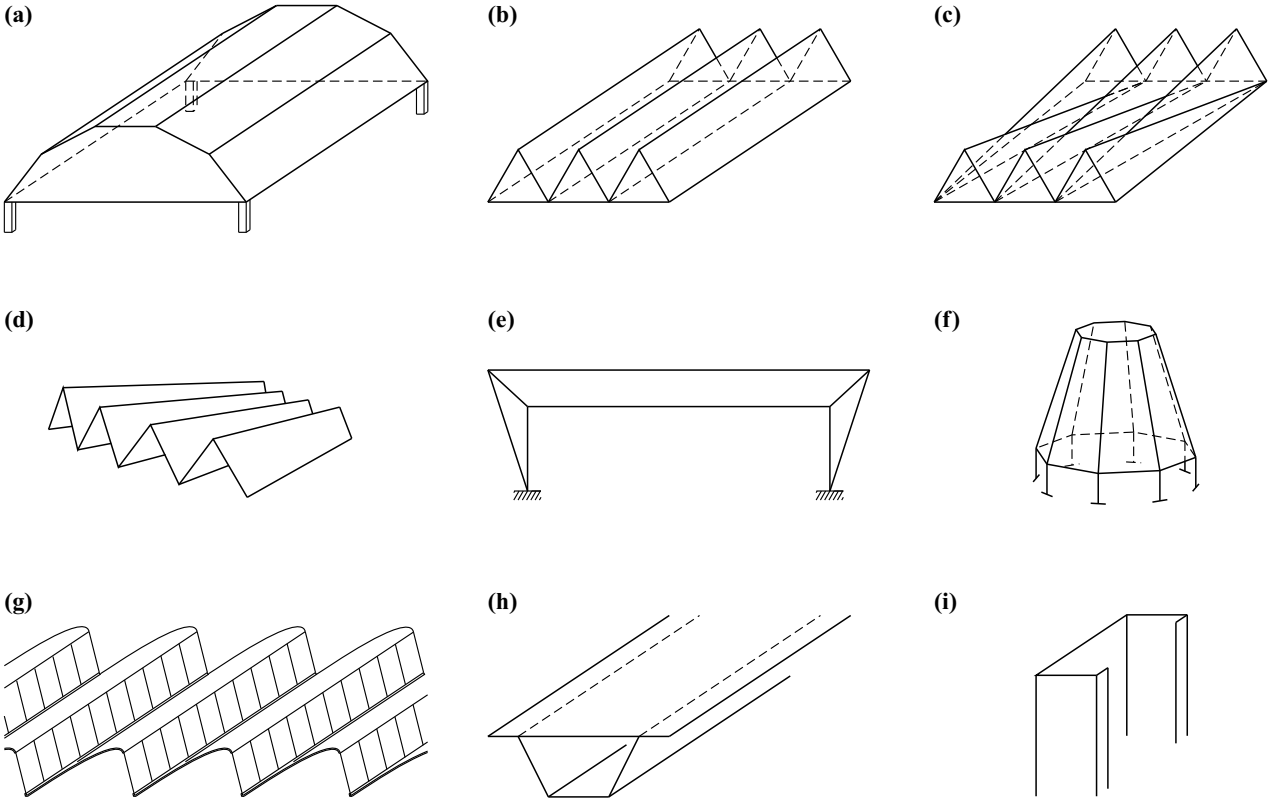

Fig. 25.1 Folded plates: (a) barrel vault, (b) to (d) sawtooth roofs, (e) frame-type folded plate, (f) cooling tower, (g) northlight roof, (h) box girder, (i) service core

Theory of Structures. First Edition. Peter Marti

Fig. 25.1(d) shows an annular area roofed over with trapezoidal elements in sawtooth form. Sawtooth roofs and folded plates with a trapezoidal cross-section can be extended to form frames according to Fig. 25.1(e), e. g. by means of appropriate folded-plate columns. Fig. 25.1(f) shows a folded plate made up of trapezoidal elements which behaves similarly to a truncated cone shell, and Fig. 25.1(g) shows a north-light roof which can be analysed as a folded plate or as a cylindrical shell. Finally, all types of profiled beams such as the box girders used for bridges, Fig. 25.1(h), and the service cores of buildings, Fig. 25.1(i), function as folded plates in principle.

The structural analysis of folded plates is mainly based on the finite element method. Methods of calculation used in the past can still provide valuable insights into the structural behaviour of folded plates, but are actually largely outdated. The aim of the following – primarily qualitative – observations is to highlight important aspects of the structural behaviour of folded plate structures, mainly with respect to their conceptual design.

25.2 Prismatic folded plates

25.2.1 Sawtooth roofs

Fig. 25.2(a) shows a section through an unbraced sawtooth roof with a single fold. The loading q creates transverse bending moments m with a minimum value of $-qb^2/2$ at the ridge plus line loads of $qb/\sin\alpha$ in each of the plates inclined at an angle α to the horizontal. In a single fold subjected to q = const, supported at the ends of its plates as a simply supported beam of span l, bending moments amounting to $ql^2b/(8\sin\alpha)$ develop at mid-span and shear forces of $qlb/(2\sin\alpha)$ at the supports. Equilibrium between the inclined shear forces at the supports and the vertical support forces of $qlb/2$ at each end requires horizontal opposing forces of $qlb/(2\tan\alpha)$ at the bottom ends of the plates. These can be assigned to a tie beam joining the supports or resisted by a transverse end frame. Solid end plates can be provided as an alternative.

The large transverse bending leads to considerable inward bending of the two free edges in the case of the unbraced single fold. Including struts or transverse frames according to Fig. 25.2(b) can help to alleviate this problem considerably. If the mutual support to the free edges is regarded as rigid, the moment at the ridge is four times smaller.

For reasons of symmetry, neither the ridges nor the valleys can be displaced laterally in the case of the inner folds shown in Fig. 25.2(c). The transverse bending moments at the ridge amount to $-qb^2/12$, i. e. one-sixth of the value of the unbraced single fold.

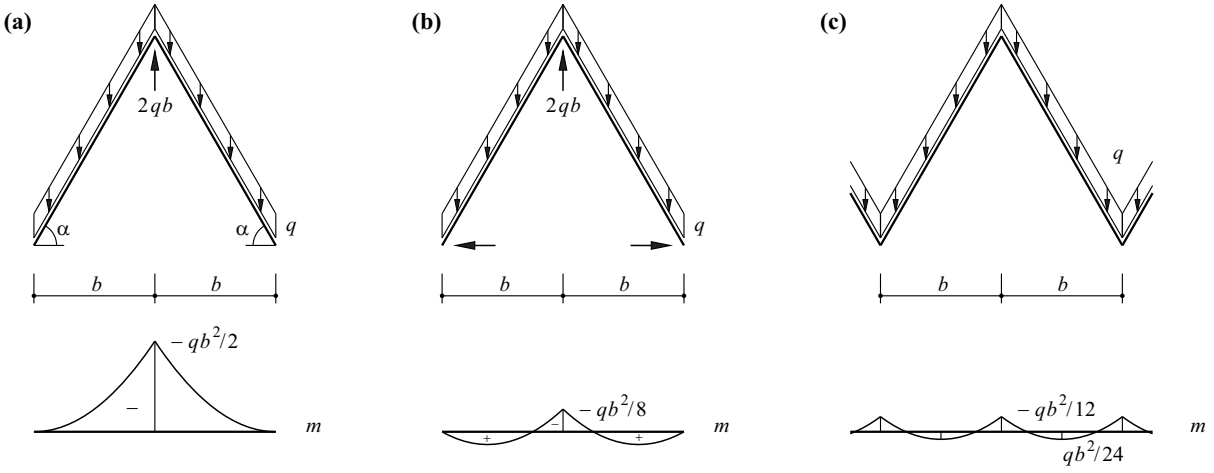

Fig. 25.2 Sawtooth roof: (a) unbraced single fold, (b) braced single fold, (c) inner fold with symmetrical loading

Sawtooth roofs are advantageous in terms of their statics and are easy to understand. The deliberations of Fig. 25.2 illustrate the principal aspects of the structural behaviour in the longitudinal and transverse directions quite clearly. In particular, it is possible to see the effects and the benefits of suitable bracing to the edge folds, which behave in a similar way to single folds. The reader will also notice secondary effects, e. g. the local bending moments and shear forces that occur for reasons of compatibility in the plates in the longitudinal direction at the transition to the end plates (or transverse end frames). These moments and forces do not need to be taken into account in the calculations, but do need to be taken into account in the detailing (e. g. by including minimum reinforcement to limit cracking).

25.2.2 Barrel vaults

25.2.2.1 Membrane theory

Let us consider a barrel-vault roof made up of n rectangular plates, see Fig. 25.3(a). The two free edges are designated with 0 and $2n$, the $n-1$ edges i with the intermediate even numbers, and the plates $i-1$ etc. with the corresponding odd numbers. The loading on the individual plates is assumed to be constant in the longitudinal direction and the plates are assumed to be connected together by some form of hinge. The plates therefore act as simply supported beams in the transverse direction. The *edge loads* q_i simply result from the corresponding support forces and can be divided into the in-plane load components $s_{i-1,i}$ and $s_{i+1,i}$ according to the plate angles α_{i-1} etc. Adding the components together at both edges results in the *in-plane loads* s_{i-1} etc.

Fig. 25.3(b) shows free body diagrams for the plates $i-1$ and $i+1$ with widths a_{i-1} or a_{i+1} which are joined together at edge i. The two plates are cut through in the middle of the span l. The unknown *edge shear forces* T_{i-2}, T_i and T_{i+2} act along the sides of the plates. The stress resultants ensuing at mid-span are given in the figure, where M_{i-1} and M_{i+1} are the bending moments in the simply supported beam due to the in-plane loads s_{i-1} or s_{i+1}. According to (13.16), the longitudinal stress for plate thicknesses h_{i-1} and h_{i+1}, cross-sectional areas $A_{i-1} = a_{i-1}h_{i-1}$, $A_{i+1} = a_{i+1}h_{i+1}$ and section moduli $W_{i-1} = a_{i-1}{}^2h_{i-1}/6$, $W_{i+1} = a_{i+1}{}^2h_{i+1}/6$ is

$$-\frac{M_{i-1}}{W_{i-1}} + 4\frac{T_i}{A_{i-1}} + 2\frac{T_{i-2}}{A_{i-1}} = \frac{M_{i+1}}{W_{i+1}} - 4\frac{T_i}{A_{i+1}} - 2\frac{T_{i+2}}{A_{i+1}}$$

at mid-span of edge i, i. e.

$$2\frac{T_{i-2}}{A_{i-1}} + 4T_i\left(\frac{1}{A_{i-1}} + \frac{1}{A_{i+1}}\right) + 2\frac{T_{i+2}}{A_{i+1}} = \frac{M_{i-1}}{W_{i-1}} + \frac{M_{i+1}}{W_{i+1}} \tag{25.1}$$

applies for the three adjacent edge shear forces T_{i-2}, T_i and T_{i+2}. Eq. (25.1) results in a set of linear equations for the $n-1$ unknown edge shear forces T_i.

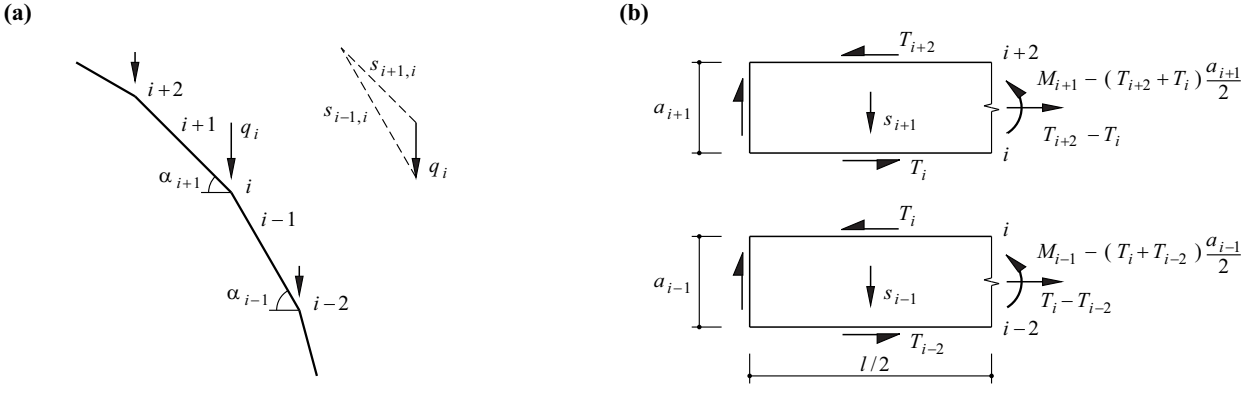

Fig. 25.3 Prismatic folded plates: (a) section, (b) individual plates

Example 25.1 Barrel vault – membrane theory

Fig. 25.4(a) shows the section through a folded plate structure with span $l = 20\,\text{m}$ and constant plate thickness $h = 160\,\text{mm}$. The action considered in this example is a dead load of $4\,\text{kN/m}^2$.

According to Fig. 25.4(b), the resulting edge loads are $q_2 = q_8 = 10/2 + 6 = 11\,\text{kN/m}$ and $q_4 = q_6 = 12/2 + 10/2 = 11\,\text{kN/m}$. We therefore get the in-plane loads $s_1 = 11\,\text{kN/m}$, $s_3 = 11 \cdot 5/3 = 18.33\,\text{kN/m}$ and $s_5 = 0$ given in Fig. 25.4(c), which cause the moments $M_1 = 11 \cdot 20^2/8 = 550\,\text{kNm}$, $M_3 = 18.33 \cdot 20^2/8 = 916.67\,\text{kNm}$ and $M_5 = 0$ at mid-span.

Putting $A_1 = 0.24\,\text{m}^2$, $A_3 = 0.4\,\text{m}^2$, $A_5 = 0.48\,\text{m}^2$ and $W_1 = 0.06\,\text{m}^3$, $W_3 = 0.167\,\text{m}^3$, eq. (25.1), taking into account $T_4 = -T_6$, results in the set of equations

$$\begin{bmatrix} 26.667 & 5 \\ 5 & 14.167 \end{bmatrix} \begin{Bmatrix} T_2 \\ T_4 \end{Bmatrix} = \begin{Bmatrix} 14.667 \\ 5.5 \end{Bmatrix} \text{MN}$$

with the solution $T_2 = 511\,\text{kN}$, $T_4 = 208\,\text{kN}$. Consequently, we get the longitudinal stresses

$$\sigma_0 = \frac{0.55}{0.06} - 2 \cdot \frac{0.511}{0.24} = 4.91\,\text{N/mm}^2$$

$$\sigma_2 = -\frac{0.55}{0.06} + 4 \cdot \frac{0.511}{0.24} = -0.65\,\text{N/mm}^2$$

$$\sigma_4 = -\frac{0.917}{0.167} + 4 \cdot \frac{0.208}{0.4} + 2 \cdot \frac{0.511}{0.4} = -0.87\,\text{N/mm}^2$$

at mid-span as given in the left part of Fig. 25.4(d). As we can see, these stresses are not distributed linearly over the depth of the cross-section (3 m).

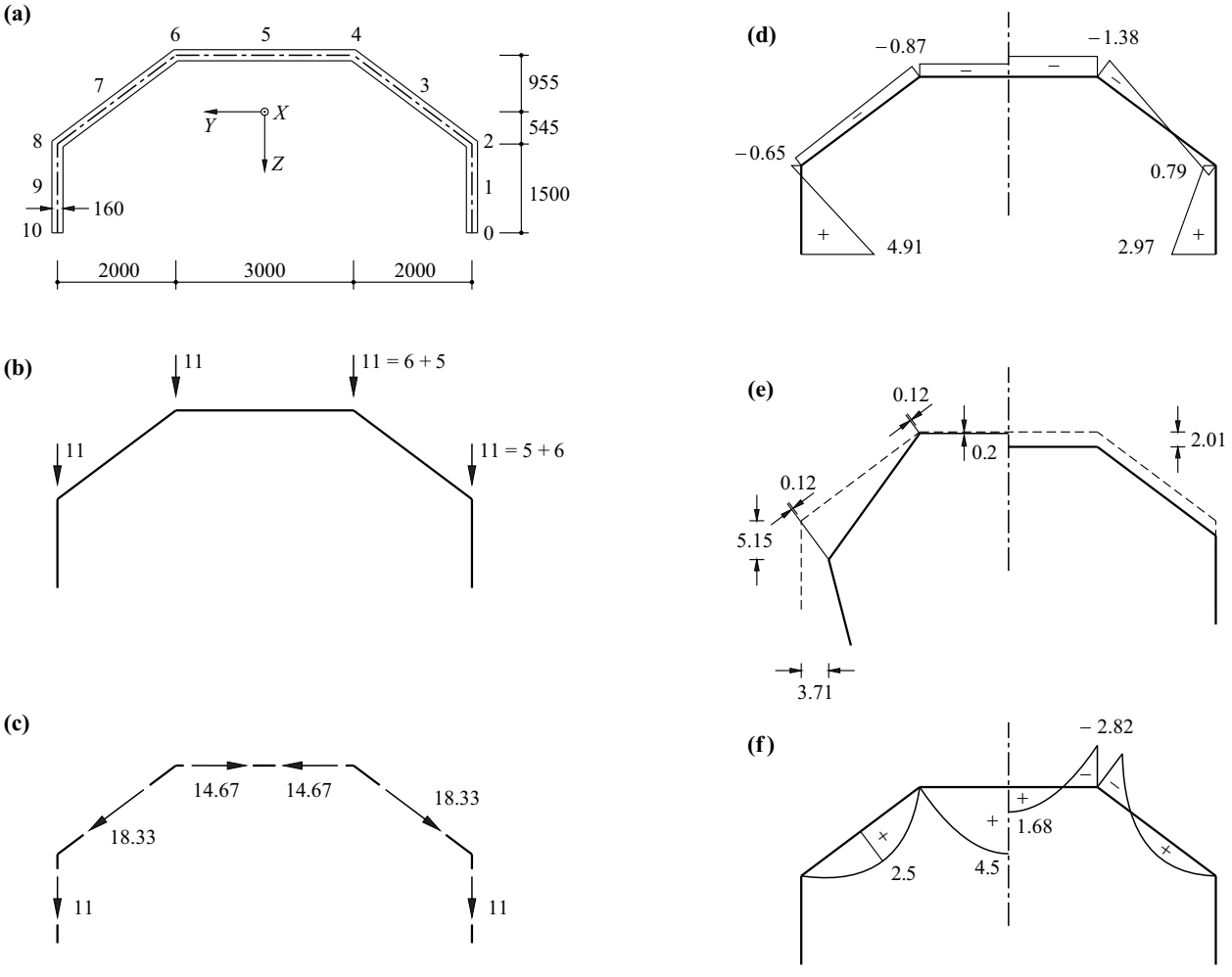

Fig. 25.4 Prismatic folded plate ($l = 20$ m): (a) notation and dimensions [mm], (b) edge loads [kN/m], (c) in-plane loads [kN/m], (d) σ_x at mid-span [N/mm^2], (e) displacements at mid-span [mm], (f) transverse bending moments [kNm/m]

The difference in the stresses $\sigma_2 - \sigma_4 = 0.22\,\mathrm{N/mm^2}$ corresponds to a curvature of plate 3 amounting to $0.22/(30 \cdot 2.5) = 0.0029\,\mathrm{mrad/m}$ at mid-span for a modulus of elasticity $E = 30\,\mathrm{kN/mm^2}$. Owing to the parabolic form of the bending moment diagram, the work equation (section 14.2) or MOHR's analogy (section 15.3.2) results in a mid-span deflection of $0.0029 \cdot 20^2/9.6 = 0.12\,\mathrm{mm}$ in the plane of the plate. For reasons of symmetry, plate 5 can only be displaced vertically and so the deflection of edge 4 (or 6) amounts to $0.12 \cdot 5/3 = 0.2\,\mathrm{mm}$, see Fig. 25.4(e).

Similarly, the difference in the stresses $\sigma_0 - \sigma_2 = 5.56\,\mathrm{N/mm^2}$ results in a curvature of plate 1 amounting to $5.56/(30 \cdot 1.5) = 0.124\,\mathrm{mrad/m}$ at mid-span and therefore a deflection of $0.124 \cdot 20^2/9.6 = 5.15\,\mathrm{mm}$. Compatibility of the displacements at edge 2 (or 8) requires that this is displaced inwards by $(5.15 - 0.2) \cdot 3/4 = 3.71\,\mathrm{mm}$, see Fig. 25.4(e).

As we can see, at edges 4 and 6 we get relative rotations of the plates which are assumed to have hinged connections along those edges. The cross-sectional form is not retained. The left half of Fig. 25.4(f) illustrates the transverse bending moments, which according to our assumptions are equal to zero at the edges and cause additional relative rotations.

If we assume that the cross-sectional form is retained, then according to beam theory, the stresses and displacements at mid-span are those shown on the right in Fig. 25.4(d) and Fig. 25.4(e). The beam with a cross-sectional area of $1.76\,\mathrm{m^2}$ and a principal moment of inertia $I_Y = 1.517\,\mathrm{m^4}$ undergoes a deflection at mid-span amounting to $5 \cdot 0.044 \cdot 20^4/(384 \cdot 30 \cdot 1.517) = 2.01\,\mathrm{mm}$ when subjected to a constant line load of 44 kN/m. The bending moment of $0.044 \cdot 20^2/8 = 2.2\,\mathrm{MNm}$ at mid-span leads to stresses of $2.2 \cdot 2.045/1.517 = 2.97\,\mathrm{N/mm^2}$ at the bottom edge of the cross-section; the other values given on the right of Fig. 25.4(d) follow from the linear variation of σ_x with Z. The analysis of a symmetrical strip of slab continuous over rigid supports in the transverse direction (statically indeterminate to the first degree) results in a value of $-79/28\,\mathrm{kNm/m} = -2.82\,\mathrm{kNm/m}$ for the transverse bending moments at edge 4 (or 6), as shown on the right of Fig. 25.4(f).

25.2.2.2 Bending theory

According to membrane theory, relative rotations of the adjoining plates ensue at hinge-type edges due to the deformation of the cross-section and the manner in which the load is carried via transverse bending of the slab. For example, according to Fig. 25.4(e), we get a rotation amounting to $3.71/1.5 = 2.473\,\mathrm{mrad}$ at mid-span of plates 3 and 7; this rotation gradually decreases to zero at the supports, affine with the deflection curve. In addition, for a slab stiffness of $30\,\mathrm{kN/mm^2} \cdot (0.16\,\mathrm{m})^3/12 = 10.24\,\mathrm{MNm}$ ($\nu = 0$), the transverse bending moments shown in Fig. 25.4(f) result in a mutual rotation of $(2.5 \cdot 2.5 + 4.5 \cdot 3)/(3 \cdot 10.24) = 0.643\,\mathrm{mrad}$ according to the work theorem; this rotation is constant over the length of the folded plate within the scope of our assumptions.

No relative rotations can develop along the edges in reality. It is possible to comply with this requirement by introducing statically indeterminate edge moments.

In the following, we shall confine ourselves to a sinusoidal loading in the longitudinal direction. In such a situation, both the bending moments and the deflections of the individual plates have a sinusoidal form, and the variation in the statically indeterminate edge moments is also sinusoidal. Contrasting with that, the shear forces and edge shear forces exhibit a cosinusoidal form.

Example 25.2 Barrel vault – bending theory

Let us replace the uniformly distributed load of $4\,\mathrm{kN/m^2}$ in example 25.1 by the first term of the FOURIER series, i. e. $(4\,\mathrm{kN/m^2}) \cdot (4/\pi) \cdot \sin(\pi x/l)$. The corresponding edge loads of $44\,\mathrm{kN/(\pi m)}$ at mid-span lead to in-plane loads of 14.006 or 23.343 kN/m in plates 1 and 3, see Fig. 25.5(a). The associated bending moments are $M_1 = 14.006 \cdot 20^2/\pi^2 = 567.6\,\mathrm{kNm}$ and $M_3 = 23.343 \cdot 20^2/\pi^2 = 946.0\,\mathrm{kNm}$.

Eq. (25.1) provides us with the set of equations

$$\begin{bmatrix} 26.667 & 5 \\ 5 & 14.167 \end{bmatrix} \begin{Bmatrix} T_2 \\ T_4 \end{Bmatrix} = \begin{Bmatrix} 15.1367 \\ 5.6763 \end{Bmatrix} \mathrm{MN}$$

with the solution $T_2 = 527.4\,\mathrm{kN}$, $T_4 = 214.5$ kN. In a similar way to example 25.1, we therefore get the longitudinal stresses $\sigma_0 = 5.07\,\mathrm{N/mm^2}$, $\sigma_2 = -0.67\,\mathrm{N/mm^2}$, $\sigma_4 = -0.89\,\mathrm{N/mm^2}$ given on the left of Fig. 25.5(e). This leads to curvatures of $(5.07 + 0.67)/(30 \cdot 1.5) = 0.127\,\mathrm{mrad/m}$ and $(0.89 - 0.67)/(30 \cdot 2.5) = 0.003\,\mathrm{mrad/m}$ at mid-span of plates 1 and 3, and therefore to corresponding deflections of $0.127 \cdot 20^2/\pi^2 = 5.17\,\mathrm{mm}$ and $0.003 \cdot 20^2/\pi^2 = 0.12\,\mathrm{mm}$, as shown on the left of Fig. 25.5(b).

The resulting value for the rotation of plates 3 and 7 is 2.481 mrad. In addition, we get rotations of $(4.5 \cdot 3 \cdot 4/\pi)/(3 \cdot 10.24) = 0.560$ mrad and $(2.5 \cdot 2.5 \cdot 4/\pi)/(3 \cdot 10.24) = 0.259$ mrad, as shown in Fig. 25.5(b), as a result of the load transfer in the transverse direction.

The figure on the left of Fig. 25.5(c) shows the variation in the transverse bending moments as a result of a moment of 1 at edges 4 and 6. The corresponding in-plane loads are given on the right of the figure. These lead to the moments $M_1 = (1/2) \cdot 20^2/\pi^2 = 20.264$ kNm/kN and $M_3 = (-5/6) \cdot 20^2/\pi^2 = -33.774$ kNm/kN. Eq. (25.1) provides us with the set of equations

$$\begin{bmatrix} 26.667 & 5 \\ 5 & 14.167 \end{bmatrix} \begin{Bmatrix} T_2 \\ T_4 \end{Bmatrix} = \begin{Bmatrix} 135.095 \\ -202.642 \end{Bmatrix}$$

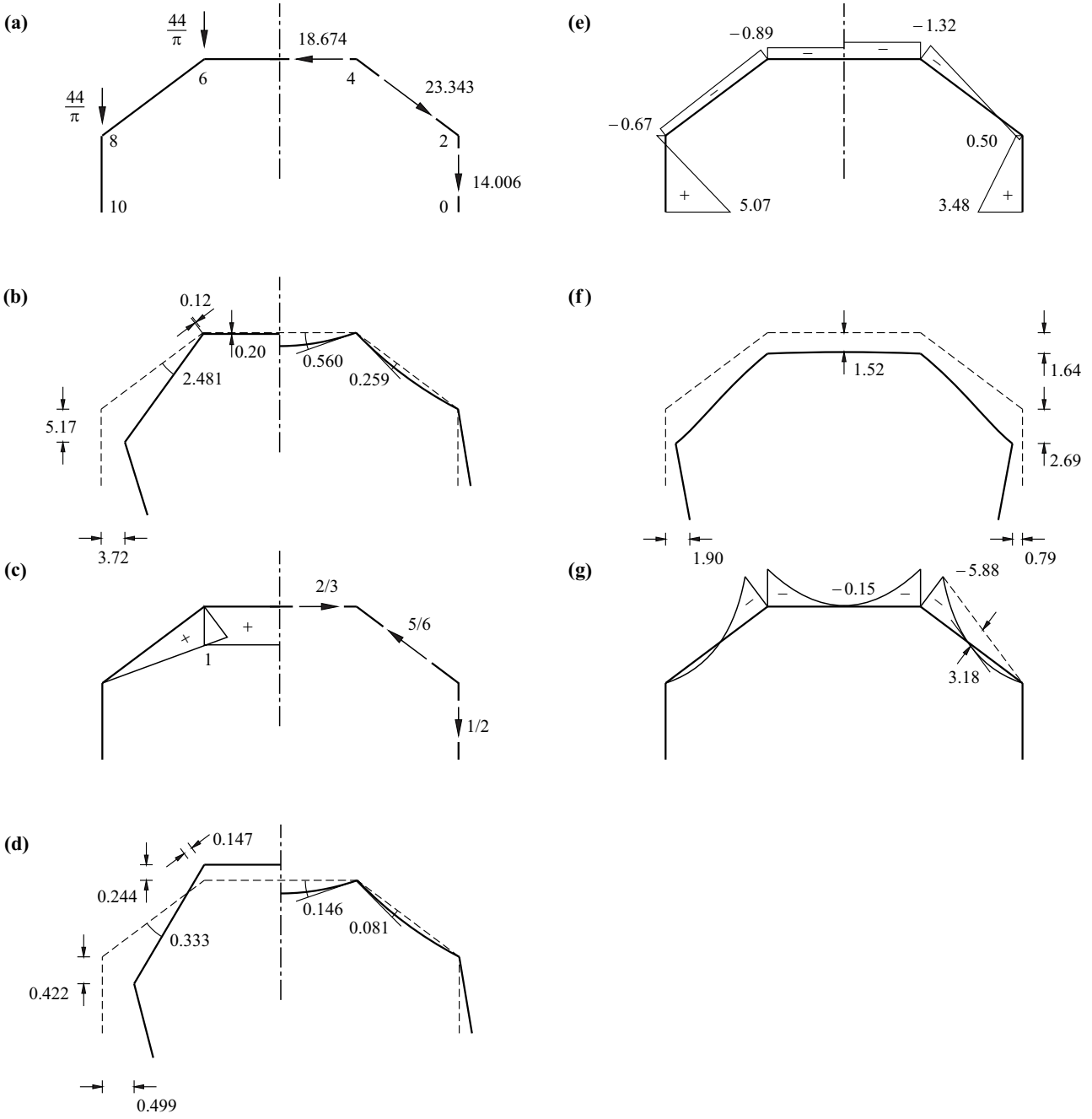

Fig. 25.5 Values at mid-span: (a) edge and in-plane loads [kN/m], (b) displacements [mm] and rotations [mrad] due to loads, (c) transverse bending moments [-] and in-plane loads [1/m] due to redundant variable = 1, (d) displacements [mm/kN] and rotations [mrad/kN] due to redundant variable = 1, (e) σ_x [N/mm^2], (f) displacements [mm], (g) transverse bending moments [kNm/m]

with the solution $T_2 = 8.297\,\text{kN/kN}$, $T_4 = -17.233\,\text{kN/kN}$, and from that we get the variables $\sigma_0 = 0.269\,(\text{N/mm}^2)/\text{kN}$, $\sigma_2 = -0.199\,(\text{N/mm}^2)/\text{kN}$ and $\sigma_4 = 0.072\,(\text{N/mm}^2)/\text{kN}$ describing a residual stresses state. The curvatures $(0.269 + 0.199)/(30 \cdot 1.5) = 0.0104$ mrad/kN and $-(0.072 + 0.199)/(30 \cdot 2.5) = -0.0036$ mrad/kN correspond to deflections of $0.0104 \cdot 20^2/\pi^2 = 0.422\,\text{mm/kN}$ and $-0.0036 \cdot 20^2/\pi^2 = -0.147\,\text{mm/kN}$ for plates 1 and 3, as shown on the left of Fig. 25.5(d). Plates 3 and 7 rotate through 0.333 mrad/kN. Added to this are the rotations $3/(2 \cdot 10.24) = 0.146\,\text{mrad/kN}$ and $2.5/(3 \cdot 10.24) = 0.081\,\text{mrad/kN}$ due to transverse bending of the slab, as shown on the right of Fig. 25.5(d).

According to (16.1), the statically indeterminate edge moment is

$$-\frac{2.481 + 0.560 + 0.259}{0.333 + 0.146 + 0.081} = -5.88\,\text{kNm/m}$$

We use superposition to get the longitudinal stress distribution at mid-span shown on the right of Fig. 25.5(e):

$$\sigma_0 = \quad 5.07 - 5.88 \cdot 0.269 = \quad 3.48\,\text{N/mm}^2$$

$$\sigma_2 = -0.67 + 5.88 \cdot 0.199 = \quad 0.50\,\text{N/mm}^2$$

$$\sigma_4 = -0.89 - 5.88 \cdot 0.072 = -1.32\,\text{N/mm}^2$$

Beam theory would result in a moment of $0.044 \cdot (4/\pi) \cdot 20^2/\pi^2 = 2.27\,\text{MNm}$ plus edge stresses of $2.27 \cdot 2.045/1.517 = 3.06\,\text{N/mm}^2$ at the bottom edge of the cross-section and $-3.06 \cdot 0.955/2.045 = -1.43\,\text{N/mm}^2$ at the level of plate 5. Comparing these values and those on the left of Fig. 25.5(e) reveals that the stresses according to bending theory lie between the results according to beam theory and those of membrane theory.

Fig. 25.5(f) illustrates the resulting displacements. Edge 4 undergoes a deflection of $0.20 + 5.88 \cdot 0.244 = 1.64\,\text{mm}$. Edge 2 deflects by $5.17 - 5.88 \cdot 0.422 = 2.69\,\text{mm}$ and experiences a horizontal inward deflection of $3.72 - 5.88 \cdot 0.499 = 0.79\,\text{mm}$. The resulting rotation at edge 4 is $-0.560 + 5.88 \cdot 0.146 = 0.30\,\text{mrad}$ clockwise, and at edge 2 that amounts to $2.481 - 5.88 \cdot 0.333 - 0.259 + 5.88 \cdot 0.081 = 0.74\,\text{mrad}$. Taking into account the transverse bending moments shown in Fig. 25.5(g), the resulting deflection at the centre of plate 5 is 1.52 mm.

Beam theory would result in a mid-span deflection of $0.044 \cdot (4/\pi) \cdot 20^4/(\pi^4 \cdot 1.517 \cdot 30) = 2.02\,\text{mm}$, and the transverse bending moment at edge 4 would be $-(79/28) \cdot (4/\pi) = -3.59\,\text{kNm/m}$. The deflections for plates 1 and 5 are somewhat larger and smaller respectively according to bending theory; however, the resulting deformation of the cross-section according to bending theory is associated with much larger negative transverse bending moments.

25.2.3 Commentary

According to bending theory, a barrel vault made up of n plates generally has $n-3$ redundant edge moments. As a result of the symmetry of both system and loading, this number can be further reduced as shown in example 25.2. It is easy to extend the procedure described with the help of example 25.2 (with the edge moments calculated according to the force method) to cover any barrel-vault roof. Higher terms of the FOURIER series can be considered for the loading if required.

As with membrane theory, bending theory also ignores the bending moments m_x and the twisting moments m_{xy}, where x = coordinate in the longitudinal direction and y = coordinate perpendicular to that in the respective plate plane. Apart from the bending moments m_y and the shear forces v_y, the other stress resultants that occur are the membrane forces n_x and n_{xy} and, as a secondary variable, n_y as well. The dimensioning for these stress resultants for folded plates of reinforced concrete can be carried out on the basis of section 24.3.2 (theory of thin plastic slabs or sandwich model).

The shallower the inclinations of the plates, the larger are the deflections of the free edges of barrel vaults and hence the associated transverse bending moments. Transverse stiffening in the form of transverse ribs or spreader bars may be necessary.

Deviation forces can be generated with the help of curved prestressing tendons to counteract the in-plane loads in the individual plates. Tensile membrane forces in the plates can therefore be reduced or avoided completely. However, the influence on the transverse bending is not so pronounced. In particular, the entire cantilever slab action remains in the perimeter plates because it is not possible to generate deviation forces perpendicular to the plane of the plate.

25.3 Non-prismatic folded plates

The huge variety of architectural design options for folded plates becomes really evident in non-prismatic structures. Simple models made of stiff paper or cardboard are helpful conceptual design aids when trying to assess the structural behaviour and the aesthetic effects. In most instances, the exploitation of the available symmetries and the skilful choice of free bodies enable crucial assertions regarding the structural response to be made just on the basis of relatively simple observations. Rough estimates at least of the principal force and deformation variables can therefore be made, and options for improving the design identified. The subsequent in-depth structural analysis, which is usually carried out with the help of the finite element method, should then essentially lead to the confirmation and refinement of the rough initial results.

25.4 Summary

1. The structural behaviour of folded plates is characterised by the interplay of slab and plate action. The edges act as (elastic) supports for the slabs that meet there.
2. Folded plates enable the realisation of a huge diversity of forms and corresponding architectural design options.
3. Simple paper or cardboard models are extremely helpful aids when trying to ascertain the structural behaviour of folded plates, assess their aesthetic effects and identify potential design improvements.
4. The examination of skilfully selected free bodies and the exploitation of available symmetries enable the principal force variables and their corresponding deformations to be estimated, at least roughly, even for complex cases.
5. The in-depth structural analysis of folded-plate structures is generally based on the finite element method.
6. Membrane theory together with eq. (25.1) permits an initial approximation of the force and deformation states of prismatic folded plates. According to bending theory, the introduction of statically redundant edge moments improves the results considerably. The longitudinal stresses are not usually distributed linearly over the cross-section because of the deformation of the folded plate cross-section.
7. The force and deformation states that become established according to beam theory – while presuming that the cross-sectional form is retained – can only occur approximately in slender folded plates with sufficient transverse bracing or lateral restraint.
8. The membrane forces occurring at the ends of folded plates must be resisted and transferred by solid or resolved end plates or sufficiently stiff transverse end frames.

25.5 Exercises

25.1 Use a conventional finite element program to analyse the barrel vault examined in examples 25.1 and 25.2. Compare the results of the calculations.

25.2 Investigate various options for extending sawtooth roofs or folded plates with a trapezoidal cross-section to form frames according to Fig. 25.1(e). Produce appropriate models and discuss the structural response (frame beam, frame corner and columns). Pay particular attention to the design of the columns, and discuss possibilities for including windows between the columns. Where should prestressing tendons be located and what advantages would they bring?

25.3 Discuss the principal flow of forces in the structure of Fig. 25.1(f) under the action of its self-weight. What types of constructional strengthening would be appropriate?

26 SHELLS

26.1 General

The term shell was introduced at the end of section 5.1.7 and the differential equation (5.51) for the thrust line was derived in section 5.3.2. The equation corresponds to a pure normal force action of bars curved in one plane and loaded in that plane. The hoop stress formula (5.52) for circular arcs with constant radial and negligible tangential loading resulted from this and was applied to two cylindrical shells in example 5.5. Annular structures rigid in shear were investigated in section 18.7. This work showed that edge disturbance problems in cylindrical shells can be simplified to the theory of beams in bending on an elastic foundation.

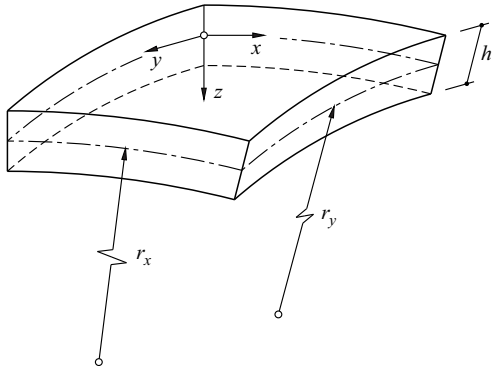

Fig. 26.1 Shell element with principal radii of curvature

If the axes x and y at one point on the middle surface of a shell, as shown in Fig. 26.1, are tangential to the lines of principal curvature, then where h = shell thickness and r_x and r_y = principal radii of curvature, the resulting stresses are

$$n_x = \int_{-h/2}^{h/2} \sigma_x \left(1 - \frac{z}{r_y}\right) \mathrm{d}z \quad , \quad n_y = \int_{-h/2}^{h/2} \sigma_y \left(1 - \frac{z}{r_x}\right) \mathrm{d}z \quad , \quad n_{xy} = \int_{-h/2}^{h/2} \tau_{xy} \left(1 - \frac{z}{r_x}\right) \mathrm{d}z$$

$$n_{yx} = \int_{-h/2}^{h/2} \tau_{yx} \left(1 - \frac{z}{r_y}\right) \mathrm{d}z$$

$$v_x = \int_{-h/2}^{h/2} \tau_{zx} \left(1 - \frac{z}{r_y}\right) \mathrm{d}z \quad , \quad v_y = \int_{-h/2}^{h/2} \tau_{zy} \left(1 - \frac{z}{r_x}\right) \mathrm{d}z$$

$$m_x = \int_{-h/2}^{h/2} \sigma_x z \left(1 - \frac{z}{r_y}\right) \mathrm{d}z \quad , \quad m_y = \int_{-h/2}^{h/2} \sigma_y z \left(1 - \frac{z}{r_x}\right) \mathrm{d}z \quad , \quad m_{xy} = \int_{-h/2}^{h/2} \tau_{xy} z \left(1 - \frac{z}{r_x}\right) \mathrm{d}z$$

$$m_{yx} = \int_{-h/2}^{h/2} \tau_{yx} z \left(1 - \frac{z}{r_y}\right) \mathrm{d}z \qquad (26.1)$$

As generally $r_x \neq r_y$, then $n_{xy} \neq n_{yx}$ and $m_{xy} \neq m_{yx}$, although $\tau_{xy} = \tau_{yx}$. However, the variables z/r_x and z/r_y for thin shells are very small, and (26.1) is simplified to the relationships (5.14) to (5.16).

The discussion below will be confined to thin shells rigid in shear. Taking this as our assumption, lines normal to the middle surface of the shell remain straight and perpendicular to the deformed middle surface; the shear forces v_x and v_y do not qualify as generalised stresses. We shall also assume linear elastic behaviour and so the relationships (8.35) and (8.43) apply for the membrane forces $n_x, n_y, n_{xy} = n_{yx}$ as well as the bending and twisting moments $m_x, m_y, m_{xy} = m_{yx}$.

Theory of Structures. First Edition. Peter Marti

The bending deformations can be ignored in many cases. The only unknowns that remain are the three membrane forces, which can be obtained from the equilibrium conditions when the loading on the shell is known, i. e. the problem is statically determinate.

The stress state described by *membrane theory* can only occur when the shell is supported at its edges in a manner compatible with a membrane. This is not usually fully possible, and the result is edge disturbances associated with bending deformations plus corresponding moments and shear forces. Similar incompatibilities can also occur within a shell, i. e. at abrupt changes in the loading intensity or the curvature or thickness of the shell. Furthermore, loads applied in concentrated form generally lead to bending deformations, and at flat points a shell can only act as a slab. Finally, bending will also have to be considered when the membrane deformation, although uninhibited, is so large that the curvatures can no longer be neglected. In all these cases, membrane theory must be replaced or supplemented by the more general *bending theory.*

The shells can be characterised with the GAUSSian curvature (total curvature)

$$K = \frac{1}{r_1 r_2} \tag{26.2}$$

where r_1, r_2 = principal radii of curvature, see section 24.1.3. *Elliptical* surfaces with $K > 0$ (e. g. dome-type shells) are very stiff when supported in a manner compatible with membranes. *Hyperbolic* surfaces with $K < 0$ (saddle forms) are less stiff and require some form of stiffening at the edges for stability. *Parabolic* surfaces in single curvature with $K = 0$ (cylindrical and conical forms) are developable and require frames or end plates to maintain their form, see section 25.2.

As with folded plates, the finite element method is mainly used for the structural analysis of shells these days. However, analytical solutions are still indispensable for acquiring a fundamental understanding of the structural behaviour of shells. A brief insight is provided below.

26.2 Membrane theory for surfaces of revolution

26.2.1 Symmetrical loading

26.2.1.1 Static relationships

Surfaces of revolution are created by rotating a planar curve, the *meridian*, about an axis lying in the *meridian plane*. A shell element is bounded by two parallels of latitude (x direction) and two adjacent meridians (y direction), see Fig. 26.2. The positions of the parallels of latitude and the meridians are measured with the angles φ and θ. The meridian plane (yz) and the plane perpendicular to this and to the shell element (xz) are the principal planes of curvature with the principal radii of curvature r_1 and r_2. The radius of the parallel of latitude is r_0. The dimensions of the sides of the shell element are $r_0 d\theta = r_2 \sin\varphi d\theta$ and $r_1 d\varphi$, and therefore the area of the element is $r_1 r_2 \sin\varphi d\varphi d\theta$.

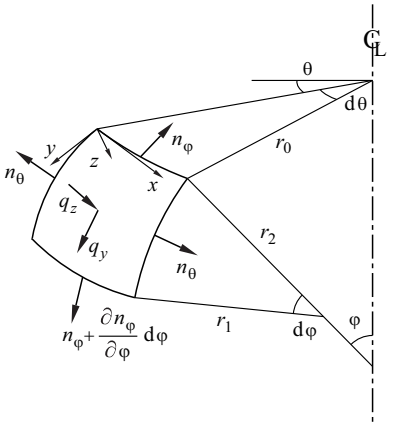

Fig. 26.2 Element of a symmetrically loaded surface of revolution

Only load components q_y, q_z in the meridian plane occur with symmetrical loading, and these are only dependent on φ. Moreover, $n_{\varphi\theta} = n_{\theta\varphi}$ must be equal to zero. The (principal) membrane forces n_φ, n_θ are likewise only dependent on φ.

Equilibrium in the z direction calls for

$$\frac{n_\varphi}{r_1} + \frac{n_\theta}{r_2} + q_z = 0 \tag{26.3}$$

A second equilibrium equation results from considering the free body above the parallel of latitude with radius $r_0 = r_2 \sin\varphi$ at point φ according to Fig. 26.3. Taking the resultant load R in the direction of the axis of rotation means that

$$2\pi r_0 n_\varphi \sin\varphi + R = 0$$

or rather

$$n_\varphi = -\frac{R}{2\pi r_2 \sin^2\varphi} \tag{26.4}$$

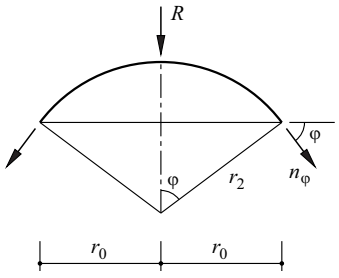

Fig. 26.3 Free body defined by φ or r_0

In contrast to an arch, which can be shaped according to the thrust line for one load case only, a shell forms a *thrust surface* for every loading. According to (26.3), the hoop forces n_θ are established in such a way that they are in equilibrium, with q_z and the meridian forces n_φ calculated with (26.4).

Example 26.1 Spherical shells

The spherical shell shown in Fig. 26.4(a), with $r_1 = r_2 = a$ and h = const, has a body load γ = const, i. e. $q_y = h\gamma\sin\varphi$, $q_z = h\gamma\cos\varphi$. The surface of the sphere above parallel of latitude φ is $2\pi a^2(1 - \cos\varphi)$, and therefore $R = 2\pi a^2 h\gamma(1 - \cos\varphi)$. Eq. (26.4) and (26.3) result in

$$n_\varphi = -\frac{ah\gamma}{1 + \cos\varphi} \quad , \quad n_\theta = -ah\gamma\left(\cos\varphi - \frac{1}{1 + \cos\varphi}\right)$$

Compression ($n_\varphi = -ah\gamma/2$ or $-ah\gamma$ for $\varphi = 0$ or $\pi/2$) always prevails along the meridians. Membrane force n_θ increases from the value $-ah\gamma/2$ at the crown ($\varphi = 0$) as φ increases and becomes positive when $\varphi > 51.8°$, i. e. we get tensile stresses.

Mounting the shell according to Fig. 26.4(b) on a supporting ring with axial stiffness EA generally results in a compatibility problem between the deformations of the supporting ring and those of the shell. The horizontal component of $n_\varphi(\varphi_1)$ must be resisted by the supporting ring. According to the hoop stress formula (5.52), the tensile force in the supporting ring is

$$T = a\sin\varphi_1 \cdot \frac{ah\gamma}{1 + \cos\varphi_1}\cos\varphi_1 = a^2 h\gamma\cot\varphi_1(1 - \cos\varphi_1)$$

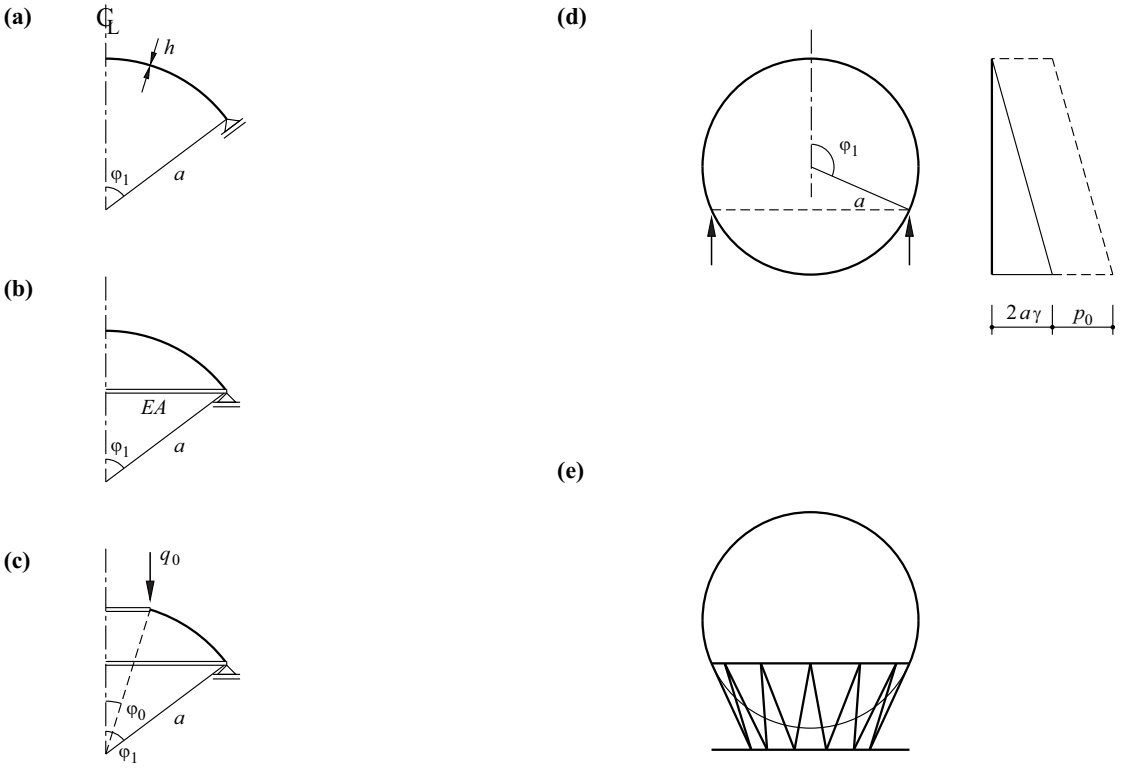

Fig. 26.4 Spherical shells: (a) membrane-compatible support, (b) supporting ring, (c) ring at crown, (d) spherical tank containing fluid (body load γ), (e) tangential support

which would correspond to a strain of $T/(EA)$. On the other hand, (8.35) results in the uninhibited perimeter strain

$$\varepsilon_\theta(\varphi_1) = \frac{n_\theta(\varphi_1) - \nu n_\varphi(\varphi_1)}{Eh} = \frac{a\gamma}{E}\left(\frac{1+\nu}{1+\cos\varphi_1} - \cos\varphi_1\right)$$

in the shell, which generally differs from $T/(EA)$. By applying a prestressing force P, it is possible to generate a strain of $-P/(EA)$ in the supporting ring and thus according to

$$\frac{-P+T}{EA} = \varepsilon_\theta(\varphi_1)$$

achieve at least approximate compatibility (exercise 26.1).

Including an opening with a perimeter ring according to Fig. 26.4(c) at the crown means that the line load q_0 results in a compressive force in this upper ring amounting to $C = q_0 a\cos\varphi_0$, and with

$$R = 2\pi a \sin\varphi_0 q_0 + 2\pi a^2 h\gamma(\cos\varphi_0 - \cos\varphi)$$

then (26.4) and (26.3) give us the membrane forces

$$n_\varphi = -\frac{ah\gamma(\cos\varphi_0 - \cos\varphi) + q_0 \sin\varphi_0}{\sin^2\varphi} \quad , \quad n_\theta = -n_\varphi - ah\gamma\cos\varphi$$

Example 26.2 Spherical tanks

The tank shown in Fig. 26.4(d) is filled with a fluid that creates a distributed load of

$$q_z = -p_0 - \gamma a(1 - \cos\varphi)$$

The pressure p_0 alone causes $n_\varphi = n_\theta = p_0 a/2$ according to (26.3) and is not considered any further here. The result for the component of q_z that exhibits a linear variation over the height is

$$n_\varphi = \frac{\gamma a^2}{6}\cdot\frac{1 + \cos\varphi - 2\cos^2\varphi}{1+\cos\varphi} \quad , \quad n_\theta = \frac{\gamma a^2}{6}\cdot\frac{5 - \cos\varphi - 4\cos^2\varphi}{1+\cos\varphi} \qquad (\varphi < \varphi_1)$$

and

$$n_\varphi = \frac{\gamma a^2}{6}\cdot\frac{5 - 5\cos\varphi + 2\cos^2\varphi}{1-\cos\varphi} \quad , \quad n_\theta = \frac{\gamma a^2}{6}\cdot\frac{1 - 7\cos\varphi + 4\cos^2\varphi}{1-\cos\varphi} \qquad (\varphi > \varphi_1)$$

We get tensile membrane forces only for $\varphi_1 \le 2\pi/3$, i. e. there is no risk of buckling. Both n_φ and n_θ exhibit an abrupt change at point φ_1 of the supporting ring; compatibility between the shell parts above and below the supporting ring must be achieved through local bending.

When only partly filled, there is a further edge disturbance problem because of the discontinuous loading.

Tangential support can improve the situation, as indicated in Fig. 26.4(e) (exercise 26.2).

Example 26.3 Conical shell

Let us consider the conical shell shown in Fig. 26.5(a), where $r_1 \to \infty$, $r_2 = r_0/\cos\alpha$ and $R = Q$. Putting $\varphi = \pi/2 - \alpha$, then (26.4) results in

$$n_\varphi = -\frac{Q}{2\pi r_0 \cos\alpha}$$

and (26.3) gives us $n_\theta = 0$ because $q_z = 0$.

Considering the shell under the action of its self-weight γh = const and assuming, similarly to Fig. 26.4(a), a form of support suitable for a membrane, then the result when $q_z = \gamma h\sin\alpha$ and $R = \pi r_0^2 h\gamma/\sin\alpha$ at the level of the parallel of latitude with radius r_0 is

$$n_\varphi = -\frac{r_0 h\gamma}{\sin(2\alpha)} \quad , \quad n_\theta = -r_0 h\gamma\tan\alpha$$

i. e. the stresses increase in proportion to the distance from the apex of the cone.

The tank shown in Fig. 26.5(b) is fully filled with a fluid (body load γ). Using (26.3) and (26.4) and taking into account $\varphi = \pi/2 + \alpha$, $r_0 = (b-\zeta)\tan\alpha$, $r_2 = r_0/\cos\alpha$, $r_1 \to \infty$, $q_z = -\gamma\zeta$ and

$$R = -\pi r_0^2\gamma[\zeta + (b-\zeta)/3]$$

results in the membrane forces

$$n_\varphi = \frac{\gamma(b+2\zeta)(b-\zeta)\tan\alpha}{6\cos\alpha} \quad , \quad n_\theta = \frac{\gamma\zeta(b-\zeta)\tan\alpha}{\cos\alpha}$$

The membrane forces vary parabolically over the height of the tank and reach maximum values at $\zeta = b/4$ and $\zeta = b/2$.

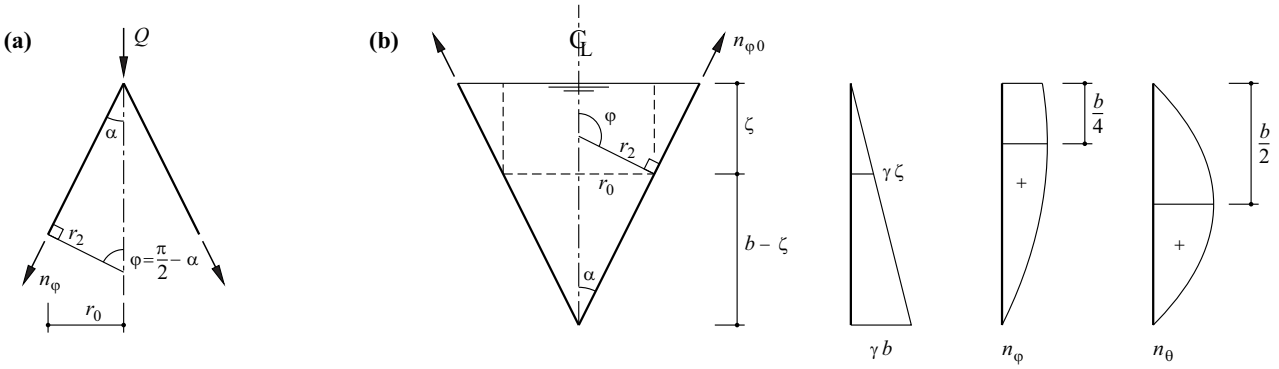

Fig. 26.5 Conical shells (a) point load at apex, (b) tank for fluids

26.2.1.2 Deformations

Referring to the notation introduced in Fig. 26.2, we get the displacements shown in Fig. 26.6 for the meridian plane. The consequence of w is that an element of length $r_1 d\varphi$ is shortened by $w d\varphi$. In addition, there is an increase in length of $(dv/d\varphi)d\varphi$, and therefore we get

$$\varepsilon_\varphi = \frac{1}{r_1} \cdot \frac{dv}{d\varphi} - \frac{w}{r_1} \tag{26.5}$$

The radius $r_0 = r_2 \sin\varphi$ of the parallel of latitude increases by $v\cos\varphi - w\sin\varphi$, i. e.

$$\varepsilon_\theta = \frac{v\cos\varphi - w\sin\varphi}{r_0} = \frac{v}{r_2}\cot\varphi - \frac{w}{r_2} \tag{26.6}$$

Eliminating w from (26.5) and (26.6) results in

$$\frac{dv}{d\varphi} - v\cot\varphi = r_1\varepsilon_\varphi - r_2\varepsilon_\theta$$

and putting

$$\varepsilon_\varphi = \frac{n_\varphi - \nu n_\theta}{Eh} \quad , \quad \varepsilon_\theta = \frac{n_\theta - \nu n_\varphi}{Eh}$$

according to (8.35), we then get

$$\frac{dv}{d\varphi} - v\cot\varphi = \frac{n_\varphi(r_1 + \nu r_2) - n_\theta(r_2 + \nu r_1)}{Eh} = f(\varphi) \tag{26.7}$$

The membrane forces $n_\varphi(\varphi)$ and $n_\theta(\varphi)$ can be determined from (26.3) and (26.4) in every case. The function $f(\varphi)$ on the right-hand side of (26.7) is thus known, and (26.7) can be integrated:

$$v = \sin\varphi\left[\int \frac{f(\varphi)}{\sin\varphi} d\varphi + C\right] \tag{26.8}$$

The integration constant C follows from the support conditions, and w follows from (26.6).

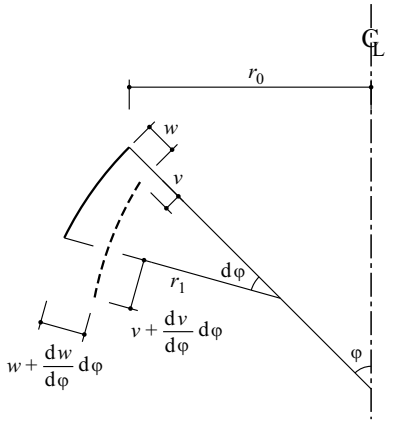

Fig. 26.6 Displacements in the meridian plane

Example 26.4 Spherical shell – dead load

The result for the spherical shell of example 26.1, with $r_1 = r_2 = a$ and subjected to a dead load γh, is

$$f(\varphi) = \frac{a^2\gamma(1+\nu)}{E}\left(\cos\varphi - \frac{2}{1+\cos\varphi}\right)$$

and (26.8) results in

$$v = \frac{a^2\gamma(1+\nu)}{E}\left[\sin\varphi \ln(1+\cos\varphi) - \frac{\sin\varphi}{1+\cos\varphi}\right] + C\sin\varphi$$

Constant C follows from the condition $v(\varphi_1) = 0$, see Fig. 26.4(a), and therefore the deformations are known.

As already discussed in example 26.1, $\varepsilon_\theta(\varphi_1)$ is known at the support and therefore it is easy to obtain $w(\varphi_1) = -a \cdot \varepsilon_\theta(\varphi_1)$ from (26.6).

26.2.2 Asymmetric loading

26.2.2.1 General relationships

Generally, the membrane forces n_φ, n_θ do not correspond to principal stresses, instead are accompanied by shear forces $n_{\varphi\theta} = n_{\theta\varphi}$. Equilibrium in the x and y directions for the element shown in Fig. 26.7 calls for

$$\frac{\partial n_\theta}{\partial \theta}\mathrm{d}\theta\, r_1\mathrm{d}\varphi + \frac{\partial (n_{\theta\varphi} r_0)}{\partial \varphi}\mathrm{d}\varphi\mathrm{d}\theta + n_{\varphi\theta} r_1 \mathrm{d}\varphi\, \mathrm{d}\theta \cos\varphi + q_x r_1 \mathrm{d}\varphi\, r_0 \mathrm{d}\theta = 0$$

$$\frac{\partial (n_\varphi r_0)}{\partial \varphi}\mathrm{d}\varphi\, \mathrm{d}\theta + \frac{\partial n_{\varphi\theta}}{\partial \theta}\mathrm{d}\theta\, r_1 \mathrm{d}\varphi - n_\theta r_1 \mathrm{d}\varphi\, \mathrm{d}\theta \cos\varphi + q_y r_1 \mathrm{d}\varphi\, r_0 \mathrm{d}\theta = 0$$

or rather

$$\begin{aligned} &\frac{\partial n_\theta}{\partial \theta} + \frac{1}{r_1}\cdot\frac{\partial (n_{\theta\varphi} r_0)}{\partial \varphi} + n_{\varphi\theta}\cos\varphi + q_x r_0 = 0 \\ &\frac{\partial n_{\varphi\theta}}{\partial \theta} + \frac{1}{r_1}\cdot\frac{\partial (n_\varphi r_0)}{\partial \varphi} - n_\theta \cos\varphi + q_y r_0 = 0 \end{aligned} \tag{26.9}$$

Relationship (26.3) still applies.

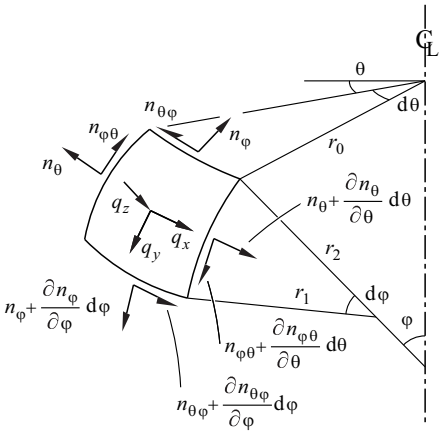

Fig. 26.7 Element of an asymmetrically loaded surface of revolution

According to (8.35), the following applies:

$$\varepsilon_\varphi = \frac{n_\varphi - \nu n_\theta}{Eh} \quad , \quad \varepsilon_\theta = \frac{n_\theta - \nu n_\varphi}{Eh} \quad , \quad \gamma_{\varphi\theta} = \frac{2(1+\nu) n_{\varphi\theta}}{Eh} \tag{26.10}$$

and (26.5) and (26.6) are generalised as follows:

$$\varepsilon_\varphi = \frac{1}{r_1}\cdot\frac{\partial v}{\partial \varphi} - \frac{w}{r_1} \quad , \quad \varepsilon_\theta = \frac{1}{r_0}\cdot\frac{\partial u}{\partial \theta} + \frac{v\cot\varphi}{r_2} - \frac{w}{r_2} \quad , \quad \gamma_{\varphi\theta} = \frac{1}{r_1}\cdot\frac{\partial u}{\partial \varphi} + \frac{1}{r_0}\cdot\frac{\partial v}{\partial \theta} \tag{26.11}$$

26.2.2.2 Wind pressure

Assuming

$$q_x = q_y = 0 \quad , \quad q_z = p\sin\varphi\cos\theta$$

then (26.9), taking into account (26.3) and $r_0 = r_2\sin\varphi$, results in the differential equations

$$\begin{aligned} &\frac{\partial n_{\varphi\theta}}{\partial \varphi} + \left(\frac{1}{r_0}\cdot\frac{\mathrm{d}r_0}{\mathrm{d}\varphi} + \frac{r_1}{r_2}\cdot\cot\varphi\right) n_{\varphi\theta} - \frac{1}{\sin\varphi}\cdot\frac{\partial n_\varphi}{\partial \theta} = -p r_1 \sin\theta \\ &\frac{\partial n_\varphi}{\partial \varphi} + \left(\frac{1}{r_0}\cdot\frac{\mathrm{d}r_0}{\mathrm{d}\varphi} + \cot\varphi\right) n_\varphi + \frac{r_1}{r_0}\cdot\frac{\partial n_{\varphi\theta}}{\partial \theta} = -p r_1 \cos\varphi\cos\theta \end{aligned} \tag{26.12}$$

for determining n_φ and $n_{\varphi\theta} = n_{\theta\varphi}$.

Example 26.5 Spherical shell – wind pressure

Taking a spherical shell with $r_1 = r_2 = a$, the two equations (26.12), with

$$n_\varphi = f(\varphi)\cdot\cos\varphi\cos\theta \quad , \quad n_{\varphi\theta} = f(\varphi)\cdot\sin\theta$$

lead to the linear differential equation

$$\frac{\mathrm{d}f}{\mathrm{d}\varphi} + 3f\cot\varphi = -pa$$

with the general solution

$$f = -\frac{pa}{3}\cdot\frac{\cos^3\varphi - 3\cos\varphi + C}{\sin^3\varphi}$$

In order to determine the integration constant C, we shall consider a hemisphere where $n_\varphi \equiv 0$ and $n_{\varphi\theta} = -paC\sin\theta/3$ at its base ($\varphi = \pi/2$). Equilibrium of forces in the direction of the diameter $\theta = 0$ at the base calls for

$$\int_0^{2\pi} n_{\varphi\theta}\sin\theta\, a\,\mathrm{d}\theta + \int_0^{2\pi}\int_0^{\pi/2} (p\sin\varphi\cos\theta)\sin\varphi\, a^2\sin\varphi\cos\theta\,\mathrm{d}\varphi\,\mathrm{d}\theta = 0$$

i. e.

$$-\frac{pa^2C}{3}\cdot\pi+pa^2\cdot\frac{2}{3}\cdot\pi=0$$

or rather $C = 2$. Taking (26.3) into account, the resulting membrane forces are therefore

$$n_\varphi=-\frac{pa\cos\theta(2\cos\varphi-3\cos^2\varphi+\cos^4\varphi)}{3\sin^3\varphi}$$

$$n_\theta=\frac{pa\cos\theta(2\cos\varphi-3\sin^2\varphi-2\cos^4\varphi)}{3\sin^3\varphi}$$

$$n_{\varphi\theta}=-\frac{pa\sin\theta(2-3\cos\varphi+\cos^3\varphi)}{3\sin^3\varphi}$$

Example 26.6 Conical shell – wind pressure

The conical shell shown in Fig. 26.8 is connected to a column at its apex; $r_1\to\infty$, $r_0 = y\sin\alpha$ and $r_2 = y\tan\alpha$. Putting $dy = r_1 d\varphi$, then $(26.12)_1$ gives us the differential equation

$$\frac{\partial n_{\varphi\theta}}{\partial y}+\frac{2n_{\varphi\theta}}{y}=-p\sin\theta$$

with the general solution

$$n_{\varphi\theta}=-\frac{1}{y^2}\left(\frac{py^3}{3}+C\right)\sin\theta$$

Integration constant C follows from the condition $n_{\varphi\theta} = 0$ at the free edge $y = l$ and is therefore $-pl^3/3$, which means that

$$n_{\varphi\theta}=\frac{p(l^3-y^3)}{3y^2}\sin\theta$$

Eq. $(26.12)_2$ results in

$$\frac{\partial n_\varphi}{\partial y}+\frac{n_\varphi}{y}+\frac{1}{y\sin\alpha}\cdot\frac{\partial n_{\varphi\theta}}{\partial\theta}=-p\sin\alpha\cos\theta$$

and therefore, taking into account the expression for $n_{\varphi\theta}$, we get the relationship

$$\frac{\partial n_\varphi}{\partial y}+\frac{n_\varphi}{y}=-p\left(\frac{l^3-y^3}{3y^3\sin\alpha}+\sin\alpha\right)\cos\theta$$

which is integrated to give us

$$n_\varphi=\frac{p\cos\theta}{\sin\alpha}\left(\frac{l^3-y^3}{3y^2}-\frac{l^2-y^2}{2y}\cos^2\alpha\right)$$

Finally, (26.3) results in

$$n_\theta=-py\sin\alpha\cos\theta$$

At the apex of the cone, n_φ and $n_{\varphi\theta}$ become infinitely large. In order to eliminate this singularity, the shell must be supported by a ring with a finite radius $r_0 = y\sin\alpha$.

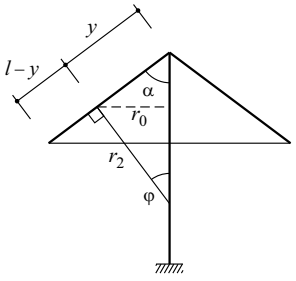

Fig. 26.8 Conical shell

26.3 Membrane theory for cylindrical shells

26.3.1 General relationships

Let us consider a cylinder with any cross-section parallel with the x axis. Fig. 26.9 shows an infinitesimal element of surface area $dx\cdot r d\varphi$ bounded by two generators (parallel with the x axis) and two profile lines (in the yz plane). Equilibrium demands

$$\frac{\partial n_x}{\partial x}dx\cdot r d\varphi+\frac{\partial n_{x\varphi}}{\partial\varphi}d\varphi\cdot dx+q_x\cdot dx\cdot r d\varphi=0$$

$$\frac{\partial n_{\varphi x}}{\partial x}dx\cdot r d\varphi+\frac{\partial n_\varphi}{\partial\varphi}d\varphi\cdot dx+q_y\cdot dx\cdot r d\varphi=0$$

$$n_\varphi dx\cdot d\varphi+q_z\cdot dx\cdot r d\varphi=0$$

or

$$\frac{\partial n_x}{\partial x}+\frac{1}{r}\cdot\frac{\partial n_{x\varphi}}{\partial\varphi}=-q_x\quad,\quad\frac{\partial n_{\varphi x}}{\partial x}+\frac{1}{r}\cdot\frac{\partial n_\varphi}{\partial\varphi}=-q_y\quad,\quad n_\varphi=-q_z r\qquad(26.13)$$

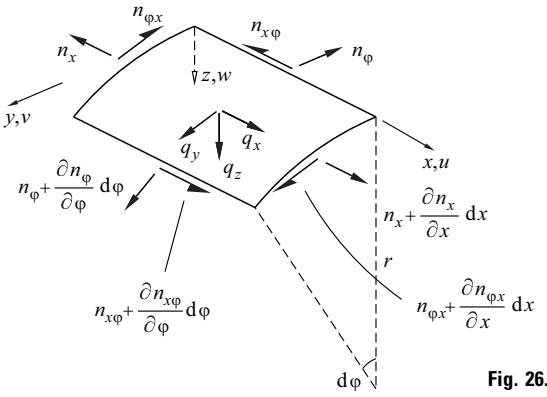

Fig. 26.9 Element of a cylindrical shell

The relationships (26.13) can be solved in succession. Eq. $(26.13)_3$ supplies n_φ and therefore we can use $(26.13)_2$ to give us the shear force $n_{\varphi x} = n_{x\varphi}$. Substituting in $(26.13)_1$ finally gives us n_x.

In a similar way to (26.10) and (26.11), we can find

$$\varepsilon_x = \frac{\partial u}{\partial x} = \frac{n_x - \nu n_\varphi}{Eh} \quad , \quad \varepsilon_\varphi = \frac{1}{r}\cdot\frac{\partial v}{\partial \varphi} - \frac{w}{r} = \frac{n_\varphi - \nu n_x}{Eh} \quad , \quad \gamma_{x\varphi} = \frac{1}{r}\cdot\frac{\partial u}{\partial \varphi} + \frac{\partial v}{\partial x} = \frac{2(1+\nu)n_{x\varphi}}{Eh} \tag{26.14}$$

Again, the relationships (26.14) can be solved one after the other by simple integration. Eq. $(26.14)_1$ provides u and therefore we can use $(26.14)_3$ to get the displacement v and, finally, w from $(26.14)_2$.

26.3.2 Pipes and barrel vaults

26.3.2.1 Cylindrical pipe filled with a fluid

The pressure on the wall of the pipe shown in Fig. 26.10 (radius a, wall thickness h) amounts to $q_z = -p_0 + \gamma a\cos\varphi$. When $q_x = q_y = 0$, eq. (26.13) gives us the membrane forces

$$n_\varphi = p_0 a - \gamma a^2\cos\varphi \quad , \quad n_{x\varphi} = -\gamma a x\sin\varphi \quad , \quad n_x = -\gamma(l^2/8 - x^2/2)\cos\varphi \tag{26.15}$$

The integration constants were chosen here in such a way that there is no torque acting on the pipe (no constant component in $n_{x\varphi}$, see section 13.4.3) and so that the normal stresses are equal to zero at the ends of the pipe, $n_x(\pm l/2) = 0$.

The membrane forces $n_{x\varphi}$ and n_x are proportional to the shear force $V = -\pi a^2\gamma x$, or rather the moment $M = \pi a^2\gamma(l^2/8 - x^2/2)$ for the simply supported beam of span l subjected to the uniformly distributed load $\pi a^2\gamma$. Using $I = \pi a^3 h$ and $S = a^2 h\sin\varphi$ allows us to determine $n_{\varphi x} = \tau_{\varphi x} h$ and $n_x = \sigma_x h$ as well via (13.37) or (13.16).

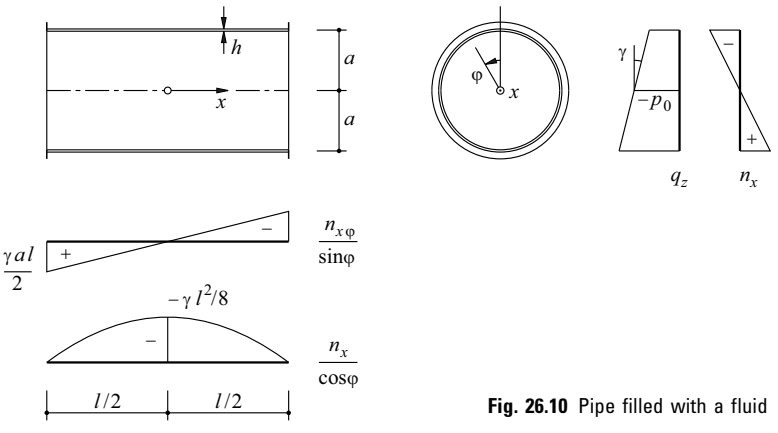

Fig. 26.10 Pipe filled with a fluid

We can use $(26.14)_1$ and (26.15), taking into account $u(x = 0) = 0$, to get

$$Ehu = -\nu p_0 a x + \gamma x\left(\nu a^2 - \frac{l^2}{8} + \frac{x^2}{6}\right)\cos\varphi \qquad (26.16)_1$$

Therefore, $(26.14)_3$, taking into account $v(x = \pm l/2) = 0$, gives us

$$Ehv = \frac{\gamma a}{8}(l^2 - 4x^2)\left(2 + \nu + \frac{5l^2 - 4x^2}{48a^2}\right)\sin\varphi \qquad (26.16)_2$$

and $(26.14)_2$ results in

$$Ehw = -p_0 a^2 + \gamma a^3\cos\varphi + \frac{\gamma a}{8}(l^2 - 4x^2)\left(2 + \frac{5l^2 - 4x^2}{48a^2}\right)\cos\varphi \qquad (26.16)_3$$

The following relationship applies for the simply supported beam subjected to the uniformly distributed load $\pi a^2\gamma$ according to example 15.1 with bending stiffness $EI = \pi a^3 hE$:

$$w = \frac{\gamma(l^2 - 4x^2)(5l^2 - 4x^2)}{384Eha}$$

The comparison with $(26.16)_2$ reveals that this expression agrees with $v(\varphi = \pm\pi/2)$ when the pipe is very slender $(l/a \to \infty)$.

The first two terms on the right in $(26.16)_3$ describe a dilatation, or rather a deformation of the cross-section at the ends of the pipe $x = \pm l/2$. The stiffening rings required there prevent these deformations and edge disturbances in the form of bending moments and shear forces occur.

26.3.2.2 Barrel vault subjected to dead load

Using (26.13) with

$$q_x = 0 \quad , \quad q_y = q\sin\varphi \quad , \quad q_z = q\cos\varphi$$

for the barrel vault shown in Fig. 26.11 results in the membrane forces

$$n_\varphi = -qa\cos\varphi \quad , \quad n_{x\varphi} = -2qx\sin\varphi \quad , \quad n_x = -\frac{q(l^2 - 4x^2)}{4a}\cos\varphi \qquad (26.17)$$

Perimeter members are necessary along the free edges $\varphi = \pm\pi/2$ in order to resist the edge shears $\mp 2qx$ that occur there, see Fig. 18.1(d). The edge member forces

$$\int_{-l/2}^{x} n_{x\varphi}\,\mathrm{d}x = q(l^2 - 4x^2)/4$$

are in equilibrium with the longitudinal compressive forces

$$\int_{0}^{\pi/2} n_x a\,\mathrm{d}\varphi = -q(l^2 - 4x^2)/4$$

in the two halves of the roof, and together they correspond to the moment

$$M = -\int_{-\pi/2}^{\pi/2} n_x a\cos\varphi\, a\,\mathrm{d}\varphi = \pi a q\frac{l^2 - 4x^2}{8}$$

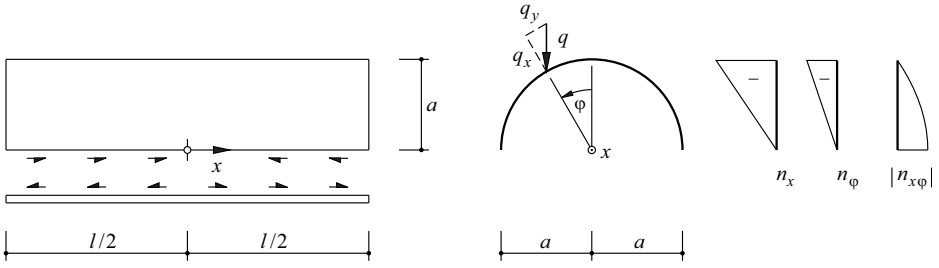

Fig. 26.11 Barrel vault subjected to dead load q [kN/m^2]

due to the line load πaq on the simply supported beam. Likewise, the membrane forces $n_{x\varphi}$ correspond to the shear force

$$V = \int_{-\pi/2}^{\pi/2} n_{\varphi x} \sin\varphi \, a \, d\varphi = -\pi aqx$$

on the simply supported beam.

Similarly to (26.16), we get the displacements

$$\begin{aligned} Ehu &= \frac{qx}{a}\left(\nu a^2 - \frac{l^2}{4} + \frac{x^2}{3}\right)\cos\varphi \\ Ehv &= \frac{q}{8}(l^2 - 4x^2)\left(4 + 3\nu + \frac{5l^2 - 4x^2}{24a^2}\right)\sin\varphi \\ Ehw &= qa^2\cos\varphi + \frac{q}{8}(l^2 - 4x^2)\left(4 + \nu + \frac{5l^2 - 4x^2}{24a^2}\right)\cos\varphi \end{aligned} \tag{26.18}$$

associated with (26.17).

26.3.3 Polygonal domes

Fig. 26.12(a) shows a dome in the form of cylindrical shell elements with generators parallel with the edges erected over a regular polygon with n corners. For reasons of symmetry, it is sufficient to consider just half OA_1B_1 of one sector when the loading exhibits the same symmetry as the structure. The ridge-type lines of intersection OB_1 between neighbouring sectors act as arch-type ribs. A perimeter beam is provided at the base A_1B_1 which functions in a similar way to the supporting ring shown in Fig. 26.4(b). There could be an opening with a (polygonal) ring in the centre of the dome similar to that of Fig. 26.4(c).

Using the surface load components q_z and q_y and noting that, for reasons of symmetry, $n_{\varphi x}$ has to disappear along OA, eq. (26.13) readily results in

$$n_\varphi = -q_z r \quad , \quad n_{x\varphi} = -x\left(q_y + \frac{1}{r}\cdot\frac{\partial n_\varphi}{\partial\varphi}\right) \tag{26.19}$$

The force in the rib S is inclined at an angle ψ to the horizontal plane xy_0, where

$$\tan\psi = \tan\varphi \cdot \cos\left(\frac{\pi}{n}\right) \tag{26.20}$$

see Fig. 26.12(b). Designating the resultant of the loads above section ABA′ in the z_0 direction with R in a similar way to Fig. 26.3 means that the following equilibrium condition applies:

$$\frac{R}{n} + S\sin\psi + 2x_\varphi n_\varphi \sin\varphi = 0 \tag{26.21}$$

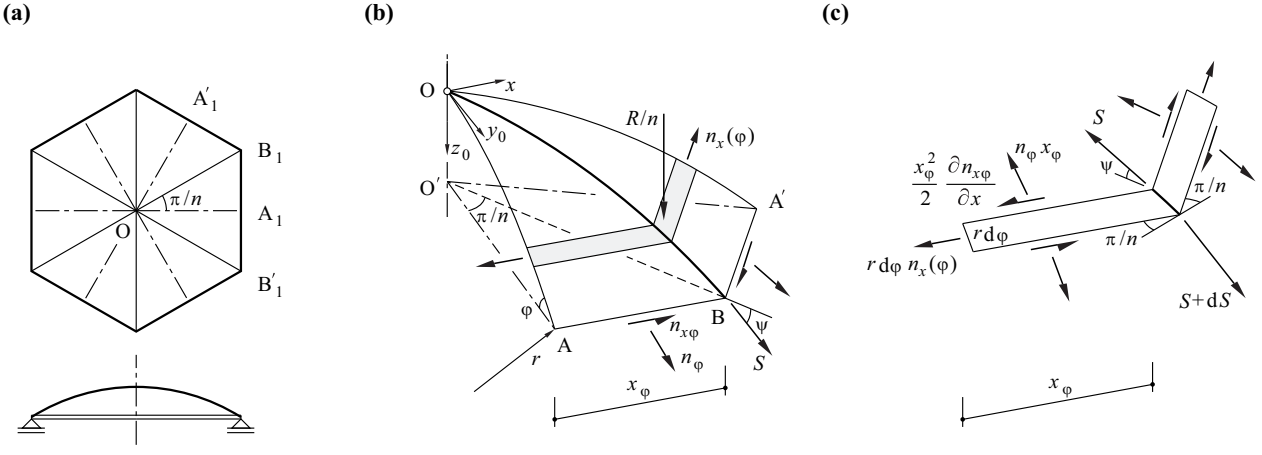

Fig. 26.12 Polygonal dome: (a) plan and section, (b) segment, (c) free body

The membrane forces $n_x(\varphi)$ required along OA in Fig. 26.12(b) can be determined via the equilibrium condition of the forces acting in direction O′B on the free body illustrated in Fig. 26.12(c):

$$-2r\mathrm{d}\varphi\sin\left(\frac{\pi}{n}\right)\cdot n_x(\varphi)+\mathrm{d}(S\cos\psi)+2\frac{\partial(n_\varphi x_\varphi\cos\varphi)}{\partial\varphi}\mathrm{d}\varphi\cos\left(\frac{\pi}{n}\right)+\frac{\partial\left(x_\varphi^2\dfrac{\partial n_{x\varphi}}{\partial x}\right)}{\partial\varphi}\mathrm{d}\varphi\sin\left(\frac{\pi}{n}\right)=0$$

or rather

$$n_x(\varphi)=\frac{\dfrac{\mathrm{d}(S\cos\psi)}{\mathrm{d}\varphi}}{2r\sin\left(\dfrac{\pi}{n}\right)}+\frac{\cot\left(\dfrac{\pi}{n}\right)}{r}\cdot\frac{\partial(n_\varphi x_\varphi\cos\varphi)}{\partial\varphi}+\frac{1}{2r}\cdot\frac{\partial\left(x_\varphi^2\dfrac{\partial n_{x\varphi}}{\partial x}\right)}{\partial\varphi}$$

Putting $\mathrm{d}x_\varphi = r\mathrm{d}\varphi\cos\varphi\tan(\pi/n)$ and using (26.20) plus (26.21) finally gives us

$$n_x(\varphi)=-\frac{\dfrac{\mathrm{d}(R\cot\varphi)}{\mathrm{d}\varphi}}{nr\sin\left(\dfrac{2\pi}{n}\right)}-\frac{\tan\left(\dfrac{\pi}{n}\right)}{r}\cdot\frac{\partial(n_\varphi x_\varphi\cos\varphi)}{\partial\varphi}+x_\varphi\cos\varphi\tan\left(\frac{\pi}{n}\right)\cdot\frac{\partial n_{x\varphi}}{\partial x}+\frac{x_\varphi^2}{2r}\cdot\frac{\partial^2 n_{x\varphi}}{\partial\varphi\partial x}\tag{26.22}$$

We have to add the result of $(26.13)_1$ and $(26.19)_2$ (where $q_x = 0$) to this value thus:

$$n_x=n_x(\varphi)+\frac{x^2}{2r}\cdot\frac{\mathrm{d}\left(q_y+\dfrac{1}{r}\cdot\dfrac{\partial n_\varphi}{\partial\varphi}\right)}{\mathrm{d}\varphi}\tag{26.23}$$

Example 26.7 Dome with circular cylindrical sectors – self-weight

Let us consider a dome made up of circular cylindrical sectors (radius a, shell thickness h, body load γ) subjected to its self-weight. Using

$q_y = \gamma h\sin\varphi \quad , \quad q_z = \gamma h\cos\varphi$

then (26.19) gives us

$n_\varphi = -ah\gamma\cos\varphi \quad , \quad n_{x\varphi} = -2hx\gamma\sin\varphi$

With $x_\varphi = a\sin\varphi\tan(\pi/n)$, then

$$R=2nah\gamma\int_0^\varphi x_\varphi\mathrm{d}\varphi=2n\gamma a^2h\tan\left(\frac{\pi}{n}\right)\cdot(1-\cos\varphi)$$

and (26.22) results in

$$n_x(\varphi)=ah\gamma\left[(1-6\sin^2\varphi)\cos\varphi\tan^2\left(\frac{\pi}{n}\right)+\frac{\sin^2\varphi-\cos\varphi}{(1+\cos\varphi)\cos^2\left(\dfrac{\pi}{n}\right)}\right]$$

Eq. (26.23) gives us

$$n_x=ah\gamma\left[\frac{x^2}{a^2}\cos\varphi+(1-6\sin^2\varphi)\cos\varphi\tan^2\left(\frac{\pi}{n}\right)+\frac{\sin^2\varphi-\cos\varphi}{(1+\cos\varphi)\cos^2\left(\dfrac{\pi}{n}\right)}\right]$$

and (26.21) results in the rib force

$$S=-2a^2h\gamma(1-\cos\varphi)(\sin^2\varphi-\cos\varphi)\frac{\tan\left(\dfrac{\pi}{n}\right)}{\sin\psi}$$

When $n\to\infty$, then n_x tends to the expression $ah\gamma(\sin^2\varphi-\cos\varphi)/(1+\cos\varphi)$ obtained in example 26.1 for n_θ, and $n_{x\varphi}$ disappears. In addition, $n_\varphi + S/(2x_\varphi)$ tends to the expression $-ah\gamma/(1+\cos\varphi)$ determined in example 26.1 for n_φ.

26.4 Membrane forces in shells of any form

26.4.1 Equilibrium conditions

Membrane theory for two special and frequently used types of shell – surfaces of revolution and cylindrical shells – was described in sections 26.2 and 26.3. The equilibrium conditions for shells of any form will now be developed in this section. The geometry of such shells is described by the function $z(x,y)$ with $\tan\alpha = \partial z/\partial x$ and $\tan\beta = \partial z/\partial y$, see Fig. 26.13.

The membrane forces n_x, n_y, n_{xy} at the shell element and their projections $\overline{n}_x$, $\overline{n}_y$, $\overline{n}_{xy}$ onto the xy plane are related by

$$n_x \cdot \frac{\mathrm{d}y}{\cos\beta} \cdot \cos\alpha = \overline{n}_x \mathrm{d}y \quad , \quad n_y \cdot \frac{\mathrm{d}x}{\cos\alpha} \cdot \cos\beta = \overline{n}_y \mathrm{d}x \quad , \quad n_{xy} \cdot \frac{\mathrm{d}x}{\cos\alpha} \cdot \cos\alpha = \overline{n}_{xy} \mathrm{d}x \quad , \quad n_{yx} \cdot \frac{\mathrm{d}y}{\cos\beta} \cdot \cos\beta = \overline{n}_{yx} \mathrm{d}y$$

or rather

$$n_x = \overline{n}_x \frac{\cos\beta}{\cos\alpha} \quad , \quad n_y = \overline{n}_y \frac{\cos\alpha}{\cos\beta} \quad , \quad n_{xy} = n_{yx} = \overline{n}_{xy} = \overline{n}_{yx} \tag{26.24}$$

With the surface area

$$\mathrm{d}A = \mathrm{d}x\mathrm{d}y\sqrt{1 + \tan^2\alpha + \tan^2\beta}$$

of the shell element, it is also the case that

$$\frac{\overline{q}_x}{q_x} = \frac{\overline{q}_y}{q_y} = \frac{\overline{q}_z}{q_z} = \frac{\mathrm{d}A}{\mathrm{d}x\mathrm{d}y} = \sqrt{1 + \tan^2\alpha + \tan^2\beta} \tag{26.25}$$

Equilibrium of the forces in the x and y directions calls for

$$\frac{\partial \overline{n}_x}{\partial x}\mathrm{d}x\mathrm{d}y + \frac{\partial \overline{n}_{xy}}{\partial y}\mathrm{d}y\mathrm{d}x + \overline{q}_x \mathrm{d}x\mathrm{d}y = 0$$

$$\frac{\partial \overline{n}_{yx}}{\partial x}\mathrm{d}x\mathrm{d}y + \frac{\partial \overline{n}_y}{\partial y}\mathrm{d}y\mathrm{d}x + \overline{q}_y \mathrm{d}x\mathrm{d}y = 0$$

or rather

$$\frac{\partial \overline{n}_x}{\partial x} + \frac{\partial \overline{n}_{xy}}{\partial y} + \overline{q}_x = 0 \quad , \quad \frac{\partial \overline{n}_{yx}}{\partial x} + \frac{\partial \overline{n}_y}{\partial y} + \overline{q}_y = 0 \tag{26.26}$$

The result in the z direction is

$$\frac{\partial}{\partial x}\left(\overline{n}_x \frac{\partial z}{\partial x}\right) + \frac{\partial}{\partial x}\left(\overline{n}_{yx} \frac{\partial z}{\partial y}\right) + \frac{\partial}{\partial y}\left(\overline{n}_y \frac{\partial z}{\partial y}\right) + \frac{\partial}{\partial y}\left(\overline{n}_{xy} \frac{\partial z}{\partial x}\right) + \overline{q}_z = 0$$

or rather

$$\overline{n}_x \frac{\partial^2 z}{\partial x^2} + 2\overline{n}_{xy} \frac{\partial^2 z}{\partial x \partial y} + \overline{n}_y \frac{\partial^2 z}{\partial y^2} = -\overline{q}_z - \left(\frac{\partial \overline{n}_x}{\partial x} + \frac{\partial \overline{n}_{xy}}{\partial y}\right)\frac{\partial z}{\partial x} - \left(\frac{\partial \overline{n}_{yx}}{\partial x} + \frac{\partial \overline{n}_y}{\partial y}\right)\frac{\partial z}{\partial y}$$

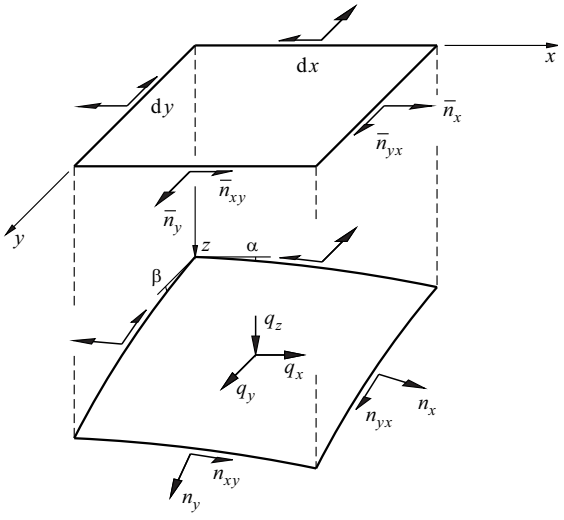

Fig. 26.13 Shell element and projection onto the *xy* plane

or when using (26.26), then

$$\overline{n}_x \frac{\partial^2 z}{\partial x^2} + 2\overline{n}_{xy} \frac{\partial^2 z}{\partial x \partial y} + \overline{n}_y \frac{\partial^2 z}{\partial y^2} = -\overline{q}_z + \overline{q}_x \frac{\partial z}{\partial x} + \overline{q}_y \frac{\partial z}{\partial y} \tag{26.27}$$

Introducing the stress function F where

$$\overline{n}_x = \frac{\partial^2 F}{\partial y^2} - \int \overline{q}_x \mathrm{d}x \quad , \quad \overline{n}_y = \frac{\partial^2 F}{\partial x^2} - \int \overline{q}_y \mathrm{d}y \quad , \quad \overline{n}_{xy} = -\frac{\partial^2 F}{\partial x \partial y} \tag{26.28}$$

enables both equations (26.26) to be satisfied, and (26.27) becomes

$$\frac{\partial^2 F}{\partial x^2}\frac{\partial^2 z}{\partial y^2} - 2\frac{\partial^2 F}{\partial x \partial y}\frac{\partial^2 z}{\partial x \partial y} + \frac{\partial^2 F}{\partial y^2}\frac{\partial^2 z}{\partial x^2} = -\overline{q}_z + \overline{q}_x \frac{\partial z}{\partial x} + \overline{q}_y \frac{\partial z}{\partial y} + \frac{\partial^2 z}{\partial x^2}\int \overline{q}_x \mathrm{d}x + \frac{\partial^2 z}{\partial y^2}\int \overline{q}_y \mathrm{d}y \tag{26.29}$$

26.4.2 Elliptical problems

As an example of an elliptical problem (positive GAUSSian curvature of the shell middle surface), we shall investigate the elliptical paraboloid shown in Fig. 26.14. This paraboloid has the equation

$$z = f_a \left(\frac{x}{a}\right)^2 + f_b \left(\frac{y}{b}\right)^2 \tag{26.30}$$

for its middle surface. Eq. (26.29) supplies the differential equation

$$\frac{f_b}{b^2} \cdot \frac{\partial^2 F}{\partial x^2} + \frac{f_a}{a^2} \cdot \frac{\partial^2 F}{\partial y^2} = -\frac{q}{2} \tag{26.31}$$

for the load case $\overline{q}_x = \overline{q}_y = 0$, $\overline{q}_z = q = \text{const}$. The boundary conditions $n_x = 0$ along $x = \pm a$ and $n_y = 0$ along $y = \pm b$ apply when we assume vertical supports to the edges, i. e. according to $(26.28)_1$ and $(26.28)_2$, the variation of F along the edges is at most linear in y or x. However, linear terms in x and y have no influence on the membrane forces and so F can be set to zero along the entire edge.

Eq. (26.31) and the boundary condition $F = 0$ along $y = \pm b$ are satisfied by

$$F = \frac{qa^2}{4f_a}(b^2 - y^2) + \sum_{n=1,3,\ldots}^{\infty} A_n \cosh\left(\frac{n\pi x}{c}\right) \cos\left(\frac{n\pi y}{2b}\right) \qquad \left(c^2 = \frac{4a^2 f_b}{f_a}\right)$$

The first term on the right in this expression can be developed into the following FOURIER series:

$$\frac{8qa^2b^2}{\pi^3 f_a} \sum_{n=1,3,\ldots}^{\infty} \frac{1}{n}(-1)^{(n-1)/2} \cdot \cos\left(\frac{n\pi y}{2b}\right)$$

The boundary condition $F = 0$ for $x = \pm a$ thus gives us the condition

$$\frac{8qa^2b^2}{\pi^3 n^3 f_a}(-1)^{(n-1)/2} + A_n \cosh\left(\frac{n\pi a}{c}\right) = 0$$

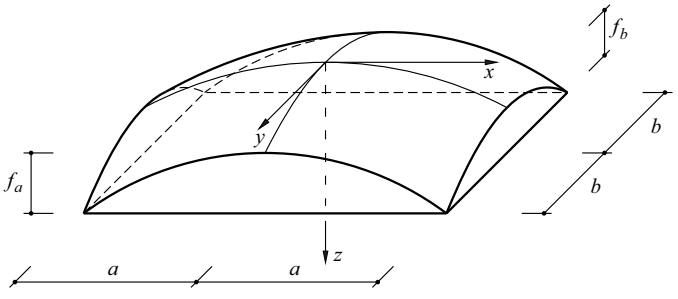

Fig. 26.14 Elliptical paraboloid

and therefore

$$F = \frac{qa^2}{4f_a}\left[b^2 - y^2 + \frac{32b^2}{\pi^3}\sum_{n=1,3,\ldots}^{\infty}(-1)^{(n+1)/2}\frac{\cosh\left(\frac{n\pi x}{c}\right)\cos\left(\frac{n\pi y}{2b}\right)}{n^3\cosh\left(\frac{n\pi a}{c}\right)}\right] \tag{26.32}$$

We can find the membrane forces n_x, n_y, n_{xy} via (26.28) and (26.24) (exercise 26.4).

Eq. (26.30) describes a *translation surface*. The two terms on the right correspond to planar curves $f(x)$ and $g(y)$. The surface $z(x,y)$ is obtained by translating one of the curves along one of the other curves. The boundary lines of a differential element therefore form a parallelogram, and the edge shear forces n_{xy} or n_{yx} are parallel, $\partial^2 z/(\partial x \partial y) = 0$, i. e. they do not contribute to equilibrium in the z direction, which is indicated by the fact that the second term of (26.29) is absent from the left side of (26.31). As $n_x = n_y = 0$ at the corners of the shell, n_{xy} theoretically tends to infinity at these points; in fact, this singularity results in considerable shear forces and corresponding moments at the corners.

26.4.3 Hyperbolic problems

26.4.3.1 Basic form

The surface shown in Fig. 26.15(a) has the equation

$$z = f\frac{xy}{ab} \tag{26.33}$$

Its generators are straight lines parallel with the edges and its twist is equal to $\partial^2 z/(\partial x \partial y) = f/(ab)$. For the load case $\overline{q}_x = \overline{q}_y = 0$, $\overline{q}_z = q = \text{const}$, (26.27) – in conjunction with $(26.24)_3$ – results in

$$n_{xy} = -\frac{qab}{2f} \tag{26.34}$$

Eq. $(26.28)_3$ supplies the stress function

$$F = \frac{qabxy}{2f} + f_1(x) + f_2(y)$$

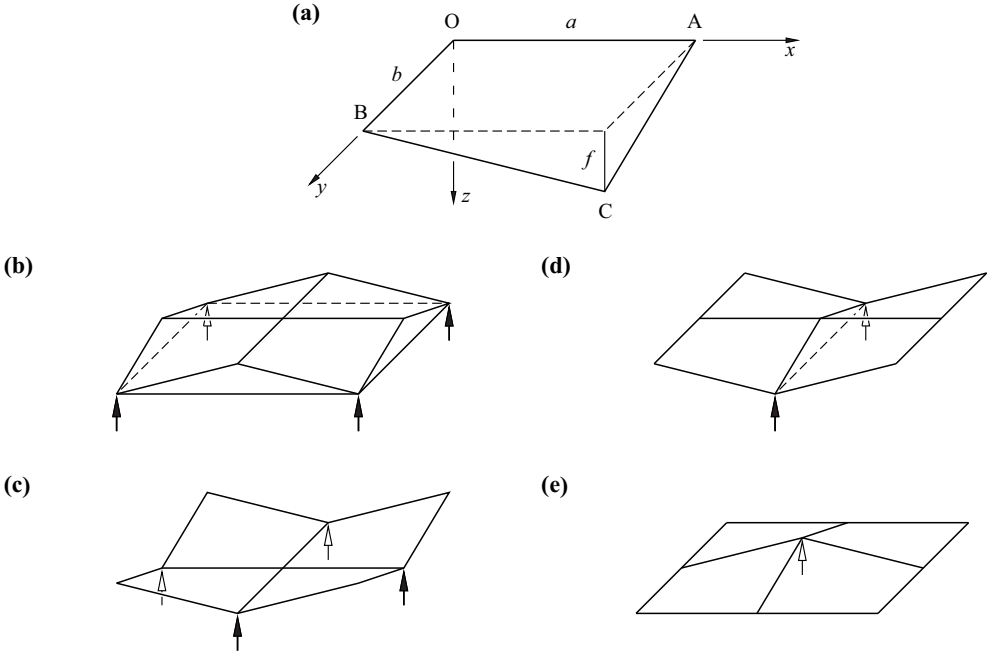

Fig. 26.15 Hyperbolic paraboloid: (a) basic form – edges parallel with generators, (b) to (e) combined forms

with two arbitrary functions f_1 and f_2. We can use $(26.28)_1$ and $(26.28)_2$ as well as $(26.24)_1$ and $(26.24)_2$ to arrive at

$$n_x = \sqrt{\frac{a^2b^2 + y^2f^2}{a^2b^2 + x^2f^2}} \cdot \frac{\mathrm{d}^2 f_2}{\mathrm{d}y^2} \quad , \quad n_y = \sqrt{\frac{a^2b^2 + x^2f^2}{a^2b^2 + y^2f^2}} \cdot \frac{\mathrm{d}^2 f_1}{\mathrm{d}x^2} \tag{26.35}$$

According to (26.34), n_{xy} is constant over the entire shell, and according to (26.35), $\overline{n}_x$ and $\overline{n}_y$ are constant along the generators. If we have $\overline{n}_x$ or $\overline{n}_y$ for one edge, the same value must occur at the opposite edge.

26.4.3.2 Combined forms

Fig. 26.15(b) shows a roof structure made up of four shells of the type shown in Fig. 26.15(a). Perimeter members must resist the shear forces n_{xy} along the edges according to (26.34). At a corner, the vertical components of the compressive forces in the two perimeter members are added together according to

$$\frac{qab}{2f}\left(\frac{f}{\sqrt{b^2+f^2}}\sqrt{b^2+f^2} + \frac{f}{\sqrt{a^2+f^2}}\sqrt{a^2+f^2}\right) = qab$$

to create vertical support forces. The corresponding horizontal components

$$\frac{qab}{2f} \cdot \frac{b}{\sqrt{b^2+f^2}}\sqrt{b^2+f^2} = \frac{qab^2}{2f} \quad , \quad \frac{qab}{2f} \cdot \frac{a}{\sqrt{a^2+f^2}}\sqrt{a^2+f^2} = \frac{qa^2b}{2f}$$

must be resisted by the ties joining the supports. Compressive forces from zero to the given values build up along the two gables from the edge to the centre of the roof; appropriate strengthening must be provided for these as well.

If we reverse the sign of the function $z(x,y)$, we then get the structure supported in the middle of each side drawn in Fig. 26.15(c). Again, the free edges function as compression members, but tensile forces with a linear variation ensue in the folds along the axes.

The form shown in Fig. 26.15(d) only requires two supports, which are connected by a tie. Tensile forces with a linear variation build up in the gable fold perpendicular to the tie, and the perimeter members experience compressive forces with a linear variation.

The structure shown in Fig. 26.15(e) – with just one support in the centre – has perimeter members in compression and folds in tension along the axes.

The loads of the perimeter members and the strengthening at the folds plus asymmetric loads cannot be handled via shell membrane forces alone. The very simple membrane stress state is only suitable for accommodating symmetric distributed loads $\overline{q}_z = q = \text{const}$. All deviations from that lead to bending stress resultants.

26.4.3.3 Hyperbolic paraboloid with edges parallel with the bisectors of the generators

The surface shown in Fig. 26.16 is described by

$$z = f_a\left(\frac{x}{a}\right)^2 - f_b\left(\frac{y}{b}\right)^2 \tag{26.36}$$

Eq. (26.29) supplies the differential equation

$$\frac{2f_b}{b^2} \cdot \frac{\partial^2 F}{\partial x^2} - \frac{2f_a}{a^2} \cdot \frac{\partial^2 F}{\partial y^2} = q \tag{26.37}$$

for the load case $\overline{q}_x = \overline{q}_y = 0$, $\overline{q}_z = q = \text{const}$, with the particular solutions

$$F_x = -\frac{qa^2y^2}{4f_a} \quad , \quad F_y = \frac{qb^2x^2}{4f_b} \tag{26.38}$$

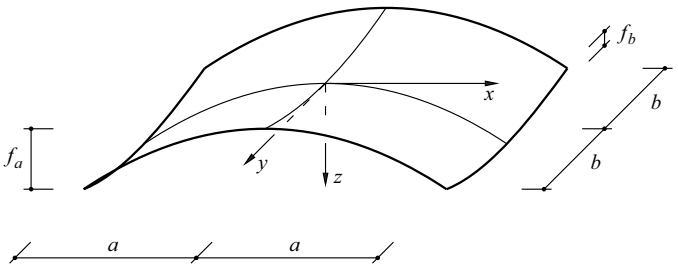

Fig. 26.16 Hyperbolic paraboloid – edges parallel with the bisectors of the generators

Fig. 26.17(a) illustrates the relationships between the second derivatives of $z(x,y)$ by means of a MOHR's circle. The curvature is equal to zero in the characteristic directions I and II inclined at an angle of

$$\alpha = \arctan\left(\frac{b}{a}\sqrt{\frac{f_a}{f_b}}\right) \tag{26.39}$$

to the principal direction x. The parallelogram-shaped network of characteristics (c = arbitrary constant) described by $y = c \mp x\tan\alpha$ corresponds to the projection of the (straight) generators of the shell surface onto the xy plane.

The shell element shown in Fig. 26.17(b) has been cut out parallel with the characteristics and forms a rhombus with side length 1 in the projection onto the xy plane. The loading $q\sin(2\alpha)$ is resisted by the shear forces s at the inclined edges of the element; the normal stresses in the characteristic directions do not contribute to equilibrium in the z direction because they pass directly through the element. Therefore,

$$4\overline{s}\left(\cos^2\alpha\frac{f_a}{a^2} + \sin^2\alpha\frac{f_b}{b^2}\right) = q\sin(2\alpha)$$

applies, or, when using (26.39), then

$$\overline{s} = \frac{qab}{4\sqrt{f_a f_b}} \tag{26.40}$$

Fig. 26.17(c) illustrates the corresponding basic stress state. Pure shear forces act on the surface elements parallel with the characteristics. The projected membrane forces $\overline{n}_x = -qa^2/(4f_a)$ and $\overline{n}_y = qb^2/(4f_b)$ are equal to half of the second derivatives of the expressions of (26.38), which means that half the load $(q/2)$ is carried via compressive arch action in the x direction and half via tensile arch action in the y direction.

Any forces in the characteristic directions can be superposed on the basic stress state without affecting equilibrium in the z direction. For example, the superposition of compressive stresses amounting to $q(a^2/f_a + b^2/f_b)/(8h)$ in the two characteristic directions (h = shell thickness) results in the stress state shown in Fig. 26.17(d), which corresponds to a pure compressive arch action in the x direction. The superposition of tensile stresses with an equal value changes the stress state from that shown in Fig. 26.17(c) to that shown in Fig. 26.17(e), which corresponds to pure tensile arch action in the y direction. Generally, we get a linear combination of the two states of Fig. 26.17(d) and (e) such that the associated load components add up to q.

According to (26.39), the generator starting at a corner of a shell intersects the opposite side of length $2a$ or $2b$ in Fig. 26.16, provided $f_a > f_b$ or $f_b > f_a$. In Fig. 26.18(a) it is assumed that $f_a > f_b$. The forces occurring at a point E on edge CD can be split into components in the direction of the characteristics EF and EI, and eliminated through superposition of the opposing forces. The incoming forces at F and I are superposed on the forces already present there. Superposing forces in the direction FG or IJ means it is possible to generate force resultants at F and I in the x or y direction as required. At G and J, the designer is free to choose the forces in direction GH or JK, too. However, the incoming forces at H and K cannot be influenced any further. In total, the transfer

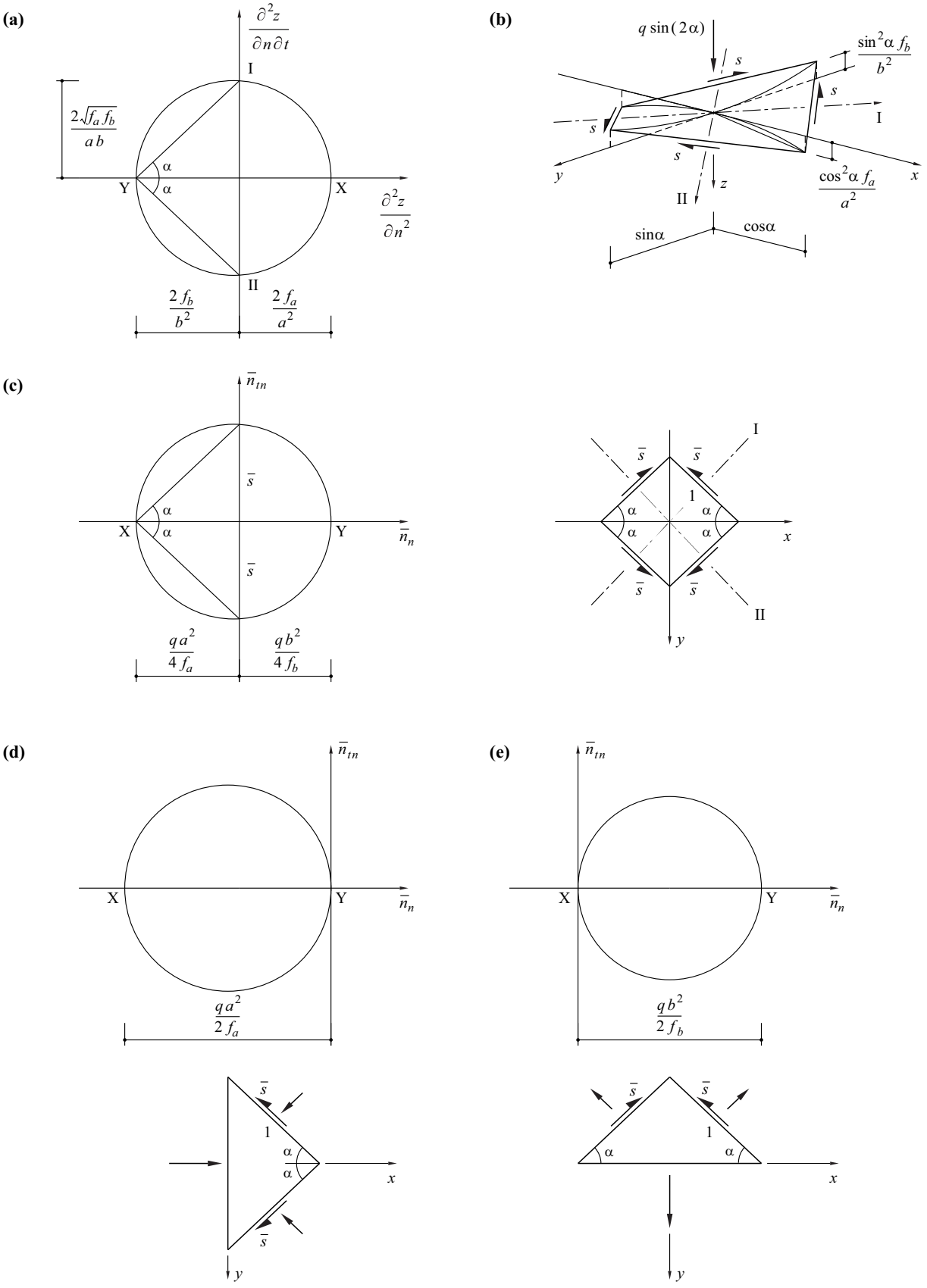

Fig. 26.17 Hyperbolic paraboloid: (a) characteristic directions, (b) shell element, (c) basic stress state, (d) compressive arch action in *x* direction, (e) tensile arch action in *y* direction

of the edge forces described here enables us to free edge CD and provide edges BC and DA with just simple supports, whereas it is necessary to resist forces in the x and y directions along AB.

As an example of an application, we shall consider shell ABCD shown in Fig. 26.18(b), where we will assume $f_a = 4f_b$, i. e. $\tan\alpha = 2b/a$, see (26.39). If we assume that the load $\overline{q}_z = q = \text{const}$ is primarily carried in the x direction, then according to $(26.38)_1$ and (26.28), we get $\overline{n}_x = -qa^2/(2f_a)$ and $\overline{n}_y = \overline{n}_{xy} = 0$ first of all. In order to free edge CD, in areas CDG and DCE we superpose two tensile stress fields inclined at an angle α to the x axis with projected membrane forces of $qa^2/(4f_a\cos^2\alpha)$, which results in the stress state $\overline{n}_y = qb^2/(2f_b)$, $\overline{n}_x = \overline{n}_{xy} = 0$ in area CDH. We want to allow only shear forces in the x direction at edges CG and DE and therefore in areas CGAE und DEBG we superpose two compressive stress fields inclined at an angle α to the x axis with projected membrane forces $qa^2/(4f_a\cos^2\alpha)$. This results in the stress state $\overline{n}_x = -qa^2/(2f_a)$, $\overline{n}_y = 0$, $\overline{n}_{xy} = -qab/[2(f_af_b)^{1/2}]$ in area CGH, whereas $\overline{n}_x = -qa^2/f_a$, $\overline{n}_y = -qb^2/(2f_b)$, $\overline{n}_{xy} = 0$ applies in area EFGH. Symmetry allows us to work out the stress state in the other areas with ease.

Referring to the example of Fig. 26.18(b), if we try to carry a load that is antisymmetric with respect to the x axis (e. g. $\overline{q}_z = q/2$ for $y > 0$ and $\overline{q}_z = -q/2$ for $y < 0$) with the help of membrane forces according to the above discussion, we will find out that this is impossible. On the other hand, we can see that this is possible when we choose a ratio of $f_a/f_b = 1$ instead of $f_a = 4f_b$. However, a shell modified in this way is not suitable for carrying symmetric loads ($\overline{q}_z = \text{const}$) via membrane forces. Generally, symmetric (antisymmetric) loads can theoretically be carried via pure membrane forces when $(f_a/f_b)^{1/2}$ is equal to an even (odd) number; however, in that scenario, antisymmetric (symmetric) loads cannot be carried via membrane forces.

The stress discontinuities connected with pure membrane force solutions, as shown in Fig. 26.18(b), correspond to incompatibilities in the deformations, which must be eliminated by way of local bending effects. This finding and the impossibility of pure membrane stress states – depending on the rise ratio – for symmetric or antisymmetric load cases shows that membrane theory can only serve as an approximation for saddle-type paraboloids and generally has to be supplemented by bending theory.

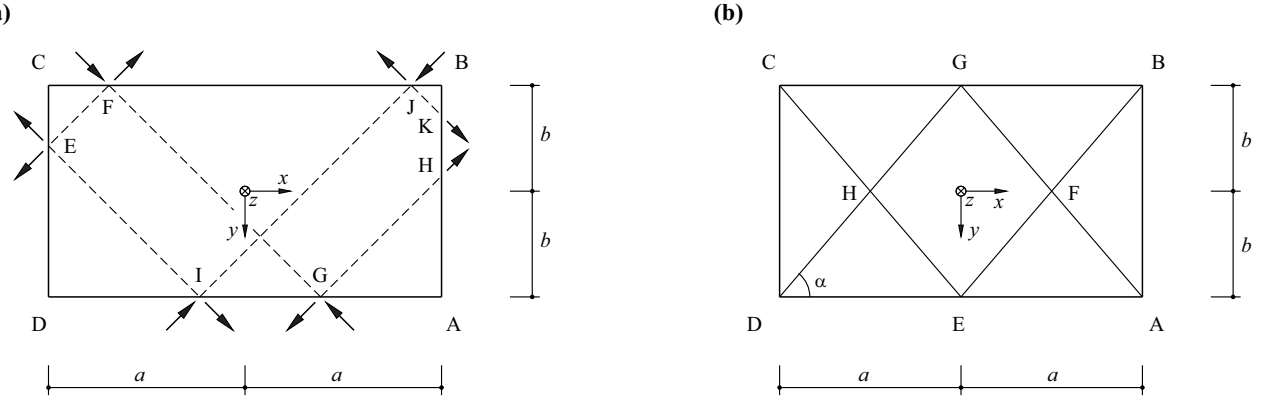

Fig. 26.18 Hyperbolic paraboloid: (a) transferring edge forces, (b) discontinuous stress field ($f_a = 4f_b$)

26.5 Bending theory for rotationally symmetric cylindrical shells

This section looks at rotationally symmetric cylindrical shells with radius a = const whose thickness h can generally vary along the cylinder axis x and which are loaded by compressive forces q_z in the radial direction only. Fig. 26.19 shows a differential shell element with the associated stress resultants. For reasons of symmetry, the shear forces v_φ, the membrane forces $n_{x\varphi} = n_{\varphi x}$ and the twisting moments $m_{x\varphi} = m_{\varphi x}$ disappear. The shear forces v_x, the membrane forces n_x and n_φ as well as the bending moments m_x and m_φ all depend on x only. The remaining non-trivial equilibrium conditions are the force-balance equations in the x and z directions as well as the moment-balance equation about the y axis, which result in

$$n_x = \text{const} \quad , \quad \frac{\mathrm{d}v_x}{\mathrm{d}x} + \frac{n_\varphi}{a} + q_z = 0 \quad , \quad \frac{\mathrm{d}m_x}{\mathrm{d}x} - v_x = 0 \tag{26.41}$$

According to $(26.41)_1$, we get n_x from the pure membrane stress state and do not need to consider this any further here, i. e. we can set n_x to zero. If necessary, it is also easy to calculate n_x for $q_x \neq 0$ as well using $(26.13)_1$.

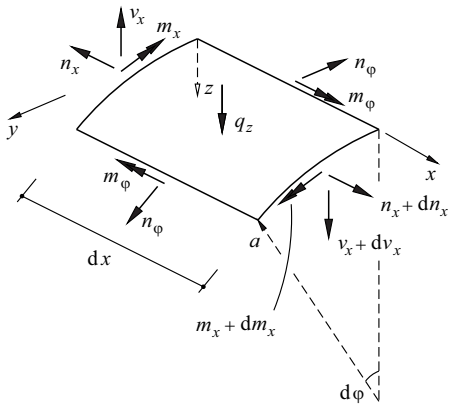

Fig. 26.19 Differential element of a rotationally symmetric cylindrical shell

The two equations $(26.41)_2$ and $(26.41)_3$ are not sufficient for determining the unknowns m_x, v_x and n_φ. Taking into account $n_x = 0$ and $\partial v/\partial\varphi = 0$, eq. $(26.14)_1$ and $(26.14)_2$ lead to

$$\frac{\mathrm{d}u}{\mathrm{d}x} = \frac{\nu w}{a} \quad , \quad n_\varphi = -\frac{Ehw}{a} \tag{26.42}$$

Owing to the rotational symmetry, only single curvature $\chi_x = -\mathrm{d}^2w/\mathrm{d}x^2$ can occur in the x direction, and therefore according to (8.43) and (8.48),

$$m_x = -D\frac{\mathrm{d}^2w}{\mathrm{d}x^2} \quad , \quad m_\varphi = \nu m_x \qquad \left[D = \frac{Eh^3}{12(1-\nu^2)}\right] \tag{26.43}$$

applies. Eliminating v_x enables $(26.41)_2$ and $(26.41)_3$ – taking into account $(26.42)_2$ and $(26.43)_1$ – to supply the differential equation

$$\frac{\mathrm{d}^2}{\mathrm{d}x^2}\left(D\frac{\mathrm{d}^2w}{\mathrm{d}x^2}\right) + \frac{Ehw}{a^2} = q_z \tag{26.44}$$

When h = const, this differential equation is simplified to

$$\frac{\mathrm{d}^4w}{\mathrm{d}x^4} + 4\beta^4 w = \frac{q_z}{D} \qquad \left[\beta^4 = \frac{3(1-\nu^2)}{a^2h^2}\right] \tag{26.45}$$

see (18.46) and (18.103). The general solution to (26.45) is made up of (18.49) and a particular solution $f(x)$.

Example 26.8 Pipe subjected to end loads

Let us consider the pipe shown in Fig. 26.20, where $f(x) = 0$ applies because $q_z = 0$. Moreover, the constants c_1 and c_2 in (18.49) must disappear because the forces v_0 and moments m_0 applied to the end of the pipe must have limited effects. So

$$w = \mathrm{e}^{-\beta x}[c_3\cos(\beta x) + c_4\sin(\beta x)]$$

The boundary conditions

$$m_x(x=0) = -D\left.\frac{\mathrm{d}^2w}{\mathrm{d}x^2}\right|_{x=0} = m_0 \quad , \quad v_x(x=0) = -D\left.\frac{\mathrm{d}^3w}{\mathrm{d}x^3}\right|_{x=0} = v_0$$

give rise to the constants

$$c_3 = -\frac{v_0 + \beta m_0}{2\beta^3 D} \quad , \quad c_4 = \frac{m_0}{2\beta^2 D}$$

The resulting relationships for the deflection and the slope of the deflection curve at the loaded end of the pipe are

$$w|_{x=0} = -\frac{v_0 + \beta m_0}{2\beta^3 D} \quad , \quad \left.\frac{\mathrm{d}w}{\mathrm{d}x}\right|_{x=0} = \frac{v_0 + 2\beta m_0}{2\beta^2 D}$$

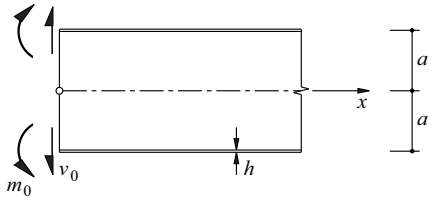

Fig. 26.20 Long pipe with end moment m_0 and end shear force v_0

Example 26.9 Cylindrical tank

The tank shown in Fig. 26.21 is free at the top and fixed at the bottom, and is loaded by the pressure

$$q_z = -\gamma(l-x)$$

of the fluid it contains. A suitable particular solution is the membrane solution

$$f(x) = -\frac{\gamma(l-x)a^2}{Eh}$$

according to $(18.99)_6$, which has the values

$$f\Big|_{x=0} = -\frac{\gamma a^2 l}{Eh} \quad , \quad \frac{\mathrm{d}f}{\mathrm{d}x}\Big|_{x=0} = \frac{\gamma a^2}{Eh}$$

that have to be eliminated by superposing end shear forces v_0 and end moments m_0 according to example 26.8. From

$$-\frac{v_0+\beta m_0}{2\beta^3 D} - \frac{\gamma a^2 l}{Eh} = 0 \quad , \quad \frac{v_0+2\beta m_0}{2\beta^2 D} + \frac{\gamma a^2}{Eh} = 0$$

it follows that

$$v_0 = -\frac{(2\beta l-1)\gamma a h}{\sqrt{12(1-\nu^2)}} \quad , \quad m_0 = \frac{\left(1-\frac{1}{\beta l}\right)\gamma a h l}{\sqrt{12(1-\nu^2)}}$$

and hence w and all other interesting variables are known from example 26.8 (exercise 26.8).

The condition of a free top edge is satisfied only approximately by the approach given here, i. e. when $x = l$, the result is generally small shear forces v_x and moments m_x. In order to satisfy the boundary conditions $v_x(l) = m_x(l) = 0$ exactly, we have to use the full formulation of (18.49) (exercise 26.9).

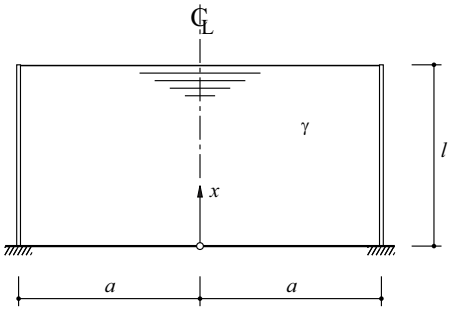

Fig. 26.21 Cylindrical tank (wall thickness h = const) completely filled with a fluid (body load γ)

Example 26.10 Pipe subjected to thermal action

A very long pipe free at its ends (radius a, wall thickness h, modulus of elasticity E, POISSON's ratio ν, coefficient of thermal expansion α_T) is subjected to a linear variation in temperature difference ΔT over its wall thickness. The corresponding uninhibited curvatures $\alpha_T \Delta T/h$ are fully inhibited outside the end regions, i. e. there are residual stress moments

$$m_x = m_\varphi = -\frac{Eh^3}{12(1-\nu)} \cdot \frac{\alpha_T \Delta T}{h} = -\frac{Eh^2 \alpha_T \Delta T}{12(1-\nu)}$$

according to (8.43), with corresponding boundary stresses of $\pm E\alpha_T \Delta T/[2(1-\nu)]$ at the outer and inner edges ($z = \mp h/2$).

In order to guarantee the condition of a free pipe end for $x = 0$, we superpose the moment

$$m_0 = \frac{Eh^2 \alpha_T \Delta T}{12(1-\nu)}$$

according to example 26.8, which results in

$$m_\varphi\Big|_{x=0} = \nu m_0 = \frac{\nu E h^2 \alpha_T \Delta T}{12(1-\nu)}$$

and by considering $(26.42)_2$ also gives us

$$n_\varphi\Big|_{x=0} = \frac{Eh}{a} \cdot \frac{m_0}{2\beta^2 D} = \frac{Eh\alpha_T \Delta T}{2\sqrt{3}} \cdot \sqrt{\frac{1+\nu}{1-\nu}}$$

The total result for $x = 0$ and $z = -h/2$ is the maximum stress

$$\sigma_\varphi = \frac{E\alpha_T \Delta T}{2}\left(1+\sqrt{\frac{1+\nu}{3(1-\nu)}}\right)$$

in the circumferential direction at the outer edge of the pipe. Putting $\nu = 0.2$ means that this stress exceeds the value outside of the end regions by 36.6 %; accordingly, cracks in the x direction may be expected, which propagate from the end of the pipe.

26.6 Bending theory for shallow shells

26.6.1 Basic concepts

26.6.1.1 Shell geometry and variables

In the vicinity of the origin, the geometry of shells with any curvature can be approximated by the quadratic function

$$z = \frac{x^2}{2} z_{,xx} + xy z_{,xy} + \frac{y^2}{2} z_{,yy} \tag{26.46}$$

The curvatures $z_{,xx} = \partial^2 z/\partial x^2$ and $z_{,yy} = \partial^2 z/\partial y^2$ plus the twist $z_{,xy} = \partial^2 z/(\partial x \partial y)$ form a symmetric tensor similar to (24.19). A MOHR's circle can be used to describe their transformation for a rotation of the system of coordinates.

The assumption of (26.46) is that the shell is shallow, i. e.

$$\left(\frac{\partial z}{\partial x}\right)^2 \ll 1 \quad , \quad \left(\frac{\partial z}{\partial y}\right)^2 \ll 1 \tag{26.47}$$

Consequently, $\cos\alpha \to 1$ and $\cos\beta \to 1$ apply for the angles in Fig. 26.13, and the difference between the real and the projected variables according to (26.24) and (26.25) no longer applies.

Based on Fig. 8.3, the behaviour of shallow shells is described by the variables

$$\boldsymbol{q} = \begin{Bmatrix} q_x \\ q_y \\ q_z \end{Bmatrix} \quad , \quad \boldsymbol{\sigma} = \begin{Bmatrix} n_x \\ n_y \\ n_{xy} \\ m_x \\ m_y \\ m_{xy} \end{Bmatrix} \quad , \quad \boldsymbol{\varepsilon} = \begin{Bmatrix} \varepsilon_x \\ \varepsilon_y \\ \gamma_{xy} \\ \chi_x \\ \chi_y \\ 2\chi_{xy} \end{Bmatrix} \quad , \quad \boldsymbol{u} = \begin{Bmatrix} u \\ v \\ w \end{Bmatrix}$$

see Fig. 26.22.

26.6.1.2 Kinematic relations

According to (26.5) and (26.6), we get strains in the middle surface amounting to $-w/r_1$ or $-w/r_2$ in the principal directions of curvature 1 and 2 of a shell because of the deflection w, where r_1 and r_2 are the principal radii of curvature. If axes x and y coincide with 1 and 2, then according to (26.46), $z_{,xx} = 1/r_1$ and $z_{,yy} = 1/r_2$, and therefore the contributions to ε_x or ε_y are $-wz_{,xx}$ and $-wz_{,yy}$. But if x and y are rotated with respect to 1 and 2, the contributions to ε_x, ε_y and $\gamma_{xy}/2$ are $-wz_{,xx}$, $-wz_{,yy}$ and $-wz_{,xy}$. Otherwise, (8.33) and (8.46) can be used. We get

$$\boldsymbol{\varepsilon} = \begin{Bmatrix} \varepsilon_x \\ \varepsilon_y \\ \gamma_{xy} \\ \chi_x \\ \chi_y \\ 2\chi_{xy} \end{Bmatrix} = \begin{bmatrix} \partial_x & 0 & -z_{,xx} \\ 0 & \partial_y & -z_{,yy} \\ \partial_y & \partial_x & -2z_{,xy} \\ 0 & 0 & -\partial_{xx} \\ 0 & 0 & -\partial_{yy} \\ 0 & 0 & -2\partial_{xy} \end{bmatrix} \begin{Bmatrix} u \\ v \\ w \end{Bmatrix} = \boldsymbol{D_k} \bullet \boldsymbol{u} \tag{26.48}$$

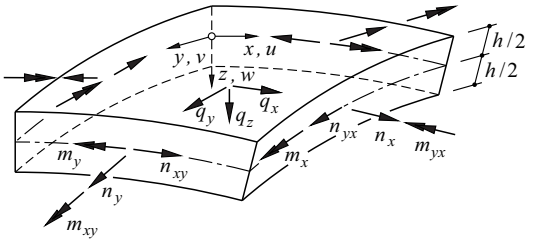

Fig. 26.22 Element of a shallow shell

26.6.1.3 Elasticity

Eq. (8.35) and (8.43) result in

$$\boldsymbol{\sigma} = \begin{Bmatrix} n_x \\ n_y \\ n_{xy} \\ m_x \\ m_y \\ m_{xy} \end{Bmatrix} = \frac{Eh}{1-\nu^2} \begin{bmatrix} 1 & \nu & 0 & 0 & 0 & 0 \\ \nu & 1 & 0 & 0 & 0 & 0 \\ 0 & 0 & \frac{1-\nu}{2} & 0 & 0 & 0 \\ 0 & 0 & 0 & \frac{h^2}{12} & \frac{\nu h^2}{12} & 0 \\ 0 & 0 & 0 & \frac{\nu h^2}{12} & \frac{h^2}{12} & 0 \\ 0 & 0 & 0 & 0 & 0 & \frac{h^2(1-\nu)}{24} \end{bmatrix} \begin{Bmatrix} \varepsilon_x \\ \varepsilon_y \\ \gamma_{xy} \\ \chi_x \\ \chi_y \\ 2\chi_{xy} \end{Bmatrix} = \boldsymbol{E} \bullet \boldsymbol{\varepsilon} \tag{26.49}$$

26.6.1.4 Equilibrium

Eq. (8.32) and (8.47), taking into account (26.27), result in

$$\boldsymbol{q} = \begin{Bmatrix} q_x \\ q_y \\ q_z \end{Bmatrix} = \begin{bmatrix} -\partial_x & 0 & -\partial_y & 0 & 0 & 0 \\ 0 & -\partial_y & -\partial_x & 0 & 0 & 0 \\ -z_{,xx} & -z_{,yy} & -2z_{,xy} & -\partial_{xx} & -\partial_{yy} & -2\partial_{xy} \end{bmatrix} \begin{Bmatrix} n_x \\ n_y \\ n_{xy} \\ m_x \\ m_y \\ m_{xy} \end{Bmatrix} = \boldsymbol{D_s} \bullet \boldsymbol{\sigma} \tag{26.50}$$

It should be noted here that the second and third terms on the right in (26.27) are dropped because according to Fig. 26.22, q_x and q_y, in contrast to Fig. 26.13, lie in the plane tangential to the middle surface of the shell.

26.6.2 Differential equation for deflection

Introducing the stress function F with

$$F_{,yy} = n_x + \int q_x \mathrm{d}x \quad , \quad F_{,xx} = n_y + \int q_y \mathrm{d}y \quad , \quad F_{,xy} = -n_{xy} \tag{26.51}$$

similarly to (26.28) means that the relationships for q_x and q_y in (26.50) are satisfied. The relationship for q_z, taking into account (8.48), results in

$$-\Gamma F + D\Delta\Delta w = q_z - z_{,xx}\int q_x \mathrm{d}x - z_{,yy}\int q_y \mathrm{d}y \tag{26.52}$$

where

$$\Gamma = z_{,xx}\partial_{yy} - 2z_{,xy}\partial_{xy} + z_{,yy}\partial_{xx} \tag{26.53}$$

designates the *shell operator* (PUCHER operator).

Eq. (26.52) contains – apart from the deflection w – the stress function F as a second unknown. In order to eliminate this, we start from the expression on the left of (24.23). Eq. (26.48) together with (26.53) results in

$$\varepsilon_{x,yy} + \varepsilon_{y,xx} - \gamma_{xy,xy} = -\Gamma w \tag{26.54}$$

Using the following relationships from (26.49) or (8.34):

$$\varepsilon_x = (n_x - \nu n_y)/(Eh) \quad , \quad \varepsilon_y = (n_y - \nu n_x)/(Eh) \quad , \quad \gamma_{xy} = 2(1+\nu)n_{xy}/(Eh)$$

and taking into account (26.51) gives us

$$\Delta\Delta F + Eh\Gamma w = \int q_{x,yy}\mathrm{d}x + \int q_{y,xx}\mathrm{d}y - \nu q_{x,x} - \nu q_{y,y} \tag{26.55}$$

Applying $\Delta\Delta$ to (26.52) and applying Γ to (26.55) followed by addition results in

$$D\Delta\Delta\Delta\Delta w + Eh\Gamma\Gamma w = \Delta\Delta q_z - \Delta\Delta(z_{,xx}\int q_x \mathrm{d}x + z_{,yy}\int q_y \mathrm{d}y) + \Gamma[\int q_{x,yy}\mathrm{d}x + \int q_{y,xx}\mathrm{d}y - \nu(q_{x,x} + q_{y,y})] \tag{26.56}$$

26.6.3 Circular cylindrical shells subjected to asymmetric loading

26.6.3.1 Differential equation

The cylindrical coordinates x, $\varphi = y/a$, z and $z_{,xx} = z_{,xy} = 0$ as well as $z_{,yy} = 1/a$ introduced in Fig. 26.19 mean that

$$\Gamma = \frac{\partial_{xx}}{a} \quad , \quad \Delta = \partial_{xx} + \frac{\partial_{\varphi\varphi}}{a^2}$$

applies, and (26.56) becomes

$$D\left(\partial_{xx} + \frac{\partial_{\varphi\varphi}}{a^2}\right)^4 w + \frac{Eh}{a^2}\frac{\partial^4 w}{\partial x^4} = \left(\partial_{xx} + \frac{\partial_{\varphi\varphi}}{a^2}\right)^2 q_z - \left(\partial_{xx} + \frac{\partial_{\varphi\varphi}}{a^2}\right)^2 \int q_\varphi \mathrm{d}\varphi + \frac{\partial_{xx}}{a}\left[\frac{1}{a^2}\int q_{x,\varphi\varphi}\mathrm{d}x + a\int q_{\varphi,xx}\mathrm{d}\varphi - \nu\left(q_{x,x} + \frac{q_{\varphi,\varphi}}{a}\right)\right] \tag{26.57}$$

Four boundary conditions per edge can be fitted to the solutions of the eighth-order differential equation (26.57). The four displacement variables u, v, w, $w_{,x}$ and the five force variables n_x, $n_{\varphi x}$, v_x, m_x, $m_{\varphi x}$ at a circular edge x = const can be considered for this, but on the other hand, u, v, w, $w_{,\varphi}/a$ and n_x, $n_{x\varphi}$, v_φ, m_φ, $m_{x\varphi}$ at a straight edge φ = const. As with slabs rigid in shear, the shear forces and the derivatives of the twisting moments parallel with the edge are combined to form edge shear forces

$$v_x + \frac{m_{\varphi x,\varphi}}{a} \quad , \quad v_\varphi + m_{x\varphi,x}$$

in order to reduce the number of edge force variables from five to four.

26.6.3.2 General solution to the homogeneous differential equation

The general solution $w(x, \varphi)$ to the homogeneous differential equation

$$D\Delta^4 w + \frac{Eh}{a^2} w_{,xxxx} = 0 \tag{26.58}$$

describes the edge disturbances in the cylindrical shell. According to (26.48) and (26.49), we get the moments

$$m_x = -D\left(w_{,xx} + \frac{\nu w_{,\varphi\varphi}}{a^2}\right) \quad , \quad m_\varphi = -D\left(\nu w_{,xx} + \frac{w_{,\varphi\varphi}}{a^2}\right) \quad , \quad m_{x\varphi} = -D(1-\nu)\frac{w_{,x\varphi}}{a} \tag{26.59}$$

from w, and according to (24.25), we get the shear forces

$$v_x = -D(\Delta w)_{,x} \quad , \quad v_\varphi = -\frac{D}{a}(\Delta w)_{,\varphi} \tag{26.60}$$

From the equilibrium condition

$$v_{x,x} + \frac{v_{\varphi,\varphi}}{a} - \frac{n_\varphi}{a} = 0$$

in the z direction it follows that

$$n_\varphi = -Da\Delta\Delta w \tag{26.61}_1$$

and hence, with the corresponding conditions according to (26.50) in the φ and x directions, in turn

$$n_{x\varphi} = D\int(\Delta\Delta w)_{,\varphi}\mathrm{d}x \quad , \quad n_x = -\frac{D}{a}\int\int(\Delta\Delta w)_{,\varphi\varphi}\mathrm{d}x^2 \tag{26.61}_{2,3}$$

Eq. (26.49) supplies

$$\varepsilon_x = \frac{n_x - \nu n_\varphi}{Eh} \quad , \quad \varepsilon_\varphi = \frac{n_\varphi - \nu n_x}{Eh}$$

and hence the result of (26.48) is

$$u = -\frac{h^2}{12(1-\nu^2)}\left[\frac{1}{a}\int\int\int(\Delta\Delta w)_{,\varphi\varphi}\mathrm{d}x^3 - \nu a\int\Delta\Delta w\,\mathrm{d}x\right]$$

$$v = -\frac{h^2}{12(1-\nu^2)}\left[a^2\int\Delta\Delta w\,\mathrm{d}\varphi - \nu\int\int(\Delta\Delta w)_{,\varphi})\mathrm{d}x^2\right] - \int w\,\mathrm{d}\varphi \tag{26.62}$$

26.6.3.3 Edge x = const

Load and displacement variables at circular edges x = const are developed into series of the following type:

$$\sum_n f(x)\cos(n\varphi)$$

Applying the corresponding formulation

$$w = e^{rx}\cos(n\varphi)$$

and using (26.58) gives us the characteristic equation

$$\left(r^2 - \frac{n^2}{a^2}\right)^4 + \frac{12(1-\nu^2)}{a^2h^2}r^4 = 0$$

whose eight roots can be presented in the form

$$\pm\frac{\beta}{2}\left[(1+\alpha) \pm i\left(1+\frac{1}{\alpha}\right)\right] \quad , \quad \pm\frac{\beta}{2}\left[(1-\alpha) \pm i\left(1-\frac{1}{\alpha}\right)\right]$$

where

$$\beta^4 = \frac{3(1-\nu^2)}{(ah)^2} \quad , \quad \alpha = \sqrt{\sqrt{\frac{4n^4}{a^4\beta^4}+1} + \frac{2n^2}{a^2\beta^2}} \quad , \quad \frac{1}{\alpha} = \sqrt{\sqrt{\frac{4n^4}{a^4\beta^4}+1} - \frac{2n^2}{a^2\beta^2}} \tag{26.63}$$

Therefore, the general solution is

$$\begin{aligned} w = \Bigg(& e^{(1+\alpha)\beta x/2}\left\{c_1\cos\left[\left(1+\frac{1}{\alpha}\right)\frac{\beta x}{2}\right] + c_2\sin\left[\left(1+\frac{1}{\alpha}\right)\frac{\beta x}{2}\right]\right\} \\ & + e^{-(1+\alpha)\beta x/2}\left\{c_3\cos\left[\left(1+\frac{1}{\alpha}\right)\frac{\beta x}{2}\right] + c_4\sin\left[\left(1+\frac{1}{\alpha}\right)\frac{\beta x}{2}\right]\right\} \\ & + e^{(1-\alpha)\beta x/2}\left\{c_5\cos\left[\left(1-\frac{1}{\alpha}\right)\frac{\beta x}{2}\right] + c_6\sin\left[\left(1-\frac{1}{\alpha}\right)\frac{\beta x}{2}\right]\right\} \\ & + e^{-(1-\alpha)\beta x/2}\left\{c_7\cos\left[\left(1-\frac{1}{\alpha}\right)\frac{\beta x}{2}\right] + c_8\sin\left[\left(1-\frac{1}{\alpha}\right)\frac{\beta x}{2}\right]\right\}\Bigg) \cdot \cos(n\varphi) \end{aligned} \tag{26.64}$$

onto which a particular solution to the inhomogeneous differential equation (26.57) has to be superposed. The coefficients c_1 to c_8 follow from the boundary conditions at two edges x = const.

Example 26.11 Chimney subjected to wind pressure

Let us consider a chimney (wall thickness h, radius $a \gg h$, height $l \gg a$, modulus of elasticity E, POISSON's ratio $\nu = 0$) fixed at its base ($x = 0$) which is subjected to a wind pressure

$$q_z = q_0 + q_1\cos\varphi + \sum_{n=2}^{\infty} q_n\cos(n\varphi)$$

constant over its height.

According to (26.45), the particular solution for the uniformly distributed load q_0 is $w = q_0a^2/(Eh)$, see $(18.99)_6$. Example 26.8 gives us the edge stress resultants

$$v_0 = \frac{q_0}{\beta} \quad , \quad m_0 = -\frac{q_0}{2\beta^2} \qquad \left[\frac{1}{\beta^2} = \frac{ah}{\sqrt{3}}\right]$$

from the boundary conditions $w(0) = w_{,x}(0) = 0$, and the result for the displacement w is

$$w = \frac{q_0a^2}{Eh}\left\{1 - e^{-\beta x}[\cos(\beta x) - \sin(\beta x)]\right\}$$

The membrane forces for the load component $q_z = q_1\cos\varphi$ are obtained from (26.13) with $q_x = q_y = 0$ and taking into account the boundary conditions $n_{x\varphi}(l) = n_x(l) = 0$:

$$n_\varphi = -aq_1\cos\varphi \quad , \quad n_{x\varphi} = q_1\sin\varphi(l-x) \quad , \quad n_x = q_1\cos\varphi(l-x)^2/(2a)$$

Eq. $(26.14)_1$ and $(26.14)_3$ with the boundary conditions $u(0) = v(0) = 0$ therefore result in

$$Ehu = q_1\cos\varphi\frac{x}{6a}(3l^2 - 3lx + x^2) \quad , \quad Ehv = q_1\sin\varphi\left[\frac{x^2}{24a^2}(6l^2 - 4lx + x^2) + 2lx - x^2\right]$$

Eq. $(26.14)_2$ gives us

$$w = v\cot\varphi + \frac{a^2 q_1 \cos\varphi}{Eh}$$

The second term on the right in this relationship is negligible with respect to the first one. According to $w = v\cot\varphi$, each ring of the chimney undergoes a rigid body displacement amounting to $v/\sin\varphi$ in the $\varphi = \pi$ direction.

The harmonic load components $q_z = q_n\cos(n\varphi)$ for $n \geq 2$ are in themselves in equilibrium, see section 18.7.3. The particular solution of (26.57)

$$w = \frac{q_n a^4}{Dn^4}\cos(n\varphi)$$

corresponds to these. The difference between this and $(18.100)_6$ is based on the fact that in contrast to $(26.50)_2$, the inclination of the shear forces was considered in the first of the three equilibrium conditions leading to (18.96). According to $(26.59)_2$ and $(26.60)_2$, the moments $m_\varphi = q_n(a/n)^2\cos(n\varphi)$ and the shear forces $v_\varphi = -q_n(a/n)\sin(n\varphi)$ belong to the particular solution. The equilibrium condition $v_{\varphi,\varphi}/a - n_\varphi/a + q_n\cos(n\varphi) = 0$ results in $n_\varphi = 0$. Consequently, as $\varepsilon_\varphi = v_{,\varphi}/a - w/a = 0$, we have the displacement

$$v = \frac{q_n a^4}{Dn^5}\sin(n\varphi)$$

Compare this with $(18.100)_5$ and note the reversed sign convention there for z, w and q_r.

As $l \gg a$, in order to satisfy the boundary conditions $u(0) = v(0) = w(0) = w_{,x}(0) = 0$ it is sufficient to consider the four terms with the coefficients c_3 to c_6 in (26.64). The coefficients c_1, c_2, c_7, c_8 concern the edge disturbances at the top of the chimney ($x = l$) and can be set to zero because the particular solution does not infringe the boundary conditions at that location. We also note that as $a \gg h$, the natural wavelength (18.54) of the functions connected with c_3 and c_4 is much smaller for the small values of n ($n = 2, 3$) interesting in this situation than that of the functions connected with c_5 and c_6, i. e. $(\alpha - 1)/(\alpha + 1) \ll 1$. Therefore, as an approximation, $c_3 = c_4 = 0$, and thus $w(0) = w_{,x}(0) = 0$ gives us the approximation $c_5 \approx -q_n a^4/(Dn^4) \approx c_6$.

26.6.3.4 Edge φ = const

Load and displacement variables at straight edges φ = const are developed into series of the following type:

$$\sum_n f(\varphi)\cos(n\pi x/l)$$

Applying the corresponding formulation

$$w = \mathrm{e}^{r\varphi}\cos\left(\frac{n\pi x}{l}\right)$$

and using (26.58) gives us the characteristic equation

$$\left(\frac{r^2}{a^2} - \frac{n^2\pi^2}{l^2}\right)^4 + \frac{12(1-\nu^2)n^4\pi^4}{a^2h^2l^4} = 0$$

whose eight roots can be presented in the form

$$\gamma\left(\pm\,\alpha_i \pm \frac{\mathrm{i}}{2\alpha_i}\right) \qquad (i = 1, 2)$$

where

$$\gamma = a\sqrt{\frac{n\pi\beta}{l}} \quad , \quad \beta^4 = \frac{3(1-\nu^2)}{(ah)^2} \quad , \quad \sqrt{2}\alpha_1 = \sqrt{\sqrt{1+\left(1+\frac{n\pi}{\beta l}\right)^2} + \left(1+\frac{n\pi}{\beta l}\right)} \quad , \quad \sqrt{2}\alpha_2 = \sqrt{\sqrt{1+\left(1-\frac{n\pi}{\beta l}\right)^2} - \left(1-\frac{n\pi}{\beta l}\right)} \tag{26.65}$$

Therefore, the general solution is

$$w = \left\{\mathrm{e}^{\alpha_1\gamma\varphi}\left[c_1\cos\left(\frac{\gamma\varphi}{2\alpha_1}\right) + c_2\sin\left(\frac{\gamma\varphi}{2\alpha_1}\right)\right] + \mathrm{e}^{-\alpha_1\gamma\varphi}\left[c_3\cos\left(\frac{\gamma\varphi}{2\alpha_1}\right) + c_4\sin\left(\frac{\gamma\varphi}{2\alpha_1}\right)\right]\right.$$
$$\left. + \mathrm{e}^{\alpha_2\gamma\varphi}\left[c_5\cos\left(\frac{\gamma\varphi}{2\alpha_2}\right) + c_6\sin\left(\frac{\gamma\varphi}{2\alpha_2}\right)\right] + \mathrm{e}^{-\alpha_2\gamma\varphi}\left[c_7\cos\left(\frac{\gamma\varphi}{2\alpha_2}\right) + c_8\sin\left(\frac{\gamma\varphi}{2\alpha_2}\right)\right]\right\} \cdot \cos\left(\frac{n\pi x}{l}\right) \tag{26.66}$$

The application of (26.66) is similar to that of (26.64) and is not pursued any further here.

26.7 Bending theory for symmetrically loaded surfaces of revolution

26.7.1 Basic concepts

Fig. 26.23 shows the shell element of Fig. 26.2 once again, but now with the addition of the (principal) moments m_θ, m_φ and the (principal) shear force v_φ. The principal radii of curvature have the same designations as in Fig. 26.1 (r_x and r_y). The coordinates given in Fig. 26.23 mean that $dx = r_x d\theta$ and $dy = r_y d\varphi$.

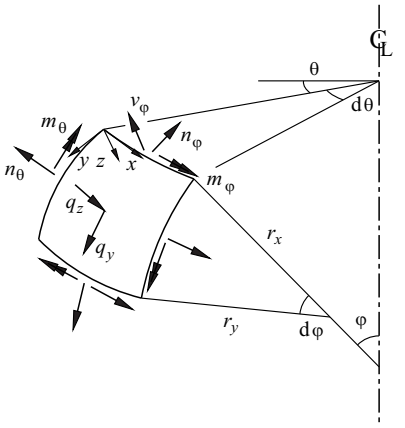

Fig. 26.23 Element of a symmetrically loaded surface of revolution

The potential edge disturbances according to section 26.2.1 are investigated below based on section 26.6. Rotational symmetry means that $q_x = 0$, $u = 0$ and $\partial_x = 0$. Moreover, the stress resultants n_{xy}, m_{xy} and the corresponding strains γ_{xy}, $2\chi_{xy}$ can be omitted. The remaining variables are

$$\boldsymbol{q} = \begin{Bmatrix} q_y \\ q_z \end{Bmatrix} \quad , \quad \boldsymbol{\sigma} = \begin{Bmatrix} n_\theta \\ n_\varphi \\ m_\theta \\ m_\varphi \end{Bmatrix} \quad , \quad \boldsymbol{\varepsilon} = \begin{Bmatrix} \varepsilon_\theta \\ \varepsilon_\varphi \\ \chi_\theta \\ \chi_\varphi \end{Bmatrix} \quad , \quad \boldsymbol{u} = \begin{Bmatrix} v \\ w \end{Bmatrix}$$

and we can use (26.48), (26.49) and (26.50) to obtain

$$\boldsymbol{\varepsilon} = \begin{Bmatrix} \varepsilon_\theta \\ \varepsilon_\varphi \\ \chi_\theta \\ \chi_\varphi \end{Bmatrix} = \begin{bmatrix} 0 & -\dfrac{1}{r_x} \\ \mathrm{d}_y & -\dfrac{1}{r_y} \\ 0 & 0 \\ 0 & -\mathrm{d}_y^2 \end{bmatrix} \begin{Bmatrix} v \\ w \end{Bmatrix} = \boldsymbol{D_k} \bullet \boldsymbol{u} \tag{26.67}$$

$$\boldsymbol{\sigma} = \begin{Bmatrix} n_\theta \\ n_\varphi \\ m_\theta \\ m_\varphi \end{Bmatrix} = \frac{Eh}{1-\nu^2} \begin{bmatrix} 1 & \nu & 0 & 0 \\ \nu & 1 & 0 & 0 \\ 0 & 0 & \dfrac{h^2}{12} & \dfrac{\nu h^2}{12} \\ 0 & 0 & \dfrac{\nu h^2}{12} & \dfrac{h^2}{12} \end{bmatrix} \begin{Bmatrix} \varepsilon_\theta \\ \varepsilon_\varphi \\ \chi_\theta \\ \chi_\varphi \end{Bmatrix} = \boldsymbol{E} \bullet \boldsymbol{\varepsilon} \tag{26.68}$$

and

$$\boldsymbol{q} = \begin{Bmatrix} q_y \\ q_z \end{Bmatrix} = \begin{bmatrix} 0 & -\mathrm{d}_y & 0 & 0 \\ -\dfrac{1}{r_x} & -\dfrac{1}{r_y} & 0 & -\mathrm{d}_y^2 \end{bmatrix} \begin{Bmatrix} n_\theta \\ n_\varphi \\ m_\theta \\ m_\varphi \end{Bmatrix} = \boldsymbol{D_s} \bullet \boldsymbol{\sigma} \tag{26.69}$$

26.7.2 Differential equation for deflection

It follows from $(26.69)_1$ that

$$n_\varphi = -\int q_y dy \tag{26.70}$$

and therefore $(26.69)_2$ is

$$-\frac{n_\theta}{r_x} - \frac{\mathrm{d}^2 m_\varphi}{\mathrm{d}y^2} = q_z - \frac{1}{r_y}\int q_y \mathrm{d}y \tag{26.71}$$

Eq. $(26.68)_1$ and $(26.68)_2$ result in

$$\varepsilon_\theta = (n_\theta - \nu n_\varphi)/(Eh) \quad , \quad \varepsilon_\varphi = (n_\varphi - \nu n_\theta)/(Eh) \tag{26.72}$$

Using $(26.67)_1$, $(26.72)_1$ and (26.70) therefore means that

$$n_\theta = -\frac{Ehw}{r_x} - \nu\int q_y \mathrm{d}y \tag{26.73}$$

applies, and we use $(26.67)_{3,4}$ and $(26.68)_{3,4}$ to obtain

$$m_\varphi = -D\frac{\mathrm{d}^2 w}{\mathrm{d}y^2} = \frac{m_\theta}{\nu} \qquad \left[D = \frac{Eh^3}{12(1-\nu^2)}\right] \tag{26.74}$$

Substituting (26.73) and (26.74) in (26.71) leads to

$$D\frac{\mathrm{d}^4 w}{\mathrm{d}y^4} + \frac{Eh}{r_x^2}w = q_z - \left(\frac{1}{r_y} + \frac{\nu}{r_x}\right)\int q_y \mathrm{d}y \tag{26.75}$$

The reader should also note that $(26.67)_2$, $(26.72)_2$, (26.70) and (26.73) result in

$$v = \left(\frac{1}{r_y} + \frac{\nu}{r_x}\right)\int w\,\mathrm{d}y - \frac{1-\nu^2}{Eh}\int\int q_y \mathrm{d}y^2 \tag{26.76}$$

and

$$v_\varphi = \frac{\mathrm{d}m_\varphi}{\mathrm{d}y} = -D\frac{\mathrm{d}^3 w}{\mathrm{d}y^3} \tag{26.77}$$

26.7.3 Spherical shells

In the case of spherical shells, $r_x = r_y = a$ = const. When $D/(Eh) = h^2/[12(1-\nu^2)]$ = const, the homogeneous part of (26.75), the only part of interest here, is simplified to the differential equation

$$\frac{\mathrm{d}^4 w}{\mathrm{d}y^4} + 4\beta^4 w = 0 \qquad \left[\beta^4 = \frac{3(1-\nu^2)}{a^2 h^2}\right]$$

with the general solution

$$w = \mathrm{e}^{\beta y}[c_1\cos(\beta y) + c_2\sin(\beta y)] + \mathrm{e}^{-\beta y}[c_3\cos(\beta y) + c_4\sin(\beta y)]$$

see (18.49) and (26.45).

Half the natural wavelength

$$\frac{\lambda}{2} = \frac{\pi}{\beta} = \frac{\pi\sqrt{ah}}{\sqrt[4]{3(1-\nu^2)}}$$

according to (18.54) is normally small when compared with the arc length $2a\varphi_1$ between two diametrically opposed edge elements (φ_1 = apex angle of shell, see Fig. 26.24). Therefore, in the expression for w we can confine ourselves to the terms containing c_3 and c_4. Consequently, apart from the direction of the shear force, we get a problem similar to example 26.8 (Fig. 26.20) for the edge force variables v_1 and m_1 plus the associated deflections w_1 and rotations ρ_1 entered in the upper part of Fig. 26.24. It is easy to use the solution developed in example 26.8 to arrive at

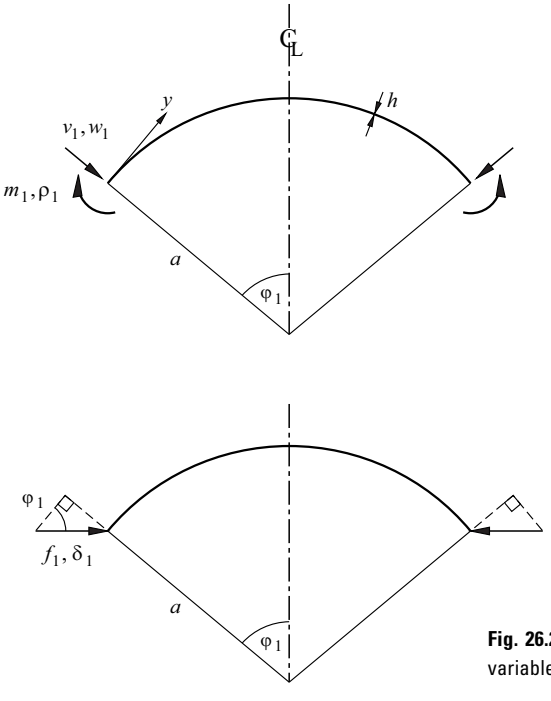

Fig. 26.24 Spherical shell subjected to edge force variables

$$\begin{Bmatrix} w_1 \\ \rho_1 \end{Bmatrix} = \frac{1}{D} \begin{bmatrix} \frac{1}{2\beta^3} & -\frac{1}{2\beta^2} \\ -\frac{1}{2\beta^2} & \frac{1}{\beta} \end{bmatrix} \begin{Bmatrix} v_1 \\ m_1 \end{Bmatrix} \tag{26.78}$$

and

$$w = \mathrm{e}^{-\beta y} \left[\frac{v_1 - \beta m_1}{2\beta^3 D} \cos(\beta y) + \frac{m_1}{2\beta^2 D} \sin(\beta y) \right] \tag{26.79}$$

Using the variables f_1, δ_1 entered in the lower part of Fig. 26.24 instead of v_1, w_1 results in

$$\begin{Bmatrix} \delta_1 \\ \rho_1 \end{Bmatrix} = \frac{1}{D} \begin{bmatrix} \frac{\sin^2\varphi_1}{2\beta^3} & -\frac{\sin\varphi_1}{2\beta^2} \\ -\frac{\sin\varphi_1}{2\beta^2} & \frac{1}{\beta} \end{bmatrix} \begin{Bmatrix} f_1 \\ m_1 \end{Bmatrix} \tag{26.80}$$

instead of (26.78).

Example 26.12 Fixed spherical shell subjected to internal pressure

We can use (26.3), with $r_1 = r_2 = a$, to obtain the membrane forces $n_\theta = n_\varphi = pa/2$ in a fixed spherical shell (Fig. 26.25) subjected to a constant internal pressure $q_z = -p$ by taking into account the symmetry at the crown ($\varphi = 0$). According to (26.72), this leads to an isotropic normal strain of $pa(1 - \nu)/(2Eh)$. At the edge of the shell (supported appropriately for a membrane), we therefore get an outward displacement of $\delta_1 = -pa^2(1 - \nu)\sin\varphi_1/(2Eh)$, but no rotation, i. e. $\rho_1 = 0$. In order to achieve $\delta_1 = 0$, we need the edge force variables

$$f_1 = \frac{p(1-\nu)}{2\beta \sin\varphi_1} \quad , \quad m_1 = \frac{f_1 \sin\varphi_1}{2\beta} = \frac{p(1-\nu)}{4\beta^2}$$

according to (26.80). Using these values and taking account of $v_1 = f_1 \sin\varphi_1$ plus (26.79), (26.73), (26.74) and (26.77) enables the calculation of the stress resultants n_θ, m_φ and v_φ (exercise 26.12).

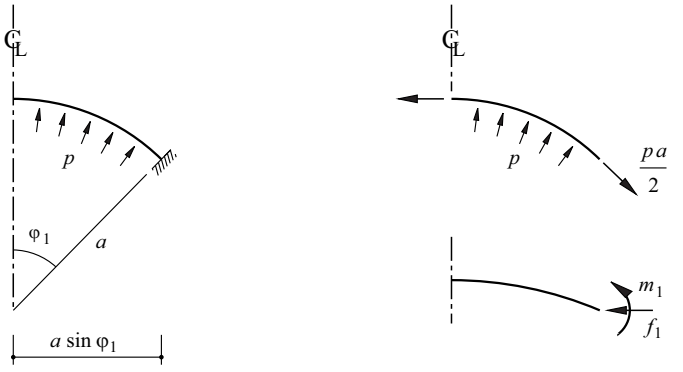

Fig. 26.25 Fixed spherical shell subjected to internal pressure p = const

Example 26.13 Pressure vessel

The pressure vessel shown in Fig. 26.26 consists of the hemispherical shell AB mounted on top of the cylindrical shell BC, see Fig. 5.28(b). Subjected to the internal pressure p = const, the membrane forces in the dome part according to example 26.12 are $n_\theta = n_\varphi = pa/2$, and the edge displacement variables in the free shell at B are $\delta_1 = -pa^2(1 - \nu)/(2Eh)$, and $\rho_1 = 0$. According to the hoop stress formula, we get a tensile force of pa in the circumferential direction in the cylinder; in the axial direction, the tensile forces of $pa/2$ coming from the dome part are transferred. The free cylindrical shell therefore extends by $(pa - \nu pa/2)/(Eh) = pa(2 - \nu)/(2Eh)$ in the circumferential direction; the edge displacement variables at B are $\delta_1 = -pa^2(2 - \nu)/(2Eh)$ and $\rho_1 = 0$.

According to (26.80) and example 26.8, putting $\varphi_1 = \pi/2$ results in the compatibility condition

$$\begin{Bmatrix} -\frac{pa^2(1-\nu)}{2Eh} \\ 0 \end{Bmatrix} + \frac{1}{D} \begin{bmatrix} \frac{1}{2\beta^3} & -\frac{1}{2\beta^2} \\ -\frac{1}{2\beta^2} & \frac{1}{\beta} \end{bmatrix} \begin{Bmatrix} f_1 \\ m_1 \end{Bmatrix} = \begin{Bmatrix} -\frac{pa^2(2-\nu)}{2Eh} \\ 0 \end{Bmatrix} - \frac{1}{D} \begin{bmatrix} \frac{1}{2\beta^3} & \frac{1}{2\beta^2} \\ \frac{1}{2\beta^2} & \frac{1}{\beta} \end{bmatrix} \begin{Bmatrix} f_1 \\ m_1 \end{Bmatrix}$$

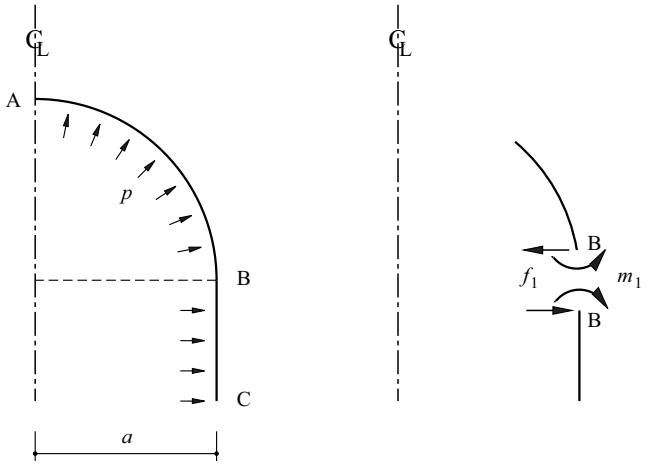

Fig. 26.26 Pressure vessel

which has the solution

$$f_1 = -\frac{p}{8\beta} \quad , \quad m_1 = 0$$

Using these values enables us to draw the diagram of the stress resultants n_θ, m_φ and v_φ (Fig. 26.23) in the spherical shell or the corresponding variables n_φ, m_x und v_x (Fig. 26.19) in the cylindrical shell (exercise 26.13). In particular, applying (18.52) results in the maximum bending moment of

$$\frac{p\mathrm{e}^{-\pi/4}}{8\sqrt{2}\beta^2} \approx 0.0403\, p/\beta^2$$

at a distance of

$$\frac{\lambda}{8} = \frac{\pi}{4\beta} \approx 0.785/\beta$$

from the transition point B between the two shells.

26.7.4 Approximation for shells of any form

Contrasting with a spherical shell, r_x in (26.75) generally varies with y. In a conical shell, for example, r_x decreases in proportion to the distance from the edge of the shell, see example 26.3. The solution for spherical shells shown in section 26.7.3 can still be used as an approximation by working with a mean value $r_x = a$. Actually, the edge disturbances according to Fig. 18.33 decrease substantially over a length of $\lambda/2 = \pi/\beta$, and r_x varies only moderately within this length for customary shell geometry.

26.8 Stability

26.8.1 General

The stability problems of framed structures addressed in chapter 22 could be treated as one-dimensional problems. However, the buckling of slabs and shells must be treated as a two-dimensional problem. Section 24.7.1 covering membrane action in elastic slabs provided the reader with a first insight into this.

The bifurcation loads of perfect elastic slabs (or plates) and shells can be calculated in a similar way to those of columns and frames by solving the associated linear eigenvalue problems. But there are also notable differences. Slabs (or plates) do not react very sensitively to imperfections and as a rule possess significant post-critical reserves due to the potential redistribution of the membrane forces. Shells, on the other hand, are very sensitive to imperfections and exhibit post-critical softening behaviour. This comes from the fact that many buckling modes are possible in shells with the same or almost the same bifurcation load, and these modes interact.

The bifurcation loads of shells have only limited significance in practical applications. In most cases the buckling failure occurs at about 20 to 40 % of the critical load of the perfect elastic shell. Attempts were made in the past to take this behaviour into account by applying reduction factors obtained from tests.

The geometric non-linear analysis of slabs (or plates) and shells is generally quite complicated and involved. Although powerful finite element programs are now available for such problems, using them properly calls for a great deal of specialist knowledge.

26.8.2 Bifurcation loads

26.8.2.1 Fundamental differential equation

Putting $q_x = q_y = q_z = 0$ and using (26.56) while including the influence of the membrane force according to (24.17) results in the relationship

$$D\Delta^4 w + Eh\Gamma^2 w - \Delta^2(n_x w_{,xx} + n_y w_{,yy} + 2n_{xy} w_{,xy}) = 0 \tag{26.81}$$

This is the fundamental differential equation for investigating the local stability of shells.

We assume below – as with Fig. 26.1 – that x and y are tangential to the principal lines of curvature, i. e. $z_{,xx} = 1/r_x$, $z_{,yy} = 1/r_y$, $z_{,xy} = 0$. Further, we set n_{xy} to zero.

Setting

$$w = w_0 \sin(\alpha x) \sin(\beta x)$$

then eq. (26.81) gives us

$$D(\alpha^2 + \beta^2)^4 + Eh\left(\frac{\alpha^2}{r_y} + \frac{\beta^2}{r_x}\right)^2 + (n_x\alpha^2 + n_y\beta^2)(\alpha^2 + \beta^2)^2 = 0 \tag{26.82}$$

Here, we assume that the shell buckles over rectangular surfaces with side lengths of π/α or π/β.

26.8.2.2 Uniaxially compressed slab

When $1/r_x = 1/r_y = 0$ and $n_y = 0$, then (26.82) results in

$$n_x = -\frac{D(\alpha^2 + \beta^2)^2}{\alpha^2} = -D\beta^2\left(\frac{\alpha}{\beta} + \frac{\beta}{\alpha}\right)^2$$

This expression takes on a minimum value for $\alpha = \beta$, i. e. $4D\beta^2$. Putting $\pi/\beta = b$, we therefore get the buckling load

$$-n_x = \frac{4\pi^2 D}{b^2} \tag{26.83}$$

see example 24.23.

26.8.2.3 Spherical shell subjected to constant external pressure

When $r_x = r_y = a$ and $n_x = n_y = -pa/2$, then (26.82) results in

$$D(\alpha^2 + \beta^2) + \frac{Eh}{a^2(\alpha^2 + \beta^2)} = \frac{pa}{2}$$

This expression is a minimum for $(\alpha^2 + \beta^2)^2 = Eh/(Da^2)$ and therefore we get the critical pressure

$$p = \frac{4\sqrt{DEh}}{a^2} \tag{26.84}$$

The associated compressive stresses in the shell are

$$\frac{pa}{2h} = \frac{Eh}{a\sqrt{3(1-\nu^2)}} \approx 0.6\,\frac{Eh}{a} \tag{26.85}$$

Assuming $\alpha = \beta$, half the buckling wavelength is equal to

$$\frac{\pi}{\alpha} = \frac{\pi\sqrt{ah}}{\sqrt[4]{3(1-\nu^2)}} \approx 2.4\sqrt{ah} \tag{26.86}$$

The ratio between the rise $\pi^2/(8\alpha^2 a)$ of the shell and length π/α is equal to $\pi/(8\alpha a) \approx 0.3\sqrt{h/a}$, i. e. the assumption of a shallow shell is justified because $h \ll a$.

26.8.2.4 Cylinder subjected to axial compression

We can use (26.82) to obtain

$$D(\alpha^2+\beta^2)^2 + \frac{Eh\alpha^4}{r_y^2(\alpha^2+\beta^2)^2} = -n_x\alpha^2$$

for cylinders subjected to axial compression, where $r_x \to \infty$, $r_y > 0$ and $n_y = 0$. Differentiating the expression on the left with respect to $(\alpha^2 + \beta^2)^2$ and equating to zero leads to

$$(\alpha^2+\beta^2)^2 = \sqrt{\frac{Eh}{D}} \cdot \frac{\alpha^2}{r_y}$$

and hence the critical compressive stress is

$$-\frac{n_x}{h} = \frac{Eh}{r_y\sqrt{3(1-\nu^2)}} \approx 0.6\frac{Eh}{r_y} \tag{26.87}$$

Buckling as a bar, i. e. global instability, governs for very long cylindrical shells. The result for this, taking the buckling length l and $I = \pi r_y^3 h$ as well as $A = 2\pi r_y h$, is

$$-\frac{n_x}{h} = \frac{\pi^2 EI}{Al^2} = \frac{\pi^2 E r_y^2}{2l^2} \tag{26.88}$$

And vice versa, the buckling stress of a bar-type strip of slab amounting to

$$-\frac{n_x}{h} = \frac{\pi^2 Eh^2}{12(1-\nu^2)l^2} \tag{26.89}$$

can be critical for very short cylindrical shells.

26.8.2.5 Cylinder subjected to radial pressure

We can use (26.82) to obtain

$$D(\alpha^2+\beta^2)^2 + \frac{Eh\alpha^4}{r_y^2(\alpha^2+\beta^2)^2} = pr_y\beta^2$$

where $r_x \to \infty$, $r_y > 0$, $n_x = 0$ and $n_y = -pr_y$. The radial pressure p is a minimum for $\pi/\alpha = l$, i. e. a half-wave always becomes established in the x direction. In the circumferential direction, on the other hand, the result is $2\pi r_y/(2\pi/\beta) = \beta r_y = n$ (whole) waves. Consequently,

$$p = \frac{Eh}{n^2 r_y}\left[\left(1+\frac{n^2l^2}{\pi^2 r_y^2}\right)^{-2} + \left(1+\frac{n^2l^2}{\pi^2 r_y^2}\right)^2 \frac{\pi^4 h^2 r_y^2}{12(1-\nu^2)l^4}\right] \tag{26.90}$$

and the critical radial pressure follows from this by minimising with respect to n or n^2 (exercise 26.16).

26.8.2.6 Cylinder subjected to axial compression and radial pressure

We can use (26.82) to obtain

$$D(\alpha^2+\beta^2)^2 + \frac{Eh\alpha^4}{r_y^2(\alpha^2+\beta^2)^2} = -n_x\alpha^2 + pr_y\beta^2$$

for cylinders subjected to axial compression and radial pressure, or rather, using the ratio,

$$\gamma = \frac{n_x}{n_y} = \frac{n_x}{-pr_y}$$

the relationship

$$p = \frac{1}{r_y(\gamma\alpha^2 + \beta^2)}\left[D(\alpha^2 + \beta^2)^2 + \frac{Eh\alpha^4}{r_y^2(\alpha^2 + \beta^2)^2}\right] \tag{26.91}$$

26.8.3 Commentary

The softening behaviour of shells and their sensitivity to imperfections can be illustrated by the bar model [3] shown in Fig. 26.27(a). The rigid pin-ended strut AB of length l is supported at B by the spring BC and loaded by the horizontal force C. We assume

$$C\tan\alpha = c_1 w - c_2 w^2 \qquad (c_1 > 0,\ c_2 > 0) \tag{26.92}$$

for the spring response according to Fig. 26.27(b), where $w = l(\sin\alpha - \sin\alpha_0)$ is measured from the (imperfect) position B_0. Therefore, the result is

$$\frac{C}{c_1 l} = \frac{\sin\alpha - \sin\alpha_0}{\sin\alpha}\left[1 - \frac{c_2 l}{c_1}(\sin\alpha - \sin\alpha_0)\right] \approx \left(1 - \frac{\alpha_0}{\alpha}\right)\left[1 - \frac{c_2 l}{c_1}(\alpha - \alpha_0)\right] \tag{26.93}$$

Fig. 26.27(c) shows the load-rotation curves for a number of assumed values of α_0. The diagram illustrates the significant influence that imperfections have on the structural behaviour. The softening of the perfect system ($\alpha_0 = 0$) takes place approximately along the straight line AB. Compared with the maximum load $c_1 l$ for the perfect system, even very small imperfections result in a severe reduction in the horizontal force C that can be accommodated. Compared with this, Fig. 22.4(b) – drawn for imperfect bars – indicates a much more accommodating behaviour.

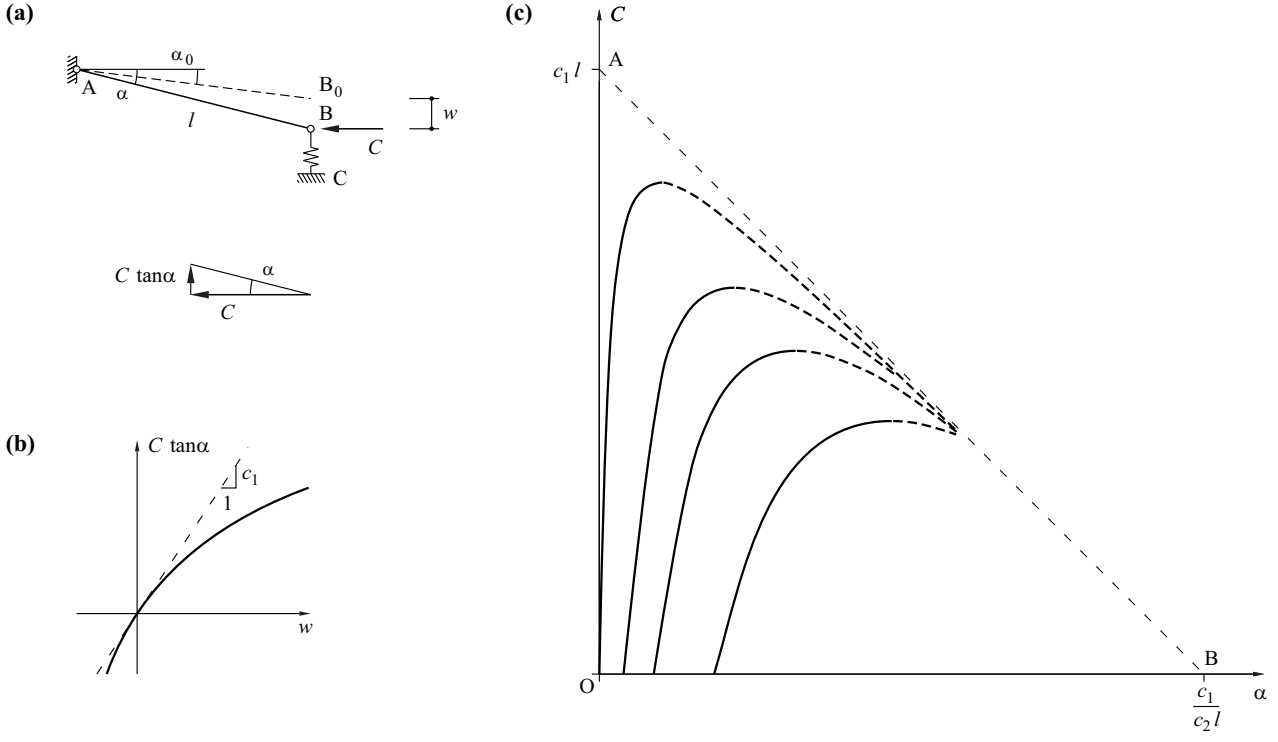

Fig. 26.27 Bar model: (a) diagram of static system and force polygon, (b) spring response, (c) load-rotation diagram

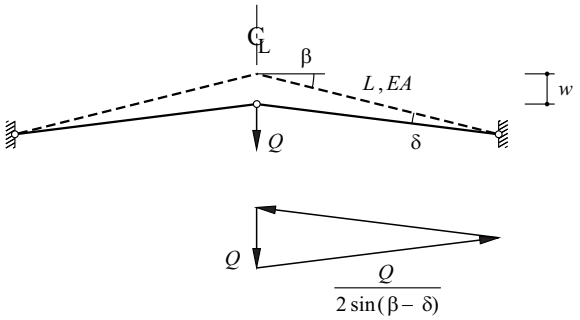

Fig. 26.28 Bar model for explaining Fig. 26.27(b)

The assumed spring response (26.92) can be explained using the bar model of Fig. 26.28. The deformed bar length is

$$\frac{L\cos\beta}{\cos(\beta-\delta)} = L - \frac{QL}{2\sin(\beta-\delta)EA} \tag{26.94}$$

and according to the sine law,

$$\frac{w}{\sin\delta} = \frac{L}{\sin\left(\frac{\pi}{2}+\beta-\delta\right)} = \frac{L}{\cos(\beta-\delta)} \tag{26.95}$$

applies. Rearranging (26.94) results in

$$Q = 2EA\tan(\beta-\delta)(\cos\beta\cos\delta + \sin\beta\sin\delta - \cos\beta)$$

Using the approximation $\cos\delta \approx 1$ and (26.95) results in

$$Q = 2EA\left[\sin\beta - \cos\beta\frac{w}{L}\cos(\beta-\delta)\right]\sin\beta\frac{w}{L} \approx c_1 w - c_2 w^2$$

As $\beta \ll 1$, then $c_1 \approx c_2\beta L$ applies, and therefore the abscissa of point B in Fig. 26.27(c) amounts to $\alpha_B \approx \beta L/l$.

26.9 Summary

1. This chapter looks at thin shells with infinite shear stiffness and membrane forces n_x, n_y, $n_{xy} = n_{yx}$ plus bending and twisting moments m_x, m_y, $m_{xy} = m_{yx}$ as generalised stresses.
2. The membrane forces can be calculated from the equilibrium conditions when the loading is known.
3. Disturbances of the membrane stress state associated with bending deformations and corresponding moments and shear forces generally result at the edges of the shell, also in the case of discontinuities in the geometry or the loading within the shell. Membrane theory must be supplemented by the bending theory of shells in order to ascertain these disturbances.
4. GAUSSian curvature (26.2) is a key feature of shell geometry. Elliptical surfaces are curved in all directions. There are two characteristic directions with negligible curvature at every point on a hyperbolic surface. Parabolic surfaces are curved in one direction only.
5. The membrane forces and deformations of symmetrically loaded surfaces of revolution are easy to calculate. An asymmetric loading leads to relationships that are somewhat more awkward to deal with.
6. Membrane theory for cylindrical shells leads to differential equations for the membrane forces and displacements which can be solved in succession through simple integration.
7. In terms of their membrane action, shells of any form can be dealt with by using the stress function introduced in (26.28).
8. The membrane forces in hyperbolic paraboloids are, advantageously, related to the (skew) network of characteristics.

9. Bending theory for rotationally symmetric cylindrical shells leads to the ordinary fourth-order differential equation (26.44) or (26.45). All the aids worked out in section 18.4.4 for the similar problem of beams in bending on an elastic foundation can be employed here.
10. The simultaneous differential equations (26.52) and (26.55) describe the structural behaviour of shallow elastic shells. Eliminating the stress function F or the deflection w results in an eighth-order differential equation for w or F, whose solutions can have four boundary conditions fitted to them.
11. The bending theory of symmetrically loaded surfaces of revolution leads to the fourth-order ordinary differential equation (26.75) for the deflection. As an approximation, the solutions presented for spherical shells can also be used for other shell forms in which the radius of curvature r_x varies along the meridian.
12. Shells are generally very sensitive to imperfections and exhibit post-critical softening behaviour. Their local stability can be investigated with the help of the differential equation (26.81). The corresponding bifurcation loads supply valuable reference values but cannot be directly applied in practice.

26.10 Exercises

26.1 Consider a concrete shell with a supporting ring according to example 26.1 ($h = 150\,\text{mm}$, $a = 40\,\text{m}$, $\gamma = 25\,\text{kN/m}^3$, $\varphi_1 = \pi/4$, $E = 30\,\text{kN/mm}^2$, $\nu = 0.2$, $A = 0.25\,\text{m}^2$). Discuss the resulting membrane forces and calculate the prestressing force P required to achieve deformation compatibility at the edge of the shell under its self-weight. What are the effects of the creep and shrinkage of the concrete and the relaxation of the prestressing steel? How would you coordinate and check the prestressing in the supporting ring and the lowering of the centering for the shell?

26.2 Verify the expressions for the membrane forces given in example 26.2 and draw a diagram of them for $\varphi_1 = 2\pi/3$. Discuss the improvement that can be achieved by providing tangential support according to Fig. 26.4(e).

26.3 Discuss the membrane forces determined in example 26.5 and their principal values for a hemispherical shell.

26.4 Calculate the membrane forces n_x, n_y, n_{xy} from (26.32) and present these graphically.

26.5 The form of a hyperbolic paraboloid shell is described by (26.36) with the values $a = b = 10\,\text{m}$ and $f_a = f_b = 2\,\text{m}$. The relationships $|x + y| = a$ and $|x - y| = a$ apply for the edges of the shell. The corners $x = \pm a$ are supported in the z direction and connected by a prestressed tie in the x direction. The corners $y = \pm b$ are free. Discuss the behaviour of the shell when subjected to $\overline{q}_z = q = 4\,\text{kN/m}^2$. Assume $h = 80\,\text{mm}$ for the shell thickness and $E = 30\,\text{kN/mm}^2$ for the modulus of elasticity.

26.6 Draw the projected membrane forces of Fig. 26.18(b) with the help of MOHR's circles and discuss the stress discontinuities that arise.

26.7 Investigate the example of Fig. 26.18(b) under the assumption that $f_a = 9f_b/4$.

26.8 Present the functions $w(x)$, $n_\varphi(x)$, $m_x(x)$ and $v_x(x)$ resulting from example 26.9 graphically for the case of $l = 10\,\text{m}$, $a = 18\,\text{m}$, $h = 0.25\,\text{m}$, $E = 30\,\text{kN/mm}^2$, $\nu = 0.2$, $\gamma = 9.81\,\text{kN/m}^3$. Compare w and n_φ with the corresponding values obtained using the membrane solution.

26.9 Work through example 26.9 exactly, i. e. with the boundary conditions $v_x(l) = m_x(l) = 0$. Compare the resulting functions with those of exercise 26.8.

26.10 Derive a differential equation similar to (26.56) for the stress function F by eliminating w from (26.52) and (26.55).

26.11 Calculate the coefficients c_3 to c_6 in example 26.11 from the four boundary conditions, compare the outcome with the approximation given in the example and discuss the course of the membrane force $n_x(x = 0, \varphi)$ for $n = 1, 2$.

26.12 Calculate the course of the stress variables n_θ, m_φ and v_φ along a meridian for example 26.12. As in exercise 26.1, use the variables $h = 150\,\text{mm}$, $a = 40\,\text{m}$, $\varphi_1 = \pi/4$ and $\nu = 0.2$.

26.13 Discuss the edge disturbance as a result of $p = 0.5\,\text{N/mm}^2$ at the transition from the cylindrical shell to the spherical shell of Fig. 5.28(b). Assume $h = 1\,\text{m}$, $a = 20\,\text{m}$ and $\nu = 0.2$.

26.14 Consider the pressure vessel of example 26.13 but assume a shallow spherical shell for the top part ($\varphi_1 < \pi/2$). Determine analytical expressions for the stress resultants f_1 and m_1 at the transition depending on φ_1. Compare the maximum bending moments for the case $\varphi_1 = \pi/4$ with those for $\varphi_1 = \pi/2$.

26.15 Use exercise 26.14 to discuss the effect of a stiffening ring at the transition between the spherical and cylindrical shells.

26.16 Present the ratio $pr_y/(Eh)$ according to (26.90) as a function of l/r_y ($1 \le l/r_y \le 100$) in a double logarithmic diagram for $\nu = 0.3$ and $r_y = 200h$, $r_y = 100h$ as well as $r_y = 50h$.

A1 DEFINITIONS

acceptance	The satisfactory handover of a structure or part thereof to the client.
accidental action	An action with a low probability of occurrence, generally of short duration but with a significant effect.
accidental design situation	A design situation that includes exceptional conditions for the structure.
accompanying action	An action additional to the leading action.
action effects	The responses of the structure to actions imposed on it (stresses, stress resultants, reactions, deformations, displacements and other action effects specific to the type of construction).
actions	Mechanical (loads, forces), other physical (temperature, humidity), chemical (salts, acids, alkalis, organic compounds) and biological (bacteria, insects, fungi, algae) actions on the structure resulting from execution, use and environmental influences.
analytical model	The coupling of physical variables (e. g. force and deformation variables) via appropriate relationships (e. g. equilibrium conditions, material laws and kinematic conditions).
basis of design	Specialist description of the implementation of the service criteria agreement specific to the construction works.
characteristic value	As a rule, the statistically founded value of an action, a geometrical variable or a construction material or subsoil property (mean value, upper or lower value), possibly also a nominal value or prudent estimate.
commissioning	The beginning of the intended use.
composition	The creation of an aesthetic manifestation by way of the spatial arrangement, shaping and choice of materials.
conceptual design	All the activities and developments, plus their results, leading from the service criteria to the structural concept.
condition assessment	Summarising analysis and assessment of the information about the current condition and the development of the condition to date linked with a prediction for the further development of the condition and its consequences over the course of a specified residual period of use.
condition survey	Acquisition of information about the current condition and the development of the condition to date with the aim of detecting significant defects, deterioration and deterioration mechanisms.
conservation	All the activities and measures required to safeguard the building stock and the material and non-material values of construction works.
construction inspection plan	A specification of the type, scope, execution and timing of construction inspections, including details of quality requirements and permissible deviations plus the regulation of responsibilities and the flow of information.
construction inspections	Checking the correct implementation of the project specifications during the execution.
construction material	A material used for a structure or construction works.

Theory of Structures. First Edition. Peter Marti

construction work	The execution of building activities according to the contract.
construction works	Output as a direct result of construction work, generally consisting of a structure and non-loadbearing components.
construction works documents	Documents specific to the construction works.
control measurement	The metrological monitoring of selected parameters.
dead load	A load due to the mass of the structure.
decommissioning	The termination or interruption of the use.
deconstruction	Systematic demolition or disassembly of construction works with sorting of components and construction materials to ensure proper disposal.
defect	The lack of a property that the structure should exhibit upon acceptance according to the contract.
deformation capacity	Ability of a structure and the structural members to deform elastically, and generally also plastically, up until failure.
design	Conceptual design, structural analysis and dimensioning.
design alternatives	Feasible variations for solving the problem underlying the conceptual design.
design boundary conditions	Spatial, temporal, legal, financial, constructional, materials-related, practical construction and operational stipulations for the design.
design criteria	Relationships to be satisfied between the action effects of relevant load cases and associated ultimate resistances or serviceability limits or between stabilising and destabilising action effects.
design situations	The physical circumstances and conditions occurring within a certain period of time for which it is necessary to verify that governing limit states are not exceeded.
design value	A value used in a verification which is determined from a characteristic or other representative value or from a function of design values in conjunction with partial and conversion factors, at best also a directly specified value.
design working life	The period of time intended for the use.
detail design	Detailed planning to provide the documents for the execution.
detailing	The specification and mutual agreement of the details of the construction works.
deterioration	Possible impairment of the material substance of a structure following acceptance.
dimensioning	Specifying the sizes, construction materials (including their properties) and detailing of a structure based on constructional or practical execution considerations or analytical verification.
draft design	The recognition, development and assessment of various design alternatives.
durability	Compliance with the requirements regarding structural safety and serviceability within the scope of the intended use and the foreseeable actions without unforeseen expenditure on maintenance and repairs.
economy	Moderate use of financial and natural resources with respect to the total duration of the design, execution and use.
effective depth	The distance of the centroidal axis of the tension reinforcement from the edge of the compression zone of the cross-section.

endurance limit	The fatigue resistance with respect to an unlimited number of stress cycles.
estimate	An approximate calculation of the mean value of a variable.
examination	A condition survey and assessment – including recommendations for remedial measures – performed for a particular reason.
execution	All the activities and measures necessary for the physical provision of the construction works, including the preparations for such.
execution documents	The contract document and other elements of the contract, construction programme, minutes of meetings and records of construction inspections plus the site diary.
failure	The exhaustion of the ultimate resistance through instability, breakage and fatigue or as a result of time-dependent action effects.
fatigue resistance	The ultimate resistance with respect to frequently repeated actions.
finite fatigue life	Fatigue resistance with respect to a limited number of stress cycles.
fixed action	An action with a specified distribution over the structure or structural member; its magnitude and direction are uniquely determined by the value at one point.
free action	An action whose distribution over the structure is not specified.
geometric variables	The intended dimensions and unintended imperfections of a structure.
hazard	A circumstance jeopardising the structural safety.
hazard scenario	A critical situation characterised by a leading hazard and associated circumstances.
imposed load	A load due to the use of the construction works.
inspection	Establishing the condition by way of specific, generally visual and simple, examinations and an assessment of the situation.
integration	The incorporation of construction works into their surroundings in a manner compatible with the natural and built environment.
leading action	The principal action in a load case.
leading hazard	The principal hazard in a hazard scenario.
limit state	A condition that, once reached, still just complies with the requirements regarding structural safety or serviceability.
load case	A physically compatible arrangement of simultaneous actions considered for a certain verification.
maintenance	Preserving the serviceability by way of simple and regular measures.
maintenance plan	Maintenance instructions specific to the construction works.
material	Metallic, non-metallic-inorganic or organic substance with properties that can be exploited for technical applications.
method of construction	The way(s) in which the construction work is performed.

modification	Intervention in the construction works for the purpose of adapting them to suit new requirements.
monitoring	Establishing and assessing the condition with recommendations for the next step(s).
monitoring plan	Monitoring instructions specific to the construction works.
nominal value	A value not based on statistics, instead fixed or based on, for example, experience or physical conditions.
observation	Checking the serviceability by means of simple and regular inspections.
observation method	In the event of basic design information of insufficient reliability, one possible method during the design, execution and use of a structure for forecasting the behaviour and specifying appropriate limit values. The method is associated with certain accepted risks and includes affiliated monitoring and safety measures.
operation instructions	Directives describing the use and operation of the technical installation(s) and intended for the owner(s) and the operator(s).
overall stability	A stable equilibrium situation for the entire structure as a rigid body.
permanent action	An action that, during a reference period, is approximately constant or changes monotonically, moving towards a limit value.
persistent design situation	A design situation that governs during a period of the same order as the design working life.
planning of remedial measures	Systematic preparation of the next operational and constructional steps based on the decision of the owner(s).
preliminary design	Drawing up the service criteria agreement and the structural concept, including an estimate of the costs, a general construction programme and a technical report.
preparation for construction	Tendering, bidding, checking of bids, concluding the contract and organising the construction work.
protection and welfare measures	Precautions taken during execution to protect persons and their health as well as property.
prudent estimate	Compared with the estimate, this is a value provided with an allowance adequate for the necessary reliability.
recommendation for remedial measures	Proposals resulting from the condition assessment for which the owner(s) must make a decision regarding the next step(s).
record of construction	A compilation of the construction works documents kept as a log of the execution.
reliability	A measure of the compliance with the requirements regarding structural safety and serviceability, usually expressed as a probability.
repair	Restoring the structural safety and serviceability for a specified length of time.
report on remedial measures	A document describing upkeep measures, including details of objectives, participants, methods, products, tests, results and costs.
representative value	The value of an action used for a verification (characteristic value, for variable actions possibly also rare, frequent or quasi permanent value).
resistance	Ability of a structure and the structural members to withstand actions during execution and use.
robustness	Ability of a structure and the structural members to limit deterioration or a failure that is disproportionate to its cause.

self-weight of non-structural elements	Loads applied by non-loadbearing components (e. g. roofing materials, floor coverings, subfloors, non-loadbearing partitions, claddings, linings, balustrades, safety barriers, spandrel panels, closures, façade components, suspended ceilings, insulation, seals) or permanent fixtures (e. g. lifts, escalators, HVAC systems, electrical installations, empty pipes, cable ducts) and, for example, earth fill or track ballast.
service criteria	Requirements for the properties and behaviour of the construction works resulting from the intended use.
service criteria agreement	Description of the usage and protection objectives of the owner(s) as well as the fundamental conditions, requirements and regulations covering the design, execution and use of the construction works.
service instructions	Directives for the use of the construction works intended for the owner(s) and operator(s).
service situations	Physical circumstances and conditions during the design working life.
serviceability	Ability of a structure and the structural members to be able to guarantee the functionality and appearance of the construction works, plus the comfort of the persons using said works, according to the serviceability limits.
serviceability limit	A specified limit for serviceability.
serviceability limit state	The condition upon reaching a boundary of serviceability.
structural analysis	Determining the action effects, possibly graduated, for the entire structure, individual structural members and local effects with the help of a structural model and various analytical models.
structural calculations	Presentation of the structural analysis and dimensioning.
structural concept	The basic idea of the structure which governs the project.
structural member	A physically distinguishable part of a structure or construction works.
structural model	The result of defining and idealising the structural system.
structural safety	Ability of a structure and the structural members to guarantee the overall stability and an adequate ultimate resistance for the assumed actions (including fatigue resistance) in accordance with a specified, necessary reliability.
structural system	Arrangement of the structural members plus the nature of their interaction.
structure	All the structural members and the subsoil necessary for maintaining the equilibrium and form of the construction works.
subsoil	Ground in the form of loose soil or solid rock in the region of a construction project or foundation.
supplementary safety measures	Requirements regarded as necessary for the specific construction works in the event of concessions regarding the structural safety in accordance with the standards.
technical report	Explanation and summary of the design work.
tender design	Further processing of the preliminary design in order to create the basis for the building approval procedure, the planning permission or the tender.
tender documents	The text of the intended contract document, specific provisions, specification or description of the works, drawings and general provisions.
transient design situation	Design situation that governs during a significantly shorter period of time than the design working life.

type of construction	The nature of the building work, determined by the main construction materials used, e. g. concrete, steel, steel-concrete composite, timber, masonry.
ultimate limit state	The condition upon reaching the boundary of structural safety.
ultimate resistance	The limit of resistance.
urgent safety measures	Directives prompted by observation or examination which are to be carried out immediately in order to protect persons, the environment and the construction works.
use	The utilisation of the construction works described in the service criteria agreement and the basis of design.
variable action	An action that is not permanently applied or not constant or does not change monotonically during a reference period.
verification	Confirmation of compliance with a design criterion.

A2 NOTATION

Latin upper-case letters

A	accidental action, area, cross-sectional area, force, constant
$\boldsymbol{A}$	force vector
B	force, constant
$\boldsymbol{B}$	force vector
C	centroid
C	serviceability limit, support force variable, product of inertia, objective function, compressive force, edge, constant
$\boldsymbol{C}$	vector of support force variables
D	dissipation function, deterioration, slab stiffness, diameter
$\boldsymbol{D}$	differential operator
E	action effect, earth pressure, modulus of elasticity
$\boldsymbol{E}$	elasticity matrix
F	action, force, stress function, LAGRANGE function
$\boldsymbol{F}$	force vector, global flexibility matrix
G	permanent action, dead load, imposed load, shear modulus, hinge force, function
H	horizontal force, LAGRANGE function
$\boldsymbol{H}$	strain interpolation matrix
I	moment of inertia, functional
I	unit matrix
J	creep function
K	bulk modulus, joint force, total curvature
$\boldsymbol{K}$	total stiffness matrix
L	initial length
M	shear centre, instantaneous centre of rotation
M	(bending) moment, "moment volume"
$\boldsymbol{M}$	moment vector, vector of bending moments
N	normal force, number of load cycles
$\boldsymbol{N}$	vector of normal forces
O	origin of coordinates
P	prestressing force, restraint parameter, bilinear form
Q	variable action, single force, load parameter, quadratic form
$\boldsymbol{Q}$	load vector
R	ultimate resistance, relaxation function, resultant force, moment, RAYLEIGH quotient
$\boldsymbol{R}$	resultant force vector, boundary displacement operator
S	surface, first moment of area, shear flow, stress resultant, cable force, force in rib
$\boldsymbol{S}$	rib force vector
T	torque, change in temperature, edge shear force, tensile force
$\boldsymbol{T}$	boundary stress operator
V	volume, shear force, degree of freedom
$\boldsymbol{V}$	displacement vector
W	work, elastic section modulus
X	property of construction material or subsoil, global coordinate, redundant variable
$\boldsymbol{X}$	vector of redundant variables, modal matrix
Y	yield function, global coordinate, function
Z	global coordinate, plastic section modulus

Theory of Structures. First Edition. Peter Marti

Latin lower-case letters

a geometrical property, distance, cross-sectional area per unit length
$\boldsymbol{a}$ kinematic transformation matrix, matrix
b width, length, distance, parameter
$\boldsymbol{b}$ static transformation matrix, matrix, vector
c cohesion, direction cosine, constant, coefficient, number of support force variables, length, support displacement variable, modulus of subgrade reaction, shear span
$\boldsymbol{c}$ transformation matrix, matrix
d differential
d length, effective depth, diameter, nullity
e base of natural logarithms
e earth pressure, deviatoric strain component, length, thickness, eccentricity
$\boldsymbol{e}$ strain deviator, transformation matrix, base vector
f strength, rise, function, flexibility, shape factor, deflection, force per unit length
$\boldsymbol{f}$ flexibility matrix
g acceleration due to gravity
g number of hinge conditions, permanent load, function
$\boldsymbol{g}$ equilibrium matrix
h height, depth, thickness, function
i imaginary unit
i radius of gyration, index
j quantity, number of floor/storey, index
k coefficient, stiffness, constant, number of joints, foundation modulus, index
$\boldsymbol{k}$ stiffness matrix
l span, length
m moment per unit length, position of free load, number
$\boldsymbol{m}$ moment tensor
n membrane force, coordinate, number, modular ratio, degree of static indeterminacy
$\boldsymbol{n}$ unit normal vector
p $-(\sigma_1 + \sigma_3)/2$, compression, force on foundation, number of plastic hinges
q force per unit volume/area/length, response factor, $(\sigma_1 - \sigma_3)/2$, shear force, imposed load, edge load
$\boldsymbol{q}$ force per unit volume/area/length, load vector
r coordinate, radius, boundary displacement, transverse bending moment, near-end bar stiffness, rank, root
$\boldsymbol{r}$ position vector, boundary displacement
s distance, deviator component, arc length, internal force variable, number of bars, longitudinal shear force, near-end bar stiffness, crack spacing, spacing, in-plane load
$\boldsymbol{s}$ stress deviator, position vector of wrench axis, vector of internal force variables, joint force vector
t coordinate, time, wall thickness, far-end bar stiffness, twisting moment
$\boldsymbol{t}$ force per unit area, stress vector, boundary stress vector, transformation matrix
u displacement in x direction, displacement, function
$\boldsymbol{u}$ displacement vector, vector
v displacement in y direction, shear force per unit length, internal deformation variable
$\boldsymbol{v}$ vector of internal deformation variables, shear force vector, vector
w displacement in z direction, deflection, crack width
$\boldsymbol{w}$ vector
x coordinate, control variable
$\boldsymbol{x}$ position vector, vector of control variables, vector
y coordinate, control variable, function
$\boldsymbol{y}$ vector of control variables, image vector, vector
z coordinate, height above ground

Greek upper-case letters

Γ shell operator (PUCHER operator)
Δ difference, distance, LAPLACE operator, bar elongation, relative displacement
$\mathbf{\Lambda}$ diagonal matrix of eigenvalues
Π potential energy, product
Σ sum
Φ stress function
Ω shape function
$\mathbf{\Omega}$ matrix of shape functions

Greek lower-case letters

α coefficient, constant, angle, ratio
β coefficient, constant, angle, ratio
γ body load, coefficient, shear strain, ratio
$\boldsymbol{\gamma}$ strain vector
δ KRONECKER symbol, deformation variable, slip, variational symbol
$\boldsymbol{\delta}$ flexibility matrix, vector of deformation variables
ε normal strain, strain, parameter
$\boldsymbol{\varepsilon}$ strain tensor, strain vector, permutation tensor
ζ coordinate, distance
η conversion factor, function, coordinate, influence ordinate
θ angle, rotation
ϑ twist
κ constant, moment distribution factor
λ LAMÉ constant, bar end rotation, coefficient, natural wavelength, constant, eigenvalue, load factor, axial force parameter, ratio, LAGRANGE multiplier
μ coefficient of friction, LAMÉ constant ($\mu = G$), moment carry-over factor, constant, amplification factor, ratio
ν POISSON's ratio
ξ damping factor, coordinate
π specific potential, ratio of circumference to diameter
ρ radius, geometric reinforcement ratio, bar end rotation, density
σ normal stress, stress component
$\boldsymbol{\sigma}$ stress tensor, stress vector
τ shear stress, time
φ angle, angle of internal friction, rotation, creep coefficient, joint rotation, function
χ ageing coefficient, curvature or twist
$\boldsymbol{\chi}$ curvature vector
ψ reduction coefficient, angle, bar rotation, stress function
$\boldsymbol{\psi}$ vector potential
ω rotation, angular frequency, approximating function, warping, constant, mechanical reinforcement ratio
$\boldsymbol{\omega}$ rotation vector

Subscripts

A	force *A*
B	force *B*
C	centroid
C	fatigue resistance
C	with respect to ***C***
D	endurance limit
E	buckling (EULER)
F	load
G	permanent action
L	threshold
M	shear centre
M	resistance, bending moment
N	normal force
P	dynamic pressure, prestressing
Q	variable action, with respect to *Q*
R	resistance
S	model uncertainty
T	temperature
V	shear force
a	age-adjusted, structural steel, arch
b	bond, bending, frame beam
c	concrete, compression, column, perpendicular to cable chord
d	design value, diagonal
e	element
e	element
e	subsoil, outer, external, elastic
e	elastic
f	importance, action, flange
g	gradient, global, geometrical
h	with respect to *h*, horizontal
i	inner, internal, transformed, index
j	index
k	characteristic value, kinematic, index
k	kinematic
l	with respect to *l*, left, index
m	construction material/subsoil, mean value, position of free load, index
m	bending
n	normalised, *n* direction, index
o	octahedral
o	octahedral
o	top, upper, orthogonal
o	orthonormal
p	prestressing steel, polar, plastic
q	as a result of *q*
r	roughness, residual, restraint, boundary displacement, right, crack, *r* direction
r	reduced degrees of freedom, residual
s	reinforcing steel, shrinkage, section, pure torsion, shear, *s* direction, direction of cable chord, static
s	static, with respect to ***s***
t	tension, boundary stress, *t* direction
u	failure, bottom, lower, limit load
u	suppressed degrees of freedom
v	strain hardening, shear force, flexural buckling
v	shear force
w	water, web, warping torsion, flexural buckling

x	x direction
y	y direction, yielding
z	z direction
cr	critical
dst	destabilising
inf	lower value, bottom
max	maximum value
min	minimum value
nom	nominal value
part	particular
rep	representative
stat	stationary
stb	stabilising
sup	upper value, top
tot	total
0	initial, reference value, rare, statically determinate
0	fundamental
1	frequent, leading action, principal value, statically indeterminate
2	quasi permanent, principal value
3	principal value
∞	final value
I	1st invariant, system component
II	2nd invariant, system component
III	3rd invariant
α	index
β	index
ζ	ζ direction
η	η direction
φ	torsional buckling
σ	load-dependent
ω	warping, index

Superscripts

A	antisymmetric
S	symmetric
T	transposition
-1	inversion
l	left
r	right
0	fixity
I	uncracked state, 1st order, system component
II	cracked state, 2nd order, system component
ω	warping, index
$*$	complementary, plastic, adjoint, single load case
$'$	effective, projected, compression, derivative with respect to x, r or s
$\cdot$	increment, derivative with respect to t
+	span, positive
–	support, negative
—	force state, complete bar end variables, equivalent stress resultant in simple beam in x direction, related stiffness/slenderness, transformed, projected
=	equivalent stress resultant in simple beam in z direction
~	similar matrix
^	congruent matrix

Special characters

$\mathbf{0}$	zero matrix
cond	condition number
const	constant
det	determinant
sp	trace
∇	HAMILTON operator
∂	partial differential
Ø	diameter
I	uncracked state, system component
II	cracked state, system component
!	factorial
$\lvert\ \rvert$	amount
$\lVert\ \rVert$	norm

Abbreviations

BL	basement level
BS	basic system
FB	free body
FBD	free-body diagram
FEM	finite element method
GF	ground floor
HVAC	heating/ventilation/air conditioning
UF	upper floor

Material	Density ρ [kg/m^3]	Modulus of elasticity E [kN/mm^2]	POISSON's ratio ν [-]	Shear modulus G [kN/mm^2]	Yield limit f_y [N/mm^2]	Tensile strength f_t [N/mm^2]	Compressive strength f_c [N/mm^2]	Elongation at failure ε_u [%]	Final shrinkage strain $\varepsilon_{s,\infty}$ [‰]	Final creep coefficient φ_∞ [-]	Coefficient of thermal expansion α_T [10^{-6}/°C]
Sandstone	1900 - 2300	10 - 40	0.2				20 - 300				2 - 12
Limestone	1700 - 2900	20 - 80	0.2				50 - 150				7
Granite	2600 - 3000	15 - 70	0.2				70 - 250				3 - 8
Softwood	470	10/0.4 [1]		0.6		80 [2]	40 [2]		3.3/1.6 [3]	1 - 2	4/35 [1]
Beech/Oak	670	13/0.9 [1]		1.0		110 [2]	50 [2]		3.6/2.0 [3]	1 - 2	4/35 [1]
Cement mortar	2400	25	0.2			2	35				12
Concrete	2400	22 - 45	0.2			1.5 - 5	20 - 80	0.2 - 0.4	0.2 - 0.7	1 - 4	10
Glass	2500	70	0.23			30	900				8
Structural steel S235	7850	210	0.3	81	250	400		25			11
Reinforcing steel B500B	7850	210	0.3		540	600		10			11
Prestressing steel Y1770	7850	210	0.3		1550	1800		5			11
Grey cast iron	7200	100	0.25			200	800	< 1			9
Aluminium 5083	2660	70	0.33		180	320		12			24
Copper	8930	120	0.35		60	200		50			17
Lead	11 300	17	0.45		10	15		100			29
E-glass	2600	73	0.18			3400		4			5
Aramid HM fibres	1450	100/5 [1]				2800		2.8			−4/17 [1]
Carbon HT fibres	1780	235/15 [1]				3400		1.4			0/10 [1]
Epoxy resin	1100 - 1250	2.8 - 3.6	0.4			70 - 90		6 - 8			60 - 70
Polypropylene	910	1.3	0.4			30		70			160
Polyvinyl chloride	1400	1 - 3.5	0.38			50 - 75		10 - 50			80
GFRP (60 % fibres by vol.)	2000	45/13 [1]	0.25	5		1000/70 [1]					7/27 [1]
CFRP (60 % fibres by vol.)	1500	140/12 [1]	0.26	5.5		1500/90 [1]					0/30 [1]

- The figures in the table are typical mean values at room temperature obtained from short-term static tests in particular. Significant deviations from the above figures are possible depending on the origin of the material or the production process and certainly when different ambient conditions (temperature, humidity) prevail.
- The figures for timber are based on a 12 % moisture content and solid timber free from defects.
- The applicable provisions of the relevant structural design, construction material and testing standards must be taken into account in each case.

[1] parallel/perpendicular to the grain/fibres
[2] parallel to the grain
[3] tangential/radial per % reduction in timber moisture content

A4 GEOMETRICAL PROPERTIES OF SECTIONS

	Cross-section	Area of section Position of centroid	Second moments of area	Shear centre Area shear factor	Torsion constant Warping constant
1		$A = bh$ $d = \frac{h}{2}$ $e = \frac{b}{2}$	$I_y = \frac{bh^3}{12}$ $I_z = \frac{hb^3}{12}$	$\alpha_v \approx \frac{5}{6}$	$I_x = \frac{hb^3}{3}\left[1 - \frac{192b}{\pi^5 h}\tanh\left(\frac{\pi h}{2b}\right)\right] \quad (h \geq b)$
2		$A = bh$ $d = \frac{h}{2}$ $e = \frac{b-c}{2}$	$I_\eta = \frac{bh^3}{12}$ $I_\zeta = \frac{bh(b^2+c^2)}{12}$ $C_{\eta\zeta} = \frac{bch^2}{12}$		
3		$A = \frac{h(a+b)}{2}$ $d = \frac{h(2a+b)}{3(a+b)}$ $e = \frac{2a^2+2ab-ac-2bc-b^2}{3(a+b)}$	$I_\eta = \frac{h^3(a^2+4ab+b^2)}{36(a+b)}$ $I_\zeta = \frac{h}{36(a+b)}\left[a^4+b^4+2ab(a^2+b^2)-c(a^3+3a^2b-3ab^2-b^3)+c^2(a^2+4ab+b^2)\right]$ $C_{\eta\zeta} = -\frac{h^2}{72(a+b)}\left[a^3+3a^2b-3ab^2-b^3-2c(a^2+4ab+b^2)\right]$		
4		$A = \frac{ah}{2}$ $d = \frac{2h}{3}$ $e = \frac{2a-c}{3}$	$I_\eta = \frac{ah^3}{36}$ $I_\zeta = \frac{ah}{36}(a^2-ac+c^2)$ $C_{\eta\zeta} = -\frac{ah^2}{72}(a-2c)$		$I_x = \frac{\sqrt{3}h^4}{45} \quad \left(c = e = \frac{h}{\sqrt{3}}\right)$
5		$A = \pi ab$	$I_y = \frac{\pi ab^3}{4}$ $I_z = \frac{\pi ba^3}{4}$	$\alpha_v \approx \frac{9}{10}$	$I_x = \frac{\pi a^3 b^3}{a^2+b^2}$
6		$A = \pi r^2$	$I = \frac{\pi r^4}{4}$	$\alpha_v \approx \frac{9}{10}$	$I_x = \frac{\pi r^4}{2}$

Theory of Structures. First Edition. Peter Marti

	Cross-section	Area of section Position of centroid	Second moments of area	Shear centre Area shear factor	Torsion constant Warping constant
7	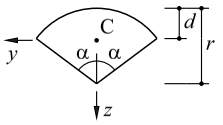	$A = \alpha r^2$ $d = r\left(1 - \frac{2\sin\alpha}{3\alpha}\right)$	$I_y = \frac{r^4}{4}\left(\alpha + \sin\alpha\cos\alpha - \frac{16\sin^2\alpha}{9\alpha}\right)$ $I_z = \frac{r^4}{4}(\alpha - \sin\alpha\cos\alpha)$		
8	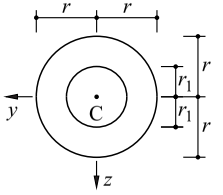	$A = \pi(r^2 - r_1^2)$	$I = \frac{\pi(r^4 - r_1^4)}{4}$		$I_x = \frac{\pi(r^4 - r_1^4)}{2}$
9	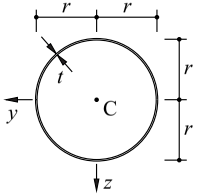	$A = 2\pi rt$	$I = \pi r^3 t$	$\alpha_v \approx \frac{1}{2}$	$I_x = 2\pi r^3 t$
10	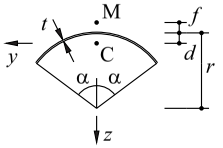	$A = 2\alpha rt$ $d = r\left(1 - \frac{\sin\alpha}{\alpha}\right)$	$I_y = r^3 t\left(\alpha + \sin\alpha\cos\alpha - \frac{2\sin^2\alpha}{\alpha}\right)$ $I_z = r^3 t(\alpha - \sin\alpha\cos\alpha)$	$f = r\frac{\sin\alpha(2 + \cos\alpha) - \alpha(1 + 2\cos\alpha)}{\alpha - \sin\alpha\cos\alpha}$	$I_x = \frac{2\alpha rt^3}{3}$ $I_\omega = \frac{2tr^5}{3}\left[\alpha^3 - \frac{6(\sin\alpha - \alpha\cos\alpha)^2}{\alpha - \sin\alpha\cos\alpha}\right]$
11	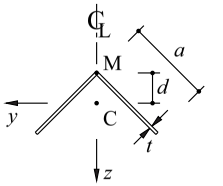	$A = 2at$ $d = \frac{a}{2\sqrt{2}}$	$I_y = \frac{a^3 t}{12}$ $I_z = \frac{a^3 t}{3}$		$I_x = \frac{2at^3}{3}$
12	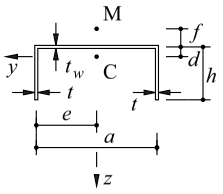	$A = 2ht + at_w$ $d = \frac{h^2 t}{2ht + at_w}$ $e = \frac{a}{2}$	$I_y = \frac{h^3 t}{3}\cdot\frac{2at_w + ht}{at_w + 2ht}$ $I_z = \frac{a^3 t_w}{12} + \frac{a^2 ht}{2}$	$f = \frac{3h^2 t}{6ht + at_w}$	$I_x = \frac{2ht^3 + at_w^3}{3}$ $I_\omega = \frac{a^2 h^3 t}{12}\cdot\frac{3ht + 2at_w}{6ht + at_w}$

	Cross-section	Area of section Position of centroid	Second moments of area	Shear centre Area shear factor	Torsion constant Warping constant
13	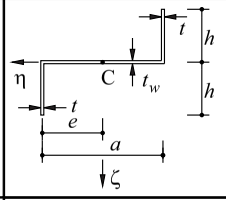	$A = 2ht + at_w$ $e = \frac{a}{2}$	$I_\eta = \frac{2h^3 t}{3}$ $I_\zeta = \frac{a^3 t_w}{12} + \frac{a^2 ht}{2}$ $C_{\eta\zeta} = -\frac{ah^2 t}{2}$		$I_x = \frac{2ht^3 + at_w^3}{3}$ $I_\omega = \frac{a^2 h^3 \left[2t(a^2 + ah + h^2) + 3aht_w\right]}{12(2h + a)^2}$
14	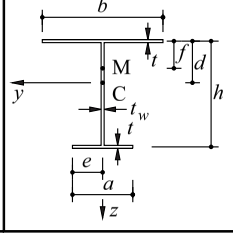	$A = (a + b)t + ht_w$ $d = \frac{h}{2} \cdot \frac{ht_w + 2at}{ht_w + at + bt}$ $e = \frac{a}{2}$	$I_y = \frac{h^2\left[12abt^2 + h^2 t_w^2 + 4htt_w(a + b)\right]}{12(at + bt + ht_w)}$ $I_z = \frac{(a^3 + b^3)t}{12}$	$f = \frac{ha^3}{a^3 + b^3}$ $\alpha_v \approx \frac{ht_w}{A}$	$I_x = \frac{(a + b)t^3 + ht_w^3}{3}$ $I_\omega = \frac{th^2}{12} \cdot \frac{a^3 b^3}{a^3 + b^3}$

A5 MATRIX ALGEBRA

A5.1 Terminology

An ($m\times n$) *matrix* (matrix of order $m\times n$) is a system of mn numbers arranged in a rectangular array of m rows and n columns:

$$\boldsymbol{a} = \begin{bmatrix} a_{11} & a_{12} & . & . & . & a_{1n} \\ a_{21} & a_{22} & . & . & . & a_{2n} \\ . & & & & & . \\ . & & & & & . \\ . & & & & & . \\ a_{m1} & a_{m2} & & & & a_{mn} \end{bmatrix} = \left[a_{ij}\right] \tag{A5.1}$$

The position of each element a_{ij} in the array is given by the row index $i = 1, 2, \ldots, m$ and the column index $j = 1, 2, \ldots, n$. It is possible to use symbols, functions and even further matrices as the elements of a matrix, as well as numbers. When the elements are themselves matrices, we speak of *partitioned matrices* and *submatrices*.

A matrix where $m = 1$ is known as a *row vector* or *row*, one where $n = 1$ as a *column vector* or *column*. A matrix in which all the elements are equal to zero is called a *zero matrix* and is given the symbol $\mathbf{0}$. A matrix where $m = n$ is *square* – and of *order* m. The sum of the main diagonal elements a_{ii} of a square matrix is known as a *trace*:

$$\mathrm{sp}\,\boldsymbol{a} = \sum_{i=1}^{m} a_{ii} \tag{A5.2}$$

The *determinant* of a square matrix is the function

$$\det \boldsymbol{a} = \begin{vmatrix} a_{11} & a_{12} & . & . & . & a_{1m} \\ a_{21} & a_{22} & . & . & . & a_{2m} \\ . & & & & & . \\ . & & & & & . \\ . & & & & & . \\ a_{m1} & a_{m2} & . & . & . & a_{mm} \end{vmatrix} = \sum(-1)^k a_{1\alpha} a_{2\beta} \cdots a_{m\omega} \tag{A5.3}$$

In this function, $\alpha, \beta, \ldots, \omega$ are computed over all the $m!$ possible permutations of the numbers $1, 2, \ldots, m$, and k denotes the number of inversions in each permutation. The *minor* of element a_{ij} is the determinant that results from the given determinant by deleting the ith row and the jth column. The *algebraic complement* A_{ij} of element a_{ij} is its minor, which is given a positive (negative) sign when the sum $i + j$ of the indices is even (odd):

$$A_{ij} = (-1)^{i+j} \begin{vmatrix} a_{11} & . & . & . & a_{1,j-1} & a_{1,j+1} & . & . & . & a_{1m} \\ . & & & & . & . & & & & . \\ . & & & & . & . & & & & . \\ . & & & & . & . & & & & . \\ a_{i-1,1} & . & . & . & a_{i-1,j-1} & a_{i-1,j+1} & . & . & . & a_{i-1,m} \\ a_{i+1,1} & . & . & . & a_{i+1,j-1} & a_{i+1,j+1} & . & . & . & a_{i+1,m} \\ . & & & & . & . & & & & . \\ . & & & & . & . & & & & . \\ . & & & & . & . & & & & . \\ a_{m1} & . & . & . & a_{m,j-1} & a_{m,j+1} & . & . & . & a_{mm} \end{vmatrix} \tag{A5.4}$$

Theory of Structures. First Edition. Peter Marti

The value of a determinant does not change when the columns and rows are transposed; therefore, all the properties formulated below for the rows also apply to the columns. The sign of a determinant changes when two rows are switched and the others retained; the determinant equals zero when one row is a linear combination of other lines (i. e. is *linearly dependent* on these). A factor common to all the elements of a row can be placed in front of the determinant. The value of the determinant remains unchanged when adding a linear combination of rows to another row. A determinant can be expanded with respect to the elements of an arbitrary row i:

$$\det \boldsymbol{a} = \sum_{j=1}^{m} a_{ij} A_{ij} \tag{A5.5}$$

The sum of the products of the elements in a row i and the algebraic complements of another row j is zero:

$$\sum_{k=1}^{m} a_{ik} A_{jk} = 0 \qquad (i \neq j) \tag{A5.6}$$

A square matrix is known as *invertible* when $\det \boldsymbol{a} \neq 0$ or *singular* when $\det \boldsymbol{a} = 0$. A singular matrix with $d \leq m$ linear-dependent rows or columns has the *rank* $r = m - d$, where d denotes the *nullity.*

A square matrix where $a_{ij} = a_{ji}$ is known as *symmetric*, one where $a_{ij} = -a_{ji}$ *antisymmetric* or *skew-symmetric*. Every square matrix can be decomposed into a symmetric and an antisymmetric submatrix according to

$$a_{ij}^{\mathrm{S}} = \frac{1}{2}(a_{ij} + a_{ji}) \quad , \quad a_{ij}^{\mathrm{A}} = \frac{1}{2}(a_{ij} - a_{ji}) \tag{A5.7}$$

Square matrices in which all the elements below (above) the main diagonal are equal to zero are known as upper or right (lower or left) *triangular matrices*. The determinant of such a matrix is equal to the product of the elements on the main diagonal (also known as leading or principal diagonal).

A *band matrix* is a square matrix whose elements not equal to zero are grouped around the main diagonal.

A *diagonal matrix* is a square matrix in which all the elements are zero apart from those on the main diagonal. And when the elements on the main diagonal all have the same value, we speak of a *scalar matrix*; if this value is 1, the matrix is an *identity matrix*, which has the symbol $\mathbf{I}$ (also known as a unit matrix).

Rectangular matrices are known as *row-regular* (where $m \leq n$) or *column-regular* (where $n \leq m$) provided their rows or columns respectively exhibit linear independence.

A5.2 Algorithms

The *transposition* of an $(m \times n)$ matrix $\boldsymbol{a}$ involves swapping (reflecting) all the rows and columns to obtain the transposed $(n \times m)$ matrix $\boldsymbol{a}^{\mathrm{T}}$. Obviously, $(\boldsymbol{a}^{\mathrm{T}})^{\mathrm{T}} = \boldsymbol{a}$ applies for all matrices, $\boldsymbol{a}^{\mathrm{T}} = \boldsymbol{a}$ for symmetric matrices and $\boldsymbol{a}^{\mathrm{T}} = -\boldsymbol{a}$ for antisymmetric matrices.

When *adding* (subtracting) two $(n \times m)$ matrices $\boldsymbol{a}$ and $\boldsymbol{b}$, all the elements in the same positions are added together (subtracted from each other):

$$c_{ij} = a_{ij} + b_{ij} \tag{A5.8}$$

Two matrices $\boldsymbol{a}$ and $\boldsymbol{b}$ are identical when they have the same order $m \times n$ and all the elements in the same positions are equal, i. e. $a_{ij} = b_{ij}$ or $\boldsymbol{a} - \boldsymbol{b} = \mathbf{0}$.

Matrix addition is commutative and associative:

$$\boldsymbol{a} + \boldsymbol{b} = \boldsymbol{b} + \boldsymbol{a} \quad , \quad (\boldsymbol{a} + \boldsymbol{b}) + \boldsymbol{c} = \boldsymbol{a} + (\boldsymbol{b} + \boldsymbol{c}) \tag{A5.9}$$

When *scaling* a matrix $\boldsymbol{a}$ with a scalar λ, all the elements of the matrix are multiplied by λ.

Multiplying an $(m\times n)$ matrix $\boldsymbol{a}$ by an $(n\times p)$ matrix $\boldsymbol{b}$ results in an $(m\times p)$ matrix $\boldsymbol{c}$, where the following applies for its elements:

$$c_{ik} = \sum_{j=1}^{n} a_{ij} b_{jk} \tag{A5.10}$$

Matrix multiplication is associative and distributive:

$$(\boldsymbol{a}\bullet\boldsymbol{b})\bullet\boldsymbol{c} = \boldsymbol{a}\bullet(\boldsymbol{b}\bullet\boldsymbol{c}) \quad , \quad \boldsymbol{a}\bullet(\boldsymbol{b}+\boldsymbol{c}) = \boldsymbol{a}\bullet\boldsymbol{b} + \boldsymbol{a}\bullet\boldsymbol{c} \tag{A5.11}$$

but generally not commutative ($\boldsymbol{a}\bullet\boldsymbol{b} \neq \boldsymbol{b}\bullet\boldsymbol{a}$). Moreover,

$$(\boldsymbol{a}\bullet\boldsymbol{b}\bullet\ldots\bullet\boldsymbol{c})^{\mathrm{T}} = \boldsymbol{c}^{\mathrm{T}}\bullet\ldots\bullet\boldsymbol{b}^{\mathrm{T}}\bullet\boldsymbol{a}^{\mathrm{T}} \tag{A5.12}$$

also applies, and $\boldsymbol{a} = \boldsymbol{a}\bullet\mathbf{I} = \mathbf{I}\bullet\boldsymbol{a}$ as well for square matrices.

Real square matrices exhibiting the property

$$\boldsymbol{a}\bullet\boldsymbol{a}^{\mathrm{T}} = \boldsymbol{a}^{\mathrm{T}}\bullet\boldsymbol{a} \tag{A5.13}$$

are known as *normal*. And if the columns (and rows, too) form a system of orthogonal unit vectors as well, i. e.

$$\boldsymbol{a}\bullet\boldsymbol{a}^{\mathrm{T}} = \boldsymbol{a}^{\mathrm{T}}\bullet\boldsymbol{a} = \mathbf{I} \tag{A5.14}$$

then we speak of *orthogonal* matrices, where $\det\boldsymbol{a} = \pm\ 1$ and $\boldsymbol{a}^{\mathrm{T}} = \boldsymbol{a}^{-1}$ apply. Where $\boldsymbol{a}$ and $\boldsymbol{b}$ are two orthogonal matrices of the same order, then their products $\boldsymbol{a}\bullet\boldsymbol{b}$ and $\boldsymbol{b}\bullet\boldsymbol{a}$ are also orthogonal.

Every invertible matrix $\boldsymbol{a}$ of order m has an invertible *inverse* $\boldsymbol{a}^{-1}$ of order m, where

$$\boldsymbol{a}\bullet\boldsymbol{a}^{-1} = \boldsymbol{a}^{-1}\bullet\boldsymbol{a} = \mathbf{I} \tag{A5.15}$$

applies. The following applies for inverses:

$$\det(\boldsymbol{a}^{-1}) = (\det\boldsymbol{a})^{-1} \quad , \quad (\boldsymbol{a}^{\mathrm{T}})^{-1} = (\boldsymbol{a}^{-1})^{\mathrm{T}} \quad , \quad (\boldsymbol{a}\bullet\boldsymbol{b}\bullet\ldots\bullet\boldsymbol{c})^{-1} = \boldsymbol{c}^{-1}\bullet\ldots\bullet\boldsymbol{b}^{-1}\bullet\boldsymbol{a}^{-1} \tag{A5.16}$$

A *coordinate transformation* for a change from one *basis* $\boldsymbol{e}$ to a new basis $\overline{\boldsymbol{e}}$ is

$$\overline{\boldsymbol{e}} = \boldsymbol{t}\bullet\boldsymbol{e} \tag{A5.17}$$

where the columns of the (invertible) *transformation matrix* $\boldsymbol{t}$ contain the components of the new basis vectors $\overline{\boldsymbol{e}}$ in the old system $\boldsymbol{e}$, and so the result is the transformation

$$\boldsymbol{x} = \boldsymbol{t}\bullet\overline{\boldsymbol{x}} \tag{A5.18}$$

for any vector $\boldsymbol{x}$. Considering a *linear mapping* (linear transformation) of a vector $\boldsymbol{x}$ to an image vector $\boldsymbol{y}$

$$\boldsymbol{y} = \boldsymbol{a}\bullet\boldsymbol{x} \tag{A5.19}$$

then

$$\overline{\boldsymbol{y}} = \boldsymbol{t}^{-1}\bullet\boldsymbol{a}\bullet\boldsymbol{t}\bullet\overline{\boldsymbol{x}} = \tilde{\boldsymbol{a}}\bullet\overline{\boldsymbol{x}} \quad , \quad \tilde{\boldsymbol{a}} = \boldsymbol{t}^{-1}\bullet\boldsymbol{a}\bullet\boldsymbol{t} \tag{A5.20}$$

applies when $\boldsymbol{y}$ transforms in the same way (*cogredient*) as $\boldsymbol{x}$ ($\boldsymbol{y} = \boldsymbol{t}\bullet\overline{\boldsymbol{y}}$). Matrices $\tilde{\boldsymbol{a}}$ and $\boldsymbol{a}$ are referred to as *similar*; $\det\tilde{\boldsymbol{a}} = \det\boldsymbol{a}$ applies.

Orthogonal transformations facilitated by orthogonal matrices are either – depending on the value of the determinant – *proper* ($\det\boldsymbol{a} = 1$) or *improper* ($\det\boldsymbol{a} = -1$). The associated mappings in the vector space correspond to a pure rotation or a rotation with reflection.

If $\boldsymbol{y}$ is not transformed in the same way as $\boldsymbol{x}$, but rather *contragredient*, i. e.

$$\overline{\boldsymbol{y}} = \boldsymbol{t}^{\mathrm{T}}\bullet\boldsymbol{y} \tag{A5.21}$$

then (A5.18) and (A5.19) are used to obtain

$$\overline{\boldsymbol{y}} = \boldsymbol{t}^{\mathrm{T}}\bullet\boldsymbol{a}\bullet\boldsymbol{t}\bullet\overline{\boldsymbol{x}} = \hat{\boldsymbol{a}}\bullet\overline{\boldsymbol{x}} \quad , \quad \hat{\boldsymbol{a}} = \boldsymbol{t}^{\mathrm{T}}\bullet\boldsymbol{a}\bullet\boldsymbol{t} \tag{A5.22}$$

Matrices $\hat{\boldsymbol{a}}$ and $\boldsymbol{a}$ are referred to as *congruent*. With a contragredient transformation, the scalar product

$$\boldsymbol{x}^{\mathrm{T}}\bullet\boldsymbol{y} = \overline{\boldsymbol{x}}^{\mathrm{T}}\bullet\boldsymbol{t}^{\mathrm{T}}\bullet\boldsymbol{y} = \overline{\boldsymbol{x}}^{\mathrm{T}}\bullet\overline{\boldsymbol{y}}$$

remains invariant, even if the transformation matrix $\boldsymbol{t}$ is not square.

The difference between similarity and congruence is irrelevant for an orthogonal transformation where $\boldsymbol{t}^{\mathrm{T}} = \boldsymbol{t}^{-1}$. The invariance of the scalar products $\boldsymbol{x}^{\mathrm{T}} \bullet \boldsymbol{x}$ and $\boldsymbol{x}^{\mathrm{T}} \bullet \boldsymbol{y}$ then signifies invariance of lengths and angles with respect to a rotation.

A5.3 Linear equations

Various direct and iterative methods of solution exist for calculating the *solution vector* $\boldsymbol{x}$ for sets of linear equations

$$\boldsymbol{a} \bullet \boldsymbol{x} = \boldsymbol{b} \tag{A5.23}$$

with an (invertible) coefficient matrix $\boldsymbol{a}$ and a given vector $\boldsymbol{b}$ on the "right-hand side". The most important direct method of solution, the GAUSS*ian algorithm*, involves transforming matrix $\boldsymbol{a}$ into an upper triangular matrix by successively eliminating the unknowns x_i, with the unknowns being calculated ascending from x_m to x_1.

A5.4 Quadratic forms

A homogeneous second-degree polynomial in m variables $x_1, x_2, \ldots, x_m$

$$Q = \sum_{i=1}^{m} x_i \sum_{k=1}^{m} a_{ik} x_k \tag{A5.24}$$

is referred to as a *quadratic form*. Where $a_{ik} = a_{ki}$ applies, then it follows that $\boldsymbol{a}^{\mathrm{T}} = \boldsymbol{a}$ and

$$Q = \boldsymbol{x}^{\mathrm{T}} \bullet \boldsymbol{a} \bullet \boldsymbol{x} \tag{A5.25}$$

The symmetric matrix $\boldsymbol{a}$ is called a matrix of form Q, and Q itself is a scalar variable, e. g. an energy expression.

Besides quadratic forms, there are also *bilinear forms*:

$$P = \boldsymbol{y}^{\mathrm{T}} \bullet \boldsymbol{a} \bullet \boldsymbol{x} \tag{A5.26}$$

which occur in two systems of variables $\boldsymbol{x}$ and $\boldsymbol{y}$, where $\boldsymbol{a}$ can be a general $(m \times n)$ matrix and P again denotes a scalar, i. e. instead of the expression on the right in (A5.26), we can also use the following transposed expression:

$$P = \boldsymbol{y}^{\mathrm{T}} \bullet \boldsymbol{a} \bullet \boldsymbol{x} = \boldsymbol{x}^{\mathrm{T}} \bullet \boldsymbol{a}^{\mathrm{T}} \bullet \boldsymbol{y} \tag{A5.27}$$

Taking into account $\partial \boldsymbol{x} / \partial x_i = \boldsymbol{e}_i$ and the fact that $\boldsymbol{a}^{\mathrm{T}} = \boldsymbol{a}$ means we can use (A5.25) to obtain the derivative

$$\frac{\partial Q}{\partial x_i} = \boldsymbol{e}_i^{\mathrm{T}} \bullet \boldsymbol{a} \bullet \boldsymbol{x} + \boldsymbol{x}^{\mathrm{T}} \bullet \boldsymbol{a} \bullet \boldsymbol{e}_i = \boldsymbol{e}_i^{\mathrm{T}} \bullet \boldsymbol{a} \bullet \boldsymbol{x} + \boldsymbol{e}_i^{\mathrm{T}} \bullet \boldsymbol{a}^{\mathrm{T}} \bullet \boldsymbol{x} = 2\, \boldsymbol{e}_i^{\mathrm{T}} \bullet \boldsymbol{a} \bullet \boldsymbol{x} \tag{A5.28}$$

or in concise form

$$\frac{\partial Q}{\partial \boldsymbol{x}} = 2\, \boldsymbol{a} \bullet \boldsymbol{x} \tag{A5.29}$$

Similarly, it follows that

$$\frac{\partial P}{\partial \boldsymbol{x}} = \boldsymbol{a}^{\mathrm{T}} \bullet \boldsymbol{y} \quad , \quad \frac{\partial P}{\partial \boldsymbol{y}} = \boldsymbol{a} \bullet \boldsymbol{x} \tag{A5.30}$$

If according to (A5.25) Q is positive for all values of $\boldsymbol{x}$ not equal to zero, then the form is known as *positive definite*, and $\boldsymbol{a}$ is invertible. But if there are finite $\boldsymbol{x}$ values where $Q = 0$ ($Q > 0$ for all other values of $\boldsymbol{x}$), then the form is called *positive semi-definite*, and $\boldsymbol{a}$ is singular.

In the vector space, Q = const represents a quadric surface. The following applies for the differential of the function Q:

$$\mathrm{d}Q = \left(\frac{\partial Q}{\partial \boldsymbol{x}} \right)^{\mathrm{T}} \bullet \mathrm{d}\boldsymbol{x} \tag{A5.31}$$

According to (A5.29), the first factor on the right in (A5.31) denotes the *gradient* of the scalar function Q, and as $\mathrm{d}Q = 0$, the gradient is perpendicular to the surface Q = const, i. e. $\boldsymbol{a} \bullet \boldsymbol{x}$ is equal to the *normal vector* on the surface.

In the three-dimensional space, a quadric surface has three *principal axes* perpendicular to each other in such a way that the position vector $\boldsymbol{x}$ and the normal vector $\boldsymbol{a}\bullet\boldsymbol{x}$ coincide at them and only at them, i. e.

$$\boldsymbol{a}\bullet\boldsymbol{x} = \lambda\boldsymbol{x} \tag{A5.32}$$

where λ designates an as yet indeterminate scalar parameter.

A5.5 Eigenvalue problems

In the following we shall confine our deliberations to *special eigenvalue problems* of the type (A5.32), which we will present in the form

$$(\boldsymbol{a} - \lambda\,\mathbf{I})\bullet\boldsymbol{x} = \mathbf{0} \tag{A5.33}$$

where $\boldsymbol{a}$ is presumed to be square but otherwise arbitrary. The matrix on the left in (A5.33) is called the *characteristic matrix* of matrix $\boldsymbol{a}$. Eq. (A5.33) has non-trivial solutions when the associated *characteristic determinant* disappears:

$$\det(\boldsymbol{a} - \lambda\,\mathbf{I}) = 0 \tag{A5.34}$$

This *characteristic equation* leads to an mth-order polynomial with respect to λ, the *characteristic polynomial*, which must disappear. The roots λ_i of equation (A5.34) are the *eigenvalues*, and the associated vectors $\boldsymbol{x}_i$ are called *eigenvectors*, which are determinate apart from their magnitude.

A matrix $\boldsymbol{a}$ only has at least one eigenvalue $\lambda = 0$ when it is singular, $\det\boldsymbol{a} = 0$. Matrix $\boldsymbol{a}$ has r eigenvalues $\neq 0$, where r denotes the rank of $\boldsymbol{a}$; the number of zero eigenvalues for $\boldsymbol{a}$ agrees with the nullity $d = m - r$. Eigenvectors for various eigenvalues exhibit linear independence. A single eigenvalue has exactly one linear-independent eigenvector, and a p-fold eigenvalue has at least one and no more than p linear-independent eigenvectors. Moreover,

$$\mathrm{sp}\,\boldsymbol{a} = \sum_{i=1}^{m}\lambda_i \quad , \quad \det\boldsymbol{a} = \prod_{i=1}^{m}\lambda_i \tag{A5.35}$$

applies. All eigenvalues are real for a symmetric $\boldsymbol{a}$, and positive when $\boldsymbol{a}$ is positive definite.

Combining the eigenvectors $\boldsymbol{x}_i$ for a symmetric $\boldsymbol{a}$ column by column in the *modal matrix* (eigenvalue matrix) $\boldsymbol{X}$ and arranging the eigenvalues λ_i in the *diagonal matrix of eigenvalues* $\boldsymbol{\Lambda}$ results in

$$\boldsymbol{a}\bullet\boldsymbol{X} = \boldsymbol{X}\bullet\boldsymbol{\Lambda} \tag{A5.36}$$

instead of (A5.33), and assuming orthonormal eigenvectors ($\boldsymbol{X}^{\mathrm{T}} = \boldsymbol{X}^{-1}$) results in

$$\boldsymbol{X}^{\mathrm{T}}\bullet\boldsymbol{a}\bullet\boldsymbol{X} = \boldsymbol{\Lambda} \tag{A5.37}$$

This congruence transformation (or similarity transformation), which is known as a *principal component analysis*, enables $\boldsymbol{a}$ to be transformed onto the diagonal matrix of eigenvalues.

The RAYLEIGH *quotient*

$$R(\boldsymbol{x}) = \frac{\boldsymbol{x}^{\mathrm{T}}\bullet\boldsymbol{a}\bullet\boldsymbol{x}}{\boldsymbol{x}^{\mathrm{T}}\bullet\boldsymbol{x}} \tag{A5.38}$$

with an eigenvector $\boldsymbol{x}_i$ results in the associated eigenvalue λ_i, which is easily confirmed by (A5.32) after first multiplying by $\boldsymbol{x}_i{}^{\mathrm{T}}$:

$$\lambda_i = R(\boldsymbol{x}_i) \tag{A5.39}$$

The function $R(x)$ takes on its extreme values for the eigenvectors $\boldsymbol{x}_i$; in fact, the derivative

$$\frac{\partial R}{\partial\boldsymbol{x}} = \frac{2\boldsymbol{a}\bullet\boldsymbol{x}}{\boldsymbol{x}^{\mathrm{T}}\bullet\boldsymbol{x}} - \frac{\boldsymbol{x}^{\mathrm{T}}\bullet\boldsymbol{a}\bullet\boldsymbol{x}\cdot 2\boldsymbol{x}}{(\boldsymbol{x}^{\mathrm{T}}\bullet\boldsymbol{x})^2} = \frac{2[\boldsymbol{a}\bullet\boldsymbol{x} - R(\boldsymbol{x})\cdot\boldsymbol{x}]}{\boldsymbol{x}^{\mathrm{T}}\bullet\boldsymbol{x}}$$

for

$$\boldsymbol{a} \bullet \boldsymbol{x} = R(\boldsymbol{x}) \cdot \boldsymbol{x} = \lambda \boldsymbol{x}$$

disappears, which corresponds precisely with the eigenvalue problem (A5.32) or (A5.33).

Considering a quadratic form (A5.25), the principal component analysis $\boldsymbol{x} = \boldsymbol{X} \bullet \boldsymbol{y}$, together with the modal matrix $\boldsymbol{X}$, leads to

$$Q = \boldsymbol{y}^{\mathrm{T}} \bullet \boldsymbol{X}^{\mathrm{T}} \bullet \boldsymbol{a} \bullet \boldsymbol{X} \bullet \boldsymbol{y} = \boldsymbol{y}^{\mathrm{T}} \bullet \boldsymbol{\Lambda} \bullet \boldsymbol{y} = \sum_{i=1}^{m} \lambda_i y_i^2 \tag{A5.40}$$

see (A5.18) and (A5.37). Comparing (A5.40) with the canonical equation for quadric surfaces reveals that the eigenvalues are proportional to the inverses of the squares of the semi-axes.

A5.6 Matrix norms and condition numbers

Various *matrix norms* and *condition numbers* are in use for estimating eigenvalue magnitudes and assessing relative errors in matrix operations. The symbol for norms is a pair of parallel lines, i. e. $\|\boldsymbol{x}\|$ for the norm of a vector $\boldsymbol{x}$ and $\|\boldsymbol{a}\|$ for the norm of a matrix $\boldsymbol{a}$. Norms must generally be positive and may only be zero for $\boldsymbol{x} = \boldsymbol{0}$ or $\boldsymbol{a} = \boldsymbol{0}$. Further, the norm of a scaled variable must be equal to the norm of the unscaled variable multiplied by the magnitude of the scalar. Finally, it is essential that the triangle inequality $\|\boldsymbol{x} + \boldsymbol{y}\| \leq \|\boldsymbol{x}\| + \|\boldsymbol{y}\|$ or $\|\boldsymbol{a} + \boldsymbol{b}\| \leq \|\boldsymbol{a}\| + \|\boldsymbol{b}\|$ should apply, and for matrix norms there is also a requirement that $\|\boldsymbol{a} \bullet \boldsymbol{b}\| \leq \|\boldsymbol{a}\| \cdot \|\boldsymbol{b}\|$.

Customary vector norms are the maximum norm, the sum norm and the EUCLIDean norm:

$$\|\boldsymbol{x}\| = \mathrm{Max}\,|x_i| \quad , \quad \|\boldsymbol{x}\| = \sum_i |x_i| \quad , \quad \|\boldsymbol{x}\| = |\boldsymbol{x}| = \sqrt{\boldsymbol{x}^{\mathrm{T}} \bullet \boldsymbol{x}} \tag{A5.41}$$

Matrix norms include the total norm, row norm, column norm and EUCLIDean norm:

$$\|\boldsymbol{a}\| = m \cdot \mathrm{Max}\,|a_{ij}| \quad , \quad \|\boldsymbol{a}\| = \mathrm{Max}_i \sum_j a_{ij} \quad , \quad \|\boldsymbol{a}\| = \mathrm{Max}_j \sum_i a_{ij} \quad , \quad \|\boldsymbol{a}\| = \sqrt{\mathrm{sp}\,\boldsymbol{a}^{\mathrm{T}} \bullet \boldsymbol{a}} \tag{A5.42}$$

A matrix norm is considered compatible with a vector norm when the inequality

$$\|\boldsymbol{a} \bullet \boldsymbol{x}\| \leq \|\boldsymbol{a}\| \cdot \|\boldsymbol{x}\| \tag{A5.43}$$

applies for all matrices $\boldsymbol{a}$ and vectors $\boldsymbol{x}$. Substituting (A5.32) in (A5.43) results in

$$\lambda \leq \|\boldsymbol{a}\| \tag{A5.44}$$

i. e. the magnitudes of the eigenvalues cannot lie outside some matrix norm.

If in a set of linear equations (A5.23) the magnitude of the determinant $\det \boldsymbol{a}$ of matrix $\boldsymbol{a}$ is very small, then small differences in large numbers occur during the elimination process, and the result is a loss of significant digits that can seriously distort the result. We speak of an *ill-conditioned* matrix in such cases; small errors in the input data are amplified in the result. The HADAMARD condition number

$$\mathrm{cond}\,\boldsymbol{a} \leq \frac{|\det \boldsymbol{a}|}{\prod_{i=1}^{m} \sqrt{\sum_{j=1}^{m} a_{ij}^2}} \tag{A5.45}$$

should be used to assess the behaviour of a matrix in this respect. This condition number can lie between 1 (optimum condition) and 0 (instability). The expression in the denominator of (A5.45) corresponds to the volume of the rectangular prism formed from the magnitudes of the row vectors.

A6 TENSOR CALCULUS

A6.1 Introduction

Many theory of structures relationships can be presented in a simple and graphic way with the help of *vector algebra* without having to refer to a particular system of coordinates. However, these methods reach their limits when other classes appear alongside scalar and vector variables. A suitable system of coordinates then becomes essential. If we then try to express the relationships that occur in such a way that they are valid in any system of coordinates (with straight or curved lines, right-angles or oblique angles), we arrive at general *tensor calculus*. We shall confine ourselves here to the essential minimum, i. e. right-handed systems of Cartesian coordinates plus corresponding Cartesian tensors. In the general spatial case, we shall refer to the $x_i = x_1, x_2, x_3$ coordinates ($x_i = x_1, x_2$ in the planar case).

A6.2 Terminology

According to (A5.17), the columns of the transformation matrix $\boldsymbol{t}$ used for the transition from an old basis $\boldsymbol{e}$ to a new basis $\overline{\boldsymbol{e}}$ contain the components of the new basis vectors in the old system. These are equal to the cosines of the angles between the x_i and $\overline{x}_{jj}$ directions and from now on are denoted with c_{ij}. Instead of (A5.18), in *symbol notation* we therefore get

$$\boldsymbol{x} = \boldsymbol{c} \bullet \overline{\boldsymbol{x}}$$

and in *index notation* (or *coordinate notation*)

$$x_i = c_{ij}\overline{x}_j \tag{A6.1}$$

when the EINSTEIN *summation convention* is agreed upon such that a Latin index occurring twice in one expression means that the expression is summed over the values 1, 2, 3 of this index. The index j occurring twice in (A6.1) is known as a *dummy*, *bound* or summation index; it disappears when the summation implied by the index has been performed.

Written out in full, expression (A6.1) encompasses three sums (two in the planar case) each with three (two) terms. Similarly, omitting the summation symbols from (A5.2), (A5.10) and (A5.24) results in the expressions a_{ii}, $a_{ij}\, b_{jk}$ and $x_i\, a_{ik}\, x_k$ for the trace of a matrix, the multiplication of two matrices and a quadratic form, for example.

Owing to the column-by-column structure with orthogonal unit vectors, the *rotation matrix* c_{ij} in (A6.1) satisfies the requirement (A5.14), i. e.

$$c_{ij}c_{ik} = \delta_{jk} \qquad \text{or} \qquad c_{ji}c_{ki} = \delta_{jk} \tag{A6.2}$$

where

$$\begin{aligned} \delta_{jk} &= 1 \quad \text{for} \quad j = k \\ \delta_{jk} &= 0 \quad \text{for} \quad j \neq k \end{aligned} \tag{A6.3}$$

denotes the KRONECKER *symbol* and corresponds to the identity matrix introduced in section A5.1.

Theory of Structures. First Edition. Peter Marti

Which Latin index is used for a dummy index is irrelevant when no other index is repeated in the same expression. For example, (A6.1) can be written in the form

$$x_i = c_{ik}\overline{x}_k$$

Multiplying this by c_{ij} and applying (A6.2) then leads to

$$\overline{x}_j = c_{ij}x_i \tag{A6.4}$$

or rather $\overline{\boldsymbol{x}} = \boldsymbol{c}^{\mathrm{T}} \bullet \boldsymbol{x}$.

A6.3 Vectors and tensors

A *vector* $\boldsymbol{v}$ is unequivocally defined by its components v_i related to its basis $\boldsymbol{e}$, or by its magnitude

$$|\boldsymbol{v}| = v = \sqrt{v_i v_i}$$

and its direction (e. g. given by its azimuth and elevation related to the basis $\boldsymbol{e}$). At the transition to a new basis $\overline{\boldsymbol{e}}$, the components v_i transform according to (A6.4), i. e.

$$\overline{v}_j = c_{ij}v_i \tag{A6.5}$$

and, vice versa,

$$v_i = c_{ij}\overline{v}_j \tag{A6.6}$$

applies in a similar way to (A6.1). The projection of $\boldsymbol{v}$ onto an arbitrary direction given by a unit vector $\boldsymbol{n}$ results in $\boldsymbol{v}\bullet\boldsymbol{n} = v_i n_i = v\cos\alpha$, where α denotes the angle included by $\boldsymbol{n}$ and $\boldsymbol{v}$; therefore, $\boldsymbol{v}$ assigns a scalar to every direction $\boldsymbol{n}$.

Where a vector with the components t_{ij} belongs to every (positive) coordinate direction x_j instead of a scalar v_j, then these vectors allocate a vector with the components

$$t_i = t_{ij}n_j \tag{A6.7}$$

to every direction $\boldsymbol{n}$. Such an allocation characterises a *tensor*. The columns of matrix t_{ij} are the values of the tensor for the coordinate directions. The transformation of t_i and n_j in (A6.7) using (A6.5) and (A6.6) results in

$$\overline{t}_k = \overline{t}_{kl}\overline{n}_l \quad , \quad \overline{t}_{kl} = c_{ik}c_{jl}t_{ij} \tag{A6.8}$$

In a Cartesian system, a tensor is therefore defined by nine variables that transform according to $(\text{A6.8})_2$ or rather $\overline{\boldsymbol{t}} = \boldsymbol{c}^{\mathrm{T}} \bullet \boldsymbol{t} \bullet \boldsymbol{c}$. Swapping indices k and l in $(\text{A6.8})_2$ results in

$$\overline{t}_{lk} = c_{il}c_{jk}t_{ij} = c_{jl}c_{ik}t_{ji}$$

i. e. t_{ji} is a tensor, too, which we call the tensor *adjoint* to t_{ij}.

Applying $(\text{A6.8})_2$ to the tensor defined by the KRONECKER symbol (A6.3) and using (A6.2) results in

$$\overline{\delta}_{kl} = c_{ik}c_{jl}\delta_{ij} = c_{ik}c_{il} = \delta_{kl}$$

i. e. δ_{ij} is a unit tensor in any system of coordinates and is isotropic.

A tensor is symmetric when $t_{ij} = t_{ji}$ and antisymmetric when $t_{ji} = -t_{ij}$. Resolving a tensor into one symmetric and one antisymmetric part is carried out in a similar way to (A5.7):

$$t_{(ij)} = t_{ij}^{\mathrm{S}} = \tfrac{1}{2}(t_{ij} + t_{ji}) \quad , \quad t_{[ij]} = t_{ij}^{\mathrm{A}} = \tfrac{1}{2}(t_{ij} - t_{ji}) \tag{A6.9}$$

Considering scalars, vectors and the aforementioned tensors as zeroth-, first- and second-order tensors, it is possible to generalise the tensor definition according to (A6.8) as follows: an nth-order tensor is determined by 3^n components (2^n in the planar case), which transform according to

$$\overline{t}_{pqr\ldots} = c_{ip}c_{jq}c_{kr}\ldots t_{ijk\ldots} \tag{A6.10}$$

The scaling and addition (subtraction) of tensors follows the algorithms for matrices discussed in section A5.2. All of the products that can be formed from one component from each of two tensors are known as *tensor products* – tensors whose order is equal to the sum of the orders of the factors. For example, the product $t_{ijk} = r_{ij}\, s_k$ of a tensor r_{ij} and a vector s_k is a third-order tensor, and the *dyadic product* $t_{ij} = u_i\, v_j$ of two vectors is a second-order tensor. It should also be noted that the dyadic product is not commutative; $t_{ji} = v_j\, u_i$ is the tensor adjoint to t_{ij}.

Equating two indices of an nth-order tensor and performing the corresponding summation results in a tensor of the $(n-2)$th order, which is the *contraction* of the initial tensor according to the equated indices. For example, we thus get the tensor's trace t_{ii} (a scalar) from the tensor t_{ij}. If a tensor product is contracted according to two indices that do not belong to the same factor, we speak of an *inner multiplication* of the initial tensors according to the equated indices. For example, the scalar product $u_i v_i$ of two vectors is their inner multiplication. Both (A6.7) and the generalisation $s_{j\ldots n} = t_{ij\ldots n}\, n_i$ correspond to inner multiplications; we get $t_{ip} t_{pj}$ for the square of a tensor and $t_{ip}\, t_{pq}\, t_{qj}$ for its cube, etc.

The permutation of certain tensor indices leads to a tensor of the same order, which can be called an *isomer* of the initial tensor. For example, the tensor t_{ji} adjoint to t_{ij} is its only isomer. A tensor is symmetric (antisymmetric) with respect to two indices when after swapping these indices it is equal (opposite and equal) to its isomer. Where $s_{\ldots i\ldots j\ldots}$ and $t_{\ldots i\ldots j\ldots}$ are symmetric or antisymmetric with respect to i and j, then their product contracted according to i and j disappears. For example, applying (A6.9) means that

$$s_{ij} t_{ij} = \left\{ s_{(ij)} + s_{[ij]} \right\} \left\{ t_{(ij)} + t_{[ij]} \right\} = s_{(ij)} t_{(ij)} + s_{[ij]} t_{[ij]} \tag{A6.11}$$

applies to any second-order tensors.

The tensor character of a certain variable can be found using the *quotient rule*. The quotient rule states that $t_{\ldots i\ldots j\ldots k\ldots}$ must be an nth-order tensor if we know that $t_{\ldots i\ldots j\ldots k\ldots} s_{ij\ldots k}$ is a tensor of the $(n-m)$th order, regardless of how the mth-order tensor $s_{ij\ldots k}$ is selected.

With the components of three non-collinear vectors u_i, v_j, w_k arranged in the columns of a (3×3) matrix, then the magnitude of their determinant (A5.3) corresponds to the volume of the parallelepiped defined by the three vectors. The sign of the determinant is positive (negative) here when the three vectors form a right-handed (left-handed) system. Introducing the variable ε_{ijk} – which takes on the values 1 (–1) or 0 depending on whether i, j, k are an even (odd) or no permutation of 1, 2, 3 – allows us to express the determinant as $\varepsilon_{ijk}\, u_i\, v_j\, w_k$. Therefore, according to the quotient rule, ε_{ijk} is a third-order tensor, which is called a *permutation tensor.*

The equation

$$t_i = \varepsilon_{ijk} t_{jk} \tag{A6.12}$$

allocates the *dual vector* t_i with the components $t_{23} - t_{32}$, ... to the tensor t_{jk}; the vector depends only on the tensor's antisymmetric part $t_{[jk]}$. The dual vector for a symmetric tensor disappears. Reversing the allocation (A6.12) results in

$$t_{jk} = \frac{1}{2} \varepsilon_{ijk} t_i \tag{A6.13}$$

i. e. an antisymmetric second-order tensor is assigned to every vector.

The dual vector

$$w_i = \varepsilon_{ijk} u_j v_k \tag{A6.14}$$

(the *vector product* $\boldsymbol{w} = \boldsymbol{u} \times \boldsymbol{v}$) corresponds to the dyadic product $u_j v_k$ of two vectors. As $u_i u_j$ ($v_i v_k$) and ε_{ijk} with respect to i and j (i and k) are symmetric and antisymmetric respectively, then $u_i w_i = v_i w_i = 0$, i. e. $\boldsymbol{w}$ is orthogonal to the plane defined by $\boldsymbol{u}$ and $\boldsymbol{v}$. Further, $w_i w_i = \varepsilon_{ijk} w_i\, u_j v_k > 0$ is equal to the volume of the prism defined by the three vectors; $\boldsymbol{u}$, $\boldsymbol{v}$ and $\boldsymbol{w}$ form a right-handed system, and the magnitude of $\boldsymbol{w}$ is equal to the area of the parallelogram defined by $\boldsymbol{u}$ and $\boldsymbol{v}$.

Placing the origin of the system of coordinates at any reference point means that the moment $\boldsymbol{M} = \boldsymbol{x} \times \boldsymbol{F}$ of a force $\boldsymbol{F}$ with point of application $\boldsymbol{x}$ related to this point can be expressed by

$$M_i = \varepsilon_{ijk} x_j F_k \tag{A6.15}$$

see (5.1). Similarly, the displacement $\boldsymbol{u} = \boldsymbol{\omega} \times \boldsymbol{x}$ of a point $\boldsymbol{x}$ for rotation with the rotation vector $\boldsymbol{\omega}$ about the origin of coordinates is

$$u_i = \varepsilon_{ijk} \omega_j x_k \tag{A6.16}$$

see (6.2).

A6.4 Principal axes of symmetric second-order tensors

Starting with (A6.7), we call n_j a *principal direction* of the symmetric tensor t_{ij} if the vector $t_{ij}\, n_j$ allocated to this direction has the direction n_i, i. e. can be expressed by $t n_i$, where t is a scalar. In a similar way to (A5.33), we obtain

$$(t_{ij} - t\delta_{ij}) n_j = 0 \tag{A6.17}$$

and we get the characteristic equation

$$\det (t_{ij} - t\delta_{ij}) = 0 \tag{A6.18}$$

as a condition for non-trivial solutions, which can also be written in the form

$$t^3 - t_{\mathrm{I}} t^2 - t_{\mathrm{II}} t - t_{\mathrm{III}} = 0 \tag{A6.19}$$

with the *basic invariants*

$$t_{\mathrm{I}} = t_{ii} \quad , \quad t_{\mathrm{II}} = \frac{1}{2}(t_{ij} t_{ji} - t_{ii} t_{jj}) \quad , \quad t_{\mathrm{III}} = \frac{1}{6} \varepsilon_{ijk} \varepsilon_{lmn} t_{il} t_{jm} t_{kn} \tag{A6.20}$$

where t_{I} is equal to the sum of the diagonal elements, or rather the trace of the tensor, t_{II} is the negative sum of the minors of these elements, and t_{III} is the determinant of the matrix t_{ij}.

The solutions $t = t_i$ to characteristic equation (A6.19) are the *principal values*, and the corresponding principal directions, orthogonal to one another, follow from

$$n_{i1} = \frac{-\, c_{i2} c_{i3}}{\sqrt{c_{i1}^2 c_{i2}^2 + c_{i1}^2 c_{i3}^2 + c_{i2}^2 c_{i3}^2}} \ , \ldots \qquad [c_{i1} = (t_{11} - t_i) t_{23} - t_{12} t_{13} \ , \ldots] \tag{A6.21}$$

where the ellipsis indicates the cyclic alternation of the indexes.

Projecting the vector (A6.7) onto direction n_j gives us the *normal component* $t_{ij}\, n_j\, n_i$ of the tensor for direction n_j. If we require the directions n_j for which the normal component is stationary, then taking into account the secondary condition $n_i\, n_i = 1$, the expression $(t_{ij} - t\delta_{ij}) n_j\, n_i$ must take on a stationary value, where t denotes a LAGRANGE multiplier. Setting the derivative of this expression to zero with respect to n_k results in

$$(t_{ij} - t\delta_{ij})(\delta_{jk} n_i + n_j \delta_{ik}) = (t_{ik} - t\delta_{ik}) n_i + (t_{kj} - t\delta_{kj}) n_j = 0 \tag{A6.22}$$

i. e. owing to the symmetry of t_{ij}, we arrive at (A6.17) again. Eq. (A6.22) makes use of the fact that the derivative of n_i (n_j) with respect to n_k is given by δ_{ik} (δ_{jk}). Summing up, stationary values of the normal components of the tensor correspond to the principal directions, and these components are given by the principal values $t = t_i$.

A6.5 Tensor fields and integral theorems

If an nth-order tensor – whose 3^n components are position functions $t_{ijk\ldots}(x_1, x_2, x_3)$ continuously changing with the position – is assigned to every point of a space, we speak of a *tensor field*. of the nth order. In the following, all the derivatives of these position functions which occur are assumed to be continuous with respect to the coordinates, and the differential operators $\partial/\partial x_p$, $\partial^2/(\partial x_p \partial x_q)$ etc. are abbreviated to ∂_p, ∂_{pq} etc. Alternatively, derivatives $\partial_p t_{ijk\ldots}$ and $\partial_{pq} t_{ijk\ldots}$ can be abbreviated with $t_{ijk\ldots,p}$ or $t_{ijk\ldots,pq}$, i. e. by adding the corresponding indices with preceding commas.

The change to $t_{ijk...}$ in the vicinity of a point x_{p0} results from a TAYLOR series $(x_p - x_{p0})t_{ijk...,p} + ...$ and is an nth-order tensor, irrespective of how $x_p - x_{p0}$ is selected. Therefore, according to the quotient rule, $t_{ijk...,p}$ is a tensor of the $(n+1)$th order. The operator ∂_p thus behaves like a vector during the coordinate transformation, operator ∂_{pq} like a second-order tensor, etc. In symbol notation, we use the "Nabla" vector or the HAMILTON operator ∇ for ∂_p.

Tensor fields of the zeroth and first orders are known as *scalar fields* φ and *vector fields* v_i respectively. These can be illustrated graphically by their *level surfaces* $\varphi = \text{const}$ or *field lines* $\mathrm{d}x_i/v_i = \text{const}$.

Applying operator ∂_i to a scalar field φ leads to the *gradient*

$$\varphi_{,i} = \nabla\varphi = \operatorname{grad}\varphi \tag{A6.23}$$

Continuing by an amount $\mathrm{d}s$ in the direction of the unit vector n_i causes φ to change by

$$\mathrm{d}\varphi = n_i\,\varphi_{,i}\,\mathrm{d}s = (\boldsymbol{n}\bullet\operatorname{grad}\varphi)\,\mathrm{d}s \tag{A6.24}$$

The gradient of φ is orthogonal to the level surface of φ at the point being considered and its magnitude is equal to the maximum slope $\mathrm{d}\varphi/\mathrm{d}s$.

Applying operator ∂_j to a vector field v_k leads to the *vector gradient* $v_{k,j}$, a second-order tensor. Continuing by an amount $\mathrm{d}s$ in the direction of the unit vector n_j causes v_k to change by

$$\mathrm{d}v_k = n_j\,v_{k,j}\,\mathrm{d}s = (\boldsymbol{n}\bullet\nabla)\,\boldsymbol{v}\,\mathrm{d}s = (\boldsymbol{n}\bullet\operatorname{grad})\,\boldsymbol{v}\,\mathrm{d}s \tag{A6.25}$$

The trace of the vector gradient is the *divergence*

$$v_{i,i} = \operatorname{div}\boldsymbol{v} = \nabla\bullet\boldsymbol{v} = \frac{\partial v_1}{\partial x_1} + \frac{\partial v_2}{\partial x_2} + \frac{\partial v_3}{\partial x_3} \tag{A6.26}$$

and the dual vector for the vector gradient is the *curl*

$$\varepsilon_{ijk}v_{k,j} = \operatorname{curl}\boldsymbol{v} = \nabla\times\boldsymbol{v} = \left(\frac{\partial v_3}{\partial x_2} - \frac{\partial v_2}{\partial x_3}\,, ...\right) \tag{A6.27}$$

Contraction of the operator ∂_{ij} leads to the LAPLACE operator

$$\partial_{ii} = \Delta = \nabla^2 = \frac{\partial^2}{\partial x_1^2} + \frac{\partial^2}{\partial x_2^2} + \frac{\partial^2}{\partial x_3^2} \tag{A6.28}$$

Using the variables introduced above, the following relationships apply:

$$\operatorname{curl}\operatorname{grad}\varphi = 0 \quad,\quad \operatorname{div}\operatorname{grad}\varphi = \Delta\varphi \quad,\quad \operatorname{div}\operatorname{curl}\boldsymbol{v} = 0 \quad,\quad \operatorname{curl}\operatorname{curl}\boldsymbol{v} = \operatorname{grad}\operatorname{div}\boldsymbol{v} - \Delta\boldsymbol{v} \tag{A6.29}$$

GAUSS' *theorem*

$$\int t_{jkl...,i}\,\mathrm{d}V = \int n_i t_{jkl...}\,\mathrm{d}S \tag{A6.30}$$

applies to any tensors for a closed surface S with outward unit normal vector $\boldsymbol{n}$, which is the boundary of a volume V, with the special cases

$$\int\operatorname{grad}\varphi\,\mathrm{d}V = \int\boldsymbol{n}\,\varphi\,\mathrm{d}S \quad,\quad \int\operatorname{div}\boldsymbol{v}\,\mathrm{d}V = \int\boldsymbol{n}\bullet\boldsymbol{v}\,\mathrm{d}S \quad,\quad \int\operatorname{curl}\boldsymbol{v}\,\mathrm{d}V = \int\boldsymbol{n}\times\boldsymbol{v}\,\mathrm{d}S \tag{A6.31}$$

And the following applies for two scalar fields φ_1, φ_2:

$$\int\varphi_1\varphi_{2,ii}\,\mathrm{d}V = \int[(\varphi_1\varphi_{2,i})_{,i} - \varphi_{1,i}\varphi_{2,i}]\,\mathrm{d}V \tag{A6.32}$$

Applying GAUSS' theorem to the first term on the right results in GREEN's *first identity*

$$\int\varphi_1\varphi_{2,ii}\,\mathrm{d}V = \int\varphi_1 n_i\varphi_{2,i}\,\mathrm{d}S - \int\varphi_{1,i}\varphi_{2,i}\,\mathrm{d}V \tag{A6.32}$$

or rather

$$\int \varphi_1 \Delta\varphi_2 \, dV = \int \varphi_1 \frac{\partial \varphi_2}{\partial n} dS - \int \text{grad}\, \varphi_1 \bullet \text{grad}\, \varphi_2 \, dV \tag{A6.33}$$

where $\partial\varphi_2/\partial n$ equals the slope of φ_2 in the direction of the normal $\boldsymbol{n}$. If we swap the roles of φ_1 and φ_2 in (A6.32) or (A6.33) and subtract the result from the initial equation, then the outcome is GREEN*'s second identity*

$$\int (\varphi_1 \varphi_{2,ii} - \varphi_2 \varphi_{1,ii}) \, dV = \int (\varphi_1 n_i \varphi_{2,i} - \varphi_2 n_i \varphi_{1,i}) \, dS \tag{A6.34}$$

or rather

$$\int (\varphi_1 \Delta\varphi_2 - \varphi_2 \Delta\varphi_1) \, dV = \int \left(\varphi_1 \frac{\partial \varphi_2}{\partial n} - \varphi_2 \frac{\partial \varphi_1}{\partial n} \right) dS \tag{A6.35}$$

A7 CALCULUS OF VARIATIONS

A7.1 Extreme values of continuous functions

According to WEIERSTRASS' theorem, every continuous function $f(x_i)$ in a closed domain of the variables x_i has a *maximum* and a *minimum* within or on the boundary of the domain. If f is differentiable in the domain considered and the extreme value is assumed to be within the domain, then all the derivatives $\partial f/\partial x_i = f_{,i}$ at the point concerned must disappear, or rather the differential $\mathrm{d}f = f_{,i}\,\mathrm{d}x_i$ must be equal to zero. The index notation introduced in section A6.2 and the abbreviated form for derivatives used in section A6.5 are employed here. However, the condition $\mathrm{d}f = f_{,i}\,\mathrm{d}x_i = 0$ only guarantees the *stationary value* of f and is not sufficient for a maximum or minimum, as the occurrence of points of inflection or saddle points shows.

Subjecting the variables x_i to side conditions $g_j(x_i) = \mathbf{0}$ allows us to form the function

$$h = f + \lambda_j g_j \tag{A7.1}$$

with the LAGRANGE multipliers λ_j and requires $h_{,i} = \mathbf{0}$, which together with the side conditions $g_j = \mathbf{0}$ permits x_i and λ_j to be determined for stationary behaviour.

A7.2 Terminology

Calculus of variations is concerned with the search for the extreme values (or merely stationary values) of *functionals*, i. e. variables

$$I = \int F(x_i, f_j, f_{j,i}, f_{j,ik}, \ldots)\,\mathrm{d}V \tag{A7.2}$$

that depend on the progression of one or more arbitrary *argument functions* f_j between certain limits and their derivatives with respect to the variables x_i. The integrand F in (A7.2) is the LAGRANGE *function*.

Those argument functions that satisfy the requirement $I = \mathrm{stat}$ are known as *extremals* of the functional. They must lie within the *domain of admissible functions*, i. e. satisfy certain continuity and differentiability requirements as well as side and boundary conditions. If I contains the nth derivative of an argument function, the admissible functions lying in a sufficiently small neighbourhood of the extremals must satisfy all the boundary conditions for the argument function and its derivatives up to the order $n-1$; these are called the *essential boundary conditions*.

The fundamental problem of calculus of variations lies in determining the extremals within the domain of admissible functions, i. e. those functions that make the functional an extreme value compared with all argument functions belonging to a sufficiently small neighbourhood.

Most *direct methods* for solving variational problems begin by solving the associated ordinary extreme value problems. This initially involves determining n parameters so that the passage to the limit $n \to \infty$ can be performed for the complete solution. The RITZ method in particular should be mentioned in this context. This method is the one most frequently used as a numerical approximation method for solving variational problems.

Theory of Structures. First Edition. Peter Marti

Indirect methods essentially simplify variational problems to associated differential equation problems. The ensuing EULER-LAGRANGE *equations* are necessary, but not sufficient, conditions for the presence of an extreme value. At points where essential boundary conditions are lacking, we get *natural boundary conditions* as well. EULER-LAGRANGE equations and natural boundary conditions together form the *equivalent conditions of the variational problem*, which are automatically satisfied by its extremals. The extremals themselves are calculated according to the indirect method of calculus of variations by integrating the EULER-LAGRANGE equations while taking into account side conditions where applicable plus the essential and natural boundary conditions.

A7.3 The simplest problem of calculus of variations

The integral

$$I = \int_{x_0}^{x_1} F(x, y, y')\,\mathrm{d}x \tag{A7.3}$$

dependent on x, $y = f(x)$ and $y' = \mathrm{d}y/\mathrm{d}x$ should take on an extreme value, where F can be continuously differentiated twice with respect to x, y and y', and x_0, x_1 as well as $y_0 = y(x_0)$, $y_1 = y(x_1)$ are given values; in addition, the second derivative y'' of the function y should be continuous. Introducing the function $\eta(x)$ with the continuous second derivative η'' and $\eta(x_0) = \eta(x_1) = 0$ together with a parameter ε results in the family of functions

$$\bar{y} = y + \varepsilon\eta = y + \delta y \tag{A7.4}$$

where y is the extremal required and δy its *variation*. For $\varepsilon = 0$, the integral $I(\bar{y})$, which can be regarded as a function $\bar{I}(\varepsilon)$, must take on an extreme value relative to all sufficiently small, non-zero values of ε, i. e. $\partial\bar{I}/\partial\varepsilon = 0$ for $\varepsilon = 0$. Differentiating the expression

$$\int_{x_0}^{x_1} F(x, y + \varepsilon\eta, y' + \varepsilon\eta')\,\mathrm{d}x$$

with respect to ε and equating to zero results in

$$\int_{x_0}^{x_1} (F_y\eta + F_{y'}\eta')\,\mathrm{d}x = 0 \tag{A7.5}$$

where, for simplicity, we have taken $F_y = \partial F/\partial y$ and $F_{y'} = \partial F/\partial y'$. Integration by parts of the second term in the integrand of (A7.5), taking into account the boundary conditions $\eta(x_0) = \eta(x_1) = 0$, results in

$$\int_{x_0}^{x_1} \eta\left(F_y - \frac{\mathrm{d}}{\mathrm{d}x}F_{y'}\right)\mathrm{d}x = 0 \tag{A7.6}$$

According to the *fundamental lemma of calculus of variations*, the identity $\varphi(\mathrm{x}) \equiv 0$ applies for continuous functions $\varphi(\mathrm{x})$ when for all functions $\eta(x)$ continuous with the first two derivatives, which disappear for x_0 and x_1, the relationship

$$\int_{x_0}^{x_1} \eta\varphi\,\mathrm{d}x = 0 \tag{A7.7}$$

holds true. Consequently, the expression in brackets in (A7.6) must disappear, i. e. the EULER-LAGRANGE equation

$$F_y - \frac{\mathrm{d}}{\mathrm{d}x}F_{y'} = 0 \tag{A7.8}$$

applies, which takes on the form

$$F_y - F_{y'y'}y'' - F_{y'y}y' - F_{y'x} = 0 \tag{A7.9}$$

when written out in full. Two integration constants that can be fitted to the boundary conditions occur in the general solution to this second-order differential equation. The differential expression on the left in (A7.8) is known as a *variational derivative*; it plays the same role as the differential quotient in ordinary extreme value problems.

We use (A7.4) to obtain the variation $\delta(y') = \varepsilon\eta'$ of the derivative y'. According to (A7.4), $(\delta y)' = \varepsilon\eta'$ also applies, and therefore

$$\delta(y') = (\delta y)' \tag{A7.10}$$

i. e. variation and differentiation are interchangeable in calculus of variations.

Considering the family of functions $y(x, \varepsilon)$ in the generalisation of (A7.4), the above deliberations are still relevant if we take

$$\eta(x) = y_\varepsilon|^{\varepsilon=0} \tag{A7.11}$$

Accordingly, the variation of y from (A7.3) results in the *first variation* of the integral I

$$\delta I = \delta \int_{x_0}^{x_1} F\,\mathrm{d}x = \varepsilon \left[\frac{\partial}{\partial\varepsilon}\int_{x_0}^{x_1} F(\varepsilon)\,\mathrm{d}x\right]_{\varepsilon=0} = \int_{x_0}^{x_1} \varepsilon\left[\frac{\partial F(\varepsilon)}{\partial\varepsilon}\right]_{\varepsilon=0}\mathrm{d}x = \int_{x_0}^{x_1}\delta F\,\mathrm{d}x \tag{A7.12}$$

i. e. variation and integration are interchangeable in calculus of variations. In (A7.12), δF is formed by the functions y and y' to be varied according to the same rules as the differential $\mathrm{d}F$ with respect to y and y':

$$\delta F = F_y\,\delta y + F_{y'}\,\delta y' \tag{A7.13}$$

Comparing (A7.5) with (A7.12) and (A7.13) reveals that the necessary condition for the occurrence of an extreme value of a functional I is the disappearance of its first variation, $\delta I = 0$.

A7.4 Second variation

The *second variation* of a function $F(y,z)$ is formed from the first variation

$$\delta F = F_y\,\delta y + F_z\,\delta z \tag{A7.14}$$

in the same way as δF is formed from F, i. e.

$$\delta^2 F = F_{yy}(\delta y)^2 + 2F_{yz}\delta y\delta z + F_{zz}(\delta z)^2 \tag{A7.15}$$

Developing F at point $y + \varepsilon\eta$, $z + \varepsilon\zeta$ into a TAYLOR series results in

$$\begin{aligned}\overline{F}(\varepsilon) &= F(y,z) + (F_y\varepsilon\eta + F_z\varepsilon\zeta) + \frac{1}{2!}[F_{yy}(\varepsilon\eta)^2 + 2F_{yz}(\varepsilon\eta)(\varepsilon\zeta) + F_{zz}(\varepsilon\zeta)^2] + \ldots \\ &= F + \delta F + \frac{1}{2!}\delta^2 F + \ldots\end{aligned} \tag{A7.16}$$

The second variation of the functional (A7.3) is formed from (A7.12) by taking into account (A7.13) in the same way, i. e.

$$\delta^2 I = \int_{x_0}^{x_1} [F_{yy}(\delta y)^2 + 2F_{yy'}(\delta y)(\delta y') + F_{y'y'}(\delta y')^2]\,\mathrm{d}x \tag{A7.17}$$

and developing I at point $y + \varepsilon\eta$ into a TAYLOR series results in

$$\bar{I}(\varepsilon) = I + \delta I + \frac{1}{2!}\delta^2 I + \ldots \tag{A7.18}$$

Necessarily, $\delta I = 0$ applies at the point of an extreme value. The difference $\bar{I} - I$ is then determined by $\delta^2 I$ because the variations of I of higher order disappear owing to the smallness of ε compared with $\delta^2 I$. If $\delta^2 I$ is positive (negative), I takes on a minimum (maximum).

Further, exploiting the arbitrariness of η allows us to demonstrate that the LEGENDRE condition $F_{y'y'} \geq 0$ for a minimum ($F_{y'y'} \leq 0$ for a maximum) persists along the extremals [5].

A7.5 Several functions required

Where

$$I = \int_{x_0}^{x_1} F(x, y, z, \ldots, y', z', \ldots)\,\mathrm{d}x \tag{A7.19}$$

should take on an extreme value, we form the families of functions $y + \varepsilon_1\eta$, $z + \varepsilon_2\zeta$, ... using the functions $\eta(x)$, $\zeta(x)$, ... (disappearing at the boundary but otherwise random) in a similar way to (A7.4), and require that the derivatives $\partial\bar{I}(\varepsilon_i)/\partial\varepsilon_j$ disappear for $\varepsilon_j = 0$. In a similar way to (A7.8), we then get the differential equations

$$F_y - \frac{\mathrm{d}}{\mathrm{d}x}F_{y'} = 0 \quad , \quad F_z - \frac{\mathrm{d}}{\mathrm{d}x}F_{z'} = 0, \ldots \tag{A7.20}$$

which take on the form

$$\begin{aligned} &F_y - F_{y'y'}y'' - F_{y'z'}z'' - \ldots - F_{y'y}y' - F_{y'z}z' - \ldots - F_{y'x} = 0, \\ &F_z - F_{z'y'}y'' - F_{z'z'}z'' - \ldots - F_{z'y}y' - F_{z'z}z' - \ldots - F_{z'x} = 0, \\ &\ldots \end{aligned} \tag{A7.21}$$

when written out in full.

A7.6 Higher-order derivatives

The integral

$$I = \int_{x_0}^{x_1} F(x, y, y', y'', \ldots, y^{(n)})\,\mathrm{d}x \tag{A7.22}$$

should take on an extreme value.All functions with continuous derivatives up to the order $2n$ are admissible for which, at the boundary, the values of the function and the values of the derivatives up to the order $n-1$ are given (essential boundary conditions, see section A7.2). We use the family of functions $y + \varepsilon\eta$ to obtain the first variation

$$\delta I = \varepsilon \int_{x_0}^{x_1} \left[F_y\eta + F_{y'}\eta' + \ldots + F_{y^{(n)}}\eta^{(n)}\right] \mathrm{d}x \tag{A7.23}$$

Repeated integration by parts causes all the derivatives of η to disappear

$$\delta I = \varepsilon \int_{x_0}^{x_1} \eta \left[F_y - \frac{\mathrm{d}}{\mathrm{d}x}F_{y'} + \frac{\mathrm{d}^2}{\mathrm{d}x^2}F_{y''} - \ldots + (-1)^n \frac{\mathrm{d}^n}{\mathrm{d}x^n}F_{y^{(n)}}\right] \mathrm{d}x \tag{A7.24}$$

and according to the fundamental lemma of calculus of variations, the EULER-LAGRANGE equation

$$F_y - \frac{\mathrm{d}}{\mathrm{d}x}F_{y'} + \frac{\mathrm{d}^2}{\mathrm{d}x^2}F_{y''} - \ldots + (-1)^n \frac{\mathrm{d}^n}{\mathrm{d}x^n}F_{y^{(n)}} = 0 \tag{A7.24}$$

must apply for an extreme value.

We obtain corresponding sets of EULER-LAGRANGE equations when several functions are to be determined in a variational problem with higher-order derivatives.

A7.7 Several independent variables

The variational problems considered hitherto for determining the extreme values of simple integrals led to ordinary differential equations. Determining the extreme values of mulitple integrals leads, similarly, to one or more partial differential equations.

For example, the double integral over a certain domain A with boundary C

$$I = \int_A F(x, y, u, u_x, u_y)\,\mathrm{d}x\,\mathrm{d}y \tag{A7.26}$$

is to be set to the extreme value using a function u (with continuous derivatives up to the second order), where the boundary values of u are given. As given above, introducing a function $\eta(x, y)$, disappearing at the boundary but otherwise random, leads, together with parameter ε, to

$$\delta I = \varepsilon \left[\frac{\partial}{\partial \varepsilon} \int_A F(u + \varepsilon\eta)\,\mathrm{d}x\,\mathrm{d}y \right]_{\varepsilon=0} = 0 \tag{A7.27}$$

i. e.

$$\delta I = \varepsilon \int_A (F_u \eta + F_{u_x}\eta_x + F_{u_y}\eta_y)\,\mathrm{d}x\,\mathrm{d}y = 0 \tag{A7.28}$$

According to GAUSS' theorem (A6.30),

$$\int_A (\eta_x F_{u_x} + \eta_y F_{u_y})\,\mathrm{d}x\,\mathrm{d}y = \int_C \eta(F_{u_x}\mathrm{d}y - F_{u_y}\mathrm{d}x) - \int_A \eta\left(\frac{\partial}{\partial x}F_{u_x} + \frac{\partial}{\partial y}F_{u_y}\right)\mathrm{d}x\,\mathrm{d}y \tag{A7.29}$$

applies, and since η disappears at C, we obtain

$$\delta I = \varepsilon \int_A \eta\left(F_u - \frac{\partial}{\partial x}F_{u_x} - \frac{\partial}{\partial y}F_{u_y}\right)\mathrm{d}x\,\mathrm{d}y \tag{A7.30}$$

instead of (A7.28). Further, according to the fundamental lemma of calculus of variations, the expression in brackets in the integrand of (A7.30) must disappear:

$$F_u - \frac{\partial}{\partial x}F_{u_x} - \frac{\partial}{\partial y}F_{u_y} = 0 \tag{A7.31}$$

which when written out in full is

$$F_u - F_{u_x u_x}u_{xx} - 2F_{u_x u_y}u_{xy} - F_{u_y u_y}u_{yy} - F_{u_x u}u_x - F_{u_y u}u_y - F_{u_x x} - F_{u_y y} = 0 \tag{A7.32}$$

We get a set of such partial differential equations when several unknown functions have to be determined. When higher-order derivatives up to order n occur, we get a differential equation of the order $2n$

$$F_u - \frac{\partial}{\partial x}F_{u_x} - \frac{\partial}{\partial y}F_{u_y} + \frac{\partial^2}{\partial x^2}F_{u_{xx}} + 2\frac{\partial^2}{\partial x \partial y}F_{u_{xy}} + \frac{\partial^2}{\partial y^2}F_{u_{yy}} + \ldots + (-1)^n \frac{\partial^n}{\partial y^n}F_{u_{yy\ldots y}} = 0 \tag{A7.33}$$

instead of (A7.31).

A7.8 Variational problems with side conditions

The argument functions of a variational problem are frequently subjected to side conditions of another kind as well as the boundary conditions.

The *isoperimetric problem* represents the simplest of such tasks. In this, the integral (A7.3) should take on an extreme value, whereas the function y is subjected to a side condition

$$\int_{x_0}^{x_1} G(x, y, y')\,\mathrm{d}x = \text{const} \tag{A7.34}$$

as well as the boundary conditions. To solve this problem, we form the LAGRANGE function

$$H = F + \lambda G \tag{A7.35}$$

with the constant LAGRANGE multiplier λ and thus obtain the EULER-LAGRANGE equation

$$H_y - \frac{\mathrm{d}}{\mathrm{d}x} H_{y'} = 0 \tag{A7.36}$$

If the integral

$$I = \int_{x_0}^{x_1} F(x, y, z, y', z')\,\mathrm{d}x \tag{A7.37}$$

subjected to the side condition

$$G(x, y, z) = 0 \tag{A7.38}$$

is to take on an extreme value, then once again we set up the LAGRANGE function (A7.35), where λ is now a function $\lambda(x)$ of x. The EULER-LAGRANGE equations

$$H_y - \frac{\mathrm{d}}{\mathrm{d}x} H_{y'} = 0 \quad , \quad H_z - \frac{\mathrm{d}}{\mathrm{d}z} H_{z'} = 0 \tag{A7.39}$$

together with (A7.38) and the boundary conditions for y and z then enable us to determine y, z and λ.

In the same way, using a multiplier $\lambda(x)$ enables us to solve cases with more general side conditions in the form

$$G(x, y, z, y', z') = 0 \tag{A7.40}$$

as well and, similarly, we can also handle problems with higher-order derivatives, several unknown functions, several side conditions and several independent variables.

A7.9 The RITZ method

It is often difficult, sometimes even impossible, to solve the EULER-LAGRANGE equations, but this problem can always be overcome by employing the approximation method devised by RITZ.

For example, in order to determine the function y in the integral (A7.22), we assume

$$y = \sum_{i=1}^{n} c_i\,\omega_i \tag{A7.41}$$

where the approximating functions ω_i must satisfy the essential boundary conditions for y. And since $\delta I = 0$, the n coefficients c_i then follow from

$$\frac{\partial I}{\partial c_1} = \frac{\partial I}{\partial c_2} = \ldots = \frac{\partial I}{\partial c_n} = 0 \tag{A7.42}$$

Example A7.1 Cantilever beam rigid in shear

A cantilever beam with infinite shear stiffness and length l is fixed at $x = 0$ and carries a line load q in the z direction. Its bending stiffness and deflection are denoted with EI and w respectively. The total potential

$$\Pi = \int_0^l \left(\frac{1}{2} EI w''^2 - qw\right) \mathrm{d}x \tag{A7.43}$$

is a minimum for the real function $w(x)$. The presence of w'' in (A7.43) means that the essential boundary conditions $w = 0$ and $w' = 0$ apply for $x = 0$, and these are satisfied by setting

$$w = \sum_{i=2}^{n} c_i\,x^i \tag{A7.44}$$

If EI and q are constant, then using $\partial\Pi/\partial c_i = 0$ with $n = 2$ gives us the value $c_2 = ql^2/(12EI)$; putting $n = 3$, the values are $c_2 = 5ql^2/(24EI)$, $c_3 = -ql/(12EI)$; and putting $n = 4$, then $c_2 = ql^2/(4EI)$, $c_3 = -ql/(6EI)$, $c_4 = -q/(24EI)$, corresponding to the exact solution

$$w = \frac{ql^4(6\xi^2 - 4\xi^3 + \xi^4)}{24EI} \qquad \left(\xi = \frac{x}{l}\right) \tag{A7.45}$$

The values $\Pi_2 = -q^2l^5/(72EI)$, $\Pi_3 = -7q^2l^5/(288EI)$ and $\Pi_4 = -q^2l^5/(40EI)$ follow for the associated approximations of the total potential, which demonstrates the successive approximation of the exact value $\Pi = \Pi_4$.

A7.10 Natural boundary conditions

Up until now we have always assumed that the argument functions to be determined take on prescribed boundary values. However, there are often no conditions for the boundary values. We then speak of *free edges* that can be dealt with by not setting the variation of the functions at the boundary to zero right from the start.

In the simplest variational problem, we thus get the condition

$$\delta I = \int_{x_0}^{x_1} \left(F_y - \frac{\mathrm{d}}{\mathrm{d}x}F_{y'}\right)\delta y\,\mathrm{d}x + F_{y'}\,\delta y\Big|_{x_0}^{x_1} = 0 \tag{A7.46}$$

instead of (A7.6). Owing to the randomness of δy, eq. (A7.8) must be satisfied on the one hand, and, on the other, the *natural boundary condition* $F_{y'} = 0$ must apply for $x = x_0$ and $x = x_1$.

Correspondingly, for (A7.19) or (A7.26) we get, apart from the EULER-LAGRANGE equations, the natural boundary conditions $F_{y'} = 0$ and $F_{z'} = 0$ for $x = x_0$ and $x = x_1$ or

$$F_{u_x}\mathrm{d}y - F_{u_y}\mathrm{d}x = 0$$

on the edge C.

Example A7.2 Cantilever beam – uniformly distributed load plus load at free end

If we apply a point load Q_0 and a moment M_0 to the free end of the cantilever beam of example A7.1 (see Fig. 8.14), then we obtain

$$\Pi = \int_0^l \left(\frac{1}{2}EIw''^2 - qw\right)\mathrm{d}x - Q_0 w\Big|^{x=l} + M_0 w'\Big|^{x=l} \tag{A7.47}$$

instead of (A7.43), where w has to satisfy the essential boundary conditions $w = 0$ and $w' = 0$ for $x = 0$. The condition

$$\delta\Pi = \int_0^l (EIw''\,\delta w'' - q\,\delta w)\,\mathrm{d}x - Q_0\,\delta w\Big|^{x=l} + M_0\,\delta w'\Big|^{x=l} = 0 \tag{A7.48}$$

can be rewritten in the form

$$\delta\Pi = -\int_0^l (M'' + q)\,\delta w\,\mathrm{d}x + (M' - Q_0)\,\delta w\Big|^{x=l} - (M - M_0)\,\delta w'\Big|^{x=l} = 0 \tag{A7.49}$$

by using $M = -EIw''$ and taking into account the boundary conditions $\delta w = \delta w' = 0$ for $x = 0$ with double integration by parts, from which we get, on the one hand, the EULER-LAGRANGE equation

$$M'' + q = -(EIw'')'' + q = 0 \tag{A7.50}$$

and, on the other, the natural boundary conditions

$$M' = -(EIw'')' = Q_0 \quad , \quad M = -EIw'' = M_0 \tag{A7.51}$$

for $x = l$.

Where EI is constant and $q = 0$, then integrating (A7.50) and taking into account the (essential and natural) boundary conditions results in

$$w = \frac{Q_0 l^3\left[3\left(1 - \dfrac{M_0}{Q_0 l}\right)\xi^2 - \xi^3\right]}{6EI} \qquad \left(\xi = \frac{x}{l}\right) \tag{A7.52}$$

REFERENCES

[1] Argyris, J. H.: Energy Theorems and Structural Analysis; *Aircraft Engineering*, vol. 26, 1954, pp. 347–356, 383–387, 394; vol. 27, 1955, pp. 42–58, 80–94, 125–134, 145–158.

[2] Bažant, Z. P.: Prediction of Concrete Creep Effects Using Age-Adjusted Effective Modulus Method; *ACI Journal*, vol. 69, No. 3, 1972, pp. 212–217.

[3] Bažant, Z. P., Cedolin, L.: Stability of Structures; Oxford University Press, 1991, 984pp.

[4] Chen, W. F.: Limit Analysis and Soil Plasticity; Elsevier, Amsterdam, 1975, 638pp.

[5] Courant, R., Hilbert, D.: Methoden der mathematischen Physik (Methods of Mathematical Physics); 1st vol., 2nd ed., Springer-Verlag, Berlin, 1931, 469pp.

[6] Flügge, W.: Stresses in Shells; 3rd printing, Springer-Verlag, New York, 1966, 499pp.

[7] Fox, E. N.: Limit Analysis for Plates: The Exact Solution for a Clamped Square Plate of Isotropic Homogeneous Material Obeying the Square Yield Criterion and Loaded by Uniform Pressure; *Philosophical Transactions of the Royal Society*, London, vol. 277, series A, 1974, pp. 121–155.

[8] Hake, E., Meskouris, K.: Statik der Flächentragwerke; 2nd ed., Springer-Verlag, Berlin/Heidelberg, 2007, 313pp.

[9] Heyman, J.: Plastic Design of Frames – 2. Applications; Cambridge University Press, 1971, 292pp.

[10] Heyman, J.: Structural Analysis – A Historical Approach; Cambridge University Press, 1998, 174pp.

[11] Hillerborg, A.: Strip Method of Design; Viewpoint Publications, Wexham Springs, 1975, 256pp.

[12] Johansen, K. W.: Yield-Line Theory; Cement and Concrete Association, London, 1962, 181pp.

[13] Krätzig, W. B., Harte, R., Meskouris, K., Wittek, U.: Tragwerke 1; 5th ed., Springer-Verlag, 2010, 300pp.

[14] Krätzig, W. B., Harte, R., Meskouris, K., Wittek, U.: Tragwerke 2; 4th ed., Springer-Verlag, 2004, 424pp.

[15] Krätzig, W. B., Başar, Y.: Tragwerke 3, Springer-Verlag, 1997, 402pp.

[16] Kurrer, K.-E.: Geschichte der Baustatik (The History of the Theory of Structures); Ernst & Sohn, Berlin, 2002, 539pp.

[17] Marti, P.: Gleichgewichtslösungen für Flachdecken; *Schweizer Ingenieur und Architekt*, vol. 99, No. 38, 1981, pp. 799–809.

[18] Marti, P.: Design of Concrete Slabs for Transverse Shear; *ACI Structural Journal*, vol. 87, No. 2, 1990, pp. 180–190.

[19] Marti, P., Monsch, O., Schilling, B.: Ingenieur-Betonbau, vdf Hochschulverlag an der ETH, Zurich, 2005, 225pp.

[20] Meskouris, K., Hake, E.: Statik der Stabtragwerke; 2nd ed., Springer-Verlag, Berlin/Heidelberg, 2009, 276pp.

[21] Meskouris, K., Butenweg, C., Hake, E., Heller, S.: Baustatik in Beispielen; Springer-Verlag, Berlin/Heidelberg, 2005, 405pp.

[22] Nielsen, M. P.: Limit Analysis of Reinforced Concrete Slabs; Acta Polytechnica Scandinavica, Civil Engineering and Building Construction Series, No. 26, 1964, 167pp.

[23] Nielsen, M. P.: Limit Analysis and Concrete Plasticity; Prentice-Hall, 1984, 420pp.

[24] Petersen, C.: Statik und Stabilität der Baukonstruktionen; Friedr. Vieweg & Sohn, Braunschweig, 1980, 960pp.

[25] Prager, W.: Probleme der Plastizitätstheorie; Birkhäuser, Basel, 1955, 100pp.

[26] Prager, W.: Einführung in die Kontinuumsmechanik; Birkhäuser, Basel/Stuttgart, 1961, 228pp.

[27] Swaczuk, A., Jaeger, T.: Grenztragfähigkeits-Theorie der Platten; Springer-Verlag, 1963, 522pp.

[28] Sayir, M. B., Dual, J., Kaufmann, S.: Ingenieurmechanik 1 – Grundlagen und Statik; B. G. Teubner Verlag, Wiesbaden, 2004, 222pp.

[29] Sayir, M. B., Dual, J., Kaufmann, S.: Ingenieurmechanik 2 – Deformierbare Körper; 2nd ed., B. G. Teubner Verlag, Wiesbaden, 2009, 335pp.

[30] Schumann, W.: On Isoperimetric Inequalities in Plasticity; *Quart. Appl. Math.*, vol. 16, 1958, pp. 309–314

[31] SIA: NORM SIA 260 – Grundlagen der Projektierung von Tragwerken; Schweizerischer Ingenieur- und Architektenverein, Zurich, 2003, 44pp.

[32] Straub, H.: Die Geschichte der Bauingenieurkunst (A History of Civil Engineering); Birkhäuser, Basel, 1992, 437 pp.

[33] Szabó, I.: Geschichte der mechanischen Prinzipien; Birkhäuser, Basel, 1977, 491pp.

[34] Timoshenko, S. P., Woinowsky-Krieger, S.: Theory of Plates and Shells; McGraw-Hill, 1959, 580pp.

[35] Timoshenko, S. P., Gere, J. M.: Theory of Elastic Stability; McGraw-Hill, 1961, 541pp.

[36] Timoshenko, S. P., Goodier, J. N.: Theory of Elasticity; McGraw-Hill, 1970, 567pp.

[37] Trost, H.: Auswirkung des Superpositionsprinzips auf Kriech- und Relaxationsprobleme bei Beton und Spannbeton; *Beton und Stahlbetonbau*, vol. 62, No. 10, 1967, pp. 230–238.

[38] Ziegler, H.: Vorlesungen über Mechanik; Birkhäuser, Basel, 1977, 445pp.
[39] Zurmühl, R.: Matrizen und ihre technischen Anwendungen; 4th ed., Springer-Verlag, Berlin/Göttingen/Heidelberg, 1964, 452pp.

NAME INDEX

AIRY, George Bidell, Sir (1801 – 1892) 492
ARCHIMEDES of Syracuse (c. 287 – c. 212 BC) 5, 329

BAUSCHINGER, Johann (1834 – 1893) 329
BERNOULLI, Daniel (1700 – 1782) 6
BERNOULLI, Jacob (1654 – 1705) 6, 108, 187
BERNOULLI, Johann (1667 – 1748) 6
BETTI, Enrico (1823 – 1892) 8, 128
BOŠCOVIĆ, Ruggiero Giuseppe (1711 – 1787) 5
BOUSSINESQ, Valentin Joseph (1842 – 1929) 99
BREDT, Rudolph (1842 – 1900) 205

CASTIGLIANO, Carlo Alberto (1847 – 1884) 8, 118, 122
CAUCHY, Augustin Louis (1789 – 1857) 8
CLAPEYRON, Benoît Pierre Emile (1799 – 1864) 8
COULOMB, Charles Augustin de (1736 – 1806) 7, 87, 517
CREMONA, Antonio Luigi Gaudenzio Giuseppe (1830 – 1903) 8, 169, 171
CROSS, Hardy (1885 – 1959) 305
CULMANN, Karl (1821 – 1881) 8, 166

D'ALEMBERT, Jean-Baptiste le Rond (1717 – 1783) 116
DA VINCI, Leonardo (1452 – 1519) 5
DE NEMORE, Jordanus (c. 1200) 5
DRUCKER, Daniel (1918 – 2001) 86

EINSTEIN, Albert (1879 – 1955) 655
ENGESSER, Friedrich (1848 – 1931) 8, 118, 124, 221, 257, 394, 456
EUCLID of Alexandria (c. 360 – c. 280 BC) 654
EULER, Leonhard (1707 – 1783) 6, 84, 452, 473, 662

FOULKES, John David Percy (1924 – 2002) 438
FOURIER, Jean Baptiste Joseph (1768 – 1830) 331, 353, 492, 535, 593

GALERKIN, Boris Grigorievic (1871 – 1945) 133, 455
GALILEO Galilei (1564 – 1642) 6
GAUSS, Carl Friedrich (1777 – 1855) 114, 305, 532, 596, 652, 659, 665
GERBER, Heinrich (1832 – 1912) 138, 160
GOODMAN, John (1862 – 1935) 98
GREEN, George (1793 – 1841) 114, 659, 660

HADAMARD, Jacques Salomon (1865 – 1963) 654
HAMILTON, William Rowan, Sir (1805 – 1865) 659
HOOKE, Robert (1635 – 1703) 6, 82

JACQUIER, François (1711 – 1788) 5

KANI, Gaspar (1910 – 1968) 305
KIRCHHOFF, Gustav Robert (1824 – 1887) 113
KOENEN, Mathias (1849 – 1924) 8
KRONECKER, Leopold (1823 – 1891) 60, 655

LAGRANGE, Joseph Louis, Comte de (1736 – 1813) 658, 661, 666
LAMÉ, Gabriel (1795 – 1870) 8, 83
LAND, Robert (1857 – 1899) 9, 179, 303
LANGER, Josef (born 1816) 139
LAPLACE, Pierre Simon de (1749 – 1827) 494, 534, 659
LE SEUR, Thomas (1703 – 1770) 5
LEGENDRE, Adrien Marie (1752 – 1833) 664
LEIBNIZ, Gottfried Wilhelm (1646 – 1716) 6
LÉVY, Maurice (1838 – 1910) 8

MAILLART, Robert (1872 – 1940) 1
MARIOTTE, Edmé (1620 – 1684) 6
MAXWELL, James Clerk (1831 – 1879) 8, 118, 125, 178, 230
MINER, Milton A. 98
MOHR, Otto Christian (1835 – 1918) 8, 54, 55, 59, 73, 89, 188, 233, 238, 526, 532
MÜLLER-BRESLAU, Heinrich Franz Bernhard (1851 – 1925) 9
MUSSCHENBROEK, Pieter van (1692 – 1761) 6

NAVIER, Claude Louis Marie Henri (1785 – 1836) 7
NEWTON, Isaac (1643 – 1727) 6, 471

OSTENFELD, Asger Skovgaard (1866 – 1931) 9

PALMGREN, Arvid G. (1890 – 1971) 98
PARENT, Antoine (1666 – 1716) 6
PAULI, Friedrich August von (1802 – 1883) 167
PERRONET, Jean Rodolphe (1708 – 1794) 7
POISSON, Siméon Denis (1781 – 1840) 8, 81, 201, 534
POLENI, Giovanni (1683 – 1761) 5
POLONCEAU, Jean Barthélémy Camille (1813 – 1859) 167
PRAGER, William (1903 – 1980) 86
PRANDTL, Ludwig (1875 – 1953) 203, 506
PRATT, Thomas Willis (born 1812) 167
PUCHER, Adolf (1902 - 1968) 616

Theory of Structures. First Edition. Peter Marti

RANKINE, William John Macquorn (1820 – 1872) 88
RAPHSON, Joseph (c. 1648 – c. 1715) 471
RAYLEIGH, John William Strutt, Baron (1842 – 1919) 454, 653
RITTER, August (1826 – 1908) 169, 172
RITTER, Karl Wilhelm (1847 – 1906) 8
RITZ, Walter (1878 – 1909) 129, 381, 455, 661, 666

SAINT-VENANT, Adhémar Jean Claude Barré de (1797 – 1886) 8
SCHWEDLER, Johann Wilhelm (1823 – 1894) 167, 168
SEIDEL, Philipp Ludwig (1821 – 1896) 305
SIMPSON, Thomas (1710 – 1761) 223
STEVIN, Simon (1548 – 1620) 5

TAYLOR, Brook (1685 – 1731) 659, 663
TIMOSHENKO, Stephen Prokofievich (1878 – 1972) 108
TRESCA, Henri (1814 – 1885) 85, 547
TRUDAINE, Daniel Charles (1703 – 1769) 7

VARIGNON, Pierre (1654 – 1722) 5
VAUBAN, Sébastien le Prêtre de (1633 – 1707) 7
VIANELLO, Luigi (1862 – 1907) 456
VIERENDEEL, Arthur (1852 – 1940) 323
VOLTERRA, Vito (1860 – 1940) 92
VON KÁRMÁN, Theodore (1891 – 1963) 576
VON MISES, Richard (1883 – 1953) 85, 547

WEIERSTRASS, Karl Theodor Wilhelm (1815 – 1897) 661
WEYRAUCH, Johann Jacob (1845 – 1917) 8
WINKLER, Emil (1835 – 1888) 8, 329
WÖHLER, August (1819 – 1914) 95

SUBJECT INDEX

A
acceptance 12, 631
accidental action 30, 631
accidental design situation 12, 32, 631
accompanying action 32, 631
action effects 12, 29, 631
actions 12, 29, 631
actions on bars 278, 283, 374
active degrees of freedom 101
active work 105, 128
adaptability 394
addition 650
adjoint 114, 656
advanced strip method 566
age-adjusted effective bulk modulus 94
age-adjusted effective elastic modulus 92
age-adjusted effective shear modulus 94
ageing coefficient 92
air-hardened 79
algebraic complement 649
alternating plasticity 266, 392, 435
amplification factor 348, 453
analogies 2
analytical model 1, 12, 31, 631
anchorage of pretensioned steel 318
angle of internal friction 87
annular structure 350
antisymmetric 650
arch 137, 345
arch action 503
area of contact 47
area of section 645
area shear factor 107, 195, 645
argument function 661
associated flow rule 84
axial force parameter 465
axial stiffness 185, 360

B
band matrix 650
bar 52, 137
bar axis 52, 137
bar cross-section 137
bar element 137
bar element rigid in shear 381
bar end rotation 144
bar extension 144, 311
bar polygon 165
bar rotation 144, 290
bar splice 319
bar substitution 170
barrel vault 589, 603
base hinge 163
basic invariants 56, 59, 658
basic system 247, 254
basis 651
basis of design 12, 15, 631
BAUSCHINGER effect 392
beam 137
beam column 131
beam in bending 326
beam in shear 321
beam mechanism 416
beam on elastic foundation 326
bending moment 51, 52, 107, 111
bending stiffness 185
bending theory 591, 596
bending-resistant tie 362
BETTI's theorem 128
bilinear form 652
bimoment 212
body force 43
body load 43
bond 311
bottom chord 167
bound index 655
boundary conditions 235
boundary displacement operator 106
boundary displacements 76, 106
boundary stress operator 106
boundary stresses 105
brittle 80
buckling 575
buckling length 454
buckling load 453, 464, 576
buckling modes 453
buckling stress curves 471, 473
bulk modulus 82

C
cable 137, 354
cable curve 356
cable equation 355
cable force 355
cable sag 356
cable stretch 354
cable-stayed bridge 139
cantilever beam 138, 161
CASTIGLIANO's theorem 118, 122
catenary 357
centroid 187, 645
chain of hinges 161
change in form 72
change in temperature 94
change in volume 72
characteristic determinant 653
characteristic equation 58, 653
characteristic matrix 653
characteristic polynomial 653
characteristic value 30, 631
chord 167
coefficient of thermal expansion 94, 643
cogredient 651
cohesion 87
cold-formed 79
collapse crack 498
column 137, 649
column deflection curve 449
column strip 545
column vector 649
column-regular 650
combined mechanism 416
commissioning 12, 631
compatibility condition 104, 201, 247, 254, 491
compatibility theorem 411
compatible 85, 104, 410
complementary internal total potential 394
complementary total potential 120
complete bar end forces 141, 281
complete bar end variables 281
complete member stiffness matrix 282
complete solution 411
completeness 386
complex truss 170
composite cross-section 190
composition 12, 14, 631
compressible 86
compressive strength 643
computation phase 287
conceptual design 11, 12, 631
condition assessment 12, 631
condition number 654
condition survey 12, 631
conformity 386
congruence transformation 105
congruent matrices 651
conjugate load 238
conjugate stress resultant 238
conjugate system 238
conservation 11, 12, 631
conservative 118
conservative system 119
constitutive equations 79, 106
constitutive relationships 79
construction detail 94

Theory of Structures. First Edition. Peter Marti

construction inspection plan 12, 631
construction inspections 12, 631
construction material 631
construction material properties 12, 31
construction work 12, 632
construction works 11, 12, 632
construction works documents 11, 12, 632
contact force 43
contained plastic deformation 390
continua 105
continuity conditions 235
continuous slab 542
contraction 657
contragredient 104, 651
control measurement 12, 632
control variable 443
convergence requirements 385
coordinate notation 655
coordinate transformation 651
coplanar deformation 72
coplanar strain state 111
coplanar stress state 54, 110
corner force 112, 528
COULOMB yield condition 87
counting scheme 143
coupling beam 161
coupling joint 333
crack spacing 319
crack width 319
creep 91
creep coefficient 91
creep deformations 90, 235
creep function 91
CREMONA diagram 171
CROSS method of moment distribution 305
cross-sectional area 107
cross-sections remain plane 187
crown 163
crown hinge 163
curl 659
curvature 107, 112, 233, 532
curvature tensor 531
curved beam 137, 193, 235
cylindrical shell 601

D

damage accumulation 96
damage accumulation hypothesis 98
dapped end 50
dead load 632
deck-stiffened polygonal arch 66, 139, 165
decommissioning 12, 632
deconstruction 11, 12, 632
defect 632
deflection 111, 531
deflection curve 233
deformation 71
deformation capacity 266, 632
deformation demand 266
deformation diagram 233, 259
deformation state 222
deformation work 104
degree of freedom 47, 141
degree of static indeterminacy 143
density 643
design 11, 12, 632
design alternatives 12, 632
design boundary conditions 12, 13, 632
design criteria 34, 632
design level 35
design situation 12, 29, 32, 632
design value 33, 632
design working life 12, 632
detail design 11, 632
detailing 12, 29, 632
deterioration 94, 632
determinacy 47, 50
determinant 649
developable 532
deviator 60
deviatoric component 60
deviatoric plane 60
diagonal matrix 650
diagonal matrix of eigenvalues 653
diagram of the static system 140
diagrams of stress resultants 159
dilatation 76
dimensioning 11, 12, 632
direct methods 661
direct stiffness method 284
direct support 510
discontinua 105
discontinuous stress field 501
discrete yield line 568
discretised structural model 140
displacement equilibrium 293
displacement field 71
displacement gradient 74
displacement method 104
displacement vector 71
displacement 106
dissipation 81
distortion 76
divergence 659
divergent 462
domain of admissible functions 661
dowelled beam 333, 342
draft design 12, 632
DRUCKER yield condition 86
dual methods 2
dual vector 657
duality theorem of linear programming 443
dummy index 655
durability 12, 14, 32, 632
dyadic product 657
dynamic action 30
dynamics 116

E

eccentrically loaded column 474
economy 12, 14, 632
edge 587
edge disturbance 353
edge force 111
edge load 589
edge shear force 113, 528, 589
effective depth 191, 632
effective strength 429
eigenvalue 653
eigenvector 653
EINSTEIN summation convention 655
elastic 79
elastic optimisation 445
elastic phase 390
elastic section modulus 398
elasticity matrix 106
elastic-plastic 409
elastic-plastic deformation 395
elastic-plastic optimisation 445
elastic-plastic phase 390
elementary mechanism 417
elliptical 532, 596
elongation at failure 643
end plate 587
endurance limit 96, 633
ENGESSER's theorem 118, 124
envelopes 265
equations of motion 3
equilibrium conditions 45
equilibrium conditions of the continuum 57
equilibrium line 393
equilibrium matrix 142
equilibrium system 45
equivalent conditions of the variational problem 662
equivalent force systems 44
equivalent frame 545
essential boundary conditions 661
estimate 633
EULER buckling load 454
EULER-LAGRANGE equations 662
examination 12, 633
exceptional case of statics 143
execution 11, 12, 633
execution documents 12, 633
expansion hinge 50
experimental statics 2
extensible cable 358
external deformation variables 1, 106, 141
external force 45
external force variables 1, 104, 105, 141
externally anchored suspension bridge 139
externally statically determinate 143
extremal 661

F

failure 633
fan action 503
fan mechanism 568
far-end bar stiffness 292
fatigue 94
fatigue behaviour 94
fatigue loading 95
fatigue loads 35, 96
fatigue resistance 12, 32, 94, 96, 633
field line 659

final creep coefficient 91, 643
final shrinkage strain 90, 643
finite element method 3, 381
finite fatigue life 633
finite fatigue life range 96
finite shear stiffness 108
first moment of area 186
first variation 663
first-order theory 71
fixed action 30, 633
fixed support 48
fixed-end forces 278
fixed-end moment 292
flat slab 543
flexibility 103
flexibility matrix 255, 256
flexibility matrix for all members 372
flexible 106
flexural buckling 482
flexural failure 513
flexural hinge 50
flexural-shear failure 514
flexural-torsional buckling 480
flow rule 84
fluctuating loading 95
folded plate structure 52
force 43
force method 103, 372, 441
force per unit area 43, 53
force per unit length 44
force per unit volume 43
force polygon 46
force state 222
force system 44
force transfer 505
force-balance equations 45
force-couple system 44
fork support 208
FOULKES diagram 438
FOULKES mechanism 439
foundation modulus 329
fracture 94
frame 163
frame beam 163
frame leg 163
framed structure 31, 51, 137
framework 137
free action 30, 633
free body 44
free cantilevering 140
free edges 667
free from warping 200
free-body diagram 44
free-body principle 1, 45, 116
full hinge 50
functional 661
fundamental angular frequency 464
fundamental lemma of calculus of variations 662
fundamental operator 128
fundamental theorem of statics 45
funicular polygon 46, 63

G

GALERKIN method 455
GAUSS' theorem 659
GAUSSian algorithm 652
GAUSSian curvature 532
general loading histories 393
generalised deformation increments 397
generalised deformation variables 85
generalised force variables 85
generalised GALERKIN method 133
generalised HOOKE's law 82
generalised stresses 397
geometric hardening 391
geometric non-linearity 72, 117
geometric reinforcement ratio 93, 191
geometric stiffness matrix 470
geometric variables 12, 31, 633
GERBER beam 138, 160
global bar end variables 285
global coordinates 140
global flexibility matrix 103
global stiffness matrix 103, 277
gradient 652, 659
graphical statics 2, 149
GREEN's first identity 659
GREEN's second identity 660
gusset plate 166

H

hanger 163
haunched beam 140
hazard 13, 633
hazard scenario 12, 13, 633
high-cycle fatigue range 96
hinge 50, 137
hinge forces 50
hinged arch 160
hinged frame 160, 163
hinged girder 138, 160
hinged support 48
homogeneous partial stress field 509
hoop stress formula 63
horizontal tension 356
hydrostatic axis 60
hydrostatic component 60
hyperbolic 532, 596
hyperelastic 80, 118

I

ideal column 130
ideal truss 101, 166
identity matrix 650
ill-conditioned 255, 654
imposed load 633
improper orthogonal transformation 651
in equilibrium 45, 104
incidence matrix 284
incidence transformation 284
incompatibility 103
incompressible 83, 85
incremental plastic failure 394
independent bar end forces 141
index notation 655
indirect methods 662
indirect support 509
inertial forces 3, 43, 116
inextensible 106
inextensible cable 357
influence line 177, 303
influence lines for deformation variables 178, 259
influence lines for force variables 178, 261
influence ordinate 177
initial deformation 452
initial length 355
initial normal strain 312
initial restraints 393
initial strain 106
initial stress 106
inner multiplication 657
in-plane forces 110
in-plane load 589
input phase 287
inspection 12, 633
instantaneous centre of rotation 156
integration 12, 14, 633
integration table 223
internal deformation variables 1, 106
internal force 45
internal force variables 1, 104, 105, 141
internally statically indeterminate 143
interpolating function 385
invariant 56
inverse 651
invertible 650
isomer 657
isoperimetric problem 665
isotropic 81, 85, 94
isotropic reinforcement 557
iterative procedure 2

J

joint 137, 417
joint equilibrium 293
joint equilibrium conditions 141
joint loads 141
joint mechanism 418
joint rotation 290

K

kern 189
kinematic boundary conditions 76
kinematic discontinuity 89
kinematic method 411, 412, 512, 567
kinematic operator 106
kinematic relations 72, 75
kinematic transformation matrix 101
kinematically admissible 76, 115
kinematically determinate 146
kinematically determinate basic system 101, 146
kinematically unstable 142
KRONECKER symbol 60, 655
K-truss 139

L
LAGRANGE function 661
LAMÉ constants 83
LANGER beam 139
lateral buckling 480
lattice girder 138
leading action 32, 633
leading hazard 32, 633
level surface 659
limit analysis 409
limit load 245, 390
limit load according to second-order theory 477
limit load program 442
limit of proportionality 79
limit state 12, 31, 633
line force 44
line load 44, 107
line load moment 62, 107
linear dependence 650
linear elastic 81
linear elastic system 125
linear mapping 651
linear statics 71
linear viscoelastic 91
linearly hardening plastic 81
load case 12, 29, 32, 633
load factor 33
load parameter 253
load train 177
load vector 255
loaded chord 177
loading processes 391
loading stress state 392
loads 105
local bar end variables 285
local coordinates 140
logarithmic spiral 519
low-cycle fatigue range 96
lower-bound theorem 393, 410

M
main cable 139
maintenance 12, 633
maintenance plan 12, 633
mass matrix 3
material 633
material non-linearity 72, 117
matrix 649
matrix norm 654
maximum 661
maximum shear stress 60
MAXWELL's generalised theorem 118, 125
MAXWELL's theorem 125, 230
mean curvature 532
mean shear strain 107, 112
mechanism 246, 390
member flexibility matrix 277
member flexibility relation 372
member stiffness matrix 277
membrane 53
membrane action 575
membrane analogy 203
membrane force 52, 530
membrane shell 53
membrane theory 589, 596
meridian 596
meridian plane 596
method of construction 12, 633
method of inequalities 420
methods of theory of structures 2
middle plane 52
middle plane of slab 531
middle strip 545
middle surface 52
middle surface of slab 531
minimal surface 532
minimum 661
minor 649
modal analysis 3
modal damping 3
modal matrix 653
model space 105
models of actions 30
modification 12, 634
modified COULOMB yield condition 88
modular ratio 93, 190
modulus of elasticity 81, 643
modulus of strain hardening 81
modulus of subgrade reaction 329
MOHR's analogy 233, 238
MOHR's circle for second moments of area 188
MOHR's envelopes 89
MOHR's sign convention 54
MOHR's strain circle 73
MOHR's stress circle 54
moment 43
moment carry-over factor 305
moment distribution factor 305
moment of inertia 107, 186
moment-balance equations 45
moment-curvature diagram 398
monitoring 12, 634
monitoring plan 12, 634
multiplication 651
multiply-connected 204
multi-span hinged arch 163
multi-span hinged frame 163
multi-stage loading 95
multi-storey frame 139, 321

N
natural boundary conditions 662, 667
natural vibration 3, 464
natural wavelength 331
near-end bar stiffness 292
necking 79
neutral 454
neutral axis 189
newton 44
nodal zones 507
nominal value 634
non-associated flow rule 84
non-concave 84
non-linear member matrix 469
non-plastic domain 84, 253
non-sway system 290
normal component 658
normal force 51, 107
normal matrix 651
normal moment yield condition 551
normal strain 72, 107
normal stress 53
normal vector 652
nullity 650
number of load cycles 94
numerical methods 3

O
observation 12, 634
observation method 221, 634
octahedral normal strain 76
octahedral normal stress 60
octahedral shear strain 76
octahedral shear stress 61
onset of yield 390
operation instructions 12, 634
optimum design 444
order 649
ordinary GALERKIN method 133
orthogonal matrix 651
orthogonal transformation 651
orthogonality conditions 257
out-of-balance moment 305
output phase 187
outrigger 333
overall stability 12, 31, 449, 634
overlapping stress fields 506
overturning moment 484

P
parabolic 532, 596
parabolic rule 225
parallel-wire cable 354
partial factor 33
partial mechanism 418
partial uplift 46
partitioned matrix 649
passive degrees of freedom 101
passive work 128
perfectly plastic 81, 83
permanent action 30, 634
permissible stress 35, 409
permutation tensor 657
persistent design situation 12, 32, 634
pin-ended strut 139
pin-jointed member 48
pipe 602
plane displacement field 72
plane subsystem 138
planning of remedial measures 12, 634
plastic 79
plastic hinge 245, 399
plastic phase 390
plastic potential 84

plastic reserve 401
plastic reserve in system 405
plastic section modulus 398
plastic strain increment 83
plastic strength of materials 426
plasticity check 414
plate 52
plate action 587
plate and shell structures 31, 52
POISSON's differential equation 201
POISSON's ratio 81, 643
polar moment of inertia 200
pole 54
polygonal domes 604
position vector 43
positive definite 652
positive semi-definite 652
post 167
potential function 118
PRAGER yield condition 86
preliminary design 11, 634
preparation for construction 12, 634
prestressing 392
primary beam 50
principal axes 186, 653
principal component analysis 653
principal directions 55, 58, 658
principal plastic directions 427
principal shear force 527
principal strains 73
principal stresses 55
principal value 658
principle of maximum dissipation energy 85, 396, 410
principle of virtual deformations 115
principle of virtual forces 115
principle of virtual work 1, 116, 410
product of inertia 186
progressive plastification 266, 392, 435
prop 163
proper orthogonal transformation 651
propped beam 138, 161
protection and welfare measures 12, 634
prudent estimate 634
pull-out test 316
punching failure 575
pure bending 61, 188
pure torsion 202
pure torsional moment 207
pylon 139, 166

Q

quadratic form 652
quotient rule 657

R

radius of gyration 189
rank 650
RAYLEIGH quotient 454, 653
reaction 43
reaction principle 1, 43, 116
rearrangement of the load 65
recommendation for remedial measures 12, 634
record of construction 12, 634
reduced degrees of freedom 376
reduced stiffness matrix 278
reduction theorem 227, 257
redundant variable 103, 247, 254
reinforced concrete plate element 496
reinforced concrete tie 318
relaxation 91
relaxation function 91
reliability 12, 14, 634
reliability theory 33
remote force 43
repair 12, 634
repeated loading 95
report on remedial measures 12, 634
representative stress 36
representative value 30, 634
residual stress 30, 94, 192, 314, 473
resistance 634
resistance factor 33
resistant 107
restraint 30, 74, 94, 298, 315, 327
restraint parameter 253
restraint state 122, 392
resultant couple 44
resultant force 44
reversed loading 95
rib 168
ridge hinge 163
rigid 106
rigid - perfectly plastic 81, 409
rigid body 31
rigid body deformations 105
rigid body equilibrium 45
rigid body motion 71
rigid in shear 106, 108, 113
rigid-plastic optimisation 444
ring 168
rise 65, 163
RITTER method of sections 172
RITZ method 129, 455, 666
robustness 12, 14, 634
rotation 71, 109
rotation matrix 655
rotation mechanism 516
rotational spring 49
rotational transformation 285
rotationally symmetric cylindrical shell 613
row 649
row deficit 103
row vector 649
row-regular 650
ruled surface 532

S

sand hill analogy 433
sandwich model 555
sandwich panel 324
sawtooth roof 588
scalar field 659
scalar matrix 650
scale effect 575
scaling 651
secant stiffness 475
secant stiffness matrix 471
second moments of area 645
second variation 663
secondary beam 50
secondary stresses 166
secondary torsion 188
second-order theory 72, 449
self-adjoint 128
self-anchored suspension bridge 139
self-weight of non-structural elements 635
semi-hinge 50
service criteria 12, 635
service criteria agreement 12, 14, 635
service instructions 12, 635
service situation 12, 13, 635
serviceability 12, 29, 635
serviceability limit 33, 635
serviceability limit state 32, 635
shakedown theorem 265, 394
shallow shell 615
shape factor 398
shape function 381, 385
shear area 107
shear centre 199, 645
shear flow 205, 527
shear force 51, 52, 107, 111
shear force potential 534
shear hinge 50
shear modulus 82, 643
shear span 434
shear stiffness 185
shear strain 72
shear stress 53
shear wall - frame system 334
shear wall connection 338
shear wall coupling beam 333
shell 53
shell operator 616
shells of any form 606, 623
shrinkage 90
shrinkage deformations 90, 235
shrinkage strain 90
sign convention I 144, 149
sign convention II 144
similar matrices 651
simple strip method 566
simple truss 170
simply supported beam 138
simply-connected 204
SIMPSON's rule 223
single-stage loading 95
singular 650
skew bending 62, 188, 426
skew-symmetric 650
slab 52, 111
slab action 587
sliding support 48
slip line 499, 519

slope-deflection method 290, 465
small deformations 71
S-N curve 95
snap-through load 462
solution vector 652
space truss 167
special eigenvalue problem 653
specific complementary energy 82, 118
specific incremental dissipation energy 84
specific strain energy 82, 118
spherical shell 621
spiral cable 354
springing 65, 163
springing hinge 163
square matrix 649
square yield condition 90
stable 45, 454
state diagrams 52, 159
state variables 52, 159
static action 30
static boundary conditions 58, 528
static discontinuity line 113, 527
static method 411, 412, 501, 557
static operator 106
static system 138
static transformation matrix 102
statically admissible 58, 115
statically determinate 45, 142
statically determinate basic system 103, 143
statically indeterminate 45, 143
statically indeterminate force variable 103
statics 116
stationary value 661
stay cable 362
stiff 106
stiff arch 66
stiffened beam with intermediate hinge 160
stiffness 103
stiffness of rotational spring 49
stiffness of translational spring 49
strain hardening 79
strain interpolation matrix 381
strain tensor 72, 75
strains 106
strains in middle plane of slab 533
strand 354
stranded cable 354
stress components 54
stress concentration factor 495
stress difference 94
stress discontinuity line 505
stress function 201, 492
stress resultants 51, 159
stress ribbon 363
stress tensor 56
stress transformation relationships 54
stress vector 43, 53
stresses 105
stress-strain diagram 79
stringer 311
stringer-panel model 501, 511
strip method 424, 563
structural analysis 11, 12, 29, 635
structural calculations 12, 29, 36, 635
structural concept 11, 12, 635
structural dynamics 3
structural engineering 1, 3
structural mechanics 1, 4
structural member 635
structural model 1, 12, 31, 138, 635
structural safety 12, 29, 635
structural system 137, 635
structure 11, 12, 635
strut 165
strut action 503
strutted beam 139
submatrix 649
subsoil 635
subsoil properties 12, 31
successive approximation of column deflection curve 456
superposition law 2, 71, 125, 254
supplementary safety measures 12, 635
support 47, 137
support envelope 47
support force variables 140, 283
support force-couple system 47
supporting plane 85
surface force 43
surface load 43
surface of revolution 569, 620
suspended beam 138, 161
suspended roof 363
suspender 139
suspension bridge 166, 368
sway mechanism 416
sway system 290
swelling deformations 90
symbol notation 655
symmetric 650
system bounds 29

T

table of the static system 140
technical report 12, 29, 38, 635
tender design 11, 635
tender documents 12, 635
tensile strength 643
tension stiffening 319
tensor 656
tensor calculus 655
tensor field 658
tensor product 657
tensorial sign convention 56
theorem of associated shear stresses 58
theorem of least complementary total potential 121
theorem of least total potential 119
theory of plastic potential 85, 410
theory of structures 1
theory of thin plastic slabs 553
thermal deformations 90, 94, 192, 235
thermally homogeneous 94
third-order theory 471
three-dimensional continua 113
three-dimensional deformation state 74
three-dimensional stress state 57
three-dimensional structure 31
three-hinged arch 139, 163
three-hinged frame 163
threshold 96
thrust line 63
thrust surface 597
tie 139, 163
top chord 167
torque 51, 109
torsion constant 109, 645
torsional buckling 482
torsional stiffness 185
torsionless 107, 421, 424
torsion-resistant 107, 422, 425
total curvature 532
total potential 119
trace 649
transfer 318
transformation matrix 651
transformed section properties 191
transient design situation 12, 32, 635
translation 71
translation surface 608
translational spring 49
translation-rotation system 71
transposition 650
trapezoidal rule 223
trapezoidal stress distribution method 329
TRESCA yield condition 85, 547
triangular cross-section 207
triangular matrix 650
truss 137, 166
truss diagonal 167
truss model 501, 503
truss types 167
twist 109, 112, 532
twisting moment 52, 111
two-hinged arch 139
two-hinged frame 139
type of construction 636

U

ultimate limit state 31, 636
ultimate resistance 12, 31, 636
ultimate resistance of subsoil 32
uncontained plastic deformation 390
uniaxial stress state 53
unit warping 212
unstable 454
upper-bound theorem 393, 411
urgent safety measures 12, 636
use 11, 12, 636

V

variable action 30, 636
variable-direction forces 460
variation 662
variational derivative 663
variational problems with side conditions 665

vector 656
vector algebra 655
vector field 659
vector gradient 659
vector product 657
verification 29, 33, 636
verification of serviceability 12, 35
verification of structural safety 12, 34
verification of ultimate load 35
VIERENDEEL girder 323
VON MISES yield condition 85, 547

W
warping 200, 211
warping constant 212, 645
warping shear stress 212
warping stress 212
warping torsion 207
warping torsional moment 207
WARREN truss 139
web crushing failure 500, 515
web member 167
well conditioned 255
wind bracing 138
work equation 104
work theorem 221
work-associated variables 1, 105
worst load position 178
wrench 71
wrench axis 71
wrench deformation 71

Y
yield condition 84
yield function 83
yield limit 79, 643
yield line 549
yield line method 567
yield locus 84, 392
yield plateau 79
yield point 79
yield slenderness ratio 472
yield surface 84
zero matrix 649